Espacenet

RSS family dossiers

Family list: WO2015136881 (A1) — 2015-09-17

4 application(s) for: WO2015136881 (A1)

1. NONAQUEOUS-ELECTROLYTE SECONDARY BATTERY					
Inventor: TAKANASHI YUU FUKUI ATSUSHI (+2)	**Applicant:** SANYO ELECTRIC CO [JP]	**CPC:** H01M10/0525 H01M10/0569 H01M10/4235 (+5)	**IPC:** H01M10/052 H01M10/0569 H01M4/36 (+2)	**Publication info:** WO2015136881 (A1) 2015-09-17 Global Dossier	**Priority date:** 2014-03-11
2. Nonaqueous-electrolyte secondary battery					
Inventor: TAKANASHI YUU FUKUI ATSUSHI (+2)	**Applicant:** SANYO ELECTRIC CO	**CPC:** H01M10/0525 H01M10/0569 H01M10/4235 (+5)	**IPC:** H01M10/052 H01M10/0569 H01M4/36 (+2)	**Publication info:** CN106104868 (A) 2016-11-09 CN106104868 (B) 2018-07-13 Global Dossier	**Priority date:** 2014-03-11
3. NONAQUEOUS ELECTROLYTE SECONDARY BATTERY					
Inventor: 高梨 優, 福井 厚史, (+2)	**Applicant:** 三洋電機株式会社	**CPC:** H01M10/0525 H01M10/0569 H01M10/4235 (+5)	**IPC:** C01G51/00 C01G53/00 H01M10/052 (+5)	**Publication info:** JPWO2015136881 (A1) 2017-04-06 JP6414589 (B2) 2018-10-31 Global Dossier	**Priority date:** 2014-03-11
4. NONAQUEOUS ELECTROLYTE SECONDARY BATTERY					
Inventor: TAKANASHI YUU [JP] FUKUI ATSUSHI [JP] (+2)	**Applicant:** SANYO ELECTRIC CO [JP]	**CPC:** H01M10/0525 H01M10/0569 H01M10/4235 (+5)	**IPC:** H01M10/0525 H01M10/0569 H01M10/42 (+1)	**Publication info:** US2017018808 (A1) 2017-01-19 US9923244 (B2) 2018-03-20 Global Dossier	**Priority date:** 2014-03-11

Espacenet

Bibliographic data: WO2015136881 (A1) — 2015-09-17

NONAQUEOUS-ELECTROLYTE SECONDARY BATTERY

Inventor(s): TAKANASHI YUU; FUKUI ATSUSHI; HASEGAWA KAZUHIRO; TSURUTA SHO ± (高梨　優, ; 福井　厚史, ; 長谷川　和弘, ; 鶴田　翔)

Applicant(s): SANYO ELECTRIC CO [JP] ± (三洋電機株式会社)

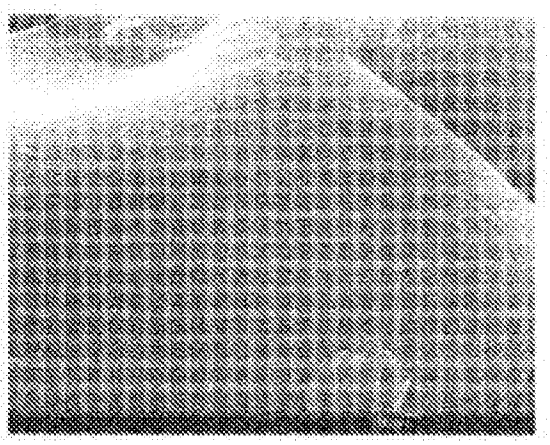
Classification: - international: ***H01M10/052; H01M10/0569; H01M4/36; H01M4/505; H01M4/525***
- cooperative: **H01M10/0525 (EP, US); H01M10/0569 (EP, US); H01M10/4235 (US); H01M4/525 (EP, US);** H01M2300/0034 (EP, US); H01M2300/0037 (EP, US); Y02E60/10 (EP); Y02T10/70 (US)

Application number: WO2015JP01075 20150302 Global Dossier

Priority number (s): JP20140047174 20140311

Also published as: CN106104868 (A) CN106104868 (B) JP6414589 (B2) JPWO2015136881 (A1) US2017018808 (A1) more

Abstract of WO2015136881 (A1)



This invention provides a nonaqueous-electrolyte secondary battery that inhibits change in the structure of a positive-electrode active material under high voltages, allowing both a high capacity and a long service life. Said nonaqueous-electrolyte secondary battery is characterized by the provision of the following: a positive electrode containing a positive-electrode active material that stores and releases lithium ions; a negative electrode containing a negative-electrode active material that stores and releases lithium ions; and a nonaqueous electrolyte. This nonaqueous-electrolyte secondary battery is also characterized in that: the positive-electrode active material is a cobalt complex oxide that contains magnesium in a lithium layer; magnesium is present in said lithium layer after the battery has been charged to a lithium-based potential of at least 4.53 V; and a magnesium-containing compound is present on the negative electrode in an amount

that is between 4.5 mol% and 10 mol%, inclusive, of the amount of magnesium in the positive electrode.

(12) 特許協力条約に基づいて公開された国際出願

(19) 世界知的所有権機関
国際事務局

(43) 国際公開日
2015 年 9 月 17 日(17.09.2015)

WIPO | PCT

(10) 国際公開番号
WO 2015/136881 A1

(51) 国際特許分類:
H01M 4/525 (2010.01) *H01M 10/052* (2010.01)
H01M 4/36 (2006.01) *H01M 10/0569* (2010.01)
H01M 4/505 (2010.01)

(21) 国際出願番号: PCT/JP2015/001075

(22) 国際出願日: 2015 年 3 月 2 日(02.03.2015)

(25) 国際出願の言語: 日本語

(26) 国際公開の言語: 日本語

(30) 優先権データ:
特願 2014-047174 2014 年 3 月 11 日(11.03.2014) JP

(71) 出願人: 三洋電機株式会社 (SANYO ELECTRIC CO., LTD.) [JP/JP]; 〒5748534 大阪府大東市三洋町１番１号 Osaka (JP).

(72) 発明者: 高梨 優(TAKANASHI, Yuu). 福井 厚史(FUKUI, Atsushi). 長谷川 和弘(HASEGAWA, Kazuhiro). 鶴田 翔(TSURUTA, Sho).

(74) 代理人: 徳田 佳昭, 外(TOKUDA, Yoshiaki et al.); 〒5718501 大阪府門真市大字門真１００６番地 パナソニック株式会社内 Osaka (JP).

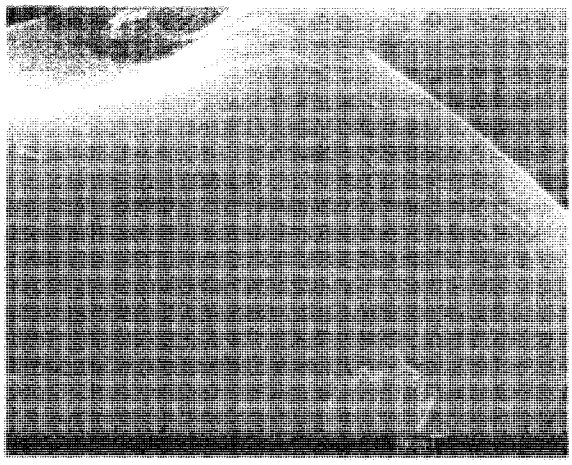
(81) 指定国 (表示のない限り、全ての種類の国内保護が可能): AE, AG, AL, AM, AO, AT, AU, AZ, BA, BB, BG, BH, BN, BR, BW, BY, BZ, CA, CH, CL, CN, CO, CR, CU, CZ, DE, DK, DM, DO, DZ, EC, EE, EG, ES, FI, GB, GD, GE, GH, GM, GT, HN, HR, HU, ID, IL, IN, IR, IS, JP, KE, KG, KN, KP, KR, KZ, LA, LC, LK, LR, LS, LU, LY, MA, MD, ME, MG, MK, MN, MW, MX, MY, MZ, NA, NG, NI, NO, NZ, OM, PA, PE, PG, PH, PL, PT, QA, RO, RS, RU, RW, SA, SC, SD, SE, SG, SK, SL, SM, ST, SV, SY, TH, TJ, TM, TN, TR, TT, TZ, UA, UG, US, UZ, VC, VN, ZA, ZM, ZW.

(84) 指定国 (表示のない限り、全ての種類の広域保護が可能): ARIPO (BW, GH, GM, KE, LR, LS, MW, MZ, NA, RW, SD, SL, ST, SZ, TZ, UG, ZM, ZW), ユーラシア (AM, AZ, BY, KG, KZ, RU, TJ, TM), ヨーロッパ (AL, AT, BE, BG, CH, CY, CZ, DE, DK, EE, ES, FI, FR, GB, GR, HR, HU, IE, IS, IT, LT, LU, LV, MC, MK, MT, NL, NO, PL, PT, RO, RS, SE, SI, SK, SM, TR), OAPI (BF, BJ, CF, CG, CI, CM, GA, GN, GQ, GW, KM, ML, MR, NE, SN, TD, TG).

添付公開書類:
— 国際調査報告（条約第 21 条(3)）

(54) **Title**: NONAQUEOUS-ELECTROLYTE SECONDARY BATTERY

(54) 発明の名称 : 非水電解質二次電池



(57) **Abstract**: This invention provides a nonaqueous-electrolyte secondary battery that inhibits change in the structure of a positive-electrode active material under high voltages, allowing both a high capacity and a long service life. Said nonaqueous-electrolyte secondary battery is characterized by the provision of the following: a positive electrode containing a positive-electrode active material that stores and releases lithium ions; a negative electrode containing a negative-electrode active material that stores and releases lithium ions; and a nonaqueous electrolyte. This nonaqueous-electrolyte secondary battery is also characterized in that: the positive-electrode active material is a cobalt complex oxide that contains magnesium in a lithium layer; magnesium is present in said lithium layer after the battery has been charged to a lithium-based potential of at least 4.53 V; and a magnesium-containing compound is present on the negative electrode in an amount that is between 4.5 mol% and 10 mol%, inclusive, of the amount of magnesium in the positive electrode.

(57) 要約:

[続葉有]

WO 2015/136881 A1

高電圧下における正極活物質の構造変化を抑制し、高容量かつ長寿命を実現できる非水電解質二次電池を提供する。非水電解質二次電池であって、リチウムイオンを吸蔵・放出する正極活物質を有する正極と、リチウムイオンを吸蔵・放出する負極活物質を有する負極と、非水電解質とを備え、前記正極活物質はリチウム層中にマグネシウムを含むコバルト複合酸化物であり、リチウム基準で電位が４．５３Ｖ以上の充電後にリチウム層にマグネシウムが存在しており、かつ負極上にマグネシウムを含む化合物が、前記正極中のマグネシウムに対して、４．５ｍｏｌ％以上１０ｍｏｌ％以下存在することを特徴とする。

明　細　書

発明の名称 ： 非水電解質二次電池

技術分野

[0001] 本発明は、非水電解質二次電池に関する。

背景技術

[0002] スマートフォンを含む携帯電話機、携帯型コンピュータ、ＰＤＡ、携帯型音楽プレイヤー等の携帯型電子機器の駆動電源として、リチウムイオン電池に代表される非水電解質二次電池が多く使用されている。さらに、電気自動車やハイブリッド電気自動車の駆動用電源、太陽光電、風力発電等の出力変動を抑制するための用途や夜間に電力をためて昼間に利用するための系統電力のピークシフト用途等の定置用蓄電池システムにおいても、非水電解質二次電池が多く使用されるようになってきている。

[0003] しかし、適用される機器の改良に伴って、さらに消費電力が高まる傾向にあり、更なる高容量化が強く望まれている。

上記、非水電解質二次電池を高容量化する方策としては、活物質の容量を高くする方策や、単位体積当たりの活物質の充填量を増やすといった方策の他、電池の充電電圧を高くするという方策がある。但し、電池の充電電圧を高くした場合には、正極活物質の結晶構造劣化や正極活物質と非水電解液との反応が生じやすくなる。

[0004] そこで、高電圧化の対策として、下記特許文献１には、正極活物質ＬｉＣｏO_2をリチウム基準で４．２～４．３Ｖで充電後、電気化学的にリチウムの一部をマグネシウムで置換することにより、リチウム層が安定化し高電圧での結晶構造が安定化することを報告している。

先行技術文献

特許文献

[0005] 特許文献1：特開２００４－２８８５７９号公報

発明の概要

発明が解決しようとする課題

[0006] しかしながら、この方法ではリチウム基準で電位が４．３Ｖ以下のリチウム引き抜き領域でリチウム層へのマグネシウム置換を行った構造となっている。この状態でさらなる高電位化のリチウム基準で電位が４．５３Ｖ以上の高電位充電を行った場合、リチウム層のマグネシウムは全て引き抜かれることになり、結晶構造が不安定化し充放電サイクルが低下する課題がある。

課題を解決するための手段

[0007] 本発明の一つの局面に係る非水電解質二次電池は、リチウムイオンを吸蔵・放出する正極活物質を有する正極と、リチウムイオンを吸蔵・放出する負極活物質を有する負極と、非水電解質とを備え、前記正極活物質は層状岩塩構造を有しリチウム層中にマグネシウムを含むコバルト複合酸化物であり、リチウム基準で電位が４．５３Ｖ以上の充電後にリチウム層にマグネシウムが存在しており、かつ負極上にマグネシウムを含む化合物が、前記正極中のマグネシウムに対して、４．５ｍｏｌ％以上１０ｍｏｌ％以下存在することを特徴とする。

[0008] （正極活物質）

本発明における正極活物質としては、一般式$Li_{1-a}Mg_aCo_{1-b}M_bO_2$(前記

一般式において、０＜ａ≦０．０５、０≦ｂ≦０．１、ＭはＡｌ、Ｍｇ、Ｍｎ、Ｎｉ、Ｆｅ、Ｔｉ、Ｚｎ、Ｍｏ、Ｖ、Ｓｒ、Ｓｎ、Ｓｂ、Ｗ、Ｔａ、Ｎｂ、Ｇｅ、ＺｒおよびＢａ

から選択される少なくとも１種の元素)で表される。

[0009] 上記リチウム層中にマグネシウムを含むコバルト複合酸化物の製造方法として、上記リチウムコバルト複合酸化物のリチウムの一部をリチウム/コバルトの組成比を１未満にした状態でマグネシウム原料を添加し焼成を行うことが好ましい。この方法により、リチウム層にマグネシウムを均一に存在させることができるため、リチウム基準で電位が４．５３Ｖ以上の高電位でリチウムを引き抜いた場合でも、リチウム層に安定的にマグネシウムを存在させ

ることでリチウム層の結晶構造を安定化し、結晶構造が大きく崩壊するＯ３構造からＨ１－３構造への相転移を抑制することができる。さらに、コバルトの一部をニッケル、マンガン、アルミニウムを同時に置換することが好ましい。ニッケルを置換することで高容量化が達成でき、さらに酸素との結合が強いマンガンやアルミニウムを置換することでリチウムが多く引き抜かれたリチウム基準で電位が４．５３Ｖ以上の充電時の場合でも遷移金属層の結晶構造を安定化させることが可能となる。

[0010] 上記一般式におけるａは０＜ａ≦０．０５が望ましい。ａ＞０．０５の場合は、リチウム量の相対的な低下による充放電容量が減少する。更に、マグネシウムの一部が遷移金属層に置換され、それにより遷移金属層内の結晶構造が不安定化するため、充放電サイクルが低下する可能性がある。また、ｂは０≦ｂ≦０．１が望ましい。ｂ＞０．１の場合においても、ニッケル、マンガン、アルミニウムを同時に置換することで、充放電サイクルを向上させることができる。

[0011] 上記リチウムコバルト複合酸化物は、充放電サイクル時に正極活物質中のリチウム層にいるマグネシウムの一部が、マグネシウムを含む化合物として負極活物質上に析出する。この時、正極活物質中のマグネシウム量に対し、４．５ｍｏｌ％以上１０ｍｏｌ％以下の範囲で、負極活物質上に析出させることが望ましい。これはマグネシウムが負極の保護膜となって存在することで、充放電サイクルでの負極の劣化を抑制することができるものと考えられる。

[0012] 上記正極活物質の表面の一部に希土類化合物もしくは酸化物が付着されていることが望ましい。正極活物質の表面に希土類元素化合物や酸化物の微粒子を分散した状態で付着させると、高電位の充放電反応を行った際の正極活物質構造変化を抑制することが可能になる。この理由は明らかでないが、希土類元素化合物や酸化物を表面に付着させることで、充電時の反応過電圧が増加し、相転移による結晶構造変化を小さくすることが可能となるためと考えられる。希土類化合物は水酸化エルビウム及びオキシ水酸化エルビウムか

らなる群から選ばれる少なくとも１種を含むことが好ましい。また、酸化物は酸化アルミニウム、酸化ジルコニウム、酸化マグネシウム、酸化銅、酸化ホウ素、酸化ランタンから選ばれる少なくとも１種を含むことが好ましい。

[0013]（負極活物質）

本発明における負極活物質としては、リチウムを吸蔵・放出可能な材料を用いるものが好ましい。例えば、リチウム金属、リチウム合金、炭素化合物、金属化合物等を挙げることが出来る。また、これらの負極活物質を一種類で使用してもよく、また二種類以上組み合わせて使用してもよい。炭素化合物としては、乱層構造を有する炭素材料、天然黒鉛、人造黒鉛、ガラス状炭素などの炭素材料が挙げられる。これらは、充放電時に生じる結晶構造の変化が非常に少なく、高い充放電容量を得ることができると共に、良好なサイクル特性を得ることが出来るので好ましい。特に、黒鉛は容量が大きく、高いエネルギー密度を得ることができるため好ましい。また、リチウム金属やリチウム合金も挙げられる。合金系は黒鉛に比べて電位が高いため、同じ電圧で電池の充放電を行った場合、正極電位も高くなるため、さらなる高容量化が期待できる。合金の金属としては、スズ、鉛、マグネシウム、アルミニウム、ホウ素、ガリウム、ケイ素、インジウム、ジルコニウム、ゲルマニウム、ビスマス、カドニウム等が挙げられ、特にケイ素およびスズの少なくとも一方を含むことが好ましい。ケイ素及び、スズはリチウムを吸蔵・放出する能力が大きく、高エネルギー密度を得ることが出来る。

[0014] スズの合金としてはスズ以外の構成元素として、鉛、マグネシウム、アルミニウム、ホウ素、ガリウム、ケイ素、インジウム、ジルコニウム、ゲルマニウム、ビスマス、カドニウム等が挙げられ、ケイ素の合金としてはケイ素以外の構成元素として、スズ、鉛、マグネシウム、アルミニウム、ホウ素、ガリウム、インジウム、ジルコニウム、ゲルマニウム、ビスマス、カドニウム等からなる少なくとも1種を挙げられる。

[0015]（非水電解質溶媒）

本発明で用いる非水電解質の溶媒は、特定のものに限定されるものではな

く、非水電解質二次電池に従来から用いられてきた溶媒を使用することが出来る。例えば、環状炭酸エステル、鎖状炭酸エステル、エステル類、環状エーテル類、鎖状エーテル類、ニトリル類、アミド類等が挙げられる。上記環状炭酸エステルとしては、エチレンカーボネート、プロピレンカーボネート、ブチレンカーボネートなどが挙げられる。上記鎖状炭酸エステルとしては、ジメチルカーボネート、エチルメチルカーボネート、ジエチルカーボネート、メチルプロピルカーボネート、エチルプロピルカーボネート、メチルイソプロピルカーボネートなどが挙げられる。上記エステル類としては、酢酸メチル、酢酸エチル、酢酸プロピル、プロピオン酸メチル、プロピオン酸エチル、γ－ブチロラクトンなどが挙げられる。上記環状エーテル類としては、１，３－ジオキソラン、４－メチル－１，３－ジオキソラン、テトラヒドロフラン、２－メチルテトラヒドロフラン、プロピレンオキシド、１，２－ブチレンオキシド、１，４－ジオキサン、１，３，５－トリオキサン、フラン、２－メチルフラン、１，８－シネオール、クラウンエーテルなどが挙げられる。上記鎖状エーテル類としては、１，２－ジメトキシエタン、ジエチルエーテル、ジプロピルエーテル、ジイソプロピルエーテル、ジブチルエーテル、ジヘキシルエーテル、エチルビニルエーテル、ブチルビニルエーテル、メチルフェニルエーテル、エチルフェニルエーテル、ブチルフェニルエーテル、ペンチルフェニルエーテル、メトキシトルエン、ベンジルエチルエーテル、ジフェニルエーテル、ジベンジルエーテル、o－ジメトキシベンゼン、１，２－ジエトキシエタン、１，２－ジブトキシエタン、ジエチレングリコールジメチルエーテル、ジエチレングリコールジエチルエーテル、ジエチレングリコールジブチルエーテル、１，１－ジメトキシメタン、１，１－ジエトキシエタン、トリエチレングリコールジメチルエーテル、テトラエチレングリコールジメチルなどが挙げられる。上記ニトリル類としては、アセトニトリル等、上記アミド類としては、ジメチルホルムアミド等が挙げられる。そして、特に、これらの水素の一部または全部をフッ素化されているものが好ましい。フッ素化により非水電解質の耐酸化性が向上するため、正極表面

の酸化雰囲気が高まる高電圧状態でも電解液の分解を防ぐことが出来る。

また、これらを単独または複数組み合わせて使用することができ、特に、環状カーボネートと鎖状カーボネートとを組み合わせた溶媒が好ましい。

[0016] （電解質塩）

非水溶媒に加えるリチウム塩としては、従来の非水電解質二次電池において電解質として一般に使用されているものを用いることができ、例えば、ＬｉＰＦ$_6$、ＬｉＢＦ$_4$、ＬｉＡｓＦ$_6$、ＬｉＣｌＯ$_4$、ＬｉＣＦ$_3$ＳＯ$_3$、ＬｉＮ（ＦＳＯ$_2$）$_2$、ＬｉＮ（ＣｌＦ$_{2l+1}$ＳＯ$_2$）（ＣｍＦ$_{2m+1}$ＳＯ$_2$）（ｌ，ｍは１以上の整数）、ＬｉＣ（ＣｐＦ$_{2p+1}$ＳＯ$_2$）（ＣｑＦ$_{2q+1}$ＳＯ$_2$）（ＣｒＦ$_{2r+1}$ＳＯ$_2$）（ｐ，ｑ，ｒは１以上の整数）、Ｌｉ［Ｂ（Ｃ$_2$Ｏ$_4$）$_2$］（ビス（オキサレート）ホウ酸リチウム（ＬｉＢＯＢ））、Ｌｉ［Ｂ（Ｃ$_2$Ｏ$_4$）Ｆ$_2$］、Ｌｉ［Ｐ（Ｃ$_2$Ｏ$_4$）Ｆ$_4$］、Ｌｉ［Ｐ（Ｃ$_2$Ｏ$_4$）$_2$Ｆ$_2$］等が挙げられ、これらのリチウム塩は一種類で使用してもよく、また二種類以上組み合わせて使用してもよい。

発明の効果

[0017] 本発明の一つの局面に係る非水電解質二次電池によれば、リチウム基準で４．５３Ｖ以上という非常に高い充電電圧で室温下（２５℃）、高温下（４５℃）であっても、正極活物質の構造変化や活物質表面での電解液との反応を抑制し、さらに、負極の劣化を抑制することができるため長寿命な非水電解質二次電池が得られる。

[0018] 前記正極活物質はリチウム/コバルトの組成比を１未満にした状態でマグネシウム原料を添加し焼成を行うことで、リチウム層にマグネシウムを均一に存在させることができる。そのため、リチウム基準で４．５３Ｖ以上の高電位で引き抜いた場合でも正極活物質中に安定的にマグネシウムを存在させ結晶構造を安定化させることができるものと考えられる。

[0019] さらに、充放電サイクル時に正極活物質ＬｉＣｏＯ$_2$のリチウム層のマグネシウムの一部を負極上に析出させ、負極保護膜となって安定化させることで、リチウム基準で電位が４．５３Ｖ以上の高電位での充放電サイクル特性を

改善できるものと考えられる。

図面の簡単な説明

[0020] [図1]希土類化合物が表面に付着した正極活物質のＳＥＭ画像である。

[図2]単極式セルの概略模式図である。

[図3]ラミネート形非水電解質二次電池の斜視図である。

[図4]図３の巻回電極体の斜視図である。

[図5]$Li_{0.99}Mg_{0.01}CoO_2$の粉末Ｘ線回折測定図である。

[図6]実験例１における高電圧充電前後の粉末Ｘ線回折測定図である。

[図7]実験例２における高電圧充電前後の粉末Ｘ線回折測定図である。

[図8]実験例３における高電圧充電前後の粉末Ｘ線回折測定図である。

[図9]実験例５における高電圧充電前後の粉末Ｘ線回折測定図である。

[図10]実験例６における高電圧充電前後の粉末Ｘ線回折測定図である。

[図11]実験例４における高電圧充電前後の粉末Ｘ線回折測定図である。

発明を実施するための形態

[0021] 以下、本発明を実施するための形態について詳細に説明する。ただし、以下に示す実施形態は、本発明の技術思想を具体化するために例示するものであって、本発明をこの実施形態に限定することを意図するものではなく、本発明は特許請求の範囲に示した技術思想を逸脱することなく種々の変更を行ったものにも均しく適用し得るものである。最初に、正極の具体的製造方法について説明する。

[0022] （実験例１）

[正極板の作製]

正極活物質は、以下のように調製した。リチウム源として炭酸リチウムを用い、コバルト源として四酸化コバルトを用い、リチウムの置換元素となるマグネシウム源として、酸化マグネシウムとを用いた。リチウム、マグネシウムのモル比を９９：１、リチウム＋マグネシウムとコバルトのモル比を１：１で乾式混合した後、粉末をペレットに成型して、空気雰囲気中において、９００℃で２４時間焼成し、正極活物質を調製した。

[0023] 次に、以下のようにして湿式法により表面に希土類化合物を付着させた。正極活物質１０００ｇを３リットルの純水と混合して撹拌し、正極活物質が分散した懸濁液を調製した。懸濁液のｐＨが９を保つように水酸化ナトリウム水溶液を添加しながら、この懸濁液に希土類化合物源としての硝酸エルビウム５水和物１．８５ｇを溶解した溶液を添加した。

[0024] なお、懸濁液のｐＨが９よりも小さいと、水酸化エルビウム及びオキシ水酸化エルビニウムが析出し難くなる。また、懸濁液のｐＨが９よりも大きいと、これらの析出する反応速度が速くなり、正極活物質表面に対する分散状態が不均一となる。

[0025] 次に、上記懸濁液を吸引濾過し、更に水洗して得られた粉末を１２０℃で乾燥し、さらに３００℃で５時間熱処理を行った。これにより、正極活物質の表面に水酸化エルビウムが均一に付着した正極活物質粉末を得た。

[0026] 図１に正極活物質の表面に希土類化合物を付着させたもののＳＥＭ像を示す。このように、正極活物質の表面に、エルビウム化合物が均一に分散した状態で付着していることが確認された。エルビウム化合物の平均粒子径は１００ｎｍ以下であった。また、高周波誘導結合プラズマ発光分光分析法（以下、ＩＣＰ）を用いてこのエルビウム化合物の付着量を測定したところ、正極活物質に対してエルビウム元素換算で０．０７質量部であった。

[0027] 上述のようにして調製された表面に希土類化合物を有する正極活物質を９６．５質量部、導電剤としてのアセチレンブラックを１．５質量部、結着剤としてのポリフッ化ビニリデン粉末を２．０質量部となるよう混合し、これをＮ－メチルピロリドン溶液と混合して正極合剤スラリーを調製した。次いで、正極合剤スラリーを正極集電体としての厚さ１５μｍのアルミニウム箔の両面にドクターブレード法により塗布して正極集電体の両面に正極活物質合剤層を形成し、乾燥した後、圧縮ローラーを用いて圧延し、所定サイズに裁断して正極板を作製した。そして、正極板の正極活物質合剤層の未形成部分に正極集電タブとしてのアルミニウムタブを取り付けて、正極板とした。正極活物質合剤層の量は３９ｍｇ／ｃｍ^{2}とし、正極合剤層の厚みは１２０μ

ｍとした。

[0028] [負極板の作製]

黒鉛と、増粘剤としてのカルボキシメチルセルロースと、結着材としてのスチレンブタジエンゴムとを、質量比で９８：１：１となるように秤量し、水に分散させて負極活物質合剤スラリーを調製した。この負極活物質合剤スラリーを、厚さ８μｍの銅製の負極芯体の両面にドクターブレード法により塗布した後、１１０℃で乾燥させて水分を除去して、負極活物質層を形成した。そして、圧縮ローラーを用いて所定の厚さに圧延し、所定サイズに裁断して負極板を作製した。

[0029] [非水電解液の調整]

非水溶媒として、フルオロエチレンカーボネート（ＦＥＣ）と、フッ素化プロピオンカーボネート（ＦＭＰ）を用意した。２５℃における体積比で、ＦＥＣ：ＦＭＰ＝２０：８０となるように混合した。この非水溶媒に、ヘキサフルオロリン酸リチウムを濃度が１ｍｏｌ／Ｌとなるように溶解して、非水電解質を調製した。

[0030] ［ラミネート形非水電解質二次電池の作製］

ラミネート形非水電解質二次電池２０は、図３及び図４に示したように、ラミネート外装体２１と、正極板と負極板とを備え偏平状に形成された巻回電極体２２と、正極板に接続された正極集電タブ２３と、負極板に接続された負極集電タブ２４とを有している。巻回電極体２２は、それぞれが帯状である正極板、負極板及びセパレーターを有し、正極板と負極板とがセパレーターを介して互いに絶縁された状態で巻回されるようにして構成されている。

[0031] ラミネート外装体２１には凹部２５が形成されており、このラミネート外装体２１の一端側がこの凹部２５の開口部分を覆うように折り返されている。凹部２５の周囲にある端部２６と折り返されて対向する部分とは溶着され、ラミネート外装体２１の内部が封止されるようになっている。封止されたラミネート外装体２１の内部には、巻回電極体２２が非水電解液とともに収

納されている。

[0032] 正極集電タブ２３及び負極集電タブ２４は、それぞれ樹脂部材２７を介して封止されたラミネート外装体２１から突出するようにして配置され、これら正極集電タブ２３及び負極集電タブ２４を介して電力が外部に供給されるようになっている。正極集電タブ２３及び負極集電タブ２４のそれぞれとラミネート外装体２１との間には、密着性向上及びラミネート材のアルミニウム合金層を介する短絡防止の目的で、樹脂部材２７が配置されている。

[0033] 上記ラミネート形非水電解質二次電池は、以下のように作製した。

即ち、上記のように作製した正極板及び負極板を、ポリエチレン製微多孔質膜からなるセパレーターを介して巻回し、最外周にポリプロピレン製のテープを張り付けて円筒状の巻回電極体を作製した。次いで、これをプレスして偏平状の巻回電極体とした。また、ポリプロピレン樹脂層／接着剤層／アルミニウム合金層／接着材層／ポリプロピレン樹脂層の５層構造からなるシート状のラミネート材を用意し、このラミネート材を折り返して底部を形成するとともにカップ状の電極体収納空間を形成した。

[0034] 次いで、アルゴン雰囲気下のグローブボックス内で偏平状の巻回電極体と非水電解質とをカップ状の電極体収納空間に挿入した。この後、ラミネート外装体内部を減圧してセパレーター内部に非水電解質を含浸させ、ラミネート外装体の開口部を封止した。このようにして、高さ６２ｍｍ、幅３５ｍｍ、厚み３．６ｍｍ(封止部を除外した寸法)のラミネート形非水電解質二次電池を作製した。なお、当該ラミネート形非水電解質二次電池を４．５０Ｖまで充電し、２．５０Ｖまで放電したときの放電容量は８００ｍＡｈであった。

[0035] [充放電サイクルの条件]

上記ラミネート形非水電解質二次電池（以下パウチセルということがある。）について、下記の条件で充放電試験を行った。

４００ｍＡの定電流で電池電圧が４．５０Ｖとなるまで充電し、電池電圧が各値に達した後は、各値の定電圧で４０ｍＡとなるまで充電を行った。そ

して、８００ｍＡの定電流で電池電圧が２．５０Ｖとなるまで放電を行い、このときに流れた電気量を測定して１回目の放電容量を求めた。負極に用いられる黒鉛の電位は、リチウム基準で約０．１Ｖである。このため、電池電圧４．５０Ｖにおいて正極電位はリチウム基準で４．５３Ｖ以上４．６０Ｖ程度となる。上記と同じ条件で充放電を繰り返して１００回目の放電容量を測定し、容量維持率を以下の式を用いて算出した。また、測定温度は２５℃及び４５℃で行った。容量維持率（％）＝（１００回目の放電容量／１回目の放電容量)×１００

[0036] [単極式セルの作製]

単極式セルの作製の製造方法について、図２を用いて説明する。単極式セル１０は、図２に示したように、正極１１、負極１２及び上記正極１１と負極１２との間にセパレーター１３が配置される測定極部１４と、参照極１５が配置される参照極部１６を有している。測定極部１４及び参照極部１６にはそれぞれ非水電解液１８が満たされている。負極１２及び参照極１５は、リチウム金属が用いられている。負極１２は、正極１１に対して対向可能な寸法となっている。作製された単極式セル１０の理論容量は１００ｍＡｈである。

[0037] [負極上へのマグネシウム化合物の析出量の算出]

負極上へのマグネシウム化合物の析出量を算出するため、上記単極式セルを０．１５Ｉｔ（＝１５ｍＡ）の定電流により、正極の電位がリチウム基準で４．６０Ｖとなるまで充電した。その後、電池を解体した後、負極のＩＣＰを行い化合物の定量を行った。負極のマグネシウム化合物割合（％）＝負極中のマグネシウム量/正極活物質中のマグネシウム量×１００で算出を行った。

[0038] （実験例２）

コバルトの置換元素源となるニッケル、マンガン源として、水酸化ニッケル、二酸化マンガンとを用いた。リチウム、マグネシウムのモル比を９９：１、コバルト、ニッケル、マンガンのモル比を９０：５：５、リチウム＋マ

グネシウムとコバルト＋ニッケル＋マンガンのモル比を１：１で乾式混合した後、粉末をペレットに成型して、空気雰囲気中において、９００℃で２４時間焼成し、正極活物質を調製した。それ以外は、上記実験例１と同様にして、単極式セル１０及びラミネート形非水電解質二次電池２０を作製した。

[0039] （実験例３）

リチウム、マグネシウムのモル比を９７：３になるように正極活物質を調製したこと以外は、実験例２と同様にして、単極式セル１０及びラミネート形非水電解質二次電池２０を作製した。

[0040] （実験例４）

マグネシウムを置換しないように正極活物質を調製したこと以外は、実験例１と同様にして単極式セル１０及びラミネート形非水電解質二次電池２０を作製した。

[0041] 下記表１に充放電サイクル結果と負極上へのマグネシウム化合物量を示す。

２５℃サイクルにおいて、実験例４は１００サイクル後で維持率が６５％に対し、実験例１～３は８８％以上と高い値となった。また、４５℃サイクルでは実験例４は４７％と室温より大幅に低下したのに対し、実験例１～３は６２％以上と実験例４を上回る値となった。これは、リチウム層にマグネシウムが安定的に存在したことで、リチウム層の結晶構造が安定化し、充放電サイクル特性が改善できたと考えられる。

さらに、実験例１～３では負極上にマグネシウム化合物が正極中のマグネシウムに対し４．６％以上析出していることを確認した。負極上に析出したマグネシウム化合物が負極の保護膜となって、充放電サイクルに伴う負極表面と電解液との反応を抑制したため、充放電サイクル特性を改善できたものと考えられる。

[0042]

[表1]

	Mg置換量 (a)	M置換量 (b)	負極中のMg量	パウチセル				
				充電電圧	温度	100サイクル後維持率	温度	100サイクル後維持率
	(mol%)	(mol%)	(% vs. 正極活物質)	(V vs. 黒鉛)	(°C)	(%)	(°C)	(%)
実験例1	1	0	7.6	4.5	25	93	45	79
実験例2	1	Ni=5 Mn=5	4.6	4.5	25	90	45	62
実験例3	3	Ni=5 Mn=5	5.1	4.5	25	88	45	73
実験例4	0	0	0	4.5	25	65	45	47

[0043] （実験例５）

リチウム、マグネシウムのモル比を９７：３になるように正極活物質を調製したこと以外は、実験例１と同様にして単極式セル１０及びラミネート形非水電解質二次電池２０を作製した。

[0044] （実験例６）

リチウム、マグネシウムのモル比を９５：５になるように正極活物質を調製したこと以外は、実験例１と同様にして単極式セル１０及びラミネート形非水電解質二次電池２０を作製した。

[0045] 表２に充放電サイクル結果を示す。２５℃サイクルにおいて、実験例４は１００サイクル後で維持率が６５％に対し、実験例１、５、６は８３％以上と高い値となった。また、４５℃サイクルでは実験例４は４７％と室温より大幅に低下したのに対し、実験例１、５、６は５０％以上と実験例４を上回る値となった。これは、マグネシウムを多く置換した場合においても、リチウム層の結晶構造が安定化し、充放電サイクル特性が改善できたと考えられる。

[0046] [表2]

	Mg置換量	パウチセル				
	(a)	充電電圧	温度	100サイクル後維持率	温度	100サイクル後維持率
	(mol%)	(V vs 黒鉛)	(℃)	(%)	(℃)	(%)
実験例1	1	4.5	25	93	45	79
実験例4	0	4.5	25	65	45	47
実験例5	3	4.5	25	83	45	51
実験例6	5	4.5	25	88	45	50

[0047] 次に、マグネシウムがリチウム層に存在しているかを確認するため、作製した正極活物質の粉末Ｘ線回折測定を行った。

[0048] [粉末Ｘ線回折測定]

実験例１の正極活物質を粉末Ｘ線回折（以下、ＸＲＤ）にて測定した結果を図５に示す。全てのピークは空間群Ｒ－３ｍに帰属可能であり、図５中３

桁の数字で示すように指数付けが可能であった。また、実験例２～６も同様の結果となった。

[0049] ［リチウム層へのマグネシウム置換確認］

次に、面指数００３と１０４の回折ピーク強度比００３/１０４を算出した。この回折強度は一般的に、リチウム層にリチウムイオン（０．７６Å）とイオン半径が近いニッケル２価のニッケルイオン（０．６９Å）が占有するカチオンミキシングの尺度であり、ピーク強度比が小さくなるとカチオンミシキングの比率が大きくなり強度比は１．３７以下と言われている。２価のマグネシウムイオン（０．７２Å）もリチウムイオンやニッケルイオンのイオン半径と近いため、強度比からマグネシウムのカチオンミキシングの可否を判断した。

[0050] 下記表３に回折ピーク強度比００３/１０４の測定結果を示す。実験例４では１．３９に対し、実験例１～３、実験例５～６は１．３７以下であり、マグネシウムがリチウム層に存在していることを確認した。

[0051] [表3]

	003/104
実験例1	1.22
実験例2	1.35
実験例3	1.37
実験例4	1.39
実験例5	1.22
実験例6	1.30

[0052] ［相転移抑制測定］

次に、作製した正極活物質が高電位充電にＯ３構造から結晶構造が大きく崩壊するＨ１－３構造に相転移を抑制しているかを確認するため充電時のＸＲＤ測定を行った。上記実験例１～６で作製した単極式セルを０．１５Ｉｔ（＝１５ｍＡ）の定電流により、正極の電位がリチウム基準で４．５０Ｖ及び４．６０Ｖとなるまで充電し、電池解体後、大気中の酸素や水分に反応するのを防ぐため、大気非暴露状態で上記実験１～６の正極活物質のＸＲＤ測定を行った。

[0053] 図６～図１１に充電後の面指数００３のＸＲＤを示す。ここで、図６～図１１中の符号３１は充電前電極、符号３２は４．５０Ｖ充電電極、符号３３は４．６０Ｖ充電電極を示す。一般的に、充電に伴い００３ピークは低角にシフトした後、高角にシフトし始めＨ１－３構造に達した時に充電前のピークよりも高角側に移動すると言われている。実験例４では、図１１に示したように、充電前電極３１のピークよりも４．６０Ｖ充電電極３３が高角側に移動していることがわかる。このため、実験例４では、４．６０Ｖ充電時にＨ１－３構造が明確に現れていることがわかる。一方、図６～図１０に示したように、実験例１～３、５～６においては、４．６０Ｖ充電電極３３が充電前電極３１よりも低角側に存在していた。このことから、実験例１～３、５～６においては、マグネシウム置換によりＯ３からＨ１－３への相転移が抑制されたものと考えられる。

産業上の利用可能性

[0054] 本発明の一局面の非水電解質二次電池は、例えば、携帯電話、ノートパソコン、スマートフォン、タブレット端末等の特に高容量かつ長寿命が必要とされる用途に適用することができる。

符号の説明

[0055] １０．単極式セル　１１．正極　１２．負極　１３．セパレータ　１４．測定極部　１５．参照極　　１６．参照極部　１８．非水電解液　２０．非水電解質二次電池　２１．ラミネート外装体　２２．巻回電極体　２３．正極集電タブ　２４．負極集電タブ３１．充電前電極　３２．４．５０Ｖ充電電

極　３３．４．６０Ｖ充電電極

請求の範囲

[請求項1] リチウムイオンを吸蔵・放出する正極活物質を有する正極と、リチウムイオンを吸蔵・放出する負極活物質を有する負極と、非水電解質とを備え、前記正極活物質は層状岩塩構造を有しリチウム層中にマグネシウムを含むコバルト複合酸化物であり、リチウム基準で電位が４．５３Ｖ以上の充電後にリチウム層にマグネシウムが存在しており、かつ負極上にマグネシウムを含む化合物が、前記正極中のマグネシウムに対して、４．５ｍｏｌ％以上１０ｍｏｌ％以下存在することを特徴とする非水電解質二次電池。

[請求項2] 前記正極の一般式が$Li_{1-a}Mg_aCo_{1-b}M_bO_2$(前記一般式において、０＜
ａ≦０．０５、０≦ｂ≦０．１、MはＡｌ、Ｍｇ、Ｍｎ、Ｎｉ、Ｆｅ、Ｍｇ、Ｔｉ、Ｚｎ、Ｍｏ、Ｖ、Ｓｒ、Ｓｎ、Ｓｂ、Ｗ、Ｔａ、Ｎｂ、Ｇｅ、ＺｒおよびＢａから選択される少なくとも1種の元素)で表される、請求項１に記載の非水電解質二次電池。

[請求項3] 前記正極活物質のＨ１−３への相転移電位がリチウム基準で４．５３Ｖ以上である、請求項１または請求項２に記載の非水電解質二次電池。

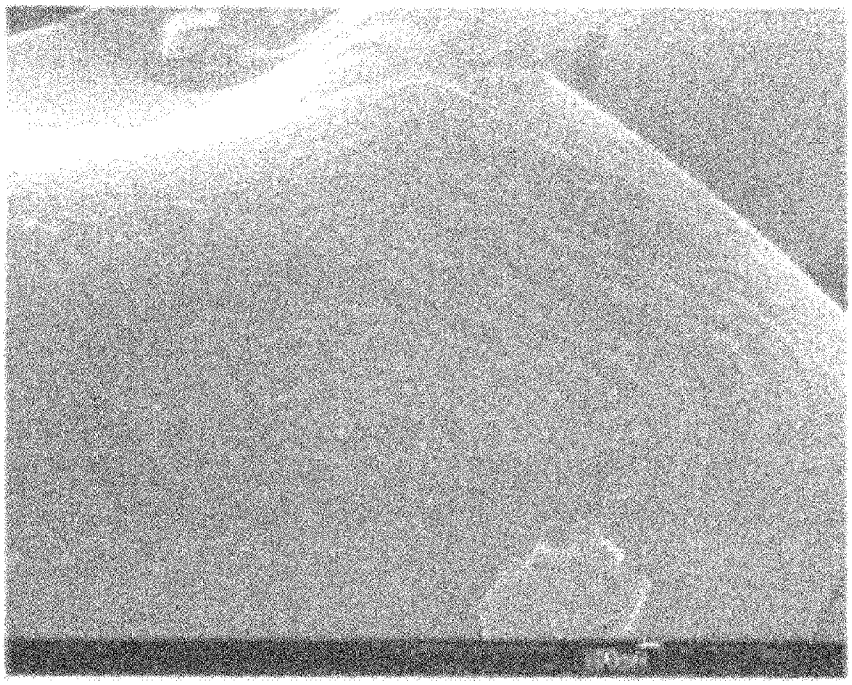
[請求項4] 前記正極の活物質表面の一部に希土類化合物が付着されている、請求項１～３のいずれか１項に記載の非水電解質二次電池。

[請求項5] 前記希土類化合物は水酸化エルビウム及びオキシ水酸化エルビウムの少なくとも１種を含む請求項４に記載の非水電解質二次電池。

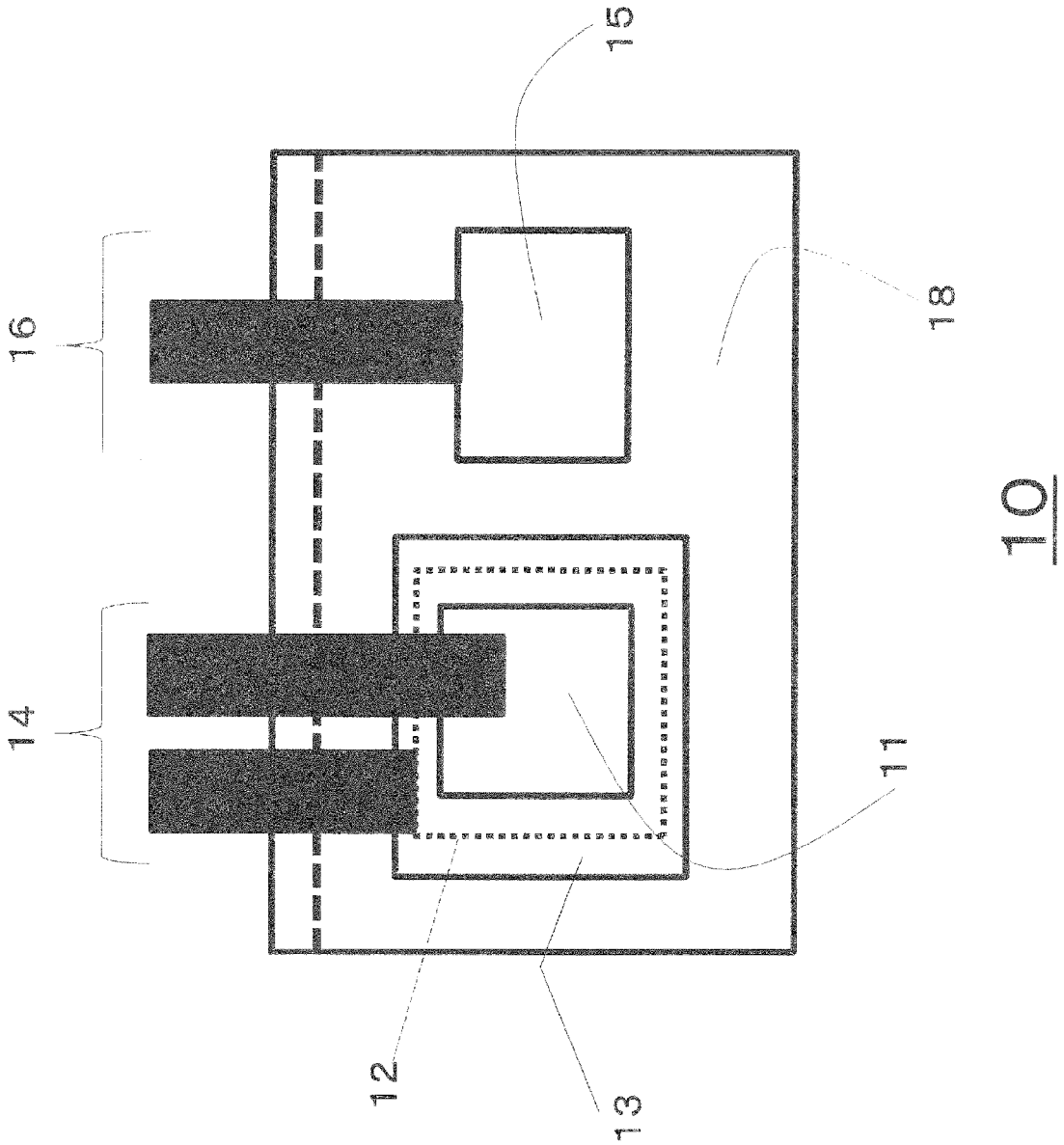
[請求項6] 前記非水電解質はフッ素化溶媒を含む請求項１～５のいずれか１項に記載の非水電解質二次電池。

[請求項7] 前記フッ素化溶媒がフルオロエチレンカーボネート、フッ素化プロピオン酸メチル及びフッ素化メチルエチルカーボネートを含む請求項６に記載の非水電解質二次電池。

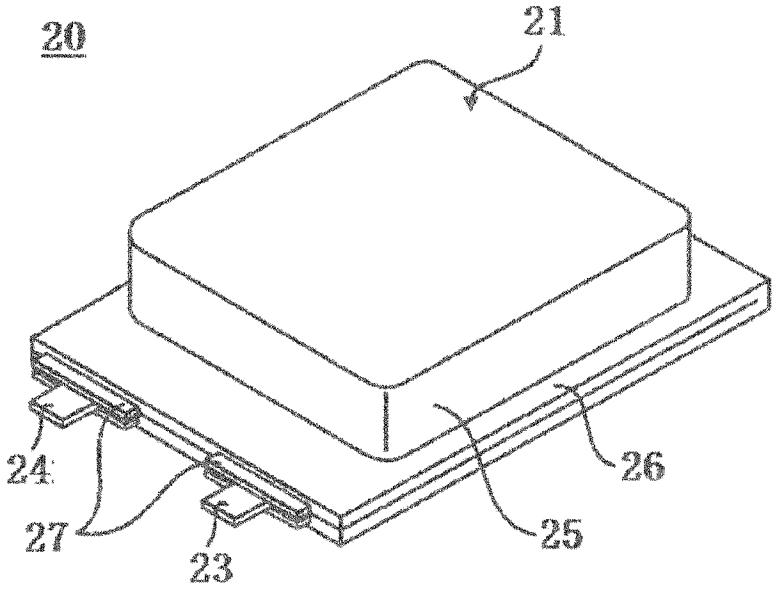
[図1]



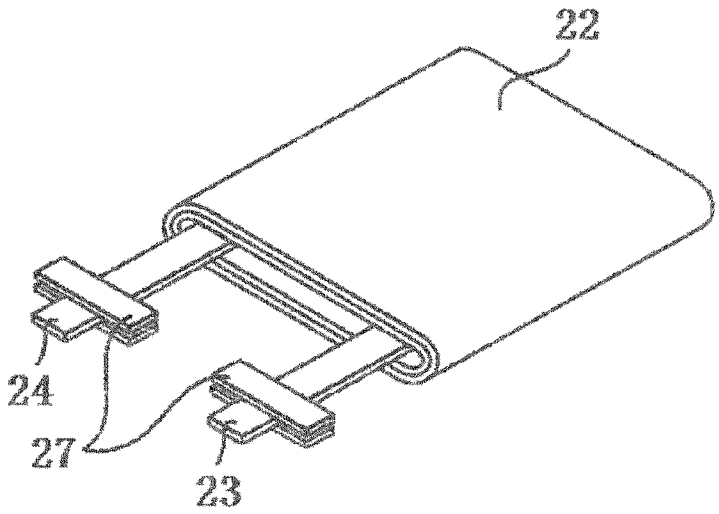
[図2]



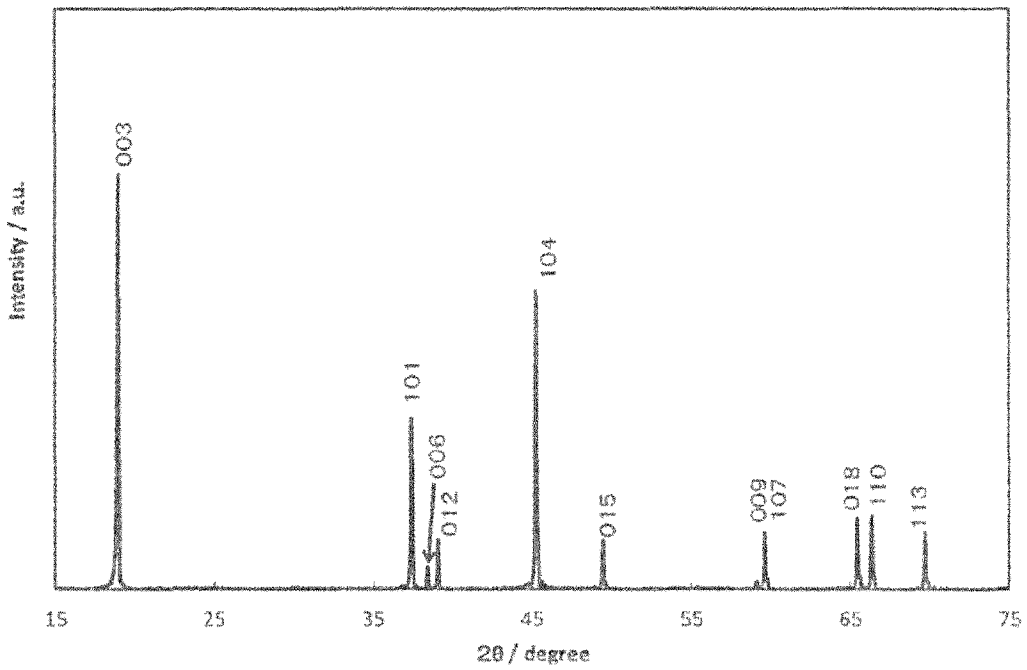
[図3]



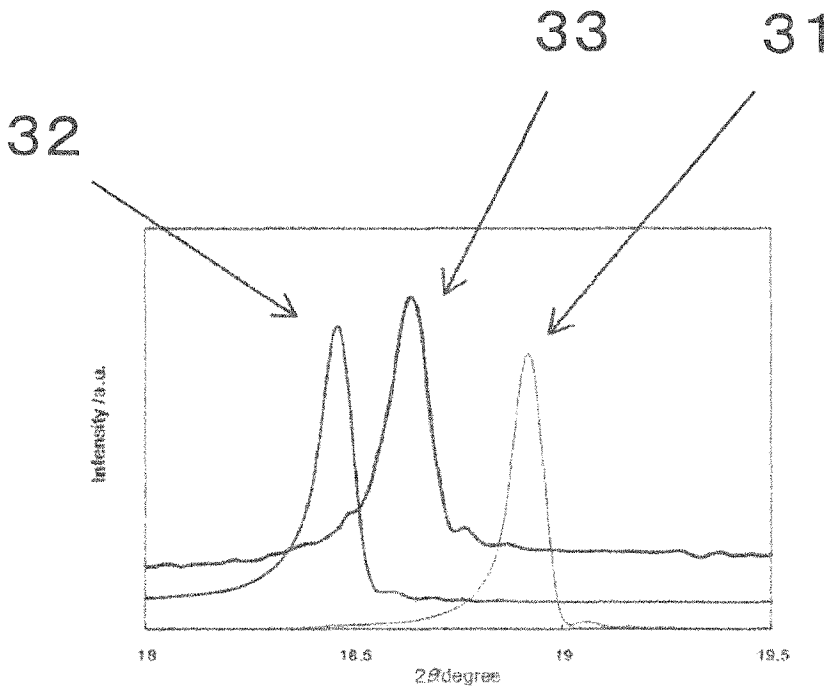
[図4]



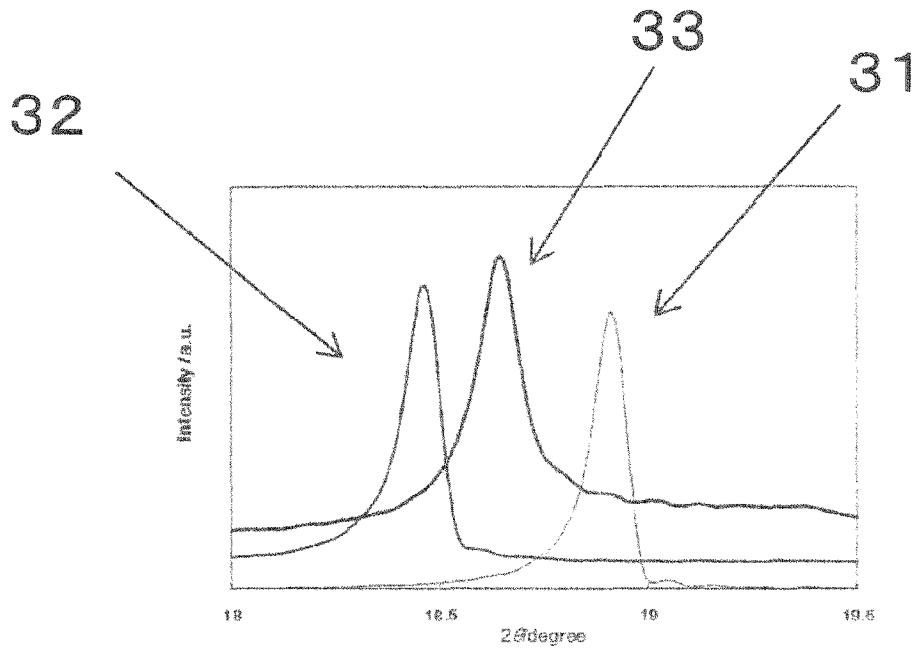
[図5]


003
101
006
012
104
015
009
107
018
110
113
Intensity / a.u.
15
25
35
45
55
65
75
2θ / degree

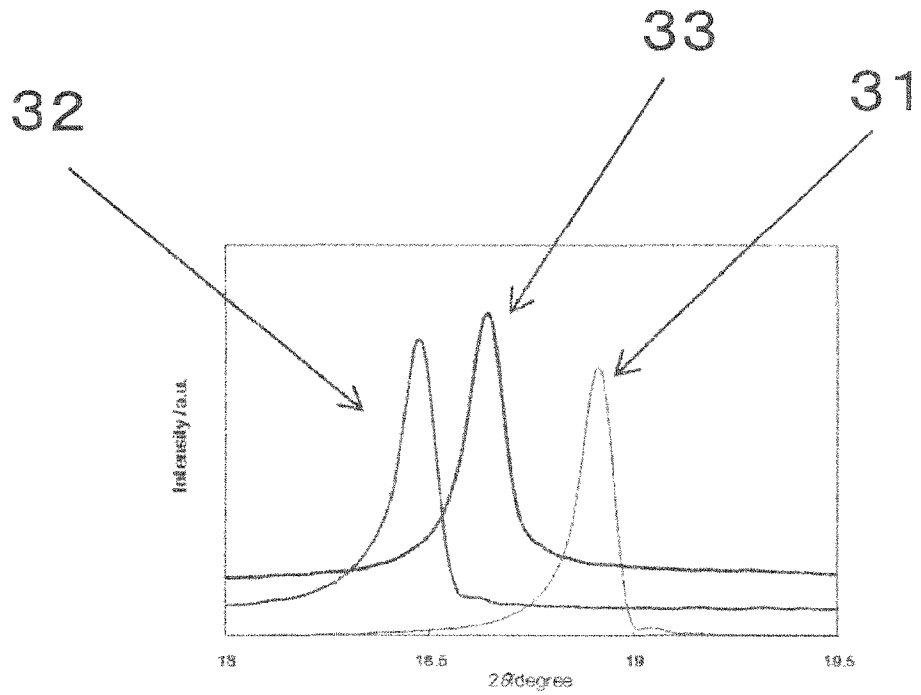
[図6]



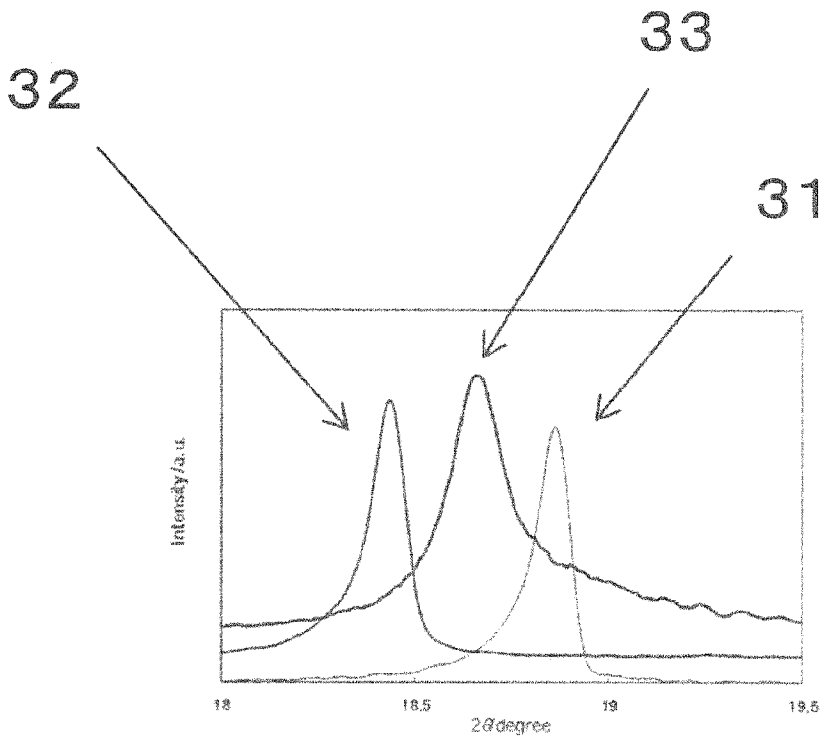
[図7]



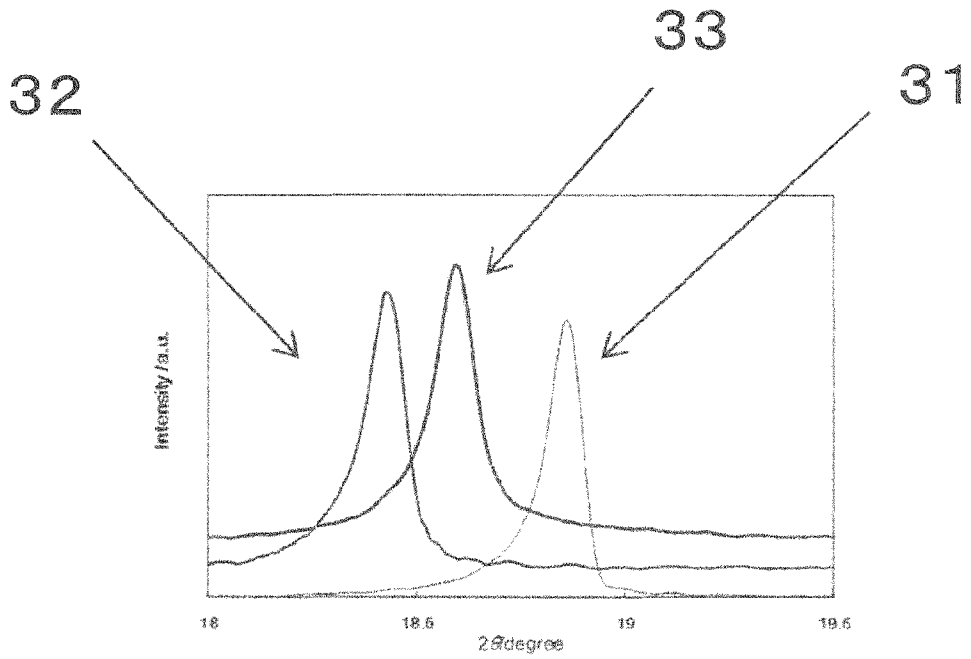
[図8]



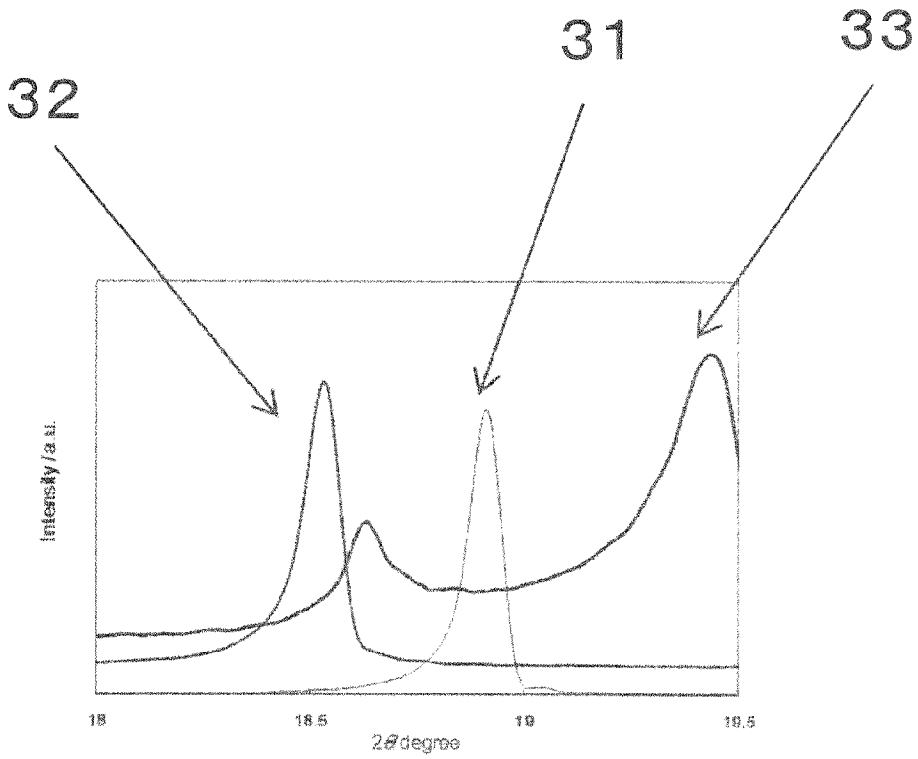
[図9]



[図10]



[図11]



INTERNATIONAL SEARCH REPORT

International application No.
PCT/JP2015/001075

A. CLASSIFICATION OF SUBJECT MATTER
H01M4/525(2010.01)i, *H01M4/36*(2006.01)i, *H01M4/505*(2010.01)i, *H01M10/052*(2010.01)i, *H01M10/0569*(2010.01)i

According to International Patent Classification (IPC) or to both national classification and IPC

B. FIELDS SEARCHED

Minimum documentation searched (classification system followed by classification symbols)
H01M4/525, H01M4/36, H01M4/505, H01M10/052, H01M10/0569

Documentation searched other than minimum documentation to the extent that such documents are included in the fields searched
Jitsuyo Shinan Koho 1922-1996 Jitsuyo Shinan Toroku Koho 1996-2015
Kokai Jitsuyo Shinan Koho 1971-2015 Toroku Jitsuyo Shinan Koho 1994-2015

Electronic data base consulted during the international search (name of data base and, where practicable, search terms used)

C. DOCUMENTS CONSIDERED TO BE RELEVANT

Category*	Citation of document, with indication, where appropriate, of the relevant passages	Relevant to claim No.
A	JP 10-241691 A (Hitachi, Ltd.), 11 September 1998 (11.09.1998), entire text; all drawings (Family: none)	1-7
A	JP 2000-123834 A (GS Melcotec Co., Ltd.), 28 April 2000 (28.04.2000), entire text; all drawings (Family: none)	1-7
A	JP 2001-256975 A (Toyota Central Research and Development Laboratories, Inc.), 21 September 2001 (21.09.2001), entire text; all drawings (Family: none)	1-7

☒ Further documents are listed in the continuation of Box C. ☐ See patent family annex.

* Special categories of cited documents:
"A" document defining the general state of the art which is not considered to be of particular relevance
"E" earlier application or patent but published on or after the international filing date
"L" document which may throw doubts on priority claim(s) or which is cited to establish the publication date of another citation or other special reason (as specified)
"O" document referring to an oral disclosure, use, exhibition or other means
"P" document published prior to the international filing date but later than the priority date claimed
"T" later document published after the international filing date or priority date and not in conflict with the application but cited to understand the principle or theory underlying the invention
"X" document of particular relevance; the claimed invention cannot be considered novel or cannot be considered to involve an inventive step when the document is taken alone
"Y" document of particular relevance; the claimed invention cannot be considered to involve an inventive step when the document is combined with one or more other such documents, such combination being obvious to a person skilled in the art
"&" document member of the same patent family

Date of the actual completion of the international search	Date of mailing of the international search report
22 May 2015 (22.05.15)	02 June 2015 (02.06.15)
Name and mailing address of the ISA/ Japan Patent Office 3-4-3,Kasumigaseki,Chiyoda-ku, Tokyo 100-8915,Japan	Authorized officer Telephone No.

Form PCT/ISA/210 (second sheet) (July 2009)

INTERNATIONAL SEARCH REPORT

International application No.
PCT/JP2015/001075

C (Continuation). DOCUMENTS CONSIDERED TO BE RELEVANT

Category*	Citation of document, with indication, where appropriate, of the relevant passages	Relevant to claim No.
A	JP 2003-346797 A (Japan Storage Battery Co., Ltd.), 05 December 2003 (05.12.2003), entire text; all drawings (Family: none)	1-7
A	JP 2004-220952 A (Matsushita Electric Industrial Co., Ltd.), 05 August 2004 (05.08.2004), entire text; all drawings & US 2004/0142240 A1 & CN 1518145 A	1-7
A	WO 2006/054604 A1 (Matsushita Electric Industrial Co., Ltd.), 26 May 2006 (26.05.2006), entire text; all drawings & JP 2006-173099 A & KR 10-2007-0085860 A & CN 101061600 A & US 2008/0118833 A1 & US 2011/0281165 A1	1-7
A	JP 2006-173137 A (Hitachi Maxell, Ltd.), 29 June 2006 (29.06.2006), entire text; all drawings (Family: none)	1-7
A	JP 2006-324235 A (Matsushita Electric Industrial Co., Ltd.), 30 November 2006 (30.11.2006), entire text; all drawings (Family: none)	1-7
P,A	JP 2014-170739 A (Samsung SDI Co., Ltd.), 18 September 2014 (18.09.2014), entire text; all drawings & US 2014/0242468 A1 & EP 2772968 A1 & KR 10-2014-0108102 A & CN 104037397 A	1-7

AMPEREX Ex. 1002

国際調査報告

国際出願番号　ＰＣＴ／ＪＰ２０１５／００１０７５

Ａ．　発明の属する分野の分類（国際特許分類（ＩＰＣ））

Int.Cl.　H01M4/525(2010.01)i, H01M4/36(2006.01)i, H01M4/505(2010.01)i, H01M10/052(2010.01)i, H01M10/0569(2010.01)i

Ｂ．　調査を行った分野

調査を行った最小限資料（国際特許分類（ＩＰＣ））

Int.Cl.　H01M4/525, H01M4/36, H01M4/505, H01M10/052, H01M10/0569

最小限資料以外の資料で調査を行った分野に含まれるもの

日本国実用新案公報	１９２２－１９９６年
日本国公開実用新案公報	１９７１－２０１５年
日本国実用新案登録公報	１９９６－２０１５年
日本国登録実用新案公報	１９９４－２０１５年

国際調査で使用した電子データベース（データベースの名称、調査に使用した用語）

Ｃ．　関連すると認められる文献

引用文献のカテゴリー＊	引用文献名　及び一部の箇所が関連するときは、その関連する箇所の表示	関連する請求項の番号
A	JP 10-241691 A (株式会社日立製作所) 1998.09.11, 全文, 全図 (ファミリーなし)	1-7
A	JP 2000-123834 A (ジーエス・メルコテック株式会社) 2000.04.28, 全文, 全図 (ファミリーなし)	1-7
A	JP 2001-256975 A (株式会社豊田中央研究所) 2001.09.21, 全文, 全図 (ファミリーなし)	1-7

☑ Ｃ欄の続きにも文献が列挙されている。　☐ パテントファミリーに関する別紙を参照。

＊　引用文献のカテゴリー
「Ａ」特に関連のある文献ではなく、一般的技術水準を示すもの
「Ｅ」国際出願日前の出願または特許であるが、国際出願日以後に公表されたもの
「Ｌ」優先権主張に疑義を提起する文献又は他の文献の発行日若しくは他の特別な理由を確立するために引用する文献（理由を付す）
「Ｏ」口頭による開示、使用、展示等に言及する文献
「Ｐ」国際出願日前で、かつ優先権の主張の基礎となる出願の日の後に公表された文献
「Ｔ」国際出願日又は優先日後に公表された文献であって出願と矛盾するものではなく、発明の原理又は理論の理解のために引用するもの
「Ｘ」特に関連のある文献であって、当該文献のみで発明の新規性又は進歩性がないと考えられるもの
「Ｙ」特に関連のある文献であって、当該文献と他の１以上の文献との、当業者にとって自明である組合せによって進歩性がないと考えられるもの
「＆」同一パテントファミリー文献

国際調査を完了した日 ２２．０５．２０１５	国際調査報告の発送日 ０２．０６．２０１５
国際調査機関の名称及びあて先 日本国特許庁（ＩＳＡ／ＪＰ） 郵便番号１００－８９１５ 東京都千代田区霞が関三丁目４番３号	特許庁審査官（権限のある職員）　４Ｘ　４８６３ 宮田　透 電話番号　０３－３５８１－１１０１　内線　３４７７

AMPEREX Ex. 1002
Page 792

Ｃ（続き）．　関連すると認められる文献

引用文献のカテゴリー＊	引用文献名　及び一部の箇所が関連するときは、その関連する箇所の表示	関連する請求項の番号
A	JP 2003-346797 A (日本電池株式会社) 2003.12.05, 全文,全図 (ファミリーなし)	1-7
A	JP 2004-220952 A (松下電器産業株式会社) 2004.08.05, 全文,全図 & US 2004/0142240 A1 & CN 1518145 A	1-7
A	WO 2006/054604 A1 (松下電器産業株式会社) 2006.05.26, 全文,全図 & JP 2006-173099 A & KR 10-2007-0085860 A & CN 101061600 A & US 2008/0118833 A1 & US 2011/0281165 A1	1-7
A	JP 2006-173137 A (日立マクセル株式会社) 2006.06.29, 全文,全図 (ファミリーなし)	1-7
A	JP 2006-324235 A (松下電器産業株式会社) 2006.11.30, 全文,全図 (ファミリーなし)	1-7
P,A	JP 2014-170739 A (三星エスディアイ株式会社) 2014.09.18, 全文,全図 & US 2014/0242468 A1 & EP 2772968 A1 & KR 10-2014-0108102 A & CN 104037397 A	1-7

Espacenet

Family list: JP2004288579 (A) — 2004-10-14

5 application(s) for: JP2004288579 (A)

1. NONAQUEOUS ELECTROLYTE SECONDARY BATTERY, POSITIVE ELECTRODE ACTIVE MATERIAL, AND ITS MANUFACTURING METHOD					
Inventor:	**Applicant:**	**CPC:**	**IPC:**	**Publication info:**	**Priority date:**
INOUE TAKAO ITAYA SHOJI (+1)	SANYO ELECTRIC CO	A01G17/10 A01G17/12 A01G7/06 (+17)	C01G45/02 C01G45/12 C01G49/00 (+9)	JP2004288579 (A) 2004-10-14 JP4404564 (B2) 2010-01-27	2003-03-25
2. Non-aqueous electrolyte secondary cell, positive pole active matter and its producing method					
Inventor:	**Applicant:**	**CPC:**	**IPC:**	**Publication info:**	**Priority date:**
TAKAO IUE [JP] MASASHISA FUJIMOTO [JP] (+1)	SANYO ELECTRIC CO [JP]	A01G17/10 A01G17/12 A01G7/06 (+17)	C01G45/02 C01G45/12 C01G49/00 (+13)	CN1532967 (A) 2004-09-29 CN1297022 (C) 2007-01-24	2003-03-25
3. NONAQUEOUS ELECTROLYTE SECONDARY BATTERY WHOSE SOME LITHIUM OF LAYERED HALITE STRUCTURE IS SUBSTITUTED WITH MAGNESIUM, CATHODE ACTIVE MATERIAL AND PREPARATION METHOD THEREOF					
Inventor:	**Applicant:**	**CPC:**	**IPC:**	**Publication info:**	**Priority date:**
INOUE TAKAO FUJIMOTO MASAHISA (+1)	SANYO ELECTRIC CO	A01G17/10 A01G17/12 A01G7/06 (+17)	C01G45/02 C01G45/12 C01G49/00 (+7)	KR20040084761 (A) 2004-10-06 KR101076501 (B1) 2011-10-24 Global Dossier	2003-03-25
4. NON-AQUEOUS ELECTROLYTE SECONDARY BATTERY, POSITIVE ELECTRODE ACTIVE MATERIAL AND METHOD OF MANUFACTURING THE SAME					
Inventor:	**Applicant:**	**CPC:**	**IPC:**	**Publication info:**	**Priority date:**
INOUE TAKAO [JP] FUJIMOTO MASAHISA [JP] (+1)	SANYO ELECTRIC CO [JP]	A01G17/10 A01G17/12 A01G7/06 (+17)	C01G45/02 C01G45/12 C01G49/00 (+10)	US2009011336 (A1) 2009-01-08 US7709151 (B2) 2010-05-04 Global Dossier	2003-03-25
5. Non-aqueous electrolyte secondary battery, positive electrode active material and method of manufacturing the same					
Inventor:	**Applicant:**	**CPC:**	**IPC:**	**Publication info:**	**Priority date:**
INOUE TAKAO [JP] FUJIMOTO MASAHISA [JP] (+1)	SANYO ELECTRIC CO [US]	A01G17/10 A01G17/12 A01G7/06 (+17)	C01G45/02 C01G45/12 C01G49/00 (+13)	US2004191628 (A1) 2004-09-30 Global Dossier	2003-03-25

Espacenet

Bibliographic data: JP2004288579 (A) — 2004-10-14

NONAQUEOUS ELECTROLYTE SECONDARY BATTERY, POSITIVE ELECTRODE ACTIVE MATERIAL, AND ITS MANUFACTURING METHOD

Inventor(s): INOUE TAKAO; ITAYA SHOJI; FUJIMOTO MASAHISA ± (INOUE TAKAO, ; ITAYA SHOJI, ; FUJIMOTO MASAHISA)

Applicant(s): SANYO ELECTRIC CO ± (SANYO ELECTRIC CO LTD)

Classification: - international: ***C01G45/02; C01G45/12; C01G49/00; C01G51/00; C01G53/00; H01M10/05; H01M4/505; H01M4/525; H01M4/58;*** (IPC1-7): H01M10/40; H01M4/02; H01M4/58

- cooperative: **A01G17/10 (KR)**; **A01G17/12 (KR)**; **A01G7/06 (KR)**; **C01G45/1228 (EP)**; **C01G49/009 (EP)**; **C01G51/42 (EP)**; **C01G51/66 (EP)**; **C01G53/42 (EP)**; **C01G53/66 (EP)**; **H01M4/1391 (EP)**; **H01M4/505 (EP)**; **H01M4/525 (EP)**; C01P2002/54 (EP); C01P2002/72 (EP); C01P2002/77 (EP); C01P2006/40 (EP); H01M10/0525 (EP); H01M4/0438 (EP); H01M4/485 (EP); Y02E60/10 (EP)

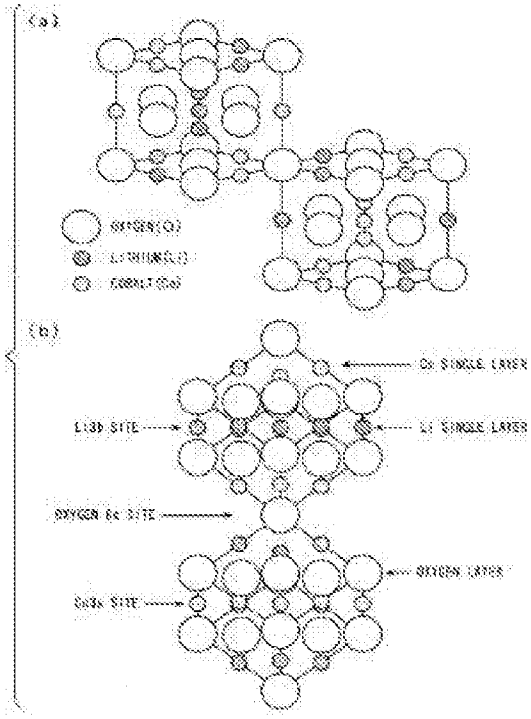
Application number: JP20030082305 20030325

Priority number(s): JP20030082305 20030325

Also published as: CN1297022 (C) CN1532967 (A) JP4404564 (B2) KR101076501 (B1) KR20040084761 (A) more

Abstract of JP2004288579 (A)

PROBLEM TO BE SOLVED: To provide a nonaqueous electrolyte battery capable of improving a capacity density, and provide a positive electrode active material and its manufacturing method. ;SOLUTION: A lithium transition metal composite oxide having a stratified salt block structure containing lithium (Li), wherein the Li is partly substituted by magnesium (Mg), is used for the active material. The composite oxide is formed by partly and chemically or electrochemically substituting Li in LiCoO<SB>2</SB>, LiMnO<SB>2</SB>, LiFeO<SB>2</SB>, LiNiO<SB>2</SB>, etc. by Mg. A cell, of which a negative electrode 2, and a positive electrode 1 including the composite oxide (the active material) are disposed in a nonaqueous electrolyte 5 containing a lithium salt are produced, and Li is partly extracted from the composite oxide by charging the cell. Then, Li is partly substituted by Mg, by replacing the electrolyte 5 containing Li with the electrolyte 5 containing Mg and discharging the cell. ;COPYRIGHT: (C) 2005,JPO&NCIPI


(a)
(b)

(19)日本国特許庁(JP)　(12)公開特許公報(A)　(11)特許出願公開番号
特開2004-288579
(P2004-288579A)
(43)公開日　平成16年10月14日(2004.10.14)

(51)Int.Cl.[7]	F I		テーマコード（参考）
H01M 4/58	H01M 4/58		5H029
H01M 4/02	H01M 4/02	C	5H050
H01M 10/40	H01M 10/40	Z	

審査請求 未請求　請求項の数 9　OL　（全 11 頁）

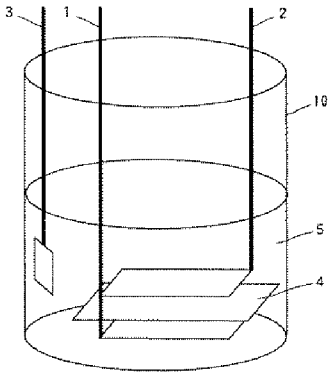
(21)出願番号　特願2003-82305(P2003-82305)
(22)出願日　平成15年3月25日(2003.3.25)

(71)出願人　000001889
三洋電機株式会社
大阪府守口市京阪本通２丁目５番５号
(74)代理人　100098305
弁理士　福島　祥人
(72)発明者　井上　尊夫
大阪府守口市京阪本通２丁目５番５号　三洋電機株式会社内
(72)発明者　板谷　昌治
大阪府守口市京阪本通２丁目５番５号　三洋電機株式会社内
(72)発明者　藤本　正久
大阪府守口市京阪本通２丁目５番５号　三洋電機株式会社内

最終頁に続く

(54)【発明の名称】非水電解質二次電池、正極活物質およびその製造方法

(57)【要約】
【課題】容量密度の向上が可能な非水電解質二次電池、正極活物質およびその製造方法を提供することである。
【解決手段】正極活物質としては、リチウム（Ｌｉ）を含有する層状岩塩構造を有しかつリチウム（Ｌｉ）の一部がマグネシウム（Ｍｇ）で置換されたリチウム遷移金属複合酸化物が用いられる。リチウム遷移金属複合酸化物は、$LiCoO_2$、$LiMnO_2$、$LiFeO_2$、$LiNiO_2$等におけるＬｉの一部をＭｇで化学的または電気化学的に置換することにより形成される。リチウム塩を含む非水電解質５中に負極２とリチウム遷移金属複合酸化物（正極活物質）を含む正極１とが配置されたセルを作製し、セルの充電を行うことによりリチウム遷移金属複合酸化物中のＬｉの一部を引き抜く。その後、Ｌｉを含む電解質をＭｇを含む電解質に交換し、セルの放電を行うことにより、リチウム遷移金属複合酸化物中のＬｉの一部をＭｇで置換する。
【選択図】　図２



【特許請求の範囲】
【請求項1】
負極と、リチウムを吸蔵および放出可能な正極活物質を含む正極と、非水電解質とを備え、
前記正極活物質は、リチウムを含有する層状岩塩構造を有しかつリチウムの一部がマグネシウムで置換された酸化物からなることを特徴とする非水電解質二次電池。
【請求項2】
前記酸化物は、組成式$Li_aMg_bM1O_2$で表されるリチウム遷移金属複合酸化物であり、前記組成式において$a+2b=1$、$0<a<1$および$0<b<0.5$であり、Ｍ１はコバルト、マンガン、鉄およびニッケルよりなる群から選択された１種以上の金属であることを特徴とする請求項１記載の非水電解質二次電池。
【請求項3】
前記酸化物は、組成式$Li_aMg_bCoO_2$で表されるリチウム遷移金属複合酸化物であり、前記組成式において$a+2b=1$、$0<a<1$および$0<b<0.5$であることを特徴とする請求項１または２記載の非水電解質二次電池。
【請求項4】
前記酸化物の前記リチウムの一部は、電気化学的にマグネシウムで置換されたことを特徴とする請求項１～３のいずれかに記載の非水電解質二次電池。
【請求項5】
前記酸化物の前記リチウムの一部は、カチオンがマグネシウムであるイミド塩またはスルホン酸塩を含む非水電解質により電気化学的にマグネシウムで置換されたことを特徴とする請求項１～４のいずれかに記載の非水電解質二次電池。
【請求項6】
前記酸化物の前記リチウムの一部は、カチオンがマグネシウムであるスルホニルイミド塩を含む非水電解質により電気化学的にマグネシウムで置換されたことを特徴とする請求項１～５のいずれかに記載の非水電解質二次電池。
【請求項7】
リチウムを吸蔵および放出可能な正極活物質であって、
リチウムを含有する層状岩塩構造を有しかつリチウムの一部がマグネシウムで置換された酸化物からなることを特徴とする正極活物質。
【請求項8】
リチウムを含有する層状岩塩構造を有する酸化物におけるリチウムの一部を電気化学的にマグネシウムで置換することを特徴とする正極活物質の製造方法。
【請求項9】
リチウム塩を含む非水電解質中に負極と前記酸化物を含む正極とが配置されたセルを作製し、前記セルの充電を行うことにより前記酸化物中のリチウムの一部を引き抜いた後、リチウム塩を含む非水電解質をマグネシウム塩を含む非水電解質に交換し、前記セルの放電を行うことによりマグネシウムを前記酸化物に挿入することを特徴とする請求項８記載の正極活物質の製造方法。

【発明の詳細な説明】
【０００１】
【発明の属する技術分野】
本発明は、非水電解質二次電池、正極活物質およびその製造方法に関する。
【０００２】
【従来の技術】
コバルト酸リチウムを始めとする層状岩塩構造を有する金属酸化物は、高い電圧を示す正極活物質として現在リチウムイオン電池に用いられている。しかし、容量密度が１２５～１５０ｍＡｈ／ｇと低いため、さらなる高容量化技術の開発および代替物質の検討が盛んに行なわれている（例えば、特許文献１および２参照）。
【０００３】

【特許文献１】
特開２００１－２４３９５１号公報
【特許文献２】
特開２００１－１５５７２９号公報
【０００４】
【発明が解決しようとする課題】
コバルト酸リチウムの理論容量密度は約２７４ｍＡｈ／ｇと高い。しかし、現在では、この理論容量密度の５５％に当たる１５０ｍＡｈ／ｇ程度が正極材料として利用できる限界であると言われている。そこで、コバルト酸リチウムの高容量密度化が望まれている。
【０００５】
本発明の目的は、容量密度の向上が可能な非水電解質二次電池、正極活物質およびその製造方法を提供することである。
【０００６】
【課題を解決するための手段および発明の効果】
コバルト酸リチウムを$Li_{1-x}CoO_2$で表し、六方晶で帰属した場合、ａ軸長は、ｘ＝０．５程度までは縮み、それ以上では伸びる傾向にある。一方、ｃ軸長は、ｘ＝０．６程度までは伸び、それ以上では縮む傾向にあり、出発物質であるｘ＝０のときより短くなるまで収縮する。つまり、コバルト酸リチウムは、ｘ＝０．６までは充電とともに格子体積が膨張し、ｘ＝０．６以上になると収縮する。０．２５≦ｘ＜０．７５の領域内のほぼ中間（ｘ＝０．４５～０．５５）の領域で次の相転移が起こり、この領域を境界としてコバルト酸リチウムの実質容量が決定される。
【０００７】
【化１】

$$R\bar{3}m \Leftrightarrow C2/m \Leftrightarrow R\bar{3}m$$

【０００８】
このようなコバルト酸リチウムの構造変化は、層状岩塩構造の３ｂサイトに位置するリチウムを過剰に引き抜くことにより構造不安定性が増加することに起因すると考えられる。
【０００９】
本発明者は、このようなコバルト酸リチウムの構造変化の原因に着目し、実験および検討を重ねた結果、層状岩塩構造の３ｂサイト（リチウム）の一部をマグネシウムで置換することにより構造安定化を図ることが可能であることを見出し、以下の発明を案出するに至った。
【００１０】
第１の発明に係る非水電解質二次電池は、負極と、リチウムを吸蔵および放出可能な正極活物質を含む正極と、非水電解質とを備え、正極活物質は、リチウムを含有する層状岩塩構造を有しかつリチウムの一部がマグネシウムで置換された酸化物からなるものである。
【００１１】
マグネシウムが層状岩塩構造における八面体３ｂサイトに位置した場合、そのイオン半径は０．８６Åであり、リチウムが八面体３ｂサイトに位置した場合のイオン半径０．９０Åと近似している。したがって、マグネシウムが八面体３ｂサイトに置換されることにより、層状岩塩構造が安定化される。それにより、過剰のリチウムを挿入および脱離しても相変化を起こし難い酸化物が得られる。その結果、酸化物の高容量密度化を図ることができ、非水電解質二次電池の容量密度を向上させることが可能となる。
【００１２】
酸化物は、組成式$Li_aMg_bM1O_2$で表されるリチウム遷移金属複合酸化物であり、組成式においてａ＋２ｂ＝１、０＜ａ＜１および０＜ｂ＜０．５であり、Ｍ１はコバルト、マンガン、鉄およびニッケルよりなる群から選択された１種以上の金属である。特に、０．５≦ａ＜１および０＜ｂ≦０．２５であることが好ましい。それにより、リチウム遷移金属複合酸化物の高容量密度化が十分に図られる。
【００１３】

酸化物は、組成式$Li_aMg_bCoO_2$で表されるリチウム遷移金属複合酸化物であり、組成式においてａ＋２ｂ＝１、０＜ａ＜１および０＜ｂ＜０．５であってもよい。特に、０．５≦ａ＜１および０＜ｂ≦０．２５であることが好ましい。それにより、コバルト酸リチウムの高容量密度化が十分に図られる。

【００１４】

酸化物のリチウムの一部は、電気化学的にマグネシウムで置換されてもよい。あるいは、酸化物のリチウムの一部は、化学的にマグネシウムで置換されてもよい。

【００１５】

酸化物のリチウムの一部は、カチオンがマグネシウムであるイミド塩またはスルホン酸塩を含む非水電解質により電気化学的にマグネシウムで置換されてもよい。特に、酸化物のリチウムの一部は、カチオンがマグネシウムであるスルホニルイミド塩を含む非水電解質により電気化学的にマグネシウムで置換されてもよい。

【００１６】

第２の発明に係る正極活物質は、リチウムを吸蔵および放出可能な正極活物質であって、リチウムを含有する層状岩塩構造を有しかつリチウムの一部がマグネシウムで置換された酸化物からなるものである。

【００１７】

本発明に係る正極活物質においては、層状岩塩構造における八面体３ｂサイトの一部をマグネシウムで置換することにより、層状岩塩構造が安定化される。それにより、過剰のリチウムを挿入および脱離しても相変化を起こし難い酸化物が得られる。その結果、酸化物からなる正極活物質の高容量密度化が図られる。

【００１８】

第３発明に係る正極活物質の製造方法は、リチウムを含有する層状岩塩構造を有する酸化物におけるリチウムの一部を電気化学的にマグネシウムで置換するものである。

【００１９】

本発明に係る正極活物質の製造方法によれば、層状岩塩構造における八面体３ｂサイトの一部をマグネシウムに置換することにより、層状岩塩構造が安定化される。それにより、過剰のリチウムを挿入および脱離しても相変化を起こし難い酸化物が得られる。その結果、酸化物の高容量密度化が図られる。

【００２０】

リチウム塩（電解質）を含む非水電解質中に負極と酸化物を含む正極とが配置されたセルを作製し、セルの充電を行うことにより酸化物中のリチウムの一部を引き抜いた後、リチウム塩（電解質）を含む非水電解質をマグネシウム塩（電解質）を含む非水電解質に交換し、セルの放電を行うことによりマグネシウムを酸化物に挿入してもよい。

【００２１】

この場合、非水電解質の交換により容易に酸化物中のリチウムの一部をマグネシウムで置換することができる。

【００２２】

【発明の実施の形態】

以下、本発明の一実施の形態に係る非水電解質二次電池およびその製造方法について説明する。

【００２３】

本実施の形態に係る非水電解質二次電池は、負極、正極および非水電解質により構成される。

【００２４】

負極としては、例えば、リチウム（Ｌｉ）を吸蔵および放出可能な黒鉛等の炭素材料、リチウム金属、リチウム合金等が用いられる。

【００２５】

正極活物質としては、リチウムを含有する層状岩塩構造を有しかつリチウムの一部がマグネシウム（Ｍｇ）で置換されたリチウム遷移金属複合酸化物が用いられる。リチウム遷移

金属複合酸化物としては、$Li_aMg_bCoO_2$、$Li_aMg_bMnO_2$、$Li_aMg_bFeO_2$、$Li_aMg_bNiO_2$等を用いることができる。これらの組成式において$a+2b=1$、$0<a<1$および$0<b<0.5$である。特に、$0.5\leqq a<1$および$0<b\leqq 0.25$であることが好ましく、例えば$a=0.8$および$b=0.1$程度とする。それにより、リチウム遷移金属複合酸化物の高容量密度化が十分に図られる。

【００２６】

上記のリチウム遷移金属複合酸化物は、後述するように、$LiCoO_2$、$LiMnO_2$、$LiFeO_2$、$LiNiO_2$等におけるリチウム（Ｌｉ）の一部をマグネシウム（Ｍｇ）で化学的または電気化学的に置換することにより形成される。

【００２７】

非水電解質の非水溶媒（有機溶媒）としては、一般の非水電解質二次電池において使用される非水溶媒（有機溶媒）を用いることができる。例えば、エチレンカーボネート、ジエチルカーボネート、ジメチルカーボネート、プロピレンカーボネート、環状エーテル、鎖状エーテル、フッ化カーボネート等から選択される少なくとも１種を用いることができる。有機溶媒に加えるリチウム塩（電解質）としては、一般の非水電解質二次電池において使用されるリチウム塩（電解質）を用いることができ、例えば、$LiBF_4$、$LiPF_6$、$LiCF_3SO_3$、$LiC_4F_9SO_3$、$LiN(CF_3SO_2)_2$、$LiN(C_2F_5SO_2)_2$、$LiN(CF_3SO_2)(COCF_3)$、$LiAsF_6$等から選択される少なくとも１種を用いることができる。非水電解質は、これに限定されず、非水電解質二次電池用の種々の非水電解質を用いることができる。

【００２８】

図１は$LiCoO_2$の層状岩塩構造を示す図であり、（ａ）はキュービック表示であり、（ｂ）はヘキサゴナル表示である。

【００２９】

図１において、酸素（Ｏ）が白丸印で表され、コバルト（Ｃｏ）が網掛けの丸印で示され、リチウム（Ｌｉ）が斜線の丸印で示されている。

【００３０】

$LiCoO_2$の層状岩塩構造は、酸素が－Ａ－Ｂ－Ｃ－積層の立方最密充填配列した基本骨格を有し、アニオンの数とカチオンの数とが等しく、酸素の八面体の間隙すべてがカチオンで占有されている。また、コバルトおよびリチウムがそれぞれ（１１１）酸素層間の八面体３ａサイトおよび八面体３ｂサイトに単独層を形成して交互に積層されている。

【００３１】

本実施の形態では、八面体３ｂサイトのリチウムの一部をマグネシウムで置換することにより、層状岩塩構造を安定化させる。それにより、過剰のリチウムを挿入および脱離しても層変化を起こし難いリチウム遷移金属複合酸化物が得られる。

【００３２】

以下、リチウム遷移金属複合酸化物のリチウムの一部をマグネシウムで電気化学的に置換することにより正極活物質を形成する方法について説明する。

【００３３】

まず、リチウム塩（電解質）を含む非水電解質中に負極とリチウム遷移金属複合酸化物（正極活物質）を含む正極とが配置されたセルを作製し、セルの充電を行うことによりリチウム遷移金属複合酸化物中のリチウムの一部を引き抜く。その後、リチウム塩（電解質）を含む非水電解質をマグネシウム塩（電解質）を含む非水電解質に交換し、セルの放電を行う。それにより、リチウム遷移金属複合酸化物中のリチウムの一部がマグネシウムで置換される。

【００３４】

この場合、マグネシウム塩（電解質）として、イミド塩またはスルホン酸塩を用いることにより電気化学的に３ｂサイトのリチウムの一部をマグネシウムで置換することが可能となる。

【００３５】

イミド塩としては、$((CF_3SO_2)_2N)_2Mg$、$((C_2F_5SO_2)_2N)_2Mg$、$((C_4F_9SO_2)(CF_3SO_2)N)_2Mg$、$((C_6F_5SO_2)(CF_3SO_2)N)_2Mg$、$((C_8F_{17}SO_2)(CF_3SO_2)N)_2Mg$、$((CF_3CH_2OSO_2)_2N)_2Mg$、$((CF_3CF_2CH_2OSO_2)_2N)_2Mg$、$((HCF_2CF_2CH_2OSO_2)_2N)_2Mg$、$(((CF_3)_2CHOSO_2)_2N)_2Mg$等を用いることができる。

【００３６】

また、スルホン酸塩としては、$(CF_3SO_3)_2Mg$、$(CH_3SO_3)_2Mg$、$(C_4F_9SO_3)_2Mg$、$(C_6F_5SO_3)_2Mg$、$(C_6H_5SO_3)_2Mg$、$(C_8F_{17}SO_3)_2Mg$等を用いることができる。

【００３７】

上記のイミド塩およびスルホン酸塩のうち１種類を用いてもよく、あるいは２種類以上を組み合わせて用いてもよい。

【００３８】

なお、この電解質は、非水溶媒（有機溶媒）に０．１～１．５Ｍの濃度で溶解されて使用され、好ましくは０．５～１．５Ｍの濃度で溶解されて使用される。

【００３９】

また、電気化学的にリチウム（Ｌｉ）をマグネシウム（Ｍｇ）で置換する際の非水溶媒（有機溶媒）としては、通常の電池用非水溶媒を用いることができる。例えば、環状炭酸エステル、鎖状炭酸エステル、エステル類、環状エーテル類、鎖状エーテル類、ニトリル類、アミド類等を用いることができる。

【００４０】

環状炭酸エステルとしては、エチレンカーボネート、プロピレンカーボネート、ブチレンカーボネート等が挙げられ、これらの水素の一部または全部がフッ素化されているものも用いることが可能であり、トリフルオロプロピレンカーボネート、フルオロエチルカーボネート等が挙げられる。

【００４１】

鎖状炭酸エステルとしては、ジメチルカーボネート、エチルメチルカーボネート、ジエチルカーボネート、メチルプロピルカーボネート、エチルプロピルカーボネート、メチルイソプロピルカーボネート等が挙げられ、これらの水素の一部または全部がフッ素化されているものも用いることが可能である。

【００４２】

エステル類としては、酢酸メチル、酢酸エチル、酢酸プロピル、プロピオン酸メチル、プロピオン酸エチル、γ－ブチロラクトン等が挙げられる。

【００４３】

環状エーテル類としては、１，３－ジオキソラン、４－メチル－１，３－ジオキソラン、テトラヒドロフラン、２－メチルテトラヒドロフラン、プロピレンオキシド、１，２－ブチレンオキシド、１，４－ジオキサン、１，３，５－トリオキサン、フラン、２－メチルフラン、１，８－シネオール、クラウンエーテル等が挙げられる。

【００４４】

鎖状エーテル類としては、１，２－ジメトキシエタン、ジエチルエーテル、ジプロピルエーテル、ジイソプロピルエーテル、ジブチルエーテル、ジヘキシルエーテル、エチルビニルエーテル、ブチルビニルエーテル、メチルフェニルエーテル、エチルフェニルエーテル、ブチルフェニルエーテル、ペンチルフェニルエーテル、メトキシトルエン、ベンジルエチルエーテル、ジフェニルエーテル、ジベンジルエーテル、ｏ－ジメトキシベンゼン、１，２－ジエトキシエタン、１，２－ジブトキシエタン、ジエチレングリコールジメチルエーテル、ジエチレングリコールジエチルエーテル、ジエチレングリコールジブチルエーテル、１，１－ジメトキシメタン、１，１－ジエトキシエタン、トリエチレングリコールジメチルエーテル、テトラエチレングリコールジメチル等が挙げられる。

【００４５】

ニトリル類としては、アセトニトリル等が挙げられ、アミド類としては、ジメチルホルムアミド等が挙げられる。

【００４６】

本実施の形態の方法により形成された正極活物質は、安定な層状岩塩構造を有する。それにより、過剰のリチウムを挿入および脱離しても相変化が起こり難い。したがって、正極活物質の高容量密度化が図られ、非水電解質二次電池の容量密度が向上される。

【００４７】

【実施例】

（実施例１）

実施例１では、図２に示す試験セルを作製し、リチウムの一部がマグネシウムで置換されたコバルト酸リチウムの放電容量を測定した。

【００４８】

図２に示すように、セル容器１０内に正極１、負極２および参照極３が配置される。正極１と負極２との間にはセパレータ４が挿入される。また、セル容器１０内には非水電解質５が注入される。

【００４９】

本実施例１では、コバルト酸リチウム（$LiCoO_2$）、炭素からなる導電剤およびポリフッ化ビニリデン（ＰＶｄＦ）からなる結着剤をそれぞれ重量比９０：５：５で混合することにより合剤を作製し、この合剤にＮ－メチル－２－ピロリドンを加え、スラリーを作製した。このスラリーをアルミニウム箔からなる集電体に塗布することにより正極１を形成した。負極２および参照極３には、金属リチウムを用いた。

【００５０】

非水電解質としては、エチレンカーボネート（ＥＣ）およびジエチルカーボネート（ＤＥＣ）の混合溶媒（体積比ＥＣ：ＤＥＣ＝５０：５０）に、溶質として六フッ化リン酸リチウム（$LiPF_6$）を１モル／リットルの割合で溶解させた非水電解質（リチウム塩を含む非水電解質）と、溶媒としてγ－ブチロラクトン（$(CH_2)_3OCO$）に溶質としてビストリフルオロメチルスルホニルイミドマグネシウム（$((CF_3SO_2)_2N)_2Mg$）を１モル／リットルの割合で溶解させた非水電解質（マグネシウム塩を含む非水電解質）とを用いた。

【００５１】

このようにして作製された試験セルを次の方法により定電流で充放電させ、正極活物質の評価を行った。非水電解質および充放電条件を表１に示す。また、マグネシウムによるリチウムの置換前後でのコバルト酸リチウムの放電曲線の測定結果を図３に示す。

【００５２】

【表１】

サイクル数	充放電状況	非水電解質	容量 mA/g	電流密度 mA/cm^2
１サイクル目	充電	$LiPF_6$ EC/DEC	120	1
	放電	$LiPF_6$ EC/DEC	110	1
２サイクル目	充電	$LiPF_6$ EC/DEC	150	1
	放電	$Mg(TFSI)_2$ γ-BL	60	0.025
	放電	$LiPF_6$ EC/DEC	124	0.025
３サイクル目	充電	$LiPF_6$ EC/DEC	135	0.05
	放電	$LiPF_6$ EC/DEC	136	0.05

【００５３】

表１において、γ－ブチロラクトンをγ－ＢＬと表記し、ビストリフルオロメチルスルホ

ニルイミドマグネシウムをＭｇ（ＴＦＳＩ）$_2$　と表記している。

【００５４】

まず、１サイクル目では、セル容器１０内に上記のリチウム塩を含む非水電解質を注入し、試験セルの充電を行った後、放電を行った。充放電時の電流密度は１ｍＡ／ｃｍ^{2}である。この場合、充電容量密度は１２０ｍＡｈ／ｇとなり、放電容量密度は１１０ｍＡｈ／ｇとなった。

【００５５】

次に、２サイクル目では、セル容器１０内に上記のリチウム塩を含む非水電解質を注入した状態で試験セルの充電を行った。それにより、正極活物質のコバルト酸リチウムからリチウム（Ｌｉ）が引き抜かれる。充電時の電流密度は１ｍＡ／ｃｍ^{2}である。

【００５６】

その後、セル容器１０内の非水電解質を上記のマグネシウム塩を含む非水電解質と入れ換え、試験セルの放電を行った。それにより、正極活物質のコバルト酸リチウムにマグネシウム（Ｍｇ）が挿入され、リチウム（Ｌｉ）の一部と置換される。この場合の放電時の電流密度は０．０２５ｍＡ／ｃｍ^{2}である。

【００５７】

次に、セル容器１０内の電解質を上記のリチウム塩を含む非水電解質と入れ換え、試験セルの放電を行った。放電時の電流密度は０．０２５ｍＡ／ｃｍ^{2}である。この場合、放電容量密度は１２４ｍＡｈ／ｇとなった。

【００５８】

さらに、３サイクル目では、セル容器１０内に上記のリチウム塩を含む非水電解質を注入した状態で試験セルの充電を行った。充電時の電流密度は０．０５ｍＡ／ｃｍ^{2}である。この場合、充電容量密度は１３５ｍＡｈ／ｇとなった。

【００５９】

次いで、試験セルの放電を行った。放電時の電流密度は０．０５ｍＡ／ｃｍ^{2}である。この場合、放電容量密度は１３６ｍＡｈ／ｇとなった。

【００６０】

このように、コバルト酸リチウムからリチウムを引き抜き、リチウムの一部をマグネシウムで置換することにより、容量密度が１２３％向上した。

【００６１】

（実施例２）

実施例２では、リチウム（Ｌｉ）の一部をマグネシウム（Ｍｇ）で置換する前後のコバルト酸リチウムの構造変化をＸＲＤ（Ｘ線回折）測定により確認した。

【００６２】

ＸＲＤ測定では、線源にＣｕ（４０ｋＶ，４０ｍＡ）を用い、スキャン速度を１度／分として2θが１０度～８０度の範囲を測定した。

【００６３】

図４はマグネシウムによるリチウムの置換前後の正極のＸＲＤパターンの測定結果を示す図である。

【００６４】

図４において、マグネシウムによるリチウムの置換前のＸＲＤパターンを細い実線で下側に示し、マグネシウムによるリチウムの置換後のＸＲＤパターンを太い実線で上側に示す。

【００６５】

黒の菱形印は、コバルト酸リチウム（$LiCoO_2$）の反射ピークであり、白の丸印は、Al_2O_3の反射ピークを示す。Al_2O_3の反射ピークは、集電体の表面の酸化アルミニウムからの反射によるものである。

【００６６】

図４に示すように、マグネシウムによるリチウムの置換前におけるリチウムCoO_2の反射ピークとマグネシウムによるリチウムの置換後におけるリチウムCoO_2　の反射ピー

クとで、変化がない。これは、マグネシウムによるリチウムの置換によりリチウムＣｏＯ$_2$　の相変化がないことを示している。

【００６７】

このように、ＬｉＣｏＯ$_2$　のリチウム（Ｌｉ）の一部をマグネシウム（Ｍｇ）で置換した場合に、構造変化が生じないことがわかる。

【図面の簡単な説明】

【図１】ＬｉＣｏＯ$_2$の層状岩塩構造を示す図である。

【図２】リチウムの一部がマグネシウムで置換されたコバルト酸リチウムを正極活物質として用いた試験セルを示す図である。

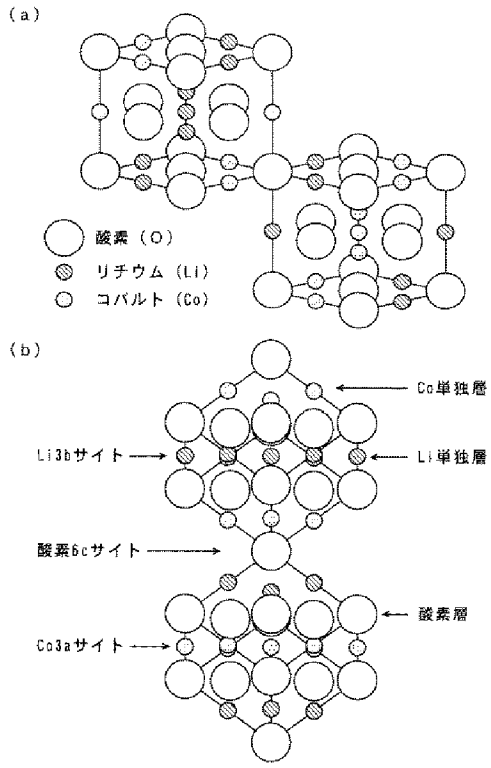
【図３】マグネシウムによるリチウムの置換前後でのコバルト酸リチウムの放電曲線の測定結果を示す図である。

【図４】マグネシウムによるリチウムの置換前後の正極のＸＲＤパターンの測定結果を示す図である。

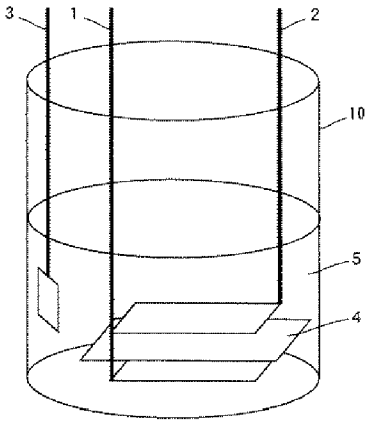
【符号の説明】

１　正極
２　負極
３　参照極
４　セパレータ
５　非水電解質
１０　セル容器

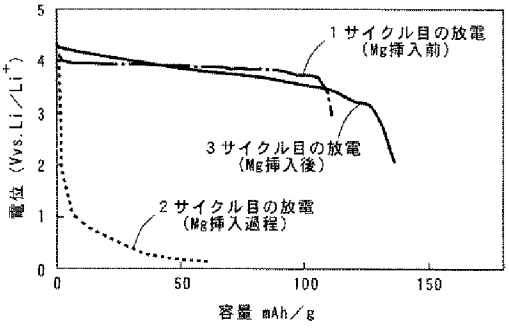
【図1】



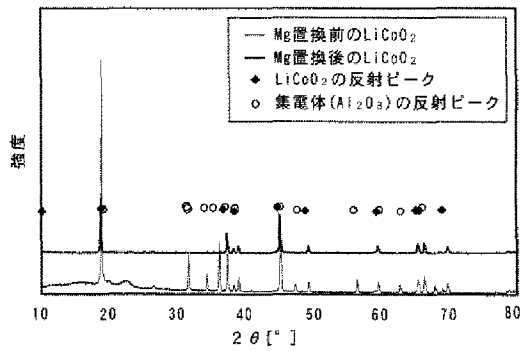
【図2】



【図3】



【図4】


Mg置換前のLiCoO2
Mg置換後のLiCoO2
LiCoO2の反射ピーク
集電体(Al2O3)の反射ピーク
強度
10
20
30
40
50
60
70
80
2θ[°]

Ｆターム(参考) 5H029 AJ03 AJ14 AK03 AL12 AM02 AM03 AM04 AM05 AM07 CJ11
CJ16 DJ17 EJ04 EJ12 HJ02
5H050 AA08 AA19 BA16 BA17 CA07 CA08 CA09 CB12 EA08 EA24
FA19 GA11 GA18 HA02

Journal of The Electrochemical Society, **154** (4) A337-A342 (2007)
0013-4651/2007/154(4)/A337/6/$20.00 © The Electrochemical Society

Phase Transitions and High-Voltage Electrochemical Behavior of $LiCoO_2$ Thin Films Grown by Pulsed Laser Deposition

H. Xia,[a] L. Lu,[b,z] Y. S. Meng,[c] and G. Ceder[c,*]

[a]*Advanced Materials for Micro- and Nano-System, Singapore-MIT Alliance, Singapore 117576*
[b]*Department of Mechanical Engineering, National University of Singapore, Singapore 117576*
[c]*Department of Materials Science and Engineering, Massachusetts Institute of Technology, Cambridge, Massachusetts 02139, USA*

The phase transitions and electrochemical behavior of $LiCoO_2$ thin-film cathodes prepared by pulsed laser deposition are studied for charging voltages ranging from 4.2 to 4.9 V. Two voltage plateaus at about 4.55 and 4.62 V are observed in the charge-discharge curves. Ex situ X-ray diffraction measurements confirm structural changes and a phase transition from the O3 to the H1-3 phase when $LiCoO_2$ is charged above 4.5 V. Thin-film $LiCoO_2$ electrodes show stable capacity retention up to 4.5 V but significant capacity fade above 4.5 V, which we attribute to damage from strain due to phase transitions and Li gradients. Li diffusion in the Li_xCoO_2 thin film up to 4.5 V is investigated by the potentiostatic intermittent titration technique. The chemical diffusion coefficient of Li reaches the maximum near $x = 0.4$ and starts to decrease when the Li content is further decreased.
© 2007 The Electrochemical Society. [DOI: 10.1149/1.2509021] All rights reserved.

Manuscript submitted September 27, 2006; revised manuscript received November 13, 2006.
Available electronically February 20, 2007.

$LiCoO_2$ is the most commonly used cathode material for rechargeable Li-ion batteries. Though its theoretical capacity is 272 mAh/g, the reversible capacity is limited to 140 mAh/g when the $LiCoO_2$ cathode is cycled between 3 and 4.2 V (measured vs Li metal), corresponding to extracting and inserting about 0.5 Li per $LiCoO_2$. In order to obtain higher capacity from $LiCoO_2$, a cutoff voltage above 4.2 V must be applied, which sometimes results in a rapid capacity loss. Because of the increasing interest in charging $LiCoO_2$ to voltage above 4.2 V, we investigate the kinetics and thermodynamic aspects of Li insertion above 4.2 V. Thin-film electrodes deposited by pulsed laser deposition (PLD) are used in this study as they can be charged and discharged without the need for binder and carbon in the electrode.

Several investigations have identified phase transitions in layered Li_xCoO_2 above 4.5 V.[1-5] Most recently, these transitions were identified as being from the O3 phase to the H1-3 phase around 4.55 V (a stage-two compound) and from the H1-3 phase to the O1 phase (CoO_2) around 4.62 V.[3,5] Some researchers have attributed poor cycling life above 4.2 V to these phase transitions, and argued that they can be inhibited by coating a metal oxide on the surface of $LiCoO_2$.[6-9] Similar improvements in high-voltage cycling after coating $LiCoO_2$ with metal oxides were reported by other groups.[10-13] However, Chen and Dahn et al.[14-16] recently pointed out that mechanical degradation through phase transitions is not a very convincing explanation for loss of capacity because $LiCoO_2$ particles do not expand further and experience no new phase transitions when cycled between 4.2 and 4.4 V. They proposed that the poor capacity retention of $LiCoO_2$ cycled to 4.4 or 4.5 V is caused by impedance growth in the cell, which apparently results from side reactions involving $LiPF_6$-based electrolytes and surface species caused by air or moisture exposure. It has been proven that, with fresh surfaces, $LiCoO_2$ cathodes can be cycled to 4.5 V and deliver a capacity of about 180 mAh/g in a $LiPF_6$-based electrolyte with excellent capacity retention.[17]

Though several groups[1-5] have done excellent work on investigating the electrochemical behavior and structural changes of Li_xCoO_2 above 4.2 V, the Li diffusion in Li_xCoO_2 ($x < 0.5$) above 4.2 V is rarely studied, though a first-principle study[18] has predicted the lithium diffusion in Li_xCoO_2 over the complete composition range $0 < x < 1$.

In this work, we report on the electrochemical behavior of $LiCoO_2$ thin-film cathodes prepared by PLD above 4.2 V. Phase transitions are studied with charge-discharge curves and ex situ X-ray diffraction (XRD). The chemical diffusion coefficient of Li in Li_xCoO_2 is measured up to 4.5 V by potentiostatic intermittent titration technique (PITT).

Experimental

$LiCoO_2$ thin films were grown by PLD on stainless steel (SS) and SiO_2/Si (SOS) substrates at a substrate temperature of 600°C in an oxygen atmosphere of 100 mTorr for 40 min. The PLD target contained 15% excess Li_2O to compensate for lithium loss during the deposition. The target-substrate distance was kept at 40 mm. A Lambda Physik KrF excimer laser beam (248 nm, 150–160 mJ/pulse) was used in the deposition with a repetition frequency of 10 Hz. A double layer of Pt/Ti was deposited on the SOS substrate, where Pt was used as current collector and Ti was used as a buffer layer to enhance the adhesion between the Pt and SiO_2. The thickness of the thin film was estimated from field emission scanning electron microscopy (FESEM, Hitachi S-4100) images for the cross sections of the films on the substrates.

The Li/$LiCoO_2$ cell was assembled with the $LiCoO_2$ thin film as the cathode and a lithium metal foil as the anode and a 1 M $LiPF_6$ in ethyl carbonate-dimethyl carbonate solution (EC/DEC, 1/1 vol %, Ozark Fluorine Specialties, Inc.) as the electrolyte. All electrochemical experiments were conducted in an Ar-filled glove box with a Solatron 1287 two-terminal cell test system. Galvanostatic charge-discharge tests were carried out in different voltage windows with a constant current density of 15 $\mu A/cm^2$. Ex situ XRD measurements of the thin-film cathodes at different charge states were measured using a Shimadzu XRD-6000 X-ray diffractometer with Cu Kα radiation. Data were collected in the 2θ range of 10–70° at a scan rate of 2°/min. To measure the chemical diffusion coefficient of Li in the Li_xCoO_2 film by PITT, a potential step of 10 mV was applied and the current was measured as a function of time. The potential step was stepped to the next level when the current dropped below 0.1 $\mu A/cm^2$. This procedure was repeated between 3.88 and 4.50 V at both increasing and decreasing potentials.

Results

Phase transitions.— In a previous paper,[19] we showed that the very smooth surface of the SOS substrate leads to almost pure (003) texture and better crystallization of the $LiCoO_2$ film resulting in well-defined plateaus in the charge-discharge voltage profiles. Figure 1 shows the charge-discharge curves of the Li/$LiCoO_2$ cell on the SOS substrate in various voltage windows. The lower cutoff voltage was fixed at 3 V and the upper cutoff voltage was varied from 4.2 to 4.9 V. The charge-discharge measurements were con-

* Electrochemical Society Active Member.
z E-mail: mpelulu@nus.edu.sg

AMPEREX Ex. 1002
Page 808

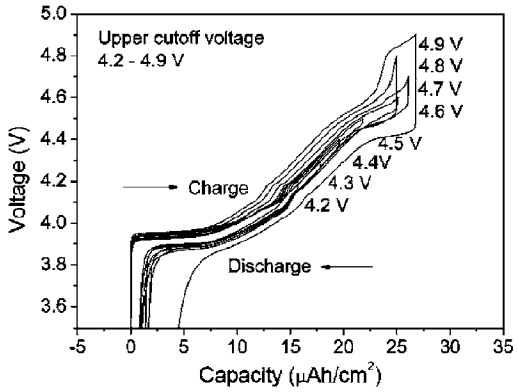


Figure 1. Charge-discharge curves of the Li/$LiCoO_2$ cell with thin-film $LiCoO_2$ cathode using various upper cutoff voltages from 4.2 to 4.8 V. The lower cutoff voltage was fixed at 3 V and the cycling current was 15 μA cm^{-2}.

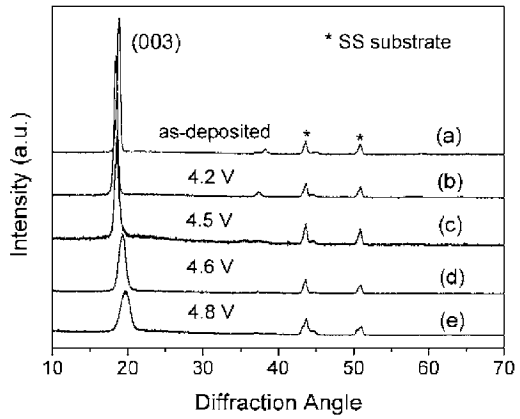


Figure 3. Ex situ XRD spectra for the $LiCoO_2$ films at different charge states: (a) as-deposited, (b) 4.2 V, (c) 4.5 V, (d) 4.6 V, and (e) 4.8 V.

tinuously done on the same cell from 4.2 to 4.9 V. Only one cycle was conducted and recorded for each potential. The thickness of the film was estimated to be about 300 nm from the FESEM on the sample after electrochemical tests. The charge and discharge capacities of the cell increased as the upper cutoff voltage increased up to 4.7 V, similar to what has been found previously on composite electrodes.[5] The polarization of the cell did not change much until 4.5 V. By increasing the upper cutoff voltage from 4.2 to 4.5 V, the capacity increased by 40%, which is slightly higher than what was obtained with the composite electrode (30%).[17] All charge-discharge curves in Fig. 1 show a large plateau at about 3.9 V and two minor plateaus between 4.05 and 4.20 V. The 3.9 V plateau corresponds to the first-order metal-insulator transition,[20,21] and the two minor plateaus correspond to the order-disorder transitions near composition $Li_{0.5}CoO_2$.[22,23] When the upper cutoff voltage was increased to 4.7 V, another two plateaus between 4.5 and 4.7 V could be observed.

The differential capacity curves were derived from the charge-discharge curves from Fig. 1. The peaks in the differential capacity, dQ/dV (Fig. 2) represent the plateaus in the charge-discharge curves in Fig. 1. No peaks are observed in the voltage range between 4.2 and 4.5 V, indicating that no phase transition occurs in this voltage range. However, the small rise of the dQ/dV curve at about 4.5 V in the charge process may signify the onset of a phase transition at 4.5 V. When the Li/$LiCoO_2$ cell was charged to 4.7 V, two peaks at 4.55 and 4.62 V were observed, corresponding to the two high-voltage plateaus above 4.5 V in the charge curves in Fig. 1. This observation agrees well with Chen and Dahn's observation on a $LiCoO_2$ composite electrode,[5] who attributed these two peaks to the phase transitions from the O3 phase to the H1-3 phase and from the H1-3 phase to the O1 phase, as predicted by Van der Ven.[3] The O3 and O1 phases are, respectively, the rhombohedral and hexagonal form of Li_xCoO_2, and the H1-3 phase is the stage II compound of Li_xCoO_2, which can be considered as a hybrid of the rhombohedral and hexagonal host. The two peaks in the discharge part of dQ/dV indicate that the phase transitions at 4.55 and 4.62 V are reversible upon charging to 4.7 V. However, after the Li/$LiCoO_2$ cell was charged to 4.9 V, the two peaks in the discharge part of dQ/dV merged into one narrow and strong peak, indicating that these reactions are only reversible under certain conditions. The staging of Li in the H1-3 structure was only stable when O3 and O1 stackings alternated along the c-axis in the structures. Thus, it is possible that structural damage induced by charging to 4.9 V prevents the Li staging upon discharge. We also found a small peak at about 4.85 V in the charge part of dQ/dV, similar to the small peak above 5 V found by Chen and Dahn,[5] which they believe is due to the electrolyte decomposition at high voltage. No such peak was found when a solid electrolyte was used,[24] consistent with the assignment of the high-voltage peak to liquid electrolyte decomposition.

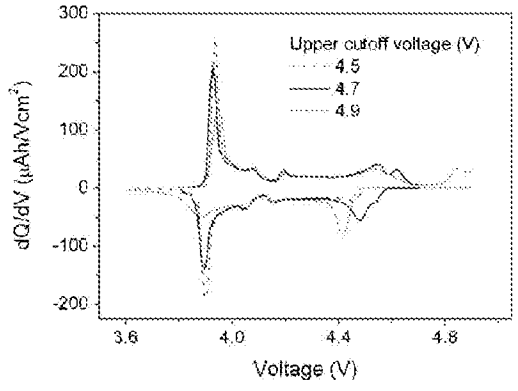


Figure 2. The differential capacity vs voltage for the Li/$LiCoO_2$ cell with different upper cutoff voltages.

To further investigate the two phase transitions between 4.5 and 4.8 V, ex situ XRD experiments were performed on the thin-film $LiCoO_2$ electrodes on SS substrates at different charge states. We prefer films on the SS substrates as they have less diffraction peaks and are easy to assemble and disassemble in our lab-made Swagelok cells. Figure 3 shows selected XRD spectra of the $LiCoO_2$ thin-film electrodes at different charge states from as-deposited ($LiCoO_2$) to 4.8 V. Due to the preferred (003) texture of the film on the SS substrate, the XRD spectrum of the as-deposited $LiCoO_2$ film shows a strong (003) peak. Other reflections have weak intensities. The shift of the (003) peak with different charge states in a selected range of angles is shown in Fig. 4. As shown in Fig. 3, the (003) peak first decreases to a lower angle when charged to 4.2 V, then increases when further charged above 4.2 V and increases significantly when charged above 4.5 V. The ex situ XRD results of $LiCoO_2$ thin film at different charge states agree well with previous reports of ex situ[1] and in situ[2,4,5] XRD of $LiCoO_2$ composite electrodes. As Li is initially removed from $LiCoO_2$, the repulsive interactions between the negatively charged oxygen planes are less compensated by the Li^+--O^{2-} interaction, resulting in an increased c-lattice parameter. When the Li content is reduced below $x = 0.5$ (above 4.2 V), the average charge on the oxygen ions decreases and the electrostatic repulsion between the oxygen ions is lowered resulting in a contraction of the host along the c axis.[23] Based on the

AMPEREX Ex. 1002
Page 809

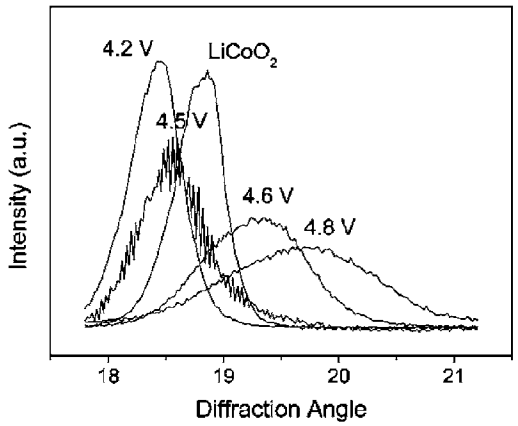


Figure 4. A selected range of the ex situ XRD spectra of the $LiCoO_2$ films at different charge states.

(003) peak position in Fig. 4, the *c*-lattice parameters at different charge states are calculated to be 14.09, 14.42, and 14.31 Å for as-deposited, 4.2, and 4.5 V, respectively. It is obvious that there is a substantial expansion in the *c*-lattice parameter when the film is charged to 4.2 V from the as-deposited state. When the film is further charged to 4.5 V, the *c*-lattice parameter starts to contract. These changes in the *c*-lattice parameter at different charge states are consistent with previous reports.[2,25]

Figure 5 shows ex situ XRD spectra of $LiCoO_2$ films charged to 4.5 and 4.8 V, respectively. In order to detect more diffraction peaks of the $LiCoO_2$ film, we purposely selected the SS substrate with rough surface, which resulted in a more randomly oriented film. All diffraction peaks for the 4.5 V charged material can be indexed based on the O3 structure, in agreement with the electrochemical data, which indicate that at 4.5 V the material still exists in the O3 structure. At 4.8 V our charge-discharge result as well as previous studies[5] indicate that the Li_xCoO_2 film should be fully delithiated and exist in the O1 structure. However, by comparison to the experimental and calculated peak positions for the H1-3 phase in Ref. 5, most diffraction peaks in our film charged to 4.8 V can be indexed as an H1-3 phase but not an O1 phase. The O1 form of CoO_2 only forms when the delithiation of lithium throughout the crystal is completed. Therefore, it may not be possible to detect this final phase through ex situ XRD because any self-discharge will turn the O1 phase into the H1-3 phase. In addition, CoO_2 phase has been

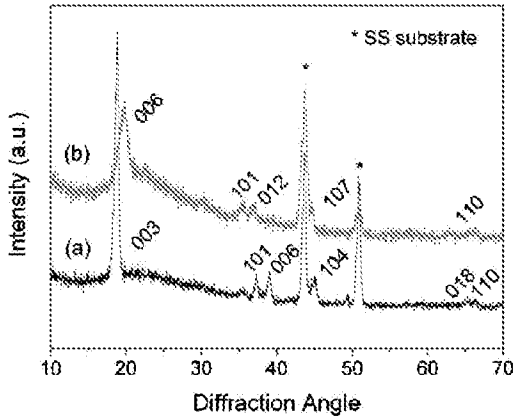


Figure 5. Ex situ XRD spectra for the $LiCoO_2$ films at different charge states: (a) 4.5 V and (b) 4.8 V.

reported to transform to other phases when exposed to air,[2] which also increases the difficulty to detect it by ex situ XRD. Ohzuku et al.,[1] who performed ex situ XRD studies on composite $LiCoO_2$ electrodes, also did not detect the CoO_2 phase.

Capacity retention.— Capacity fade has been extensively investigated in $LiCoO_2$.[7,17,26-29] Possible capacity fade mechanisms have been suggested by different groups. According to Wang et al.,[7] the capacity fade is rapid when cycled to above 4.2 V, and is generally attributed to mechanical failure process associated with structural changes at $x < 0.5$. According to Amatucci[26] and Kim et al.,[27] the fast capacity fade of $LiCoO_2$ electrodes when cycled to 4.4 or 4.5 V is probably due to cobalt dissolution correlated with structural changes. Aurbach et al.,[28] and Chen and Dahn[17] attributed the capacity loss of $LiCoO_2$ electrodes to the impedance growth caused by the formation of a surface layer. Such an electronically resistive surface film may form even quicker when the electrode is cycled to 4.5 V. It seems now generally accepted that below 4.4 or 4.5 V capacity fade is due to impedance growth from side reactions involving $LiPF_6$-based electrolytes and surface species caused by air or moisture exposure. Chen and Dahn[17] indicated that, by creating fresh surfaces, either through grinding or by heating, very good cycle life could be obtained, and they attributed the beneficial effects of coating to the accompanying removal of surface species. Above 4.5 V, the more likely reason for the capacity fade of $LiCoO_2$ is structural phase transitions. According to a transmission electron microscope (TEM) study by Yazami et al.,[29] $LiCoO_2$ electrodes cycled to 4.7 V show an irreversible structural phase transition from hexagonal to cubic spinel, accompanying by increased density of dislocations and internal strains.

Because our $LiCoO_2$ films were grown in a vacuum chamber with in situ heating, without any binder or carbon black, they likely had a fresh surface and are an excellent tool to study the hypothesis of capacity fade. Figure 6a shows the discharge capacity vs cycle number for the Li/$LiCoO_2$ cell ($LiCoO_2$ film on SS substrate) in various voltage windows (10 cycles for each voltage window). Figure 6b shows the capacity fade for the cell as a function of the upper cutoff voltage. It can be seen that the capacity retention of the cell is good for a cutoff voltage below 4.4 V, degrades slightly when cycled to 4.5 V, and significantly deteriorates for voltages above 4.5 V. Ten charge-discharge curves of the cell between 3–4.5 and 3–4.7 V are shown in Fig. 7. The charge-discharge curves of the cell cycled between 3 and 4.7 V show a larger polarization growth with cycling. Figure 8 shows the cycle performance of the cell cycled between 3 and 4.5 V with a constant current of 15 $\mu A/cm^2$ for 50 cycles. The cell exhibits good cycle performance with a capacity fade rate of about 0.2% per cycle. Except for the first several cycles, the charge capacity and discharge capacity are highly reversible with a coulombic efficiency >95%. Jang et al.[24] reported even better cycle performance of their $LiCoO_2$ thin films cycled to 4.4 V in all-solid-state thin-film batteries using the Lipon electrolyte. The improvement of capacity retention is probably because they used solid electrolyte, which avoids the formation of surface films caused by reactions with the liquid electrolyte. In addition, they used a lower cutoff voltage of 4.4 V. Our results seem to give further evidence to the capacity-fade mechanisms previously proposed. Because the thin-film cell has a clean surface, little or no fade exists up to 4.4 to 4.5 V. The structural phase transitions in that regime are mild and accompanied by small changes in lattice parameters. Above 4.5 V, capacity fade is caused by the phase transitions to H1-3 and O1 and occurs in all $LiCoO_2$ electrodes regardless of surface chemistry.

Li diffusion.— Lithium diffusion in the electrode materials is a key factor that determines the rate at which a battery can be charged and discharged. Li diffusion in $LiCoO_2$ has been studied by cyclic voltammetry (CV), electrical impedance spectroscopy (EIS), and potentiostatic intermittent titration technique (PITT).[30-32] However, previous studies of Li diffusion in Li_xCoO_2 have been limited to

AMPEREX Ex. 1002
Page 810

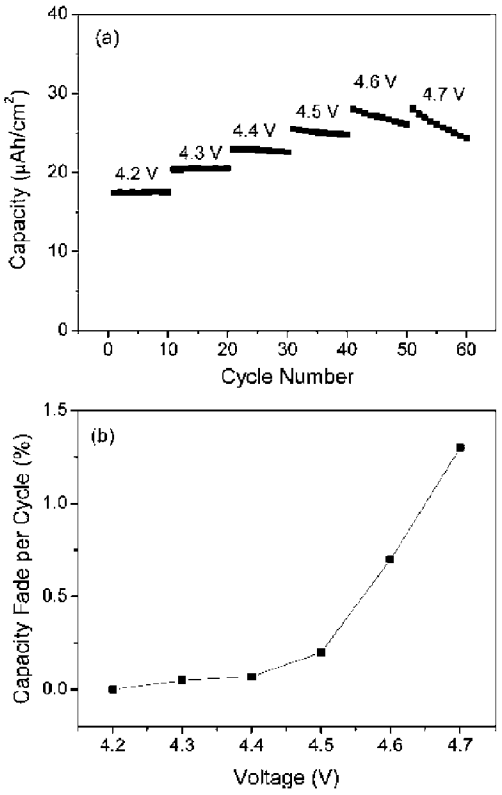


Figure 6. (a) Discharge capacity vs cycle number for the thin-film $LiCoO_2$ electrode with various upper cutoff voltages from 4.2 to 4.7 V and (b) capacity fade per cycle for the thin film $LiCoO_2$ electrode as a function of the upper cutoff voltage.

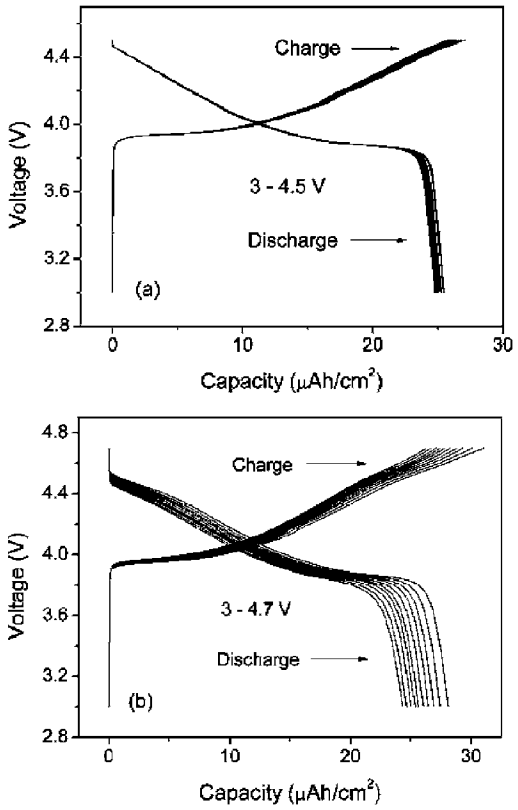


Figure 7. Charge-discharge curves for the thin-film $LiCoO_2$ electrode cycled in different voltage windows: (a) 3–4.5 V and (b) 3–4.7 V.

$x > 0.5$, corresponding to a charge cutoff of about 4.2 V. In this paper we included the region up to $V = 4.5$ V because this potential region could be reversibly accessed in our thin-film electrodes. The chemical diffusion coefficients of Li were measured using PITT. In a single phase region, the current after each potential step decayed exponentially with time according to the expression

$$I(t) = \frac{2Fa(C_S - C_0)\tilde{D}}{L} \exp\left(-\frac{\pi^2 \tilde{D} t}{4L^2}\right) \quad [1]$$

Here, F is the Faraday constant, a is the active surface area of the electrode, L is the thickness of the cathode film, and $(C_s\text{-}C_0)$ is the change in Li concentration at the cathode-electrolyte interface during each potential step. The chemical diffusion coefficient, $\tilde{D}_{Li}$, can be calculated from the slope of the linear region in the plot of $\ln[I(t)]$ vs t, where

$$\tilde{D} = -\frac{d\ln(I)}{dt}\frac{4L^2}{\pi^2} \quad [2]$$

Figure 9a shows the chemical diffusion coefficients obtained from PITT as a function of electrode potential during both charge and discharge. The values of $\tilde{D}_{Li}$ in the potential range between 3.88 and 4.50 V vary from 10^{-12} to 10^{-11} cm^2 s^{-1}, similar to values obtained previously in the potential range between 3.88 and 4.20 V.[31,32] Three minima exist in $\tilde{D}_{Li}$ near 3.9, 4.1, and 4.2 V, respectively. The minimum near 3.9 V is due to the two-phase region and the standard Cottrell analysis to extract $\tilde{D}_{Li}$ may not be appropriate.[33] The other two minima near 4.1 and 4.2 V are associated with the order-disorder phase transitions near $Li_{0.5}CoO_2$. Such minima were also observed in Jang's report, and in our previous study.[32,34] Figure 9b shows $\tilde{D}_{Li}$ vs x of Li_xCoO_2 in the composition region $0.14 < x < 0.75$. The chemical diffusion coefficient of Li initially increases with decreasing Li content, is maximal at about $x = 0.4$, and then starts to decrease with decreasing Li content. The chemical diffusion coefficient of Li in Li_xCoO_2 is expected to be influenced by several factors: (*i*) the concentration of vacancy sites available for lithium ions, (*ii*) the activation barrier for lithium ions to jump, and (*iii*) the thermodynamic factor. The concentration of vacancy sites increases with decreasing Li content. As discussed by Van den Ven and

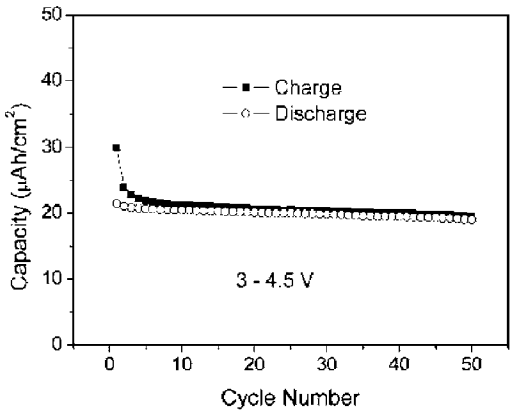


Figure 8. Charge-discharge capacities vs cycle number for the thin-film $LiCoO_2$ electrode cycled between 3 and 4.5 V with a current of 15 μA cm^{-2}.

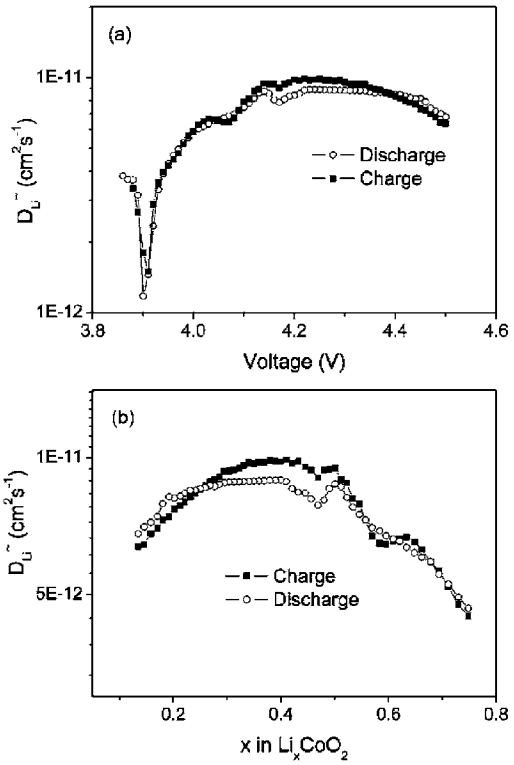


Figure 9. (a) Chemical diffusion coefficients of Li vs potential during charge and discharge states and (b) chemical diffusion coefficients of Li vs x in Li_xCoO_2 during charge and discharge states as obtained with PITT.

Ceder,[18] the variation of the activation barrier can be attributed to two factors. One is the c-lattice parameter. A drop of the c-lattice parameter reduces the distance between the oxygen planes, and compresses the tetrahedral site, resulting in an increase in the activation barrier. A second factor is the change in effective valence of the cobalt ions with x. As x is reduced, the effective positive charge on Co increases, causing the activation barrier to increase.[18,35] The thermodynamic factor is a measure of the deviation of the chemical potential from that for an ideal solution. In the composition range $0.5 < x < 0.75$, the c-lattice parameter increases only slightly with decreasing Li content and the activation barrier does not change much.[18] Therefore, in this composition range, the chemical diffusion coefficient of Li is mainly influenced by the increasing concentration of Li vacancies. For $x < 0.5$, the c-lattice parameter decreases, and the charge on Co increases with decreasing Li content, resulting in a significant increase in the activation barrier energy.[18]

Though there is a good agreement between the experimental result and previously calculated results[18] for the Li diffusivity in $LiCoO_2$, some discrepancies exist. The experimental result shows a maximum at about $x = 0.5$, whereas the calculation result shows a minimum at about $x = 0.5$. The chemical diffusion coefficient $\tilde{D}_{Li}$ is a product of the self-diffusion coefficient D_{Li} and the thermodynamic factor Θ.[36] Θ is proportional to $-dV/dx$, which will have minima at the phase boundaries near the composition $Li_{0.5}CoO_2$ and a maximum at composition $Li_{0.5}CoO_2$. As discussed by Van der Ven and Ceder,[18] the self-diffusion coefficient, D_{Li}, should have a minimum at $x = 0.5$ due to the higher activation energy associated with Li jumps in ordered $Li_{0.5}CoO_2$. Whether the chemical diffusivity, $\tilde{D}_{Li}$, is maximal or minimal depends on the balance between the thermodynamic factor and the self-diffusion coefficient. A less-ordered $Li_{0.5}CoO_2$ cathode will exhibit a less deep minimum of D_{Li}, as there would be less limitation to Li jumping. The thermodynamic factor, is an averaged quantity and is likely to be less drastically influenced by the state of order. Hence, in real samples, which are less ordered than in simulations,[32] the thermodynamic factor may dominate and lead to a maximum. For both experimental and calculation results, $\tilde{D}_{Li}$ starts to drop with decreasing x when $x < 0.4$. However, the drop of $\tilde{D}_{Li}$ in the calculation result is much more pronounced than in the experiments. We attribute this discrepancy to the difference of c-lattice parameter change between calculations and experiments. In previous first- principle calculation,[23] the calculated c-lattice parameter of the O3 host is systematically smaller than the experimentally observed value by approximately 4% and drops more significantly in the composition region $0.15 < x < 0.5$ than in our experimental results: In the calculated result, the c-lattice parameter changes from 13.8 to 12.9 Å when x decreases from 0.5 to 0.15. For our thin-film experimental result, the c-lattice parameter changes from 14.42 to 14.31 Å when x decreases from 0.5 to 0.15 (4.2 to 4.5 V). This large discrepancy is likely due to the overestimation of the van der Waals forces in the local density approximation, which keeps the oxygen layers together as Li is removed.

Discussion

Our thin-film $LiCoO_2$ electrodes show electrochemical behavior that is consistent with composite $LiCoO_2$ electrodes studied previously.[2-5] Two voltage plateaus between 4.5 and 4.7 V are observed for both charge and discharge curves, which likely correspond to the O3 to the H1-3, and the H1-3 to the O1 transitions. We find that the stability of these two phase transitions is highly dependent on the cutoff voltage. As shown in Fig. 2, two peaks between 4.5 and 4.7 V can be observed for both charge and discharge when using the cutoff voltage of 4.7 V. After the cutoff voltage has been raised to 4.9 V, the two peaks for the charge become weak, and the two peaks for the discharge become one narrow and strong peak. The increased difference between these two peaks for charge and discharge indicates that the irreversibility of these two reactions increases as the cutoff voltage increases. We also find that charging the film to very high voltage such as 4.9 V will induce further damage to the structure of the film. As shown in the dQ/dV curve for 4.9 V in Fig. 2, besides the changes of the two peaks at high voltage, the 3.9, 4.1, and 4.2 V peaks all become broad and weak for the discharge process. Especially, the 3.9 V peak for the discharge is much weaker than that for the charge, which indicates that dramatic structure degradation occurs when the film is charged to 4.9 V. As shown in Fig. 1, the polarization of the cell increases gradually as the cutoff voltage is increased from 4.5 to 4.8 V. However, a sudden increase of the cell polarization occurs with a dramatic increase of irreversible capacity when the cutoff voltage is increased from 4.8 to 4.9 V. At the same time, there is a new voltage plateau emerging at about 4.85 V for the charge, which can be attributed to electrolyte decomposition. In this case, we speculate that the electrolyte decomposition probably accelerates the degradation of the crystal structure of the film or impedance growth at the interface between the film and electrolyte and contributes to the large polarization of the cell.

Our work confirms the results obtained by Chen and Dahn,[17] which attributed capacity fade for $LiCoO_2$ electrodes cycled at voltage <4.5 V to the impedance growth of the cell induced by the formation of a surface layer, and not to phase transformations. In agreement, we find that structural changes between 4.2 and 4.5 V are small and that the order-disorder transitions, which occur at 4.1 and 4.2 V, are reversible. The fact that the lattice parameters change little between 4.2 and 4.5 V, and that the Li diffusivity is high, makes it unlikely that capacity degradation through mechanical stress occurs in this voltage region, which is further confirmed by our cycling tests. Below 4.5 V (Fig. 6), very little capacity loss is observed. Because the surfaces of our $LiCoO_2$ films are likely to be

AMPEREX Ex. 1002
Page 812

free of contamination, the lack of capacity loss between 4.2 and 4.5 V seems consistent with the mechanism proposed by Aurbach et al.[28] and Dahn and Chen.[17]

Rapid capacity fade is found when $LiCoO_2$ is cycled to higher voltages such as 4.6 or 4.7 V. In this voltage regime phase transitions occur with a substantial effect on the lattice parameters. Phase transitions together with the decreasing Li diffusivity, which makes Li composition gradients larger, likely leads to large internal strains, and subsequent mechanical degradation of the material. The above conclusion is evidenced in our materials by the lack of clear phase transitions in the charge-discharge cycle after exposure to high potential. Li vacancy ordering is likely to be most sensitive to structure defects. It is therefore not surprising that the plateaus at 4.1 and 4.2 V are significantly deteriorated after a charge to 4.9 V. Yazami et al.,[29] as well as Wang et al.,[7] observed significant amounts of cracking, dislocations, and other extended defects in samples charged to high potential. Cumulative damage of this nature may be responsible for capacity fade during overcharging or in long-term cycling of $LiCoO_2$ electrodes. In addition, CoO_2 has been reported to decompose through loss of oxygen, and the decomposition of CoO_2 may also contribute to the capacity fade when $LiCoO_2$ cycled to 4.7 V.

Lattice parameter changes due to phase transitions or compositional variations are most detrimental when they occur with high Li composition gradients, as this leads to large compatibility strains in the crystallites. Li diffusivity is the key factor which controls the homogeneity (at the particle level) of the charge-discharge process. We observe a drop of the Li chemical diffusion coefficient in Li_xCoO_2 for $x < 0.4$, which is probably caused by the drop of c-lattice parameter and the increased charge on Co. Though it is difficult to measure the chemical diffusion coefficient of Li above 4.5 V (PITT is only meaningful in a single phase region), it is reasonable to believe that an even faster drop of the Li diffusion will occur when the $LiCoO_2$ film is further charged to 4.6 or 4.7 V. According to both experimental[2] and calculation[3] results, the c-lattice drops more significantly when $LiCoO_2$ goes through the two phase transitions from the O3 to the H1-3 phase and from the H1-3 to the O1 phase. As discussed previously, a drop of the c-lattice parameter slows down the Li diffusion. Therefore, the sluggish Li diffusion accompanying the large internal strains above 4.5 V for $LiCoO_2$ may limit the use of $LiCoO_2$ electrodes at high voltages above 4.5 V.

Conclusions

We have used thin-film $LiCoO_2$ electrodes without binder or carbon to study the phase transitions, Li diffusion, and capacity fade above 4.2 V. Two voltage plateaus above 4.5 V are observed in the charge-discharge curves. Ex situ XRD indicated that one of these phase transitions converts the O3 into the H1-3 phase. The $LiCoO_2$ film shows good capacity retention up to a cutoff voltage of 4.5 V, but rapid capacity fade occurs when cycled to 4.6 or 4.7 V. The structural changes between 4.2 and 4.5 V have no obvious effect on the capacity fade, while the structural changes between 4.5 and 4.7 V combined with the decrease of Li diffusivity probably lead to the fast capacity fade of $LiCoO_2$ when cycled to such a high voltage. The chemical diffusion coefficient of Li in Li_xCoO_2 decreases with decreasing Li content for $0.14 < x < 0.4$. The decrease of the chemical diffusion coefficient of Li in Li_xCoO_2 is attributed to the increase of activation barrier of Li jumping at low Li content. An even faster drop of Li diffusion is likely to occur at voltage above 4.5 V. Our present studies provide further evidence that it is very possible to raise the cutoff voltage of $LiCoO_2$ to 4.5 V without sacrificing the capacity retention.

Acknowledgments

This research was supported by Advanced Materials for Micro- and Nano- System (AMM&NS) program under Singapore-MIT Alliance (SMA) and by National University of Singapore.

National University of Singapore assisted in meeting the publication costs of this article.

References

1. T. Ohzuku and A. Ueda, *J. Electrochem. Soc.*, **141**, 2972 (1994).
2. G. G. Amatucci, J. M. Tarascon, and L. C. Klein, *J. Electrochem. Soc.*, **143**, 1114 (1996).
3. A. Van der Ven, M. K. Aydinol, and G. Ceder, *J. Electrochem. Soc.*, **145**, 2149 (1998).
4. X. Sun, X. Q. Yang, J. McBreen, Y. Gao, M. V. Yakovleva, X. K. Xing, and M. L. Daroux, *J. Power Sources*, **97–98**, 374 (2001).
5. Z. H. Chen, Z. H. Lu, and J. R. Dahn, *J. Electrochem. Soc.*, **149**, A1604 (2002).
6. T. Ohzuku, A. Ueda, M. Nagayama, Y. Iwakoshi, and H. Komori, *Electrochim. Acta*, **38**, 1159 (1993).
7. H. Wang, Y. Jang, B. Huang, D. R. Sadoway, and Y. Chang, *J. Electrochem. Soc.*, **146**, 473 (1999).
8. J. Cho, Y. J. Kim, T. J. Kim, and B. Park, *Angew. Chem., Int. Ed.*, **40**, 3367 (2001).
9. J. Cho and G. Kim, *Electrochem. Solid-State Lett.*, **2**, 253 (1999).
10. Z. Wang, C. Wu, L. Liu, L. Chen, and X. Huang, *Solid State Ionics*, **148**, 335 (2002).
11. Z. Wang, C. Wu, L. Liu, L. Chen, and X. Huang, *J. Electrochem. Soc.*, **149**, A466 (2002).
12. L. Liu, Z. Wang, F. Wu, L. Chen, and X. Huang, *Solid State Ionics*, **152**, 341 (2002).
13. A. M. Kannan, L. Rabenberg, and A. Manthiram, *Electrochem. Solid-State Lett.*, **7**, A16 (2002).
14. Z. H. Chen and J. R. Dahn, *Electrochem. Solid-State Lett.*, **5**, A213 (2002).
15. Z. H. Chen and J. R. Dahn, *Electrochem. Solid-State Lett.*, **6**, A221 (2003).
16. Z. H. Chen and J. R. Dahn, *Electrochem. Solid-State Lett.*, **7**, A11 (2004).
17. Z. H. Chen and J. R. Dahn, *Electrochim. Acta*, **49**, 1079 (2004).
18. A. Van der Ven and G. Ceder, *Electrochem. Solid-State Lett.*, **3**, 301 (2000).
19. H. Xia, L. Lu, and G. Ceder, *J. Alloys Compd.*, **417**, 304 (2006).
20. C. A. Maianetti, G. Kotliar, and G. Ceder, *Nat. Mater.*, **3**, 627 (2004).
21. J. Molenda, A. Stoklosa, and T. Bak, *Solid State Ionics*, **36**, 53 (1989).
22. J. N. Reimers, J. R. Dahn, and U. von Sacken, *J. Electrochem. Soc.*, **140**, 2091 (1992).
23. A. Van der Ven, M. K. Aydinol, and G. Ceder, *Phys. Rev. B.*, **58**, 2975 (1998).
24. Y. I. Jang, N. J. Dudney, D. A. Blom, and L. F. Allard, *J. Power Sources*, **119–121**, 295 (2003).
25. J. Cho, Y. J. Kim, and B. Park, *Chem. Mater.*, **12**, 3788 (2000).
26. G. G. Amatucci, J. M. Tarascon, and L. C. Klein, *Solid State Ionics*, **83**, 167 (1996).
27. Y. J. Kim, H. Kim, B. Kim, D. Ahn, J. G. Lee, T. J. Kim, D. Son, J. Cho, Y. W. Kim, and B. Park, *Chem. Mater.*, **15**, 1505 (2003).
28. D. Aurbach, B. Markovsky, A. Rodkin, E. Levi, Y. S. Cohen, H. J. Kim, and M. Schmidt, *Electrochim. Acta*, **47**, 4291 (2002).
29. R. Yazami, Y. Ozawa, H. Gabrisch, and B. Fultz, *Electrochim. Acta*, **50**, 385 (2004).
30. Y. Iriyama, M. Inaba, T. Abe, and Z. Ogumi, *J. Power Sources*, **94**, 175 (2001).
31. M. D. Levi, G. Salitra, B. Markovsky, H. Teller, D. Aurbach, U. Heider, and L. Heider, *J. Electrochem. Soc.*, **146**, 1279 (1999).
32. Y. I. Jang, B. J. Neudecker, and N. J. Dudney, *Electrochem. Solid-State Lett.*, **4**, A74 (2001).
33. B. C. Han, A. Van der Ven, D. Morgan, and G. Ceder, *Electrochim. Acta*, **49**, 4691 (2004).
34. H. Xia, L. Lu, and G. Ceder, *J. Power Sources*, **159**, 1422 (2006).
35. K. Kang, Y. S. Meng, J. Breger, C. P. Grey, and G. Ceder, *Science*, **311**, 977 (2006).
36. W. Weppner and R. A. Huggins, *J. Electrochem. Soc.*, **124**, 1569 (1977).

AMPEREX Ex. 1002
Page 813

Journal of The Electrochemical Society, **156** (12) A1005-A1010 (2009)
0013-4651/2009/156(12)/A1005/6/$25.00 © The Electrochemical Society

Role of AlF_3 Coating on $LiCoO_2$ Particles during Cycling to Cutoff Voltage above 4.5 V

Yang-Kook Sun,[a,*,z] Chong Seung Yoon,[b] Seoung-Taek Myung,[c,*] Ilias Belharouak,[d,*] and Khalil Amine[d,*]

[a]*Department of Energy Engineering and* [b]*Division of Materials Science and Engineering, Hanyang University, Seoul 133-791, South Korea*
[c]*Department of Chemical Engineering, Iwate University, Iwate 020-8551, Japan*
[d]*Electrochemical Technology Program, Chemical Sciences and Engineering Division, Argonne National Laboratory, Argonne, Illinois 60439, USA*

Cell tests demonstrated that the use of an AlF_3 coating enabled a $LiCoO_2$ electrode to deliver a higher discharge capacity (208 mAh g^{-1}) at an upper cutoff voltage of 4.54 V. About 94% of the initial capacity was retained after 50 cycles, while the capacity retention of pristine $LiCoO_2$ was only 60% at 4.5 V. The improved electrochemical performance with the AlF_3 coating was attributed to the delay of structural degradation of $LiCoO_2$ during cycling. A structural analysis of the cycled $LiCoO_2$ electrode revealed that the pristine $LiCoO_2$ transforms to a cubic spinel phase via an intermediate phase triggered by progressive chemical leaching of Co during cycling. The AlF_3 coating protected $LiCoO_2$ from the chemical attack by HF and thus helped to delay the eventual phase transformation to a spinel phase. By delaying this transformation, the AlF_3 coating was able to reduce the charge-transfer resistance and maintain the structural stability when cycled above 4.5 V.
© 2009 The Electrochemical Society. [DOI: 10.1149/1.3236501] All rights reserved.

Manuscript submitted July 9, 2009; revised manuscript received August 27, 2009. Published October 9, 2009.

In recent decades, the demand for small, high capacity batteries to power portable equipment, such as cellular phones and notebook computers, has dramatically risen. Because lithium-ion batteries offer high energy and power density, they have become the most widely used power sources for portable electronic devices and, more recently, hybrid electric vehicles (HEVs) and plug-in HEVs.[1] The most common cathode material for commercial lithium-ion batteries is $LiCoO_2$ due to its high tap density, excellent cycling performance, and high rate capability. Though $LiCoO_2$ has a high theoretical capacity of 274 mAh g^{-1}, its reversible capacity is limited to only 140 mAh g^{-1} when cycled between 3.0 and 4.2 V vs Li metal.

To increase the reversible capacity of $LiCoO_2$, an upper cutoff voltage above 4.2 V should be applied to extract lithium ions beyond $Li_{0.5}CoO_2$. However, as expected, this elevated charge voltage leads to severe capacity loss. Some research groups have reported that the poor cycling performance above 4.2 V is caused by structural instability induced by a phase transition from the hexagonal phase to a monoclinic phase, accompanying a volume change of ~2.6% along the *c*-axis.[2-4] To overcome the above problems, many researchers have modified the $LiCoO_2$ cathode particle surface with metal oxide[5-7] and metal fluoride[8,9] to reduce the catalytic activity of the Co ions with a high oxidation state. Cho et al. reported that ZrO_2-coated $LiCoO_2$, the so-called zero-strain material, delivered a capacity of 170 mAh g^{-1} with an excellent capacity retention after 70 cycles in the voltage range between 2.75 and 4.4 V.[6] Chen and Dahn reported that the capacity loss of $LiCoO_2$ below 4.5 V is mainly due to the interfacial impedance growth between the cathode and electrolyte, which results from side reactions involving $LiPF_6$-based electrolyte and surface impurities caused by air or moisture exposure.[10,11] Recently, Sun et al. also reported that the poor capacity retention of $LiCoO_2$ cycled to 4.5 V stemmed from the increase in charge-transfer resistance and in Co dissolution caused by an HF attack on the cathode surface.[8] More recently, Xia et al. reported that a $LiCoO_2$ thin film (300 nm) shows good capacity retention up to a cutoff voltage of 4.5 V, as no phase transition occurred in the voltage range between 4.2 and 4.5 V.[12]

Structural phase transition and dissolution of a highly oxidized Co^{4+} are responsible for the capacity loss of $LiCoO_2$ above 4.5 V.[13] Van der Ven and Ceder calculated the phase diagram of Li_xCoO_2 ($x < 0.5$) and correlated the phase transition from the O3 phase to the H1-3 phase at around 4.55 V (a stage 2 compound) and from the H1-3 phase to the O1 phase at around 4.62 V.[3] Yazami et al. reported that an aged $LiCoO_2$ electrode charged to 4.7 V underwent the irreversible phase change from a hexagonal to a cubic spinel phase, and the crystals that experienced this phase transformation showed an increased dislocation density and internal strains.[14] Until now, the reason for the enhanced electrochemical performance of the metal-oxide- and metal-fluoride-coated $LiCoO_2$ cathode materials with above 4.5 V cutoff voltage has not been investigated through a detailed structural analysis of the coated cathode during extended cycling.

In this study, we report the excellent capacity exhibited by AlF_3-coated $LiCoO_2$ in the voltage range between 4.5 and 4.6 V and the relation between crystal structure and electrochemical performance at a high cutoff voltage. A pristine $LiCoO_2$ was also tested and characterized at 4.5 V to confirm the capacity fading mechanism.

Experimental

To prepare AlF_3-coated $LiCoO_2$, 0.1 g ammonium fluoride (Aldrich) and 3.91 g aluminum nitrate nonahydrate (Aldrich) were separately dissolved in distilled water. After 50 g $LiCoO_2$ (Nippon Chemical Co.) powders were immersed in the aluminum nitrate nonahydrate solution, the ammonium fluoride solution was slowly added to the resulting solution. The amount of AlF_3 in the solution was 2 mol % of the $LiCoO_2$ powders. After the solution containing the cathode powders was constantly stirred at 80°C for 5 h, it was filtered by distilled water. The obtained $LiCoO_2$ powders were heated at 400°C for 5 h in flowing nitrogen to avoid the formation of Al_2O_3. Details of the coating method are provided in our previous paper.[8,9]

The electrochemical properties of the prepared powder were evaluated with coin-type half-cells (CR2032). Cells were constructed with the electrodes separated by a porous polypropylene film. The electrolyte was a 1:1 mixture of ethylene carbonate (EC) and diethyl carbonate (DEC) containing 1 M $LiPF_6$ by volume (Ukseung Chemical Co., Ltd., Korea). The cathode was fabricated with a mixture of 84 wt % of the prepared powder, 8 wt % carbon black, and 8 wt % poly(vinylidene difluoride) binder on an aluminum current collector. The anode was lithium metal. The cell assembly was carried out in an argon-filled glove box. The capacity and the capacity retention were measured by applying constant currents of 32 mA g^{-1} (0.2 C rate) and 80 mA g^{-1} (0.5 C rate), respectively, between 3.0 and 4.5--4.6 V vs Li/Li^+.

* Electrochemical Society Active Member.
z E-mail: yksun@hanyang.ac.kr

AMPEREX Ex. 1002
Downloaded on 2017-04-02 to IP 61.197.236.153 address. Redistribution subject to ECS terms of use (see ecsdl.org/site/terms_use) unless CC License in place (see abstract).

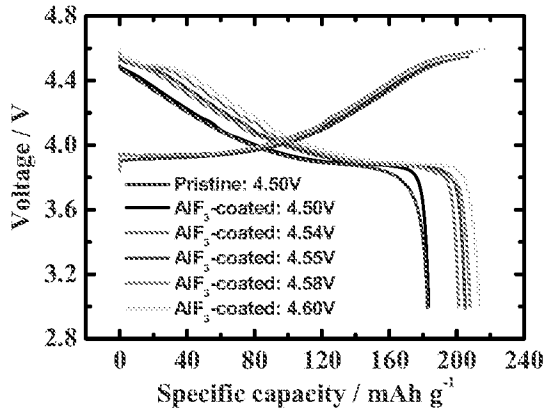


Figure 1. (Color online) Initial charge–discharge curves of Li/pristine $LiCoO_2$ with cutoff voltage of 4.5 V and AlF_3-coated $LiCoO_2$ with cutoff voltages of 4.5–4.6 V at a current density of 32 mA g^{-1} (0.2 C rate).

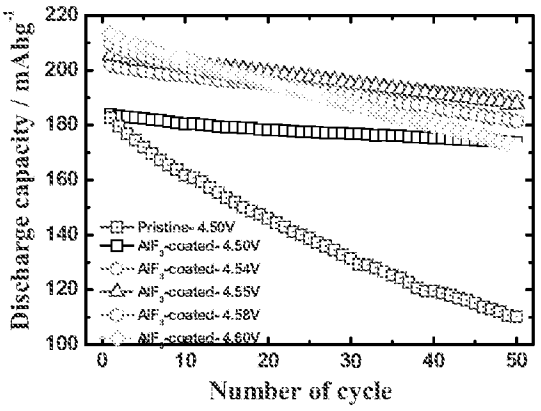


Figure 2. (Color online) Cycling performance of Li/pristine $LiCoO_2$ with cutoff voltage of 4.5 V and AlF_3-coated $LiCoO_2$ with cutoff voltages of 4.5–4.6 V at a current density of 80 mA g^{-1} (0.5 C rate).

AC impedance measurements were performed using a Zahner Elektrik IM6 impedance analyzer over the frequency range of 1 MHz–5 mHz with an amplitude of 10 mV_{rms}. The experiment was carried out for the AlF_3-coated $LiCoO_2$ in a charged state of above 4.5 V as a function of cycle number. To measure the dissolved amount of Co, the coin-type half-cells containing pristine $LiCoO_2$ charged to 4.5 V and AlF_3-coated $LiCoO_2$ charged to an upper cutoff voltage of above 4.5 V were carefully disassembled in a glove box. The recovered cathode active materials were stored in electrolyte at 55°C, and the amount of Co dissolution into electrolyte with storage time was measured by atomic absorption spectroscopy (AAS) (Analytik Jena AG, Vario 6). Transmission electron microscopy (TEM) (JEOL 2010) was employed to observe the phase evolution of the AlF_3-coated Li_xCoO_2 with an upper cutoff voltage above 4.5 V.

Results and Discussion

Figure 1 shows the initial charge/discharge curves of the Li/AlF_3-coated $LiCoO_2$ cells that were obtained by applying a constant current of 32 mA g^{-1} (0.2 C rate) and cutoff voltages between 3.0 and 4.5–4.6 V vs Li/Li$^+$. For comparison, Fig. 1 shows the initial charge/discharge curve of the Li/pristine $LiCoO_2$ cell charged to 4.5 V. All cells had stable and smooth charge/discharge curves, even above 4.5 V. The discharge capacity of the AlF_3-coated $LiCoO_2$ increased with increasing upper cutoff voltage. The discharge capacity increased by 35% from 4.2 V (140 mAh g^{-1}) to 4.5 V (189 mAh/g) and by 19% from 4.5 to 4.6 V (225 mAh g^{-1}). Also, the AlF_3-coated $LiCoO_2$ delivered a capacity of 208 mAh g^{-1} at a cutoff voltage of 4.54 V. The AlF_3-coated $LiCoO_2$ also had a higher discharge curve than that of the pristine one (cutoff voltage of 4.5 V), especially at the end of discharge, indicating a reduction in the cathode/electrolyte interface resistance, which leads to an increase in energy density of the cell in terms of Wh.[9]

Figure 2 shows the discharge capacity vs cycle number of the Li/AlF_3-coated $LiCoO_2$ cells with various cutoff voltages and the Li/pristine $LiCoO_2$ cell at a 4.5 V cutoff voltage, with a constant current of 80 mA g^{-1} (0.5 C rate). The capacity retention of the AlF_3-coated $LiCoO_2$ decreased as the upper cutoff voltage was raised, especially at 4.6 V. The capacity retention values of the cells at 4.55, 4.58, and 4.6 V after 50 cycles were 91.4, 86.6, and 80.8%, respectively. The capacity retention of the cell with a cutoff voltage of 4.54 V reached 94.3%, which is similar to the 94.4% at 4.5 V. The capacity retention of 94.3% for the cell charged to 4.54 V after 50 cycles is higher than that of 91.4% for the cell charged to 4.55 V even though the charging voltage difference is only 0.01 V. As expected, the pristine $LiCoO_2$ charged to 4.5 V suffers from a severe capacity loss, having a capacity retention of only 61% after 50 cycles.

Figure 3 shows the differential capacity ($dQ\ dV^{-1}$) vs the cell voltage of pristine $LiCoO_2$ and AlF_3-coated $LiCoO_2$ as a function of upper cutoff voltage at the 1st, 10th, 25th, and 50th cycles. The AlF_3-coated $LiCoO_2$ cell exhibited a sharp oxidation peak at 3.94 V. Two minor peaks appeared at 4.08 and 4.20 V during charging due to the multiphase transitions (Fig. 3a). The corresponding reduction peaks are present at 3.88, 4.05, and 4.16 V. The major 3.94 V peak corresponds to the phase transition between the two O3 phases, and two minor peaks correspond to the order–disorder transitions.[2-4] These variations in redox peaks were negligible for the AlF_3-coated $LiCoO_2$ with an upper cutoff voltage of 4.5 and 4.54 V during extensive cycling. No peaks were observed between 4.2 and 4.5 V, suggesting no phase transition in this voltage region and the Li_xCoO_2 still being O3 phase.[12] This result suggests that the AlF_3 coating on the cathode particle does not contribute to the suppression of structural change induced by the phase transition and is quite different from the report on zero-strain materials by Cho et al.[9] In contrast, for the pristine $LiCoO_2$ cycled at 4.5 V, the redox peaks were more polarized and became broader with cycling.[11]

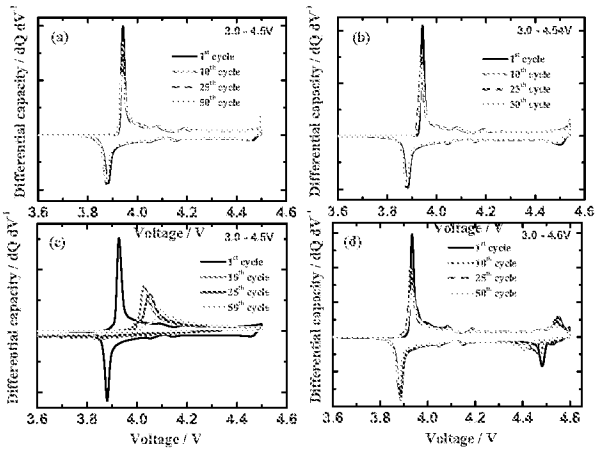


Figure 3. (Color online) Differential capacity vs voltage curves of Li/AlF_3-coated $LiCoO_2$ cells with cutoff voltages of (a) 4.5 and (b) 4.54 V, (c) pristine $LiCoO_2$ with cutoff voltage of 4.5 V, and (d) AlF_3-coated $LiCoO_2$ with cutoff voltage of 4.6 V. Current density of 80 mA g^{-1} (0.5 C rate).

AMPEREX Ex. 1002
Downloaded on 2017-04-02 to IP 61.197.236.153 address. Redistribution subject to ECS terms of use (see ecsdl.org/site/terms_use) unless CC License in place (see abstract).

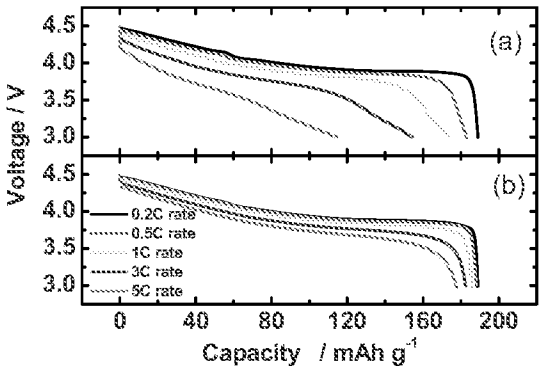


Figure 4. (Color online) Charge/discharge curves of the (a) pristine $LiCoO_2$ and (b) AlF_3-coated $LiCoO_2$ as a function of C rates.

When the upper cutoff voltage was increased to 4.6 V for the AlF_3-coated $LiCoO_2$ (Fig. 3d), a new peak appeared at 4.55 V, which corresponds to the phase transition from the O3 phase to H1-3 phase.[11,12,15] In addition, the redox peaks at 4.55 and 4.48 V changed to a more polarized state, became smaller, and shifted farther apart as the electrochemical cycling proceeded. It is believed that this phase transition from O3 to H1-3 phase is responsible for the capacity fading above an upper cutoff voltage of 4.55 V. Recently, Xia et al. reported that the capacity retention of their $LiCoO_2$ film cell is excellent at an upper cutoff voltage below 4.4 V, degrades slightly when cycled to 4.5 V, and significantly deteriorates above 4.5 V, in which the capacity fade is caused by the structural phase transitions to H1-3 regardless of surface chemistry.[12]

Figure 4 shows the discharge capacities of the Li/pristine and AlF_3-coated $LiCoO_2$ cells as a function of C rate between 3.0 and 4.5 V vs Li. The cells were charged galvanostatically with a 0.2 C rate before each discharge testing, and then discharged at different C rates from 0.2 to 5 C rates (32–800 mA g^{-1}). Clearly, the AlF_3-coated $LiCoO_2$ delivered a higher discharge capacity than the pristine $LiCoO_2$, especially at all the tested C rates. Although the pristine $LiCoO_2$ showed an abrupt discharge capacity at higher currents above a 1 C rate, the AlF_3-coated $LiCoO_2$ electrode retained its higher discharge capacity. At a 5 C rate, the obtained discharge capacity of the AlF_3-coated $LiCoO_2$ was about 93.5%, compared to that of a 0.2 C rate, while the pristine electrode showed a capacity retention of only 60.6% at the same C rate. This result clearly shows the AlF_3-coating impact on the electrochemical performance.

To correlate the structural degradation with interfacial impedance at the interface between the cathode and the electrolyte, electrochemical impedance spectroscopy (EIS) was performed in the AlF_3-coated $LiCoO_2$ charged to different upper cutoff voltages as a function of cycle number, as shown in Fig. 5. The Nyquist plots for the electrodes present two semicircles, one in the high-to-medium frequency region and the other in the low frequency region. According to our previous equivalent circuit concerning EIS,[7,6] the high-to-medium frequency semicircle is attributed to the resistance of the surface film (R_{sf}) covering the cathode particles, and the low frequency one reflects the charge-transfer resistance (R_{ct}) coupled with a double-layer capacitance. The R_{sf} of the AlF_3-coated $LiCoO_2$ electrodes was almost the same, irrespective of the upper cutoff voltage. However, the R_{ct} value increased with an increase in upper cutoff voltage as well as cycle number at each cutoff voltage; the R_{ct} values at the first cycle were 5.9 Ω at a cutoff voltage of 4.5 V, 10.4 Ω at 4.54 V, and 15.9 Ω at 4.58 V. Table I gives the values obtained for R_{ct} as a function of the number of cycles of the AlF_3-coated $LiCoO_2$ electrodes with different cutoff voltages. As shown by the data, the charge-transfer resistance for the electrode charged to 4.58 V rapidly increased with cycling, while that for the electrodes charged to 4.5 and 4.54 V remained nearly constant. Based on Fig. 3

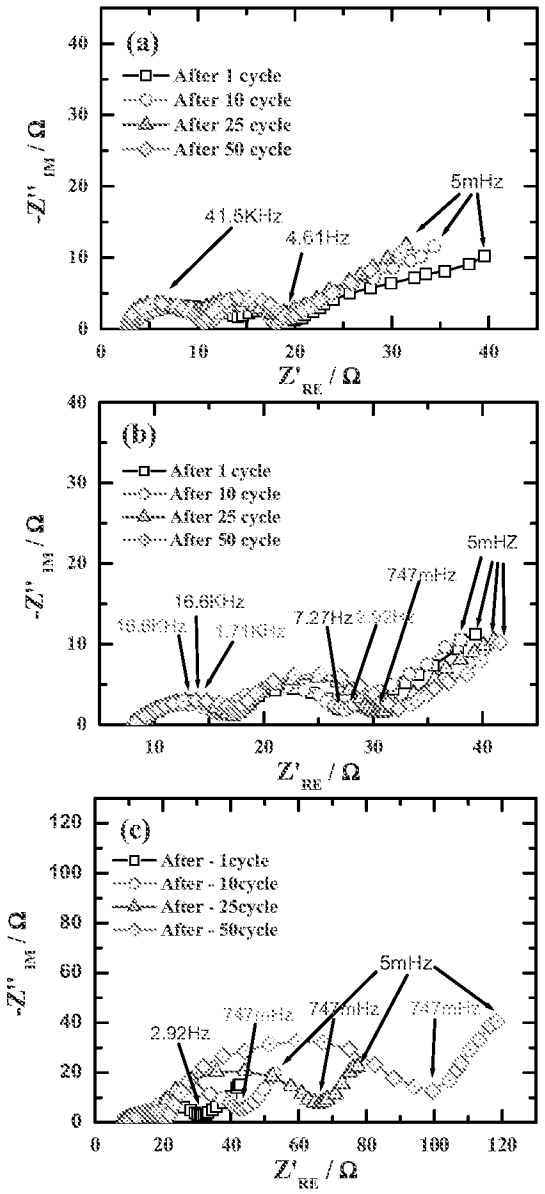


Figure 5. (Color online) Nyquist plots of the Li/AlF_3-coated $LiCoO_2$ with cutoff voltages of (a) 4.5, (b) 4.54, and (c) 4.58 V as a function of cycle number.

and 5, it is speculated that the impedance growth for pristine $LiCoO_2$ cycled at 4.5 V and AlF_3-coated $LiCoO_2$ cycled at 4.58 V

Table I. Charge-transfer resistance (R_{ct}) for AlF_3-coated $LiCoO_2$ cells with different cutoff voltages as a function of cycle number.

	Charge-transfer resistance (Ω)		
Cycle number	4.5 V	4.54 V	4.58 V
1	5.9	10.4	15.9
15	6.8	11.3	26.1
25	8.3	13.5	48.1
50	8.5	14.5	78.4

AMPEREX Ex. 1002
Downloaded on 2017-04-02 to IP 61.197.236.153 address. Redistribution subject to ECS terms of use (see ecsdl.org/site/terms_use) unless CC License in place (see abstract).

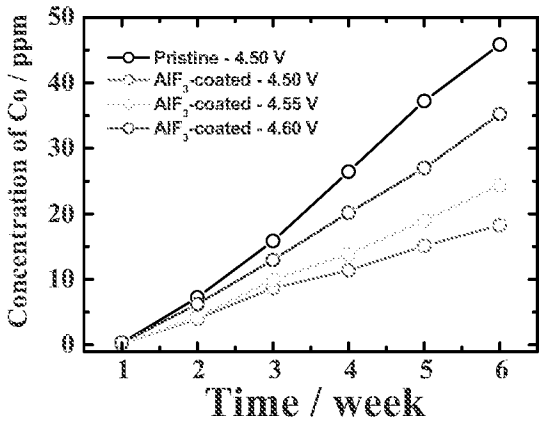


Figure 6. (Color online) Amount of Co dissolution of the pristine and AlF_3-coated $LiCoO_2$ charged to various cutoff voltages as a function of storage time in electrolyte at 55°C.

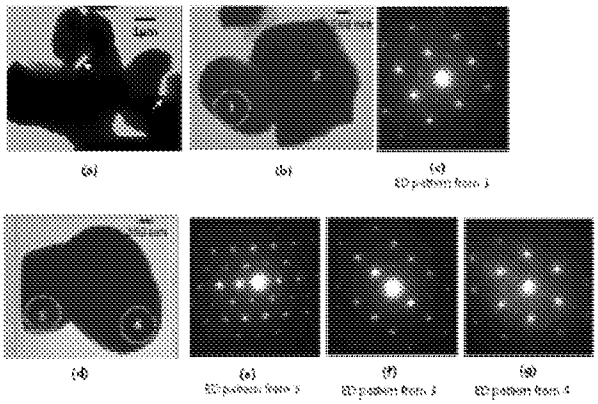


Figure 7. Analytical results of the pristine $LiCoO_2$ after 50 cycles at 4.5 V: (a) TEM image of damaged $LiCoO_2$ particles with arrows showing holes created by a chemical attack during cycling, (b) TEM image of a phase formed on the pre-existing $LiCoO_2$ particle (particle 1 corresponds to this phase, whereas particle 2 is the pre-existing $LiCoO_2$ particle), (c) electron diffraction pattern from particle 1, (d) TEM image showing multiple phases found in the cycled $LiCoO_2$ at 4.5 V, (e) and (f) electron diffraction patterns from particle 3 in two orientations, and (g) electron diffraction pattern from particle 4 indicating a cubic spinel structure (111 zone).

stems from the interface degradation between the cathode and the electrolyte caused by the structural deterioration of the cathode materials.

According to Amatucci et al.,[13] the capacity fading of $LiCoO_2$ cycled between 4.1 and 4.5 V is directly related to cobalt dissolution, which is correlated with large anisotropic structural changes. After testing, the pristine and AlF_3-coated $LiCoO_2$ cathodes were carefully disassembled in a glove box. The recovered cathode materials were stored in their electrolyte [1 M $LiFP_6$ in EC:DEC (1:1 vol %)] at 55°C, and the amount of dissolved Co in the electrolyte solution was measured by AAS. Figure 6 plots the amount of Co dissolution from the pristine and the AlF_3-coated $LiCoO_2$ as a function of storage time. The dissolved amount of Co from the pristine $LiCoO_2$ and AlF_3-coated $LiCoO_2$ increased almost linearly with storage time. However, the Co dissolution from the AlF_3-coated $LiCoO_2$ was substantially suppressed compared with the pristine material, and the amount of Co dissolution was dependent on the upper cutoff voltage, which was consistent with the capacity loss shown in Fig. 2. The Co dissolutions from AlF_3-coated $LiCoO_2$ charged to 4.5, 4.55, and 4.6 V after 6 weeks were 18.3, 24.4, and 35.3 ppm, respectively, which are significantly lower than that for the pristine $LiCoO_2$ charged to 4.5 V (45.5 ppm).

We employed TEM to further analyze the capacity degradation mechanism of the pristine $LiCoO_2$ electrode cycled at 4.5 V. The TEM images of the pristine $LiCoO_2$ particles after 50 cycles revealed that they severely eroded during cycling, which agrees with the Co dissolution data in Fig. 7. A massive Co dissolution from the $LiCoO_2$ electrode can be clearly seen in the TEM bright-field image of the cycled $LiCoO_2$ electrode in Fig. 7a. The particle surface has become rounded, and micrometer-sized voids have formed in the interior of the particles, as indicated by the arrows in Fig. 7a. The image is in striking contrast with those for the as-prepared $LiCoO_2$ electrode before cycling, whose constituent particles are elongated and have straight sides. Figure 7a visually confirms the electrochemical leaching of Co from the electrode when repeatedly cycled at 4.5 V.

In addition to the chemical attack, we observed a phase developing on the surface of the cycled electrode, as shown in Fig. 7b. The particle, labeled 2 in Fig. 7b, has rough edges, indicative of the gradual chemical erosion of a cycled $LiCoO_2$ particle. Particle 1, which appears attached to particle 2, is round and has a smooth surface in contrast to particle 2. The appearance of particle 1 suggests that it nucleated on the pre-existing $LiCoO_2$ particle. The electron diffraction pattern from particle 1, shown in Fig. 7c, could not be indexed to the original $R\bar{3}m$ structure of $LiCoO_2$. The pattern did not match the cubic spinel structure, which was previously observed from the cycled $LiCoO_2$ electrode at 4.7 V.[14] The pattern also did not match either CoO or CoO_2, which are possible phases that can appear during the redox reaction of $LiCoO_2$ with acid.[17] Because this phase could not be detected from X-ray diffraction, the exact crystal structure could not be unambiguously determined. It is believed that a distinctively different phase was formed on the electrode surface during cycling, resulting from a phase transition induced by the progressive Co dissolution. The formation of such a phase is likely responsible for the increased impedance between cathode and electrolyte, thus accelerating the capacity fade of $LiCoO_2$ at 4.5 V. Another example of the coexistence of multiple phases is shown in Fig. 7d. In an attempt to identify particle 3 in Fig. 7d, we conducted electron diffraction of it from two orientations, as shown in Fig. 7e and f; however, neither pattern could be indexed to the original layered structure of $LiCoO_2$ or to the cubic spinel structure. The two patterns appear similar to those of CoO_2 ($P\bar{3}m1$, $a = 2.82$ Å, $c = 4.24$ Å);[18] however, the c/a ratio appears to differ from that of CoO_2 substantially so that the patterns failed to match CoO_2. The electron diffraction pattern from particle 4 matched the 111 zone of a cubic spinel structure. We conjectured that $LiCoO_2$, when cycled at a high cutoff voltage, first transforms to an intermediate phase, yet to be identified, and then to the spinel structure, which is the energetically most stable state for $LiCoO_2$. The phase transformation is most likely triggered by the progressive loss of Co during cycling.

Figure 8 indicates that the AlF_3 coating of the $LiCoO_2$ electrode protects the material from HF attack during cycling. Indeed, a TEM image of the AlF_3-coated $LiCoO_2$ electrode after 50 cycles at 4.5 V in Fig. 8a shows that the particle surface remains intact during cycling, and no severe damage is observed, unlike the pristine counterpart in Fig. 7. Unlike the pristine $LiCoO_2$ electrode, a particle with the original $R\bar{3}m$ structure was rather easily found in the AlF_3-coated $LiCoO_2$ sample. A typical diffraction pattern in the 100 zone of the layered $LiCoO_2$ structure is shown in Fig. 8b. A TEM image of the AlF_3 coating layer remaining after 50 cycles is included in Fig. 8c, which indicates that the AlF_3 coating provides effective protection against the chemical attack from HF in the electrolyte through the electrode's cycle life. Failure to locate the intermediate phase in the AlF_3-coated $LiCoO_2$ sample cycled at 4.5 V suggests that the AlF_3 protection against the Co dissolution also

AMPEREX Ex. 1002
Downloaded on 2017-04-02 to IP 61.197.236.153 address. Redistribution subject to ECS terms of use (see ecsdl.org/site/terms_use) unless CC License in place (see abstract).

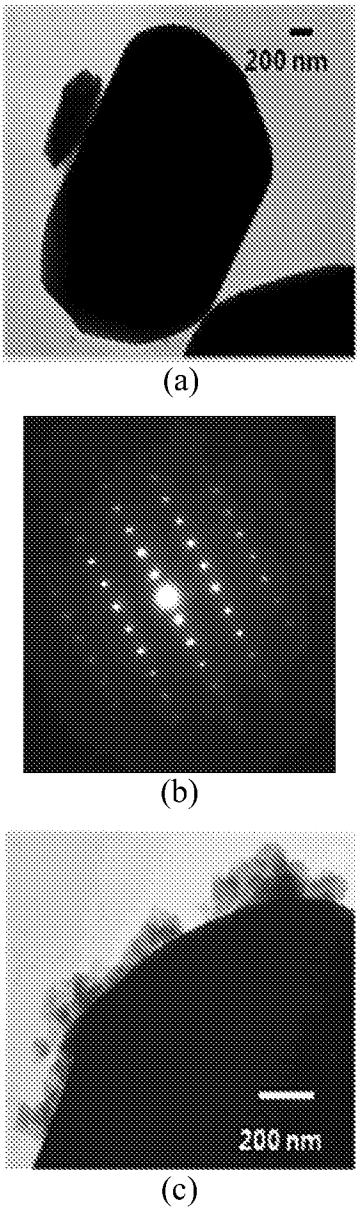


Figure 8. Analytical results of the AlF_3-coated $LiCoO_2$ after 50 cycles at 4.5 V: (a) TEM image showing undamaged particle surface of the AlF_3-coated $LiCoO_2$ electrode, (b) electron diffraction pattern from (a) with the $R\bar{3}m$ structure in 100 zone, and (c) TEM image of AlF_3 coating remaining on the $LiCoO_2$ surface after 50 cycles.

prevented the formation of the secondary phase on the particle surface, blocking the transition to the eventual spinel phase and the accompanying reversible capacity fade.

As the cycling voltage was increased to 4.54 V, the AlF_3-coated $LiCoO_2$ electrode after 50 cycles also started to exhibit formation of an intermediate phase resulting from the Co loss, as shown in Fig. 9. The TEM image in Fig. 9a shows two $LiCoO_2$ particles, which appear to be joined together. It is believed that the particles are in a partially transformed state so that region 1 in Fig. 9a, which appears to be a remnant of the $LiCoO_2$ electrode, retained the original $R\bar{3}m$ structure of $LiCoO_2$, whereas region 2 is the product of the phase transformation. Electron diffraction patterns from each region are

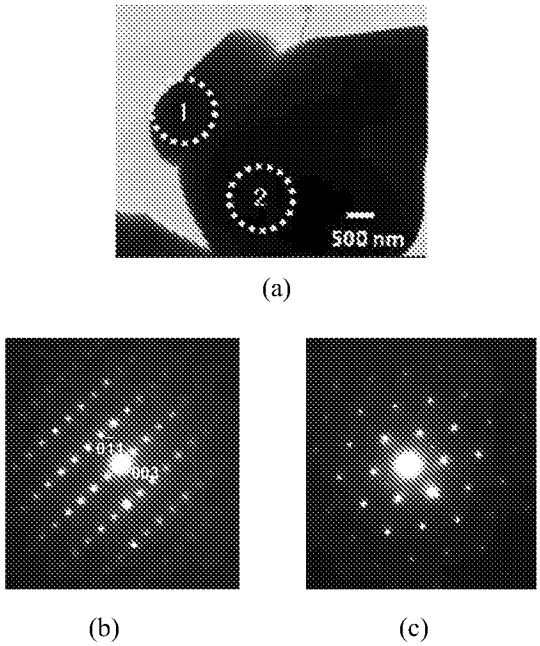


Figure 9. Analytical results from the AlF_3-coated $LiCoO_2$ after 50 cycles at 4.54 V: (a) TEM image of partially transformed $LiCoO_2$ particle, (b) electron diffraction pattern from region 1 in (a), and (c) electron diffraction pattern from region 2 in (a).

presented in Fig. 9b and c. Figure 9b taken from region 1 is unequivocally indexed to the 100 zone of the layered $LiCoO_2$, whereas the diffraction pattern in Fig. 9c cannot be indexed to $R\bar{3}m$ or cubic spinel structures. The interplanar distances estimated from the two diffraction patterns do not coincide, indicating that the two patterns are likely from different crystal structures. As the upper cutoff voltage further increases to 4.55 V, a cubic spinel phase starts to appear in the cycled electrode.

Figure 10a is a TEM image of three distinct regions observed in AlF_3-coated $LiCoO_2$ after 50 cycles at 4.55 V. The electron diffraction patterns in Fig. 10b-d demonstrate that the three regions differ from each other in their crystal structure. Regions 1 and 3 have a cubic spinel phase, and the diffraction patterns are indexed to the 100 and 211 zones of the cubic spinel phase, respectively. Meanwhile, the diffraction pattern from the midregion remains unassigned and is believed to belong to the intermediate phase. In this case, the increased Co dissolution from cycling at 4.55 V induces the increasing conversion of $LiCoO_2$ into the intermediate phase, which was followed by transformation to a spinel phase. At an increased cutoff voltage to 4.58 V, similar to the pristine sample, the AlF_3-coated $LiCoO_2$ was subjected to a severe chemical attack, as can be seen in Fig. 10e. The particle surface is irregular and serrated from extended chemical leaching. The ability of the AlF_3 coating to protect the $LiCoO_2$ electrode from Co dissolution and the accompanying transformations progressively decreases with increasing cutoff voltage.

The TEM analysis of the cycled electrodes shows that when cycled at 4.5 V, the pristine $LiCoO_2$ undergoes a phase transition to a cubic spinel phase via an as-yet unidentified intermediate phase. The transformation is the most likely culprit for the capacity fade observed at 4.5 V by increasing the charge-transfer resistance and thereby decreasing the intrinsic discharge capacity. It is believed that the transformation is triggered by a gradual loss of the Co from the surfaces of the $LiCoO_2$ particles. The AlF_3 coating is effective in protecting $LiCoO_2$ from the dissolution of Co and thus helps to delay the eventual phase transformation to a spinel phase. By delay-

AMPEREX Ex. 1002
Downloaded on 2017-04-02 to IP 61.197.236.153 address. Redistribution subject to ECS terms of use (see ecsdl.org/site/terms_use) unless CC License in place (see abstract).

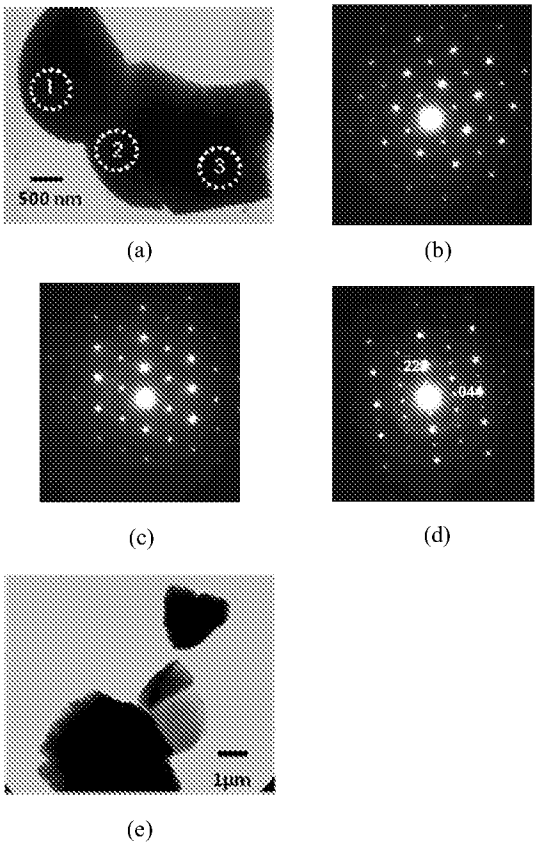


Figure 10. Analytical results from the AlF_3-coated $LiCoO_2$ after 50 cycles at 4.55 and 4.58 V: (a) TEM image of transformed $LiCoO_2$ particle at 4.55 V, [(b), (c), and (d)] electron diffraction patterns from regions 1, 2, and 3, respectively, and (e) TEM image of damaged $LiCoO_2$ particles at 4.58 V.

ing the transformation, the AlF_3 coating allows the $LiCoO_2$ electrode to maintain the reversible capacity above 4.5 V.

Conclusions

The effect of an AlF_3 coating on $LiCoO_2$ electrodes cycled at cutoff voltages above 4.5 V was investigated. The AlF_3 coating enabled the $LiCoO_2$ electrode to achieve a capacity retention greater than 90% after 50 cycles, even at a 4.55 V cutoff, while the pristine $LiCoO_2$ exhibited a capacity retention of only 60% at 4.5 V. The improved electrochemical performance with the AlF_3 coating was attributed to the lowered charge-transfer resistance caused by the delay of the structural degradation of the electrode. The Co dissolution data, together with the TEM analysis, explicitly demonstrated that the AlF_3 coating protects $LiCoO_2$ from the dissolution of Co and thus helps to delay the eventual phase transformation to a spinel phase during cycling. By delaying the transformation, the AlF_3 coating reduces the charge-transfer resistance and allows the electrode to maintain its structural stability when cycled above 4.5 V.

Acknowledgments

This work was supported by the Global Research Network Program and by a World Class University (WCU) program through the Korea Science and Engineering Foundation by Education, Science, and Technology (R31-2008-000-10092).

Hanyang University assisted in meeting the publication costs of this article.

References

1. K. Amine, C. H. Chen, J. Liu, M. Hammond, A. Jansen, D. Dees, I. Bloom, D. Vissers, and G. Henriksen, *J. Power Sources*, **97–98**, 684 (2001).
2. J. N. Reimers and J. R. Dahn, *J. Electrochem. Soc.*, **139**, 2091 (1992).
3. A. Van der Ven, M. K. Aydinol, G. Ceder, G. Kresse, and J. Hafner, *Phys. Rev. B*, **58**, 2975 (1998).
4. T. Ohzuku and A. Ueda, *J. Electrochem. Soc.*, **141**, 2972 (1994).
5. H.-J. Kweon, G.-B. Kim, and D.-G. Park, K.R. Pat. 0,420,034 (2004).
6. J. Cho, Y. J. Kim, T. J. Kim, and B. Park, *Angew. Chem., Int. Ed.*, **40**, 3367 (2001).
7. Y.-K. Sun, Y.-S. Lee, M. Yoshio, and K. Amine, *Electrochem. Solid-State Lett.*, **5**, A99 (2002).
8. Y.-K. Sun, J.-M. Han, S.-T. Myung, S.-W. Lee, and K. Amine, *Electrochem. Commun.*, **8**, 821 (2006).
9. Y.-K. Sun, S.-W. Cho, S.-T. Myung, K. Amine, and J. Prakash, *Electrochim. Acta*, **53**, 1013 (2007).
10. Z. H. Chen and J. R. Dahn, *Electrochem. Solid-State Lett.*, **6**, A221 (2003).
11. Z. H. Chen and J. R. Dahn, *Electrochim. Acta*, **49**, 1079 (2004).
12. H. Xia, L. Lu, Y. S. Meng, and G. Ceder, *J. Electrochem. Soc.*, **154**, A337 (2007).
13. G. G. Amatucci, J. M. Tarascon, and L. C. Klein, *Solid State Ionics*, **83**, 167 (1996).
14. R. Yazami, Y. Ozawa, H. Gabrisch, and B. Fultz, *Electrochim. Acta*, **50**, 385 (2004).
15. Z. Chen, Z. Lu, and J. R. Dahn, *J. Electrochem. Soc.*, **149**, A1604 (2002).
16. Y.-K. Sun, S.-T. Myung, C. S. Yoon, and D.-W. Kim, *Electrochem. Solid-State Lett.*, **12**, A163 (2009).
17. R. J. Gummow, M. M. Thackeray, W. I. F. David, and S. Hull, *Mater. Res. Bull.*, **27**, 327 (1992).
18. T. Motohashi, T. Ono, Y. Katsumata, R. Kanno, M. Karppinen, and H. Yamauchi, *J. Appl. Phys.*, **103**, 07C902 (2008).

AMPEREX Ex. 1002
Downloaded on 2017-04-02 to IP 61.197.238.153 address. Redistribution subject to ECS terms of use (see ecsdl.org/site/terms_use) unless CC License in place (see abstract).

Journal of Power Sources 269 (2014) 236–243

Contents lists available at ScienceDirect

Journal of Power Sources

journal homepage: www.elsevier.com/locate/jpowsour

Electrochemical properties of $LiNi_{1/3}Co_{1/3}Mn_{1/3}O_2$ cathode material modified by coating with Al_2O_3 nanoparticles

Kazuhiro Araki [a, *], Noboru Taguchi [b], Hikari Sakaebe [b, **], Kuniaki Tatsumi [b], Zempachi Ogumi [a]

[a] Office of Society-Academia Collaboration for Innovation, Kyoto University, Gokasho, Uji, Kyoto 611-0011, Japan
[b] Research Institute for Ubiquitous Energy Devices, AIST, 1-8-31 Midorigaoka, Ikeda, Osaka 563-8577, Japan

HIGHLIGHTS

- We succeeded in suppressing the power fade using mechano-chemical bonding technology.
- Crack formation of NCM correlated with the ASI (10 s) increase.
- Coating with Al_2O_3 can be an effective technique for improving the power fade.

ARTICLE INFO

Article history:
Received 29 January 2014
Received in revised form
10 June 2014
Accepted 16 June 2014
Available online 25 June 2014

Keywords:
Lithium ion batteries
$LiNi_{1/3}Co_{1/3}Mn_{1/3}O_2$
Al_2O_3 coating
Nano particle
Mechano-chemical bonding technology
Crack

ABSTRACT

$LiNi_{1/3}Co_{1/3}Mn_{1/3}O_2$ particles were coated with Al_2O_3 nanoparticles by means of a mechanochemical bonding process; SEM confirmed that the Al_2O_3 particles were uniformly coated over the surface of the $LiNi_{1/3}Co_{1/3}Mn_{1/3}O_2$ powder. During subsequent electrochemical testing using pouch cells, uncoated $LiNi_{1/3}Co_{1/3}Mn_{1/3}O_2$ exhibited a gradual capacity fading and an increase in area specific impedance (ASI) at a 50% state of charge. Under the same conditions, the increase in ASI of the Al_2O_3 modified samples was significantly suppressed, although the initial performance (charge/discharge capacity and ASI) slightly deteriorated. The Al_2O_3 coating was also effective in improving the cyclability of $LiNi_{1/3}Co_{1/3}Mn_{1/3}O_2$ at elevated temperatures by reducing the extent of cracking.

© 2014 Elsevier B.V. All rights reserved.

1. Introduction

The recent emergence of hybrid and electric vehicles onto the market has highlighted the limitations of conventional lithium ion batteries in terms of their energy density, durability, electrochemical performance, and cost. As a result, $LiNi_{1/3}Co_{1/3}Mn_{1/3}O_2$ (NCM) has been considered as an alternative cathode material for such applications, as it offers a significant cost benefit over conventional $LiCoO_2$. However, NCM also experiences appreciable degradation during cycling at elevated temperatures [1]. The use of coatings is well known as an effective technique for improving the cyclability of positive active-materials at elevated temperatures and therefore several metal oxide coatings have been intensively studied for the surface modification of cathode materials, e.g., Al_2O_3 [2–5], ZrO_2, MgO, and ZnO [6–9]; metal phosphates like $AlPO_4$ [10,11]; and metal fluorides like AlF_3 [12,13]. These techniques have been demonstrated to greatly enhance electrochemical properties, such as cyclability and rate capability, with Jung et al. reporting that these films can minimize Co dissolution or suppress surface reactions with the electrolyte [14]. Moreover, Cho et al. have shown that the expansion of the *c*-axis is sharply reduced during cycling, and that this results in negligible strain and microcrack formation [5]. However, the mechanism by which the cyclability is enhanced by this coating is still unclear, and subject to discussion.

In this work, (NCM) was coated with Al_2O_3 nanoparticles via a mechanochemical bonding technology [15] in order to investigate their effect on the electrochemical performance, surface characteristics, structure and morphology of NCM. By comparing these

* Corresponding author. Present address: Honda R&D Co., Ltd., 4630 Shimotakanezawa, Haga-machi, Haga-gun, Tochigi 321-3393, Japan. Tel.: +81 80 4871 4817; fax: +81 28 677 7460.
** Corresponding author. Tel.: +81 72 751 9673; fax: +81 72 751 9609.
E-mail addresses: kazuhiro_araki@n.t.rd.honda.co.jp (K. Araki), hikari.sakaebe@aist.go.jp (H. Sakaebe).

http://dx.doi.org/10.1016/j.jpowsour.2014.06.161
0378-7753/© 2014 Elsevier B.V. All rights reserved.

results with those of uncoated NCM, the mechanisms behind any observed improvement are discussed.

2. Experimental

A mechanochemical bonding process (AMS-MINI, Hosokawa Micron Corp.) was used to coat NCM (supplied by Toda Kogyo Corp.) 50 nm Al_2O_3 nanoparticles (Aldrich). This bonding process allows a variety of powders to be hybridized by a mechanochemical reaction that utilizes only mechanical energy; the basic principles and a schematic illustration of the essential components are shown in Fig. 1 [15]. In this process the powder is pressed against the inner wall of the rotor by centrifugal force, thus generating compressive and shear forces in the powder as it passes through the gap between the rotor and inner component. The amount of Al_2O_3 coated onto the NCM powders was 3.0 or 7.5 wt%, with Table 1 providing a detailed overview of the coating procedure.

The morphology of the powder particles was confirmed using a scanning electron microscope (SEM; S5000, Hitachi) and scanning-transmission electron microscope (STEM; Hitachi, S-5500). A cross-section polisher (E-3500, Hitachi) was used to prepare cross-sectional samples of the powder for imaging. Each electrode was held between two sheets of cover glass for microscope and cut by an argon-ion beam polisher at a constant power of 0.65 W (5 kV and 0.13 mA) under gas flow rate of 0.1 mL min^{-1} for 90 min. Oriented image mapping was reconstructed from an electron backscatter diffraction (EBSD) pattern (TSL Solutions KK). For this, the electron beam was scanned over the sample, with the EBSD pattern measured at each point then indexed to ascertain the orientation of the crystal lattice. A high-speed CCD camera (1500M-T1-GE-EX) and the software package TSL OIM Data Collection 6 were used for the pattern acquisition and mapping image reconstruction, respectively. X-ray diffractometry (XRD; Rigaku, RINT 2200) was employed to characterize the crystal structure of the powder sample. XRD data were obtained using Cu Kα radiation (λ = 0.15406 nm) in continuous scan mode across a 2θ range of 10–80°, with a step size of 0.02° and a scan rate of 2° per minute. X-ray photoelectron spectroscopy (XPS, ULVAC-PHI QuanteraSXM with Al Kα radiation, hν = 1486.71 eV) measurements (about φ100 μm) were performed to investigate the surface of the electrodes before and after cycling. For this, all cells were first disassembled in a dry box filled with argon gas in which the dew point was below −50 °C. Next, the electrodes were washed with diethyl carbonate (DEC), dried, and then transported for analysis under an inert atmosphere. Physical properties were assessed using a microcompression testing machine (MCT-510, Shimadzu) with a 50 μmφ flat indenter (load: 9.8–55 mN, displacement: 0–100 μm) to determine the compressive strength. Tensile strength was also obtained from the load–displacement curve.

Electrochemical performance was evaluated using pouch-type full cells (49 cm^2) in which the positive electrode consisted of 90 wt% coated or uncoated NCM combined with 5 wt% of carbon

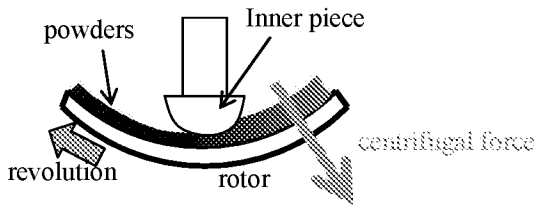


Fig. 1. Schematic illustration of the primary components of a Hosokawa mechanochemical bonding coating device [15].

Table 1
Process of coating Al_2O_3 nanoparticles onto NCM-10.

Step no.	Step rotation number (rpm)	Step time (min.)	3.0 wt% Al_2O_3	7.5 wt% Al_2O_3
1	4000	1	mixing of 81 g NCM, with 1.250 g Al_2O_3	mixing of 81 g NCM, with 1.312 g Al_2O_3
2	4000	1	adding 1.250 g Al_2O_3	adding 1.312 g Al_2O_3
3	4000	1		adding 1.312 g Al_2O_3
4	4000	1		adding 1.312 g Al_2O_3
5	4000	1		adding 1.312 g Al_2O_3

black (Super-P(Li), TIMCAL) and 5 wt% of polyvinylidene fluoride (PVDF) (KLF#1120, Kureha). The negative electrode consisted of 93 wt% hard-carbon (Carbotron-P(J), Kureha) and 7 wt% PVDF (KLF#9130, Kureha). All electrodes were dried under vacuum at 160 °C for 12 h prior to cell assembly. For the assembly, a porous polypropylene membrane (#2500, Celgard) was used as a separator and 1.0 mol dm^{-3} $LiPF_6$/ethylene carbonate-dimethyl carbonate-ethylmethyl carbonate (1:1:1 by volume) served as the electrolyte. A three-electrode electrochemical cell was also assembled to compare the potential of uncoated positive and negative electrodes, in which a Li reference electrode was inserted in between the electrodes of the cell. Assembly of all cells was carried out in a dry room, after which they were charged and discharged for three cycles at a rate of 1C within a voltage range of 4.2–2.7 V at 25 °C using a multi-channel charge–discharge device (TOSCAT-3000, Toyo System Co., Ltd.). The area specific impedance (ASI) was evaluated at a 50% state of charge (SOC), which corresponds to a cell voltage of 3.615 V. ASI was measured at 3, 5, 8 and 12C for 12 s at each pulse current rate rest for 10 min in order to attain linearity at room temperature, following the previously reported procedure [18]. The voltage after 1 or 10 s (V_{1s} or V_{10s}) was recorded at each current pulse, and plots of V_{1s}–I and V_{10s}–I were obtained in which (I) corresponds to the absolute current for each pulse. The each decision coefficient is over 0.999 on the slopes of the V_{1s}–I and V_{10s}–I. The state of relaxation of the cell has a small influence on the V–I plots under our experimental conditions. The absolute values of the slopes of these V–I plots, as normalized by the electrode area, were used to determine the ASI values at 10 and 1 s intervals, which are hereafter denoted as ASI(10s) and ASI(1s), respectively. The rate capability was tested by discharging at current densities of 1, 5, 10, 20, 30 and 50C. Cycling performance was evaluated in the voltage range of 2.7–4.2 V using a constant current/constant voltage (CC/CV) method for charging to 4.2 V with a typical test current of 110 mA g^{-1}, and a CC method for discharging to 2.7 V with a typical test current of 110 mA g^{-1} at 50 °C. Monitoring of the discharge capacity, ASI(10s) and ASI(1s) was conducted at 25 °C for 100 and 250 cycles.

3. Results and discussion

Fig. 2 shows SEM images of the surfaces of uncoated and coated NCM particles. From this, we can see that the concave regions are the first to be filled with coating material, with the convex parts only being covered when the amount of coating is increased. Thus, the enclosed section corresponding to the convex region of NCM was apparently less covered in the case of 3.0 wt% coated particles (Fig. 2(b)), whereas the surface of the 7.5 wt% coated particles was so completely covered by Al_2O_3 nanoparticles that the morphology of the original uncoated particle could no longer be seen (Fig. 2(c)). Fig. 2(d) shows a cross-sectional STEM image of the surface region of the particle coated by 7.5 wt% Al_2O_3, in which the thickness of coating can be seen to vary from 150 to 300 nm.

AMPEREX Ex. 1002
Page 821

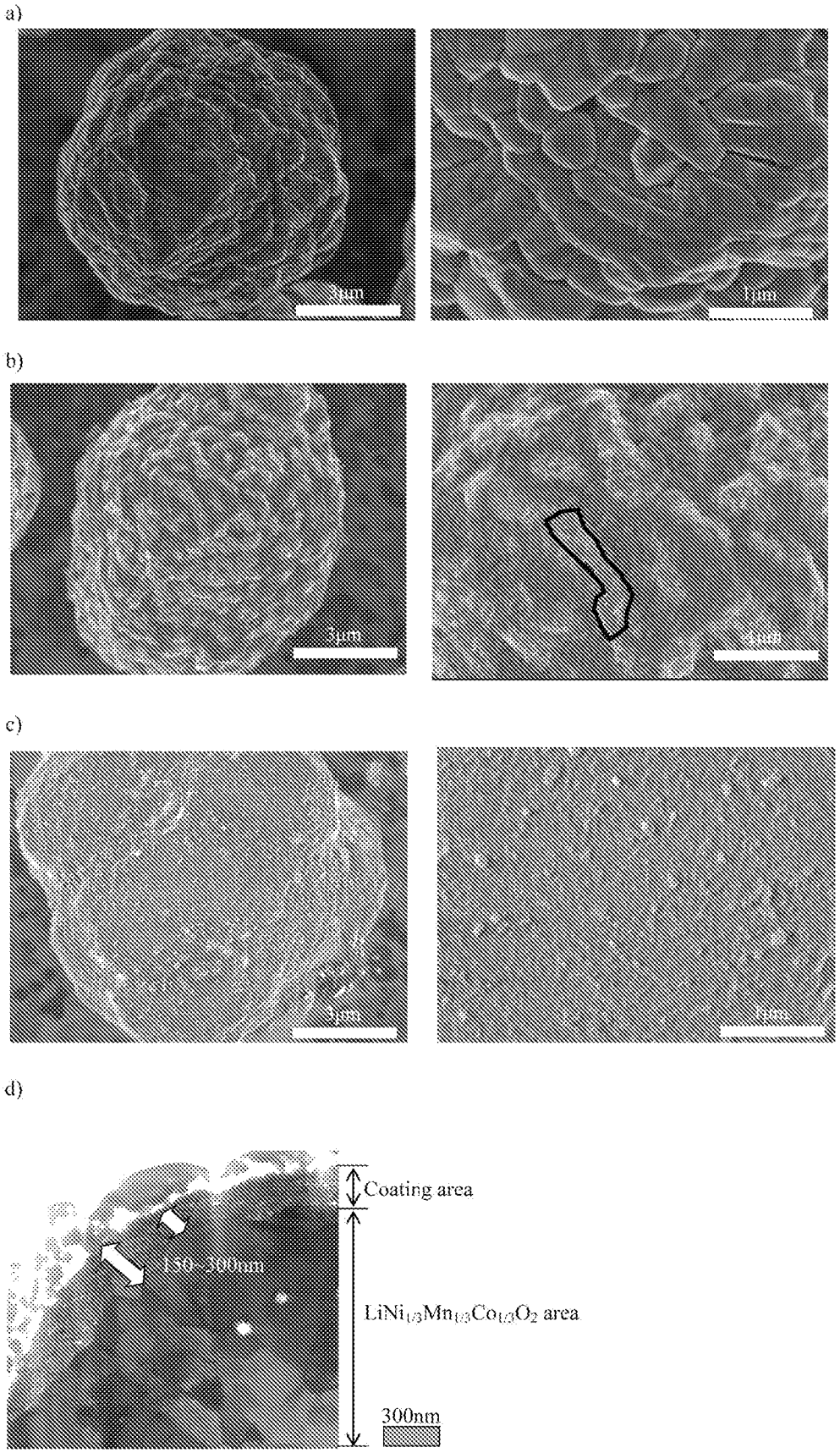


Fig. 2. SEM and TEM images of $LiNi_{1/3}Co_{1/3}Mn_{1/3}O_2$ powder (a) uncoated, (b) coated with 3.0 wt% Al_2O_3, and (c) coated with 7.5 wt% Al_2O_3. (d) Cross-sectional STEM image of the particle in (c).

AMPEREX Ex. 1002
Page 822

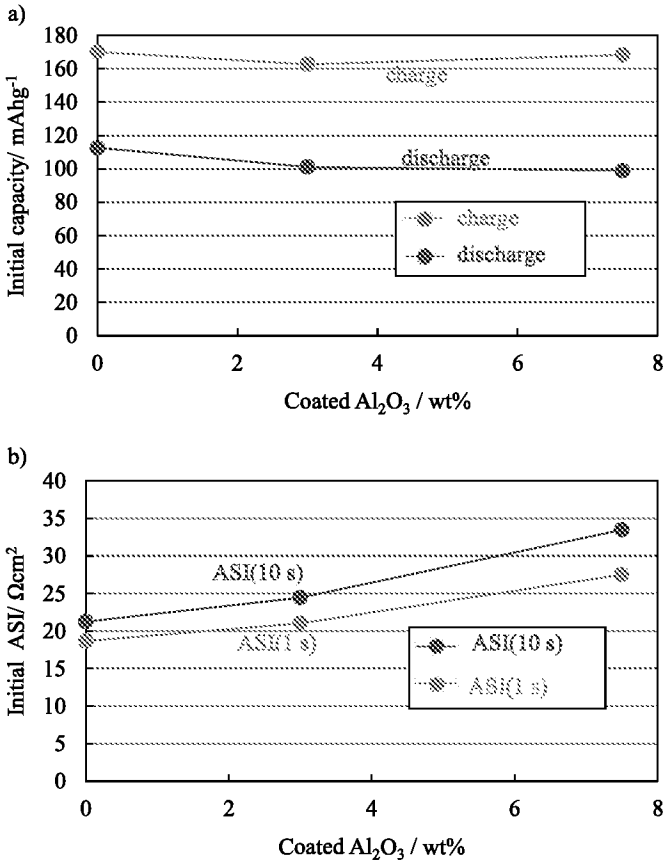


Fig. 3. Correlation between the initial electrochemical performance at 25 °C of coated/uncoated $LiNi_{1/3}Co_{1/3}Mn_{1/3}O_2$ and (a) charge/discharge capacity and (b) area specific impedance ASI(10 s) and ASI(1s).

Fig. 3 illustrates the correlation between the initial charge/discharge capacity and area specific impedance (ASI) with Al_2O_3 loading. In this, the full cell was charged at a current density of 22 mA g^{-1}(0.2C-rate) up to 4.2 V, revealing that the discharge capacity of the coated sample undergoes a perceptible capacity loss. Furthermore, the initial ASI(10s) and ASI(1s) is gradually increased with Al_2O_3 loading, which can be ascribed to a decrease in contact area between each active material particle, and also between particles of active material and carbon black.

A comparison of the rate capabilities of uncoated, 3.0 and 7.5 wt % Al_2O_3-modified NCM is shown in Fig. 4. This shows that the

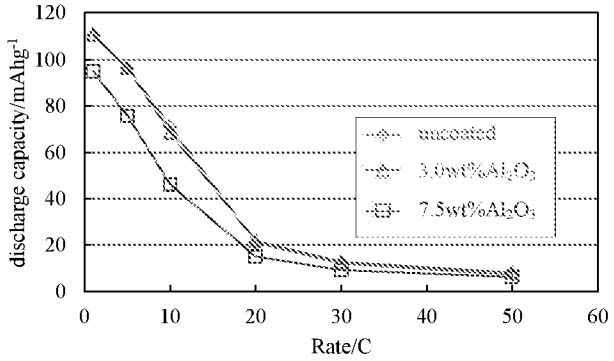


Fig. 4. Rate capability of ◇uncoated, △3.0 wt% Al_2O_3-coated, and □7.5 wt% Al_2O_3-coated samples.

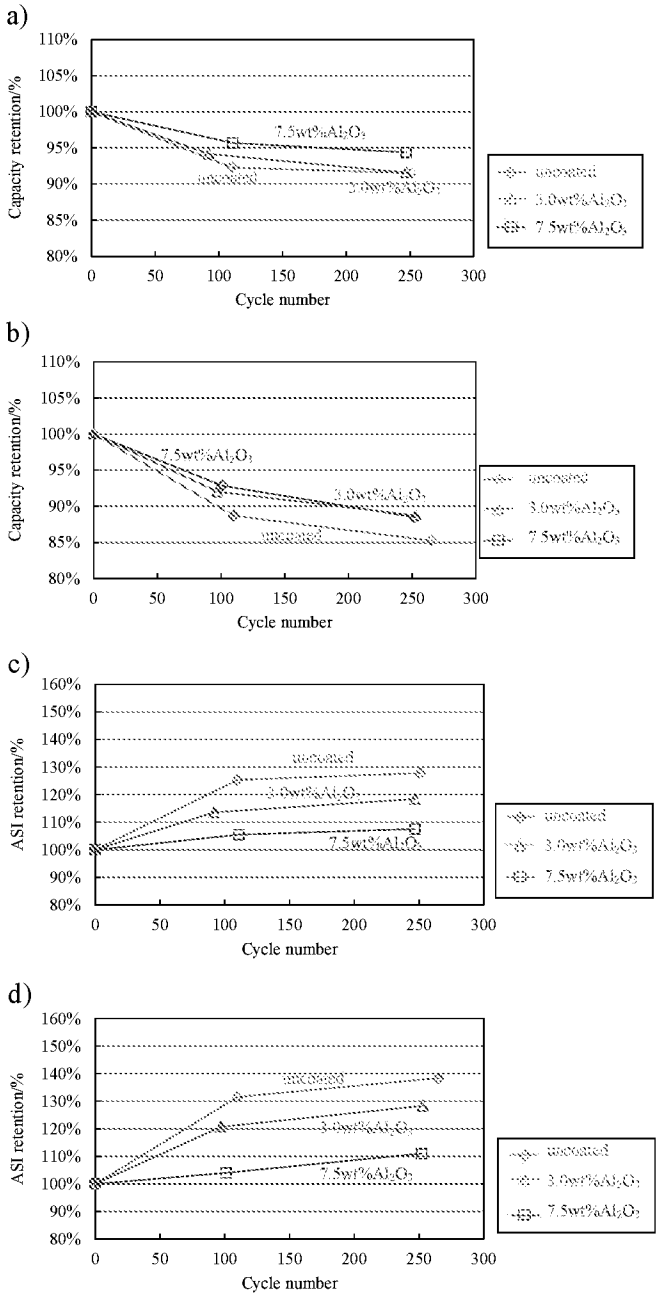


Fig. 5. Cycling performance of coated/uncoated samples. (a) Capacity retention during cycling at 35 °C, (b) capacity retention during cycling at 50 °C, (c) ASI(10s) ratio during cycling at 35 °C, and (d) ASI(10s) ratio during cycling at 50 °C.

capacity of uncoated NCM at 10C is 71 mAh g^{-1}, which corresponds to about 65% of that at 1C. In contrast, the capacity of 3 wt% Al_2O_3-coated NCM is 68.5 mAh g^{-1} at 10C, or about 62% of that at 1C, whereas the capacity at 7.5 wt% Al_2O_3 of 46.1 mAh g^{-1} at 10C corresponds to only about 49% of that at 1C. This obvious difference in the rate capability of the 7.5 wt% Al_2O_3-modified NCM is most likely caused by the reduced contact area between the conductor and the active materials.

Fig. 5 shows the dependency of capacity retention and ASI(10s) of cells containing coated samples on the number of cycles. These results clearly indicate that Al_2O_3 modification suppresses the increase in ASI(10s) with cycling, and although the capacity retention gradually decreased with an increasing number of cycles, the rate of

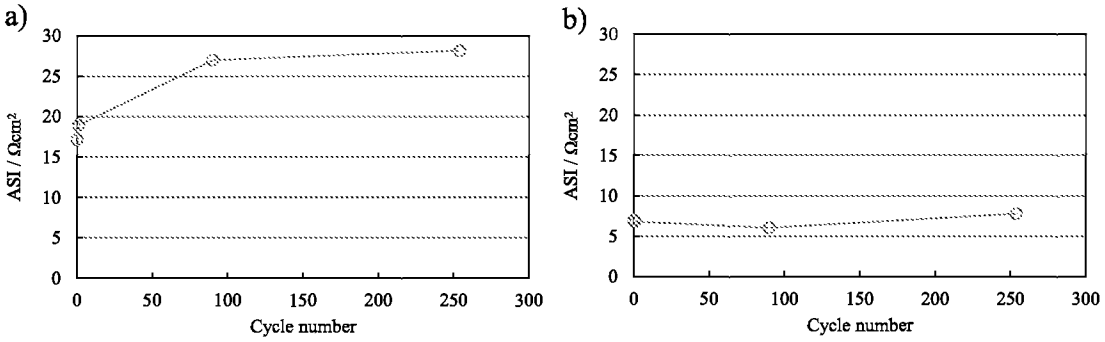


Fig. 6. Increase in ASI(10s) of a three-electrode electrochemical cell containing (a) an uncoated positive electrode and (b) a negative electrode.

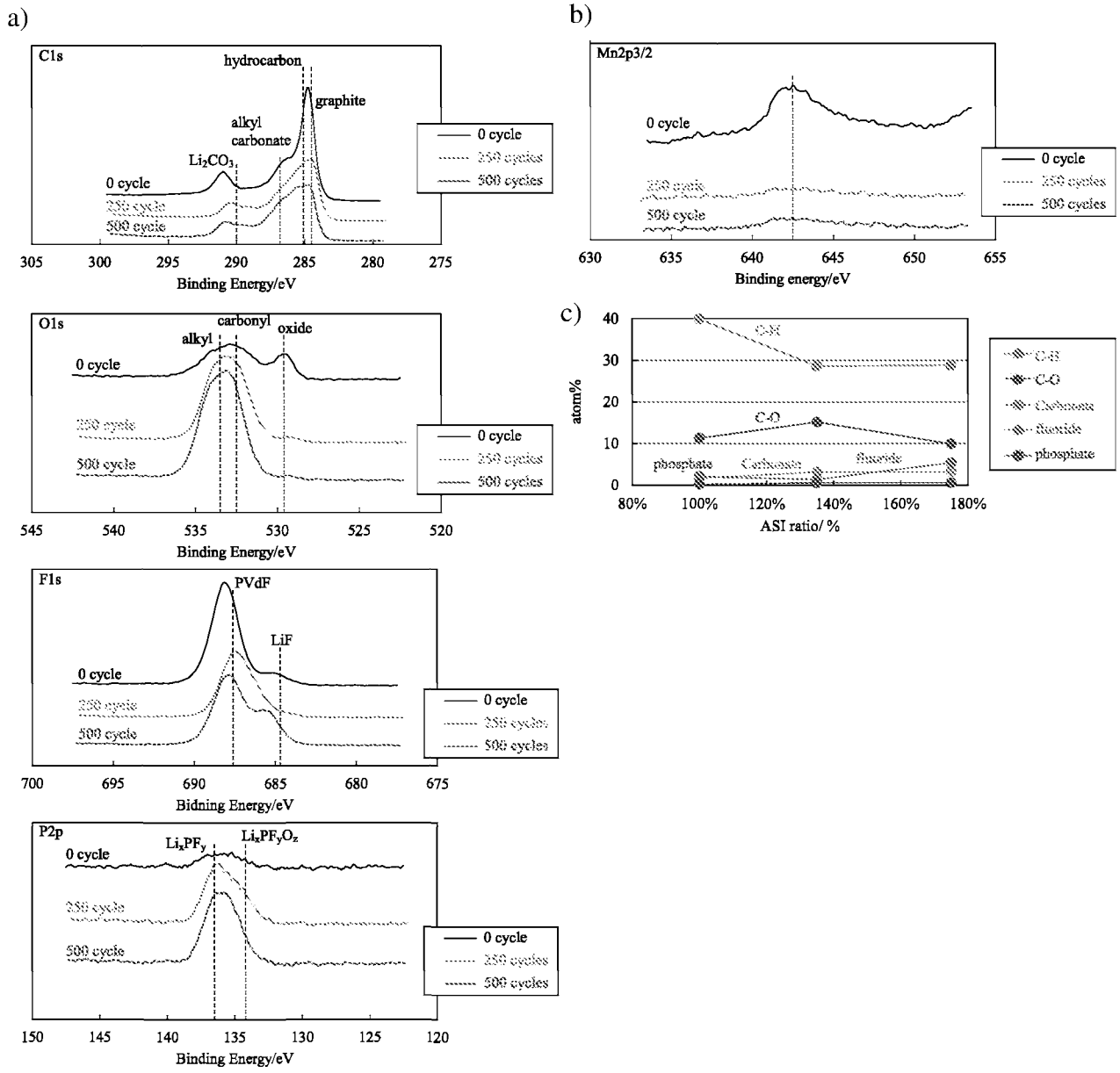


Fig. 7. XPS correlation of degradation (a) XPS spectra of an uncoated sample after 0, 250 and 500 cycles on a positive electrode, (b) XPS spectra of an uncoated sample after 0, 250 and 500 cycles on a negative electrode, (c) ratio of SEI compounds on a positive electrode.

Table 2
Concentration of Mn on the negative electrode surface, as determined by the peak area ratio of Mn 2p3/2 spectrum to the total area of detected elements.

Sample	ASI(10s) ratio (%)	Mn (at%)
Fresh	100%	0.1%
35 °C, 250 cycles	122%	0.6%
50 °C, 250 cycles	135%	0.6%
50 °C, 250 cycles	175%	0.8%

decrease did not significantly differ between uncoated and coated samples.

The electrochemical behavior of the uncoated and 7.5 wt% coated positive and negative electrodes was examined in detail using a three-electrode cell at 50 °C. Through this, a change in the ASI(10s) was observed at 25 °C after the 100th and 250th cycles, as illustrated in Fig. 6. This increase in the ASI(10s) is attributed mainly to the increase of the positive electrode, with the Al_2O_3 coating effectively suppressing the ASI(10s) increase with degradation.

XPS analysis was used to identify the chemical species present on the surface of the electrodes by comparing the peaks obtained against those identified in the literature [18,20]. In the O_{1s} spectra (Fig. 7(a)), a small signal attributable to metal oxide is clearly discernible at 529.6 eV in each cycled sample. The peaks at 532.5 and 533.5 eV correspond to carbonyl oxygen and oxygen for alkyl group, respectively. In the P_{2p} spectra (Fig. 7(a)), the peaks for Li_xPF_y at 136.5 eV and $Li_xPF_yO_z$ at 134.2 eV are both clearly evident. It can therefore be inferred from these results that by cycling at 50 °C, a solid electrolyte interphase (SEI) film is produced that covers the surface of the active material. Moreover, the Mn $2P_{3/2}$ spectra (Fig. 7(b)) of the negative electrodes suggest the presence of a Mn compound at 642.5 eV with increased cycles [21]. We therefore looked at the area ratio of the decomposition products of the electrolyte (C–H and C–O signals from carbonate, fluoride, and phosphate signals) on the positive electrode, and the Mn species originating from NCM that were deposited on the negative electrode. Fig. 7(c) shows the correlation in intensity of these peaks from the surface of the positive electrode and the ASI ratio, indicating that none of the chemical species from the SEI has a close relationship with the ratio of ASI(10s). Furthermore, the results shown in Table 2 indicate that the atomic concentration of Mn on the negative electrode of ASI(10s) at ratios of 122 and 135% was the same. Since it is well-known that the charge compensation and oxygen vacancy mechanism drives Mn dissolution, resulting in the reduction of Mn^{4+} to Mn^{3+} in positive active materials [22], it seems likely that the Mn ions migrating to the negative electrode are deposited on the surface of the carbon. This phenomenon degrades cell performance, and so if Mn dissolution is indeed responsible for the ASI(10s) degradation then we would expect there to be more Mn in the cell with the higher ASI(10s) ratio. The fact that the observed results deviate from this expectation

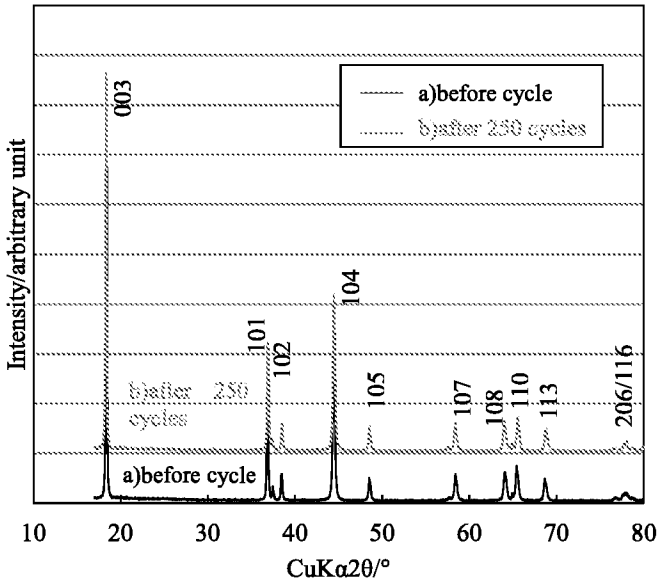


Fig. 8. XRD patterns for an electrode (a) before cycling, and (b) after 250 cycles.

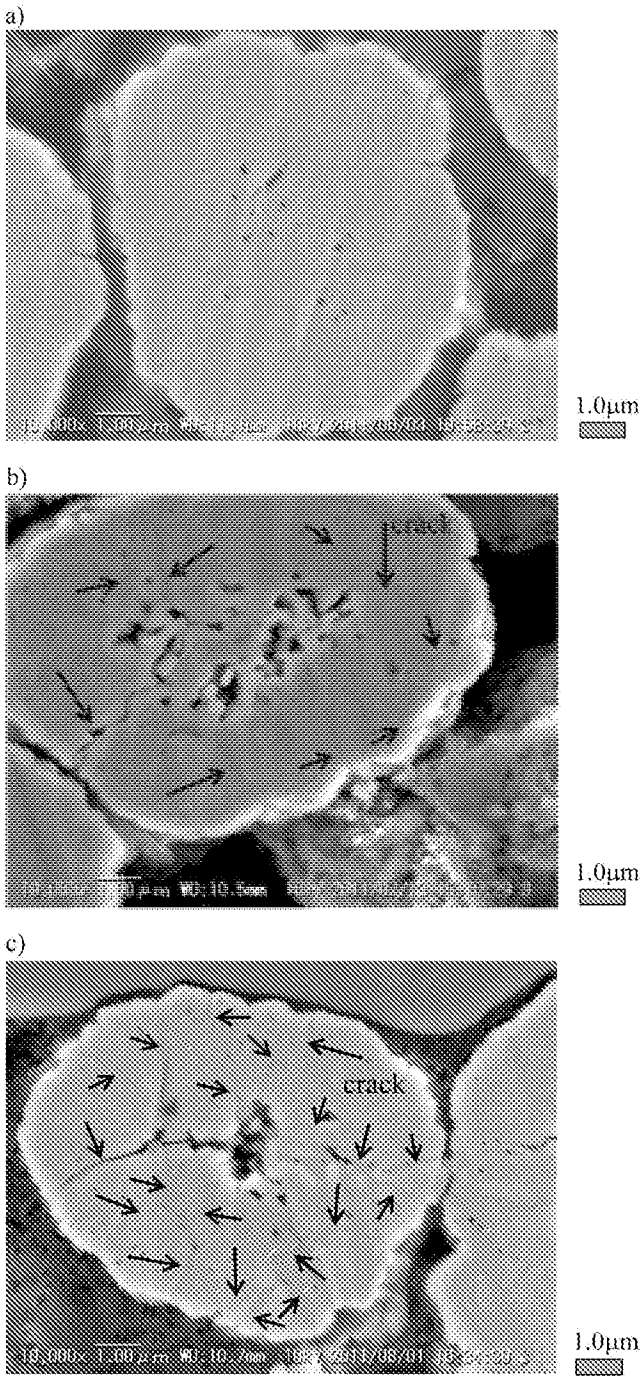


Fig. 9. Cross-sectional SEM images of uncoated electrodes (a) before cycling, (b) after 100 cycles with an ASI(10s) ratio of 121%, and (c) after 250 cycles with an ASI(10s) ratio of 128%.

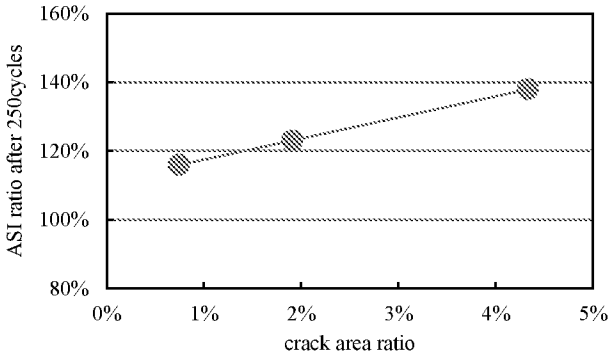


Fig. 10. Correlation between ASI(10s) ratio and crack area ratio in uncoated positive electrode particles.

suggests that Mn dissolution can not be a significant factor in degradation.

To evaluate any change in the bulk structure, the XRD patterns of electrodes before and after 250 cycles were compared (Fig. 8). In this, both the original and cycled uncoated electrode can be identified as a layered α-$NaFeO_2$ structure, with a space group of R-3m. The calculated cell parameters were $a = b = 2.84$ Å and $c = 14.36$ Å. Although the detailed cell parameters differed slightly due to the use of a 2-electrode full cell, no additional peaks were found in the electrode after cycling. The bulk structure was also found to have no significant relationship with the observed degradation.

Fig. 9 shows a cross-sectional image of a representative single-particle in a cycled positive-electrode (uncoated NCM) of a three-electrode cell. In this, the cracks (indicated by arrows) can be seen to increase dramatically with cycling. Fig. 10 illustrates the dependence of ASI(10s) on the crack area ratio, which is defined as the ratio of cracks/total area of the particle as calculated by image processing techniques. It is evident from this that the area of cracks inside particles shows a clear correlation with ASI(10s) in the uncoated positive electrode of the three-electrode cell. It should also be noted that this crack area ratio was estimated from 10 representative particles of an SEM view containing more than 40 particles in total. Itou et al. have suggested that in the case of $LiNi_{0.8}Co_{0.15}Al_{0.05}O_2$ the degradation mechanism of the positive electrode is an increase of resistance caused by morphological change of the particles [16]. With this in mind, it can be concluded

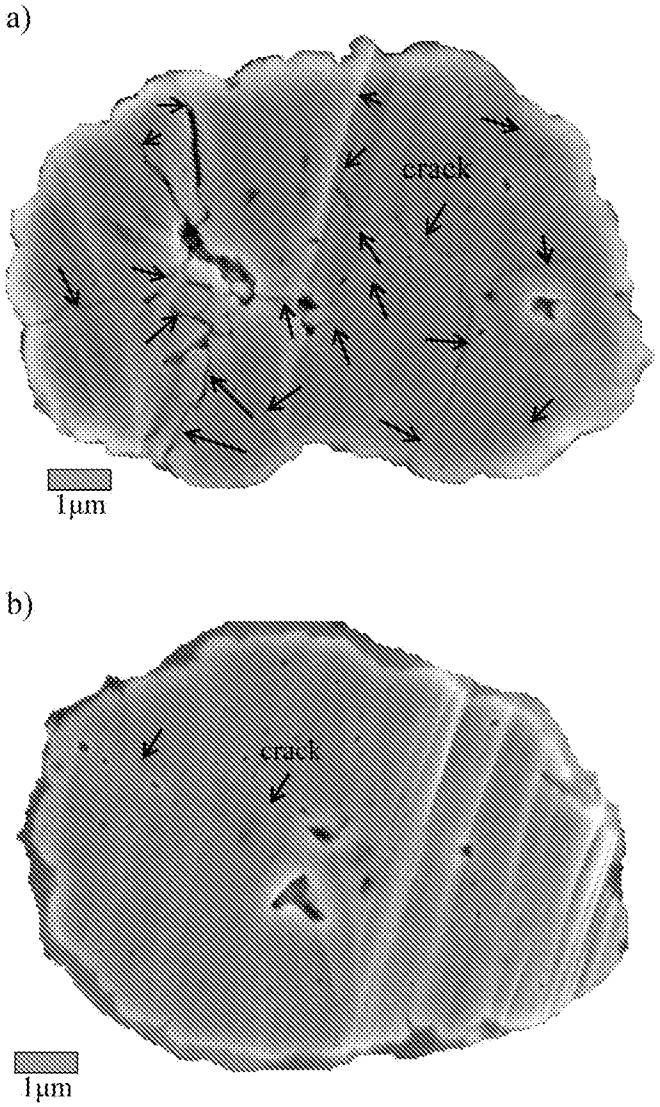


Fig. 12. Cross-sectional SEM images of electrodes cycled 250 times at 50 °C: (a) uncoated and (b) 7.5 wt% Al_2O_3 coated.

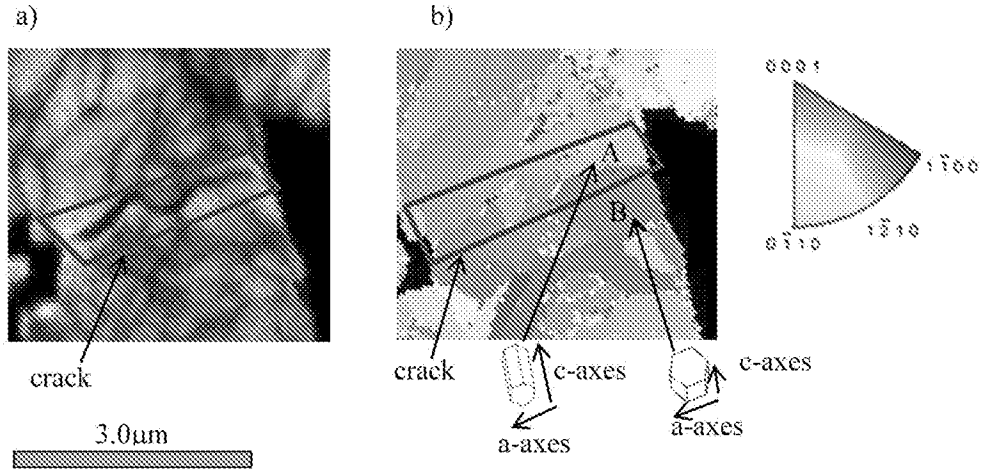


Fig. 11. Backscatter electron images of ground sections of cracks in an uncoated particle cycled 250 times at 50 °C: (a) SEM image and (b) EBSD image.

Table 3
Strength of uncoated and 7.5 wt% Al_2O_3-coated NCM particles.

Sample	Particle strength (MPa)
Uncoated NCM	128
NCM coated by 7.5 wt% Al_2O_3	168

that the increase in ASI(10s) is caused by increasing evolution of cracks leading to degradation of the electrochemical properties.

Since the reason why these cracks increase is very important, the internal structure of the particles was investigated further using EBSD. Fig. 11 shows an EBSD image of uncoated NCM particles after 250 cycles, in which the different colors represent different crystal orientations. The figure shows that the primary particles facing the notch, for example in the boxed area, are in a different crystal orientation. The crystal *c*-axes of primary particles A and B are almost mutually orthogonal. The lattice parameters are changed to a completely opposite direction during the charge/discharge process, and the stress concentrated at the grain boundary of two primary particles during such a change is the most likely cause of cracking.

Fig. 12 shows cross-sectional images of coated and non-coated NCM after 250 cycles at 50 °C, each image indicating a representative secondary particle from an SEM view containing more than 40 particles. The ASI ratios of uncoated NCM and NCM coated with 7.5 wt% Al_2O_3 were 138 and 111%, respectively. Thus, for a given number of cycles, it is clear that the number of cracks in coated NCM is dramatically less than that of an uncoated sample.

Cho et al. reported that a thin-film coating of high-fracture-toughness oxides suppresses the *c*-axis expansion (or phase transition) of $LiCoO_2$, thereby preventing capacity fading during electrochemical cycling [17]. In contrast, Itou et al. reported that occurrence of cracking in $LiNi_{0.8}Co_{0.15}Al_{0.05}O_2$ was one of the factors in its increased resistance [18]. The particle strengths of the uncoated and coated samples were therefore measured a using a microcompression testing machine. The results in Table 3 indicate that the average particle strength of coated particles is slightly higher than that of uncoated NCM. We can speculate from this enhancement of particle strength that the suppressed cracking during the charge/discharge cycle is at least one factor in determining capacity fade, but that other factors need to be taken into account.

4. Conclusions

This study has revealed that the increase of ASI in an NCM-based cell is due to the increased ASI of the active material at the positive electrode, which in turn is caused by the formation of cracks in secondary particles. We succeeded in suppressing this increase of ASI by coating NCM with Al_2O_3 nanoparticles using a mechanochemical bonding technology. This confirmed that crack formation inside the secondary particles of NCM correlates to the ASI increase. Moreover, the Al_2O_3 nanoparticle coating enhanced the particle strength, and this contributed to reducing the degree of crack growth inside the particles. Coating with Al_2O_3 therefore provides an effective technique for improving the life and power fade of Li-ion cells that utilize NCM as the positive electrode material.

Acknowledgments

This work was financially supported by the "Research & Development Initiative for Scientific Innovation of New Generation Batteries (RISING)" project of the New Energy and Industrial Technology Development Organization (NEDO).

References

[1] K. Amine, Z. Chen, Z. Zhang, J. Liu, W. Lu, Y. Qin, J. Lu, L. Curtis, Y. Sun, J. Mater. Chem. 21 (2011) 17754–17759.
[2] Y. Huang, J. Chen, F. Cheng, W. Wan, W. Liu, H. Zhou, X. Zhang, J. Power Sources 195 (2010) 8267–8274.
[3] S. Park, S. Lee, W.I. Cho, B.W. Cho, Met. Mater. Int. 16 (1) (2010) 93–98.
[4] L. Liu, L. Chen, X. Huang, X. Yang, W. Yoon, H.S. Lee, J. McBreen, J. Electrochem. Soc. 151 (2004) A1344–A1351.
[5] J. Cho, Y.J. Kim, B. Park, Chem. Mater. 12 (2000) 3788–3791.
[6] Y. Huang, J. Chen, J. Ni, H. Zhou, X. Zhang, J. Power Sources 188 (2009) 538–545.
[7] S. Hu, C. Cheng, M. Cheng, B. Hwang, R. Santhanam, J. Power Sources 188 (2009) 564–569.
[8] B.J. Hwang, C.Y. Chen, M.Y. Cheng, R. Santhanam, R. Kagavendran, J. Power Sources 195 (2010) 4255–4265.
[9] G.Q. Liu, H.T. Kuo, P.S. Liu, C.H. Shen, D.S. Shy, X.K. Xing, J.M. Chen, J. Alloys Compd. 496 (2010) 512–516.
[10] Y. Cho, J. Eom, J. Cho, J. Electrochem. Soc. 157 (2010) A617–A624.
[11] J.Y. Shi, C. Yi, K. Kim, J. Power Sources 195 (2010) 6860–6866.
[12] S.-U. Woo, C.S. Yoon, K. Amine, I. Belharouak, Y.-K. Sun, J. Electrochem. Soc. 154 (2007) A1005–A1009.
[13] S. Lee, C.S. Yoon, K. Amine, Y. Sun, J. Power Sources 234 (2013) 201–207.
[14] Y.S. Jung, A.S. Cavanagh, A.C. Dillon, M.D. Groner, S.M. George, S. Lee, J. Electrochem. Soc. 157 (2010) A75–A81.
[15] A.D. Pasquier, C.C. Huang, T. Spitler, J. Power Sources 186 (2009) 508–514.
[16] Y. Itou, Y. Ukyo, J. Power Sources 146 (2005) 39–44.
[17] J. Cho, Y.J. Kim, T. Kim, B. Park, Angew. Chem. Int. 40 (18) (2001) 3367–3369.
[18] H. Kobayashi, M. Shikano, S. Koike, H. Sakaebe, K. Tatsumi, J. Power Sources 174 (2007) 380–386.
[19] A.M. Andersson, D.P. Abraham, R. Haasch, S. Maclaren, J. Liu, K. Amine, J. Electrochem. Soc. 149 (2002) A1358–A1369.
[20] N. Dupré, J.-P. Martin, J. Oliveri, P. Soudan, A. Yamada, R. Kanno, D. Guyomard, J. Power Sources 196 (2011) 4791–4800.
[21] M. Shikano, H. Kobayashi, S. Koike, H. Sakaebe, Y. Saito, H. Nori, H. Kageyama, K. Tatsumi, J. Power Sources 196 (2011) 6881–6885.
[22] Z. Lu, D.D. MacNeil, J.R. Dahn, Electrochem. Solid State Lett. 4 (2001) A191–A194.

AMPEREX Ex. 1002
Page 827

Journal of Electroanalytical Chemistry 782 (2016) 168–173

Contents lists available at ScienceDirect

Journal of Electroanalytical Chemistry

journal homepage: www.elsevier.com/locate/jelechem

Capacity fading behavior of Ni-rich layered cathode materials in Li-ion full cells

Hyang-Rim Kim [a], Sang-Gil Woo [a,*], Jae-Hun Kim [b,*], Woosuk Cho [a], Young-Jun Kim [a,c]

[a] Advanced Batteries Research Center, Korea Electronics Technology Institute, Seongnam, Gyeonggi 13509, Republic of Korea
[b] School of Advanced Materials Engineering, Kookmin University, Seoul 02707, Republic of Korea
[c] SKKU Advanced Institute of Nanotechnology (SAINT), Sungkyunkwan University, Gyeonggi 16419, Republic of Korea

ARTICLE INFO

Article history:
Received 24 August 2016
Received in revised form 10 October 2016
Accepted 17 October 2016
Available online 18 October 2016

Keywords:
Capacity fading
Failure mechanism
Li-ion battery
Ni-rich cathode
Full cell

ABSTRACT

We report the failure mechanism of a Ni-rich layered cathode material ($LiNi_{0.8}Co_{0.1}Mn_{0.1}O_2$) in Li-ion full cells. Laminated pouch-type full cells were cycled 300 times, after which the cells exhibited 16.3% capacity fading. After 1, 100, 200, and 300 cycles, each full cell was disassembled and the cathode was investigated via a half-cell test, X-ray diffraction (XRD), and field emission scanning electron microscopy (FE-SEM). XRD analysis showed loss of the active lithium source in the cathode, and FE-SEM observation exhibited traces of mechanical failure in the Ni-rich secondary particles. Particle strength measurements on the cathode materials by applying compressive force demonstrated that the mechanical strength of particles significantly weakened after full-cell cycling. Thus, the capacity of the Ni-rich cathode may deteriorate during full-cell cycling because of decreases in compressive particle strength. This issue should be considered in materials preparation processes.

© 2016 Elsevier B.V. All rights reserved.

1. Introduction

With the rapid development of electric vehicles and large-scale energy storage systems, the demand for rechargeable batteries has grown explosively. Although research on next-generation batteries with high-energy density, such as Li-S and Li-air systems, has recently attracted attention, Li-ion batteries (LIBs) continue to dominate the market. Therefore, the development of advanced LIBs with improved energy density has been proposed to meet the increasing energy demands. To increase the energy density of current LIBs, adoption of high-capacity electrode materials is essential. Layered lithium transition-metal oxide materials are representative cathode materials for LIBs. In the early days of LIB commercialization, $LiCoO_2$ was mainly used because of its moderate capacity, ease of synthesis, and good cycle performance [1]. Recently, $LiCoO_2$ has been replaced in part with three-component layered $LiNi_xCo_yMn_zO_2$ oxides ($x + y + z = 1$) because of their lower cost and relatively high capacity [1–4]. As the Ni content of a cathode material increases, its specific capacity further increases with its material cost reduction [5]. Higher Ni contents are required for increasing the specific capacity of layered transition-metal oxide cathodes, which is needed for enhancing the energy density of lithium-ion batteries to enable the aforementioned large-scale applications.

Considering its benefits, however, large amounts of Ni in the cathode material result in structural and thermal instabilities. When Li cells are charged to voltages higher than 4 V vs. Li^+/Li, high-Ni-containing cathode materials show a transition from a hexagonal to monoclinic phase, leading to the distortion in the layered structure [6–8]. In addition, oxygen in the material becomes unstable at elevated temperatures, causing safety concerns via the exothermic thermal runaway [9–13]. To address the aforementioned issues, several strategies have been proposed and demonstrated [2,3]. Among these strategies, the surface modification by coating with materials such as metal oxide [14–16], metal phosphate [17,18], and metal fluoride [19,20] has been mainly studied. In general, a coating can prevent undesirable reactions between the active materials and the organic electrolyte, thereby improving the structural and thermal stability of the cathode material. In relevant works, the materials and electrochemical performance of the cathode are usually evaluated in half-cell tests using a Li metal counter and reference electrode. In this case, however, sufficient Li ions are provided to the cathode materials, such that the cathode degradation observed in practical full-cell conditions cannot be evaluated. Full-cell tests can provide operating conditions similar to those found in the practical use of rechargeable batteries. Some important factors that can be evaluated in full-cell tests include active material loading level, electrode density, heat produced in a large-scale cell, mechanical degradation by electrode swelling, and supply limitation of Li to the cathode by irreversible consumption in the graphite anode. From the postmortem analysis of electrodes cycled in full cells, we can observe the actual fading behavior of batteries in various applications [21–26].

In this study, we prepared pouch-type full cells by employing commercial graphite as a negative electrode (anode) material and high-Ni layered oxide ($LiNi_{0.8}Co_{0.1}Mn_{0.1}O_2$) as a positive electrode (cathode)

* Corresponding authors.
E-mail addresses: blackdragon@keti.re.kr (S.-G. Woo), jaehunkim@kookmin.ac.kr (J.-H. Kim).

http://dx.doi.org/10.1016/j.jelechem.2016.10.032
1572-6657/© 2016 Elsevier B.V. All rights reserved.

material. The capacity fading of full cells with graphite anodes can be mainly attributed to the loss of active Li ions by irreversible consumption through solid electrolyte interphase (SEI) formation/repairing on the graphite surface and physical degradation of the graphite electrode induced by volume changes during Li intercalation/deintercalation reactions [27–32]. If high-Ni oxide materials are adopted in full cells, they may also suffer capacity fading and material degradation. Here, we introduce a commercial-grade high-Ni oxide without surface coating and investigate the cause of cathode material failure during full-cell cycling through postmortem analyses.

2. Experimental

Commercial-grade graphite (BTR New Energy Materials Inc.) and high-Ni layered oxide ($LiNi_{0.8}Co_{0.1}Mn_{0.1}O_2$, NCM811, GS Energy) were used as anode and cathode materials, respectively. Anodes were prepared by coating slurries containing the active materials (graphite, 96 wt%) and a binder (styrene-butadiene rubber (SBR, Zeon)/carboxymethylcellulose (CMC, Daichi), 4 wt%) dissolved in de-ionized water onto copper foil substrates. Cathodes were also prepared by coating slurries consisting of the active material (NCM811, 95 wt%), a conducting agent (Super P®, carbon black, 2 wt%) and a binder (polyvinylidene fluoride, Kureha, 3 wt%) dissolved in n-methyl pyrrolidinone onto aluminum foil substrates. These electrodes were pressed and dried under vacuum for 12 h at 120 °C. The electrodes were then cut into rectangular shapes (30 × 40 mm) and the average mass loading for anode and cathode materials was about 9.5 and 15.3 mg cm^{-2}, respectively. Pouch-type 230 mAh cells were prepared by stacking five anodes and four cathodes. First, a single-side coated anode was placed, and double-side coated cathodes and anodes were stacked sequentially. Finally, another single-side coated anode was placed to face the cathode. Polyethylene separators (Toray, 16 μm thickness) were inserted between anode and cathode to prevent physical contact and short-circuit. The total capacity of the graphite anode was designed to be 1.07 times larger than that of the Ni-rich oxide cathode to prevent Li metal deposition on the anode surface. The full cells were sealed in an aluminum-laminated polymer film box (Dai Nippon Printing) with an electrolyte composed of 1 M $LiPF_6$ in ethylene carbonate (EC)/ethyl methyl carbonate (EMC) (3:7 v/v, Panax Etec) containing 2 wt% vinylene carbonate as an additive. This additive helps the formation of a stable SEI on the anode surface and facilitates observations of cathode degradation. All cell fabrication processes were performed in a dry room. After assembly, the cells were subjected to a formation cycle by charging and discharging at a constant current. In this pre-cycle, all cells were first charged in constant current (CC) mode to 4.2 V vs. Li^+/Li at a constant current of 46 mA (0.2C, 1C rate = 230 mA) and then charged in constant voltage (CV) mode until the current reached 4.6 mA. The cells were discharged to 2.75 V vs. Li^+/Li in CC mode with a constant current of 46 mA. Each cell was subsequently cycled 1, 100, 200, and 300 times within the voltage range of 2.75–4.2 V at 1C.

For cathode analysis, the pouch-type full cells were dismantled in the fully discharged state in an Ar-filled glovebox. The electrodes were washed in pure EMC solution (Panax Etec) and dried under vacuum to eliminate the effect of surface impurities. To evaluate the specific capacity of the cycled cathode, coin-type half-cell tests (CR2032) were galvanostatically conducted in fresh electrolyte using lithium metal foil (Honjyo Chemical) as the counter/reference electrode. The cycled electrodes were cut into a 12 mm-diameter disc for the coin-cell tests. For in-situ X-ray diffraction (XRD) analysis, a special laboratory-made pouch cell consisting of an anode and a cathode was used and XRD patterns were obtained at each potential step after the first, 100th, 200th, and 300th cycle. XRD measurements were carried out on the electrode using a PANalytical Empyrean XRD system with Cu-Kα radiation (40 kV, 30 mA). The lattice parameters were obtained by Rietveld refinement using HighScore Plus software. Inductively coupled plasma mass spectrometry (ICP-MS, Bruker Aurora M90) was used to quantify the ratio of transition metal elements (i.e., Ni, Co, Mn) in the cathode material after cycling. Instrumental errors for the composition are typically below 1%. The morphology and microstructure of the electrodes were examined by using a field emission scanning electron microscope (FE-SEM, JEOL JSM-7000F). For cross-sectional SEM observation, the electrodes were cut using a cross-section polisher (CP, JEOL SM-09010). After washing in pure EMC solution in an Ar-filled glovebox, the cycled electrodes were protected from air using a tightly sealed polyvinyl bag during transfer to the polisher and SEM chamber. To evaluate particle strength, the compression strength of the particle was measured by a micro-compression tester (Shimadzu MCT-W500). For in-situ internal pressure monitoring, cells consisting of an electrode charged to 4.3 V vs. Li^+/Li and fresh electrolyte (10 μL) were heated up to 95 °C for 3 h and then stored at a constant temperature for an additional 9 h in an oven. The internal pressure of the cell was then recorded by a pressure sensor (GE).

3. Results and discussion

Fig. 1a shows the voltage profiles of the pouch full cells measured at a rate of 0.2 C. The full cells were first cycled 1, 100, 200, and 300 times at 1 C, respectively and the profiles were then obtained at the very next cycle at 0.2 C. It was confirmed that the cell capacity at the first cycle was about 230 mA. The profiles obtained are typical of graphite/NCM811 full cells, and the average voltage for discharge was about 3.6 V [33]. As the cycle number increased, a slight increase in polarization, which could be attributed to an increase in internal resistance, was observed. The cycling performance of the full cell at 1 C shows gradual capacity fading (Fig. 1b). After 100, 200, and 300 cycles, the capacity retention ratios were about 89.9%, 86.1%, and 83.7%, respectively. In the early stages of cycling, capacity fading occurred first rapidly and then more gradually. Capacity fading in full cells with graphite anodes can be mainly ascribed to the loss of active Li ions in the graphite electrode. As cycling is performed, Li ions are irreversibly consumed on the graphite surface by SEI formation and repair, and the physical degradation of graphite occurs by volume changes through Li intercalation and deintercalation processes [27–32]. Although deterioration of the graphite electrodes largely affects full cells, the cathode also exhibits degradations in terms of both material and capacity. In particular, layered oxides with high Ni contents require further investigation when they are employed in full cells [21,22,34,35].

Fig. 1c shows the voltage profiles of NCM811 electrodes tested with a Li metal counter/reference electrode in the half cells. The half cells were galvanostatically tested at 0.2 C after disassembly of the full cells that had been cycled 1, 100, 200, and 300 times. Similar to the full cell profiles, the shapes obtained in the figure are typical of high-Ni layered oxide electrodes, and increased polarization was observed with increasing cycle numbers. The specific discharge capacities of the cathodes measured in half-cells after full-cell cycling are displayed in Fig. 1d. After the first cycle, the electrode exhibited a discharge capacity of 208.4 mAh g^{-1}, and the capacity retention ratios of electrodes cycled 100, 200, and 300 times in full cells were about 96.8%, 94.8%, and 93.0%, respectively. The capacity retention ratios of the cathode were higher than those of the full cells; however, the Ni-rich cathodes also showed considerable capacity fading even at half-cell test conditions, where the fresh Li counter electrode provides sufficient Li ions. Thus, to examine the cause of cathode degradation, several analytical methods were applied.

In-situ XRD measurement was performed to achieve detailed investigations on the structural changes of the cathode materials during cycling. Fig. 2a shows the in-situ XRD patterns obtained from the laboratory-made cells after 1, 100, 200, and 300 full-cell cycles. The crystal structure of $LiNi_{0.8}Co_{0.1}Mn_{0.1}O_2$ is indexed to a hexagonal α-$NaFeO_2$ type structure, with a space group $R\bar{3}m$. This material has several

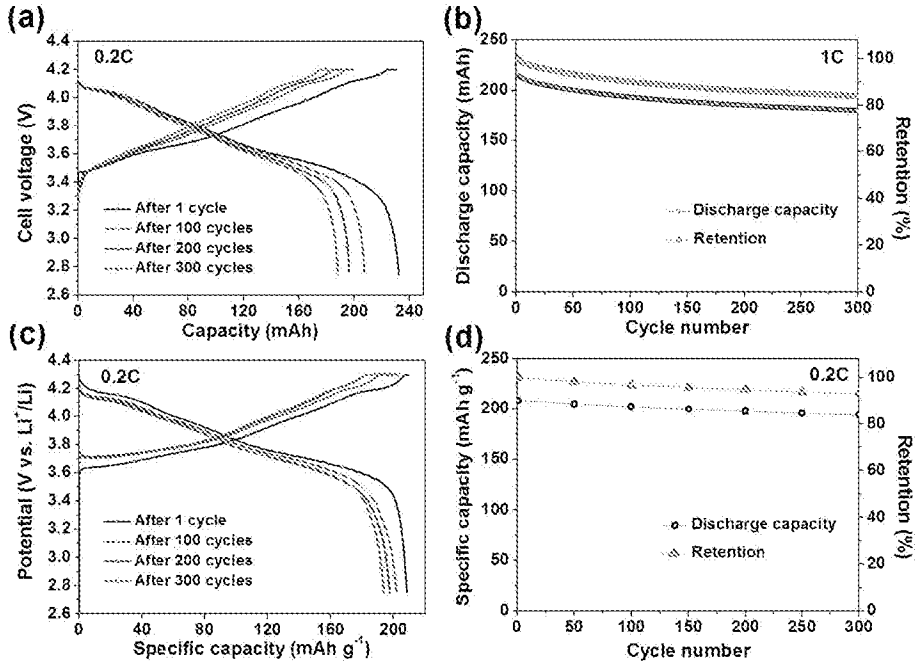


Fig. 1. Electrochemical test results: (a) voltage profiles of graphite/NCM811 full cells at 0.2 C, (b) cycle performance of graphite/NCM811 full cells at 1 C, (c) voltage profiles of half cells with cathodes cycled in full cells, and (d) discharge capacity of cathodes cycled in full cells as a function of cycle number.

characteristic diffraction peaks and the (003) reflection was selected for analysis because it clearly shows the structural variation. All of the electrodes showed similar behavior during cycling. When the cells were charged from 2.75 to 4.2 V vs. Li^+/Li, during which Li^+ extraction occurs, the (003) peak shifted first to a lower angle. Above 3.98 V, the peak shifted back toward a higher angle up to 4.2 V. This peak shift can be attributed to the phase transition of the cathode material from hexagonal to monoclinic and then back to hexagonal, as reported in the literature [6–8]. During Li^+ insertion (discharge) process, the peak initially shifted toward a lower angle and then returned to a higher angle; this pattern corresponds to reversible reactions into the fully lithiated state. All of the peak variations are in good accordance with previous reports [7,36].

To compare the XRD patterns obtained clearly, the lattice parameter of the c-axis at each potential step was calculated using the patterns,

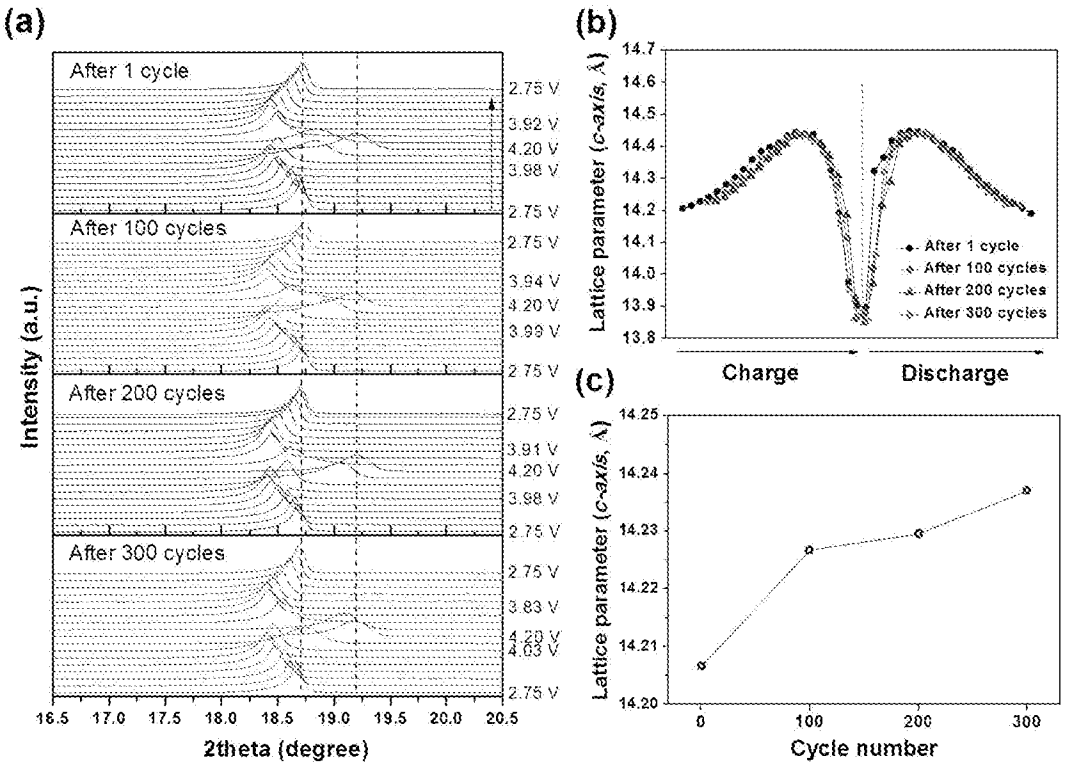


Fig. 2. (a) In-situ XRD patterns of cathodes cycled in full cells after the first, 100th, 200th, and 300th cycles, (b) lattice parameter variation of the c-axis during Li^+ extraction and insertion, and (c) lattice parameter variation of the c-axis at the fully discharged state after full-cell cycling.

Table 1
Atomic percentage of Ni, Co, and Mn in cathode materials.

	Fresh	After the first cycle	After the 100th cycle	After the 200th cycle	After the 300th cycle
Ni	80.6%	80.2%	80.5%	80.4%	80.1%
Co	10.1%	10.7%	10.5%	10.8%	10.8%
Mn	9.3%	9.1%	9.0%	8.8%	9.1%

and the results are presented in Fig. 2b. The variation in lattice parameter is similar among the electrodes, and minor differences were observed only at the initial state of each cycle, which was obtained from fully discharged full cells. As shown in Fig. 2c, the initial position of the (003) peak shifted toward a higher angle with increasing cycle number, which indicates that lattice expansion occurred. The lattice parameter increased from 14.207 to 14.237 Å during full-cell cycling, which is evidence of Li deficiency in the fully discharged cathode. This result implies that some amount of Li^+ ions could not return to the cathode materials upon cycling, which could be related to the loss of active Li in graphite anodes, as reported in the literature [27–32]. The loss of active Li is not directly connected to cathode material degradation. In-situ XRD analysis revealed that the structural degradation of high-Ni cathode materials upon Li insertion and extraction is not remarkable. To investigate the chemical state of the cathode material during cycling, X-ray photoelectron spectroscopy was performed; however, significant differences were not observed (data not shown). ICP-MS was performed to examine the dissolution of Ni from the Ni-rich cathode material after cycling. As shown in Table 1, the Ni content of the system remained nearly invariant upon cycling, which indicates that Ni dissolution exerts a limited influence on cathode degradation.

FE-SEM was used to evaluate the morphological changes of the high-Ni cathode after full-cell cycling. Fig. 3 shows the surface and cross-sectional FE-SEM images of electrodes cycled 1, 100, 200, and 300 times. The surface images shown in Fig. 3a–d reveal no notable difference in morphology between the cycled electrodes. When we compared low-magnification cross-sectional images of the electrodes (Fig. 3e–h), no remarkable difference was obtained. However, high-magnification cross-sectional images of the materials exhibited important morphological changes (Fig. 3i–l). As the cycle number increased, microcracks became more evident, and this morphological variation could lead to the capacity fading of the cathode material as reported in the literature [37–40]. To verify this, mechanical properties of the cathode material were examined.

Fig. 4a presents the compressive stress-displacement curves of the cathode particles, which were obtained from cycled electrodes. To acquire the curves, a controlled force was exerted on the particles and their displacement was recorded. In the initial stages of the test, the displacement increased rapidly with the compressive force. Thereafter, slower growth of the displacement was observed. Finally, the particles were broken at a critical point and displacement rose sharply at nearly constant stress. The particle strength was calculated by measuring the breaking force and cross-sectional area of particles. Fig. 4b shows changes in particle strength with increasing cycle number. In the first 50 cycles, the compressive strength of the particles abruptly decreased and then the decreasing rate became slower. These mechanical test results demonstrate the relationship between particle strength and the capacity fading of the cathode. The strength of active material particles influences the electrochemical properties of the cathode when it is cycled in full cells at room temperature. As cycling proceeds, high-Ni-containing particles suffer mechanical stress upon Li insertion and extraction. This phenomenon is significant in the first stages of cycling [37], which results in microcrack formation in the particles. These microcracks can lead to increased interfacial area and irreversible degradation of the material surface via side reactions with the electrolyte.

To examine the surface stability of the cathode upon the full-cell cycling, the internal pressure of a cell consisting of a delithiated NCM811 cathode obtained after cycling in full cells and fresh electrolyte was recorded at an elevated temperature of 95 °C. Because the interfacial stability between the high-Ni cathode and electrolyte affects the internal pressure through gas evolution reactions on the material surface, monitoring the internal pressure at the high temperature can provide information on material stability after long-term cycling [41,42]. Fig. 5 shows the measurement results of cell internal pressure. As temperature increased for the first 3 h of the test, the internal pressure drastically

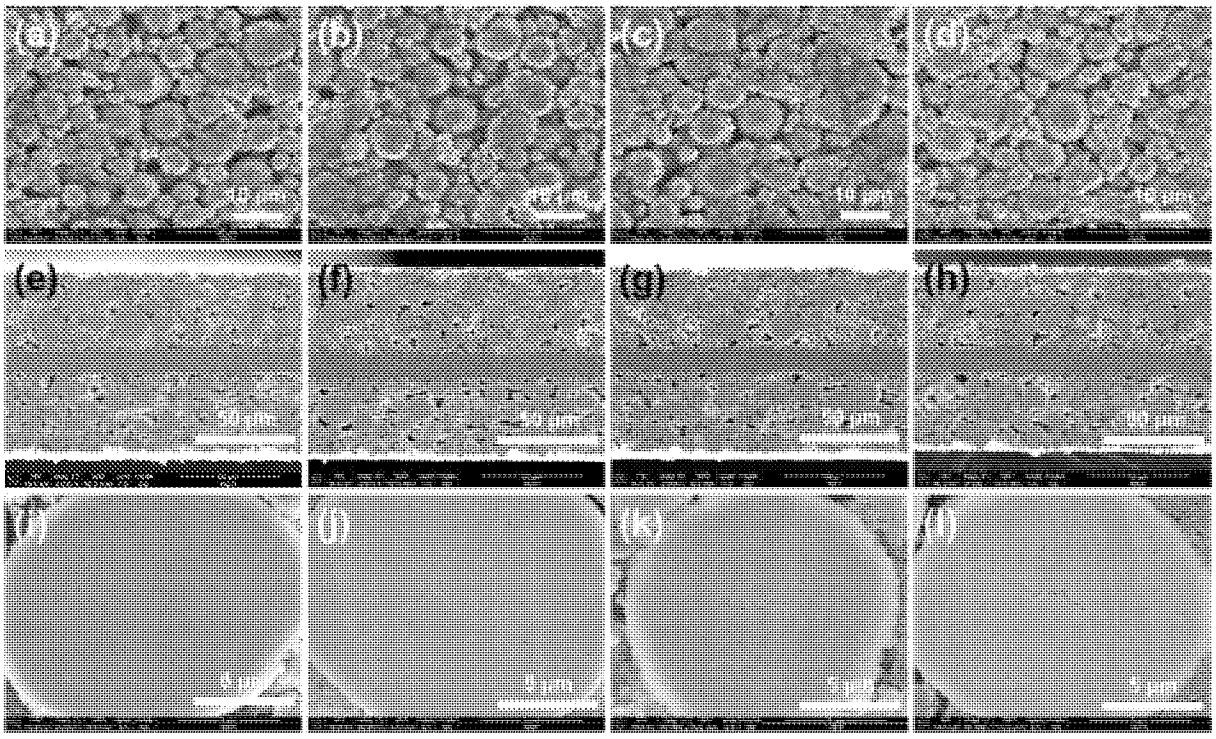


Fig. 3. FE-SEM images of the (a–d) surface, (e–h) low-magnification cross-section, and (i–l) high- magnification cross-section of the cathode after 1, 100, 200, and 300 cycles in full cells.

AMPEREX Ex. 1002
Page 831

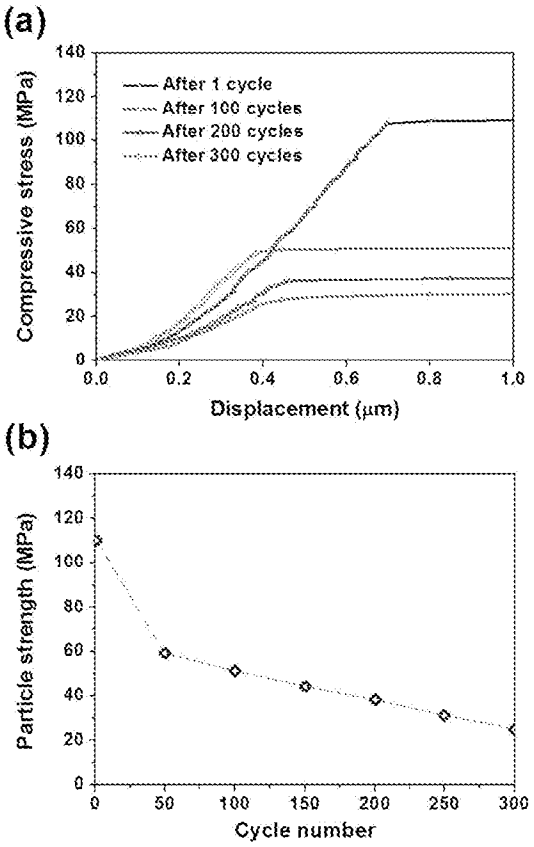


Fig. 4. (a) Compressive stress–displacement curves and (b) particle strength of the cathode materials after 1, 100, 200, and 300 cycles in full cells.

increased owing to vaporization of the electrolyte and expansion of internal gas; this tendency was similar for all of the cells observed. However, as time increased from 3 to 12 h, notable differences between the cells were observed. As the cycle number increased, a higher internal pressure was observed; this increase in pressure can be attributed to the decrement of the cathode surface stability. The cathode obtained after the first cycle in full cells showed the lowest internal pressure, and the difference in pressure among cathodes cycled 100–300 times was relatively small. This result is in good agreement with the measurement results of particle strength described above.

During the first stage of full-cell cycling, the electrolyte can penetrate into the microcracks of the cathode particles, thereby weakening the bonding strength between primary particles. Increases in interfacial

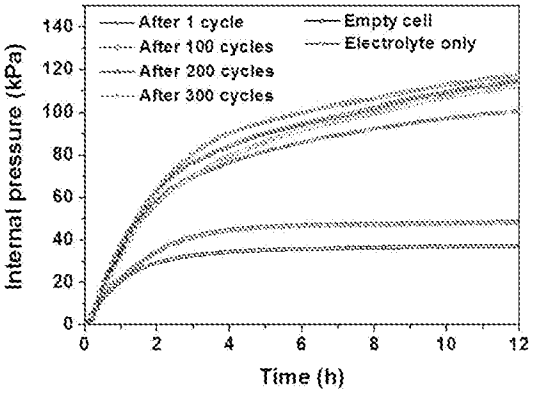


Fig. 5. Internal pressure measurement results at 95 °C. The cathode charged to 4.3 V vs. Li^+/Li was used for the measurement. The 4.3 V vs. Li^+/Li is equivalent to the upper potential limit of 4.2 V in full cells because the operating potential of the graphite anode is about 0.1 V vs. Li^+/Li.

area with the electrolyte may cause undesirable reactions that promote capacity fading. As cycling proceeds, more of the fresh cathode surface is gradually exposed to the electrolyte, and the capacity of the cathode slowly decreases. To prevent capacity fading of the high-Ni-containing layered cathode during full-cell cycling, improvements in secondary particle strength are recommended. As recently reported, these improvements could be achieved by addition of an agent that can enhance the bonding strength between primary particles to the material preparation process [43].

4. Conclusions

Pouch-type full cells consisting of commercial graphite and NCM811 electrodes were prepared and cycled 300 times at room temperature. After 1, 100, 200, and 300 cycles, each full cell was dismantled and the Ni-rich cathode was examined. Half-cell evaluation exhibited a high discharge capacity of 208.4 mAh g^{-1} after the first cycle and a capacity retention of 93.0% after 300 cycles. FE-SEM analysis demonstrated increasing microcrack formation in the Ni-rich secondary particles during cycling. Particle strength measurement results of the cathode materials indicated that the mechanical strength of secondary particles was significantly weakened after full-cell cycling. Increases in interfacial area induced by microcracks may cause undesirable reactions between the cathode material and the electrolyte, thereby promoting capacity fading. Thus, the strength of secondary particles should be further carefully considered in materials preparation processes.

Acknowledgements

The work was supported by the Technology Innovation Program (Project No. 10049170 and 10050568) funded By the Ministry of Trade, Industry and Energy (MI, Korea). This work was also supported by the National Research Foundation of Korea (NRF) Grant funded by the Korean Government (MSIP, 2015R1A5A7037615).

References

[1] M.S. Whittingham, Lithium batteries and cathode materials, Chem. Rev. 104 (2004) 4271–4302.
[2] W. Liu, P. Oh, X. Liu, M.-J. Lee, W. Cho, S. Chae, Y. Kim, J. Cho, Nickel-rich layered lithium transition-metal oxide for high-energy lithium-ion batteries, Angew. Chem. Int. Ed. 54 (2015) 4440–4457.
[3] A. Manthiram, J.C. Knight, S.-T. Myung, S.-M. Oh, Y.-K. Sun, Nickel-rich and lithium-rich layered oxide cathodes: progress and perspectives, Adv. Energy Mater. 6 (2016) 1501010.
[4] P. Rozier, J.M. Tarascon, Review—Li-rich layered oxide cathodes for next-generation Li-ion batteries: chances and challenges, J. Electrochem. Soc. 162 (2015) A2490–A2499.
[5] H.-J. Noh, S. Youn, C.S. Yoon, Y.-K. Sun, Comparison of the structural and electrochemical properties of layered $Li[Ni_xCo_yMn_z]O_2$ (x = 1/3, 0.5, 0.6, 0.7, 0.8 and 0.85) cathode material for lithium-ion batteries, J. Power Sources 233 (2013) 121–130.
[6] T. Ohzuku, A. Ueda, M. Nagayama, Electrochemistry and structural chemistry of $LiNiO_2$ (R3m) for 4 volt secondary lithium cells, J. Electrochem. Soc. 140 (1993) 1862–1870.
[7] W. Li, J.N. Reimers, J.R. Dahn, In situ x-ray diffraction and electrochemical studies of $Li_{1-x}NiO_2$, Solid State Ionics 67 (1993) 123–130.
[8] H. Arai, S. Okada, H. Ohtsuka, M. Ichimura, J. Yamaki, Characterization and cathode performance of $Li_{1-y}Ni_{1+y}O_2$ prepared with the excess lithium method, Solid State Ionics 80 (1995) 261–269.
[9] J.R. Dahn, E.W. Fuller, M. Obrovac, U. von Sacken, Thermal stability of Li_xCoO_2, Li_xNiO_2 and λ-MnO_2 and consequences for the safety of Li-ion cells, Solid State Ionics 69 (1994) 265–270.
[10] H. Arai, S. Okada, Y. Sakurai, J.-i. Yamaki, Thermal behavior of $Li_{1-y}NiO_2$ and the decomposition mechanism, Solid State Ionics 109 (1998) 295–302.
[11] D.P. Abraham, R.D. Twesten, M. Balasubramanian, I. Petrov, J. McBreen, K. Amine, Surface changes on $LiNi_{0.8}Co_{0.2}O_2$ particles during testing of high-power lithium-ion cells, Electr. Commun. 4 (2002) 620–625.
[12] H. Arai, M. Tsuda, K. Saito, M. Hayashi, Y. Sakurai, Thermal reactions between delithiated lithium nickelate and electrolyte solutions, J. Electrochem. Soc. 149 (2002) A401–A406.
[13] H. Arai, S. Okada, Y. Sakurai, J.I. Yamaki, Electrochemical and thermal behavior of $LiNi_{1-y}M_yO_2$ (M = Co, Mn, Ti), J. Electrochem. Soc. 144 (1997) 3117–3125.
[14] J. Cho, T.-J. Kim, Y.J. Kim, B. Park, High-performance ZrO_2-coated $LiNiO_2$ cathode material, Electrochem. Solid-State Lett. 4 (2001) A159–A161.

[15] S.-G. Woo, J.-H. Han, K.J. Kim, J.-H. Kim, J.-S. Yu, Y.-J. Kim, Surface modification by sulfated zirconia on high-capacity nickel-based cathode materials for Li-ion batteries, Electrochim. Acta 153 (2015) 115–121.
[16] W. Cho, S.-M. Kim, J.H. Song, T. Yim, S.-G. Woo, K.-W. Lee, J.-S. Kim, Y.-J. Kim, Improved electrochemical and thermal properties of nickel rich $LiNi_{0.6}Co_{0.2}Mn_{0.2}O_2$ cathode materials by SiO_2 coating, J. Power Sources 282 (2015) 45–50.
[17] W. Cho, S.-M. Kim, K.-W. Lee, J.H. Song, Y.N. Jo, T. Yim, H. Kim, J.-S. Kim, Y.-J. Kim, Investigation of new manganese orthophosphate $Mn_3(PO_4)_2$ coating for nickel-rich $LiNi_{0.6}Co_{0.2}Mn_{0.2}O_2$ cathode and improvement of its thermal properties, Electrochim. Acta 198 (2016) 77–83.
[18] G.-R. Hu, X.-R. Deng, Z.-D. Peng, K. Du, Comparison of $AlPO_4$- and $Co_3(PO_4)_2$-coated $LiNi_{0.8}Co_{0.2}O_2$ cathode materials for Li-ion battery, Electrochim. Acta 53 (2008) 2567–2573.
[19] J.-H. Kim, M.-S. Park, J.-H. Song, D.-J. Byun, Y.-J. Kim, J.-S. Kim, Effect of aluminum fluoride coating on the electrochemical and thermal properties of $0.5Li_2MnO_3 \cdot 0.5LiNi_{0.5}Co_{0.2}Mn_{0.3}O_2$ composite material, J. Alloys Compd. 517 (2012) 20–25.
[20] S.-U. Woo, C.S. Yoon, K. Amine, I. Belharouak, Y.-K. Sun, Significant Improvement of electrochemical performance of AlF_3-coated $Li[Ni_{0.8}Co_{0.1}Mn_{0.1}]O_2$ cathode materials, J. Electrochem. Soc. 154 (2007) A1005–A1009.
[21] R. Kostecki, F. McLarnon, Degradation of $LiNi_{0.8}Co_{0.2}O_2$ cathode surfaces in high-power lithium-ion batteries, Electrochem. Solid-State Lett. 5 (2002) A164–A166.
[22] D.P. Abraham, R.D. Twesten, M. Balasubramanian, J. Kropf, D. Fischer, J. McBreen, I. Petrov, K. Amine, Microscopy and spectroscopy of lithium nickel oxide-based particles used in high power lithium-ion cells, J. Electrochem. Soc. 150 (2003) A1450–A1456.
[23] K. Striebel, J. Shim, A. Sierra, H. Yang, X. Song, R. Kostecki, K. McCarthy, The development of low cost $LiFePO_4$-based high power lithium-ion batteries, J. Power Sources 146 (2005) 33–38.
[24] D.S. Lu, L.B. Yuan, J.L. Li, R.Q. Huang, J.H. Guo, Y.P. Cai, Failure mechanism for high voltage graphite/$LiNi_{0.5}Mn_{1.5}O_4$ (LNMO) Li-ion cells stored at elevated temperature, J. Electroanal. Chem. 758 (2015) 33–38.
[25] D. Li, D.L. Danilov, L. Gao, Y. Yang, P.H.L. Notten, Degradation mechanisms of C_6/$LiFePO_4$ batteries: experimental analyses of cycling-induced aging, Electrochim. Acta 210 (2016) 445–455.
[26] H. Hahn, R. Wagner, F. Schappacher, M. Winter, S. Nowak, In operando X-shaped cell online electrochemical mass spectrometry (OEMS): new online analysis enables insight into lab scale lithium ion batteries during operation, J. Electroanal. Chem. 772 (2016) 52–57.
[27] L.J. Hardwick, M. Marcinek, L. Beer, J.B. Kerr, R. Kostecki, An investigation of the effect of graphite degradation on irreversible capacity in lithium-ion cells, J. Electrochem. Soc. 155 (2008) A442–A447.
[28] M. Safari, C. Delacourt, Aging of a commercial graphite/$LiFePO_4$ cell, J. Electrochem. Soc. 158 (2011) A1123–A1135.
[29] L. Castro, R. Dedryvère, J.-B. Ledeuil, J. Bréger, C. Tessier, D. Gonbeau, Aging mechanisms of $LiFePO_4$//graphite cells studied by XPS: redox reaction and electrode/electrolyte interfaces, J. Electrochem. Soc. 159 (2012) A357–A363.
[30] J.-H. Kim, S.C. Woo, M.-S. Park, K.J. Kim, T. Yim, J.-S. Kim, Y.-J. Kim, Capacity fading mechanism of $LiFePO_4$-based lithium secondary batteries for stationary energy storage, J. Power Sources 229 (2013) 190–197.
[31] L. Tan, L. Zhang, Q. Sun, M. Shen, Q. Qu, H. Zheng, Capacity loss induced by lithium deposition at graphite anode for $LiFePO_4$/graphite cell cycling at different temperatures, Electrochim. Acta 111 (2013) 802–808.
[32] H. Zheng, L. Tan, L. Zhang, Q. Qu, Z. Wan, Y. Wang, M. Shen, H. Zheng, Correlation between lithium deposition on graphite electrode and the capacity loss for $LiFePO_4$/graphite cells, Electrochim. Acta 173 (2015) 323–330.
[33] Y. Bi, W. Yang, R. Du, J. Zhou, M. Liu, Y. Liu, D. Wang, Correlation of oxygen non-stoichiometry to the instabilities and electrochemical performance of $LiNi_{0.8}Co_{0.1}Mn_{0.1}O_2$ utilized in lithium ion battery, J. Power Sources 283 (2015) 211–218.
[34] R. Kostecki, F. McLarnon, Local-probe studies of degradation of composite $LiNi_{0.8}Co_{0.15}Al_{0.05}O_2$ cathodes in high-power lithium-ion cells, Electrochem. Solid-State Lett. 7 (2004) A380–A383.
[35] X. Zhang, P.N. Ross, R. Kostecki, F. Kong, S. Sloop, J.B. Kerr, K. Striebel, E.J. Cairns, F. McLarnon, Diagnostic characterization of high power lithium-ion batteries for use in hybrid electric vehicles, J. Electrochem. Soc. 148 (2001) A463–A470.
[36] H. Yu, S. Qian, L. Yan, P. Li, X. Lin, M. Luo, N. Long, M. Shui, J. Shu, Morphological, electrochemical and in-situ XRD study of $LiNi_{0.5}Co_{0.2}Mn_{0.1}Al_{0.1}O_2$ as high potential cathode material for rechargeable lithium-ion batteries, J. Alloys Compd. 667 (2016) 58–64.
[37] S. Zheng, R. Huang, Y. Makimura, Y. Ukyo, C.A.J. Fisher, T. Hirayama, Y. Ikuhara, Microstructural changes in $LiNi_{0.8}Co_{0.15}Al_{0.05}O_2$ positive electrode material during the first cycle, J. Electrochem. Soc. 158 (2011) A357–A362.
[38] D.J. Miller, C. Proff, J.G. Wen, D.P. Abraham, J. Bareño, Observation of microstructural evolution in Li battery cathode oxide particles by in situ electron microscopy, Adv. Energy Mater. 3 (2013) 1098–1103.
[39] E.-J. Lee, Z. Chen, H.-J. Noh, S.C. Nam, S. Kang, D.H. Kim, K. Amine, Y.-K. Sun, Development of microstrain in aged lithium transition metal oxides, Nano Lett. 14 (2014) 4873–4880.
[40] S. Watanabe, M. Kinoshita, T. Hosokawa, K. Morigaki, K. Nakura, Capacity fade of $LiAl_yNi_{1-x-y}Co_xO_2$ cathode for lithium-ion batteries during accelerated calendar and cycle life tests (surface analysis of $LiAl_yNi_{1-x-y}Co_xO_2$ cathode after cycle tests in restricted depth of discharge ranges), J. Power Sources 258 (2014) 210–217.
[41] K.S. Kang, S. Choi, J. Song, S.-G. Woo, Y.N. Jo, J. Choi, T. Yim, J.-S. Yu, Y.-J. Kim, Effect of additives on electrochemical performance of lithium nickel cobalt manganese oxide at high temperature, J. Power Sources 253 (2014) 48–54.
[42] T. Yim, K.S. Kang, J. Mun, S.H. Lim, S.-G. Woo, K.J. Kim, M.-S. Park, W. Cho, J.H. Song, Y.-K. Han, J.-S. Yu, Y.-J. Kim, Understanding the effects of a multi-functionalized additive on the cathode-electrolyte interfacial stability of Ni-rich materials, J. Power Sources 302 (2016) 431–438.
[43] S.-H. Han, J.H. Song, T. Yim, Y.-J. Kim, J.-S. Yu, S. Yoon, Communication—improvement of structural stability during high-voltage cycling in high-nickel cathode materials with B_2O_3 addition, J. Electrochem. Soc. 163 (2016) A748–A750.

AMPEREX Ex. 1002
Page 833

nature COMMUNICATIONS

ARTICLE

Received 19 Nov 2013 | Accepted 28 Feb 2014 | Published 27 Mar 2014

DOI: 10.1038/ncomms4529

Surface reconstruction and chemical evolution of stoichiometric layered cathode materials for lithium-ion batteries

Feng Lin[1], Isaac M. Markus[1,2], Dennis Nordlund[3], Tsu-Chien Weng[3], Mark D. Asta[2], Huolin L. Xin[4] & Marca M. Doeff[1]

The present study sheds light on the long-standing challenges associated with high-voltage operation of $LiNi_xMn_xCo_{1-2x}O_2$ cathode materials for lithium-ion batteries. Using correlated ensemble-averaged high-throughput X-ray absorption spectroscopy and spatially resolved electron microscopy and spectroscopy, here we report structural reconstruction (formation of a surface reduced layer, $R\bar{3}m$ to $Fm\bar{3}m$ transition) and chemical evolution (formation of a surface reaction layer) at the surface of $LiNi_xMn_xCo_{1-2x}O_2$ particles. These are primarily responsible for the prevailing capacity fading and impedance buildup under high-voltage cycling conditions, as well as the first-cycle coulombic inefficiency. It was found that the surface reconstruction exhibits a strong anisotropic characteristic, which predominantly occurs along lithium diffusion channels. Furthermore, the surface reaction layer is composed of lithium fluoride embedded in a complex organic matrix. This work sets a refined example for the study of surface reconstruction and chemical evolution in battery materials using combined diagnostic tools at complementary length scales.

[1] Environmental Energy Technologies Division, Lawrence Berkeley National Laboratory, Berkeley, California 94720, USA. [2] Department of Materials Science and Engineering, University of California, Berkeley, California 94720, USA. [3] Stanford Synchrotron Radiation Lightsource, SLAC National Accelerator Laboratory, Menlo Park, California 94025, USA. [4] Center for Functional Nanomaterials, Brookhaven National Laboratory, Upton, New York 11973, USA. Correspondence and requests for materials should be addressed to F.L. (email: flin@lbl.gov) or to H.L.X. (email: hxin@bnl.gov).

© 2014 Macmillan Publishers Limited. All rights reserved.

Chemical evolution and structural transformations at the surface of a material directly influence characteristics relevant to a wide range of prominent applications including heterogeneous catalysis[1–3] and energy storage[4,5]. Structural and/or chemical rearrangements at surfaces determine the way a material interacts with its surrounding environment, thus controlling the functionalities of the material[6–10]. Specifically, the surfaces of lithium-ion battery electrodes evolve simultaneously with charge–discharge cycling (that is, *in situ* surface reconstruction and formation of a surface reaction layer (SRL)) that can lead to deterioration of performance[4,5,11]. An improved understanding of *in situ* surface reconstruction phenomena imparts knowledge not only for understanding degradation mechanisms for battery electrodes but also to provide insights into the surface functionalization for enhanced cyclability[12,13].

The investigation of *in situ* surface reconstruction of layered cathode materials, such as stoichiometric $LiNi_xMn_xCo_{1-2x}O_2$ (that is, NMC), lithium-rich $Li(Li_yNi_{x-y}Mn_xCo_{1-2x})O_2$, lithium-rich/manganese-rich (composite layered–layered) $xLi_2MnO_3 \cdot (1-x)LiMO_2$ (M = Mn, Ni, Co, and so on) materials, is technologically significant as they represent a group of materials with the potential to improve energy densities and reduce costs for plug-in hybrid electric vehicles and electric vehicles[14–17]. Practical implementation of some of these materials is thwarted by their high first-cycle coulombic inefficiencies[17–20], capacity fading[18,21] and voltage instability[20–22], especially during high-voltage operation. Specifically, high-voltage charge capacities achieved in lithium-rich/manganese-rich layered cathodes are directly associated with various irreversible electrochemical processes including oxygen loss and concomitant lithium ion removal[23] and electrode/electrolyte reactions[24]. With respect to regular NMC materials, although improved high-voltage cyclability (2.0–4.7 V versus Li^+/Li) was recently achieved when a small percentage of Co was substituted with Ti (<4%), capacity fading still occurred after extended charge–discharge cycles[18]. Due to the structural and chemical complexities of these layered structures, their fading mechanisms have not been fully resolved. Electron microscopy studies indicated that, in lithium and manganese-rich materials, the capacity fading and voltage decay were partially attributed to structural reconstruction inducing a transition from the layered structure to spinel and/or rock-salt structures at the surface and/or in the bulk[5,17,25,26]. A recent study investigated the atomic structure of Li_2MnO_3 after partial delithiation and re-lithiation to enable improved understanding of lithium-rich/manganese-rich materials[27]. However, these studies were mainly performed using spatially resolved techniques, thereby inevitably lacking relevance to large-scale battery electrodes and failing to account for the inhomogeneous nature of battery electrodes[28–30]. In addition, the role of electrode–electrolyte interactions in the surface reconstruction and chemical evolution has been rarely studied. The elucidation of the surface reconstruction of stoichiometric NMC materials should provide insights into the fading mechanisms not only for these compounds but also complement the mechanistic paradigm for more complex layered structures including lithium-rich and manganese-rich materials. In order to achieve a statistically viable and spatially visible elucidation (in real space) for surface phenomena on electrode materials, diagnostic techniques with complementary length scales should be implemented, including high-throughput synchrotron X-ray absorption spectroscopy (XAS) and atomic-scale scanning transmission electron microscopy (STEM) and electron energy loss spectroscopy (EELS).

Here, we report the surface reconstruction and chemical evolution of stoichiometric NMC layered structures, using ensemble-averaged synchrotron XAS coupled with atomic-scale STEM-EELS, where the surface reconstruction and chemical evolution refer to the formations of surface reduced layer ($R\bar{3}m$ to $Fm\bar{3}m$ transition) and SRL, respectively. Our results reveal that the surface reconstruction occurs simultaneously with charge–discharge cycles and is strongly determined by the upper voltage limits used during cycling, electrolyte exposure and crystal orientations. Furthermore, the major lithium-containing phase in the SRL is identified as lithium fluoride (LiF) embedded in a complex amorphous organic matrix. The present study provides insights into the surface reconstruction and chemical evolution in NMC materials and directly illustrates the origin(s) of the long-standing challenges involved in cycling NMC materials to high voltages, such as capacity fading, impedance increases and first-cycle coulombic inefficiency. Finally, the study complements the mechanistic understanding of the surface reconstruction in layered materials and sheds light on the possible advantages of conformal functionalization on the surfaces of NMC particles.

Results

Characterization of pristine materials. $LiNi_{0.4}Mn_{0.4}Co_{0.18}Ti_{0.02}O_2$ (abbreviated NMC hereafter) powders with different particle size distributions were used for this study, because previous studies have shown that partial Ti substitution in NMCs results in higher practical specific capacities, better capacity retention upon cycling to 4.7 V versus Li^+/Li, and decreased first-cycle coulombic inefficiencies compared with baseline electrodes[18,19]. The ratio of transition metals was verified to be close to stoichiometric $LiNi_{0.4}Mn_{0.4}Co_{0.18}Ti_{0.02}O_2$ (Supplementary Fig. 1). Extensive analysis was performed on the pristine materials to verify the homogeneity of the surface and bulk prior to electrochemical implementation. The combinatorial evaluation was done using a variety of X-ray and electron-based techniques and is shown in Fig. 1. The irregularly shaped primary particles of the NMC powder ranged in size from ~100–250 nm across (Fig. 1a), indicating that the surface is terminated with various crystal orientations.

The specific surface area of the material was measured to be 9 $m\,g^{-2}$ by N_2 physisorption using the Brunauer–Emmett–Teller method (Supplementary Fig. 2). An extensive number of atomic resolution annular dark-field STEM (ADF-STEM) images were obtained and representative ones are shown in Fig. 1b,c. STEM-EELS analysis was performed for the particle shown in Fig. 1b, and it was found that the transition metal oxidation state remains constant from the surface to the bulk (Supplementary Fig. 3). Because ADF-STEM images approximately reflect the Z-contrast of materials, the images demonstrate that the material exhibits a well-defined layered structure, and the position of transition metals (*3b* sites) are atomically resolved along the [100] zone axis (Fig. 1c). Note that lithium (*3a* sites) and oxygen (*6c* sites) are not visible in the Z-contrast ADF-STEM image due to their low atomic masses. Powder X-ray diffraction (XRD) confirmed that the NMC has the expected $R\bar{3}m$ layered structure (Fig. 1d). The refined lattice parameters are consistent with those reported previously for this composition[18] and are summarized in Supplementary Table 1. Depth profiling of the electronic structure was carried out using XAS and STEM-EELS. Transition metal L-edge XAS and EELS measure the dipole allowed transitions from metal *2p* orbitals to unoccupied metal *3d* orbitals[31–33] and indirectly probe the local hybridization states for metal-oxygen octahedral units[34] in an NMC material. Transition metal L-edge XAS is superior to K-edge XAS in terms of resolving local hybridization states, as the former directly probes the unoccupied *3d* states in the metal *3d*-oxygen *2p* hybridized octahedral crystal field. Furthermore, L-edge XAS allows different sample depths to be probed from surface to bulk, depending on

© 2014 Macmillan Publishers Limited. All rights reserved.
AMPEREX EX. 1002
Page 835

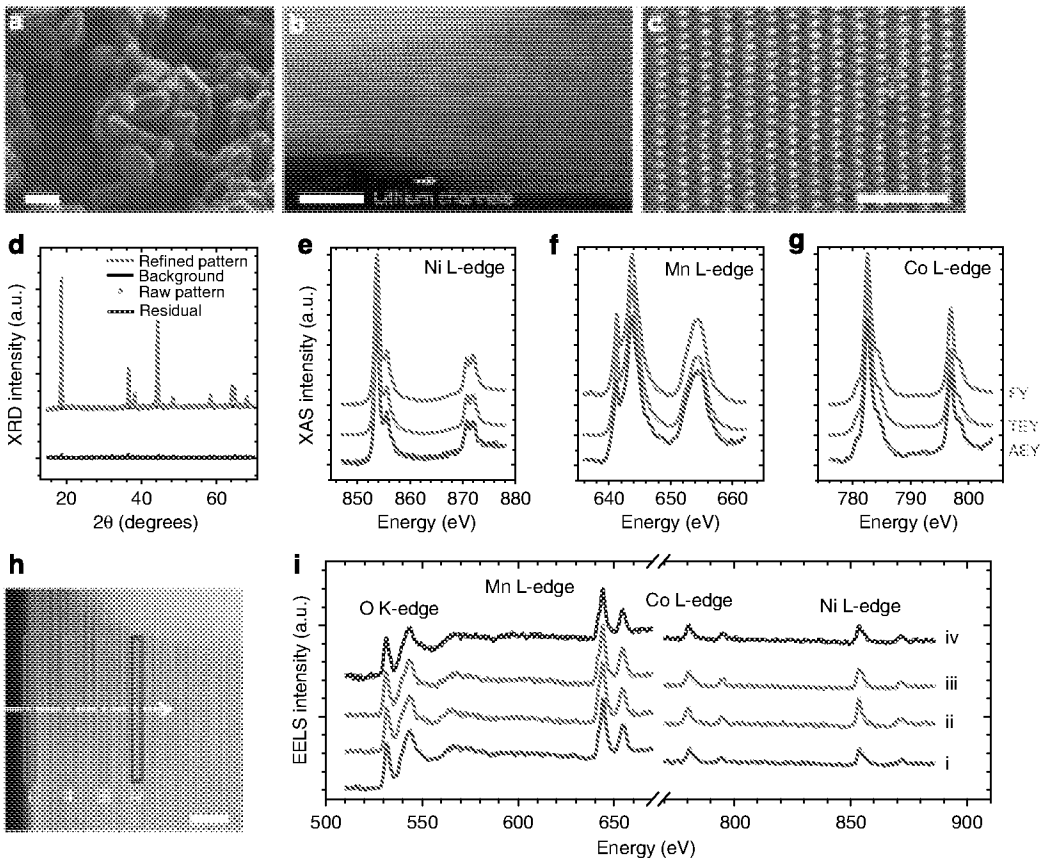


Figure 1 | Crystal structure and electronic structure of pristine NMC materials. (**a**) SEM image. (**b**) High-resolution Z-contrast ADF-STEM image. (**c**) Atomic resolution Z-contrast ADF-STEM image along the [100] zone axis, with the R$\bar{3}$m *3a* and *3b* sites indicated in the image. (**d**) XRD pattern with Rietveld refinement (fitted parameters are given in Supplementary Table 1). XAS spectra of (**e**) Ni L-edge, (**f**) Mn L-edge and (**g**) Co L-edge using AEY (blue), TEY (red) and FY (green) modes. (**h**,**i**) EELS spectra integrated from areas (i), (ii), (iii) and (iv); see also Supplementary Fig. 3 for the spectroscopic imaging of the pristine surface. The scale bars in **a**,**b**,**c** and **h** are 200 nm, 5 nm, 2 nm and 5 nm, respectively.

the detection modes. In the configuration used for this study, Auger electron yield (AEY), total electron yield (TEY) and fluorescence yield (FY) yield information about the chemical environments with depth sensitivities of 1–2 nm, 2–5 nm and 50 nm, respectively. Note that the FY probing depth is smaller than the particle size of the NMC materials, thus the signal primarily originates from the NMC particles on the top layer of the electrode rather than in the bulk of the composite electrode (typical thickness $\sim$ 76 μm, Supplementary Fig. 4). XAS L-edge spectra of the transition metals exhibit almost identical shapes (for example, Ni3p$_{3/2}$ and Ni3p$_{1/2}$ splitting features) and L2,3 normalized intensities in AEY, TEY and FY modes (Fig. 1e–g), which suggest an ensemble-averaged chemical homogeneity in the NMC material. Finally, the formal oxidation states of Ni, Mn and Co are determined to be +2, +4 and +3, respectively, as expected[31,35–37]. Furthermore, the formal oxidation state of Ti is +4, and the shape of L-edge verifies the Ti substitution in the R$\bar{3}$m layered lattice (Supplementary Fig. 5). A series of EELS area integrated spectra was recorded to directly assess the homogeneity of the chemical environment in a single NMC particle (Fig. 1h) and representative ones are displayed in Fig. 1i. The corresponding transition metal L-edge spectra exhibit no variation in the shapes or L3/L2 ratios at different probing positions. Furthermore, the O K-edge shows identical pre-edge peaks that are associated with the transitions from O 1*s* to O 2*p*-metal 3*d* hybridized states and are sensitive to the oxidation states of transition metals[38,39], which implies that the average oxidation states of transition metals remain constant from the top surfaces to volumes deep in the bulk. The above ensemble-averaged and spatially resolved spectroscopic studies allow us to conclude that the pristine NMC material exhibits a well-defined R$\bar{3}$m crystal structure with a homogenous distribution of the electronic structure. Furthermore, the homogeneity is not affected by the NMC particle size (Supplementary Fig. 6). Such comprehensive investigation of homogeneity is rarely reported in the literature, although its establishment is critical for resolving the effects of electrochemistry on surface reconstruction and chemical evolution.

Electrochemical tests of NMC materials. The electrochemical performances of the NMC materials were evaluated in lithium half-cells, and the cycled electrodes were collected for the subsequent synchrotron X-ray and electron spectroscopy based investigation. There are distinct differences in behaviour between the high-voltage cycling (2.0–4.7 V) and lower-voltage cycling (2.0–4.3 V). The NMC material shows a gradually sloping charge profile with no evidence of the high-voltage plateau associated with irreversible loss of lithium and oxygen, commonly seen during electrochemical oxidation of lithium-excess compounds under these conditions[16,22]. Nevertheless, when repeatedly charged to 4.7 V versus Li^+/Li, the capacity of the NMC electrode decreased with each cycle, while it fades very little during cycling between 2.0–4.3 V (Fig. 2a–c). Furthermore, the potential hysteresis between lithium deintercalation (charging) and intercalation (discharging) increased gradually during

© 2014 Macmillan Publishers Limited. All rights reserved.
AMPEREX Ex. 1002
Page 836

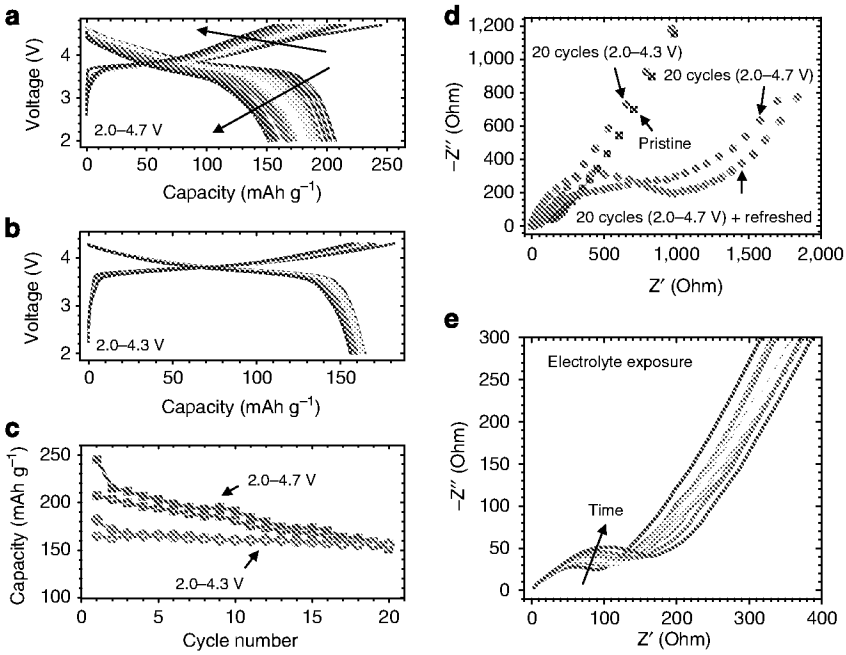


Figure 2 | Battery cycling performance of NMC materials. (**a**) Charge–discharge profiles at 2.0–4.7 V for 20 cycles at C/20, where the arrows indicate the gradual capacity fading and potential hysteresis. (**b**) Charge–discharge profiles at 2.0–4.3 V for 20 cycles at C/20. (**c**) Charge and discharge capacities as functions of cycle number at 2.0–4.7 V (blue square) and 2.0–4.3 V (red circle), respectively. The solid and open data points represent charge and discharge capacities, respectively. (**d**) Nyquist plots of impedance data obtained on cells containing electrodes in the pristine state, cycled at 2.0–4.3 V for 20 cycles, cycled at 2.0–4.7 V for 20 cycles and in the refreshed state (that is, rinsed with DMC, reassembled with fresh electrolyte after 20 cycles at 2.0–4.7 V). (**e**) A series of Nyquist plots for a pristine NMC electrode exposed to electrolytic solution for various periods up to 7 days. The exposure durations were 0 h (pristine), 5 h, 10 h, 1 day, 2 days, 3 days, 4 days, 5 days and 7 days.

high-voltage cycling (indicated by the arrows in Fig. 2a); namely, larger overpotentials were observed for both processes. Because cycling was carried out between set voltage limits, this impedance rise also contributed to the apparent capacity fading. In contrast, capacity retention was much better when using a lower-voltage limit on charge, that is, when cycling between 2.0–4.3 V (Fig. 2b,c). Such pronounced dependence on the voltage cutoff is partially caused by increased cell impedance under the high-voltage cycling conditions, as shown in Fig. 2d. The Nyquist plots of the impedance data are composed of a semicircle at high frequencies and Warburg tails at low frequencies, which correspond to charge transfer resistance and mass transfer resistance, respectively. Both charge transfer resistance and mass transfer resistance markedly increased after the extended high-voltage cycling indicated by the increased semicircle radius and the decreased slope of Warburg tail (Fig. 2d). In contrast, the charge transfer resistance slightly decreased after lower-voltage cycling between 2.0–4.3 V (Fig. 2d), which is likely attributed to cell conditioning and minimal surface reconstruction between 2.0–4.3 V (discussed below). An impedance rise was also observed when the NMC electrode was exposed to the electrolytic solution for an extended period (Fig. 2e) without being cycled. The similarities in the behaviour suggest that the NMC electrodes undergo similar modifications under conditions of cycling and electrolytic solution exposure, although to a lesser degree for the latter.

Post analysis of NMC materials. A correlated study using XAS, EELS and STEM imaging was performed to elucidate the mechanism of capacity fading and impedance rise in NMC cathodes under high-voltage cycling conditions. XAS/TEY is suitable for probing electronic structures at the top few nanometres due to the limited penetration depth of soft X-rays[40]. Because the measurements were performed on electrodes in the fully discharged state, nickel consistently showed a formal oxidation state of +2 after extended charge–discharge cycles (Supplementary Fig. 7). In contrast, manganese and cobalt underwent significant changes upon cycling. The contribution from the low-energy shoulders of Mn L3- and Co L3-edges grew gradually with increasing numbers of cycles (Fig. 3a,b), indicating an evolution of transition metal 3*d* bands to higher occupancies, that is, reduced oxidation states[35,36,41]. Furthermore, the oxidation states of transition metals exhibited depth-dependent characteristics, as shown by the direct comparison of AEY, TEY and FY spectra in Fig. 3c,d. The low-energy components of Mn L-edge and Co L-edge spectra were more obvious in the AEY mode than those in the TEY and FY modes. Therefore, the reduced Mn and Co species are primarily located at the surface. However, the high-energy component of the L3-edge was always present even in the surface-sensitive AEY mode, which suggests that the reduced Mn and Co species were not evenly distributed on individual NMC particles at the surfaces of the NMC electrodes. This observation coincides with previous studies that show that the charge distribution on the electrode surfaces is inhomogeneous in nature[30]. It is plausible that the reduced species were dominant on certain facets of individual NMC crystals, and that some surfaces exposed to incident X-rays retained the pristine electronic structure. Our subsequent investigation by ADF-STEM imaging further supports this hypothesis. An EELS line scanning profile was obtained on a particle cycled five times (Fig. 3e–h). The variation of the Mn oxidation state along the scanning direction is evident by the blue shift of the absolute energy onset and the reduced L3/L2 ratio[33]. A calculation based on the linear combination of Mn^{2+} and Mn^{4+} was performed and the corresponding concentration profiles are presented in Fig. 3h. The concentrations of Mn^{2+} and Mn^{4+} were inversely correlated along the scanning

© 2014 Macmillan Publishers Limited. All rights reserved.
AMPEREX EX. 1002
Page 837

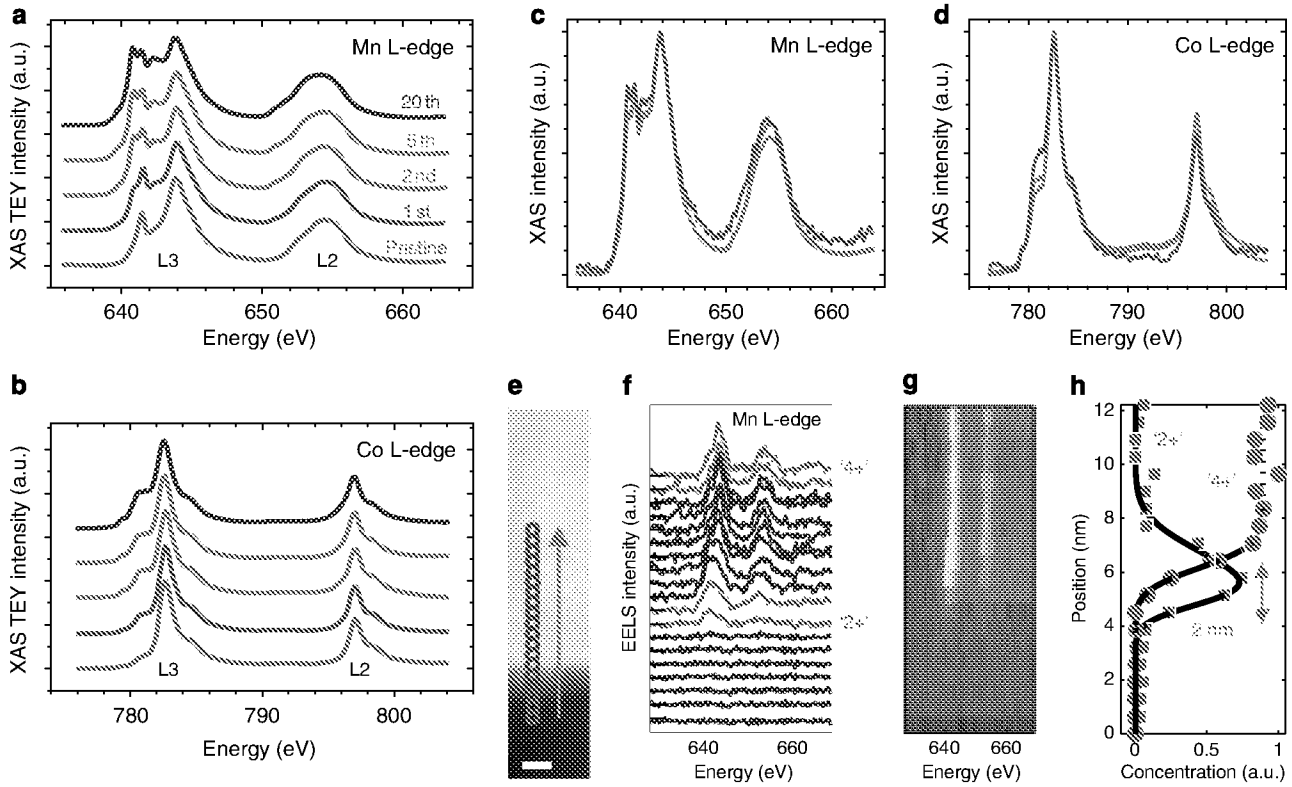


Figure 3 | Surface reconstruction and chemical evolution. (**a**) Mn L-edge XAS/TEY spectra and (**b**) Co L-edge XAS/TEY spectra after the designated number of cycles. (**c**) Mn L-edge XAS spectra and (**d**) Co L-edge XAS spectra for an electrode after two charge–discharge cycles in the AEY (blue), TEY (red) and FY (green) modes. EELS line scan profile for an NMC particle along the 〈001〉 direction after five cycles: (**e**) STEM image for the scanning pathway, (**f**) Mn L-edge EELS spectra along the scanning pathway, (**g**) 2D EELS map visualizing the peak shift and (**h**) concentration profiles for Mn^{2+} and Mn^{4+} obtained from the data using a linear combination method. All the measurements were performed on electrodes in the fully discharged state after cycled between 2–4.7 V versus Li^+/Li. The scale bar in (**e**) is 2 nm.

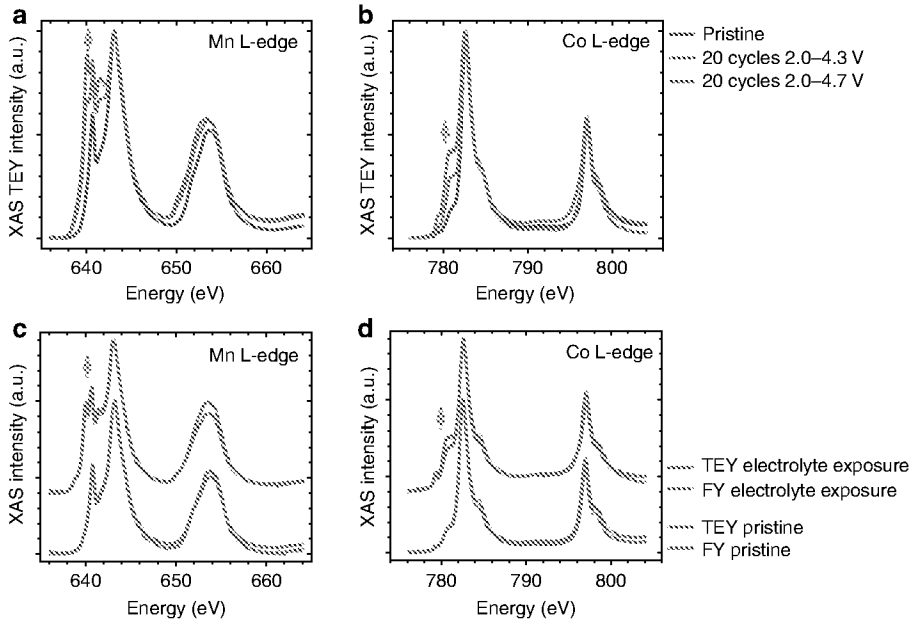


Figure 4 | Effects of cycling voltages and electrolyte exposure. (**a**) Mn L-edge XAS/TEY spectra and (**b**) Co L-edge XAS/TEY spectra of pristine and cycled electrodes (20 cycles). (**c**) Mn L-edge XAS/TEY/FY spectra and (**d**) Co L-edge XAS/TEY/FY spectra of a pristine electrode and one exposed to electrolytic solution for 7 days. The blue arrows in (**a**–**d**) indicate the increase of transition metals having low oxidation states.

direction, with Mn^{2+} primarily dominant on the surface. The thickness of the surface reduced layer was 2 nm for this particle, determined by using the intersections of Mn^{2+} and Mn^{4+} concentration profiles (Fig. 3h). An equivalent experimental protocol was applied to an NMC particle cycled 20 times. Along the identical crystal orientation, the thickness of the surface

© 2014 Macmillan Publishers Limited. All rights reserved.

reduced layer increased to ~3.4 nm (Supplementary Fig. 8). However, low-voltage cycling (2.0–4.3 V) yielded a surface reduced layer with a thickness of 2 nm after 20 cycles (Supplementary Fig. 9). Another NMC material with identical composition yet smaller particle size was studied to probe the effect of particle size on the surface reduced layer, and the results show that the particle size imposes negligible effects on surface reduced layer within the range in this study (Supplementary Fig. 10), and had similar cycling behaviour (Supplementary Fig. 11).

In addition to the surface reduced layer on the active NMC materials, a surface reaction layer (SRL) was observed after extended charge–discharge cycles (Supplementary Fig. 12). EELS revealed that the SRL consisted of a LiF phase in a complex organic matrix (Supplementary Fig. 12). The SRL buildup is partially responsible for the impedance rise (Fig. 2d). The emergence of the SRL is mainly attributed to the repeated high-voltage electrochemical processes, because it was barely observed in the electrode that was cycled to the low voltage (Supplementary Fig. 13) or exposed to the $LiPF_6$/EC-DMC solution for 7 days, without being cycled (Supplementary Fig. 14).

The capacity retention of NMC materials is compromised when high-voltage cycling, such as 4.7 V versus Li/Li^+, is used. Here we show that the surface reduced layer is related to the inferior capacity retention observed under high-voltage cycling conditions. As shown in Fig. 4a,b, the relative amounts of reduced transition metals were higher after high-voltage cycling (2.0–4.7 V versus Li/Li^+) than after lower-voltage cycling (2.0–4.3 V versus Li/Li^+). These results suggest that the layered lattice is disrupted at high voltages resulting in a formation of a metastable phase that is readily reduced under discharging conditions. Presumably, the surface reduced layer creates a passivation layer that inhibits efficient lithium diffusion, thus adversely impacting capacity retention. This hypothesis is further justified by several control experiments. First, after high-voltage cycling, the electrodes could not be revitalized to the initial state by reassembling the cell with fresh electrolytic solution (Supplementary Fig. 15a), because this did not reduce the impedance (Fig. 2d). Second, the capacity normally obtained with low-voltage cycling (2.0–4.3 V versus Li/Li^+) could not be restored after high-voltage cycling (Supplementary Fig. 15b). Third, the high-voltage capacity could be improved only by using an extremely slow charge–discharge rate even after 20 high-voltage cycles (Supplementary Fig. 15c). These observations indicate that the cycling losses imposed by high-voltage cycling are mainly due to the impedance rise caused by the surface reduced layer and SRL rather than changes in the bulk electrode material.

Previous studies have attributed the surface reduced layer mainly to electrochemical processes with little attention dedicated to the effects of electrode–electrolyte reactivity[4,5,17]. Here we found that a surface reduced layer similar to the ones observed during high-voltage cycling is also created after an NMC electrode was immersed in the electrolyte (Fig. 4c,d), although it is thinner. In addition, its buildup leads to gradually increased charge transfer resistance (Fig. 2e). After extended cycling, the surface reduced layer originates from dual effects involving both the electrode–electrolyte reactivity and electrochemical activation. The immediate generation of the reduced surface upon exposure to electrolyte may also be responsible for the first-cycle coulombic inefficiencies that are usually observed with NMC electrodes even when cycled conservatively, using voltage limits well below the oxidative stability limit of the electrolytic solution.

In the above discussion, XAS and EELS spectroscopies provided correlated evidence for the surface reduced layer and chemical evolution via the elucidation of local electronic structures primarily at the vicinity of NMC particle surfaces. The changes in electronic structures must be associated with the collapse and rearrangement of local crystal structures; that is, lattice reconstruction. The atomic resolution ADF-STEM imaging allows the visualization of the localized structural rearrangements

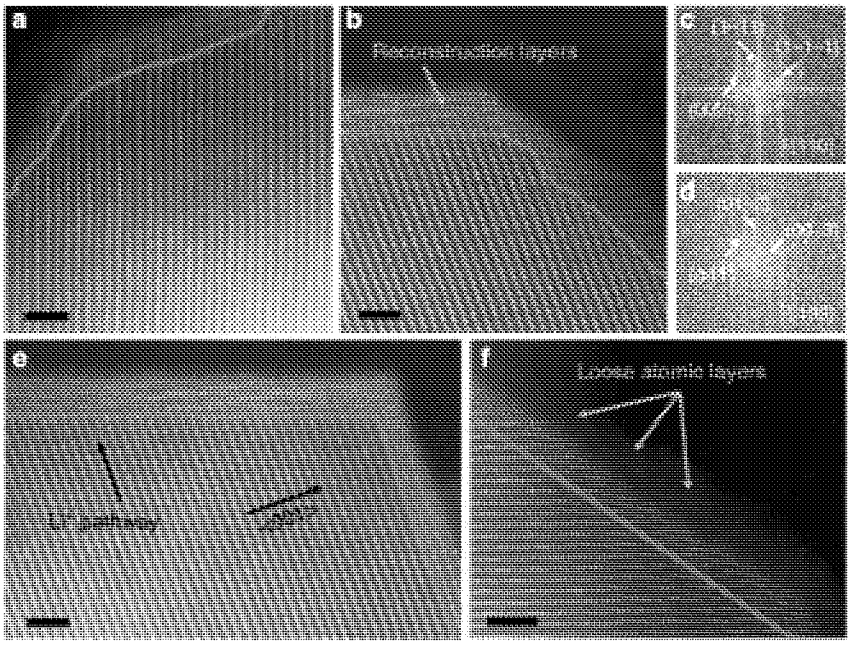


Figure 5 | Atomic resolution ADF-STEM images of NMC particles. (**a**) After electrolyte exposure (the exposure time is ~30 h, equivalent to the time used for one full cycle in this study). (**b**) After 1 cycle (2.0–4.7 V); the blue arrow indicates the surface reconstruction layer. (**c**,**d**) FFT results showing the surface reconstruction layer ($Fm\bar{3}m$ [110] zone axis) and the NMC layered structure ($R\bar{3}m$ [100] zone axis), respectively in (**b**). (**e**) Showing variation of the surface reconstruction layer thickness on orientation after 1 cycle (2.0–4.7 V). (**f**) Image showing loose atomic layers on an NMC particle, after 1 cycle (2.0–4.7 V). The blue lines indicate the boundaries between the NMC layered structure and surface reconstruction layer in all images. The scale bars are 2 nm in all images.

© 2014 Macmillan Publishers Limited. All rights reserved.
AMPEREX EX. 1002
Page 839

at surfaces with the sensitivity of a single atom. A surface reconstruction layer is readily observed after the electrolyte exposure experiment (Fig. 5a), where the blue line indicates the boundary between the NMC R$\bar{3}$m layered structure and the surface reconstruction layer. This instantaneously generated reconstruction layer adversely impacts the capacity and first-cycle coulombic efficiency. The thickness of the surface reconstruction layer increased after one complete cycle between 2.0–4.7 V (Fig. 5b) relative to that observed on the particle that was exposed to the electrolytic solution without electrochemical cycling (although the duration of the two experiments was identical). The observation visually validates our previous conclusion that this layer originated from dual effects involving both electrode–electrolyte reactivity and electrochemical activation. The crystal structure of the reconstruction layer consists primarily of an Fm$\bar{3}$m rock-salt structure (Fig. 5c,d), with a few atomic layers of spinel structure as a 'bridge' between the layered structure (containing Ni^{2+}, Mn^{4+} and Co^{3+}) and rock-salt structure (containing Ni^{2+}, Mn^{2+} and Co^{2+}). By analysing a large number of ADF-STEM images, we found that the surface reconstruction layer was greatly influenced by crystal orientations. Figure 5e shows a typical example of orientation-dependent surface reconstruction (more relevant images are available in Supplementary Fig. 16). Furthermore, reconstruction-poor and -rich surfaces are occasionally observed on the same NMC particle after cycling (Supplementary Fig. 16). Due to the random orientation of NMC particles on the electrode surfaces, surface-sensitive XAS spectroscopy (that is, AEY, TEY) yields an average of the electronic structures for reconstruction-poor and -rich surfaces, and thus the high-energy components of XAS/AEY and XAS/TEY are still present in the electrodes that have been cycled (Fig. 3c,d). In general, the thicker surface reconstruction layers are observed along the lithium diffusion channels relative to other orientations (for example, $\langle 001 \rangle$), suggesting that surface reconstruction is promoted by lithium removal during charging, and the reconstruction is more severe in the regions that undergo dynamic lithium transport. Interestingly, we also observed dangling layers (that is, loose atomic layers) of the cubic rock-salt structure (indicated by blue arrows in Fig. 5f) at the external surface of reconstruction layers. These loosely attached atomic layers are susceptible to dissolution into electrolytes and coincide with the suspected Mn^{2+} dissolution in a variety of Mn-containing cathodes[42–44]. It has been shown in Supplementary Fig. 15c that, after 20 high-voltage cycles, the discharge capacity could be nearly recovered at a slow rate (190 mAh g^{-1}, compared with the first-cycle discharge capacity of 210 mAh g^{-1}). Therefore, the transition metal dissolution accounts for a capacity loss of no more than 20 mAh g^{-1}.

Finally, we performed density functional theory (DFT) calculation for the formation energy of the rock-salt structure from the layered structure as a function of lithium concentration (Supplementary Fig. 17). Under oxygen partial pressure ranging from 10^{-12} atm to 1 atm, we found that after about 60% of lithium has been removed from the NMC structure, it becomes favourable to form the rock-salt structure (that is, negative formation energy). This supports the above results showing that the high-voltage cycling (that is, more lithium ions are removed) leads to a much more severe buildup of the surface reduced layer (that is, rock-salt structure). Our experimental results showed that the R$\bar{3}$m to Fm$\bar{3}$m transition primarily occurred at the surface and direct exposure to electrolytic solution assisted the kinetics of this phase transition.

Discussion

We correlated cycling performance with the observation of structural reconstruction and chemical evolution at the surfaces of stoichiometric NMC materials using statistically viable high-throughput ensemble-averaged XAS as well as spatially resolved EELS and atomically resolved ADF-STEM imaging. The structural reconstruction was directly evidenced by the changes in the transition metal oxidation states and the atomic packing, which were achieved by synchrotron XAS and ADF-STEM, respectively. Our findings show that the challenge of achieving stable high-voltage cycling of the NMC electrodes lies with structural and chemical metastability at the surfaces. Upon cycling and/or electrolyte exposure, the surfaces of NMC particles undergo progressive reconstruction (that is, lower transition metal oxidation states, Fig. 3a,b) from an R$\bar{3}$m–layered structure to an Fm$\bar{3}$m rock-salt structure in addition to the buildup of a complex SRL containing LiF and organic components (that is, chemical evolution). These observations provide new insights into the capacity degradation and impedance buildup in stoichiometric NMC materials undergoing high-voltage cycling conditions. Interestingly, the structural reconstruction at the surface is highly anisotropic, and primarily occurs along the lithium ion transport direction. This phenomenon would have been omitted without such a study at complementary length scales. This finding suggests that conformal protection coatings on certain orientations of NMC particles should be more beneficial than those on other orientations provided that the conformal coating is capable of inhibiting surface reconstruction and allows for efficient lithium diffusion.

Methods

Preparation of electrode materials. $LiNi_{0.4}Mn_{0.4}Co_{0.18}Ti_{0.02}O_2$ materials were synthesized using a co-precipitation method. For the synthesis of $LiNi_{0.4}Mn_{0.4}Co_{0.18}Ti_{0.02}O_2$, 250 ml of an aqueous solution of transition metal nitrates (0.16 M $Ni(NO_3)_2$, 0.16 M $Mn(NO_3)_2$, 0.072 M $Co(NO_3)_2$), 0.008 M $TiO(SO_4)\bullet xH_2O$ and 250 ml of 0.8 M LiOH aqueous solution were dripped simultaneously into a beaker using a Masterflex C/L peristaltic pump and stirred continuously. The precipitate was collected, filtered and washed with DI water, and then dried overnight at 100 °C in the oven. The dried precipitate was ball-milled with LiOH or Li_2CO_3 and then heated in air at 900 °C for 3 h with a ramp of 2 °C min^{-1}. The use of Li_2CO_3 led to smaller NMC particles than that of LiOH. In the main text and Supplementary Information, the small and large NMC particles represent the materials made with Li_2CO_3 and LiOH, respectively.

Coin cell preparation and electrochemical measurements. Composite electrodes were prepared with 84 wt% active material, 8 wt% polyvinylidene fluoride (Kureha Chemical), 4 wt% acetylene carbon black (Denka, 50% compressed) and 4 wt% SFG-6 synthetic graphite (Timcal, Graphites and Technologies) in *N*-methyl-2-pyrrolidinone and cast onto carbon-coated aluminium current collectors (Exopack Advanced Coatings (http://www.exopackadvancedcoatings.com) with typical active material loadings of 6–7 mg cm^{-2}. 2032 coin cells were assembled in a helium-filled glove box using the composite electrode as the positive electrode and Li metal as the negative electrode. A Celgard 2400 separator and 1 M $LiPF_6$ electrolyte solution in 1:2 w/w ethylene carbonate/dimethyl carbonate (Ferro Corporation) were used to fabricate the coin cells. Battery testing was performed on a computer controlled VMP3 potentiostat/galvanostat (BioLogic). 1C was defined as fully charging a cathode in 1 h, corresponding to a specific current density of 280 mA g^{-1}. Electrochemical impedance spectra were collected using a 10 mV AC signal ranging from 10 mHz to 100 kHz using this same instrument. The electrodes were removed from coin cells, rinsed with dimethyl carbonate and dried in a helium-filled glove box for further study. The electrodes were sealed under helium and then transferred to the synchrotron beamline using a homemade system to prevent air exposure. For electron microscopy and spectroscopy measurements, the electrode particles were scratched off and deposited onto TEM grids.

Materials characterization. X-ray diffraction (XRD) on powder samples was performed on a Bruker D2 Phaser diffractometer using CuKα radiation. Scanning electron microscopy (SEM) was performed on a JEOL JSM-7000F with a Thermo Scientific. EDS (energy dispersive X-ray spectroscopy) detector.

XAS measurements were performed on the 31-pole wiggler beamline 10-1 at Stanford Synchrotron Radiation Lightsource using a ring current of 350 mA and a 1,000 l mm^{-1} spherical grating monochromator with 20 μm entrance and exit slits, providing ~1011 ph s^{-1} at 0.2 eV resolution in a 1 mm^2 beam spot. During the measurements, all battery electrode samples were attached to an aluminium sample holder using conductive carbon. Data were acquired under ultrahigh vacuum

© 2014 Macmillan Publishers Limited. All rights reserved.
AMPEREX EX. 1002
Page 840

(10^{-9} Torr) in a single load at room temperature using TEY, AEY and FY. The sample drain current was collected for TEY. AEY was collected with a Cylindrical Mirror Analyzer using pass energy of 200 eV and a kinetic energy window of 2 eV near the main Auger for oxygen and nitrogen, respectively. A silicon diode (IRD AXUV-100) was used to collect the FY positioned near the sample surface. Contributions from visible light were carefully minimized before the acquisition, and all spectra were normalized by the current from freshly evaporated gold on a fine grid positioned upstream of the main chamber. XAS signals were collected at several positions on individual electrodes to ensure that data were representative of the sample.

A 200 keV and 300 keV probe-corrected field-emission scanning/transmission electron microscopes (S/TEM) were used for ADF-STEM imaging and spatially resolved EELS. Spectroscopic imaging was performed with an Enfina spectrometer on a Hitachi 2700C dedicated STEM.

Calculation method. The calculations were carried out using Kohn–Sham DFT with the projector augmented wave method, as implemented in the Vienna *ab initio* Simulation Package. For the exchange and correlation functional, we use a standard DFT + U framework with spin-dependent generalized gradient approximation of Perdew, Burke and Ernzerhof (PBE)[45–50]. The electron states were sampled using a k-point grid of $2 \times 2 \times 2$ centred at the origin. The electronic wave functions were expanded in a plane wave basis set with an energy cutoff of 500 eV, and the ionic positions were optimized until the forces on the ions were converged to 10 meV/Å. The layered NMC material was modelled employing 27 unit cells with a superstructure with space group $P3_112$, while the rock-salt structured used space group $Fm\bar{3}m$ employing the same configurational order for the cations as the NMC material. The generalized gradient approximation + U formalism developed by Dudarev *et al.*[51] was employed for the 3*d* electrons of each transition metal cation species. The values of these Hubbard-U parameters for Ni, Mn and Co were initially determined from previous computational work on Li intercalation compounds[52], and subsequently optimized by iteratively calculating the voltage profile as described by Meng and Dompablo[53], to the values of 5.5 eV, 7.0 eV and 5.0 eV, respectively.

In order to determine the relative stability of the layered versus rock-salt structure, the reaction free energy was calculated for the following reaction at different initial lithium concentrations.

$$2Li_x\left(Ni_{\frac{1}{3}}Co_{\frac{1}{3}}Mn_{\frac{1}{3}}\right)O_2 \rightarrow 2\left(Ni_{\frac{1}{3}}Co_{\frac{1}{3}}Mn_{\frac{1}{3}}\right)O + O_2 + 2xLi \qquad (1)$$

The Gibbs free energy for solid species were approximated by the zero temperature energies, neglecting vibrational contributions and assuming that the configurational disorder in the Ni, Co and Mn sublattice is frozen in at the temperatures of interest. For the oxygen molecule energy, the Gibbs free energy was computed using a standard '*ab initio* thermodynamics' formalism, in which the free energy is decomposed into three parts: (i) a zero temperature energy calculated from DFT, and corrected by an overbinding error as described in ref. 54 (ii) the zero-point energy of the oxygen molecule, (iii) finite temperature contributions arising from vibrational, translational and orientational motion, and taken from experimental measurements corresponding to a temperature of 298 K and a partial pressure of 1 atm[55], and (iv) a term $RT \ln p_{o_2}$ to account for variations of the oxygen partial pressure for 1 atm, 10^{-6} atm and 10^{-12} atm.

References

1. Bell, A. T. The impact of nanoscience on heterogeneous catalysis. *Science* **299,** 1688–1691 (2003).
2. Chen, M. S. & Goodman, D. W. The structure of catalytically active gold on titania. *Science* **306,** 252–255 (2004).
3. Cadigan, C. A. *et al.* Nanoscale (111) faceted rock-salt metal oxides in catalysis. *Catal. Sci. Technol.* **3,** 900–911 (2013).
4. Zheng, J. *et al.* Corrosion/fragmentation of layered composite cathode and related capacity/voltage fading during cycling process. *Nano Lett.* **13,** 3824–3830 (2013).
5. Boulineau, A., Simonin, L., Colin, J.-F., Bourbon, C. & Patoux, S. First evidence of manganese-nickel segregation and densification upon cycling in Li-Rich layered oxides for lithium batteries. *Nano Lett.* **13,** 3857–3863 (2013).
6. Toda, Y. *et al.* Activation and splitting of carbon dioxide on the surface of an inorganic electride material. *Nat. Commun.* **4,** 2378 (2013).
7. Chen, X., Liu, L., Yu, P. Y. & Mao, S. S. Increasing solar absorption for photocatalysis with black hydrogenated titanium dioxide nanocrystals. *Science* **331,** 746–750 (2011).
8. Doeff, M. M., Hu, Y., McLarnon, F. & Kostecki, R. Effect of surface carbon structure on the electrochemical performance of $LiFePO_4$. *Electrochem. Solid-State Lett.* **6,** A207–A209 (2003).
9. Stamenkovic, V. R., Mun, B. S., Mayrhofer, K. J. J., Ross, P. N. & Markovic, N. M. Effect of surface composition on electronic structure, stability, and electrocatalytic properties of Pt-transition metal alloys: Pt-skin versus Pt-skeleton surfaces. *J. Am. Chem. Soc.* **128,** 8813–8819 (2006).
10. Lu, X. *et al.* New insight into the atomic structure of electrochemically delithiated O3-$Li_{(1-x)}CoO_2$ ($0 \leq x \leq 0.5$) nanoparticles. *Nano Lett.* **12,** 6192–6197 (2012).
11. Jung, S.-K. *et al.* Understanding the degradation mechanisms of $LiNi_{0.5}Co_{0.2}Mn_{0.3}O_2$ cathode material in lithium ion batteries. *Adv. Energy Mater.* **4,** 1300787 (2014).
12. Leung, K. *et al.* Using atomic layer deposition to hinder solvent decomposition in lithium ion batteries: first-principles modeling and experimental studies. *J. Am. Chem. Soc.* **133,** 14741–14754 (2011).
13. Zhang, X. *et al.* Structural and electrochemical study of Al_2O_3 and TiO_2 coated $Li_{1.2}Ni_{0.13}Mn_{0.54}Co_{0.13}O_2$ cathode material using ALD. *Adv. Energy Mater.* **3,** 1299–1307 (2013).
14. Nam, K.-W. *et al.* Combining *in situ* synchrotron x-ray diffraction and absorption techniques with transmission electron microscopy to study the origin of thermal instability in overcharged cathode materials for lithium-ion batteries. *Adv. Funct. Mater.* **23,** 1047–1063 (2013).
15. Fell, C. R. *et al.* Correlation between oxygen vacancy, microstrain, and cation distribution in lithium-excess layered oxides during the first electrochemical cycle. *Chem. Mater.* **25,** 1621–1629 (2013).
16. Thackeray, M. M. *et al.* Li_2MnO_3-stabilized $LiMO_2$ (M = Mn, Ni, Co) electrodes for lithium-ion batteries. *J. Mater. Chem.* **17,** 3112–3125 (2007).
17. Xu, B., Fell, C. R., Chi, M. & Meng, Y. S. Identifying surface structural changes in layered Li-excess nickel manganese oxides in high voltage lithium ion batteries: a joint experimental and theoretical study. *Energy Environ. Sci.* **4,** 2223–2233 (2011).
18. Kam, K. C., Mehta, A., Heron, J. T. & Doeff, M. M. Electrochemical and physical properties of Ti-substituted layered nickel manganese cobalt oxide (NMC) cathode materials. *J. Electrochem. Soc.* **159,** A1383–A1392 (2012).
19. Kam, K. C. & Doeff, M. M. Aliovalent titanium substitution in layered mixed Li Ni–Mn–Co oxides for lithium battery applications. *J. Mater. Chem.* **21,** 9991–9993 (2011).
20. Yu, H. & Zhou, H. High-energy cathode materials (Li_2MnO_3–$LiMO_2$) for lithium-ion batteries. *J. Phys. Chem. Lett.* **4,** 1268–1280 (2013).
21. Mohanty, D. *et al.* Structural transformation of a lithium-rich $Li_{1.2}Co_{0.1}Mn_{0.55}Ni_{0.15}O_2$ cathode during high voltage cycling resolved by *in situ* X-ray diffraction. *J. Power Sources* **229,** 239–248 (2013).
22. Thackeray, M. M., Wolverton, C. & Isaacs, E. D. Electrical energy storage for transportation—approaching the limits of, and going beyond, lithium-ion batteries. *Energy Environ. Sci.* **5,** 7854–7863 (2012).
23. Armstrong, A. R. *et al.* Demonstrating oxygen loss and associated structural reorganization in the lithium battery cathode $Li[Ni_{0.2}Li_{0.2}Mn_{0.6}]O_2$. *J. Am. Chem. Soc.* **128,** 8694–8698 (2006).
24. Jiang, M., Key, B., Meng, Y. S. & Grey, C. P. Electrochemical and structural study of the layered, 'Li-Excess' lithium-ion battery electrode material $Li[Li_{1/9}Ni_{1/3}Mn_{5/9}]O_2$. *Chem. Mater.* **21,** 2733–2745 (2009).
25. Gu, M. *et al.* Formation of the spinel phase in the layered composite cathode used in Li-ion batteries. *ACS Nano* **7,** 760–767 (2013).
26. Tran, N. *et al.* Mechanisms associated with the 'plateau' observed at high voltage for the overlithiated $Li_{1.12}(Ni_{0.425}Mn_{0.425}Co_{0.15})_{0.88}O_2$ system. *Chem. Mater.* **20,** 4815–4825 (2008).
27. Wang, R. *et al.* Atomic structure of Li_2MnO_3 after partial delithiation and re-lithiation. *Adv. Energy Mater.* **3,** 1358–1367 (2013).
28. Chueh, W. C. *et al.* Intercalation pathway in many-particle $LiFePO_4$ electrode revealed by nanoscale state-of-charge mapping. *Nano Lett.* **13,** 866–872 (2013).
29. Harris, S. J. & Lu, P. Effects of inhomogeneities—nanoscale to mesoscale—on the durability of Li-Ion batteries. *J. Phys. Chem. C* **117,** 6481–6492 (2013).
30. Kerlau, M., Marcinek, M., Srinivasan, V. & Kostecki, R. M. Studies of local degradation phenomena in composite cathodes for lithium-ion batteries. *Electrochim. Acta* **52,** 5422–5429 (2007).
31. Lin, F. *et al.* Origin of electrochromism in high-performing nanocomposite nickel oxide. *ACS Appl. Mater. Interfaces* **5,** 3643–3649 (2013).
32. Lin, F. *et al.* Hole doping in Al-containing nickel oxide materials to improve electrochromic performance. *ACS Appl. Mater. Interfaces* **5,** 301–309 (2013).
33. Graetz, J., Ahn, C., Ouyang, H., Rez, P. & Fultz, B. White lines and d-band occupancy for the 3d transition-metal oxides and lithiumtransition-metal oxides. *Phys. Rev. B* **69,** 235103 (2004).
34. Van Veenendaal, M. & Sawatzky, G. Doping dependence of Ni 2p X-ray-absorption spectra of $M_xNi_{1-x}O$ (M = Li,Na). *Phys. Rev. B* **50,** 11326–11331 (1994).
35. Gilbert, B. *et al.* Multiple scattering calculations of bonding and X-ray absorption spectroscopy of manganese oxides. *J. Phys. Chem. A* **107,** 2839–2847 (2003).
36. Hy, S., Su, W.-N., Chen, J.-M. & Hwang, B.-J. Soft X-ray absorption spectroscopic and Raman studies on $Li_{1.2}Ni_{0.2}Mn_{0.6}O_2$ for lithium-ion batteries. *J. Phys. Chem. C* **116,** 25242–25247 (2012).
37. Yoon, W.-S. *et al.* Oxygen contribution on Li-Ion intercalation—deintercalation in $LiCoO_2$ investigated by O K-Edge and Co L-Edge X-ray absorption spectroscopy. *J. Phys. Chem. B* **106,** 2526–2532 (2002).
38. Hu, Z. *et al.* Hole distribution between the Ni 3d and O 2p orbitals in $Nd_{2-x}Sr_xNiO_{4-\delta}$. *Phys. Rev. B* **61,** 3739–3744 (2000).

© 2014 Macmillan Publishers Limited. All rights reserved.

AMPEREX EX. 1002
Page 841

39. Yoon, W.-S. *et al.* Investigation of the charge compensation mechanism on the electrochemically Li-Ion deintercalated $Li_{1-x}Co_{1/3}Ni_{1/3}Mn_{1/3}O_2$ electrode system by combination of soft and hard X-ray absorption spectroscopy. *J. Am. Chem. Soc.* **127,** 17479–17487 (2005).
40. Frazer, B. H., Gilbert, B., Sonderegger, B. R. & De Stasio, G. The probing depth of total electron yield in the sub-keV range: TEY-XAS and X-PEEM. *Surf. Sci.* **537,** 161–167 (2003).
41. Liang, Y. *et al.* Covalent hybrid of spinel manganese-cobalt oxide and graphene as advanced oxygen reduction electrocatalysts. *J. Am. Chem. Soc.* **134,** 3517–3523 (2012).
42. Aurbach, D. *et al.* Capacity fading of $Li_xMn_2O_4$ spinel electrodes studied by XRD and electroanalytical techniques. *J. Power Sources* **81,** 472–479 (1999).
43. Goodenough, J. B. & Kim, Y. Challenges for rechargeable Li Batteries. *Chem. Mater.* **22,** 587–603 (2010).
44. Zheng, H., Sun, Q., Liu, G., Song, X. & Battaglia, V. S. Correlation between dissolution behavior and electrochemical cycling performance for $LiNi_{1/3}Co_{1/3}Mn_{1/3}O_2$-based cells. *J. Power Sources* **207,** 134–140 (2012).
45. Blöchl, P. E. Projector augmented-wave method. *Phys. Rev. B* **50,** 17953–17979 (1994).
46. Kresse, G. & Furthmüller, J. Efficient iterative schemes for *ab initio* total-energy calculations using a plane-wave basis set. *Phys. Rev. B* **54,** 11169–11186 (1996).
47. Kresse, G. & Furthmüller, J. Efficiency of *ab initio* total energy calculations for metals and semiconductors using a plane-wave basis set. *Comp. Mater. Sci.* **6,** 15–50 (1996).
48. Kresse, G. & Hafner, J. *Ab initio* molecular dynamics for liquid metals. *Phys. Rev. B* **47,** 558–561 (1993).
49. Kresse, G. & Joubert, D. From Ultrasoft pseudopotentials to the projector augmented-wave method. *Phys. Rev. B* **59,** 1758–1775 (1999).
50. Perdew, J. P., Burke, K. & Ernzerhof, M. Generalized gradient approximation made simple. *Phys. Rev. Lett.* **77,** 3865–3868 (1996).
51. Dudarev, S. L., Botton, G. A., Savrasov, S. Y., Humphreys, C. J. & Sutton, A. P. Electron-energy-loss spectra and the structural stability of nickel oxide: an LSDA + U study. *Phys. Rev. B* **57,** 1505–1509 (1998).
52. Wang, L., Maxisch, T. & Ceder, G. Oxidation energies of transition metal oxides within the GGA + U framework. *Phys. Rev. B* **73,** 195107 (2006).
53. Meng, Y. S. & Dompablo, M. First principles computational materials design for energy storage materials in lithium ion batteries. *Energy Environ. Sci.* **2,** 589–609 (2009).
54. Zhou, F., Cococcioni, M., Marianetti, C. A., Morgan, D. & Ceder, G. First-principles prediction of redox potentials in transition-metal compounds with LDA + U. *Phys. Rev. B* **70,** 235121 (2004).
55. Rogal, J. & Reuter, K. in: *Experiment, Modeling and Simulation of Gas-surface Interactions for Reactive Flows in Hypersonic Flights, RTO-AVT-142, VKI Lecture Series* Ch. 2, 1–18. (Rhode St. Genèse, Belgium, 2006).

Acknowledgements

This work was supported by the Assistant Secretary for Energy Efficiency and Renewable Energy, Office of Vehicle Technologies of the U.S. Department of Energy under Contract No. DE-AC02-05CH11231 under the Batteries for Advanced Transportation Technologies (BATT) Program. The synchrotron X-ray portions of this research were carried out at the Stanford Synchrotron Radiation Lightsource, a Directorate of SLAC National Accelerator Laboratory and an Office of Science User Facility operated for the US Department of Energy Office of Science by Stanford University. S/TEM and EELS experiments were performed at the Center for Functional Nanomaterials, Brookhaven National Laboratory, which is supported by the US Department of Energy, Office of Basic Energy Sciences under Contract No. DE-AC02-98CH10886, and at National Center for Electron Microscopy (NCEM) of the Lawrence Berkeley National Laboratory (LBNL), which is supported by the US Department of Energy (DOE) under Contract No. DE-AC02-05CH11231. This work made use of computational resources provided by the National Energy Research Supercomputer Center (NERSC), which is supported by the Office of Science of the US Department of Energy under Contract DE-AC03-76SF00098 and the Extreme Science and Engineering Discovery Environment (XSEDE), which is supported by National Science Foundation grant number OCI-1053575. I.M.M. acknowledges the support of the NSF graduate research fellowship programme. H.L.X conducted a portion of the TEM work when he was a postdoctoral fellow in Dr. Haimei Zheng's group at LBNL. H.L.X. thanks Dr. Haimei Zheng for her full support and cordial advice on this project.

Author contributions

F.L., I.M.M., H.L.X. and M.M.D. participated in conceiving and designing the experiments. F.L. performed the materials syntheses, electrochemical measurements and prepared the samples for material characterization with assistance from I.M.M. F.L., I.M.M., D.N. and T.-C.W. performed the synchrotron X-ray absorption experiments. H.L.X. performed S/TEM and EELS experiments. I.M.M. performed DFT calculation under the supervision of M.A. F.L. prepared the figures and wrote the manuscript with assistance from all authors. M.M.D. supervised the project. All authors participated in discussions and know the implications of the work.

Additional information

Supplementary Information accompanies this paper at http://www.nature.com/naturecommunications

Competing financial interests: The authors declare no competing financial interests.

Reprints and permission information is available online at http://www.npg.nature.com/reprintsandpermissions/

How to cite this article: Lin, F. *et al.* Surface reconstruction and chemical evolution of stoichiometric layered cathode materials for lithium-ion batteries. *Nat. Commun.* 5:3529 doi: 10.1038/ncomms4529 (2014).

© 2014 Macmillan Publishers Limited. All rights reserved.

Focus Issue of Selected Presentations from IMLB 2014

Surface Structure and High-Voltage Charge/Discharge Characteristics of Al-Oxide Coated $LiNi_{1/3}Co_{1/3}Mn_{1/3}O_2$ Cathodes

Akira Yano,[a,z] Shigeo Aoyama,[a,c] Masahiro Shikano,[a] Hikari Sakaebe,[a,*,z] Kuniaki Tatsumi,[a,*] and Zempachi Ogumi[b,]**

[a]*Research Institute for Ubiquitous Energy Devices, National Institute of Advanced Industrial Science and Technology (AIST), Ikeda, Osaka 563–8577, Japan*
[b]*Office of Society-Academia Collaboration for Innovation, Kyoto University, Uji, Kyoto 611-0011, Japan*

A sol-gel method was used to fabricate Al-oxide coated $LiNi_{1/3}Co_{1/3}Mn_{1/3}O_2$ cathodes and their surface structure and high-voltage charge/discharge characteristics were evaluated with a view to their potential use in Li-ion batteries. Scanning transmission electron microscopy (STEM) revealed that a solid solution of $LiAlO_2$-$LiNi_{1/3}Co_{1/3}Mn_{1/3}O_2$ is uniformly formed to a depth of several nanometers from the surface of Al-oxide coated $LiNi_{1/3}Co_{1/3}Mn_{1/3}O_2$. Furthermore, the discharge capacity and average discharge voltage of Al-oxide coated $LiNi_{1/3}Co_{1/3}Mn_{1/3}O_2$ is equal to or higher than uncoated $LiNi_{1/3}Co_{1/3}Mn_{1/3}O_2$ at a charge voltage of 4.5 to 4.9 V. It was also found that the Al-oxide coating significantly improves the cycle performance at a charge voltage of 4.5 to 4.7 V. A substantial fade in capacity observed during the cycling of bare $LiNi_{1/3}Co_{1/3}Mn_{1/3}O_2$ is attributed to an increase in polarization due to an increased charge transfer resistance (R_{ct}), which is indicative of degradation of the interface between the electrode and electrolyte. However, this increase in polarization and R_{ct} is effectively suppressed in the Al-oxide coated $LiNi_{1/3}Co_{1/3}Mn_{1/3}O_2$. This can be explained by an inhibition of the formation of a rock-salt-structured phase in the surface region of bare $LiNi_{1/3}Co_{1/3}Mn_{1/3}O_2$ during cycling, as confirmed by STEM and electron energy loss spectrometry.
© The Author(s) 2015. Published by ECS. This is an open access article distributed under the terms of the Creative Commons Attribution Non-Commercial No Derivatives 4.0 License (CC BY-NC-ND, http://creativecommons.org/licenses/by-nc-nd/4.0/), which permits non-commercial reuse, distribution, and reproduction in any medium, provided the original work is not changed in any way and is properly cited. For permission for commercial reuse, please email: oa@electrochem.org. [DOI: 10.1149/2.0131502jes] All rights reserved.

Manuscript submitted September 12, 2014; revised manuscript received December 9, 2014. Published January 17, 2015. This was Paper 102 presented at the Como, Italy, Meeting of the IMLB, June 10–14, 2014. *This paper is part of the Focus Issue of Selected Presentations from IMLB 2014.*

With an increasing demand for high-capacity Li-ion batteries, layered rock-salt-structured materials such as $LiCoO_2$ and its derivatives show great promise for use as a cathode material by virtue of their high theoretical capacity of 270–280 mAh g^{-1}.[1–3] When used in commercial Li-ion batteries, however, the actual capacity is typically only about 60% of this theoretical capacity at most. Furthermore, the charge voltage is limited to no more than 4.4V (versus Li/Li^+), as the electrodes rapidly degrade due to the large quantity of Li that is deintercalated at higher charge voltage.

This destruction of the crystalline structure is particularly problematic in the case of $LiCoO_2$, as voltages above 4.5V can induce phase transitions from a rhombohedral structure to H1–3 and O1 phases.[4–6] Consequently, $LiNi_{1/3}Co_{1/3}Mn_{1/3}O_2$ presents a promising alternative to $LiCoO_2$ not just because of its lower cost, but also its high structural and thermal stability and high capacity.[7,8] Indeed, the fact that $LiNi_{1/3}Co_{1/3}Mn_{1/3}O_2$ can be charged to as high as 5.0 V without a phase transition[9] makes it particularly well suited to high-voltage use.

The degradation of electrode surfaces has received greatly increased attention over recent years, as it is now considered to be the major cause of capacity fade. Specifically, it has been reported that the surface structure of $LiCoO_2$ undergoes transformation to a tetrahedral spinel from a layered rock-salt structure during cycling.[10] Moreover, a rock-salt-structured-phase is typically formed near the surface of $LiNi_{0.8}Co_{0.2}O_2$, $LiNi_{0.8}Co_{0.15}Al_{0.05}O_2$, and $LiNi_{1/3}Co_{1/3}Mn_{1/3}O_2$ active materials.[11–13] In most of these studies, high resolution transmission electron microscopy (HR-TEM) was used to analyze the surface structure, this being a powerful analytical technique for directly identifying the atomic species present and their relative position within the crystal structure.[14,15]

The electrochemical stability of active materials can be improved by surface modification techniques such as applying a thin layer of an oxide, phosphate, or fluoride coating.[16–19] Al-based coatings such as Al_2O_3, $AlPO_4$, and $LiAlO_2$ are the most effective coating materials.[20–28] Although these Al-oxides exhibit poor electrical and ionic conductivity, the capacity fade during cycling at high voltages is significantly reduced, which means that durability of the active materials can be improved by its optimization. Recently, X-ray photoelectron spectrometry revealed that Al-based coatings form solid-solution interphases at the surface;[24–26] however, the detailed nature of their surface structure and mechanisms of Li-ion conductivity and capacity fade have not yet been fully evaluated. To solve the detailed nature, a technique of coating thin and uniform Al-oxides layer has been required.

Given this deficiency in the current understanding, this study examines the surface structure of an Al-oxide coated $LiNi_{1/3}Co_{1/3}Mn_{1/3}O_2$ electrode prepared by an original sol-gel method in fine detail by utilizing scanning electron microscopy (SEM), scanning transmission electron microscopy (STEM) with energy dispersive X-ray spectroscopy (EDX) and electron energy loss spectroscopy (EELS). In addition, we also investigate the effect of this Al-oxide coating on the electrochemical characteristics at a charge voltage excess of 4.5 V, and discuss the mechanisms of Li-ion conductivity and capacity fade in relation to its potential use in Li-ion batteries.

Experimental

Al-oxide coating.— The Al-oxide coating was applied by the sol-gel method, with a $LiNi_{1/3}Co_{1/3}Mn_{1/3}O_2$ powder with a particle diameter of 10 μm (Toda Kogyo Corp.) providing the active material. In this process, a heptanes solution containing Al-isopropoxide as a precursor and dipropylenglycol as a chelating agent was first mixed by stirring. By substituting the isopropoxide ligand of the precursor with dipropylenglycol, the subsequent hydrolysis reaction is homogenized and a uniform coating layer is formed. Into this solution the $LiNi_{1/3}Co_{1/3}Mn_{1/3}O_2$ powder was added, followed by $NH_3 \cdot H_2O$ (1 wt%). The resulting mixture was then dried at 80°C under vacuum to evaporate the solvents. Finally, the mixture was calcined at

*Electrochemical Society Active Member.
**Electrochemical Society Fellow.
[c]Present address: Hitachi Maxell, Ltd., Ibaraki, Osaka 567–8567, Japan
[z]E-mail: akira-yano@aist.go.jp; hikari.sakaebe@aist.go.jp

AMPEREX Ex. 1002

500°C for 2hr. The Al content was controlled at 0.5%, based on the assumption that the Al-oxide is present only as Al_2O_3.

Electrode and cell preparation.— Cathodes were prepared by first dissolving polyvinylidene fluoride (PVDF) in N-methyl-2-pyrrolidone (NMP) to act as a binder. A black, viscous slurry consisting of 90 wt% $LiNi_{1/3}Co_{1/3}Mn_{1/3}O_2$, 5 wt% acetylene black, and 5 wt% PVDF was then cast onto aluminum foils with a blade. The NMP was evaporated at 80°C for 1 h, with the electrodes then dried under vacuum at 120°C for 12 h. Once dry, the electrodes were punched to form 20 mm × 20 mm square samples that were used to fabricate laminated-type cells in a dry room (< −45°C dew point). Lithium metal foil, a polypropylene membrane (Celgard 2500), and 1 M of $LiPF_6$ dissolved in a 1:1:1 solution of ethylene carbonate (EC):dimethyl carbonate (DMC):ethyl methyl carbonate (EMC) were used as the negative electrode, the separator, and the electrolyte, respectively.

Electrochemical testing.— The initial charge/discharge performance was measured by the following procedure. First, the cell was charged to a maximum voltage (V_{max}) at a constant current density of 0.05 C (0.06 mA cm^{-2}), continued to be charged at V_{max} until the current tapered down to 0.005 C, and was then discharged down to 2.5 V at 0.05 C. This cycle was repeated three times. Following this assessment of initial performance, the cycle performance was measured by charging to V_{max} at 1 C, holding at V_{max} until the current tapered down to 0.1 C, and then discharging down to 2.5 V at 1 C. This cycle was repeated one hundred times. The cell was then tested after cycling using the same procedure as for the initial measurement. Here, 1 C was defined as 278mAh g^{-1}, which is the theoretical capacity of $LiNi_{1/3}Co_{1/3}Mn_{1/3}O_2$.

Finally, the Li-ion conductivity characteristics were studied by AC impedance spectroscopy (Solartron 1287 potentiostat) over a frequency range of 10^6 to 10^{-2} Hz. All electrochemical measurements were carried out at 20°C.

Structural characterization.— The surface structure of the bare and Al-oxide coated $LiNi_{1/3}Co_{1/3}Mn_{1/3}O_2$ was evaluated by SEM (JEOL, JSM7100F, 3kV) and by Cs-corrected STEM analysis (JEOL, JEM-ARM200F, 200 kV) with EDX (Thermo fisher scientific, NORAN System 7) and, EELS (Gatan, GIF Quantum). The samples for STEM analysis were prepared by focused ion-beam milling (FEI, Versa-3d, liquid-nitrogen cooled).

Results and Discussion

Structure of the Al-oxide coating layer.— Figure 1a shows typical SEM images of bare and Al-oxide-coated $LiNi_{1/3}Co_{1/3}Mn_{1/3}O_2$. No significant difference is discernible between these, with both clearly composed of primary particles no bigger than about 1 μm in diameter. Deposited materials are also scarcely observed on the coated $LiNi_{1/3}Co_{1/3}Mn_{1/3}O_2$ particles. Figure 1b shows EDX elemental maps of the Al-oxide coated $LiNi_{1/3}Co_{1/3}Mn_{1/3}O_2$, demonstrating that Al is uniformly distributed over the $LiNi_{1/3}Co_{1/3}Mn_{1/3}O_2$ particles.

Figure 2a and Fig. 2b show typical cross-sectional STEM-EDX maps and a concentration depth profile of the Al-oxide coated $LiNi_{1/3}Co_{1/3}Mn_{1/3}O_2$, respectively. In this, a continuous layer with a high concentration of Al can be seen to be formed from the surface to a depth of several nanometers. The concentration of Al is about 45 at% at the outermost surface, with Ni, Co and Mn all coexistent with Al; however, this Al concentration is continuously reduced with depth to a value of almost zero at 10 nm in depth. From these SEM and STEM-EDX results, it is evident that a thin coating layer is uniformly formed over the whole of surface of the Al-oxide coated $LiNi_{1/3}Co_{1/3}Mn_{1/3}O_2$.

Figure 3a shows a high-resolution, high-angle annular dark field (HAADF) STEM image of the Al-oxide coated $LiNi_{1/3}Co_{1/3}Mn_{1/3}O_2$. This reveals layers in which bright spots are arranged linearly alternating with dark layers in which this bright spot stacking is not observed. Since the brightness of HAADF spots are relative to atomic number, the bright layers indicate atomic columns of transition metals, whereas the dark layers are Li. Fast Fourier transform patterns of the surface area (FFT1) and inside area (FFT2) are also shown in the inset image in Fig. 3a. Both of these are consistent with the calculated electron diffraction pattern (Fig. 3b), assuming a [−1−10] zone axis for the $R\bar{3}m$ symmetry of an α-$NaFeO_2$ type structure.

These results indicate that a solid solution of $LiAlO_2$-$LiNi_{1/3}Co_{1/3}Mn_{1/3}O_2$ is formed within a region existing to a depth of several nanometers from the surface of Al-oxide coated $LiNi_{1/3}Co_{1/3}Mn_{1/3}O_2$.

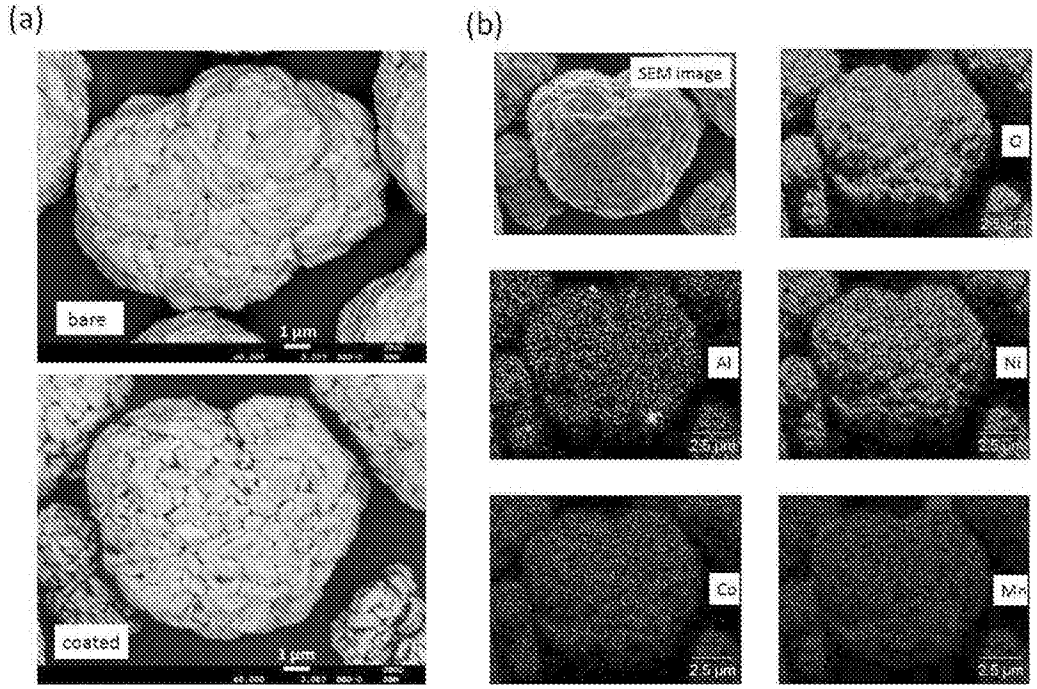


Figure 1. (a) SEM images of bare and Al-oxide coated $LiNi_{1/3}Co_{1/3}Mn_{1/3}O_2$. (b) EDX elemental maps of Al-oxide coated $LiNi_{1/3}Co_{1/3}Mn_{1/3}O_2$.

AMPEREX Ex. 1002
Page 844

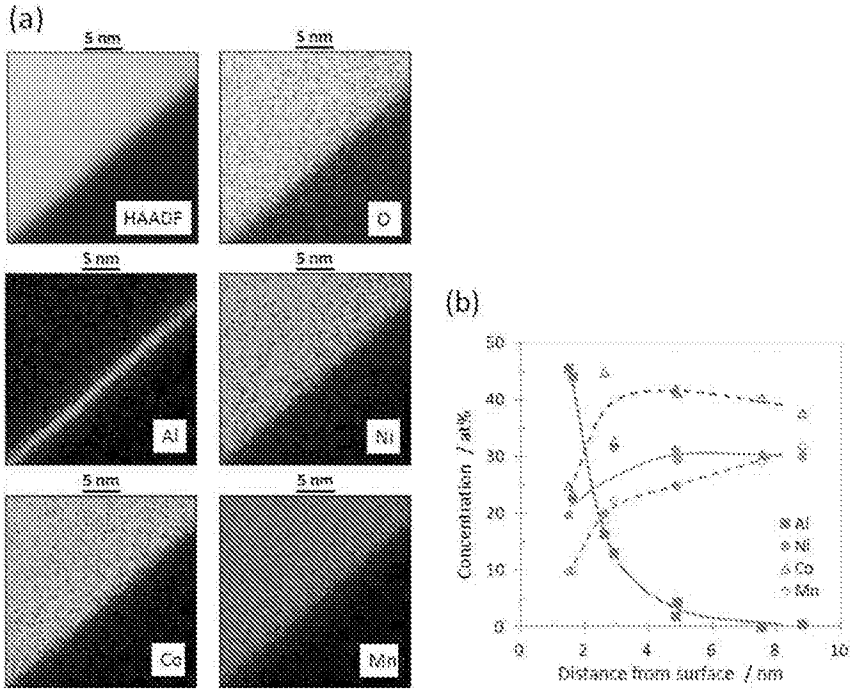


Figure 2. (a) Cross-sectional STEM-EDX maps and (b) concentration depth profile of Al-oxide coated $LiNi_{1/3}Co_{1/3}Mn_{1/3}O_2$.

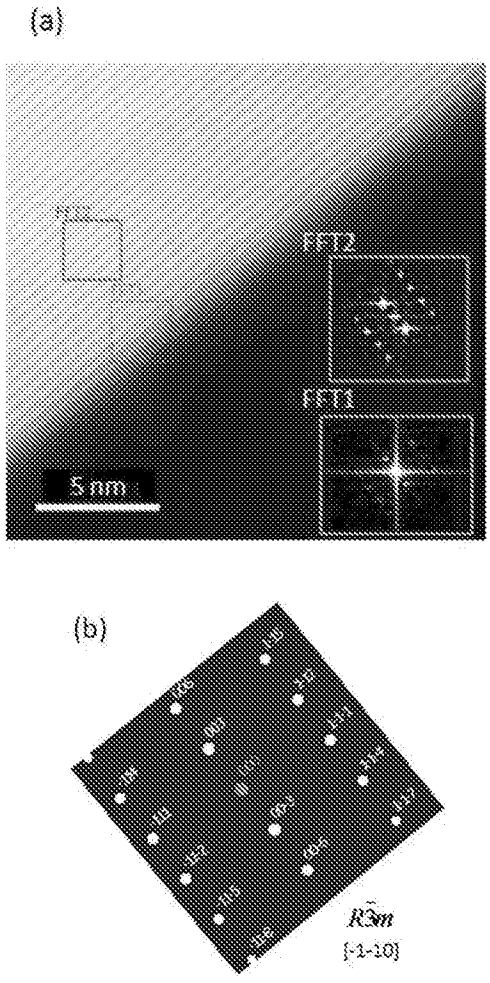


Figure 3. (a) High resolution STEM image of Al-oxide coated $LiNi_{1/3}Co_{1/3}Mn_{1/3}O_2$. The insets show fast Fourier transform patterns of a surface area (FFT1) and an inside area (FFT2). (b) Calculated electron diffraction pattern assuming a [-1-10] zone axis for the $R\bar{3}m$ symmetry.

This seems perfectly plausible given that Li-Al-oxide has the same $R\bar{3}m$ structure as α-$LiAlO_2$, and forms a solid solution between $LiAlO_2$ and $LiNiO_2$, or between $LiAlO_2$ and $LiCoO_2$.[29,30] Furthermore, the aforementioned formation of a solid solution of $LiAlO_2$-$LiNi_{1/3}Co_{1/3}Mn_{1/3}O_2$ at the surface ensures diffusion of Li-ions into the bulk through the Li sites of this solid solution.

Electrochemical characteristics.— Figure 4 shows the discharge capacity, Coulombic efficiency, and average discharge voltage for bare and Al-oxide coated $LiNi_{1/3}Co_{1/3}Mn_{1/3}O_2$ as a function of V_{max} following the first cycle. This demonstrates that the discharge capacity and average discharge voltage increase linearly as V_{max} is increased from 4.5 to 4.7 V, but plateaus above 4.8 V. Furthermore, the discharge capacity and average discharge voltage of the bare and Al-oxide coated $LiNi_{1/3}Co_{1/3}Mn_{1/3}O_2$ is almost equal within the range of 4.5 to 4.9 V. The values of the discharge capacity, average discharge voltage, and energy density at 4.7 V for Al-oxide coated $LiNi_{1/3}Co_{1/3}Mn_{1/3}O_2$ are 210 mAh g^{-1}, 3.98 V, and 834 Wh kg^{-1}, respectively. From this, we can see that the Coulombic efficiency decreases slightly as V_{max} is increased from 4.5 to 4.7 V, but decreases rapidly above 4.7V. The coulombic efficiency of Al-oxide coated $LiNi_{1/3}Co_{1/3}Mn_{1/3}O_2$ is slightly higher than that of bare $LiNi_{1/3}Co_{1/3}Mn_{1/3}O_2$.

Figure 5 shows the cycle performance of bare and Al-oxide coated $LiNi_{1/3}Co_{1/3}Mn_{1/3}O_2$ at a V_{max} of 4.5, 4.6, and 4.7 V. This demonstrates that the cycle performance is quite effectively improved by the Al-oxide coating regardless of V_{max}. Moreover, while the discharge capacity retention after 100 cycles at 4.5, 4.6, and 4.7 V of bare $LiNi_{1/3}Co_{1/3}Mn_{1/3}O_2$ is 25, 16, and 32%, respectively; the Al-oxide coated $LiNi_{1/3}Co_{1/3}Mn_{1/3}O_2$ achieves values of 98, 90, and 71%, respectively. It is also evident in Fig. 5 that the capacity during the initial cycle of Al-oxide coated $LiNi_{1/3}Co_{1/3}Mn_{1/3}O_2$ is higher than that of bare $LiNi_{1/3}Co_{1/3}Mn_{1/3}O_2$ at every value of V_{max}, the reason for which is discussed further on.

Figure 6 shows charge/discharge curves for a low current of 0.05 C before (i.e. the third cycle of the initial test) and after the cycle-test at V_{max} of 4.7 V. It should be noted that most of the capacity is recovered even for bare $LiNi_{1/3}Co_{1/3}Mn_{1/3}O_2$, the capacity of which decreased to 32% during cycle-testing. On the basis of this initial capacity, the capacity recovery rates of bare and Al-oxide coated $LiNi_{1/3}Co_{1/3}Mn_{1/3}O_2$ are 87 and 91%, respectively. However, in the case of bare $LiNi_{1/3}Co_{1/3}Mn_{1/3}O_2$, the charge/discharge curve

AMPEREX Ex. 1002
Page 845

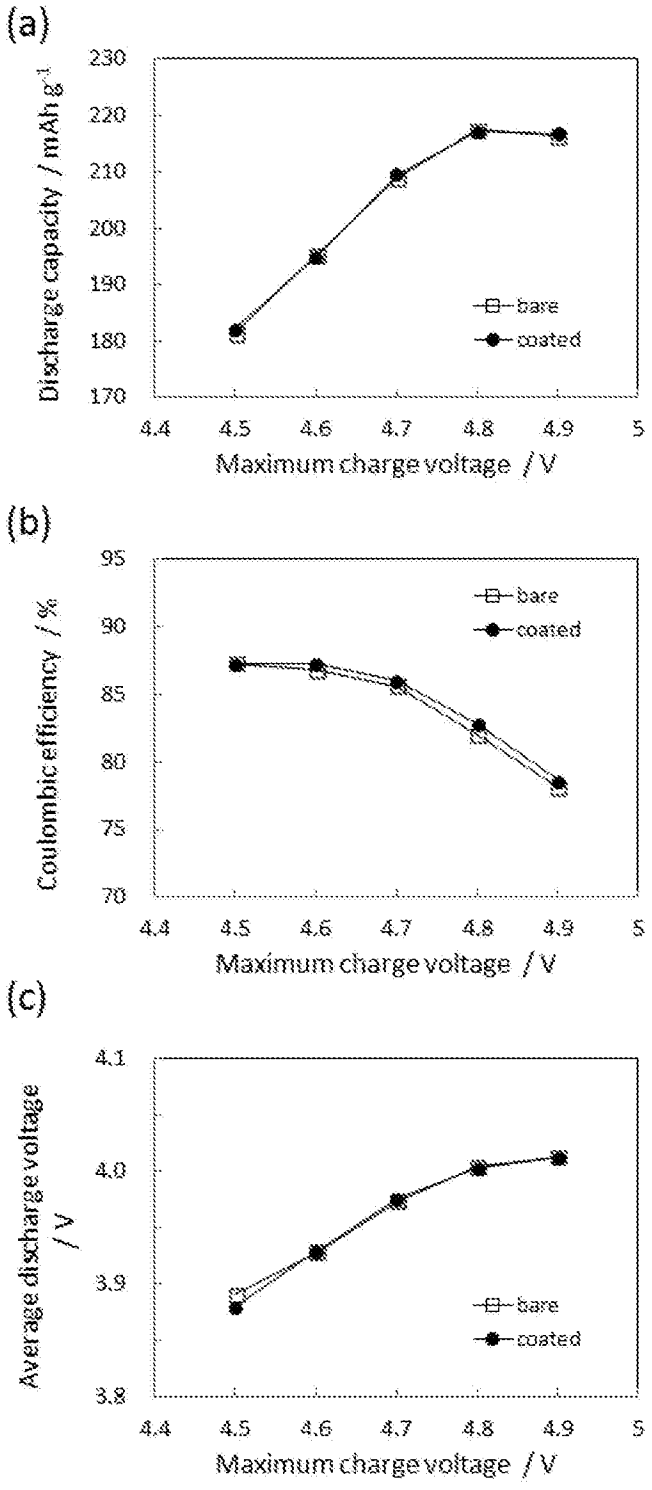


Figure 4. (a) Discharge capacity, (b) Coulombic efficiency, and (c) average discharge voltage for bare and Al-oxide coated $LiNi_{1/3}Co_{1/3}Mn_{1/3}O_2$ at the first cycle as a function of maximum charge voltage.

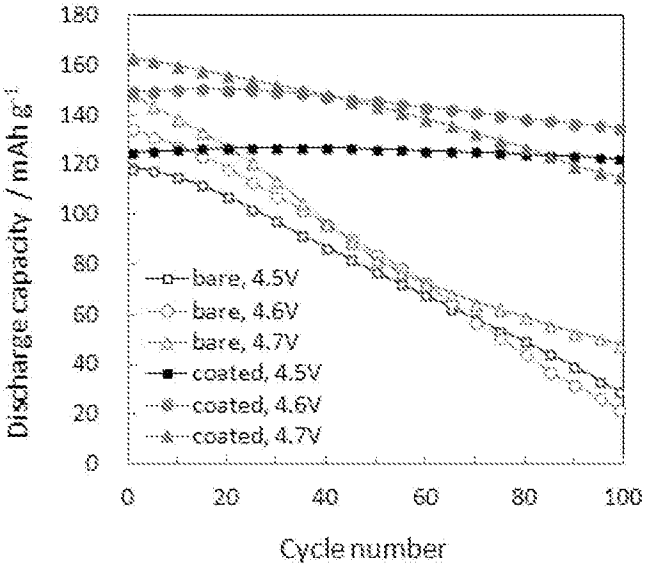


Figure 5. Cycle performance examined at maximum charge voltages of 4.5, 4.6, and 4.7 V for bare and Al-oxide coated $LiNi_{1/3}Co_{1/3}Mn_{1/3}O_2$.

after cycle-testing shows a substantially larger polarization. This indicates that a reduction in the depth of charge/discharge attributable to an increase in polarization causes the capacity fade during cycle-testing. In addition, most of the Li sites in the bulk of the bare $LiNi_{1/3}Co_{1/3}Mn_{1/3}O_2$ appear to be still active after the cycle-test, but the resistance of the Li-ion diffusion paths is markedly increased.

The impedance spectra dependence on electrode potential was measured to evaluate the resistance of Li-ion conductivity. Figure 7a shows Nyquist plots of bare $LiNi_{1/3}Co_{1/3}Mn_{1/3}O_2$ at various open circuit voltage (OCV) values prior to the cycle-test, in which two very different types of semicircle are observed. Those semicircles in the low frequency region, which have characteristic frequencies of 0.5 to 4 Hz, depend greatly on OCV; and, hence, they are attributed to charge transfer resistance.[31,32] In contrast, Figure 7b shows the Nyquist plots in the high frequency region, which hardly depend on OCV. Instead, the considerable distortion suggests the existence of plural resistance components. These high frequency semicircles are therefore attributed to the resistances of the Li negative electrode and the surface films of the $LiNi_{1/3}Co_{1/3}Mn_{1/3}O_2$ electrode.[32,33] Each resistance was quantitatively evaluated by fitting it with an equivalent circuit, as shown in Fig. 7c. In these equivalent circuits, R_{ct} represents the charge transfer resistance; whereas R_{f1} and R_{f2} correspond to the resistances of the highest and second highest frequency, respectively.

Figure 8a and Fig. 8b show R_{f1}, R_{f2} and, R_{ct} plotted against OCV for bare and Al-oxide coated $LiNi_{1/3}Co_{1/3}Mn_{1/3}O_2$ prior to cycle-testing. This demonstrates that R_{ct} is larger than R_{f1} and R_{f2} at the OCV value tested; whereas the minimum R_{ct} around 4 V, which is near to the average discharge voltage, is about 8 Ω for both the bare and coated $LiNi_{1/3}Co_{1/3}Mn_{1/3}O_2$. The Li-ion conductivity of Al-oxide coated $LiNi_{1/3}Co_{1/3}Mn_{1/3}O_2$ is also equivalent to that of bare $LiNi_{1/3}Co_{1/3}Mn_{1/3}O_2$. Figure 8c and Fig. 8d show the resistances of the bare and Al oxide coated $LiNi_{1/3}Co_{1/3}Mn_{1/3}O_2$ after the cycle-test, respectively. In this we see that although R_{f1} and R_{f2} show no significant change during the cycle-test, R_{ct} is increased for both the bare and coated $LiNi_{1/3}Co_{1/3}Mn_{1/3}O_2$. Of particular note, however, is that the minimum R_{ct} of the bare $LiNi_{1/3}Co_{1/3}Mn_{1/3}O_2$ is 406 Ω after the cycle-test, which is much larger than the 48 Ω of the Al-oxide coated $LiNi_{1/3}Co_{1/3}Mn_{1/3}O_2$. The large increase in polarization of the bare $LiNi_{1/3}Co_{1/3}Mn_{1/3}O_2$ after cycle-testing can therefore be explained by this increase in R_{ct}, which is suppressed in the coated $LiNi_{1/3}Co_{1/3}Mn_{1/3}O_2$. Moreover, since R_{ct} represents the transfer resistance of Li-ions and electrons at the interfaces between the electrode surface and electrolyte, this large increase in R_{ct} suggests that the interface is degraded.

The reason for R_{ct} showing minimum value at medium OCV region in Fig. 8 is explained as follows. The charge-transfer reaction at electrode/electrolyte interface is interpreted as the reaction expressed by the Butler-Volmer equation. According to this equation, charge transfer resistance R_{ct} and exchange current density i_0 are expressed

AMPEREX Ex. 1002
Page 846

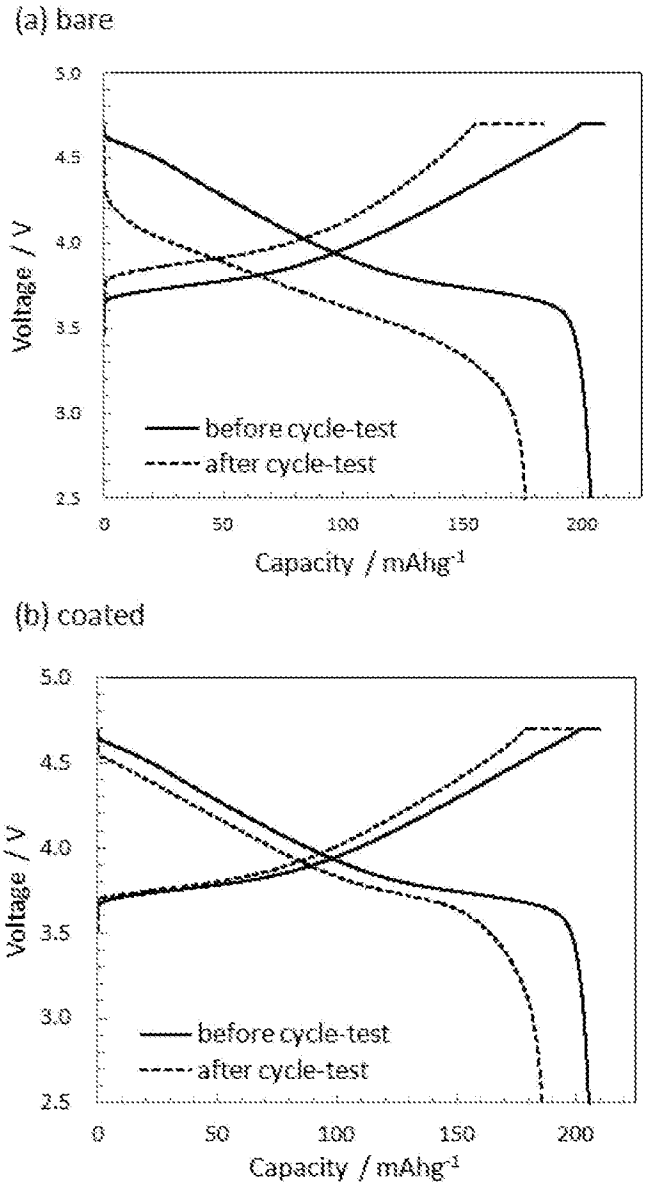


Figure 6. Charge/discharge curves at low current of 0.05 C before and after cycle-test at maximum charge voltage of 4.7V for (a) bare and (b) Al-oxide coated $LiNi_{1/3}Co_{1/3}Mn_{1/3}O_2$.

as shown below.

$$R_{ct} \propto \frac{1}{i_0} \quad [1]$$

$$i_0 \propto Fk \cdot x^{\alpha} \cdot \{(1-x)C_{Li}\}^{1-\alpha} \quad [2]$$

where F, k, x, $(1-x)$, $C_{Li,}$ and α are Faraday's constant, reaction rate constant, concentration of Li^+ in electrode, concentration of Li^+ vacancy in electrode, concentration of Li^+ in electrolyte, and a transference coefficient, respectively. In case of higher voltage limitation, x approaches to 0, that is, R_{ct} becomes larger. On the other hand, in the case of lower voltage limitation, $(1-x)$ is approaches to 0, then R_{ct} also becomes larger.

Figure 9 shows the R_{ct} values for bare and Al-oxide coated $LiNi_{1/3}Co_{1/3}Mn_{1/3}O_2$ in the high voltage region prior to the cycle-test. From this, we can see that the R_{ct} of bare $LiNi_{1/3}Co_{1/3}Mn_{1/3}O_2$ is greater than that of the coated $LiNi_{1/3}Co_{1/3}Mn_{1/3}O_2$ at 4.3 V, with this difference in R_{ct} increasing at higher voltage. This higher R_{ct} value in turn causes a greater IR-drop during charging, thus reducing

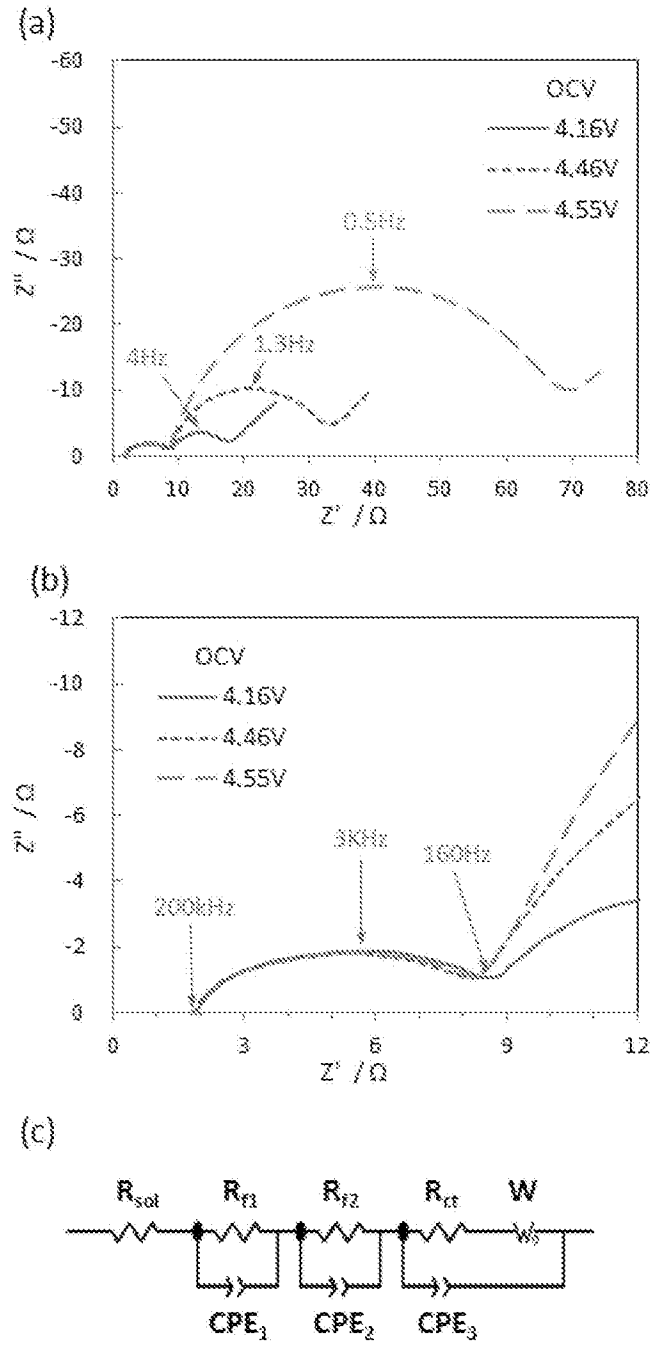


Figure 7. (a) Nyquist plots of bare $LiNi_{1/3}Co_{1/3}Mn_{1/3}O_2$ before cycle-test at various open circuit voltage. (b) Nyquist plots in high frequency region. (c) Equivalent circuit used for fitting.

the effective charge capacity. If we assume that the difference in R_{ct} at 4.7 V is 100 Ω, then the difference in IR-drop at 0.1 C (i.e., the cutoff current for the cycle-test) is estimated to about 0.05 V. This difference in the effective charge capacity during charging provides an explanation for the difference observed in the capacity of the bare and coated $LiNi_{1/3}Co_{1/3}Mn_{1/3}O_2$ during the initial cycle of testing (Fig. 5.) Meanwhile, the larger R_{ct} for bare $LiNi_{1/3}Co_{1/3}Mn_{1/3}O_2$ at high voltage suggests a greater structural change occurs at the interface between the electrode surface and electrolyte during charging when compared with coated $LiNi_{1/3}Co_{1/3}Mn_{1/3}O_2$.

Figure 10 shows a HAADF-STEM image of bare $LiNi_{1/3}Co_{1/3}Mn_{1/3}O_2$ discharged at a low rate of 0.05 C after the cycle-test. In this, a layered structure can be observed inside the $LiNi_{1/3}Co_{1/3}Mn_{1/3}O_2$;

AMPEREX Ex. 1002
Page 847

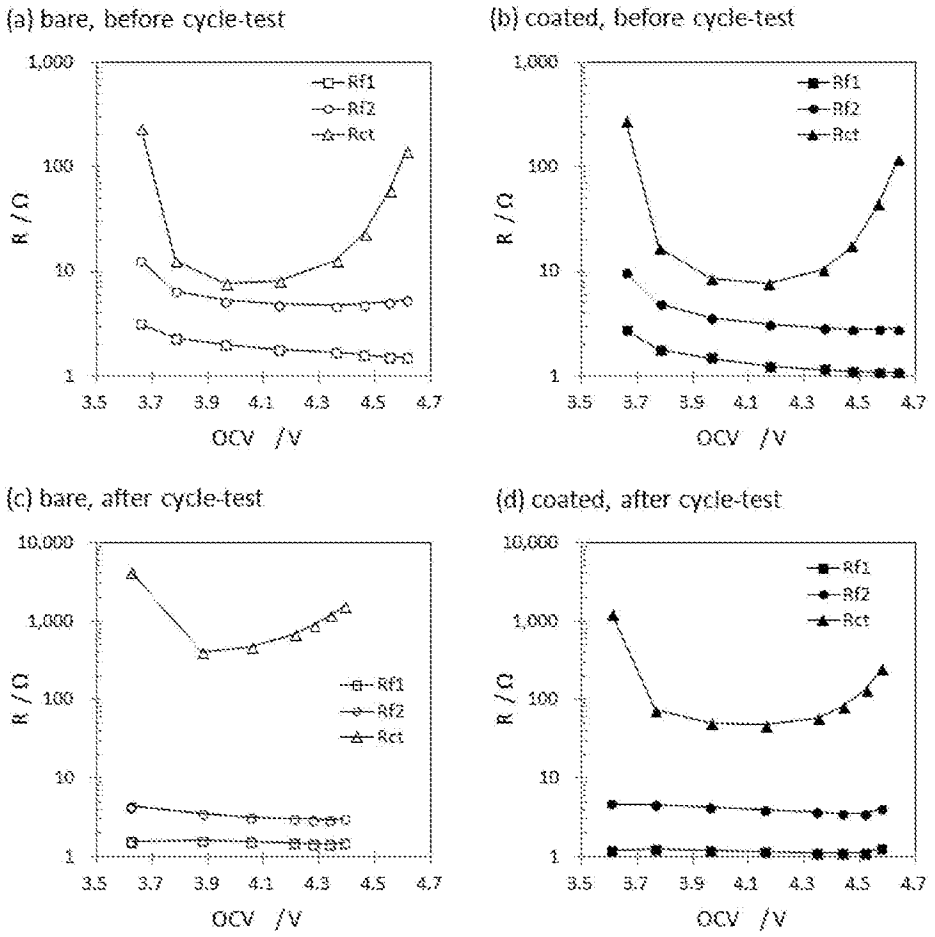


Figure 8. R_{f1}, R_{f2} and, R_{ct} plotted against OCV. (a) Bare and (b) Al-oxide coated $LiNi_{1/3}Co_{1/3}Mn_{1/3}O_2$ before cycle-test. (c) Bare and (d) Al oxide coated $LiNi_{1/3}Co_{1/3}Mn_{1/3}O_2$ after cycle-test.

however, the period of bright spots from the surface to a thickness of about 2 nm thick is about half that of the inside. Figure 11 shows EELS spectrum profiles (0.5nm pitch in depth) of Mn, Co and Ni, which correspond to the line shown in the inset in the Fig. 10. In the surface region where the layered structure changes, the peak positions of Mn and Co can be seen to shift to a lower energy by about 3 or 2 eV, respectively. This reveals that the expected discharge-state valences[34] of Mn^{4+} and Co^{3+} are actually more reduced at the surface.[35,36] This change in the layered structure and valence indicates the formation of a rock-salt-structured phase in the surface region. Since there is no diffusion path for Li-ions in the rock-salt-structure, this structural change results in a decrease in the number of sites at which the insertion of Li-ions can occur. Furthermore, the existence of this

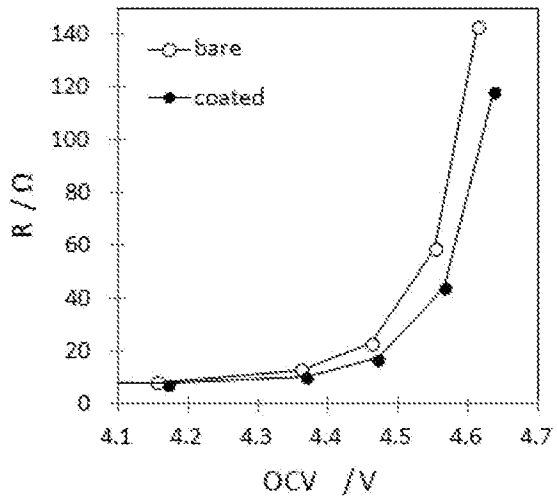


Figure 9. R_{ct} of bare and Al-oxide coated $LiNi_{1/3}Co_{1/3}Mn_{1/3}O_2$ in high voltage region before cycle-test.

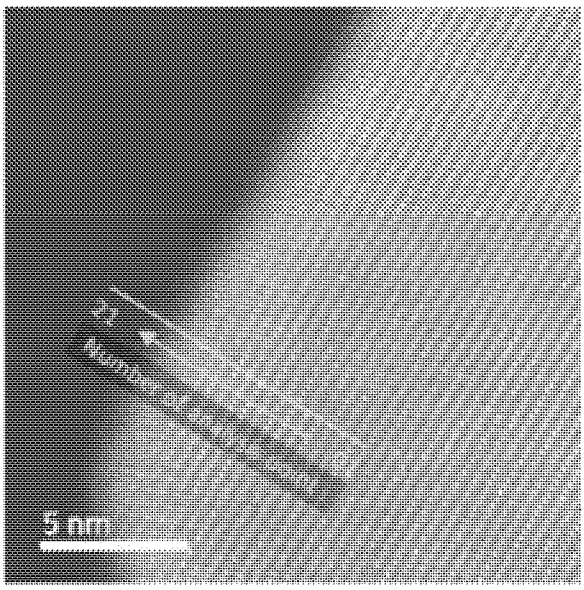


Figure 10. HAADF-STEM image of bare $LiNi_{1/3}Co_{1/3}Mn_{1/3}O_2$ discharged at low rate of 0.05 C after cycle-test.

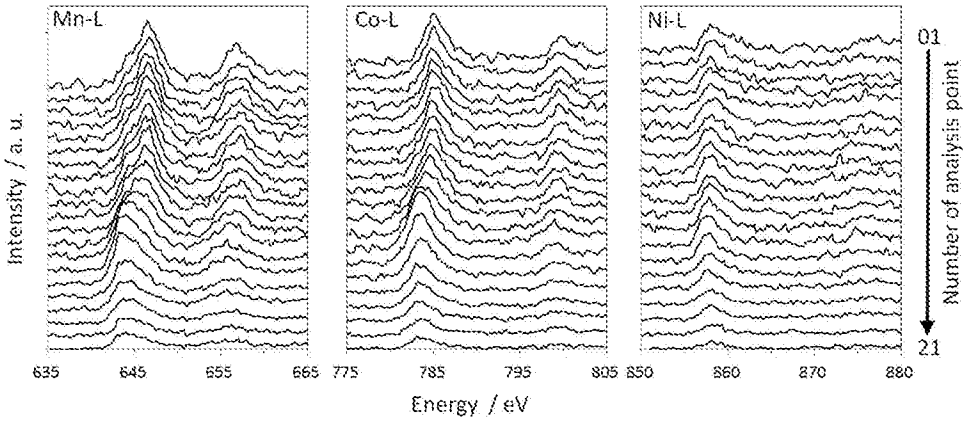


Figure 11. EELS spectrum profiles of bare $LiNi_{1/3}Co_{1/3}Mn_{1/3}O_2$ discharged at low rate of 0.05 C after cycle-test.

deteriorated phase may distort neighboring normal lattices, thereby inducing a large increase in R_{ct} and substantial capacity fade during cycle testing. This formation of a rock-salt-structured phase at the surface of degraded electrodes is in agreement with previous reports of other researchers.[11–13]

Using in-situ X-ray absorption spectroscopy and a thin-film $LiCoO_2$ electrode, Takamatsu et al. identified that Co at the surface of $LiCoO_2$ is reduced by immersion in organic electrolyte solution, and an irreversible structural change begins at the surface at the first charge/discharge.[37] Based on these findings and the above mentioned results, the mechanism of degradation and suppression is considered to be as follows. When $LiNi_{1/3}Co_{1/3}Mn_{1/3}O_2$ is charged at high voltage, most of the Li-ions are deintercalated and the majority of the transition metal (TM) cations are oxidized to tetravalent forms. These TM cations can easily move to the Li layers and TM-O phases of the rock-salt structure formed by the reduction of TM, the detachment of oxygen, and the oxidation of electrolyte as follows:

$$\text{Charge} : Li^{+}TM^{3+}O^{2-}{}_2 \rightarrow Li^{+} + e^{-} + V_L TM^{4+}O^{2-}{}_2 \qquad [3]$$

$$\text{Degradation} : V_L TM^{4+}O^{2-}{}_2 + E \rightarrow TM^{2+}O^{2-} + E^{2+}O^{2-} \qquad [4]$$

where V_L represents a vacancy in the Li layer and E is the electrolyte.

Conversely, since trivalent Al cations are electrochemically inactive it is difficult to detach both Li and oxygen from $LiAlO_2$, even with a high voltage charge.[29,38] Moreover, because Al shares O with TM as an octahedral coordination of MO_6 (where M is Al or TM) in a solid solution of $LiAlO_2$-$LiNi_{1/3}Co_{1/3}Mn_{1/3}O_2$, the detachment of O is suppressed. We therefore believe that the solid solution of $LiAlO_2$-$LiNi_{1/3}Co_{1/3}Mn_{1/3}O_2$ formed near the surface effectively suppress the destruction of the surface structure that typically occurs during charging, as shown by Formula (4). The structure of the Al-oxide coated $LiNi_{1/3}Co_{1/3}Mn_{1/3}O_2$ after cycle testing, and a detailed understanding of the mechanism of this suppression of degradation, are currently being investigated.

Acknowledgments

This work was supported by the "Research and Development Initiative for Scientific Innovation of New Generation Batteries (RISING project)" of the New Energy and Industrial Technology Development Organization (NEDO), Japan. The authors thank Yasuo Kikuzono for preparing the coating materials, Naomi Fukiya for the electrochemical measurements, and Taguchi Noboru for valuable discussions.

References

1. K. Mizushima, P. C. Jones, P. J. Wiseman, and J. B. Goodenough, *Materials Research Bulletin*, **15**(6), 783 (1980).
2. T. Ohzuku, A. Ueda, and M. Nagayama, *Journal of the Electrochemical Society*, **140**(7), 1862 (1993).
3. T. Ohzuku and A. Ueda, *Solid State Ionics*, **69**(3–4), 201 (1994).
4. A. Van der Ven, M. K. Aydinol, and G. Ceder, *Journal of the Electrochemical Society*, **145**(6), 2149 (1998).
5. Z. H. Chen, Z. H. Lu, and J. R. Dahn, *Journal of the Electrochemical Society*, **149**(12), A1604 (2002).
6. H. Xia, L. Lu, Y. S. Meng, and G. Ceder, *Journal of the Electrochemical Society*, **154**(4), A337 (2007).
7. T. Ohzuku and Y. Makimura, *Chemistry Letters*, (7), 642 (2001).
8. N. Yabuuchi and T. Ohzuku, *Journal of Power Sources*, **119**, 171 (2003).
9. N. Yabuuchi, Y. Makimura, and T. Ohzuku, *Journal of the Electrochemical Society*, **154**(4), A314 (2007).
10. H. F. Wang, Y. I. Jang, B. Y. Huang, D. R. Sadoway, and Y. T. Chiang, *Journal of the Electrochemical Society*, **146**(2), 473 (1999).
11. D. P. Abraham, R. D. Twesten, M. Balasubramanian, J. Kropf, D. Fischer, J. McBreen, I. Petrov, and K. Amine, *Journal of the Electrochemical Society*, **150**(11), A1450 (2003).
12. S. Muto, Y. Sasano, K. Tatsumi, T. Sasaki, K. Horibuchi, Y. Takeuchi, and Y. Ukyo, *Journal of the Electrochemical Society*, **156**(5), A371 (2009).
13. M. Shikano, H. Kobayashi, S. Koike, H. Sakaebe, Y. Saito, H. Hori, H. Kageyama, and K. Tatsumi, *Journal of Power Sources*, **196**(16), 6881 (2011).
14. S. J. Zheng, R. Huang, Y. Makimura, Y. Ukyo, C. A. J. Fisher, T. Hirayama, and Y. Ikuhara, *Journal of the Electrochemical Society*, **158**(4), A357 (2011).
15. N. Taguchi, T. Akita, H. Sakaebe, K. Tatsumi, and Z. Ogumi, *Journal of the Electrochemical Society*, **160**(11), A2293 (2013).
16. C. Li, H. P. Zhang, L. J. Fu, H. Liu, Y. P. Wu, E. Ram, R. Holze, and H. Q. Wu, *Electrochimica Acta*, **51**(19), 3872 (2006).
17. J. Cho, Y. J. Kim, and B. Park, *Journal of the Electrochemical Society*, **148**(10), A1110 (2001).
18. Z. H. Chen and J. R. Dahn, *Electrochimica Acta*, **49**(7), 1079 (2004).
19. B. C. Park, H. B. Kim, S. T. Myung, K. Amine, I. Belharouak, S. M. Lee, and Y. K. Sun, *Journal of Power Sources*, **178**(2), 826 (2008).
20. J. Cho, Y. J. Kim, and B. Park, *Chemistry of Materials*, **12**(12), 3788 (2000).
21. H. Cao, B. J. Xia, Y. Zhang, and N. X. Xu, *Solid State Ionics*, **176**(9), 911 (2005).
22. Y. Kim, H. S. Kim, and S. W. Martin, *Electrochimica Acta*, **52**(3), 1316 (2006).
23. Y. Y. Huang, J. T. Chen, F. Q. Cheng, W. Wan, W. Liu, H. H. Zhou, and X. X. Zhang, *Journal of Power Sources*, **195**(24), 8267 (2010).
24. A. T. Appapillai, A. N. Mansour, J. Cho, and Y. Shao-Horn, *Chemistry of Materials*, **19**(23), 5748 (2007).
25. S. Verdier, L. El Ouatani, R. Dedryvere, F. Bonhomme, P. Biensan, and D. Gonbeau, *Journal of the Electrochemical Society*, **154**(12), A1088 (2007).
26. L. DaheFron, R. Dedryvère, H. Martinez, D. Flahaut, M. Ménétrier, C. Delmas, and D. Gonbeau, *Chemistry of Materials*, **21**(23), 5607 (2009).
27. G. T. K. Fey, C. S. Chang, and T. P. Kumar, *Journal of Solid State Electrochemistry*, **14**(1), 17 (2010).
28. L. A. Riley, S. Van Ana, A. S. Cavanagh, Y. F. Yan, S. M. George, P. Liu, A. C. Dillon, and S. H. Lee, *Journal of Power Sources*, **196**(6), 3317 (2011).
29. T. Ohzuku, A. Ueda, and M. Kouguchi, *Journal of the Electrochemical Society*, **142**(12), 4033 (1995).
30. Y. I. Jang, B. Y. Huang, H. F. Wang, D. R. Sadoway, G. Ceder, Y. M. Chiang, H. Liu, and H. Tamura, *Journal of the Electrochemical Society*, **146**(3), 862 (1999).

31. D. Aurbach, M. D. Levi, E. Levi, H. Teller, B. Markovsky, G. Salitra, U. Heider, and L. Heider, *Journal of the Electrochemical Society*, **145**(9), 3024 (1998).
32. M. D. Levi, G. Salitra, B. Markovsky, H. Teller, D. Aurbach, U. Heider, and L. Heider, *Journal of the Electrochemical Society*, **146**(4), 1279 (1999).
33. P. G. Bruce and M. Y. Saidi, *Journal of Electroanalytical Chemistry*, **322**(1–2), 93 (1992).
34. A. Deb, U. Bergmann, S. P. Cramer, and E. J. Cairns, *Journal of Applied Physics*, **97**(11), (2005).
35. D. B. Loomer, T. A. Al, L. Weaver, and S. Cogswell, *American Mineralogist*, **92**(1), 72 (2007).
36. Y. A. Zhao, T. E. Feltes, J. R. Regalbuto, R. J. Meyer, and R. F. Klie, *Journal of Applied Physics*, **108**(6), 063704 (2010).
37. D. Takamatsu, Y. Koyama, Y. Orikasa, S. Mori, T. Nakatsutsumi, T. Hirano, H. Tanida, H. Arai, Y. Uchimoto, and Z. Ogumi, *Angewandte Chemie- International Edition*, **51**(46), 11597 (2012).
38. M. Guilmard, A. Rougier, A. Grune, L. Croguennec, and C. Delmas, *Journal of Power Sources*, **115**(2), 305 (2003).

Journal of The Electrochemical Society, **163** (2) A75-A82 (2016)
0013-4651/2016/163(2)/A75/8/$33.00 © The Electrochemical Society

Surface Structure and High-Voltage Charging/Discharging Performance of Low-Content Zr-Oxide-Coated $LiNi_{1/3}Co_{1/3}Mn_{1/3}O_2$

Akira Yano,[a,z] Atsushi Ueda,[a,*,c] Masahiro Shikano,[a] Hikari Sakaebe,[a,*,z] and Zempachi Ogumi[b,]**

[a]*Research Institute of Electrochemical Energy, National Institute of Advanced Industrial Science and Technology (AIST), Ikeda, Osaka 563-8577, Japan*
[b]*Office of Society-Academia Collaboration for Innovation, Kyoto University, Uji, Kyoto 611-0011, Japan*

The surface structures, high-voltage charging/discharging performances, and Li-ion transfer at the electrode/electrolyte interface of $LiNi_{1/3}Co_{1/3}Mn_{1/3}O_2$ coated with small amounts of Zr oxide by the sol-gel method were investigated. Island-like ZrO_2 grains as well as grain-free (sea-like) zones were observed on the surfaces of the coated $LiNi_{1/3}Co_{1/3}Mn_{1/3}O_2$ samples. The ratio of the area of these sea-like zones to the total surface area of the $LiNi_{1/3}Co_{1/3}Mn_{1/3}O_2$ sample increased from 44 to 85% when the Zr oxide content was decreased from 1.0 to 0.125 wt%. A compound oxide phase containing Zr, Ni, Co, and Mn was formed uniformly on the sea-like zones; the depth of this phase was approximately 2 nm. The initial discharge capacities of the coated $LiNi_{1/3}Co_{1/3}Mn_{1/3}O_2$ samples were equal to that of bare $LiNi_{1/3}Co_{1/3}Mn_{1/3}O_2$. Further, the cycling performances of the coated $LiNi_{1/3}Co_{1/3}Mn_{1/3}O_2$ samples were significantly higher, as were their discharge capacities and discharge voltages, while their charge-transfer resistances (R_{ct}) were lower. It was also found that the coated $LiNi_{1/3}Co_{1/3}Mn_{1/3}O_2$ samples had lower activation energies (E_a) for charge transfer than the bare $LiNi_{1/3}Co_{1/3}Mn_{1/3}O_2$. Thus, it can be surmised that the area and structure of the sea-like zones determined the R_{ct} and E_a values and cycling performances of the coated $LiNi_{1/3}Co_{1/3}Mn_{1/3}O_2$ samples.
© 2015 The Electrochemical Society. [DOI: 10.1149/2.0211602jes] All rights reserved.

Manuscript submitted September 4, 2015; revised manuscript received October 21, 2015. Published November 5, 2015.

With the demand for high-energy-density Li-ion batteries increasing, it has become necessary to develop positive electrode materials that exhibit superior performances. Layered rock-salt-like active materials such as $LiCoO_2$ and its derivatives have a theoretical capacity as high as 270–280 mA h g^{-1} and an average discharging voltage of approximately 4 V.[1–3] However, their actual capacity in commercial Li-ion batteries is typically limited to approximately 60% of their theoretical capacity, while their charging voltage is no more than 4.4 V (versus Li/Li^+). This is because the electrodes rapidly degrade at higher charging voltages. Of the various layered rock-salt-like materials available, $LiNi_{1/3}Co_{1/3}Mn_{1/3}O_2$ is one of the most promising ones for use at high voltages, owing to its highly stable crystal structure, which results in high electrochemical and thermal stability.[4,5] For instance, $LiNi_{1/3}Co_{1/3}Mn_{1/3}O_2$ can be charged to voltages as high as 5.0 V without undergoing a phase transition.[6]

In addition to the stability of the bulk of the active material, the stability of the interface between the electrode and the electrolyte is also of great importance. It has been reported that the surface structure of $LiCoO_2$ changes from layered rock-salt-like to tetrahedral spinel-like during cycling.[7] Moreover, a rock-salt-like phase with a NaCl-type structure is typically formed near the surfaces of the active materials $LiNi_{0.8}Co_{0.2}O_2$, $LiNi_{0.8}Co_{0.15}Al_{0.05}O_2$, and $LiNi_{1/3}Co_{1/3}Mn_{1/3}O_2$.[8–11] It is thus believed that the degradation of this electrode/electrolyte interface is the primary cause of capacity fading.

Surface coatings are often deposited on active materials in order to prevent the degradation of the electrode/electrolyte interface. Various kinds of coating materials have been studied, such as oxides, phosphates, and fluorides.[12–17] Zr-based oxides are one of the most effective coating materials.[18–24] However, their surface structures and the effects of their structure on Li-ion transfer at the electrode/electrolyte interface have not yet been elucidated. This is because analyzing the surface structure of powdered active materials with micrometer-size particles is difficult and because the reaction that occurs at the electrode/electrolyte interface is a complex one. Recently, to overcome these issues, Zr oxide coatings deposited on thin-film electrodes or on active materials with nanometer-sized particles have been analyzed. It has been reported that the surface region extending to a depth of several atomic layers play an intrinsic role in the charge/discharge reaction.[25,26] However, additional studies based on practical electrodes consisting of powdered active materials are needed.

Generally, in the case of Zr oxide coatings, because the Zr cations do not readily diffuse into the active material, the Zr oxide particles are deposited on the surface of the active material.[19–21,24] Since Zr oxide in itself exhibits poor electrical and ionic conductivities, when it is deposited as a coating in a large amount, the Li-ion transfer resistance between the electrode and the electrolyte increases. Coatings with a lower Zr oxide content are preferable in this regard. On the other hand, lowering the amount of Zr oxide in the coating can cause the coating to become nonuniform. Thus, to achieve high-performance coatings, it is necessary that uniform coatings are formed using the optimal amount of Zr oxide.

In a previous study, we had used the sol-gel method to deposit an Al oxide coating on $LiNi_{1/3}Co_{1/3}Mn_{1/3}O_2$. We could obtain a uniform coating that extended to a depth of several nanometers from the surface. Further, the coating effectively suppressed the cycling-related degradation of the underling active material even at 4.7 V.[13] In this study, we attempted to form a uniform coating of Zr oxide on $LiNi_{1/3}Co_{1/3}Mn_{1/3}O_2$ using the sol-gel method, while keeping the Zr oxide content as low as possible, in order to ensure that the performance of the coated material was high. We examined the surface structures of the Zr-oxide-coated $LiNi_{1/3}Co_{1/3}Mn_{1/3}O_2$ samples in detail by using scanning electron microscopy (SEM) and scanning transmission electron microscopy (STEM) in combination with energy-dispersive X-ray spectroscopy (EDX). In addition, we also investigated the effects of the Zr oxide coating on the charging/discharging performance of the active material at a charging voltage of 4.6 V. Finally, we discuss the mechanisms determining the transfer of Li ions at the electrode/electrolyte interface on the basis of the results of an electrochemical impedance analysis.

Experimental

Sample preparation.— The Zr oxide coating was formed using the sol-gel method.[11] A $LiNi_{1/3}Co_{1/3}Mn_{1/3}O_2$ powder with a secondary particle diameter of 10 μm (Toda Kogyo Corp.) was used as the active material. Zr tetrapropoxide and dipropylenglycol were used as the precursor and the chelating agent, respectively. By substituting the isopropoxide ligand of the precursor with dipropylenglycol, a homogenous hydrolysis reaction was made to occur during the sol-gel process; this resulted in the formation of a uniform coating. The

*Electrochemical Society Active Member.
**Electrochemical Society Fellow.
[c]Present address: Hitachi Maxell, Ltd., Ibaraki, Osaka 567–8567, Japan.
[z]E-mail: akira-yano@aist.go.jp; hikari-sakaebe@aist.go.jp

AMPEREX Ex. 1002
Page 851

sol-gel-coated $LiNi_{1/3}Co_{1/3}Mn_{1/3}O_2$ samples were calcined at 500°C for 2 h. Based on the assumption that the only Zr oxide present was ZrO_2, it was determined that the Zr oxide content was 0.125–1.0 wt%.

Positive electrodes were fabricated using a mixture of 90 wt% $LiNi_{1/3}Co_{1/3}Mn_{1/3}O_2$, 5 wt% acetylene black, and 5 wt% polyvinylidene fluoride. The electrodes were punched to form squares with dimensions of 20 mm × 20 mm, which were used to fabricate pouch cells. Lithium metal foil, a polypropylene membrane (Celgard 2500), and 1 M of $LiPF_6$ dissolved in a 1:2 (vol%) solution of ethylene carbonate (EC)/diethyl carbonate (DEC) were used as the negative electrode, the separator, and the electrolyte, respectively.

Electrochemical testing.— To evaluate the initial charging/discharging performance of the fabricated cells, the cells were charged to 4.6 V at a constant current density of 0.05 C (0.08 mA cm^{-2}); they were charged to 4.6 V until the current tapered down to 0.005 C. They were then discharged to 2.5 V at 0.05 C. Following this initial charging/discharging cycle, the cycle performances were measured by charging the cells to 4.6 V at 1 C, holding them at 4.6 V until the current tapered to 0.1 C, and then discharging them to 2.5 V at 1 C. This cycle was repeated 100 times. Here, 1 C was defined as 278 mA h g^{-1}, which is the theoretical capacity of $LiNi_{1/3}Co_{1/3}Mn_{1/3}O_2$.

The transfer of Li ions at the electrode/electrolyte interface was studied using alternating current impedance spectroscopy (Solartron 1287 potentiostat) for frequencies ranging from 10^6 to 10^{-2} Hz. The dependency of the Li-ion transfer resistance on the electrode potential and temperature was evaluated. Before performing the impedance measurements, the cell voltages were changed to the desired values and the cells were relaxed in the open-circuit mode for 1 h. All the electrochemical measurements, except those related to the temperature dependency of the Li-ion transfer resistance, were performed at 25°C. Other details are mentioned in the Results and discussion section.

Structural characterization.— The surface structures of the Zr-oxide-coated $LiNi_{1/3}Co_{1/3}Mn_{1/3}O_2$ samples were evaluated using SEM (Hitachi, S-4800, 1.5 kV), SEM/EDX (JEOL, JSM7100F, 3 kV), and spherical aberration corrected (Cs)-STEM (JEOL, JEM-ARM200F, 200 kV) in combination with EDX (Thermo Fisher Scientific, NORAN System 7). The samples for the STEM analysis were prepared using focused ion-beam milling (FEI, Versa-3D, liquid-nitrogen cooled).

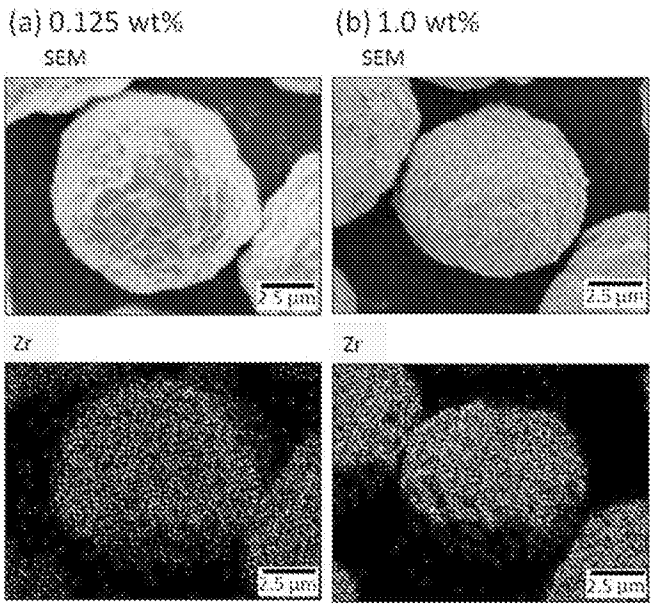


Figure 1. Low-magnification SEM images and EDX maps of Zr-oxide-coated $LiNi_{1/3}Co_{1/3}Mn_{1/3}O_2$ particles with Zr oxide content of (a) 0.125 and (b) 1.0 wt%.

Results and Discussion

SEM analysis.— Figure 1 shows low-magnification SEM images and the corresponding EDX maps of the Zr-oxide-coated $LiNi_{1/3}Co_{1/3}Mn_{1/3}O_2$ samples with Zr oxide contents of 0.125 and 1.0 wt%. Zr was uniformly distributed over the secondary particles of both $LiNi_{1/3}Co_{1/3}Mn_{1/3}O_2$ samples.

Figure 2a shows mid-magnification SEM images of the Zr-oxide-coated $LiNi_{1/3}Co_{1/3}Mn_{1/3}O_2$ samples with Zr oxide contents of 0.125, 0.25, 0.5, and 1.0 wt%. Primary particles of $LiNi_{1/3}Co_{1/3}Mn_{1/3}O_2$ with diameters in the submicron range and the coating deposited on these particles can be observed. The deposited material was distributed uniformly over the primary particles in the case of all the samples. Figure 2b show high-magnification SEM images of these samples. The deposited coatings consisted of island-like grains 10–20 nm in diameter; further, areas over which the coatings were not deposited (i.e., the sea-like zones) were also observed. With a decrease in the Zr oxide content, the amount of the island-like grains decreased, while the sea-like zones increased in size. The results of X-ray diffraction and STEM analyses indicated that these island-like grains were crystals of ZrO_2 and did not contain Li, as shown in Supporting Information.

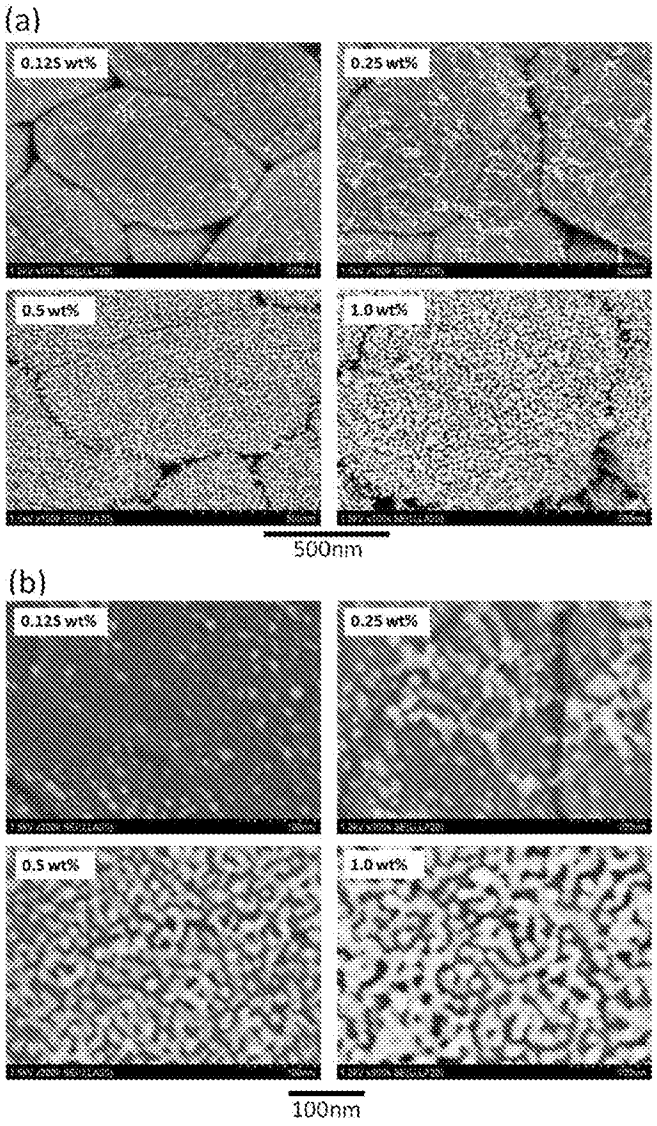


Figure 2. SEM images of Zr-oxide-coated $LiNi_{1/3}Co_{1/3}Mn_{1/3}O_2$ with Zr oxide content of 0.125, 0.25, 0.5, and 1.0 wt%. (a) Mid-magnification (100k) and (b) high-magnification (300k) images.

AMPEREX Ex. 1002
Page 852

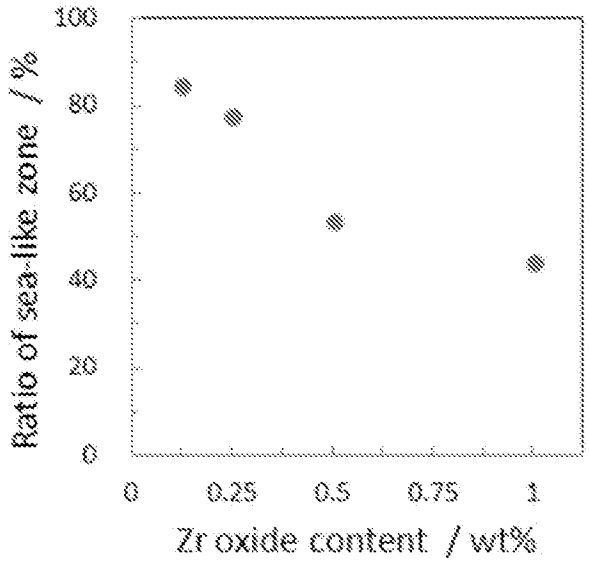


Figure 3. Ratio of sea-like zone of Zr-oxide-coated $LiNi_{1/3}Co_{1/3}Mn_{1/3}O_2$ as a function of Zr oxide content.

Since ZrO_2 crystals exhibit very poor Li-ion conductivity, it can be assumed that sea-like zones were the electrode/electrolyte interface where the transfer of Li ions took place.

Figure 3 shows the values of the ratio of the area of the sea-like zone to the total surface area of $LiNi_{1/3}Co_{1/3}Mn_{1/3}O_2$, as estimated by digitally analyzing the SEM images. With a decrease in the Zr oxide content from 1.0 to 0.125 wt%, the ratio increased from 44 to 85%. Thus, it can be surmised that increasing the area of the sea-like zones resulted in an expansion of the area of the effective electrode/electrolyte interface.

Electrochemical characteristics.— Figure 4 shows the discharge capacities, Coulombic efficiencies, and average discharge voltages for the first cycle for the Zr-oxide-coated $LiNi_{1/3}Co_{1/3}Mn_{1/3}O_2$ samples as functions of the Zr oxide content; the values for bare $LiNi_{1/3}Co_{1/3}Mn_{1/3}O_2$ are also shown for comparison. The discharge capacity of the Zr-oxide-coated $LiNi_{1/3}Co_{1/3}Mn_{1/3}O_2$ samples was approximately 200 mA h g^{-1} regardless of the Zr oxide content. Further, that of the bare $LiNi_{1/3}Co_{1/3}Mn_{1/3}O_2$ sample was almost similar. The Coulombic efficiencies of all the coated $LiNi_{1/3}Co_{1/3}Mn_{1/3}O_2$ samples were also equal and similar to that of the bare $LiNi_{1/3}Co_{1/3}Mn_{1/3}O_2$ samples. Further, the average discharge voltages of the $LiNi_{1/3}Co_{1/3}Mn_{1/3}O_2$ samples coated with 0.125–0.5 wt% Zr oxide were slightly higher than that of the bare $LiNi_{1/3}Co_{1/3}Mn_{1/3}O_2$ sample.

Figure 5 shows the discharge capacities and average discharge voltages of the bare and Zr-oxide-coated $LiNi_{1/3}Co_{1/3}Mn_{1/3}O_2$ samples during cycling. The reversibility of both the discharge capacity and the average discharge voltage increased markedly after the deposition of the Zr oxide coating; this was true regardless of the amount of Zr oxide coated. Further, while the retentions of the discharge capacity and average discharge voltage after 100 cycles for the bare $LiNi_{1/3}Co_{1/3}Mn_{1/3}O_2$ sample were 25 and 73%, respectively, those for the Zr-oxide-coated $LiNi_{1/3}Co_{1/3}Mn_{1/3}O_2$ samples were 63–67% and 86–91%, respectively. It can also be seen from Fig. 5 that there were differences in the capacities and voltages of the bare and Zr-oxide-coated $LiNi_{1/3}Co_{1/3}Mn_{1/3}O_2$ samples for fewer cycles as well.

Figure 6 shows the discharge capacities and average discharge voltages of the bare and Zr-oxide-coated $LiNi_{1/3}Co_{1/3}Mn_{1/3}O_2$ samples as determined early during the cycling test. Both the capacities and the voltages of the $LiNi_{1/3}Co_{1/3}Mn_{1/3}O_2$ samples coated with smaller amounts of Zr oxide (0.125–0.25 wt%) were higher than those of the bare $LiNi_{1/3}Co_{1/3}Mn_{1/3}O_2$ sample, as well as those of the

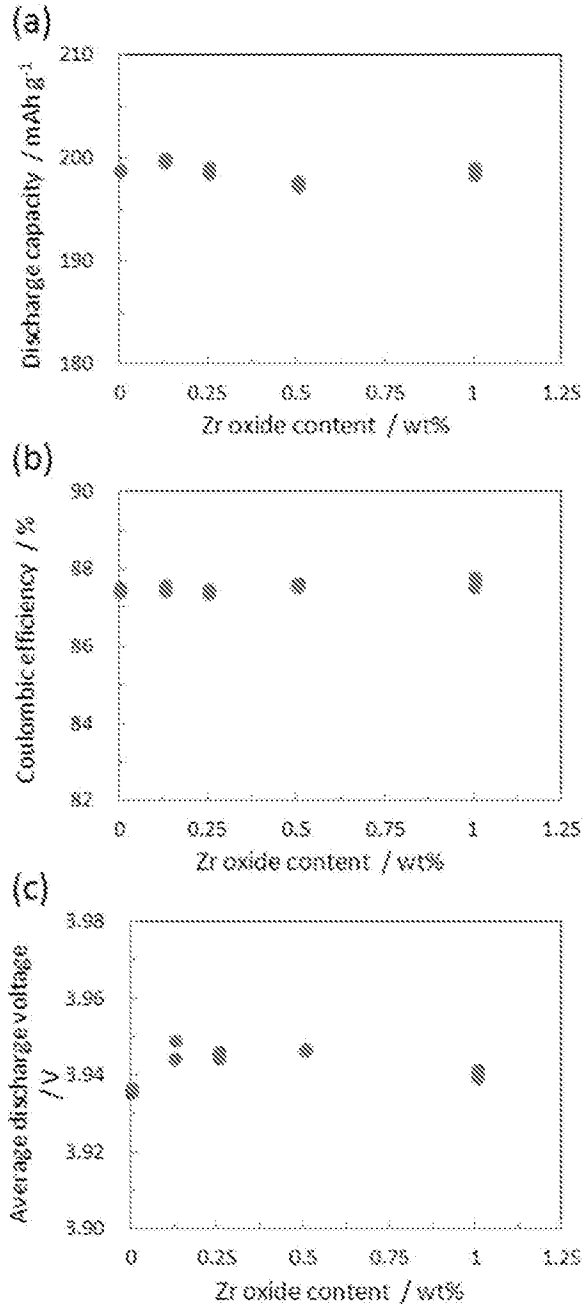


Figure 4. (a) Discharge capacities, (b) Coulombic efficiencies, and (c) average discharge voltages for bare and Zr-oxide-coated $LiNi_{1/3}Co_{1/3}Mn_{1/3}O_2$ for the first cycle as a function of Zr oxide content.

$LiNi_{1/3}Co_{1/3}Mn_{1/3}O_2$ samples coated with larger amounts of Zr oxide (0.5–1.0 wt%). This result indicates that coating $LiNi_{1/3}Co_{1/3}Mn_{1/3}O_2$ with smaller amounts of Zr oxide resulted in larger sea-like zones as well as improvements in the charging/discharging performance at high current rates.

The dependence of the impedance spectra of the coated $LiNi_{1/3}Co_{1/3}Mn_{1/3}O_2$ samples on the electrode potential was determined in order to evaluate the Li-ion transfer resistances at the electrode/electrolyte interface of the samples. Figures 7a and 7b show the Nyquist plots of the bare and 0.125-wt%-Zr-oxide-coated $LiNi_{1/3}Co_{1/3}Mn_{1/3}O_2$ samples, respectively, for various open-circuit voltages (OCVs) for the second cycle (i.e. after the initial charge/discharge cycle). Two types of semicircles can be observed in both figures. The semicircles in the low-frequency region, which have

AMPEREX Ex. 1002
Page 853

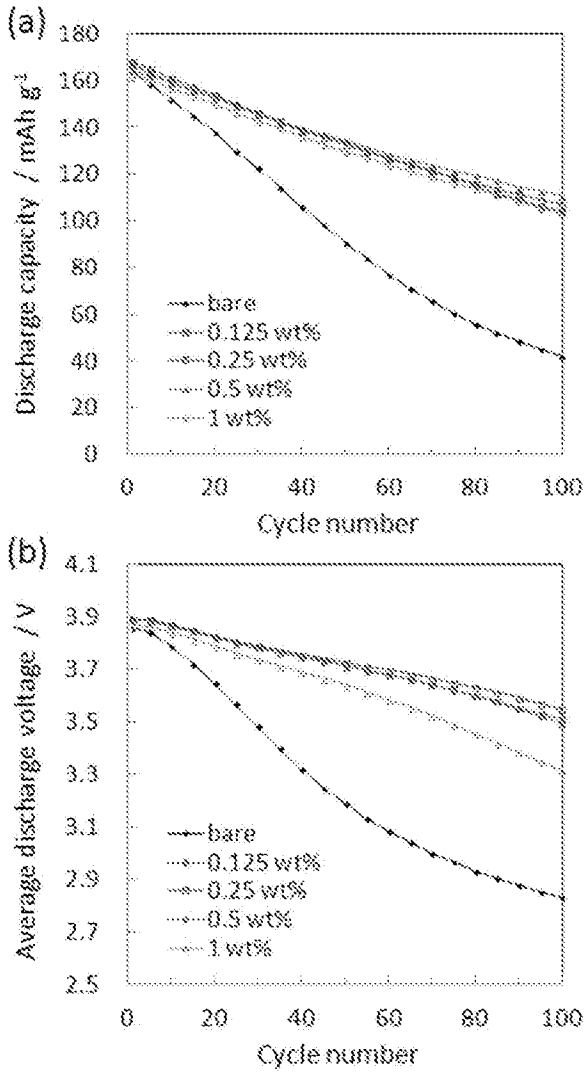


Figure 5. (a) Discharge capacities and (b) average discharge voltages during cycling of bare and Zr-oxide-coated $LiNi_{1/3}Co_{1/3}Mn_{1/3}O_2$.

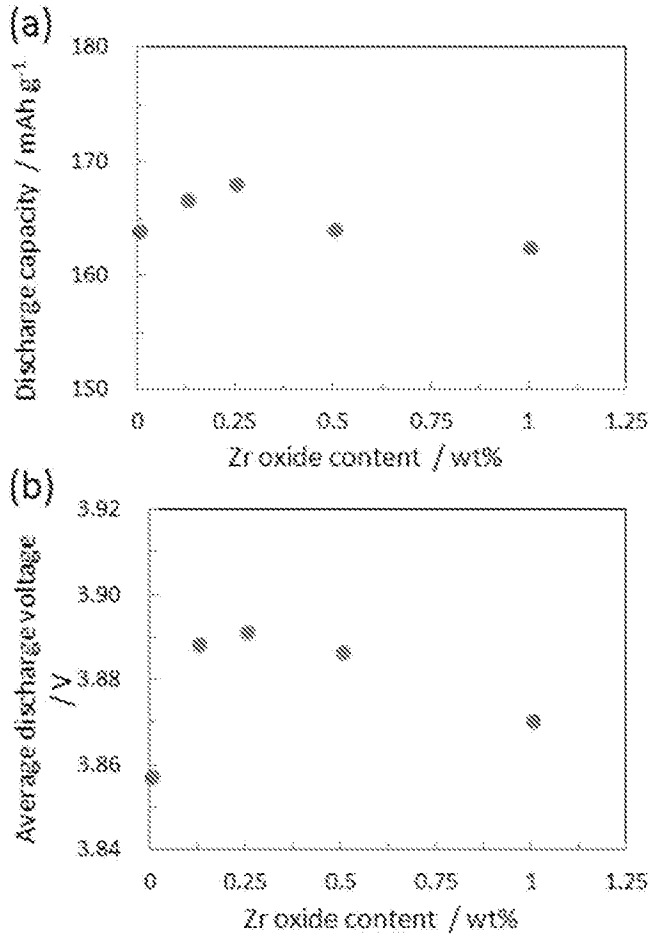


Figure 6. (a) Discharge capacities and (b) average discharge voltages at the initial cycle during cycling test of bare and Zr-oxide-coated $LiNi_{1/3}Co_{1/3}Mn_{1/3}O_2$.

characteristic frequencies of 2–20 Hz, depend greatly on the OCV. The charge-transfer reaction at the electrode/electrolyte interface can be represented by the Butler-Volmer equation. When the activities of Li^+ in the electrode and electrolyte are approximated by their concentrations, using this equation, the relationship between the charge-transfer resistance, R_{ct}, and the exchange current density, i_0, can be expressed as shown below.

$$R_{ct} = \frac{RT}{nFi_0} \quad [1]$$

where R, T, n, and F are the gas constant, absolute temperature, number of electrons, and Faraday's constant, respectively.

$$i_0 = nF \cdot k \cdot x^{\alpha} \cdot \{(1-x)C_{Li}\}^{1-\alpha} \quad [2]$$

where k, x, $(1-x)$, C_{Li}, and α are the reaction-rate constant, the concentration of Li^+ in the electrode, the concentration of Li^+ vacancies in the electrode, the concentration of Li^+ in the electrolyte, and a transference coefficient, respectively. It can be seen from Eqs. 1 and 2 that R_{ct} depends on x, which is the factor that determines the electrode potential in the Nernst equation. Therefore, the low-frequency semicircles, which depend on the OCV, represent R_{ct}. In contrast, the semicircles in the high-frequency region, which correspond to frequencies of 2.5 kHz, do not depend on the OCV. Moreover, the fact that they exhibit considerable distortion suggests the existence of multiple resistance components. These high-frequency semicircles are therefore attributable to the resistances of the Li negative electrode and the surface film formed on the $LiNi_{1/3}Co_{1/3}Mn_{1/3}O_2$ positive electrode.[27,28] Each resistance was quantitatively evaluated through fitting with an equivalent circuit, as shown in Fig. 7c. In these equivalent circuits, R_{f1} and R_{f2} represent the resistances corresponding to the highest and second-highest frequency, respectively.

Figure 8 shows the plots of R_{ct} against OCV for the bare and Zr-oxide-coated $LiNi_{1/3}Co_{1/3}Mn_{1/3}O_2$ samples for the second cycle. It can be seen that the R_{ct} values of the $LiNi_{1/3}Co_{1/3}Mn_{1/3}O_2$ samples coated with 0.125 and 0.25 wt% Zr oxide are lower than that of the bare $LiNi_{1/3}Co_{1/3}Mn_{1/3}O_2$; this is true for the entire range of OCVs. A low R_{ct} value in the high-OCV region results in a decrease in the degree of polarization during charging. This increases the effective charge capacity, resulting in an increase in the discharge capacity as well as the discharge voltage. Moreover, a low R_{ct} in the middle-to-low OCV region increases the discharge voltage. This difference in the R_{ct} values is a possible reason for the observed differences in the discharge capacities and average discharge voltages in the initial stage of the cycling test (Fig. 6). It also should be noted that the differences in the R_{ct} values for the entire OCV range (i.e. corresponding to the entire x region) mean that there is a difference in the values of the constant k (see Eq. 2) for the coated and bare samples. This, in turn, implies that the rates of transfer of Li ions and electrons at the electrode/electrolyte interface are different for the two types of samples.

In order to determine the reason for this difference in the values of k, the temperature dependence of R_{ct} was measured for temperatures of 0–40°C. For the measurements, a low-concentration (0.1 M) solution

AMPEREX Ex. 1002
Page 854

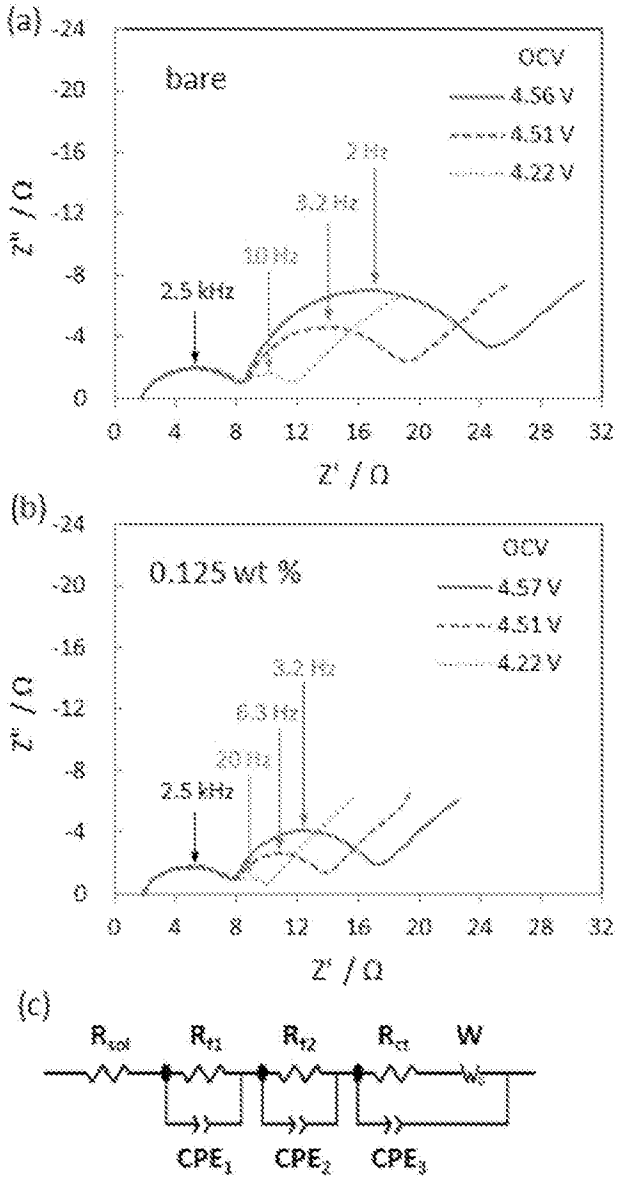


Figure 7. Nyquist plots of (a) bare and (b) Zr-oxide coated $LiNi_{1/3}Co_{1/3}Mn_{1/3}O_2$ with 0.125 wt% at various open circuit voltages in the second cycle. (c) Equivalent circuit used for fitting.

of $LiPF_6$ in EC/DEC was used as the electrolyte. Because a lower C_{Li}, means a decrease in i_0 and an increase in R_{ct} as per Eqs. 1 and 2, the accuracy of the R_{ct} measurements was high. Figure 9a shows the Arrhenius plots of R_{ct} for the bare and Zr-oxide-coated $LiNi_{1/3}Co_{1/3}Mn_{1/3}O_2$ samples for an OCV of 4.2 V for the second cycle. It can be seen that there are differences in the gradients of the lines. Figure 9b shows the values of the activation energy, E_a, which was calculated from the gradients using the following expression:

$$\frac{1}{R_{ct}} \propto k = A \cdot \exp\left(\frac{-E_a}{RT}\right) \quad [3]$$

where A is the frequency factor. The E_a value of the Zr-oxide-coated $LiNi_{1/3}Co_{1/3}Mn_{1/3}O_2$ samples were 5–10 kJ mol^{-1} lower than that of the bare $LiNi_{1/3}Co_{1/3}Mn_{1/3}O_2$ sample. Because A should be proportional to the area of the effective electrode/electrolyte interface, it can be assumed that the electrode based on the Zr-oxide-coated $LiNi_{1/3}Co_{1/3}Mn_{1/3}O_2$ sample with a lower Zr oxide content (0.125–0.25 wt%), for which the sea-like zones constituted 80% of the surface (Fig. 3), had an A value comparable to that of the bare

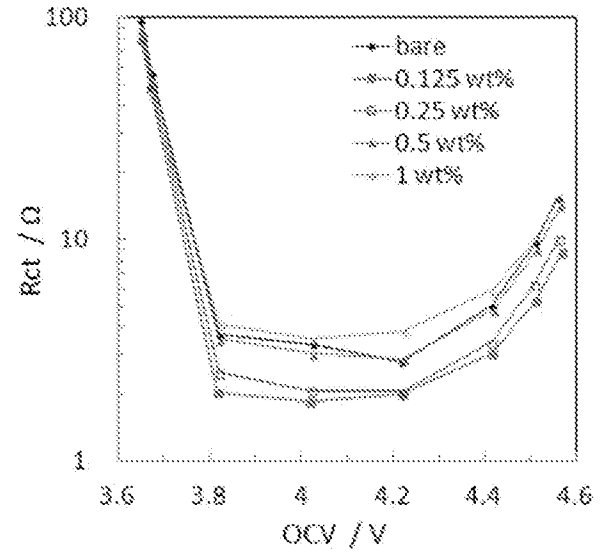


Figure 8. R_{ct} plotted against OCV of bare and Zr-oxide-coated $LiNi_{1/3}Co_{1/3}Mn_{1/3}O_2$ for the second cycle.

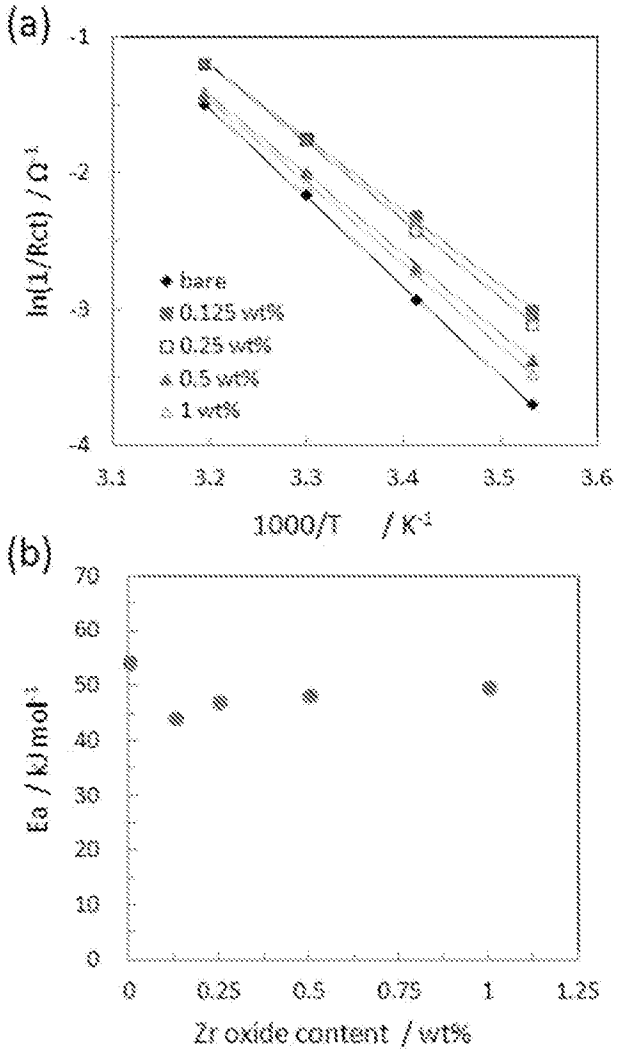


Figure 9. (a) Temperature dependence of R_{ct} and (b) coating content dependence of E_a of bare and Zr-oxide-coated $LiNi_{1/3}Co_{1/3}Mn_{1/3}O_2$ for the second cycle.

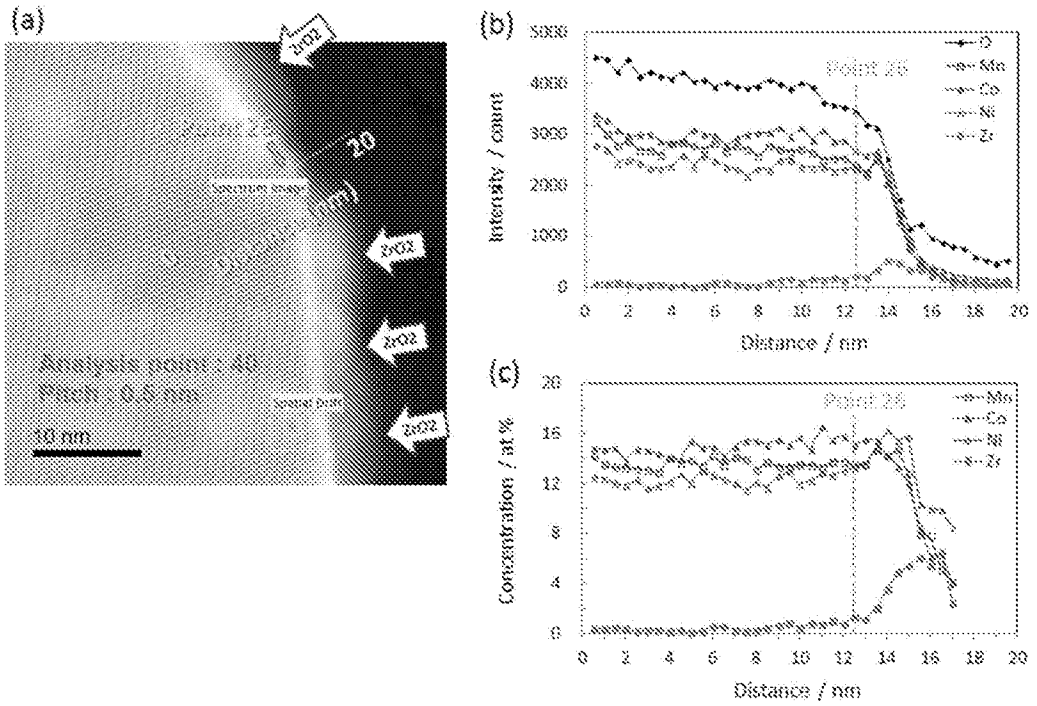


Figure 10. (a) HAADF-STEM image and (b and c) concentration depth profiles of Zr-oxide- coated $LiNi_{1/3}Co_{1/3}Mn_{1/3}O_2$ with 0.125 wt%. Vertical axes of (b) and (c) are intensity and atomic concentration, respectively.

$LiNi_{1/3}Co_{1/3}Mn_{1/3}O_2$ sample. Therefore, we can surmise that the lower R_{ct} values of the Zr-oxide-coated $LiNi_{1/3}Co_{1/3}Mn_{1/3}O_2$ samples with the lower Zr oxide content (see Fig. 8) were because their E_a values were lower and their A values were comparable to those of the bare $LiNi_{1/3}Co_{1/3}Mn_{1/3}O_2$ sample.

Based on the reaction mechanism termed the "adatom model", which was proposed by Bruce et al., the primary elementary processes involved in the reaction that takes place at the Li-insertion electrode/electrolyte interface can be considered to be the following: (1) the solvated Li ions in the electrolyte get absorbed onto the electrode surface and are desolvated (i.e., they undergo adsorption and desolvation) and (2) the desolvated Li ions are incorporated into the electrode material (i.e., they undergo lattice incorporation).[28] That the E_a values of the Zr-oxide-coated $LiNi_{1/3}Co_{1/3}Mn_{1/3}O_2$ samples were lower than that of the bare $LiNi_{1/3}Co_{1/3}Mn_{1/3}O_2$ sample indicated that the coated $LiNi_{1/3}Co_{1/3}Mn_{1/3}O_2$ samples exhibited a lower activation barrier for the lattice incorporation of Li ions.

High-resolution STEM analysis.— Figure 10a shows a cross-sectional high-angle annular dark field (HAADF) image of the Zr-oxide-coated $LiNi_{1/3}Co_{1/3}Mn_{1/3}O_2$ sample with a 0.125 wt% Zr oxide content. In addition to the island-like grains, sea-like zones, where the grains were not deposited, were also observed. Figures 10b and 10c show the concentration depth profiles (0.5 nm pitch in depth) for the sample; these correspond to the line across the sea-like zone shown in the inset in Fig. 10a. The vertical axes in Figs. 10b and 10c represent the intensity and atomic concentration, respectively. Zr was detected in the region extending from the surface to a depth of approximately 2 nm, and so were Ni, Co, Mn, and O. This indicates that a compound oxide phase containing Zr, Ni, Co, and Mn was formed in the surface region of the sea-like zones. The Zr concentration at the outmost surface of this region was almost comparable to those of the other metal elements.

Figure 11a shows a cross-sectional annular bright field (ABF) image of the Zr-oxide-coated $LiNi_{1/3}Co_{1/3}Mn_{1/3}O_2$ sample with a Zr oxide content of 0.125 wt% (this image shows a different view from that seen in Fig. 10). In this image, too, one can see the island-like grains and the sea-like zones. In this case, the $LiNi_{1/3}Co_{1/3}Mn_{1/3}O_2$ sample has a surface step in the direction of the electron beam, as shown in the schematic in Fig. 11c. Figure 11b shows the EDX map for Zr corresponding to the area selected in the inset in Fig. 11a. It can be seen that a continuous layer with a high concentration of Zr formed from the surface of the sea-like zone to a depth of approximately 2 nm. It is evident from these STEM-EDX results that a uniform thin coating of a compound oxide containing Zr was formed over the surface of the sea-like zones of the Zr-oxide-coated $LiNi_{1/3}Co_{1/3}Mn_{1/3}O_2$ sample. Further, it can be surmised that this thin coating contributes to the observed decrease in the R_{ct} and E_a values as well as the improvement in the cycling performance.

Surface structure and Li-ion transfer mechanism.— As mentioned above, a thin layer of a compound oxide containing Zr was formed uniformly over the surface of the sea-like zones. The formation mechanism of this layer can be considered to be the following. First, a uniform gel-like network containing Zr and O is formed on the surface of $LiNi_{1/3}Co_{1/3}Mn_{1/3}O_2$ during the sol-gel process. During the subsequent calcining process, the atoms in the gel-net and those in $LiNi_{1/3}Co_{1/3}Mn_{1/3}O_2$ mix, and a compound oxide layer is formed at the surface. Because the ionic radius (r_i) and valency of the Zr cation (Zr^{4+}, $r_i = 0.072$ nm) are different from those of the cations in $LiNi_{1/3}Co_{1/3}Mn_{1/3}O_2$, it is difficult for the Zr cations to diffuse into the bulk of $LiNi_{1/3}Co_{1/3}Mn_{1/3}O_2$ and substitute the other cations. (If the discharge-state valences are Li^+, Ni^{2+}, Co^{3+}, and Mn^{4+}, the values of r_i are 0.076, 0.069, 0.055, and 0.053 nm, respectively.) In the surface region, however, the degree of freedom of the atoms is higher than that in the bulk, and the equilibrium conditions there are different from that in the bulk. Therefore, a certain amount of Zr cations can diffuse into the surface region. However, at the same time, the excess Zr cations in the gel-net that cannot mix into the surface region are deposited on the surfaces of the $LiNi_{1/3}Co_{1/3}Mn_{1/3}O_2$ as ZrO_2 particles. If we assume that a ZrO_2-like gel-net of uniform thickness is formed on the surface of the $LiNi_{1/3}Co_{1/3}Mn_{1/3}O_2$, then, on the basis of the specific surface area of the $LiNi_{1/3}Co_{1/3}Mn_{1/3}O_2$ sample, a Zr oxide content of 0.125 wt% can be said to be equivalent to a gel-net thickness of approximately 1 nm. Since the lattice parameters of the ZrO_2 crystals

AMPEREX Ex. 1002
Page 856

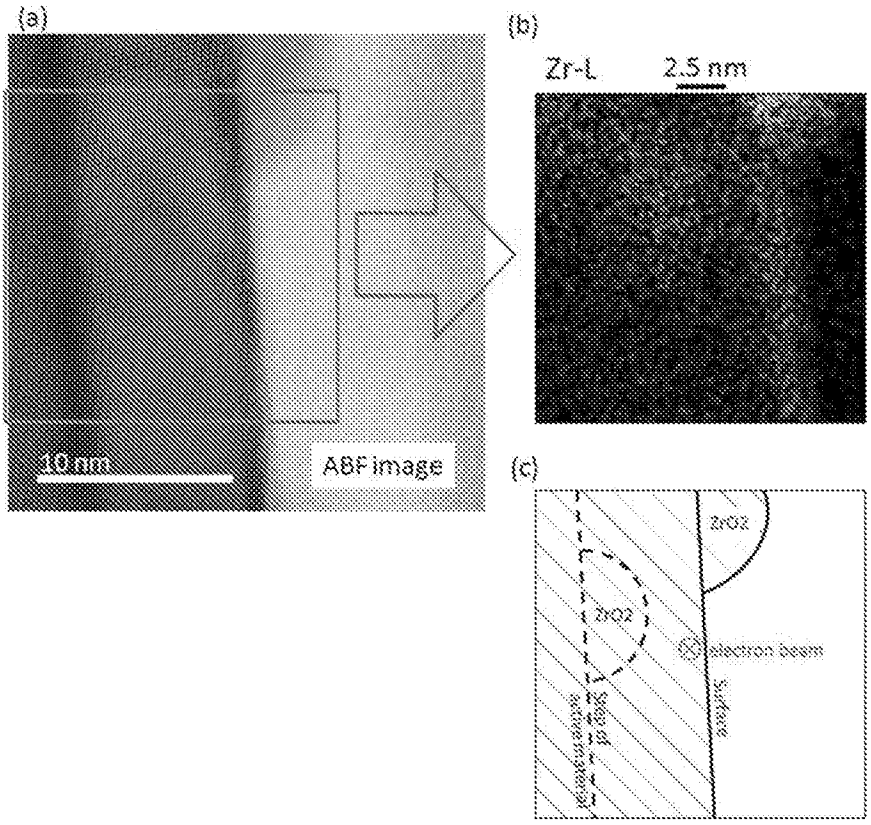


Figure 11. (a) ABF-STEM image of Zr-oxide-coated $LiNi_{1/3}Co_{1/3}Mn_{1/3}O_2$ with 0.125 wt%, (b) EDX map of Zr corresponding to the selected area, and (c) Schematic diagram of the ABF-STEM image.

are slightly greater than 0.5 nm, a coating content of 0.125 wt% is almost the lower limit at which a continuous gel-net can be formed.

It is assumed that the compound oxide layer decreases the activation energy of lattice incorporation ($E_{a,i}$). Although the mechanism responsible for this decrease in $E_{a,i}$ is not clear at this moment, it is possible that it is caused by one of the following factors. Since the Zr-O bond is more ionic in nature than the Ni-O, Co-O, and Mn-O bonds, the mixing of Zr into the surface region changes the electronic state of the octahedral MO_6 (M is Ni, Co, Mn, or Zr) there. The change in the electronic state should affect the activation barrier when the Li ions desolvated on the surface are incorporated into the Li sites between MO_6s; this means that the $E_{a,i}$ value changes. Furthermore, using in-situ X-ray scattering and thin-film electrodes of various active materials Hirayama et al. found that the surface atomic arrangements of active materials change when they are soaked in electrolyte solutions and that they are reconstructed during the first charging process.[29–32] Consequently, it is the reconstructed surface that is the effective interface. Thus, $E_{a,i}$ depends on the reconstructed atomic arrangement. Further, because the mixing of Zr cations into the surface region affects the reconstructed atomic arrangement, it probably also changes $E_{a,i}$.

The compound oxide layer is also probably responsible for the observed improvement in cycling performance. A major cause for cycling-related degradation of $LiNi_{1/3}Co_{1/3}Mn_{1/3}O_2$ is the formation of a rock-salt-like phase at the surface region during charging.[10,11] This rock-salt-like phase forms because of the change in the valency of M and the detachment of O:

$$M^{4+}O_2^{2-} + E \rightarrow M^{2+}O^{2-} + E^{2+}O^{2-} \quad [4]$$

where E is the electrolyte. Because the tetravalent Zr cations do not change their valency readily, the detachment of O is suppressed by the sharing of O by Zr with Ni, Co, and Mn in the compound oxide phase in the form of octahedral MO_6. Therefore, we believe that the compound oxide phase containing Zr suppresses the formation of the rock-salt-like phase and improves the cycling performance.

Acknowledgments

This work was supported by the "Research and Development Initiative for Scientific Innovation of New Generation Batteries (RISING project)" of the New Energy and Industrial Technology Development Organization (NEDO), Japan. The authors thank Yasuo Kikuzono for preparing the coating materials and Naomi Fukiya for the electrochemical measurements.

References

1. K. Mizushima, P. C. Jones, P. J. Wiseman, and J. B. Goodenough, *Mater. Res. Bull.*, **15**(6), 783 (1980).
2. T. Ohzuku, A. Ueda, and M. Nagayama, *J. Electrochem. Soc.*, **140**(7), 1862 (1993).
3. T. Ohzuku and A. Ueda, *Solid State Ionics*, **69**(3-4), 201 (1994).
4. T. Ohzuku and Y. Makimura, *Chem. Lett.*, (7), 642 (2001).
5. N. Yabuuchi and T. Ohzuku, *J. Power Sources*, **119**, 171 (2003).
6. N. Yabuuchi, Y. Makimura, and T. Ohzuku, *J. Electrochem. Soc.*, **154**(4), A314 (2007).
7. H. F. Wang, Y. I. Jang, B. Y. Huang, D. R. Sadoway, and Y. T. Chiang, *J. Electrochem. Soc.*, **146**(2), 473 (1999).
8. D. P. Abraham, R. D. Twesten, M. Balasubramanian, J. Kropf, D. Fischer, J. McBreen, I. Petrov, and K. Amine, *J. Electrochem. Soc.*, **150**(11), A1450 (2003).
9. S. Muto, Y. Sasano, K. Tatsumi, T. Sasaki, K. Horibuchi, Y. Takeuchi, and Y. Ukyo, *J. Electrochem. Soc.*, **156**(5), A371 (2009).
10. M. Shikano, H. Kobayashi, S. Koike, H. Sakaebe, Y. Saito, H. Hori, H. Kageyama, and K. Tatsumi, *J. Power Sources*, **196**(16), 6881 (2011).
11. A. Yano, S. Aoyama, M. Shikano, H. Sakaebe, K. Tatsumi, and Z. Ogumi, *J. Electrochem. Soc.*, **162**(2), A3137 (2015).
12. C. Li, H. P. Zhang, L. J. Fu, H. Liu, Y. P. Wu, E. Ram, R. Holze, and H. Q. Wu, *Electrochim. Acta*, **51**(19), 3872 (2006).
13. J. Cho, Y. J. Kim, and B. Park, *J. Electrochem. Soc.*, **148**(10), A1110 (2001).
14. Z. H. Chen and J. R. Dahn, *Electrochim. Acta*, **49**(7), 1079 (2004).
15. A. T. Appapillai, A. N. Mansour, J. Cho, and Y. Shao-Horn, *Chem. Mater.*, **19**(23), 5748 (2007).
16. L. Dahéron, R. Dedryvère, H. Martinez, D. Flahaut, M. Ménétrier, C. Delmas, and D. Gonbeau, *Chem. Mater.*, **21**(23), 5607 (2009).
17. B. C. Park, H. B. Kim, S. T. Myung, K. Amine, I. Belharouak, S. M. Lee, and Y. K. Sun, *J. Power Sources*, **178**(2), 826 (2008).
18. J. Cho, Y. J. Kim, T. J. Kim, and B. Park, *Angewandte Chemie-International Edition*, **40**(18), 3367 (2001).

AMPEREX Ex. 1002
Page 857

19. Z. H. Chen and J. R. Dahn, *Electrochemical and Solid State Letters*, **5**(10), A213 (2002).
20. M. M. Thackeray, C. S. Johnson, J. S. Kim, K. C. Lauzze, J. T. Vaughey, N. Dietz, D. Abraham, S. A. Hackney, W. Zeltner, and M. A. Anderson, *Electrochem. Commun.*, **5**(9), 752 (2003).
21. S. M. Lee, S. H. Oh, J. P. Ahn, W. I. Cho, and H. Jang, *J. Power Sources*, **159**(2), 1334 (2006).
22. G. T. K. Fey, C. L. Hsiao, and P. Muralidharan, *J. Power Sources*, **189**(1), 837 (2009).
23. Y. Y. Huang, J. T. Chen, J. F. Ni, H. H. Zhou, and X. X. Zhang, *J. Power Sources*, **188**(2), 538 (2009).
24. B. J. Hwang, C. Y. Chen, M. Y. Cheng, R. Santhanam, and K. Ragavendran, *J. Power Sources*, **195**(13), 4255 (2010).
25. D. Takamatsu, S. Mori, Y. Orikasa, T. Nakatsutsumi, Y. Koyama, H. Tanida, H. Arai, Y. Uchimoto, and Z. Ogumi, *J. Electrochem. Soc.*, **160**(5), A3054 (2013).
26. N. Taguchi, H. Sakaebe, T. Akita, K. Tatsumi, and Z. Ogumi, *J. Electrochem. Soc.*, **161**(10), A1521 (2014).
27. M. D. Levi, G. Salitra, B. Markovsky, H. Teller, D. Aurbach, U. Heider, and L. Heider, *J. Electrochem. Soc.*, **146**(4), 1279 (1999).
28. P. G. Bruce and M. Y. Saidi, *J. Electroanal. Chem*, **322**(1-2), 93 (1992).
29. M. Hirayama, N. Sonoyama, T. Abe, M. Minoura, M. Ito, D. Mori, A. Yamada, R. Kanno, T. Terashima, M. Takano, K. Tamura, and J. Mizuki, *J. Power Sources*, **168**(2), 493 (2007).
30. M. Hirayama, K. Sakamoto, T. Hiraide, D. Mori, A. Yamada, R. Kanno, N. Sonoyama, K. Tamura, and J. Mizuki, *Electrochim. Acta*, **53**(2), 871 (2007).
31. K. Sakamoto, M. Hirayama, H. Konishi, N. Sonoyama, N. Dupre, D. Guyomard, K. Tamura, J. Mizuki, and R. Kanno, *PCCP*, **12**(15), 3815 (2010).
32. M. Hirayama, H. Ido, K. Kim, W. Cho, K. Tamura, J. Mizuki, and R. Kanno, *J. Am. Chem. Soc.*, **132**(43), 15268 (2010).

Electronic Acknowledgement Receipt

EFS ID:	40607239
Application Number:	16923494
International Application Number:	
Confirmation Number:	3273
Title of Invention:	POSITIVE ELECTRODE ACTIVE MATERIAL, METHOD FOR MANUFACTURING POSITIVE ELECTRODE ACTIVE MATERIAL, AND SECONDARY BATTERY
First Named Inventor/Applicant Name:	Teruaki OCHIAI
Customer Number:	26171
Filer:	John F. Hayden/Alexis Bailey
Filer Authorized By:	John F. Hayden
Attorney Docket Number:	12732-2003004
Receipt Date:	18-SEP-2020
Filing Date:	08-JUL-2020
Time Stamp:	22:20:39
Application Type:	Utility under 35 USC 111(a)

Payment information:

Submitted with Payment	no

File Listing:

Document Number	Document Description	File Name	File Size(Bytes)/ Message Digest	Multi Part /.zip	Pages (if appl.)
1	Information Disclosure Statement (IDS) Form (SB08)	IDS_12732-2003004.pdf	170318 3500b142a44e49b2684e47584405e836633c4ec3	no	4

Warnings:

Information:					
This is not an USPTO supplied IDS fillable form					
2	Foreign Reference	JP2011-082133A.pdf	1423687 ea6392ff57144174137bea42264df8383950d75f	no	34
Warnings:					
Information:					
3	Foreign Reference	JP2011-210694A.pdf	741173 51ef1242afa20492d356b860039a67704463bd65	no	34
Warnings:					
Information:					
4	Foreign Reference	JP2014-116111A.pdf	1664120 cee417e4a1079700c9e8a2e58c70a455169d4292	no	39
Warnings:					
Information:					
5	Foreign Reference	JP2018-147726A.pdf	668703 888d1ac9be4b23dd822590734412f670051f9282	no	18
Warnings:					
Information:					
6	Foreign Reference	JP2012-043794A.pdf	703453 e09d0a2db44be5951d1dd5b4863c84a67c79d356	no	19
Warnings:					
Information:					
7	Foreign Reference	WO2014-061653A.pdf	2474323 2695f05e8c065590d09739eae3d65a71abb3f647	no	46
Warnings:					
Information:					
8	Foreign Reference	WO2015-163356A.pdf	4264179 b29a75fcc5a1bd3209d42759dfa9fffc16baa17a	no	180
Warnings:					
Information:					

9	Foreign Reference	WO2015-136881A.pdf	2166059 463d7d095748f8ecc63495d26d50a6d970a47884	no	39
Warnings:					
Information:					
10	Foreign Reference	JP2004-288579A.pdf	532454 9284581fc6ba07b2dfc80acc1d837d332642dd81	no	14
Warnings:					
Information:					
11	Non Patent Literature	JES_154_A337.pdf	231012 cfcad7d9fe267a68c764317474d38a4f1d9d4399	no	6
Warnings:					
Information:					
12	Non Patent Literature	JES_156_A1005.pdf	567295 e30b989147c33b7de09fc1fad32cc9ba25591175	no	6
Warnings:					
Information:					
13	Non Patent Literature	JPowerSources_269_236.pdf	1776038 4e4eb0757d761d8181ab5902c23e8faa82cfb14d	no	8
Warnings:					
Information:					
14	Non Patent Literature	JElectroanalChem_782_168.pdf	1260950 ededc99a60474d924f71548d508b6ba63409ea20	no	6
Warnings:					
Information:					
15	Non Patent Literature	ncomms_5_3529.pdf	856807 f619979c4572d162bac9f5cbbbfb1d629981bd9c	no	9
Warnings:					
Information:					

16	Non Patent Literature	JES_162_A3137.pdf	1422402 ab97be21be334faa3f5a5cb7cad7917b45567bdb	no	8
Warnings:					
Information:					
17	Non Patent Literature	JES_163_A75.pdf	1254770 d12e68df117fcfb28b94e414763f06d04d78d893	no	8
Warnings:					
Information:					
			Total Files Size (in bytes):	22177743	

This Acknowledgement Receipt evidences receipt on the noted date by the USPTO of the indicated documents, characterized by the applicant, and including page counts, where applicable. It serves as evidence of receipt similar to a Post Card, as described in MPEP 503.

New Applications Under 35 U.S.C. 111

If a new application is being filed and the application includes the necessary components for a filing date (see 37 CFR 1.53(b)-(d) and MPEP 506), a Filing Receipt (37 CFR 1.54) will be issued in due course and the date shown on this Acknowledgement Receipt will establish the filing date of the application.

National Stage of an International Application under 35 U.S.C. 371

If a timely submission to enter the national stage of an international application is compliant with the conditions of 35 U.S.C. 371 and other applicable requirements a Form PCT/DO/EO/903 indicating acceptance of the application as a national stage submission under 35 U.S.C. 371 will be issued in addition to the Filing Receipt, in due course.

New International Application Filed with the USPTO as a Receiving Office

If a new international application is being filed and the international application includes the necessary components for an international filing date (see PCT Article 11 and MPEP 1810), a Notification of the International Application Number and of the International Filing Date (Form PCT/RO/105) will be issued in due course, subject to prescriptions concerning national security, and the date shown on this Acknowledgement Receipt will establish the international filing date of the application.

To: PATDOCTC@fr.com,,
From: PAIR_eOfficeAction@uspto.gov
Cc: PAIR_eOfficeAction@uspto.gov
Subject: Private PAIR Correspondence Notification for Customer Number 26171

Sep 21, 2020 03:55:24 AM

Dear PAIR Customer:

FISH & RICHARDSON P.C. (DC)
P.O. BOX 1022
MINNEAPOLIS, MN 55440-1022
UNITED STATES

The following USPTO patent application(s) associated with your Customer Number, 26171 , have new outgoing correspondence. This correspondence is now available for viewing in Private PAIR.

The official date of notification of the outgoing correspondence will be indicated on the form PTOL-90 accompanying the correspondence.

Disclaimer:
The list of documents shown below is provided as a courtesy and is not part of the official file wrapper. The content of the images shown in PAIR is the official record.

Application	Document	Mailroom Date	Attorney Docket No.
16923494	CTNF	09/21/2020	12732-2003004
	892	09/21/2020	12732-2003004
	1449	09/21/2020	12732-2003004

To view your correspondence online or update your email addresses, please visit us anytime at https://sportal.uspto.gov/secure/myportal/privatepair.

If you have any questions, please email the Electronic Business Center (EBC) at EBC@uspto.gov with 'e-Office Action' on the subject line or call 1-866-217-9197 during the following hours:

Monday - Friday 6:00 a.m. to 12:00 a.m.

Thank you for prompt attention to this notice,

UNITED STATES PATENT AND TRADEMARK OFFICE

PATENT APPLICATION INFORMATION RETRIEVAL SYSTEM

PTO/SB/08A (07-06)
Approved for use through 03/31/2007. OMB 0651-0031
U.S. Patent and Trademark Office; U.S. DEPARTMENT OF COMMERCE

Under the Paperwork Reduction Act of 1995, no persons are required to respond to a collection of information unless it contains a valid OMB control number.

Substitute for form 1449/PTO

INFORMATION DISCLOSURE STATEMENT BY APPLICANT

(Use as many sheets as necessary)

Sheet 1 of 2

Complete if Known	
Application Number	16/923,494
Filing Date	July 8, 2020
First Named Inventor	Teruaki OCHIAI
Art Unit	1725
Examiner Name	S.CULLEN
Attorney Docket Number	12732-2003004

U. S. PATENT DOCUMENTS

Examiner Initials*	Cite No.[1]	Document Number Number-Kind Code[2] (if known)	Publication Date MM-DD-YYYY	Name of Patentee or Applicant of Cited Document	Pages, Columns, Lines, Where Relevant Passages or Relevant Figures Appear
		US-2014/0242463	08-28-2014	Song.J et al.	

FOREIGN PATENT DOCUMENTS

Examiner Initials*	Cite No.[1]	Foreign Patent Document Country Code[3] -Number[4] -Kind Code[5] (if known)	Publication Date MM-DD-YYYY	Name of Patentee or Applicant of Cited Document	Pages, Columns, Lines, Where Relevant Passages or Relevant Figures Appear	T[6]
		KR-2013-0033154A	04-03-2013			Abst.
		KR-2011-0134852A	12-15-2011			Abst.
		EP-2763218A	08-06-2014			Eng.
		WO-2011/155781	12-15-2011			Abst.
		JP-2015-088450A	05-07-2015			Abst.

Examiner Signature		Date Considered	

*EXAMINER: Initial if reference considered, whether or not citation is in conformance with MPEP 609. Draw line through citation if not in conformance and not considered. Include copy of this form with next communication to applicant. 1 Applicant's unique citation designation number (optional). 2 See Kinds Codes of USPTO Patent Documents a www.uspto.gov or MPEP 901.04. 3 Enter Office that issued the document, by the two-letter code (WIPO Standard ST.3). 4 For Japanese patent documents, the indication of the year of the reign of the Emperor must precede the serial number of the patent document. 5 Kind of document by the appropriate symbols as indicated on the document under WIPO Standard ST.16 if possible. 6 Applicant is to place a check mark here if English language Translation is attached.

This collection of information is required by 37 CFR 1.97 and 1.98. The information is required to obtain or retain a benefit by the public which is to file (and by the USPTO to process) an application. Confidentiality is governed by 35 U.S.C. 122 and 37 CFR 1.14. This collection is estimated to take 2 hours to complete, including gathering, preparing, and submitting the completed application form to the USPTO. Time will vary depending upon the individual case. Any comments on the amount of time you require to complete this form and/or suggestions for reducing this burden, should be sent to the Chief Information Officer, U.S. Patent and Trademark Office, P.O. Box 1450, Alexandria, VA 22313-1450. DO NOT SEND FEES OR COMPLETED FORMS TO THIS ADDRESS. **SEND TO: Commissioner for Patents, P.O. Box 1450, Alexandria, VA 22313-1450.**

If you need assistance in completing the form, call 1-800-PTO-9199 (1-800-786-9199) and select option 2.

PTO/SB/08A (07-06)
Approved for use through 03/31/2007. OMB 0651-0031
U.S. Patent and Trademark Office; U.S. DEPARTMENT OF COMMERCE

Under the Paperwork Reduction Act of 1995, no persons are required to respond to a collection of information unless it contains a valid OMB control number.

Substitute for form 1449/PTO

INFORMATION DISCLOSURE STATEMENT BY APPLICANT

(Use as many sheets as necessary)

Sheet 2 of 2

Complete if Known	
Application Number	16/923,494
Filing Date	July 8, 2020
First Named Inventor	Teruaki OCHIAI
Art Unit	1725
Examiner Name	S.CULLEN
Attorney Docket Number	12732-2003004

NON PATENT LITERATURE DOCUMENTS

Examiner Initials*	Cite No.[1]	Include name of the author (in CAPITAL LETTERS), title of the article (when appropriate), title of the item (book, magazine, journal, serial, symposium, catalog, etc.), date, page(s), volume-issue number(s), publisher, city and/or country where published.	T[2]
		Ding.Y et al., "Preparation of nano-structured LiFePO4/graphene composites by co-precipitation method", ELECTROCHEMISTRY COMMUNICATIONS, 2010, Vol. 12, No. 1, pp. 10-13, ELSEVIER.	Eng.

Examiner Signature		Date Considered	

*EXAMINER: Initial if reference considered, whether or not citation is in conformance with MPEP 609. Draw line through citation if not in conformance and not considered. Include copy of this form with next communication to applicant.

1 Applicant's unique citation designation number (optional). 2 Applicant is to place a check mark here if English language Translation is attached.

This collection of information is required by 37 CFR 1.97 and 1.98. The information is required to obtain or retain a benefit by the public which is to file (and by the USPTO to process) an application. Confidentiality is governed by 35 U.S.C. 122 and 37 CFR 1.14. This collection is estimated to take 2 hours to complete, including gathering, preparing, and submitting the completed application form to the USPTO. Time will vary depending upon the individual case. Any comments on the amount of time you require to complete this form and/or suggestions for reducing this burden, should be sent to the Chief Information Officer, U.S. Patent and Trademark Office, U.S. Department of Commerce, P.O. Box 1450, Alexandria, VA 22313-1450. DO NOT SEND FEES OR COMPLETED FORMS TO THIS ADDRESS. **SEND TO: Commissioner for Patents, P.O. Box 1450, Alexandria, VA 22313-1450.**

If you need assistance in completing the form, call 1-800-PTO-9199 (1-800-786-9199) and select option 2.

IN THE UNITED STATES PATENT AND TRADEMARK OFFICE

First Named Inventor	:	Teruaki OCHIAI	Art Unit	:	1725
Application No.	:	16/923,494	Examiner	:	Sean P. Cullen
Filed	:	July 8, 2020	Conf. No.	:	3273
Title	:	POSITIVE ELECTRODE ACTIVE MATERIAL, METHOD FOR MANUFACTURING POSITIVE ELECTRODE ACTIVE MATERIAL, AND SECONDARY BATTERY			

Commissioner for Patents
P.O. Box 1450
Alexandria, VA 22313-1450

INFORMATION DISCLOSURE STATEMENT

Please consider the references listed on the enclosed disclosure form. Copies of the documents required under 37 C.F.R. § 1.98(a)(2) are being submitted with this statement.

Each item of information in this information disclosure statement, with the exception of EP2763218, US2014/0242463, and WO2011/155781, was first cited in communications from foreign patent offices in counterpart foreign applications dated July 27, 2020, and August 18, 2020, neither of which is more than three months prior to the filing of this information disclosure statement. See 37 CFR 1.97(e)(1).

KR2013-0033154, KR2011-0134852, and Ding.Y et al., "Preparation of nano-structured LiFePO4/graphene composites by co-precipitation method", ELECTROCHEMISTRY COMMUNICATIONS, 2010, Vol. 12, No. 1, pp. 10-13, ELSEVIER, were cited in an office action dated July 27, 2020, from the Korea Intellectual Property Office in counterpart Korean Application No. 2019-7034933.

JP2015-088450 was cited in office actions dated August 18, 2020, from the Japan Patent Office in counterpart Japanese Application Nos. 2020-067736 and 2020-088842.

EP2763218 and US2014/0242463 are English-language documents corresponding to KR2013-0033154; and WO2011/155781 corresponds to KR2011-0134852.

This statement is being filed within three months of the filing date of the application. Please apply any charges or credits to Deposit Account No. 06-1050, referencing the above attorney docket number.

Respectfully submitted,

Date: September 24, 2020

/John F. Hayden/
John F. Hayden
Reg. No. 37640

Customer Number 26171
Fish & Richardson P.C.
Telephone: (202) 783-5070
Facsimile: (877) 769-7945

100256264.doc

Espacenet

RSS family dossiers

Family list: KR20130033154 (A) — 2013-04-03

5 application(s) for: KR20130033154 (A)

Inventor:	Applicant:	CPC:	IPC:	Publication info:	Priority date:
1. POSITIVE ACTIVE MATERIAL, PREPARATION METHOD THEREOF AND LITHIUM SECONDARY BATTERY COMPRISING THE SAME					
SONG JUN HO [KR] KIM YOUNG JUN [KR] (+4)	KOREA ELECTRONICS TECHNOLOGY [KR]	C01G53/50 C01P2002/85 C01P2004/03 (+19)	H01M10/052 H01M4/505 H01M4/525 (+1)	KR20130033154 (A) 2013-04-03 Global Dossier	2011-09-26
2. CATHODE ACTIVE MATERIAL FOR A LITHIUM SECONDARY BATTERY, METHOD FOR MANUFACTURING SAME, AND LITHIUM SECONDARY BATTERY INCLUDING SAME					
SONG JUN HO [KR] KIM YOUNG JUN [KR] (+4)	KOREA ELECTRONICS TECHNOLOGY [KR]	C01G53/50 C01P2002/85 C01P2004/03 (+19)	C01G53/00 H01M4/04 H01M4/131 (+7)	EP2763218 (A2) 2014-08-06 EP2763218 (A4) 2015-07-22 EP2763218 (B1) 2016-08-31 Global Dossier	2011-09-26
3. CATHODE ACTIVE MATERIAL FOR A LITHIUM SECONDARY BATTERY, METHOD FOR MANUFACTURING SAME, AND LITHIUM SECONDARY BATTERY INCLUDING SAME					
ソン, ジュンホ, キム, ユンジュン, (+4)	コリア エレクトロニクス テクノロジ インスティチュート	C01G53/50 C01P2002/85 C01P2004/03 (+19)	H01M10/052 H01M4/36 H01M4/505 (+1)	JP2014531718 (A) 2014-11-27 JP6251679 (B2) 2017-12-20 Global Dossier	2011-09-26
4. CATHODE ACTIVE MATERIAL FOR A LITHIUM SECONDARY BATTERY, METHOD FOR MANUFACTURING SAME, AND LITHIUM SECONDARY BATTERY INCLUDING SAME					
SONG JUN HO [KR] KIM YOUNG JUN [KR] (+4)	KOREA ELECTRONICS TECHNOLOGY [KR]	C01G53/50 C01P2002/85 C01P2004/03 (+19)	H01M4/04 H01M4/1391 H01M4/36	US2014242463 (A1) 2014-08-28 Global Dossier	2011-09-26
5. CATHODE ACTIVE MATERIAL FOR A LITHIUM SECONDARY BATTERY, METHOD FOR MANUFACTURING SAME, AND LITHIUM SECONDARY BATTERY INCLUDING SAME					

Inventor:	Applicant:	CPC:	IPC:	Publication info:	Priority date:
SONG JUN HO [KR] KIM YOUNG JUN [KR] (+4)	KOREA ELECTRONICS TECHNOLOGY [KR]	C01G53/50 C01P2002/85 C01P2004/03 (+19)		WO2013048048 (A2) 2013-04-04 WO2013048048 (A3) 2013-05-23 WO2013048048 (A8) 2013-06-13 Global Dossier	2011-09-26

Espacenet

Bibliographic data: KR20130033154 (A) — 2013-04-03

POSITIVE ACTIVE MATERIAL, PREPARATION METHOD THEREOF AND LITHIUM SECONDARY BATTERY COMPRISING THE SAME

Inventor(s): SONG JUN HO [KR]; KIM YOUNG JUN [KR]; KIM JEOM SOO [KR]; CHO WOO SUK [KR]; KIM JAE HUN [KR]; KIM JIN HWA [KR] + (SONG, JUN HO, ; KIM, YOUNG JUN, ; KIM, JEOM SOO, ; CHO, WOO SUK, ; KIM, JAE HUN, ; KIM, JIN HWA)

Applicant(s): KOREA ELECTRONICS TECHNOLOGY [KR] + (KOREA ELECTRONICS TECHNOLOGY INSTITUTE)

Classification: - international: ***H01M10/052; H01M4/505; H01M4/525; H01M4/58***
- cooperative: **C01G53/50 (EP); H01M10/052 (KR); H01M10/0525 (KR); H01M4/0402 (EP, US); H01M4/0471 (EP, US); H01M4/131 (EP, KR); H01M4/1391 (EP, KR, US); H01M4/364 (KR); H01M4/366 (EP, US); H01M4/382 (KR); H01M4/505 (EP, KR); H01M4/525 (EP, KR); H01M4/58 (KR); H01M4/62 (EP);** C01P2002/85 (EP); C01P2004/03 (EP); C01P2004/61 (EP); C01P2004/80 (EP); C01P2006/40 (EP); H01M10/0525 (EP); H01M2004/021 (EP, US); H01M2220/30 (EP, US)

Application number: KR20110097058 20110926 Global Dossier

Priority number(s): KR20110097058 20110926

Also published as: EP2763218 (A2) EP2763218 (A4) EP2763218 (B1) JP2014531718 (A) JP6251679 (B2) more

Abstract of KR20130033154 (A)

PURPOSE: A positive electrode active material for a lithium secondary battery is provided to minimize the side reaction of a positive electrode active material and electrolyte and to suppress the elution of manganese and degradation at charging and discharging. CONSTITUTION: A positive electrode active material for a lithium secondary battery includes a lithium metal composite oxide core represented by chemical formula 1, Li_wNi_xCo_yMn_(1-x-y-z)M_zO_2; and a coating layer containing fluorine compounds on the lithium metal composite oxide core. In chemical formula 1, 1.2<=w<=1.5, 0<x<1, 0y<1, 0.5<=1-x-y-z, and M is one or more metals selected from Al, Mg, Fe, Cu, Zn, Cr, Ag, Ca, Na, K, In, Ga, Ge, V, Mo, Nb, Si, Ti, and Zr. [Reference numerals] (AA) Lithium-rich metal complex oxide; (BB) Metal salt; (CC) Fluorine compound; (DD) Coating step; (EE) Thermal treatment step; (FF) Providing positive electrode active materials surface-modified with a fluorine compound;

(19) 대한민국특허청(KR)
(12) 공개특허공보(A)

(11) 공개번호 10-2013-0033154
(43) 공개일자 2013년04월03일

(51) 국제특허분류(Int. Cl.)
H01M 4/525 (2010.01) *H01M 4/505* (2010.01)
H01M 10/052 (2010.01) *H01M 4/58* (2010.01)
(21) 출원번호 10-2011-0097058
(22) 출원일자 2011년09월26일
심사청구일자 없음

(71) 출원인
전자부품연구원
경기도 성남시 분당구 새나리로 25 (야탑동)
(72) 발명자
송준호
경기 성남시 분당구 수내2동 파크대림아파트 106동 101호
김영준
경기도 용인시 기흥구 용구대로2469번길 20, 죽전택지개발지구 아파트 428호 (보정동, 죽전자이2차)
(뒷면에 계속)
(74) 대리인
유미특허법인

전체 청구항 수 : 총 14 항

(54) 발명의 명칭 **리튬 이차전지용 양극 활물질, 그의 제조방법 및 그를 포함하는 리튬이차전지**

(57) 요 약

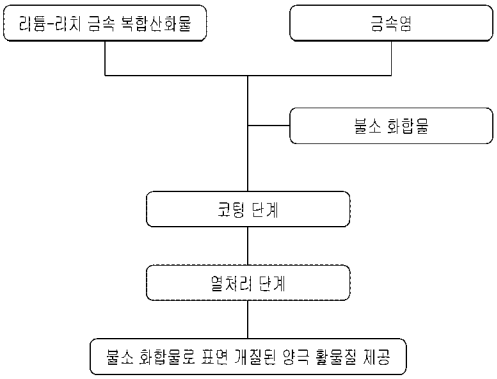
리튬 이차전지용 양극 활물질, 그의 제조방법 및 그를 포함하는 리튬 이차전지에 관한 것으로, 하기 화학식 1로 표시되는 리튬 금속 복합산화물 코어; 및 상기 리튬 금속 복합산화물 코어 위에 불소 화합물을 함유하는 코팅층을 포함하는, 리튬 이차전지용 양극 활물질을 제공한다.

[화학식 1]

$Li_wNi_xCo_yMn_{1-x-y-z}M_zO_2$

(1.2≤w≤1.5, 0<x<1, 0y<1, 0.5≤1-x-y-z, M은 Al, Mg, Fe, Cu, Zn, Cr, Ag, Ca, Na, K, In, Ga, Ge, V, Mo, Nb, Si, Ti 및 Zr으로 이루어진 군으로부터 선택되는 1 종 이상의 금속).

대 표 도 - 도1



AMPEREX Ex. 1002
Page 872

(72) 발명자

김점수

경기도 화성시 반월동 860 신영통현대3차아파트 310동 104호

조우석

경기도 성남시 분당구 판교로 393, 이지더원 214동 1202호 (삼평동)

김재헌

경기 용인시 수지구 상현1동 서원마을현대홈타운아파트 201동 203호

김진화

경기도 성남시 분당구 새나리로6번길 18, 103호 (야탑동, 탑하이빌)

이 발명을 지원한 국가연구개발사업

과제고유번호	10037921
부처명	지식경제부
연구사업명	WPM 사업
연구과제명	전기자동차용 고에너지 LIB용 Li-rich 양극 전구체 개발
주관기관	(주)엘앤에프신소재
연구기간	2010.09.01~2019.03.31

AMPEREX Ex. 1002
Page 873

특허청구의 범위

청구항 1

하기 화학식 1로 표시되는 리튬 금속 복합산화물 코어; 및

상기 리튬 금속 복합산화물 코어 위에 불소 화합물을 함유하는 코팅층을 포함하는, 리튬 이차전지용 양극 활물질.

[화학식 1]

$Li_wNi_xCo_yMn_{1-x-y-z}M_zO_2$

(1.2≤w≤1.5, 0<x<1, 0y<1, 0.5≤1-x-y-z, M은 Al, Mg, Fe, Cu, Zn, Cr, Ag, Ca, Na, K, In, Ga, Ge, V, Mo, Nb, Si, Ti 및 Zr으로 이루어진 군으로부터 선택되는 1 종 이상의 금속)

청구항 2

제1항에 있어서,

상기 불소 화합물은 CsF, KF, LiF, NaF, RbF, TiF, AgF, AgF, BaF_2, CaF_2, CuF_2, CdF_2, FeF_2, HgF_2, HgF, MnF, MgF, NiF, PbF, SnF_2, SrF_2, XeF_2, ZnF_2, AlF_3, BF_3, BiF_3, CeF_3, CrF_3, DyF_3, EuF_3, GaF_3, GdF_3, FeF_3, HoF_3, InF_3, LaF_3, LuF_3, MnF_3, NdF_3, VOF_3, PrF_3, SbF_3, ScF_3, SmF_3, TbF_3, TiF_3, TmF_3, YF_3, YbF_3, TIF_3, CeF_3, GeF_3, HfF_3, SiF_3, SnF_3, TiF_4, VF_4, ZrF_4, NbF_5, SbF_5, TaF_5, BiF_5, MoF_5, ReF_5, SF_5 및 WF_5으로 이루어진 군으로부터 선택되는 하나 이상인, 리튬 이차전지용 양극 활물질.

청구항 3

제1항에 있어서,

상기 코팅층의 함량이 상기 리튬 금속 복합산화물 코어 총 중량에 대하여 0.2 내지 1.5 중량%인, 양극활물질.

청구항 4

제1항에 있어서,

상기 코팅층의 두께가 5 내지 20nm인, 리튬 이차전지용 양극 활물질.

청구항 5

제1항에 있어서,

상기 코팅층은 ZrO_2, SnO_2 또는 이들의 혼합물을 더 포함하는, 리튬 이차전지용 양극 활물질.

청구항 6

제1항에 있어서,

상기 리튬 금속 복합산화물 코어의 평균 입경(D50)이 10 내지 20㎛인, 양극 활물질.

청구항 7

제1항에 있어서,

상기 화학식 1의 w가 1.3 내지 1.5인, 리튬 이차전지용 양극 활물질.

청구항 8

제1항에 있어서,

AMPEREX Ex. 1002
Page 874

AMPEREX Ex. 1002
Page 875

상기 리튬 금속 복합산화물 코어가 $Li_{1.3}Ni_{0.2}Co_{0.1}Mn_{0.7}O_2$, $Li_{1.3}Ni_{0.25}Mn_{0.75}O_2$, $Li_{1.3}Ni_{0.25}Co_{0.05}Mn_{0.7}O_2$ 및 $Li_{1.3}Ni_{0.2}Co_{0.1}Al_{0.05}Mn_{0.65}O_2$로 이루어진 군에서 선택되는 하나인, 리튬 이차전지용 양극 활물질.

청구항 9

a) 하기 화학식 1로 표시되는 리튬 금속 복합산화물 코어를 제공하는 단계;

[화학식 1]

$Li_wNi_xCo_yMn_{1-x-y-z}M_zO_2$

($1.2 \leq w \leq 1.5$, $0<x<1$, $0y<1$, $0.5 \leq 1-x-y-z$, M은 Al, Mg, Fe, Cu, Zn, Cr, Ag, Ca, Na, K, In, Ga, Ge, V, Mo, Nb, Si, Ti 및 Zr으로 이루어진 군으로부터 선택되는 1 종 이상의 금속).

b) 불소 화합물이 포함된 용액을 제공하는 단계;

c) 상기 단계 a)의 리튬 금속 복합산화물 코어를 b) 단계의 불소 화합물을 포함하는 용액으로 코팅하는 단계; 및

d) 상기 단계 c)의 코팅된 리튬 금속 복합산화물을 열처리하는 단계를 포함하는,

리튬 이차전지용 양극 활물질의 제조방법.

청구항 10

제9항에 있어서,

상기 단계 c)는 상기 불소 화합물이 포함된 용액을 리튬 금속 복합산화물에 코팅 후, 120℃ 내지 150℃의 온도에서 용액을 증발시키는 것을 포함하는, 리튬 이차전지용 양극 활물질의 제조방법.

청구항 11

제9항에 있어서,

상기 단계 d)에서, 열처리는 비활성 분위기에서 380℃ 내지 460℃의 온도에서 1 내지 10 시간 동안 실시되는, 리튬 이차전지용 양극 활물질의 제조방법.

청구항 12

제9항에 있어서,

상기 단계 b)에서, 리튬 금속 복합산화물 코어를 약 5 내지 약 20nm의 두께로 코팅하는, 리튬 이차전지용 양극 활물질의 제조방법.

청구항 13

제9항에 있어서,

상기 단계 b)에서, 상기 용액은 ZrO_2, SnO_2 또는 이들의 혼합물을 추가로 포함하는, 리튬 이차전지용 양극 활물질의 제조방법.

청구항 14

제1항 내지 제8항에 따른 양극 활물질을 포함하는 양극;

리튬 이온의 삽입/탈리가 가능한 음극 활물질을 포함하는 음극;

상기 양극과 음극 사이에 존재하는 세퍼레이터; 및

비수성 전해질을 포함하는 리튬 이차 전지로서,

AMPEREX Ex. 1002
Page 876

방전 용량이 220mAhg^{-1} 이상인 리튬 이차전지.

명 세 서

기 술 분 야

[0001] 리튬 이차전지용 양극 활물질, 그의 제조방법 및 그를 포함하는 리튬이차전지에 관한 것이다.

배 경 기 술

[0002] 휴대용의 소형 전기 전자기기의 보급이 확산됨에 따라 니켈수소전지나 리튬 이차전지와 같은 신형 이차전지 개발이 활발하게 진행되고 있다. 이 중 리튬 이차전지는 흑연 등의 카본을 음극 활물질로 사용하고, 리튬이 포함되어 있는 금속 산화물을 양극 활물질로 사용하며, 비수 용매를 전해액으로 사용하는 전지이다. 리튬은 매우 이온화 경향이 큰 금속이기 때문에, 고전압 발현이 가능하여 에너지 밀도가 높은 전지 개발이 이루어지고 있다.

[0003] 리튬 이차전지에 사용되는 양극 활물질로는 리튬을 함유하고 있는 리튬 전이금속산화물이 주로 사용되고 있으며, 코발트계, 니켈계 및 코발트, 니켈, 망간이 공존하는 삼성분계 등의 층상계 리튬 전이금속산화물이 90% 이상 사용되고 있다.

[0004] 그러나 종래 양극 활물질로 많이 사용되고 있는 층상계 리튬 전이금속산화물은 사용할 수 있는 가역용량이 200mAhg^{-1} 이하이기 때문에 에너지밀도에 있어서 한계가 있었다. 따라서, 양극의 가역용량의 제한으로 인한 리튬 이차전지의 문제점을 해결하는 수단으로서 일반 층상계 리튬 전이금속산화물 대신, 리튬을 과량으로 포함하는 리튬-리치 층상계 산화물(Lithium-rich layered oxide: OLO)에 대한 연구가 진행되고 있다.

[0005] 리튬-리치 층상계 산화물을 포함하는 양극 활물질은, 기존 층상계 리튬 전이금속산화물에 Li_2MnO_3 상이 복합화되어 있는 고용체 구조를 가지며, 4.6V 로 초기 충전하면, Li_2MnO_3 에서 산소가 탈리되고, 리튬이 추출됨으로써 200mAhg^{-1} 이상의 고용량을 발현할 수 있다.

[0006] 따라서, 리튬-리치 층상계 산화물이 전기 화학적으로 활성화되기 위해서는 초기 고전압으로 충전하는 과정이 필수적이다. 그러나, 고전압 충전 과정에서 리튬-리치 금속 복합산화물이 전해액과 반응하게 되면, 열화 현상이 발생하고, 고온 및 고전압에서의 망간(Mn) 용출 문제가 보다 심각해져, 전지 성능 및 수명특성이 저하되는 문제점이 발생하였다.

[0007] 따라서, 본원에서는 상기 종래 문제점을 해결하기 위하여, 리튬-리치 금속 복합산화물을 표면 개질하여, 수명특성이 우수한 양극 활물질 및 그를 포함하는 리튬 이차전지를 제공하고자 하였다.

발명의 내용

해결하려는 과제

[0008] 본 발명의 일 구현예는 양극 활물질과 전해액의 부반응을 억제함으로써, 충방전시 열화 현상 및 망간의 용출을 억제하는 양극 활물질을 제공한다.

[0009] 본 발명의 다른 구현예는 상기 양극 활물질을 제조하는 신규한 제조방법을 제공한다.

[0010] 본 발명의 또 다른 구현예는 상기 양극 활물질을 이용한 이차전지로서, 사이클 특성이 우수하며, 220mAhg^{-1} 이상의 방전 용량을 가지는 리튬 이차전지를 제공한다.

과제의 해결 수단

[0011] 본 발명의 일 구현예는, 하기 화학식 1로 표시되는 리튬 금속 복합산화물 코어; 및 상기 리튬 금속 복합산화물 코어 위에 불소 화합물을 함유하는 코팅층을 포함하는, 리튬 이차전지용 양극 활물질을 제공한다.

[0012] [화학식 1]

[0013] $Li_wNi_xCo_yMn_{1-x-y-z}M_zO_2$

[0014] ($1.2 \leq w \leq 1.5$, $0<x<1$, $0y<1$, $0.5 \leq 1-x-y-z$, M은 Al, Mg, Fe, Cu, Zn, Cr, Ag, Ca, Na, K, In, Ga, Ge, V, Mo, Nb, Si, Ti 및 Zr으로 이루어진 군으로부터 선택되는 1 종 이상의 금속).

[0015] 상기 불소 화합물은 CsF, KF, LiF, NaF, RbF, TiF, AgF, AgF, BaF_2, CaF_2, CuF_2, CdF_2, FeF_2, HgF_2, HgF, MnF, MgF, NiF, PbF, SnF_2, SrF_2, XeF_2, ZnF_2, AlF_3, BF_3, BiF_3, CeF_3, CrF_3, DyF_3, EuF_3, GaF_3, GdF_3, FeF_3, HoF_3, InF_3, LaF_3, LuF_3, MnF_3, NdF_3, VOF_3, PrF_3, SbF_3, ScF_3, SmF_3, TbF_3, TiF_3, TmF_3, YF_3, YbF_3, TlF_3, CeF_3, GeF_3, HfF_3, SiF_3, SnF_3, TiF_4, VF_4, ZrF_4, NbF_5, SbF_5, TaF_5, BiF_5, MoF_5, ReF_5, SF_5 및 WF_5으로 이루어진 군으로부터 선택되는 하나 이상일 수 있다.

[0016] 상기 코팅층의 함량은 상기 리튬 금속 복합산화물 코어 총 중량에 대하여 약 0.2 내지 약 1.5 중량% 일 수 있다.

[0017] 상기 코팅층의 두께는 약 5 내지 약 20nm 일 수 있다.

[0018] 상기 코팅층은 ZrO_2, SnO_2 또는 이들의 혼합물을 더 포함할 수 있다.

[0019] 상기 리튬 금속 복합산화물 코어의 평균 입경(D50)이 약 10 내지 약 20㎛일 수 있다.

[0020] 상기 화학식 1에서, w는 약 1.3 내지 약 1.5일 수 있다.

[0021] 상기 리튬 금속 복합산화물 코어는 $Li_{1.3}Ni_{0.2}Co_{0.1}Mn_{0.7}O_2$, $Li_{1.3}Ni_{0.25}Mn_{0.75}O_2$, $Li_{1.3}Ni_{0.25}Co_{0.05}Mn_{0.7}O_2$ 및 $Li_{1.3}Ni_{0.2}Co_{0.1}Al_{0.05}Mn_{0.65}O_2$로 이루어진 군에서 선택되는 하나일 수 있다.

[0022] 본 발명의 다른 구현예는, a) 하기 화학식 1로 표시되는 리튬 금속 복합산화물 코어를 제공하는 단계;

[0023] [화학식 1]

[0024] $Li_wNi_xCo_yMn_{1-x-y-z}M_zO_2$

[0025] ($1.2 \leq w \leq 1.5$, $0<x<1$, $0y<1$, $0.5 \leq 1-x-y-z$, M은 Al, Mg, Fe, Cu, Zn, Cr, Ag, Ca, Na, K, In, Ga, Ge, V, Mo, Nb, Si, Ti 및 Zr으로 이루어진 군으로부터 선택되는 1 종 이상의 금속)

[0026] b) 불소 화합물이 포함된 용액을 제공하는 단계; c) 상기 단계 a)의 리튬 금속 복합산화물 코어에 b) 단계의 불소 화합물을 코팅하는 단계; 및 d) 상기 단계 c)의 코팅된 리튬 금속 복합산화물을 열처리하는 단계를 포함하는, 리튬 이차전지용 양극 활물질의 제조방법을 제공한다.

[0027] 상기 단계 c)에서, 상기 불소 화합물이 포함된 용액을 리튬 금속 복합산화물에 코팅한 뒤, 약 120℃ 내지 약 150℃의 온도에서 용액을 증발시킬 수 있다.

[0028] 상기 단계 d) 의 열처리는 약 380℃ 내지 약 460℃의 온도에서 약 1 내지 약 10시간 동안 실시될 수 있다.

[0029] 상기 단계 b)에서, 리튬 금속 복합산화물 코어를 약 5 내지 약 20nm의 두께로 코팅할 수 있다.

[0030] 상기 단계 b)에서, 불소 화합물이 포함된 용액에는 ZrO_2, SnO_2 또는 이들의 혼합물이 더 포함될 수 있다.

[0031] 본 발명의 또 다른 구현예는, 양극 활물질을 포함하는 양극; 리튬 이온의 삽입/탈리가 가능한 음극 활물질을 포함하는 음극; 상기 양극과 음극 사이에 존재하는 세퍼레이터; 및 비수성 전해질을 포함하는 리튬 이차전지로서, 방전 용량이 $220mAhg^{-1}$ 이상인 리튬 이차전지를 제공한다.

발명의 효과

[0032] 리튬 금속 복합산화물 코어를 불소 화합물로 코팅한 양극 활물질은 리튬 금속 복합산화물과 전해액 간의 부반응을 억제하고, 망간 용출 및 열화 현상을 억제하는 양극 활물질을 제공한다.

[0033] 또한, 리튬 금속 복합산화물 코어 표면에 불소 화합물이 균일하게 코팅되도록 하는, 리튬 이차전지용 양극 활물질의 제조방법을 제공한다.

AMPEREX Ex. 1002
Page 877

[0034] 상기 제조방법에 의하여 제조된 리튬 이차전지용 양극 활물질을 이용하는 리튬 이차전지는 220mAhg^{-1} 이상의 방전 용량을 구현하는 동시에 우수한 수명 특성을 가진다.

도면의 간단한 설명

[0035] 도 1은 불소 화합물로 표면 개질된 코팅된 양극 활물질의 제조방법의 흐름도를 나타낸 것이다.

도 2는 실시예 1에서 제조된 양극 활물질의 SEM 사진 및 EDS 분석 결과를 나타낸 것이다.

도 3은 비교예 1에서 제조된 양극 활물질의 SEM 사진 및 EDS 분석 결결과를 나타낸 것이다.

도 4는 실시예 1, 비교예 1 및 비교예 2에서 제조된 양극 활물질의 충방전 실험 결과를 나타낸 것이다.

발명을 실시하기 위한 구체적인 내용

[0036] 리튬 이차전지용 양극 활물질, 그의 제조방법 및 그를 포함하는 리튬이차전지를 제공한다.

[0037] 이하, 본 발명의 구현예를 상세히 설명하기로 한다. 다만, 이는 예시로서 제시되는 것으로, 이에 의해 본 발명이 제한되지는 않으며 본 발명은 후술할 청구항의 범주에 의해 정의될 뿐이다.

[0038] 본 발명의 일 구현예는 하기 화학식 1로 표시되는 리튬 금속 복합산화물 코어; 및 상기 리튬 금속 복합산화물 코어 위에 불소 화합물을 함유하는 코팅층을 포함하는, 리튬 이차전지용 양극 활물질을 제공한다.

[0039] [화학식 1]

[0040] $Li_wNi_xCo_yMn_{1-x-y-z}M_zO_2$

[0041] ($1.2 \leq w \leq 1.5$, $0<x<1$, $0y<1$, $0.5 \leq 1-x-y-z$, M은 Al, Mg, Fe, Cu, Zn, Cr, Ag, Ca, Na, K, In, Ga, Ge, V, Mo, Nb, Si, Ti 및 Zr으로 이루어진 군으로부터 선택되는 1 종 이상의 금속).

[0042] 상기 화학식 1로 표시되는 리튬 금속 복합산화물 코어는 약 1.2 몰 이상 약 1.5몰 이하의 리튬을 포함하는 리튬-리치 층상계 금속 복합산화물로, 리튬 금속 복합산화물과 Li_2MnO_3가 고용체로 존재하는 구조를 가진다. 상기 리튬 금속 복합산화물을 양극 활물질로 사용하여, 약 4.5 내지 5.0 V에서 전지를 충전하는 경우, Li_2MnO_3가 전기화학적으로 활성화되어, 220mAhg^{-1} 이상의 방전 용량을 구현할 수 있다. 이때, 상기 리튬 금속 복합산화물은 양극 전위를 기준으로 4.6V 이상의 고전압에서 충전시 약 4.6 내지 약 5V의 부근에서 평탄준위구간을 가지면서 산소를 발생시킨다. 이 때, 충전방법은 특별히 제한하지 아니하며, 본 기술분야에서 공지된 방법을 이용하여도 무방하다.

[0043] 상기 리튬 금속 복합산화물 코어는 니켈, 코발트, 망간을 포함할 수 있으며, 니켈, 코발트 및 망간의 몰비는 목적에 따라 적절히 조절될 수 있었다. 망간은 리튬을 제외한 금속에 대해 0.5몰 이상으로 포함될 수 있으며, 리튬 금속 복합산화물의 구조적 안정성을 향상시키며, 상기 망간 중 일부는 수명 특성을 연장시키기 위하여 다른 원소로 치환될 수도 있다. 치환될 수 있는 금속으로는 전이금속 또는 희토류 금속 등이 있으며, 예를 들면, Al, Mg, Fe, Cu, Zn, Cr, Ag, Ca, Na, K, In, Ga, Ge, V, Mo, Nb, Si, Ti 및 Zr으로 이루어진 군으로부터 선택되는 1 종 이상의 금속일 수 있다.

[0044] 상기 리튬 금속 복합산화물 코어는, a) 수용액을 포함하는 공침 반응기에 니켈 원료, 코발트 원료, 망간 원료를 원하는 당량비로 첨가하여 금속 복합 수용액을 제조하는 단계; b) 상기 금속 복합 수용액에 암모니아수 및 수산화나트륨을 첨가하여 제조된 용액의 pH를 10 내지 12로 유지하면서 교반하여, 망간 이온의 분포도를 조절하는 단계; c) 상기 용액을 소정의 온도에서 소정의 시간 동안 시효처리(aging)시켜 금속 복합산화물 전구체를 얻는 단계를 포함하는, 리튬 이차전지용 전구체의 제조방법에 의하여 제조될 수 있다.

[0045] 상기 니켈 원료로는 예를 들면, 황산니켈염, 질산니켈염, 염산니켈염, 초산니켈염 등을 사용할 수 있으며, 코발트 원료로는 예를 들면, 황산코발트염, 질산코발트염, 염산코발트염, 초산코발트염 등을 사용할 수 있으며, 망간 원료로는 예를 들면, 황산망간염, 질산망간염, 염산망간염, 초산망간염 등을 사용할 수 있다.

[0046] 상기 리튬 이차전지용 양극 활물질 전구체의 제조방법에서, 상기 전구체 입자 내의 망간 이온의 분포도를 조절하기 위한 방법으로 공침 반응기의 형태, 공침 반응기의 직경 및 깊의 비율, 교반속도(rpm), 반응액의 pH 등의 여러 변수를 조절할 수 있다.

AMPEREX Ex. 1002
Page 878

[0047] 상기 리튬 이차전지용 전구체의 제조방법 중, 단계 b)에서, 상기 용액을 약 1000 내지 약 3000rpm로 교반할 수 있다. 만약, 공침 전구체 제조시 교반 속도를 1000rpm 미만으로 설정하는 경우, 균일한 교반이 일어나지 않아 특히 내부의 조성 균일도가 현저히 낮아지는 문제점이 있으며, 3000rpm 초과하여 설정하는 경우, 생성된 구형의 전구체가 파괴되는 문제점이 있다.

[0048] 상기 리튬 이차전지용 전구체의 제조방법 중, 단계 c)에서, 상기 용액을 약 10℃ 내지 약 60℃에서 4 내지 20시간 동안 시효처리할 수 있으며, 예를 들면, 약 30℃에서 약 10 시간 동안 시효처리하는 것이 바람직하다. 만약, 공침 전구체 제조시 온도를 60℃ 이상으로 하는 경우, 투입되는 암모니아수의 지속적인 휘발로 인한 pH 제어의 문제점이 있으며, 시간을 20시간 이상으로 하는 경우 생산성이 낮아짐과 동시에 구형의 입자의 과다 성장 및 이로인한 구형 깨짐 현상이 발생하는 문제점이 있다.

[0049] 상기 리튬 금속 복합산화물 코어를 코팅하는 불소 화합물은 CsF, KF, LiF, NaF, RbF, TiF, AgF, AgF_2, BaF_2, CaF_2, CuF_2, CdF_2, FeF_2, HgF_2, Hg_2F_2, MnF_2, MgF_2, NiF_2, PbF_2, SnF_2, SrF_2, XeF_2, ZnF_2, AlF_3, BF_3, BiF_3, CeF_3, CrF_3, DyF_3, EuF_3, GaF_3, GdF_3, FeF_3, HoF_3, InF_3, LaF_3, LuF_3, MnF_3, NdF_3, VOF_3, PrF_3, SbF_3, ScF_3, SmF_3, TbF_3, TiF_3, TmF_3, YF_3, YbF_3, TlF_3, CeF_3, GeF_3, HfF_3, SiF_3, SnF_3, TiF_4, VF_4, ZrF_4, NbF_5, SbF_5, TaF_5, BiF_5, MoF_5, ReF_5, SF_5 및 WF_5으로 이루어진 군으로부터 선택되는 하나 이상일 수 있으며, 예를 들면 AlF_3, BF_3, ZrF_4 등 일 수 있다.

[0050] 본 발명의 일 구현예에 있어서, 상기 불소 화합물은 상기 리튬 금속 복합산화물의 표면에 약 5 내지 약 20nm의 두께로 코팅될 수 있으며, 상기 코팅층은, 금속염을 포함하는 용액과 플루오르계 화합물을 포함하는 용액을 혼합하여 제조한 불소 화합물 수용액에 리튬 금속 복합산화물을 침지하거나 또는 상기 불소 화합물 수용액을 리튬 금속 복합산화물에 스프레이 건조하는 방법으로 제조될 수 있으며, 그 밖에 공지된 코팅 방법을 사용할 수도 있다. 코팅층의 두께가 약 5 내지 약 20nm인 경우, 양극 활물질의 도전성을 낮추지 않으면서, 망간 용출을 억제하는 효과를 얻을 수 있다 코팅층의 두께가 5nm 이하가 되면 표면상의 코팅층원 분포도가 상대적으로 낮아져서 망간 용출의 억제효과를 볼 수 없으며, 반대로 코팅층이 20nm 이상이 되면 리튬이온의 통과가 어렵게 되어 출력특성에 제한을 받게될 뿐만 아니라 첫 충전에서의 전기화학적 활성화에도 제한을 받게 된다.

[0051] 상기 코팅층의 함량은 상기 리튬 금속 복합산화물 코어 총 중량에 대하여 약 0.2 내지 약 1.5 중량%일 수 있다.

[0052] 상기 코팅층은 ZrO_2, SnO_2 또는 이들의 혼합물을 더 포함할 수 있다.

[0053] 상기 리튬 금속 복합산화물 코어의 평균입경(D50)은 약 10 내지 약 20㎛일 수 있다. 양극 활물질의 평균입경이 상기 수치 범위 내인 경우, 입도 분포가 균일하고, 구형화도가 높으며, 내부 치밀도가 높은 양극 활물질을 제조할 수 있으며, 이는 리튬 이차전지 제조시 높은 방전 용량을 구현할 수 있다.

[0054] 상기 화학식 1에서 w는 1.3 내지 1.5 일 수 있으며, 상기 리튬 금속 복합산화물 코어는 $Li_{1.3}Ni_{0.2}Co_{0.1}Mn_{0.7}O_2$, $Li_{1.3}Ni_{0.25}Mn_{0.75}O_2$, $Li_{1.3}Ni_{0.25}Co_{0.05}Mn_{0.7}O_2$ 및 $Li_{1.3}Ni_{0.2}Co_{0.1}Al_{0.05}Mn_{0.65}O_2$로 이루어진 군에서 선택되는 하나일 수 있다. 이와 같이, 리튬이 약 1.2 몰, 예를 들면 약 1.3 몰 이상인 경우, 고용량 양극 활물질을 제공할 수 있다.

[0055] 본 발명의 또 다른 구현예는, 리튬 금속 복합산화물 코어 및 불소 화합물 코팅층을 포함하는 양극 활물질의 제조방법을 제공한다.

[0056] 상기 양극 활물질의 구체적인 제조방법은 a) 하기 화학식 1로 표시되는 리튬 금속 복합산화물 코어를 제공하는 단계;

[0057] [화학식 1]

[0058] $Li_wNi_xCo_yMn_{1-x-y-z}M_zO_2$

[0059] ($1.2 \leq w \leq 1.5$, $0<x<1$, $0y<1$, $0.5 \leq 1-x-y-z$, M은 Al, Mg, Fe, Cu, Zn, Cr, Ag, Ca, Na, K, In, Ga, Ge, V, Mo, Nb, Si, Ti 및 Zr으로 이루어진 군으로부터 선택되는 1 종 이상의 금속).

[0060] b) 불소 화합물이 포함된 용액을 제공하는 단계; c) 상기 단계 a)의 리튬 금속 복합산화물 코어를 b) 단계의 불소 화합물을 포함하는 용액으로 코팅하는 단계; 및 d) 상기 단계 c)의 코팅된 리튬 금속 복합산화물을 열처리하는 단계를 포함한다.

AMPEREX Ex. 1002
Page 879

[0061] 상기 단계 c)에서, 상기 불소 화합물이 포함된 용액을 리튬 금속 복합산화물에 코팅한 뒤, 약 120℃ 내지 약 150℃의 온도에서 용액을 증발시킬 수 있다.

[0062] 상기 단계 d) 의 열처리는 약 380℃ 내지 약 460℃의 온도에서 약 1 내지 약 10 시간 동안 실시될 수 있다.

[0063] 상기 단계 b)에서, 리튬 금속 복합산화물 코어를 약 5 내지 약 20nm의 두께로 코팅할 수 있다. 코팅층의 두께가 약 5 내지 약 20nm인 경우, 양극 활물질의 도전성을 낮추지 않으면서, 망간 용출을 억제하는 효과를 얻을 수 있다. 코팅층의 두께가 약 5nm 이하가 되면 표면상의 코팅층의 분포도가 상대적으로 낮아져서 망간 용출의 억제 효과를 볼 수 없으며, 반대로 코팅층이 약 20nm 이상이 되면 리튬 이온 잘 통과하지 못해 출력특성에 제한을 받게 될 뿐만 아니라, 첫 충전에서의 전기화학적 활성화에도 제한을 받게 된다.

[0064] 상기 단계 b)에서, 불소 화합물이 포함된 용액에는 ZrO_2, SnO_2 또는 이들의 혼합물이 더 포함될 수 있다.

[0065] 본 발명의 또 다른 구현예는 상기 화학식 1로 표시되는 리튬 금속 복합산화물 코어; 및 상기 리튬 금속 복합산화물 코어 위에 불소 화합물을 함유하는 코팅층을 포함하는 양극 활물질을 포함하는 양극; 리튬 이온의 삽입/탈리가 가능한 음극 활물질을 포함하는 음극; 상기 양극과 음극 사이에 존재하는 세퍼레이터; 및 비수성 전해질을 포함하는 리튬 이차 전지로서, 방전 용량이 $220mAhg^{-1}$ 이상인 리튬 이차전지를 제공한다.

[0066] 상기 리튬 이차전지의 형태는 코인, 버튼, 시트, 원통형, 각형 등 어느 것이라도 좋다. 상기 리튬 이차전지들은 공지된 방법으로 제조될 수 있으며, 이러한 제조방법에 대한 구체적인 설명은 생략하기로 한다. 또한, 양극 극판의 제작 및 리튬 이차전지의 구성에 대해 간단하게 설명하지만, 이것들에 한정되는 것은 아니다.

[0067] 상기 양극은 상기 화학식 2로 표시되는 양극 활물질을 도전재, 바인더와 기타 첨가제, 예를 들면 필러, 분산제, 이온 도전재, 압력 증강제 등의 1종 이상의 첨가제와 함께 적절한 유기용매에 용해시킨 후, 슬러리 또는 페이스트(paste)로 제조하여, 이를 전류 집전체 위에 도포, 건조, 프레스함으로써 제조될 수 있다.

[0068] 상기 양극은 전류 집전체 및 상기 화학식 2로 표시되는 양극 활물질 층을 포함하며, 상기 양극 활물질 표면에 코팅층을 갖는 것도 사용할 수 있고, 또는 상기 양극 활물질과 코팅층을 갖는 화합물을 혼합하여 사용할 수도 있다. 상기 코팅층은 코팅 원소 화합물로서, Mg, Al, Co, K, Na, Ca, Si, Ti, V, Sn, Ge, Ga, B, As, Zr의 산화물 또는 이들의 혼합물을 사용할 수 있다.

[0069] 상기 바인더는 폴리비닐알콜, 카르복시메틸셀룰로즈, 히드록시프로필셀룰로즈, 디아세틸셀룰로즈, 폴리비닐클로라이드, 카르복실화된 폴리비닐클로라이드, 폴리비닐플루오라이드, 에틸렌 옥사이드를 포함하는 폴리머, 폴리비닐피롤리돈, 폴리우레탄, 폴리테트라플루오로에틸렌, 폴리비닐리덴 플루오라이드, 폴리에틸렌, 폴리프로필렌, 스티렌-부타디엔 러버, 아크릴레이티드 스티렌-부타디엔 러버, 에폭시 수지, 나일론 등이 사용될 수 있으나, 이에 한정되는 것은 아니다.

[0070] 상기 도전재는 전극에 도전성을 부여하기 위해 사용되는 것으로서, 구성되는 전지에 있어서, 화학변화를 야기하지 않고 전자 전도성 재료이면 어떠한 것도 사용가능하며, 그 예로 천연 흑연,인조 흑연, 카본 블랙, 아세틸렌 블랙, 케첸블랙, 탄소섬유, 구리, 니켈, 알루미늄, 은 등의 금속 분말, 금속 섬유 등을 사용할 수 있고, 또한 폴리페닐렌 유도체 등의 도전성 재료를 1종 또는 1종 이상을 혼합하여 사용할 수 있다.

[0071] 상기 양극의 전류 집전체로는 동, 니켈, 스텐레스강철, 알루미늄 등의 박, 시트 혹은 탄소섬유 등이 사용될 수 있다.

[0072] 상기 음극은 집전체 및 상기 집전체 위에 형성된 음극 활물질층을 포함한다.

[0073] 상기 음극 활물질로는 리튬 이온을 가역적으로인터칼레이션/디인터칼레이션할 수 있는 흑연 등의 카본물질 또는 전이금속의 복합 산화물 등의 1종 혹은 2종 이상을 사용할 수 있다. 그 외, 실리콘, 주석 등도 음극재료로서 사용할 수 있다.

[0074] 상기 음극 활물질 층은 또한 바인더를 포함하며, 선택적으로 도전재를 더욱 포함할 수도 있다.

[0075] 상기 바인더는 음극 활물질 입자들을 서로 잘 부착시키고, 또한 음극 활물질을 전류 집전체에 잘 부착시키는 역할을 하며, 그 대표적인 예로 폴리비닐알콜, 카르복시메틸셀룰로즈, 히드록시프로필셀룰로즈, 폴리비닐클로라이드, 카르복실화된 폴리비닐클로라이드, 폴리비닐플루오라이드, 에틸렌 옥사이드를 포함하는 폴리머, 폴리비닐피

롤리돈, 폴리우레탄, 폴리테트라플루오로에틸렌, 폴리비닐리덴 플루오라이드, 폴리에틸렌, 폴리프로필렌, 스티렌-부타디엔 러버, 아크릴레이티드 스티렌-부타디엔 러버, 에폭시 수지, 나일론 등을 사용할 수 있으나, 이에 한정되는 것은 아니다.

[0076] 상기 도전재의 예로는, 천연 흑연,인조 흑연, 카본 블랙, 아세틸렌 블랙, 케첸블랙, 탄소섬유 등의 탄소계 물질; 구리, 니켈, 알루미늄, 은 등의 금속 분말 또는 금속 섬유 등의 금속계 물질; 폴리페닐렌 유도체 등의 도전성 폴리머; 또는 이들의 혼합물을 포함하는 도전성 재료를 사용할 수 있다.

[0077] 상기 음극 집전체로는 구리 박, 니켈 박, 스테인레스강 박, 티타늄 박, 니켈 발포체(foam), 구리 발포체, 전도성 금속이 코팅된 폴리머 기재, 또는 이들의 조합을 사용할 수 있다.

[0078] 상기 전해질은 비수성 유기 용매와 리튬염을 포함한다.

[0079] 상기 비수성 유기용매로는 카보네이트계, 에스테르계, 에테르계, 케톤계, 알코올계 또는 비양성자성 용매를 사용할 수 있다. 상기 카보네이트계 용매로는 디메틸 카보네이트(DMC), 디에틸 카보네이트(DEC), 디프로필 카보네이트(DPC), 메틸프로필 카보네이트(MPC), 에틸프로필 카보네이트(EPC), 메틸에틸 카보네이트(MEC), 에틸렌 카보네이트(EC), 프로필렌 카보네이트(PC), 부틸렌 카보네이트(BC) 등이 사용될 수 있으며, 상기 에스테르계 용매로는 메틸 아세테이트, 에틸 아세테이트, n-프로필 아세테이트, 디메틸아세테이트, 메틸프로피오네이트, 에틸프로피오네이트, -부티로락톤, 데카놀라이드(decanolide), 발레로락톤, 메발로노락톤(mevalonolactone), 카프로락톤(caprolactone) 등이 사용될 수 있다. 상기 에테르계 용매로는 디부틸 에테르, 테트라글라임, 디글라임, 디메톡시에탄, 2-메틸테트라히드로퓨란, 테트라히드로퓨란 등이 사용될 수 있으며, 상기 케톤계 용매로는 시클로헥사논 등이 사용될 수 있다. 또한 상기 알코올계 용매로는 에틸알코올, 이소프로필 알코올 등이 사용될 수 있으며, 상기 비양성자성 용매로는 R-CN(R은 C2 내지 C20의 직쇄상, 분지상 또는 환 구조의 탄화수소기이며, 이중결합 방향 환 또는 에테르 결합을 포함할 수 있다) 등의 니트릴류, 디메틸포름아미드 등의 아미드류, 1,3-디옥솔란 등의 디옥솔란류, 설포란(sulfolane)류 등이 사용될 수 있다.

[0080] 상기 비수성 유기 용매는 단독으로 또는 하나 이상 혼합하여 사용할 수 있으며, 하나 이상 혼합하여 사용하는 경우의 혼합 비율은 목적하는 전지 성능에 따라 적절하게 조절할 수 있고, 이는 당해 분야에 종사하는 사람들에게는 널리 이해될 수 있다.

[0081] 이러한 용매에 용해하는 리튬염으로는 LiClO, LiBF, $LiPF_6$, $LiAlCl_4$, $LiSbF_6$, LiSCN, $LiCF_3SO$, $LiCF_3CO$, $Li(CF_3SO)$, $LiAsF_6$, $LiN(CF_3SO)$, $LiB_{10}Cl_{10}$, LiBOB(Lithium Bis(oxalato)borate), 저급 지방족 카르본산 리튬(Lithium), 클로로 보란 리튬(chloro borane Lithium), LiN(CF3SO2), $Li(C_2F_5SO_2)$, $LiN(CF_3SO_2)_2$, $LiN(C_2F_5SO_2)_2$, $LiN(CF_3SO_2)(C_4F_9SO_2)$등의 이미드(imide)류 등을 들 수 있다. 이것들은 사용하는 전해액 등에 각각 단독으로 또는 본 발명의 효과를 손상시키지 않은 범위에서 임의로 조합시키고 사용할 수 있다. 이중에서, 특별히 $LiPF_6$을 포함시키는 것이 보다 바람직하다. 또, 전해액을 불연성으로 하기 위해 사염화탄소, 삼불화 염화 에틸렌(ethylene), 혹은인이 포함된인산염 등을 전해액에 포함시킬 수 있다.

[0082] 세퍼레이터로는 폴리에틸렌, 폴리프로필렌, 폴리비닐리덴 플루오라이드 또는 이들의 2층 이상의 다층막이 사용될 수 있으며, 폴리에틸렌/폴리프로필렌 2층 세퍼레이터, 폴리에틸렌/폴리프로필렌/폴리에틸렌 3층 세퍼레이터, 폴리프로필렌/폴리에틸렌/폴리프로필렌 3층 세퍼레이터 등과 같은 혼합 다층막이 사용될 수 있다.

[0083] 이하 본 발명의 실시예 및 비교예를 기재한다. 하기 실시예는 본 발명의 일 실시예일뿐 본 발명이 하기한 실시예에 한정되는 것은 아니다.

[0084] **실시예 1**

[0085] **<u>리튬 금속 복합산화물 코어의 제조</u>**

[0086] 황산니켈염, 황산코발트염, 황산망간염을 0.20 : 0.10 : 0.70의 몰비로, 물이 들어 있는 공침 반응기에 10mL/min의 속도로 첨가하여, 1M의 금속 복합 수용액을 제조하였다. 상기 공침 반응기는 원통형 구조를 가지는 것으로, 상기 공침 반응기의 직경 및 깊이를 적절히 조절하여 사용하였으며, 상기 금속 복합 수용액이 담긴 공침 반응기에 1M의 암모니아수를 5mL/min의 속도로 투입시키면서, pH 제어기를 통해 pH가 11이 되도록 유지하면서 수산화나트륨을 첨가하였다. 상기 금속 복합 수용액을 1000 rpm으로 교반하고, 10 시간 시효시켜, 구형 전구

AMPEREX Ex. 1002
Page 881

체를 제조하였다. 상기 제조된 전구체를 30℃이상의 초순수로 pH가 8이하가 될 때까지 수세한 후에 80℃에서 12시간 건조하였다. 건조된 공침전구체에 대하여 1.3 당량비의 탄산리튬을 첨가하여 혼합하였다. 이를 900℃에서 10시간 공기 중에서 열처리하여, $Li_{1.3}Ni_{0.2}Co_{0.1}Mn_{0.7}O_2$을 제조하였다.

[0087] **리튬 금속 복합산화물 코어의 코팅**

[0088] 알루미늄염을 포함하는 수용액에 NH_4F(Aldrich)를 포함하는 수용액을 용해시킨 후, 10 분 이상 교반하여 균일한 혼합용액을 제조하였다. 얻어진 혼합용액을 상기 제조된 $Li_{1.3}Ni_{0.2}Co_{0.1}Mn_{0.7}O_2$에 스프레이 코팅한 뒤, 비활성 분위기 하에서, 400℃로 5시간 동안 열처리하였다. 상기 제조방법에 의하여 얻은 양극 활물질에 코팅된 코팅층은 두께가 10㎚이었으며, 코팅층의 함량은 리튬 금속복합 산화물의 총량에 대하여 0.5중량%이었다.

[0089] **리튬 이차전지의 제조**

[0090] 상기 제조된 양극 활물질의 평균입자 크기 입경이 25㎛가 되도록 분급하고, 상기 양극 활물질 90 중량%, 도전재로 아세틸렌 블랙 5 중량%, 바인더로 PVdF 5 중량%를 NMP에 용해시켜, 슬러리를 제조하였다. 이 슬러리를 두께 20㎛의 알루미늄 포일(foil)에 도포하여 건조 후 프레스로 압밀화시킨 뒤, 진공에서 120℃로 16시간 건조해 직경 16㎜의 원판으로 전극을 제조하였다. 상대극으로는 직경 16㎜로 펀칭(punching)한 리튬 금속박을 사용하고, 분리막으로는 PP 필름을 사용하였다. 전해액으로는 1M의 $LiPF_6$의 EC/DME 1:1 v/v의 혼합 용액을 사용하였다. 전해액을 분리막에 함침시킨 후, 이 분리막을 작용극과 상대극 사이에 끼운 후 케이스(모델명 CR2032, SUS사)를 사용하여 리튬 이차전지를 제조하였다.

[0091] **실시예 2**

[0092] 코팅층의 함량을 리튬 금속복합 산화물의 총량에 대하여 1.0중량%인 것을 제외하고, 상기 실시예 1과 동일한 방법을 사용하여, 양극 활물질 및 그를 포함하는 이차전지를 제조하였다.

[0093] **비교예 1**

[0094] 리튬 금속 복합산화물을, 알루미늄염을 포함하는 수용액에 NH_4F(Aldrich)를 포함하는 수용액을 용해시킨 후, 10 분 이상 교반하여 균일한 혼합용액으로 코팅하는 단계를 제외하고, 상기 실시예 1과 동일한 방법을 사용하여, $Li_{1.3}Ni_{0.2}Co_{0.1}Mn_{0.7}O_2$을 제조하였으며, 이를 포함하는 이차전지를 제조하였다.

[0095] .

[0096] **비교예 2**

[0097] 코팅된 리튬 금속 복합산화물을 350℃로 열처리 하는 것을 제외하고, 상기 실시예 1과 동일한 방법을 사용하여, 양극 활물질 및 그를 포함하는 이차전지를 제조하였다.

[0098] **비교예 3**

[0099] 코팅된 리튬 금속 복합산화물을 400℃로 열처리 하는 것을 제외하고, 상기 실시예 1과 동일한 방법을 사용하여, 양극 활물질 및 그를 포함하는 이차전지를 제조하였다.

[0100] **비교예 4**

[0101] 코팅된 리튬 금속 복합산화물을 350℃로 열처리 하는 것을 제외하고, 상기 실시예 2와 동일한 방법을 사용하여, 양극 활물질 및 그를 포함하는 이차전지를 제조하였다.

AMPEREX Ex. 1002
Page 882

[0102] **비교예 5**

[0103] 코팅된 리튬 금속 복합산화물을 400℃로 열처리 하는 것을 제외하고, 상기 실시예 2와과 동일한 방법을 사용하여, 양극 활물질 및 그를 포함하는 이차전지를 제조하였다.

[0104] 표 1은 실시예 1 및 실시예 2와 비교예 1 내지 5의 실험 조건, 코팅층에 함유된 불소 화합물의 종류 및 코어 총량에 대한 코팅층의 함량(중량%)을 하기 표 1에 나타내었다.

[0105] 표 1

	불소 화합물	코팅층의 함량 (중량 %)	코팅 후 열처리 온도 (℃)
실시예 1	AlF_3	0.5	400
실시예 2	AlF_3	1.0	400
비교예 1	N	0.0	N
비교예 2	AlF_3	0.5	350
비교예 3	AlF_3	0.5	450
비교예 4	AlF_3	1.0	350
비교예 5	AlF_3	1.0	450

[0106] **실험예**

[0107] SEM 촬영 및 EDS 분석

[0108] JSM-7000F(Jeol사) 이용하여 실시예 1 및 비교예 2에서 제조된 공침 전구체의 SEM 사진을 촬영하고, 양극 활물질의 표면에 분포하는 금속(Mn, Co, Ni, Al, F)의 분산도를 측정하기 위하여, EDS(Energy dispersive spectroscopy, Oxford) 분석을 실시하여, 그 결과를 도 2 및 도 3에 도시하였다.

[0109] 도 2 및 도 3에 도시된 양극 활물질은 리튬 금속복합 산화물을 코어로 포함하고, 표면에는 불소 화합물을 함유하는 코팅층을 가진다. 도 2와 도 3을 비교할 때, 실시예 1에서 제조된 양극 활물질은 비교예 1에서 제조된 양극 활물질에 비하여 Al 및 F의 원소의 분포도가 더욱 균일한 것을 알 수 있다. 이로부터 실시예 1의 제조방법에 의하는 경우에, 불소 화합물을 포함하는 코팅층이 매우 균일하게 코팅될 수 있음을 알 수 있다.

[0110] **전지 용량 평가**

[0111] 실시예 1, 실시예 2 및 비교예 1 내지 5에서 제조된 리튬 이차전지를 25℃ 환경 하에서, 25mA/g의 정전류로 4.6V가 되기까지 충전을 행한 뒤, 4.6V의 정전압으로 2.5mA/g가 되기까지 충전을 행한 후, 25mA/g의 정전류로 2.0V가 되기까지 방전을 행했을 때의 전지 용량을 구하였다.

[0112] **사이클 특성 평가**

[0113] 실시예 1, 실시예 2 및 비교예 1 내지 5에서 제조된 리튬 이차전지를 30회 충방전 반복하였다. 구체적으로, 실시예 1, 실시예 2 및 비교예 1 내지 5에서 제조된 리튬 이차전지를, 60℃ 환경 하에서, 25mA/g의 정전류로 전압값이 4.6V가 되기까지 충전을 행하며, 그 후, 4.6V의 정전압으로 전류값이 5mA/g가 되기까지 충전을 행한 뒤, 25mA/g의 정전류로 전압값이 2.0V가 되기까지 방전을 한다. 이를 1 사이클로 하여, 이 사이클을 30 사이클 반복하고, 용량 유지율을 평가하였다. 용량 유지율은 하기 식으로 산출하였다.

[0114] 용량 유지율 (%) = 30 사이클의 용량/ 1 사이클의 용량 X 100

[0115] 상기 실험을 통하여, 실시예 1, 실시예 2 및 비교예 1 내지 5에서 제조된 리튬 이차전지에 대한 방전 용량 및 30 사이클 용량 유지율을 하기 표 2에 나타내었다.

AMPEREX Ex. 1002
Page 883

[0116] 표 2

	25°C에서 초기 방전용량 ($mAhg^{-1}$)	60°C에서, 30 사이클 용량 유지율(%)
실시예 1	234	90.4
실시예 2	226	90.2
비교예 1	240	81.7
비교예 2	231	85.8
비교예 3	238	84.1
비교예 4	215	86.4
비교예 5	224	85.4

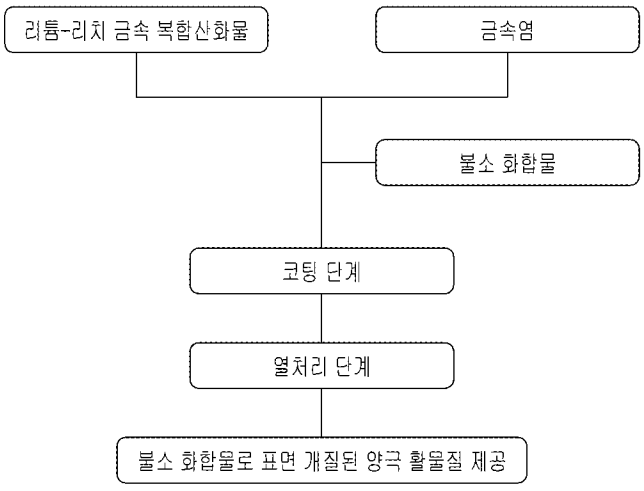
[0117] 상기 표 2에서 알 수 있듯이, 실시예 1 및 2의 경우 초기 방전 용량이 $220mAhg^{-1}$ 이상으로 높았으며, 30 사이클 후에도 용량 유지율은 모두 90% 이상으로 상당히 높았다. 그에 반해, 코팅층을 포함하지 않는 비교예 1의 양극 활물질은 초기 방전 용량이 $240mAhg^{-1}$으로 높은 반면, 30 사이클 후의 용량은 초기 방전 용량은 81.7%로 매우 낮음을 확인하였다. 이로부터 불소 화합물로 코팅된 리튬-리치 금속 복합산화물을 포함하는 양극 활물질은 수명 특성이 개선됨을 알 수 있다. 도 5는 실시예 1, 비교예 1 및 비교예 2에서 제조된 양극 활물질의 사이클 특성을 나타낸 그래프이다.

[0118] 상기 표 2에 나타낸 바와 같이, 실시예 1 및 실시예 2에서 제조된 양극 활물질은 비교예 2 내지 5에서 제조된 양극 활물질에 비하여, 사이클 특성이 우수하였다. 실시예 1 및 실시예 2의 경우 용량 유지율이 90%이상인 반면, 비교예 2 내지 비교예 5는 용량 유지율이 약 81 내지 85%에 불과하였다. 이는 본원의 제조방법에 의하는 경우, 불소 화합물이 리튬 금속 복합산화물 코어에 균일하게 분포되기 때문인 것으로, 코팅층이 코어에 균일하게 피복되면 리튬-리치 층상계 금속 복합산화물과 전해액 간의 부반응이 방지되어 사이클 특성이 향상될 수 있다.

[0119] 한편, 본 명세서와 도면에 개시된 본 발명의 실시예들은 이해를 돕기 위해 특정 예를 제시한 것에 지나지 않으며, 본 발명의 범위를 한정하고자 하는 것은 아니다. 여기에 개시된 실시예들 이외에도 본 발명의 기술적 사위에 바탕을 둔 다른 변형예들이 실시 가능하다는 것은, 본 발명이 속하는 기술분야에서 통상의 지식을 가진 자에게 자명한 것이다.

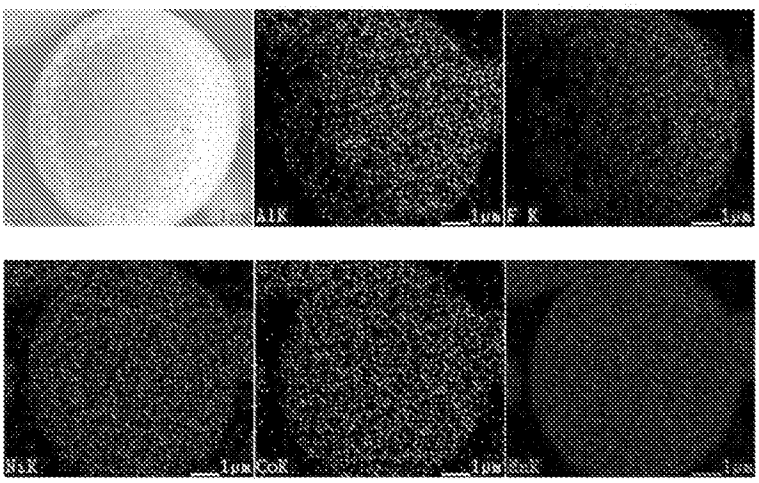
도면

도면1

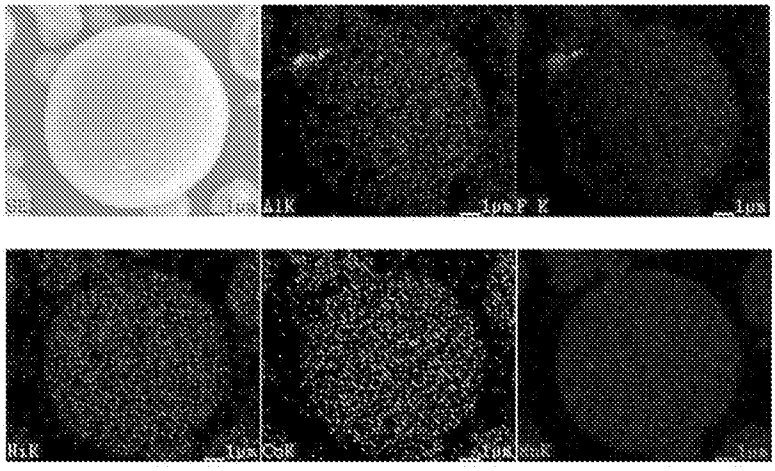


AMPEREX Ex. 1002
Page 884

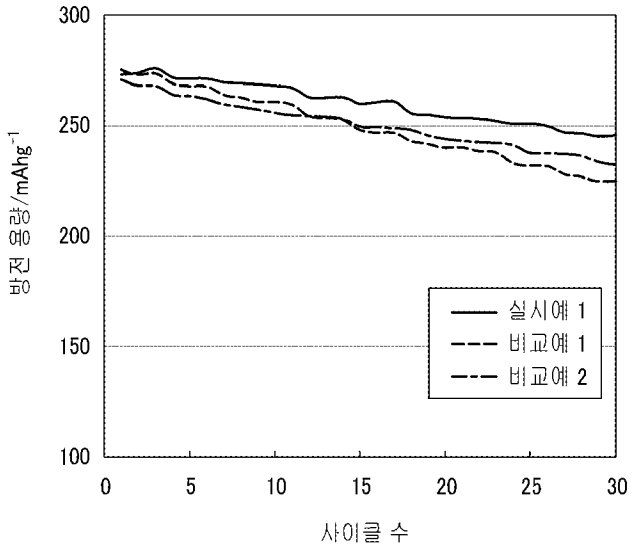
도면2



도면3



도면



AMPEREX Ex. 1002
Page 886

Espacenet

Family list: KR20110134852 (A) — 2011-12-15

2 application(s) for: KR20110134852 (A)

1. CATHODE ACTIVE MATERIAL FOR LITHIUM SECONDARY BATTERY, MANUFACTURING METHOD FOR THE SAME AND LITHIUM SECONDARY BATTERY COMPRISING THE SAME					
Inventor: HONG JI JUN [KR] BYUN KI TAEK [KR] (+1)	**Applicant:** ROUTE JJ CO LTD [KR]	**CPC:** C01G23/005 C01G45/1235 C01G49/009 (+20)	**IPC:** H01M4/485 H01M4/505 H01M4/525 (+1)	**Publication info:** KR20110134852 (A) 2011-12-15 KR101393651 (B1) 2014-05-13 Global Dossier	**Priority date:** 2010-06-09
2. POSITIVE ELECTRODE ACTIVE MATERIAL FOR A LITHIUM SECONDARY BATTERY, METHOD FOR PRODUCING SAME AND LITHIUM SECONDARY BATTERY COMPRISING SAME					
Inventor: HONG JI JUN [KR] BYUN KI TAEK [KR] (+1)	**Applicant:** ROUTE JJ CO LTE [KR] HONG JI JUN [KR] (+2)	**CPC:** C01G23/005 C01G45/1235 C01G49/009 (+20)	**IPC:** H01M4/485 H01M4/505 H01M4/525 (+1)	**Publication info:** WO2011155781 (A2) 2011-12-15 WO2011155781 (A3) 2012-04-19 Global Dossier	**Priority date:** 2010-06-09

Espacenet

Bibliographic data: KR20110134852 (A) — 2011-12-15

CATHODE ACTIVE MATERIAL FOR LITHIUM SECONDARY BATTERY, MANUFACTURING METHOD FOR THE SAME AND LITHIUM SECONDARY BATTERY COMPRISING THE SAME

Inventor(s): HONG JI JUN [KR]; BYUN KI TAEK [KR]; KIM HYO WON [KR] ± (HONG, JI JUN, ; BYUN, KI TAEK, ; KIM, HYO WON)

Applicant(s): ROUTE JJ CO LTD [KR] ± (ROUTE JJ CO., LTD)

Classification: - international: ***H01M4/485; H01M4/505; H01M4/525; H01M4/583***
- cooperative: **C01G23/005 (EP)**; **C01G45/1235 (EP)**; **C01G49/009 (EP)**; **C01G51/40 (EP)**; **C01G51/52 (EP)**; **C01G53/40 (EP)**; **C01G53/52 (EP)**; **H01M4/131 (EP)**; **H01M4/364 (EP)**; **H01M4/485 (EP, KR)**; **H01M4/505 (EP, KR)**; **H01M4/525 (EP, KR)**; **H01M4/583 (KR)**; **H01M4/587 (EP)**; C01P2002/50 (EP); C01P2002/72 (EP); C01P2004/03 (EP); C01P2004/61 (EP); C01P2004/62 (EP); C01P2006/10 (EP); C01P2006/40 (EP); H01M10/052 (EP); H01M4/625 (EP)

Application number: KR20110055678 20110609 Global Dossier

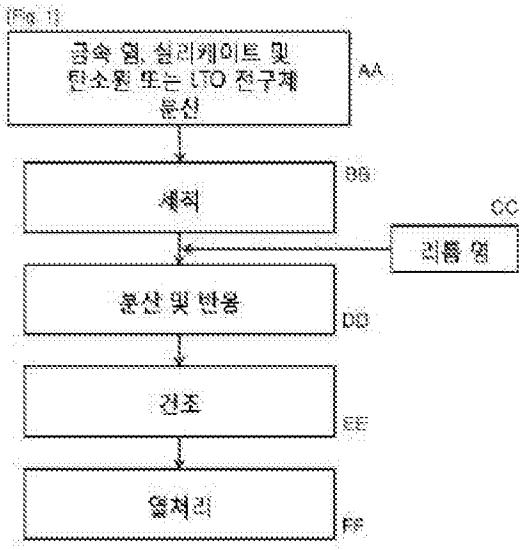
Priority number(s): KR20100054224 20100609

Also published as: KR101393651 (B1) WO2011155781 (A2) WO2011155781 (A3)

Abstract of KR20110134852 (A)

PURPOSE: A cathode active material for lithium secondary battery has moderate energy density for secondary battery, excellent stability and safety, and long cycle life maintaining excellent battery characteristic. CONSTITUTION: A cathode active material for lithium secondary battery comprises LinMO4/x composite. M is one or more element selected from the group consisting of Mn, Fe, Co, Ni, Al, Mn, V, Cr, Fe, Co, Zn, Zr, Nb, Mo, Ag, Ge, Sn, Mg, Si, S, Ca, Ti, Cu, Ba, W and Pb. X is carbon source or lithium titanium oxide or mixture thereof, n is integer. The carbon source is one or more kind selected from the group consisting of carbon nanotubes, carbon nanowires, carbon nanofiber, graphite, and graphene.

[Fig. 1]



AA ... Metal salt, silicate and carbon source or LTO precursor dispersion
BB ... Cleaning
CC ... Lithium salt
DD ... Dispersion and reaction
EE ... Drying
FF ... Heat treatment

(19) 대한민국특허청(KR)
(12) 공개특허공보(A)

(11) 공개번호 10-2011-0134852
(43) 공개일자 2011년12월15일

(51) Int. Cl.
H01M 4/505 (2010.01) *H01M 4/525* (2010.01)
H01M 4/485 (2010.01) *H01M 4/583* (2010.01)
(21) 출원번호 10-2011-0055678
(22) 출원일자 2011년06월09일
심사청구일자 2011년06월09일
(30) 우선권주장
1020100054224 2010년06월09일 대한민국(KR)

(71) 출원인
주식회사 루트제이제이
경기 시흥시 정왕동 1261-3 시화공단2나 304호
(72) 발명자
홍지준
서울특별시 강남구 개포동 172-3 현대아파트 501-502
변기택
서울특별시 강서구 등촌1동 631-9 대동황토방아파트 101동 1204호
김효원
경기도 시흥시 정왕동 1366-14 파인힐오피스텔 C동 409호
(74) 대리인
엄명용

전체 청구항 수 : 총 11 항

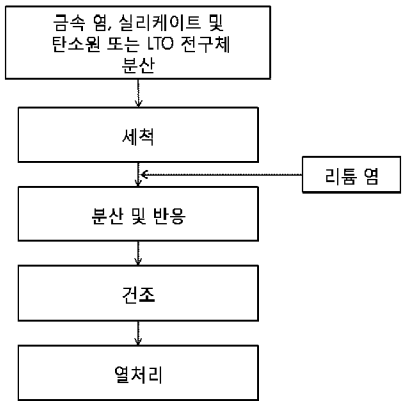
(54) 리튬 이차전지용 양극 활 물질, 그 제조방법 및 이를 포함하는 리튬 이차전지

(57) 요 약

리튬 이차전지용 양극 활 물질, 그 제조방법 및 이를 포함하는 리튬 이차전지가 제공된다.

본 발명에 따른 리튬 이차전지용 양극 활 물질은 Li_nMO_4 / X의 복합체를 포함하며, 여기에서 M은 Mn, Fe, Co, Ni, Al, Mn, V, Cr, Fe, Co, Zn, Zr, Nb, Mo, Ag, Ge, Sn, Mg, Si, S, Ca, Ti, Cu, Ba, W 및 Pb로 이루어진 군으로부터 선택된 1종 또는 2종 이상의 원소이며, X는 탄소원 또는 리튬티탄산화물(Lithium Titanium Oxide, $Li_4Ti_5O_{12}$) 또는 이들의 혼합물인 것을 특징으로 하며, 본 발명에 따르면, 경제적인 방식으로 우수한 전기 전도도 및 기계적 특성을 갖는 리튬이차전지용 양극 활 물질이 제조될 수 있다. 특히, 상기 Li_nMO_4 입자상 표면에 균일하게 분산, 함유된 탄소원 또는 리튬티탄산화물(LTO)은 리튬이차전지용 양극 활 물질 복합체로 하여금 향상된 전기 전도도를 갖게 한다. 또한, 본 발명에 따른 양극 활 물질은 이차전지에 적용하기 적합한 에너지 밀도를 가지고, 안정성과 안전성이 뛰어나며, 우수한 전지특성을 유지하면서도 사이클 수명이 긴 장점을 갖는다.

대 표 도 - 도1



AMPEREX Ex. 1002
Page 890

특허청구의 범위

청구항 1

리튬이차전지용 양극 활 물질로서, 상기 양극 활 물질은

Li_nMO_4 / X의 복합체를 포함하며, 여기에서 M은 Mn, Fe, Co, Ni, Al, Mn, V, Cr, Fe, Co, Zn, Zr, Nb, Mo, Ag, Ge, Sn, Mg, Si, S, Ca, Ti, Cu, Ba, W 및 Pb로 이루어진 군으로부터 선택된 1종 또는 2종 이상의 원소이며, X는 탄소원 또는 리튬티탄산화물(Lithium Titanium Oxide, $Li_4Ti_5O_{12}$) 또는 이들의 혼합물이고, n은 정수인 것을 특징으로 하는 리튬이차전지용 양극 활 물질.

청구항 2

제 1항에 있어서,

상기 M은 mm'이며, 여기에서 m은 Mn, Fe, Co 및 Ni로 이루어진 군으로부터 선택되며, m'는 Al, V, Cr, Zn, Zr, Nb, Mo, Ag, Ge, Sn, Mg, Si, S, Ca, Ti, Cu, Ba, W 및 Pb로 이루어진 군으로부터 선택된 1종 이상의 원소인 것을 특징으로 하는 리튬이차전지용 양극 활 물질.

청구항 3

제 1항에 있어서,

상기 탄소원은 탄소나노튜브, 탄소나노와이어, 탄소나노섬유, 흑연, 활성탄 및 그래핀으로 이루어진 군으로부터 선택된 1종 이상인 것을 특징으로 하는 리튬이차전지용 양극 활 물질.

청구항 4

제 3항에 있어서,

상기 탄소원은 탄소나노튜브, 탄소나노와이어, 탄소나노섬유, 흑연, 활성탄 및 그래핀으로 이루어진 군으로부터 선택된 1종 이상의 물질 및 글루코스(glucose), 스쿠로스(scurose), 폴리에틸렌글리콜(poly ethylene glycol), 폴리비닐알콜(poly vinyl alcohol), 폴리비닐클로라이드(poly vinyl chloride), 구연산(citric acid)으로 이루어진 군으로부터 선택된 1종 이상의 물질을 모두 포함하는 것을 특징으로 하는 리튬이차전지용 양극 활 물질.

청구항 5

제 1항에 있어서,

상기 탄소원 또는 리튬티탄산화물은 Li_nMO_4 입자 표면을 코팅하는 것을 특징으로 하는 리튬이차전지용 양극 활 물질.

청구항 6

제 1항 내지 제 5항 중 어느 한 항에 따른 리튬이차전지용 양극 활 물질을 포함하는 리튬이차전지용 양극 활 물질.

청구항 7

(a) Li_nMO_4 중 MO_4 를 이루는 금속 또는 무기 염 또는 이들의 혼합 염과 탄소원 또는 리튬티탄산화물 또는 이들의 혼합물을 용액에 혼합하여, 분산시키는 단계;

(b) 상기 혼합물을 세척하는 단계;

(c) 상기 세척된 혼합물에 리튬염을 혼합하는 단계;

(d) 상기 리튬염이 혼합된 상기 혼합물을 용액에 분산시킨 후, 반응시키는 단계;

AMPEREX Ex. 1002
Page 891

(e) 상기 반응의 반응물을 건조하는 단계; 및

(f) 상기 건조된 반응물을 열처리 하는 단계를 포함하며, 여기에서 (a) 단계의 M은 Mn, Fe, Co, Ni, Al, Mn, V, Cr, Fe, Co, Zn, Zr, Nb, Mo, Ag, Ge, Sn, Mg, Si, S, Ca, Ti, Cu, Ba, W 및 Pb로 이루어진 군으로부터 선택된 1종 이상의 원소이고, n은 정수인 것을 특징으로 하는 리튬이차전지용 양극 활 물질 제조방법.

청구항 8

제 7항에 있어서,

상기 (a) 및 (d) 단계 중 적어도 어느 하나의 단계에서 상기 분산은 초음파 가진 또는 기계적 교반 방식으로 수행되는 것을 특징으로 하는 리튬이차전지용 양극 활 물질 제조방법.

청구항 9

제 7항에 있어서,

상기 M은 mm'이며, 여기에서 m은 Mn, Fe, Co 및 Ni로 이루어진 군으로부터 선택되며, m'는 Al, V, Cr, Zn, Zr, Nb, Mo, Ag, Ge, Sn, Mg, Si, S, Ca, Ti, Cu, Ba, W 및 Pb로 이루어진 군으로부터 선택된 1종 이상의 원소인 것을 특징으로 하는 리튬이차전지용 양극 활 물질 제조방법.

청구항 10

제 7항에 있어서,

상기 탄소원은 탄소나노튜브, 탄소나노와이어, 탄소나노섬유, 흑연, 활성탄 및 그래핀으로 이루어진 군으로부터 선택된 1종 이상인 것을 특징으로 하는 리튬이차전지용 양극 활 물질 제조방법.

청구항 11

제 10항에 있어서,

상기 탄소원은 탄소나노튜브, 탄소나노와이어, 탄소나노섬유, 흑연, 활성탄 및 그래핀으로 이루어진 군으로부터 선택된 1종 이상의 물질 및 글루코스(glucose), 스쿠로스(scurose), 폴리에틸렌글리콜(poly ethylene glycol), 폴리비닐알콜(poly vinyl alcohol), 폴리비닐클로라이드(poly vinyl chloride), 구연산(citric acid)으로 이루어진 군으로부터 선택된 1종 이상의 물질을 포함하는 것을 특징으로 하는 리튬이차전지용 양극 활 물질 제조방법.

명 세 서

기 술 분 야

[0001] 본 발명은 리튬 이차전지용 양극 활 물질 및 그 제조방법에 관한 것으로서, 더욱 상세하게는 $Li_2MM'O_4$ 입자상 표면에 균일하게 분산, 함유된 탄소원 또는 리튬티탄산화물(LTO)에 의하여 향상된 비용량과 전기전도도를 갖는 리튬이차전지용 양극 활 물질 복합체, 그 제조방법 및 이를 포함하는 리튬이차전지에 관한 것이다.

배 경 기 술

[0002] 최근 휴대전화, 휴대용 개인정보단말기(PDA), 노트북 PC, MP3 등의 휴대용 소형 전자기기 및 전기 자동차 등의 전원 및 동력원으로서의 리튬 이차전지의 수요가 급격히 늘어나고 있다. 이에 따라 리튬 이차전지의 고용량화와 사이클 수명 연장에 대한 요구도 증가하고 있다.

[0003] 리튬 이차전지의 양극 활 물질로서는 리튬 코발트 산화물($LiCoO_2$), 리튬 니켈 산화물($LiNiO_2$) 및 리튬 복합금속 산화물 등이 사용되고 있다. 그 외에도 저가격 고안정성의 스피넬형 리튬 망간 산화물($LiMn_2O_4$), 올리빈형 인산철, 인산 망간 및 인산 복합금속 리튬 화합물도 주목받고 있다.

[0004] 하지만, 리튬 코발트 산화물이나 리튬 니켈 산화물, 리튬 복합금속 산화물은 기본적인 전지 특성은 우수하지만, 열 안정성과 과충전 안전성 등이 충분하지 않다. 따라서 이를 개선하기 위한 별도의 안전장치가 추가로 필요하며, 또한 활 물질 자체의 가격이 비싼 단점이 있다.

AMPEREX Ex. 1002
Page 892

[0005] 또한, 리튬 망간 산화물 $LiMn_2O_4$의 경우 +3가의 망간 양이온에 기인하는 얀-텔러 뒤틀림 (Jahn-Teller distortion)이라는 구조변이 때문에 수명 특성이 좋지 않다는 치명적인 단점을 나타낸다. 이는 또한 낮은 전기 용량으로 인해 고에너지 밀도에 대한 요구를 충분히 만족시키지 못한다. 올리빈형 인산철 및 인산망간 리튬 화합물은 전기 전도성이 상당히 낮기 때문에 우수한 전지 특성을 기대하기 어렵고 또한 평균 작동전위가 낮아 고용량화에 대한 요구를 충분히 만족시키지 못한다.

[0006] 이에 반해 오르쏘실리케이트계 화합물(orthosilicate, Li_2MSiO_4, M=Fe, Mn, Ni, Co)은 가격이 저렴할 뿐만 아니라 높은 열안정성을 가지며 및 환경친화적인 물질로 여겨지고 있다. 더 나아가, Li_2MSiO_4는 330 mAh/g로 올리빈형 보다 높은 이론적 용량을 가지고 있다고 알려져 있지만, 전기전도성이 나쁘다는 단점을 가지고 있다.

발명의 내용

해결하려는 과제

[0007] 따라서, 본 발명이 해결하려는 과제는 높은 전기 전도성을 갖는 $Li_2MM'SiO_4$ 기반의 리튬이차전지용 양극 활 물질을 제공하는 것이다.

[0008] 본 발명이 해결하려는 또 다른 과제는 높은 전기 전도성을 갖는 $Li_2MM'SiO_4$ 기반의 리튬이차전지용 양극 활 물질의 경제적인 제조방법을 제공하는 것이다.

[0009] 본 발명이 해결하려는 또 다른 과제는 높은 전도성 및 기계적 특성의 양극 활 물질을 포함하는 리튬이차전지를 제공하는 것이다.

과제의 해결 수단

[0010] 상기 과제를 해결하기 위하여, 본 발명은 리튬이차전지용 양극 활 물질로서, 상기 양극 활 물질은 Li_nMO_4 / X의 복합체를 포함하며, 여기에서 M은 Mn, Fe, Co, Ni, Al, Mn, V, Cr, Fe, Co, Zn, Zr, Nb, Mo, Ag, Ge, Sn, Mg, Si, S, Ca, Ti, Cu, Ba, W 및 Pb로 이루어진 군으로부터 선택된 1종 또는 2종 이상의 원소이며, X는 탄소원 또는 리튬티탄산화물(Lithium Titanium Oxide, $Li_4Ti_5O_{12}$) 또는 이들의 혼합물이고, n은 정수인 것을 특징으로 하는 리튬이차전지용 양극 활 물질을 제공한다.

[0011] 본 발명의 일 실시예에서 상기 M은 mm'이며, 여기에서 m은 Mn, Fe, Co 및 Ni로 이루어진 군으로부터 선택되며, m'는 Al, V, Cr, Zn, Zr, Nb, Mo, Ag, Ge, Sn, Mg, Si, S, Ca, Ti, Cu, Ba, W 및 Pb로 이루어진 군으로부터 선택된 1종 이상의 원소이며, 상기 탄소원은 탄소나노튜브, 탄소나노와이어, 탄소나노섬유, 흑연, 활성탄 및 그래핀으로 이루어진 군으로부터 선택된 1종 이상이다 .

[0012] 본 발명의 또 다른 일 실시예에서 상기 탄소원은 탄소나노튜브, 탄소나노와이어, 탄소나노섬유, 흑연, 활성탄 및 그래핀으로 이루어진 군으로부터 선택된 1종 이상의 물질 및 글루코스(glucose), 수크로스(scurose), 폴리에틸렌글리콜(poly ethylene glycol), 폴리비닐알콜(poly vinyl alcohol), 폴리비닐클로라이드(poly vinyl chloride), 구연산(citric acid)으로 이루어진 군으로부터 선택된 1종 이상의 물질을 모두 포함하며, 상기 탄소원 또는 리튬티탄산화물은 Li_nMO_4 입자 표면을 코팅한다.

[0013] 본 발명은 또한 상술한 리튬이차전지용 양극 활 물질을 포함하는 리튬이차전지용 양극 활 물질을 제공한다.

[0014] 본 발명은 상기 또 다른 과제를 해결하기 위하여, (a) Li_nMO_4 중 MO_4 를 이루는 금속 또는 무기 염 또는 이들의 혼합 염과 탄소원 또는 리튬티탄산화물 또는 이들의 혼합물을 용액에 혼합하여, 분산시키는 단계; (b) 상기 혼합물을 세척하는 단계; (c) 상기 세척된 혼합물에 리튬염을 혼합하는 단계; (d) 상기 리튬염이 혼합된 상기 혼합물을 용액에 분산시킨 후, 반응시키는 단계; (e) 상기 반응의 반응물을 건조하는 단계; 및 (f) 상기 건조된 반응물을 열처리 하는 단계를 포함하며, 여기에서 (a) 단계의 M은 Mn, Fe, Co, Ni, Al, Mn, V, Cr, Fe, Co, Zn, Zr, Nb, Mo, Ag, Ge, Sn, Mg, Si, S, Ca, Ti, Cu, Ba, W 및 Pb로 이루어진 군으로부터 선택된 1종 이상의 원소이고, n은 정수인 것을 특징으로 하는 리튬이차전지용 양극 활 물질 제조방법을 제공한다.

[0015] 본 발명은 또 다른 일 실시예에서 상기 (a) 및 (d) 단계 중 적어도 어느 하나의 단계에서 상기 분산은 초음파 가진 또는 기계적 교반 방식으로 수행되며, 상기 M은 mm'이며, 여기에서 m은 Mn, Fe, Co 및 Ni로 이루어진 군으

AMPEREX Ex. 1002
Page 893

로부터 선택되며, m'는 Al, V, Cr, Zn, Zr, Nb, Mo, Ag, Ge, Sn, Mg, Si, S, Ca, Ti, Cu, Ba, W 및 Pb로 이루어진 군으로부터 선택된 1종 이상의 원소이다.

[0016] 본 발명의 일 실시예에서 상기 탄소원은 탄소나노튜브, 탄소나노와이어, 탄소나노섬유, 흑연, 활성탄 및 그래핀으로 이루어진 군으로부터 선택된 1종 이상이며, 상기 탄소원은 탄소나노튜브, 탄소나노와이어, 탄소나노섬유, 흑연, 활성탄 및 그래핀으로 이루어진 군으로부터 선택된 1종 이상의 물질 및 글루코스(glucose), 스쿠로스(scurose), 폴리에틸렌글리콜(poly ethylene glycol), 폴리비닐알콜(poly vinyl alcohol), 폴리비닐클로라이드(poly vinyl chloride), 구연산(citric acid)으로 이루어진 군으로부터 선택된 1종 이상의 물질을 포함한다.

발명의 효과

[0017] 본 발명에 따르면, 경제적인 방식으로 우수한 전기 전도도 및 기계적 특성을 갖는 리튬이차전지용 양극 활 물질이 제조될 수 있다. 특히, 상기 Li_nMO_4 입자상 표면에 균일하게 분산, 함유된 탄소원 또는 리튬티탄산화물(LTO)은 리튬이차전지용 양극 활 물질 복합체로 하여금 향상된 전기 전도도를 갖게 한다. 또한, 본 발명에 따른 양극 활 물질은 이차전지에 적용하기 적합한 에너지 밀도를 가지고, 안정성과 안전성이 뛰어나며, 우수한 전지특성을 유지하면서도 사이클 수명이 긴 장점을 갖는다.

도면의 간단한 설명

[0018] 도 1은 본 발명의 일 실시예에 따른 리튬이차전지용 양극 활 물질 제조방법의 단계도이다.

도 2는 본 발명에 따라 제조된 복합 양극 활물질의 구조를 X선 회절계(XRD, Rigaku)를 사용하여 분석한 결과이다.

도 3 내지 6은 본 발명에 따라 제조된 복합 양극 활물질의 입자형태를 FE-SEM(전계 주사현미경)으로 관찰한 결과이다.

도 7은 본 발명에 따라 제조된 복합 양극 활물질을 포함하는 리튬 이차전지에 대한 충방전 특성 분석 결과이다.

발명을 실시하기 위한 구체적인 내용

[0019] 이하, 본 발명을 도면을 참조하여 상세하게 설명하고자 한다. 다음에 소개되는 실시예들은 당업자에게 본 발명의 사상이 충분히 전달될 수 있도록 하기 위해 예로서 제공되는 것이다. 따라서 본 발명은 이하 설명된 실시예들에 한정되지 않고 다른 형태로 구체화될 수도 있다. 그리고 도면들에 있어서, 구성요소의 폭, 길이, 두께 등은 편의를 위하여 과장되어 표현될 수도 있으며, 명세서 전체에 걸쳐서 동일한 참조번호들은 동일한 구성요소들을 나타낸다.

[0020] 본 발명은 상술한 바와 같이 리튬이차전지용 양극 활 물질로서 Li_nMO_4 / X 형태의 복합체를 제공한다. 특히 본 발명은 Li 계열의 활성 입자 상에 X로 표시되는 탄소원(여기에서 탄소원은 탄소를 구성원소로 포함하는 임의의 탄소 화합물을 모두 지칭하며, 예를 들면, 탄소나노튜브, 탄소나노섬유, 탄소나노와이어, 그래핀, 흑연 등이 상기 탄소원에 속한다) 또는 리튬티탄산화물($Li_4Ti_5O_{12}$) 또는 이들의 혼합물을 코팅시킴으로써, 활성 입자로 하여금 높은 전도성을 갖게 한다. 여기에서 M은 Mn, Fe, Co, Ni, Al, V, Cr, Zn, Zr, Nb, Mo, Ag, Ge, Sn, Mg, Si, S, Ca, Ti, Cu, Ba, W 및 Pb로 이루어진 군으로부터 선택된 1종 이상의 원소이다. 본 발명의 일 실시예에서 상기 M은 두 종류의 원소(mm')로 이루어지며, 여기에서 m은 Mn, Fe, Co 및 Ni로 이루어진 군으로부터 선택되며, m'는 Al, V, Cr, Zn, Zr, Nb, Mo, Ag, Ge, Sn, Mg, Si, S, Ca, Ti, Cu, Ba, W 및 Pb로 이루어진 군으로부터 선택된 1종 이상의 원소이며, 본 발명의 일 실시예에서 상기 m'는 실리콘(Si), m은 Mn, Fe, Co 및 Ni로 이루어진 군으로부터 선택되었으나, 본 발명의 범위는 이에 제한되지 않는다. 또한 n은 정수로서, 1, 2, 3 등을 포함한다.

[0021] 본 발명의 일 실시예에서 상기 탄소원은 상술한 바와 같이 탄소를 구성원소로 하는 임의 형태의 화합물로, 예를 들면 탄소나노튜브, 탄소나노와이어, 탄소나노섬유 및 그래핀으로 이루어진 군으로부터 선택된 1종 이상이 될 수 있다. 본 발명의 또 다른 일 실시예에서 상기 탄소원은 탄소를 구성성분으로 포함하는 전구체 형태로서 글루코스(glucose), 스쿠로스(scurose), 폴리에틸렌글리콜(poly ethylene glycol), 폴리비닐알콜(poly vinyl alcohol), 폴리비닐클로라이드(poly vinyl chloride), 구연산(citric acid)의 일종 또는 이종 이상, 바람직하게는 글루코스, 스쿠로스 및 구연산으로 이루어진 군으로부터 선택된 하나 이상일 수 있다. 본 발명의 일 실시예에서는 탄소나노튜브, 탄소나노와이어, 탄소나노섬유 및 그래핀으로 이루어진 군에서 선택되는 제 1 탄소원과 글루코스(glucose), 스쿠로스(scurose), 폴리에틸렌글리콜(poly ethylene glycol), 폴리비닐알콜(poly vinyl

AMPEREX Ex. 1002
Page 894

alcohol), 폴리비닐클로라이드(poly vinyl chloride), 구연산(citric acid)으로 이루어진 군에서 선택되는 제 2 탄소원을 혼합 사용하여, 활성 입자를 코팅하는 경우, 매우 우수한 전지 특성을 나타내었다.

[0022] 본 발명은 상기 또 다른 과제를 해결하기 위하여, 상술한 양극 활 물질의 제조방법을 제공한다.

[0023] 도 1은 본 발명의 일 실시예에 따른 양극 활 물질의 단계도이다.

[0024] 도 1을 참조하면, 먼저 상술한 Li_nMO_4 중 MO_4 를 이루는 금속 또는 무기 염 또는 이들의 혼합 염과 탄소원 또는 리튬티탄산화물 또는 이들의 혼합물을 용액에 혼합하여, 분산시킨다. 이때 상기 분산은 초음파의 가진 또는 기계적 교반 방식 또는 이 둘 다가 모두 사용될 수 있다. 즉, 본 발명에서 전구체 분말(금속염 등)은 탄소원 또는 리튬티탄산화물과 습식혼합되는 단계로부터 양극 활 물질이 제조된다.

[0025] 이후, 상기 분산되어 습식 혼합된 혼합물은 세척된다. 다시, 상기 세척된 혼합물에 리튬염이 혼합되며, 상기 리튬염이 혼합된 상기 혼합물은 다시 용액에 혼입되어, 분산된 후, 반응과정을 거치게 된다. 본 발명의 일 실시예에서 상기 리튬염은 Li_2NO_3, Li_2CO_3, LiOH 등을 사용하였다. 특히 본 발명의 일 실시예에서는 상기 분산 및 반응과정에서 일정한 에너지를 음파 형태로 공급하는 음향화학(Sonochemistry) 기반의 초음파 가진 공정이 독립적으로 또는 기계적 교반과 함께 사용되어, 입자상에 탄소원 등이 코팅된 양극 활 물질 복합체를 효과적이고 경제적인 방식으로 제조하였다. 이후, 상기 반응물은 건조되며, 상기 건조된 반응물은 열처리된다.

[0026] 본 발명에 따른 상기 습식 혼합은 전구체 분말을 수용액에 혼입한 후, 이를 분산시키는 방식인데, 상기 분산은 초음파 가진(음향화학, Sonochemistry), 또는 기계적 교반 방식으로 수행될 수 있다. 상기 열처리 공정은 비활성 또는 환원분위기에서 수행되어 상기 금속 화합물, 예를 들면 철이 산화되는 것을 억제하는 것이 바람직하며, 온도 조건은 500~1000 ℃에서 0.5~10 시간 열처리하여 얻어지는 입자 크기가 500nm 이하가 되도록 하는 것이 바람직하다. 왜냐하면, 500nm를 초과하는 경우, 각 성분들간의 균일한 밀도를 얻기 어렵기 때문이다.

[0027] 실시예 1

[0028] $Mn(Ac)2 \cdot 6H_2O$ 0.3M 수용액 중에 나노 중공 섬유형 탄소인 탄소나노튜브(CNT) 2 중량%를 균일하게 분산시켜 분산액을 제조한다. 나노 중공 섬유형 탄소의 분산은 초음파 분산 방법 과 고압분산 방법을 이용하였다. 이어서 상기 분산액을 연속적으로 흘려주면서 $Na_2SiO_3 \cdot 12H_2O$ 0.15M을 이용, 분사하여 $MnSiO_3$를 형성시키며, 원심분리기를 이용하여 Na을 제거하였다. Na가 제거된 염에 LiOH 0.1M, 수크로스(sucrose), 구연산(citric acid(Li2MnSiO3:citricacid:sucrose=1:0.3:0.05)) 수용액을 $MnSiO_3$ 수용액에 첨가 한 후 1시간 교반 후, 반응기 내의 반응계를 저속으로 충분히 교반하거나 또는 상기 반응계에 초음파를 1시간 가진(음향화학, Sonochemistry)하였다. 이때 순환식항온조를 이용하여 반응기 내 온도를 30℃로 유지하고, 운전 주파수는 200 kHz 강도는 300 W, 반응기 내의 압력을 3 atm으로 일정하게 가압하였으며, 반응기 내부에는 아르곤 가스를 이용하였다. 반응 후 스프레이 건조기에서 150도에서 건조하였다. 건조 후 질소 분위기에서 750℃에서 24시간 소성하였다. 이로써, Li_2MnSiO_4 활성입자 상에 탄소나노튜브 및 수크로스와 같은 탄소원이 코팅된 복합 양극 활 물질을 제조하였다.

[0029] 실시예 2

[0030] $Mn(Ac)2 \cdot 6H_2O$ 0.28M에 $Fe(NO_3)$ 0.02M을 소량 첨가한 것을 제외하고는 실시예 1과 동일한 방식으로 리튬 이차전지용 복합 양극 활 물질을 제조하였다.

[0031] 실시예 3

[0032] 탄소나노튜브 대신 LiOH, TiO_2를 넣은 것을 제외하고는 실시예 1과 동일한 방법으로 복합 양극 활 물질을 제조하였다.

[0033] 비교예 1

[0034] 실시예 1에서 sucrose, citric acid, CNT와 같은 탄소원을 넣지 않은 것을 제외하고는 실시예 1과 동일한 방법으로 복합 양극 활 물질을 제조하였다.

[0035] 시험예 1

[0036] X선 회절 분석

[0037] 실시예에서 제조된 복합 양극 활물질의 구조를 X선 회절계(XRD, Rigaku)를 사용하여 분석하고, 그 결과를 도 2에 나타내었다. 도 2의 결과로부터 알 수 있는 바와 같이, 본 발명에 따라 제조된 복합 양극 활물질에서 Li_2MnSiO_4의 특성 피크와 아주 잘 일치하는 것을 알 수 있다.

[0038] 시험예 2

[0039] FE-SEM

[0040] FE-SEM(전계 주사현미경)으로 실시예에서 제조된 복합 양극 활물질의 입자형태를 관찰하였으며, 그 결과를 도 3 내지 도 6에 나타내었다. 도 3 내지 6에서 보는 바와 같이 복합 양극 활물질의 입자에 CNT가 잘 분산되어 있으며, 입자 평균 입자 크기가 약 10 마이크로 나타나는 것을 알 수 있다.

[0041] 시험예 3

[0042] 입도 분석

[0043] 레이저회절식의 입도 분포계를 이용하여 재료의 입도 분석을 하였다. 누적 입도 분포의 결과로부터 누적 제적이 10%, 50% 및 90%에 도달하는 지점에서의 입도를 확인하여, 각각 d10, d50, 및 d90으로 하였으며, 이에 대한 결과는 표 1에 나타내었다.

[0044] 표 1

Sample		입자 크기 (μm)	탭 밀도 (g/cc)
실시예 1	d10	6.0	1.2
	d50	10.4	
	d90	14.2	
실시예 2	d10	5.5	1.2
	d50	10.0	
	d90	13.0	
실시예 3	d10	5.4	1.3
	d50	9.2	
	d90	12.3	
비교예 1	d10	4.5	1.3
	d50	11.0	
	d90	12.5	

[0045] 시험예 4

[0046] 탭 밀도

[0047] 탭 밀도는 실린더에 재료 50g을 투입하고, 탭 횟수 2000회 후의 부피를 측정하여 탭 밀도를 계산하였으며, 그 결과를 상기 표 1에 나타내었다. 복합 양극 활물질에 탄소물질과 CNT가 포함될수록 탭 밀도는 다소 감소하나, 최종적인 전지 평가에 나타난 전지 성능은 제 1 탄소원(수크로스)과 제 2 탄소원인 CNT가 포함될수록 전지 성능은 증가하였다. 따라서, 상기 결과는 본 발명에 따른 양극 활 물질은 망간의 문제점인 전기 전도성을 향상시켜, 우수한 전지 성능을 발생시키는 점을 나타낸다. 특히 탄소나노튜브와 탄소원인 수크로스를 함께 사용한 경우, 그 효과는 보다 명확해진다.

AMPEREX Ex. 1002
Page 896

[0048] 시험예 5

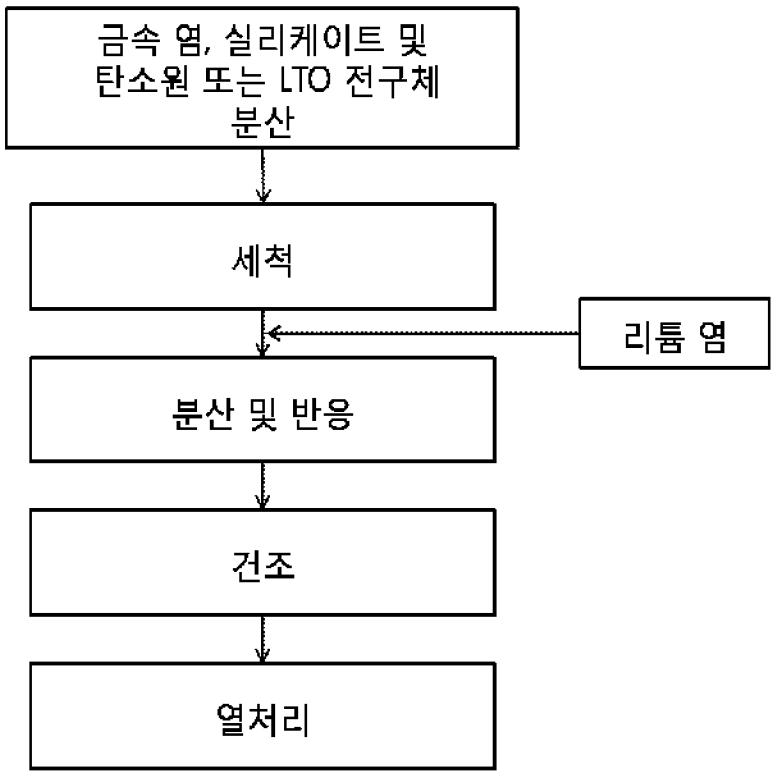
[0049] 전지 평가

[0050] 전지 평가를 위하여 본 발명에 따라 제조된 복합 양극 활물질 : 도전재 : 바인더를 85 : 8 : 7의 중량 비율로 칭량하였다. 혼합된 물질을 슬러리화한 후 알루미늄 박막에 도포 후 120℃에서 8시간 건조 하여 극판을 제조하였으며, 제조된 극판을 프레스 하였다. 음극으로는 Li 메탈을 이용하고, 2030 형 코인 셀을 제조하였으며, 전해액으로 1M-LiPF6를 EC-DEC(체적비1 : 1)에 용해시킨 것을 이용하였다. 충전 조건을 4.4V, 방전 조건을 3.0V로 충방전을 실시하였고, 그 결과를 도 7에 나타내었다.

[0051] 도 7에서 나타난 바와 같이 탄소물질과 CNT를 동시에 포함하지 않는 양극 활물질은 방전 비용량이 아주 좋지 않음을 알 수 있으며, CNT와 탄소물질이 동시에 포함 복합 양극 활물질이 아주 좋은 방전 비용량을 가진다. 이는 탄소물질과 CNT가 전기 전도성을 향상 시켜 주는 것을 알 수 있다. 또한, 탄소 물질과 LTO가 동시에 첨가된 실시예 1에서 아주 좋은 비용량을 보였다. 이는 LTO가 전극물질의 안정성을 높여 일어난 현상으로 보인다.

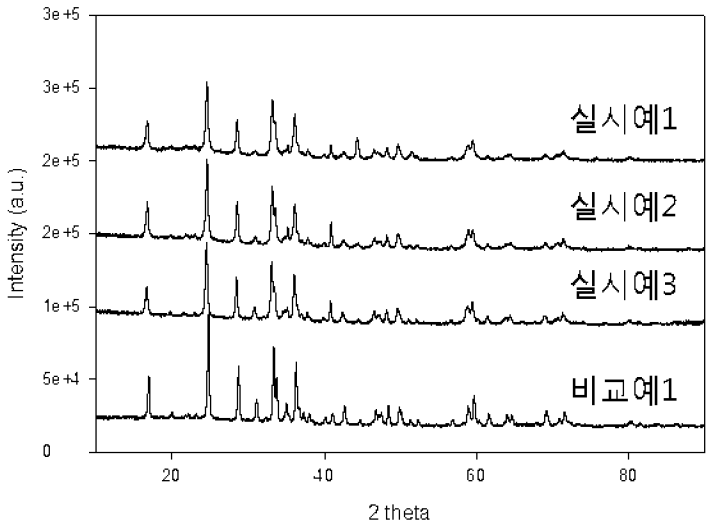
도면

도면1

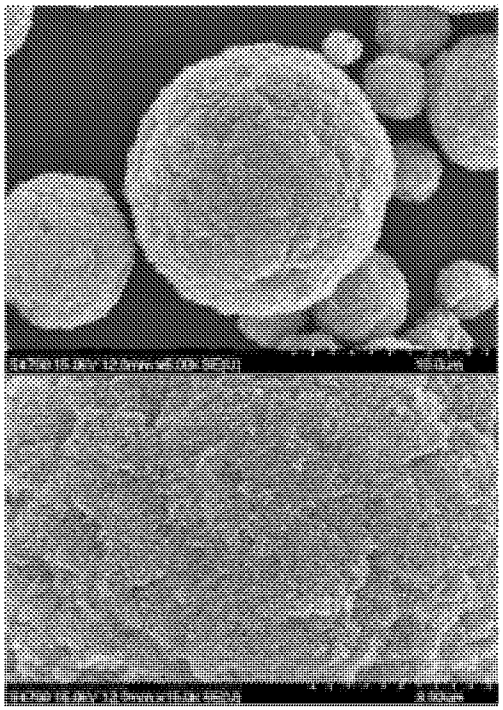


AMPEREX Ex. 1002
Page 897

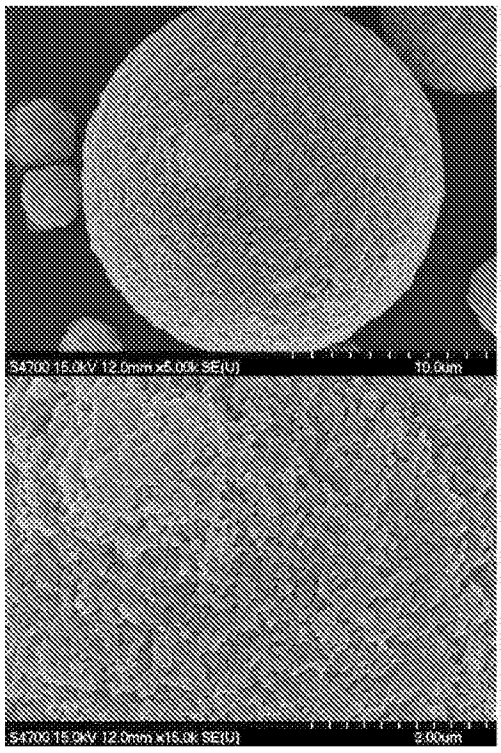
도면2


3e+5
3e+5
2e+5
2e+5
1e+5
5e+4
0
Intensity (a.u.)
실시예1
실시예2
실시예3
비교예1
20
40
60
80
2 theta

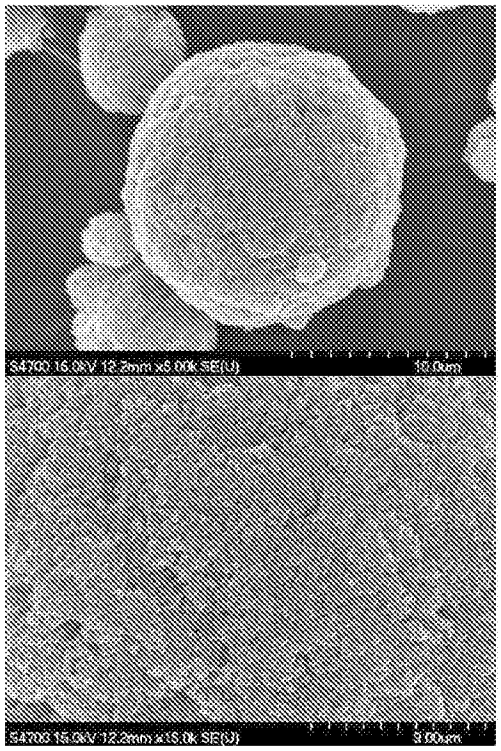
도면3



도면4

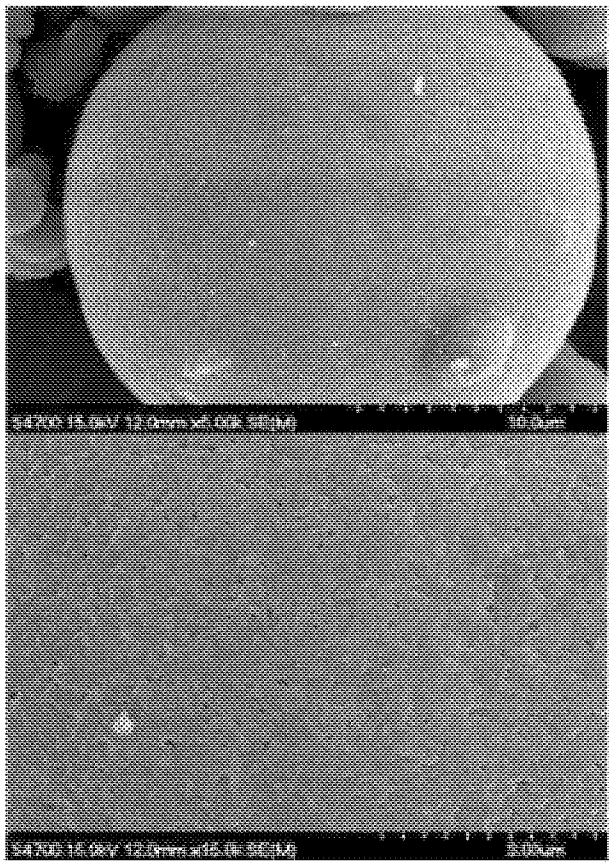


도면5

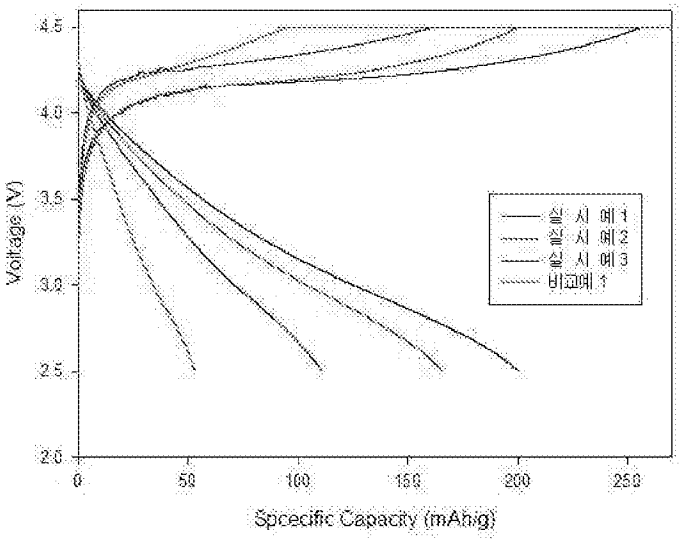


AMPEREX Ex. 1002
Page 899

도면6



도면7



AMPEREX Ex. 1002
Page 900

(19) Europäisches Patentamt
European Patent Office
Office européen des brevets

(11) EP 2 763 218 A2

(12) EUROPEAN PATENT APPLICATION
published in accordance with Art. 153(4) EPC

(43) Date of publication:
06.08.2014 Bulletin 2014/32

(21) Application number: 12834643.4

(22) Date of filing: 18.09.2012

(51) Int Cl.:
H01M 4/505 (2010.01) *H01M 10/052* (2010.01)
H01M 4/58 (2010.01)

(86) International application number:
PCT/KR2012/007457

(87) International publication number:
WO 2013/048048 (04.04.2013 Gazette 2013/14)

(84) Designated Contracting States:
AL AT BE BG CH CY CZ DE DK EE ES FI FR GB GR HR HU IE IS IT LI LT LU LV MC MK MT NL NO PL PT RO RS SE SI SK SM TR

(30) Priority: 26.09.2011 KR 20110097058

(71) Applicant: Korea Electronics Technology Institute
Kyunggi-do 463-816 (KR)

(72) Inventors:
- SONG, Jun Ho
  Seongnam-si
  Gyeonggi-do 463-727 (KR)
- KIM, Young Jun
  Yongin-si
  Gyeonggi-do 446-913 (KR)
- KIM, Jeom-Soo
  Hwaseong-si
  Gyeonggi-do 445-984 (KR)
- CHO, Woo Suk
  Seongnam-si
  Gyeonggi-do 463-400 (KR)
- KIM, Jae-Hun
  Yongin-si
  Gyeonggi-do 448-520 (KR)
- KIM, Jin Hwa
  Seongnam-si
  Gyeonggi-do 463-816 (KR)

(74) Representative: Land, Addick Adrianus Gosling et al
Arnold & Siedsma
Sweelinckplein 1
2517 GK Den Haag (NL)

(54) CATHODE ACTIVE MATERIAL FOR A LITHIUM SECONDARY BATTERY, METHOD FOR MANUFACTURING SAME, AND LITHIUM SECONDARY BATTERY INCLUDING SAME

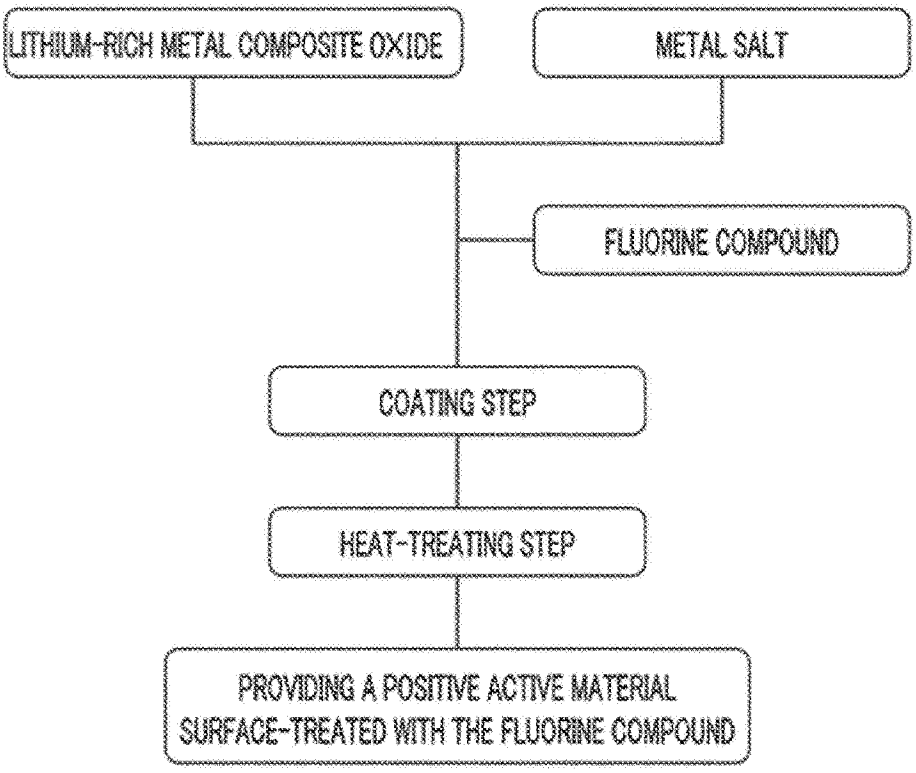
(57) The present invention provides a positive active material for a secondary lithium battery, a method of preparing the positive active material, and a secondary lithium battery including the positive active material, wherein the positive active material includes a lithium metal composite oxide core represented by the following Chemical Formula 1, and a coating layer including a fluorine compound and positioned at a shell of the lithium metal composite oxide core.

[Chemical Formula 1] $Li_wNi_xCo_yMn_{1-x-y-z}M_zO_2$

($1.2 \leq w \leq 1.5$, $0 < x < 1$, $0 \leq y < 1$, $0.5 \leq 1-x-y-z$, and M is at least one metal selected from the group consisting of Al, Mg, Fe, Cu, Zn, Cr, Ag, Ca, Na, K, In, Ga, Ge, V, Mo, Nb, Si, Ti, and Zr).

EP 2 763 218 A2

FIG.1



AMPEREX Ex. 1002
Page 902

Description

BACKGROUND OF THE INVENTION

(a) Field of the Invention

[0001] A positive active material for a secondary lithium battery, a preparation method thereof, and a secondary lithium battery including the same are disclosed.

(b) Description of the Related Art

[0002] As use of small portable electric/electronic devices has widely increased, a new secondary battery such as a nickel hydrogen battery or a secondary lithium battery has been actively developed. The secondary lithium battery uses carbon such as graphite and the like as a negative active material, a metal oxide including lithium as a positive active material, and a non-aqueous solvent as an electrolyte solution. The lithium is a metal having high ionization tendency and may realize a high voltage, and thus is used to develop a battery having high energy density.

[0003] The secondary lithium batteries mainly use a lithium transition metal oxide including lithium as a positive active material, and specifically, 90 % or more use a layered lithium transition metal oxide such as cobalt-based and nickel-based lithium transition metal oxides, a three component-based lithium transition metal oxide in which cobalt, nickel, and manganese coexist, and the like.

[0004] However, the layered lithium transition metal oxide that is widely used as a conventional positive active material has reversible capacity of less than or equal to 200 mAh/g^{-1} and thus has a limit in terms of energy density. Accordingly, in order to solve the problem of a secondary lithium battery due to the limited reversible capacity of a positive electrode, research on a lithium-rich layered oxide (OLO) excessively including lithium instead of the layered lithium transition metal oxide being undertaken.

[0005] A positive active material including the lithium-rich layered oxide has a solid solution structure in which a Li_2MnO_3 phase is combined with the conventional layered lithium transition metal oxide, and may realize high capacity of greater than or equal to 200 mAh/g^{-1} since oxygen is dissociated from the Li_2MnO_3, and lithium is extracted therefrom when initially charged at 4.6 V.

[0006] However, the lithium-rich layered oxide is necessarily charged at an initial high voltage for electrochemical activation, but the lithium-rich-based composite metal oxide reacts with an electrolyte solution during the high voltage charge and thus deteriorates the positive active material and aggravates manganese (Mn) elution at a high temperature and a high voltage, and resultantly deteriorates battery performance and cycle-life characteristics.

[0007] Accordingly, the present invention provides a positive active material having excellent cycle-life characteristics by surface-modifying a lithium-rich-based composite metal oxide in order to solve the conventional problem, and a secondary lithium battery including the same.

SUMMARY OF THE INVENTION

[0008] One embodiment of the present invention provides a positive active material suppressing deterioration and manganese elution during charge and discharge by suppressing a side reaction between the positive active material and an electrolyte solution.

[0009] Another embodiment of the present invention provides a novel method of preparing the positive active material.

[0010] Yet another embodiment of the present invention provides a secondary battery using the positive active material and having excellent cycle characteristics and discharge capacity of greater than or equal to 220 mAh/g^{-1}.

[0011] One embodiment of the present invention provides a positive active material for a secondary lithium battery, including: a lithium metal composite oxide core represented by the following Chemical Formula 1; and a coating layer positioned on the lithium metal composite oxide core and including a fluorine compound.

[Chemical Formula 1] $Li_wNi_xCo_yMn_{1-x-y-z}M_zO_2$

[0012] In the above Chemical Formula 1, $1.2 \le w \le 1.5$, $0 < x < 1$, $0 \le y < 1$, $0.5 \le 1-x-y-z$, and M is at least one metal selected from the group consisting of Al, Mg, Fe, Cu, Zn, Cr, Ag, Ca, Na, K, In, Ga, Ge, V, Mo, Nb, Si, Ti, and Zr.

[0013] The fluorine compound may be one or more selected from the group consisting of CsF, KF, LiF, NaF, RbF, TiF, AgF, AgF_2, BaF_2, CaF_2, CuF_2, CdF_2, FeF_2, HgF_2, Hg_2F_2, MnF_2, MgF_2, NiF_2, PbF_2, SnF_2, SrF_2, XeF_2, ZnF_2, AlF_3, BF_3, BiF_3, CeF_3, CrF_3, DyF_3, EuF_3, GaF_3, GdF_3, FeF_3, HoF_3, InF_3, LaF_3, LuF_3, MnF_3, NdF_3, VOF_3, PrF_3, SbF_3, ScF_3, SmF_3, TbF_3, TiF_3, TmF_3, YF_3, YbF_3, TlF_3, CeF_3, GeF_3, HfF_3, SiF_3, SnF_3, TiF_4, VF_4, ZrF_4, NbF_5, SbF_5, TaF_5, BiF_5, MoF_5, ReF_5, SF_5, and WF_5.

AMPEREX Ex. 1002
Page 903

[0014] The coating layer may be included in an amount of about 0.2 to about 1.5 wt% based on the total weight of the lithium metal composite oxide core.

[0015] The coating layer may have a thickness of about 5 to about 20 nm.

[0016] The coating layer may further include ZrO_2, SnO_2, or a mixture thereof.

[0017] The lithium metal composite oxide core may have an average particle diameter (D50) of about 10 to about 20 μm.

[0018] In the above Chemical Formula 1, w may be about 1.3 to about 1.5.

[0019] The lithium metal composite oxide core may be one selected from the group consisting of $Li_{1.3}Ni_{0.2}Co_{0.1}Mn_{0.7}O_2$, $Li_{1.3}Ni_{0.25}Mn_{0.75}O_2$, $Li_{1.3}Ni_{0.25}Co_{0.05}Mn_{0.7}O_2$, and $Li_{1.3}Ni_{0.2}Co_{0.1}Mn_{0.65}O_2$.

[0020] Another embodiment of the present invention provides a method of preparing the positive active material including: a) providing a lithium metal composite oxide core represented by the following Chemical Formula 1

[Chemical Formula 1] $Li_wNi_xCo_yMn_{1-x-y-z}M_zO_2$

wherein $1.2 \le w \le 1.5$, $0 < x < 1$, $0 \le y < 1$, $0.5 \le 1-x-y-z$, and M is at least one metal selected from the group consisting of Al, Mg, Fe, Cu, Zn, Cr, Ag, Ca, Na, K, In, Ga, Ge, V, Mo, Nb, Si, Ti, and Zr;

[0021] b) preparing a solution including a fluorine compound; c) coating the fluorine compound included in the solution of b) on the lithium metal composite oxide core of a); and d) heat-treating the coated lithium metal composite oxide in the step c).

[0022] The solution including the fluorine compound may be evaporated at about 120 to about 150 ° C after coating the solution including the fluorine compound on the lithium metal composite oxide in the step c).

[0023] The heat-treating of the step d) may be performed at about 380 to about 460 ° C for about 1 to about 10 hours.

[0024] The lithium metal composite oxide core may be coated to have a thickness of about 5 to about 20 nm in the step b).

[0025] The solution including the fluorine compound in the step b) may further include ZrO_2, SnO_2, or a mixture thereof.

[0026] Another embodiment of the present invention provides a secondary lithium battery that includes: a positive electrode including a positive active material; a negative electrode including a negative active material being capable of intercalating and deintercalating lithium ions; a separator interposed between the positive electrode and the negative electrode; and a non-aqueous electrolyte, wherein the battery has a discharge capacity of greater than or equal to 220 mAh/g^{-1}.

[0027] The positive active material including the lithium metal composite oxide core coated with the fluorine compound may be suppressed from a side reaction between the lithium metal composite oxide and an electrolyte solution, and thus from manganese elution and deterioration.

[0028] According to the method of preparing the positive active material for a secondary lithium battery, the fluorine compound may be uniformly coated on the surface of the lithium metal composite oxide core.

[0029] In addition, a secondary lithium battery using the positive active material prepared according to the method realizes discharge capacity of greater than or equal to 220 $mAhg^{-1}$, and simultaneously has excellent cycle-life characteristics.

BRIEF DESCRIPTION OF THE DRAWINGS

[0030]

FIG. 1 is a flowchart showing a method of preparing a positive active material surface-treated by coating a fluorine compound thereon.

FIG. 2 shows scanning electron microscope (SEM) photographs and energy dispersive spectroscopy (EDS) analysis of the positive active material according to one embodiment of the present invention.

FIG. 3 shows scanning electron microscope (SEM) photographs and energy dispersive spectroscopy (EDS) analysis of a positive active material according to a comparative example.

FIG. 4 shows charge and discharge experiment results of the positive active materials.

DETAILED DESCRIPTION

[0031] A positive active material for a secondary lithium battery, a preparation method thereof, and a secondary lithium battery including the same are provided.

[0032] Hereinafter, embodiments of the present invention are described in detail. However, these embodiments are exemplary, and this disclosure is not limited thereto.

[0033] One embodiment of the present invention provides a positive active material for a secondary lithium battery including a lithium metal composite oxide core represented by the following Chemical Formula 1, and a coating layer positioned on the lithium metal composite oxide core and including a fluorine compound.

AMPEREX Ex. 1002
Page 904

[Chemical Formula 1] $Li_wNi_xCo_yMn_{1-x-y-z}M_zO_2$

[0034] In the above Chemical Formula 1, $1.2 \leq w \leq 1.5$, $0 < x < 1$, $0 \leq y < 1$, $0.5 \leq 1-x-y-z$, and M is at least one metal selected from the group consisting of Al, Mg, Fe, Cu, Zn, Cr, Ag, Ca, Na, K, In, Ga, Ge, V, Mo, Nb, Si, Ti, and Zr.

[0035] The lithium metal composite oxide core represented by the above Chemical Formula 1 is a lithium-rich layered metal composite oxide including lithium in an amount of greater than or equal to about 1.2 mol and less than or equal to about 1.5 mol, and has a structure in which a lithium metal composite oxide and Li_2MnO_3 form a solid solution. When a battery using the lithium metal composite oxide as a positive active material is charged at about 4.5 to 5.0 V, the Li_2MnO_3 is electrochemically activated, realizing discharge capacity of greater than or equal to 220 $mAhg^{-1}$. Herein, the lithium metal composite oxide has a plateau region around about 4.6 to about 5 V, and generates oxygen when charged at a high voltage of greater than or equal to 4.6 V based on a positive electrode potential. The charging is not particularly limited, and may be performed in any conventional method in a related art.

[0036] The lithium metal composite oxide core may include nickel, cobalt, and manganese, and the nickel, cobalt, and manganese may be included in a mole ratio appropriately adjusted depending on a purpose. The manganese may be included in an amount of greater than and equal to 0.5 mol based on the total weight of the metals except for lithium, and thus improves structural stability of the lithium metal composite oxide, and may also be partly substituted with other elements to prolong cycle-life characteristics. The substituted metal elements may include a transition metal, a rare earth element, or the like, and for example, at least one metal selected from the group consisting of Al, Mg, Fe, Cu, Zn, Cr, Ag, Ca, Na, K, In, Ga, Ge, V, Mo, Nb, Si, Ti, and Zr may be used.

[0037] The lithium metal composite oxide core may be prepared in a method of preparing a precursor for a secondary lithium battery including: a) preparing a metal composite aqueous solution by adding a nickel raw material, a cobalt raw material, and a manganese raw material in a desired equivalent ratio to an aqueous solution in a co-precipitation reactor; b) adjusting a distribution degree of manganese ions by adding an ammonia solution and sodium hydroxide to the metal composite aqueous solution and agitating the mixed solution while maintained a pH of 10 to 12; and c) aging the solution at a predetermined temperature for a predetermined time.

[0038] The nickel raw material may be, for example, a nickel sulfate salt, a nickel nitrate salt, a nickel hydrochlorate salt, a nickel acetate salt, and the like, the cobalt raw material may be, for example, a cobalt sulfate salt, a cobalt nitrate salt, a cobalt hydrochlorate salt, a cobalt acetate salt, and the like, and the manganese raw material may be, for example, a manganese sulfate salt, a manganese nitrate salt, a manganese hydrochlorate salt, a manganese acetate salt, and the like.

[0039] In the method of preparing a positive active material precursor for a secondary lithium battery precursor, the adjustment of distribution degree of manganese ions in a precursor particle may be performed by using various factors such as shape of a co-precipitation reactor, a ratio between diameter and depth of the co-precipitation reactor, an agitation speed (rpm), pH of a reaction solution, and the like.

[0040] In the step b) of the method of preparing a precursor for a secondary lithium battery, the solution may be agitated at about 1000 to about 3000 rpm. When the agitation speed is set at less than 1000 rpm during the preparation of a co-precipitation precursor, the agitation may not be uniformly performed and may remarkably deteriorate internal composition uniformity, while when the agitation is set at greater than 3000 rpm, the spherically-produced precursor may be destroyed.

[0041] In the step c) of the method of preparing a precursor for a secondary lithium battery, the solution may be aged at about 10 °C to about 60 °C for 4 to 20 hours, for example, at about 30 °C for about 10 hours. When the temperature is set at greater than 60 °C during the preparation of a co-precipitation precursor, the added ammonia solution may be constantly volatilized and thus may cause difficulty in controlling pH, and when the aging is performed for greater than 20 hours, there may be a problem of decreasing productivity, and simultaneously a problem of excessive growth of spherical particles, thus destroying the spherical shape.

[0042] The fluorine compound that coats the lithium metal composite oxide core may be one or more selected from the group consisting of CsF, KF, LiF, NaF, RbF, TiF, AgF, AgF_2, BaF_2, CaF_2, CuF_2, CdF_2, FeF_2, HgF_2, Hg_2F_2, MnF_2, MgF_2, NiF_2, PbF_2, SnF_2, SrF_2, XeF_2, ZnF_2, AlF_3, BF_3, BiF_3, CeF_3, CrF_3, DyF_3, EuF_3, GaF_3, GdF_3, FeF_3, HoF_3, InF_3, LaF_3, LuF_3, MnF_3, NdF_3, VOF_3, PrF_3, SbF_3, SnF_3, SmF_3, TbF_3, TlF_3, TmF_3, YF_3, YbF_3, TlF_3, CeF_3, GeF_3, HfF_3, SnF_3, SnF_3, TiF_4, VF_4, ZrF_4, NbF_5, SbF_5, TaF_5, BiF_5, MoF_5, ReF_5, SF_5, and WF_5, for example AlF_3, BF_3, ZrF_4, and the like.

[0043] In one embodiment of the present invention, the fluorine compound may be coated to be about 5 to about 20 nm thick on the surface of the lithium metal composite oxide, and the coating layer may be formed by dipping the lithium metal composite oxide in a fluorine compound aqueous solution obtained by mixing a metal salt-including solution and a fluoro-based compound-including solution, spraying the fluorine compound aqueous solution onto the lithium metal composite oxide and drying it, or using any other conventional coating method. When the coating layer has a thickness of about 5 to about 20 nm, conductivity of a positive active material may not only be decreased, but manganese elution may also be suppressed.

[0044] When the coating layer has a thickness of less than or equal to 5 nm, the manganese elution may not be

AMPEREX Ex. 1002
Page 905

effectively suppressed due to a relatively low distribution degree of the coating layer on the surface, while when the coating layer has a thickness of greater than or equal to 20 nm, the coating layer may hardly pass lithium ions and thus limits electrochemical activation at the first charge as well as output characteristics.

[0045] The coating layer may be about 0.2 to about 1.5 wt% based on the total weight of the lithium metal composite oxide core.

[0046] The coating layer may further include ZrO_2, SnO_2, or a mixture thereof.

[0047] The lithium metal composite oxide core may have an average particle diameter (D50) of about 10 to about 20 μm. When the positive active material has an average particle diameter within the range, the positive active material may have a uniform particle distribution, a high sphericality degree, and high internal dimension density and thus realize a secondary lithium battery having high discharge capacity.

[0048] In the above Chemical Formula 1, w may be 1.3 to 1.5, and the lithium metal composite oxide core may be one selected from $Li_{1.3}Ni_{0.2}Co_{0.1}Mn_{0.7}O_2$, $Li_{1.3}Ni_{0.25}Mn_{0.75}O_2$, $Li_{1.3}Ni_{0.25}Co_{0.05}Mn_{0.7}O_2$, and $Li_{1.3}Ni_{0.2}Co_{0.05}Mn_{0.65}O_2$. In this way, when lithium is included in an amount of greater than or equal to about 1.2 mol, for example, greater than or equal to about 1.3 mol, a high-capacity positive active material may be provided.

[0049] Yet another embodiment of the present invention provides a method of preparing a positive active material including a lithium metal composite oxide core and a fluorine compound coating layer.

[0050] Specifically, the method of preparing a positive active material includes: a) providing lithium metal composite oxide core represented by the following Chemical Formula 1.

[Chemical Formula 1] $Li_wNi_xCo_yMn_{1-x-y-z}M_zO_2$

wherein, in the above Chemical Formula 1, $1.2 \le w \le 1.5$, $0 < x < 1$, $0 \le y < 1$, $0.5 \le 1-x-y-z$, and M is at least one metal selected from the group consisting of Al, Mg, Fe, Cu, Zn, Cr, Ag, Ca, Na, K, In, Ga, Ge, V, Mo, Nb, Si, Ti, and Zr;

[0051] b) preparing a solution including a fluorine compound; c) coating a) the lithium metal composite oxide core with b) the fluorine compound-including solution; and d) heat-treating the coated lithium metal composite oxide formed in the step c).

[0052] After coating the lithium metal composite oxide with the fluorine compound-including solution in the step c), the solution may be evaporated at about 120 to about 150 °C.

[0053] The heat-treating of the step d) may be performed at about 380 to about 460 °C for about 1 to about 10 hours.

[0054] In the step b), the lithium metal composite oxide core may be coated to be about 5 to about 20 nm thick. When the coating layer has a thickness of about 5 to about 20 nm, manganese elution may be suppressed without decreasing conductivity of the positive active material, but when the coating layer has a thickness of less than or equal to about 5 nm, the manganese elution may not be effectively suppressed due to relatively decreased distribution of the coating layer on the core, while when the coating layer has a thickness of greater than or equal to about 20 nm, the coating layer may hardly pass lithium ions and thus limits electrochemical activation at the first charge as well as output characteristics.

[0055] In the step b), the fluorine compound-including solution may further include ZrO_2, SnO_2, or a mixture thereof.

[0056] Yet another embodiment of the present invention provides a secondary lithium battery including: a positive electrode including a positive active material including a lithium metal composite oxide core represented by the above Chemical Formula 1; a coating layer including a fluorine compound on the lithium metal composite oxide core; a negative electrode including a negative active material being capable of intercalating and deintercalating lithium ions; a separator interposed between the positive and negative electrodes; and a non-aqueous electrolyte, and having discharge capacity of greater than or equal to 220 mAh/g^{-1}.

[0057] The secondary lithium battery may have any shape such as a coin, a button, a sheet, a cylinder, a prism, and the like. The variously-shaped secondary lithium batteries may be prepared in a conventional method, which will not be illustrated in detail. In addition, manufacture of the positive electrode and constitution of the secondary lithium battery are briefly illusirated, but the present invention is not limited thereto.

[0058] The positive electrode may be prepared by dissolving the positive active material along with a conductive material, a binder, and other additives, for example, at least one additive selected from a filler, a dispersing agent, an ion conductive material, a pressure enhancer, and the like in an appropriate organic solvent to prepare a slurry or paste, coating the slurry or paste on a current collector, and drying and compressing it.

[0059] The positive electrode includes a current collector and the positive active material layer, and the positive active material layer may be formed by using the positive active material having a coating layer on the surface or by mixing the positive active material with a compound having a coating layer. The coating layer may be formed by using an oxide of Mg, Al, Co, K, Na, Ca, Si, Ti, V, Sn, Ge, Ga, B, As, or Zr, or a mixture thereof, as a coating element compound.

[0060] The binder may be polyvinyl alcohol, carboxylmethyl cellulose, hydroxypropyl cellulose, diacetyl cellulose, polyvinylchloride, carboxylated polyvinylchloride, polyvinylfluoride, an ethylene oxide-containing polymer, polyvinylpyrrolidone, polyurethane, polytetrafluoroethylene, polyvinylidene fluoride, polyethylene, polypropylene, a styrene-butadiene rubber, an acrylated styrene-butadiene rubber, an epoxy resin, nylon, and the like, but is not limited thereto.

AMPEREX Ex. 1002
Page 906

[0061] The conductive material improves conductivity of an electrode, any electrically conductive material may be used as the conductive material unless it causes a chemical change, and examples thereof may be one or more of natural graphite, artificial graphite, carbon black, acetylene black, ketjen black, a carbon fiber, a metal powder, a metal fiber, and the like of copper, nickel, aluminum, silver, and the like, and a conductive material such as a polyphenylene derivative and the like.

[0062] The current collector of the positive electrode may be a foil, a sheet, and the like of copper, nickel, stainless steel, aluminum, and the like, or a carbon fiber and the like.

[0063] The negative electrode includes a current collector and a negative active material layer formed on the current collector.

[0064] As the negative active material, one or two kinds of a composite oxide and the like of a carbon material such as graphite and the like or a transition metal capable of reversibly intercalating/deintercalating lithium ions may be used. Other than these materials, silicon, tin, and the like may be used as the negative electrode material.

[0065] The negative active material layer includes a binder, and may optionally include a conductive material.

[0066] The binder improves binding properties of negative active material particles with one another and with a current collector, examples thereof may be polyvinyl alcohol, carboxylmethyl cellulose, hydroxypropyl cellulose, polyvinylchloride, carboxylated polyvinylchloride, polyvinylfluoride, an ethylene oxide-containing polymer, polyvinylpyrrolidone, polyurethane, polytetrafluoroethylene, polyvinylidene fluoride, polyethylene, polypropylene, a styrene-butadiene rubber, an acrylated styrene-butadiene rubber, an epoxy resin, nylon, and the like, but are not limited thereto.

[0067] Examples of the conductive material may be a carbon-based material such as natural graphite, artificial graphite, carbon black, acetylene black, ketjen black, carbon fiber, and the like; a metal-based material such as a metal powder or a metal fiber and the like of copper, nickel, aluminum, silver, and the like; a conductive polymer such as a polyphenylene derivative and the like; and a mixture thereof.

[0068] The negative current collector may be a copper foil, a nickel foil, a stainless steel foil, a titanium foil, a nickel foam, a copper foam, a polymer substrate coated with a conductive metal, or a combination thereof.

[0069] The electrolyte includes a non-aqueous organic solvent and a lithium salt.

[0070] The non-aqueous organic solvent may include a carbonate-based, ester-based, ether-based, ketone-based, alcohol-based, or aprotic solvent. The carbonate-based solvent may include dimethyl carbonate (DMC), diethyl carbonate (DEC), dipropyl carbonate (DPC), methylpropyl carbonate (MPC), ethylpropyl carbonate (EPC), methylethyl carbonate (MEC), ethylene carbonate (EC), propylene carbonate (PC), butylene carbonate (BC), and the like, and the ester-based solvent may include methyl acetate, ethyl acetate, n-propyl acetate, dimethyl acetate, methyl propionate, ethyl propionate, γ-butyrolactone, decanolide, valerolactone, mevalonolactone, caprolactone, and the like. The ether-based solvent may be dibutyl ether, tetraglyme, diglyme, dimethoxyethane, 2-methyltetrahydrofuran, tetrahydrofuran, and the like, and the ketone-based solvent may be cyclohexanone and the like. The alcohol-based solvent may be ethanol, isopropyl alcohol, and the like, and the aprotic solvent may be nitriles of R-CN (R is a C2 to C20 linear, branched, or cyclic structured hydrocarbon group, and may include a double bond aromatic ring or an ether bond) and the like, amides of dimethylformamide and the like, dioxolanes such as 1,3-dioxolane and the like, or sulfolanes and the like.

[0071] The non-aqueous organic solvent may be used singularly or in a mixture, and when the organic solvent is used in a mixture, the mixture ratio may be controlled in accordance with a desirable battery performance.

[0072] A lithium salt dissolved in such a solvent may include $LiClO_4$, $LiBF_4$, $LiPF_6$, $LiAlCl_4$, $LiSbF_6$, LiSCN, $LiCF_3SO_3$, $LiCF_3CO_2$, $Li(CF_3SO_2)_2$, $LiAsF_6$, $LiN(CF_3SO_2)_2$, $LiB_{10}Cl_{10}$, LiBOB (lithium bis(oxalato)borate), a lower aliphatic lithium carbonate, chloroborane lithium, imides of $LiN(CF_3SO_2)$, $Li(C_2F_5SO_2)$, $LiN(CF_3SO_2)_2$, $LiN(C_2F_5SO_2)_2$, $LiN(CF_3SO_2)(C_4F_9SO_2)$, and the like. These lithium salts may be used alone or may be randomly combined in an electrolyte solution and the like unless they damage the effect of the present invention. Particularly, $LiPF_6$ may be preferably included. In addition, carbon tetrachloride, trifluorochloroethylene, or a phosphate salt and the like including phosphorus may be included in the electrolyte solution so as to make the electrolyte solution nonflammable.

[0073] The separator may be polyethylene, polypropylene, polyvinylidene fluoride, or a multi-layer of the above, and a mixed multi-layer such as a polyethylene/polypropylene double-layered separator, a polyethylene/polypropylene/polyethylene triple-layered separator, a polypropylene/polyethylene/polypropylene triple-layered separator, and the like may be used.

[0074] Hereinafter, examples of the present invention and comparative examples are described. These examples, however, are not in any sense to be interpreted as limiting the scope of the invention.

Example 1

Manufacture of Lithium Metal Composite Oxide Core

[0075] A 1 M metal composite aqueous solution was prepared by adding nickel sulfate salt, cobalt sulfate salt, and manganese sulfate salt in a mole ratio of 0.20:0.10:0.70 to water in a co-precipitation reactor at a speed of 10 mL/min.

AMPEREX Ex. 1002
Page 907

Then, a 1 M ammonia solution was added to the obtained metal composite aqueous solution in the co-precipitation reactor at a speed of 5 mL/min, and sodium hydroxide was added thereto while pH of the mixture was maintained to be 11 by using a pH controller, and herein, the co-precipitation reactor had a cylindrical structure, and the diameter and depth of the co-precipitation reactor were appropriately adjusted. The metal composite aqueous solution was agitated at 1000 rpm and aged for 10 hours, obtaining a spherical shape precursor. The obtained precursor was washed with ultra pure water at greater than or equal to 30 °C until its pH became less than or equal to 8, and was dried at 80 °C for 12 hours. Lithium carbonate was added in an equivalent ratio of 1.3 with the dried co-precipitation precursor. The mixture was heat-treated at 900 °C for 10 hours in the air, preparing $Li_{1.3}Ni_{0.2}Co_{0.1}Mn_{0.7}O_2$.

Coating of Lithium Metal Composite Oxide Core

[0076] A uniform mixed solution was obtained by dissolving an aqueous solution including NH_4F (Sigma-Aldrich Co. Ltd.) in an aqueous solution including an aluminum salt and agitating the mixture for greater than or equal to 10 minutes. The mixed solution was spray-coated on the prepared $Li_{1.3}Ni_{0.2}Co_{0.1}Mn_{0.7}O_2$, and then heat-treated under an in an inert atmosphere at 400 °C for 5 hours. The coating layer coated on a positive active material according to the preparing method was 10 nm thick and was 0.5 wt% based on the total amount of the lithium metal composite oxide.

Manufacture of Secondary Lithium Battery Cell

[0077] The positive active material was allocated to have an average particle diameter of 25 μm, and then 90 wt% of the positive active material, 5 wt% of acetylene black as a conductive material, and 5 wt% of polyvinylidene fluoride (PVdF) as a binder were dissolved in N-methyl-2-pyrrolidone (NMP), preparing a slurry. This slurry was coated on a 20 μm-thick aluminum foil, dried and compressed with a press, and then dried in a vacuum at 120 °C for 16 hours, preparing a disk electrode having a diameter of 16 mm. As a counter electrode, a lithium metal film punched to have a diameter of 16 mm was used, and a PP film was used for a separation membrane. An electrolyte solution was prepared by mixing ethylene carbonate (EC)/dimethylether (DME) in a ratio of 1:1 (v/v) and dissolving 1 M $LiPF_6$ therein. The electrolyte solution was impregnated into a separation membrane, the separation membrane was inserted between a working electrode and a counter electrode, and a CR2032 SUS case was used, preparing a secondary lithium battery cell.

Example 2

[0078] A positive active material and a secondary battery cell were prepared according to the same method as Example 1, except for using 1.0 wt% of the coating layer based on the total amount of the lithium metal composite oxide.

Comparative Example 1

[0079] $Li_{1.3}Ni_{0.2}Co_{0.1}Mn_{0.7}O_2$ was prepared according to the same method as Example 1, except for dissolving an aqueous solution including NH_4F (Sigma-Aldrich Co. Ltd.) in an aqueous solution including an aluminum salt, agitating the solution for greater than or equal to 10 minutes, and coating the lithium metal composite oxide with the uniform mixed solution, preparing a secondary battery cell including the same.

Comparative Example 2

[0080] A positive active material and a secondary battery cell including the same were prepared according to the same method as Example 1, except for heating the coated lithium metal composite oxide at 350 °C.

Comparative Example 3

[0081] A positive active material and a secondary battery cell including the same were prepared according to the same method as Example 1, except for heat-treating the coated lithium metal composite oxide at 400 °C.

Comparative Example 4

[0082] A positive active material and a secondary battery cell including the same were prepared according to the same method as Example 2, except for heat-treating the coated lithium metal composite oxide at 350 °C.

AMPEREX Ex. 1002
Page 908

Comparative Example 5

[0083] A positive active material and a secondary battery cell including the same were prepared according to the same method as Example 2, except for heat-treating the coated lithium metal composite oxide at 400 °C.

[0084] Experiment conditions of Examples 1 and 2 and Comparative Examples 1 to 5, a kind of fluorine compound included in a coating layer, and amount (wt%) of the coating layer based on the total amount of a core are provided in the following Table 1.

[Table 1]

	Fluorine compound	Amount of coating layer (wt%)	Heat-treating temperature after coating (° C)
Example 1	AlF_3	0.5	400 ° C
Example 2	AlF_3	1.0	400 ° C
Comparative Example 1	N	0.0	N
Comparative Example 2	AlF_3	0.5	350 ° C
Comparative Example 3	AlF_3	0.5	450 ° C
Comparative Example 4	AlF_3	1.0	350 ° C
Comparative Example 5	AlF_3	1.0	450 ° C

Experimental Example

SEM Photograph and EDS Analysis

[0085] The co-precipitation precursors of Example 1 and Comparative Example 2 were photographed with a SEM using JSM-7000F (Jeol Ltd.) equipment, energy dispersive spectroscopy (EDS, Oxford) analysis was performed to measure polydispersity of metals (Mn, Co, Ni, Al, and F) on the surface of the positive active materials, and the results are provided in FIGS. 2 and 3.

[0086] The positive active materials shown in FIGS. 2 and 3 included a lithium metal composite oxide as a core and a coating layer including a fluorine compound on the surface of the core. Comparing FIG. 2 with FIG. 3, the positive active material of Example 1 showed more uniform distribution of Al and F elements than the positive active material of Comparative Example 1. Accordingly, the positive active material of Example 1 showed that the coating layer including a fluorine compound was further uniformly formed.

Battery Capacity

[0087] The secondary lithium battery cells according to Examples 1 and 2 and Comparative Examples 1 to 5 were charged at a constant current of 25 mA/g up to 4.6 V at 25 ° C and at a constant voltage of 4.6 V to 2.5 mA/g, and then discharged at a constant current of 25 mA/g down to 2.0 V, and capacity of the battery cells was measured.

Cycle Characteristics

[0088] The secondary lithium battery cells according to Examples 1 and 2 and Comparative Examples 1 to 5 were repeatedly charged and discharged 30 times. Specifically, the secondary lithium battery cells according to Examples 1 and 2 and Comparative Examples 1 to 5 were charged at a constant current of 25 mA/g up to a voltage of 4.6 at 60 ° C and at a constant voltage of 4.6 V to a current of 5 mA/g, and then discharged at a constant current of 25 mA/g down to a voltage of 2.0 V. The charge and discharge as one cycle was repeated 30 times, and capacity retention of the battery cells was evaluated. The capacity retention was calculated according to the following formula.

AMPEREX Ex. 1002
Page 909

Capacity Retention (%) = Capacity at 30th cycle/ Capacity at 1st cycle X 100

[0089] The experiment results of discharge capacity and 30 cycle capacity retention of the secondary lithium battery cells according to Examples 1 and 2 and Comparative Examples 1 to 5 are provided in the following table.

[Table 2]

	Initial discharge capacity at 25 °C (mAh/g^{-1})	30 cycle capacity retention at 60 °C (%)
Example 1	234	90.4
Example 2	226	90.2
Comparative Example 1	240	81.7
Comparative Example 2	231	85.8
Comparative Example 3	238	84.1
Comparative Example 4	215	86.4
Comparative Example 5	224	85.4

[0090] As shown in Table 2, the secondary lithium battery cells according to Examples 1 and 2 showed high initial discharge capacity of greater than or equal to 220 mAhg^{-1}, and considerably high capacity retention of greater than or equal to 90 % after 30 cycles. On the contrary, the positive active material including no coating layer according to Comparative Example 1 showed high initial discharge capacity of 240 mA/g^{-1}, but very low initial discharge capacity of 81.7 % after 30 cycles. Accordingly, the positive active material including a lithium-rich metal composite oxide coated with a fluorine compound showed improved cycle-life characteristics. FIG. 4 is a graph showing cycle characteristics of the positive active materials according to Example 1 and Comparative Examples 1 and 2.

[0091] As shown in Table 2, the positive active materials of Examples 1 and 2 showed excellent cycle characteristics compared with the positive active materials of Comparative Examples 2 to 5. The positive active materials of Examples 1 and 2 showed capacity retention of greater than or equal to 90 %, while the positive active materials of Comparative Examples 2 to 5 showed only capacity retention of about 81 to 85 %. The reason it that a fluorine compound was uniformly coated on a lithium metal composite oxide core in the positive active material of the present invention, and when the core was uniformly coated with a coating layer, the coating layer prevented a side reaction between the lithium-rich layer-based metal composite oxide and an electrolyte solution and improved cycle characteristics.

[0092] Exemplary embodiments of the present invention illustrated in the specification and drawings are provided to facilitate understanding but do not limit the range of the present invention. Other exemplary variations based on a technology of the present invention other than the exemplary embodiments are clearly understood and accepted by those who have ordinary skill in this art to the present invention.

Claims

1. A positive active material for a secondary lithium battery, comprising:

   a lithium metal composite oxide core represented by the following Chemical Formula 1; and
   a coating layer positioned on the lithium metal composite oxide core and comprising a fluorine compound:

   [Chemical Formula 1] $Li_wNi_xCo_yMn_{1-x-y-z}M_zO_2$

   wherein, in the above Chemical Formula 1, $1.2 \le w \le 1.5$, $0 < x < 1$, $0 \le y < 1$, $0.5 \le 1-x-y-z$, and M is at least one metal selected from the group consisting of Al, Mg, Fe, Cu, Zn, Cr, Ag, Ca, Na, K, In, Ga, Ge, V, Mo, Nb, Si, Ti, and Zr.

2. The positive active material for a secondary lithium battery of claim 1, wherein the fluorine compound is one or more selected from the group consisting of CsF, KF, LiF, NaF, RbF, TlF, AgF, AgF_2, BaF_2, CaF_2, CuF_2, CdF_2, FeF_2, HgF_2, Hg_2F_2, MnF_2, MgF_2, NiF_2, PbF_2, SnF_2, SrF_2, XeF_2, ZnF_2, AlF_3, BF_3, BiF_3, CeF_3, CrF_3, DyF_3, EuF_3, GaF_3, GdF_3, FeF_3, HoF_3, InF_3, LaF_3, LuF_3, MnF_3, NdF_3, VOF_3, PrF_3, SbF_3, ScF_3, SmF_3, TbF_3, TiF_3, TmF_3, YF_3, YbF_3, TlF_3, CeF_3, GeF_3, HfF_3, SiF_3, SnF_3, TiF_4, VF_4, ZrF_4, NbF_5, SbF_5, TaF_5, BiF_5, MoF_5, ReF_5, SF_5, and WF_5.

AMPEREX Ex. 1002
Page 910

3. The positive active material of claim 1, wherein the coating layer is included in an amount of 0.2 wt% to 1.5 wt% based on the total weight of the lithium metal composite oxide core.

4. The positive active material of claim 1, wherein the coating layer has a thickness of 5 nm to 20 nm.

5. The positive active material of claim 1, wherein the coating layer further comprises ZrO_2, SnO_2, or a mixture thereof.

6. The positive active material of claim 1, wherein the lithium metal composite oxide core has an average particle diameter (D50) of 10 μm to 20 μm.

7. The positive active material of claim 1, wherein w in the above Chemical Formula 1 is 1.3 to 1.5.

8. The positive active material of claim 1, wherein the lithium metal composite oxide core is one selected from the group consisting of $Li_{1.3}Ni_{0.2}Co_{0.1}Mn_{0.7}O_2$, $Li_{1.3}Ni_{0.25}Mn_{0.75}O_2$, $Li_{1.3}Ni_{0.25}Co_{0.05}Mn_{0.7}O_2$, and $Li_{1.3}Ni_{0.2}Co_{0.1}Mn_{0.65}O_2$.

9. A method of preparing the positive active material for a secondary lithium battery, comprising

a) preparing a lithium metal composite oxide core represented by the following Chemical Formula 1

[Chemical Formula 1] $Li_wNi_xCo_yMn_{1-x-y-z}M_zO_2$

wherein, in the above Chemical Formula 1, $1.2 \leq w \leq 1.5$, $0 < x < 1$, $0 \leq y < 1$, $0.5 \leq 1-x-y-z$, and M is at least one metal selected from the group consisting of Al, Mg, Fe, Cu, Zn, Cr, Ag, Ca, Na, K, In, Ga, Ge, V, Mo, Nb, Si, Ti, and Zr;
b) preparing a solution including a fluorine compound;
c) coating a) the lithium metal composite oxide core b) the solution comprising a fluorine compound; and
d) heat-treating the coated lithium metal composite oxide in the step c).

10. The method of claim 9, wherein the coating step c) comprises evaporation of the solution at a temperature of 120 ° C to 150 ° C, after coating the lithium metal composite oxide with the solution including a fluorine compound.

11. The method of claim 9, wherein the heat-treatment is performed at 380 ° C to 460 ° C under an inert atmosphere for 1 to 10 hours in the step (d).

12. The method of claim 9, wherein the solution of b) is coated to be 5 nm to 20 nm thick on the lithium metal composite oxide core.

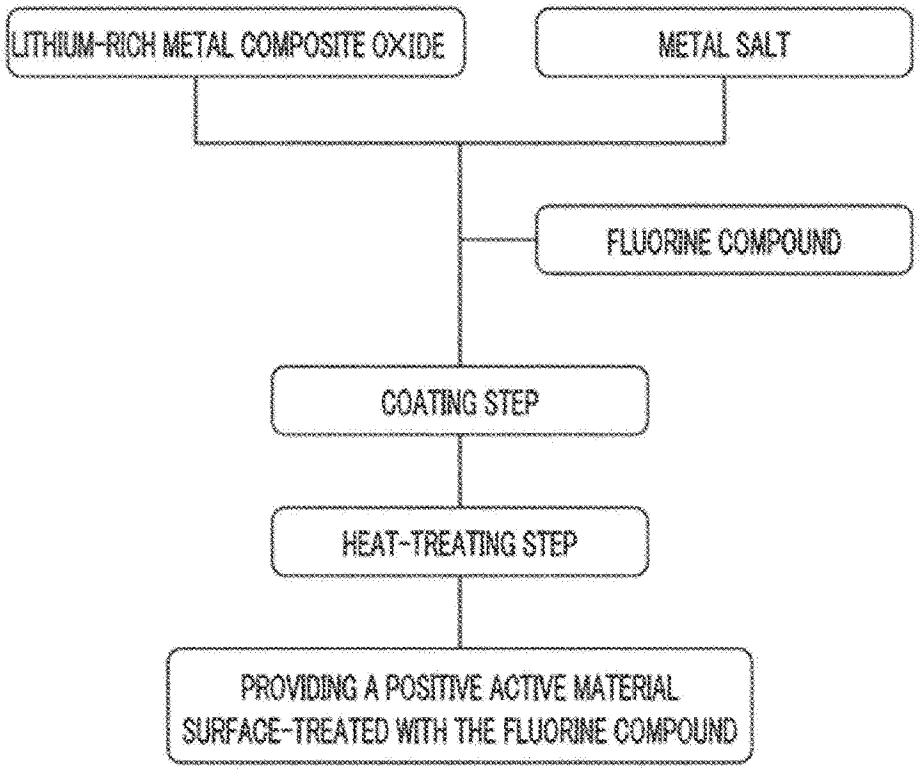
13. The method of claim 9, wherein the solution including a fluorine compound in b) additionally comprises ZrO_2, SnO_2, or a mixture thereof.

14. A secondary lithium battery, comprising:

a positive electrode including the positive active material of any one of claim 1 to claim 8;
a negative electrode including a negative active material being capable of intercalating and deintercalating lithium ions;
a separator interposed between the positive electrode and the negative electrode; and
a non-aqueous electrolyte,
wherein the secondary lithium battery has a discharge capacity of greater than or equal to 220 $mAhg^{-1}$.

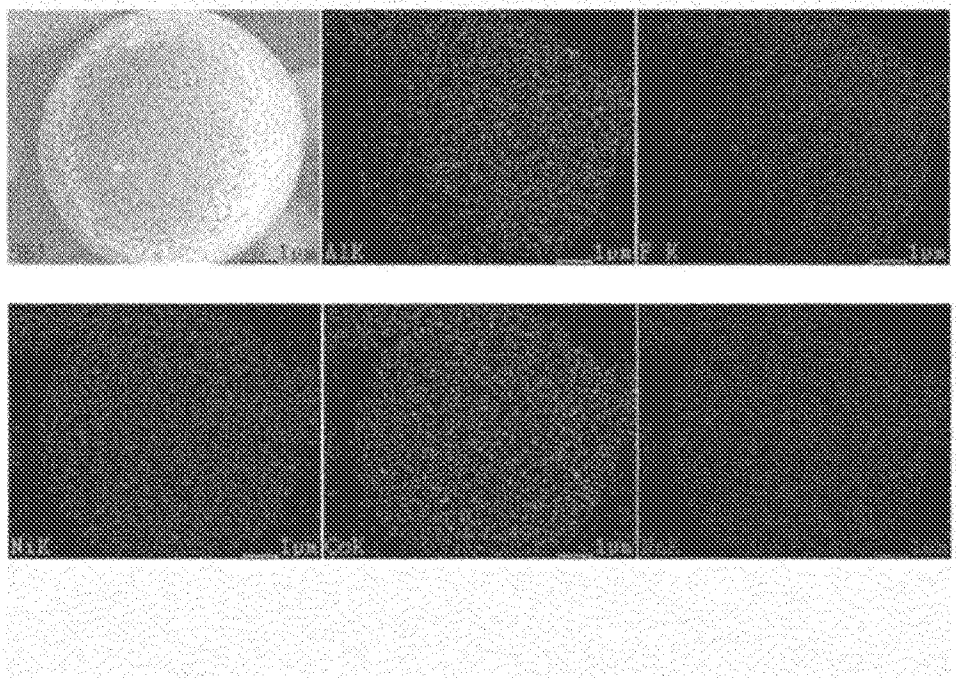
AMPEREX Ex. 1002
Page 911

FIG.1



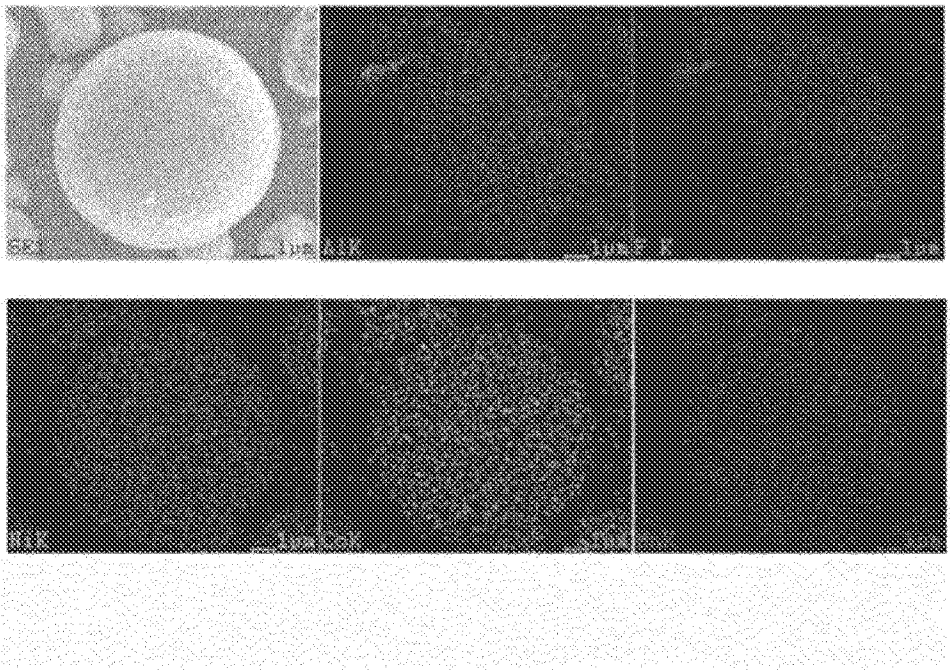
AMPEREX Ex. 1002
Page 912

FIG.2



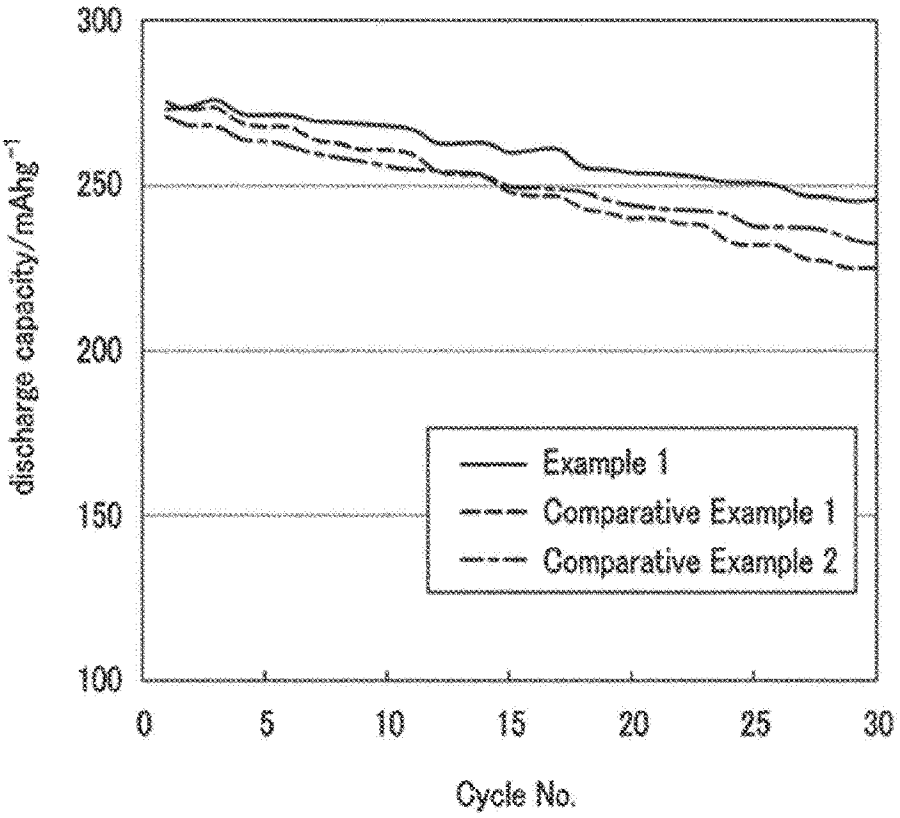
AMPEREX Ex. 1002
Page 913

FIG.3



AMPEREX Ex. 1002
Page 914

FIG.4



AMPEREX Ex. 1002
Page 915

Espacenet

Bibliographic data: WO2011155781 (A2) — 2011-12-15

POSITIVE ELECTRODE ACTIVE MATERIAL FOR A LITHIUM SECONDARY BATTERY, METHOD FOR PRODUCING SAME AND LITHIUM SECONDARY BATTERY COMPRISING SAME

Inventor(s): HONG JI JUN [KR]; BYUN KI TAEK [KR]; KIM HYO WON [KR] ± (HONG, JI JUN, ; BYUN, KI TAEK, ; KIM, HYO WON)

Applicant(s): ROUTE JJ CO LTE [KR]; HONG JI JUN [KR]; BYUN KI TAEK [KR]; KIM HYO WON [KR] ± (ROUTE JJ CO., LTE, ; HONG, JI JUN, ; BYUN, KI TAEK, ; KIM, HYO WON)

Classification: - international: ***H01M4/485; H01M4/505; H01M4/525; H01M4/583***
- cooperative: **C01G23/005 (EP); C01G45/1235 (EP); C01G49/009 (EP); C01G51/40 (EP); C01G51/52 (EP); C01G53/40 (EP); C01G53/52 (EP); H01M4/131 (EP); H01M4/364 (EP); H01M4/485 (EP, KR); H01M4/505 (EP, KR); H01M4/525 (EP, KR); H01M4/583 (KR); H01M4/587 (EP);** C01P2002/50 (EP); C01P2002/72 (EP); C01P2004/03 (EP); C01P2004/61 (EP); C01P2004/62 (EP); C01P2006/10 (EP); C01P2006/40 (EP); H01M10/052 (EP); H01M4/625 (EP)

Application number: WO2011KR04239 20110609 Global Dossier

Priority number(s): KR20100054224 20100609

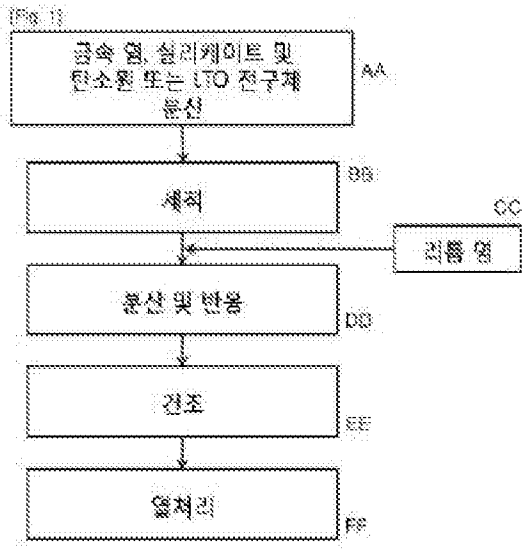
Also published as: WO2011155781 (A3) KR101393651 (B1) KR20110134852 (A)

Abstract of WO2011155781 (A2)

The present invention relates to a positive electrode active material for a lithium secondary battery, a method for producing the same and to a lithium secondary battery comprising the same. The positive electrode active material for a lithium secondary battery according to the present invention comprises a Li2MO4 / X composite, wherein M is one or two or more elements selected from a group consisting of Mn, Fe, Co, Ni, Al, Mn, V, Cr, Fe, Co, Zn, Zr, Nb, Mo, Ag, Ge, Sn, Mg, Si, S, Ca, Ti, Cu, Ba, W and Pb, and X is a carbon source, lithium titanium oxide (Li4Ti5O12) or a mixture thereof. According to the present invention, positive electrode active material having superior electrical conductivity and mechanical characteristics can be produced in an economically advantageous manner. Particularly, the carbon source or lithium titanium oxide (LTO) uniformly dispersed on or contained in the particulate surface of Li2MM'O4 provides the composite of the positive electrode active material for a lithium secondary battery with improved electrical conductivity. In addition, the positive electrode active

material according to the present invention has energy density suitable for a secondary battery, and superior stability and safety, and has a long life cycle while maintaining excellent battery characteristics.

[Fig. 1]



AA ... Metal salt, silicate and carbon source or LTO precursor dispersion
BB ... Cleaning
CC ... Lithium salt
DD ... Dispersion and reaction
EE ... Drying
FF ... Heat treatment

(12) 특허협력조약에 의하여 공개된 국제출원

(19) 세계지식재산권기구
국제사무국

(43) 국제공개일
2011 년 12 월 15 일 (15.12.2011)

PCT

(10) 국제공개번호
WO 2011/155781 A2

(51) 국제특허분류:
H01M 4/505 (2010.01) *H01M 4/485* (2010.01)
H01M 4/525 (2010.01) *H01M 4/583* (2010.01)

(21) 국제출원번호: PCT/KR2011/004239

(22) 국제출원일: 2011 년 6 월 9 일 (09.06.2011)

(25) 출원언어: 한국어

(26) 공개언어: 한국어

(30) 우선권정보:
10-2010-0054224 2010 년 6 월 9 일 (09.06.2010) KR

(71) 출원인 (US 을(를) 제외한 모든 지정국에 대하여): **주식회사 루트제이제이 (ROUTE JJ CO., LTD)** [KR/KR]; 경기도 시흥시 정왕동 1261-3 서화상단 2 나 304 호, 429-450 Gyeonggi-do (KR).

(72) 발명자; 겸
(75) 발명자/출원인 (US 에 한하여): **홍지준 (HONG, Ji Jun)** [KR/KR]; 서울 강남구 개포동 172-3 현대아파트 501-502, 135-240 Seoul (KR). **변기택 (BYUN, Ki Taek)** [KR/KR]; 서울 강서구 등촌 1 동 631-9 대동화포탑아파트 101-1204, 157-839 Seoul (KR). **김효원 (KIM, Hyo Won)** [KR/KR]; 경기도 시흥시 정왕동 1366-14 파인힐오피스텔 C 동 409 호, 429-450 Gyeonggi-do (KR).

(74) 대리인: **엄명용 (EOM, Myung Yong)**; 서울 서초구 서초동 1503-9 메강빌딩 4 층, 137-070 Seoul (KR).

(81) 지정국 (별도의 표시가 없는 한, 가능한 모든 종류의 국내 권리의 보호를 위하여): AE, AG, AL, AM, AO, AT, AU, AZ, BA, BB, BG, BH, BR, BW, BY, BZ, CA, CH, CL, CN, CO, CR, CU, CZ, DE, DK, DM, DO, DZ, EC, EE, EG, ES, FI, GB, GD, GE, GH, GM, GT, HN, HR, HU, ID, IL, IN, IS, JP, KE, KG, KM, KN, KP, KZ, LA, LC, LK, LR, LS, LT, LU, LY, MA, MD, ME, MG, MK, MN, MW, MX, MY, MZ, NA, NG, NI, NO, NZ, OM, PE, PG, PH, PL, PT, RO, RS, RU, SC, SD, SE, SG, SK, SL, SM, ST, SV, SY, TH, TJ, TM, TN, TR, TT, TZ, UA, UG, US, UZ, VC, VN, ZA, ZM, ZW.

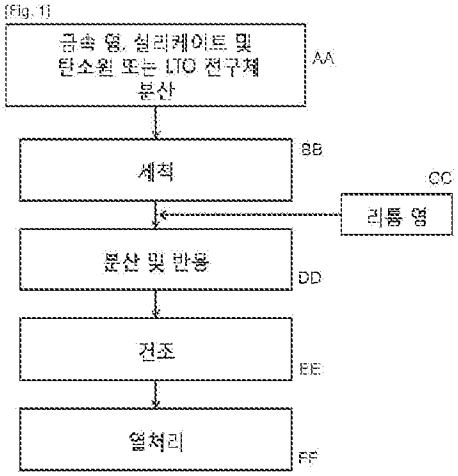
(84) 지정국 (별도의 표시가 없는 한, 가능한 모든 종류의 역내 권리의 보호를 위하여): ARIPO (BW, GH, GM, KE, LR, LS, MW, MZ, NA, SD, SL, SZ, TZ, UG, ZM, ZW), 유라시아 (AM, AZ, BY, KG, KZ, MD, RU, TJ, TM), 유럽 (AL, AT, BE, BG, CH, CY, CZ, DE, DK, EE, ES, FI, FR, GB, GR, HR, HU, IE, IS, IT, LT, LU, LV, MC, MK, MT, NL, NO, PL, PT, RO, RS, SE, SI, SK, SM, TR), OAPI (BF, BJ, CF, CG, CI, CM, GA, GN, GQ, GW, ML, MR, NE, SN, TD, TG).

[다음 쪽 계속]

(54) Title: POSITIVE ELECTRODE ACTIVE MATERIAL FOR A LITHIUM SECONDARY BATTERY, METHOD FOR PRODUCING SAME AND LITHIUM SECONDARY BATTERY COMPRISING SAME

(54) 발명의 명칭 : 리튬 이차전지용 양극 활 물질, 그 제조방법 및 이를 포함하는 리튬 이차전지

[Fig. 1]



AA ... Metal salt, silicate and carbon source or LTO precursor dispersion
BB ... Cleaning
CC ... Lithium salt
DD ... Dispersion and reaction
EE ... Drying
FF ... Heat treatment

(57) **Abstract**: The present invention relates to a positive electrode active material for a lithium secondary battery, a method for producing the same and to a lithium secondary battery comprising the same. The positive electrode active material for a lithium secondary battery according to the present invention comprises a Li_2MO_4 / X composite, wherein M is one or two or more elements selected from a group consisting of Mn, Fe, Co, Ni, Al, Mn, V, Cr, Fe, Co, Zn, Zr, Nb, Mo, Ag, Ge, Sn, Mg, Si, S, Ca, Ti, Cu, Ba, W and Pb, and X is a carbon source, lithium titanium oxide ($Li_xTi_yO_{12}$) or a mixture thereof. According to the present invention, positive electrode active material having superior electrical conductivity and mechanical characteristics can be produced in an economically advantageous manner. Particularly, the carbon source or lithium titanium oxide (LTO) uniformly dispersed on or contained in the particulate surface of $Li_2MM'O_4$ provides the composite of the positive electrode active material for a lithium secondary battery with improved electrical conductivity. In addition, the positive electrode active material according to the present invention has energy density suitable for a secondary battery, and superior stability and safety, and has a long life cycle while maintaining excellent battery characteristics.

(57) 요약서:

[다음 쪽 계속]

WO 2011/155781 A2

공개:

---- 국제조사보고서 없이 공개하며 보고서 접수 후 이를 별도 공개함 (규칙 48.2(g))

리튬 이차전지용 양극 활 물질, 그 제조방법 및 이를 포함하는 리튬 이차전지가 제공된다. 본 발명에 따른 리튬 이차전지용 양극 활 물질은 Li_2MO_4 / X 의 복합체를 포함하며, 여기에서 M 은 Mn, Fe, Co, Ni, Al, Mn, V, Cr, Fe, Co, Zn, Zr, Nb, Mo, Ag, Ge, Sn, Mg, Si, S, Ca, Ti, Cu, Ba, W 및 Pb 로 이루어진 군으로부터 선택된 1 종 또는 2 종 이상의 원소이며, X 는 탄소원 또는 리튬티탄산화물(Lithium Titanium Oxide, $Li_4Ti_5O_{12}$) 또는 이들의 혼합물인 것을 특징으로 하며, 본 발명에 따르면, 경제적인 방식으로 우수한 전기 전도도 및 기계적 특성을 갖는 리튬이차전지용 양극 활 물질이 제조될 수 있다. 특히, 상기 $Li_2MM'O_4$ 일차상 표면에 균일하게 분산, 함유된 탄소원 또는 리튬티탄산화물(LTO)은 리튬이차전지용 양극 활 물질 복합체로 하여금 향상된 전기 전도도를 갖게 한다. 또한, 본 발명에 따른 양극 활 물질은 이차전지에 적용하기 적합한 에너지 밀도를 가지고, 안정성과 안전성이 뛰어나며, 우수한 전지특성을 유지하면서도 사이클 수명이 긴 장점을 갖는다.

명세서

발명의 명칭: 리튬 이차전지용 양극 활 물질, 그 제조방법 및 이를 포함하는 리튬 이차전지

기술분야

[1] 본 발명은 리튬 이차전지용 양극 활 물질 및 그 제조방법에 관한 것으로서, 더욱 상세하게는 $Li_2MM'O_4$ 입자상 표면에 균일하게 분산, 함유된 탄소원 또는 리튬티탄산화물(LTO)에 의하여 향상된 비용량과 전기전도도를 갖는 리튬이차전지용 양극 활 물질 복합체, 그 제조방법 및 이를 포함하는 리튬이차전지에 관한 것이다.

배경기술

[2] 최근 휴대전화, 휴대용 개인정보단말기(PDA), 노트북 PC, MP3 등의 휴대용 소형 전자기기 및 전기 자동차 등의 전원 및 동력원으로서의 리튬 이차전지의 수요가 급격히 늘어나고 있다. 이에 따라 리튬 이차전지의 고용량화와 사이클 수명 연장에 대한 요구도 증가하고 있다.

[3] 리튬 이차전지의 양극 활 물질로서는 리튬 코발트 산화물($LiCoO_2$), 리튬 니켈 산화물($LiNiO_2$) 및 리튬 복합금속 산화물 등이 사용되고 있다. 그 외에도 저가격 고안정성의 스피넬형 리튬 망간 산화물($LiMn_2O_4$), 올리빈형 인산철, 인산 망간 및 인산 복합금속 리튬 화합물도 주목받고 있다.

[4] 하지만, 리튬 코발트 산화물이나 리튬 니켈 산화물, 리튬 복합금속 산화물은 기본적인 전지 특성은 우수하지만, 열 안정성과 과충전 안전성 등이 충분하지 않다. 따라서 이를 개선하기 위한 별도의 안전장치가 추가로 필요하며, 또한 활 물질 자체의 가격이 비싼 단점이 있다.

[5] 또한, 리튬 망간 산화물 $LiMn_2O_4$의 경우 +3가의 망간 양이온에 기인하는 얀-텔러 뒤틀림 (Jahn-Teller distortion)이라는 구조변이 때문에 수명 특성이 좋지 않다는 치명적인 단점을 나타낸다. 이는 또한 낮은 전기용량으로 인해 고에너지 밀도에 대한 요구를 충분히 만족시키지 못한다. 올리빈형 인산철 및 인산망간 리튬 화합물은 전기 전도성이 상당히 낮기 때문에 우수한 전지 특성을 기대하기 어렵고 또한 평균 작동전위가 낮아 고용량화에 대한 요구를 충분히 만족시키지 못한다.

[6] 이에 반해 오르쏘실리케이트계 화합물(orthosilicate, Li_2MSiO_4, M=Fe, Mn, Ni, Co)은 가격이 저렴할 뿐만 아니라 높은 열안정성을 가지며 및 환경친화적인 물질로 여겨지고 있다. 더 나아가, Li_2MSiO_4는 330 mAh/g로 올리빈형 보다 높은 이론적 용량을 가지고 있다고 알려져 있지만, 전기전도성이 나쁘다는 단점을 가지고 있다.

발명의 상세한 설명

기술적 과제

[7] 따라서, 본 발명이 해결하려는 과제는 높은 전기 전도성을 갖는 $Li_2MM'SiO_4$ 기반의 리튬이차전지용 양극 활 물질을 제공하는 것이다.

[8] 본 발명이 해결하려는 또 다른 과제는 높은 전기 전도성을 갖는 $Li_2MM'SiO_4$ 기반의 리튬이차전지용 양극 활 물질의 경제적인 제조방법을 제공하는 것이다.

[9] 본 발명이 해결하려는 또 다른 과제는 높은 전도성 및 기계적 특성의 양극 활 물질을 포함하는 리튬이차전지를 제공하는 것이다.

과제 해결 수단

[10] 상기 과제를 해결하기 위하여, 본 발명은 리튬이차전지용 양극 활 물질로서, 상기 양극 활 물질은 Li_nMO_4 / X의 복합체를 포함하며,여기에서 M은 Mn, Fe, Co, Ni, Al, Mn, V, Cr, Fe, Co, Zn, Zr, Nb, Mo, Ag, Ge, Sn, Mg, Si, S, Ca, Ti, Cu, Ba, W 및 Pb로 이루어진 군으로부터 선택된 1종 또는 2종 이상의 원소이며, X는 탄소원 또는 리튬티탄산화물(Lithium Titanium Oxide, $Li_4Ti_5O_{12}$) 또는 이들의 혼합물이고, n은 정수인 것을 특징으로 하는 리튬이차전지용 양극 활 물질을 제공한다.

[11] 본 발명의 일 실시예에서 상기 M은 mm'이며, 여기에서 m은 Mn, Fe, Co 및 Ni로 이루어진 군으로부터 선택되며, m'는 Al, V, Cr, Zn, Zr, Nb, Mo, Ag, Ge, Sn, Mg, Si, S, Ca, Ti, Cu, Ba, W 및 Pb로 이루어진 군으로부터 선택된 1종 이상의 원소이며, 상기 탄소원은 탄소나노튜브, 탄소나노와이어, 탄소나노섬유, 흑연, 활성탄 및 그래핀으로 이루어진 군으로부터 선택된 1종 이상이다 .

[12] 본 발명의 또 다른 일 실시예에서 상기 탄소원은 탄소나노튜브, 탄소나노와이어, 탄소나노섬유, 흑연, 활성탄 및 그래핀으로 이루어진 군으로부터 선택된 1종 이상의 물질 및 글루코스(glucose), 스쿠로스(scurose), 폴리에틸렌글리콜(poly ethylene glycol), 폴리비닐알콜(poly vinyl alcohol), 폴리비닐클로라이드(poly vinyl chloride), 구연산(citric acid)으로 이루어진 군으로부터 선택된 1종 이상의 물질을 모두 포함하며, 상기 탄소원 또는 리튬티탄산화물은 Li_nMO_4 입자 표면을 코팅한다.

[13] 본 발명은 또한 상술한 리튬이차전지용 양극 활 물질을 포함하는 리튬이차전지용 양극 활 물질을 제공한다.

[14] 본 발명은 상기 또 다른 과제를 해결하기 위하여, (a) Li_nMO_4 중 MO_4를 이루는 금속 또는 무기 염 또는 이들의 혼합 염과 탄소원 또는 리튬티탄산화물 또는 이들의 혼합물을 용액에 혼합하여, 분산시키는 단계; (b) 상기 혼합물을 세척하는 단계; (c) 상기 세척된 혼합물에 리튬염을 혼합하는 단계; (d) 상기 리튬염이 혼합된 상기 혼합물을 용액에 분산시킨 후, 반응시키는 단계; (e) 상기 반응의 반응물을 건조하는 단계; 및 (f) 상기 건조된 반응물을 열처리 하는 단계를 포함하며, 여기에서 (a) 단계의 M은 Mn, Fe, Co, Ni, Al, Mn, V, Cr, Fe, Co, Zn, Zr, Nb, Mo, Ag, Ge, Sn, Mg, Si, S, Ca, Ti, Cu, Ba, W 및 Pb로 이루어진 군으로부터 선택된 1종 이상의 원소이고, n은 정수인 것을 특징으로 하는 리튬이차전지용 양극 활 물질 제조방법을 제공한다.

[15] 본 발명은 또 다른 일 실시예에서 상기 (a) 및 (d) 단계 중 적어도 어느 하나의 단계에서 상기 분산은 초음파 가진 또는 기계적 교반 방식으로 수행되며, 상기 M은 mm'이며, 여기에서 m은 Mn, Fe, Co 및 Ni로 이루어진 군으로부터 선택되며, m'는 Al, V, Cr, Zn, Zr, Nb, Mo, Ag, Ge, Sn, Mg, Si, S, Ca, Ti, Cu, Ba, W 및 Pb로 이루어진 군으로부터 선택된 1종 이상의 원소이다.

[16] 본 발명의 일 실시예에서 상기 탄소원은 탄소나노튜브, 탄소나노와이어, 탄소나노섬유, 흑연, 활성탄 및 그래핀으로 이루어진 군으로부터 선택된 1종 이상이며, 상기 탄소원은 탄소나노튜브, 탄소나노와이어, 탄소나노섬유, 흑연, 활성탄 및 그래핀으로 이루어진 군으로부터 선택된 1종 이상의 불질 및 글루코스(glucose), 스쿠로스(scurose), 폴리에틸렌글리콜(poly ethylene glycol), 폴리비닐알콜(poly vinyl alcohol), 폴리비닐클로라이드(poly vinyl chloride), 구연산(citric acid)으로 이루어진 군으로부터 선택된 1종 이상의 물질을 포함한다.

발명의 효과

[17] 본 발명에 따르면, 경제적인 방식으로 우수한 전기 전도도 및 기계적 특성을 갖는 리튬이차전지용 양극 활 물질이 제조될 수 있다. 특히, 상기 Li_aMO_4 입사상 표면에 균일하게 분산, 함유된 탄소원 또는 리튬티탄산화물(LTO)은 리튬이차전지용 양극 활 물질 복합체로 하여금 향상된 전기 전도도를 갖게 한다. 또한, 본 발명에 따른 양극 활 물질은 이차전지에 적용하기 적합한 에너지 밀도를 가지고, 안정성과 안전성이 뛰어나며, 우수한 전지특성을 유지하면서도 사이클 수명이 긴 장점을 갖는다.

도면의 간단한 설명

[18] 도 1은 본 발명의 일 실시예에 따른 리튬이차전지용 양극 활 물질 제조방법의 단계도이다.

[19] 도 2는 본 발명에 따라 제조된 복합 양극 활물질의 구조를 X선 회절계(XRD, Rigaku)를 사용하여 분석한 결과이다.

[20] 도 3 내지 6은 본 발명에 따라 제조된 복합 양극 활물질의 입자형태를 FE-SEM(전계 주사현미경)으로 관찰한 결과이다.

[21] 도 7은 본 발명에 따라 제조된 복합 양극 활물질을 포함하는 리튬 이차전지에 대한 충방전 특성 분석 결과이다.

발명의 실시를 위한 최선의 형태

[22] 이하, 본 발명을 도면을 참조하여 상세하게 설명하고자 한다. 다음에 소개되는 실시예들은 당업자에게 본 발명의 사상이 충분히 전달될 수 있도록 하기 위해 예로서 제공되는 것이다. 따라서 본 발명은 이하 설명된 실시예들에 한정되지 않고 다른 형태로 구체화될 수도 있다. 그리고 도면들에 있어서, 구성요소의 폭, 길이, 두께 등은 편의를 위하여 과장되어 표현될 수도 있으며, 명세서 전체에 걸쳐서 동일한 참조번호들은 동일한 구성요소들을 나타낸다

[23] 본 발명은 상술한 바와 같이 리튬이차전지용 양극 활 물질로서 Li_nMO_4 / X 형태의 복합체를 제공한다. 특히 본 발명은 Li 계열의 활성 입자 상에 X로 표시되는 탄소원(여기에서 탄소원은 탄소를 구성원소로 포함하는 임의의 탄소 화합물을 모두 지칭하며, 예를 들면, 탄소나노튜브, 탄소나노섬유, 탄소나노와이어, 그래핀, 흑연 등이 상기 탄소원에 속한다) 또는 리튬티탄산화물($Li_4Ti_5O_{12}$) 또는 이들의 혼합물을 코팅시킴으로써, 활성 입자로 하여금 높은 전도성을 갖게 한다. 여기에서 M은 Mn, Fe, Co, Ni, Al, V, Cr, Zn, Zr, Nb, Mo, Ag, Ge, Sn, Mg, Si, S, Ca, Ti, Cu, Ba, W 및 Pb로 이루어진 군으로부터 선택된 1종 이상의 원소이다. 본 발명의 일 실시예에서 상기 M은 두 종류의 원소(mm')로 이루어지며, 여기에서 m은 Mn, Fe, Co 및 Ni로 이루어진 군으로부터 선택되며, m'는 Al, V, Cr, Zn, Zr, Nb, Mo, Ag, Ge, Sn, Mg, Si, S, Ca, Ti, Cu, Ba, W 및 Pb로 이루어진 군으로부터 선택된 1종 이상의 원소이며, 본 발명의 일 실시예에서 상기 m'는 실리콘(Si), m은 Mn, Fe, Co 및 Ni로 이루어진 군으로부터 선택되었으나, 본 발명의 범위는 이에 제한되지 않는다. 또한 n은 정수로서, 1, 2, 3 등을 포함한다.

[24] 본 발명의 일 실시예에서 상기 탄소원은 상술한 바와 같이 탄소를 구성원소로 하는 임의 형태의 화합물로, 예를 들면 탄소나노튜브, 탄소나노와이어, 탄소나노섬유 및 그래핀으로 이루어진 군으로부터 선택된 1종 이상이 될 수 있다. 본 발명의 또 다른 일 실시예에서 상기 탄소원은 탄소를 구성성분으로 포함하는 전구체 형태로서 글루코스(glucose), 스쿠로스(scurose), 폴리에틸렌글리콜(poly ethylene glycol), 폴리비닐알콜(poly vinyl alcohol), 폴리비닐클로라이드(poly vinyl chloride), 구연산(citric acid)의 일종 또는 이종 이상, 바람직하게는 글루코스, 스쿠로스 및 구연산으로 이루어진 군으로부터 선택된 하나 이상일 수 있다. 본 발명의 일 실시예에서는 탄소나노튜브, 탄소나노와이어, 탄소나노섬유 및 그래핀으로 이루어진 군에서 선택되는 제 1 탄소원과 글루코스(glucose), 스쿠로스(scurose), 폴리에틸렌글리콜(poly ethylene glycol), 폴리비닐알콜(poly vinyl alcohol), 폴리비닐클로라이드(poly vinyl chloride), 구연산(citric acid)으로 이루어진 군에서 선택되는 제 2 탄소원을 혼합 사용하여, 활성 입자를 코팅하는 경우, 매우 우수한 전지 특성을 나타내었다.

[25] 본 발명은 상기 또 다른 과제를 해결하기 위하여, 상술한 양극 활 물질의 제조방법을 제공한다.

[26] 도 1은 본 발명의 일 실시예에 따른 양극 활 물질의 단계도이다.

[27] 도 1을 참조하면, 먼저 상술한 Li_nMO_4 중 MO_4를 이루는 금속 또는 무기 염 또는 이들의 혼합 염과 탄소원 또는 리튬티탄산화물 또는 이들의 혼합물을 용액에 혼합하여, 분산시킨다. 이때 상기 분산은 초음파의 가진 또는 기계적 교반 방식 또는 이 둘 다가 모두 사용될 수 있다. 즉, 본 발명에서 전구체 분말(금속염 등)은 탄소원 또는 리튬티탄산화물과 습식혼합되는 단계로부터 양극 활 물질이 제조된다.

[28] 이후, 상기 분산되어 습식 혼합된 혼합물은 세척된다. 다시, 상기 세척된 혼합물에 리튬염이 혼합되며, 상기 리튬염이 혼합된 상기 혼합물은 다시 용액에 혼입되어, 분산된 후, 반응과정을 거치게 된다. 본 발명의 일 실시예에서 상기 리튬염은 Li_2NO_3, Li_2CO_3, LiOH 등을 사용하였다. 특히 본 발명의 일 실시예에서는 상기 분산 및 반응 과정에서 일정한 에너지를 음파 형태로 공급하는 음향화학(Sonochemistry) 기반의 초음파 가진 공정이 독립적으로 또는 기계적 교반과 함께 사용되어, 입자상에 탄소원 등이 코팅된 양극 활 물질 복합체를 효과적이고 경제적인 방식으로 제조하였다. 이후, 상기 반응물은 건조되며, 상기 건조된 반응물은 열처리된다.

[29] 본 발명에 따른 상기 습식 혼합은 전구체 분말을 수용액에 혼입한 후, 이를 분산시키는 방식인데, 상기 분산은 초음파 가진(음향화학, Sonochemistry), 또는 기계적 교반 방식으로 수행될 수 있다. 상기 열처리 공정은 비활성 또는 환원분위기에서 수행되어 상기 금속 화합물, 예를 들면 철이 산화되는 것을 억제하는 것이 바람직하며, 온도 조건은 500~1000 ℃에서 0.5~10 시간 열처리하여 얻어지는 입자 크기가 500nm 이하가 되도록 하는 것이 바람직하다. 왜냐하면, 500nm를 초과하는 경우, 각 성분들간의 균일한 밀도를 얻기 어렵기 때문이다.

[30]

발명의 실시를 위한 형태

[31] 실시예 1

[32] $Mn(Ac)2{\cdot}6H_2O$ 0.3M 수용액 중에 나노 중공 섬유형 탄소인 탄소나노튜브(CNT) 2 중량%를 균일하게 분산시켜 분산액을 제조한다. 나노 중공 섬유형 탄소의 분산은 초음파 분산 방법 과 고압분산 방법을 이용하였다. 이어서 상기 분산액을 연속적으로 흘려주면서 $Na_2SiO_3{\cdot}12H_2O$ 0.15M을 이용, 분사하여 $MnSiO_3$를 형성시키며, 원심분리기를 이용하여 Na을 제거하였다. Na가 제거된 염에 LiOH 0.1M, 수크로스(sucrose), 구연산(citric acid($Li2MnSiO_3$:citricacid:sucrose=1:0.3:0.05)) 수용액을 $MnSiO_3$ 수용액에 침가 한 후 1시간 교반 후, 반응기 내의 반응계를 지속으로 충분히 교반하거나 또는 상기 반응계에 초음파를 1시간 가진(음향화학, Sonochemistry)하였다. 이때 순환식항온조를 이용하여 반응기 내 온도를 30℃로 유지하고, 운전 주파수는 200 kHz 강도는 300 W, 반응기 내의 압력을 3 atm으로 일정하게 가압하였으며, 반응기 내부에는 아르곤 가스를 이용하였다. 반응 후 스프레이 건조기에서 150도에서 건조하였다. 건조 후 질소 분위기에서 750℃에서 24시간 소성하였다. 이로써, Li_2MnSiO_4 활성입자 상에 탄소나노튜브 및 수크로스와 같은 탄소원이 코팅된 복합 양극 활 물질을 제조하였다.

[33]

[34] 실시예 2

[35] $Mn(Ac)2{\cdot}6H_2O$ 0.28M에 $Fe(NO_3)$ 0.02M을 소량 첨가한 것을 제외하고는 실시예 1과 동일한 방식으로 리튬 이차전지용 복합 양극 활 물질을 제조하였다.

[36]

[37] 실시예 3

[38] 탄소나노튜브 대신 LiOH, TiO_2를 넣은 것을 제외하고는 실시예 1과 동일한 방법으로 복합 양극 활 물질을 제조하였다.

[39]

[40] 비교예 1

[41] 실시예 1에서sucrose, citric acid, CNT와 같은 탄소원을 넣지 않은 것을 제외하고는 실시예 1과 동일한 방법으로 복합 양극 활 물질을 제조하였다.

[42]

[43] 시험예 1

[44] X선 회절 분석

[45] 실시예에서 제조된 복합 양극 활물질의 구조를 X선 회절계(XRD, Rigaku)를 사용하여 분석하고, 그 결과를 도 2에 나타내었다. 도 2의 결과로부터 알 수 있는 바와 같이, 본 발명에 따라 제조된 복합 양극 활물질에서 Li_2MnSiO_4의 특성 피크와 아주 잘 일치하는 것을 알 수 있다.

[46]

[47] 시험예 2

[48] FE-SEM

[49] FE-SEM(전계 주사현미경)으로 실시예에서 제조된 복합 양극 활물질의 입자형태를 관찰하였으며, 그 결과를 도 3 내지 도 6에 나타내었다. 도 3 내지 6에서 보는 바와 같이 복합 양극 활물질의 입자에 CNT가 잘 분산되어 있으며, 입자 평균 입자 크기가 약 10 마이크로 나타나는 것을 알 수 있다.

[50]

[51] 시험예 3

[52] 입도 분석

[53] 레이저회절식의 입도 분포계를 이용하여 재료의 입도 분석을 하였다. 누적 입도 분포의 결과로부터 누적 체적이 10%, 50% 및 90%에 도달하는 지점에서의 입도를 확인하여, 각각 d10, d50, 및 d90으로 하였으며, 이에 대한 결과는 표 1에 나타내었다.

[54] 표 1

Sample		입자 크기(μm)	탭 밀도(g/cc)
실시예 1	d10	6.0	1.2
	d50	10.4	
	d90	14.2	
실시예 2	d10	5.5	1.2
	d50	10.0	
	d90	13.0	
실시예 3	d10	5.4	1.3
	d50	9.2	
	d90	12.3	
비교예 1	d10	4.5	1.3
	d50	11.0	
	d90	12.5	

[55]

[56] 시험예 4

[57] 탭 밀도

[58] 탭 밀도는 실린더에 재료 50g을 투입하고, 탭 횟수 2000회 후의 부피를 측정하여 탭 밀도를 계산하였으며, 그 결과를 상기 표 1에 나타내었다. 복합 양극 활물질에 탄소물질과 CNT가 포함될수록 탭 밀도는 다소 감소하나, 최종적인 전지 평가에 나타난 전지 성능은 제 1 탄소원(수크로스)과 제 2 탄소원인 CNT가 포함될수록 전지 성능은 증가하였다. 따라서, 상기 결과는 본 발명에 따른 양극 활 물질은 망간의 문제점인 전기 전도성을 향상시켜, 우수한 전지 성능을 발생시키는 점을 나타낸다. 특히 탄소나노튜브와 탄소원인 수크로스를 함께 사용한 경우, 그 효과는 보다 명확해진다.

[59]

[60] 시험예 5

[61] 전지 평가

[62] 전지 평가를 위하여 본 발명에 따라 제조된 복합 양극 활물질 : 도전재 : 바인더를 85 : 8 : 7의 중량 비율로 칭량하였다. 혼합된 물질을 슬러리화한 후 알루미늄 박막에 도포 후 120℃에서 8시간 건조 하여 극판을 제조하였으며, 제조된 극판을 프레스 하였다. 음극으로는 Li 메탈을 이용하고, 2030 형 코인 셀을 제조하였으며, 전해액으로 1M-LiPF6를 EC-DEC(체적비1 : 1)에 용해시킨 것을 이용하였다. 충전 조건을 4.4V, 방전 조건을 3.0V로 충방전을 실시하였고, 그 결과를 도 7에 나타내었다.

[63] 도 7에서 나타난 바와 같이 탄소물질과 CNT를 동시에 포함하지 않는 양극 활물질은 방전 비용량이 아주 좋지 않음을 알 수 있으며, CNT와 탄소물질이 동시에 포함 복합 양극 활물질이 아주 좋은 방전 비용량을 가진다. 이는 탄소물질과 CNT가 전기 전도성을 향상 시켜 주는 것을 알 수 있다. 또한, 탄소물질과 LTO가 동시에 첨가된 실시예 1에서 아주 좋은 비용량을 보였다. 이는 LTO가 전극물질의 안정성을 높여 일어난 현상으로 보인다.

산업상 이용가능성

[64] 본 발명법에 의하여 경제적인 방식으로 우수한 전기 전도도 및 기계적 특성을 갖는 리튬이차전지용 양극 활 물질이 제조될 수 있다.

청구범위

[청구항 1] 리튬이차전지용 양극 활 물질로서, 상기 양극 활 물질은 Li_nMO_4 / X의 복합체를 포함하며,여기에서 M은 Mn, Fe, Co, Ni, Al, Mn, V, Cr, Fe, Co, Zn, Zr, Nb, Mo, Ag, Ge, Sn, Mg, Si, S, Ca, Ti, Cu, Ba, W 및 Pb로 이루어진 군으로부터 선택된 1종 또는 2종 이상의 원소이며, X는 탄소원 또는 리튬티탄산화물(Lithium Titanium Oxide, $Li_4Ti_5O_{12}$) 또는 이들의 혼합물이고, n은 정수인 것을 특징으로 하는 리튬이차전지용 양극 활 물질.

[청구항 2] 제 1항에 있어서,
상기 M은 mm'이며, 여기에서 m은 Mn, Fe, Co 및 Ni로 이루어진 군으로부터 선택되며, m'는 Al, V, Cr, Zn, Zr, Nb, Mo, Ag, Ge, Sn, Mg, Si, S, Ca, Ti, Cu, Ba, W 및 Pb로 이루어진 군으로부터 선택된 1종 이상의 원소인 것을 특징으로 하는 리튬이차전지용 양극 활 물질.

[청구항 3] 제 1항에 있어서,
상기 탄소원은 탄소나노튜브, 탄소나노와이어, 탄소나노섬유, 흑연, 활성탄 및 그래핀으로 이루어진 군으로부터 선택된 1종 이상인 것을 특징으로 하는 리튬이차전지용 양극 활 물질.

[청구항 4] 제 3항에 있어서,
상기 탄소원은 탄소나노튜브, 탄소나노와이어, 탄소나노섬유, 흑연, 활성탄 및 그래핀으로 이루어진 군으로부터 선택된 1종 이상의 물질 및 글루코스(glucose), 스쿠로스(scurose), 폴리에틸렌글리콜(poly ethylene glycol), 폴리비닐알콜(poly vinyl alcohol), 폴리비닐클로라이드(poly vinyl chloride), 구연산(citric acid)으로 이루어진 군으로부터 선택된 1종 이상의 물질을 모두 포함하는 것을 특징으로 하는 리튬이차전지용 양극 활 물질.

[청구항 5] 제 1항에 있어서,
상기 탄소원 또는 리튬티탄산화물은 Li_nMO_4 입자 표면을 코팅하는 것을 특징으로 하는 리튬이차전지용 양극 활 물질.

[청구항 6] 제 1항 내지 제 5항 중 어느 한 항에 따른 리튬이차전지용 양극 활 물질을 포함하는 리튬이차전지용 양극 활 물질.

[청구항 7] (a) Li_nMO_4 중 MO_4를 이루는 금속 또는 무기 염 또는 이들의 혼합염과 탄소원 또는 리튬티탄산화물 또는 이들의 혼합물을 용액에 혼합하여, 분산시키는 단계;
(b) 상기 혼합물을 세척하는 단계;
(c) 상기 세척된 혼합물에 리튬염을 혼합하는 단계;
(d) 상기 리튬염이 혼합된 상기 혼합물을 용액에 분산시킨 후,

반응시키는 단계;
(e) 상기 반응의 반응물을 건조하는 단계; 및
(f) 상기 건조된 반응물을 열처리 하는 단계를 포함하며, 여기에서 (a) 단계의 M은 Mn, Fe, Co, Ni, Al, Mn, V, Cr, Fe, Co, Zn, Zr, Nb, Mo, Ag, Ge, Sn, Mg, Si, S, Ca, Ti, Cu, Ba, W 및 Pb로 이루어진 군으로부터 선택된 1종 이상의 원소이고, n은 정수인 것을 특징으로 하는 리튬이차전지용 양극 활 물질 제조방법.

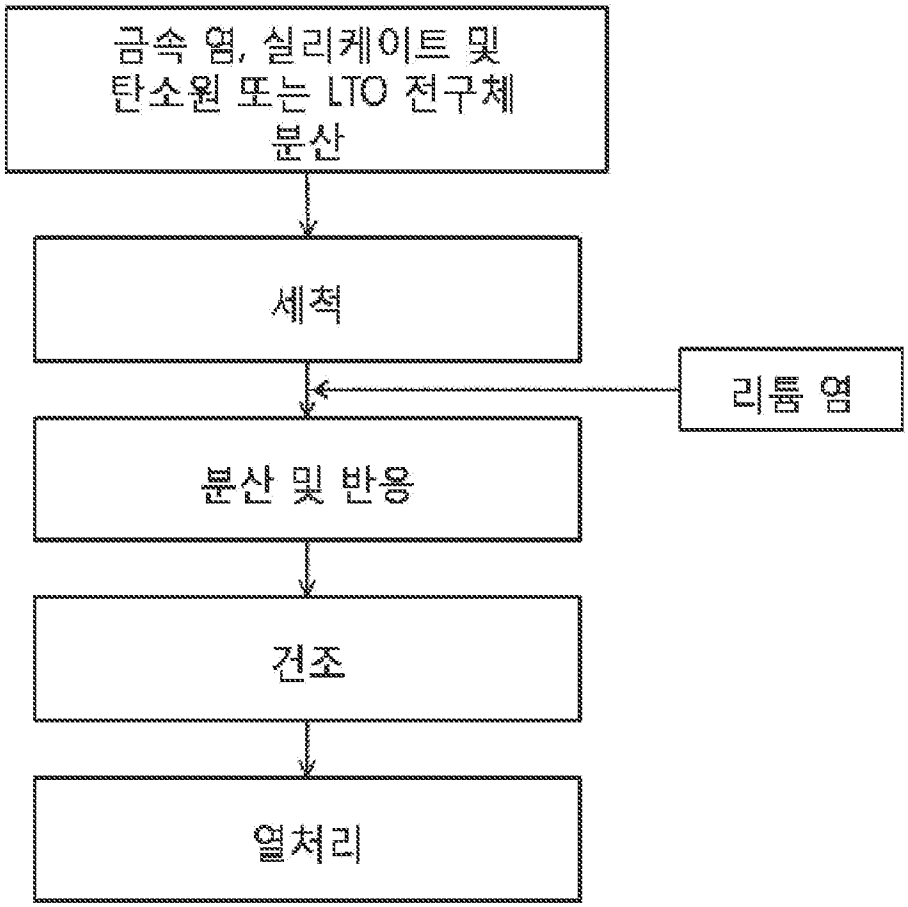
[청구항 8] 제 7항에 있어서,
상기 (a) 및 (d) 단계 중 적어도 어느 하나의 단계에서 상기 분산은 초음파 가진 또는 기계적 교반 방식으로 수행되는 것을 특징으로 하는 리튬이차전지용 양극 활 물질 제조방법.

[청구항 9] 제 7항에 있어서,
상기 M은 mm'이며, 여기에서 m은 Mn, Fe, Co 및 Ni로 이루어진 군으로부터 선택되며, m'는 Al, V, Cr, Zn, Zr, Nb, Mo, Ag, Ge, Sn, Mg, Si, S, Ca, Ti, Cu, Ba, W 및 Pb로 이루어진 군으로부터 선택된 1종 이상의 원소인 것을 특징으로 하는 리튬이차전지용 양극 활 물질 제조방법.

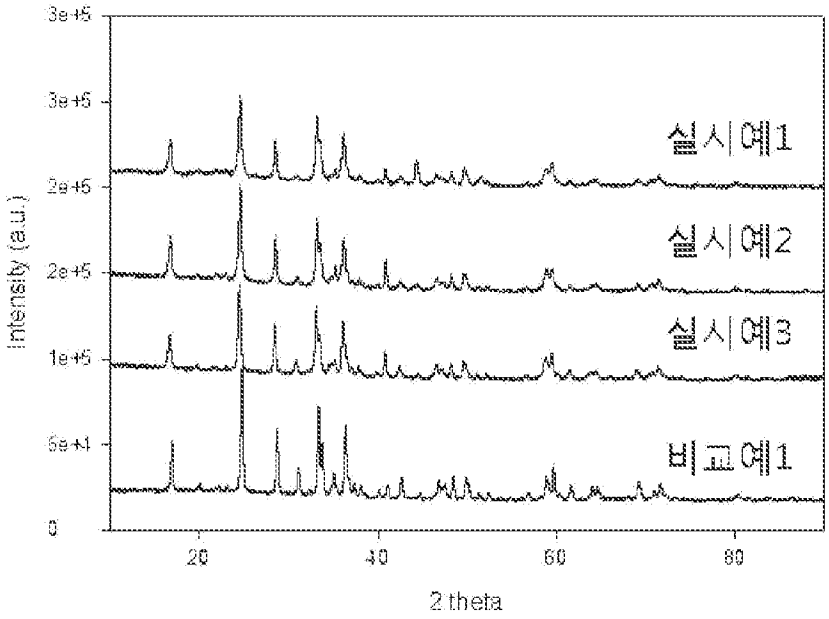
[청구항 10] 제 7항에 있어서,
상기 탄소원은 탄소나노튜브, 탄소나노와이어, 탄소나노섬유, 흑연, 활성탄 및 그래핀으로 이루어진 군으로부터 선택된 1종 이상인 것을 특징으로 하는 리튬이차전지용 양극 활 물질 제조방법.

[청구항 11] 제 10항에 있어서,
상기 탄소원은 탄소나노튜브, 탄소나노와이어, 탄소나노섬유, 흑연, 활성탄 및 그래핀으로 이루어진 군으로부터 선택된 1종 이상의 물질 및 글루코스(glucose), 스쿠로스(scurose), 폴리에틸렌글리콜(poly ethylene glycol), 폴리비닐알콜(poly vinyl alcohol), 폴리비닐클로라이드(poly vinyl chloride), 구연산(citric acid)으로 이루어진 군으로부터 선택된 1종 이상의 물질을 포함하는 것을 특징으로 하는 리튬이차전지용 양극 활 물질 제조방법.

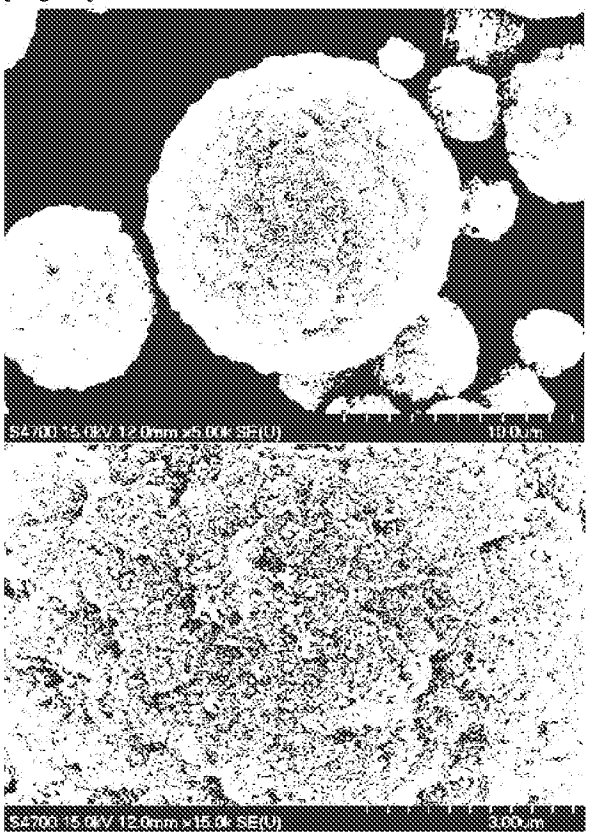
[Fig. 1]


금속 염, 실리케이트 및
탄소원 또는 LTO 전구체
분산
세척
리튬 염
분산 및 반응
건조
열처리

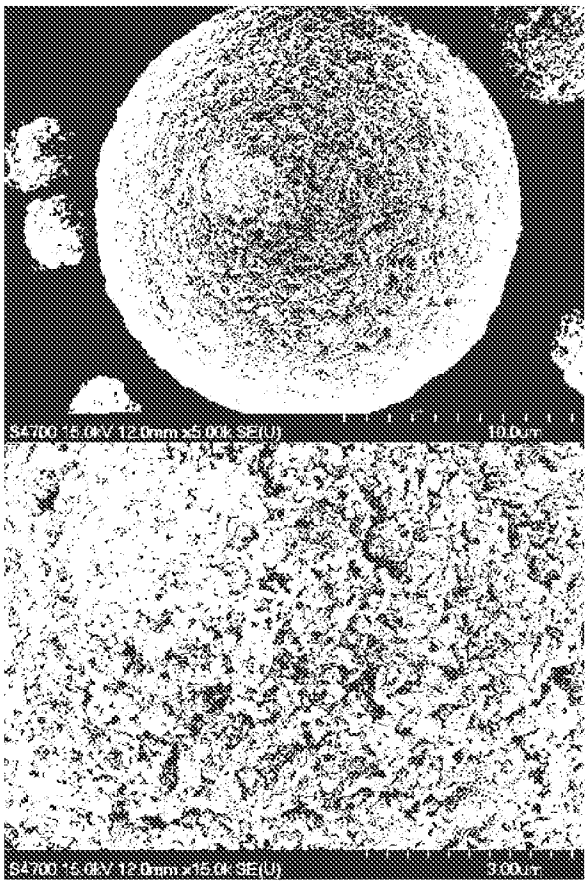
[Fig. 2]


3e+5
3e+5
2e+5
2e+5
1e+5
5e+4
0
Intensity (a.u.)
20
40
60
80
2 theta
실시예1
실시예2
실시예3
비교예1

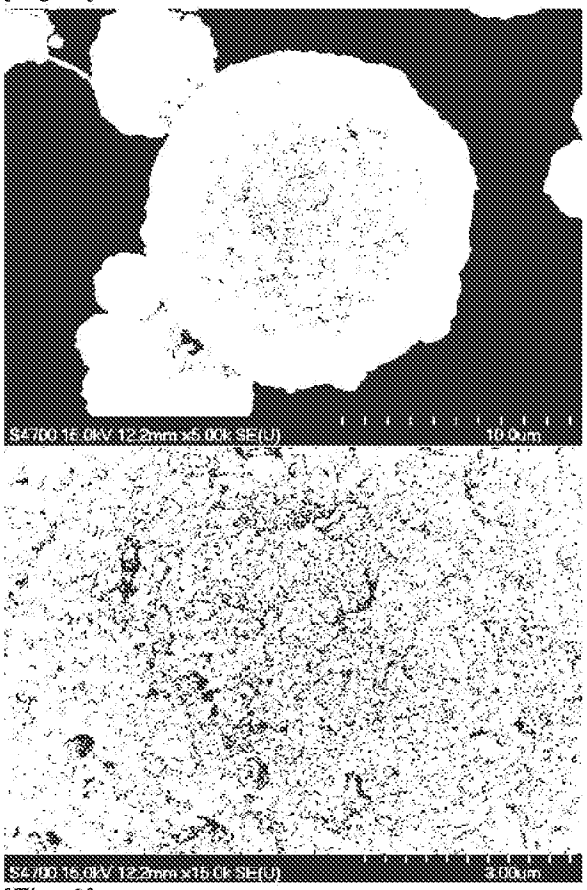
[Fig. 3]


S4700 5.0kV 12.0mm x5.00k SE(U) 10.0μm
S4700 5.0kV 12.0mm x15.0k SE(U) 3.00μm

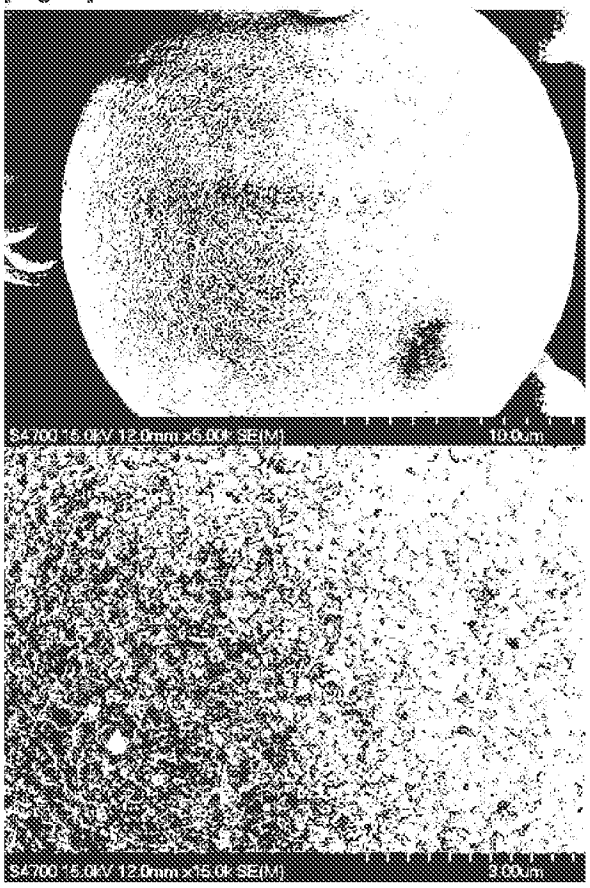
[Fig. 4]


S4700 5.0kV 12.0mm x5.00k SE(U) 10.0μm
S4700 5.0kV 12.0mm x15.0k SE(U) 3.00μm

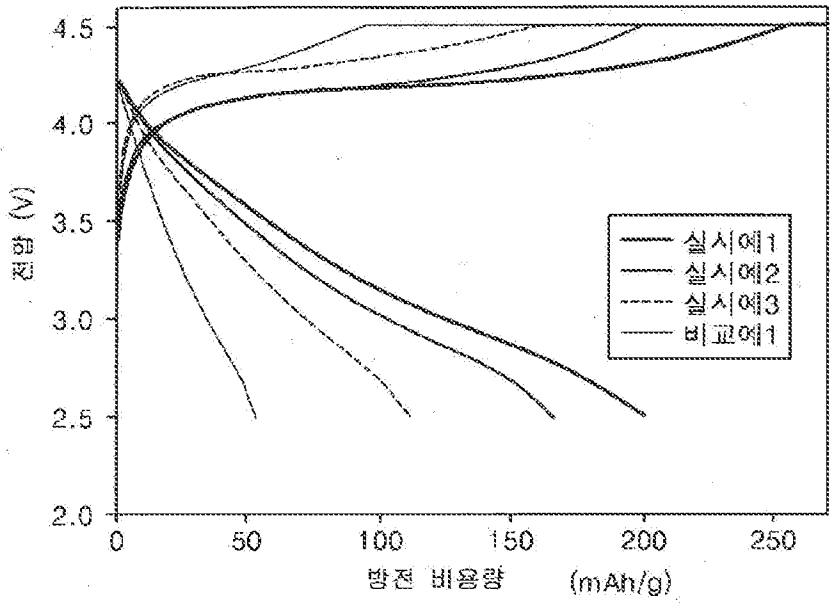
[Fig. 5]



[Fig. 6]



[Fig. 7]


4.5
4.0
3.5
3.0
2.5
2.0
전압 (V)
0
50
100
150
200
250
방전 비용량 (mAh/g)
실시예1
실시예2
실시예3
비교예1

Espacenet

Family list: JP2015088450 (A) — 2015-05-07

1 application(s) for: JP2015088450 (A)

1. LITHIUM ION SECONDARY BATTERY					
Inventor: SHINMYO KENICHI TERANISHI RIE (+1)	**Applicant:** SEKISUI CHEMICAL CO LTD	**CPC:**	**IPC:** H01M4/13 H01M4/36 H01M4/48 (+1)	**Publication info:** JP2015088450 (A) 2015-05-07 JP6302322 (B2) 2018-03-28 Global Dossier	**Priority date:** 2013-09-26

Espacenet

Bibliographic data: JP2015088450 (A) — 2015-05-07

LITHIUM ION SECONDARY BATTERY

Inventor(s): SHINMYO KENICHI; TERANISHI RIE; TOYOKAWA TAKUYA ± (新明 健一, ; 寺西 利絵, ; 豊川 卓也)

Applicant(s): SEKISUI CHEMICAL CO LTD ± (積水化学工業株式会社)

Classification: **- international:** ***H01M4/13; H01M4/36; H01M4/48; H01M4/62***
- cooperative:

Application number: JP20140068328 20140328 Global Dossier

Priority number (s): JP20130200106 20130926 ; JP20140068328 20140328

Also published as: JP6302322 (B2)

Abstract of JP2015088450 (A)

PROBLEM TO BE SOLVED: To provide a lithium ion secondary battery having a high capacity appearance rate and a capacity maintenance rate.SOLUTION: The lithium ion secondary battery includes: a negative electrode active material formed by using a negative electrode material formed by mixing silicon oxide, a particulate conductive assistant, a fiber-like conductive assistant, and a binder; and a negative electrode to which lithium is pre-doped.

(19)日本国特許庁(JP)　(12)公開特許公報(A)　(11)特許出願公開番号
特開2015-88450
(P2015-88450A)
(43)公開日　平成27年5月7日(2015.5.7)

(51)Int.Cl.		F I			テーマコード（参考）
H01M 4/13	***(2010.01)***	H01M	4/13		5H050
H01M 4/62	***(2006.01)***	H01M	4/62	Z	
H01M 4/48	***(2010.01)***	H01M	4/48		
H01M 4/36	***(2006.01)***	H01M	4/36	B	

審査請求 未請求　請求項の数 4　ＯＬ　（全 27 頁）

(21)出願番号　特願2014-68328(P2014-68328)
(22)出願日　平成26年3月28日(2014.3.28)
(31)優先権主張番号　特願2013-200106(P2013-200106)
(32)優先日　平成25年9月26日(2013.9.26)
(33)優先権主張国　日本国(JP)

(71)出願人　000002174
積水化学工業株式会社
大阪府大阪市北区西天満２丁目４番４号
(74)代理人　100146835
弁理士　佐伯　義文
(74)代理人　100134544
弁理士　森　隆一郎
(74)代理人　100147267
弁理士　大槻　真紀子
(74)代理人　100119091
弁理士　豊山　おぎ
(72)発明者　新明　健一
茨城県つくば市和台３２番地　積水化学工業株式会社内

最終頁に続く

(54)【発明の名称】リチウムイオン二次電池

(57)【要約】
【課題】容量発現率及び容量維持率が高いリチウムイオン二次電池の提供。
【解決手段】酸化ケイ素、粒子状導電助剤、繊維状導電助剤及びバインダーが配合されてなる負極材を用いて形成された負極活物質層を有し、且つリチウムがプレドープされている負極を備えたことを特徴とするリチウムイオン二次電池。
【選択図】なし

【特許請求の範囲】
【請求項１】
酸化ケイ素、粒子状導電助剤、繊維状導電助剤及びバインダーが配合されてなる負極材を用いて形成された負極活物質層を有し、且つリチウムがプレドープされている負極を備えたことを特徴とするリチウムイオン二次電池。
【請求項２】
前記粒子状導電助剤がカーボンブラックであり、前記繊維状導電助剤がカーボンナノチューブであることを特徴とする請求項１に記載のリチウムイオン二次電池。
【請求項３】
前記酸化ケイ素の粒径が０．１μｍ～２０μｍの大きさであることを特徴とする請求項１又は２に記載のリチウムイオン二次電池。
【請求項４】
前記負極材を形成する前記酸化ケイ素、前記粒子状導電助剤、前記繊維状導電助剤及び前記バインダーの総質量に対する、該バインダーの割合が１０～２０質量％であることを特徴とする請求項１～３のいずれか一項に記載のリチウムイオン二次電池。
【発明の詳細な説明】
【技術分野】
【０００１】
本発明は、リチウムイオン二次電池に関する。
【背景技術】
【０００２】
リチウムイオン二次電池は、正極、負極及び電解質を備えて構成される。そして、正極及び負極、すなわち電極は、電極活物質が配合されて構成され、通常はさらに、導電助剤及びバインダーが配合されて構成される。なかでも電極活物質は、リチウムイオン二次電池の容量に関わる重要な因子であり、負極活物質として従来は、主に黒鉛（グラファイト）が使用されている。
【０００３】
これに対して、より高容量のリチウムイオン二次電池を実現し得る負極活物質として、ケイ素が注目されている。リチウムイオン二次電池の理論容量は、例えば、負極活物質として黒鉛を用いた場合には３７２ｍＡｈ／ｇであるのに対して、ケイ素を用いた場合には４１９９ｍＡｈ／ｇである。
【０００４】
しかし、ケイ素を用いて負極を構成した場合、充放電時におけるリチウムイオンの吸蔵及び放出過程で、負極が膨張及び収縮することが知られている。負極では、１個のケイ素原子に対して４個のリチウムイオンの吸蔵及び放出が可能であり、二次電池が作動する際に、負極は４倍膨張及び収縮し得る。充放電時におけるこの膨張及び収縮により、負極は集電性が低下して、放電容量が大きく低下してしまう。このように、負極活物質としてケイ素を用いたリチウムイオン二次電池は、充放電を繰り返し行ったときの容量維持率が低いという問題点があった。
【０００５】
これに対して、負極活物質として酸化ケイ素を用いた負極が開示されている（特許文献１参照）。このような負極を備えたリチウムイオン二次電池では、充放電を繰り返し行ったときの容量維持率の低下を抑制できるものの、初期充電工程においてリチウムが酸化ケイ素と不可逆的に反応してリチウムシリケート（Li_4SiO_4）等の副生成物が生じ、このリチウムは以降、放電に関与することができず、放電容量が低下してしまうという問題点があった。
【０００６】
このような放電容量の低下を解決できるものとして、酸化ケイ素を真空蒸着法又はスパッタリング法により成膜して負極を構成する手法が開示されている（特許文献２参照）。
【先行技術文献】

【特許文献】
【０００７】
【特許文献１】特開平６－３２５７６５号公報
【特許文献２】特開２００４－３４９２３７号公報
【発明の概要】
【発明が解決しようとする課題】
【０００８】
しかし、特許文献２で開示されている手法では、リチウムイオン二次電池の定格容量に対する１サイクル目の放電容量の割合、いわゆる容量発現率が８０％程度にとどまり、不十分であるという問題点があった。
【０００９】
本発明は上記事情に鑑みてなされたものであり、容量発現率及び容量維持率が高いリチウムイオン二次電池を提供することを課題とする。
【課題を解決するための手段】
【００１０】
上記課題を解決するため、本発明は、酸化ケイ素、粒子状導電助剤、繊維状導電助剤及びバインダーが配合されてなる負極材を用いて形成された負極活物質層を有し、且つリチウムがプレドープされている負極を備えたことを特徴とするリチウムイオン二次電池を提供する。
本発明のリチウムイオン二次電池は、前記粒子状導電助剤がカーボンブラックであり、前記繊維状導電助剤がカーボンナノチューブであることが好ましい。
【発明の効果】
【００１１】
本発明によれば、容量発現率及び容量維持率が高いリチウムイオン二次電池が提供される。
【図面の簡単な説明】
【００１２】
【図１】本発明に係るリチウムイオン二次電池の要部を模式的に例示する正面図である。
【図２】製造例１における^{1}Ｈ－ＮＭＲデータであり、（ａ）は比較用の三フッ化ホウ素ジエチルエーテル錯体の^{1}Ｈ－ＮＭＲデータ、（ｂ）は得られたシュウ酸リチウム－三フッ化ホウ素錯体の^{1}Ｈ－ＮＭＲデータである。
【図３】製造例１における^{19}Ｆ－ＮＭＲデータであり、（ａ）は比較用の三フッ化ホウ素ジエチルエーテル錯体の^{19}Ｆ－ＮＭＲデータ、（ｂ）は得られたシュウ酸リチウム－三フッ化ホウ素錯体の^{19}Ｆ－ＮＭＲデータである。
【図４】製造例１におけるＩＲデータであり、（ａ）は比較用のシュウ酸リチウムのＩＲデータ、（ｂ）は得られたシュウ酸リチウム－三フッ化ホウ素錯体のＩＲデータである。
【図５】実施例１で得られた負極前駆体における負極活物質層の、走査型電子顕微鏡（ＳＥＭ）で取得した撮像データである。
【発明を実施するための形態】
【００１３】
＜リチウムイオン二次電池＞
本発明に係るリチウムイオン二次電池は、酸化ケイ素、粒子状導電助剤、繊維状導電助剤及びバインダーが配合されてなる負極材を用いて形成された負極活物質層を有し、且つリチウムがプレドープされている負極を備えたことを特徴とする。
かかるリチウムイオン二次電池は、粒子状導電助剤及び繊維状導電助剤を併用し、さらにリチウムがプレドープされている負極を用いたことにより、容量発現率と、充放電を繰り返し行ったときの容量維持率とが共に高く、充放電特性に優れる。
【００１４】
本明細書において、リチウムイオン二次電池における「容量発現率」とは、定格容量に対する１サイクル目の放電容量の割合（％）を意味し、式「｛［１サイクル目の放電容量

（ｍＡｈ）］／［定格容量（ｍＡｈ）］}×１００」により算出される。
また、本明細書において、リチウムイオン二次電池における「容量維持率」とは、充放電サイクルを繰り返し行ったときの、１サイクル目の放電容量に対する特定のサイクル数での放電容量の割合（％）を意味し、式「{［特定のサイクル数での放電容量（ｍＡｈ）］／［１サイクル目の放電容量（ｍＡｈ）］}×１００）」により算出される。ここで、「特定のサイクル数」は、好ましくは５０サイクル以上である。

【００１５】

［負極材］

本発明において、前記負極材は、酸化ケイ素、粒子状導電助剤、繊維状導電助剤及びバインダーが配合されてなるものであり、酸化ケイ素に対して、粒子状導電助剤及び繊維状導電助剤を必須成分として併用する点で、従来の負極材とは相違するものである。

【００１６】

（酸化ケイ素）

前記酸化ケイ素としては、一般式「SiO_z（式中、ｚは０．５～１．５のいずれかの数である。）」で表されるものが例示できる。ここで酸化ケイ素を「ＳｉＯ」単位で見た場合、このＳｉＯは、アモルファス状のＳｉＯであるか、又はＳｉ：SiO_2のモル比が約１：１となるように、ナノクラスターのＳｉの周囲にSiO_2が存在する、Ｓｉ及びSiO_2の複合物である。SiO_2は、充放電時におけるＳｉの膨張及び収縮に対して緩衝作用を有すると推測される。

【００１７】

前記酸化ケイ素は、粉末状であることが好ましく、粒子状であることがより好ましく、例えば、平均粒子径が３０μｍ以下であることが好ましく、２０μｍ以下であることがより好ましく、１０μｍ以下であることが特に好ましく、２．０μｍ以下であることが最も好ましい。また、酸化ケイ素とバインダーの配合比率にもよるが、前記平均粒子径が１．０μｍ以下であると最も好ましい傾向がある。このような微粉末状の酸化ケイ素を用いることで、粒子状導電助剤及び繊維状導電助剤の併用による効果が、より顕著に得られる。

酸化ケイ素の平均粒子径は、例えば、電子顕微鏡を用いて、任意の酸化ケイ素の粒子約１００個について粒子径を計測し、その平均値を算出することで求められる。

酸化ケイ素は、例えば、ボールミル等を用いる公知の手法で粉砕することにより、平均粒子径を所望の値に調節できる。

【００１８】

前記負極材において、酸化ケイ素、粒子状導電助剤、繊維状導電助剤及びバインダーの総配合量に対する、酸化ケイ素の配合量の割合は、４０～８５質量％であることが好ましく、５５～８０質量％であることがより好ましい。酸化ケイ素の前記配合量の割合が前記下限値以上であることで、リチウムイオン二次電池は放電容量がより向上し、酸化ケイ素の前記配合量の割合が前記上限値以下であることで、負極構造の安定した維持が容易となる。

【００１９】

（粒子状導電助剤）

前記粒子状導電助剤は、導電助剤として機能する粒子状のものであれば特に限定されないが、好ましいものとしては、アセチレンブラック、ケッチェンブラック等のカーボンブラック；黒鉛（グラファイト）；フラーレン等が例示できる。

【００２０】

粒子状導電助剤は、平均粒子径が１０～１００ｎｍであることが好ましく、１５～６０ｎｍであることがより好ましい。また、粒子状導電助剤は、各々の粒子が数珠つなぎになったもの等、互いに連なった構造を形成していることが好ましい。このような平均粒子径又は構造を形成している粒子状導電助剤を用いることで、繊維状導電助剤との併用による効果がより顕著に得られる。

粒子状導電助剤の平均粒子径は、上記の酸化ケイ素の平均粒子径の場合と同様の方法で求められ、調節できる。

【００２１】
粒子状導電助剤は、後述する負極活物質層中において、そのナノ粒子等の微粒子が連なった構造を形成し、酸化ケイ素と後述する繊維状導電助剤との接触面積を高めることで、導電性の向上に寄与していると推測される。
【００２２】
前記粒子状導電助剤は、一種を単独で用いてもよいし、二種以上を併用してもよく、二種以上を併用する場合には、その組み合わせ及び比率は目的に応じて適宜選択すればよい。
【００２３】
前記負極材において、酸化ケイ素、粒子状導電助剤、繊維状導電助剤及びバインダーの総配合量に対する、粒子状導電助剤の配合量の割合は、３～３０質量％であることが好ましく、５～２０質量％であることがより好ましい。粒子状導電助剤の前記配合量の割合が前記下限値以上であることで、粒子状導電助剤を用いたことによる効果がより顕著に得られ、粒子状導電助剤の前記配合量の割合が前記上限値以下であることで、繊維状導電助剤との併用による効果がより顕著に得られる。
【００２４】
（繊維状導電助剤）
前記繊維状導電助剤は、導電助剤として機能する繊維状のものであれば特に限定されないが、好ましいものとしては、カーボンナノチューブ、カーボンナノホーンが例示できる。
【００２５】
繊維状導電助剤は、平均繊維径が５ｎｍ～３００ｎｍであることが好ましく、１０ｎｍ～１５０ｎｍであることがより好ましい。また、繊維状導電助剤は、平均繊維長が０．１μｍ～３０μｍであることが好ましく、０．５μｍ～２０μｍであることがより好ましい。このような繊維状導電助剤を用いることで、粒子状導電助剤との併用による効果がより顕著に得られる。
繊維状導電助剤の平均繊維径は、例えば、電子顕微鏡を用いて、任意の繊維状導電助剤約１００本について繊維径を計測し、その平均値を算出することで求められる。同様に、繊維状導電助剤の平均繊維長は、例えば、電子顕微鏡を用いて、任意の繊維状導電助剤約１００本について繊維長を計測し、その平均値を算出することで求められる。
【００２６】
繊維状導電助剤は、後述する負極活物質層中において、好ましくは負極活物質層全体に、網目構造を形成することで、負極活物質層の構造安定化に寄与すると共に、負極活物質層中に導電ネットワークを形成して、導電性の向上に寄与している推測される。
【００２７】
前記繊維状導電助剤は、一種を単独で用いてもよいし、二種以上を併用してもよく、二種以上を併用する場合には、その組み合わせ及び比率は目的に応じて適宜選択すればよい。
【００２８】
前記負極材において、酸化ケイ素、粒子状導電助剤、繊維状導電助剤及びバインダーの総配合量に対する、繊維状導電助剤の配合量の割合は、１～２５質量％であることが好ましく、２～１５質量％であることがより好ましい。繊維状導電助剤の前記配合量の割合が前記下限値以上であることで、繊維状導電助剤を用いたことによる効果がより顕著に得られ、繊維状導電助剤の前記配合量の割合が前記上限値以下であることで、粒子状導電助剤との併用による効果がより顕著に得られる。
【００２９】
前記負極材において、「粒子状導電助剤：繊維状導電助剤」の配合量の質量比率（配合質量比）は、９０：１０～３０：７０であることが好ましく、８０：２０～４０：６０であることがより好ましい。粒子状導電助剤及び繊維状導電助剤の配合質量比がこのような範囲であることで、粒子状導電助剤及び繊維状導電助剤の併用による効果がより顕著に得

られる。
【００３０】
（バインダー）
前記バインダーは公知のものでよく、好ましいものとしては、ポリアクリル酸（ＰＡＡ）、ポリアクリル酸リチウム（ＰＡＡＬｉ）、ポリフッ化ビニリデン（ＰＶＤＦ）、ポリフッ化ビニリデン－六フッ化プロピレン共重合体（ＰＶＤＦ－ＨＦＰ）、スチレンブタジエンゴム（ＳＢＲ）、ポリビニルアルコール（ＰＶＡ）、ポリエチレンオキサイド（ＰＥＯ）、ポリエチレングリコール（ＰＥＧ）、カルボキシメチルセルロース（ＣＭＣ）、ポリアクリルニトリル（ＰＡＮ）、ポリイミド（ＰＩ）等が例示できる。
前記バインダーは、一種を単独で用いてもよいし、二種以上を併用してもよく、二種以上を併用する場合には、その組み合わせ及び比率は目的に応じて適宜選択すればよい。
【００３１】
前記負極材において、酸化ケイ素、粒子状導電助剤、繊維状導電助剤及びバインダーの総配合量に対する、バインダーの配合量の割合は、３～３０質量％であることが好ましく、５～２０質量％であることがより好ましい。バインダーの前記配合量の割合が前記下限値以上であることで、負極構造がより安定して維持され、バインダーの前記配合量の割合が前記上限値以下であることで、放電容量がより向上する。
【００３２】
（その他の成分）
前記負極材は、酸化ケイ素、粒子状導電助剤、繊維状導電助剤及びバインダー以外に、これらに該当しないその他の成分がさらに配合されてなるものでもよい。
前記その他の成分は、特に限定されず、目的に応じて任意に選択でき、好ましいものとしては、前記配合成分（酸化ケイ素、粒子状導電助剤、繊維状導電助剤、バインダー）を溶解又は分散させるための溶媒が例示できる。
このような、さらに溶媒が配合されてなる負極材は、使用時において流動性を有する液状組成物であることが好ましい。
【００３３】
前記溶媒は、前記配合成分の種類に応じて任意に選択でき、好ましいものとしては、水、有機溶媒が例示できる。
前記有機溶媒で好ましいものとしては、メタノール、エタノール、１－プロパノール、２－プロパノール等のアルコール；Ｎ－メチルピロリドン（ＮＭＰ）、Ｎ，Ｎ－ジメチルホルムアミド（ＤＭＦ）等の鎖状又は環状アミド；アセトン等のケトンが例示できる。
前記溶媒は、一種を単独で用いてもよいし、二種以上を併用してもよく、二種以上を併用する場合には、その組み合わせ及び比率は目的に応じて適宜選択すればよい。
【００３４】
負極材における前記溶媒の配合量は、特に限定されず、目的に応じて適宜調節すればよい。例えば、溶媒が配合された液状組成物である負極材を塗工及び乾燥させて、後述する負極活物質層を形成する場合には、この液状組成物が塗工に適した粘度となるように、溶媒の配合量を調節すればよい。具体的には、負極材において、配合成分の総量に対する、溶媒以外の配合成分の総量の割合が、好ましくは５～６０質量％、より好ましくは１０～３５質量％となるように、溶媒の配合量を調節するとよい。
【００３５】
前記その他の成分として、前記溶媒以外の成分（その他の固体成分）を配合する場合、前記負極材において、溶媒以外の配合成分の総量に対する、その他の固体成分の配合量の割合は、１０質量％以下であることが好ましく、５質量％以下であることがより好ましい。
【００３６】
前記負極材は、前記粒子状導電助剤がカーボンブラックであり、前記繊維状導電助剤がカーボンナノチューブであるものが特に好ましい。
【００３７】

前記負極材は、前記酸化ケイ素、粒子状導電助剤、繊維状導電助剤、バインダー、及び必要に応じてその他の成分を配合することで製造できる。

各成分の配合時には、これら成分を添加して、各種手段により十分に混合することが好ましい。

各成分は、これらを順次添加しながら混合してもよいし、全成分を添加してから混合してもよく、配合成分が均一に混合されればよい。

【００３８】

前記その他の成分として前記溶媒を配合する場合、この溶媒は、少なくとも一部を、前記酸化ケイ素、粒子状導電助剤、繊維状導電助剤、バインダー、及びその他の固体成分からなる群から選択される一種以上とあらかじめ混合して、これら成分の溶液又は分散液として、配合してもよい。このような溶液又は分散液の調製に用いる溶媒は、全量であってもよい。

【００３９】

各成分の混合方法は、特に限定されず、例えば、撹拌子、撹拌翼、ボールミル、スターラー、超音波分散機、超音波ホモジナイザー、自公転ミキサー等を使用する公知の方法を適用すればよい。そして、複数種の方法を組み合わせて行ってもよい。

混合温度、混合時間等の混合条件は、各種方法に応じて適宜設定すればよい。通常は、混合時の温度は１０～５０℃であることが好ましく、１５～３５℃であることがより好ましい。また、混合時間は３～４０分であることが好ましく、５～２０分であることがより好ましい。

【００４０】

各成分を添加及び混合して得られた組成物は、そのまま負極材として用いてもよいし、例えば、配合した前記溶媒の一部を留去等によって除去するなど、得られた組成物に何らかの操作を追加して行って得られたものを、負極材として用いてもよい。

【００４１】

［負極］

本発明において、前記負極は、前記負極材を用いて形成された負極活物質層を有し、且つリチウムがプレドープされているものであり、例えば、前記負極活物質層を集電体（負極集電体）上に備えて構成される。

かかる負極は、前記負極材を用いること以外は、公知の負極と同様の方法で製造できる。

【００４２】

集電体は、公知のものでよく、その材質で好ましいものとしては、銅（Ｃｕ）、アルミニウム（Ａｌ）、チタン（Ｔｉ）、ニッケル（Ｎｉ）、ステンレス鋼等の導電性を有するものが例示できる。

また、前記集電体はシート状であることが好ましく、その厚さは、５～２０μｍであることが好ましい。

【００４３】

負極活物質層の厚さは、特に限定されないが、５～１００μｍであることが好ましく、１０～６０μｍであることがより好ましい。

【００４４】

負極活物質層は、前記負極材を用いて集電体上に形成すればよい。

例えば、負極材として、溶媒が配合されてなる液状組成物を用いる場合には、この液状組成物を塗工及び乾燥させることで、負極活物質層を形成できる。

【００４５】

液状組成物の塗工方法としては、バーコーター、グラビアコーター、コンマコーター、リップコーター等の各種コーターを用いる方法；ドクターブレード法；ディッピング法等の、各種塗布方法が例示できる。

【００４６】

液状組成物の乾燥は、公知の方法で常圧下又は減圧下で行えばよい。そして、乾燥温度

は、４０～１８０℃であることが好ましい。乾燥温度が前記下限値以上であることで、短時間で乾燥させることができ、乾燥温度が前記上限値以下であることで、集電体の酸化等を抑制する効果が高くなる。乾燥時間は、乾燥温度に応じて適宜調節すればよいが、例えば、１２～４８時間とすることができる。

【００４７】

負極活物質層は、集電体上に直接形成して設けてもよいし、他の基材上に形成してから集電体上に移動させ、集電体上に圧着させて設けてもよい。そして、負極活物質層は、集電体上に直接形成する場合にも、集電体上に圧着させてもよい。

【００４８】

本発明において、前記負極は、さらにリチウムがプレドープされているものであり、少なくとも負極活物質層にリチウムがプレドープされているものである。

リチウムがプレドープされている負極の製造方法は、特に限定されないが、負極活物質層を有する、リチウムがプレドープされていない負極（以下、「負極前駆体」と略記することがある）、好ましくは前記負極前駆体の負極活物質層を電解液と接触させ、負極前駆体のこの電解液との接触面をさらに金属リチウムと接触させることにより行うのが好ましい。このような方法を適用することで、負極前駆体中の広範囲に、より容易にリチウムをプレドープできる。接触させる前記電解液は、この負極を用いてリチウムイオン二次電池を製造する際に用いる電解液と同じであることが好ましい。

接触させる金属リチウムは、シート状（金属リチウム箔）であることが好ましい。

リチウムのプレドープは、リチウムイオン（Li^+）ではなく金属リチウム（Ｌｉ）を用いて行う必要がある。

【００４９】

負極にプレドープされているリチウムの量は、負極活物質層中の二酸化ケイ素（SiO_2）に対して、１～４倍モル量であることが好ましく、２～４倍モル量であることがより好ましく、３～４倍モル量であることが特に好ましい。

【００５０】

前記負極は、リチウムがプレドープされていることにより、このリチウムが負極活物質層中の二酸化ケイ素と不可逆的に反応して、あらかじめリチウムシリケート（Li_4SiO_4）を生成していると推測される。そして、このような負極を備えた本発明に係るリチウムイオン二次電池は、初期充電工程において負極にリチウムが吸蔵されても、負極活物質層中の酸化ケイ素との上記反応が抑制されるため、放電時の放出が妨げられることがなく、放電容量の低下が抑制されると推測される。本発明に係るリチウムイオン二次電池は、後述するように、充放電特性に優れたものである。

【００５１】

本発明に係るリチウムイオン二次電池は、前記負極を備えたことを特徴とし、前記負極を備えた点以外は、従来のリチウムイオン二次電池と同様の構成とすることができ、例えば、前記負極、正極、及び電解液、ゲル電解質又は固体電解質を備えて構成され、さらに必要に応じて、負極と正極との間に、セパレータを備えていてもよい。

【００５２】

［正極］

前記正極は、公知のものでよく、正極活物質、バインダー及び溶媒、並びに必要に応じて導電助剤等が配合されてなる正極材を用いて形成された正極活物質層を、集電体（正極集電体）上に備えたものが例示できる。正極としては、市販品を用いてもよい。

【００５３】

正極におけるバインダー、溶媒及び集電体は、いずれも負極におけるバインダー、溶媒及び集電体と同様のものでよい。

【００５４】

正極における導電助剤は公知のものでよく、好ましいものとしては、黒鉛（グラファイト）；ケッチェンブラック、アセチレンブラック等のカーボンブラック；カーボンナノチューブ；カーボンナノホーン；グラフェン；フラーレン等が例示できる。

正極における前記導電助剤は、一種を単独で用いてもよいし、二種以上を併用してもよく、二種以上を併用する場合には、その組み合わせ及び比率は目的に応じて適宜選択すればよい。

【００５５】

正極活物質としては、一般式「LiM_xO_y（式中、Ｍは金属であり；ｘ及びｙは、金属Ｍと酸素Ｏとの組成比である。）」で表される金属酸リチウム化合物が例示できる。

このような金属酸リチウム化合物としては、コバルト酸リチウム（$LiCoO_2$）、ニッケル酸リチウム（$LiNiO_2$）、マンガン酸リチウム（$LiMn_2O_4$）等が例示でき、類似の組成であるオリビン型リン酸鉄リチウム（$LiFePO_4$）を用いることもできる。

前記金属酸リチウム化合物は、前記一般式において、Ｍが複数種のものであってもよく、このような金属酸リチウム化合物としては、一般式「$LiM^1_pM^2_qM^3_rO_y$（式中、M^1、M^2及びM^3は互いに異なる種類の金属であり；ｐ、ｑ、ｒ及びｙは、金属M^1、M^2及びM^3と酸素Ｏとの組成比である。）」で表されるものが例示できる。ここで、ｐ＋ｑ＋ｒ＝ｘである。

このような金属酸リチウム化合物としては、$LiNi_{0.33}Mn_{0.33}Co_{0.33}O_2$等が例示できる。

正極活物質は、一種を単独で用いてもよいし、二種以上を併用してもよく、二種以上を併用する場合には、その組み合わせ及び比率は目的に応じて適宜選択すればよい。

【００５６】

前記正極材における、配合成分の総量に対する、前記正極活物質、バインダー、溶媒、及び導電助剤のそれぞれの配合量の割合は、前記負極材における、配合成分の総量に対する、前記負極活物質、バインダー、溶媒、及び導電助剤のそれぞれの配合量の割合と同様とすることができる。

【００５７】

正極活物質層の厚さは、特に限定されないが、２０～６０μｍであることが好ましい。

【００５８】

正極活物質層は、前記負極材に代えて正極材を用いる点以外は、負極活物質層の場合と同様の方法で形成できる。

【００５９】

［電解液］

前記電解液としては、（Ａ）カルボン酸リチウム塩、（Ｂ）三フッ化ホウ素及び／又は三フッ化ホウ素錯体、並びに（Ｃ）有機溶媒が配合されてなるもの（以下、「第一の電解液」と略記することがある）が例示できる。

【００６０】

（Ａ）カルボン酸リチウム塩は、電解質であり、カルボキシ基がリチウム塩（－Ｃ（＝Ｏ）－ＯＬｉ）を構成しているものであれば、脂肪族カルボン酸、脂環式カルボン酸及び芳香族カルボン酸のいずれのリチウム塩でもよく、１価カルボン酸及び多価カルボン酸のいずれのリチウム塩でもよい。そして、（Ａ）カルボン酸リチウム塩は、リチウム塩を構成するカルボキシ基の数は、特に限定されない。例えば、カルボキシ基の数が２以上である場合には、すべてのカルボキシ基がリチウム塩を構成していてもよいし、一部のカルボキシ基のみがリチウム塩を構成していてもよい。

【００６１】

（Ａ）カルボン酸リチウム塩で好ましいものとしては、ギ酸リチウム（ＨＣＯＯＬｉ）、酢酸リチウム（CH_3COOLi）、プロピオン酸リチウム（CH_3CH_2COOLi）、酪酸リチウム（$CH_3(CH_2)_2COOLi$）、イソ酪酸リチウム（$(CH_3)_2CHCOOLi$）、吉草酸リチウム（$CH_3(CH_2)_3COOLi$）、イソ吉草酸リチウム（$(CH_3)_2CHCH_2COOLi$）、カプロン酸リチウム（$CH_3(CH_2)_4COOLi$）等の１価カルボン酸のリチウム塩；シュウ酸リチウム（$(COOLi)_2$）、マロン酸リチウム（$LiOOCCH_2COOLi$）、コハク酸リチウム（$(CH_2CO$

ＯＬｉ）$_2$）、グルタル酸リチウム（ＬｉＯＯＣ（ＣＨ$_2$）$_3$ＣＯＯＬｉ）、アジピン酸リチウム（（ＣＨ$_2$ＣＨ$_2$ＣＯＯＬｉ）$_2$）等の２価カルボン酸のリチウム塩；乳酸リチウム（ＣＨ$_3$ＣＨ（ＯＨ）ＣＯＯＬｉ）等の水酸基を有する１価カルボン酸のリチウム塩；酒石酸リチウム（（ＣＨ（ＯＨ）ＣＯＯＬｉ）$_2$）、リンゴ酸リチウム（ＬｉＯＯＣＣＨ$_2$ＣＨ（ＯＨ）ＣＯＯＬｉ）等の水酸基を有する２価カルボン酸のリチウム塩；マレイン酸リチウム（ＬｉＯＯＣＣＨ＝ＣＨＣＯＯＬｉ、ｃｉｓ体）、フマル酸リチウム（ＬｉＯＯＣＣＨ＝ＣＨＣＯＯＬｉ、ｔｒａｎｓ体）等の不飽和２価カルボン酸のリチウム塩；クエン酸リチウム（ＬｉＯＯＣＣＨ$_2$Ｃ（ＣＯＯＬｉ）（ＯＨ）ＣＨ$_2$ＣＯＯＬｉ）等の３価カルボン酸のリチウム塩（水酸基を有する３価カルボン酸のリチウム塩）が例示でき、ギ酸リチウム、酢酸リチウム、シュウ酸リチウム、コハク酸リチウムがより好ましく、シュウ酸リチウムが特に好ましい。

【００６２】

（Ａ）カルボン酸リチウム塩は、一種を単独で用いてもよいし、二種以上を併用してもよい。二種以上を併用する場合には、その組み合わせ及び比率は目的に応じて適宜選択すればよい。

【００６３】

（Ｂ）三フッ化ホウ素及び三フッ化ホウ素錯体は、（Ａ）カルボン酸リチウム塩と錯形成反応を行うものであり、三フッ化ホウ素錯体は、三フッ化ホウ素（ＢＦ$_3$）が別の成分に配位結合したものである。

【００６４】

好ましい前記三フッ化ホウ素錯体としては、三フッ化ホウ素ジメチルエーテル錯体（ＢＦ$_3$・Ｏ（ＣＨ$_3$）$_2$）、三フッ化ホウ素ジエチルエーテル錯体（ＢＦ$_3$・Ｏ（Ｃ$_2$Ｈ$_5$）$_2$）、三フッ化ホウ素ジｎ－ブチルエーテル錯体（ＢＦ$_3$・Ｏ（Ｃ$_4$Ｈ$_9$）$_2$）、三フッ化ホウ素ジｔｅｒｔ－ブチルエーテル錯体（ＢＦ$_3$・Ｏ（（ＣＨ$_3$）$_3$Ｃ）$_2$）、三フッ化ホウ素ｔｅｒｔ－ブチルメチルエーテル錯体（ＢＦ$_3$・Ｏ（（ＣＨ$_3$）$_3$Ｃ）（ＣＨ$_3$））、三フッ化ホウ素テトラヒドロフラン錯体（ＢＦ$_3$・ＯＣ$_4$Ｈ$_8$）等の三フッ化ホウ素アルキルエーテル錯体；三フッ化ホウ素メタノール錯体（ＢＦ$_3$・ＨＯＣＨ$_3$）、三フッ化ホウ素プロパノール錯体（ＢＦ$_3$・ＨＯＣ$_3$Ｈ$_7$）、三フッ化ホウ素フェノール錯体（ＢＦ$_3$・ＨＯＣ$_6$Ｈ$_5$）等の三フッ化ホウ素アルコール錯体が例示できる。

（Ｂ）三フッ化ホウ素及び／又は三フッ化ホウ素錯体としては、取り扱いが容易で、錯形成反応がより円滑に進行する点から、前記三フッ化ホウ素錯体を用いることが好ましい。

【００６５】

（Ｂ）三フッ化ホウ素及び／又は三フッ化ホウ素錯体としては、一種を単独で用いてもよいし、二種以上を併用してもよい。二種以上を併用する場合には、その組み合わせ及び比率は目的に応じて適宜選択すればよい。

【００６６】

（Ｂ）三フッ化ホウ素及び／又は三フッ化ホウ素錯体の配合量は特に限定されず、（Ｂ）三フッ化ホウ素及び／又は三フッ化ホウ素錯体や（Ａ）カルボン酸リチウム塩の種類に応じて適宜調節すればよい。通常は、［（Ｂ）三フッ化ホウ素及び／又は三フッ化ホウ素錯体の配合量（モル数）］／［配合された（Ａ）カルボン酸リチウム塩中のリチウム原子のモル数］のモル比が０．５以上であることが好ましく、０．７以上であることがより好ましい。このような範囲とすることで、（Ｃ）有機溶媒に対する（Ａ）カルボン酸リチウム塩の溶解度がより向上する。また、前記モル比の上限値は本発明の効果を妨げない限り特に限定されないが、２．０であることが好ましく、１．５であることがより好ましい。

【００６７】

（Ｃ）有機溶媒は特に限定されないが、好ましいものとして具体的には、エチレンカーボネート、プロピレンカーボネート、ブチレンカーボネート、ジメチルカーボネート、エチルメチルカーボネート、ジエチルカーボネート、ビニレンカーボネート等の炭酸エステル化合物；γ－ブチロラクトン等のラクトン化合物；ギ酸メチル、酢酸メチル、プロピオ

ン酸メチル等のカルボン酸エステル化合物；テトラヒドロフラン、ジメトキシエタン等のエーテル化合物；アセトニトリル等のニトリル化合物；スルホラン等のスルホン化合物が例示できる。

（Ｃ）有機溶媒は、一種を単独で用いてもよいし、二種以上を併用してもよい。二種以上を併用する場合には、その組み合わせ及び比率は目的に応じて適宜選択すればよい。

【００６８】

（Ｃ）有機溶媒は、エチレンカーボネート、プロピレンカーボネート、ブチレンカーボネート、ジメチルカーボネート、エチルメチルカーボネート、ジエチルカーボネート、ビニレンカーボネート、γ－ブチロラクトン、テトラヒドロフラン、ジメトキシエタン、ギ酸メチル、酢酸メチル、プロピオン酸メチル、アセトニトリル及びスルホランからなる群から選択される一種以上であることが好ましい。

二種以上を併用した（Ｃ）有機溶媒としては、プロピレンカーボネート及びビニレンカーボネートが配合されたもの、プロピレンカーボネート及びエチレンカーボネートが配合されたもの、並びにエチレンカーボネート及びジメチルカーボネートが配合されたものが好ましい。

【００６９】

前記電解液における（Ｃ）有機溶媒の配合量は特に限定されず、例えば、電解質の種類に応じて、適宜調節すればよい。通常は、リチウム原子（Ｌｉ）の濃度が、好ましくは０．２～３．０モル／ｋｇ、より好ましくは０．４～２．０モル／ｋｇとなるように、配合量を調節することが好ましい。

【００７０】

第一の電解液としては、（Ｅ）カルボン酸リチウム塩－三フッ化ホウ素錯体、及び（Ｃ）有機溶媒が配合されてなるものも例示できる。

（Ｅ）カルボン酸リチウム塩－三フッ化ホウ素錯体としては、カルボン酸リチウム塩中の少なくとも１個のカルボキシ基又はリチウム塩となっているカルボキシ基に、三フッ化ホウ素（BF_3）が配位結合したものが例示できる。

（Ｅ）カルボン酸リチウム塩－三フッ化ホウ素錯体を構成するカルボン酸リチウム塩としては、（Ａ）カルボン酸リチウム塩と同様のものが例示できる。

【００７１】

（Ｅ）カルボン酸リチウム塩－三フッ化ホウ素錯体は、例えば、（Ａ）カルボン酸リチウム塩、（Ｂ）三フッ化ホウ素及び／又は三フッ化ホウ素錯体、並びに（Ｃ’）溶媒を配合して、（Ａ）カルボン酸リチウム塩と、（Ｂ）三フッ化ホウ素及び／又は三フッ化ホウ素錯体と、を反応させる工程（以下、「反応工程」と略記する）と、前記反応後の反応液から、（Ｃ’）溶媒と、（Ｂ）三フッ化ホウ素及び／又は三フッ化ホウ素錯体に由来する不純物と、を除去する工程（以下、「除去工程」と略記する）と、を有する製造方法で製造できる。かかる製造方法で得られた（Ｅ）カルボン酸リチウム塩－三フッ化ホウ素錯体は、（Ａ）カルボン酸リチウム塩と（Ｂ）三フッ化ホウ素及び／又は三フッ化ホウ素錯体とが、錯形成反応して、形成されたものである。

【００７２】

この製造方法において、（Ａ）カルボン酸リチウム塩、（Ｂ）三フッ化ホウ素及び／又は三フッ化ホウ素錯体は、上記のものと同じである。すなわち、（Ｅ）カルボン酸リチウム塩－三フッ化ホウ素錯体における「カルボン酸リチウム塩」は、（Ａ）カルボン酸リチウム塩と同じものである。

【００７３】

（Ｅ）カルボン酸リチウム塩－三フッ化ホウ素錯体は、一種を単独で使用してもよいし、二種以上を併用してもよい。二種以上を併用する場合には、その組み合わせ及び比率は目的に応じて適宜選択すればよい。

【００７４】

前記（Ｃ’）溶媒は、前記反応工程における、（Ａ）カルボン酸リチウム塩と（Ｂ）三フッ化ホウ素及び／又は三フッ化ホウ素錯体との錯形成反応を妨げず、これらを溶解可能

なものであれば、特に限定されないが、有機溶媒が好ましく、常圧下又は減圧下での留去が可能なものが好ましい。

【００７５】

（Ｃ’）溶媒の沸点は、２０℃以上であることが好ましく、３０℃以上であることがより好ましく、３５℃以上であることが特に好ましい。そして、（Ｃ’）溶媒の沸点は、１８０℃以下であることが好ましく、１５０℃以下であることがより好ましく、１２０℃以下であることが特に好ましい。（Ｃ’）溶媒の沸点が前記下限値以上であることで、前記反応工程における反応液を常温で撹拌することができるので、前記反応工程をより容易に行うことができる。また、（Ｃ’）溶媒の沸点が前記上限値以下であることで、前記除去工程での留去により、（Ｃ’）溶媒をより容易に除去できる。

【００７６】

（Ｃ’）溶媒における好ましい前記有機溶媒としては、ジメチルカーボネート、エチルメチルカーボネート、ジエチルカーボネート等の鎖状炭酸エステル化合物（鎖状構造中に、炭酸エステル結合を有する化合物）；アセトニトリル等のニトリル化合物；テトラヒドロフラン等の環状エーテル化合物（環状構造中にエーテル結合を有する化合物）；ジエチルエーテル、１，２－ジメトキシエタン等の鎖状エーテル化合物（鎖状構造中にエーテル結合を有する化合物）；酢酸エチル、酢酸イソプロピル等のカルボン酸エステル化合物が例示できる。

これらの中でも、前記有機溶媒としては、鎖状炭酸エステル化合物、ニトリル化合物、環状エーテル化合物が好ましい。

【００７７】

（Ｃ’）溶媒は、一種を単独で使用してもよいし、二種以上を併用してもよい。二種以上を併用する場合には、その組み合わせ及び比率は目的に応じて適宜選択すればよい。

【００７８】

前記除去工程において、前記不純物としては、（Ａ）カルボン酸リチウム塩と反応せずに残存した、過剰量の（Ｂ）三フッ化ホウ素及び／又は三フッ化ホウ素錯体や、これから生じた副生物が挙げられ、前記副生物としてより具体的には、（Ｂ）成分である三フッ化ホウ素錯体において、反応前に元々三フッ化ホウ素に配位結合していた成分等が例示できる。これら不純物は、留去が可能なものである。

【００７９】

（Ｅ）カルボン酸リチウム塩－三フッ化ホウ素錯体を用いた第一の電解液は、例えば、（Ａ）カルボン酸リチウム塩、並びに（Ｂ）三フッ化ホウ素及び／又は三フッ化ホウ素錯体を配合するのに代えて、（Ｅ）カルボン酸リチウム塩－三フッ化ホウ素錯体を配合することにより、（Ａ）カルボン酸リチウム塩、並びに（Ｂ）三フッ化ホウ素及び／又は三フッ化ホウ素錯体が配合されてなる上記の第一の電解液と同様の方法で得られる。例えば、（Ｃ）有機溶媒の配合量は特に限定されないが、リチウム原子（Ｌｉ）の濃度が、好ましくは０．２～３．０モル／ｋｇ、より好ましくは０．４～２．０モル／ｋｇとなるように、配合量を調節することが好ましい。

【００８０】

また、前記電解液としては、電解質として六フッ化リン酸リチウム（$LiPF_6$）、四フッ化ホウ素リチウム（$LiBF_4$）、リチウムビスフルオロスルホニルイミド（ＬｉＦＳＩ）、ビス（トリフルオロメタンスルホニル）イミドリチウム（$LiN(SO_2CF_3)_2$、ＬｉＴＦＳＩ）等の、（Ａ）カルボン酸リチウム塩以外の公知のリチウム塩が有機溶媒に溶解されてなるもの（以下、「第二の電解液」と略記することがある）も例示できる。

【００８１】

第二の電解液における前記電解質は、一種を単独で用いてもよいし、二種以上を併用してもよい。二種以上を併用する場合には、その組み合わせ及び比率は目的に応じて適宜選択すればよい。

【００８２】

第二の電解液における前記有機溶媒としては、第一の電解液における（Ｃ）有機溶媒と同じのものが例示できる。

また、第二の電解液におけるリチウム原子（Ｌｉ）の濃度も、第一の電解液の場合と同様である。

【００８３】

第一及び第二の電解液は、いずれも、上記の必須成分（第一の電解液における（Ａ）カルボン酸リチウム塩、（Ｂ）三フッ化ホウ素及び／又は三フッ化ホウ素錯体、（Ｅ）カルボン酸リチウム塩－三フッ化ホウ素錯体、（Ｃ）有機溶媒；第二の電解液におけるリチウム塩、有機溶媒）以外に、本発明の効果を損なわない範囲内において、任意成分が配合されてなるものでもよい。

前記任意成分は、目的に応じて適宜選択すればよく、特に限定されない。

【００８４】

第一及び第二の電解液は、前記必須成分、及び必要に応じて任意成分を配合することで製造できる。各成分の配合方法は、前記負極材の製造時における各成分の配合方法と同様である。ただし、混合時の組成は特に限定されない。

【００８５】

本発明において、前記電解液は、（Ａ）カルボン酸リチウム塩並びに（Ｂ）三フッ化ホウ素及び／又は三フッ化ホウ素錯体、あるいは（Ｅ）カルボン酸リチウム塩－三フッ化ホウ素錯体が配合されてなるもの、すなわち第一の電解液であることが好ましい。

【００８６】

［ゲル電解質］

前記ゲル電解質としては、（Ａ）カルボン酸リチウム塩、（Ｂ）三フッ化ホウ素及び／又は三フッ化ホウ素錯体、（Ｃ）有機溶媒、並びに（Ｄ）マトリクスポリマーが配合されてなるもの；（Ｅ）カルボン酸リチウム塩－三フッ化ホウ素錯体、（Ｃ）有機溶媒、及び（Ｄ）マトリクスポリマーが配合されてなるものが例示でき、必要に応じて、前記第一及び第二の電解液における任意成分が配合されてなるものでもよい。また、前記ゲル電解質としては、第一の電解液に、さらに（Ｄ）マトリクスポリマーが配合されてなるものも例示できる。ここで、（Ａ）カルボン酸リチウム塩、（Ｂ）三フッ化ホウ素及び／又は三フッ化ホウ素錯体、（Ｅ）カルボン酸リチウム塩－三フッ化ホウ素錯体、並びに（Ｃ）有機溶媒は、いずれも第一の電解液におけるものと同じである。

【００８７】

ゲル電解質は、型を用いて所望の形状に成型してもよい。

ゲル電解質では、（Ｄ）マトリクスポリマー以外の成分（電解液）が、マトリクスポリマー中に保持される。

【００８８】

ゲル電解質は、配合した（Ｃ）有機溶媒の一部が、乾燥等によって除去されたものでもよく、製造時において、ゲル電解質中に主として残存する（Ｃ）有機溶媒とは異なる有機溶媒（希釈用有機溶媒）が別途配合され、この希釈用有機溶媒が上記の乾燥時に除去されたものであってもよい。

【００８９】

（Ｄ）マトリクスポリマーは、特に限定されず、固体電解質分野で公知のものが適宜使用できる。

好ましい（Ｄ）マトリクスポリマーとしては、ポリエチレンオキシド、ポリプロピレンオキシド等のポリエーテル系ポリマー（ポリエーテル骨格を有するポリマー）；ポリフッ化ビニル、ポリフッ化ビニリデン、ポリフッ化ビニリデン－六フッ化プロピレン共重合体、ポリフッ化ビニリデン－六フッ化アセトン共重合体、ポリテトラフルオロエチレン等のフッ素系ポリマー（フッ素原子を有するポリマー）；ポリ（メタ）アクリル酸メチル、ポリ（メタ）アクリル酸エチル、ポリアクリルアミド、エチレンオキシドユニットを含むポリアクリレート等のポリアクリル系ポリマー（（メタ）アクリル酸エステル又はアクリルアミドから誘導される構成単位を有するポリマー）；ポリアクリロニトリル；ポリホスフ

ァゼン；ポリシロキサンが例示できる。

【００９０】

（Ｄ）マトリクスポリマーは、一種を単独で用いてもよいし、二種以上を併用してもよい。二種以上を併用する場合には、その組み合わせ及び比率は目的に応じて適宜選択すればよい。

【００９１】

（Ｄ）マトリクスポリマーは、ポリエチレンオキシド、ポリプロピレンオキシド、ポリフッ化ビニル、ポリフッ化ビニリデン、ポリフッ化ビニリデン－六フッ化プロピレン共重合体、ポリフッ化ビニリデン－六フッ化アセトン共重合体、ポリテトラフルオロエチレン、ポリアクリロニトリル、ポリホスファゼン及びポリシロキサンからなる群から選択される一種以上であることが好ましい。

【００９２】

ゲル電解質において、（Ｄ）マトリクスポリマーの配合量は特に限定されず、その種類に応じて適宜調節すればよいが、配合成分の総量に対する（Ｄ）マトリクスポリマーの配合量の割合は、２～５０質量％であることが好ましい。（Ｄ）マトリクスポリマーの配合量が前記下限値以上であることで、ゲル電解質の強度がより向上し、（Ｄ）マトリクスポリマーの配合量が前記上限値以下であることで、リチウムイオン二次電池はより優れた電池性能を示す。

【００９３】

前記希釈用有機溶媒は、配合成分のいずれかを十分に溶解又は分散させることができるものが好ましく、具体的には、アセトニトリル等のニトリル化合物；テトラヒドロフラン等のエーテル化合物：ジメチルホルムアミド等のアミド化合物が例示できる。

希釈用有機溶媒は、一種を単独で用いてもよいし、二種以上を併用してもよい。二種以上を併用する場合には、その組み合わせ及び比率は目的に応じて適宜選択すればよい。

【００９４】

ゲル電解質は、リチウムイオン二次電池が通常使用される４０℃以下の環境において、流動性を示さないものが好ましい。

【００９５】

ゲル電解質製造時における各成分の配合方法は、前記電解液の場合と同様でよい。

希釈用有機溶媒を除去するときの乾燥方法は、特に限定されず、例えば、ドライボックス、真空デシケータ、減圧乾燥機等を使用する公知の方法を適用すればよい。

【００９６】

［固体電解質］

前記固体電解質としては、（Ａ）カルボン酸リチウム塩、（Ｂ）三フッ化ホウ素及び／又は三フッ化ホウ素錯体、希釈用有機溶媒、並びに（Ｄ）マトリクスポリマーが配合されて得られた組成物；（Ｅ）カルボン酸リチウム塩－三フッ化ホウ素錯体、希釈用有機溶媒、及び（Ｄ）マトリクスポリマーが配合されて得られた組成物から、乾燥により前記希釈用有機溶媒が除去されてなるものが例示でき、必要に応じて、前記第一及び第二の電解液における任意成分が配合されてなるものでもよい。ここで、（Ａ）カルボン酸リチウム塩、（Ｂ）三フッ化ホウ素及び／又は三フッ化ホウ素錯体、（Ｅ）カルボン酸リチウム塩－三フッ化ホウ素錯体、並びに（Ｃ）有機溶媒は、いずれも第一の電解液におけるものと同じであり、希釈用有機溶媒及び（Ｄ）マトリクスポリマーは、前記ゲル電解質におけるものと同じである。

【００９７】

固体電解質は、型を用いて所望の形状に成型してもよい。

【００９８】

固体電解質において、（Ｄ）マトリクスポリマーの配合量は特に限定されず、その種類に応じて適宜調節すればよいが、配合成分の総量に対する（Ｄ）マトリクスポリマーの配合量の割合は、２～６５質量％であることが好ましい。（Ｄ）マトリクスポリマーの配合量が前記下限値以上であることで、固体電解質（電解質膜）の強度がより向上し、（Ｄ）

マトリクスポリマーの配合量が前記上限値以下であることで、リチウムイオン二次電池はより優れた電池性能を示す。

【００９９】

固体電解質製造時における各成分の配合方法は、前記電解液の場合と同様でよい。

また、希釈用有機溶媒を除去するときの乾燥方法は、前記ゲル電解質の場合と同様でよい。

【０１００】

［セパレータ］

前記セパレータの材質は特に限定されないが、微多孔性の高分子膜、不織布、ガラスファイバー等が例示でき、これら材質からなる群から選択される一種以上であることが好ましい。

【０１０１】

図１は、本発明に係るリチウムイオン二次電池の要部を模式的に例示する正面図である。

ここに示すリチウムイオン二次電池１は、シート状の負極３及び正極４が、セパレータ２を介して積層されたものである。セパレータ２は、単層からなるものでもよいし、二層以上が積層された複数層からなるものでもよい。図１において、電解液は図示を省略している。電解液に代えてゲル電解質又は固体電解質を用いたリチウムイオン二次電池としては、セパレータ２に代えてゲル電解質又は固体電解質を、あるいはセパレータを含むゲル電解質又は固体電解質を備えたものが例示できる。

【０１０２】

ここでは、負極３及び正極４をそれぞれ１枚ずつ示しているが、負極３、セパレータ２及び正極４がこの順に積層された積層構造を繰り返し単位として、この順を繰り返すように、これら繰り返し単位の間にさらにセパレータ２が介在して、前記積層構造が複数個繰り返し積層された構成であってもよい。

なお、ここに示すリチウムイオン二次電池１は、本発明の一実施形態を例示するものであり、本発明に係るリチウムイオン二次電池はこれに限定されるものではない。

【０１０３】

前記リチウムイオン二次電池は、公知の方法に従って、例えば、グローブボックス内又は乾燥空気雰囲気下で、前記電解液、ゲル電解質又は固体電解質、及び電極等を用いて製造すればよい。

例えば、ゲル電解質を備えたリチウムイオン二次電池であれば、加熱して液状としたゲル電解質を、負極及び正極のいずれか一方又は両方の電極面上に塗工し、次いで、このゲル電解質を備えた負極及び正極を、これらの電極面が対向するようにゲル電解質を介して積層し、必要に応じてこれらの電極面間にセパレータを介在させることで、容易に製造できる。液状のゲル電解質は、例えば、バーコーター等の各種コーターを用いる方法で、電極面上に塗工できる。

また、例えば、電解液を備えたリチウムイオン二次電池であれば、ゲル電解質に代えてこの電解液を、負極及び正極の電極面に接触するように配置すること以外は、上記のゲル電解質を備えたリチウムイオン二次電池と同様の方法で、容易に製造できる。

【０１０４】

前記リチウムイオン二次電池の形状は、特に限定されず、円筒型、角型、コイン型、シート型等、種々のものに調節できる。

【０１０５】

リチウムイオン二次電池は、（Ａ）カルボン酸リチウム塩並びに（Ｂ）三フッ化ホウ素及び／又は三フッ化ホウ素錯体、あるいは（Ｅ）カルボン酸リチウム塩－三フッ化ホウ素錯体を用いた場合、初期充電時に負極表面上において、フッ化リチウム（ＬｉＦ）を含む界面皮膜（以下、「ＳＥＩ」と略記する）を形成する。このＳＥＩは、充放電時にリチウムイオンに溶媒和された溶媒分子が負極中に進入するのを阻止し、負極構造の破壊を抑制して、リチウムイオン二次電池のサイクル特性の向上に寄与する。

【０１０６】
本発明に係るリチウムイオン二次電池は、容量発現率が高く、好ましくは８３％以上、より好ましくは８７％以上となる。
また、本発明に係るリチウムイオン二次電池は、優れたサイクル特性を示す。例えば、充放電サイクルを繰り返し行ったときの、１００サイクルでの容量維持率の値が、好ましくは８５％以上、より好ましくは９０％以上となる。
【実施例】
【０１０７】
以下、具体的実施例により、本発明についてさらに詳しく説明する。ただし、本発明は、以下に示す実施例に何ら限定されるものではない。
【０１０８】
（１）使用した原料
本実施例で使用した原料を以下に示す。
・導電助剤
アセチレンブラック（電気化学工業社製「ＨＳ－１００」、平均粒子径４８ｎｍ）
カーボンナノチューブ（保土谷化学社製「ＮＴ－７」、平均繊維径６５ｎｍ、平均繊維長６μｍ以上）
・バインダー
スチレン－ブタジエン樹脂（以下、「ＳＢＲ」と略記する）（ＪＳＲ社製）
ポリイミド（Ｉ．Ｓ．Ｔ社製「ＤＲＥＡＭＢＯＮＤ」）
・（Ａ）カルボン酸リチウム塩
シュウ酸リチウム（Ａｌｆａ社製）
・（Ｂ）三フッ化ホウ素錯体
三フッ化ホウ素ジエチルエーテル錯体（BF_3・Ｏ（C_2H_5）$_2$）（アルドリッチ社製）
・（Ｃ）有機溶媒
エチレンカーボネート（以下、「ＥＣ」と略記する）（キシダ化学社製）
プロピレンカーボネート（以下、「ＰＣ」と略記する）（キシダ化学社製）
・（Ｃ’）溶媒
ジメチルカーボネート（以下、「ＤＭＣ」と略記する）（キシダ化学社製）
【０１０９】
＜（Ｅ）有機酸リチウム塩－三フッ化ホウ素錯体の製造＞
［製造例１］（シュウ酸リチウム－三フッ化ホウ素錯体の製造）
シュウ酸リチウム（２２．３ｇ、２２３ｍｍｏｌ）を丸底フラスコに量り取り、これを２００ｍＬのＤＭＣに懸濁させた。これに２３℃で三フッ化ホウ素ジエチルエーテル錯体（６３．３ｇ、４４６ｍｍｏｌ）をゆっくりと滴下した後、室温（２３℃）で２４時間撹拌し、反応液が透明になって不溶物が見られず、均一な溶液となったことを確認した。次いで、ロータリーエバポレーターを用いて、反応液から溶媒及び不純物を留去した。その後、析出した白色の固体を５０℃にて乾燥させることにより、白色粉末のシュウ酸リチウム－三フッ化ホウ素錯体（（ＣＯＯＬｉ）$_2$・（BF_3）$_2$）を得た（収率９６．５％）。
【０１１０】
得られたシュウ酸リチウム－三フッ化ホウ素錯体について、ＮＭＲ、ＩＲにより、その構造を確認した。得られたデータを図２～４に示す。図２中、（ａ）は比較用の三フッ化ホウ素ジエチルエーテル錯体（BF_3・Ｏ（C_2H_5）$_2$）の^{1}Ｈ－ＮＭＲデータ、（ｂ）は得られたシュウ酸リチウム－三フッ化ホウ素錯体（（ＣＯＯＬｉ）$_2$・（BF_3）$_2$）の^{1}Ｈ－ＮＭＲデータである。また、図３中、（ａ）は比較用の三フッ化ホウ素ジエチルエーテル錯体（BF_3・Ｏ（C_2H_5）$_2$）の^{19}Ｆ－ＮＭＲデータ、（ｂ）は得られたシュウ酸リチウム－三フッ化ホウ素錯体の^{19}Ｆ－ＮＭＲデータである。そして、図４中、（ａ）は比較用のシュウ酸リチウムのＩＲデータ、（ｂ）は得られたシュウ酸リチウ

ム－三フッ化ホウ素錯体のＩＲデータである。

【０１１１】

図２（ａ）において観測された、三フッ化ホウ素ジエチルエーテル錯体（BF_3・$O(C_2H_5)_2$）のジエチルエーテルに由来するメチル水素（－CH_3）及びメチレン水素（－Ｏ－CH_2－）のピークが、図２（ｂ）では観測されておらず、これは、得られたシュウ酸リチウム－三フッ化ホウ素錯体に、三フッ化ホウ素ジエチルエーテル錯体、ジエチルエーテル等の不純物が混入していないことを支持していた。

また、図３（ａ）及び（ｂ）において観測されたフッ素のケミカルシフトに違いがみられることから、三フッ化ホウ素（BF_3）の配位環境が互いに異なることが確認され、これは、目的物であるシュウ酸リチウム－三フッ化ホウ素錯体が得られたことを支持していた。さらに、図３（ｂ）において不純物ピークが観測されなかったことや、三フッ化ホウ素の単体（BF_3）の沸点が－１００℃であることから、過剰量使用して反応工程で残存した三フッ化ホウ素ジエチルエーテル錯体が除去工程で除去され、得られたシュウ酸リチウム－三フッ化ホウ素錯体に、三フッ化ホウ素ジエチルエーテル錯体が混入していないと考えられた。

また、図４（ａ）及び（ｂ）でスペクトルに違いがみられることから、カルボニル基の配位環境が互いに異なることが確認され、これは、目的物であるシュウ酸リチウム－三フッ化ホウ素錯体が得られたことを支持していた。

以上から、目的物であるシュウ酸リチウム－三フッ化ホウ素錯体が得られ、これには、三フッ化ホウ素ジエチルエーテル錯体、ジエチルエーテル等の不純物が混入していないことを確認できた。

【０１１２】

＜リチウムイオン二次電池の製造＞

［実施例１］（負極材の製造）

一酸化ケイ素（ＳｉＯ、平均粒子径０．８μｍ、６９質量部）、アセチレンブラック（１０質量部）、カーボンナノチューブ（６質量部）、ポリアクリル酸リチウム（全酸基の５０モル％がリチウム塩とされたもの、以下、「ＰＡＡＬｉ」と略記することがある、１０質量部）、及びＳＢＲ（５質量部）を試薬瓶に入れ、さらにここに蒸留水を添加して濃度調整した後、自公転ミキサーを用いてこの濃度調整したものを２０００ｒｐｍで３分間混合した。次いで、超音波ホモジナイザーを用いてこの混合物を１０分間分散処理した後、再度、自公転ミキサーを用いてこの分散物を２０００ｒｐｍで３分間混合することにより、負極材を得た。ここまでの操作は、すべて２５℃で行った。このときの各配合成分と、配合成分の総量に対する各配合成分の割合（質量％）とを表１に示す。

【０１１３】

（電解液の製造）

有機溶媒として、ＥＣ及びＰＣの混合溶媒（ＥＣ：ＰＣ＝３０：７０（体積比））をサンプル瓶に量り取り、ここにシュウ酸リチウム－三フッ化ホウ素錯体（１．８２ｇ）を加えて、シュウ酸リチウム－三フッ化ホウ素錯体中のリチウム原子の濃度が１．０モル／ｋｇとなるようにし、２３℃で混合することにより、電解液を得た。

【０１１４】

（負極の製造）

バーコーターを用いて、厚さ１５μｍの銅箔の両面に得られた負極材を塗布し、５０℃のホットプレート上でこれを乾燥させた後、ロールプレス機を用いて１ｋＮでプレスすることにより、集電体である銅箔上に厚さ２５μｍの負極活物質層を形成して、負極前駆体を得た。

【０１１５】

図５は、得られた負極前駆体における負極活物質層の、走査型電子顕微鏡（ＳＥＭ）で取得した撮像データである。図５中、（ａ）は負極活物質層の１００００倍の撮像データであり、（ｂ）は（ａ）中の丸囲み領域ａ１の拡大撮像データであり、（ｃ）は（ｂ）中の丸囲み領域ｂ１の拡大撮像データである。図５（ａ）～（ｃ）から明らかなように、Ｓ

ｉＯ（酸化ケイ素）は負極活物質層中で均一に分散しており、一方で、カーボンナノチューブ（繊維状導電助剤）は、負極活物質層中において、負極活物質層全体に網目構造を形成していた。また、アセチレンブラック（粒子状導電助剤）は、負極活物質層中のＳｉＯの周辺部においてそのナノ粒子が連なった構造を形成し、ＳｉＯとアセチレンブラックとの接触面積を高めていた。

【０１１６】

得られた負極前駆体の負極活物質層上に、上記で得られた電解液を、滴下量が５０μＬ／ｃｍ^{2}となるように滴下し、その滴下面上に厚さ２００μｍのリチウム箔を重ねて、この状態で２４時間静置することにより、負極前駆体にリチウムをプレドープして、負極を得た。このリチウム箔は、プレドープ後、負極から取り除いた。

【０１１７】

（正極の製造）

ニッケル・コバルト・マンガン酸リチウム（Ｎｉ：Ｃｏ：Ｍｎ＝１：１：１、ＬｉＮＭＣ）（９３質量部）と、ポリフッ化ビニリデン（ＰＶＤＦ）（３質量部）と、導電助剤であるカーボンブラック（４質量部）とを混合して正極合材を調製し、これをＮ－メチルピロリドン（ＮＭＰ）中に分散させて、正極材（スラリー）を調製した。次いで、この正極材を厚さ１５μｍのアルミニウム箔の両面にバーコーターを用いて塗布し、１００℃、０．１ＭＰａ、１０時間の条件で減圧乾燥させた後、ロールプレスすることにより、集電体であるアルミニウム箔上に厚さ６０μｍの正極活物質層を形成して、正極を得た。

【０１１８】

（リチウムイオン二次電池の製造）

上記で得られた負極及び正極を直径１６ｍｍの円盤状に打ち抜いた。また、セパレータとしてガラスファイバーからなるものを用い、これを直径１７ｍｍの円盤状に打ち抜いた。これら円盤状の正極、セパレータ及び負極を、この順にＳＵＳ製の電池容器（ＣＲ２０３２）内で積層し、上記で得られた電解液を、セパレータ、負極及び正極に含浸させ、さらに負極上に、ＳＵＳ製の板（厚さ１．２ｍｍ、直径１６ｍｍ）を載せ、蓋をすることにより、リチウムイオン二次電池としてコイン型セルを製造した。

【０１１９】

［実施例２］（負極材の製造）

一酸化ケイ素（ＳｉＯ、平均粒子径０．８μｍ、６９質量部）、アセチレンブラック（１０質量部）、カーボンナノチューブ（６質量部）、及びポリイミド（１５質量部）を試薬瓶に入れ、さらにここにＮＭＰを添加して濃度調整した後、自公転ミキサーを用いてこの濃度調整したものを２０００ｒｐｍで３分間混合した。次いで、超音波ホモジナイザーを用いてこの混合物を１０分間分散処理した後、再度、自公転ミキサーを用いてこの分散物を２０００ｒｐｍで３分間混合することにより、負極材を得た。ここまでの操作は、すべて２５℃で行った。このときの各配合成分と、配合成分の総量に対する各配合成分の割合（質量％）とを表１に示す。

【０１２０】

（電解液、負極、正極及びリチウムイオン二次電池の製造）

実施例１と同じ方法で電解液を製造し、さらに得られた負極材を用いた点以外は、実施例１と同じ方法で負極、正極及びリチウムイオン二次電池を製造した。

【０１２１】

［比較例１］

表１に示すように、負極前駆体に対してリチウムをプレドープしなかった点以外は、実施例１と同じ方法でリチウムイオン二次電池を製造した。

【０１２２】

［比較例２］

表１に示すように、負極前駆体に対してリチウムをプレドープしなかった点以外は、実施例２と同じ方法でリチウムイオン二次電池を製造した。

【０１２３】

［比較例３］（負極材の製造）
一酸化ケイ素（ＳｉＯ、平均粒子径０．８μｍ、７５質量部）、アセチレンブラック（１０質量部）、ＰＡＡＬｉ（全酸基の５０モル％がリチウム塩とされたもの、１０質量部）、及びＳＢＲ（５質量部）を試薬瓶に入れ、さらにここに蒸留水を添加して濃度調整した後、自公転ミキサーを用いてこの濃度調整したものを２０００ｒｐｍで３分間混合した。次いで、超音波ホモジナイザーを用いてこの混合物を１０分間分散処理した後、再度、自公転ミキサーを用いてこの分散物を２０００ｒｐｍで３分間混合することにより、負極材を得た。ここまでの操作は、すべて２５℃で行った。このときの各配合成分と、配合成分の総量に対する各配合成分の割合（質量％）とを表１に示す。なお、表１において、「－」との記載は、その成分が配合されていないことを意味する。

【０１２４】
（電解液、負極、正極及びリチウムイオン二次電池の製造）
実施例１と同じ方法で電解液を製造し、さらに得られた負極材を用いた点以外は、実施例１と同じ方法で負極、正極及びリチウムイオン二次電池を製造した。

【０１２５】
［比較例４］（負極材の製造）
一酸化ケイ素（ＳｉＯ、平均粒子径０．８μｍ、７５質量部）、アセチレンブラック（１０質量部）、及びポリイミド（１５質量部）を試薬瓶に入れ、さらにここにＮＭＰを添加して濃度調整した後、自公転ミキサーを用いてこの濃度調整したものを２０００ｒｐｍで３分間混合した。次いで、超音波ホモジナイザーを用いてこの混合物を１０分間分散処理した後、再度、自公転ミキサーを用いてこの分散物を２０００ｒｐｍで３分間混合することにより、負極材を得た。ここまでの操作は、すべて２５℃で行った。このときの各配合成分と、配合成分の総量に対する各配合成分の割合（質量％）とを表１に示す。

【０１２６】
（電解液、負極、正極及びリチウムイオン二次電池の製造）
実施例１と同じ方法で電解液を製造し、さらに得られた負極材を用いた点以外は、実施例１と同じ方法で負極、正極及びリチウムイオン二次電池を製造した。

【０１２７】

【表１】

	負極材の配合成分（質量%）				リチウムのプレドープ
	酸化ケイ素	粒子状導電助剤	繊維状導電助剤	バインダー	
実施例１	ＳｉＯ（６９）	アセチレンブラック（１０）	カーボンナノチューブ（６）	ＰＡＡＬｉ/ＳＢＲ（１０）/（５）	あり
実施例２				ポリイミド（１５）	あり
比較例１				ＰＡＡＬｉ/ＳＢＲ（１０）/（５）	なし
比較例２				ポリイミド（１５）	なし
比較例３	ＳｉＯ（７５）	アセチレンブラック（１０）	－	ＰＡＡＬｉ/ＳＢＲ（１０）/（５）	あり
比較例４				ポリイミド（１５）	あり

【０１２８】

＜リチウムイオン二次電池の充放電特性の評価＞

上記各実施例及び比較例で得られたリチウムイオン二次電池について、２５℃において０．２Ｃの定電流定電圧充電を、上限電圧４．２Ｖとして電流値が０．１Ｃに収束するまで行った後、０．２Ｃの定電流放電を２．７Ｖまで行った。次いで、充放電電流を１Ｃとして同様の方法で、充放電サイクルを数回～数十回繰り返し行い、リチウムイオン二次電池の状態を安定させた。次いで、充放電電流を１Ｃとして同様の方法で、充放電サイクルを繰り返し行い、容量発現率（{［１サイクル目の放電容量（ｍＡｈ）］／［定格容量（ｍＡｈ）］}×１００）（%）、及び１００サイクルでの容量維持率（{［１００サイクル目の放電容量（ｍＡｈ）］／［１サイクル目の放電容量（ｍＡｈ）］}×１００）（%）を算出した。結果を表２に示す。

【０１２９】

【表２】

	評価結果	
	容量発現率（％）	１００サイクルでの容量維持率（％）
実施例１	９５．８	９６．４
実施例２	８９．４	９５．０
比較例１	６０．４	９０．４
比較例２	４７．２	８３．５
比較例３	８８．３	２５．１
比較例４	８４．７	１８．４

【０１３０】
上記結果から明らかなように、粒子状導電助剤及び繊維状導電助剤を併用し、リチウムがプレドープされている負極を用いた実施例１～２のリチウムイオン二次電池は、バインダーの種類が異なっていても、容量発現率及び１００サイクルでの容量維持率が共に十分に高く、充放電特性に優れていた。
これに対して、リチウムがプレドープされていない負極を用いた比較例１～２のリチウムイオン二次電池は、バインダーの種類によらず、特に容量発現率が不十分であった。また、繊維状導電助剤を併用していない負極を用いた比較例３～４のリチウムイオン二次電池は、バインダーの種類によらず、特に１００サイクルでの容量維持率が不十分であった。
【０１３１】
［実施例３］
＜平均粒子径（D50）の異なる酸化ケイ素粒子の製造＞
一酸化ケイ素（D50＝６μｍ、大阪チタニウムテクノロジーズ社製）１００ｇ、φ１ｍｍジルコニアボール５６０ｇ、２－プロパノール１２０ｇを専用ジルコニア容器に入れ、遊星型ボールミル（P-６：FRITSCH）を使用して酸化ケイ素を粉砕し、平均粒子径（D50）（メジアン径）が１．５μｍの一酸化ケイ素粒子の２－プロパノール分散液を得た。
得られた分散液について遠心分離機による分離及び回収を行い、一酸化ケイ素粒子（ＳｉＯ、平均粒子径１．５μｍ）のウェットケーキ（固形分７０％）を得た。
【０１３２】
上記で得られた一酸化ケイ素粒子を使用して、実施例１と同様の方法で負極材を得た。それらの操作は、すべて２５℃で行った。このときの各配合成分と、配合成分の総量に対する各配合成分の割合（質量％）とを表３に示す。
【０１３３】
＜リチウムイオン二次電池の作製と評価＞
上記の様に一酸化ケイ素の粒径を変化させたこと以外は、実施例１と同じ方法でリチウムイオン二次電池を作製した。その評価については、１００サイクルでの容量維持率に加えて、２００サイクルでの容量維持率（{［２００サイクル目の放電容量（ｍＡｈ）］／［１サイクル目の放電容量（ｍＡｈ）］}×１００）（％）を算出した。その結果を表４に示す。

【０１３４】
［実施例４］
実施例３の粉砕条件を変更して、平均粒子径（D50）が０．９μｍの一酸化ケイ素粒子を得た。この粒子を使用した以外は、実施例３と同様にリチウムイオン二次電池を作製して評価した。実施例４の負極材の各配合成分と、配合成分の総量に対する各配合成分の割合（質量％）とを表３に示す。また、評価結果を表４に示す。
【０１３５】
［実施例５］
実施例３の粉砕条件を変更して、平均粒子径（D50）が０．６μｍの一酸化ケイ素粒子を得た。この粒子を使用した以外は、実施例３と同様にリチウムイオン二次電池を作製して評価した。実施例５の負極材の各配合成分と、配合成分の総量に対する各配合成分の割合（質量％）とを表３に示す。また、評価結果を表４に示す。
【０１３６】
［実施例６］
実施例３の負極材における各成分の配合において、一酸化ケイ素粒子の配合量を６５質量％に減量し、カーボンナノチューブの配合量を１０質量％に増量した以外は、実施例３と同様にリチウムイオン二次電池を作製して評価した。実施例６の負極材の各配合成分と、配合成分の総量に対する各配合成分の割合（質量％）とを表３に示す。また、評価結果を表４に示す。
【０１３７】
［実施例７］
実施例４の負極材における各成分の配合において、一酸化ケイ素粒子の配合量を６５質量％に減量し、カーボンナノチューブの配合量を１０質量％に増量した以外は、実施例４と同様にリチウムイオン二次電池を作製して評価した。実施例７の負極材の各配合成分と、配合成分の総量に対する各配合成分の割合（質量％）とを表３に示す。また、評価結果を表４に示す。
【０１３８】
［実施例８］
実施例６の負極材における各成分の配合において、一酸化ケイ素粒子の配合量を６２質量％に減量し、バインダー成分のＰＡＡＬｉを６質量％に減量した一方、バインダー成分のＳＢＲを１２質量％に増量した以外は、実施例６と同様にリチウムイオン二次電池を作製して評価した。実施例８の負極材の各配合成分と、配合成分の総量に対する各配合成分の割合（質量％）とを表３に示す。また、評価結果を表４に示す。
【０１３９】
［実施例９］
実施例７の負極材における各成分の配合において、一酸化ケイ素粒子の配合量を６２質量％に減量し、バインダー成分のＰＡＡＬｉを６質量％に減量した一方、バインダー成分のＳＢＲを１２質量％に増量した以外は、実施例７と同様にリチウムイオン二次電池を作製して評価した。実施例９の負極材の各配合成分と、配合成分の総量に対する各配合成分の割合（質量％）とを表３に示す。また、評価結果を表４に示す。
【０１４０】

【表３】

		負極材の配合成分（質量%）				リチウムのプレドープ
	酸化ケイ素の平均粒子径（μm）	酸化ケイ素	粒子状導電助剤	繊維状導電助剤	バインダー	
実施例3	１．５	ＳｉＯ（６９）	アセチレンブラック（１０）	カーボンナノチューブ（６）	ＰＡＡＬｉ／ＳＢＲ（１０）/（５）	あり
実施例4	０．９				ＰＡＡＬｉ／ＳＢＲ（１０）/（５）	あり
実施例5	０．６				ＰＡＡＬｉ／ＳＢＲ（１０）/（５）	あり
実施例6	１．５	ＳｉＯ（６５）	アセチレンブラック（１０）	カーボンナノチューブ（１０）	ＰＡＡＬｉ／ＳＢＲ（１０）/（５）	あり
実施例7	０．９					
実施例8	１．５	ＳｉＯ（６２）	アセチレンブラック（１０）	カーボンナノチューブ（１０）	ＰＡＡＬｉ／ＳＢＲ（6）/（１２）	あり
実施例9	０．９					

【０１４１】

【表４】

	評価結果	
	１００サイクルでの容量維持率（%）	２００サイクルでの容量維持率（%）
実施例３	８１．７	４７．１
実施例４	９３．９	８１．３
実施例５	９６．０	９０．０
実施例６	９６．６	５７．１
実施例７	９９．５	９７．３
実施例８	９９．５	９８．３
実施例９	８３．１	３３．０

【０１４２】

上記結果において、実施例３～５を比較すると、一酸化ケイ素粒子の平均粒子径が１μ

m以下の実施例４，５において特に容量維持率の向上が見られた。

また、一酸化ケイ素粒子の平均粒子径が同じ、実施例３と６、および実施例４と７を各々比べると、繊維状導電助剤の割合を増やした実施例６，７においてサイクル特性の向上が見られた。この理由の一つとして、酸化ケイ素粒子の平均粒子径が変化すると、導電ネットワークを上手く機能させるための繊維状導電助剤の好適な割合が変化することが考えられる。

【０１４３】

実施例６～９を比較検討すると、平均粒子径が比較的大きい場合（実施例６，８）には、それに応じてバインダーの配合量が多い方（実施例８）が容量維持率を高められた。一方、平均粒子径が比較的小さい場合（実施例７，９）には、それに応じてバインダーの配合量が少ない方（実施例７）が容量維持率を高められた。

このように、酸化ケイ素粒子の平均粒子径（大きさ）に応じてバインダー量を調節することにより、さらなる容量維持率の向上が確認された。

普通に考えれば、酸化ケイ素粒子の平均粒子径が大きくなる程、その粒子群の総質量に対する表面積の割合が小さくなるため、バインダー量は少なくて済むと考えられる。ところが、本実施例は、それと逆の結果を示していた。すなわち、酸化ケイ素粒子の平均粒子径が大きい場合には、バインダー量を多めにすることが好ましく、酸化ケイ素粒子の平均粒子径が小さい場合には、バインダー量を少なめにすることが好ましいことが確認された。

【産業上の利用可能性】

【０１４４】

本発明は、リチウムイオン二次電池の分野で利用可能である。

【符号の説明】

【０１４５】

１・・・リチウムイオン二次電池、２・・・セパレータ、３・・・負極、４・・・正極

【図１】

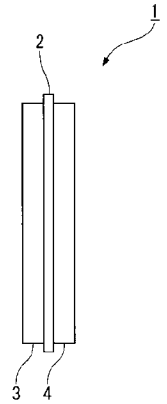


図１

【図２】

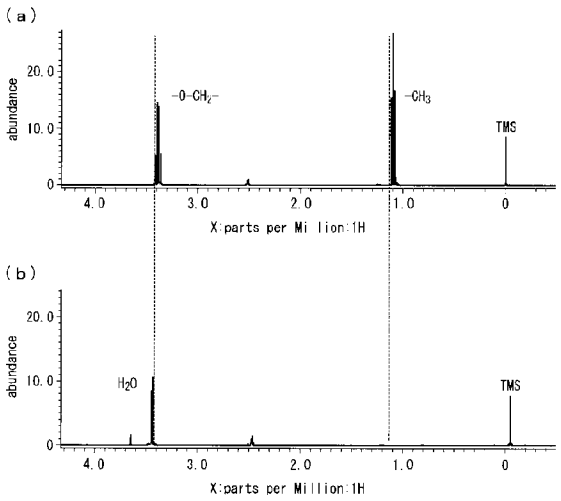


図２

【図３】

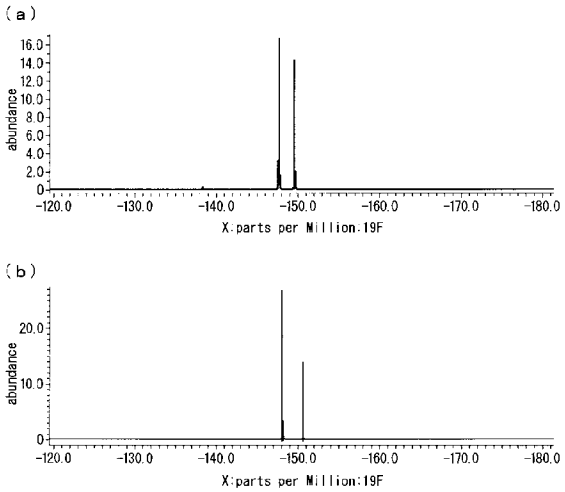

(a)
abundance
16.0
14.0
12.0
10.0
8.0
6.0
4.0
2.0
0
-120.0
-130.0
-140.0
-150.0
-160.0
-170.0
-180.0
X-parts per Million:19F
(b)
abundance
20.0
10.0
0
-120.0
-130.0
-140.0
-150.0
-160.0
-170.0
-180.0
X-parts per Million:19F

図３

【図４】

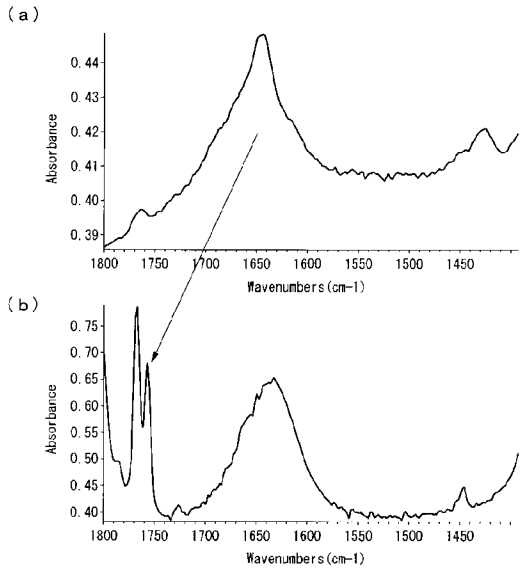

(a)
Absorbance
0.44
0.43
0.42
0.41
0.40
0.39
1800
1750
1700
1650
1600
1550
1500
1450
Wavenumbers(cm-1)
(b)
Absorbance
0.75
0.70
0.65
0.60
0.55
0.50
0.45
0.40
1800
1750
1700
1650
1600
1550
1500
1450
Wavenumbers(cm-1)

図４

【図５】

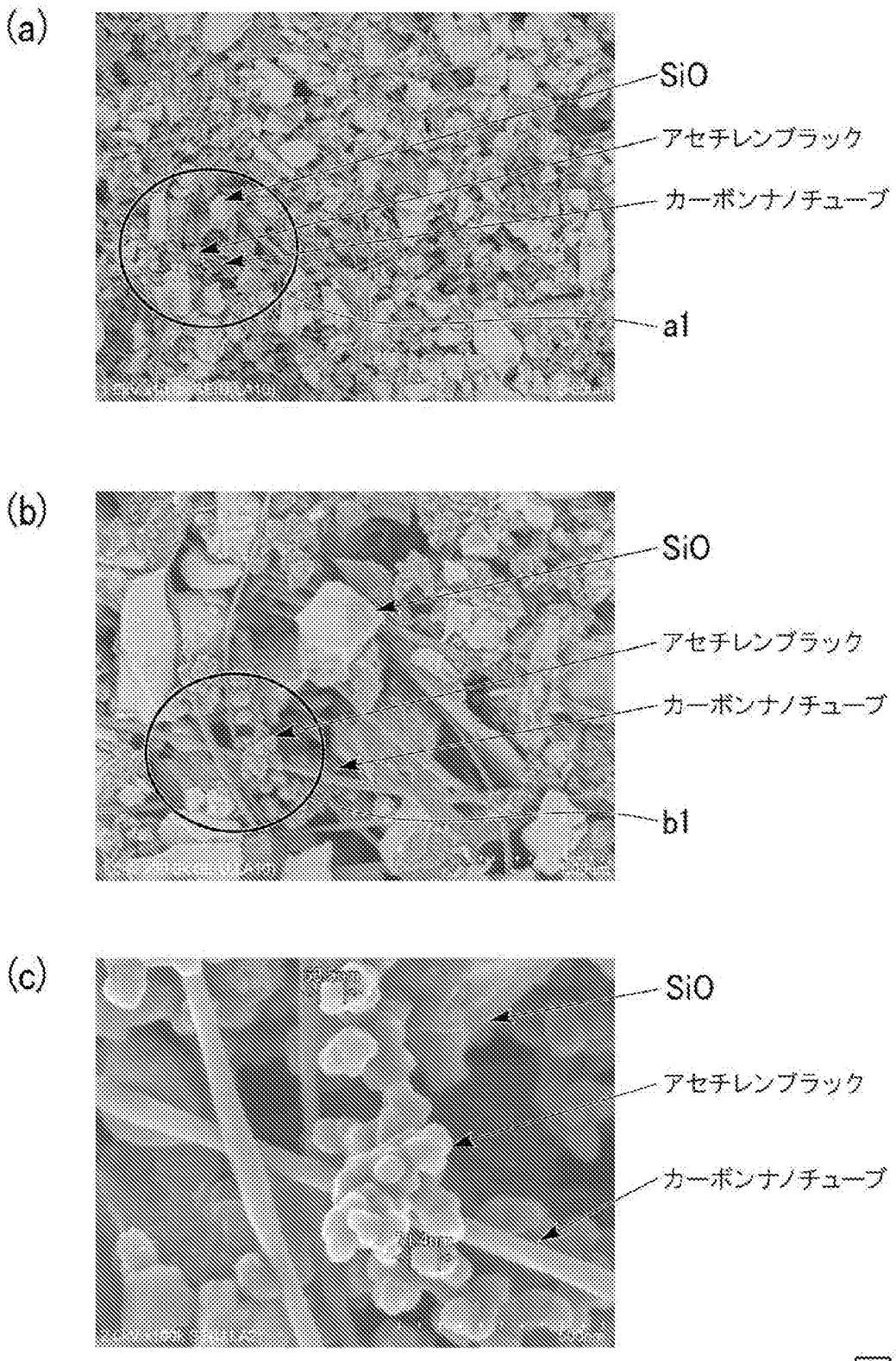

(a)
SiO
アセチレンブラック
カーボンナノチューブ
a1
(b)
SiO
アセチレンブラック
カーボンナノチューブ
b1
(c)
SiO
アセチレンブラック
カーボンナノチューブ

図５

フロントページの続き

(72)発明者　寺西　利絵
茨城県つくば市和台３２番地　積水化学工業株式会社内
(72)発明者　豊川　卓也
茨城県つくば市和台３２番地　積水化学工業株式会社内

Ｆターム(参考) 5H050 AA07 AA08 BA15 CA01 CA07 CA08 CA09 CB02 CB11 DA10
DA11 EA08 EA09 EA10 EA23 EA24 EA25 EA28 FA16 FA17
GA10 GA16 HA01 HA05

Electrochemistry Communications 12 (2010) 10–13

Contents lists available at ScienceDirect

Electrochemistry Communications

journal homepage: www.elsevier.com/locate/elecom

Preparation of nano-structured $LiFePO_4$/graphene composites by co-precipitation method

Y. Ding [a,b,*], Y. Jiang [a,b], F. Xu [a,b], J. Yin [a,b], H. Ren [a,b], Q. Zhuo [b], Z. Long [a,b], P. Zhang [a,b,*]

[a] Institute of Rheology Mechanics, Xiangtan University, Hunan 411105, China
[b] College of Civil Engineering and Mechanics, Xiangtan University, Hunan 411105, China

ARTICLE INFO

Article history:
Received 17 August 2009
Received in revised form 15 October 2009
Accepted 16 October 2009
Available online 21 October 2009

Keywords:
$LiFePO_4$/graphene composite
Nanostructure
Electrochemical property

ABSTRACT

Graphene materials with superior electrical conductivities and high surface area would be advantageous for application in energy storage. And $LiFePO_4$ has been a promising electrode material however its poor conductivity limits its practical application. To improve the electronic conductivity, we prepare $LiFePO_4$/graphene composites in a co-precipitation method, in which graphene nanosheets are used as additives. The composites were characterized by X-ray diffraction (XRD) and atomic force microscopy (AFM), and their electrochemical properties were investigated by galvanostatic charge and discharge tests. The experimental results show that the capacity delivery and cycle performances of $LiFePO_4$ could be improved considerably by adding graphene. Therefore, $LiFePO_4$/graphene composites are a promising candidate for lithium secondary batteries.

© 2009 Elsevier B.V. All rights reserved.

1. Introduction

Recently, much research has been conducted to explore the promising properties of the graphene nanosheets after Geim and co-workers at Manchester University first isolated a single-layer graphene from graphite [1,2]. The graphene and its ramifications can be applied to energy storage, nanoelectronic devices, nanomachines and composite materials because of their remarkable properties, such as high values of Young's modules, fracture strength, specific surface area (2630 $m^2 g^{-1}$) and mobility of charge carriers (200,000 $cm^2 V^{-1} s^{-1}$) [3,4]. The Olivine-type $LiFePO_4$ has been recognized as a promising candidate for lithium secondary batteries cathode because of its low cost, environmental compatibility, cycling stability and high theoretical capacity of 170 mA h g^{-1} [5–7]. The main limitation of the $LiFePO_4$ for applications is its poor conductivity, and it originated from the low lithium–ion diffusion rate and the low electronic conductivity. To improve the electronic conductivity, many attempts such as cation-doping [8], carbon-coating [9,10] and particle-size controlling [11] have been directed to overcome the drawbacks of $LiFePO_4$. Among them, carbon-coating is most effective and facile to improve the conductivity of $LiFePO_4$.

Graphene, which has a high specific surface area, is superior to other carbon-sources for the coating of $LiFePO_4$. In this paper, we reported a novel co-precipitation method for preparation of $LiFePO_4$/graphene composites with high electrochemical properties. The structure, morphology and electrochemical properties of the materials will be studied in the following sections.

2. Experimental

2.1. Preparation of materials

Typically, graphene was synthesized from natural graphite powder by a modified Hummers method [12]. Natural graphite powder was first oxidized by reacting them with concentrated nitric acid and sulfuric acid (1:2, v/v). The reaction unit was immersed in an ice bath, and potassium chlorate was added slowly. Then the ice bath was removed and replaced by a water bath, and the mixture was heated to 65 °C. The reaction was maintained for 120 h in order to increase the oxidation degree of the graphite powder. Graphite oxide (GO) was obtained by thoroughly washing and filtering using de-ionized water until pH 7. The GO suspended in a mixture of ethanol and water was exfoliated through ultrasonication for 2 h. Then the exfoliated GO was reduced to graphene by hydrazine hydrate at 100 °C for 24 h. The final products were centrifuged, washed, and finally vacuum-dried.

The $LiFePO_4$/graphene composites were prepared using a co-precipitation method in de-ionized water at room temperature. Aqueous solution of $(NH_4)_2Fe(SO_4)_26H_2O$ and $NH_4H_2PO_4$ was added to a Suspension of graphene. Then aqueous solution of LiOH was added to the mixture with blowing nitrogen gas into the solution. The obtained green color deposit was washed with the de-ionized water and separated by the high-speed centrifugation separator. The deposit was put into pellets, and then the pellets

* Corresponding authors. Address: Institute of Rheology Mechanics, Xiangtan University, Hunan 411105, China. Tel./fax: +86 731 58293240 (Y. Ding).
E-mail address: yhding@xtu.edu.cn (Y. Ding).

1388-2481/$ - see front matter © 2009 Elsevier B.V. All rights reserved.
doi:10.1016/j.elecom.2009.10.023

were heated to 120 °C for 5 h and finally sintered at 700 °C for 18 h in a tubular furnace under argon flow. Cooling to room temperature and grinding the resulting product, the $LiFePO_4$/graphene composites were obtained. For comparison, we also synthesize the $LiFePO_4$ follow the same procedure except that no graphene was added.

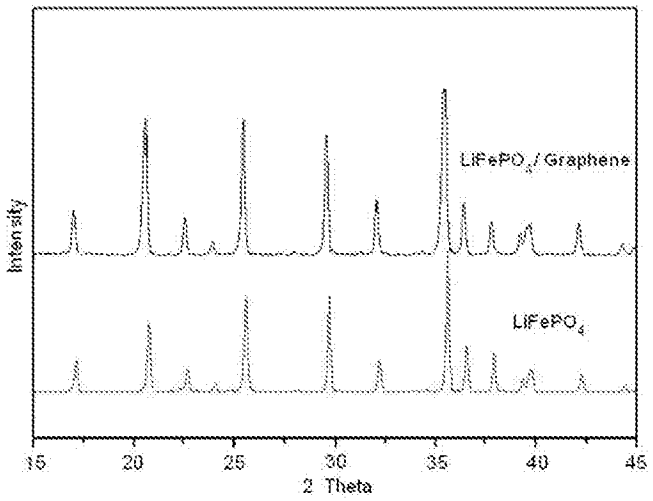


Fig. 1. XRD patterns of $LiFePO_4$ and $LiFePO_4$/graphene composites.

2.2. Measurements

Powder X-ray diffraction was carried out using a Rigaku Rotaflex D/max-3C X-ray diffractometer with a graphite monochromator and Cu Kα radiation operated at 40 kV and 30 mA. The morphology of $LiFePO_4$/graphene composites was characterized by atomic force microscopy (Veeco Instruments Inc., USA).

For electrochemical testing, the cathode was prepared by mixing the active materials with carbon black and PTFE in a weight ratio of 80:10:10. The mixture was pressed onto Al foils and pressing at 16 MPa before drying for 24 h at 120 °C. The cells were assembled with the cathode as prepared, lithium metal as anode and Celgard 2300 film as separator. The electrolytes were 1 M $LiPF_6$ dissolved in EC + DMC (1:1, v/v). Test cells were assembled in an argon-filled glove box. Charge–discharge experiments were performed in Lixin battery cycler over a voltage of 2.4–4.2 V at 35 °C (Lixin Instruments, China).

3. Results and discussion

The contents of graphene were determined by a solution method and the three average results show it was near 1.5 wt.%. The XRD patterns of $LiFePO_4$ and $LiFePO_4$/graphene composites are shown in Fig. 1. For both samples, all Bragg peaks can be indexed as a well-crystallized $LiFePO_4$ phase with an orthorhombic structure with the space group of *Pnma*. No evidence of diffraction peaks for graphene appears in the diffraction pattern and its presence

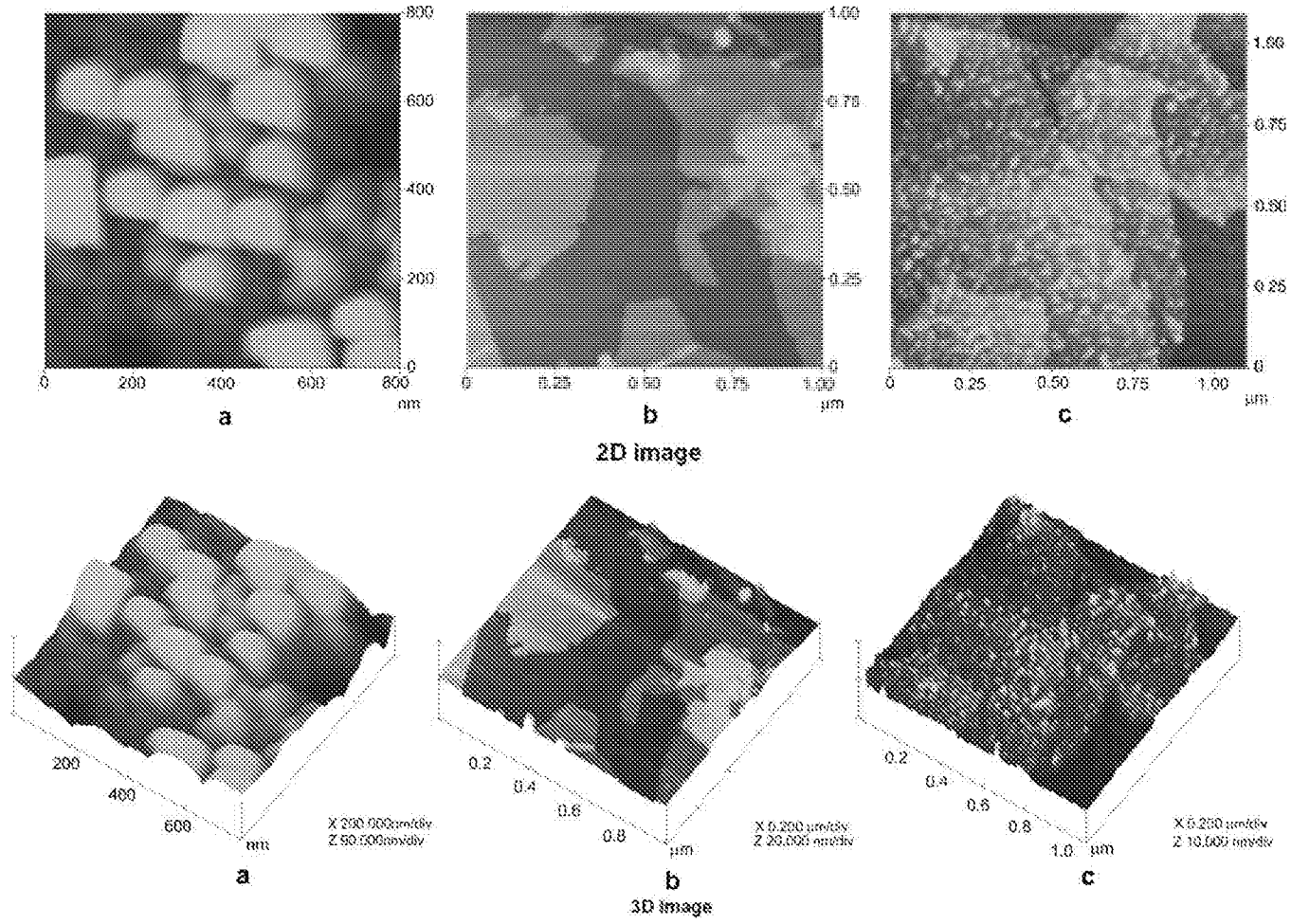


Fig. 2. Morphology of $LiFePO_4$, graphene and $LiFePO_4$/graphene composites. (a) $LiFePO_4$; (b) graphene; and (c) $LiFePO_4$/graphene composites.

AMPEREX Ex. 1002
Page 964

does not influence the structure of $LiFePO_4$, which could be ascribed to the low contents of graphene. The crystal lattice parameters are $a = 1.029$ nm, $b = 0.602$ nm, $c = 0.468$ nm for pristine $LiFePO_4$, and $a = 1.032$ nm, $b = 0.601$ nm, $c = 0.469$ nm for $LiFePO_4$/graphene composites. Both sets of parameters are very close to each other and consistent with the previously reported results [13,14]. The crystal sizes calculated by the Scherrer's equation are about 20 nm for $LiFePO_4$/graphene and 70 nm for $LiFePO_4$.

The morphological features of $LiFePO_4$, graphene and $LiFePO_4$/graphene composites were characterized by AFM and the results are shown in Fig. 2. The $LiFePO_4$ prepared from co-precipitation method has spherical shapes and their average particle-sizes are about 100 nm. Fig. 2b displays an atomic force microscopy (AFM) image of primitive graphene nanosheets on atomically flat mica surfaces. Analysis of a larger number of AFM images reveals graphene sheets with lateral dimensions of 200–2000 nm and heights in the range of 0.6–4 nm. Approximately 80% of the graphene sheets display a smooth surface and a height of 0.6–2 nm. As can be seen from Fig. 2c, the surface of graphene nanosheets is covered with $LiFePO_4$ nanoparticles with the diameter less than 10 nm. By controlling the precipitation conditions, the deposit could be attached to the graphene sheets by using graphene as additives. Though there are also some unattached and aggregated $LiFePO_4$ particles in the composites. Obviously, the particle-graphene sheets are homogeneous without large-diameter $LiFePO_4$ particles. The particle-sizes are basically matched to the calculated result from the Scherrer's equation. The data of BET surface area of $LiFePO_4$/graphene composite and graphene sheet are 112.8 and 684.4 $m^2 g^{-1}$, respectively. The specific surface area of graphene is much lower than the theoretical value of 2630 $m^2 g^{-1}$ due to the restacking of the graphene sheets under the van der Waals forces. By comparison, the measured surface area of $LiFePO_4$/graphene composites is also lower than that of graphene.

Fig. 3 shows the voltage profiles as a function of the specific capacity for the prepared $LiFePO_4$ and $LiFePO_4$/graphene composites at 0.2 C. The corresponding potential capacity diagram for the first cycle shows the typical flat potential plateau at 3.4 V versus Li/Li^+. Furthermore, the discharge curve of $LiFePO_4$/graphene composites is more flattened than that of $LiFePO_4$. It means energy can be used more effectively in $LiFePO_4$/graphene composites. The samples deliver a specific capacity of 160 and 113 mA h g^{-1} for $LiFePO_4$/graphene composites and $LiFePO_4$, respectively. The specific capacity and charge–discharge efficiency of $LiFePO_4$ increases dramatically with low content of graphene nanosheets. One possibility is that the adding of graphene at co-precipitation controls the particle-diameter of precursor. As shown in the insert, another possible reason is that graphene nanosheets act as conducting routes between the $LiFePO_4$ nanoparticles and the contact resistance is reduced. In addition, graphene itself has been reported as high capacity anode materials for rechargeable lithium secondary batteries [15]. It is beneficial in the improvement of reversible capacity of $LiFePO_4$.

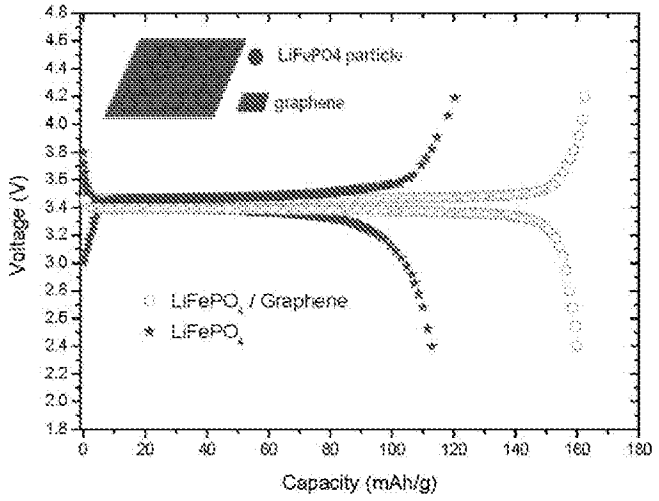


Fig. 3. Voltage profiles as a function of the specific capacity for the $LiFePO_4$ and $LiFePO_4$/graphene composites at 0.2 C.

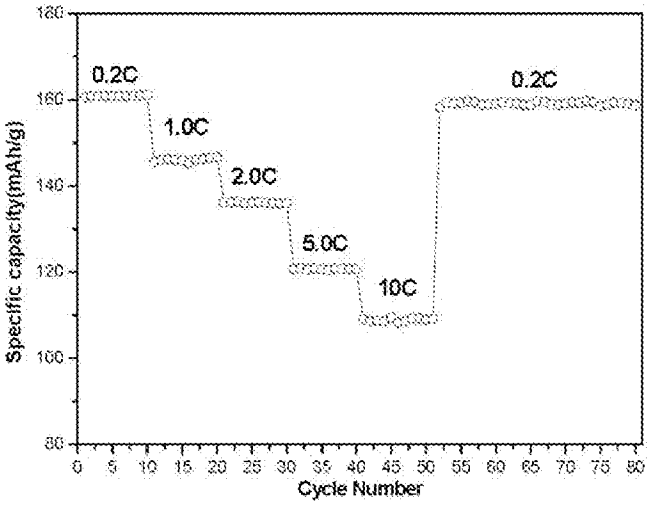


Fig. 4. Cycle characterizations of the $LiFePO_4$/graphene cell at various rates.

The cycle characterizations of the $LiFePO_4$/graphene cell at various rates from 0.2 to 10 C are presented in Fig. 4. The discharge capacity of $LiFePO_4$/graphene is about 160, 146, 136, 120 and 109 mA h g^{-1} at 0.2, 1.0, 2.0, 5.0 and 10 C, respectively. After 80 cycles under various conditions, the test cells deliver about 97% of the initial capacity. The rate performance and cycling stability of the $LiFePO_4$/graphene could be attributed to the fact that nanosize particle with surface area and improved conductivity through a superior graphene conductor. The capacities of $LiFePO_4$/graphene decrease from 160 to 109 mA h g^{-1} by increasing the discharge rates from 0.2 to 10 C. The decrease of discharge capacity with higher rate can be ascribed to the Li^+ diffusion in the interface between $LiFePO_4$ and $FePO_4$.

4. Conclusion

In this paper, a novel route for synthesis of $LiFePO_4$/graphene composites with high electrochemical performance has been reported. The graphene nanosheets were used as scaffolds with $LiFePO_4$ nanoparticles growing on the surface. The composites delivered an initial discharge capacity of 160 mA h g^{-1} at 0.2 C and the capacity retained 110 mA h g^{-1} even at high rate of 10 C with only 1.5 wt.% of graphene. Based on the results, we believe that the $LiFePO_4$/graphene composites may be a promising candidate for lithium secondary batteries.

Acknowledgments

The financial support from the Scientific Research Fund of Hunan Provincial Education Department (No. 08C892) and Undergraduate Innovation Foundation of Education Ministry of China (Nos. 081053019 and 091053021) is greatly acknowledged.

AMPEREX Ex. 1002
Page 965

References

[1] K.S. Novoselov, A.K. Geim, S.V. Morozov, D. Jiang, Y. Zhang, S.V. Dubonos, I.V. Grigorieva, A.A. Firsov, Science 306 (2004) 666.
[2] S. Park, R.S. Ruoff, Nat. Nanotechnol. 4 (2009) 217.
[3] K.I. Bolotin, Solid State Commun. 146 (2008) 351.
[4] M.D. Stoller, S. Park, Y. Zhu, J. An, R.S. Ruoff, Nano Lett. 8 (2008) 3498.
[5] A.K. Padhi, K.S. Nanjundaswamy, C. Masquelier, S. Okada, J.B. Goodenough, J. Electrochem. Soc. 144 (1997) 1609.
[6] Y. Yang, X.-Z. Liao, Z.-F. Ma, B.-F. Wang, L. He, Y.-S. He, Electrochem. Commun. 11 (2009) 1277.
[7] K.S. Park, J.T. Son, H.T. Chung, S.J. Kim, C.H. Lee, H.G. Kim, Electrochem. Commun. 5 (2003) 839.
[8] S.Y. Chung, J.T. Bloking, Y.M. Chiang, Nat. Mater. 1 (2002) 123.
[9] Z.R. Chang, H.J. Lv, H.W. Tang, H.J. Li, X.Z. Yuan, H. Wang, Electrochim. Acta 54 (2009) 4595.
[10] K.S. Park, S.B. Schougaard, J.B. Goodenough, Adv. Mater. 19 (2007) 848.
[11] P.P. Prosini, M. Carewska, S. Scaccia, P. Wisniewski, M. Pasquali, Electrochim. Acta 48 (2003) 4205.
[12] W.S. Hummers, R.E. Offeman, J. Am. Chem. Soc. 80 (1958) 1339.
[13] C.S. Sun, Z. Zhou, Z.G. Xu, D.G. Wang, J.P. Wei, X.K. Bian, J. Yan, J. Power Sour. 193 (2009) 841.
[14] M. Takhashi, S. Tobishima, K. Takei, Y. Sakurai, J. Power Sour. 97 (2001) 508.
[15] E.J. Yoo, J. Kim, E. Hosono, H.-S. Zhou, T. Kudo, I. Honma, Nano Lett. 8 (2008) 2277.

Electronic Acknowledgement Receipt

EFS ID:	40661560
Application Number:	16923494
International Application Number:	
Confirmation Number:	3273
Title of Invention:	POSITIVE ELECTRODE ACTIVE MATERIAL, METHOD FOR MANUFACTURING POSITIVE ELECTRODE ACTIVE MATERIAL, AND SECONDARY BATTERY
First Named Inventor/Applicant Name:	Teruaki OCHIAI
Customer Number:	26171
Filer:	John F. Hayden/Alexis Bailey
Filer Authorized By:	John F. Hayden
Attorney Docket Number:	12732-2003004
Receipt Date:	24-SEP-2020
Filing Date:	08-JUL-2020
Time Stamp:	16:59:33
Application Type:	Utility under 35 USC 111(a)

Payment information:

Submitted with Payment	no

File Listing:

Document Number	Document Description	File Name	File Size(Bytes)/ Message Digest	Multi Part /.zip	Pages (if appl.)
1	Information Disclosure Statement (IDS) Form (SB08)	IDS_12732-2003004.pdf	166596 dcb5daac2d7223ed1aad55b5f9cc4117b96c6536	no	4

Warnings:

Information:					
This is not an USPTO supplied IDS fillable form					
2	Foreign Reference	KR1020130033154A.pdf	1170440 b49e1e8d5baebf080d538619da267f76781ede13	no	19
Warnings:					
Information:					
3	Foreign Reference	KR1020110134852A.pdf	1030335 12148ccaf8c612d75e24de7f355c62ee32a71828	no	14
Warnings:					
Information:					
4	Foreign Reference	EP2763218A2.pdf	13292723 0af743e5c84b7248fece76e2d8b18612422060cc	no	15
Warnings:					
Information:					
5	Foreign Reference	WO2011155781A2.pdf	10968040 565c2c2f7df4c0a839ef5fbf6ed706846b6e4897	no	18
Warnings:					
Information:					
6	Foreign Reference	JP2015-088450.pdf	617313 870842504fde451e5578485ab0630e67997fd53d	no	29
Warnings:					
Information:					
7	Non Patent Literature	ElectrochemistryCom_12_10.pdf	271823 f88b5a3f3e7eff3e8e041ee041cabc166d1a9c87	no	4
Warnings:					
Information:					
			Total Files Size (in bytes):	27517270	

This Acknowledgement Receipt evidences receipt on the noted date by the USPTO of the indicated documents, characterized by the applicant, and including page counts, where applicable. It serves as evidence of receipt similar to a Post Card, as described in MPEP 503.

New Applications Under 35 U.S.C. 111

If a new application is being filed and the application includes the necessary components for a filing date (see 37 CFR 1.53(b)-(d) and MPEP 506), a Filing Receipt (37 CFR 1.54) will be issued in due course and the date shown on this Acknowledgement Receipt will establish the filing date of the application.

National Stage of an International Application under 35 U.S.C. 371

If a timely submission to enter the national stage of an international application is compliant with the conditions of 35 U.S.C. 371 and other applicable requirements a Form PCT/DO/EO/903 indicating acceptance of the application as a national stage submission under 35 U.S.C. 371 will be issued in addition to the Filing Receipt, in due course.

New International Application Filed with the USPTO as a Receiving Office

If a new international application is being filed and the international application includes the necessary components for an international filing date (see PCT Article 11 and MPEP 1810), a Notification of the International Application Number and of the International Filing Date (Form PCT/RO/105) will be issued in due course, subject to prescriptions concerning national security, and the date shown on this Acknowledgement Receipt will establish the international filing date of the application.

PTO/SB/08A (07-06)
Approved for use through 03/31/2007. OMB 0651-0031
U.S. Patent and Trademark Office; U.S. DEPARTMENT OF COMMERCE

Under the Paperwork Reduction Act of 1995, no persons are required to respond to a collection of information unless it contains a valid OMB control number.

Substitute for form 1449/PTO

INFORMATION DISCLOSURE STATEMENT BY APPLICANT

(Use as many sheets as necessary)

Sheet 1 of 1

Complete if Known	
Application Number	16/923,494
Filing Date	July 8, 2020
First Named Inventor	Teruaki OCHIAI
Art Unit	1725
Examiner Name	S.CULLEN
Attorney Docket Number	12732-2003004

U. S. PATENT DOCUMENTS

Examiner Initials*	Cite No.[1]	Document Number Number-Kind Code[2] (if known)	Publication Date MM-DD-YYYY	Name of Patentee or Applicant of Cited Document	Pages, Columns, Lines, Where Relevant Passages or Relevant Figures Appear
		US-2016/0013478	01-14-2016	Satow.T et al.	
		US-2013/0230770	09-05-2013	Oya.M et al.	

FOREIGN PATENT DOCUMENTS

Examiner Initials*	Cite No.[1]	Foreign Patent Document Country Code[3] -Number[4] -Kind Code[5] (if known)	Publication Date MM-DD-YYYY	Name of Patentee or Applicant of Cited Document	Pages, Columns, Lines, Where Relevant Passages or Relevant Figures Appear	T[6]
		CN-105024047A	11-04-2015			FULL
		KR-10-0696619	03-19-2007			Abst.

Examiner Signature		Date Considered	

*EXAMINER: Initial if reference considered, whether or not citation is in conformance with MPEP 609. Draw line through citation if not in conformance and not considered. Include copy of this form with next communication to applicant. 1 Applicant's unique citation designation number (optional). 2 See Kinds Codes of USPTO Patent Documents at www.uspto.gov or MPEP 901.04. 3 Enter Office that issued the document, by the two-letter code (WIPO Standard ST.3). 4 For Japanese patent documents, the indication of the year of the reign of the Emperor must precede the serial number of the patent document. 5 Kind of document by the appropriate symbols as indicated on the document under WIPO Standard ST.16 if possible. 6 Applicant is to place a check mark here if English language Translation is attached.

This collection of information is required by 37 CFR 1.97 and 1.98. The information is required to obtain or retain a benefit by the public which is to file (and by the USPTO to process) an application. Confidentiality is governed by 35 U.S.C. 122 and 37 CFR 1.14. This collection is estimated to take 2 hours to complete, including gathering, preparing, and submitting the completed application form to the USPTO. Time will vary depending upon the individual case. Any comments on the amount of time you require to complete this form and/or suggestions for reducing this burden, should be sent to the Chief Information Officer, U.S. Patent and Trademark Office, P.O. Box 1450, Alexandria, VA 22313-1450. DO NOT SEND FEES OR COMPLETED FORMS TO THIS ADDRESS. **SEND TO: Commissioner for Patents, P.O. Box 1450, Alexandria, VA 22313-1450.**

If you need assistance in completing the form, call 1-800-PTO-9199 (1-800-786-9199) and select option 2.

IN THE UNITED STATES PATENT AND TRADEMARK OFFICE

First Named Inventor	:	Teruaki OCHIAI	Art Unit	:	1725
Application No.	:	16/923,494	Examiner	:	Sean P. Cullen
Filed	:	July 8, 2020	Conf. No.	:	3273
Title	:	POSITIVE ELECTRODE ACTIVE MATERIAL, METHOD FOR MANUFACTURING POSITIVE ELECTRODE ACTIVE MATERIAL, AND SECONDARY BATTERY			

Commissioner for Patents
P.O. Box 1450
Alexandria, VA 22313-1450

INFORMATION DISCLOSURE STATEMENT

Please consider the references listed on the enclosed disclosure form. Copies of the documents required under 37 C.F.R. § 1.98(a)(2) are being submitted with this statement.

Applicant notes that this information disclosure statement includes KR-10-0696619, which was listed on the information disclosure statement filed on August 3, 2020. As noted by the Examiner in the office action dated September 21, 2020, that information disclosure statement erroneously indicated that this reference had been provided in the parent application. Applicant is providing a copy of the reference now to correct that error.

This statement is being filed after a first action on the merits, but before receipt of a final action or a notice of allowance. A late submission fee in the amount of $260 specified by 37 CFR §1.17(p), is being paid with this statement. Please apply any charges or credits to Deposit Account No. 06-1050, referencing the above attorney docket number.

Respectfully submitted,

Date: October 21, 2020

/John F. Hayden/
John F. Hayden
Reg. No. 37640

Customer Number 26171
Fish & Richardson P.C.
Telephone: (202) 783-5070
Facsimile: (877) 769-7945

100275944.doc

(19)中华人民共和国国家知识产权局

(12)发明专利申请

(10)申请公布号 CN 105024047 A
(43)申请公布日 2015.11.04

(21)申请号 201410165123.0

(22)申请日 2014.04.23

(71)申请人 宁德时代新能源科技有限公司
地址 352100 福建省宁德市蕉城区漳湾镇新港路1号科研楼1F-西

(72)发明人 来佑磊 杨同欢 金海族 朱凌波 陈伟峰

(74)专利代理机构 北京五洲洋和知识产权代理事务所(普通合伙) 11387
代理人 张向琨

(51)Int.Cl.
H01M 4/36(2006.01)
H01M 4/58(2010.01)
H01M 4/525(2010.01)
H01M 10/0525(2010.01)

权利要求书2页 说明书10页 附图4页

(54)发明名称

锂离子二次电池及其复合正极活性材料及制备方法

(57)摘要

本发明提供一种锂离子二次电池及其复合正极活性材料及制备方法。所述复合正极活性材料由锂钴系列氧化物和磷酸锰锂(LMP)复合而成。所述复合正极活性材料具有填充式结构;所述填充式结构为所述磷酸锰锂(LMP)的一次颗粒填充复合到所述锂钴系列氧化物的二次颗粒的表面缝隙和凹坑中;所述锂钴系列氧化物的化学通式为$LiA_xCo_{1-x}O_2$,其中,$0 \leq x<1$,A为Ni、Mn、Al、Mg、Ca、Cr、Zr、Mo、Ag、Nb中的至少一种;所述磷酸锰锂(LMP)的化学通式为$LiB_yMn_{1-y}PO_4$,其中,$0 \leq y<1$,B为Ni、Co、Fe、Al、Ca、Zn、Mg、Mo、Pb、Zr中的至少一种。所述锂离子二次电池包括上述复合正极活性材料。本发明的锂离子二次电池具有良好的容量密度、倍率性能、循环性能、存储性能以及安全性能。

CN 105024047 A

1.一种锂离子二次电池的复合正极活性材料，由锂钴系列氧化物和磷酸锰锂（LMP）复合而成，其特征在于，

所述复合正极活性材料具有填充式结构；

所述填充式结构为所述磷酸锰锂（LMP）的一次颗粒填充复合到所述锂钴系列氧化物的二次颗粒的表面缝隙和凹坑中；

所述锂钴系列氧化物的化学通式为 $LiA_xCo_{1-x}O_2$，其中，$0 \leqslant x<1$，A 为 Ni、Mn、Al、Mg、Ca、Cr、Zr、Mo、Ag、Nb 中的至少一种；

所述磷酸锰锂（LMP）的化学通式为 $LiB_yMn_{1-y}PO_4$，其中，$0 \leqslant y<1$，B 为 Ni、Co、Fe、Al、Ca、Zn、Mg、Mo、Pb、Zr 中的至少一种。

2.根据权利要求 1 所述的锂离子二次电池的复合正极活性材料，其特征在于，所述锂钴系列氧化物的二次颗粒的颗粒不规则系数 BET×D50>3.5。

3.根据权利要求 1 所述的锂离子二次电池的复合正极活性材料，其特征在于，所述磷酸锰锂（LMP）在所述复合正极活性材料中的质量百分含量为 1% ～ 40%。

4.根据权利要求 3 所述的锂离子二次电池的复合正极活性材料，其特征在于，所述磷酸锰锂（LMP）在所述复合正极活性材料中的质量百分含量为 10% ～ 20%。

5.根据权利要求 1 所述的锂离子二次电池的复合正极活性材料，其特征在于，所述磷酸锰锂（LMP）的一次颗粒的粒径为 0.1nm ～ 50nm，BET 比表面积 $>20m^2/g$。

6.一种锂离子二次电池的复合正极活性材料的制备方法，用于制备根据权利要求 1-5 中任一项所述的锂离子二次电池的复合正极活性材料，包括步骤：

（1）将分散剂去离子水与磷酸锰锂（LMP）的一次颗粒以 1:1 ～ 3:1 的体积比混合球磨，然后在 800r/min ～ 1000r/min 的转速下球磨分散 1h ～ 2h，得到磷酸锰锂（LMP）的一次颗粒的分散浆料，其中，所述磷酸锰锂（LMP）的化学通式为 $LiB_yMn_{1-y}PO_4$，其中，$0 \leqslant y<1$，B 为 Ni、Co、Fe、Al、Ca、Zn、Mg、Mo、Pb、Zr 中的至少一种；

（2）将分散剂去离子水与锂钴系列氧化物的二次颗粒以 1:1 ～ 3:1 的体积比混合球磨，然后在 200r/min ～ 400r/min 的转速下球磨分散 1h ～ 3h，将锂钴系列氧化物的二次颗粒分散到分散剂中，得到锂钴系列氧化物的二次颗粒的分散浆料，其中，所述锂钴系列氧化物的化学通式为 $LiA_xCo_{1-x}O_2$，其中，$0 \leqslant x<1$，A 为 Ni、Mn、Al、Mg、Ca、Cr、Zr、Mo、Ag、Nb 中的至少一种；

（3）将磷酸锰锂（LMP）的一次颗粒的分散浆料加入到锂钴系列氧化物的二次颗粒的分散浆料中，继续在 200r/min ～ 400r/min 的转速下球磨分散 2h ～ 4h，使磷酸锰锂（LMP）的一次颗粒的分散浆料与锂钴系列氧化物的二次颗粒的分散浆料充分混合，随后逐渐降低球磨转速，当球磨转速降至 50r/min ～ 200r/min 时继续球磨分散 0.5h ～ 4h，进行材料复合，沉淀后除去上层清液，将余下的混合物在 100℃～ 200℃下鼓风干燥 12h，即得到锂离子二次电池的复合正极活性材料，其中，所述复合正极活性材料具有填充式结构，所述填充式结构为所述磷酸锰锂（LMP）的一次颗粒填充复合到所述锂钴系列氧化物的二次颗粒的表面缝隙和凹坑中。

7.一种锂离子二次电池，包括：

正极片，含有正极活性材料；

负极片；

AMPEREX Ex. 1002
Page 973

隔离膜，间隔于正极片和负极片之间；

非水电解液；以及

锂离子二次电池壳体，包含压力安全阀；

其特征在于，所述正极活性材料为根据权利要求 1-5 中任一项所述的锂离子二次电池的复合正极活性材料。

8. 根据权利要求 7 所述的锂离子二次电池，其特征在于，所述压力安全阀为压力限制阀。

9. 根据权利要求 8 所述的锂离子二次电池，其特征在于，所述压力安全阀的压力范围为 2MPa ～ 4MPa。

10. 根据权利要求 7 所述的锂离子二次电池，其特征在于，所述压力安全阀的内侧为金属限压层，外侧为聚合物保护层。

AMPEREX Ex. 1002
Page 974

锂离子二次电池及其复合正极活性材料及制备方法

技术领域

[0001] 本发明涉及电池领域，尤其涉及一种锂离子二次电池及其复合正极活性材料及制备方法。

背景技术

[0002] 锂离子二次电池由于具有良好的电化学性能而被广泛应用于各个领域，如手机、电脑、电动工具、电动车等。锂离子二次电池的安全性能是除电化学性能外最重要的性能，其决定了使用锂离子二次电池的设备的安全性以及可靠性，与广大消费者的生命财产安全息息相关。

[0003] 锂离子二次电池的安全问题主要是各种形式的热失控问题，如内短路点温度升高导致的锂离子二次电池起火爆炸等。

[0004] 常见的过渡金属氧化物正极活性材料通常具有良好的电化学性能，但是其中绝大多数在高温下会分解释放出氧，在密闭的锂离子二次电池内作为电解液和隔离膜等易燃部件的助燃剂，导致锂离子二次电池燃烧爆炸。

[0005] 目前，为了解决这个问题，满足安全需求，通常采用安全性好但电化学性能较差的正极活性材料，如磷酸盐系列的正极活性材料(诸如橄榄石结构的磷酸铁锂)。磷酸盐系列的正极活性材料在高温下不会产生大量的氧，从而不会与电解液发生副反应。在密封的锂离子二次电池内部，电解液即使达到燃点，因无氧气的供给故不会使锂离子二次电池发生燃烧爆炸，但当电解液的蒸发气化达到一定程度时会使锂离子二次电池产生膨胀爆炸。通常的解决方式是在锂离子二次电池上设置压力安全阀，以控制锂离子二次电池内的电解液的蒸发气化产生的压力，当锂离子二次电池内的压力超过临界值时，压力安全阀打开，气化的电解液可释放到锂离子二次电池的外部，气化的电解液外喷后，锂离子二次电池内部因电解液的流失而干涸，极片间的离子传递介质消失，进而锂离子二次电池内的反应终止，不会发生燃烧、爆炸进而保证了锂离子二次电池甚至当其在电池组中使用时整个电池组的安全。

[0006] 但是，磷酸盐系列的正极活性材料电化学性能较差，导致使用磷酸盐系列正极活性材料的锂离子二次电池的倍率性能受到严重的限制，进而限制了其作为动力电池在相关领域的发展。

[0007] 目前动力锂离子二次电池采用的高电化学性能的正极活性材料，主要有锂镍钴锰氧(NCM)三元材料、锂镍钴铝氧(NCA)等，虽然其具有较高的电化学性能，但安全性能较差，限制了高性能锂离子二次电池的应用。

发明内容

[0008] 鉴于背景技术中存在的问题，本发明的目的在于提供一种锂离子二次电池及其复合正极活性材料及制备方法，所述锂离子二次电池具有良好的容量密度、倍率性能、循环性能以及存储性能，同时还具有良好的安全性能以及热稳定性。

AMPEREX Ex. 1002
Page 975

[0009] 为了实现上述目的，在本发明的第一方面，本发明提供了一种锂离子二次电池的复合正极活性材料，其由锂钴系列氧化物和磷酸锰锂（LMP）复合而成。所述复合正极活性材料具有填充式结构；所述填充式结构为所述磷酸锰锂（LMP）的一次颗粒填充复合到所述锂钴系列氧化物的二次颗粒的表面缝隙和凹坑中；所述锂钴系列氧化物的化学通式为 $LiA_xCo_{1-x}O_2$，其中，$0 \leqslant x<1$，A 为 Ni、Mn、Al、Mg、Ca、Cr、Zr、Mo、Ag、Nb 中的至少一种；所述磷酸锰锂（LMP）的化学通式为 $LiB_yMn_{1-y}PO_4$，其中，$0 \leqslant y<1$，B 为 Ni、Co、Fe、Al、Ca、Zn、Mg、Mo、Pb、Zr 中的至少一种。

[0010] 在本发明的第二方面，本发明提供了一种锂离子二次电池的复合正极活性材料的制备方法，用于制备根据本发明第一方面所述的锂离子二次电池的复合正极活性材料，其包括步骤：（1）将分散剂去离子水与磷酸锰锂（LMP）的一次颗粒以 1:1 ～ 3:1 的体积比混合球磨，然后在 800r/min ～ 1000r/min 的转速下球磨分散 1h ～ 2h，得到磷酸锰锂（LMP）的一次颗粒的分散浆料，其中，所述磷酸锰锂（LMP）的化学通式为 $LiB_yMn_{1-y}PO_4$，其中，$0 \leqslant y<1$，B 为 Ni、Co、Fe、Al、Ca、Zn、Mg、Mo、Pb、Zr 中的至少一种；（2）将分散剂去离子水与锂钴系列氧化物的二次颗粒以 1:1 ～ 3:1 的体积比混合球磨，然后在 200r/min ～ 400r/min 的转速下球磨分散 1h ～ 3h，将锂钴系列氧化物的二次颗粒分散到分散剂中，得到锂钴系列氧化物的二次颗粒的分散浆料，其中，所述锂钴系列氧化物的化学通式为 $LiA_xCo_{1-x}O_2$，其中，$0 \leqslant x<1$，A 为 Ni、Mn、Al、Mg、Ca、Cr、Zr、Mo、Ag、Nb 中的至少一种；（3）将磷酸锰锂（LMP）的一次颗粒的分散浆料加入到锂钴系列氧化物的二次颗粒的分散浆料中，继续在 200r/min ～ 400r/min 的转速下球磨分散 2h ～ 4h，使磷酸锰锂（LMP）的一次颗粒的分散浆料与锂钴系列氧化物的二次颗粒的分散浆料充分混合，随后逐渐降低球磨转速，当球磨转速降至 50r/min ～ 200r/min 时继续球磨分散 0.5h ～ 4h，进行材料复合，沉淀后除去上层清液，将余下的混合物在 100℃～ 200℃下鼓风干燥 12h，即得到锂离子二次电池的复合正极活性材料，其中，所述复合正极活性材料具有填充式结构，所述填充式结构为所述磷酸锰锂（LMP）的一次颗粒填充复合到所述锂钴系列氧化物的二次颗粒的表面缝隙和凹坑中。

[0011] 在本发明的第三方面，本发明提供了一种锂离子二次电池，包括：正极片，含有正极活性材料；负极片；隔离膜，间隔于正极片和负极片之间；非水电解液；以及锂离子二次电池壳体，包含压力安全阀。所述正极活性材料为根据本发明第一方面所述的锂离子二次电池的复合正极活性材料。

[0012] 本发明的有益效果如下：

[0013] 1. 本发明的锂离子二次电池的复合正极活性材料可以减缓电解液和锂钴系列氧化物之间的副反应，提高锂离子二次电池的循环性能以及存储性能。复合正极活性材料良好的高温稳定性，还使得锂离子二次电池热失控时电解液的蒸发气化过程成为主导，电解液气化后从锂离子二次电池的压力安全阀外喷而排出，电解液与正极片的氧化还原反应停止，从而降低了锂离子二次电池在碰撞、穿刺过程中的燃烧、爆炸的风险，从而提高了锂离子二次电池的安全性能。

[0014] 2. 本发明的锂离子二次电池的复合正极活性材料可以用少量的磷酸锰锂（LMP）的一次颗粒通过简单的方法填充复合到锂钴系列氧化物的二次颗粒的表面缝隙和凹坑中，由于磷酸锰锂（LMP）不是完全包覆锂钴系列氧化物，因而保持了锂钴系列氧化物的高倍率性能，并且由于磷酸锰锂（LMP）的用量较少，不会降低锂离子二次电池的能量密度。同时，复

AMPEREX Ex. 1002
Page 976

合正极活性材料中的磷酸锰锂(LMP)覆盖锂钴系列氧化物表面的活性点,使复合正极活性材料具有较好的热稳定性以及化学稳定性,因此锂离子二次可同时具有良好的倍率性能、较高的能量密度以及良好的安全性能。

附图说明

[0015] 图 1 是使用本发明的复合正极活性材料的锂离子二次电池的结构示意图。

[0016] 图 2 是本发明的实施例 1 的磷酸锰锂($LiFe_{0.1}Mn_{0.9}PO_4$)的一次颗粒以及锂钴系列氧化物($LiNi_{0.4}Co_{0.4}Mn_{0.2}O_2$)的二次颗粒的扫描电镜照片。

[0017] 图 3 是本发明的实施例 1 的复合正极活性材料的颗粒在相同倍数下的不同位置的扫描电镜照片,其中,A 为磷酸锰锂($LiFe_{0.1}Mn_{0.9}PO_4$)的一次颗粒,B 为锂钴系列氧化物($LiNi_{0.4}Co_{0.4}Mn_{0.2}O_2$)的二次颗粒。

[0018] 图 4 是复合正极活性材料的传统完全包覆结构以及本发明的填充式结构的示意图。

具体实施方式

[0019] 下面详细说明根据本发明的锂离子二次电池及其复合正极活性材料及制备方法以及实施例、对比例以及测试结果。

[0020] 首先说明根据本发明第一方面的锂离子二次电池的复合正极活性材料。

[0021] 根据本发明第一方面的锂离子二次电池的复合正极活性材料,由锂钴系列氧化物和磷酸锰锂(LMP)复合而成。所述复合正极活性材料具有填充式结构;所述填充式结构为所述磷酸锰锂(LMP)的一次颗粒填充复合到所述锂钴系列氧化物的二次颗粒的表面缝隙和凹坑中;所述锂钴系列氧化物的化学通式为 $LiA_xCo_{1-x}O_2$,其中,$0 \leqslant x<1$,A 为 Ni、Mn、Al、Mg、Ca、Cr、Zr、Mo、Ag、Nb 中的至少一种;所述磷酸锰锂(LMP)的化学通式为 $LiB_yMn_{1-y}PO_4$,其中,$0 \leqslant y<1$,B 为 Ni、Co、Fe、Al、Ca、Zn、Mg、Mo、Pb、Zr 中的至少一种。

[0022] 在根据本发明第一方面所述的锂离子二次电池的复合正极活性材料中,所述锂钴系列氧化物的二次颗粒是由一次颗粒聚集形成,所述锂钴系列氧化物的二次颗粒的表面粗糙不平(表面存在缝隙和凹坑)且二次颗粒的比表面积大于一次颗粒的比表面积。因而可明显提升复合正极活性材料的倍率性能。单独使用本发明的锂钴系列氧化物的不足之处在于:(1)安全问题更加严重,本发明的锂钴系列氧化物的二次颗粒的颗粒界面与一次颗粒的边缘之间的表面能较高,在锂离子二次电池热失控时受热失氧更快,进而氧气与电解液反应可释放出大量的热,导致锂离子二次电池燃烧爆炸,因此安全性能较差;(2)循环性能和存储性能有所下降,由于本发明的锂钴系列氧化物具有高的表面能,导致其与电解液之间的副反应的反应速度加快,产生烷烃、烯烃、二氧化碳等气体,导致锂离子二次电池的循环性能和存储性能下降。

[0023] 单独使用磷酸锰锂(LMP)时,由于磷酸盐离子结构的化学稳定性较高,因此磷酸锰锂(LMP)的热稳定性和化学稳定性较高,即使锂离子二次电池处于高温环境中,其释放氧气的可能性也十分小。此外,磷酸锰锂(LMP)在充放电过程中晶格参数的变化较小,其与电解液的副反应的反应速度也非常缓慢,因此锂离子二次电池的循环性能和存储性能更好。但是也存在一些不足之处:(1)磷酸锰锂(LMP)的电导率较低,使用其作为正极活性材料的锂

AMPEREX Ex. 1002
Page 977

离子二次电池的倍率性能较差，不能满足锂离子二次电池作为动力电池的参数需求；(2)磷酸锰锂(LMP)的较低的电导率使得其需要被制成一次颗粒以增加其导电性，因此其比表面积大幅度增加，使用其作为正极活性材料的锂离子二次电池所需的导电剂和粘结剂的用量也大幅度增加，导致正极片的比容量降低，影响锂离子二次电池的容量密度和能量密度。

[0024] 而在本发明中，由锂钴系列氧化物和磷酸锰锂(LMP)填充复合而成的复合正极活性材料，可以避免两者各自的缺点，同时发挥二者的优点，既具有良好的容量密度以及倍率性能，又具有良好的稳定性、循环性能以及存储性能。其中，参照图4的右图，磷酸锰锂(LMP)的一次颗粒不是简单的混合，也不是完全的包覆，而是填充复合到锂钴系列氧化物的二次颗粒的表面缝隙和凹坑中。如果只是简单的混合，则磷酸锰锂(LMP)对锂钴系列氧化物与电解液之间的副反应的抑制作用并不明显，不能给电解液蒸发外喷排出提供足够的时间，因而不能达到预期的提升安全性能的效果。如果采用传统完全包覆的方式，参照图4的左图，则锂离子二次电池的安全性能可明显提升，然而由于包覆结构中磷酸锰锂(LMP)完全覆盖在锂钴系列氧化物的表面，使得锂钴系列氧化物的表面特性表现为磷酸锰锂(LMP)的特性，降低了复合正极活性材料的倍率性能。

[0025] 在根据本发明第一方面所述的锂离子二次电池的复合正极活性材料中，所述锂钴系列氧化物的二次颗粒的颗粒不规则系数BET×D50可>3.5。常见锂钴系列氧化物的一次颗粒的颗粒不规则系数BET×D50为2.0～3.0。也就是说相同粒径的锂钴系列氧化物，本发明的锂钴系列氧化物的二次颗粒比常见锂钴系列氧化物的一次颗粒的比表面积大25%～100%，因而可明显提升复合正极活性材料的倍率性能。

[0026] 在根据本发明第一方面所述的锂离子二次电池的复合正极活性材料中，所述磷酸锰锂(LMP)在所述复合正极活性材料中的质量百分含量可为1%～40%。

[0027] 在根据本发明第一方面所述的锂离子二次电池的复合正极活性材料中，所述磷酸锰锂(LMP)在所述复合正极活性材料中的质量百分含量可为10%～20%。

[0028] 在根据本发明第一方面所述的锂离子二次电池的复合正极活性材料中，所述磷酸锰锂(LMP)的一次颗粒的粒径可为0.1nm～50nm，BET比表面积可>20m^2/g。

[0029] 其次说明根据本发明第二方面的锂离子二次电池的复合正极活性材料的制备方法。

[0030] 根据本发明第二方面的锂离子二次电池的复合正极活性材料的制备方法，用于制备本发明第一方面的锂离子二次电池的复合正极活性材料，包括步骤：(1)将分散剂去离子水与磷酸锰锂(LMP)的一次颗粒以1:1～3:1的体积比混合球磨，然后在800r/min～1000r/min的转速下球磨分散1h～2h，得到磷酸锰锂(LMP)的一次颗粒的分散浆料，其中，所述磷酸锰锂(LMP)的化学通式为$LiB_yMn_{1-y}PO_4$，0≤y<1，B为Ni、Co、Fe、Al、Ca、Zn、Mg、Mo、Pb、Zr中的至少一种；(2)将分散剂去离子水与锂钴系列氧化物的二次颗粒以1:1～3:1的体积比混合球磨，然后在200r/min～400r/min的转速下球磨分散1h～3h，将锂钴系列氧化物的二次颗粒分散到分散剂中，得到锂钴系列氧化物的分散浆料，其中，所述锂钴系列氧化物的化学通式为$LiA_xCo_{1-x}O_2$，其中，0≤x<1，A为Ni、Mn、Al、Mg、Ca、Cr、Zr、Mo、Ag、Nb中的至少一种；(3)将磷酸锰锂(LMP)的一次颗粒的分散浆料加入到锂钴系列氧化物的二次颗粒的分散浆料中，继续在200r/min～400r/min的转速下球磨分散2h～4h，使磷酸锰锂(LMP)的一次颗粒的分散浆料与锂钴系列氧化物的二次颗粒的分散浆料充分混合，随后逐

AMPEREX Ex. 1002
Page 978

渐降低球磨转速，当球磨转速降至50r/min～200r/min时继续球磨分散0.5h～4h，进行材料复合，沉淀后除去上层清液，将余下的混合物再在100℃～200℃下鼓风干燥12h，即得到锂离子二次电池的复合正极活性材料，其中，所述复合正极活性材料具有填充式结构，所述填充式结构为所述磷酸锰锂(LMP)的一次颗粒填充复合到所述锂钴系列氧化物的二次颗粒的表面缝隙和凹坑中。

[0031] 再次说明根据本发明第二方面的锂离子二次电池。

[0032] 根据本发明第三方面的锂离子二次电池，参照图1，包括：正极片，含有正极活性材料；负极片；隔离膜，间隔于正极片和负极片之间；非水电解液；以及锂离子二次电池壳体(图未示出)，包含压力安全阀(图未示出)。其中，所述正极活性材料为根据本发明第一方面所述的锂离子二次电池的复合正极活性材料。

[0033] 在根据本发明第三方面所述的锂离子二次电池中，所述正极片可包含正极集流体以及正极膜片。

[0034] 在根据本发明第三方面所述的锂离子二次电池中，所述正极膜片可包含复合正极活性材料、粘结剂、导电剂以及分散剂。

[0035] 在根据本发明第三方面所述的锂离子二次电池中，所述正极集流体可为铝箔。

[0036] 在根据本发明第三方面所述的锂离子二次电池中，所述正极膜片中的粘结剂可为聚偏氟乙烯(PVDF)。

[0037] 在根据本发明第三方面所述的锂离子二次电池中，所述正极膜片中的导电剂可为导电炭黑、乙炔黑、高导碳、石墨微片或石墨纤维。

[0038] 在根据本发明第三方面所述的锂离子二次电池中，所述正极膜片中的分散剂可为N-甲基吡咯烷酮。

[0039] 在根据本发明第三方面所述的锂离子二次电池中，所述负极片可包括负极集流体以及负极膜片。

[0040] 在根据本发明第三方面所述的锂离子二次电池中，所述负极膜片可包含负极活性材料、粘结剂、导电剂以及分散剂。

[0041] 在根据本发明第三方面所述的锂离子二次电池中，所述负极集流体可为铜箔。

[0042] 在根据本发明第三方面所述的锂离子二次电池中，所述负极膜片中的粘结剂可为丁苯橡胶。

[0043] 在根据本发明第三方面所述的锂离子二次电池中，所述负极膜片中的导电剂可为导电炭黑、乙炔黑、高导碳、石墨微片或石墨纤维。

[0044] 在根据本发明第三方面所述的锂离子二次电池中，所述负极膜片中的分散剂可为去离子水。

[0045] 在根据本发明第三方面的锂离子二次电池中，所述负极片可包含存储和释放锂离子的材料。

[0046] 在根据本发明第三方面所述的锂离子二次电池中，所述负极片中存储和释放锂离子的材料可为金属锂、石墨、硬碳或钛酸锂。

[0047] 在根据本发明第三方面的锂离子二次电池中，所述隔离膜可为PP膜、PE膜或PP/PE复合膜。

[0048] 在根据本发明第三方面的锂离子二次电池中，所述压力安全阀可为压力限制阀，

AMPEREX Ex. 1002
Page 979

其可以很好地控制锂离子二次电池内部的压力，大幅度降低由于锂离子二次电池内部的压力升高而导致膨胀爆炸的风险，如锂离子二次电池在高温下工作时副反应产生的气体导致的内部的压力的升高。当锂离子二次电池内部的压力达到一定数值时，压力安全阀打开，锂离子二次电池内的气体外喷排出。

[0049] 在根据本发明第三方面的锂离子二次电池中，所述压力安全阀的压力范围可为2MPa～4MPa。

[0050] 在根据本发明第三方面的锂离子二次电池中，所述压力安全阀的内侧可为金属限压层，外侧可为聚合物保护层。所述压力安全阀的内侧的金属限压层可通过调节金属的厚度来满足不同的压力范围。

[0051] 在根据本发明第三方面的锂离子二次电池中，所述锂离子二次电池可采用叠层结构，参照图1，在负极片上叠加一层隔离膜，随后在隔离膜上叠加一层正极片，随后再叠加一层负极片，如此重复叠加直至达到需要的层数，之后将极耳分别焊接到正极片和负极片的集流体上，构成锂离子二次电池正极和负极。

[0052] 在根据本发明第三方面的锂离子二次电池中，所述锂离子二次电池也可采用卷绕结构。

[0053] 本发明的锂离子二次电池的复合正极活性材料减少了氧气的产生，减缓了氧气与电解液之间发生的副反应的反应速度，同时电解液在温度升高时转变为普通蒸发，而蒸发后的气体可通过压力安全阀外喷排出，降低了锂离子二次电池在碰撞、穿刺过程中燃烧和爆炸的风险，使得使用复合正极活性材料和压力安全阀的锂离子二次电池具有良好的容量密度、倍率性能以及循环性能，同时具有良好的安全性能。且只有压力安全阀配合复合正极活性材料共同使用，才能够在锂离子二次电池热失控时抑制电解液和复合正极活性材料之间的副反应，进而使电解液蒸发并从压力安全阀外喷排出，解决锂离子二次电池的安全问题。

[0054] 接下来说明根据本发明的锂离子二次电池及其复合正极活性材料及制备方法的实施例及对比例。

[0055] 实施例1

[0056] 1.制备锂离子二次电池的复合正极活性材料

[0057] (1)将分散剂去离子水与磷酸锰锂($LiFe_{0.1}Mn_{0.9}PO_4$)的一次颗粒(图2)以1:1的体积比在行星式球磨机上混合球磨，然后在800r/min的转速下球磨分散1h，得到磷酸锰锂($LiFe_{0.1}Mn_{0.9}PO_4$)的一次颗粒的分散浆料，其中，磷酸锰锂($LiFe_{0.1}Mn_{0.9}PO_4$)的一次颗粒的粒径为3nm～10nm，BET比表面积>25m^2/g；

[0058] (2)将分散剂去离子水与锂钴系列氧化物($LiNi_{0.4}Co_{0.4}Mn_{0.2}O_2$)的二次颗粒(图2)以1:1的体积比在行星式球磨机上混合球磨，然后在200r/min的转速下球磨分散1h，得到锂钴系列氧化物($LiNi_{0.4}Co_{0.4}Mn_{0.2}O_2$)的二次颗粒的分散浆料，其中，锂钴系列氧化物($LiNi_{0.4}Co_{0.4}Mn_{0.2}O_2$)的二次颗粒的颗粒不规则系数BET×D50为4.39；

[0059] (3)将磷酸锰锂($LiFe_{0.1}Mn_{0.9}PO_4$)的一次颗粒的分散浆料加入到锂钴系列氧化物($LiNi_{0.4}Co_{0.4}Mn_{0.2}O_2$)的二次颗粒的分散浆料中，继续在200r/min的转速下球磨分散2h，使磷酸锰锂($LiFe_{0.1}Mn_{0.9}PO_4$)的一次颗粒的分散浆料与锂钴系列氧化物($LiNi_{0.4}Co_{0.4}Mn_{0.2}O_2$)的二次颗粒的分散浆料充分混合，随后逐渐降低球磨转速，当球磨转速降至50r/min时继

AMPEREX Ex. 1002
Page 980

续球磨分散 1h，进行材料复合，沉淀后除去上层清液，将余下的混合物在 150℃下鼓风干燥 12h，即得到锂离子二次电池的复合正极活性材料（图 3），其中，磷酸锰锂（$LiFe_{0.1}Mn_{0.9}PO_4$）在复合正极活性材料中的质量百分含量为 10%。

[0060] 2. 制备锂离子二次电池的正极片

[0061] 将上述复合正极活性材料、粘结剂（PVDF）、导电剂（导电炭黑）按照重量比 90:5:5 在分散剂（N- 甲基吡咯烷酮）中混合均匀，制成正极浆料，随后将正极浆料均匀涂布正极集流体铝箔（厚度为 20μm）的两面，两面涂布重量为 15mg/cm^2，干燥后经辊压、裁切、焊接极耳，制成锂离子二次电池的正极片。

[0062] 3. 制备锂离子二次电池的负极片

[0063] 将负极活性物质石墨、导电剂（乙炔黑）、粘结剂（丁苯橡胶）、增稠剂（CMC）按照重量比 95:2:2:1 在分散剂（去离子水）中充分搅拌混合均匀后，制成负极浆料，随后将负极浆料涂覆在负极集流体铜箔（厚度为 20μm）的两面，两面涂布重量为 7mg/cm^2，干燥后经辊压、裁切、焊接极耳，制成锂离子二次电池的负极片。

[0064] 4. 制备锂离子二次电池

[0065] 将制备的正极片、隔离膜（20μm 的 PE 膜）、负极片按顺序叠好，叠层得到裸电芯，之后封入金属密闭壳体中，注入非水电解液（1mol/l LiPF6，EC:DEC:EMC 的体积比为 1:1:1）并封装，得到锂离子二次电池。

[0066] 实施例 2

[0067] 1. 制备锂离子二次电池的复合正极活性材料

[0068] （1）将分散剂去离子水与磷酸锰锂（$LiFe_{0.3}Mn_{0.7}PO_4$）的一次颗粒以 1.5:1 的体积比在行星式球磨机上混合球磨，然后在 1000r/min 的转速下球磨分散 2h，得到磷酸锰锂（$LiFe_{0.3}Mn_{0.7}PO_4$）的一次颗粒的分散浆料，其中，磷酸锰锂（$LiFe_{0.3}Mn_{0.7}PO_4$）的一次颗粒的粒径为 5nm ～ 12nm，BET 比表面积 >20m^2/g；

[0069] （2）将分散剂去离子水与锂钴系列氧化物（$LiCoO_2$）的二次颗粒以 3:1 的体积比在行星式球磨机上混合球磨，然后在 400r/min 的转速下球磨分散 3h，得到锂钴系列氧化物（$LiCoO_2$）的二次颗粒的分散浆料，其中，锂钴系列氧化物（$LiCoO_2$）的二次颗粒的颗粒不规则系数 BET×D50 为 3.6；

[0070] （3）将磷酸锰锂（$LiFe_{0.3}Mn_{0.7}PO_4$）的一次颗粒的分散浆料加入到锂钴系列氧化物（$LiCoO_2$）的二次颗粒的分散浆料中，继续在 200r/min 的转速下球磨分散 2h，使磷酸锰锂（$LiFe_{0.3}Mn_{0.7}PO_4$）的一次颗粒的分散浆料与锂钴系列氧化物（$LiCoO_2$）的二次颗粒的分散浆料充分混合，随后逐渐降低球磨转速，当球磨转速降至 50r/min 时继续球磨分散 1h，进行材料复合，沉淀后除去上层清液，将余下的混合物在 150℃下鼓风加热 12h，即得到锂离子二次电池复合正极活性材料，其中，磷酸锰锂（$LiFe_{0.3}Mn_{0.7}PO_4$）的质量百分含量为 10%。

[0071] 2. 制备锂离子二次电池的正极片

[0072] 同实施例 1。

[0073] 3. 制备锂离子二次电池的负极片

[0074] 同实施例 1。

[0075] 4. 制备锂离子二次电池

[0076] 同实施例 1。

AMPEREX Ex. 1002
Page 981

[0077] 对比例 1

[0078] 依照实施例 1 的方法制备锂离子二次电池，只是在锂离子二次电池的复合正极活性材料的制备(即步骤 1)中，仅采用锂钴系列氧化物($LiNi_{0.4}Co_{0.4}Mn_{0.2}O_2$)的二次颗粒(BET×D50 为 4.39)作为锂离子二次电池的正极活性材料。

[0079] 对比例 2

[0080] 依照实施例 1 的方法制备锂离子二次电池，只是在锂离子二次电池的复合正极活性材料的制备(即步骤 1)中，将二次颗粒的颗粒不规则系数 BET×D50 为 4.39 的锂钴系列氧化物($LiNi_{0.4}Co_{0.4}Mn_{0.2}O_2$)与一次颗粒的粒径为 4μm～9μm 且 BET=8.2m^2/g 的磷酸锰锂($LiFe_{0.1}Mn_{0.9}PO_4$)直接混合，不进行材料复合处理。

[0081] 对比例 3

[0082] 依照实施例 1 的方法制备锂离子二次电池，只是在锂离子二次电池的复合正极活性材料的制备(即步骤 1)中，磷酸锰铁($LiFe_{0.1}Mn_{0.9}PO_4$)在复合正极活性材料中的质量百分含量为 70%。

[0083] 对比例 4

[0084] 依照实施例 1 的方法制备锂离子二次电池，只是在锂离子二次电池的复合正极活性材料的制备(即步骤 1)中，采用一次颗粒的颗粒不规则系数 BET×D50 为 2.4 的常见锂钴系列氧化物($LiNi_{0.4}Co_{0.4}Mn_{0.2}O_2$)作为锂离子二次电池的正极活性材料。

[0085] 最后说明本发明的锂离子二次电池及其复合正极活性材料及制备方法的测试过程以及测试结果。

[0086] (1)锂离子二次电池的充放电测试

[0087] 在常温下以 1C 倍率恒定电流充电至电压为 4.1V，随后在 4.1V 恒定电压下充电至电流为 0.05C；之后用 1C 倍率恒定电流放电至电压为 2.8V。测试锂离子二次电池的首次放电容量作为初始容量。

[0088] (2)锂离子二次电池的倍率性能测试

[0089] 在常温下以 1C 倍率恒定电流充电至电压为 4.1V，随后在 4.1V 恒定电压下充电至电流为 0.05C；之后用不同倍率(0.5C、1C、2C、3C、5C)恒定电流放电至电压为 2.8V。

[0090] 不同倍率下锂离子二次电池的容量保持率 = 不同倍率下锂离子二次电池的放电容量 / 锂钴系列氧化物作为正极活性材料的锂离子二次电池 0.5C 倍率下的放电容量 ×100%。

[0091] (3)锂离子二次电池的安全性能测试

[0092] 安全测试项目和测试标准参考《中华人民共和国汽车行业标准 / 电动汽车用锂二次蓄电池》QC/T743-2006。

[0093] (4)锂离子二次电池的循环性能测试

[0094] 在常温下以 1C 倍率恒定电流充电至电压为 4.1V，随后在 4.1V 恒定电压下充电至电流为 0.05C；之后用 1C 恒定电流放电至电压为 2.8V。以上流程为一个充放电循环，重复该流程 1000 次。

[0095] 第 1000 次循环的容量保持率 = 第 1000 次循环后的放电容量 / 首次放电容量 ×100%。

[0096] (5)锂离子二次电池的存储性能测试

AMPEREX Ex. 1002
Page 982

[0097] 将锂离子二次电池充电至 4.1V，之后在 25℃下恒温存储，测试存储 100 天后锂离子二次电池的残余电量，作为锂离子二次电池第 100 天存储后的放电容量。

[0098] 第 100 天的容量保持率 = 第 100 天存储后的放电容量 / 首次放电容量 ×100%。

[0099] (6) 锂离子二次电池的放热量测试

[0100] 加热锂离子二次电池至 500℃，进行 DSC 测试，对比锂离子二次电池的放热量与理论放热量。

[0101] 表 1 给出实施例 1-2 和对比例 1-4 的性能测试结果。

[0102] 从表 1 中可以看出，在本发明的磷酸锰锂 (LMP) 和锂钴系列氧化物填充复合而成的复合正极活性材料中，使用少量的磷酸锰锂 (LMP) 的一次颗粒填充复合到锂钴系列氧化物的二次颗粒的表面缝隙和凹坑中，制备出的锂离子二次电池具备良好的容量性能以及倍率性能，并兼备磷酸锰锂 (LMP) 的热稳定性、良好的循环性能以及存储性能。同时，锂离子二次电池还使用压力安全阀。锂钴系列氧化物的一次颗粒形成的二次颗粒的表面缝隙和凹坑被磷酸锰锂 (LMP) 的一次颗粒填充，抑制了锂离子二次电池热失控时复合正极活性材料产生氧气，进而减少了复合正极活性材料与电解液之间的副反应，且气化的电解液的气液混合物可从压力安全阀外喷排出，使锂离子二次电池的副反应停止，从而改善锂离子二次电池的安全性能。从实施例 1 和对比例 3 的对比中可以看出，当磷酸锰铁 ($LiFe_{0.1}Mn_{0.9}PO_4$) 在复合正极活性材料中的质量百分含量过高时，锂离子二次电池的倍率性能、循环性能以及存储性能均恶化，因此，当磷酸锰铁在复合正极活性材料中的质量百分含量不宜过高。

[0103] 因此，本发明的锂离子二次电池具有良好的容量密度、倍率性能、循环性能以及存储性能，同时具有良好的安全性能以及热稳定性。

AMPEREX Ex. 1002
Page 983

[0104]

表1 实施例1-2和对比例1-4的性能测试结果

	倍率性能					安全性能							循环性能	存储性能	DSC放热量			
	不同倍率下的容量保持率(%)					穿钉测试	挤压测试	跌落测试	加热测试	短路测试	过放测试	过充测试	第1000次循环后的容量保持率(%)	第100天的容量保持率(%)	放热峰(℃)	放热量(J/g)	放热变化量(%)	理论放热量加和(J/g)
	0.5C	1C	2C	3C	5C													
实施例1	100	98	98	98	98	通过	通过	通过	通过	通过	通过	通过	91	92	301.10	642.15	-19	793
实施例2	99	94	93	91	88	失败	失败	通过	通过	通过	通过	通过	89	89	320.60	689.00	-13	793
对比例1	100	98	98	98	99	失败	失败	通过	失败	通过	通过	失败	86	88	334.50	858.30	0	858
对比例2	99	98	97	97	96	失败	失败	通过	失败	通过	通过	失败	72	77	327.00	710.23	-9	793
对比例3	90	87	85	80	67	通过	通过	通过	通过	通过	通过	通过	65	66	包峰	213.50	-75	213
对比例4	100	96	93	91	89	失败	失败	通过	失败	通过	通过	失败	88	89	334.50	858.30	0	858

AMPEREX Ex. 1002
Page 984

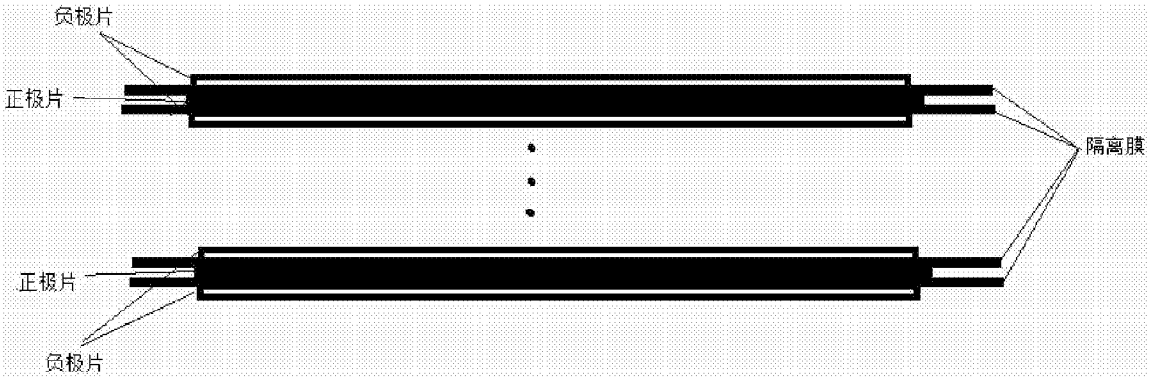
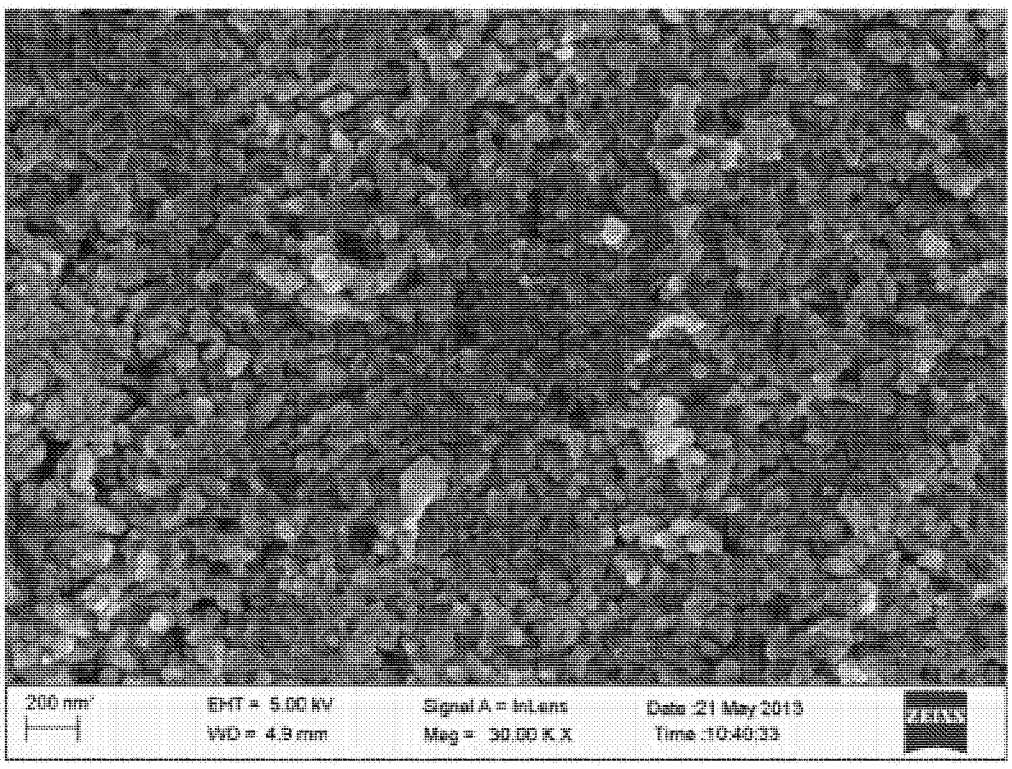


图 1

AMPEREX Ex. 1002
Page 985

$LiFe_{0.1}Mn_{0.9}PO_4$



$LiNi_{0.4}Co_{0.4}Mn_{0.2}O_2$

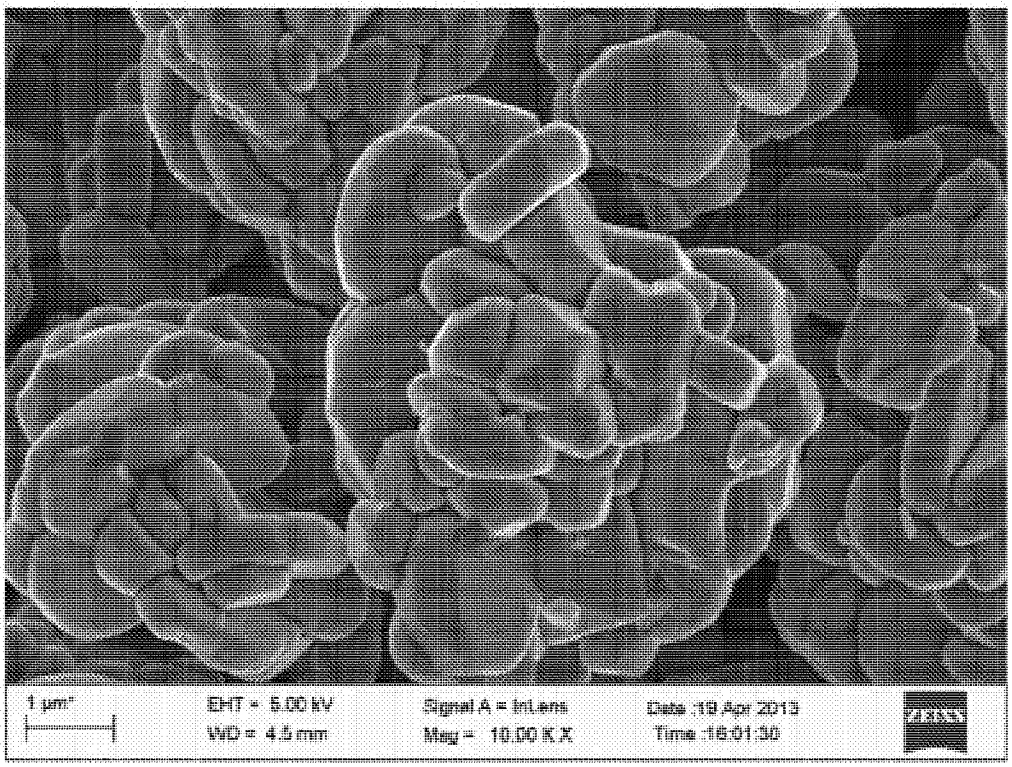


图 2

AMPEREX Ex. 1002
Page 986

复合正极活性材料

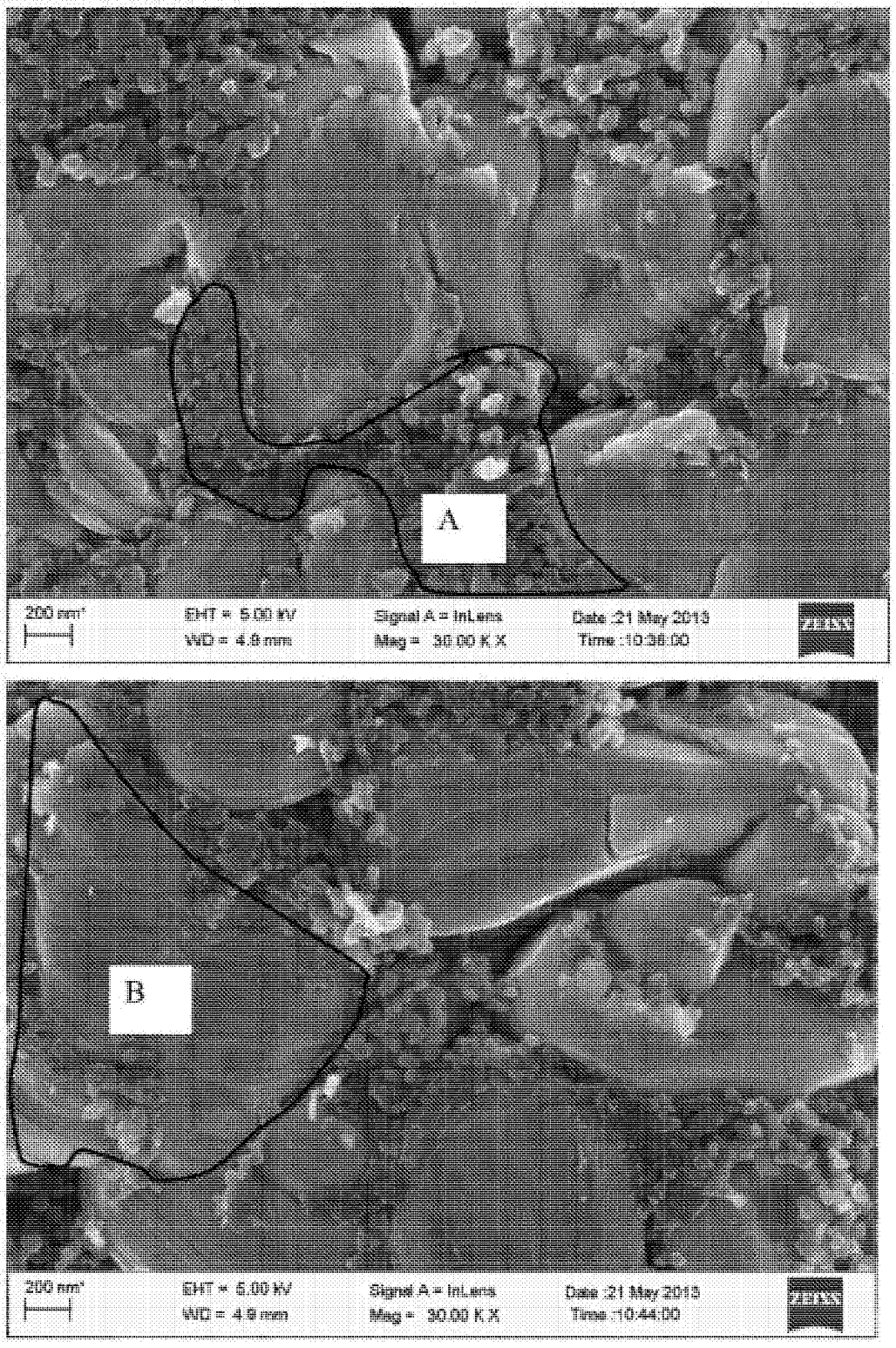


图 3

AMPEREX Ex. 1002
Page 987

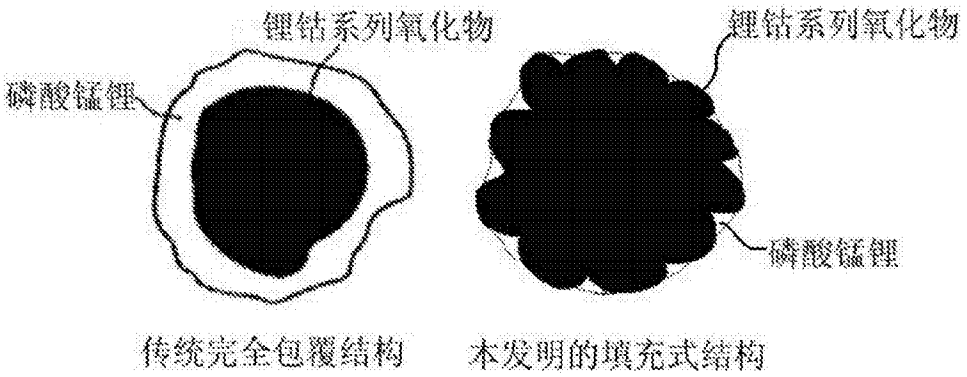


图 4

AMPEREX Ex. 1002
Page 988

CN105024047A Lithium ion secondary battery, composite positive electrode active material thereof and preparation method

The EPO does not accept responsibility for the accuracy of data originating from authorities other than the EPO, nor does it guarantee that such data is complete, up-to-date or fit for specific purposes.

[0001] Technical field

[0002] The present invention relates to the field of batteries, and in particular to a lithium ion secondary battery and a composite positive active material thereof and a preparation method thereof.

[0003] Background technique

[0004] Lithium ion secondary batteries are widely used in various fields due to their good electrochemical performance, such as mobile phones, computers, power tools, and electric vehicles. The safety performance of lithium ion secondary batteries is the most important performance in addition to electrical and chemical properties, which determines the safety and reliability of equipment using lithium ion secondary batteries, and is closely related to the safety of life and property of consumers.

[0005] The safety problem of lithium ion secondary batteries is mainly caused by various types of thermal runaway problems, such as lithium ion secondary battery fire and explosion caused by an increase in the temperature of the internal short circuit.

[0006] Common transition metal oxide positive active materials generally have good electrochemical properties, but most of them decompose and release oxygen at high temperatures, and are used as flammable components such as electrolytes and separators in sealed lithium ion secondary batteries. The combustion improver causes the lithium ion secondary battery to burn and explode.

[0007] At present, in order to solve this problem and to meet safety requirements, a positive electrode active material having good safety but poor electrochemical performance, such as a positive electrode active material of a phosphate series (such as lithium iron phosphate having an olivine structure), is usually used. The positive electrode active material of the phosphate series does not generate a large amount of oxygen at a high temperature, so that it does not react with the electrolyte. In the sealed lithium ion secondary battery, even if the electrolyte reaches the ignition point, the lithium ion secondary battery will not be burned and exploded due to the supply of no oxygen, but the lithium ion will be generated when the evaporation of the electrolyte reaches a certain level. The secondary battery produces an expansion explosion. A common solution is to provide a pressure relief valve on a lithium ion secondary battery to control the pressure generated by the vaporization of the electrolyte in the lithium ion secondary battery. When the pressure in the lithium ion secondary battery exceeds a critical value, When the pressure safety valve is opened, the vaporized electrolyte can be released to the outside of the lithium ion secondary battery, and after the vaporized electrolyte is externally sprayed, the interior of the lithium ion secondary battery is dried due to the loss of the electrolyte, and the ion transfer between the pole pieces is performed. The medium disappears, and the reaction in the lithium ion secondary battery is terminated, and

combustion and explosion do not occur, thereby ensuring the safety of the entire battery pack of the lithium ion secondary battery even when it is used in the battery pack.

[0008] However, the electrochemical activity of the positive electrode active material of the phosphate series is inferior, and the rate performance of the lithium ion secondary battery using the phosphate series positive electrode active material is severely limited, thereby limiting its development as a power battery in related fields.

[0009] At present, the high electrochemical performance positive electrode active materials used in power lithium ion secondary batteries mainly include lithium nickel cobalt manganese oxide (NCM) ternary materials, lithium nickel cobalt aluminum oxide (NCA), etc., although they have higher electrochemical properties. Performance, but poor safety performance, limits the application of high performance lithium ion secondary batteries.

[0010] Summary of the invention

[0011] In view of the problems in the background art, an object of the present invention is to provide a lithium ion secondary battery, a composite positive electrode active material thereof, and a preparation method thereof, which have good capacity density, rate performance, cycle performance, and Storage performance, while also having good security and thermal stability.

[0012] In order to achieve the above object, in a first aspect of the invention, the present invention provides a composite positive electrode active material of a lithium ion secondary battery which is composed of a lithium cobalt series oxide and a lithium manganese

phosphate (LMP). The composite positive active material has a packed structure; the filled structure is that the primary particles of the lithium manganese phosphate (LMP) are filled and composited into surface gaps and pits of the secondary particles of the lithium cobalt series oxide; The lithium cobalt series oxide has a chemical formula of LiA x Co 1-x O 2 , wherein $0 \leq x < 1$, and A is Ni, Mn, Al, Mg, Ca, Cr, Zr, Mo, Ag, Nb. At least one of the lithium manganese phosphate (LMP) has a chemical formula of LiB y Mn 1-y PO 4 , wherein $0 \leq y < 1$, and B is Ni, Co, Fe, Al, Ca, Zn, At least one of Mg, Mo, Pb, and Zr.

[0013] In a second aspect of the invention, the present invention provides a method for preparing a composite positive active material for a lithium ion secondary battery, which is used for preparing a composite positive active material for a lithium ion secondary battery according to the first aspect of the present invention. The method comprises the steps of: (1) mixing the dispersing agent deionized water with the primary particles of lithium manganese phosphate (LMP) in a volume ratio of 1:1 to 3:1, and then rotating at a speed of 800 r/min to 1000 r/min. The ball mill is dispersed for 1 h to 2 h to obtain a dispersion slurry of primary particles of lithium manganese phosphate (LMP), wherein the lithium manganese phosphate (LMP) has a chemical formula of LiB y Mn 1-y PO 4 , wherein $0 \leq y < 1$, B is at least one of Ni, Co, Fe, Al, Ca, Zn, Mg, Mo, Pb, Zr; (2) dispersing agent deionized water and secondary particles of lithium cobalt series oxide The volume ratio of 1:1~3:1 is mixed with ball mill, then ball milled at 200r/min~400r/min for 1h~3h, and the secondary particles of lithium cobalt series oxide are dispersed into dispersant to obtain lithium cobalt. a dispersion slurry of secondary particles of a series of oxides, wherein the chemistry of the lithium cobalt series oxide The general formula is LiA x Co 1-x O 2 , wherein $0 \leq x < 1$, and A is at least one of Ni, Mn, Al, Mg, Ca, Cr, Zr, Mo, Ag, Nb; (3) Adding a dispersion slurry of primary particles of lithium manganese phosphate (LMP) to a dispersion slurry of secondary particles of lithium

cobalt series oxide, and continuously performing ball milling dispersion at a rotation speed of 200 r/min to 400 r/min for 2 to 4 hours. The dispersed slurry of the primary particles of lithium manganese phosphate (LMP) is thoroughly mixed with the dispersed slurry of the secondary particles of the lithium cobalt series oxide, and then the ball milling speed is gradually lowered, and the ball milling speed is decreased to 50 r/min to 200 r/min. The ball mill is dispersed for 0.5 h to 4 h, and the material is compounded. After the precipitation, the supernatant liquid is removed, and the remaining mixture is air-dried at 100 ° C to 200 ° C for 12 h to obtain a composite positive electrode active material of a lithium ion secondary battery. The composite positive electrode active material has a packed structure in which primary particles of the lithium manganese phosphate (LMP) are filled and compounded into surface slits and pits of secondary particles of the lithium cobalt series oxide.

[0014] In a third aspect of the invention, the present invention provides a lithium ion secondary battery comprising: a positive electrode sheet containing a positive electrode active material; a negative electrode sheet; a separator, spaced between the positive electrode sheet and the negative electrode sheet; and a nonaqueous electrolyte And a lithium ion secondary battery case containing a pressure relief valve. The positive active material is a composite positive active material of a lithium ion secondary battery according to the first aspect of the present invention.

[0015] The beneficial effects of the present invention are as follows:

[0016] 1.The composite positive electrode active material of the lithium ion secondary battery of the present invention can alleviate side reactions between the electrolyte and the lithium cobalt series oxide, and improve the cycle performance and storage performance of

the lithium ion secondary battery. The high temperature stability of the composite positive electrode active material also makes the evaporation and gasification process of the electrolyte become dominant when the lithium ion secondary battery is out of control, and the electrolyte is vaporized and discharged from the pressure safety valve of the lithium ion secondary battery. The redox reaction of the electrolyte and the positive electrode sheet is stopped, thereby reducing the risk of burning and explosion of the lithium ion secondary battery during collision and puncture, thereby improving the safety performance of the lithium ion secondary battery.

[0017] 2.The composite positive electrode active material of the lithium ion secondary battery of the present invention can be filled into the surface gaps and pits of the secondary particles of the lithium cobalt series oxide by a simple method using a small amount of primary particles of lithium manganese phosphate (LMP). Since lithium manganese phosphate (LMP) is not completely coated with lithium cobalt series oxides, it maintains high rate performance of lithium cobalt series oxides, and since lithium manganese phosphate (LMP) is used in a small amount, lithium ions are not reduced twice. The energy density of the battery. At the same time, the lithium manganese phosphate (LMP) in the composite positive active material covers the active sites on the surface of the lithium cobalt oxide, so that the composite positive active material has good thermal stability and chemical stability, so the lithium ion can have two times at the same time. Good rate performance, high energy density and good safety.

[0018] DRAWINGS

[0019] Fig. 1 is a schematic view showing the structure of a lithium ion secondary battery using the composite positive electrode active material of the present invention.

[0020] Fig. 2 is a scanning electron micrograph of primary particles of lithium manganese phosphate (LiFe 0.1 Mn 0.9 PO 4) and secondary particles of lithium cobalt series oxide (LiNi 0.4 Co 0.4 Mn 0.2 O 2) according to Example 1 of the present invention.

[0021] 3 is a scanning electron micrograph of different positions of particles of the composite positive electrode active material of Example 1 of the present invention at the same multiple, wherein A is a primary particle of lithium manganese phosphate (LiFe 0.1 Mn 0.9 PO 4), and B is lithium. Secondary particles of a cobalt series oxide (LiNi 0.4 Co 0.4 Mn 0.2 O 2).

[0022] Fig. 4 is a schematic view showing a conventional full-clad structure of a composite positive electrode active material and a packed structure of the present invention.

[0023] Detailed ways

[0024] Hereinafter, a lithium ion secondary battery and a composite positive electrode active material thereof according to the present invention, a preparation method thereof, and examples, comparative examples, and test results will be described in detail.

[0025] First, a composite positive electrode active material of a lithium ion secondary battery according to the first aspect of the invention will be described.

[0026] The composite positive electrode active material of the lithium ion secondary battery according to the first aspect of the present invention is a composite of a lithium cobalt oxide and a lithium manganese phosphate (LMP). The composite positive active material has a packed structure; the filled structure is that the primary particles of the lithium manganese phosphate (LMP) are filled and composited into surface gaps and pits of the secondary particles of the lithium cobalt series oxide; The lithium cobalt series oxide has a chemical formula of LiA x Co 1-x O 2 , wherein $0 \leq x < 1$, and A is Ni, Mn, Al, Mg, Ca, Cr, Zr, Mo, Ag, Nb. At least one of the lithium manganese phosphate (LMP) has a chemical formula of LiB y Mn 1-y PO 4 , wherein $0 \leq y < 1$, and B is Ni, Co, Fe, Al, Ca, Zn, At least one of Mg, Mo, Pb, and Zr.

[0027] In the composite positive electrode active material of the lithium ion secondary battery according to the first aspect of the present invention, the secondary particles of the lithium cobalt series oxide are formed by aggregation of primary particles, and the secondary of the lithium cobalt series oxide The surface of the particles is rough (there are gaps and pits on the surface) and the specific surface area of the secondary particles is larger than the specific surface area of the primary particles. Therefore, the rate performance of the composite positive electrode active material can be remarkably improved. The disadvantages of using the lithium cobalt series oxide of the present invention alone are: (1) the safety problem is more serious, and the surface energy between the particle interface of the secondary particles of the lithium cobalt series oxide of the present invention and the edge of the primary particle is higher. High, when the lithium ion secondary battery is out of control, it loses heat more quickly, and then oxygen reacts with the electrolyte to release a large amount of heat, causing the lithium ion secondary battery to burn and explode, so the safety performance is poor; (2) cycle performance And the storage performance is degraded. Since

the lithium cobalt series oxide of the present invention has high surface energy, the reaction speed of the side reaction between the electrolyte and the electrolyte is accelerated, and a gas such as an alkane, an olefin or a carbon dioxide is generated, resulting in lithium ion II. The cycle performance and storage performance of the secondary battery are degraded.

[0028] When lithium manganese phosphate (LMP) is used alone, the thermal stability and chemical stability of lithium manganese phosphate (LMP) are high due to the high chemical stability of the phosphate ion structure, even if the lithium ion secondary battery is in a high temperature environment. The possibility of releasing oxygen is also very small. In addition, lithium manganese phosphate (LMP) has a small change in lattice parameters during charge and discharge, and its reaction rate with the side reaction of the electrolyte is also very slow, so the cycle performance and storage performance of the lithium ion secondary battery are better. However, there are also some shortcomings: (1) Lithium manganese phosphate (LMP) has low conductivity, and the lithium ion secondary battery using it as a positive electrode active material has poor rate performance and cannot satisfy lithium ion secondary battery as power. The parameter requirements of the battery; (2) The lower conductivity of lithium manganese phosphate (LMP) makes it necessary to be made into primary particles to increase its conductivity, so its specific surface area is greatly increased, and lithium is used as a positive electrode active material. The amount of the conductive agent and the binder required for the ion secondary battery is also greatly increased, resulting in a decrease in the specific capacity of the positive electrode sheet, affecting the capacity density and energy density of the lithium ion secondary battery.

[0029] In the present invention, the composite positive electrode active material which is compounded by lithium cobalt series oxide and lithium manganese phosphate (LMP) can

avoid the disadvantages of both, and at the same time exert the advantages of both, and has good capacity density. And rate performance, but also good stability, cycle performance and storage performance. Referring to the right diagram of FIG. 4, the primary particles of lithium manganese phosphate (LMP) are not simply mixed, nor completely coated, but filled with surface gaps and pits of secondary particles compounded to the lithium cobalt series oxide. in. If it is only a simple mixing, the inhibitory effect of lithium manganese phosphate (LMP) on the side reaction between the lithium cobalt series oxide and the electrolyte is not obvious, and it can not provide enough time for the electrolyte to evaporate and discharge, so that it cannot be reached. Expected improvements in safety performance. If the conventional full coating method is adopted, referring to the left diagram of FIG. 4, the safety performance of the lithium ion secondary battery can be remarkably improved, however, since the lithium manganese phosphate (LMP) completely covers the lithium cobalt series oxide in the cladding structure. The surface makes the surface characteristics of the lithium cobalt series oxides be characterized by lithium manganese phosphate (LMP), which lowers the rate performance of the composite positive electrode active material.

[0030] In the composite positive electrode active material of the lithium ion secondary battery according to the first aspect of the invention, the particle irregularity BET × D50 of the secondary particles of the lithium cobalt series oxide may be >3.5. The primary particles of the lithium-cobalt series oxide have a particle irregularity coefficient BET × D50 of 2.0 to 3.0. That is to say, the lithium cobalt series oxide of the same particle diameter, the secondary particle of the lithium cobalt series oxide of the invention is 25% to 100% larger than the specific surface area of the primary particles of the common lithium cobalt series oxide, thereby significantly improving the composite The rate performance of the positive active material.

[0031] In the composite positive electrode active material of the lithium ion secondary battery according to the first aspect of the present invention, the mass percentage of the lithium manganese phosphate (LMP) in the composite positive electrode active material may be 1% to 40%. .

[0032] In the composite positive electrode active material of the lithium ion secondary battery according to the first aspect of the present invention, the mass percentage of the lithium manganese phosphate (LMP) in the composite positive electrode active material may be 10% to 20%. .

[0033] In the composite positive electrode active material of the lithium ion secondary battery according to the first aspect of the present invention, the primary particles of the lithium manganese phosphate (LMP) may have a particle diameter of 0.1 nm to 50 nm, and the BET specific surface area may be >20 m 2 . /g.

[0034] Next, a method of preparing a composite positive electrode active material of a lithium ion secondary battery according to a second aspect of the present invention will be described.

[0035] A method for preparing a composite positive electrode active material for a lithium ion secondary battery according to a second aspect of the present invention, which is used for preparing a composite positive electrode active material for a lithium ion secondary battery of the first aspect of the invention, comprising the steps of: (1) dispersing a dispersant The primary particles of deionized water and lithium manganese phosphate (LMP) are mixed by a

ball mill at a volume ratio of 1:1 to 3:1, and then ball-milled at 800 r/min to 1000 r/min for 1 h to 2 h to obtain lithium manganese phosphate (a primary particle dispersion slurry of LMP), wherein the lithium manganese phosphate (LMP) has a chemical formula of LiB y Mn 1-y PO 4 , $0 \leq y < 1$, and B is Ni, Co, Fe, Al, At least one of Ca, Zn, Mg, Mo, Pb, and Zr; (2) mixing the dispersing agent deionized water and the secondary particles of the lithium cobalt series oxide in a volume ratio of 1:1 to 3:1 by ball milling, Then, the ball is dispersed at a rotation speed of 200 r/min to 400 r/min for 1 to 3 hours, and the secondary particles of the lithium cobalt series oxide are dispersed in a dispersant to obtain a dispersion slurry of a lithium cobalt series oxide, wherein the lithium The chemical formula of the cobalt series oxide is LiA x Co 1-x O 2 , wherein $0 \leq x < 1$, A is Ni, At least one of Mn, Al, Mg, Ca, Cr, Zr, Mo, Ag, Nb; (3) adding a dispersion slurry of primary particles of lithium manganese phosphate (LMP) to the lithium cobalt series oxide In the dispersed slurry of the particles, the ball mill is continuously dispersed at a rotation speed of 200 r/min to 400 r/min for 2 to 4 hours, so that the primary particle dispersion slurry of lithium manganese phosphate (LMP) and the secondary particles of the lithium cobalt series oxide are used. The dispersed slurry is thoroughly mixed, and then the ball milling speed is gradually decreased. When the ball milling speed is reduced to 50 r/min to 200 r/min, the ball milling is continued for 0.5 h to 4 h, the material is compounded, and the supernatant is removed after precipitation, and the remaining mixture is further The composite cathode active material of the lithium ion secondary battery is obtained by blast drying at 100 ° C to 200 ° C for 12 hours, wherein the composite cathode active material has a packed structure, and the filled structure is the lithium manganese phosphate (LMP) The primary particle filling is compounded into the surface gaps and pits of the secondary particles of the lithium cobalt series oxide.

[0036] A lithium ion secondary battery according to a third aspect of the invention will be described again.

[0037] A lithium ion secondary battery according to a third aspect of the present invention, comprising: a positive electrode sheet containing a positive electrode active material; a negative electrode sheet; a separator, spaced between the positive electrode sheet and the negative electrode sheet; a nonaqueous electrolyte; and lithium An ion secondary battery case (not shown) includes a pressure relief valve (not shown). The positive electrode active material is a composite positive electrode active material of the lithium ion secondary battery according to the first aspect of the invention.

[0038] In the lithium ion secondary battery according to the third aspect of the invention, the positive electrode sheet may include a positive electrode current collector and a positive electrode film.

[0039] In the lithium ion secondary battery according to the third aspect of the invention, the positive electrode film may comprise a composite positive electrode active material, a binder, a conductive agent, and a dispersant.

[0040] In the lithium ion secondary battery according to the third aspect of the invention, the cathode current collector may be an aluminum foil.

[0041] In the lithium ion secondary battery according to the third aspect of the invention, the binder in the positive electrode film may be polyvinylidene fluoride (PVDF).

[0042] In the lithium ion secondary battery according to the third aspect of the invention, the electroconductive agent in the positive electrode film may be conductive carbon black, acetylene black, high carbon, graphite microplate or graphite fiber.

[0043] In the lithium ion secondary battery according to the third aspect of the invention, the dispersing agent in the positive electrode film may be N-methylpyrrolidone.

[0044] In the lithium ion secondary battery according to the third aspect of the invention, the negative electrode sheet may include a negative electrode current collector and a negative electrode film.

[0045] In the lithium ion secondary battery according to the third aspect of the invention, the negative electrode film may include a negative electrode active material, a binder, a conductive agent, and a dispersing agent.

[0046] In the lithium ion secondary battery according to the third aspect of the invention, the anode current collector may be a copper foil.

[0047] In the lithium ion secondary battery according to the third aspect of the invention, the binder in the negative electrode film may be styrene-butadiene rubber.

[0048] In the lithium ion secondary battery according to the third aspect of the invention, the conductive agent in the negative electrode film may be conductive carbon black, acetylene black, high carbon, graphite microplate or graphite fiber.

[0049] In the lithium ion secondary battery according to the third aspect of the invention, the dispersing agent in the negative electrode membrane may be deionized water.

[0050] In the lithium ion secondary battery according to the third aspect of the invention, the negative electrode sheet may contain a material that stores and releases lithium ions.

[0051] In the lithium ion secondary battery according to the third aspect of the invention, the material for storing and releasing lithium ions in the negative electrode sheet may be metallic lithium, graphite, hard carbon or lithium titanate.

[0052] In the lithium ion secondary battery according to the third aspect of the invention, the separator may be a PP film, a PE film or a PP/PE composite film.

[0053] In the lithium ion secondary battery according to the third aspect of the present invention, the pressure relief valve may be a pressure limiting valve which can well control the pressure inside the lithium ion secondary battery and greatly reduce the lithium ion secondary battery The internal pressure rises to cause a risk of expansion and explosion, such as an increase in internal pressure caused by a gas generated by a side reaction when a lithium ion secondary battery operates at a high temperature. When the pressure inside the lithium ion secondary battery reaches a certain value, the pressure relief valve is opened, and the gas outside the lithium ion secondary battery is discharged.

[0054] In the lithium ion secondary battery according to the third aspect of the invention, the pressure relief valve may have a pressure in the range of 2 MPa to 4 MPa.

[0055] In the lithium ion secondary battery according to the third aspect of the invention, the inside of the pressure relief valve may be a metal pressure limiting layer, and the outer side may be a polymer protective layer. The metal pressure limiting layer on the inside of the pressure relief valve can be adjusted to different pressure ranges by adjusting the thickness of the metal.

[0056] In the lithium ion secondary battery according to the third aspect of the present invention, the lithium ion secondary battery may have a laminated structure. Referring to FIG. 1, a separator is superposed on the negative electrode sheet, and then a positive electrode is laminated on the separator. The sheet is then superposed with a layer of negative electrode, and the stack is repeated until the desired number of layers is reached, and then the tabs are respectively welded to the current collectors of the positive electrode and the negative electrode to constitute a positive electrode and a negative electrode of the lithium ion secondary battery.

[0057] In the lithium ion secondary battery according to the third aspect of the invention, the lithium ion secondary battery may also adopt a winding structure.

[0058] The composite positive electrode active material of the lithium ion secondary battery of the invention reduces the generation of oxygen, slows down the reaction speed of the side reaction between the oxygen and the electrolyte, and at the same time, the electrolyte changes to ordinary evaporation and evaporates when the temperature rises. The rear gas can be discharged through the pressure safety valve, which reduces the risk of burning and explosion of the lithium ion secondary battery during collision and puncture, so that the lithium ion secondary battery using the composite positive active material and the pressure safety valve

has good performance. Capacity density, rate performance and cycle performance, while having good safety performance. Only when the pressure safety valve is used together with the composite positive active material can the side reaction between the electrolyte and the composite positive active material be suppressed during the thermal runaway of the lithium ion secondary battery, thereby evaporating the electrolyte and spraying from the pressure safety valve. Discharge, solve the safety problem of lithium ion secondary batteries.

[0059] Next, examples and comparative examples of the lithium ion secondary battery, the composite positive electrode active material thereof, and the preparation method according to the present invention will be described.

[0060] Example 1

[0061] 1.Composite cathode active material for preparing lithium ion secondary battery

[0062] (1) The dispersing agent deionized water and the primary particles of lithium manganese phosphate (LiFe 0.1 Mn 0.9 PO 4) (Fig. 2) were mixed in a planetary ball mill at a volume ratio of 1:1, and then ball milled at 800 r/min. 1h, a dispersion slurry of primary particles of lithium manganese phosphate (LiFe 0.1 Mn 0.9 PO 4) is obtained, wherein the primary particles of lithium manganese phosphate (LiFe 0.1 Mn 0.9 PO 4) have a particle diameter of 3 nm to 10 nm, and the BET specific surface area > 25m 2 /g;

[0063] (2) Dispersing agent deionized water and lithium cobalt series oxide (LiNi 0.4 Co 0.4 Mn 0.2 O 2) secondary particles (Fig. 2) were mixed in a planetary ball mill at a volume ratio of 1:1, then at 200 r/min. The ball mill was dispersed at a rotation speed for 1 hour to

obtain a dispersion slurry of a secondary particle of a lithium cobalt series oxide (LiNi 0.4 Co 0.4 Mn 0.2 O 2), wherein the lithium cobalt series oxide (LiNi 0.4 Co 0.4 Mn 0.2 O 2) The particle irregularity coefficient BET × D50 of the secondary particles is 4.39;

[0064] （3） A dispersion slurry of primary particles of lithium manganese phosphate (LiFe 0.1 Mn 0.9 PO 4) is added to a dispersion slurry of secondary particles of lithium cobalt series oxide (LiNi 0.4 Co 0.4 Mn 0.2 O 2), and continues at 200 r/ The ball mill was dispersed at a speed of min for 2 h to disperse the slurry of the primary particles of lithium manganese phosphate (LiFe 0.1 Mn 0.9 PO 4) and the secondary particles of lithium cobalt series oxide (LiNi 0.4 Co 0.4 Mn 0.2 O 2). The material is thoroughly mixed, and then the ball milling speed is gradually reduced. When the ball milling speed is reduced to 50 r/min, the ball milling is continued for 1 h, the material is compounded, the supernatant is removed after precipitation, and the remaining mixture is blast dried at 150 ° C for 12 h. A composite positive electrode active material of a lithium ion secondary battery (Fig. 3), wherein lithium manganese phosphate (LiFe 0.1 Mn 0.9 PO 4) has a mass percentage of 10% in the composite positive electrode active material.

[0065] 2.Preparation of positive electrode sheets for lithium ion secondary batteries

[0066] The composite positive electrode active material, the binder (PVDF), and the conductive agent (conductive carbon black) are uniformly mixed in a dispersing agent (N-methylpyrrolidone) at a weight ratio of 90:5:5 to prepare a positive electrode slurry, and then The positive electrode slurry was uniformly coated on both sides of a positive electrode current collector aluminum foil (thickness: 20 μm), and the coating weight on both sides was

15 mg/cm 2 . After drying, the roller was pressed, cut, and welded to form a lithium ion secondary battery. Positive electrode sheet.

[0067] 3.Preparation of negative electrode sheets for lithium ion secondary batteries

[0068] The anode active material graphite, the conductive agent (acetylene black), the binder (styrene-butadiene rubber), and the thickener (CMC) are thoroughly stirred and mixed in a dispersing agent (deionized water) at a weight ratio of 95:2:2:1. After uniformization, a negative electrode slurry was prepared, and then the negative electrode slurry was coated on both sides of a negative electrode current collector copper foil (thickness: 20 μm), and the coating weight on both sides was 7 mg/cm 2 , and after drying, rolling, cutting, and welding were performed. The ear piece is made into a negative electrode sheet of a lithium ion secondary battery.

[0069] 4.Preparation of lithium ion secondary battery

[0070] The prepared positive electrode sheet, separator (20 μm PE film), and negative electrode sheet were stacked in this order, laminated to obtain a bare cell, and then sealed in a metal sealed case, and a non-aqueous electrolyte (1 mol/l LiPF6, EC: DEC: EMC has a volume ratio of 1:1:1) and is packaged to obtain a lithium ion secondary battery.

[0071] Example 2

[0072] 1.Composite cathode active material for preparing lithium ion secondary battery

[0073] （1）The primary particles of dispersant deionized water and lithium manganese phosphate (LiFe 0.3 Mn 0.7 PO 4) were mixed by a ball mill in a volume ratio of 1.5:1 on a planetary ball mill, and then ball milled at 1000 r/min for 2 h to obtain phosphoric acid. a dispersion slurry of primary particles of lithium manganese (LiFe 0.3 Mn 0.7 PO 4), wherein the primary particles of lithium manganese phosphate (LiFe 0.3 Mn 0.7 PO 4) have a particle diameter of 5 nm to 12 nm and a BET specific surface area of >20 m 2 /g ;

[0074] （2）The dispersant deionized water and the secondary particles of lithium cobalt series oxide (LiCoO 2) were mixed in a planetary ball mill at a volume ratio of 3:1, and then ball milled at 400 r/min for 3 h to obtain lithium cobalt. a dispersion of secondary particles of a series of oxides (LiCoO 2), wherein the secondary particles of the lithium cobalt series oxide (LiCoO 2) have a particle irregularity coefficient BET × D50 of 3.6;

[0075] （3）A dispersion slurry of primary particles of lithium manganese phosphate (LiFe 0.3 Mn 0.7 PO 4) is added to a dispersion slurry of secondary particles of lithium cobalt series oxide (LiCoO 2), and ball milling dispersion is continued at a rotation speed of 200 r/min. 2h, the dispersion slurry of the primary particles of lithium manganese phosphate (LiFe 0.3 Mn 0.7 PO 4) and the secondary particles of the lithium cobalt series oxide (LiCoO 2) are thoroughly mixed, and then the ball milling speed is gradually lowered, when the ball mill When the rotation speed is reduced to 50r/min, the ball milling is continued for 1 hour, and the material is compounded. After the precipitation, the supernatant liquid is removed, and the remaining mixture is heated by blasting at 150 ° C for 12 hours to obtain a lithium ion secondary battery composite cathode active material. The mass percentage of lithium manganese phosphate (LiFe 0.3 Mn 0.7 PO 4) was 10%.

[0076] 2.Preparation of positive electrode sheets for lithium ion secondary batteries

[0077] Same as Example 1.

[0078] 3.Preparation of negative electrode sheets for lithium ion secondary batteries

[0079] Same as Example 1.

[0080] 4.Preparation of lithium ion secondary battery

[0081] Same as Example 1.

[0082] Comparative example 1

[0083] A lithium ion secondary battery was prepared according to the method of Example 1, except that in the preparation of the composite positive electrode active material of the lithium ion secondary battery (ie, step 1), only lithium cobalt series oxide (LiNi 0.4 Co 0.4 Mn 0.2 O 2 was used). The secondary particles (BET × D50 is 4.39) are used as a positive electrode active material of a lithium ion secondary battery.

[0084] Comparative example 2

[0085] A lithium ion secondary battery was prepared according to the method of Example 1, except that in the preparation of the composite positive electrode active material of the lithium ion secondary battery (ie, step 1), the lithium particle having an irregular coefficient

of BET × D50 of 4.39 was used. The cobalt series oxide (LiNi 0.4 Co 0.4 Mn 0.2 O 2) is directly mixed with lithium manganese phosphate (LiFe 0.1 Mn 0.9 PO 4) having a primary particle diameter of 4 μm to 9 μm and a BET=8.2 m 2 /g, and no material is used. Compound processing.

[0086] Comparative example 3

[0087] A lithium ion secondary battery was prepared according to the method of Example 1, except that in the preparation of the composite positive electrode active material of the lithium ion secondary battery (ie, step 1), the ferromanganese phosphate (LiFe 0.1 Mn 0.9 PO 4) was used in the composite positive electrode active material. The mass percentage in the medium is 70%.

[0088] Comparative example 4

[0089] A lithium ion secondary battery was prepared according to the method of Example 1, except that in the preparation of the composite positive electrode active material of the lithium ion secondary battery (ie, step 1), the common lithium having a particle irregularity coefficient BET × D50 of 2.4 was used. A cobalt series oxide (LiNi 0.4 Co 0.4 Mn 0.2 O 2) is used as a positive electrode active material of a lithium ion secondary battery.

[0090] Finally, the testing process and test results of the lithium ion secondary battery of the present invention and the composite positive electrode active material and the preparation method thereof will be described.

[0091] （1）Charge and discharge test of lithium ion secondary battery

[0092] The battery was charged at a constant current of 1 C at a normal temperature to a voltage of 4.1 V, and then charged to a current of 0.05 C at a constant voltage of 4.1 V; thereafter, a constant current was discharged at a rate of 1 C to a voltage of 2.8 V. The first discharge capacity of the lithium ion secondary battery was tested as the initial capacity.

[0093] （2）Magnification performance test of lithium ion secondary battery

[0094] At a constant temperature, the battery is charged at a constant current of 1 C to a voltage of 4.1 V, and then charged to a current of 0.05 C at a constant voltage of 4.1 V; thereafter, a constant current is discharged to a voltage with different magnifications (0.5 C, 1 C, 2 C, 3 C, 5 C). It is 2.8V.

[0095] Capacity retention rate of lithium ion secondary battery at different magnifications = discharge capacity of lithium ion secondary battery at different magnifications / lithium cobalt secondary oxide discharge capacity at 0.5C rate of lithium ion secondary battery as positive electrode active material × 100% .

[0096] （3）Safety test of lithium ion secondary battery

[0097] The safety test items and test standards refer to "Automotive Industry Standards of the People's Republic of China / Lithium Secondary Batteries for Electric Vehicles" QC/T743-2006.

[0098] (4) Cyclic performance test of lithium ion secondary battery

[0099] It was charged at a constant current of 1 C at a normal temperature to a voltage of 4.1 V, and then charged to a current of 0.05 C at a constant voltage of 4.1 V; thereafter, it was discharged with a constant current of 1 C to a voltage of 2.8 V. The above process is a charge and discharge cycle, and the process is repeated 1000 times.

[0100] Capacity retention rate at the 1000th cycle = discharge capacity after the 1000th cycle / first discharge capacity × 100%.

[0101] (5) Storage performance test of lith ium ion secondary battery

[0102] The lithium ion secondary battery was charged to 4.1 V, and then stored at a constant temperature at 25 ° C, and the residual electric quantity of the lithium ion secondary battery after 100 days of storage was tested as the discharge capacity after storage on the 100th day of the lithium ion secondary battery.

[0103] Capacity retention rate on the 100th day = discharge capacity after storage on the 100th day / initial discharge capacity × 100%.

[0104] (6) Lithium ion seco ndary battery heat release test

[0105] The lithium ion secondary battery was heated to 500 ° C, and a DSC test was performed to compare the heat release amount and the theoretical heat release amount of the lithium ion secondary battery.

[0106] Table 1 gives the performance test results of Examples 1-2 and Comparative Examples 1-4.

[0107] As can be seen from Table 1, in the composite positive electrode active material in which the lithium manganese phosphate (LMP) and the lithium cobalt series oxide of the present invention are filled and filled, a small amount of primary particles of lithium manganese phosphate (LMP) are used to fill and compound. In the surface gaps and pits of the secondary particles of the lithium cobalt series oxide, the prepared lithium ion secondary battery has good capacity performance and rate performance, and has thermal stability and good circulation of lithium manganese phosphate (LMP). Performance and storage performance. At the same time, lithium ion secondary batteries also use pressure relief valves. The surface gaps and pits of the secondary particles formed by the primary particles of the lithium cobalt series oxide are filled with primary particles of lithium manganese phosphate (LMP), which suppress the generation of oxygen in the composite positive active material when the lithium ion secondary battery is thermally out of control, thereby reducing A side reaction between the composite positive electrode active material and the electrolyte, and the gas-liquid mixture of the vaporized electrolyte can be discharged from the outside of the pressure safety valve to stop the side reaction of the lithium ion secondary battery, thereby improving the lithium ion secondary Battery safety performance. From the comparison of Example 1 and Comparative Example 3, it can be seen that when the mass percentage of ferromanganese phosphate ($LiFe_{0.1}Mn_{0.9}PO_4$) in the composite positive electrode active material is too high, the rate performance of the lithium ion secondary battery The cycle performance and storage performance are deteriorated. Therefore, the mass

percentage of ferromanganese phosphate in the composite positive electrode active material should not be too high.

[0108] Therefore, the lithium ion secondary battery of the present invention has good capacity density, rate performance, cycle performance, and storage performance, and has good safety performance and thermal stability.

Espacenet

Family list: KR100696619 (B1) — 2007-03-19

5 application(s) for: KR100696619 (B1)

1. A POSITIVE ACTVIVE MATERIAL FOR A LITHIUM SECONDARY BATTERY AND A METHOD OF PREPARING THE SAME					
Inventor: JUNG WON IL [KR] KWON HO JIN [KR] (+1)	**Applicant:** SAMSUNG SDI CO LTD [KR]	**CPC:**	**IPC:** H01M4/36 H01M4/505 H01M4/525 (+1)	**Publication info:** KR20020024521 (A) 2002-03-30 KR100696619 (B1) 2007-03-19 Global Dossier	**Priority date:** 2000-09-25
2. Positive active material for rechargeable lithium cell and preparation process thereof					
Inventor: HO-CHIN KWON [KR] JUN-MOON SU [KR] (+1)	**Applicant:** SAMSUNG SDI CO LTD [KR]	**CPC:** C01G45/1221 C01G45/1228 C01G45/1242 (+18)	**IPC:** C01G45/00 C01G51/00 C01G53/00 (+10)	**Publication info:** CN1346160 (A) 2002-04-24 CN1263182 (C) 2006-07-05	**Priority date:** 2000-09-25
3. POSITIVE ELECTRODE ACTIVE MATERIAL FOR LITHIUM SECONDARY BATTERY, AND MANUFACTURING METHOD THEREFOR					
Inventor: KWEON HO-JIN SUH JOON-WON (+1)	**Applicant:** SAMSUNG SDI CO LTD	**CPC:**	**IPC:** H01M4/36 H01M4/505 H01M4/525	**Publication info:** JP2009152214 (A) 2009-07-09 JP5753650 (B2) 2015-07-22 Global Dossier	**Priority date:** 2000-09-25
4. LITHIUM SECONDARY CELL POSITIVE ELECTRODE ACTIVATOR, AND MANUFACTURING METHOD OF THE SAME					
Inventor: KWEON HO-JIN SUH JOON-WON (+1)	**Applicant:** SAMSUNG SDI CO LTD	**CPC:** C01G45/1221 C01G45/1228 C01G45/1242 (+18)	**IPC:** C01G45/00 C01G51/00 C01G53/00 (+13)	**Publication info:** JP2002158011 (A) 2002-05-31	**Priority date:** 2000-09-25
5. Positive active material for rechargeable lithium batteries and method for preparing same					
Inventor: KWEON HO-JIN [KR] SUH JUN-WON [KR] (+1)	**Applicant:** KWEON HO-JIN, SUH JUN-WON, (+2)	**CPC:** C01G45/1221 C01G45/1228 C01G45/1242 (+18)	**IPC:** C01G45/00 C01G51/00 C01G53/00 (+15)	**Publication info:** US2002110736 (A1) 2002-08-15 US6753111 (B2) 2004-06-22	**Priority date:** 2000-09-25

Espacenet

Bibliographic data: KR100696619 (B1) — 2007-03-19

A POSITIVE ACTVIVE MATERIAL FOR A LITHIUM SECONDARY BATTERY AND A METHOD OF PREPARING THE SAME

Inventor(s): 권호진, ; 서준원, ; 정원일

Applicant(s): SAMSUNG SDI CO., LTD

Classification: **- international:*H01M4/36; H01M4/505; H01M4/52; H01M4/525***
- cooperative:

Application number: KR20010036767 20010626 Global Dossier

Priority number(s): KR20000056246 20000925

Also published as: JP2009152214 (A) JP5753650 (B2) KR20020024521 (A)

Abstract of KR20020024521 (A)

PURPOSE: Provided is a cathode active material for a lithium secondary battery, which has improved thermal stability, cycle lifetime property, and discharge potential property and contains a core containing a lithium compound with secondary particles and a metal oxide layer formed on the core. CONSTITUTION: The cathode active material contains: the core containing the lithium compound(formula: LixMn1-yM'yA2) having the secondary particles with an average particle size of 1-10 micrometer, wherein the secondary particles are formed by assembling at least one primary particles with an average particle size of 1-2 micrometer; a metal oxide layer coated on the core, wherein the metal of the metal oxide is selected from the group consisting of Mg, Al, Co, K, Na, Ca, Si, Ti, Sn, V, Ge, Ga, B, As, and Zr. And the cathode active material is produced by a process comprising the steps of: coating the lithium compound with a metal organic solution or a metal water solution; heat-treating the coated compound. In the formula, x is more than 0.95 and less than 1.1, y is more than 0 and less than 0.5, M' is Al, Ni, Co, Cr, Fe, Mg, and etc., and A is O, F, S, and P.

(19)대한민국특허청(KR)
(12) 등록특허공보(B1)

(51) 。Int. Cl.
H01M 4/52 (2006.01)

(45) 공고일자 2007년03월19일
(11) 등록번호 10-0696619
(24) 등록일자 2007년03월12일

(21) 출원번호 10-2001-0036767
(22) 출원일자 2001년06월26일
심사청구일자 2006년05월12일

(65) 공개번호 10-2002-0024521
(43) 공개일자 2002년03월30일

(30) 우선권주장 1020000056246 2000년09월25일 대한민국(KR)

(73) 특허권자 삼성에스디아이 주식회사
정기 수원시 영통구 신동 575

(72) 발명자 권호진
충청남도천안시신부동동아태조아파트101동1102호

서준원
충청남도천안시쌍용동주공아파트201동402호

정원일
충청남도천안시두정동극동늘푸른아파트112동2004호

(74) 대리인 유미특허법인

(56) 선행기술조사문헌
JP09050810 A
KR1019990071411 A
KR1020000061755 A
1020000028033
JP09055210 A
KR1019990079408 A
1019990071411
* 심사관에 의하여 인용된 문헌

심사관 : 최병철

전체 청구항 수 : 총 10 항

(54) 리튬 이차 전지용 양극 활물질 및 그 제조 방법

(57) 요약

본 발명은 리튬 이차 전지용 양극 활물질 및 그의 제조 방법을 제공하는 것으로서, 이 양극 활물질은 평균 입도가 1 내지 2 ㎛인 하나 이상의 일차 입자가 조립되어 형성되는 평균 입도가 1㎛ 이상, 10㎛ 미만인 이차 입자를 가지는 리튬 화합물을 포함하는 코어; 및 상기 코어 위에 코팅된 금속 산화물 층을 포함한다. 이 양극 활물질은 평균 입도가 1 내지 2㎛인 하나 이상의 일차 입자가 조립된 평균 입도가 1㎛ 이상, 10㎛ 미만인 이차 입자로 형성된 리튬 화합물을 금속 알콕사이드 용액, 금속염 유기 용액 또는 금속 수용액으로 코팅하고, 상기 금속 알콕사이드 용액 또는 금속 수용액이 코팅된 화합물을 열처리하여 제조된다.

AMPEREX Ex. 1002
Page 1017

대표도

도 3

특허청구의 범위

청구항 1.

평균 입도가 1 내지 2㎛인 하나 이상의 일차 입자가 모여 평균 입도가 1㎛ 이상, 10㎛ 미만인 이차 입자를 형성하는 리튬 화합물을 포함하는 코어; 및

상기 코어 위에 코팅된 금속 산화물 층

을 포함하는 리튬 이차 전지용 양극 활물질.

청구항 2.

제1항에 있어서, 상기 리튬 화합물이 하기 화학식 1 내지 11로 이루어진 군에서 선택되는 하나 이상의 화합물인 리튬 이차 전지용 양극 활물질.

[화학식 1]

$Li_xMn_{1-y}M'_yA_2$

[화학식 2]

$Li_xMn_{1-y}M'_yO_{2-z}A_z$

[화학식 3]

$Li_xMn_2O_{4-z}A_z$

[화학식 4]

$Li_xMn_{2-y}M'_yA_4$

[화학식 5]

$Li_xM_{1-y}M''_yA_2$

[화학식 6]

$Li_xMO_{2-z}A_z$

[화학식 7]

$Li_xNi_{1-y}Co_yO_{2-z}A_z$

[화학식 8]

$Li_xNi_{1-y-z}Co_yM''_zA_\alpha$

[화학식 9]

$Li_xNi_{1-y-z}Co_yM''_zO_{2-\alpha}A_\alpha$

[화학식 10]

$Li_xNi_{1-y-z}Mn_yM'_zA_\alpha$

[화학식 11]

$Li_xNi_{1-y-z}Mn_yM'_zO_{2-\alpha}A_\alpha$

(상기 식에서, $0.95 \leq x \leq 1.1$, $0 \leq y \leq 0.5$, $0 \leq z \leq 0.5$, $0 < \alpha \leq 2$이고, M은 Ni 또는 Co이고, M'은 Al, Ni, Co, Cr, Fe, Mg, Sr, V, Sc, Y, La, Ce, Pr, Nd, Pm, Sm, Eu, Gd, Tb, Dy, Ho, Er, Tm, Yb, Lu, Ac, Th, Pa, U, Np, Pu, Am, Cm, Bk, Cf, Es, Fm, Md, No, 및 Lr로 이루어진 군에서 선택되는 하나 이상의 원소이고, M''은 Al, Cr, Mn, Fe, Mg, Sr, V, Sc, Y, La, Ce, Pr, Nd, Pm, Sm, Eu, Gd, Tb, Dy, Ho, Er, Tm, Yb, Lu, Ac, Th, Pa, U, Np, Pu, Am, Cm, Bk, Cf, Es, Fm, Md, No, 및 Lr로 이루어진 군에서 선택되는 하나 이상의 원소이며, A는 O, F, S 및 P로 이루어진 군에서 선택되는 원소임.)

청구항 3.

제1항에 있어서, 상기 금속 산화물은 Mg, Al, Co, K, Na, Ca, Si, Ti, V, Ge, Ga, B, As 및 Zr로 이루어진 군에서 선택되는 금속의 산화물인 리튬 이차 전지용 양극 활물질.

청구항 4.

제1항에 있어서, 상기 금속 산화물 층내의 금속의 함량은 양극 활물질에 대하여 2×10^{-5} 내지 1 중량%인 리튬 이차 전지용 양극 활물질.

청구항 5.

제3항에 있어서, 상기 금속 산화물 층내의 금속의 함량은 양극 활물질에 대하여 0.001 내지 1 중량%인 리튬 이차 전지용 양극 활물질.

청구항 6.

평균 입도가 1 내지 2㎛인 하나 이상의 일차 입자가 조립된 평균 입도가 1㎛ 이상, 10㎛ 미만인 이차 입자로 형성된 리튬 화합물을 금속 유기 용액 또는 금속 수용액으로 코팅하는 단계; 및

상기 코팅된 화합물을 열처리하는 단계

를 포함하는 리튬 이차 전지용 양극 활물질의 제조방법.

AMPEREX Ex. 1002
Page 1019

청구항 7.

제6항에 있어서, 상기 리튬 화합물이 하기 화학식 1 내지 11로 이루어진 군에서 선택되는 하나 이상의 화합물인 리튬 이차 전지용 양극 활물질의 제조방법.

[화학식 1]

$Li_xMn_{1-y}M'_yA_2$

[화학식 2]

$Li_xMn_{1-y}M'_yO_{2-z}A_z$

[화학식 3]

$Li_xMn_2O_{4-z}A_z$

[화학식 4]

$Li_xMn_{2-y}M'_yA_4$

[화학식 5]

$Li_xM_{1-y}M''_yA_2$

[화학식 6]

$Li_xMO_{2-z}A_z$

[화학식 7]

$Li_xNi_{1-y}Co_yO_{2-z}A_z$

[화학식 8]

$Li_xNi_{1-y-z}Co_yM''_zA_\alpha$

[화학식 9]

$Li_xNi_{1-y-z}Co_yM''_zO_{2-\alpha}A_\alpha$

[화학식 10]

$Li_xNi_{1-y-z}Mn_yM'_zA_\alpha$

[화학식 11]

$Li_xNi_{1-y-z}Mn_yM'_zO_{2-\alpha}A_\alpha$

AMPEREX Ex. 1002
Page 1020

(상기 식에서, $0.95 \leq x \leq 1.1$, $0 \leq y \leq 0.5$, $0 \leq z \leq 0.5$, $0 < a \leq 2$이고, M은 Ni 또는 Co이고, M'은 Al, Ni, Co, Cr, Fe, Mg, Sr, V, Sc, Y, La, Ce, Pr, Nd, Pm, Sm, Eu, Gd, Tb, Dy, Ho, Er, Tm, Yb, Lu, Ac, Th, Pa, U, Np, Pu, Am, Cm, Bk, Cf, Es, Fm, Md, No, 및 Lr로 이루어진 군에서 선택되는 하나 이상의 원소이고, M"은 Al, Cr, Mn, Fe, Mg, Sr, V, Sc, Y, La, Ce, Pr, Nd, Pm, Sm, Eu, Gd, Tb, Dy, Ho, Er, Tm, Yb, Lu, Ac, Th, Pa, U, Np, Pu, Am, Cm, Bk, Cf, Es, Fm, Md, No, 및 Lr로 이루어진 군에서 선택되는 하나 이상의 원소이며, A는 O, F, S 및 P로 이루어진 군에서 선택되는 원소임.)

청구항 8.

제6항에 있어서, 상기 금속 유기 용액 또는 금속 수용액내의 금속, 금속 알콕사이드, 금속염 또는 금속 산화물의 농도는 0.1 내지 50 중량%인 리튬 이차 전지용 양극 활물질의 제조방법.

청구항 9.

제8항에 있어서, 상기 금속 유기 용액 또는 금속 수용액내의 금속, 금속 알콕사이드, 금속염 또는 금속 산화물의 농도는 1 내지 20 중량%인 리튬 이차 전지용 양극 활물질의 제조방법.

청구항 10.

제6항에 있어서, 상기 열처리 공정은 공기 또는 산소 분위기 하에서 300 내지 800℃의 온도로 5 내지 15시간 동안 실시하는 것인 제조 방법.

명세서

발명의 상세한 설명

발명의 목적

발명이 속하는 기술 및 그 분야의 종래기술

[산업상 이용 분야]

본 발명은 리튬 이차 전지용 양극 활물질 및 그 제조 방법에 관한 것으로서, 더욱 상세하게는 열적 안정성이 우수한 양극 활물질 및 그 제조 방법에 관한 것이다.

[종래 기술]

리튬 이차 전지는 가역적으로 리튬 이온의 삽입 및 탈리가 가능한 물질을 양극 및 음극으로 사용하고, 상기 양극과 음극 사이에 유기 전해액 또는 폴리머 전해액을 충전시켜 제조하며, 리튬 이온이 양극 및 음극에서 삽입/탈리될 때의 산화, 환원 반응에 의하여 전기 에너지를 생성한다.

리튬 이차 전지의 음극 활물질로는 리튬 금속을 사용하였으나, 리튬 금속을 사용할 경우 덴드라이트(dendrite)의 형성으로 인한 전지 단락에 의해 폭발 위험성이 있어서 리튬 금속 대신 비정질 탄소 또는 결정질 탄소 등의 탄소계 물질로 대체되어 가고 있다. 특히, 최근에는 탄소계 물질의 용량을 증가시키기 위하여 탄소계 물질에 보론을 첨가하여 보론 코팅된 그라파이트(BOC)를 제조하고 있다.

양극 활물질로는 칼코게나이드(chalcogenide) 화합물이 사용되고 있으며, 그 예로 $LiCoO_2$, $LiMn_2O_4$, $LiNiO_2$, $LiNi_{1-x}Co_xO_2(0<x<1)$, $LiMnO_2$ 등의 복합 금속 산화물들이 연구되고 있다. 상기 양극 활물질 중 $LiMn_2O_4$, $LiMnO_2$ 등의 Mn계 양극 활물질은 합성하기도 쉽고, 값이 비교적 싸며, 환경에 대한 오염도 적어 매력이 있는 물질이기는 하나, 용량이 작다는

AMPEREX Ex. 1002
Page 1021

단점을 가지고 있다. $LiCoO_2$는 양호한 전기 전도도와 높은 전지 전압 그리고 우수한 전극 특성을 보이며, 현재 Sony사 등에서 상업화되어 시판되고 있는 대표적인 양극 활물질이나, 가격이 비싸다는 단점을 내포하고 있다. $LiNiO_2$는 위에서 언급한 양극 활물질 중 가장 값이 싸며, 가장 높은 방전 용량의 전지 특성을 나타내고 있으나 합성하기가 어려운 단점을 안고 있다.

이 중에서 양극 활물질로는 $LiCoO_2$가 주로 사용되며, 최근 Sony에서 Al_2O_3를 약 1 내지 5 중량% 도핑한 $LiCo_{1-x}Al_xO_2$를 개발하였으며, A&TB에서는 SnO_2를 도핑한 $LiCoO_2$를 개발하였다.

상술한 양극 및 음극 활물질로 구성된 리튬 이차 전지는 사용하는 세퍼레이터와 전해질의 종류에 따라 리튬 이온 전지, 리튬 이온 폴리머 전지 및 리튬 폴리머 전지로 분류할 수 있다. 리튬 이온 전지는 세퍼레이터로 다공성 폴리프로필렌/폴리에틸렌 필름을 사용하며, 전해질로는 리튬염이 용해된 카보네이트 계열의 유기 용매를 사용하는 전지를 말한다. 리튬 이온 폴리머 전지는 전해질로 다공성 SiO_2 등과 폴리비닐리덴 플루오라이드 계열의 폴리머 기재에 상기 유기 용매를 함침(impregnation)시킨 것을 사용하며, 이 전해질이 세퍼레이터의 역할도 하므로, 별도의 세퍼레이터를 사용할 필요는 없다. 또한, 리튬 폴리머 전지는 전해질로 순수한 리튬 이온 도전성을 갖는 SO_2 계열의 무기 물질 또는 유기 물질을 사용하는 전지를 말한다.

상기 구성의 리튬 이차 전지의 형태로는 원통형, 각형, 코인형 등이 있다. 원통형 전지는 리튬 이온 이차 전지를 예로 들어 설명하면, 양극, 음극과 세퍼레이터를 와인딩하여 젤리 롤 타입(jelly-roll type)의 극판군을 제조하고, 이 극판군을 원통형 전지 케이스에 넣은 후, 전해액을 주입한 전지를 말한다. 각형 전지는 상기 극판군을 각형 전지 케이스에 넣어서 제조한 전지를 말하며, 코인형 전지는 상기 극판군을 코인형 전지 케이스에 넣어서 제조한 전지를 말한다. 또한, 케이스의 재질에 따라 스틸 또는 Al 재질의 캔을 사용한 전지와 파우치(pouch) 전지로 구별할 수 있다. 캔 전지는 상기 전지 케이스가 스틸 또는 Al의 얇은 판으로 제조된 것으로 말하며, 파우치 전지는 비닐 백과 같은 다층 구조로 이루어진 1㎜ 이내 두께의 유연한 재질에 상기 극판군을 넣어 제조된 전지로서, 전지의 두께가 캔 전지에 비해 얇고, 유연한 구조를 갖는 전지를 말한다.

이러한 리튬 이차 전지는 최근 전자 기기가 소형화 및 경량화됨에 따라 점점 고용량, 장수명 등의 전기 화학적 특성이 우수한 전지를 개발하기 위한 연구가 진행되고 있다.

발명이 이루고자 하는 기술적 과제

본 발명은 상술한 문제점을 해결하기 위한 것으로서, 본 발명의 목적은 사이클 수명 특성과 방전 전위 특성이 향상된 리튬 이차 전지용 양극 활물질을 제공하는 것이다.

본 발명의 다른 목적은 상기 리튬 이차 전지용 양극 활물질의 제조 방법을 제공하는 것이다.

발명의 구성

상기 본 발명의 목적을 달성하기 위하여, 본 발명은 평균 입도가 1 내지 2㎛인 하나 이상의 일차 입자가 조립되어 형성되는 평균 입도가 1㎛ 이상, 10㎛ 미만 이차 입자를 가지는 리튬 화합물을 포함하는 코어; 및 상기 코어 위에 코팅된 금속 산화물 층을 포함하는 리튬 이차 전지용 양극 활물질을 제공한다.

또한, 본 발명은 상기 양극 활물질의 제조 방법으로서, 평균 입도가 1 내지 2㎛인 하나 이상의 일차 입자가 조립되어 형성되는 평균 입도가 1㎛ 이상, 10㎛ 미만인 이차 입자를 가지는 리튬 화합물을 금속 알콕사이드 용액, 금속염 유기 용액 또는 금속 수용액으로 코팅하고; 상기 코팅된 화합물을 열처리하는 공정을 포함하는 리튬 이차 전지용 양극 활물질의 제조 방법을 제공한다.

이하, 본 발명을 더욱 상세히 설명한다.

본 발명의 리튬 이차 전지용 양극 활물질은 평균 입도가 1 내지 2㎛인 하나 이상의 일차 입자가 조립되어 형성되는 평균 입도가 1㎛ 이상, 10㎛ 미만 이차 입자를 가지는 리튬 화합물을 포함하는 코어; 및 상기 코어 위에 코팅된 금속 산화물 층을 포함한다.

AMPEREX Ex. 1002
Page 1022

AMPEREX Ex. 1002
Page 1023

본 발명의 양극 활물질의 코어를 이루는 리튬 화합물은 평균 입도가 1 내지 2㎛인 일차 입자 하나 이상이 조립되어 이루어진 평균 입도가 1㎛ 이상 10㎛ 미만인 이차 입자로 구성된다. 본 발명의 양극 활물질에서, 일차 입자의 평균 입도 조건은 큰 의미를 부여하지 않으며, 이차 입자의 평균 입도 조건이 중요하다. 이차 입자의 평균 입도가 1㎛ 보다 작은 것을 사용할 경우에는, Li^+의 반응 속도(kinetics)에 있어 문제가 있어 열적 안정성이 나빠져 전지 시스템의 안전성이 취약해지는 문제점이 있고, 10㎛ 이상인 것은 고율(high current) 조건에서 특성이 나빠지는 문제점이 있어 바람직하지 않다. 본 명세서에서 일차 입자란 평균 입도가 1 내지 2㎛로 작은 미세 입자를 말하며, 이러한 일차 입자 하나 이상이 조립된 입자를 사용한다.

상기 리튬 화합물로는 하기 화학식 1 내지 11로 이루어진 군에서 선택되는 하나 이상의 화합물이 바람직하게 사용될 수 있다. 이들 화합물중 리튬-코발트 칼코게나이드, 리튬-망간 칼코게나이드, 리튬-니켈 칼코게나이드 또는 리튬-니켈-망간 칼코게나이드 화합물이 본 발명에 더 바람직하게 사용될 수 있다.

[화학식 1]

$Li_xMn_{1-y}M'_yA_2$

[화학식 2]

$Li_xMn_{1-y}M'_yO_{2-z}A_z$

[화학식 3]

$Li_xMn_2O_{4-z}A_z$

[화학식 4]

$Li_xMn_{2-y}M'_yA_4$

[화학식 5]

$Li_xM_{1-y}M''_yA_2$

[화학식 6]

$Li_xMO_{2-z}A_z$

[화학식 7]

$Li_xNi_{1-y}Co_yO_{2-z}A_z$

[화학식 8]

$Li_xNi_{1-y-z}Co_yM''_zA_\alpha$

[화학식 9]

$Li_xNi_{1-y-z}Co_yM''_zO_{2-\alpha}A_\alpha$

[화학식 10]

$Li_xNi_{1-y-z}Mn_yM'_zA_\alpha$

[화학식 11]

$Li_xNi_{1-y-z}Mn_yM'_zO_{2-\alpha}A_\alpha$

(상기 식에서, $0.95 \leq x \leq 1.1$, $0 \leq y \leq 0.5$, $0 \leq z \leq 0.5$, $0 < \alpha \leq 2$이고, M은 Ni 또는 Co이고, M'은 Al, Ni, Co, Cr, Fe, Mg, Sr, V, Sc, Y, La, Ce, Pr, Nd, Pm, Sm, Eu, Gd, Tb, Dy, Ho, Er, Tm, Yb, Lu, Ac, Th, Pa, U, Np, Pu, Am, Cm, Bk, Cf, Es, Fm, Md, No, 및 Lr로 이루어진 군에서 선택되는 하나 이상의 원소이고, M"은 Al, Cr, Mn, Fe, Mg, Sr, V, Sc, Y, La, Ce, Pr, Nd, Pm, Sm, Eu, Gd, Tb, Dy, Ho, Er, Tm, Yb, Lu, Ac, Th, Pa, U, Np, Pu, Am, Cm, Bk, Cf, Es, Fm, Md, No, 및 Lr로 이루어진 군에서 선택되는 하나 이상의 원소이며, A는 O, F, S 및 P로 이루어진 군에서 선택되는 원소이다.)

상기 리튬 화합물의 표면에 형성되는 하나 이상의 금속 산화물은 Mg, Al, Co, K, Na, Ca, Si, Ti, V, Ga, Ge, B, As 및 Zr로 이루어진 군에서 선택되는 금속의 산화물인 것이 바람직하다.

상기 하나 이상의 금속 산화물 층내의 금속의 함량은 양극 활물질에 대하여 2×10^{-5} 내지 1 중량%인 것이 바람직하고, 0.001 내지 1 중량%인 것이 더 바람직하다.

본 발명의 양극 활물질은 발열 온도가 높고 발열량이 작아 열적 안정성이 우수하다.

본 발명에서는 리튬 화합물의 코팅 용액으로 금속을 포함하는 유기 용액 또는 금속 수용액을 사용한다.

상기 코팅 용액 제조시 사용되는 금속으로는 유기 용매 또는 물에 용해되는 것은 어떠한 것도 사용할 수 있으며, 그 대표적인 예로 Mg, Al, Co, K, Na, Ca, Si, Ti, V, Sn, Ge, Ga, B, As 또는 Zr이 있다.

상기 금속 유기 용액은 금속, 금속 알콕사이드, 금속염, 금속산화물 등을 유기 용매에 용해시켜 제조하거나, 이 혼합물을 환류시켜 제조할 수 있다. 상기 금속 수용액은 금속염 또는 금속산화물을 물에 용해시켜 제조하거나, 이 혼합물을 환류시켜 제조할 수 있다. 유기 용매 또는 물에 용해되는 적당한 금속의 형태는 이 분야의 통상의 지식에 의하여 선택될 수 있다. 예를 들어 보론을 포함하는 코팅 용액은 $HB(OH)_2$, B_2O_3, H_3BO_3 등을 유기 용매 또는 물에 용해시켜 제조할 수 있다.

상기 코팅 용액중 금속 유기 용액 제조시 사용가능한 유기 용매로는 메탄올, 에탄올 또는 이소프로판올과 같은 알코올, 헥산, 클로로포름, 테트라하이드로퓨란, 에테르, 메틸렌 클로라이드, 아세톤 등이 있다.

상기 금속 유기 용액중 금속 메톡사이드, 금속 에톡사이드 또는 금속 이소프로폭사이드와 같은 금속 알콕사이드를 알코올에 용해시켜 제조한 금속 알콕사이드 용액이 본 발명에 바람직하게 사용될 수 있다. 이러한 금속 알콕사이드 용액의 예로, Si 알콕사이드 용액으로는 Aldrich사에서 시판하는 테트라에틸오르토실리케이트(tetraethylorthosilicate) 용액 또는 실리케이트를 에탄올에 용해하여 제조한 테트라에틸오르토실리케이트 용액이 있다.

상기 코팅 용액중 금속 수용액 제조시 사용될 수 있는 금속염 또는 금속 산화물의 대표적인 예로는 암모늄 바나데이트($NH_4(VO_3)$)와 같은 바나듐산염, 바나듐 옥사이드(V_2O_5) 등이 있다.

금속 유기 용액 또는 금속 수용액 제조시 첨가되는 금속, 금속 알콕사이드, 금속염, 또는 금속산화물의 양은 유기 용액 또는 수용액에 대하여 0.1 내지 50 중량%이며, 더 바람직하게는 1 내지 20 중량%이다. 상기 금속, 금속 알콕사이드, 금속염 또는 금속산화물의 농도가 0.1 중량%보다 낮으면 금속 유기 용액 또는 금속 수용액으로 리튬 화합물을 코팅하는 효과가 나타나지 않으며, 상기 금속, 금속 알콕사이드, 금속염, 또는 금속산화물의 농도가 50 중량%를 초과하면 코팅층의 두께가 너무 두꺼워져 바람직하지 않다.

이와 같이 제조된 금속 유기 용액 또는 금속 수용액으로 평균 입도가 1 내지 2㎛인 하나 이상의 일차 입자가 조립되어 형성되는 평균 입도가 1㎛ 이상, 10㎛ 미만인 이차 입자를 가지는 리튬 화합물을 코팅(encapsulation)한다.

AMPEREX Ex. 1002
Page 1024

상기 코팅 방법으로는 스퍼터링법, CVD(Chemical Vapor Deposition)법, 딥 코팅(dip coating)법 등 범용 코팅 방법을 사용할 수 있으나, 가장 간편한 코팅법으로서 단순히 분말을 코팅 용액에 담그었다가 빼내는 딥 코팅법을 사용하는 것이 바람직하다.

이와 같이 금속 유기 용액 또는 금속 수용액이 코팅된 분말을 120℃ 오븐에서 약 5시간 동안 건조시키는 것이 바람직하다. 이 건조 공정은 분말 내에 리튬 염을 더욱 균일하게 분포시키는 역할을 한다.

금속 유기 용액 또는 금속 수용액이 코팅된 리튬 화합물 분말을 300 내지 800℃로 5 내지 15시간 동안 열처리한다. 더욱 균일한 결정성 활물질을 제조하기 위해 상기 열처리 공정은 건조 공기 또는 산소를 블로잉하는(blowing) 조건하에서 수행하는 것이 바람직하다. 이때, 열처리 온도가 300℃보다 낮으면 코팅된 금속 알콕사이드 용액이 결정화되지 않으므로 이 활물질을 전지에 적용하면 리튬 이온의 이동이 방해를 받을 수 있다. 또한, 상기 열처리 온도가 800℃보다 높으면 Li 증발(evaporation)에 의하여, 원하는 당량비가 얻어지지 않으며 결정 구조에 문제가 있는 활물질이 합성되어 바람직하지 않다.

상기 열처리 공정으로 금속 유기 용액 또는 금속 수용액이 금속 산화물로 변화하여, 평균 입도가 1 내지 2㎛인 하나 이상의 일차 입자가 조립되어 형성되는 평균 입도가 1㎛ 이상, 10㎛ 미만인 이차 입자를 가지는 리튬 화합물의 표면에 금속 산화물이 코팅된 활물질이 제조된다.

활물질 표면에 형성된 금속 산화물은 상기 리튬 화합물의 금속, 및 금속 유기 용액 또는 금속 수용액으로부터 유래된 금속의 복합 금속 산화물, 및/또는 금속 유기 용액 또는 금속 수용액으로부터 유래된 금속의 산화물 등이다. 예를 들면, $LiCoO_2$를 알루미늄 알콕사이드 졸로 코팅한 후 열처리하면 코발트와 알루미늄의 복합 금속 산화물 및/또는 알루미늄의 산화물로 표면 처리된 양극 활물질을 얻을 수 있다.

상기 코팅 및 열처리 공정은 하나 이상의 금속을 포함하는 유기 용액 또는 수용액을 사용하여 실시하여 하나의 코팅층에 하나 이상의 금속이 포함되도록 할 수 있다. 또한 하나 이상의 금속을 포함하는 제1 유기 용액 또는 수용액으로 1차 코팅한 후 열처리하고, 하나 이상의 금속을 포함하는 제2 유기 용액 또는 수용액으로 2차 코팅한 후 열처리하여 이중층을 형성할 수도 있다. 하나 이상의 금속을 포함하는 유기 용액 또는 수용액으로 순차적으로 3회 이상 코팅 및 열처리하여 금속 산화물 코팅층이 3개 이상이 되도록 할 수도 있다.

본 발명에서 사용한 리튬 화합물은 상업적으로 유통되는 평균 입도가 1 내지 2㎛인 것을 조립하여 사용할 수도 있고, 합성된 리튬 화합물 분말중 평균 입도가 1 내지 2㎛인 것을 선별한 후 이를 조립하여 사용할 수도 있으며, 이들 리튬 화합물을 혼합하여 사용할 수도 있다.

상기 리튬 화합물을 합성방법은 다음과 같다. 우선 리튬염 및 금속염을 원하는 당량비대로 혼합한다. 상기 리튬염으로는 일반적으로 망간계 리튬 이차 전지용 양극 활물질을 제조하는 데 사용되는 것은 어떠한 것도 사용할 수 있으며, 그 대표적인 예로 리튬 나이트레이트, 리튬 아세테이트, 리튬 하이드록사이드 등을 사용할 수 있다. 상기 금속염으로는 망간염, 코발트염, 니켈염 또는 니켈 망간염을 사용할 수 있다. 상기 망간염으로는 망간 아세테이트, 망간 디옥사이드 등을 사용할 수 있고, 상기 코발트염으로는 코발트 옥사이드, 코발트 나이트레이트 또는 코발트 카보네이트 등을 사용할 수 있으며, 니켈염으로는 니켈 하이드록사이드, 니켈 나이트레이트 또는 니켈 아세테이트 등을 사용할 수 있다. 상기 니켈 망간염은 니켈염과 망간염을 공침 방법으로 침전시켜 제조된 것을 사용할 수 있다. 금속염으로 망간염, 코발트염, 니켈염, 또는 니켈 망간염과 함께 불소염, 황염 또는 인염을 함께 침전시킬 수도 있다. 상기 불소염으로는 망간 플루오라이드, 리튬 플루오라이드 등이 사용될 수 있으며, 상기 황 염으로는 망간 설파이드, 리튬 설파이드 등을 사용할 수 있고, 상기 인염으로는 H_3PO_4를 사용할 수 있다. 상기 망간염, 코발트염, 니켈염, 니켈 망간염, 불소염, 황염 및 인염이 상기 화합물에 한정되는 것은 아니다.

혼합 방법은 예를 들면, 몰타르 그라인더 혼합(mortar grinder mixing)을 사용할 수 있고, 이때, 리튬염 및 금속염의 반응을 촉진하기 위하여, 에탄올, 메탄올, 물, 아세톤 등 적절한 용매를 첨가하고 용매가 거의 없어질 때까지(solvent-free) 몰타르 그라인더 혼합을 실시하는 것이 바람직하다.

얻어진 혼합물을 약 400 내지 600℃의 온도에서 열처리하여 준 결정성(semi-crystalline) 상태의 리튬 화합물 전구체 분말을 제조한다. 열처리 온도가 400℃보다 낮으면 리튬염과 금속염의 반응이 충분하지 않다는 문제점이 있다. 또한 열처리하여 제조된 전구체 분말을 건조시킨 후, 또는 열처리 과정 후에 건조 공기를 블로잉(blowing)하면서 상기 전구체 분말을 상온에서 재혼합(remixing)시켜 리튬염을 균일하게 분포시킬 수도 있다.

AMPEREX Ex. 1002
Page 1025

AMPEREX Ex. 1002
Page 1026

얻어진 준 결정성 전구체 분말을 700 내지 900℃의 온도로 약 10 내지 15시간 동안 2차 열처리한다. 2차 열처리 온도가 700℃보다 낮으면 결정성 물질이 형성되기 어려운 문제점이 있다. 상기 열처리 공정은 건조 공기 또는 산소를 블로잉(blowing)하는 조건하에서 1 내지 5℃/분의 속도로 승온하여 실시하고, 각 열처리 온도에서 일정 시간 동안 유지한 후 자연 냉각하는 것으로 이루어진다.

이어서, 제조된 리튬 화합물의 분말을 상온에서 재혼합(remixing)시켜 리튬 염을 더욱 균일하게 분포시키는 것이 바람직하다.

상기 방법으로 제조한 리튬 화합물 분말중 일차 입자의 평균 입도가 1 내지 2㎛인 리튬 화합물 분말은 조립되어 평균 입도가 1㎛ 이상, 10㎛ 미만인 이차 입자를 형성한다.

다음은 본 발명의 이해를 돕기 위하여 바람직한 실시예를 제시한다. 그러나 하기의 실시예들은 본 발명을 보다 쉽게 이해하기 위하여 제공되는 것일 뿐 본 발명이 하기의 실시예에 한정되는 것은 아니다.

(실시예 1)

Al-이소프로폭사이드 분말을 에탄올에 첨가하여 5 중량% 농도를 갖는 Al-이소프로폭사이드 용액을 제조하였다.

평균입경이 1~2㎛인 일차 입자가 조립되어 형성된 이차 입자의 평균 입경이 5㎛인 $LiCoO_2$ 분말 100g을 상기 Al-이소프로폭사이드 용액에 첨가하고, 교반기로 약 10분간 저어 주어 상기 Al-이소프로폭사이드 용액이 $LiCoO_2$ 분말의 표면에 골고루 코팅되도록 하였다. 이렇게 제조된 슬러리를 약 30분간 방치하여 슬러리와 Al-이소프로폭사이드 용액을 분리한 후, Al-이소프로폭사이드 용액을 제거하여, 슬러리만을 열처리용 로에 넣었다.

상기 로에서 3℃/분의 승온 속도로 건조 공기를 블로잉하면서 500℃에서 10시간 열처리한 후, 로 내에서 냉각시켜 표면에 알루미늄 산화물 층이 형성된 리튬 이차 전지용 양극 활물질을 제조하였다.

제조된 양극 활물질과 슈퍼 P 카본 도전재 및 폴리비닐리덴 플루오라이드 바인더를 94 : 3 : 3의 중량비로 측정한 후, N-메틸피롤리돈 용매에 첨가하여 양극 활물질 슬러리를 제조하였다. 이 슬러리를 Al-포일 위에 캐스팅하고 건조한 후 프레싱하여 양극 극판을 제조하였다.

음극 활물질로 Petoka사의 MCF(mesocarbon fiber)와, 폴리비닐리덴 플루오라이드 바인더를 96 : 4의 중량비로 혼합하여 N-메틸 피롤리돈 용매에 첨가하여 음극 활물질 슬러리를 제조하였다. 이 음극 활물질 슬러리를 Cu-포일 위에 캐스팅하고 건조한 후 프레싱하여 음극 극판을 제조하였다.

상기 양극 극판 및 음극 극판을 사용하여 통상의 방법으로 각형의 리튬 이온 전지를 제조하였다. 이때, 전해액으로는 1M $LiPF_6$가 용해된 에틸렌 카보네이트, 디메틸 카보네이트와 디에틸 카보네이트의 혼합 용매를 사용하였다.

(실시예 2)

열처리 온도를 500℃에서 300℃로 변경한 것을 제외하고는 상기 실시예 1과 동일한 방법으로 실시하여 각형의 리튬 이온 전지를 제조하였다.

(실시예 3)

열처리 온도를 500℃에서 700℃로 변경한 것을 제외하고는 상기 실시예 1과 동일한 방법으로 실시하여 각형의 리튬 이온 전지를 제조하였다.

(실시예 4)

Al-이소프로폭사이드 용액 대신에 $Al(NO_3)_3$를 물에 첨가하여 제조한 5 중량%의 알루미늄 나이트레이트 용액을 사용한 것을 제외하고는 상기 실시예 1과 동일한 방법으로 실시하여 각형의 리튬 이온 전지를 제조하였다.

(실시예 5)

Al-이소프로폭사이드 용액 대신에, $Al(NO_3)_3$를 물에 첨가하여 제조한 5 중량%의 알루미늄 나이트레이트 용액을 사용하고, 열처리 온도를 500℃에서 300℃로 변경한 것을 제외하고는 상기 실시예 1과 동일한 방법으로 실시하여 각형의 리튬 이온 전지를 제조하였다.

(실시예 6)

Al-이소프로폭사이드 용액 대신에, $Al(NO_3)_3$를 물에 첨가하여 제조한 5 중량%의 알루미늄 나이트레이트 용액을 사용하고, 열처리 온도를 500℃에서 700℃로 변경한 것을 제외하고는 상기 실시예 1과 동일한 방법으로 실시하여 각형의 리튬 이온 전지를 제조하였다.

(대조예 1)

Al-이소프로폭사이드 용액으로 $LiCoO_2$ 분말을 코팅하지 않은 것을 제외하고는 상기 실시예 1과 동일하게 실시하여 각형의 리튬 이온 전지를 제조하였다.

(비교예 1)

평균 입경이 10㎛인 $LiCoO_2$ 분말을 사용한 것을 제외하고는 상기 실시예 1과 동일하게 실시하여 각형의 리튬 이온 전지를 제조하였다.

(비교예 2)

Al-이소프로폭사이드 용액으로 $LiCoO_2$ 분말을 코팅하지 않은 것을 제외하고는 상기 비교예 1과 동일하게 실시하여 각형의 리튬 이온 전지를 제조하였다.

상기 실시예 1과 대조예 1의 방법으로 제조된 양극 활물질의 SEM 사진을 도 1a 및 도 1b에 각각 나타내었다. 또한, 상기 비교예 1 및 2의 방법으로 제조된 양극 활물질의 SEM 사진을 도 2a 및 도 2b에 각각 나타내었다.

상기 실시예 1, 대조예 1 및 비교예 1~2의 방법으로 제조된 각형의 리튬 이온 전지를 4.2V~2.75V 사이에서 충방전을 실시하였다. 충방전은 0.2C-속도로 화성(formation)을 거친 전지를 충전은 모두 0.2C-속도로 실시한 후 방전을 0.5C, 1C 및 2C로 하여 C-속도 변화에 따른 방전 특성을 측정하였다. 도 3은 실시예 1과 비교예 1의 측정 결과를 나타내고, 도 4는 실시예 1과 대조예 1의 측정 결과를 나타낸다. 도 4에서 방전 용량은 각 전지의 최대 방전 용량을 100%로 환산하여 나타내었다.

도 3에 나타낸 것과 같이, 동일하게 Al-이소프로폭사이드 용액으로 $LiCoO_2$를 코팅하여 표면에 알루미늄 산화물 층이 형성된 양극 활물질이라도, 사용한 $LiCoO_2$ 크기에 따라 방전 특성이 다르게 나타남을 알 수 있다. $LiCoO_2$ 이차 입자의 크기가 5㎛인 것을 사용한 실시예 1의 전지가 10㎛인 것을 사용한 비교예 1의 전지에 비해 고율(1.0C 및 2.0C)에서 방전 전압이 높게 나타나는 것으로부터 본 발명에 따른 실시예 1의 방전 특성이 비교예 1보다 우수함을 알 수 있다.

또한, 도 4에 나타낸 것과 같이, 동일한 크기의 $LiCoO_2$ 분말을 사용하였을지라도 알루미늄 산화물 층이 형성된 실시예 1의 양극 활물질이 알루미늄 산화물 층이 형성되지 않은 대조예 1의 양극 활물질에 비하여 고율(1.0C 및 2.0C)에서 방전 특성이 우수함을 알 수 있다.

이러한 결과로부터, 리튬 금속 산화물, 예를 들어 $LiCoO_2$의 입자 크기가 작을수록 방전 전압 특성이 우수하며, 표면에 금속 산화물 층이 코팅되어 있는 것이 코팅되지 않은 것보다 방전 특성이 더 우수하게 나타남을 알 수 있다.

(실시예 7)

AMPEREX Ex. 1002
Page 1027

Al-이소프로폭사이드 용액 대신에 10 중량%의 보론 에톡사이드 용액을 사용한 것을 제외하고는 상기 실시예 1과 동일한 방법으로 실시하여 각형의 리튬 이온 전지를 제조하였다.

(실시예 8)

Al-이소프로폭사이드 용액 대신에, 10 중량%의 보론 에톡사이드 용액을 사용하고, 열처리 온도를 500℃에서 300℃로 변경한 것을 제외하고는 상기 실시예 1과 동일한 방법으로 실시하여 각형의 리튬 이온 전지를 제조하였다.

(실시예 9)

Al-이소프로폭사이드 용액 대신에, 10 중량%의 보론 에톡사이드 용액을 사용하고, 열처리 온도를 500℃에서 700℃로 변경한 것을 제외하고는 상기 실시예 1과 동일한 방법으로 실시하여 각형의 리튬 이온 전지를 제조하였다.

실시예 7~9 및 비교예 1의 각형 리튬 이온 전지 20개에 대하여 연소, 열노출, 과충전 시험을 하였다. 연소시험은 버너로 전지를 가열하여 전지의 파열률을 계산하였고, 열노출 시험은 150℃에서 전지를 열노출시킬 경우 전지가 파열되는 시간을 측정하였고, 과충전 시험은 전지를 1C로 과충전할 경우 누액률을 조사하였다. 그 결과를 하기 표 1에 기재하였다.

[표 1]

	비교예 1	실시예 7	실시예 8	실시예 9
연소시 파열률	90%	0%	0%	0%
열노출시 전지의 파열시간(평균)	11분	15분	12분	20분
1C 과충전 누액률	100%	10%	30%	0%

(실시예 10)

$LiCoO_2$ 대신 평균입경이 1~2㎛인 일차 입자가 조립되어 형성된 이차 입자의 평균 입경이 5㎛인 $Li_{1.03}Ni_{0.69}Mn_{0.19}Co_{0.1}Al_{0.07}Mg_{0.07}O_2$를 1 중량%의 보론 에톡사이드 용액으로 코팅한 후, 700℃에서 열처리한 것을 제외하고 상기 실시예 1과 동일한 방법으로 보론 산화물 층이 형성된 양극 활물질 분말을 제조하였다.

상기 양극 활물질 분말, 슈퍼 P 카본 도전재 및 폴리비닐리덴 플루오라이드 바인더를 94 : 3 : 3의 질량비로 측정한 후 N-메틸피롤리돈 용매에 녹여서 양극 활물질 슬러리를 제조하였다. 이 슬러리를 Al-포일 위에 캐스팅하고 건조한 후 프레싱하여 코인 전지용 양극 극판을 제조하였다.

제조된 양극 극판과 대극으로 리튬 금속을 사용하여 Ar-제거된(purged) 글로브 박스에서 코인 타입의 반쪽 전지를 제조하였다. 이때 전해액은 1M $LiPF_6$가 용해된 에틸렌 카보네이트와 디메틸 카보네이트의 혼합 용매(1 : 1 부피비)의 표준 전해액을 사용하였다.

(실시예 11)

$LiCoO_2$ 대신 평균입경이 1~2㎛인 일차 입자가 조립되어 형성된 이차 입자의 평균 입경이 5㎛인 $LiNi_{0.9}Co_{0.1}Sr_{0.002}O_2$를 1 중량%의 보론 에톡사이드 용액으로 코팅한 후 700℃에서 열처리한 것을 제외하고 상기 실시예 10과 동일한 방법으로 코인-타입의 반쪽 전지를 제조하였다.

(실시예 12)

AMPEREX Ex. 1002
Page 1028

$LiCoO_2$ 대신 평균입경이 1~2㎛인 일차 입자가 조립되어 형성된 이차 입자의 평균 입경이 5㎛인 $LiMn_2O_4$를 사용한 것을 제외하고 1 중량%의 보론 에톡사이드 용액으로 코팅한 후 700℃에서 열처리한 것을 제외하고 상기 실시예 10과 동일한 방법으로 코인-타입의 반쪽 전지를 제조하였다.

(비교예 3)

평균 입경이 10㎛이고 코팅되지 않은 $LiCoO_2$ 분말을 양극 활물질로 사용한 것을 제외하고 실시예 7과 동일한 방법으로 코인-타입의 반쪽 전지를 제조하였다.

(비교예 4)

평균 입경이 10㎛이고 코팅되지 않은 $Li_{1.03}Ni_{0.69}Mn_{0.19}Co_{0.1}Al_{0.07}Mg_{0.07}O_2$를 양극 활물질로 사용한 것을 제외하고 상기 실시예 7과 동일한 방법으로 반쪽 전지를 제조하였다.

(비교예 5)

평균 입경이 10㎛이고 코팅되지 않은 $LiNi_{0.9}Co_{0.1}Sr_{0.002}O_2$를 사용한 것을 제외하고 양극 활물질로 사용한 것을 제외하고 상기 실시예 7과 동일한 방법으로 반쪽 전지를 제조하였다.

(비교예 6)

평균 입경이 20㎛이고 코팅되지 않은 $LiMn_2O_4$를 사용한 것을 제외하고 양극 활물질로 사용한 것을 제외하고 상기 실시예 7과 동일한 방법으로 반쪽 전지를 제조하였다.

실시예 7~12 및 비교예 3~6의 방법으로 제조된 코인 전지에 대하여 연속적으로 0.1C(1사이클), 0.2C(3사이클), 0.5C (10사이클) 및 1C(6사이클) 순서로 C rate를 변화시키면서 4.3V~2.75V의 전압범위에서 충방전을 실시하여 방전용량을 측정하였다. 이중 실시예 11과 비교예 5의 코인 전지에 대한 사이클에 따른 용량 특성을 도 5에 도시하였다. 도 5에서 보는 바와 같이 실시예 11의 코인 전지가 비교예 5에 비하여 우수한 사이클 용량 특성과 높은 방전전위를 보였다.

상기 실시예 7~12 및 비교예 3~6의 방법으로 제조된 코인 전지를 4.3V까지 충전하였다. 충전이 완료된 전지를 글로브 박스에서 해체한 후, 극판에서 활물질만 10mg을 채취하여 시료로 사용하였다. 이 시료를 이용하여 3℃/분의 속도로 공기 분위기 하에서 25 내지 300℃까지 DSC(differential scanning calorimetry) 스캔하여 양극 활물질의 열적 안정성을 측정하였다. 실시예 10과 비교예 4의 양극 활물질의 DSC 측정 결과는 도 6에 나타나 있다. 도 7은 실시예 11과 비교예 5의 양극 활물질의 DSC 측정 결과를 도시한 도면이다.

상기 실시예 7~12 및 비교예 3~6의 방법으로 제조된 코인 전지를 4.45V까지 과충전한 다음 글로브 박스에서 해체한 후, 극판에서 활물질만 10mg을 채취하여 시료로 사용하였다. 이 시료를 이용하여 3℃/분의 속도로 공기 분위기 하에서 25 내지 300℃까지 DSC 스캔하였다. 도 8에는 과충전 후 실시예 10과 비교예 4의 양극 활물질에 대한 DSC 측정 결과를 도시되어 있다.

DSC 분석은 충전된 양극 활물질의 열적 안정성을 확인하기 위해 실시한 것이다. 일반적으로 리튬 이차 전지의 안전성(safety)은 여러 가지 메카니즘에 의하여 진행되는데, 특히 충전 상태에서 못으로 관통시키는 실험이 가장 중요한 안전성 실험 중의 하나로 알려져 있다. 이때 충전된 전지의 안전성에 영향을 미치는 인자로서 여러 가지가 있는데, 특히 충전된 양극과 이 극판에 함침되어 있는 전해액의 반응에 의한 발열 반응이 중요한 역할을 한다고 알려져 있다. 이러한 현상을 비교 판단하는 방법으로 코인 전지를 제조한 후, 일정 전위로 충전시켜 $Li_{1-x}CoO_2$의 상태로 만든 후 이 충전 상태의 물질에 대한 DSC 측정을 통하여 나타나는 발열 온도와 발열량 및 발열 커브의 결과를 바탕으로 안전성 여부를 판단할 수 있다.

이를, $LiCoO_2$를 예를 들어 설명하면, $LiCoO_2$는 충전 상태에서 $Li_{1-x}CoO_2$의 구조를 가지게 된다. 이러한 구조를 가지는 활물질은 불안정하기 때문에 전지 내부의 온도가 높아지면 금속 즉, 코발트와 결합되어 있는 산소가 금속으로부터 유리된다. 유리된 산소는 전지 내부에서 전해액과 반응하여 전지가 폭발할 수 있는 기회를 제공할 가능성이 높다. 그러므로 산소 분해 온도와 이때의 발열량은 전지의 안정성을 나타내는 중요한 인자라 할 수 있다.

AMPEREX Ex. 1002
Page 1029

도 6에 도시된 바와 같이, 비교예 4의 발열피크는 약 220℃에서 크게 나타났으나 실시예 10의 발열 커브는 거의 수평에 가까운 것으로 발열피크를 보이지 않았다. 이것은 비교예 4의 양극 활물질보다 실시예 10의 양극 활물질이 발열량이 훨씬 감소된 것을 나타내는 것이며, 이로부터 본원발명에 따른 양극 활물질의 열적 안정성이 훨씬 우수함을 알 수 있다. 이러한 결과는 실시예 11과 비교예 5의 DSC 측정결과를 도시한 도 7에서도 확인할 수 있다. 또한 과충전 후 DSC 측정 결과인 도 8로부터 비교예 4와 실시예 10의 발열 피크의 면적의 격차가 더 심해짐을 알 수 있다.

발명의 효과

상술한 바와 같이, 본 발명의 리튬 이차 전지용 양극 활물질은 평균입경이 1~2㎛인 일차 입자가 조립되어 형성된 이차 입자의 평균 입경이 10㎛ 미만으로 작고, 표면에 금속 산화물 층이 형성되어 있어 우수한 방전 특성을 나타낸다. 이러한 방전 특성이 향상됨에 따라, 본 발명의 리튬 이차 전지용 양극 활물질을 사용한 전지는 충방전 사이클 진행에 따른 우수한 전력 특성을 발휘할 수 있으며, 이러한 전지를 전자 제품에 적용할 경우 사용시간을 늘릴 수 있다. 또한 본 발명의 리튬 이차 전지용 양극 활물질은 일정 범위의 입자 크기를 가지며, 표면에 금속 산화물 층을 포함하여 열적 안정성이 대폭 향상되고 따라서 전지 시스템에서의 안전성 향상에 큰 영향을 미치는 효과를 얻을 수 있다.

도면의 간단한 설명

도 1a 및 도 1b는 본 발명의 실시예 1 및 대조예 1의 방법으로 제조된 양극 활물질의 표면 상태를 각각 나타내는 SEM 사진.

도 2a 및 도 2b는 비교예 1 및 비교예 2의 방법으로 제조된 양극 활물질의 표면 상태를 각각 나타내는 SEM 사진.

도 3은 본 발명의 실시예 1 및 비교예 1의 방법으로 제조된 양극 활물질의 방전 용량을 나타낸 그래프.

도 4는 본 발명의 실시예 1 및 대조예 1의 방법으로 제조된 양극 활물질의 방전 용량을 나타낸 그래프.

도 5는 실시예 11과 비교예 5의 코인 전지에 대한 사이클에 따른 용량 특성을 도시한 그래프.

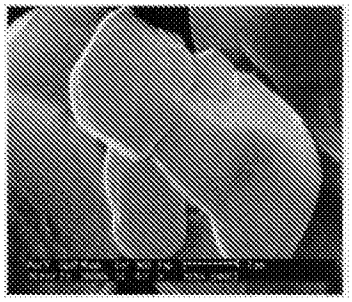
도 6은 실시예 10과 비교예 4의 양극 활물질에 대한 DSC 측정 결과를 나타낸 도면.

도 7은 실시예 11과 비교예 5의 양극 활물질에 대한 DSC 측정 결과를 도시한 도면.

도 8은 실시예 10과 비교예 4의 양극 활물질에 대한 과충전 후 DSC 측정 결과를 도시한 도면.

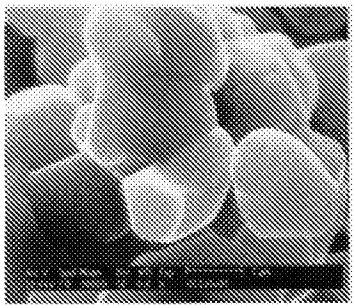
도면

도면1a

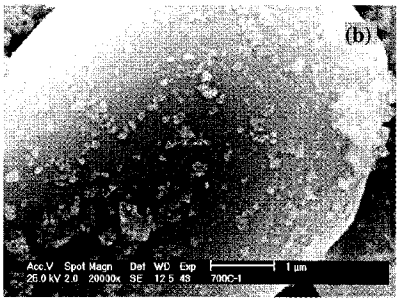


AMPEREX Ex. 1002
Page 1030

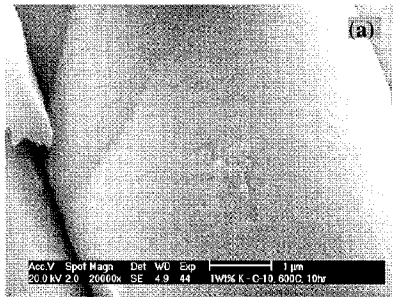
도면1b



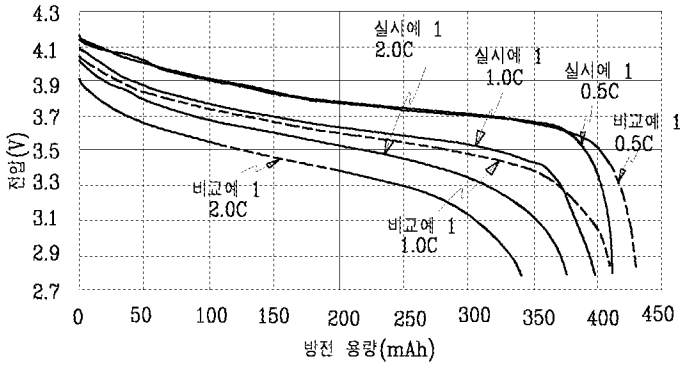
도면2a



도면2b

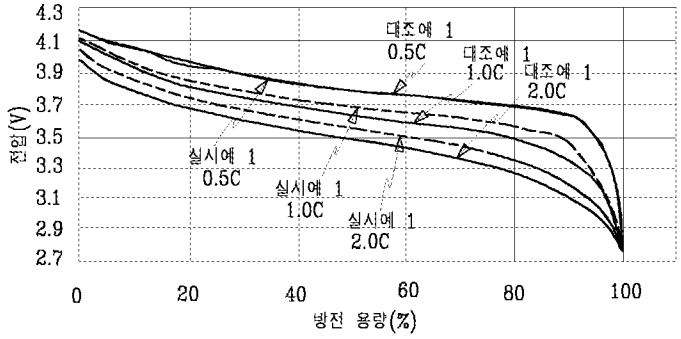


도면3

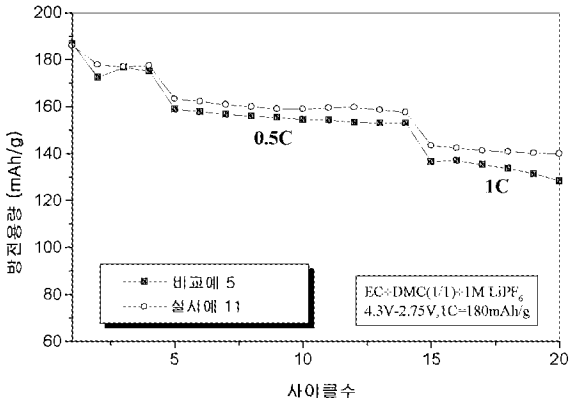


AMPEREX Ex. 1002
Page 1031

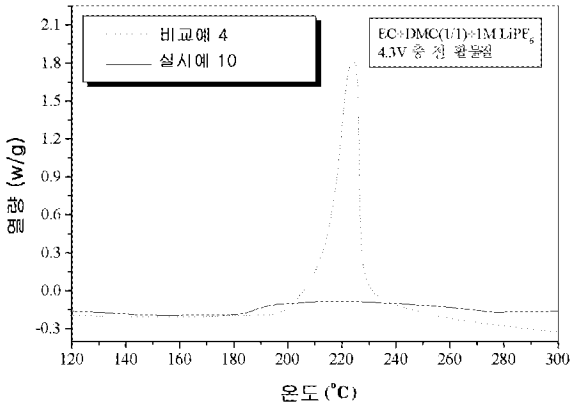
도면4



도면5

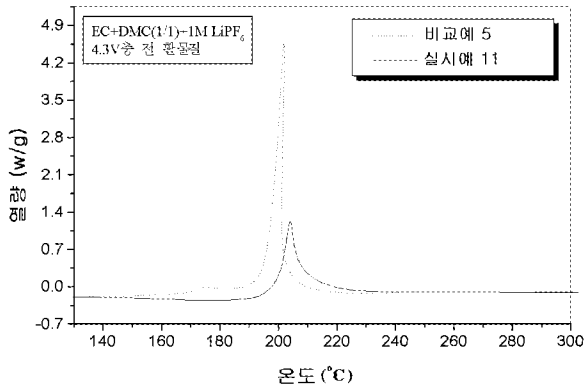


도면6

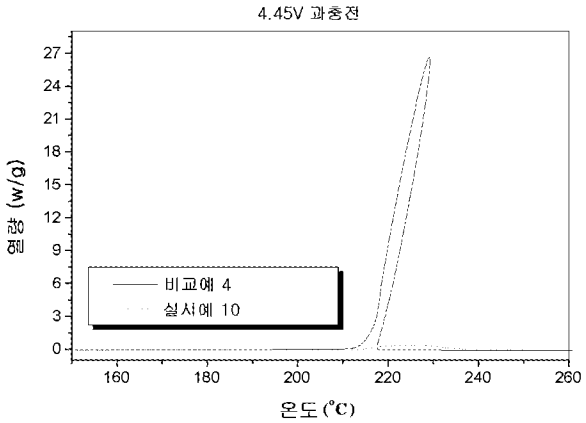


AMPEREX Ex. 1002
Page 1032

도면7


EC+DMC(1/1)+1M LiPF6
4.3V충 전 활물질
비교예 5
실시예 11
열량 (w/g)
온도 (°C)

도면8


4.45V 과충전
비교예 4
실시예 10
열량 (w/g)
온도 (°C)

Electronic Patent Application Fee Transmittal

Application Number:	16923494
Filing Date:	08-Jul-2020
Title of Invention:	POSITIVE ELECTRODE ACTIVE MATERIAL, METHOD FOR MANUFACTURING POSITIVE ELECTRODE ACTIVE MATERIAL, AND SECONDARY BATTERY
First Named Inventor/Applicant Name:	Teruaki OCHIAI
Filer:	John F. Hayden/Alexis Bailey
Attorney Docket Number:	12732-2003004

Filed as Large Entity

Filing Fees for Utility under 35 USC 111(a)

Description	Fee Code	Quantity	Amount	Sub-Total in USD($)
Basic Filing:				
Pages:				
Claims:				
Miscellaneous-Filing:				
Petition:				
Patent-Appeals-and-Interference:				
Post-Allowance-and-Post-Issuance:				
Extension-of-Time:				

Description	Fee Code	Quantity	Amount	Sub-Total in USD($)
Miscellaneous:				
SUBMISSION- INFORMATION DISCLOSURE STMT	1806	1	260	260
		Total in USD ($)		**260**

Electronic Acknowledgement Receipt

EFS ID:	40907982
Application Number:	16923494
International Application Number:	
Confirmation Number:	3273
Title of Invention:	POSITIVE ELECTRODE ACTIVE MATERIAL, METHOD FOR MANUFACTURING POSITIVE ELECTRODE ACTIVE MATERIAL, AND SECONDARY BATTERY
First Named Inventor/Applicant Name:	Teruaki OCHIAI
Customer Number:	26171
Filer:	John F. Hayden/Alexis Bailey
Filer Authorized By:	John F. Hayden
Attorney Docket Number:	12732-2003004
Receipt Date:	21-OCT-2020
Filing Date:	08-JUL-2020
Time Stamp:	16:23:17
Application Type:	Utility under 35 USC 111(a)

Payment information:

Submitted with Payment	yes
Payment Type	DA
Payment was successfully received in RAM	$260
RAM confirmation Number	E20200KG23325667
Deposit Account	
Authorized User	

The Director of the USPTO is hereby authorized to charge indicated fees and credit any overpayment as follows:

File Listing:

Document Number	Document Description	File Name	File Size(Bytes)/ Message Digest	Multi Part /.zip	Pages (if appl.)
1	Information Disclosure Statement (IDS) Form (SB08)	IDS_12732-2003004.pdf	160246 08ae12e61c0288d444e7e60e5d63231b83ebd2f7	no	2
Warnings:					
Information:					
This is not an USPTO supplied IDS fillable form					
2	Foreign Reference	CN105024047A.pdf	2548763 780892f151876307510d00bb7219b58220a74db5	no	43
Warnings:					
Information:					
3	Foreign Reference	KR100696619.pdf	1024428 043919922011cc0586a35a6f65391c72efb94b2a	no	19
Warnings:					
Information:					
4	Fee Worksheet (SB06)	fee-info.pdf	30638 1efadb663918352bc9b6228580c6c8627fa10142	no	2
Warnings:					
Information:					
		Total Files Size (in bytes):	3764075		

This Acknowledgement Receipt evidences receipt on the noted date by the USPTO of the indicated documents, characterized by the applicant, and including page counts, where applicable. It serves as evidence of receipt similar to a Post Card, as described in MPEP 503.

New Applications Under 35 U.S.C. 111

If a new application is being filed and the application includes the necessary components for a filing date (see 37 CFR 1.53(b)-(d) and MPEP 506), a Filing Receipt (37 CFR 1.54) will be issued in due course and the date shown on this Acknowledgement Receipt will establish the filing date of the application.

National Stage of an International Application under 35 U.S.C. 371

If a timely submission to enter the national stage of an international application is compliant with the conditions of 35 U.S.C. 371 and other applicable requirements a Form PCT/DO/EO/903 indicating acceptance of the application as a national stage submission under 35 U.S.C. 371 will be issued in addition to the Filing Receipt, in due course.

New International Application Filed with the USPTO as a Receiving Office

If a new international application is being filed and the international application includes the necessary components for an international filing date (see PCT Article 11 and MPEP 1810), a Notification of the International Application Number and of the International Filing Date (Form PCT/RO/105) will be issued in due course, subject to prescriptions concerning national security, and the date shown on this Acknowledgement Receipt will establish the international filing date of the application.

UNITED STATES PATENT AND TRADEMARK OFFICE

UNITED STATES DEPARTMENT OF COMMERCE
United States Patent and Trademark Office
Address: COMMISSIONER FOR PATENTS
P.O. Box 1450
Alexandria, Virginia 22313-1450
www.uspto.gov

APPLICATION NUMBER	FILING OR 371(C) DATE	FIRST NAMED APPLICANT	ATTY. DOCKET NO./TITLE
16/923,494	07/08/2020	Teruaki OCHIAI	12732-2003004

CONFIRMATION NO. 3273

26171
FISH & RICHARDSON P.C. (DC)
P.O. BOX 1022
MINNEAPOLIS, MN 55440-1022

PUBLICATION NOTICE

OC000000121003038

Title:POSITIVE ELECTRODE ACTIVE MATERIAL, METHOD FOR MANUFACTURING POSITIVE ELECTRODE ACTIVE MATERIAL, AND SECONDARY BATTERY

Publication No.US-2020-0343530-A1
Publication Date:10/29/2020

NOTICE OF PUBLICATION OF APPLICATION

The above-identified application will be electronically published as a patent application publication pursuant to 37 CFR 1.211, et seq. The patent application publication number and publication date are set forth above.

The publication may be accessed through the USPTO's publically available Searchable Databases via the Internet at www.uspto.gov. The direct link to access the publication is currently http://www.uspto.gov/patft/.

The publication process established by the Office does not provide for mailing a copy of the publication to applicant. A copy of the publication may be obtained from the Office upon payment of the appropriate fee set forth in 37 CFR 1.19(a)(1). Orders for copies of patent application publications are handled by the USPTO's Public Records Division. The Public Records Division can be reached by telephone at (571) 272-3150 or (800) 972-6382, by facsimile at (571) 273-3250, by mail addressed to the United States Patent and Trademark Office, Public Records Division, Alexandria, VA 22313-1450 or via the Internet.

In addition, information on the status of the application, including the mailing date of Office actions and the dates of receipt of correspondence filed in the Office, may also be accessed via the Internet through the Patent Electronic Business Center at www.uspto.gov using the public side of the Patent Application Information and Retrieval (PAIR) system. The direct link to access this status information is currently https://portal.uspto.gov/pair/PublicPair. Prior to publication, such status information is confidential and may only be obtained by applicant using the private side of PAIR.

Further assistance in electronically accessing the publication, or about PAIR, is available by calling the Patent Electronic Business Center at 1-866-217-9197.

Office of Data Managment, Application Assistance Unit (571) 272-4000, or (571) 272-4200, or 1-888-786-0101

AMPEREX Ex. 1002
Page 1039

To: PATDOCTC@fr.com,,
From: PAIR_eOfficeAction@uspto.gov
Cc: PAIR_eOfficeAction@uspto.gov
Subject: Private PAIR Correspondence Notification for Customer Number 26171

Oct 30, 2020 04:34:13 AM

Dear PAIR Customer:

FISH & RICHARDSON P.C. (DC)
P.O. BOX 1022
MINNEAPOLIS, MN 55440-1022
UNITED STATES

The following USPTO patent application(s) associated with your Customer Number, 26171 , have new outgoing correspondence. This correspondence is now available for viewing in Private PAIR.

The official date of notification of the outgoing correspondence will be indicated on the form PTOL-90 accompanying the correspondence.

Disclaimer:
The list of documents shown below is provided as a courtesy and is not part of the official file wrapper. The content of the images shown in PAIR is the official record.

Application	Document	Mailroom Date	Attorney Docket No.
16923494	NTC.PUB	10/29/2020	12732-2003004

To view your correspondence online or update your email addresses, please visit us anytime at https://sportal.uspto.gov/secure/myportal/privatepair.

If you have any questions, please email the Electronic Business Center (EBC) at EBC@uspto.gov with 'e-Office Action' on the subject line or call 1-866-217-9197 during the following hours:

Monday - Friday 6:00 a.m. to 12:00 a.m.

Thank you for prompt attention to this notice,

UNITED STATES PATENT AND TRADEMARK OFFICE

PATENT APPLICATION INFORMATION RETRIEVAL SYSTEM

PTO/SB/08A (07-06)
Approved for use through 03/31/2007. OMB 0651-0031
U.S. Patent and Trademark Office; U.S. DEPARTMENT OF COMMERCE

Under the Paperwork Reduction Act of 1995, no persons are required to respond to a collection of information unless it contains a valid OMB control number.

Substitute for form 1449/PTO

INFORMATION DISCLOSURE STATEMENT BY APPLICANT

(Use as many sheets as necessary)

Sheet 1 of 3

Complete if Known	
Application Number	16/923,494
Filing Date	July 8, 2020
First Named Inventor	Teruaki OCHIAI
Art Unit	1725
Examiner Name	S. CULLEN
Attorney Docket Number	12732-2003004

U. S. PATENT DOCUMENTS

Examiner Initials*	Cite No.[1]	Document Number Number-Kind Code[2] (if known)	Publication Date MM-DD-YYYY	Name of Patentee or Applicant of Cited Document	Pages, Columns, Lines, Where Relevant Passages or Relevant Figures Appear
		US-9,105,926	08-11-2015	Fujiki.S et al.	
		US-2014/0212759	07-31-2014	Blangero.M et al.	
		US-8,951,448	02-10-2015	Toyama.T et al.	
		US-10,777,815	09-15-2020	Kanada.S et al.	
		US-2016/0336595	11-17-2016	Choi.S et al.	
		US-7,504,180	03-17-2009	Tatsumi.K et al.	
		US-9,614,225	04-04-2017	Park.J	
		US-9,812,709	11-07-2017	Endoh.K et al.	
		US-2004/0142241	07-22-2004	Nagayama.M	
		US-2006/0263690	11-23-2006	Suhara.M et al.	
		US-2009/0017383	01-15-2009	Suhara.M et al.	
		US-2010/0294985	11-25-2010	Suhara.M et al.	
		US-2016/0276659	09-22-2016	Choi.S et al.	
		US-2018/0034045	02-01-2018	Xia.X et al.	
		US-2013/0052534	02-28-2013	Fujiki.S et al.	
		US-2013/0089786	04-11-2013	Jeong.C et al.	
		US-2018/0190976	07-05-2018	Blangero.M et al.	
		US-2010/0086854	04-08-2010	Kumar.S et al.	
		US-9,871,246	01-16-2018	Kim.J et al.	

FOREIGN PATENT DOCUMENTS

Examiner Initials*	Cite No.[1]	Foreign Patent Document Country Code[3] -Number[4] -Kind Code[5] (if known)	Publication Date MM-DD-YYYY	Name of Patentee or Applicant of Cited Document	Pages, Columns, Lines, Where Relevant Passages or Relevant Figures Appear	T[6]
		CN-001715193A	01-04-2006			Abst.
		CN-103490060A	01-01-2014			Abst.
		JP-2003-068306A	03-07-2003			Abst.
		JP-2008-060033A	03-13-2008			Abst.
		JP-2013-087040A	05-13-2013			Abst.
		KR-2016-0092946A	08-05-2016			Abst.

Examiner Signature		Date Considered	

*EXAMINER: Initial if reference considered, whether or not citation is in conformance with MPEP 609. Draw line through citation if not in conformance and not considered. Include copy of this form with next communication to applicant. 1 Applicant's unique citation designation number (optional). 2 See Kinds Codes of USPTO Patent Documents at www.uspto.gov or MPEP 901.04. 3 Enter Office that issued the document, by the two-letter code (WIPO Standard ST.3). 4 For Japanese patent documents, the indication of the year of the reign of the Emperor must precede the serial number of the patent document. 5 Kind of document by the appropriate symbols as indicated on the document under WIPO Standard ST.16 if possible. 6 Applicant is to place a check mark here if English language Translation is attached.

This collection of information is required by 37 CFR 1.97 and 1.98. The information is required to obtain or retain a benefit by the public which is to file (and by the USPTO to process) an application. Confidentiality is governed by 35 U.S.C. 122 and 37 CFR 1.14. This collection is estimated to take 2 hours to complete, including gathering, preparing, and submitting the completed application form to the USPTO. Time will vary depending upon the individual case. Any comments on the amount of time you require to complete this form and/or suggestions for reducing this burden, should be sent to the Chief Information Officer, U.S. Patent and Trademark Office, P.O. Box 1450, Alexandria, VA 22313-1450. DO NOT SEND FEES OR COMPLETED FORMS TO THIS ADDRESS. **SEND TO: Commissioner for Patents, P.O. Box 1450, Alexandria, VA 22313-1450.**

If you need assistance in completing the form, call 1-800-PTO-9199 (1-800-786-9199) and select option 2.

PTO/SB/08A (07-06)
Approved for use through 03/31/2007. OMB 0651-0031
U.S. Patent and Trademark Office; U.S. DEPARTMENT OF COMMERCE

Under the Paperwork Reduction Act of 1995, no persons are required to respond to a collection of information unless it contains a valid OMB control number.

Substitute for form 1449/PTO

INFORMATION DISCLOSURE STATEMENT BY APPLICANT

(Use as many sheets as necessary)

Sheet 2 of 3

Complete if Known	
Application Number	16/923,494
Filing Date	July 8, 2020
First Named Inventor	Teruaki OCHIAI
Art Unit	1725
Examiner Name	S. CULLEN
Attorney Docket Number	12732-2003004

U. S. PATENT DOCUMENTS

Examiner Initials*	Cite No.[1]	Document Number Number-Kind Code[2] (if known)	Publication Date MM-DD-YYYY	Name of Patentee or Applicant of Cited Document	Pages, Columns, Lines, Where Relevant Passages or Relevant Figures Appear
		US-6,277,521	08-21-2001	Gao.Y et al.	
		US-6,589,499	07-08-2003	Gao.Y et al.	
		US-6,878,490	04-12-2005	Gao.Y et al.	
		US-6,127,065	10-03-2000	Yamamoto.Y et al.	

FOREIGN PATENT DOCUMENTS

Examiner Initials*	Cite No.[1]	Foreign Patent Document Country Code[3] -Number[4] -Kind Code[5] (if known)	Publication Date MM-DD-YYYY	Name of Patentee or Applicant of Cited Document	Pages, Columns, Lines, Where Relevant Passages or Relevant Figures Appear	T[6]
		CN-102779976A	11-14-2012			Abst.
		CN-102339998A	02-01-2012			Abst.
		CN-102447107A	05-09-2012			Abst.
		CN-103022502A	04-03-2013			Abst.
		CN-104701534A	06-10-2015			Abst.
		CN-106099098A	11-09-2016			Abst.

Examiner Signature		Date Considered	

*EXAMINER: Initial if reference considered, whether or not citation is in conformance with MPEP 609. Draw line through citation if not in conformance and not considered. Include copy of this form with next communication to applicant. 1 Applicant's unique citation designation number (optional). 2 See Kinds Codes of USPTO Patent Documents at www.uspto.gov or MPEP 901.04. 3 Enter Office that issued the document, by the two-letter code (WIPO Standard ST.3). 4 For Japanese patent documents, the indication of the year of the reign of the Emperor must precede the serial number of the patent document. 5 Kind of document by the appropriate symbols as indicated on the document under WIPO Standard ST.16 if possible. 6 Applicant is to place a check mark here if English language Translation is attached.

This collection of information is required by 37 CFR 1.97 and 1.98. The information is required to obtain or retain a benefit by the public which is to file (and by the USPTO to process) an application. Confidentiality is governed by 35 U.S.C. 122 and 37 CFR 1.14. This collection is estimated to take 2 hours to complete, including gathering, preparing, and submitting the completed application form to the USPTO. Time will vary depending upon the individual case. Any comments on the amount of time you require to complete this form and/or suggestions for reducing this burden, should be sent to the Chief Information Officer, U.S. Patent and Trademark Office, P.O. Box 1450, Alexandria, VA 22313-1450. DO NOT SEND FEES OR COMPLETED FORMS TO THIS ADDRESS. **SEND TO: Commissioner for Patents, P.O. Box 1450, Alexandria, VA 22313-1450.**

If you need assistance in completing the form, call 1-800-PTO-9199 (1-800-786-9199) and select option 2.

PTO/SB/08A (07-06)
Approved for use through 03/31/2007. OMB 0651-0031
U.S. Patent and Trademark Office; U.S. DEPARTMENT OF COMMERCE

Under the Paperwork Reduction Act of 1995, no persons are required to respond to a collection of information unless it contains a valid OMB control number.

Substitute for form 1449/PTO

INFORMATION DISCLOSURE STATEMENT BY APPLICANT

(Use as many sheets as necessary)

Sheet 3 of 3

Complete if Known	
Application Number	16/923,494
Filing Date	July 8, 2020
First Named Inventor	Teruaki OCHIAI
Art Unit	1725
Examiner Name	S. CULLEN
Attorney Docket Number	12732-2003004

NON PATENT LITERATURE DOCUMENTS

Examiner Initials*	Cite No.[1]	Include name of the author (in CAPITAL LETTERS), title of the article (when appropriate), title of the item (book, magazine, journal, serial, symposium, catalog, etc.), date, page(s), volume-issue number(s), publisher, city and/or country where published.	T[2]
		Antolini.E, "LiCoO2: formation, structure, lithium and oxygen nonstoichiometry, electrochemical behaviour and transport properties", Solid State Ionics, 2004, Vol. 170, No. 3-4, pp. 159-171.	Eng.
		Ceder.G et al., "Identification of cathode materials for lithium batteries guided by first-principles calculations", NATURE, April 16, 1998, Vol. 392, pp. 694-696.	Eng.
		Gopukumar.S et al., "Synthesis and electrochemical performance of tetravalent doped LiCoO2 in lithium rechargeable cells", Solid State Ionics, 2003, Vol. 159, pp. 223-232, ELSEVIER.	Eng.

Examiner Signature		Date Considered	

*EXAMINER: Initial if reference considered, whether or not citation is in conformance with MPEP 609. Draw line through citation if not in conformance and not considered. Include copy of this form with next communication to applicant.
1 Applicant's unique citation designation number (optional). 2 Applicant is to place a check mark here if English language Translation is attached.

This collection of information is required by 37 CFR 1.97 and 1.98. The information is required to obtain or retain a benefit by the public which is to file (and by the USPTO to process) an application. Confidentiality is governed by 35 U.S.C. 122 and 37 CFR 1.14. This collection is estimated to take 2 hours to complete, including gathering, preparing, and submitting the completed application form to the USPTO. Time will vary depending upon the individual case. Any comments on the amount of time you require to complete this form and/or suggestions for reducing this burden, should be sent to the Chief Information Officer, U.S. Patent and Trademark Office, U.S. Department of Commerce, P.O. Box 1450, Alexandria, VA 22313-1450. DO NOT SEND FEES OR COMPLETED FORMS TO THIS ADDRESS. **SEND TO: Commissioner for Patents, P.O. Box 1450, Alexandria, VA 22313-1450.**

If you need assistance in completing the form, call 1-800-PTO-9199 (1-800-786-9199) and select option 2.

PTO/SB/08A (07-06)
Approved for use through 03/31/2007. OMB 0651-0031
U.S. Patent and Trademark Office; U.S. DEPARTMENT OF COMMERCE

Under the Paperwork Reduction Act of 1995, no persons are required to respond to a collection of information unless it contains a valid OMB control number.

Substitute for form 1449/PTO

INFORMATION DISCLOSURE STATEMENT BY APPLICANT

(Use as many sheets as necessary)

Sheet 1 of 1

Complete if Known	
Application Number	16/923,494
Filing Date	July 8, 2020
First Named Inventor	Teruaki OCHIAI
Art Unit	1725
Examiner Name	S. CULLEN
Attorney Docket Number	12732-2003004

U. S. PATENT DOCUMENTS

Examiner Initials*	Cite No.[1]	Document Number Number-Kind Code[2] (if known)	Publication Date MM-DD-YYYY	Name of Patentee or Applicant of Cited Document	Pages, Columns, Lines, Where Relevant Passages or Relevant Figures Appear
		US-9,385,366	07-05-2016	Yamakaji.M et al.	

FOREIGN PATENT DOCUMENTS

Examiner Initials*	Cite No.[1]	Foreign Patent Document Country Code[3] -Number[4] -Kind Code[5] (if known)	Publication Date MM-DD-YYYY	Name of Patentee or Applicant of Cited Document	Pages, Columns, Lines, Where Relevant Passages or Relevant Figures Appear	T[6]
		KR-2009-0111130A	10-26-2009			Abst.

Examiner Signature		Date Considered	

*EXAMINER: Initial if reference considered, whether or not citation is in conformance with MPEP 609. Draw line through citation if not in conformance and not considered. Include copy of this form with next communication to applicant. 1 Applicant's unique citation designation number (optional). 2 See Kinds Codes of USPTO Patent Documents at www.uspto.gov or MPEP 901.04. 3 Enter Office that issued the document, by the two-letter code (WIPO Standard ST.3). 4 For Japanese patent documents, the indication of the year of the reign of the Emperor must precede the serial number of the patent document. 5 Kind of document by the appropriate symbols as indicated on the document under WIPO Standard ST.16 if possible. 6 Applicant is to place a check mark here if English language Translation is attached.

This collection of information is required by 37 CFR 1.97 and 1.98. The information is required to obtain or retain a benefit by the public which is to file (and by the USPTO to process) an application. Confidentiality is governed by 35 U.S.C. 122 and 37 CFR 1.14. This collection is estimated to take 2 hours to complete, including gathering, preparing, and submitting the completed application form to the USPTO. Time will vary depending upon the individual case. Any comments on the amount of time you require to complete this form and/or suggestions for reducing this burden, should be sent to the Chief Information Officer, U.S. Patent and Trademark Office, P.O. Box 1450, Alexandria, VA 22313-1450. DO NOT SEND FEES OR COMPLETED FORMS TO THIS ADDRESS. **SEND TO: Commissioner for Patents, P.O. Box 1450, Alexandria, VA 22313-1450.**

If you need assistance in completing the form, call 1-800-PTO-9199 (1-800-786-9199) and select option 2.

IN THE UNITED STATES PATENT AND TRADEMARK OFFICE

First Named Inventor	:	Teruaki OCHIAI	Art Unit	:	1725
Application No.	:	16/923,494	Examiner	:	Sean P. Cullen
Filed	:	July 8, 2020	Conf. No.	:	3273
Title	:	POSITIVE ELECTRODE ACTIVE MATERIAL, METHOD FOR MANUFACTURING POSITIVE ELECTRODE ACTIVE MATERIAL, AND SECONDARY BATTERY			

Commissioner for Patents
P.O. Box 1450
Alexandria, VA 22313-1450

INFORMATION DISCLOSURE STATEMENT

Please consider the references listed on the enclosed disclosure form. Copies of the documents required under 37 C.F.R. § 1.98(a)(2) are being submitted with this statement.

This statement is being filed after a first action on the merits, but before receipt of a final action or a notice of allowance. A late submission fee in the amount of $260 specified by 37 CFR §1.17(p), is being paid with this statement. Please apply any charges or credits to Deposit Account No. 06-1050, referencing the above attorney docket number.

Respectfully submitted,

Date: December 21, 2020

/Heather L. Flanagan/
Heather L. Flanagan
Reg. No. 54,101

Customer Number 26171
Fish & Richardson P.C.
Telephone: +1 512-226-8156
Facsimile: (877) 769-7945

62490932.doc

Espacenet

Family list: CN1715193 (A) — 2006-01-04

1 application(s) for: CN1715193 (A)

1. New process for preparing high quality Co3O4					
Inventor: HU GUORONG [CN]	**Applicant:** RUIXIANG NEW MATERIAL CO LTD H [CN]	**CPC:**	**IPC:** C01G51/04	**Publication info:** CN1715193 (A) 2006-01-04 CN100398454 (C) 2008-07-02	**Priority date:** 2004-06-28

Espacenet

Bibliographic data: CN1715193 (A) — 2006-01-04

New process for preparing high quality Co3O4

Inventor(s): HU GUORONG [CN] ± (GUORONG HU, ; HU GUORONG)

Applicant(s): RUIXIANG NEW MATERIAL CO LTD H [CN] ± (RUIXIANG NEW MATERIAL CO., LTD., HUNAN, ; NANTONG RESHINE NEW MATERIAL CO., LTD)

Classification: **- international:** ***C01G51/04***
- cooperative:

Application number: CN20041023350 20040628

Priority number (s): CN20041023350 20040628

Also published as: CN100398454 (C)

Abstract of CN1715193 (A)

In the new process of preparing high quality Co3O4 product, Co salt with crystalline water is loaded into corundum crucible or other special container at normal pressure, roasted at 250-900 deg.c in special reaction furnace for 5-20 hr for growing complete crystal grain, and finally cooled naturally, so as to obtain Co3O4 powder in single polygonal cube structure and with complete crystal form and high density. The production process is environment friendly, short in time, low in cost, high in yield and high in product quality.

[19] 中华人民共和国国家知识产权局

[51] Int. Cl.
C01G 51/04 (2006.01)

[12] 发明专利申请公开说明书

[21] 申请号 200410023350.6

[43] 公开日 2006 年 1 月 4 日

[11] 公开号 CN 1715193A

[22] 申请日 2004.6.28
[21] 申请号 200410023350.6
[71] 申请人 湖南瑞翔新材料有限公司
地址 410100 湖南省长沙市经济技术开发区天华路
[72] 发明人 胡国荣

[74] 专利代理机构 长沙正奇专利事务所有限责任公司
代理人 魏国先

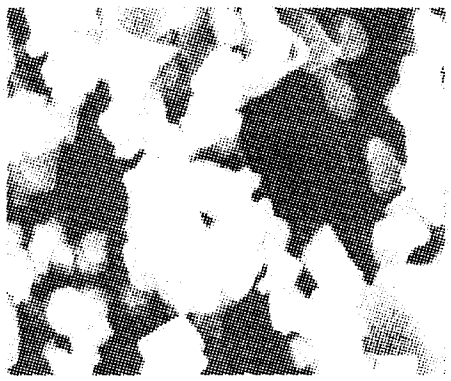
权利要求书 1 页 说明书 6 页 附图 3 页

[54] 发明名称

制备高品质四氧化三钴的新方法

[57] 摘要

一种制备高品质四氧化三钴的新方法，采用带结晶水的钴盐，在常压下用刚玉坩埚等专用容器盛装，载入专用的反应炉，在 250℃ ~ 900℃ 的高温下，焙烧 5 – 20 小时，促使颗粒晶型生长完整，最后经自然冷却收集成粒度好、形貌单一且为多面立方体结构、晶型结构完整、振实密度高的四氧化三钴粉体。 本发明生产稳定，无污水排出，有利环境保护，设备投资少，流程短，成本低，产量高，质量好，工艺成熟，技术先进。



1. 一种制备高品质四氧化三钴的新方法，其特征在于采用带结晶水的钴盐，在常压下用专用容器盛装载入专用的反应炉，经烧结，制成高品质四氧化三钴粉体。

2. 根据权利要求 1 所述的制备高品质四氧化三钴的新方法，其特征在于采用带结晶水的钴盐为 $CoCl_2 \cdot xH_2O$，$Co(NO_3)_2 \cdot xH_2O$，$CoSO_4 \cdot xH_2O$，$Co(AC)_2 \cdot xH_2O$，（x=1~6）中的至少一种。

3. 根据权利要求 1 所述的制备高品质四氧化三钴的新方法，其特征在于所述的专用容器可采用刚玉坩埚或陶瓷坩埚或石墨坩埚或粘土坩埚。

4. 根据权利要求 1 所述的制备高品质四氧化三钴的专用反应炉，其特征在于包括煅烧部分和尾气处理回收部分，煅烧部分的炉体由铁壳外墙内砌耐火材料构成，炉体内的下部和侧部安装有电加热装置，电加热装置与炉膛之间用耐火挡板隔开，炉体中段的上部具有垂直通气道和气体缓冲室，炉膛上部通过垂直通气道与气体缓冲室连通，气体缓冲室的烟气出口连接尾气处理回收部分，炉体内分为预热区、蒸发区、反应分解区、降温区四个部分，炉口处设有气墙，炉体内还安装有推板；尾气处理回收部分由管道依次连接的引风机、冷凝器、吸收塔构成，冷凝器还具有冷凝水入口和冷凝水出口，吸收塔为喷淋吸收塔，还连接安装有由回收罐、循环泵、循环管道连接连通构成的循环、回收装置。

5. 根据权利要求 1 所述的制备高品质四氧化三钴的新方法，其特征在于专用的反应炉其升温速度为 2—10℃/分钟，炉内温度为 250℃—900℃，带结晶水的钴盐在专用的反应炉内烧结时间为 5—20 小时。

AMPEREX Ex. 1002
Page 1049

制备高品质四氧化三钴的新方法

技术领域

本发明涉及一种金属氧化物的制造技术，具体涉及一种水合钴盐一步直接焙烧制备高品质四氧化三钴的方法。

背景技术

新能源二次锂离子技术的广泛应用，推动了我国用于锂离子电池正极材料、尤其是以电池级四氧化三钴为主体原料的钴酸锂材料制备技术和生产规模的迅速扩张。作为正极材料的首选原料，电池级四氧化三钴的制备技术也成为了正极材料制备技术的关键问题之一。目前制备四氧化三钴主要有两种途径，一是采用钴盐溶液的喷雾焙烧(以比利时的 Umicore 公司为首)，其优点是流程简单，易于控制，产品质量稳定，但这种方法设备投资非常大，大约需要 1000~2000 万美元，同时制作焙烧溶液所带来的能耗也非常大，这在国内很难实现，还有其焙烧出来的四氧化三钴粉末中的阴离子很难洗涤干净。二是采用钴盐预先沉淀为钴的氢氧化物，然后再热分解该沉淀物来生产四氧化三钴（以美国的 OMG 公司为首），其优点是设备投资相对上一种方法较少，产品形貌和粒度控制好，但是这种方法在制备氢氧化物过程中存在着流程长、沉淀相态不稳定，且在沉淀中的钠等杂质离子很难洗涤干净和在沉淀过程中易带入铁、钙、镁等其他杂质，以及生产的母液含有大量的铵盐和氯根离子给环境造成污染等缺点；目前国内的方法大多是采用氯化钴溶液用碳酸氢氨或草酸氨等沉淀剂沉淀钴盐（以金川和赣州钴钨有限公司为代表），生成碳酸钴或草酸钴等沉淀物，然后热分解碳酸钴、草酸钴等沉淀物来制备四氧化三钴粉末，这种方法制备的四氧化三钴，

AMPEREX Ex. 1002
Page 1050

其粒度、形貌、比表面积和振实密度难以达到制备钴酸锂的要求，且生产过程易带入铁、钠、镁、钙等杂质。锂离子电池正极材料钴酸锂的制备对其原材料四氧化三钴提出了严格要求，主要包括：粒度要求小且分布均匀；形貌单一为多面立方结构；表面活性高；振实密度大，产品杂质含量低；原料易于得到，而且价廉。传统方法制备的四氧化三钴主要用于硬质合金和陶瓷领域，其在形貌上为无定形，粒度分布宽，振实密度低且表面活性差等缺点，很难满足现在制备锂离子二次电池用正极材料钴酸锂的制备要求。

发明内容

本发明所要解决的技术问题是：解决传统工艺喷雾焙烧和沉淀—烧结方法制备四氧化三钴存在的设备投入大、流程长、能耗高、环境污染严重、成本高、生产不稳定、产品形貌和粒度难以控制、无法满足制造钴酸锂要求等问题；而提供一种工艺先进、生产稳定、无污水排出、产生的少量酸性气体能吸收成为副产品、有利保护环境、设备投资少、生产成本低、流程短、能耗低、产品质量好、产量高的制备高品质四氧化三钴的新方法。

本发明采用的技术方案是：采用带结晶水的钴盐，在常压下用专用容器盛装载入专用的反应炉，经烧结，制成高品质四氧化三钴粉体。

上述技术方案中，采用带结晶水的钴盐为 $CoCl_2 \cdot xH_2O$，$Co(NO_3)_2 \cdot xH_2O$，$CoSO_4 \cdot xH_2O$，$Co(AC)_2 \cdot xH_2O$，（x=1~6）中的至少一种。

上述技术方案中，所述的专用容器可采用刚玉坩埚或陶瓷坩埚或石墨坩埚或粘土坩埚。

上述技术方案中，所述的专用的反应炉为现有电热窑炉的改进，包括煅烧部分和尾气处理回收部分，煅烧部分的炉体由铁壳外墙内砌耐火材料构成，炉体内的下部和侧部安装有电加热装置，电加热装置与炉膛之间用耐火挡板隔开，

AMPEREX Ex. 1002
Page 1051

炉体中段的上部具有垂直通气道和气体缓冲室，炉膛上部通过垂直通气道与气体缓冲室连通，气体缓冲室的烟气出口连接尾气处理回收部分，炉体内分为预热区、蒸发区、反应分解区、降温区四个部分，炉口处设有气墙，炉体内还安装有推板，原料由推板推入反应炉内焙烧，制成高品质四氧化三钴，尾气处理回收部分由管道依次连接的引风机、冷凝器、吸收塔构成，冷凝器还具有冷凝水入口和冷凝水出口，吸收塔为喷淋吸收塔，还连接安装有由回收罐、循环泵、循环管道连接连通构成的循环、回收装置。

上述技术方案中，专用的反应炉其升温速度为 2—10℃/分钟，炉内温度为250℃—900℃，带结晶水的钴盐在专用的反应炉内烧结时间为 5—20 小时。

本发明提供了一种以钴盐为前驱体、直接进入特殊设计的专用反应炉中烧结分解的制备工艺，采用本发明制备四氧化三钴的工艺，可取代现有的喷雾焙烧和沉淀—烧结法生产四氧化三钴的工艺，本发明继承了喷雾焙烧法的优点，在工艺流程上完全不经历传统工艺的湿法沉淀部分，因而生产稳定，同时无污水排出，只产生少量酸性气体，该酸性气体又经本发明的特殊处理，百分之百得到吸收，并可作为副产品出售，环境大为改善，设备投资少，远远低于喷雾焙烧设备和沉淀——烧结流程的设备投入，大幅降低生产成本，也简化了生产的过程控制和设备的维修，大大提高了生产效率，实现了生产过程流程短、低能耗、无污染、高产量、低成本等目标。特别是制备的四氧化三钴质量好、粒度合理、形貌单一、振实密度大，为高品质电池级四氧化三钴。粒度为 3—8μm，形貌单一且为多面立方体结构，晶型结构完整，从粉体 X—射线衍射图上看无杂相，振实密度为 2.2—2.8g/cm^3，完全能满足制备锂离子二次电池用正极材料钴酸锂的要求。

AMPEREX Ex. 1002
Page 1052

附图说明

图 1 为本发明制备的四氧化三钴的 SEM 图

图 2 为本发明制备的四氧化三钴的 XRD 图

图 3 为专用的反应炉纵向结构示意图

图 4 为图 3 中 A—A 剖面示图

图 5 为图 3 中 B—B 剖面示图

图 6 为图 3 中 C—C 剖面示图

具体实施方式

本发明提出的一种制备高品质四氧化三钴的新方法是水合钴盐一步直接焙烧法，即从原料出发只需要一个焙烧过程就可直接得到完全符合制备钴酸锂要求的四氧化三钴粉体。

本发明采用带有结晶水的钴盐，如 $CoCl_2 \cdot xH_2O$，$Co(NO_3)_2 \cdot xH_2O$，$CoSO_4 \cdot xH_2O$，$Co(AC)_2 \cdot xH_2O$，（x=1~6）等中的至少一种，特别优先采用 $CoCl_2 \cdot xH_2O$，在常压下用特制容器如刚玉坩埚或陶瓷坩埚或石墨坩埚或粘土坩埚盛装，盛装物料厚度以 2—5cm 为最佳，载入经特别改进设计的专用反应炉中，这种专用的反应炉为隧道窑、推板窑、回转窑、箱式炉中至少一种的改进，带结晶水钴盐的专用的反应炉中，以 2—10℃/分钟的升温速度升到 250℃—900℃，特别优先 500℃—850℃，使钴盐快速分解得到粒度分布均匀的颗粒，再通过保持一定的烧结时间 5—20 小时，特别优先 15—20 小时，促使颗粒晶型进一步生长完整，最后产物经自然冷却收集，最终得到粒度为 3—8μm、形貌单一且为多面立方体结构，如图 1 所示，晶型结构完整，从粉体 X—射线衍射图上看无杂相，如图 2 所示，振实密度为 2.2—2.8g/cm^3 的四氧化三钴粉体。工艺过程中产生的酸性气体经本发明专用反应炉中尾气处理回收部分的引风机引入冷凝器

AMPEREX Ex. 1002
Page 1053

中冷却，再经吸收塔循环吸收，完全吸收后作为副产品。

参见图 3、图 4，本发明专用的反应炉为现有电热窑炉的改进，如推板窑、箱式炉、隧道窑、回转窑等的改进，本发明专用的反应炉包括煅烧部分和尾气处理回收部分，煅烧部分的炉体 1 为铁壳外墙 2 内砌耐火材料 3 构成，这些耐火材料 3 为保温层，可采用莫来石纤维或高铝纤维、轻质刚玉莫来石、陶瓷纤维、低铁氧化铝聚轻高铝砖、重刚玉莫来石、碳化硅等耐火材料，炉体内的下部和侧部安装电加热装置，取消传统窑炉的上部加热方式，这些电加热装置为电阻丝 4 和电加热硅碳棒 5，电加热装置与炉膛之间用耐火砖挡板 6 隔开，以此加强对加热元件的保护，炉体中段的上部具有垂直通气道 7 和气体缓冲室 8，炉膛上部通过垂直通气道 7 与气体缓冲室 8 连通，气体缓冲室 8 的烟气出口 9 连接连通尾气处理回收部分，炉体 1 内分为预热区 10、蒸发区 11、反应分解区 12、降温区 13 四个部分，炉口处 14 设有两到三个气墙，成 90° 交叉摆放，由空气喷咀喷射形成气墙。炉体 1 内还设置有推板 15，推板由机械推动或液压机械传动。带结晶水的钴盐原料由推板 15 推入反应炉内，首先在预热区预热 2—3 小时，脱去部分结晶水：

$$CoCl_2 \cdot 6H_2O \xrightarrow{\triangle} CoCl_2 \cdot 4H_2O + 2H_2O\uparrow$$

然后进入蒸发区 3—5 小时，再脱去部分结晶水：

$$CoCl_2 \cdot 4H_2O \xrightarrow{\triangle} CoCl_2 \cdot 2H_2O + 2H_2O\uparrow$$

上述脱出的结晶水以水蒸汽的形式由垂直通气道 7 进入气体缓冲室 8，最后进入尾气处理回收部分，钴盐原料进入反应分解区 4—6 小时，发生剧烈反应，生成四氧化三钴和酸性气体：$6(CoCl_2 \cdot H_2O) + O_2 \xrightarrow{\triangle} 2Co_3O_4 + 12HCl\uparrow$ 酸性气体也由垂直通气道 7 进入气体缓冲室 8，四氧化三钴颗粒晶型进一步生长完整后，最后进入炉体内的降温区约 4—6 小时，经自然冷却收集，最终得到

AMPEREX Ex. 1002
Page 1054

高品质的电池级四氧化三钴粉体。前述的水蒸汽和酸性气体由引风机 16 通过管道引入冷凝器 17 中冷却并预回收，冷凝器 17 内材质为石墨或钛钢，并连接有冷却水入口 18 和冷却水出口 19，经冷凝器后的剩余气体引入喷淋吸收塔 20 循环反复吸收，直至酸性气体完全吸收后剩余气体由引风机 24 及管道引出排空，与喷淋吸收塔 20 相配套连接安装有回收罐 21 及循环泵 22，经循环吸收后，母液回收由管道 23 输出。

本发明提出的水合钴盐一步直接焙烧制备电池级高品质四氧化三钴粉末的方法，在提高产品质量的同时省略了传统工艺中湿法沉钴的部分和烧结后破碎分级过程，简化了工艺流程，在大大节约了生产设备投入的同时，也简化了生产过程控制和设备维修，并大大提高了产量，保护了环境。

前述的冷凝器、喷淋吸收塔、回收罐、循环泵、引风机均可采用现有的环保设备。

实施例

将含有结晶水的钴盐 $CoCl_2 \cdot xH_2O$ 或 $Co(NO_3)_2 \cdot xH_2O$ 或 $CoSO_4 \cdot xH_2O$ 或 $Co(AC)_2 \cdot xH_2O$，（x=1~6）以刚玉坩埚盛好，推入本发明专用反应炉内，以 5℃/分钟的升温速度升到 850℃下煅烧 15 小时，使颗粒晶型进一步生长完整，最后经自然冷却收集，得到平均粒径为 3—8μm 的粉体，振实密度为 2.2—2.8g/cm^3，射线衍射物相分析表明，粉体为纯相的 Co_3O_4；焙烧中所产生的气体由引风机先引入冷凝器中冷却并预收集，然后通入特制的吸收装置中完全吸收制作成酸，作为副产品，所得粉体完全能满足制备锂离子二次电池用正极材料钴酸锂的要求。

AMPEREX Ex. 1002
Page 1055

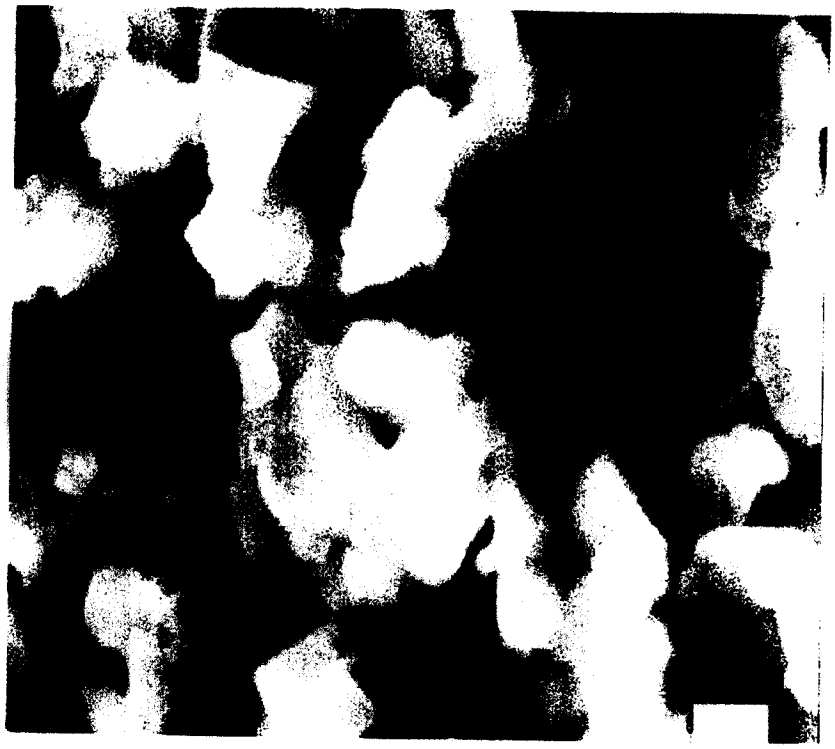


图 1

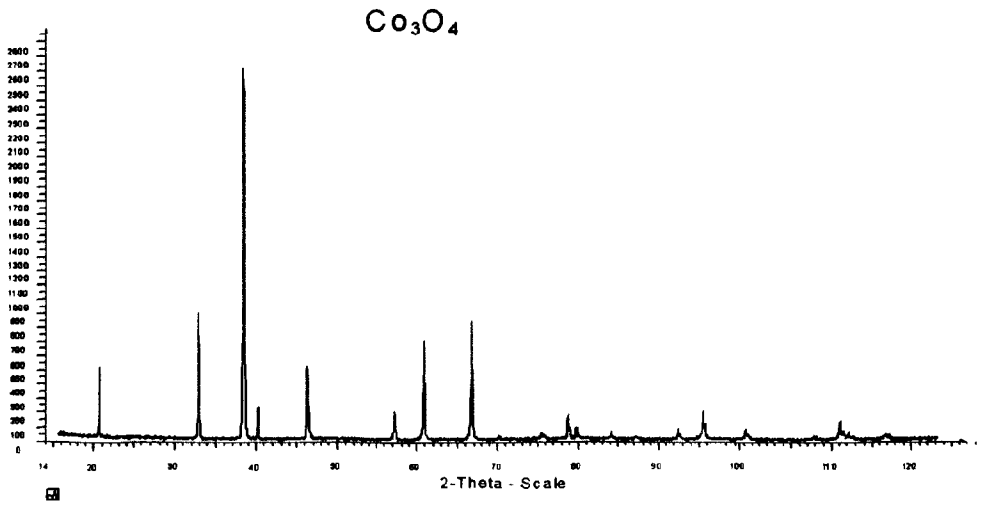


图 2

AMPEREX Ex. 1002
Page 1056

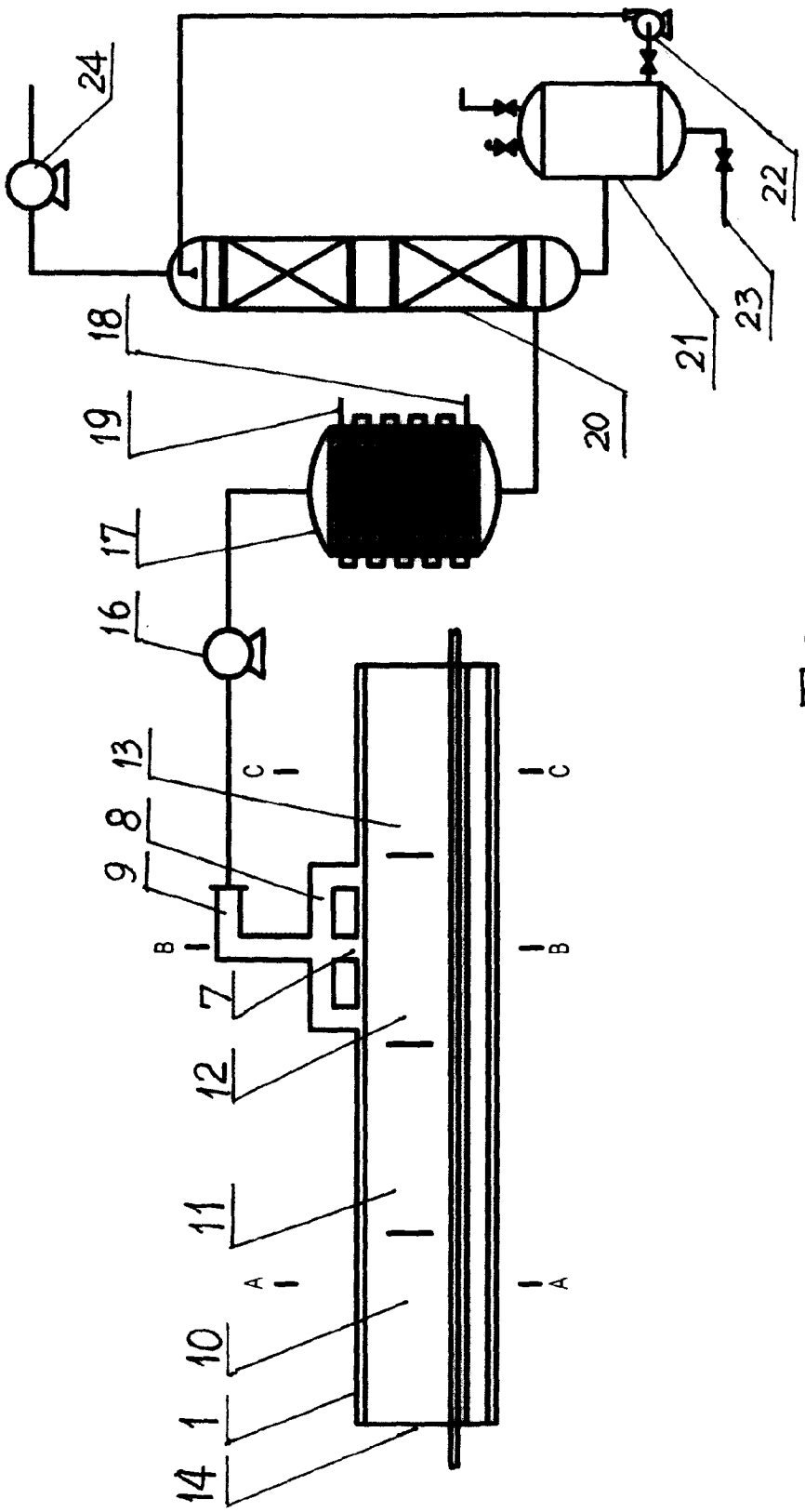


图 3

AMPEREX Ex. 1002
Page 1057

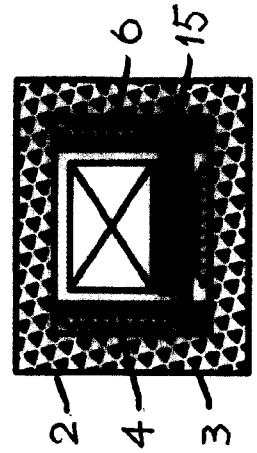


图 6

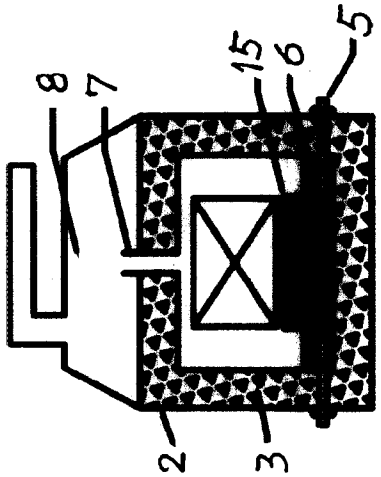


图 5

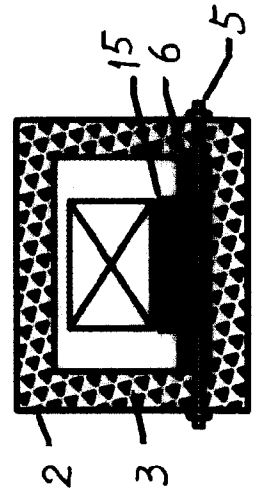


图 4

AMPEREX Ex. 1002
Page 1058

Espacenet

Family list: JP2013087040 (A) — 2013-05-13

1 application(s) for: JP2013087040 (A)

1. LITHIUM COMPOUND OXIDE AND PRODUCTION METHOD OF THE SAME, AND LITHIUM ION SECONDARY BATTERY					
Inventor: TERAJIMA JUNPEI	**Applicant:** TOYOTA MOTOR CORP	**CPC:** Y02E60/10	**IPC:** C01G53/00 H01M10/052 H01M4/36 (+3)	**Publication info:** JP2013087040 (A) 2013-05-13 Global Dossier	**Priority date:** 2011-10-21

Espacenet

Bibliographic data: JP2013087040 (A) — 2013-05-13

LITHIUM COMPOUND OXIDE AND PRODUCTION METHOD OF THE SAME, AND LITHIUM ION SECONDARY BATTERY

Inventor(s): TERAJIMA JUNPEI ± (TERAJIMA JUNPEI)

Applicant(s): TOYOTA MOTOR CORP ± (TOYOTA MOTOR CORP)

Classification: - **international:** ***C01G53/00; H01M10/052; H01M4/36; H01M4/485; H01M4/505; H01M4/525***
- **cooperative:** Y02E60/10 (EP)

Application number: JP20110231734 20111021 Global Dossier

Priority number (s): JP20110231734 20111021

Abstract of JP2013087040 (A)

PROBLEM TO BE SOLVED: To provide a production method of a lithium compound oxide that is suitable as a positive electrode active substance of a lithium ion secondary battery and can effectively improve a capacity retention rate and a capacity recovery rate.SOLUTION: A method for producing a lithium compound oxide comprising a matrix oxide expressed by general formula of LiMOwith addition of at least one alkaline earth metal is provided; and the method comprises carrying out steps of: (A) preparing an acidic metal salt solution containing metal salts of the whole structural metal elements of the lithium compound oxide; (B) gelling the metal salt solution by maintaining the solution at a temperature lower than a firing temperature in the following step (C); and (C) firing the obtained gel product after the step (B). In the above general formula, M represents at least one transition metal having an average valence of 4+ or more and comprises at least one selected from the group consisting of Ti, V, Cr, Mn, Fe, Co Ni and Cu; and x and y satisfy 0<x<2 and 0<y≤1.

(19)日本国特許庁(JP)　(12)公開特許公報(A)　(11)特許出願公開番号
特開2013-87040
(P2013-87040A)
(43)公開日　平成25年5月13日(2013.5.13)

(51)Int.Cl.		F I			テーマコード（参考）
C01G 53/00	(2006.01)	C01G	53/00	A	4G048
H01M 4/485	(2010.01)	H01M	4/48	102	5H029
H01M 4/505	(2010.01)	H01M	4/50	102	5H050
H01M 4/525	(2010.01)	H01M	4/52	102	
H01M 4/36	(2006.01)	H01M	4/36	C	

審査請求 未請求　請求項の数 15　ＯＬ　（全 28 頁）　最終頁に続く

(21)出願番号　特願2011-231734 (P2011-231734)
(22)出願日　平成23年10月21日 (2011.10.21)

(71)出願人　000003207
トヨタ自動車株式会社
愛知県豊田市トヨタ町１番地
(74)代理人　100103894
弁理士　家入　健
(72)発明者　寺島　純平
愛知県豊田市トヨタ町１番地　トヨタ自動車株式会社内

Ｆターム(参考)　4G048 AA04 AB02 AC06 AD03 AE08
5H029 AJ02 AJ05 AJ14 AK03 AL01
AL02 AL04 AL06 AL07 AL12
AM03 AM05 AM07 AM11 CJ01
CJ02 DJ17 HJ02 HJ10 HJ14
HJ17 HJ18 HJ19

最終頁に続く

(54)【発明の名称】リチウム複合酸化物とその製造方法、及びリチウムイオン二次電池

(57)【要約】
【課題】リチウムイオン二次電池の正極活物質用として好適なものであり、容量維持率、及び容量回復率を効果的に向上することが可能なリチウム複合酸化物の製造方法を提供する。
【解決手段】本発明は、下記式で表される母体酸化物に、少なくとも１種のアルカリ土類金属が添加されたリチウム複合酸化物の製造方法に関する。リチウム複合酸化物のすべての構成金属元素の金属塩を含む、酸性の金属塩溶液を調製する工程（Ａ）と、金属塩溶液を工程（Ｃ）の焼成温度より低い温度で保持してゲル化させる工程（Ｂ）と、工程（Ｂ）後に得られたゲル化物を焼成する工程（Ｃ）とを実施する。
一般式：$Li_xM_yO_2$（式中、Ｍは平均価数が４＋である少なくとも１種の遷移金属であり、Ｔｉ、Ｖ、Ｃｒ、Ｍｎ、Ｆｅ、Ｃｏ、Ｎｉ、及びＣｕからなる群より選ばれた少なくとも１種を含む。
$0<x<2$、$0<y\leqq 1$）
【選択図】なし

【特許請求の範囲】
【請求項１】
下記式で表される母体酸化物に、少なくとも１種のアルカリ土類金属が添加されたリチウム複合酸化物の製造方法であって
前記リチウム複合酸化物のすべての構成金属元素の金属塩を含む、酸性の金属塩溶液を調製する工程（Ａ）と、
前記金属塩溶液を工程（Ｃ）の焼成温度より低い温度で保持してゲル化させる工程（Ｂ）と、
工程（Ｂ）後に得られたゲル化物を焼成する工程（Ｃ）とを有するリチウム複合酸化物の製造方法。
一般式：$Li_xM_yO_2$
（式中、Ｍは平均価数が４＋である少なくとも１種の遷移金属であり、Ｔｉ、Ｖ、Ｃｒ、Ｍｎ、Ｆｅ、Ｃｏ、Ｎｉ、及びＣｕからなる群より選ばれた少なくとも１種を含む。
$0<x<2$、$0<y\leqq 1$）
【請求項２】
工程（Ａ）において、前記リチウム複合酸化物のすべての構成金属元素に対する前記アルカリ土類金属の添加量を２．５ｍｏｌ％以下とする請求項１に記載のリチウム複合酸化物の製造方法。
【請求項３】
工程（Ａ）において、前記リチウム複合酸化物のすべての構成金属元素に対する前記アルカリ土類金属の添加量を１．０ｍｏｌ％以下とする請求項２に記載のリチウム複合酸化物の製造方法。
【請求項４】
工程（Ａ）において、金属塩溶液のｐＨを３以下とする請求項１～３のいずれかに記載のリチウム複合酸化物の製造方法。
【請求項５】
工程（Ｂ）において、ゲル化温度を４５～１００℃とする請求項１～４のいずれかに記載のリチウム複合酸化物の製造方法。
【請求項６】
工程（Ｃ）が、４５０～７５０℃で仮焼成する工程（Ｃ１）と、７５０～９００℃で本焼成する工程（Ｃ２）とを有する請求項１～５のいずれかに記載のリチウム複合酸化物の製造方法。
【請求項７】
工程（Ｃ１）と工程（Ｃ２）との間に、工程（Ｃ１）後に得られた仮焼成物を粒子状に粉砕する工程（Ｄ）を有し、工程（Ｄ）後に得られた粉砕物に対して工程（Ｃ２）を実施する請求項６に記載のリチウム複合酸化物の製造方法。
【請求項８】
前記リチウム複合酸化物が、リチウムイオン二次電池に用いられる正極活物質用である請求項１～７のいずれかに記載のリチウム複合酸化物の製造方法。
【請求項９】
請求項１～８のいずれかにに記載のリチウム複合酸化物の製造方法により製造されたリチウム複合酸化物。
【請求項１０】
下記式で表される母体酸化物に、少なくとも１種のアルカリ土類金属が添加されたリチウム複合酸化物であって、
前記リチウム複合酸化物の表面に、前記アルカリ土類金属を含む、前記リチウム複合酸化物に主として存在する結晶相とは異なる結晶相を有し、かつ、当該結晶相が、前記リチウム複合酸化物の表面全体に略均一な分布で存在しているリチウム複合酸化物。
一般式：$Li_xM_yO_2$
（式中、Ｍは平均価数が４＋である少なくとも１種の遷移金属であり、Ｔｉ、Ｖ、Ｃｒ、

Ｍｎ、Ｆｅ、Ｃｏ、Ｎｉ、及びＣｕからなる群より選ばれた少なくとも１種を含む。
０＜ｘ＜２、０＜ｙ≦１）
【請求項１１】
前記リチウム複合酸化物のすべての構成金属元素に対する前記アルカリ土類金属の添加量が２．５ｍｏｌ％以下である請求項１０に記載のリチウム複合酸化物。
【請求項１２】
前記リチウム複合酸化物のすべての構成金属元素に対する前記アルカリ土類金属の添加量が１．０ｍｏｌ％以下である請求項１１に記載のリチウム複合酸化物。
【請求項１３】
請求項９～１２のいずれかに記載のリチウム複合酸化物を正極活物質として用いたリチウムイオン二次電池。
【請求項１４】
２５℃、充電電圧４．６Ｖ、放電電圧２．５Ｖ、及び、電流密度３００ｍＡ／ｇの条件で１サイクルの充放電を行った後の放電容量と、下記のサイクル充放電を行った後の放電容量との比から求められる容量維持率が、７９．０％以上である請求項１３に記載のリチウムイオン二次電池。
サイクル充放電条件：２５℃、充電電圧４．６Ｖ、放電電圧２．５Ｖ、及び、電流密度１５ｍＡ／ｇの条件で３サイクルの充放電を行い、引き続き、同温度、同充電電圧、同放電電圧、及び、電流密度３００ｍＡ／ｇの条件で５０サイクルの充放電を行う。
【請求項１５】
下記のサイクル充放電を行った後、さらに２５℃、充電電圧４．６Ｖ、放電電圧２．５Ｖ、及び、電流密度５０ｍＡ／ｇの条件で１サイクルの充放電を行った後の放電容量から、下記のサイクル充放電の最終サイクルの充電容量を除して求められる容量回復率が、５８．０％以上である請求項１３又は１４に記載のリチウムイオン二次電池。
サイクル充放電条件：２５℃、充電電圧４．６Ｖ、放電電圧２．５Ｖ、及び、電流密度１５ｍＡ／ｇの条件で３サイクルの充放電を行い、引き続き、同温度、同充電電圧、同放電電圧、及び、電流密度３００ｍＡ／ｇの条件で５０サイクルの充放電を行う。
【発明の詳細な説明】
【技術分野】
【０００１】
本発明は、リチウム複合酸化物とその製造方法、及びリチウムイオン二次電池に関するものである。
【背景技術】
【０００２】
リチウムイオン二次電池は、リチウムイオンを可逆的に脱挿入可能な正極及び負極と、液状、ゲル状もしくは固体状の電解質とから概略構成され、高出力及び高エネルギー密度などの利点を有している。
【０００３】
リチウムイオン二次電池の正極活物質としては、$LiCoO_2$、$LiNiO_2$、あるいはこれらの置換系など、式$LiMO_2$（式中、Ｍは平均価数が４＋である少なくとも１種の遷移金属）で表される層状岩塩型構造のリチウム複合酸化物が広く用いられている。
【０００４】
高性能なリチウムイオン二次電池では、高電位での充放電でも高容量で、かつ充放電を繰り返しても安定的に充放電が可能であることが求められる。
【０００５】
上記の層状岩塩型構造のリチウム複合酸化物を正極に用いたリチウムイオン電池において、４．５Ｖ以上の高電位の充電とその放電を繰り返す場合、正極活物質が膨張と収縮を繰り返し、層状構造の不安定に起因して、正極活物質の構造が崩れて正極が劣化し、容量維持率の低下が生じる恐れがある。
【０００６】

層状岩塩型構造の材料の中で、式$Li_{1+x}M_{1-x}O_2$（式中、Mは上記と同様、0＜x）で表されるリチウム過剰系の材料では、４．５Ｖ以上の高電位の充電とその放電を繰り返しても層状構造を比較的保つことができる。しかしながら、結晶格子の膨張収縮が大きく、容量維持率の低下が生じる恐れがある。

【０００７】

高電位の充電とその放電を繰り返しても高容量で安定的に充放電が可能なリチウムイオン二次電池を提供することを目的として、以下の特許文献にリチウムイオン二次電池用の正極活物質が開示されている。

【０００８】

特許文献１には、Ｍｎに対して１０モル％未満のアルカリ金属及びアルカリ土類金属からなる群から選ばれる少なくとも一種の金属元素（但し、Ｌｉを除く）を含有するリチウムマンガン複合酸化物を含有する正極活物質が開示されている（請求項１）。

特許文献１には、上記金属元素が、リチウムマンガン複合酸化物粒子の表面近傍に偏在することが好ましいと記載されている（請求項３、段落０００９等）。

特許文献１には、サイクル充放電特性が向上することが記載されている（段落０００５等）。

【０００９】

特許文献１には、層状岩塩型構造及びスピネル型構造等に適用可能であることが記載されている（段落００１０）。

ただし、特許文献１の[実施例]の項では、金属元素Ｍとしてアルカリ金属であるセシウムを含むスピネル型構造のリチウム複合酸化物のみが製造されており、層状岩塩型構造のリチウム複合酸化物の具体的な製造については記載がない。

金属元素Ｍとしてアルカリ金属であるセシウムを含むスピネル型構造のリチウム複合酸化物の具体的な製造方法は、段落００２３に記載されている。

【００１０】

特許文献２には、下記式で表される正極活物質が開示されている（請求項２）。

$Li\{Li_xNi_yMn_zM_b\}O_{2-a}$

（式中、$0<x<0.4$、$0.12<y<0.5$、$0.3<z<0.62$、$0\leqq a<0.5$、Ｍは原子価２～６の少なくとも１つの金属元素、$x>(1-2y)/3$、$1/4\leqq y/z\leqq 1.0$、$0<b/(y+z)\leqq 0.1$、$1.0\leqq x+y+z+b\leqq 1.1$）

【００１１】

特許文献２には、金属元素Ｍとして、Ｍｇ，Ａｌ，Ｚｒ，Ｔｉ，Ｎｂ，Ｗ，及びＭｏから選ばれる少なくとも１種が挙げられている（請求項３）。

特許文献２には、初期充放電効率と放電容量が向上することが記載されている（段落００７９等）。

【００１２】

特許文献２の［実施例］の項における正極活物質の具体的な製造方法は、段落００２０に記載されている。

【先行技術文献】

【特許文献】

【００１３】

【特許文献１】特開2001-068109号公報

【特許文献２】特開2007-242581号公報

【非特許文献】

【００１４】

【非特許文献１】Marcel Poubaix, 1974, National Association of Corrosion Engineers, "Atlas of electrochemical equilibria in aqueous solutions"

【発明の概要】

【発明が解決しようとする課題】

【００１５】

特許文献１、２には、Ｍｎ、Ｃｏ、及びＮｉを含む３元系のリチウム複合酸化物において、アルカリ土類金属を添加することで、サイクル充放電特性が向上することが記載されている。特許文献１には、アルカリ土類金属がリチウム複合酸化物の表面に偏在することが好ましいことが記載されている。

【００１６】

特性のばらつきを抑制し、サイクル充放電特性を効果的に向上するには、アルカリ土類金属がリチウム複合酸化物の表面全体に略均一な分布で存在していることが好ましいと考えられる。

しかしながら、本発明者が検討を行ったところ、特許文献１、２に記載のリチウム複合酸化物の製造方法では、アルカリ土類金属をリチウム複合酸化物の表面全体に略均一な分布で存在させることが難しく、サイクル充放電特性を効果的に向上することが難しいことが明らかとなった（後記比較例４を参照）。

【００１７】

プラグインハイブリッド車（ＰＨＶ）あるいは電気自動車（ＥＶ）等に搭載される二次電池では、高電位・高電流密度で充放電を繰り返した際の容量維持率の他、高電位・高電流密度で充放電を繰り返し、その後高電位・低電流密度で充放電を行った際の容量回復率も重要である。特許文献１、２の構成では、容量維持率と容量回復率のいずれについても、向上に限界がある。

本明細書において、高電位は「４．５Ｖ以上」と定義する。

【００１８】

本発明は上記事情に鑑みてなされたものであり、リチウムイオン二次電池の正極活物質用として好適なものであり、高電位・高電流密度で充放電を繰り返した際の容量維持率、及び、高電位・高電流密度で充放電を繰り返し、その後高電位・低電流密度で充放電を行った際の容量回復率を効果的に向上することが可能なリチウム複合酸化物とその製造方法を提供することを目的とするものである。

【課題を解決するための手段】

【００１９】

本発明のリチウム複合酸化物の製造方法は、

下記式で表される母体酸化物に、少なくとも１種のアルカリ土類金属が添加されたリチウム複合酸化物の製造方法であって

前記リチウム複合酸化物のすべての構成金属元素の金属塩を含む、酸性の金属塩溶液を調製する工程（Ａ）と、

前記金属塩溶液を工程（Ｃ）の焼成温度より低い温度で保持してゲル化させる工程（Ｂ）と、

工程（Ｂ）後に得られたゲル化物を焼成する工程（Ｃ）とを有するものである。

一般式：$Li_xM_yO_2$

（式中、Ｍは平均価数が４＋である少なくとも１種の遷移金属であり、Ｔｉ、Ｖ、Ｃｒ、Ｍｎ、Ｆｅ、Ｃｏ、Ｎｉ、及びＣｕからなる群より選ばれた少なくとも１種を含む。

$0<x<2$、$0<y\leqq 1$）

【００２０】

本発明の第１のリチウム複合酸化物は、上記のリチウム複合酸化物の製造方法により製造されたものである。

【００２１】

本発明の第２のリチウム複合酸化物は、

下記式で表される母体酸化物に、少なくとも１種のアルカリ土類金属が添加されたリチウム複合酸化物であって、

前記リチウム複合酸化物の表面に、前記アルカリ土類金属を含む、前記リチウム複合酸化物に主として存在する結晶相とは異なる結晶相を有し、かつ、当該結晶相が、前記リチウム複合酸化物の表面全体に略均一な分布で存在しているものである。

一般式：$Li_xM_yO_2$

（式中、Ｍは平均価数が４＋である少なくとも１種の遷移金属であり、Ｔｉ、Ｖ、Ｃｒ、Ｍｎ、Ｆｅ、Ｃｏ、Ｎｉ、及びＣｕからなる群より選ばれた少なくとも１種を含む。
０＜ｘ＜２、０＜ｙ≦１）

【００２２】

リチウム複合酸化物に主として存在する結晶相とは異なる結晶相の同定及びその分布状態は、ＸＰＳ分析（Ｘ線光電子分光分析）、ＨＡＡＤＦ-ＳＴＥＭ分析（高角度散乱暗視野走査透過電子顕微鏡分析）、及びＥＤＸ分析（エネルギー分散型蛍光Ｘ線分光分析）等の分析によって行うことができる。

【００２３】

ＨＡＡＤＦ-ＳＴＥＭ像において、ＥＤＸ分析によるアルカリ土類金属のマッピングを行い、アルカリ土類金属がリチウム複合酸化物の表面全体に渡って分布していれば、アルカリ土類金属を含む結晶相がリチウム複合酸化物の表面全体に略均一な分布で存在していると言える（後記[実施例]の項の図３Ａを参照）。

具体的な分析については、後記［実施例］の項を参照されたい。

【００２４】

本発明の第１、第２のリチウム複合酸化物は、リチウムイオン二次電池に用いられる正極活物質用として好適である。

【００２５】

本発明のリチウムイオン二次電池は、上記の本発明のリチウム複合酸化物を正極活物質として用いたものである。

【発明の効果】

【００２６】

本発明によれば、リチウムイオン二次電池の正極活物質用として好適なものであり、高電位・高電流密度で充放電を繰り返した際の容量維持率、及び、高電位・高電流密度で充放電を繰り返し、その後高電位・低電流密度で充放電を行った際の容量回復率を効果的に向上することが可能なリチウム複合酸化物とその製造方法を提供することができる。

【図面の簡単な説明】

【００２７】

【図１Ａ】実施例１で得られた正極活物質のＸＲＤパターンである。
【図１Ｂ】実施例２で得られた正極活物質のＸＲＤパターンである。
【図１Ｃ】実施例３で得られた正極活物質のＸＲＤパターンである。
【図１Ｄ】実施例４で得られた正極活物質のＸＲＤパターンである。
【図１Ｅ】実施例５で得られた正極活物質のＸＲＤパターンである。
【図１Ｆ】実施例６で得られた正極活物質のＸＲＤパターンである。
【図１Ｇ】比較例１で得られた正極活物質のＸＲＤパターンである。
【図１Ｈ】比較例２で得られた正極活物質のＸＲＤパターンである。
【図１Ｉ】比較例３で得られた正極活物質のＸＲＤパターンである。
【図２】実施例１～３で得られた正極活物質のＸＰＳスペクトルである。
【図３Ａ】実施例２で得られた正極活物質について得られたＨＡＡＤＦ-ＳＴＥＭ像及びその表面におけるＥＤＸ分析によるＣａマッピングの写真である。
【図３Ｂ】実施例２で得られた正極活物質における析出物のＥＤＸスペクトルである。
【図４】Ｃａ添加量と容量維持率との関係を示すグラフである。

【発明を実施するための形態】

【００２８】

以下、本発明について詳述する。

【００２９】

[リチウム複合酸化物とその製造方法]

本発明のリチウム複合酸化物の製造方法は、

下記式で表される母体酸化物に、少なくとも１種のアルカリ土類金属が添加されたリチウム複合酸化物の製造方法であって

前記リチウム複合酸化物のすべての構成金属元素の金属塩を含む、酸性の金属塩溶液を調製する工程（Ａ）と、
前記金属塩溶液を工程（Ｃ）の焼成温度より低い温度で保持してゲル化させる工程（Ｂ）と、
工程（Ｂ）後に得られたゲル化物を焼成する工程（Ｃ）とを有するものである。
一般式：$Li_xM_yO_2$
（式中、Ｍは平均価数が４＋である少なくとも１種の遷移金属であり、Ｔｉ、Ｖ、Ｃｒ、Ｍｎ、Ｆｅ、Ｃｏ、Ｎｉ、及びＣｕからなる群より選ばれた少なくとも１種を含む。
$0<x<2$、$0<y\leqq 1$）

【００３０】
＜母体酸化物＞
母体酸化物としては、下記式で表される少なくとも１種のリチウム複合酸化物が用いられる。
一般式：$Li_xM_yO_2$
（式中、Ｍは平均価数が４＋である少なくとも１種の遷移金属であり、Ｔｉ、Ｖ、Ｃｒ、Ｍｎ、Ｆｅ、Ｃｏ、Ｎｉ、及びＣｕからなる群より選ばれた少なくとも１種を含む。
$0<x<2$、$0<y\leqq 1$）

【００３１】
Ｍは、Ｍｎ、Ｃｏ、及びＮｉからなる群より選ばれた少なくとも１種を含むことがより好ましい。
母体酸化物は、ＭとしてＭｎ、Ｃｏ、及びＮｉを含む３元系が特に好ましい。

【００３２】
上記母体酸化物は層状岩塩型構造を有し、Ｃｕ電球を用いたＸＲＤパターンが$2\theta=20\sim24°$にピークを有する。

【００３３】
＜アルカリ土類金属＞
添加元素としては、少なくとも1種のアルカリ土類金属が用いられる。
アルカリ土類金属としては、Ｍｇ、Ｃａ、Ｓｒ、及びＢａからなる群より選ばれる少なくとも１種が好ましい。
層状岩塩型構造のリチウム複合酸化物に少なくとも１種のアルカリ土類金属を添加することで、サイクル充放電の特性を向上することができる。

【００３４】
＜工程（Ａ）＞
はじめに、最終的に製造するリチウム複合酸化物のすべての構成金属元素（母体酸化物の構成金属、及びアルカリ土類金属）の金属塩をそれぞれ用意する。
母体酸化物の構成金属の金属塩、及びアルカリ土類金属の金属塩としては例えば、酢酸塩等が好ましい。

【００３５】
最終的に製造するリチウム複合酸化物のすべての構成金属元素の金属塩をそれぞれ所望の金属組成比で配合し、水等を用いて溶解させる。溶液は酸を用いて、ｐＨを酸性にする。
本発明者は、金属塩溶液のｐＨを酸性とすることで、金属塩溶液中に金属の酸化物及び水酸化物が生成されることが抑制され、金属イオンを液中に安定的に存在させることができることができること、これにより各金属が良好に分散した金属塩溶液が得られることを見出している。
金属塩溶液のｐＨは酸性であればよく、具体的には６未満が好ましく、３以下が特に好ましい。

【００３６】
例えば、母体酸化物がＭｎ、Ｃｏ、及びＮｉを含む３元系であれば、Ｍｎ、Ｃｏ、及びＮｉの各イオンが金属塩溶液中に安定的に存在するようにする。

【００３７】
［背景技術］の項で挙げた非特許文献１のｐ.２９０には、Ｍｎを含む溶液において、酸化マンガン及び水酸化マンガンが生成するｐＨと電位が記載されている。水溶液中では、図中のラインａからラインｂの範囲内にある物質が安定に存在する。原料中のＭｎの価数は２＋である。金属塩溶液中にこのＭｎイオンがイオンのまま安定に存在するには、ライン１２、１６、１８、２０よりも左側の条件である必要がある。ｐＨ８以下でライン１２より左側の条件にすることができる。ライン１６、１８、２０は、空気中の酸素とＭｎが反応可能な領域を示している。高濃度の酸素ガス雰囲気の条件であれば、ライン２０を超える場合があり得るが、通常の空気雰囲気ではライン２０を超えることはない。ライン１６、１８を超えないようにするには、溶液のｐＨは６未満が好ましく、３以下が特に好ましいことが示されている。

【００３８】
同文献のｐ.３２５、ｐ.３３３には、ＣｏとＮｉについても同様の図が示されている。Ｍｎと同様、金属塩溶液中にＣｏイオン及びＮｉイオンがイオンのまま安定に存在するには、ｐＨは６未満が好ましく、３以下が特に好ましいことが示されている。

【００３９】
母体酸化物中の遷移金属Ｍの選択肢として挙げた他のいずれの金属についても、金属イオンが金属塩溶液中に安定的に存在する条件は、Ｍｎ、Ｃｏ、及びＮｉと同様である。

【００４０】
ｐＨ調整に用いる酸は特に制限されず、硝酸、塩酸、硫酸、過塩素酸、及びこれらの組合わせ等が挙げられる。

【００４１】
本発明において、最終的に製造するリチウム複合酸化物のすべての構成金属元素に対するアルカリ土類金属の添加量は２．５ｍｏｌ％以下が好ましく、１ｍｏｌ％以下が特に好ましい。

【００４２】
層状岩塩型構造のリチウム複合酸化物にアルカリ土類金属を添加することで、サイクル充放電特性を向上することができる。ただし、添加量が多くなりすぎると、母体酸化物の量が相対的に低下することに起因して、電池性能が低下する恐れがある。したがって、アルカリ土類金属の添加量を上記規定内とすることが好ましい。

【００４３】
＜工程（Ｂ）＞
次に、上記工程で得られた酸性の金属塩溶液を後の工程（Ｃ）の焼成温度より低い温度で保持してゲル化させる。
ゲル化温度は特に制限なく、例えば４５～１００℃が好ましい。
例えば、上記工程で得られた酸性の金属塩溶液を４５～１００℃で約一晩保持して、ゲル化させることができる。
このゲル化工程を経ることで、金属イオンの均一な分散状態を維持しつつ、次の焼成工程を進めることができる。

【００４４】
＜工程（Ｃ）、工程（Ｄ）＞
次に、上記工程後に得られたゲル化物を焼成する（工程（Ｃ））。
本発明では、金属塩溶液のｐＨを酸性とし、これをゲル化してから焼成することで、金属が均一に分散された焼成物を生成することができる。

【００４５】
焼成雰囲気は特に制限されず、大気雰囲気でもよいし、Ａｒ雰囲気等の不活性雰囲気でもよい。

【００４６】
焼成工程（Ｃ）は１段階で実施してもよいし、複数段階で実施してもよい。
１段階の焼成工程後、複数段階の最終焼成工程後、あるいは複数段階の焼成工程の間に

、粉砕工程（Ｄ）を実施することができる。

【００４７】

例えば、焼成工程（Ｃ）は仮焼成工程（Ｃ１）と本焼成工程（Ｃ２）の２段階で行い、これらの間に粉砕工程（Ｄ）を実施することが好ましい。

仮焼成温度及び本焼成温度は特に制限されない。

良好な結晶化を進め、かつ所望でない結晶の生成を抑制するには、例えば、仮焼成温度は４５０～７５０℃、特に５５０～６５０℃が好ましく、本焼成温度は７５０～９００℃、特に８００～９００℃が好ましい。

【００４８】

焼成物（仮焼成物の場合もある）の粉砕方法は特に制限されず、ボールミルを用いた粉砕等が好ましい。

ボールミルによる粉砕時間は特に制限なく、１～１０時間が好ましく、１～３時間が特に好ましい。

【００４９】

以上のようにして、下記式で表されるリチウム複合酸化物を母体酸化物とし、少なくとも１種のアルカリ土類金属が添加されたリチウム複合酸化物を製造することができる。

一般式：$Li_xM_yO_2$

（式中、Ｍは平均価数が４＋である少なくとも１種の遷移金属であり、Ｔｉ、Ｖ、Ｃｒ、Ｍｎ、Ｆｅ、Ｃｏ、Ｎｉ、及びＣｕからなる群より選ばれた少なくとも１種を含む。$0<x<2$、$0<y\leqq1$）

【００５０】

本発明の製造方法では、母体結晶の構成金属よりもイオン半径の大きいアルカリ土類金属を添加している。そのため、アルカリ土類金属は母体結晶に容易に固溶せず、異相として析出させることができる。

この異相は、二次電池の電気化学反応には関与しないと考えられる。そして、４．５Ｖ以上の高電位の充電とその放電を繰り返した場合、この電気化学反応に関与しない結晶相が母体酸化物の膨張収縮によって発生する応力を緩和する機能を発現すると考えられる。

【００５１】

本発明の製造方法では、前駆体を含む金属塩溶液を酸性にして、金属の酸化物及び水酸化物の析出を抑制し、その後にゲル化工程を経て、焼成を行うことで、略均一に反応を進めることができ、リチウム複合酸化物の表面全体に渡って、略均一にアルカリ土類金属を含む異相を分布させることができる。

【００５２】

本発明の製造方法によれば、リチウム複合酸化物の表面に、アルカリ土類金属を含む、リチウム複合酸化物に主として存在する結晶相とは異なる結晶相を有し、かつ、当該結晶相が、リチウム複合酸化物の表面全体に略均一な分布で存在したリチウム複合酸化物を安定的に製造することができる。

【００５３】

本発明の製造方法では、アルカリ土類金属を含む異相を、リチウム複合酸化物の表面全体に略均一に分散させることができるので、「背景技術」の項で挙げたいずれの特許文献よりも、特性のばらつきが抑制され、サイクル充放電特性を効果的に向上することができる。

【００５４】

本発明の製造方法によれば、４．５Ｖ以上の高電位の充電とその放電を繰り返しても、正極活物質に発生するクラックが抑制されて、正極の劣化が抑制され、容量維持率と容量回復率の両方を向上することができる。

【００５５】

母体酸化物に対するアルカリ土類金属の添加量が多くなりすぎると、二次電池の電気化学反応には関与する母体結晶相の量が相対的に少なくなることに起因して、電池容量が低下すると考えられる。したがって、アルカリ土類金属の添加量は、リチウム複合酸化物の

すべての構成金属元素に対して、２．５ｍｏｌ％以下が好ましく、１．０ｍｏｌ％以下が特に好ましい。

【００５６】

本発明の製造方法により製造されたリチウム複合酸化物は、リチウムイオン二次電池の正極活物質として好ましく利用することができる。

【００５７】

以上説明したように、本発明によれば、リチウムイオン二次電池の正極活物質用として好適なものであり、高電位・高電流密度で充放電を繰り返した際の容量維持率、及び、高電位・高電流密度で充放電を繰り返し、その後高電位・低電流密度で充放電を行った際の容量回復率を効果的に向上することが可能なリチウム複合酸化物とその製造方法を提供することができる。

【００５８】

充放電の繰り返しにおける充電電位は特に制限なく、例えば４．５～５．０Ｖが好ましい。本発明では、４．５Ｖ以上の高電位の充電とその放電を繰り返しても、良好な電池性能が得られる。

【００５９】

［リチウムイオン二次電池］

本発明のリチウムイオン二次電池は、本発明の製造方法により製造されたリチウム複合酸化物を正極活物質として用いたものである。

正極と負極とセパレータと非水電解質と外装体を用い、公知方法により、リチウムイオン二次電池を製造することができる。

【００６０】

＜正極＞

正極は、公知の方法により、アルミニウム箔などの正極集電体に正極活物質を塗布して、製造することができる。

【００６１】

本発明では、上記の本発明の製造方法により製造されたリチウム複合酸化物を正極活物質として用いる。

【００６２】

正極活物質として、上記の本発明の製造方法により製造されたリチウム複合酸化物以外の公知の正極活物質を併用しても構わない。ただし、上記の本発明の製造方法により製造されたリチウム複合酸化物の使用量が多い程、より高い効果が得られる。

公知の正極活物質としては特に制限なく、例えば、$LiCoO_2$、$LiMnO_2$、$LiMn_2O_4$、$LiNiO_2$、$LiNi_xCo_{(1-x)}O_2$、及び$LiNi_xCo_yMn_{(1-x-y)}O_2$等のリチウム含有複合酸化物等が挙げられる（式中、$0<x<1$、$0<y<1$）。

【００６３】

例えば、Ｎ－メチル－２－ピロリドン等の分散剤を用い、正極活物質と、炭素粉末等の導電剤と、ポリフッ化ビニリデン（ＰＶＤＦ）等の結着剤とを混合して、スラリーを得、このスラリーをアルミニウム箔等の集電体上に塗布し、乾燥し、プレス加工して、正極を得ることができる。

正極の目付は特に制限なく、１．５～１５ｍｇ／ｃｍ^{2}が好ましい。正極の目付が過小では均一な塗布が難しく、過大では集電体から剥離する恐れがある。

【００６４】

＜負極＞

負極活物質としては特に制限なく、Ｌｉ／Ｌｉ＋基準で２．０Ｖ以下にリチウム吸蔵能力を持つものが好ましく用いられる。負極活物質としては、黒鉛等の炭素、金属リチウム、リチウム合金、リチウムイオンのドープ・脱ドープが可能な遷移金属酸化物／遷移金属窒化物／遷移金属硫化物、及び、これらの組合わせ等が挙げられる。

【００６５】

負極は例えば、公知の方法により、銅箔などの負極集電体に負極活物質を塗布して、製造することができる。

例えば、水等の分散剤を用い、負極活物質と、変性スチレンーブタジエン共重合体ラテックス等の結着剤と、必要に応じてカルボキシメチルセルロースＮａ塩（ＣＭＣ）等の増粘剤とを混合して、スラリーを得、このスラリーを銅箔等の集電体上に塗布し、乾燥し、プレス加工して、負極を得ることができる。

負極の目付は特に制限なく、１．５～１５ｍｇ／ｃｍ^{2}が好ましい。負極の目付が過小では均一な塗布が難しく、過大では集電体から剥離する恐れがある。

【００６６】

負極活物質として金属リチウム等を用いる場合、金属リチウム等をそのまま負極として用いることができる。

【００６７】

＜非水電解質＞

非水電解質としては公知のものが使用でき、液状、ゲル状もしくは固体状の非水電解質が使用できる。

例えば、プロピレンカーボネートあるいはエチレンカーボネート等の高誘電率カーボネート溶媒と、ジエチルカーボネート、メチルエチルカーボネート、ジメチルカーボネート等の低粘度カーボネート溶媒との混合溶媒に、リチウム含有電解質を溶解した非水電界液が好ましく用いられる。

混合溶媒としては例えば、エチレンカーボネート（ＥＣ）／ジメチルカーボネート（ＤＭＣ）／エチルメチルカーボネート（ＥＭＣ）の混合溶媒が好ましく用いられる。

リチウム含有電解質としては例えば、$LiPF_6$、$LiBF_4$、$LiClO_4$、$LiAsF_6$、Li_2SiF_6、$LiOSO_2C_kF_{(2k+1)}$（ｋ＝１～８の整数）、$LiPF_n\{C_kF_{(2k+1)}\}_{(6-n)}$（ｎ＝１～５の整数、ｋ＝１～８の整数）等のリチウム塩、及びこれらの組合わせが挙げられる。

【００６８】

＜セパレータ＞

セパレータは、正極と負極とを電気的に絶縁し、かつリチウムイオンが透過可能な膜であればよく、多孔質高分子フィルムが好ましく使用される。

セパレータとしては例えば、ＰＰ（ポリプロピレン）製多孔質フィルム、ＰＥ（ポリエチレン）製多孔質フィルム、あるいは、ＰＰ（ポリプロピレン）－ＰＥ（ポリエチレン）の積層型多孔質フィルム等のポリオレフィン製多孔質フィルムが好ましく用いられる。

【００６９】

＜外装体＞

外装体としては公知のものが使用できる。

二次電池の型としては、円筒型、コイン型、角型、あるいはフィルム型等があり、所望の型に合わせて外装体を選定することができる。

【００７０】

本発明のリチウムイオン二次電池は、正極活物質として上記の本発明の製造方法により製造されたリチウム複合酸化物を用いたものである。

本発明によれば、高電位・高電流密度で充放電を繰り返した際の容量維持率、及び、高電位・高電流密度で充放電を繰り返し、その後高電位・低電流密度で充放電を行った際の容量回復率を効果的に向上することが可能なリチウムイオン二次電池を提供することができる。

【００７１】

本発明によれば、２５℃、充電電圧４．６Ｖ、放電電圧２．５Ｖ、及び、電流密度３００ｍＡ／ｇの条件で１サイクルの充放電を行った後の放電容量と、下記のサイクル充放電を行った後の放電容量との比から求められる容量維持率が、７９．０％以上であるリチウムイオン二次電池を提供することができる（［実施例］の項の表１を参照）。

【００７２】

本発明によれば、下記のサイクル充放電を行った後、さらに２５℃、充電電圧４．６Ｖ、放電電圧２．５Ｖ、及び、電流密度５０ｍＡ／ｇの条件で１サイクルの充放電を行った後の放電容量から、下記のサイクル充放電の最終サイクルの充電容量を除して求められる容量回復率が、５８．０％以上であるリチウムイオン二次電池を提供することができる（［実施例］の項の表１を参照）。

【００７３】

サイクル充放電条件：２５℃、充電電圧４．６Ｖ、放電電圧２．５Ｖ、及び、電流密度１５ｍＡ／ｇの条件で３サイクルの充放電を行い、引き続き、同温度、同充電電圧、同放電電圧、及び、電流密度３００ｍＡ／ｇの条件で５０サイクルの充放電を行う。

【実施例】

【００７４】

本発明に係る実施例及び比較例について説明する。

【００７５】

（実施例１）

＜正極活物質の合成＞

Ｌｉ源として酢酸リチウム・２水和物、Ｍｎ源として酢酸マンガン・４水和物、Ｃｏ源として酢酸コバルト・４水和物、Ｎｉ源として酢酸ニッケル・４水和物、Ｃａ源として酢酸カルシウム・１水和物（いずれもナカライテスク（株）社製）を用いた。

これらの原料を、Ｌｉ／Ｍｎ／Ｃｏ／Ｎｉ／Ｃａ＝６０／２６．７５／６．５／６．５／０．０２５（モル比）となるようにそれぞれ秤量して純水で溶解した。

溶液は、硝酸を用いて、ｐＨを３に調整した。

得られた溶液を撹拌しながら、８０℃で一晩保持し、ゲルを得た。

【００７６】

＜焼成＞

上記で得られたゲルを大気雰囲気下で２段階焼成した。

まず６００℃で５時間仮焼成した。その後、常温まで冷却後にボールミルを用いて１時間粒子状に粉砕し、その後、再度９００℃で本焼成した。

以上のようにして、３元系のリチウム複合酸化物粒子からなる正極活物質を得た。

【００７７】

＜正極の製造＞

分散剤としてＮ－メチル－２－ピロリドン（（株）和光純薬工業社製）を用い、上記のリチウム複合酸化物粒子からなる正極活物質と、導電剤であるアセチレンブラック（電気化学工業（株）社製ＨＳ－１００）と、結着剤であるＰＶＤＦ（（株）クレハ社製ＫＦポリマー＃１１２０）とを、８５／１０／５（質量比）で混合して、スラリーを得た。

上記スラリーを集電体であるアルミニウム箔上にドクターブレード法で塗布し、１５０℃で３０分間乾燥し、プレス機械を用いてプレス加工して、正極を得た。正極は、目付５．５ｍｇ／ｃｍ^2、厚み１８μｍとした。

【００７８】

＜負極＞

負極活物質として、金属リチウムを用いた。

これをそのまま負極として用いた。

【００７９】

＜セパレータ＞

ＰＰ（ポリプロピレン）製多孔質フィルムからなる市販のセパレータを用意した。

【００８０】

＜非水電解質＞

エチレンカーボネート（ＥＣ）／ジメチルカーボネート（ＤＭＣ）／エチルメチルカーボネート＝３／３／４（体積比）の混合溶液を溶媒とし、電解質としてリチウム塩である$LiPF_6$を１ｍｏｌ／Ｌの濃度で溶解して、非水電界液を調製した。

【００８１】

＜外装体＞
外装体として、ＳＵＳ製２０３２型コインセルを用意した。
【００８２】
＜リチウムイオン二次電池の製造＞
上記の正極と負極とセパレータと非水電解液と外装体を用い、公知方法により、リチウムイオン二次電池を製造した。
【００８３】
（実施例２～６、比較例１～４）
正極活物質の合成において下記組成比とした以外は、実施例１と同様にして、リチウムイオン二次電池を製造した。
【００８４】
（実施例２）
Ｌｉ／Ｍｎ／Ｃｏ／Ｎｉ／Ｃａ＝６０／２６．５／６．５／６．５／０．５（モル比）
（実施例３）
Ｌｉ／Ｍｎ／Ｃｏ／Ｎｉ／Ｃａ＝６０／２６／６．５／６．５／１（モル比）
（実施例４）
Ｌｉ／Ｍｎ／Ｃｏ／Ｎｉ／Ｍｇ＝６０／２６．５／６．５／６．５／０．５（モル比）
（実施例５）
Ｌｉ／Ｍｎ／Ｃｏ／Ｎｉ／Ｍｇ＝６０／２６／６．５／６．５／１（モル比）
（実施例６）
Ｌｉ／Ｍｎ／Ｃｏ／Ｎｉ／Ｓｒ＝６０／２６／６．５／６．５／１（モル比）
（実施例７）
Ｌｉ／Ｍｎ／Ｃｏ／Ｎｉ／Ｃａ＝６０／２４．５／６．５／６．５／２．５（モル比）
【００８５】
（比較例１）
Ｌｉ／Ｍｎ／Ｃｏ／Ｎｉ＝６０／２７／６．５／６．５（モル比）
（比較例２）
Ｌｉ／Ｍｎ／Ｃｏ／Ｎｉ／Ｔｉ＝６０／２６／６．５／６．５／１．０（モル比）
（比較例３）
Ｌｉ／Ｍｎ／Ｃｏ／Ｎｉ／Ｆｅ＝６０／２６／６．５／６．５／１．０（モル比）
【００８６】
（比較例４）
はじめに、「背景技術」の項で挙げた特許文献２の実施例１と同様の共沈法にて、正極活物質の前駆体を製造した。具体的には、Ｍｎの硫酸塩とＣｏの硫酸塩とＮｉの硫酸塩との混合溶液に水酸化リチウムを加え共沈させることにより、Ｍｎ／Ｃｏ／Ｎｉ複合水酸化物を得た。
【００８７】
次に、炭酸リチウムと炭酸マグネシウムと上記で得た複合水酸化物を下記組成比となるように混合した。
Ｌｉ／Ｍｎ／Ｃｏ／Ｎｉ／Ｃａ＝６０／２６／６．５／６．５／１（モル比）
【００８８】
得られた混合物を大気雰囲気下で２段階焼成した。
まず６００℃で５時間仮焼成した。その後、常温まで冷却後にボールミルを用いて１時間粒子状に粉砕し、その後、再度９００℃で本焼成した。
以上のようにして、リチウム複合酸化物粒子からなる正極活物質を得た。
この正極活物質を用い、実施例１と同様にして、リチウムイオン二次電池を製造した。
【００８９】
（評価）
＜ＸＲＤ分析＞
実施例１～６及び比較例１～３において得られた正極活物質について、Ｘ線回折（ＸＲ

AMPEREX Ex. 1002
Page 1073

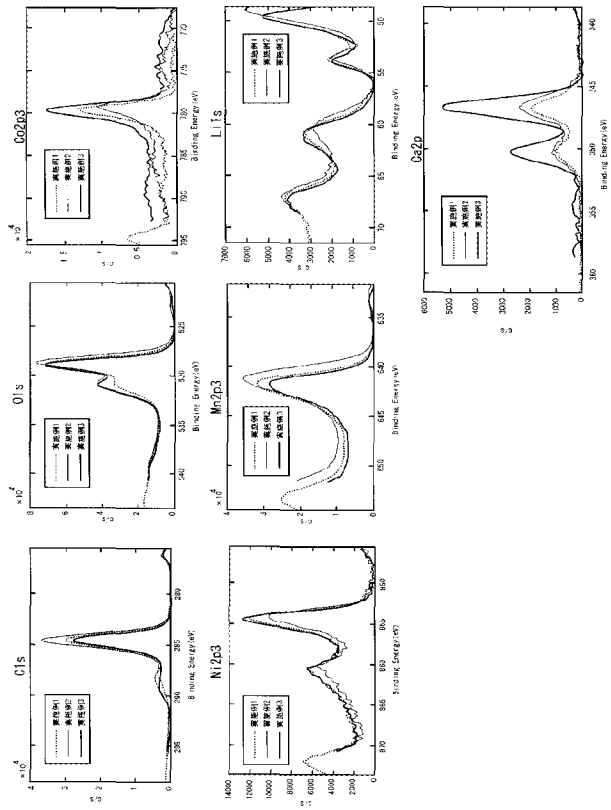
Ｄ）装置を用いて、粉末ＸＲＤパターンを得、結晶相の同定を行った。
測定装置としてリガクＵｌｔｉｍａ４を用い、ＣｕＫα線を用い、一次検出器を用いて測定を行った。測定条件は、２θ＝１０～８０°、１０°／ｍｉｎ、３回積算とした。
【００９０】
＜ＸＰＳ分析＞
実施例１～３で得られた正極活物質の表面について、アルバックファイ社製ＰＨＩ５８００を用いて、ＸＰＳ分析（Ｘ線光電子分光分析）を実施した。線源Ｍｇ、４００Ｗの条件で測定を実施した。
【００９１】
＜ＨＡＡＤＦ-ＳＴＥＭ分析とＥＤＸ分析＞
実施例２で得られた正極活物質について、ＦＥＩ社製ＴＩＴＡＮ８０－３００を用いて、ＨＡＡＤＦ-ＳＴＥＭ分析（高角度散乱暗視野走査透過電子顕微鏡分析）とＥＤＸ分析（エネルギー分散型蛍光Ｘ線分光分析）を実施した。加速電圧は３００ｋＶとした。
【００９２】
＜容量維持率及び容量回復率の測定＞
各例において得られたリチウムイオン二次電池に対して、下記のサイクル充放電を実施した。
２５℃の恒温槽内で、充電電圧４．６Ｖ（ｖｓ．Ｌｉ／Ｌｉ＋）、放電電圧２．５Ｖ（ｖｓ．Ｌｉ／Ｌｉ＋）、及び、電流密度１５ｍＡ／ｇの条件で３サイクルの充放電を行い、引き続き、同温度の恒温槽内で、同充電電圧、同放電電圧、及び、電流密度５０ｍＡ／ｇの条件で５０サイクルの充放電を行った。
【００９３】
上記と同温度の恒温槽内で、同充電電圧、同放電電圧、及び、電流密度３００ｍＡ／ｇの条件で１サイクルの充放電を行った後の放電容量と、上記のサイクル充放電を行った後の放電容量との比を、容量維持率として求めた。
【００９４】
上記のサイクル充放電を行った後、さらに２５℃、充電電圧４．６Ｖ、放電電圧２．５Ｖ、及び、電流密度５０ｍＡ／ｇの条件で１サイクルの充放電を行った後の放電容量から、上記のサイクル充放電の最終サイクルの充電容量を除した値を、容量回復率として求めた。
【００９５】
（結果）
図１Ａ～図１Ｉに、実施例１～６及び比較例１～３のＸＲＤパターンを示す。いずれも所望の結晶構造（層状岩塩型構造）が得られた。
【００９６】
図２に、実施例１～３で得られた正極活物質のＸＰＳスペクトルを示す。
実施例１～３で得られた正極活物質の表面に、Ｃａが存在することが確認された。
【００９７】
図３Ａに、実施例２で得られた正極活物質について得られたＨＡＡＤＦ-ＳＴＥＭ像及びその表面におけるＥＤＸ分析によるＣａマッピングの写真を示す。図中、白っぽく見える部分が、Ｃａを含む結晶相が存在しているところである。図３Ｂに、このＣａを含む結晶相のＥＤＸスペクトルを示す。図３Ｂ中のＣｕのピークは基板由来のものである。
実施例２で得られた正極活物質においては、母体結晶の表面全体に略均一にＣａを含む結晶相が分布しており、その組成がＣａＯであることが確認された。ＣａＯは母体結晶とは異なる結晶相を有する。
【００９８】
ＸＰＳ、ＨＡＡＤＦ-ＳＴＥＭ、及びＥＤＸの分析結果は、Ｃａを用いた実施例１～３、７、及び、Ｃａ以外のアルカリ土類金属を用いた実施例４～６において同様であり、母体結晶の表面全体に略均一にアルカリ土類金属を含む結晶相が分布しており、その組成がアルカリ土類金属の酸化物であることが確認された。

【００９９】
各例におけるアルカリ土類金属の種類と添加量、及び、容量維持率と容量回復率の測定結果を表１に示す。Ｃａ添加量と容量維持率との関係を図４に示す。図４はＣａ添加なしの比較例１及びＣａ添加ありの実施例１～３、７の結果をプロットしたものである。
【０１００】
表１及び図４に示すように、アルカリ土類金属を添加した実施例１～７では、金属元素を添加しなかった比較例１よりも、高い容量維持率と高い容量回復率が得られた。
特に、アルカリ土類金属を０．２５～１．０ｍｏｌ％添加した実施例１～６では、金属元素を添加しなかった比較例１、アルカリ土類金属以外の金属元素を添加した比較例２、３よりも、高い容量維持率と高い容量回復率が得られた。
【０１０１】
正極活物質の添加金属として、比較例２、３ではＦｅあるいはＴｉを用いた。これらの金属元素は、母体結晶をなすＮｉ、Ｍｎ、及びＣｏとイオン半径が近いため、母体酸化物の結晶構造に容易に固溶すると考えられる。そのため、表面に異相として析出させることが難しい。
【０１０２】
一方、実施例１～７で用いたアルカリ土類金属は、Ｎｉ、Ｍｎ、及びＣｏよりもイオン半径が大きく、異相として析出させることができると考えられる。この異相は、二次電池の電気化学反応には関与しないと考えられる。そして、４．５Ｖ以上の高電位の充電とその放電を繰り返した場合、この電気化学反応に関与しない結晶相が母体酸化物の膨張収縮によって発生する応力を緩和する機能を発現すると考えられる。その結果、４．５Ｖ以上の高電位の充電とその放電を繰り返しても、正極活物質に発生するクラックが抑制されて、正極の劣化が抑制され、容量維持率と容量回復率の両方が向上されると考えられる。
【０１０３】
母体酸化物に対するアルカリ土類金属の添加量が多くなりすぎると、二次電池の電気化学反応には関与する母体結晶相の量が相対的に少なくなることに起因して、電池容量が低下すると考えられる。したがって、アルカリ土類金属の添加量は、リチウム複合酸化物のすべての構成金属元素に対して、２．５ｍｏｌ％以下が好ましく、１．０ｍｏｌ％以下が特に好ましい。
【０１０４】
【表１】

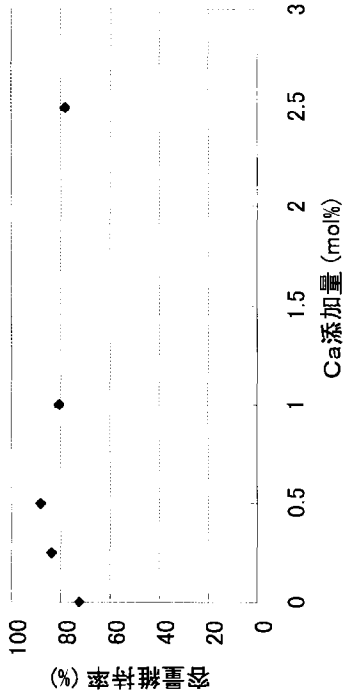
	添加元素	添加量 (mol%)	容量維持率 (%)	容量回復率 (%)
実施例1	Ca	0.25	83.8	59.1
実施例2	Ca	0.5	88.3	72
実施例3	Ca	1	80.5	63
実施例4	Mg	0.5	81.1	60.8
実施例5	Mg	1	79.3	58.1
実施例6	Sr	1	83.7	62.9
実施例7	Ca	2.5	78.0	55.5
比較例1	なし	0	72.6	55.3
比較例2	Ti	1	77.8	53
比較例3	Fe	1	78.1	49.3
比較例4	Mg	1	72.3	56.7

【産業上の利用可能性】
【０１０５】
本発明のリチウム複合酸化物の製造方法は、プラグインハイブリッド車（ＰＨＶ）あるいは電気自動車（ＥＶ）に搭載されるリチウムイオン二次電池等に好ましく適用できる。

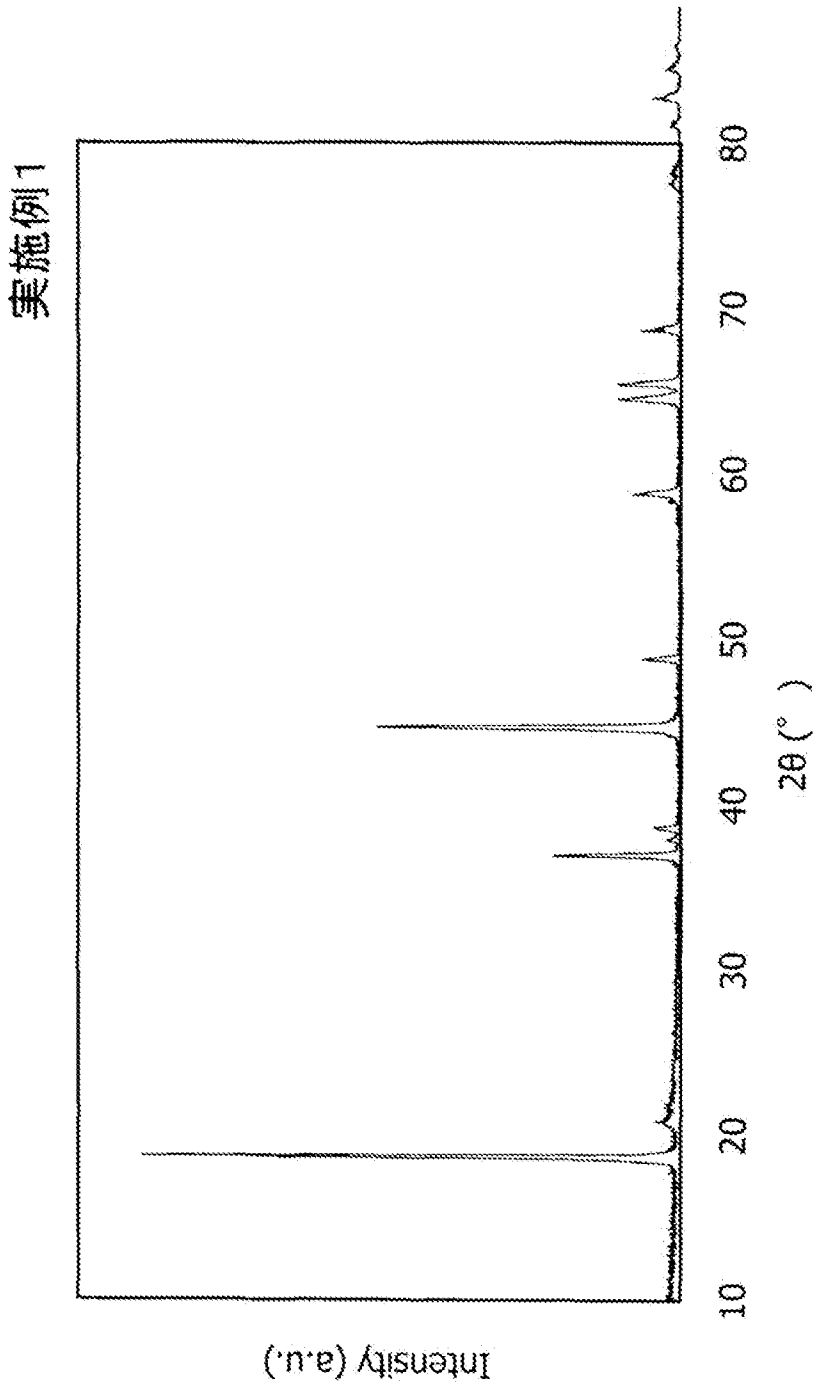
【図２】


Co2p3
Li1s
O1s
Mn2p3
Ca2p
C1s
Ni2p3
Binding Energy (eV)

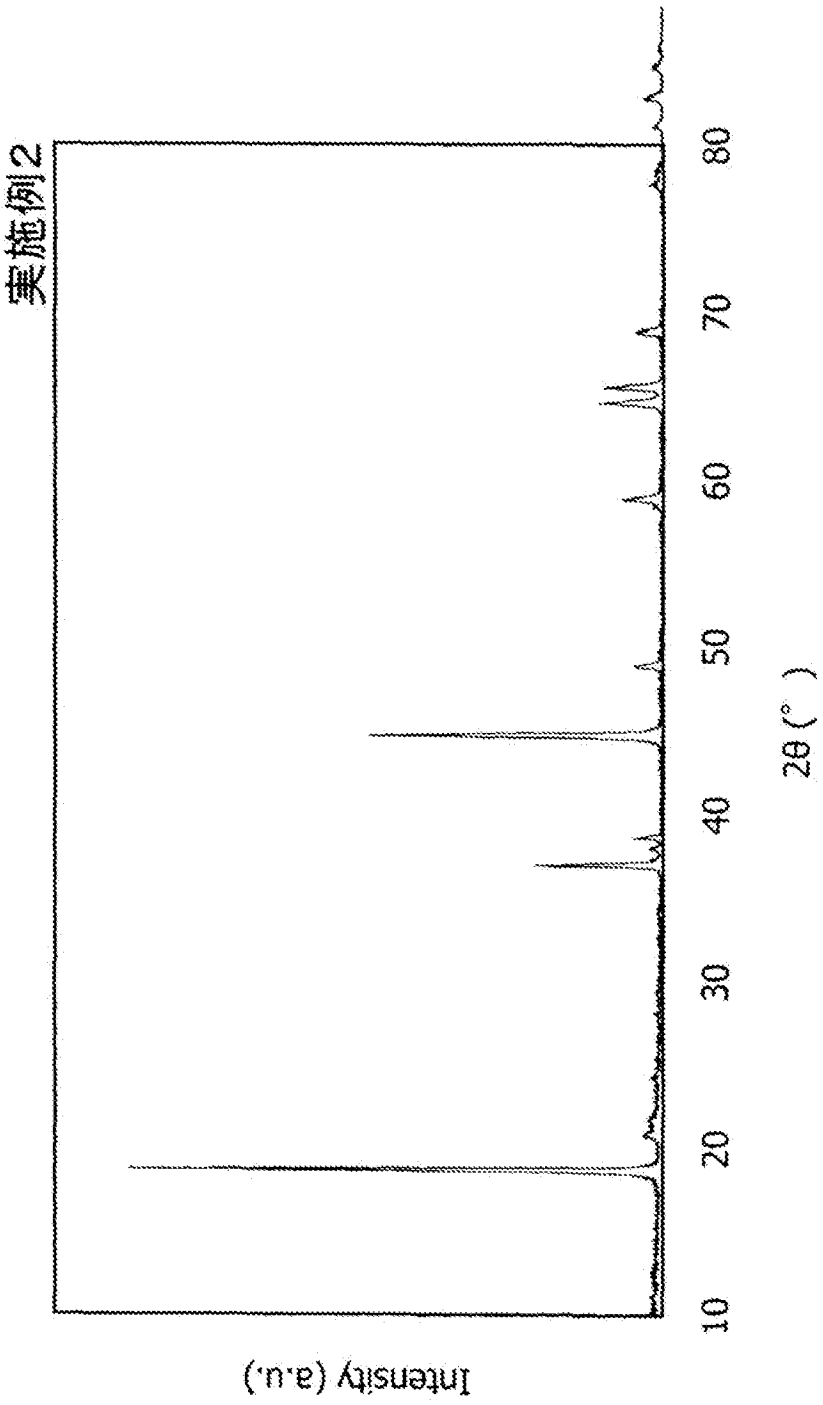
【図４】


容量維持率 (%)
Ca添加量 (mol%)
0
20
40
60
80
100
0
0.5
1
1.5
2
2.5
3

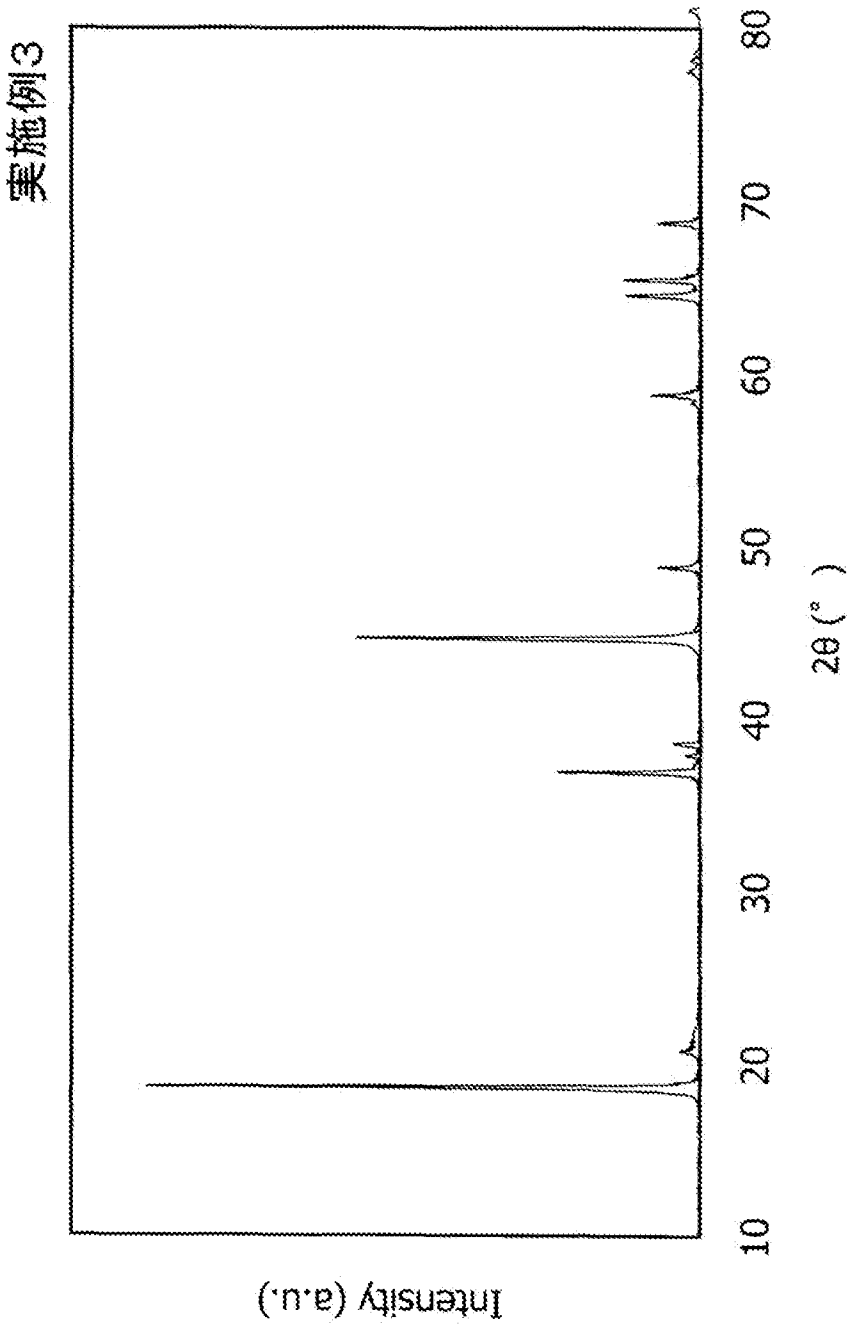
【図１Ａ】



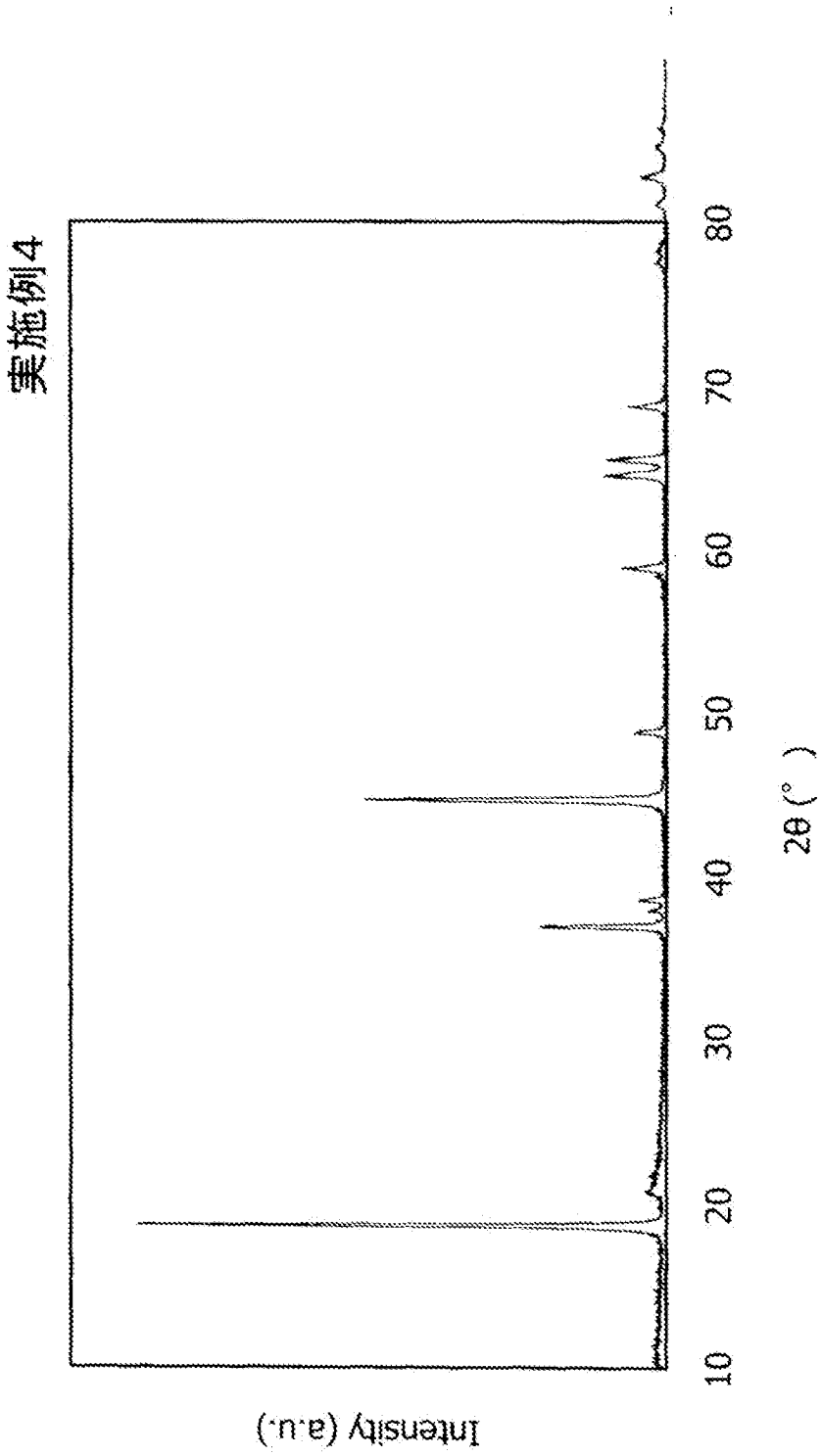
【図１Ｂ】



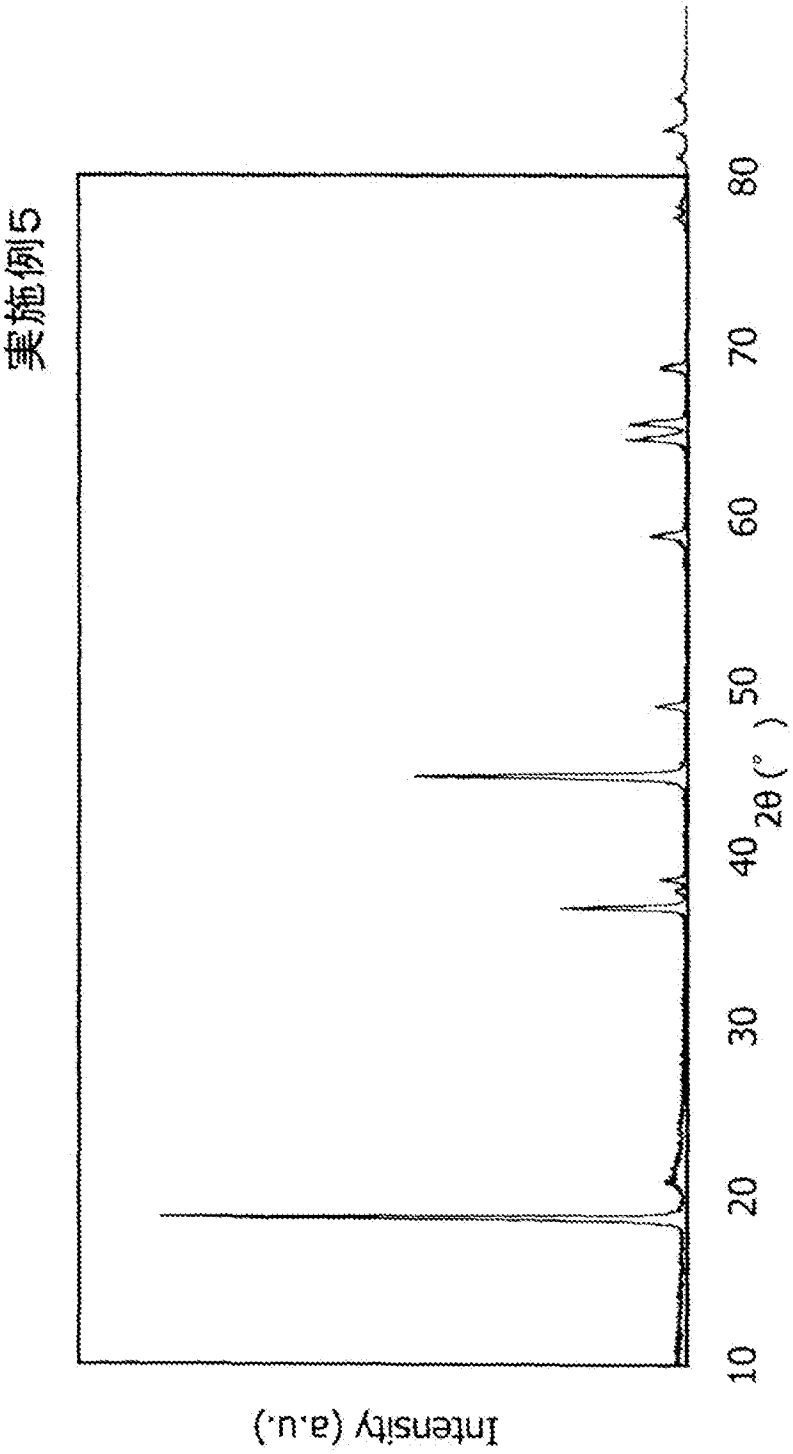
【図１Ｃ】



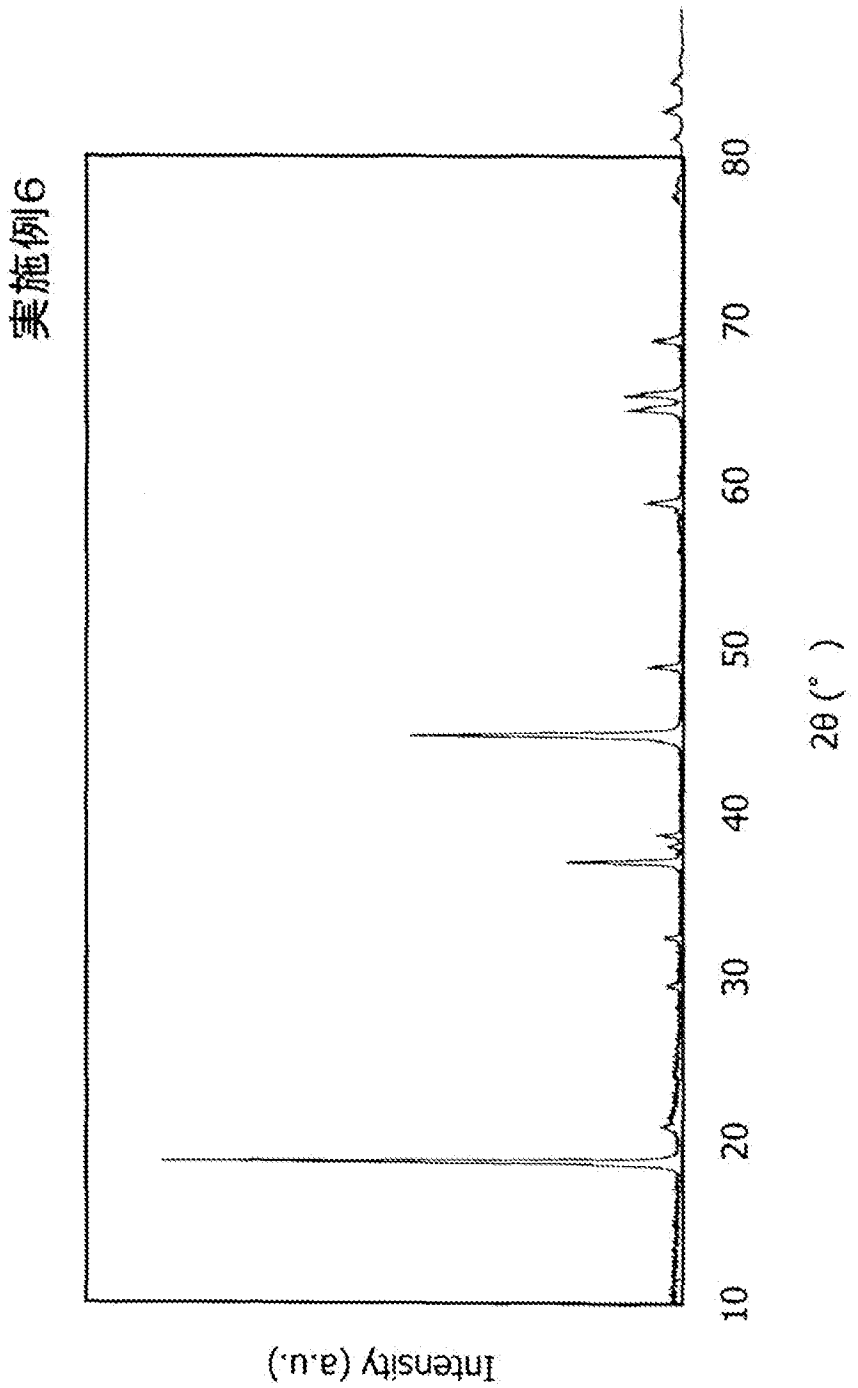
【図１Ｄ】



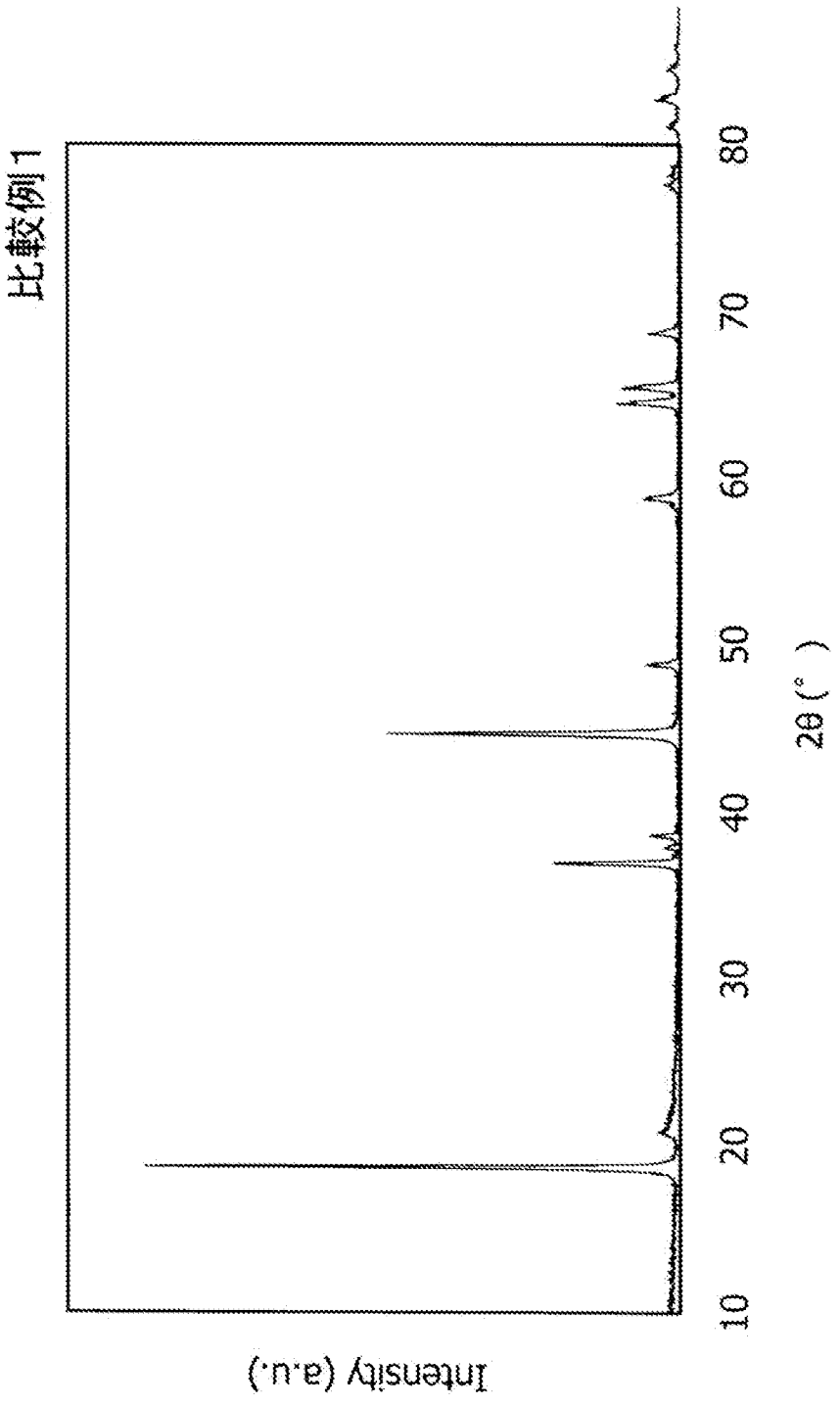
【図１Ｅ】



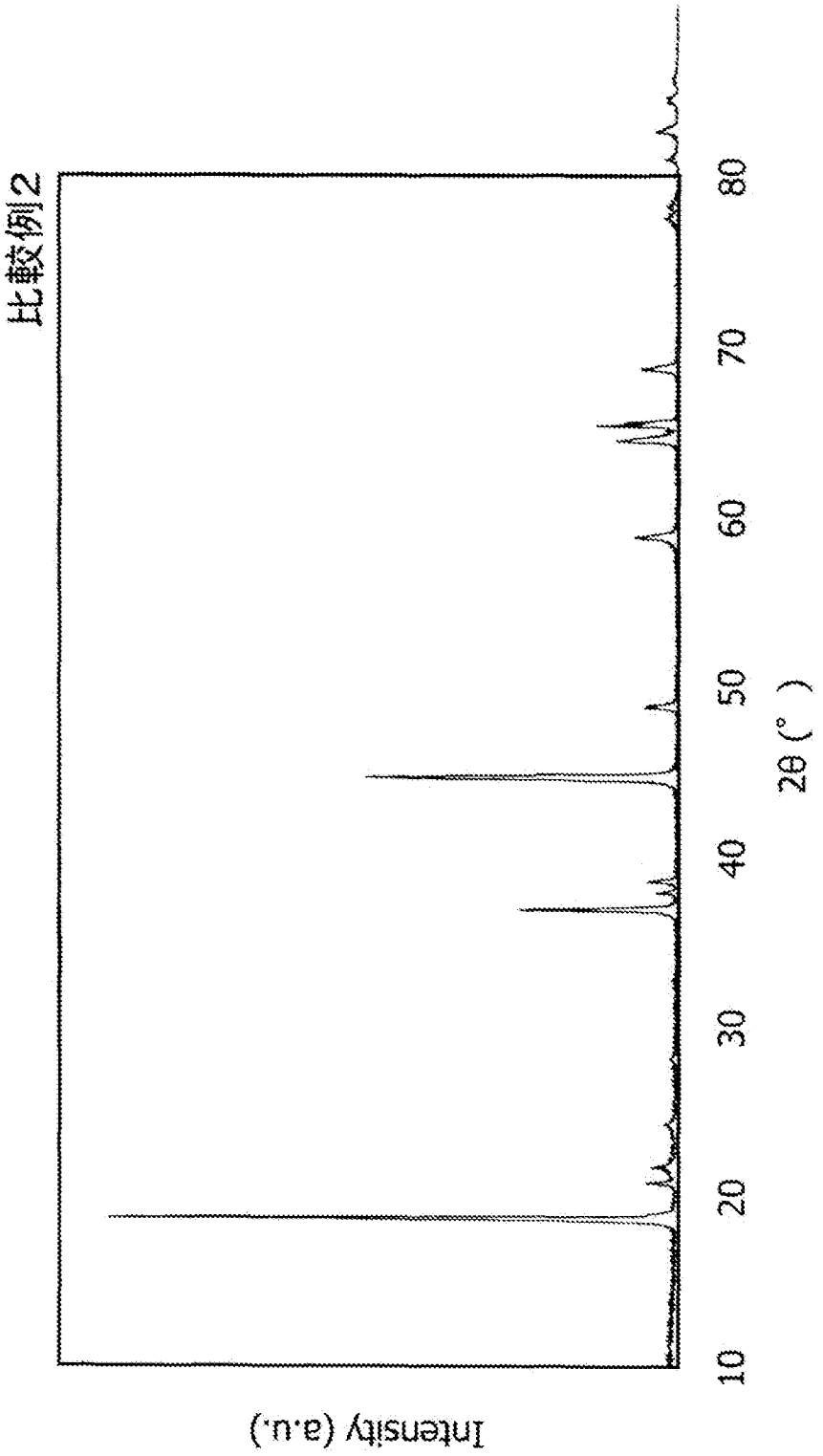
【図１Ｆ】



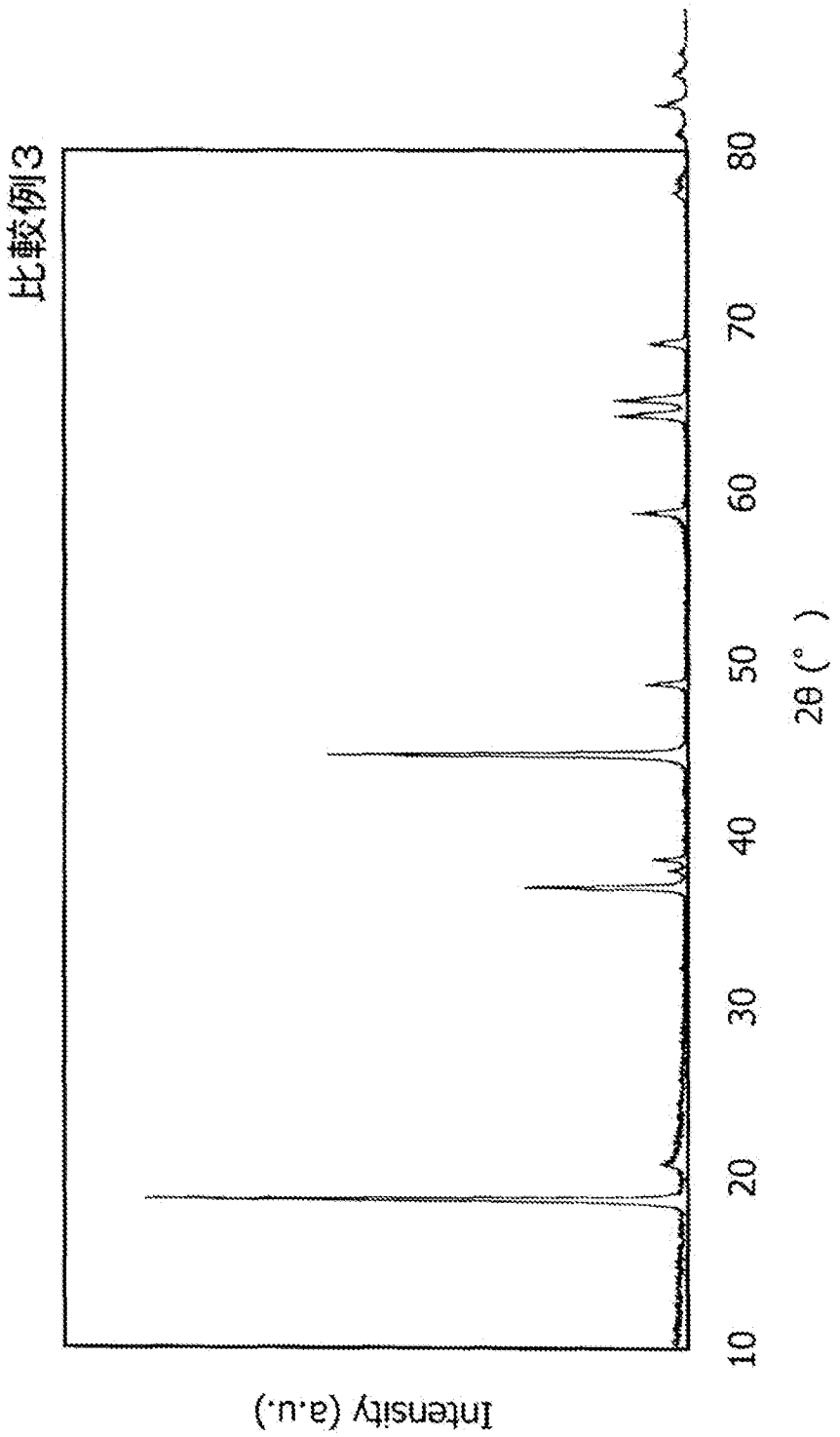
【図１Ｇ】



【図１Ｈ】

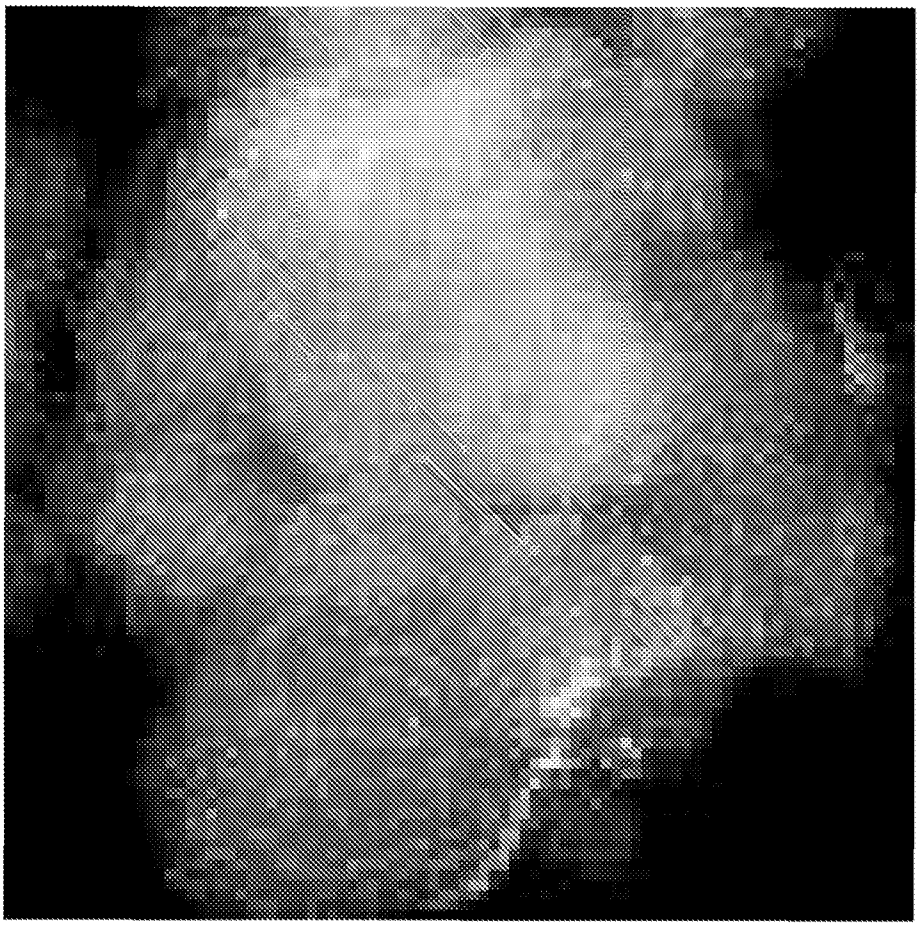


【図１１】

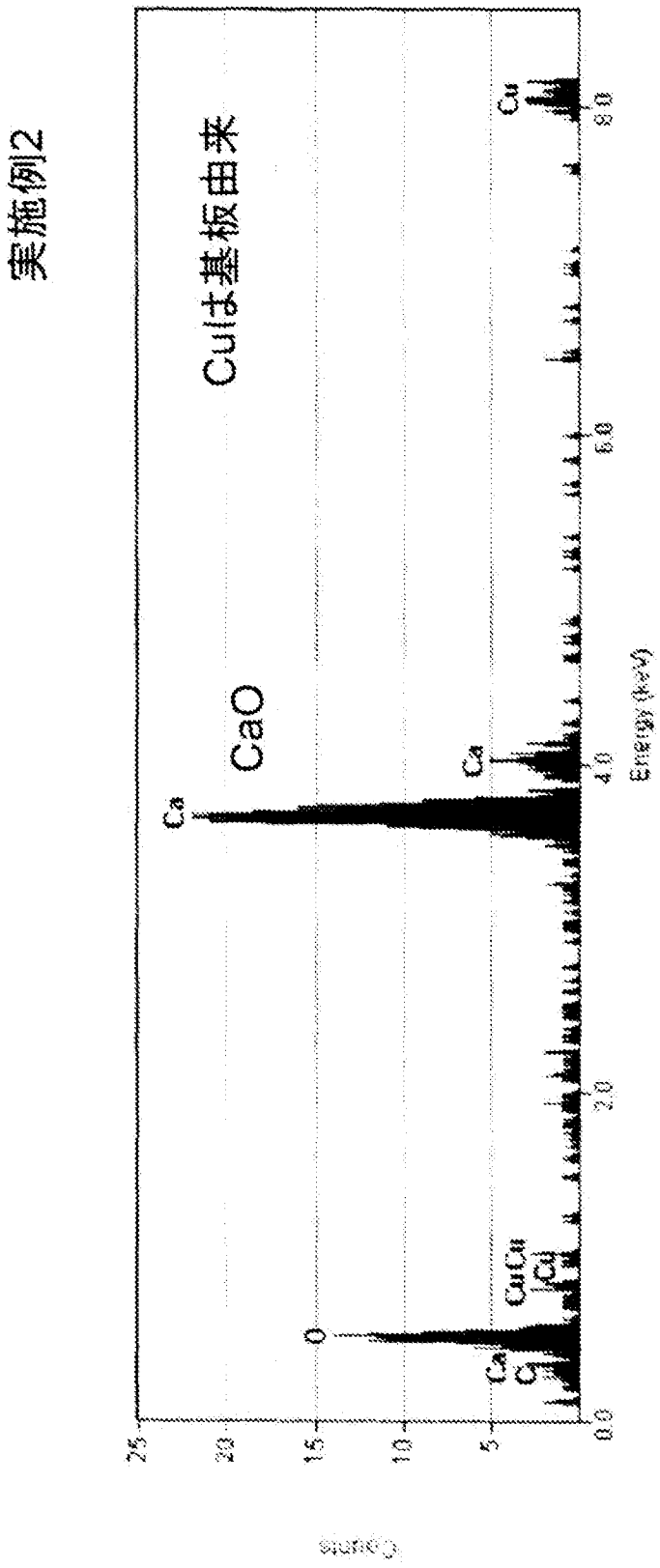


【図３Ａ】

実施例2



【図３Ｂ】


実施例2
Cu基板由来
CaO
Ca
Cu
O
Cu Cu
Cl
Ca
Energy (keV)
Counts
0.0
2.0
4.0
6.0
8.0
5
10
15
20
25

フロントページの続き

(51)Int.Cl.	F I	テーマコード（参考）
H01M 10/052 (2010.01)	H01M 10/00 102	

Fターム(参考) 5H050 AA02 AA07 AA19 BA16 BA17 CA07 CA08 CA09 CB01 CB02
CB05 CB07 CB08 CB12 EA10 EA24 GA02 GA05 GA14 HA02
HA10 HA14

Espacenet

Family list: JP2008060033 (A) — 2008-03-13

1 application(s) for: JP2008060033 (A)

1. POSITIVE-ELECTRODE ACTIVE MATERIAL, POSITIVE ELECTRODE USING THE SAME, NONAQUEOUS ELECTROLYTE SECONDARY BATTERY, AND POSITIVE-ELECTRODE ACTIVE MATERIAL MANUFACTURING METHOD					
Inventor: MORITA KOSHI YAMAGUCHI HIROYUKI (+2)	**Applicant:** SONY CORP	**CPC:**	**IPC:** H01M10/05 H01M4/02 H01M4/505 (+1)	**Publication info:** JP2008060033 (A) 2008-03-13 Global Dossier	**Priority date:** 2006-09-04

Espacenet

Bibliographic data: JP2008060033 (A) — 2008-03-13

POSITIVE-ELECTRODE ACTIVE MATERIAL, POSITIVE ELECTRODE USING THE SAME, NONAQUEOUS ELECTROLYTE SECONDARY BATTERY, AND POSITIVE-ELECTRODE ACTIVE MATERIAL MANUFACTURING METHOD

Inventor(s): MORITA KOSHI; YAMAGUCHI HIROYUKI; NAKAI HIDEKI; SAGANE MASAYOSHI ± (MORITA KOSHI, ; YAMAGUCHI HIROYUKI, ; NAKAI HIDEKI, ; SAGANE MASAYOSHI)

Applicant(s): SONY CORP ± (SONY CORP)

Classification: **- international:** ***H01M10/05; H01M4/02; H01M4/505; H01M4/525***
- cooperative:

Application number: JP20060238791 20060904 Global Dossier

Priority number (s): JP20060238791 20060904

Abstract of JP2008060033 (A)

PROBLEM TO BE SOLVED: To provide a positive-electrode active material excellent in charge/discharge cycle characteristics, a positive electrode using the same, a nonaqueous electrolyte secondary battery, and a positive-electrode active material manufacturing method. ;SOLUTION: The positive electrode 2 has the positive-electrode active material. In the positive-electrode active material, a peak intensity ratio (LiMeF+/LiMeO+) in the cross-section of a compound oxide particle between LiMeF+ and LiMeO+ obtained by positive ion analysis executed by a time-of-flight secondary ion mass spectrometer is within the range of 0.01-0.3. The LiMeF+ exists even at the center part of the compound oxide particle. ;COPYRIGHT: (C)2008,JPO&INPIT

(19)日本国特許庁(JP)　(12)公開特許公報(A)　(11)特許出願公開番号
特開2008-60033
(P2008-60033A)
(43)公開日　平成20年3月13日(2008.3.13)

(51)Int.Cl.		F I		テーマコード（参考）
H01M 4/58	(2006.01)	H01M 4/58		5H029
H01M 10/40	(2006.01)	H01M 10/40	Z	5H050
H01M 4/02	(2006.01)	H01M 4/02	C	

審査請求 未請求　請求項の数 15　ＯＬ　（全 23 頁）

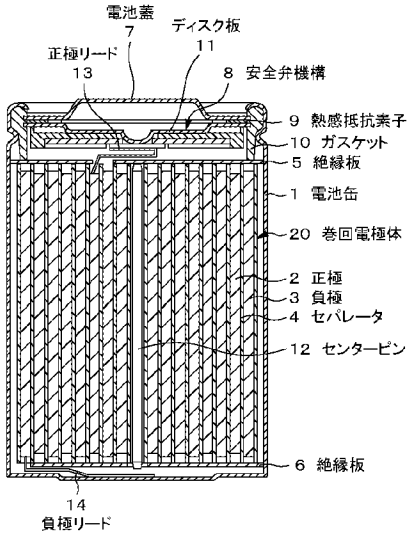
(21)出願番号　特願2006-238791 (P2006-238791)
(22)出願日　平成18年9月4日 (2006.9.4)

(71)出願人　000002185
ソニー株式会社
東京都港区港南１丁目７番１号
(74)代理人　100082762
弁理士　杉浦　正知
(72)発明者　森田　耕詩
東京都品川区北品川６丁目７番３５号　ソニー株式会社内
(72)発明者　山口　裕之
東京都品川区北品川６丁目７番３５号　ソニー株式会社内
(72)発明者　中井　秀樹
東京都品川区北品川６丁目７番３５号　ソニー株式会社内

最終頁に続く

(54)【発明の名称】正極活物質、これを用いた正極および非水電解質二次電池、並びに正極活物質の製造方法

(57)【要約】
【課題】充放電サイクル特性に優れた正極活物質、これを用いた正極および非水電解質二次電池、並びに正極活物質の製造方法を提供する。
【解決手段】正極２は、正極活物質を有する。正極活物質は、複合酸化物粒子の断面において、飛行時間型二次イオン質量分析装置による正イオン分析で得られるＬｉＭｅＦ＋のＬｉＭｅＯ＋に対するピーク強度比（ＬｉＭｅＦ＋／ＬｉＭｅＯ＋）が０．０１～０．３の範囲内であり、且つ複合酸化物粒子の中心部にまでＬｉＭｅＦ＋が存在することを特徴とする。
【選択図】図１



【特許請求の範囲】
【請求項１】
平均組成が化１で表される複合酸化物粒子であり、
上記複合酸化物粒子の断面において、飛行時間型二次イオン質量分析装置による正イオン分析で得られるＬｉＭｅＦ＋のＬｉＭｅＯ＋に対するピーク強度比（ＬｉＭｅＦ＋／ＬｉＭｅＯ＋）が０．０１～０．３の範囲内であり、且つ
上記複合酸化物粒子の中心部にまでＬｉＭｅＦ＋が存在すること
を特徴とする正極活物質。
〔Ｍｅは、２族～１５族の元素から選ばれた何れかを示す。〕
（化１）
$Li_pNi_{(1-q-r)}Mn_qM1_rO_{(2-y)}X_z$
（Ｍ１はＮｉ、Ｍｎを除く２族～１５族から選ばれる元素のうち少なくとも一種を、Ｘはフッ素を示す。ｐ、ｑ、ｒ、ｙ、ｚは０≦ｐ≦１．５、０≦ｑ≦１．０、０≦ｒ≦１．０、－０．１０≦ｙ≦０．２０、０＜ｚ≦０．２の範囲内の値である。）
【請求項２】
上記複合酸化物粒子の表面におけるフッ素量が１ａｔｏｍｉｃ％～２０ａｔｏｍｉｃ％であること
を特徴とする請求項１記載の正極活物質。
【請求項３】
上記複合酸化物粒子は、化２で平均組成が表されること
を特徴とする請求項１記載の正極活物質。
（化２）
$Li_{(1+p)}Co_{(1-q)}M_qO_{(2-y)}F_z$
（式中、Ｍはコバルトを除く２族～１５族から選ばれる元素のうち少なくとも一種を示す。ｐ、ｑ、ｙ、ｚは、－０．１０≦ｐ≦０．１０、０≦ｑ＜０．３、－０．１０≦ｙ≦０．２０、０＜ｚ≦０．２の範囲内の値である。）
【請求項４】
平均組成が化１で表される複合酸化物粒子を有し、
上記複合酸化物粒子の断面において、飛行時間型二次イオン質量分析装置による正イオン分析で得られるＬｉＭｅＦ＋のＬｉＭｅＯ＋に対するピーク強度比（ＬｉＭｅＦ＋／ＬｉＭｅＯ＋）が０．０１～０．３の範囲内であり、且つ
上記複合酸化物粒子の中心部にまでＬｉＭｅＦ＋が存在すること
を特徴とする正極。
〔Ｍｅは、２族～１５族の元素から選ばれた何れかを示す。〕
（化１）
$Li_pNi_{(1-q-r)}Mn_qM1_rO_{(2-y)}X_z$
（Ｍ１はＮｉ、Ｍｎを除く２族～１５族から選ばれる元素のうち少なくとも一種を、Ｘはフッ素を示す。ｐ、ｑ、ｒ、ｙ、ｚは０≦ｐ≦１．５、０≦ｑ≦１．０、０≦ｒ≦１．０、－０．１０≦ｙ≦０．２０、０＜ｚ≦０．２の範囲内の値である。）
【請求項５】
上記複合酸化物粒子の表面におけるフッ素量が１ａｔｏｍｉｃ％～２０ａｔｏｍｉｃ％であること
を特徴とする請求項４記載の正極。
【請求項６】
上記複合酸化物粒子は、化２で平均組成が表されること
を特徴とする請求項４記載の正極。
（化２）
$Li_{(1+p)}Co_{(1-q)}M_qO_{(2-y)}F_z$
（式中、Ｍはコバルトを除く２族～１５族から選ばれる元素のうち少なくとも一種を示す。ｐ、ｑ、ｙ、ｚは、－０．１０≦ｐ≦０．１０、０≦ｑ＜０．３、－０．１０≦ｙ≦０．２

AMPEREX Ex. 1002
Page 1092

０、０＜ｚ≦０．２の範囲内の値である。）

【請求項７】

正極と、負極と、電解質とを有し、

上記正極は、

平均組成が化１で表される複合酸化物粒子を有し、

上記複合酸化物粒子の断面において、飛行時間型二次イオン質量分析装置による正イオン分析で得られるＬｉＭｅＦ＋のＬｉＭｅＯ＋に対するピーク強度比（ＬｉＭｅＦ＋／ＬｉＭｅＯ＋）が０．０１～０．３の範囲内であり、且つ

上記複合酸化物粒子の中心部にまでＬｉＭｅＦ＋が存在すること

を特徴とする非水電解質二次電池。

〔Ｍｅは、２族～１５族の元素から選ばれた何れかを示す。〕

（化１）

$Li_pNi_{(1-q-r)}Mn_qM1_rO_{(2-y)}X_z$

（Ｍ１はＮｉ、Ｍｎを除く２族～１５族から選ばれる元素のうち少なくとも一種を、ＸはＦを示す。ｐ、ｑ、ｒ、ｙ、ｚは０≦ｐ≦１．５、０≦ｑ≦１．０、０≦ｒ≦１．０、－０．１０≦ｙ≦０．２０、０＜ｚ≦０．２の範囲内の値である。）

【請求項８】

上記複合酸化物粒子は、化２で平均組成が表されること

を特徴とする請求項７記載の非水電解質二次電池。

（化２）

$Li_{(1+p)}Co_{(1-q)}M_qO_{(2-y)}F_z$

（式中、ＭはＣｏを除く２族～１５族から選ばれる元素のうち少なくとも一種を示す。ｐ、ｑ、ｙ、ｚは、－０．１０≦ｐ≦０．１０、０≦ｑ＜０．３、－０．１０≦ｙ≦０．２０、０＜ｚ≦０．２の範囲内の値である。）

【請求項９】

上記複合酸化物粒子の表面におけるフッ素量が１ａｔｏｍｉｃ％～２０ａｔｏｍｉｃ％であること

を特徴とする請求項７記載の非水電解質二次電池。

【請求項１０】

化３または化４で表される複合酸化物粒子を高温環境下でフッ素化を行うこと

を特徴とする正極活物質の製造方法。

（化３）

$Li_pNi_{(1-q-r)}Mn_qM1_rO_{(2-y)}$

（Ｍ１はＮｉ、Ｍｎを除く２族～１５族から選ばれる元素のうち少なくとも一種を示す。ｐ、ｑ、ｒ、ｙは０≦ｐ≦１．５、０≦ｑ≦１．０、０≦ｒ≦１．０、－０．１０≦ｙ≦０．２０の範囲内の値である。）

（化４）

$Li_{(1+p)}Co_{(1-q)}M_qO_{(2-y)}$

（式中、ＭはＣｏを除く２族～１５族から選ばれる元素のうち少なくとも一種を示す。ｐ、ｑ、ｙ、は、－０．１０≦ｐ≦０．１０、０≦ｑ＜０．３、－０．１０≦ｙ≦０．２０の範囲内の値である。）

【請求項１１】

上記フッ素化を１００℃～３００℃の温度環境下、フッ素ガスの分圧が０．００２ＭＰａ～０．５ＭＰａで行うこと

を特徴とする請求項１０記載の正極活物質の製造方法。

【請求項１２】

化３または化４で表される複合酸化物粒子を常温でフッ素化した後、加熱処理を行うこと

を特徴とする正極活物質の製造方法。

（化３）

$Li_pNi_{(1-q-r)}Mn_qM1_rO_{(2-y)}$
（Ｍ１はＮｉ、Ｍｎを除く２族～１５族から選ばれる元素のうち少なくとも一種を示す。ｐ、ｑ、ｒ、ｙは０≦ｐ≦１．５、０≦ｑ≦１．０、０≦ｒ≦１．０、－０．１０≦ｙ≦０．２０の範囲内の値である。）
（化４）
$Li_{(1+p)}Co_{(1-q)}M_qO_{(2-y)}$
（式中、ＭはＣｏを除く２族～１５族から選ばれる元素のうち少なくとも一種を示す。ｐ、ｑ、ｙ、は、－０．１０≦ｐ≦０．１０、０≦ｑ＜０．３、－０．１０≦ｙ≦０．２０の範囲内の値である。）
【請求項１３】
上記加熱処理を加熱温度２００℃～１０００℃で０．５時間～１０時間行うこと
を特徴とする請求項１２記載の正極活物質の製造方法。
【請求項１４】
化３または化４で表される複合酸化物粒子を高温環境下でフッ素化を行った後、加熱処理を行うこと
を特徴とする正極活物質の製造方法。
（化３）
$Li_pNi_{(1-q-r)}Mn_qM1_rO_{(2-y)}$
（Ｍ１はＮｉ、Ｍｎを除く２族～１５族から選ばれる元素のうち少なくとも一種を示す。ｐ、ｑ、ｒ、ｙは０≦ｐ≦１．５、０≦ｑ≦１．０、０≦ｒ≦１．０、－０．１０≦ｙ≦０．２０の範囲内の値である。）
（化４）
$Li_{(1+p)}Co_{(1-q)}M_qO_{(2-y)}$
（式中、ＭはＣｏを除く２族～１５族から選ばれる元素のうち少なくとも一種を示す。ｐ、ｑ、ｙ、は、－０．１０≦ｐ≦０．１０、０≦ｑ＜０．３、－０．１０≦ｙ≦０．２０の範囲内の値である。）
【請求項１５】
上記フッ素化を１００℃～３００℃の温度環境下、フッ素ガスの分圧が０．００２ＭＰａ～０．５ＭＰａで行い、
上記加熱処理を加熱温度２００℃～１０００℃で０．５時間～１０時間行うこと
を特徴とする請求項１４記載の正極活物質の製造方法。
【発明の詳細な説明】
【技術分野】
【０００１】
この発明は、正極活物質、これを用いた正極および非水電解質二次電池、並びに正極活物質の製造方法に関する。さらに詳しくは、フッ素化処理がなされた正極活物質、これを用いた正極および非水電解質二次電池、並びに正極活物質の製造方法に関する。
【背景技術】
【０００２】
携帯機器の多機能化・高性能化につれて、機器の消費電力は高まりつつあり、電源となる電池は、より一層の高容量が要求されている。経済性と機器の小型軽量化の観点から、高エネルギー密度の二次電池が強く要望されている。代表的な二次電池としては、鉛蓄電池、アルカリ蓄電池、リチウムイオン二次電池等が知られている。
【０００３】
二次電池の中でも、特にリチウムイオン二次電池は、高出力、高エネルギー密度などの利点を有している。リチウムイオン二次電池は、リチウムイオンを可逆的に脱挿入可能な正極と負極と、非水電解液あるいはゲル、固体電解質とから構成される。
【０００４】
リチウムイオン二次電池用の正極材料としては、リチウムイオンをインターカレート・デインターカレートできる$LiCoO_2$、$LiNiO_2$あるいはこれらのリチウム含有遷移

金属化合物に金属元素を一部置換した複合酸化物が用いられる。また、スピネル構造を有するＬｉＭｎ$_2$Ｏ$_4$は、高エネルギー密度、高電圧を有するため、よく使用されており、高電圧を有する安価な材料として開発が進められている。

【０００５】

通常、リチウムイオン二次電池では、正極にコバルト酸リチウムおよび負極には炭素材料が使用されており、作動電圧が４．２Ｖから２．５Ｖの範囲で用いられる。単電池において、端子電圧を４．２Ｖまで上げられるのは、非水電解質材料やセパレータ等の優れた電気化学的安定性によるところが大きい。

【０００６】

現状、最大４．２Ｖで作動するリチウムイオン二次電池では、それに用いられるコバルト酸リチウム等の正極活物質は、その理論容量に対して６割程度の容量を活用しているに過ぎない。リチウムイオン二次電池については、コスト低減以外に、高エネルギー密度化、高信頼性化および長寿命化が望まれている。

【０００７】

これらの特性、特に電池のエネルギー密度を向上する方法としては、充電の上限電圧を高く設定することが挙げられる。充電電圧を高くすると正極活物質であるリチウム複合酸化物からより多くのリチウムがデインターカレート・インターカレートされるため、高容量化が可能となる。

【０００８】

このように充電電圧を上げることにより、残存容量を活用することが、原理上可能であり、実際、例えば、特許文献１にて開示されているように、充電時の電圧を４．２５Ｖ以上にすることにより、高エネルギー密度化を実現できることが知られている。

【０００９】

【特許文献１】国際公開第０３／０１９７１３号パンフレット

【００１０】

ところで、充電電圧を高くした二次電池では、Ｌｉ$_x$ＣｏＯ$_2$（０＜ｘ≦１．０）、Ｌｉ$_x$ＮｉＯ$_2$（０＜ｘ≦１．０）などが、高電位、安定性、長寿命という点から最も有望である。このなかでも、ＬｉＣｏＯ$_2$を主体とする正極活物質は、高電位を示す正極活物質であり、充電電圧を高め、エネルギー密度を高めることが期待されるが、充電電圧を高くした電池は充放電サイクル寿命が低下したり、高温特性が劣化してしまうことが問題となっている。

【００１１】

また、ＬｉＮｉＯ$_2$で表されるリチウムニッケル複合酸化物やニッケル（Ｎｉ）の一部をコバルト（Ｃｏ）やマンガン（Ｍｎ）で置換したリチウムニッケル複合酸化物はＬｉＣｏＯ$_2$に比べて高電位での安定性が高いとされているが、ＬｉＣｏＯ$_2$に比べて放電電位の低下や体積密度の低下によりエネルギー密度を高めるには不利となっている。

【００１２】

そこで、ＬｉＣｏＯ$_2$を主体とする活物質を安定化させるために、アルミニウム（Ａｌ）やマグネシウム（Ｍｇ）、ジルコニウム（Ｚｒ）、チタン（Ｔｉ）等の異種元素を固溶させたり（特許文献２参照）、ＬｉＭｎ$_{1/3}$Ｃｏ$_{1/3}$Ｎｉ$_{1/3}$Ｏ$_2$などを少量混合して用いること、ＬｉＣｏＯ$_2$表面をスピネルマンガン酸リチウムやスピネルチタン酸リチウム、ニッケルコバルト複合酸化物で表面被覆を行うことなどが提案されている。（特許文献３および特許文献４参照）

【００１３】

【特許文献２】特開２００４－３０３５９１号公報

【特許文献３】特開２０００－１６４２１４号公報

【特許文献４】特開２００２－１５１０７８号公報

【００１４】

また、金属元素の置換や被覆ではなく、フッ素（Ｆ）や硫黄（Ｓ）といったハロゲン元素やカルコゲン元素を用いた処理により活物質の安定化を図ることも提案されている。（

特許文献５～特許文献７参照）
【００１５】
【特許文献５】特許第３１４１８５８号公報
【特許文献６】特許第３１５７４１３号公報
【特許文献７】特開２００５－１１６８８号公報
【発明の開示】
【発明が解決しようとする課題】
【００１６】
しかしながら、特許文献５～特許文献７で提案されている正極活物質のフッ素処理による改質では、改質された正極活物質を用いて、特に充電上限電圧が４．２５Ｖ以上の高充電電圧になるような電池を作製して、高容量で充放電を繰り返すと、容量劣化が生じるため電池寿命が短くなる問題があった。
【００１７】
したがって、この発明の目的は、充放電サイクル特性に優れた正極活物質、これを用いた正極および非水電解質二次電池、並びに正極活物質の製造方法を提供することにある。
【課題を解決するための手段】
【００１８】
上述した課題を解決するために、第１の発明は、
平均組成が化１で表される複合酸化物粒子であり、
複合酸化物粒子の断面において、飛行時間型二次イオン質量分析装置による正イオン分析で得られるＬｉＭｅＦ＋のＬｉＭｅＯ＋に対するピーク強度比（ＬｉＭｅＦ＋／ＬｉＭｅＯ＋）が０．０１～０．３の範囲内であり、且つ
複合酸化物粒子の中心部にまでＬｉＭｅＦ＋が存在すること
を特徴とする正極活物質である。
〔Ｍｅは、２族～１５族の元素から選ばれた何れかを示す。〕
（化１）
$Li_pNi_{(1-q-r)}Mn_qM1_rO_{(2-y)}X_z$
（Ｍ１はＮｉ、Ｍｎを除く２族～１５族から選ばれる元素のうち少なくとも一種を、Ｘはフッ素を示す。ｐ、ｑ、ｒ、ｙ、ｚは$0 \leqq p \leqq 1.5$、$0 \leqq q \leqq 1.0$、$0 \leqq r \leqq 1.0$、$-0.10 \leqq y \leqq 0.20$、$0 < z \leqq 0.2$の範囲内の値である。）
【００１９】
第２の発明は、
平均組成が化１で表される複合酸化物粒子を有し、
複合酸化物粒子の断面において、飛行時間型二次イオン質量分析装置による正イオン分析で得られるＬｉＭｅＦ＋のＬｉＭｅＯ＋に対するピーク強度比（ＬｉＭｅＦ＋／ＬｉＭｅＯ＋）が０．０１～０．３の範囲内であり、且つ
複合酸化物粒子の中心部にまでＬｉＭｅＦ＋が存在すること
を特徴とする正極である。
〔Ｍｅは、２族～１５族の元素から選ばれた何れかを示す。〕
（化１）
$Li_pNi_{(1-q-r)}Mn_qM1_rO_{(2-y)}X_z$
（Ｍ１はＮｉ、Ｍｎを除く２族～１５族から選ばれる元素のうち少なくとも一種を、Ｘはフッ素を示す。ｐ、ｑ、ｒ、ｙ、ｚは$0 \leqq p \leqq 1.5$、$0 \leqq q \leqq 1.0$、$0 \leqq r \leqq 1.0$、$-0.10 \leqq y \leqq 0.20$、$0 < z \leqq 0.2$の範囲内の値である。）
【００２０】
第３の発明は、
正極と、負極と、電解質とを有し、
正極は、
平均組成が化１で表される複合酸化物粒子を有し、
複合酸化物粒子の断面において、飛行時間型二次イオン質量分析装置による正イオン分

析で得られるＬｉＭｅＦ＋のＬｉＭｅＯ＋に対するピーク強度比（ＬｉＭｅＦ＋／ＬｉＭｅＯ＋）が０．０１～０．３の範囲内であり、且つ
　複合酸化物粒子の中心部にまでＬｉＭｅＦ＋が存在すること
を特徴とする非水電解質二次電池である。
〔Ｍｅは、２族～１５族の元素から選ばれた何れかを示す。〕
（化１）
$Li_pNi_{(1-q-r)}Mn_qM1_rO_{(2-y)}X_z$
（Ｍ１はＮｉ、Ｍｎを除く２族～１５族から選ばれる元素のうち少なくとも一種を、ＸはＦを示す。ｐ、ｑ、ｒ、ｙ、ｚは０≦ｐ≦１．５、０≦ｑ≦１．０、０≦ｒ≦１．０、－０．１０≦ｙ≦０．２０、０＜ｚ≦０．２の範囲内の値である。）

【００２１】
　第４の発明は、
　化３または化４で表される複合酸化物粒子を高温環境下でフッ素化を行うこと
を特徴とする正極活物質の製造方法である。
（化３）
$Li_pNi_{(1-q-r)}Mn_qM1_rO_{(2-y)}$
（Ｍ１はＮｉ、Ｍｎを除く２族～１５族から選ばれる元素のうち少なくとも一種を示す。ｐ、ｑ、ｒ、ｙは０≦ｐ≦１．５、０≦ｑ≦１．０、０≦ｒ≦１．０、－０．１０≦ｙ≦０．２０の範囲内の値である。）
（化４）
$Li_{(1+p)}Co_{(1-q)}M_qO_{(2-y)}$
（式中、ＭはＣｏを除く２族～１５族から選ばれる元素のうち少なくとも一種を示す。ｐ、ｑ、ｙ、は、－０．１０≦ｐ≦０．１０、０≦ｑ＜０．３、－０．１０≦ｙ≦０．２０の範囲内の値である。）

【００２２】
　第５の発明は、
　化３または化４で表される複合酸化物粒子を常温でフッ素化した後、加熱処理を行うこと
を特徴とする正極活物質の製造方法である。
（化３）
$Li_pNi_{(1-q-r)}Mn_qM1_rO_{(2-y)}$
（Ｍ１はＮｉ、Ｍｎを除く２族～１５族から選ばれる元素のうち少なくとも一種を示す。ｐ、ｑ、ｒ、ｙは０≦ｐ≦１．５、０≦ｑ≦１．０、０≦ｒ≦１．０、－０．１０≦ｙ≦０．２０の範囲内の値である。）
（化４）
$Li_{(1+p)}Co_{(1-q)}M_qO_{(2-y)}$
（式中、ＭはＣｏを除く２族～１５族から選ばれる元素のうち少なくとも一種を示す。ｐ、ｑ、ｙ、は、－０．１０≦ｐ≦０．１０、０≦ｑ＜０．３、－０．１０≦ｙ≦０．２０の範囲内の値である。）

【００２３】
　第６の発明は、
　化３または化４で表される複合酸化物粒子を高温環境下でフッ素化を行った後、加熱処理を行うこと
を特徴とする正極活物質の製造方法である。
（化３）
$Li_pNi_{(1-q-r)}Mn_qM1_rO_{(2-y)}$
（Ｍ１はＮｉ、Ｍｎを除く２族～１５族から選ばれる元素のうち少なくとも一種を示す。ｐ、ｑ、ｒ、ｙは０≦ｐ≦１．５、０≦ｑ≦１．０、０≦ｒ≦１．０、－０．１０≦ｙ≦０．２０の範囲内の値である。）
（化４）

$Li_{(1+p)}Co_{(1-q)}M_qO_{(2-y)}$
（式中、ＭはＣｏを除く２族～１５族から選ばれる元素のうち少なくとも一種を示す。ｐ、ｑ、ｙ、は、－０．１０≦ｐ≦０．１０、０≦ｑ＜０．３、－０．１０≦ｙ≦０．２０の範囲内の値である。）
【００２４】
この発明では、フッ素（Ｆ）が複合酸化物粒子の内部にまで拡散されているので、その表面でのリチウム（Ｌｉ）の吸蔵放出性能を低下させることなく、正極活物質の安定性を高めることが可能になっていると考えられる。これにより、非水電解質二次電池に用いた場合に、優れたサイクル特性を得ることができる。
【００２５】
第３の発明～第６の発明では、表面のＬｉＦ量を減少させるとともに、粒子の内部までＬｉ－Ｍｅ－Ｆ結合を有する正極活物質を作製できる。
【発明の効果】
【００２６】
この発明によれば、優れた充放電サイクル特性を得ることができる。
【発明を実施するための最良の形態】
【００２７】
この発明の一実施形態による正極活物質は、平均組成が化１、好ましくは化２で表される複合酸化物粒子であり、複合酸化物粒子の中心部にまで、Ｌｉ－Ｍｅ－Ｆ結合が存在していることを特徴とする。ここで、Ｍｅは、２族～１５族の元素から選ばれた何れかを示す。
【００２８】
（化１）
$Li_pNi_{(1-q-r)}Mn_qM1_rO_{(2-y)}X_z$
（Ｍ１はＮｉ、Ｍｎを除く２族～１５族から選ばれる元素のうち少なくとも一種を、ＸはＦを示す。ｐ、ｑ、ｒ、ｙ、ｚは０≦ｐ≦１．５、０≦ｑ≦１．０、０≦ｒ≦１．０、－０．１０≦ｙ≦０．２０、０＜ｚ≦０．２の範囲内の値である。）
（化２）
$Li_{(1+p)}Co_{(1-q)}M_qO_{(2-y)}F_z$
（式中、ＭはＣｏを除く２族～１５族から選ばれる元素のうち少なくとも一種を示す。ｐ、ｑ、ｙ、ｚは、－０．１０≦ｐ≦０．１０、０≦ｑ＜０．３、－０．１０≦ｙ≦０．２０、０＜ｚ≦０．２の範囲内の値である。）
【００２９】
化１、好ましくは化２で表される複合酸化物粒子において、粒子中に存在するＬｉ－Ｍｅ－Ｆ結合の存在は、化１、好ましくは化２で表された複合酸化物粒子について、ＴＯＦ－ＳＩＭＳ（Time of Flight secondary Ion Mass Spectrometry;飛行時間型２次イオン質量分析法）による断面分析を行い、Ｌｉ－Ｍｅ－Ｆ結合を表すＬｉＭｅＦ＋を測定することで評価できる。また、Ｌｉ－Ｍｅ－Ｏ結合を表すＬｉＭｅＯ＋イオンを測定し、ＬｉＭｅＦ＋のＬｉＭｅＯ＋に対するピーク強度比（ＬｉＭｅＦ＋／ＬｉＭｅＯ＋）を求めることで、フッ素化の程度を評価することができる。
【００３０】
一実施形態による正極活物質として、ピーク強度比（ＬｉＭｅＦ＋／ＬｉＭｅＯ＋）は、０．０１～０．３の範囲内に選ばれる。０．０１未満の場合にはフッ素化の程度が弱く、正極活物質の安定性を向上させることができなくなり、ＬｉＭｅＦ＋の割合が０．３を超えると、正極の容量低下の原因となるからである。
【００３１】
さらに、一実施形態による正極活物質としては、表面のフッ素量がｌａｔｏｍｉｃ％～２０ａｔｏｍｉｃ％であるものが好ましい。フッ素（Ｆ）の量がｌａｔｏｍｉｃ％より小さい場合には、活物質の安定化効果が小さく、十分な特性を得ることができないからである。また、フッ素（Ｆ）が２０ａｔｏｍｉｃ％を超えて存在するような場合には、表面のＬ

ｉイオンの吸蔵放出性能の低下の原因となり、この場合にも正極活物質として十分な特性を得ることができないからである。ここで、粒子表面のフッ素量の測定はＥＳＣＡ（走査型Ｘ線光電子分光装置）を用いて行うことができる。

【００３２】

例えば、正極活物質を常温環境下でフッ素（Ｆ）ガス中にさらすようにしてフッ素（Ｆ）ガス処理を行い作製した場合などでは、表面に偏った状態でフッ素（Ｆ）が存在するため表面のフッ素（Ｆ）量が多くなってしまう。これに対し、熱処理等を行ってフッ素（Ｆ）を内部にまで拡散させることによって、表面でのリチウム（Ｌｉ）の吸蔵放出性能を低下させることなく、正極活物質の安定性を高めることが可能になっていると考えられる。

【００３３】

この発明の一実施形態による正極活物質は、例えば、化３、好ましくは化４で平均組成が表されるリチウム複合酸化物を、フッ素化処理を行うことで作製できる。

（化３）

$Li_pNi_{(1-q-r)}Mn_qM1_rO_{(2-y)}$

（Ｍ１はＮｉ、Ｍｎを除く２族～１５族から選ばれる元素のうち少なくとも一種を示す。ｐ、ｑ、ｒ、ｙは$0 \leqq p \leqq 1.5$、$0 \leqq q \leqq 1.0$、$0 \leqq r \leqq 1.0$、$-0.10 \leqq y \leqq 0.20$の範囲内の値である。）

（化４）

$Li_{(1+p)}Co_{(1-q)}M_qO_{(2-y)}$

（式中、ＭはＣｏを除く２族～１５族から選ばれる元素のうち少なくとも一種を示す。ｐ、ｑ、ｙは、$-0.10 \leqq p \leqq 0.10$、$0 \leqq q < 0.3$、$-0.10 \leqq y \leqq 0.20$の範囲内の値である。）

【００３４】

フッ素化処理を行う方法としては、従来ではフッ素（Ｆ）ガスやフッ素（Ｆ）を含むガス（NF_3など）を直接接触させる方法、ＬｉＦやＣＦ、NiF_2などの金属フッ化物で被覆処理を施す方法などが提案されていた。しかしながら、従来の方法で処理を行った場合には、正極活物質の粒子表面にＬｉＦのような金属フッ化物が存在してしまうので、正極活物質のＬｉイオンの吸蔵放出特性を低下させる原因となり、被覆材に用いた金属フッ化物によって、充放電容量が低下してしまう問題があった。

【００３５】

そこで、本願発明者らは、加温状態でフッ素（Ｆ）ガスと反応させることでフッ素化を行う方法や、フッ素化後に再熱処理を行う方法などを見出した。すなわち、この発明の一実施形態による正極活物質を製造する方法は、第１の例としては、化３、好ましくは化４で表される複合酸化物粒子を、高温環境下でフッ素（Ｆ）ガスと反応させることでフッ素化を行うことで一実施形態による正極活物質を製造することを特徴とする。フッ素（Ｆ）ガスとの反応は、例えば１００℃～３００℃、フッ素ガスの分圧が０．００２ＭＰａ～０．５ＭＰａの条件下で行うことが好ましい。また、フッ素ガスの分圧としては、０．０１ＭＰａ～０．１ＭＰａの範囲で行うことがより好ましい。これはフッ素ガスの分圧が低すぎるとフッ素ガス処理が進まず処理時間も長くなり、また、フッ素分圧が高い場合にはフッ素化が急激に進み反応の制御が困難となるためである。

【００３６】

また、第２の例としては、化３、好ましくは化４で表される複合酸化物粒子を、常温でフッ素化した後、このフッ素化した複合酸化物を加熱処理することを特徴とする。加熱処理は、例えば２００℃～１０００℃の加熱温度で、０．５時間～１０時間で行うことが好ましい。また、加熱温度としては、３００℃～９００℃の範囲で行うことがより好ましい。これは加熱温度が低すぎるとフッ素の内部への拡散が進みにくく、十分な効果が得られず、また、加熱温度が高すぎる場合には複合酸化物粒子自体の容量低下を引き起こすためである。

【００３７】

さらに、第３の例としては、化３、好ましくは化４で表される複合酸化物粒子を、高温

環境下でフッ素（Ｆ）ガスと反応させることでフッ素化を行い、このフッ素化した複合酸化物を加熱処理することを特徴とする。フッ素（Ｆ）ガスとの反応は、例えば１００℃～３００℃、フッ素ガスの分圧が０．００２ＭＰａ～０．５ＭＰａの条件下で行うことが好ましい。加熱処理は、例えば２００℃～１０００℃の加熱温度で、０．５時間～１０時間行うことが好ましい。

【００３８】

第１の例～第３の例で説明したような正極活物質の製造方法を用いることによって、表面のＬｉＦ量を減少させるとともに、粒子の内部までＬｉ－Ｍｅ－Ｆ結合を有する正極活物質を作製することができ、容量低下などを引き起こすことなく、サイクル特性の劣化を抑制できる。

【００３９】

次に、この発明の一実施形態による正極活物質を用いた非水電解質二次電池について説明する。図１は、この発明の一実施形態による正極活物質を用いた非水電解質二次電池の第１の例の断面構造を表している。

【００４０】

この電池では、上限充電電圧を４．２０Ｖ以上４．８０Ｖ以下、下限放電電圧を２．００Ｖ以上３．３０Ｖ以下とすることが好ましい。この発明の一実施形態による正極活物質は、従来の材料に比較して安定であるため、充放電を繰り返し行った際の容量劣化を抑制できるとともに，充電電圧を従来の非水電解液電池よりも高く設定し、高いエネルギー密度実現した場合でも良好な高温特性を得ることができる。

【００４１】

この電池は、いわゆる円筒型といわれるものであり、ほぼ中空円柱状の電池缶１の内部に、帯状の正極２と帯状の負極３とがセパレータ４を介して巻回された巻回電極体２０を有している。

【００４２】

電池缶１は、例えばニッケル（Ｎｉ）のめっきがされた鉄（Ｆｅ）により構成されており、一端部が閉鎖され他端部が開放されている。電池缶１の内部には、巻回電極体２０を挟むように巻回周面に対して垂直に一対の絶縁板５，６がそれぞれ配置されている。

【００４３】

電池缶１の開放端部には、電池蓋７と、この電池蓋７の内側に設けられた安全弁機構８および熱感抵抗素子（Positive Temperature Coefficient；ＰＴＣ素子）９とが、ガスケット１０を介してかしめられることにより取り付けられており、電池缶１の内部は密閉されている。電池蓋７は、例えば、電池缶１と同様の材料により構成されている。安全弁機構８は、熱感抵抗素子９を介して電池蓋７と電気的に接続されており、内部短絡あるいは外部からの加熱等により電池の内圧が一定以上となった場合にディスク板１１が反転して電池蓋７と巻回電極体２０との電気的接続を切断するようになっている。熱感抵抗素子９は、温度が上昇すると抵抗値の増大により電流を制限し、大電流による異常な発熱を防止するものである。ガスケット１０は、例えば、絶縁材料により構成されており、表面にはアスファルトが塗布されている。

【００４４】

巻回電極体２０は、例えば、センターピン１２を中心に巻回されている。巻回電極体２０の正極２には、例えばアルミニウム（Ａｌ）等よりなる正極リード１３が接続されており、負極３には、例えばニッケル（Ｎｉ）等よりなる負極リード１４が接続されている。正極リード１３は、安全弁機構８に溶接されることにより電池蓋７と電気的に接続されており、負極リード１４は、電池缶１に溶接され電気的に接続されている。

【００４５】

［正極］

図２は、図１に示した巻回電極体２０の一部を拡大して表すものである。図２に示すように、正極２は、例えば、対向する一対の面を有する正極集電体２Ａと、正極集電体２Ａの両面に設けられた正極合剤層２Ｂとを有している。なお、正極集電体２Ａの片面のみに

正極合剤層２Ｂが設けられた領域を有するようにしてもよい。正極集電体２Ａは、例えば、アルミニウム（Ａｌ）箔等の金属箔により構成されている。正極合剤層２Ｂは、例えば、正極活物質を含んでおり、必要に応じてグラファイト等の導電剤と、ポリフッ化ビニリデン等の結着剤とを含んでいてもよい。正極活物質としては、上述の構成を有するリチウム複合酸化物を用いる。

【００４６】

［負極］

図２に示すように、負極３は、例えば、対向する一対の面を有する負極集電体３Ａと、負極集電体３Ａの両面に設けられた負極合剤層３Ｂとを有している。なお、負極集電体３Ａの片面のみに負極合剤層３Ｂが設けられた領域を有するようにしてもよい。負極集電体３Ａは、例えば銅（Ｃｕ）箔等の金属箔により構成されている。負極合剤層３Ｂは、例えば、負極活物質を含んでおり、必要に応じてポリフッ化ビニリデン等の結着剤を含んでいてもよい。

【００４７】

負極活物質としては、対リチウム金属２．０Ｖ以下の電位で電気化学的にリチウムをドープ脱ドープする材料であればいずれも用いることができる。例示するならば難黒鉛化性炭素、人造黒鉛、天然黒鉛、熱分解炭素類、コークス類（ピッチコークス、ニードルコークス、石油コークス等）、グラファイト類、ガラス状炭素類、有機高分子化合物焼成体（フェノール樹脂、フラン樹脂等を適当な温度で焼成し炭素化したもの）、炭素繊維、活性炭、カーボンブラック類等の炭素質材料を挙げることができる。またリチウムと合金を形成可能な金属およびその合金や金属間化合物も用いることができる。酸化鉄、酸化ルテニウム、酸化モリブデン、酸化タングステン、酸化チタン、酸化スズ等の比較的電位が卑な電位でリチウムをドープおよび脱ドープする酸化物やその他窒化物等も同様に用いることができる。

【００４８】

［電解液］

電解液としては、非水溶媒に電解質塩を溶解させた非水電解液を用いることができる。非水溶媒と電解質塩とを適宜組み合わせて調製されるが、これら非水溶媒としては、この種の電池に用いられるものであればいずれも使用可能である。例示するならば、プロピレンカーボネート、エチレンカーボネート、ジエチルカーボネート、ジメチルカーボネート、１，２－ジメトキシエタン、１，２－ジエトキシエタン、γ－ブチロラクトン、テトラヒドロフラン、２－メチルテトラヒドロフラン、１，３－ジオキソラン、４－メチル－１，３ジオキソラン、ジエチルエーテル、スルホラン、メチルスルホラン、アセトニトリル、プロピオニトリル、アニソール、酢酸エステル、酪酸エステル、プロピオン酸エステル等である。

【００４９】

電解質塩であるリチウム塩としては、この種の電池に用いられるものであればいずれも使用可能である。例示するならば、$LiClO_4$、$LiAsF_6$、$LiPF_6$、$LiBF_4$、$LiB(C_6H_5)_4$、$LiCH_3SO_3$、$LiCF_3SO_3$、ＬｉＣｌ、ＬｉＢｒ等である。

【００５０】

［セパレータ］

セパレータ４は、例えばポリエチレン（ＰＥ）あるいはポリプロピレン（ＰＰ）等のポリオレフィン系の材料よりなる多孔質膜により構成されている。セパレータ４は、２種以上の多孔質膜を積層した構造とされていてもよい。

【００５１】

次に、非水電解質二次電池の第１の例の製造方法について説明する。以下、一例として円筒型の非水電解質二次電池を挙げて、非水電解質二次電池の製造方法について説明する。

【００５２】

正極２は、以下に述べるようにして作製する。まず、例えば、正極活物質と、導電剤と

、結着剤とを混合して正極合剤を調製し、この正極合剤をＮ－メチル－２－ピロリドン等の溶剤に分散させて正極合剤スラリーとする。

【００５３】

次に、この正極合剤スラリーを正極集電体２Ａに塗布し溶剤を乾燥させた後、ロールプレス機等により圧縮成型して正極合剤層２Ｂを形成し、正極２を作製する。

【００５４】

負極３は、以下に述べるようにして作製する。まず、例えば、負極活物質と、結着剤とを混合して負極合剤を調製し、この負極合剤をＮ－メチル－２－ピロリドン等の溶剤に分散させて負極合剤スラリーとする。

【００５５】

次に、この負極合剤スラリーを負極集電体３Ａに塗布し溶剤を乾燥させた後、ロールプレス機等により圧縮成型して負極合剤層３Ｂを形成し、負極３を作製する。

【００５６】

次に、正極集電体２Ａに正極リード１３を溶接等により取り付けると共に、負極集電体３Ａに負極リード１４を溶接等により取り付ける。次に、正極２と、負極３とをセパレータ４を介して巻回し、正極リード１３の先端部を安全弁機構８に溶接すると共に、負極リード１４の先端部を電池缶１に溶接して、巻回した正極２および負極３を一対の絶縁板５，６で挟み電池缶１の内部に収納する。

【００５７】

次に、電解液を電池缶１の内部に注入し、電解液をセパレータ４に含浸させる。次に、電池缶１の開口端部に電池蓋７、安全弁機構８および熱感抵抗素子９を、ガスケット１０を介してかしめることにより固定する。以上により、非水電解質二次電池が作製される。

【００５８】

次に、この発明の一実施形態による正極活物質を用いた非水電解質二次電池の第２の例について説明する。図３は、この発明の一実施形態による正極活物質を用いた非水電解質二次電池の第２の例の構造を示す。図３に示すように、この非水電解質二次電池は、電池素子３０を防湿性ラミネートフィルムからなる外装材３７に収容し、電池素子３０の周囲を溶着することにより封止してなる。電池素子３０には、正極リード３２および負極リード３３が備えられ、これらのリードは、外装材３７に挟まれて外部へと引き出される。正極リード３２および負極リード３３のそれぞれの両面には、外装材３７との接着性を向上させるために樹脂片３４および樹脂片３５が被覆されている。

【００５９】

［外装材］

外装材３７は、例えば、接着層、金属層、表面保護層を順次積層した積層構造を有する。接着層は高分子フィルムからなり、この高分子フィルムを構成する材料としては、例えばポリプロピレン（ＰＰ）、ポリエチレン（ＰＥ）、無延伸ポリプロピレン（ＣＰＰ）、直鎖状低密度ポリエチレン（ＬＬＤＰＥ）、低密度ポリエチレン（ＬＤＰＥ）が挙げられる。金属層は金属箔からなり、この金属箔を構成する材料としては、例えばアルミニウム（Ａｌ）が挙げられる。また、金属箔を構成する材料としては、アルミニウム（Ａｌ）以外の金属を用いることも可能である。表面保護層を構成する材料としては、例えばナイロン（Ｎｙ）、ポリエチレンテレフタレート（ＰＥＴ）が挙げられる。なお、接着層側の面が、電池素子３０を収納する側の収納面となる。

【００６０】

［電池素子］

この電池素子３０は、例えば、図４に示すように、両面にゲル電解質層４５が設けられた帯状の負極４３と、セパレータ４４と、両面にゲル電解質層４５が設けられた帯状の正極４２と、セパレータ４４とを積層し、長手方向に巻回されてなる巻回型の電池素子３０である。

【００６１】

正極４２は、帯状の正極集電体４２Ａと、この正極集電体４２Ａの両面に形成された正

極合剤層４２Ｂとからなる。正極集電体４２Ａは、例えばアルミニウム（Ａｌ）等からなる金属箔である。正極合剤層４２Ｂは、上述した構成を有する正極活物質を含んでいる。

【００６２】

正極４２の長手方向の一端部には、例えばスポット溶接または超音波溶接で接続された正極リード３２が設けられている。この正極リード３２の材料としては、例えばアルミニウム等の金属を用いることができる。

【００６３】

負極４３は、帯状の負極集電体４３Ａと、この負極集電体４３Ａの両面に形成された負極合剤層４３Ｂとからなる。負極集電体４３Ａは、例えば、銅（Ｃｕ）箔、ニッケル箔あるいはステンレス箔等の金属箔により構成されている。

【００６４】

また、負極４３の長手方向の一端部にも正極４２と同様に、例えばスポット溶接または超音波溶接で接続された負極リード３３が設けられている。この負極リード３３の材料としては、例えば銅（Ｃｕ）、ニッケル（Ｎｉ）等を用いることができる。

【００６５】

ゲル電解質層４５以外のことは、上述の第１の例と同様であるので、以下ではゲル電解質層４５について説明する。

【００６６】

ゲル電解質層４５は、電解液と、この電解液を保持する保持体となる高分子化合物とを含み、いわゆるゲル状となっている。ゲル電解質層４５は高いイオン伝導率を得ることができるとともに、電池の漏液を防止できるので好ましい。電解液の構成（すなわち液状の溶媒、電解質塩）は、非水電解質二次電池の第１の例と同様である。

【００６７】

ゲル電解質層４５のマトリックスとしては、電解液を吸収してゲル化するものであれば種々の高分子が利用できる。例えば、ポリ（ビニリデンフルオロライド）やポリ（ビニリデンフルオロライド-co-ヘキサフルオロプロピレン）等のフッ素系高分子、ポリ（エチレンオキサイド）や同架橋体等のエーテル系高分子、またポリ（アクリロニトリル）等を使用できる。特に酸化還元安定性から、フッ素系高分子を用いることが望ましい。電解質塩を含有させることによりイオン導電性を賦与する。

【００６８】

次に、この発明の一実施形態による正極活物質を用いた非水電解質二次電池の第２の例の製造方法について説明する。まず、正極４２および負極４３のそれぞれに、溶媒と、電解質塩と、高分子化合物と、混合溶剤とを含む前駆溶液を塗布し、混合溶剤を揮発させてゲル電解質層４５を形成する。なお、予め正極集電体の端部に正極リード３２を溶接により取り付けるとともにに、負極集電体４３Ａの端部に負極リード３３を溶接により取り付けるようにする。

【００６９】

次に、ゲル電解質層４５が形成された正極４２と負極４３とを、セパレータ４４を介して積層し積層体とした後、この積層体をその長手方向に巻回して、巻回型の電池素子３０を形成する。

【００７０】

次に、ラミネートフィルムからなる外装材３７を深絞り加工することで凹部３６を形成し、電池素子３０をこの凹部３６に挿入し、外装材３７の未加工部分を凹部３６上部に折り返し、凹部３６の外周部分を熱溶着し密封する。以上により、非水電解質二次電池が作製される。

【実施例】

【００７１】

以下、この発明の具体的な実施例について説明する。ただし、この発明はこれらの実施例のみに限定されるものではない。

【００７２】

＜実施例１＞

レーザ散乱法により測定した平均粒子径が１３μｍのコバルト酸リチウム（平均化学組成分析値：$Li_{1.03}CoO_2$）１０００重量部をステンレス（ＳＵＳ）容器に入れ、真空ポンプで減圧した。次に、フッ素（Ｆ）ガスを０．０１ＭＰａの分圧となるようにＳＵＳ容器中へ入れ、そのまま常温で１時間放置するようにして、フッ素化処理を行った。

【００７３】

次に、フッ素化処理を行ったコバルト酸リチウムの加熱処理を、毎分３℃の速度で７００℃まで昇温し、７００℃で３時間保持するようにして行い、その後徐冷し、実施例１の正極活物質を作製した。

【００７４】

なお、得られた実施例１の正極活物質粉末について、ＣｕＫαを用いた粉末Ｘ線回折パターンを測定したところ、得られたパターンは層状岩塩構造を有する$LiCoO_2$に相当する回折ピークのみが得られ、ＬｉＦをはじめとする不純物は確認されなかった。

＜実施例２＞

実施例１と同様にして、実施例２の正極活物質を作製した。

【００７５】

＜実施例３＞

フッ素（Ｆ）化処理の際、フッ素（Ｆ）ガスの分圧を０．０２ＭＰａとした点以外は、実施例１と同様にして、実施例３の正極活物質を作製した。

【００７６】

＜実施例４＞

コバルト酸リチウム（$Li_{1.03}CoO_2$）の代わりに、$LiCo_{0.98}Al_{0.01}Mg_{0.01}O_2$を用いた点以外は、実施例３と同様にして、実施例４の正極活物質を作製した。

【００７７】

＜実施例５＞

フッ素（Ｆ）化処理の際、フッ素（Ｆ）ガスの分圧を０．０３ＭＰａとした点以外は、実施例１と同様にして、実施例５の正極活物質を作製した。

【００７８】

＜実施例６＞

レーザ散乱法により測定した平均粒子径が１３μｍのコバルト酸リチウム（平均化学組成分析値：$Li_{1.03}CoO_2$）１０００重量部をＳＵＳの容器に入れ、真空ポンプで減圧した。次に、フッ素（Ｆ）ガスを０．０１ＭＰａの分圧となるようにＳＵＳ容器中に入れ、その後、この反応容器であるＳＵＳ容器を２００℃に加熱した状態で１時間放置するようにして、フッ素化処理を行い実施例６の正極活物質を作製した。

【００７９】

なお、実施例６の正極活物質粉末についてＣｕＫαを用いた粉末Ｘ線回折パターンを測定したところ、得られたパターンは、層状岩塩構造を有する$LiCoO_2$に相当する回折ピークのみが得られ、ＬｉＦをはじめとする不純物は確認されなかった。

【００８０】

＜実施例７＞

レーザ散乱法により測定した平均粒子径が１３μｍのコバルト酸リチウム（平均化学組成分析値：$Li_{1.03}CoO_2$）１０００重量部を、ＳＵＳの容器に入れ、真空ポンプで減圧した。次に、フッ素（Ｆ）ガスを０．０１ＭＰａの分圧となるようにＳＵＳ容器中へ入れ、その後、この反応容器であるＳＵＳ容器を２００℃に加熱した状態で１時間放置するようにして、フッ素化処理を行った。

【００８１】

次に、フッ素化処理を行ったコバルト酸リチウムの加熱処理を、毎分３℃の速度で７００℃まで昇温し、７００℃で３時間保持するようにして行い、その後徐冷し、実施例７の正極活物質を作製した。

【００８２】

なお、実施例７の正極活物質粉末について、ＣｕＫαを用いた粉末Ｘ線回折パターンを測定したところ、得られたパターンは、層状岩塩構造を有する$LiCoO_2$に相当する回折ピークのみが得られ、ＬｉＦをはじめとする不純物は確認されなかった。

【００８３】

＜実施例８＞

レーザ散乱法により測定した平均粒子径が１３μｍのコバルト酸リチウム（平均化学組成分析値：$Li_{1.03}CoO_2$）１０００重量部を、ＳＵＳの容器に入れ、真空ポンプで減圧した。次に、フッ素（Ｆ）ガスを０．０１ＭＰａの分圧となるようにＳＵＳ容器中へ入れ、その後、そのまま常温で１時間放置するようにして、フッ素化処理を行った。

【００８４】

次に、フッ素化処理を行ったコバルト酸リチウムの加熱処理を、毎分３℃の速度で５００℃まで昇温し、５００℃で３時間保持するようにして行い、その後徐冷し、実施例８の正極活物質を作製した。

【００８５】

なお、実施例８の正極活物質粉末についてＣｕＫαを用いた粉末Ｘ線回折パターンを測定したところ、得られたパターンは層状岩塩構造を有する$LiCoO_2$に相当する回折ピークのみが得られ、ＬｉＦをはじめとする不純物は確認されなかった。

【００８６】

＜実施例９＞

まず、市販の硝酸ニッケル、硝酸コバルト、硝酸マンガンを水溶液として、Ｎｉ（ニッケル）、Ｃｏ（コバルト）、Ｍｎ（マンガン）のモル比率がそれぞれ１／３、１／３、１／３となるように混合し、十分攪拌しながらアンモニア水を滴下して複合水酸化物を得た。

【００８７】

次に、これを水酸化リチウムと混合し、酸素気流中、９００℃で１０時間焼成した後に粉砕し、リチウム遷移金属複合酸化物を作製した。このリチウム遷移金属複合酸化物粉末を原子吸光分析により分析したところ、$LiNi_{1/3}Co_{1/3}Mn_{1/3}O_2$の組成が確認された。

【００８８】

また、このリチウム遷移金属複合酸化物の粒径をレーザ回折法により測定したところ、平均粒径は１３μｍであった。さらに、この粉末のＸ線回折測定を行ったところ、得られたパターンは、ＩＣＤＤの０９－００６３にある$LiNiO_2$のパターンに類似しており、$LiNiO_2$と同様の層状岩塩構造を形成している事が確認された。さらに、ＳＥＭ（Scanning Electoron Microscope）により粉末を観察したところ、粒径０．１μｍ～５μｍの１次粒子が凝集した球状の粒子が観察された。

【００８９】

次に、このリチウム遷移金属複合酸化物１０００重量部をＳＵＳの容器に入れ、真空ポンプで減圧した。次に、フッ素（Ｆ）ガスを０．０１ＭＰａの分圧となるようにＳＵＳ容器中へ入れ、そのまま常温で１時間放置するようにして、フッ素化処理を行った。次に、フッ素化処理を行ったリチウム遷移金属複合酸化物の加熱処理を、毎分３℃の速度で７００℃まで昇温し、７００℃で３時間保持するようにして行い、その後徐冷し、実施例９の正極活物質を作製した。

【００９０】

＜実施例１０＞

加熱処理の際、焼成温度を７５０℃とした点以外は、実施例１と同様にして、実施例１０の正極活物質を作製した。

【００９１】

＜比較例１＞

コバルト酸リチウム（平均化学組成分析値：$Li_{1.03}CoO_2$）を比較例１の正極活物質とした。

【００９２】
＜比較例２＞
コバルト酸リチウム（平均化学組成分析値：$Li_{1.03}CoO_2$）を比較例２の正極活物質とした。
【００９３】
＜比較例３＞
レーザ散乱法により測定した平均粒子径が１３μｍのコバルト酸リチウム正極活物質（平均化学組成分析値：$Li_{1.03}CoO_2$）１０００重量部を、ＳＵＳの容器に入れ、真空ポンプで減圧した。次に、フッ素（Ｆ）ガスを０．０１ＭＰａの分圧となるようにＳＵＳ容器中へ入れ、そのまま常温で１時間放置するようにして、フッ素化処理を行い、比較例３の正極活物質を作製した。
【００９４】
＜比較例４＞
レーザ散乱法により測定した平均粒子径が１３μｍのコバルト酸リチウム正極活物質（平均化学組成分析値：$Li_{1.03}CoO_2$）１０００重量部を、ＳＵＳの容器に入れ、真空ポンプで減圧した。次に、フッ素（Ｆ）ガスを０．０３ＭＰａの分圧となるようにＳＵＳ容器中へ入れ、そのまま常温で１時間放置するようにして、フッ素化処理を行い、比較例４の正極活物質を作製した。
【００９５】
＜比較例５＞
ＬｉＦ粉末１０ｍｏｌ％とコバルト酸リチウム正極活物質（$Li_{1.03}CoO_2$）９０ｍｏｌ％とをメカノフュージョン装置によって１時間処理を行い、コバルト酸リチウム表面にＬｉＦを被着させ、比較例５の正極活物質を得た。
【００９６】
＜比較例６＞
市販の硝酸ニッケル、硝酸コバルト、硝酸マンガンを水溶液として、Ｎｉ、Ｃｏ、Ｍｎのモル比率がそれぞれ１／３、１／３、１／３となるように混合し、十分攪拌しながらアンモニア水を滴下して複合水酸化物を得た。これを水酸化リチウムと混合し、酸素気流中、９００℃で１０時間焼成した後に粉砕し、比較例６の正極活物質を作製した。
【００９７】
比較例６の正極活物質粉末を原子吸光分析により分析したところ、$LiNi_{1/3}Co_{1/3}Mn_{1/3}O_2$の組成が確認された。また、レーザ回折法により粒径を測定したところ、平均粒径は１３μｍであった。さらに、この粉末のＸ線回折測定を行ったところ、得られたパターンはＩＣＤＤの０９－００６３にある$LiNiO_2$のパターンに類似しており、$LiNiO_2$と同様の層状岩塩構造を形成している事が確認された。さらに、ＳＥＭにより粉末を観察したところ、０．１～５μｍの１次粒子が凝集した球状の粒子が観察された。
【００９８】
＜比較例７＞
レーザ散乱法により測定した平均粒子径が１３μｍのコバルト酸リチウム（平均化学組成分析値：$Li_{1.03}CoO_2$）１０００重量部を、ＳＵＳの容器に入れ、真空ポンプで減圧した。次に、フッ素（Ｆ）ガスを０．００１ＭＰａの分圧となるようにＳＵＳ容器中へ入れ、そのまま常温で１０分間放置するようにしてフッ素化処理を行った。次に、フッ素化処理を行ったコバルト酸リチウムの加熱処理を、毎分３℃の速度で７００℃まで昇温し、７００℃で３時間保持するようにして行い、その後徐冷し、比較例７の正極活物質を得た。
【００９９】
＜比較例８＞
レーザ散乱法により測定した平均粒子径が１３μｍのコバルト酸リチウム（平均化学組成分析値：$Li_{1.03}CoO_2$）１０００重量部を、ＳＵＳの容器に入れ、真空ポンプで減圧した。次に、フッ素（Ｆガス）を０．０３ＭＰａの分圧となるようにＳＵＳ容器中へ入

れ、その後、この反応容器であるＳＵＳ容器を２００℃に加熱した状態で３ｈ放置するようにして、フッ素化処理を行った。

【０１００】

次に、フッ素化処理を行ったコバルト酸リチウムの加熱処理を、毎分３℃の速度で７００℃まで昇温し、７００℃で３時間保持するようにして行い、その後徐冷し、比較例８の正極活物質を得た。

【０１０１】

なお、比較例８の正極活物質粉末についてＣｕＫαを用いた粉末Ｘ線回折パターンを測定したところ、得られたパターンは、層状岩塩構造を有する$LiCoO_2$に相当する回折ピークのみが得られ、ＬｉＦをはじめとする不純物は確認されなかった。

【０１０２】

次に、実施例１～実施例１０および比較例１～比較例８の正極活物質について、以下に説明するようにして、ＴＯＦ－ＳＩＭＳによる分析およびＥＳＣＡによる分析を行った。

【０１０３】

ＴＯＦ－ＳＩＭＳによる分析

測定装置は、「ＩＯＮ－ＴＯＦ社製のＴＯＦ－ＳＩＭＳ　Ｖ」を用い、以下の測定条件で行った。

〔測定条件〕

一次イオン１９７Ａｕ＋、イオン銃加速電圧２５ｋｅＶ、アンバンチング、照射イオン電流０．５ｐＡ（パルスビームでの計測）、パルス周波数５０ｋＨｚ、質量範囲１～２００ａｍｕ、走査範囲２５×２５μｍで行い、空間分解能は０．２μｍである。

【０１０４】

ＥＳＣＡによる分析

走査型Ｘ線光電子分光装置（アルバック・ファイ社製、ＱｕａｎｔｅｒａＳＸＭ）を用いて行った。測定する粒子試料を金属インジウム片に埋め込み、その試料片を板バネで試料台に固定した。Ｘ線源は、単色化Ａｌ－Ｋα線（１４８６．６ｅＶ）を用い、アルゴンイオン銃、電子中和銃を用いて測定試料表面を自動モードで帯電補正しながら測定した。

【０１０５】

次に、実施例１～実施例１０および比較例１～比較例８の正極活物質を用いて、以下に説明するようにして、円筒型電池を作製した。

【０１０６】

まず、正極活物質を８６重量％と、導電剤としてグラファイトを１０重量％と、結着剤としてポリフッ化ビニリデンを４重量％とを混合して、溶剤であるＮ－メチル－２－ピロリドン（ＮＭＰ）に分散させて、正極合剤スラリーとした。

【０１０７】

この正極合剤スラリーを厚さ２０μｍの帯状のアルミニウム（Ａｌ）箔の両面に均一に塗布・乾燥後、ローラープレス機で圧縮して帯状の正極を得た。この際、電極中の空隙は体積比率にして２６％となるように調節した。

【０１０８】

次に、負極として、粉末状の人造黒鉛９０重量％にポリフッ化ビニリデン（ＰＶｄＦ）を１０重量％混合し、Ｎ－メチル－２－ピロリドン（ＮＭＰ）に分散させて負極合剤スラリーとした。この負極合剤スラリーを厚さ１０μｍの銅（Ｃｕ）箔の両面に均一に塗布し、乾燥後にローラープレス機で圧縮することで帯状の負極を得た。

【０１０９】

次に、正極および負極を作製した後、多孔性のポリオレフィンフィルムをセパレータとして用い、このセパレータと、正極と負極とを、負極、セパレータ、正極、セパレータの順に積層し、渦巻型に多数回巻回することにより、渦巻き型の巻回電極体を作製した。

【０１１０】

次に、この巻回電極体をニッケルめっきを施した鉄製電池缶に収納し、巻回電極体の上下両面に絶縁板を配設した。アルミニウム製の正極リードを正極集電体から導出して、電

池蓋と電気的な導通が確保された安全弁の突起部に溶接した。ニッケル製の負極リードを負極集電体から導出して電池缶の底部に溶接した。

【０１１１】

次に、上述の電極体が組み込まれた電池缶内に電解液を注入した後、絶縁封口ガスケットを介して電池缶をかしめることにより、安全弁、ＰＴＣ素子ならびに電池蓋を固定し、外径が１８ｍｍで高さが６５ｍｍの円筒型電池を作製した。なお、電解液は、エチレンカーボネートとジエチルカーボネートとの体積混合比が１：１である混合溶液に１ｍｏｌ／ｄｍ^{3}の濃度になるように$LiPF_6$を溶解して非水電解液を調製した。

【０１１２】

次に、上述のようにして、実施例１～実施例１０、比較例１～比較例８の正極活物質を用いて作製した電池について、初期容量および容量維持率の測定を行った。

【０１１３】

初期容量測定

初期容量は、充電を環境温度４５℃、１０００ｍＡの定電流で電池電圧が所定電圧（実施例１および比較例１では４．２０Ｖ、実施例２～実施例１０および比較例２～比較例８では４．４０Ｖ）に達した時点で、定電圧充電に切り替え、充電時間の総計が２．５時間に達するまで行い、こののちに、８００ｍＡの定電流で終止電圧３．０Ｖで放電を行って測定した。

【０１１４】

容量維持率の測定

初期容量測定と同様の条件で、充放電を繰り返し、２００サイクル目の放電容量を測定して、初期容量に対する容量維持率を求めた。

【０１１５】

表１に、ＴＯＦ－ＳＩＭＳでの分析による（ＬｉＣｏＦ＋／ＬｉＣｏＯ＋）の値、ＥＳＣＡの分析による表面Ｆ量、作製した二次電池の初期容量および容量維持率を示す。

【０１１６】

また、図５に実施例１の正極活物質の断面におけるＴＯＦ－ＳＩＭＳ像を示す。図６に比較例３の正極活物質の断面におけるＴＯＦ－ＳＩＭＳ像を示す。図５と図６の比較により、実施例１の正極活物質は、ＬｉＣｏＦ結合の割合が多いことが確認できる。

【０１１７】

【表１】

	母材	フッ素化処理	熱処理	LiCoF+/LiCoO+	表面F量[at%]	初回容量[Wh]	容量維持率[%]	充電電圧[V]
実施例1	$Li_{1.03}CoO_2$	常温-0.01MPa	700℃-3h	0.09	3.8	8.1	89	4.20
実施例2	$Li_{1.03}CoO_2$	常温-0.01MPa	700℃-3h	0.09	3.8	9.2	82	4.40
実施例3	$Li_{1.03}CoO_2$	常温-0.02MPa	700℃-3h	0.11	4.3	9.2	81	4.40
実施例4	$LiCo_{0.98}Al_{0.01}Mg_{0.01}O_2$	常温-0.02MPa	700℃-3h	0.10	3.9	9.2	85	4.40
実施例5	$Li_{1.03}CoO_2$	常温-0.03MPa	700℃-3h	0.12	7.7	9.2	83	4.40
実施例6	$Li_{1.03}CoO_2$	200℃-0.01MPa	—	0.15	17.1	9.2	78	4.40
実施例7	$Li_{1.03}CoO_2$	200℃-0.01MPa	700℃-3h	0.24	4.8	9.2	77	4.40
実施例8	$Li_{1.03}CoO_2$	常温-0.01MPa	500℃-3h	0.03	10.4	9.2	77	4.40
実施例9	$LiNi_{1/3}Co_{1/3}Mn_{1/3}O_2$	常温-0.01MPa	700℃-3h	0.05	4.6	8.5	91	4.40
実施例10	$Li_{1.03}CoO_2$	常温-0.01MPa	750℃-3h	0.11	1.2	9.2	80	4.40
比較例1	$Li_{1.03}CoO_2$	—	—	0.00	0	8.1	72	4.20
比較例2	$Li_{1.03}CoO_2$	—	—	0.00	0	9.2	50	4.40
比較例3	$Li_{1.03}CoO_2$	常温-0.01MPa	—	0.006	25.3	9.2	52	4.40
比較例4	$Li_{1.03}CoO_2$	常温-0.03MPa	—	0.009	33.7	9.2	45	4.40
比較例5	$Li_{1.03}CoO_2$	LiF被覆処理	—	0.00	39.6	8.8	34	4.40
比較例6	$LiNi_{1/3}Co_{1/3}Mn_{1/3}O_2$	—	—	0.00	0	8.5	76	4.40
比較例7	$Li_{1.03}CoO_2$	常温-0.001MPa	700℃-3h	0.003	0.7	9.2	47	4.40
比較例8	$Li_{1.03}CoO_2$	200℃-0.03MPa	700℃-3h	0.32	8.3	8.6	61	4.40

【０１１８】

表１に示すように、ピーク強度比（ＬｉＣｏＦ＋／ＬｉＣｏＯ＋）の値が、０．０１～０．３、表面フッ素量が１ａｔｏｍｉｃ％～２０ａｔｏｍｉｃ％の実施例１～実施例１０では、上記数値範囲を満たさない比較例１～比較例８より、容量維持率および初回容量が大きかった。すなわち、ピーク強度比（ＬｉＣｏＦ＋／ＬｉＣｏＯ＋）の値が０．０１～０．３である正極活物質を用いることで、高容量で優れた充放電サイクル特性を有する電池を得られることがわかった。また、表面フッ素量は、１ａｔｏｍｉｃ％～２０ａｔｏｍｉｃ％がより好ましいことがわかった。

【０１１９】

この発明は、上述したこの発明の実施形態に限定されるものでは無く、この発明の要旨を逸脱しない範囲内で様々な変形や応用が可能である。例えば、電池形状については特に限定されることはなく、円筒型、角型、コイン型、ボタン型、ラミネートシール型等の種々の形状にすることできる。また、例えば、電極体は、正極および負極とセパレータとを順次積層する積層方式等によって作製してもよい。

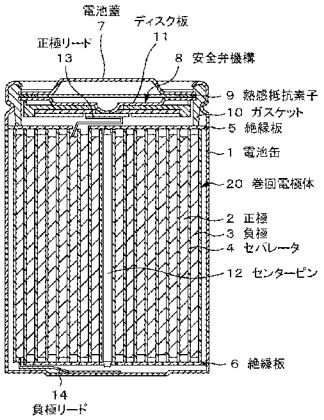
【０１２０】

さらに、例えば、正極、負極の作製方法は、上述した例に限定されない。例えば、材料に公知の結着剤等を添加して加熱して塗布する方法、材料単独、あるいは導電性材料、さらには、結着剤と混合して成型等の処理を施して集電体上に成型体電極を作製する方法が採られるが、これに限定されるものではない。より具体的には、結着剤、有機溶剤等と混合されたスラリー状にされた後、集電体上に塗布、乾燥させて作製することができる。あるいは、結着剤有無にかかわらず、活物質に熱を加えたまま加圧成型することにより、高度を有した電極を作製することも可能である。

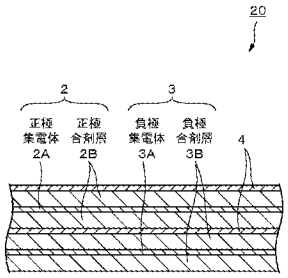
【０１２１】
さらに、例えば、電池の作製方法として、正極と負極との間にセパレータを介して巻芯の周囲に巻回する作製方法、電極とセパレータを順次積層する積層方式等が取られる。角型電池を作成する際に、巻回する方式が採られる場合にも有効である。
【０１２２】
また、電池の第１の例では、電解質として、電解液を有する非水電解質二次電池、電池の第２の例では、電解質として、ゲル電解質を有する非水電解質二次電池について説明したがこれらに限定されるものではない。例えば、電解質として、電解質塩を含有させた固体電解質を用いることもできる。固体電解質としては、リチウムイオン導電性を有する材料であれば無機固体電解質、高分子固体電解質いずれも用いることができる。無機固体電解質として、窒化リチウム、ヨウ化リチウム等が挙げられる。高分子固体電解質は、電解質塩とそれを溶解する高分子化合物からなり、その高分子化合物は、ポリ（エチレンオキサイド）や同架橋体等のエーテル系高分子、ポリ（メタクリレート）エステル系、アクリレート系等を単独あるいは分子中に共重合、または混合して用いることができる。
【図面の簡単な説明】
【０１２３】
【図１】この発明の一実施形態による正極活物質を用いた非水電解質二次電池の概略断面図である。
【図２】図１に示した巻回電極体の一部の拡大断面図である。
【図３】この発明の一実施形態による正極活物質を用いた非水電解質二次電池の構造を示す概略図である。
【図４】図３に示した電池素子の一部の拡大断面図である。
【図５】実施例１の正極活物質の断面におけるＴＯＦ－ＳＩＭＳ像である。
【図６】比較例３の正極活物質の断面におけるＴＯＦ－ＳＩＭＳ像である。
【符号の説明】
【０１２４】
１・・・電池缶
２・・・正極
２Ａ・・・正極集電体
２Ｂ・・・正極合剤層
３Ａ・・・負極集電体
３Ｂ・・・負極合剤層
３・・・負極
４・・・セパレータ
５，６・・・絶縁板
７・・・電池蓋
８・・・安全弁機構
９・・・熱感抵抗素子
１０・・・ガスケット
１１・・・ディスク板
１２・・・センターピン
１３・・・正極リード
１４・・・負極リード
２０・・・巻回電極体
３０・・・電池素子
３２・・・正極リード
３３・・・負極リード
３４，３５・・・樹脂片
３６・・・凹部
３７・・・外装材

４２・・・正極
４２Ａ・・・正極集電体
４２Ｂ・・・正極合剤層
４３・・・負極
４３Ａ・・・負極集電体
４３Ｂ・・・負極合剤層
４４・・・セパレータ
４５・・・ゲル電解質層

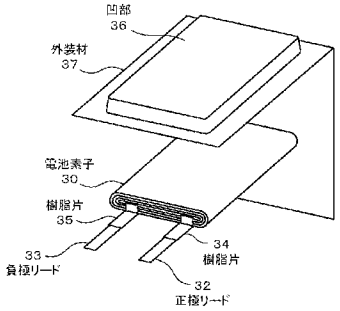
【図１】



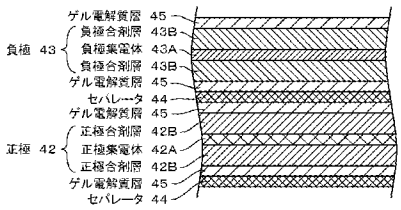
【図２】



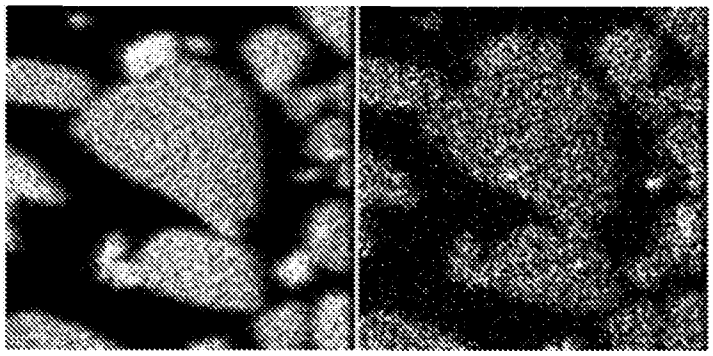
【図３】



【図４】



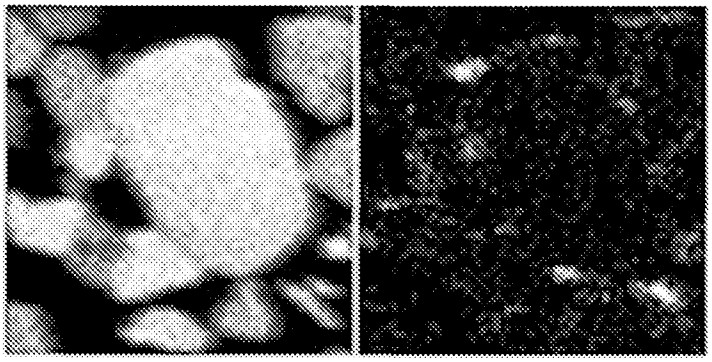
【図５】



LiCoO
tc:166921

LiCoF
tc:18138

【図６】



LiCoO
tc:452816

LiCoF
tc:4203

フロントページの続き

(72)発明者　砂金　正芳
東京都品川区北品川６丁目７番３５号　ソニー株式会社内

Ｆターム(参考) 5H029 AJ05 AK03 AL01 AL02 AL06 AL07 AL11 AM03 AM04 AM07
CJ02 CJ21 CJ28 DJ16 HJ00 HJ02 HJ13 HJ14 HJ15
5H050 AA07 BA17 CA07 CA08 CB01 CB02 CB07 CB08 CB11 DA02
EA09 EA24 FA17 GA02 GA21 GA27 HA02 HA13 HA14 HA15
HA20

Espacenet

KR20090111130A POSITIVE ACTIVE MATERIAL FOR LITHIUM SECONDARY BATTERY, METHOD FOR PREPARING THE SAME, AND LITHIUM SECONDARY BATTERY USING THE SAME

Applicants: LS MTRON LTD [KR]

Inventors: HAN JUNG MIN [KR],HAN KYUNG HEE [KR],KIM JONG SUNG [KR],OH JEONG HUN [KR],YOUM CHUL [KR]

Classifications:
IPC ***H01M10/052; H01M4/525;***

CPC **C01G51/006 (KR); H01M10/052 (KR); H01M4/58 (KR);** C01P2006/40 (KR); H01M4/136 (KR); Y02E60/10 (EP,KR);

Priorities: KR20080036739A 2008-04-21

Application: KR20090111130A·2008-04-21

Publication: KR20090111130A·2009-10-26

Published as: KR20090111130A

POSITIVE ACTIVE MATERIAL FOR LITHIUM SECONDARY BATTERY, METHOD FOR PREPARING THE SAME, AND LITHIUM SECONDARY BATTERY USING THE SAME

Abstract

PURPOSE: A cathode active material for lithium secondary battery and a method for manufacturing the same are provided to prevent structure change and improve structural stability. CONSTITUTION: A method for manufacturing a cathode active material for lithium secondary battery comprises: a step of uniformly mixing lithium composite, cobalt oxide, metal oxide (or metal hydroxide) and fluoride (S100); a step of heating the mixture; and a step of synthesizing lithium cobalt complex oxide (S120).

(19) 대한민국특허청(KR)
(12) 공개특허공보(A)

(11) 공개번호 10-2009-0111130
(43) 공개일자 2009년10월26일

(51) Int. Cl.
H01M 4/58 (2006.01) *H01M 4/40* (2006.01)
H01M 4/52 (2006.01)
(21) 출원번호 10-2008-0036739
(22) 출원일자 2008년04월21일
심사청구일자 2008년04월21일

(71) 출원인
엘에스엠트론 주식회사
경기 안양시 동안구 호계1동 1026-6
(72) 발명자
한정민
경기 김포시 감정동 무지개회영아파트 101동 105호
오정훈
경기 안양시 동안구 부림동 공작부영아파트 308동 806호
(뒷면에 계속)
(74) 대리인
특허법인필앤온지

전체 청구항 수 : 총 14 항

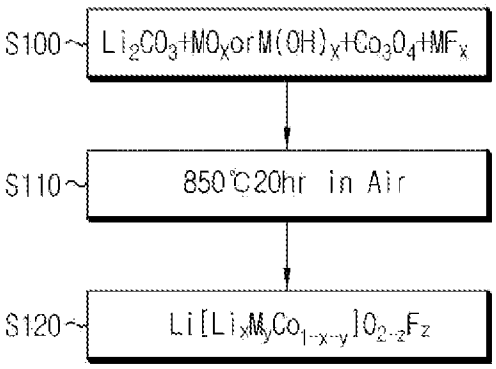
(54) 리튬 이차전지용 양극 활물질 및 그 제조방법과 이를이용한 리튬 이차전지

(57) 요 약

본 발명에 따른 리튬 이차전지용 양극 활물질은 불소화합물에 의해 코발트 원자의 일부가 금속원자로 치환됨과 동시에 산소 원자 일부가 불소 원자로 치환되고, 조성식이 $Li[Li_xM_yCo_{1-x-y}]O_{2-z}F_z$ (M은 Zr, Al, Mg 및 알칼리 토금속 원소로 이루어진 군에서 선택된 적어도 하나의 원소, $0 \leq x \leq 0.1$, $0 \leq y \leq 0.2$, $0 \leq z \leq 0.2$)인 것을 특징으로 한다.

본 발명에 의하면 고전압에서 충/방전 횟수에 따라 구조변이가 발생하지 않아 사이클 특성 및 율(C-rate) 특성, 열적 안정성 등이 우수한 리튬 이차전지를 제조할 수 있다.

대 표 도 - 도1



AMPEREX Ex. 1002
Page 1115

(72) 발명자

김종성

서울 구로구 구로6동 74-30 신구로현대아파트 2동 301호

염철

경기 수원시 영통구 매탄1동 172-33 301호

한경희

경기 성남시 중원구 상대원동 산19-4 산호아파트 913호

AMPEREX Ex. 1002
Page 1116

특허청구의 범위

청구항 1

리튬 이차전지용 양극 활물질에 있어서,

불소화합물에 의해 코발트 원자의 일부가 금속 원자로 치환됨과 동시에 산소 원자 일부가 불소 원자로 치환되고, 리튬 코발트 복합산화물 형태를 갖는 것을 특징으로 하는 리튬 이차전지용 양극 활물질.

청구항 2

제1항에 있어서,

상기 리튬 코발트 복합산화물의 조성식이 $Li[Li_xM_yCo_{1-x-y}]O_{2-z}F_z$ (M은 Zr, Al, Mg 및 알칼리 토금속 원소로 이루어진 군에서 선택된 적어도 하나의 원소, $0 \leq x \leq 0.1$, $0 \leq y \leq 0.2$, $0 \leq z \leq 0.2$)인 것을 특징으로 하는 리튬 이차전지용 양극 활물질.

청구항 3

제2항에 있어서,

상기 불소화합물은 CsF, KF, NaF, RbF, TlF, AgF, AgF_2 , BaF_2, CaF_2, CuF_2, CdF_2, FeF_2, HgF_2, Hg_2F_2, MnF_2, MgF_2, NiF_2, PbF_2, SnF_2, SrF_2, XeF_2, ZnF_2, AlF_3, BF_3, BiF_3, CeF_3, CrF_3, DyF_3, EuF_3, GaF_3, GdF_3, FeF_3, HoF_3, InF_3, LaF_3, LuF_3, MnF_3, NdF_3, VOF_3, PrF_3, SbF_3, ScF_3, SmF_3, TbF_3, TiF_3, TmF_3, YF_3, YbF_3, TlF_3, CeF_4, GeF_4, HfF_4, SiF_4, SnF_4, TiF_4, VF_4, ZrF_4, NbF_5, SbF_5, TaF_5, BiF_5, MoF_6, ReF_6, SF_6 및 WF_6 으로 이루어진 군에서 선택된 적어도 하나 이상인 것을 특징으로 하는 리튬 이차전지용 양극 활물질.

청구항 4

제1항 또는 제2항에 있어서,

상기 코발트 원자의 다른 일부는 금속산화물 또는 금속수산화물에 의해 금속 원자로 치환된 것을 특징으로 하는 리튬 이차전지용 양극 활물질.

청구항 5

리튬 이차전지용 양극 활물질 제조방법에 있어서,

리튬복합물, 코발트산화물, 금속산화물(또는 금속수산화물) 및 불소화합물을 균일하게 혼합한 후 그라인딩(grinding)하여 혼합물을 제조하는 단계; 및

상기 혼합물을 열처리하여, 불소화합물에 의해 코발트 원자의 일부가 금속 원자로 치환됨과 동시에 산소 원자 일부가 불소 원자로 치환된 리튬 코발트 복합산화물을 합성하는 단계;를 포함하는 것을 특징으로 하는 리튬 이차전지용 양극 활물질 제조방법.

청구항 6

제5항에 있어서,

상기 리튬 코발트 복합산화물의 조성식이 $Li[Li_xM_yCo_{1-x-y}]O_{2-z}F_z$ (M은 Zr, Al, Mg 및 알칼리 토금속 원소로 이루어진 군에서 선택된 적어도 하나의 원소, $0 \leq x \leq 0.1$, $0 \leq y \leq 0.2$, $0 \leq z \leq 0.2$)인 것을 특징으로 하는 리튬 이차전지용 양극 활물질 제조방법.

청구항 7

제6항에 있어서,

상기 리튬복합물은 Li_2CO_3이고, 상기 코발트산화물은 Co_3O_4인 것을 특징으로 하는 리튬 이차전지용 양극 활물질 제조방법.

AMPEREX Ex. 1002
Page 1117

청구항 8

제5항에 있어서,

상기 혼합물을 700~1000℃에서 10~30시간 동안 산화성 분위기, 환원성 분위기 또는 진공상태 하에서 하소하여 상기 열처리를 수행하는 것을 특징으로 하는 리튬 이차전지용 양극 활물질 제조방법.

청구항 9

제5항에 있어서,

상기 혼합물을 800~900℃에서 15~25시간 동안 산화성 분위기하에서 하소하여 상기 열처리를 수행하는 것을 특징으로 하는 리튬 이차전지용 양극 활물질 제조방법.

청구항 10

제5항 내지 제9항 중 어느 한 항의 제조방법에 의해 제조된 양극 활물질을 포함하는 리튬 이차전지.

청구항 11

리튬 이차전지에 있어서,

불소화합물에 의해 코발트 원자의 일부가 금속 원자로 치환됨과 동시에 산소 원자 일부가 불소 원자로 치환되고, 리튬 코발트 복합산화물 형태를 갖는 것을 특징으로 하는 양극 활물질을 포함하는 리튬 이차전지.

청구항 12

제11항에 있어서,

상기 리튬 코발트 복합산화물의 조성식이 $Li[Li_xM_yCo_{(1-x-y)}]O_{(2-z)}F_z$ (M은 Zr, Al, Mg 및 알칼리 토금속 원소로 이루어진 군에서 선택된 적어도 하나의 원소, $0 \leq x \leq 0.1$, $0 \leq y \leq 0.2$, $0 \leq z \leq 0.2$)인 것을 특징으로 하는 리튬 이차전지.

청구항 13

제11항 또는 제12항에 있어서,

상기 불소화합물은 CsF, KF, NaF, RbF, TlF, AgF, AgF_2 , BaF_2, CaF_2, CuF_2, CdF_2, FeF_2, HgF_2, Hg_2F_2, MnF_2, MgF_2, NiF_2, PbF_2, SnF_2, SrF_2, XeF_2, ZnF_2, AlF_3, BF_3, BiF_3, CeF_3, CrF_3, DyF_3, EuF_3, GaF_3, GdF_3, FeF_3, HoF_3, InF_3, LaF_3, LuF_3, MnF_3, NdF_3, VOF_3, PrF_3, SbF_3, ScF_3, SmF_3, TbF_3, TiF_3, TmF_3, YF_3, YbF_3, TlF_3, CeF_4, GeF_4, HfF_4, SiF_4, SnF_4, TiF_4, VF_4, ZrF_4, NbF_5, SbF_5, TaF_5, BiF_5, MoF_6, ReF_6, SF_6 및 WF_6 으로 이루어진 군에서 선택된 적어도 하나 이상인 것을 특징으로 하는 리튬 이차전지.

청구항 14

제11항에 있어서,

상기 코발트 원자의 다른 일부는 금속산화물 또는 금속수산화물에 의해 금속 원자로 치환된 것을 특징으로 하는 리튬 이차전지.

명 세 서

발명의 상세한 설명

기 술 분 야

<1> 본 발명은 리튬 이차전지용 양극 활물질에 관한 것으로서, 더욱 상세하게는 고전압 충전이 가능한 구성을 가진 리튬 코발트 복합산화물 형태의 양극 활물질 및 그 제조방법과 이를 이용한 리튬 이차전지에 관한 것이다.

AMPEREX Ex. 1002
Page 1118

배경 기술

<2> 최근 휴대전화, 휴대용개인정보단말기(PDA), 노트북 등 정보통신용 휴대용 전자기기나, 디지털카메라, 캠코더, MP3 등의 휴대용 전자기기, 전기자전거, 전기자동차 등의 전원으로 사용되는 이차전지의 수요가 급증함에 따라 소형, 경량이면서도 고에너지 밀도를 갖는 리튬 이차전지와 같은 비수 전해액 이차전지에 대한 요구가 점점 높아지고 있다.

<3> 리튬 이차전지는 4V급의 높은 전압이 얻어지기 때문에 고에너지 밀도를 갖는 장점이 있다. 이러한 리튬 이차전지의 양극 활물질로는 $LiCoO_2$, $LiNiO_2$, $LiMn_2O_4$, $LiFeO_2$ 등의 리튬 복합산화물이 널리 사용되고 있다. 그 중에서도 $LiCoO_2$는 각종 전기화학적 특성이 다른 복합산화물에 비해 우수하여 선호되고 있으나, 코발트(Co) 자원이 부족하고 가격이 비싼 문제가 있어 $LiCoO_2$를 양극 활물질로 사용하기 위해서는 지속적인 고성능화와 고수명화가 요구되고 있다.

<4> 최근에는 코발트(Co)를 대체하는 다른 전이원소를 사용하여 코발트(Co)를 사용한 경우와 동등하거나 그 이상의 각종 전기화학적 특성을 제공하는 양극 활물질에 대한 연구개발이 활발히 이루어지고 있다.

<5> 예를 들어, 일본 공개특허공보 평4-319260호에는 $LiCoO_2$에 지르코늄(Zr), 마그네슘(Mg) 등의 이종 원소를 첨가함으로써 우수한 충방전 특성과 사이클 특성을 나타내는 방법이 개시되어 있다.

<6> 일본 공개특허공보 제2004-299975호에는 $LiCoO_2$에 첨가하는 이종원소로서 지르코늄(Zr), 마그네슘(Mg) 뿐만 아니라, 티타늄(Ti)이나 불소(F)를 첨가하여 사이클 특성을 향상시키는 기술이 개시되어 있다.

<7> 일본 공개특허공보 평3-201368호에는 코발트(Co) 원자의 5~35%를 텅스텐(W), 망간(Mn), 탄탈(Ta), 티타늄(Ti) 또는 니오브(Nb)로 치환함으로써 사이클 특성을 향상시키는 기술이 개시되어 있다.

<8> 또한, 최근 문헌[*Chem. Mater. 2005,17,1284-1286*]에는 4.5V의 고전압에서 사용가능한 리튬 이차전지용 양극 활물질인 $LiM_{0.05}Co_{0.95}O_2$ [M = Cr, Bi, Sn, and Zr]재료가 제시되어 있으며, 문헌[*Journal of Power Sources 148 (2005) 90-94*]에는 $LiCo_{1-x}Zr_{x/2}Mg_{x/2}O_2$ [x = 0, 0.02, 0.06, 0.1, 0.2]에는 코발트(Co) 원자에 지르코늄(Zr), 마그네슘(Mg)을 동시에 첨가하는 방법이 제시되어 있다.

발명의 내용

해결 하고자하는 과제

<9> 본 발명은 위와 같은 양극 활물질의 개발 상황을 바탕으로 하여 창안된 것으로서, 고전압에서 더욱 향상된 구조 안정성과 열적 안정성을 갖도록 불소화합물에 의한 원소 치환을 통해 리튬 복합산화물의 구조가 개선된 리튬 이차전지용 양극 활물질 및 그 제조방법과 이를 이용한 리튬 이차전지를 제공하는 데 목적이 있다.

과제 해결수단

<10> 상기와 같은 목적을 달성하기 위해 본 발명은, 리튬 이차전지용 양극 활물질에 있어서, 불소화합물에 의해 코발트 원자의 일부가 금속 원자로 치환됨과 동시에 산소 원자 일부가 불소 원자로 치환되고, 리튬 코발트 복합산화물 형태를 갖는 것을 특징으로 하는 양극 활물질을 개시한다.

<11> 상기 리튬 코발트 복합산화물의 조성식은 $Li[Li_xM_yCo_{1-x-y}]O_{2-z}F_z$ (M은 Zr, Al, Mg 및 알칼리 토금속 원소로 이루어진 군에서 선택된 적어도 하나의 원소, $0 \le x \le 0.1$, $0 \le y \le 0.2$, $0 \le z \le 0.2$)인 것이 바람직하다.

<12> 상기 불소화합물은 CsF, KF, NaF, RbF, TlF, AgF, AgF_2 , BaF_2, CaF_2, CuF_2, CdF_2, FeF_2, HgF_2, Hg_2F_2, MnF_2, MgF_2, NiF_2, PbF_2, SnF_2, SrF_2, XeF_2, ZnF_2, AlF_3, BF_3, BiF_3, CeF_3, CrF_3, DyF_3, EuF_3, GaF_3, GdF_3, FeF_3, HoF_3, InF_3, LaF_3, LuF_3, MnF_3, NdF_3, VOF_3, PrF_3, SbF_3, ScF_3, SmF_3, TbF_3, TiF_3, TmF_3, YF_3, YbF_3, TlF_3, CeF_4, GeF_4, HfF_4, SiF_4, SnF_4, TiF_4, VF_4, ZrF_4, NbF_5, SbF_5, TaF_5, BiF_5, MoF_6, ReF_6, SF_6 및 WF_6 으로 이루어진 군에서 선택된 적어도 하나 이상인 것이 바람직하다.

<13> 상기 코발트 원자의 다른 일부는 금속산화물 또는 금속수산화물에 의해 금속 원자로 치환될 수 있다.

AMPEREX Ex. 1002
Page 1119

<14> 본 발명의 다른 측면에 따르면, 리튬복합물, 코발트산화물, 금속산화물(또는 금속수산화물) 및 불소화합물을 균일하게 혼합한 후 그라인딩(grinding)하여 혼합물을 제조하는 단계; 및 상기 혼합물을 열처리하여, 불소화합물에 의해 코발트 원자의 일부가 금속 원자로 치환됨과 동시에 산소 원자 일부가 불소 원자로 치환된 리튬 코발트 복합산화물을 합성하는 단계;를 포함하는 것을 특징으로 하는 리튬 이차전지용 양극 활물질 제조방법이 제공된다.

<15> 상기 리튬 코발트 복합산화물의 조성식은 $Li[Li_xM_yCo_{1-x-y}]O_{2-z}F_z$ (M은 Zr, Al, Mg 및 알칼리 토금속 원소로 이루어진 군에서 선택된 적어도 하나의 원소, $0 \le x \le 0.1$, $0 \le y \le 0.2$, $0 \le z \le 0.2$)인 것이 바람직하다.

<16> 상기 열처리는, 상기 혼합물을 700~1000℃에서 10~30시간 동안 산화성 분위기, 환원성 분위기 또는 진공상태 하에서 하소함으로써 수행될 수 있다. 보다 바람직하게, 상기 열처리는, 상기 혼합물을 800~900℃에서 15~25시간 동안 산화성 분위기하에서 하소함으로써 수행될 수 있다.

<17> 상기 리튬복합물은 Li_2CO_3이고, 상기 코발트산화물은 Co_3O_4인 것이 바람직하다.

<18> 본 발명의 또 다른 측면에 따르면, 불소화합물에 의해 코발트 원자의 일부가 금속 원자로 치환됨과 동시에 산소 원자 일부가 불소 원자로 치환되고, 리튬 코발트 복합산화물 형태를 갖는 것을 특징으로 하는 양극 활물질을 포함하는 리튬 이차전지가 제공된다.

효 과

<19> 본 발명에 따르면, 입자의 결정성이 우수하고, 고전압 충전 시 발생하는 구조적 변형이 방지되어 구조적 안정성이 향상된 리튬 이차전지용 양극 활물질을 얻을 수 있다. 특히 불소 원자의 함유로 인해 양극 활물질의 표면 뿐만 아니라 입자 내부에 강한 불소 결합물이 형성되어 양극 활물질 근처에서 생성되는 산에 대한 영향력을 감소시킬 수 있으며, 이차전지에 적용 시에는 양극 활물질과 전해액 간의 반응이 억제됨으로써 전지의 용량이 급격하게 줄어드는 현상을 방지할 수 있다.

<20> 따라서, 본 발명은 충방전 특성, 수명특성, 고전압, 율(C-rate) 특성, 열적 안정성 등이 우수한 양극 활물질을 제공할 수 있으며, 4.5V 이상의 고전압으로 충전이 가능한 리튬 이차전지를 제공할 수 있는 장점이 있다.

발명의 실시를 위한 구체적인 내용

<21> 이하, 첨부된 도면을 참조하여 본 발명의 바람직한 실시예를 상세히 설명하기로 한다. 이에 앞서, 본 명세서 및 청구범위에 사용된 용어나 단어는 통상적이거나 사전적인 의미로 한정해서 해석되어서는 아니되며, 발명자는 그 자신의 발명을 가장 최선의 방법으로 설명하기 위해 용어의 개념을 적절하게 정의할 수 있다는 원칙에 입각하여 본 발명의 기술적 사상에 부합하는 의미와 개념으로 해석되어야만 한다. 따라서, 본 명세서에 기재된 실시예와 도면에 도시된 구성은 본 발명의 가장 바람직한 일 실시예에 불과할 뿐이고 본 발명의 기술적 사상을 모두 대변하는 것은 아니므로, 본 출원시점에 있어서 이들을 대체할 수 있는 다양한 균등물과 변형예들이 있을 수 있음을 이해하여야 한다.

<22> 도 1은 본 발명의 바람직한 실시예에 따른 리튬 이차전지용 양극 활물질의 제조방법을 도시한 흐름도이다.

<23> 도 1을 참조하면, 본 발명의 바람직한 실시예에 따른 리튬 이차전지용 양극 활물질의 제조방법은 고상법(solid state reaction method)을 통해 수행되며, 출발물질을 혼합하는 혼합물 형성 공정(단계 S100)과, 혼합물을 열처리하여 코발트 원자의 일부가 금속 원자로 치환되는 동시에 산소 원자의 일부가 불소 원자로 치환된 $Li[Li_xM_yCo_{1-x-y}]O_{2-z}F_z$ 형태의 리튬 코발트 복합산화물을 합성하는 공정(단계 S110, S120)을 포함한다. 여기서, M은 Zr, Al, Mg 및 알칼리 토금속 원소로 이루어진 군에서 선택된 적어도 하나의 원소이며, x, y, z의 범위는 각각 $0 \le x \le 0.1$, $0 \le y \le 0.2$, $0 \le z \le 0.2$로 정해진다.

<24> 혼합물 형성 공정(단계 S100)에서는 출발물질로 리튬복합물(Li_2CO_3), 코발트산화물(Co_3O_4), 금속산화물(MO_k) 및 불소화합물(MF_k)을 사용하는 것이 바람직하다. 여기서, 불소화합물(MF_k)은 $Li[Li_xM_yCo_{1-x-y}]O_{2-z}F_z$에 있어 산소 원자의 일부를 불소 원자로 치환하고, 코발트 원자의 일부를 금속 원자로 치환하기 위해 사용된다. 금속산화물(MO_k)은 불소화합물(MF_k)에 의해 치환되는 금속 원자의 부족분을 보충하기 위한 용도로 사용된다. 즉, 예를 들어 Li_2CO_3, ZrO_2, ZrF_4 및 Co_3O_4를 사용하여 리튬 코발트 복합산화물인 $LiZr_{0.05}Co_{0.95}O_{1.95}F_{0.05}$를 합성하는 경우, 불소

AMPEREX Ex. 1002
Page 1120

원자는 모두 ZrF_4로부터 제공되며, 금속 원자는 ZrO_2와 ZrF_4로부터 제공된다. 상기 금속산화물(MO_x)은 금속수산화물($M(OH)_x$)로 대체될 수 있다.

<25> 바람직하게, 금속산화물로는 ZrO_2이 사용되고, 불소화합물(MF_x)로는 ZrF_4이 사용될 수 있으나, 본 발명이 이러한 예에 한정되지 않음은 물론이다. 그 밖의 불소화합물(MF_x)로는 CsF, KF, NaF, RbF, TiF, AgF, AgF_2, BaF_2, CaF_2, CuF_2, CdF_2, FeF_2, HgF_2, Hg_2F_2, MnF_2, MgF_2, NiF_2, PbF_2, SnF_2, SrF_2, XeF_2, ZnF_2, AlF_3, BF_3, BiF_3, CeF_3, CrF_3, DyF_3, EuF_3, GaF_3, GdF_3, FeF_3, HoF_3, InF_3, LaF_3, LuF_3, MnF_3, MoF_3, VOF_3, PrF_3, SbF_3, ScF_3, SmF_3, TbF_3, TiF_3, TmF_3, YF_3, YbF_3, TlF_3, CeF_4, GeF_4, HfF_4, SiF_4, SnF_4, TiF_4, VF_4, NbF_5, SbF_5, TaF_5, BiF_5, MoF_6, ReF_6, SF_6, WF_6 등이 사용 가능하다.

<26> 혼합물 형성 공정(단계 S100)에서는 리튬함유물(Li_2CO_3), 코발트산화물(Co_3O_4), 금속산화물(MO_x) 및 불소화합물(MF_x)을 균일하게 혼합(mixing)한 후 그라인딩(grinding)하여 혼합물을 형성한다. 혼합물을 균일하게 혼합하기 위한 장비로는 공지의 모르타르 아게이트(Mortar agate), 믹서(Mixer) 등이 채용되는 것이 바람직하다.

<27> 리튬 코발트 복합 혼합물을 형성한 후에는, 혼합물을 바람직하게 850℃에서 20시간 동안 산화성 분위기하에서 하소(calcine)하여 열처리하는 공정을 수행하고(단계 S110), 이후 파우더의 입자 사이즈 제어나 불순물 제거를 위해 그라인딩을 수행하여 층상구조(layered structure)를 가진 $Li[Li_xM_yCo_{(1-x-y)}]O_{2-z}F_z$를 합성한다(단계 S120). 여기서, 열처리 조건은 700~1000℃에서 10~30시간 동안 산화성 분위기, 환원성 분위기 또는 진공상태 하에서 수행하면 충분하고, 더욱 바람직하게는 800~900℃에서 15~25시간 동안 산화성 분위기하에서 수행한다.

<28> 본 발명에 따라 제조된 양극 활물질을 이용하여 리튬 이차전지를 제조할 경우에는 전해질로서 에스테르(ester)가 사용되는 것이 바람직하다. 예를 들면, 에틸렌 카보네이트(ethylene carbonate)(EC), 프로필렌 카보네이트(propylene carbonate)(PC), 부틸렌 카보네이트(butylene carbonate)(BC) 및 비닐렌 카보네이트(carbonate)(VC)등의 환상 카보네이트(carbonate), 디메틸 카보네이트(dimethyl carbonate)(DMC), 디에틸 카보네이트(diethyl carbonate)(DEC), 에틸 메틸 카보네이트(ethyl methyl carbonate)(EMC) 및 지푸로필카보네토(DPC) 등의 비환상 카보네이트(carbonate), 포름산 메틸(methyl)(MF), 초산메틸(MA), 프로피온산 메틸(methyl)(MP) 및 프로피온산 에틸(ethyl)(MA)등의 지방족 카르본산 에스테르(ester), 무틸로 락톤(lactone)(GBL)등의 환상 카르본산 에스테르(ester)가 사용될 수 있다. 환상 카보네이트(carbonate)로는 EC, PC, VC 등이 사용되는 것이 바람직하다. 또한, 필요에 따라 지방족 카르본산 에스테르(ester)를 20% 이하의 범위에서 사용하는 것도 바람직하다.

<29> 상기와 같은 용매에 용해하는 리튬염으로는 $LiClO_4$, $LiBF_4$, $LiPF_6$, $LiAlCl_4$, $LiSbF_6$, LiSCN, $LiCF_3SO_3$, $LiCF_3CO_2$, $Li(CF_3SO_2)_2$, $LiAsF_6$, $LiN(CF_3SO_2)_2$, $LiB_{10}Cl_{10}$, LiBOB(Lithium Bis(oxalato)borate), LiBoB, 저급 지방족 카르본산 리튬, 클로로 보란 리튬, 사페닐붕산리튬, 그리고 $LiN(CF_3SO_2)$ $(C_2F_5SO_2)$, $LiN(CF_3SO_2)_2$, $LiN(C_2F_5SO_2)_2$, $LiN(CF_3SO_2)(C_4F_9SO_2)$등의 이미드(imide)류 등을 사용할 수 있다. 상기 리튬염은 각각 단독으로 또는 본 발명의 효과를 손상시키지 않은 범위에서 임의로 조합하여 사용할 수 있으며, 그 중에서도 $LiPF_6$을 사용하는 것이 바람직하다.

<30> 전해액에는 불연성을 부여하기 위해 사염화탄소, 삼불화 염화 에틸렌, 혹은 인이 포함된 인산염 등이 더 포함될 수 있다.

<31> 한편, 전해질로는 무기 또는 유기 고체 전해질이 사용될 수도 있다. 무기 고체 전해질로는 Li_4SiO_4, Li_4SiO_4-LiAl-LiOH, $xLi_3PO_{4-(1.5)x}Li_4SiO_4$, Li_2SiS_2, Li_3PO_4-Li_2S-SiS_2, 황화인 화합물 등이 유효하다. 유기 고체 전해질로는 폴리에틸렌 옥사이드, 폴리프로필렌 옥사이드, 폴리비닐 알코올, 폴리불화비닐리덴, 폴루오르프로필렌 등이나 이러한 유도체, 혼합물, 복합체 등의 폴리머 재료가 유효하다.

<32> 리튬 이차전지의 세퍼레이터(separator)는 다공성 폴리에틸렌과 같은 폴리에틸렌계 혹은 폴리프로필렌계 폴리머를 주로 사용한다.

<33> 리튬 이차전지의 음극재료로는 리튬, 리튬합금, 합금/금속 간 화합물, 탄소, 유기 화합물, 무기 화합물, 금속착체, 유기 고분자 화합물 등 리튬이온을 흡착, 방출할 수 있는 화합물을 사용한다. 상기의 화합물을 각각 단독으

AMPEREX Ex. 1002
Page 1121

로, 또는 본 발명의 효과를 손상시키지 않은 범위에서 임의로 조합하여 사용할 수 있다.

<34> 리튬합금으로는, Li-Al계 합금, Li-Al-Mn계 합금, Li-Al-Mg계 합금, Li-Al-Sn계 합금, Li-Al-In계 합금, Li-Al-Cd계 합금, Li-Al-Te계 합금, Li-Ga계 합금, Li-Cd계 합금, Li-In계 합금, Li-Pb계 합금, Li-Bi계 합금 및 Li-Mg계 합금 등을 사용할 수 있다. 합금/금속 간 화합물로는 천이금속과 규소의 화합물이나 천이금속과 주석의 화합물 등을 사용할 수 있고, 특히 니켈과 규소의 화합물이 바람직하다.

<35> 탄소성질 재료로는, 코르스(cokes), 열분해 탄소류, 천연 흑연, 인조 흑연, 메소 카본마이크로 비즈(carbon micro beads), 흑연화 메소 페이즈(phase) 소구체, 유리상 탄소류, 탄소섬유(폴리 아크릴로나트릴(poly acrylonitrile)계, 피치(pitch)계, 셀룰로오스(cellulose)계, 기상 성장 탄소계), 무정형 탄소 및 유기물이 소성되는 탄소 등을 들 수 있다. 이것들은 각각 단독으로, 또는 본 발명의 효과를 손상시키지 않은 범위에서 임의로 조합하여 사용할 수 있다.

<36> 리튬 이차전지의 외장재로는 금속캔 또는 알루미늄과 수지의 폴리머층으로 구성된 포장재를 주로 사용한다.

<37> 이하에서는 리튬 이차전지용 양극 활물질의 구체적인 제조방법과 그에 따라 제조된 양극 활물질의 특성을 설명하기로 한다.

<38> 출발물질로 탄산리튬(Li_2CO_3), 코발트 산화물(Co_3O_4) 및 지르코늄 산화물 (ZrO_2), 지르코늄 불소화합물 (ZrF_4)을 사용하였다. 상기 출발물질들을 조성비에 대해 0.2몰로 정량하여 모르타르 아게이트(mortar agate)로 일정시간 균일하게 그라인딩하여 혼합물을 제조하였다. 이 혼합물을 알루미나 용기에 넣고 850℃에서 20시간동안 하소한 후 그라인딩하여 최종 리튬 코발트 복합산화물인 $Li[Li_xZr_yCo_{1-x-y}]O_{2-z}F_z$ ($0 \le x \le 0.1$, $0 \le y \le 0.2$, $0 \le z \le 0.2$)을 수득하였다. 치환하는 지르코늄(Zr)과 불소(F)의 양을 다양하게 하여 최적 조성을 찾고자 다양한 조성의 리튬 코발트 복합산화물을 제조하였다.

<39> 상기와 같이 제조된 리튬 코발트 복합산화물의 XRD 특성을 확인하기 위해, X선 회절 분석장치(상표명: Rint-2000, 회사명: Rigaku, Japan)를 이용하여 X선 회절 패턴을 측정하였다. 도 2 및 도 3을 참조하면, 코발트 원자의 일부를 치환하는 금속원자인 지르코늄(Zr)의 양이 증가함에 따라 X선 회절 패턴에서 지르코늄(Zr)을 명확히 관찰할 수 있다. 도 2에서 $Li[Li_xZr_yCo_{1-x-y}]O_{2-z}F_z$의 y와 z는 각각 $0.005 \le y \le 0.05$, $0.005 \le z \le 0.2$의 범위로 조절하였다. 도 3에서 $Li[Li_xZr_yCo_{1-x-y}]O_{2-z}F_z$의 z는 0.05로 고정하고, y는 $0.02 \le y \le 0.05$의 범위로 조절하였다.

<40> 도 4 및 도 5에는 상기 제조된 리튬 코발트 복합산화물의 FE-SEM(Field Emission Scanning Electron Microscopy, 상표명: JSM 6400, 회사명: JEOL, Japan) 사진이 나타나 있다. 도 4 및 도 5를 참조하면, 코발트 원자의 일부를 치환하는 지르코늄(Zr)과 산소원자의 일부를 치환하는 불소(F)의 양이 증가함에 따라 형태(morphology)가 변하는 것을 관찰할 수 있으며, 특히 지르코늄(Zr)은 고정하고, 불소(F)의 양을 증가시키는 경우에는 결정성이 더욱 향상되는 것을 관찰할 수 있다(도 4 참조).

<41> 리튬 이차전지용 양극을 제조하기 위하여, 상기 방법으로 제조된 리튬 코발트 복합산화물과, 도전재인 아세틸렌 블랙과, 결합제인 폴리비닐리덴 플루오라이드(PVdF)를 80:10:10의 중량비로 혼합하여 슬러리를 제조하였다. 이 슬러리를 20㎛ 두께의 알루미늄박에 균일하게 도포하고, 120℃에서 진공 건조하여 리튬 이차전지용 양극을 제조하였다.

<42> 상기 방법으로 제조된 양극과 리튬호일을 상대전극으로 하며, 다공성 폴리에틸렌막(Celgard 2300, 두께: 25㎛)을 세퍼레이터로 하고, 에틸렌 카보네이트:디메틸 카보네이트 = 1:1(부피비) 혼합용매의 1몰 LiPF6 용액을 액체 전해액으로 사용하여 리튬 전지의 통상적인 제조공정에 따라 2032 규격의 코인 전지(coin cell)를 제조하였다.

<43> 상기 제조된 전지의 특성을 평가하기 위하여 전기화학 분석장치(Toyo사 Toscat3000U, Japan)를 이용하여 상온(30℃), 3.0-4.5V의 전위영역에서 처음 2 사이클까지는 0.2mA/㎠, 3 사이클부터는 0.8mA/㎠의 전류밀도 조건에서 충, 방전 실험을 하였다. 도 6 및 도 7에는 사이클에 따른 방전 용량 변화가 나타나 있다. 도 6 및 도 7을 참조하면, 본 발명은 전반적으로 30 사이클까지 용량 감소가 거의 없는 매우 우수한 사이클 특성을 나타내는 반면에, 단순히 $LiCoO_2$의 조성을 갖는 양극 활물질을 채용한 전지는 용량이 급격히 감소하는 것을 확인할 수 있다. 본 발명은 양극 활물질 표면에서 전해액 부반응에 의해 생성되는 산에 대한 영향력을 감소시키거나, 양극 활물질과 전해액 간의 반응을 억제하여 전지의 용량이 급격하게 줄어드는 현상을 개선할 수 있다. 도 6 및 도 7에서, 30 사이클 이후에 용량이 전체적으로 감소하는 이유는 불소를 함유하고 있는 양극 활물질의 경우 고전압에서 0.5C 이상의 전류밀도로 충,방전 시 상대 전극인 리튬 금속의 부식이 빠르게 진행될 수 있기 때문이다.

AMPEREX Ex. 1002
Page 1122

<44> 상기 제조된 전지의 율(C-rate) 특성을 평가하기 위하여 전기화학 분석장치(Toyo사 Toscat3000U, Japan)를 이용하여 상온(30℃), 3.0~4.5V의 전위영역에서 다양한 전류밀도 조건으로 충, 방전 실험을 수행하였다. 도 8의 (A)에는 사이클에 따른 용량 변화가 나타나 있으며, 도 8의 (B)에는 20mA/g 전류밀도 대비 용량이 %단위로 나타나 있다. 도 8을 참조하면, $Li[Li_xZr_yCo_{1-x-y}]O_{2-z}F_z$ ($0 \leq x \leq 0.1$, $0 \leq y \leq 0.2$, $0 \leq z \leq 0.2$)의 양극 활물질 조성을 갖는 본 발명은 단순히 $LiCoO_2$의 조성을 갖는 양극 활물질을 채용한 전지에 비해 다양한 전류밀도 조건에서 매우 우수한 용량 특성을 나타내며, 20mA/g 전류밀도를 기준으로 비교했을 때 고율로 갈수록 더 우수한 출력 특성을 나타내는 것으로 확인되었다(도 8의 (B) 참조).

<45> 상기 제조된 리튬 코발트 복합산화물 $Li[Li_xZr_yCo_{1-x-y}]O_{2-z}F_z$ ($0 \leq x \leq 0.1$, $0 \leq y \leq 0.2$, $0 \leq z \leq 0.2$)의 열적 안정성을 평가하기 위하여 상술한 바와 같이 코인 전지를 제조하여 4.5V까지 충전시킨 후 전극을 분리하여 시차 열중량분석법(Differential Scanning Calorimetry; DSC, NETZSCH-TA4, Germany)으로 열 분석하였다. 도 9의 (A)와 (B)를 참조하면, 종래기술에 따른 $LiCoO_2$의 경우 241℃ 근방에서 주 발열피크가 나타나지만, 본 발명의 실시예에 따른 $LiZr_{0.05}Co_{0.95}O_{1.95}F_{0.05}$ 경우에는 약 242℃ 에서 주 발열피크가 나타났다. 대체로, 본 발명에 따라 제조된 리튬 코발트 복합산화물의 발열피크의 위치는 종래기술에 따른 $LiCoO_2$에 비해 발열량(J/g)이 낮은 것으로 확인되었다.

<46> 실시예 1

<47> 리튬 코발트 복합산화물 $LiZr_{0.05}Co_{0.95}O_{1.95}F_{0.05}$를 제조하기 위하여 출발물질로 탄산리튬($Li_2CO_3$), 코발트 산화물($Co_3O_4$), 지르코늄 산화물($ZrO_2$) 및 지르코늄 불소화합물($ZrF_4$)을 사용하였다. 상기 출발물질을 조성비에 대해 0.2 몰로 정량하여 모르타르 아게이트(mortar agate)로 일정시간 균일하게 그라인딩하여 혼합물을 제조하였다. 이 혼합물을 알루미나 용기에 넣고 850℃ 20시간동안 하소한 후 그라인딩하여 최종 산화물인 리튬 코발트 복합산화물 $LiZr_{0.05}Co_{0.95}O_{1.95}F_{0.05}$을 수득하였다.

<48> 실시예 2

<49> 출발물질로서 탄산리튬(Li_2CO_3), 코발트 산화물(Co_3O_4), 알루미늄 수산화물($Al(OH)_3$), 알루미늄 불소화합물(AlF_3)을 사용하여 정량하는 것을 제외하고는 실시예 1과 동일한 방법으로 리튬 코발트 복합산화물 $LiAl_{0.05}Co_{0.95}O_{1.95}F_{0.05}$를 수득하였다.

<50> 실시예 3

<51> 출발물질로서 탄산리튬(Li_2CO_3), 코발트 산화물(Co_3O_4), 마그네슘 수산화물($Mg(OH)_2$) 및 마그네슘 불소화합물(MgF_2)을 사용하여 정량하는 것을 제외하고는 실시예 1과 동일한 방법으로 리튬 코발트 복합산화물 $LiMg_{0.05}Co_{0.95}O_{1.95}F_{0.05}$를 수득하였다.

<52> 본 발명의 실시예 1 내지 3에 따라 제조된 리튬 코발트 복합산화물의 XRD 특성을 확인하기 위해, X선 회절 분석장치(상표명: Rint-2000, 회사명: Rigaku, Japan)를 이용하여 X선 회절 패턴을 측정하였다. 도 10을 참조하면, 코발트 원자의 일부를 치환하는 금속원자인 지르코늄(Zr), 알루미늄(Al), 마그네슘(Mg) 등을 X선 회절 패턴에서 관찰할 수 있다.

<53> 도 11에는 본 발명의 실시예 1 내지 3에 따라 제조된 리튬 코발트 복합산화물의 FE-SEM(Field Emission Scanning Electron Microscopy, 상표명: JSM 6400, 회사명: JEOL, Japan) 사진이 나타나 있다. 도 11을 참조하면, 코발트 원자의 일부를 치환하는 금속원자(Mg,Al,Zr)에 따라 다른 morphology를 관찰할 수 있다.

<54> 본 발명의 실시예 1 내지 3에 따라 제조된 리튬 코발트 복합산화물을 이용하여 양극을 제조한 후 이를 적용하여 코인 전지를 제조하였다.

<55> 상기 제조된 코인 전지의 특성을 평가하기 위하여 전기화학 분석장치(Toyo사 Toscat3000U, Japan)를 이용하여 상온(30℃), 3.0~4.5V의 전위영역에서 처음 2 사이클까지는 0.2mA/㎠, 3 사이클부터는 0.8mA/㎠의 전류밀도 조건에서 충, 방전 실험을 하여 사이클에 따른 용량 변화를 도 12에 나타내었다. 도 12를 참조하면, 본 발명의 실시예 1 내지 3에 따라 제조된 전지는 사이클 횟수에 따른 용량감소가 적어 고전압에서의 수명 특성이 매우 우수한 것을 확인할 수 있다.

AMPEREX Ex. 1002
Page 1123

<56> 비교예 1

<57> 금속 원자나 산소 원자의 일부가 치환되지 않은 리튬 이차전지용 양극 활물질인 $LiCoO_2$을 실시예 1과 동일한 방법으로 제조하고 특성을 평가하였다. 그 특성은 도 2, 4, 6~18에 나타나 있다.

<58> 비교예 2

<59> 산소 원자의 일부가 불소 원자로 치환되지 않은 리튬 이차전지용 양극 활물질인 $Li[Li_xZr_yCo_{(1-x-y)}]O_2$ ($0 \le x \le 0.1$, $0 \le y \le 0.2$)을 실시예 1과 동일한 방법으로 제조하고, 실시예 1과 동일한 조건하에서 충, 방전 특성을 평가하여 사이클에 따른 용량 변화를 도 13 내지 15에 나타내었다. 도면에 나타난 바와 같이, 코발트 원자의 일부를 치환하는 지르코늄(Zr)의 양이 0.005 또는 0.01과 같이 적을 경우(도 13 및 14 참조), 비교예 2는 실시예 1에 비해 사이클 특성이 좋기 않은 것으로 나타났으며, 지르코늄(Zr)의 양이 0.05일 경우(도 15 참조)에는 비교예 2와 실시예 1이 비슷한 사이클 특성을 나타내었다. 이는 비교예 2와는 달리 실시예 1에 따른 리튬 코발트 복합산화물은 코발트 원자의 일부가 금속 원자로 치환되고 산소 원자의 일부는 불소 원자로 치환되는 특성상, 소량만 치환되어도 양극 활물질 근처에서 전해액 부반응에 의해 생성되는 산에 대한 영향력을 감소시키거나, 양극 활물질과 전해액과의 반응성을 억제하여 전지의 용량이 급격하게 줄어드는 현상을 개선할 수 있기 때문이다.

<60> 율(C-rate)특성을 평가하기 위하여 전기화학 분석장치(Toyo사 Toscat3000U, Japan)를 이용하여 상온(30℃), 3.0~4.5V의 전위영역, 다양한 전류밀도 조건에서 충, 방전 실험을 하여 사이클에 따른 용량 변화를 도 16 및 17에 나타내었다. 도면을 참조하면, 비교예 2는 코발트 원자의 일부를 금속 원자로 치환하기만 하는 특성상 실시예 1에 비해 용량 특성이 좋지 않은 것을 확인할 수 있다.

<61> 비교예 3

<62> 마그네슘 수산화물($Mg(OH)_2$)과 리튬 불소화합물(LiF)을 이용하여 리튬 이차전지용 양극 활물질인 $LiMg_{0.05}Co_{0.95}O_{1.95}F_{0.05}$을 실시예 3과 동일한 방법으로 제조하고 동일한 조건하에서 특성을 평가하였다. 도 18을 참조하면, 리튬불소화합물(LiF)을 이용하여 산소원자의 일부를 불소원자로 치환하는 비교예 3은, 불소화합물(MgF_2)을 이용하여 코발트 원자와 산소 원자 일부를 마그네슘 원자와 불소원자로 치환하는 실시예 3에 비해 고전압에서 사이클 특성이 좋지 않은 것을 확인할 수 있다.

<63> 이상에서 본 발명은 비록 한정된 실시예와 도면에 의해 설명되었으나, 본 발명은 이것에 의해 한정되지 않으며 본 발명이 속하는 기술분야에서 통상의 지식을 가진 자에 의해 본 발명의 기술사상과 아래에 기재될 특허청구범위의 균등범위 내에서 다양한 수정 및 변형이 가능함은 물론이다.

도면의 간단한 설명

<64> 본 명세서에 첨부되는 다음의 도면들은 본 발명의 바람직한 실시예를 예시하는 것이며, 상술한 발명의 상세한 설명과 함께 본 발명의 기술사상을 더욱 이해시키는 역할을 하는 것이므로, 본 발명은 그러한 도면에 기재된 사항에만 한정되어 해석되어서는 아니된다.

<65> 도 1은 본 발명의 바람직한 실시예에 따른 리튬 이차전지용 양극 활물질의 제조방법을 도시한 흐름도이다.

<66> 도 2는 본 발명의 실시예(조성식에서, $0.005 \le y \le 0.05$, $0.005 \le z \le 0.2$)와 비교예에 따라 제공되는 리튬 코발트 복합산화물의 조성별 XRD 패턴을 나타낸 그래프이다.

<67> 도 3은 본 발명의 실시예(조성식에서, $0.02 \le y \le 0.05$, $z=0.05$)와 비교예에 따라 제공되는 리튬 코발트 복합산화물의 조성별 XRD 패턴을 나타낸 그래프이다.

<68> 도 4는 본 발명의 실시예(조성식에서, $0.005 \le y \le 0.05$, $0.005 \le z \le 0.2$)와 비교예에 따라 제공되는 리튬 코발트 복합산화물의 조성별 FE-SEM 사진이다.

<69> 도 5는 본 발명의 실시예(조성식에서, $0.02 \le y \le 0.05$, $z=0.05$)와 비교예에 따라 제공되는 리튬 코발트 복합산화물의 조성별 FE-SEM 사진이다.

<70> 도 6은 본 발명의 실시예(조성식에서, $0.005 \le y \le 0.05$, $0.005 \le z \le 0.2$)와 비교예에 따라 제공되는 리튬 이차전지의 사이클에 따른 용량 특성을 리튬 코발트 복합산화물의 조성별로 나타낸 그래프이다.

<71> 도 7은 본 발명의 실시예(조성식에서, $0.02 \le y \le 0.05$, $z=0.05$)와 비교예에 따라 제공되는 리튬 이차전지의 사이

AMPEREX Ex. 1002
Page 1124

클에 따른 용량 특성을 리튬 코발트 복합산화물의 조성별로 나타낸 그래프이다.

<72> 도 8은 본 발명의 실시예(조성식에서, $0.005 \le y \le 0.05$, $0.005 \le z \le 0.2$)와 비교예에 따라 제공되는 리튬 이차전지의 사이클에 따른 용량 특성과 C-rate에 따른 용량 특성을 리튬 코발트 복합산화물의 조성별로 나타낸 그래프와 테이블이다.

<73> 도 9는 본 발명의 실시예(조성식에서, $0.005 \le y \le 0.05$, $0.005 \le z \le 0.2$)와 비교예에 따라 제공되는 리튬 코발트 복합산화물에 대하여 수행된 시차열중량분석법(DSC)에 의한 열 분석 결과를 리튬 코발트 복합산화물의 조성별로 나타낸 그래프와 테이블이다.

<74> 도 10은 본 발명의 실시예(조성식에서, y=0.05, z=0.05)와 비교예에 따라 제공되는 리튬 코발트 복합산화물 조성에 따른 XRD 패턴을 나타낸 그래프이다.

<75> 도 11은 본 발명의 실시예(조성식에서, y=0.05, z=0.05)와 비교예에 따라 제공되는 리튬 코발트 복합산화물의 조성에 따른 FE-SEM 사진이다.

<76> 도 12는 본 발명의 실시예(조성식에서, y=0.05, z=0.05)와 비교예에 따라 제공되는 리튬 이차전지의 사이클에 따른 용량 특성을 리튬 코발트 복합산화물의 조성별로 나타낸 그래프이다.

<77> 도 13은 본 발명의 실시예(조성식에서, y=0.005 z=0.005)와 비교예에 따라 제공되는 리튬 이차전지의 사이클에 따른 용량 특성을 리튬 코발트 복합산화물의 조성별로 나타낸 그래프이다.

<78> 도 14는 본 발명의 실시예(조성식에서, y=0.01, z=0.01)와 비교예에 따라 제공되는 리튬 이차전지의 사이클에 따른 용량 특성을 리튬 코발트 복합산화물의 조성별로 나타낸 그래프이다.

<79> 도 15는 본 발명의 실시예(조성식에서, y=0.05 z=0.05)와 비교예에 따라 제공되는 리튬 이차전지의 사이클에 따른 용량 특성을 리튬 코발트 복합산화물의 조성별로 나타낸 그래프이다.

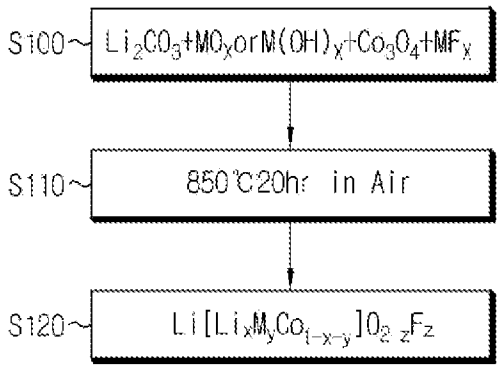
<80> 도 16은 본 발명의 실시예(조성식에서, y=0.005, z=0.005)와 비교예에 따라 제공되는 리튬 이차전지의 사이클에 따른 용량 특성과 C-rate에 따른 용량 특성을 리튬 코발트 복합산화물의 조성별로 나타낸 그래프와 테이블이다.

<81> 도 17은 본 발명의 실시예(조성식에서, y=0.01, z=0.01)와 비교예(조성식에서, y=0.01)에 따라 제공되는 리튬 이차전지의 사이클에 따른 용량 특성과 C-rate에 따른 용량 특성을 리튬 코발트 복합산화물의 조성별로 나타낸 그래프와 테이블이다.

<82> 도 18은 본 발명의 실시예(조성식에서, M=Mg, y=0.05, z=0.05)와 비교예에 따라 제공되는 리튬 이차전지의 사이클에 따른 용량 특성을 리튬 코발트 복합산화물의 조성별로 나타낸 그래프이다.

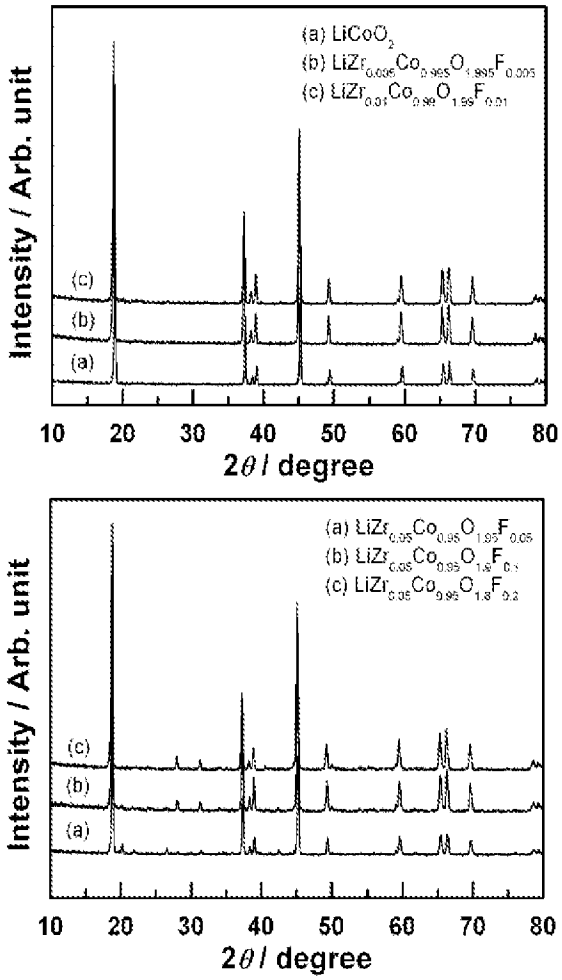
도면

도면1



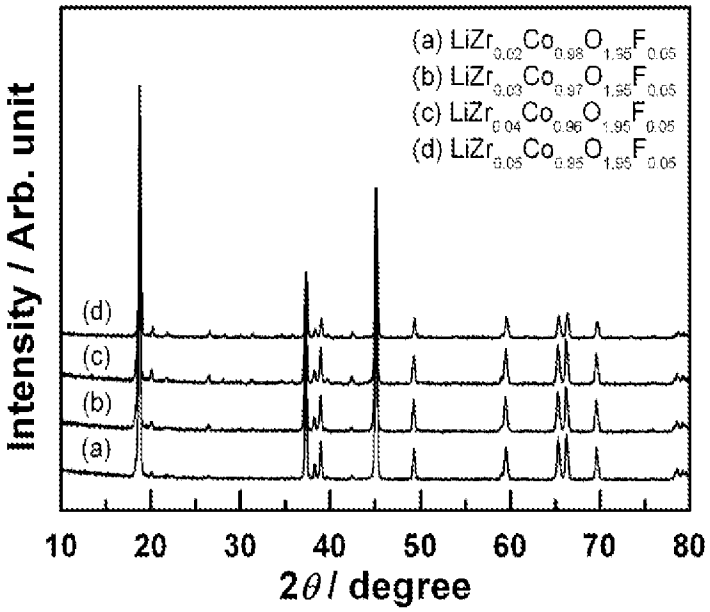
AMPEREX Ex. 1002
Page 1125

도면2



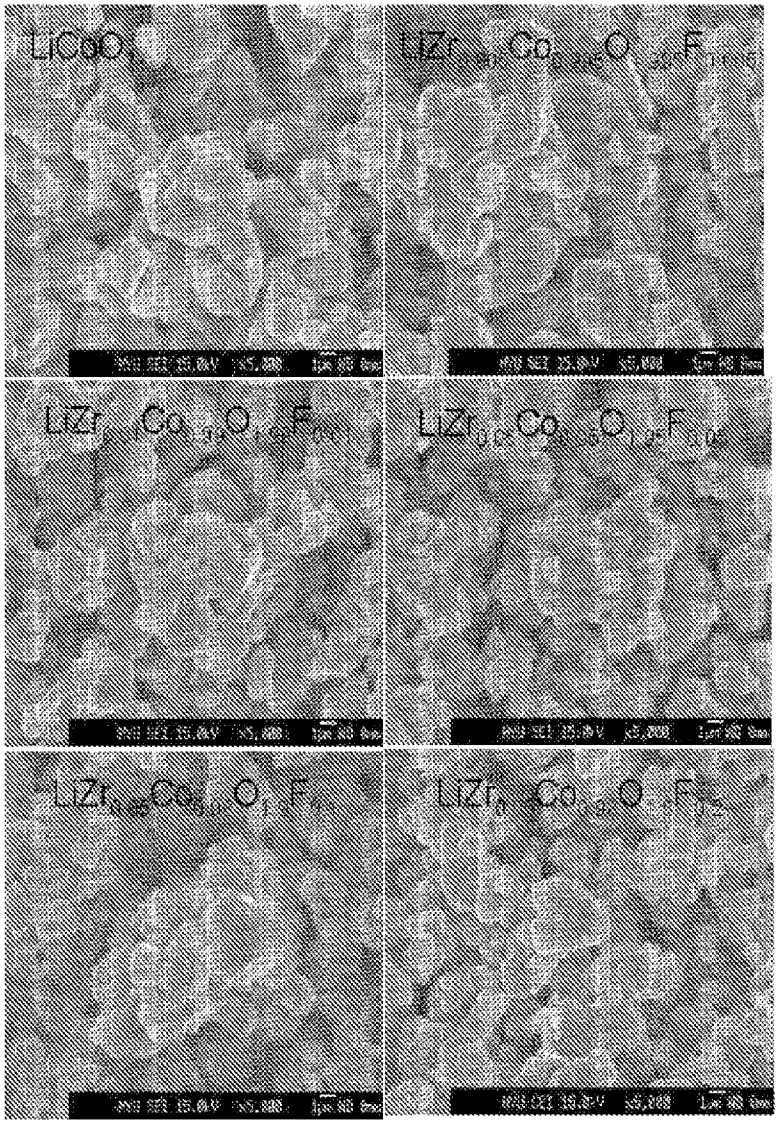
AMPEREX Ex. 1002
Page 1126

도면3

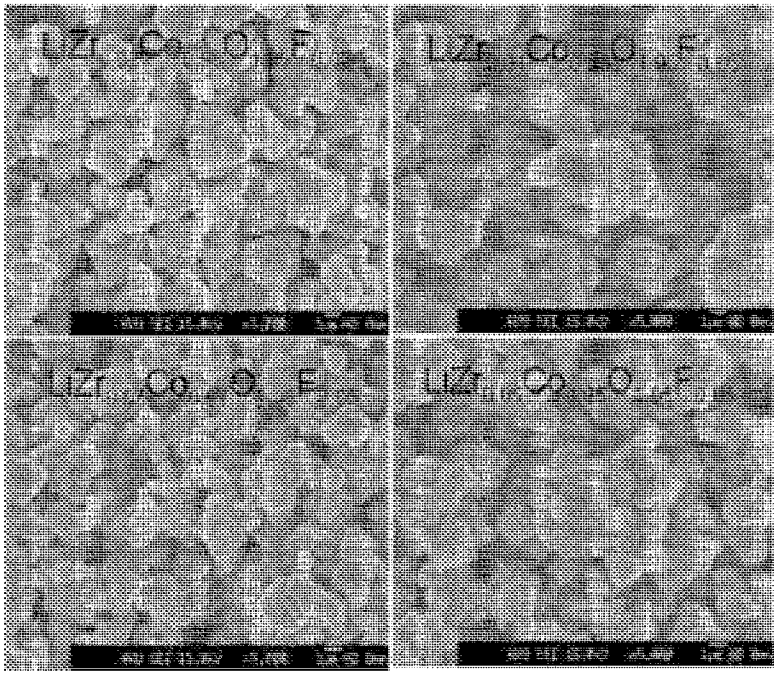


AMPEREX Ex. 1002
Page 1127

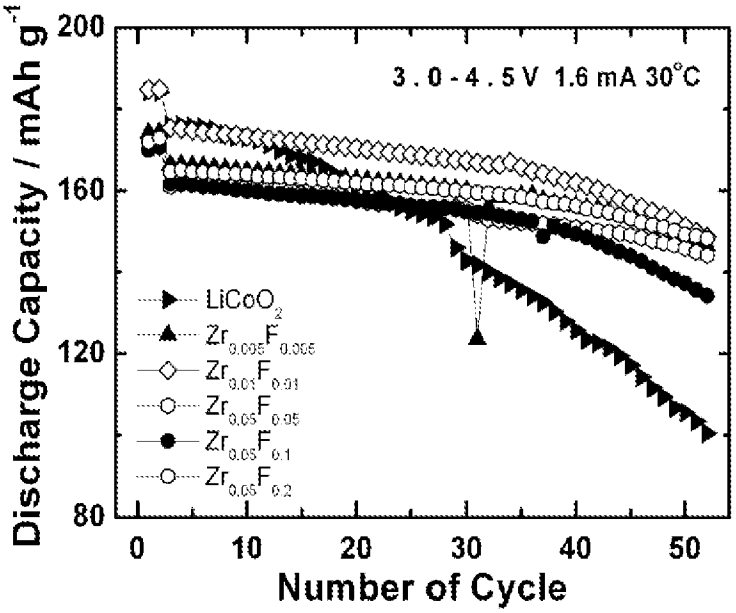
도면4


LiCoO2
LiZr0.001Co0.999O1.999F0.001
LiZr0.01Co0.99O1.99F0.01
LiZr0.02Co0.98O1.98F0.02
LiZr0.04Co0.96O1.96F0.04
LiZr0.08Co0.92O1.92F0.08

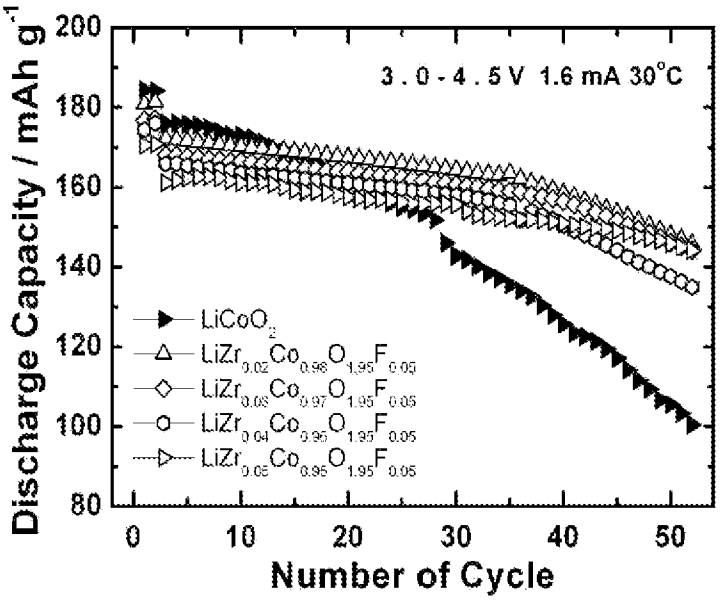
도면5



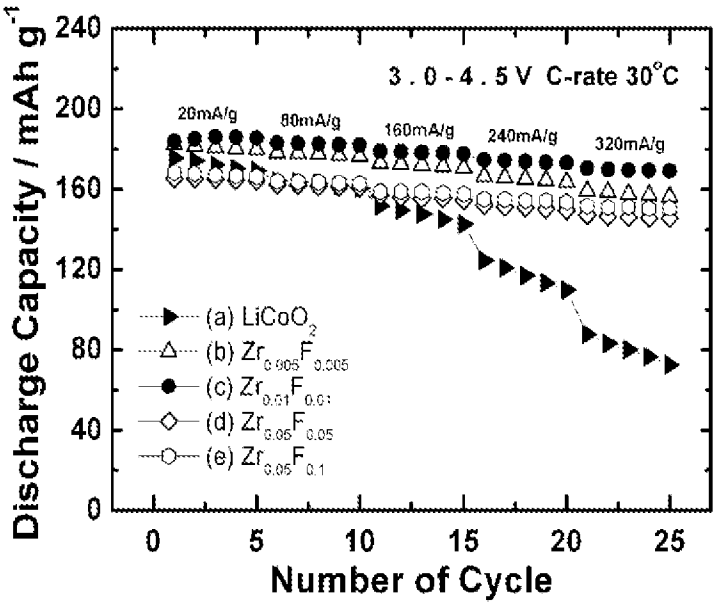
도면6


3.0-4.5V 1.6mA 30°C
Discharge Capacity / mAh g-1
Number of Cycle
200
160
120
80
0
10
20
30
40
50
LiCoO2
Zr0.005F0.005
Zr0.01F0.01
Zr0.05F0.05
Zr0.05F0.1
Zr0.05F0.2

도면7


3.0 - 4.5 V 1.6 mA 30°C
Discharge Capacity / mAh g-1
Number of Cycle
200
180
160
140
120
100
80
0
10
20
30
40
50
LiCoO2
LiZr0.02Co0.98O1.95F0.05
LiZr0.03Co0.97O1.95F0.05
LiZr0.04Co0.96O1.95F0.05
LiZr0.05Co0.95O1.95F0.05

도면8



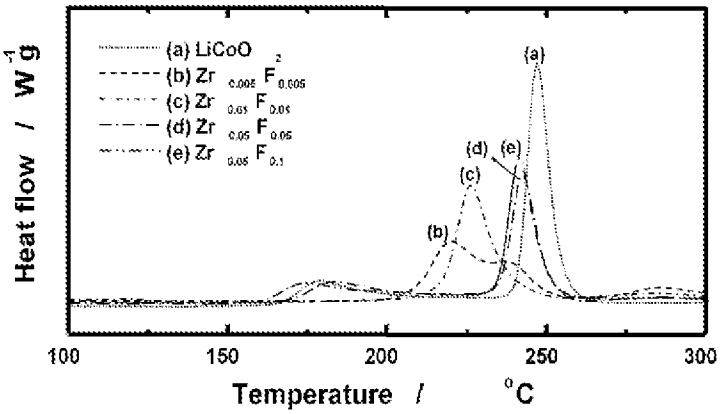
(A)

	(a)	(b)	(c)	(d)	(e)
0.5C	93.5	97.8	99.5	98	97.4
1C	86.4	95	97.2	94.9	94.3
2C	71	91.3	94.9	92.1	92.1
3C	50	87.3	92.6	89	89.9

20mA/g 대비 용량 (%)

(B)

도면9

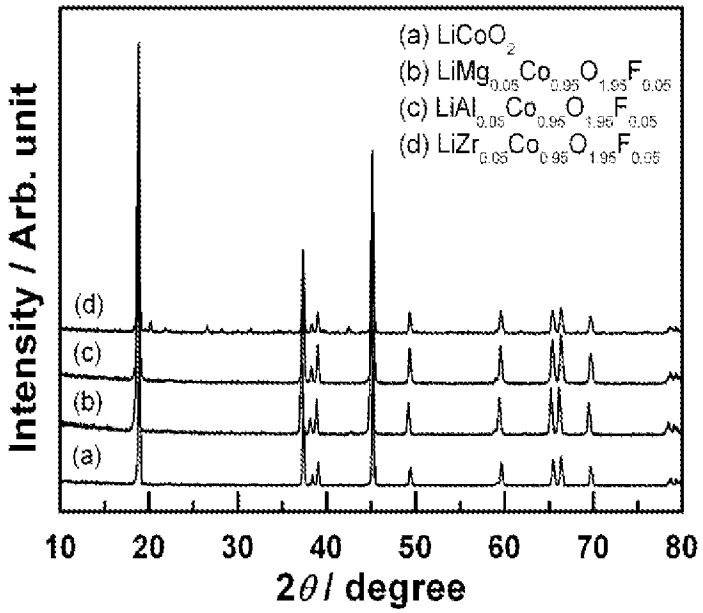


(A)

	(a)	(b)	(c)	(d)	(e)
Onset (°C)	241.4	207.4	226.3	242.5	241.6
발열량 (J/g)	3108	2351	2566	1872	2093

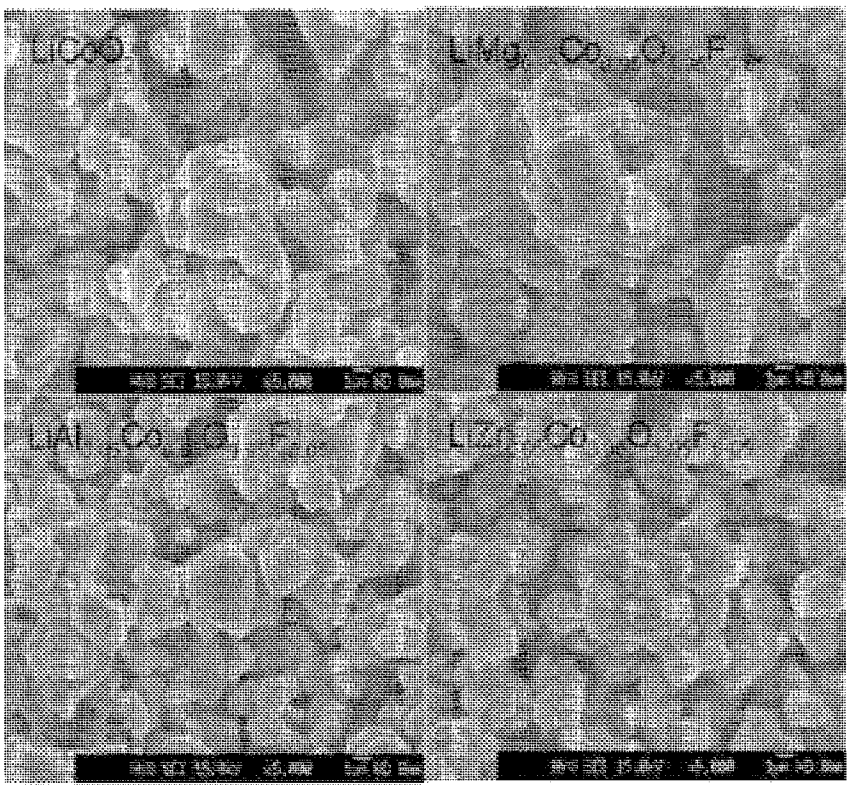
(B)

도면10

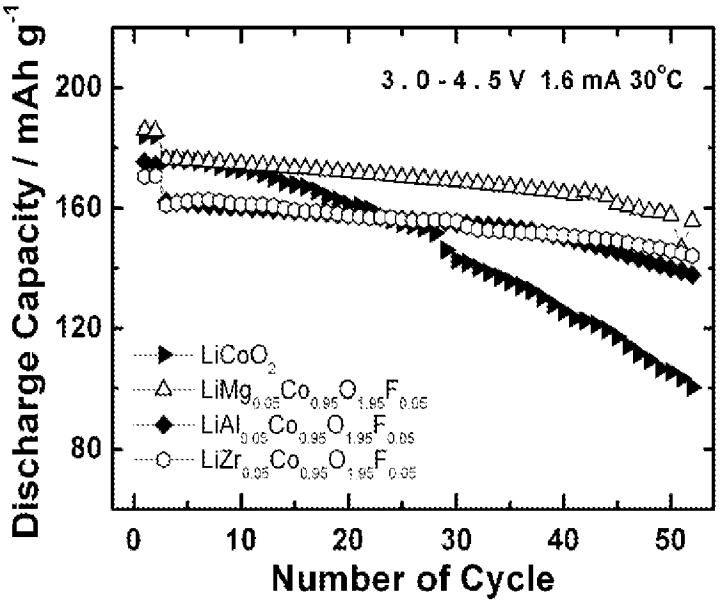


AMPEREX Ex. 1002
Page 1132

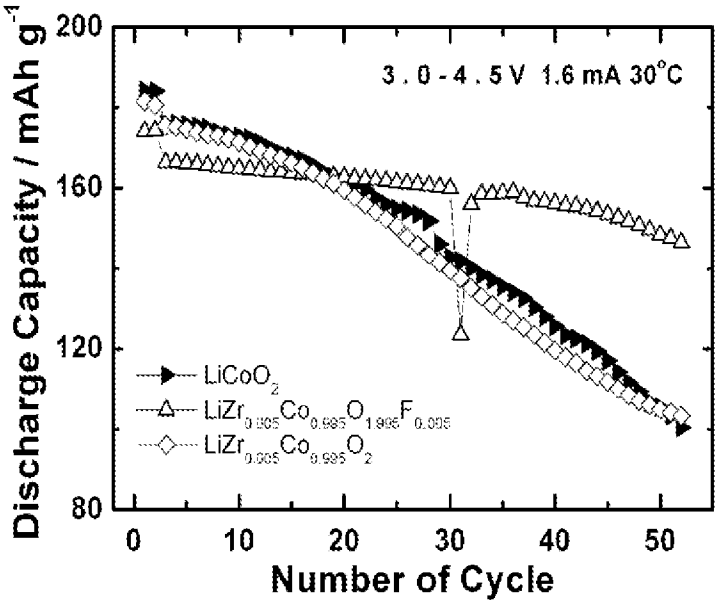
도면11



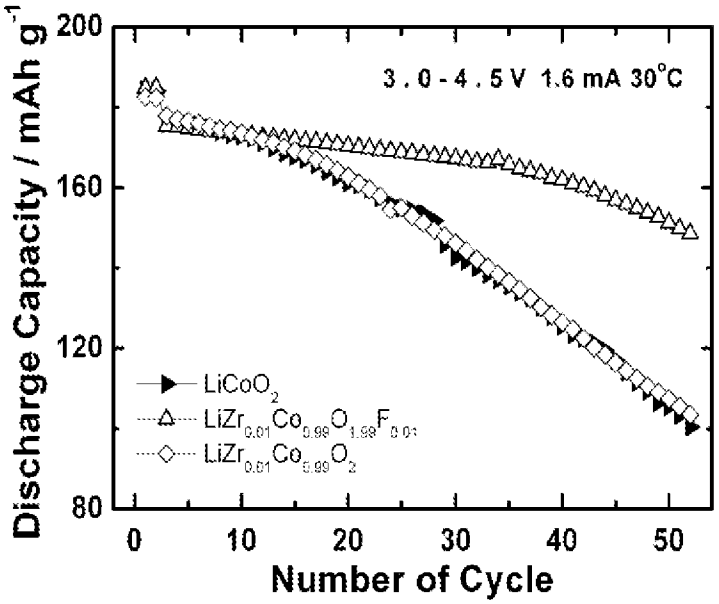
도면12


3.0-4.5V 1.6mA 30°C
Discharge Capacity / mAh g-1
Number of Cycle
200
160
120
80
0
10
20
30
40
50
LiCoO2
LiMg0.05Co0.95O1.95F0.05
LiAl0.05Co0.95O1.95F0.05
LiZr0.05Co0.95O1.95F0.05

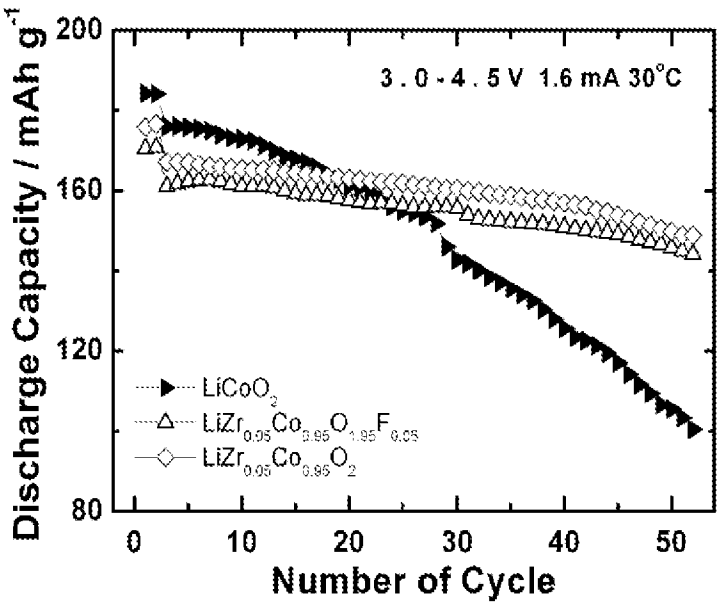
도면13


3.0-4.5V 1.6mA 30°C
Discharge Capacity / mAh g-1
Number of Cycle
200
160
120
80
0
10
20
30
40
50
LiCoO2
LiZr0.005Co0.995O1.995F0.005
LiZr0.005Co0.995O2

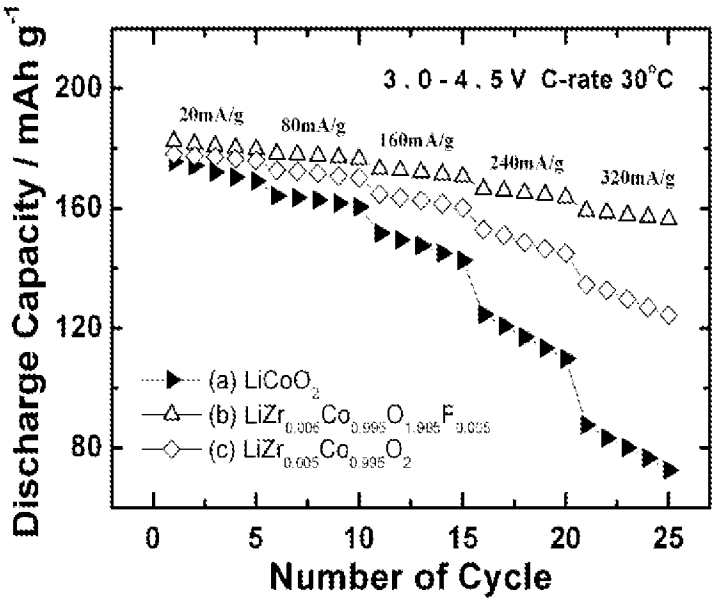
도면14


3.0-4.5V 1.6mA 30°C
Discharge Capacity / mAh g-1
Number of Cycle
200
160
120
80
0
10
20
30
40
50
LiCoO2
LiZr0.01Co0.99O1.98F0.01
LiZr0.01Co0.99O2

도면15


3.0-4.5V 1.6mA 30°C
Discharge Capacity / mAh g-1
Number of Cycle
200
160
120
80
0
10
20
30
40
50
LiCoO2
LiZr0.05Co0.95O1.95F0.05
LiZr0.05Co0.95O2

도면16



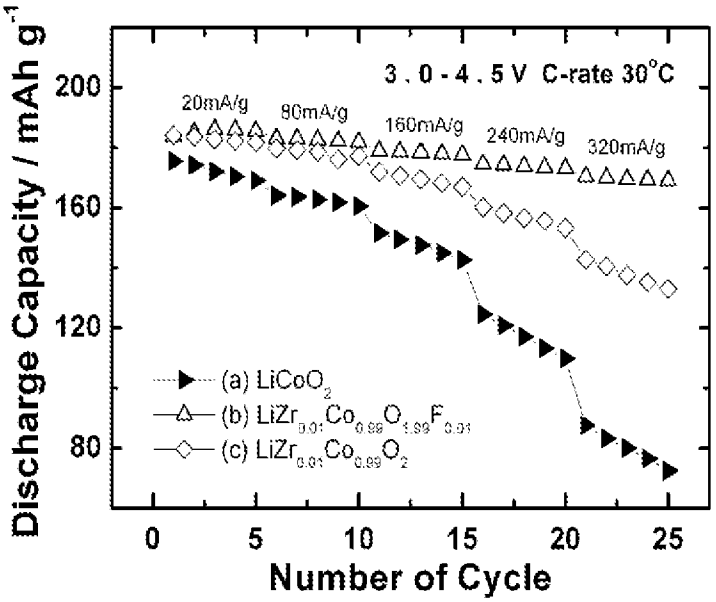
(A)

	(a)	(b)	(c)
0.5C	93.5	97.8	97
1C	86.4	95	92.5
2C	71	91.3	85.9
3C	50	87.3	75.5

20mA/g 대비 용량 (%)

(B)

도면17



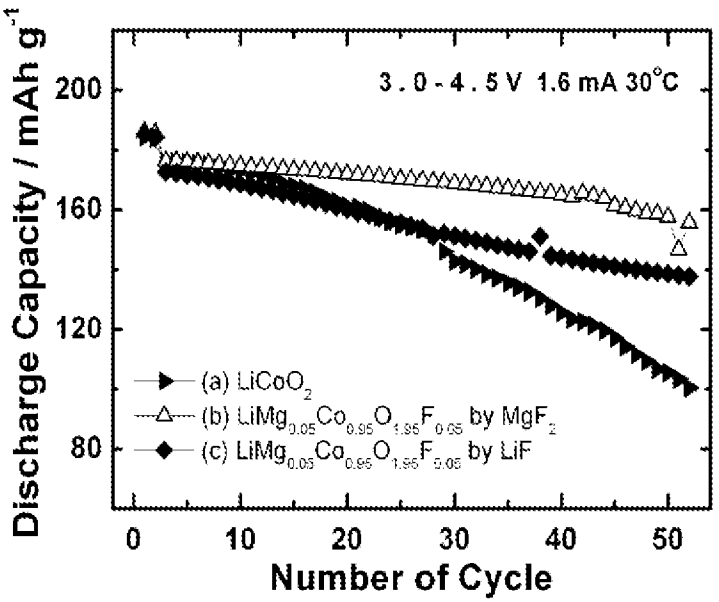
(A)

	(a)	(b)	(c)
0.5C	93.5	99.6	97.6
1C	86.4	97.3	93.3
2C	71	94.9	87
3C	50	92.6	77.5

20mA/g 대비 용량 (%)

(B)

도면18


3.0-4.5V 1.6mA 30°C
Discharge Capacity / mAh g-1
Number of Cycle
200
160
120
80
0
10
20
30
40
50
(a) LiCoO2
(b) LiMg0.05Co0.95O1.95F0.05 by MgF2
(c) LiMg0.05Co0.95O1.95F0.05 by LiF

Espacenet

RSS family document

Family list: CN102339998 (A) — 2012-02-01

1 application(s) for: CN102339998 (A)

1. Positive material for lithium ion battery and its preparation method

Inventor:	Applicant:	CPC:	IPC:	Publication info:	Priority date:
YANBIN CHEN WEI YU (+2)	BEIJING EASPRING MATERIAL TECHNOLOGY CO LTD	Y02E60/10	H01M10/0525 H01M4/131 H01M4/1391 (+1)	CN102339998 (A) 2012-02-01 CN102339998 (B) 2016-06-22 Global Dossier	2010-07-21

Espacenet

Bibliographic data: CN102339998 (A) — 2012-02-01

Positive material for lithium ion battery and its preparation method

Inventor(s): YANBIN CHEN; WEI YU; YUANYUAN WEI; YAFEI LIU ± (CHEN YANBIN, ; YU WEI, ; WEI YUANYUAN, ; LIU YAFEI, ; 陈彦彬, ; 于微, ; 魏媛媛, ; 刘亚飞)

Applicant(s): BEIJING EASPRING MATERIAL TECHNOLOGY CO LTD ± (BEIJING EASPRING MATERIAL TECHNOLOGY CO., LTD, ; 北京当升材料科技股份有限公司)

Classification: - international: ***H01M10/0525; H01M4/131; H01M4/1391; H01M4/525***

- cooperative: Y02E60/10 (EP)

Application number: CN201010232749 20100721 Global Dossier

Priority number (s): CN201010232749 20100721

Also published as: CN102339998 (B)

Abstract of CN102339998 (A)

The invention discloses a positive material for a lithium ion battery and its preparation method, concretely relates to a modified cobalt acid lithium material and its preparation method, and relates to a lithium ion battery containing the material. The general formula of the material is LiMxLyNwCozO2, wherein 0.001<=x<=0.1, 0.005<=y<=0.05, 0<=w<=0.05, 1-x-y-w<=z<=1, M is one or more transition metals selected from Mn, Ni, Ti, Zr, Cr, Fe, Cu, Zn, Y, Ce, Sm, Pr, La, Mo or Nb and the like, L is one or more main group metal elements selected from Na, K, Ca, Mg, Sr, Ba, B, Ga, Sn, Sb, Bi or Al and the like; N is one or more of Li, Mn, Ni, Zr, Ti, Y, Ce, Sm, Mo, Nb, Na, K, Ca, Mg, Sr, Ba, B or Al. The material has the advantages of high specific capacity, excellent cycle performance and heat stability, simple preparation method and easy industrialization production.

(19)中华人民共和国国家知识产权局

(12)发明专利申请

(10)申请公布号 CN 102339998 A
(43)申请公布日 2012.02.01

(21)申请号 201010232749.0

(22)申请日 2010.07.21

(71)申请人 北京当升材料科技股份有限公司
地址 100044 北京市西城区西直门外文兴街1号

(72)发明人 陈彦彬 于微 魏媛媛 刘亚飞

(51)Int.Cl.
H01M 4/525(2010.01)
H01M 4/131(2010.01)
H01M 4/1391(2010.01)
H01M 10/0525(2010.01)

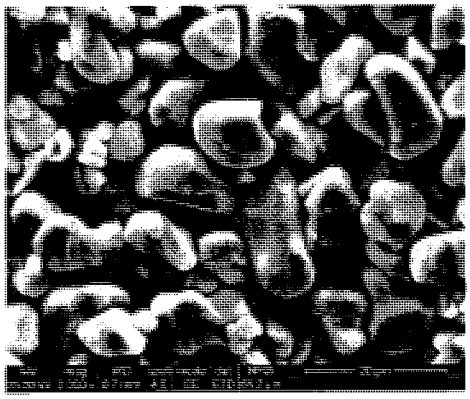
权利要求书 1 页 说明书 4 页 附图 2 页

(54)发明名称

一种锂离子电池正极材料及其制备方法

(57)摘要

本发明公开了一种锂离子电池正极材料及其制备方法，具体地讲涉及一种改性钴酸锂材料及其制备方法，还涉及一种含该材料的锂离子电池。该材料通式为 $LiM_xL_yN_wCo_zO_2$，其中 $0.001 \leqslant x \leqslant 0.1$，$0.005 \leqslant y \leqslant 0.05$，$0 \leqslant w \leqslant 0.05$，$1-x-y-w \leqslant z \leqslant 1$，M 为 Mn、Ni、Ti、Zr、Cr、Fe、Cu、Zn、Y、Ce、Sm、Pr、La、Mo 或 Nb 等副族过渡金属中的一种或几种，L 为 Na、K、Ca、Mg、Sr、Ba、B、Ga、Sn、Sb、Bi 或 Al 等主族金属元素中的一种或几种；N 为 Li、Mn、Ni、Zr、Ti、Y、Ce、Sm、Mo、Nb、Na、K、Ca、Mg、Sr、Ba、B、Al 中的一种或几种。该材料在保持较高的比容量的同时，具有优异的循环性能和热稳定性，制备方法简单，易于工业化生产。



CN 102339998 A

1. 一种锂离子电池正极材料，其特征在于通式为 $LiM_xL_yN_wCo_zO_2$，其中，$0.001 \leqslant x \leqslant 0.01$，$0.005 \leqslant y \leqslant 0.05$，$0 \leqslant w \leqslant 0.05$，$1-x-y-w \leqslant z \leqslant 1$；M 和 L 为包覆或梯度掺杂元素，N 为掺杂元素；M 为 Mn、Ni、Zr、Cr、Fe、Ti、Cu、Zn、Y、Ce、Sm、Pr、La、Mo 或 Nb 中的一种或几种，L 为 Na、K、Ca、Mg、Sr、Ba、B、Ga、Sn、Sb、Bi 或 Al 中的一种或几种，N 为 Li、Mn、Ni、Zr、Ti、Y、Ce、Sm、Mo、Nb、Na、K、Ca、Mg、Sr、Ba、B、Al 中的一种或几种。

2. 根据权利要求 1 所述锂离子电池正极材料，其特征为一次粒子中粒径为 12 ～ 25μm。

3. 根据权利要求 2 所述锂离子电池正极材料，其特征为一次粒子中粒径为 12 ～ 18μm。

4. 一种权利要求 1 所述锂离子电池正极材料的制备方法，其特征在于包括如下步骤：

(1) 将含锂化合物、含钴化合物混合均匀，在 700℃～ 1200℃下烧结，破碎后得到前驱体；

(2) 将前驱体与含 M 和 L 的化合物混合均匀，在 300℃～ 900℃下进行热处理，破碎后得到产物。

5. 根据权利要求 4 所述锂离子电池正极材料的制备方法，其特征为步骤 (1) 中将含锂化合物、含钴化合物以及含 N 的化合物混合。

6. 根据权利要求 4 或 5 所述锂离子电池正极材料的制备方法，其特征为步骤 (1) 中含 N 化合物以及步骤 (2) 中含 M 和含 L 的化合物为氧化物、氢氧化物、羟基氧化物、碳酸盐、草酸盐、氟化物、氯化物、磷酸盐、硫酸盐中的一种或几种。

7. 根据权利要求 4 所述锂离子电池正极材料的制备方法，其特征为步骤 (1) 中含锂化合物为碳酸锂或氢氧化锂中的一种或几种，含钴化合物为四氧化三钴、氧化亚钴、碳酸钴、草酸钴、氢氧化钴或羟基氧化钴中的一种或几种。

8. 根据权利要求 4 所述锂离子电池正极材料的制备方法，其特征为步骤 (1) 中锂、钴摩尔比为 0.95 ： 1 ～ 1.08 ： 1。

9. 一种锂离子电池，其特征在于包括含有权利要求 1 ～ 3 中任意一项所述的锂离子电池正极材料的正极；负极；隔膜；电解质。

10. 根据权利要求 9 所述的锂离子电池，其特征为 0.2C 放电比容量为 153 ～ 156mAh/g，300 周容量保持率大于 85%，85℃高温存储 4h 的容量损失率小于 5%。

AMPEREX Ex. 1002
Page 1142

一种锂离子电池正极材料及其制备方法

技术领域

[0001] 本发明涉及一种锂离子电池正极材料及其制备方法，具体地讲涉及一种改性钴酸锂材料及其制备方法。

[0002] 本发明还涉及一种含该材料的锂离子电池。

背景技术

[0003] 锂离子电池与传统的绿色二次电池相比，具有工作电压高、体积小、比能量高、质量轻、无记忆效应、自放电小、污染少、寿命长等优点。锂离子二次电池以其卓越的高性能价格比优势在笔记本电脑、移动电话、摄像机、数码相机、武器装备等小型电池领域占据了主导地位，拥有可观的市场销量。

[0004] 层状钴酸锂 $LiCoO_2$ 具有电压高 (3.6V)、放电平稳、比容量较高 (140mAh/g 左右)、循环性能优异、倍率性能好、制备工艺简单等优点，被认为是小型锂离子电池的理想正极材料，随着小型电池对容量、循环以及安全性能的要求逐渐提高，促使钴酸锂材料朝着高容量、高密度和大颗粒方向发展。

[0005] 影响容量、循环性能和热稳定性的主要因素是粒径和改性方式。一般来说，相同的改性工艺，大颗粒的循环性能和热稳定性比小颗粒更优异。改性方式分为掺杂和包覆两种：对于大颗粒钴酸锂来说，单靠元素掺杂可以增加材料的首次充放电比容量，但对提高材料的循环性能和热稳定性等效果却不明显；而单种元素包覆根据包覆剂的性质不同，形成的效果有两种：一种相当于均相掺杂，是比较均匀地分布在颗粒内部及表面，可以提高材料的首次充放电比容量，但是对材料的循环性能和热稳定性没有提升作用；一种相当于梯度掺杂，颗粒表面的改性剂避免了 $LiCoO_2$ 与电解液的直接接触，抑制了循环期间的晶格膨胀，提升了材料的循环性能和热稳定性，但是导致材料比容量降低。中国专利 CN0214607.1 公开了一种单元素包覆的改性钴酸锂材料，制备出的锂离子电池只改进了循环性能，但热稳定性和容量的改进并不明显。中国专利 CN200710060049.6 公开了锆、磷掺杂型钴酸锂及其制备方法，循环性能有所改进，但是首次放电容量有所减低。综上可知，由掺杂和单种元素包覆制备出的钴酸锂材料很难同时满足小型锂电高端客户对容量、循环性能和热稳定性的要求。

发明内容

[0006] 为了克服上述现有技术的缺点，本发明目的是在不影响比容量的前提下，提供一种循环性能优良、热稳定性更好的锂离子电池正极材料及其制备方法，另外还提供一种含该材料的锂离子电池。

[0007] 本发明的解决方案是采用对钴酸锂或掺杂型钴酸锂前驱体进行表面共包覆的方法，采用此种方法制备的改性钴酸锂保持较高比容量的同时，具有优异的循环性能和热稳定性。该材料通式为 $LiM_xL_yN_wCo_zO_2$，其中，$0.001 \leqslant x \leqslant 0.01$，$0.005 \leqslant y \leqslant 0.05$，$0 \leqslant w \leqslant 0.05$，$1-x-y-w \leqslant z \leqslant 1$；M 和 L 为包覆或梯度掺杂元素，N 为掺杂元素；M 为 Mn、Ni、

AMPEREX Ex. 1002
Page 1143

Zr、Cr、Fe、Ti、Cu、Zn、Y、Ce、Sm、Pr、La、Mo 或 Nb 等副族过渡金属中的一种或几种，L 为 Na、K、Ca、Mg、Sr、Ba、B、Ga、Sn、Sb、Bi 或 Al 中的一种或几种，N 为 Li、Mn、Ni、Zr、Ti、Y、Ce、Sm、Mo、Nb、Na、K、Ca、Mg、Sr、Ba、B、Al 中的一种或几种，N 与 M、L 一般不为同一种元素的化合物。本发明制备的锂离子电池正极材料，具有均匀的粒径分布和光滑的微观形貌，一次粒子中粒径约为 12 ～ 25um，优选为 12 ～ 18um。

[0008] 本发明的锂离子电池正极材料的制备方法如下：

[0009] (1) 将含锂化合物、含钴化合物混合均匀，在 700℃～ 1200℃下烧结，破碎后得到前驱体，其中锂、钴摩尔比约为 0.95 ： 1 ～ 1.08 ： 1；

[0010] (2) 将前驱体与含 M 和 L 的化合物混合均匀，在 300℃～ 900℃下进行热处理，使改性剂充分浸润到前驱体材料表面，将热处理后得到的材料破碎，得到产物。

[0011] 步骤 (1) 中也可以将含 N 的化合物与含锂化合物、含钴化合物混合均匀，然后再依照步骤 (1) 的条件下进行烧结、破碎，得到掺杂的前驱体。

[0012] 步骤 (1) 中含锂化合物为碳酸锂或氢氧化锂中的一种或几种，含钴化合物为四氧化三钴、氧化亚钴、碳酸钴、草酸钴、氢氧化钴或羟基氧化钴中的一种或几种。

[0013] 步骤 (1) 中含 N 化合物以及步骤 (2) 中含 M 和含 L 的化合物可为氧化物、氢氧化物、羟基氧化物、碳酸盐、草酸盐、氟化物、氯化物、磷酸盐、硫酸盐中的一种或几种。

[0014] 一种锂离子电池，包括含有该锂离子电池正极材料的正极；负极；隔膜；电解质。其电性能为在 0.2C 下放电比容量为 153 ～ 156mAh/g 左右，300 周容量保持率达到 85％以上，85℃高温存储 4h 的容量损失率小于 5％。

[0015] 本发明具有下述优点：

[0016] (1) 对钴酸锂或掺杂型钴酸锂的前驱体进行合适的表面共包覆，根据不同改性剂的不同性质，使改性剂在钴酸锂表面和内部呈现不同的状态分布，在不降低比容量的前提下，抑制循环过程中晶格的膨胀，并经过特定的热处理工艺，得到了循环性能和热稳 定性良好的钴酸锂正极材料。

[0017] (2) 通过采用该改性过的钴酸锂材料，制备出的锂离子电池循环性能和热稳定性良好。

[0018] (3) 材料的制备方法简单，易于工业化生产。

附图说明

[0019] 图 1 是实施例 1 中制备的锂离子电池正极材料的 SEM 图。

[0020] 图 2 是实施例 1 和对比例 1 中制备的锂离子电池的循环性能曲线对比图。

[0021] 图 3 是实施例 1 和对比例 1 中制备的锂离子电池的高温存储容量损失率对比图。

实施例

[0022] 下面通过具体的对比例、实施例并结合附图对本发明作进一步详细的描述。

[0023] 对比例 1

[0024] 将 Li ： Co 摩尔比为 1.04 ： 1 的碳酸锂、四氧化三钴混合 6h，将混合均匀的物料于 1000℃烧结 14h，冷却至室温，破碎过筛即得钴酸锂材料，一次粒子中粒径约为 12 ～ 14um，产品电性能见表 1。

AMPEREX Ex. 1002
Page 1144

[0025] 对比例 2

[0026] 将 Li ： (Co+Al) 摩尔比为 1.04 ： 1 的碳酸锂、四氧化三钴、氢氧化铝混合 6h，于 1000℃烧结 14h，冷却至室温，破碎过筛即得钴酸锂材料，一次粒子中粒径约为 12 ～ 16um，产品电性能见表 1。

[0027] 实施例 1

[0028] 按 Li ： Co 摩尔比为 1.04 ： 1 的碳酸锂、羟基氧化钴混合 6h，于 700℃烧结 14h，冷却至室温，破碎过筛即得前驱体。

[0029] 将摩尔比为 1 ： 0.01 ： 0.005 的前驱体、MnO_2、Al_2O_3 混合 4h，于 900℃烧结 6h，冷却至室温，破碎过筛即得改性钴酸锂材料，如图 1 所示，一次粒子中粒径约为 12 ～ 25μm，其产品电性能见表 1。

[0030] 实施例 2

[0031] 将 Li ： Co ： Mn 摩尔比为 0.95 ： 1 ： 0.02 的氢氧化锂、草酸钴、二氧化锰混合 5h，于 1200℃烧结 14h，冷却至室温，破碎过筛即得前驱体。

[0032] 将摩尔比为 1 ： 0.001 ： 0.05 的前驱体、ZrO_2、$K_2C_2O_4 \cdot H_2O$ 混合 4h，于 300℃烧结 6h，冷却至室温，破碎过筛即得改性钴酸锂材料，一次粒子中粒径约为 12 ～ 18um，其产品电性能见表 1。

[0033] 实施例 3

[0034] 将 Li ： Co ： B 摩尔比为 1.08 ： 1 ： 0.05 的碳酸锂、四氧化三钴、五氧化二硼混合 8h，于 1000℃烧结 14h，冷却至室温，破碎过筛即得前驱体。

[0035] 将摩尔比为 1 ： 0.005 ： 0.01 的前驱体、Y_2O_3、$Mg(OH)_2$ 混合 4h，于 900℃烧结 6h，冷却至室温，破碎过筛即得改性钴酸锂材料，一次粒子中粒径约为 12 ～ 18um，其产品电性能见表 1。

[0036] 实施例 4

[0037] 按 Li ： Co 摩尔比为 1.05 ： 1 的氢氧化锂、氧化亚钴和四氧化三钴混合 5h，于 700℃烧结 14h，冷却至室温，破碎过筛即得前驱体。

[0038] 将该摩尔比为 1 ： 0.001 ： 0.02 的前驱体、$NiCl_2$、$CaSO_4$ 混合 4h，于 600℃烧结 6h，冷却至室温，破碎过筛即得改性钴酸锂材料，一次粒子中粒径约为 12 ～ 19um，其产品电性能见表 1。

[0039] 实施例 1-4 和对比例 1-2 中的钴酸锂材料与炭黑、聚偏氟乙烯 (PVDF) 按 94％ ： 3％ ： 3％重量比配料并拉浆成极片，负极采用人造石墨，中间加隔膜卷绕、并注液后，加工成 053048 方型铝壳电池；测试电池的电化学性能：

[0040] 根据锂离子电池国家标准 GB/T18287-2000：C 是额定容量，表示以 5h 率放电至终止电压所应提供的电量，单位为 Ah 或 mAh。1C5A 充放电循环是指在 20±5℃条件下，以 1C5A 充电至 4.2V，转恒压充电至充电电流≤ 0.01C5A，再以 1C5A 放电至 2.75V，形成 1 个周期，之后再重复 1C5A 充 / 放电过程。1C5A 高温充放电循环是指在 60±2℃条件下，以 1C5A 充电至 4.2V，转恒压充电至充电电流≤ 0.01C5A，再以 1C5A 放电至 2.75V，形成 1 个周期，之后再重复 1C5A 充 / 放电过程。放电比容量是指 0.2C5A 充放电时，放电状态下每克正极材料释放的容量，单位是 mAh/g。

[0041] 85℃存储的测试方法为：1、根据电池制作要求，选择活化过程中 1C 恒流放电容量

AMPEREX Ex. 1002
Page 1145

在平均值范围内的电池 3 只，把放电容量记为 C_1，从电池柜卸下之后，测试每只电池的存储前的内阻和电压，确保内阻在 50mΩ 以下，电压在 4.17V 以上。如所选电池不满足要求，则重新选取直至 3 只电池均满足。2、把选好的电池放进烘箱，升温至 85℃，并使温度稳定 10min。设定烘箱恒温时间 4h，恒温 4h 终止后立即将电池取出在空气中冷却至室温，重新检测电池的厚度、内阻和开路电压，并记录。3、将电池装到电池检测仪，1C 恒流放电到 2.75V，再按各体系循环 6 次放电完全后记录电池各次放电容量，存储完的第一周放电容量记为 C_2。$(1-C_2/C_1)$ 即为高温存储容量损失率。

[0042] 表 1 为实施例 1-4 和对比例 1-2 的电性能测试结果。

[0043] 表 1 电性能测试结果

[0044]

样品	放电比容量 (mAh/g)	300 周容量保持率	85℃高温存储容量损失率
实施例 1	154	88.54%	4.52%
实施例 2	153	86.24%	3.36%
实施例 3	156	89.29%	3.02%
实施例 4	155	87.78%	4.23%
对比例 1	152	63.26%	17.03%
对比例 2	150	81.45%	10.49%

AMPEREX Ex. 1002
Page 1146

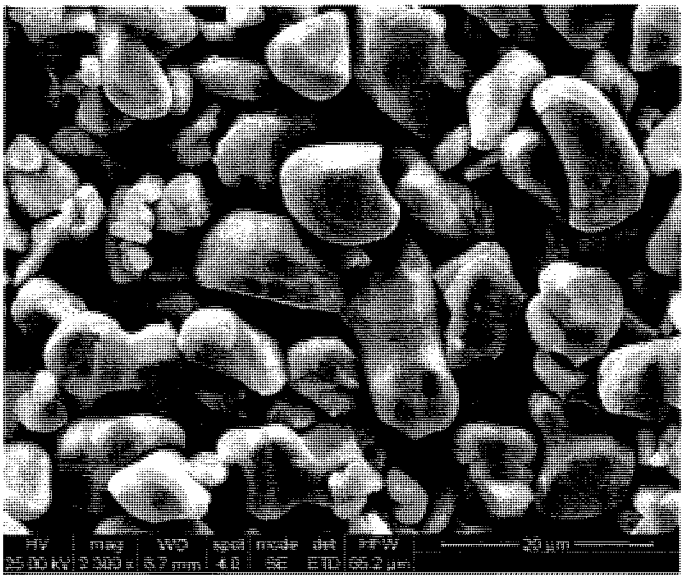


图 1

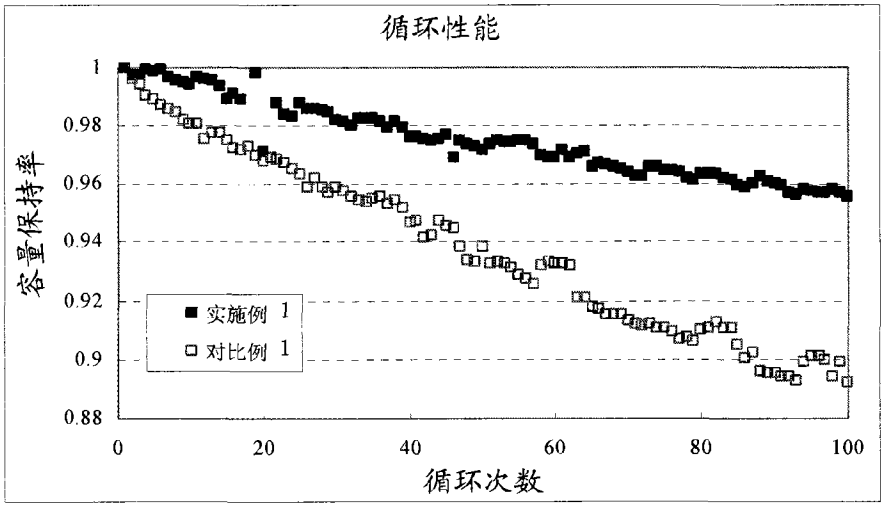


图 2

AMPEREX Ex. 1002
Page 1147

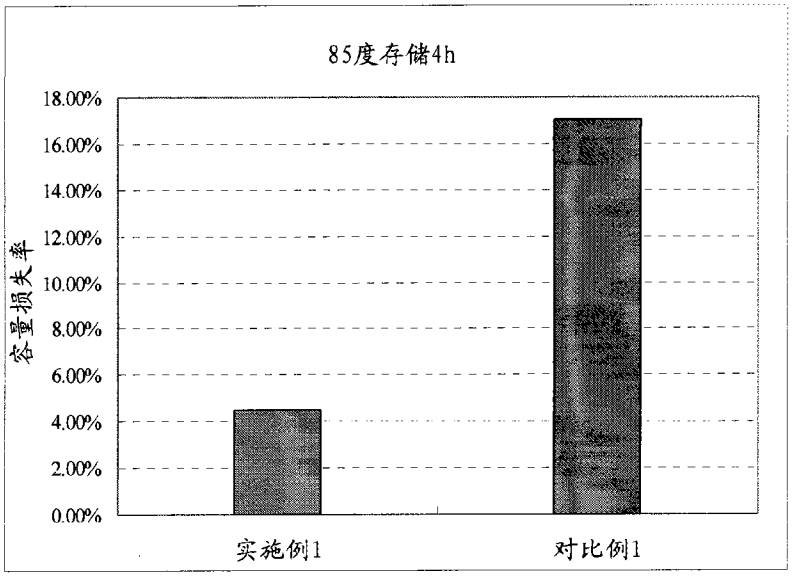


图 3

AMPEREX Ex. 1002
Page 1148

Available online at www.sciencedirect.com

SCIENCE DIRECT®

Solid State Ionics 170 (2004) 159–171

SOLID STATE IONICS

www.elsevier.com/locate/ssi

$LiCoO_2$: formation, structure, lithium and oxygen nonstoichiometry, electrochemical behaviour and transport properties

Ermete Antolini*

Scuola di Scienza dei Materiali, Via 25 aprile 22, 16016 Cogoleto, Genova, Italy

Received 10 November 2003; received in revised form 26 March 2004; accepted 1 April 2004

Abstract

The formation, structure and transport properties of $LiCoO_2$ are described. $LiCoO_2$ exhibits two crystal structures, depending on both the preparation method and synthesis temperature. High temperature lithium cobalt oxide (HT-$LiCoO_2$) has a hexagonal layered structure, while the low temperature oxide (LT-$LiCoO_2$) has a cubic spinel-related structure. The dependence of the morphological characteristics (grain size, size distribution, crystallinity) of $LiCoO_2$ on synthesis method as well as their effect on the electrochemical properties are extensively reviewed. As the electrochemical properties and the electrical conductivity strongly depend on the structure of the oxide, primary attention is given to lithium cobalt oxide with defect structure and lithium and oxygen nonstoichiometry.
© 2004 Elsevier B.V. All rights reserved.

Keywords: $LiCoO_2$; Crystal structure; Defects; Electrical conductivity; Li-batteries

1. Introduction

Lithium cobalt oxide ($LiCoO_2$) has been attracting worldwide interest for its application as cathode material in lithium ion batteries because this material exhibits high specific capacity, low self discharge and excellent cycle life [1–3]. This material is also used in molten carbonate fuel as the coating of NiO cathode with $LiCoO_2$ improves its stability during cell operation [4–6]. Finally, thin films of $LiCoO_2$ are used as electrochromic material [7]. The crystallinity, the average particle size and particle size distribution of this material are important factors in achieving high performance rechargeable lithium batteries, and depend strongly on starting materials and/or preparation method. Many researchers prepared $LiCoO_2$ by solid-state reaction. Using this method, owing to insufficient mixing and the low reactivity of the starting materials, calcination at 850–900 °C for several hours is required to synthesize $LiCoO_2$. The prolonged calcination at elevated temperatures causes the inevitable coarsening of the powder and the evaporation of lithium species, which significantly impair the electrochemical properties of the product. For these reasons, to obtain ultrafine well-crystallized $LiCoO_2$ powders with uniform size distribution, many efforts have been addressed to investigate various synthesis methods, as sol–gel method, spray-drying method, combustion synthesis, hydrothermal synthesis, and so on. The crystal structure and magnetic properties of the complex oxides of the $LiMO_2$ series (M = transition 3d metal) were reviewed by Kellerman [8]. The present work deals on the formation, structure and transport properties of lithium cobalt oxide, with particular attention to nonstoichiometric $LiCoO_2$.

2. Structure and formation

$LiCoO_2$ exhibits two forms, a hexagonal structure and a cubic structure. The definition, used also in this paper, regarding the two types of $LiCoO_2$ as low temperature (LT-$LiCoO_2$), the cubic form, and high temperature (HT-$LiCoO_2$), the hexagonal form, lithium cobalt oxide is not appropriate, considering that HT-$LiCoO_2$ is obtained also at very low temperatures. The hexagonal and cubic structures are based on the same oxide sublattice, and are distinguished by the spatial arrangement of cations. In the following we have reviewed the method of preparation and the structural and morphological characteristics of lithium cobalt oxides in three separated sections: LT-$LiCoO_2$, HT-$LiCoO_2$ and defective and non-stoichiometric $LiCoO_2$.

* Tel.: +39-109182880; fax: +39-109182368.
E-mail address: ermantol@libero.it (E. Antolini).

0167-2738/$ - see front matter © 2004 Elsevier B.V. All rights reserved.
doi:10.1016/j.ssi.2004.04.003

2.1. Low temperature lithium cobalt oxide (LT-$LiCoO_2$)

Gummow et al. [9,10] using neutron diffraction data showed that the structure of LT-$LiCoO_2$ is not ideally layered, and 6% of the cobalt ions resides in the octahedral (8a) sites of the lithium layers. According to Rossen et al. [11], LT-$LiCoO_2$ is believed to adopt a spinel-relate structure (space group $Fd3m$) based on a cubic closed packed oxygen network with alternating cation layers of 0.75 Co, 0.25 Li and 0.75 Li, 0.25 Co composition perpendicular to each of the four cubic [111] direction. The cell parameters reported by Gummow et al. [9] are 2.8297(6) Å for the a-value and 13.868(4) Å for the c-value. The aspect ratio of the spinel (c/a in the range 4.900–4.914) is close to that of the ideal cubic close packing oxygen array ($c/a = 4.899$). Efforts to obtain lithiated $Li_2[Co_2]O_4$ spinel structure with the ideal c/a ratio were unsuccessful [13]. Because the cation distribution in this compound is intermediate between layered and spinel type structure and because of the strong resemblance of the X-ray and neutron diffraction patterns to that of a lithiated spinel structure $Li_2[Co_2]O_4$, it is referred as a quasi-spinel phase [12,13].

The preparation methods and the morphological characteristics of LT-$LiCoO_2$ are reported in Table 1. In most of the reports concerning LT-$LiCoO_2$, the characterized product was contaminated with an appreciable amount of HT phase and/or unreacted Co_3O_4, Li_2CO_3, or $LiNO_3$, depending upon the starting compounds and synthesis procedure. High-level mixing of the starting materials is very important in preparing single-phase LT-$LiCoO_2$. Also, synthesis temperature needs to be kept below 400 °C to avoid HT phase formation. It appears that as temperature increased, structural change occurred (LT-to-HT phase). As previously theorized by Antolini [20], from X-ray diffraction (XRD) and transmission electron microscope (TEM) data Shao-Horn et al. [21] found that $Li_2[Co_2]O_4$ (LT-$LiCoO_2$) nucleates from an intermediate $Li_xCo_{1-x}[Co_2]O_4$ spinel product before transforming more slowly into layered $LiCoO_2$. They observed also that layered $LiCoO_2$ is more stable at 400 °C than the lithiated-spinel structure. According to the authors, the non-ideal cation distribution in $Li_2[Co_2]O_4$, nonstoichiometry and kinetic factors restrict the transformation of the lithiated-spinel structure to layered $LiCoO_2$ at this temperature.

2.2. High temperature lithium cobalt oxide (HT-$LiCoO_2$)

The structure of HT-$LiCoO_2$ belongs to the trigonal system (space group $R3m$, O_3 phase) with an ideal G-$NaFeO_2$ layered structure, in which Co and Li planes alternate in the ABCABC oxygen stacking [22]. The cell parameters reported in literature are in the range 2.815–2.816 Å for the a value (intralayer metal–metal distance), and in the range 14.05–14.08 Å for the c-value (interslab distance) [22–27]. The value of c/a ratio is in the range 4.98–5.00 and is significantly larger than that of an ideal cubic closed packed lattice ($c/a = 4.899$). By the Rietveld refinement of X-ray and neutron diffraction spectra [28], both the presence of Co in the Li site and the presence of tetrahedral Li and Co ions were excluded. At first, $LiCoO_2$ was prepared by solid state reaction. Solid state synthesis is a simple and inexpensive method of producing a ceramic powder, the precursor being simply ground and mixed together before being calcined at 850–900 °C. $LiCoO_2$ solid state synthesis may start from many different precursors: Li_2O_2 and CoO [27], Li_2CO_3 and Co_3O_4 [29], Li_2CO_3 and Co [30], $LiOH{\cdot}H_2O$ and $CoCO_3$ [31], Li_2CO_3 and $CoCO_3$ [32,33], $Li(CH_3COO){\cdot}2H_2O$ and $Co(CH_3COO)_2{\cdot}4H_2O$ [34,35]. Independent of Co precursor, $LiCoO_2$ formation reaction goes through the reaction of Li precursor and Co_3O_4 [30,35,36]. Using acetates as starting materials yields HT-$LiCoO_2$ below 500 °C, owing to the formation and the fast reaction at low temperature of intermediates compounds [34,35]. The kinetics of $LiCoO_2$ formation is largely influenced by the reactant particle size [33]. Lungblad and Bergman [37] found that CO_2 and O_2 partial pressure of the calcination atmosphere have a significant effect on the particle size of $LiCoO_2$ obtained by solid state reaction. Calcination at 900 °C for several hours lead to the formation of single-phase $LiCoO_2$, but with particle size >1

Table 1
Preparation methods and synthesis temperature and time, phase composition and morphological characteristics of LT-$LiCoO_2$, ordered with decreasing synthesis temperature

Reagents	Preparation method and synthesis temperature and time	Phase composition and morphological characteristics	References
$LiCl–Li_2CO_3$, $CoCl_2$	Molten salt synthesis 550 °C, 600 °C, 1 h	Mixed LT- and HT-$LiCoO_2$ 53% at 550 °C, 26% at 600 °C, particle size 10.95 μm at 600 °C	[14]
Li and Co nitrates	Sol–gel with maleic acid, 500 °C, 1 h	Polycrystalline LT-$LiCoO_2$, ultrafine particle size 0.03 μm	[15]
Li_2CO_3, $Co(NO_3)_2$	Citrate sol–gel method 400 °C, 120 h	Mixed LT- and HT-$LiCoO_2$, particle size <1 μm	[16]
LiOH, $CoCO_3$	Solid state synthesis 400 °C, 90 h	Mixed LT- and HT-$LiCoO_2$	[11]
LiOH, CoOOH	Mechanical activation 400 °C, 4 h	LT-$LiCoO_2$	[17]
Formate(f), acetate(a) and nitrate(n) as Li and Co precursors	Freeze drying synthesis 300–350 C (f, a), 1–2 h 250C(a, n), 1–2 h	Single phase LT-$LiCoO_2$	[18]
Li_2CO_3, Co_3O_4	Citric acid in the solid state reaction 300 °C, 100 h	Single phase LT-$Li_{1+x}CoO_2$ ($x = -0.2, 0.0, 0.2, 0.4$) BET surface area 19 $m^2\ g^{-1}$	[19]

AMPEREX Ex. 1002
Page 1150

μm. Indeed, the prolonged calcination at elevated temperatures causes the inevitable coarsening of the powder, which significantly impair the electrochemical properties of the material. Moreover, high temperature firing for an elongated period causes non-homogeneity, irregular morphology and a broader particle size distribution of $LiCoO_2$ powder. For these reasons, $LiCoO_2$ preparation by solid state synthesis using activated precursors or by other synthesis methods has

Table 2

Reagents	Preparation method and synthesis temperature and time	Phase composition and morphological characteristics	References
(a) Preparation methods, phase composition and morphological characteristics of HT-$LiCoO_2$, ordered with decreasing synthesis temperature (T in the range 900–750 °C)			
LiOH, Li_2O_2 and Co acetate	Co^{2+} oxidation reaction in solution, 900 °C, 3 days	HT-$LiCoO_2$	[38]
Li and Co nitrates	Emulsion dry method, 900 °C, 24 h	High crystalline HT-$LiCoO_2$, particle size <1 μm	[39]
LiOH, $Co(NO_3)_2$	Cobalt–organic acid complexes route, 900 °C, 20 h	Well-crystallised HT-$LiCoO_2$	[40]
Li and Co acetates	Water-in-oil emulsion process, 900 °C, 1 s	Monophasic HT-$LiCoO_2$, narrow size distribution 0.2–0.4 μm	[41]
Li_2CO_3, Co_3O_4, Li/Co 1.00–1.05	Hydrothermally precipitated Co_3O_4, followed by solid state synthesis, 800–900 °C, 10 h	Monodispersed HT-$LiCoO_2$, particle size 3 μm (Li/Co 1.00) to 8 μm (1.05)	[42]
Li_2CO_3 and Co acetate	Spray-dry method, followed by sintering in single or two steps at 800–900 °C for 12–20 h	Plate-like shaped HT-$LiCoO_2$, particle size 10 μm (single sintering step), 3–6 μm (two sintering steps)	[43]
Li and Co acetates	Freeze drying synthesis 850 °C, 24 h	Single phase HT-$LiCoO_2$	[18]
Li and Co acetates	Spray-dry method 800 °C, 4 h	HT-$LiCoO_2$, particle size 0.2–0.7 μm	[44]
Li and Co acetates	Aqueous solution based process, followed by sintering 800 °C, 2 h	HT-$LiCoO_2$ with regular cuboidal shape, crystallite size 0.4–0.6 μm	[45]
Li and Co nitrates	Non-aqueous solution process with tetramethyl ammonium oxalate, 800 °C	HT-$LiCoO_2$	[46]
Li_2CO_3, LiCl and $CoCl_2$	Molten salt synthesis 700–900 °C, 1 h	Single phase HT-$LiCoO_2$, particle size distribution shown in Fig. 1, particle size 7–14 μm	[14]
Li and Co nitrates	Polyacrylic acid sol–gel method, 750 °C, 10 h	Monodispersed rectangular HT-$LiCoO_2$, particle size 0.5 μm	[47]
(b) Preparation methods, phase composition and morphological characteristics of HT-$LiCoO_2$, ordered with decreasing synthesis temperature (T in the range 700–100 °C)			
Lithium and cobalt 2-ethylhexanoate	Metallorganic decomposition route, 700 °C, 8 h	Well organised HT-$LiCoO_2$, specific surface area 7.4 $m^2\ g^{-1}$	[48]
Li and Co nitrates	Solution-combustion method with starch, 700 °C, 3 h	Plate-like HT-$LiCoO_2$, narrow size distribution <1.6 μm	[49]
Li and Co nitrates	Microprecipitation in molten acid stearic, 700 °C, 6 h	Well ordered HT-$LiCoO_2$ with uniform shape, narrow size distribution, particle size <1 μm	[50]
Li and Co nitrates	Combustion synthesis with urea 600, 700 °C, 12 h	Single phase HT-$LiCOO_2$, particle size 0.15 μm	[51]
Li and Co acetates	Sol–gel method with acrylic acid 600 and 700 °C, 10 h	Single phase HT-$LiCoO_2$, particle size <1 μm	[52]
LiCl and $Co(OH)_2$	LiCl-flux method 650 °C, 4 days	Layered HT-$LiCoO_2$, particle size 1–5 μm	[53]
Li and Co acetates	Microwave synthesis 600 °C, 10 min	Fine and uniformly grained single-phase HT-$LiCoO_2$	[54]
Li and Co nitrates	Sol–gel method with maleic acid, 600 °C, 1 h	Polycrystalline HT-$LiCoO_2$, ultrafine particle size 0.06 μm	[15]
$LiNO_3$ and $Co(CH_3COO)_2$	Sol–gel method 600 °C, 5 h	HT-$LiCoO_2$, particle size 0.016 μm	[55]
LiOH and $Co(OH)_2$	Mechanical alloying 600 °C, 2 h	HT-$LiCoO_2$	[56]
Li and Co acetates	Citrate sol–gel method 550 and 750 °C, 10 h	Mono-dispersed spherical HT-$LiCoO_2$, particle size 0.03–0.05 μm	[57]
Li and Co nitrates	Sol–gel method with polyacrylic acid 550 °C, 1 h	Ultrafine uniformly sized HT-$LiCoO_2$, particle size 0.03–0.05 μm	[58]
LiOH and $Co(NO_3)_2$	Precipitation process in aqueous solution, 400 °C, 2 h	Layered HT-$LiCoO_2$	[59]
Li_2CO_3, $Co(NO_3)_2$	Thermal pyrolysis of Co/Li citrate compositions, 400 °C	HT-$LiCoO_2$, particle size 0.07–12 μm	[60]
LiOH and $Co(NO_3)_2$	Supercritical water synthesis 400 °C, 1 min	High crystalline HT-$LiCoO_2$, particle size <1 μm	[61]
LiOH and CoOOH	Hydrothermal reaction method, 150–250 °C, 0.5–24 h	Well crystallised plate-like HT-$LiCoO_2$, particle size 0.07–0.2 μm	[62]
LiOH and $Co(OH)_2$	Reflux reaction method 130–200 °C, 6–48 h	Well crystallised HT-$LiCoO_2$, particle size 0.1 μm	[63]
LiOH and CoOOH	Ion exchange reaction 100 °C, 3 days	Impurity containing HT-$LiCoO_2$, particle size 0.08–0.2 μm	[64]

AMPEREX Ex. 1002
Page 1151

been investigated, as reported in Table 2. As can be seen in Table 2, the sol–gel preparation method requires a much lower calcination temperature (550–750 °C) and shorter calcination time (1–10 h) than the solid-state reaction where the calcination temperature is almost 900 °C and the calcination time is more than 24 h, resulting in a lower $LiCoO_2$ particle size. Low temperature methods have been developed to obtain HT-$LiCoO_2$, using highly reactive precursors, as CoOOH and $Co(OH)_2$. Synthesis temperature was in the range 100 to 250 °C, without formation of LT-$LiCoO_2$ phase. On the other hand, HT-$LiCoO_2$ preparation by water-in-oil emulsion process, supercritical water synthesis and microwave synthesis required very low synthesis times, 1 s (soak at 900 °C), 1 min (total process) and 10 min (calcination at 600–900 °C), respectively (Fig. 1).

Most preparation methods, as sol–gel and low temperature synthesis, lead to the formation of ultrafine $LiCoO_2$ powders with submicron average particle size. As can be seen in Table 2, the molten salt synthesis, instead, lead to formation of $LiCoO_2$ with the highest particle size. Antolini et al. [65] investigated the effect of the presence of molten Li_2CO_3 on $LiCoO_2$ particle size during the synthesis of non-stoichiometric lithium cobalt oxide (Li/Co>1) from $CoCO_3$ and excess Li_2CO_3. As shown in Fig. 2, at 800 °C and in the presence of excess Li_2CO_3 (Li_2CO_3 melting point 723 °C) a remarkable decrease of the specific surface area of the samples takes place, the molten Li_2CO_3 acting as a flux medium during the synthesis. This could to low the electrochemical performance of the material. But, unlikely from the opinion of many authors, which focused their efforts to obtain ultrafine $LiCoO_2$ powders, regarding the detrimental effect of $LiCoO_2$ powders with large particle size on Li-batteries operation, according to Levasseur et al. [66] the increase of particle size increases battery security in charge state, and according to Han et al. [14] a large particle size improves the specific capacity and cycle life of the powder in Li-batteries.

As it can be inferred from the results of the various $LiCoO_2$ synthesis process, there exist different reaction mechanisms in the formation of HT-$LiCoO_2$, depending

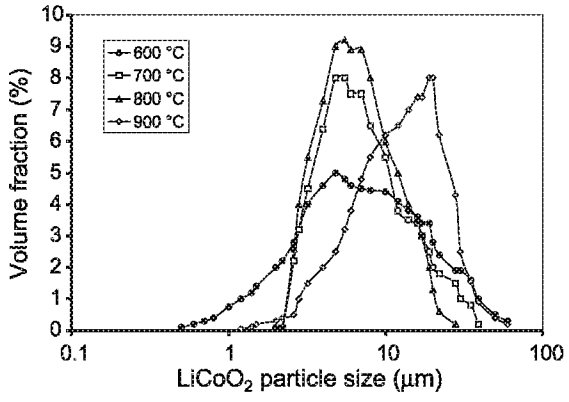


Fig. 1. Particle size distribution in $LiCoO_2$ samples prepared at various temperatures for 24 h [14].

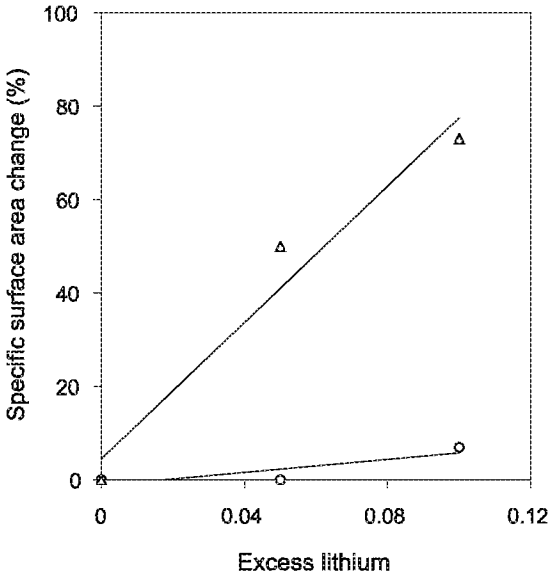


Fig. 2. Change of $LiCoO_2$ specific surface area, referred to excess lithium = 0, vs. excess lithium at 700 (○) and 800 (△) °C [65].

on the preparation method. By solid state reaction and low temperature synthesis using cobalt hydroxides, layered $LiCoO_2$ is obtained without the formation of intermediates lithium cobalt compounds. By other synthesis methods, as combustion synthesis, mechanical activation, freeze-drying and molten salt synthesis, hexagonal $LiCoO_2$ is formed by the transformation of LT in HT lithium cobalt oxide. By cobalt oxidation reaction in solution HT-$LiCoO_2$ is obtained through the formation of lithium overstoichiometric $Li_{1+x}Co_{1-x}O_2$.

3. Defect structure and non-stoichiometry in $LiCoO_2$

Many efforts have been devoted to synthesize $LiCoO_2$ with structural disordering. The structure of these materials should be more stable to intercalation/deintercalation of lithium ions in the course of discharge/charge processes in Li-batteries, thus providing better electrochemical behaviour and preventing structural distortion. Structural disordered $LiCoO_2$ can be achieved by cation or anion nonstoichiometry, cation mixing, and a disturbance of oxygen layers stacking. Generally, it corresponds to the weakening of *d*-ions correlation, resulting in the full localization of *d* electrons on the transition metals ions.

3.1. Defect structure

The preparation method and the structural characteristics of some defective $LiCoO_2$ compounds are reported in Table 3. The unusual O_2-type (the letter O describes the alkali ion site (O = octahedral) and the number 2 indicates the number of slabs within the hexagonal cell) $LiCoO_2$ phase was characterized by by Rietveld refinement of the X-ray and

AMPEREX Ex. 1002
Page 1152

Table 3
Preparation methods and the structural characteristics of some defective $LiCoO_2$

Reagents	Preparation method	Characteristics	References
P2–$Na_{0.7}CoO_2$	Li/Na ion exchange	O_2LiCoO_2 phase	[67]
LiOH, COOH	Mechanical activation 400/600 °C	Defective HT-$LiCoO_2$ (oxygen vacancy, O^- ions)	[17]
Li_2CO_3, $Co(NO_3)_2$	Solution-combustion 350/850 °C, 5 min/6 h	HT-$LiCoO_2$, anomalous cell parameters	[68]
LiCl, $Co(OH)_2$	Flux method, 650 °C	HT-$Li_{0.88}CoO_2$, anomalous peak intensity	[53]
HT-$LiCoO_2$	Ball milling	Disordered $Li_xCo_{1-x}O$ rock salt phase	[69]
HT-$LiCoO_2$	Non-reactive grinding	Disordered $Li_xCo_{1-x}O$ rock salt phase	[17]

neutron diffraction patterns. In the O_2 packing, the lithium ions occupy only the octahedral sites, even if the strong Li^+–Co^{3+} electrostatic repulsion occurring through the common face of the CoO_6 and LiO_6 octahedra leads to small displacement of the lithium and cobalt ions from the center of their octahedra. Magnetic measurements and ^7Li MAS NMR confirm a composition very close to the ideal one for O_2 phase. The O_2–$LiCoO_2$ phase is metastable and transforms to well-crystallized O_3–$LiCoO_2$ upon heating [67].

Disordered HT-$LiCoO_2$ synthesized by Kosova et al. [17] was characterized by $Co^{3+}O_6$ octahedra less perfect than those of ceramic $LiCoO_2$. In as-prepared $LiCoO_2$ the main electronic state of cobalt ions is a low-spin $[Co^{3+}]_{Oh}$ with some oxygen crystal field nonhomogeneity, probably due to the formation of oxygen defects. Diffuse reflectance electron spectroscopy measurements indicated that all observed *d*-electrons are localized. The main reason is probably the formation of definite mechanochemically induced defects (e.g., oxygen vacancies, O^- ions), which are preserved even after heating at 600 °C. These defects appeared to act as traps for delocalized electrons, producing cobalt ions with localized electrons.

Layered lithium cobalt oxides with anomalous cell parameters [68] or anomalous XRD peak intensity ratio [53], related to a defective or oriented structure, were synthesised by Rodrigues et al. and Tang et al., respectively. A discharge capacity close to the theoretical value and a high discharge/charge efficiency of this compound in Li-batteries was observed by Tang et al. [53].

By mechanical activation [69] and non-reactive grinding [17] of HT-$LiCoO_2$, owing to lithium and oxygen loss, due to noticeable instability of $LiCoO_2$ under mechanical loading, disordered cubic $Li_xCo_{1-x}O$ structures were obtained.

3.2. Nonstoichiometry

3.2.1. Li/Co<1

3.2.1.1. Spinel structure. Some preparation methods of LT-$LiCoO_2$ with Li/Co<1 are reported in Table 4. Elec-

Table 4
Preparation methods and phase composition of non-stoichiometric $LiCoO_2$, reported in the following order: LT-$LiCoO_2$ (Li/Co<1), HT-$LiCoO_2$ (Li/Co<1), HT-$LiCoO_2$ (Li/Co>1) and HT-$LiCoO_{2-\delta}$

Reagents	Preparation method	Phase composition	References
	LT-$LiCoO_2$ with Li/Co<1		
Li_2Co_3, $CoCO_3$	Solid state synthesis 400 °C, 1 week	LT-$Li_{1-x}Co_{1+x}O_2$ $x=0.02$	[9]
LT-$LiCoO_2$	Electrochemical Li extraction	LT-Li_xCoO_2 $0.1<x<1$	[9]
LT-$LiCoO_2$	Chemical Li extraction with $Na_2S_2O_8$	$Li[Co_2]O4$	[70]
LT-$LICoO_2$	Chemical Li extraction with NO_2BF_4	$Li_{1-x}[Co_2]O_{4-\delta}$ $0.44 \le (1-x) \le 1$	[71]
HT-$LiCoO_2$	Chemical Li extraction	LT-Li_xCoO_2, $x<1$	[72]
Li, Co precursors Li/Co <1	Solid state reaction	LT-Li_xCoO_2, $x<1$	[72]
HT-$LiCoO_2$	Electrochemical Li extraction	LT-Li_xCoO_2, $x<1$	[73]
	HT-$LiCoO_2$ with Li/Co<1		
Li_2CO_3, Co_3O_4 Li/Co=0.90	Solid state synthesis at 900 °C	HT-$Li_yCo_{2-y}O_2$ (stable at T>860 °C), $0.82<y<1$	[74]
HT-$LiCoO_2$	Thermal treatment at T>900 °C	HT-$Li_yCo_{2-y}O_2$ (stable at T>860 °C)	[75,76]
Li, Co precursors Li/Co<1	Solid state reaction at 900 °C	HT-Li_xCoO_2 $0.9<x\le 1$	[28,77]
HT-$LiCoO_2$	Electrochemical Li extraction	HT-Li_xCoO_2 $0.5\le x<1$	[23,25,78–82]
HT-$LiCoO_2$	Chemical extraction	HT-$Li_{0.5}CoO_2$	[70]
	HT-$LiCoO_2$ with Li/Co>1		
Li_2CO_3, Co_3O_4 Li/Co>1	Solid state synthesis 900 °C	HT-Li_xCoO_2 $1<x\le 1.30$	[28,83]
Li_2CO_3, $CoCO_3$ Li/Co>1	Solid state synthesis 900 °C	HT-Li_xCoO_2 $x=1.065$	[77]
LiOH, Co_3O_4	Solid state synthesis 850 °C	HT-Li_xCoO_2	[84,85]
	HT-$LiCoO_{2-\delta}$		
Li_2CO_3, Co Li/Co 0.11 and 0.25	Solid state synthesis 900–1200 °C	HT-$LiCoO_{2-\delta}$ $\delta=0.09$–0.14	[87]
HT-$LlCoO_2$	Oxygen extraction by thermal treatment under reduced O_2 pressure	HT-$LiCoO_{2-\delta}$	[66,88,89]

AMPEREX Ex. 1002
Page 1153

trochemical lithium extraction from LT-$LiCoO_2$ revealed the existence of a two-phase domain for Li_xCoO_2 ($0.1 < x < 0.95$). The two-phase behaviour of LT-$LiCoO_2$ electrode is consistent with a phase transition between a rock salt structure in which the cations occupy only octahedral sites and a spinel-type structure in which the cations occupy both octahedral and tetrahedral sites. The essentially ideal cubic close packing oxygen array surprisingly is maintained during lithium extraction [9]. Efforts to obtain ideal $Li[Co_2]O_4$ spinel structure from a starting mixture with Li/Co atomic ratio 0.5 at low temperature were unsuccessful [13]. $Li[Co_2]O_4$ and $Li_{1-x}[Co_2]O_{4-\delta}$ spinel oxides were obtained by chemically extracting lithium from LT-$LiCoO_2$ [70,71]. The $Li[Co_2]O_4$ spinel is metastable, and it disproportionates with the loss of oxygen to give $LiCoO_2$ and Co_3O_4 on heating at $T>200$ °C. Rietveld analysis of the X-ray diffraction data revealed that the $Li_{1-x}[Co_2]O_{4-\delta}$ samples adopt the normal cubic spinel structure. Redox iodometric titration data indicated that the LT-$LiCoO_2$ tends to lose oxygen on extracting lithium, and, as a consequence, the delithiated spinel samples are oxygen deficient [70].

Recent studies carried out using Raman scattering spectroscopy on Li_xCoO_2 obtained both by solid state reaction using precursors with Li/Co < 1 and by chemical delithiation of HT-$LiCoO_2$ indicated the formation of spinel lithium cobalt oxide on the grain surface [72]. Such changes, affecting only the grain surface, may not be observable by diffraction.

The formation of the spinel phase upon electrochemical lithium deintercalation from layered $LiCoO_2$ was proposed by Gabrisch et al. [73]. According to the authors, a transmission electron microscopy study of this material after a large number of charge/discharge cycles (344 cycles between 4.2 and 2.9 V) showed that the initial HT-$LiCoO_2$ transformed partially to a cubic spinel phase, especially on the surface of the particles.

3.2.1.2. Layered structure. There are two kinds of layered $LiCoO_2$ with Li/Co < 1: (a) $Li_yCo_{2-y}O_2$ solid solution of CoO in $LiCoO_2$ (Li + Co = O, presence of Co^{2+} ions); (b) Li_xCoO_2 (Li + Co < O, presence of Li vacancies and Co^{4+} ions). Table 4 shows some preparation methods and phase composition of HT-$LiCoO_2$ with Li/Co < 1.

From X-ray diffraction and thermogravimetric measurements Moore and White [74] postulated the formation of layered $Li_y{Co^{3+}}_y{Co^{2+}}_{2(1-y)}O_2$ solid solution from Li_2CO_3 and Co_3O_4 with Li/Co = 0.90 at temperature higher than 860 °C. According to the authors, the value of y for Co saturated $Li_yCo_{2-y}O_2$ is 0.82. The value of y increases with decreasing temperature, transforming $Li_yCo_{2-y}O_2$ to stoichiometric $LiCoO_2 + Co_3O_4$.

Li_xCoO_2 is obtained by chemical delithiation of HT-$LiCoO_2$ and by electrochemical cycling of HT-$LiCoO_2$ in Li-batteries. Its formation by synthesis from precursors within Li/Co atomic ratio <1 and by heat treatment of $LiCoO_2$ at $T>900$ °C is doubtful.

Many works have been devoted to the study of phase changes upon lithium deintercalation from HT-$LiCoO_2$ [23,25,78–82]. The cyclic voltamogram shown in Fig. 3 attests the structural changes of $LiCoO_2$ in the potential region from 3.5 to 4.2 V vs. Li/Li^+. The three cathodic and anodic peaks correspond to as many $LiCoO_2$ structural changes. The first peak at 3.970 V is related to the existence of a two-phase domain for Li_xCoO_2 ($0.75 < x < 0.94$) and the third peak at 4.195 V to the presence of a monoclinic distortion for $x = 0.5$ due to an interslab Li/vacancy ordering. The phase change related to the second peak at 4.086 V, observed only on $LiCoO_2$ sample prepared by supercritical water synthesis [61], is unidentified. In layered $LiCoO_2$, removal of lithium ions upon electrochemical cycling decreases the electrostatic shielding between O–Co–O sheets which leads to an increase in c/a ratio from 4.99 at full Li content to 5.13 in $Li_{0.5}CoO_2$ [81]. Evolution of the cell parameters during lithium deintercalation in LT-$LiCoO_2$, HT-$LiCoO_2$ and $Li_{1.1}CoO_2$ is shown in Fig. 4. The c-parameter of HT-$LiCoO_2$ and $Li_{1.1}CoO_2$ increases due to the increase of the electrostatic repulsion between adjacent oxygen layers, while the a-parameter decreases owing to cobalt oxidation. The cell parameters of LT-$LiCoO_2$, instead, maintain the same value during lithium deintercalation.

Lithium and vacancy ordering phenomenon and the monoclinic distortion in $Li_{0.5}CoO_2$ was studied by Shao-Horn et al. [82] using X-ray and electron diffraction measurements. They showed that the observed peak splitting, indicative of monoclinic distortion, is due primarily to the shearing of the rhombohedral oxygen lattice. Experimental electron diffraction studies of a monoclinic $Li_{0.5}CoO_2$ sample revealed additional reflections that were consistent with the in-plane ordering configuration of lithium and vacancy proposed previously by Reimers and Dahn [78]. They also assumed that the electron diffraction pattern

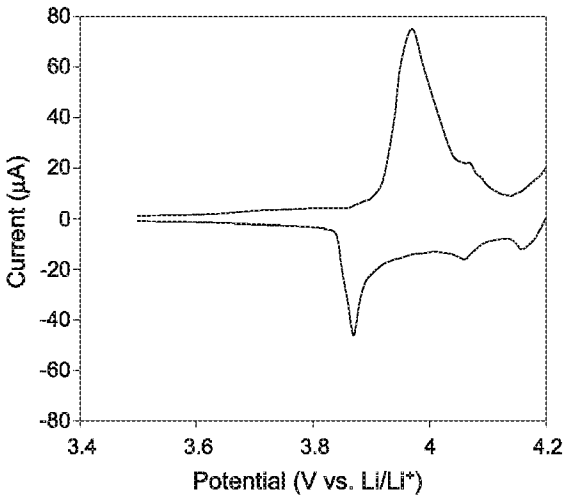


Fig. 3. Cyclic voltammogram of $LiCoO_2$ prepared by supercritical water synthesis in a mixed solvent of diethyl carbonate and ethylene carbonate with 1.0 mol dm^{-3} $LiClO_4$ at 1.0 mV min^{-1} [61].

AMPEREX Ex. 1002
Page 1154

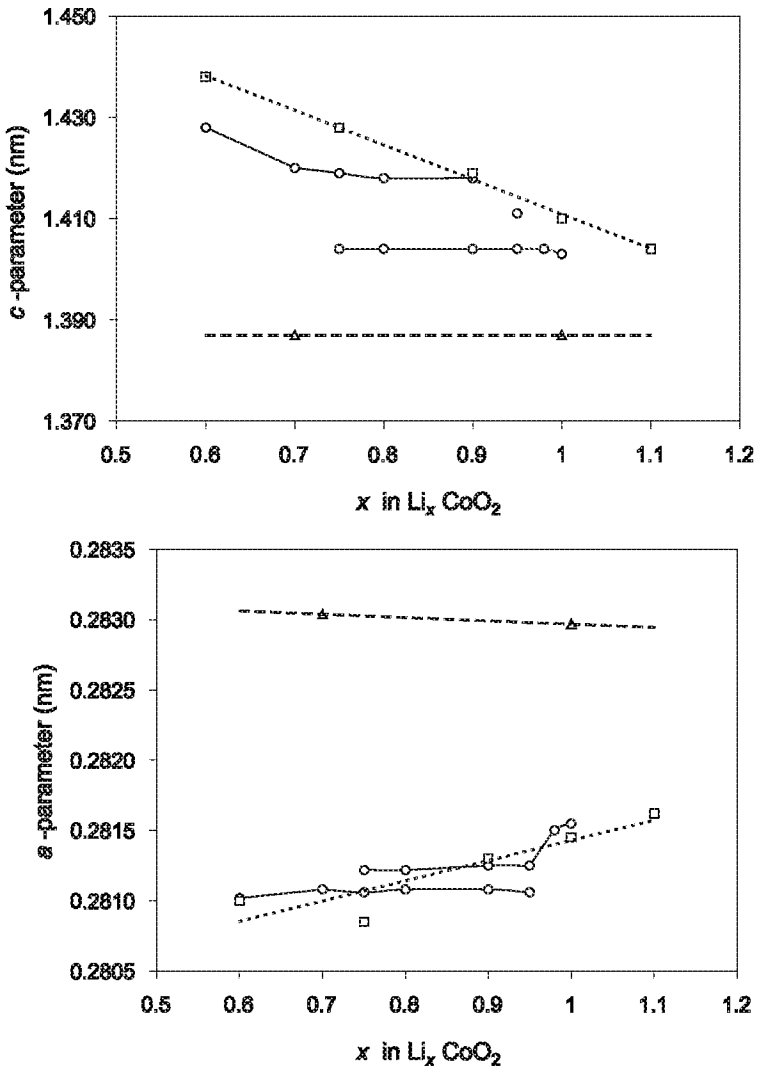


Fig. 4. Variation of the cell parameters for LT-$LiCoO_2$ (△) [9], HT-$LiCoO_2$ (○) [80] and lithium overstoichiometric $Li_{1.1}CoO_2$ (△) [28] deintercalated samples ($0.60 \leq x \leq 1.10$).

with appearances resembling those of the spinel structure could be explained fully by the formation of mazed microstructure and lithium ordering in $Li_{0.5}CoO_2$. According to the authors, there was no evidence of the layered to spinel transformation in the Li_xCoO_2 system. To confirm this assertion, according to Choi and Manthiran [70], $Li_{0.5}CoO_2$ maintains the layered structure even after heating at 200 °C.

3.2.2. Li/Co> 1

Lithium overstoichiometry in $LiCoO_2$ was first mentioned by Carewka et al. [83]. The preparation methods of Li_xCoO_2 with $x>1$ are presented in Table 4. As previously denoted, the presence of excess Li_2CO_3, acting a flux medium during the synthesis, increases the particle size (approximately 20 μm for Li_xCoO_2 with $x=1.10$ [28]). The lattice parameters of Li_xCoO_2 ($x>1$) are similar to those of stoichiometric $LiCoO_2$ [28]. By a detailed ^6Li and ^7Li NMR study of Li_xCoO_2, Carewska et al. [83] found that only a small amount of lithium (<20% of the excess) enters the structure ionically while reducing the formal Co valence. Most of the excess consists of unreacted Li_2CO_3. Another small portion of the excess Li (about 10%) appears to enter interstitial sites in close proximity to paramagnetic Co^{2+} ions. Moreover, they observed a decreasing average cobalt oxidation state with increasing nominal Li/Co ratio. By ^7Li and ^{59}Co NMR measurements, Peeters et al. [77] provided evidence of the existence of paramagnetic Co species in overlithiated Li_xCoO_2. Ganguly et al. [86], by a ^{59}Co NMR study, proposed the presence of Co^{2+} species in Li_xCoO_2 with $x>1$. ^7Li MAS NMR spectra showed three new signals in addition to the signal resulting from the presence of diamagnetic Co^{3+} ions, suggesting the presence of divalent cobalt ions in the low-spin configuration. X-ray and neutron diffraction results excluded the presence of interstitial lithium ions in these materials. Simulations of X-ray patterns of Li_xCoO_2 ($x>1$) materials allowed us to reject the hypothesis of the existence of stacking faults. On these bases Levasseur et al. [28] hypothesized the presence of

AMPEREX Ex. 1002
Page 1155

structural defects involving low-spin Co^{2+} ions and a simultaneous cobalt and oxygen deficiency leading to the chemical formulae $[Li]_{interslab}[Co_{1-t}\square_t]_{slab}[O_{2-\delta}]$ or $[Li]_{interslab}[Co_{1-t}Li_t]_{slab}[O_{2-\delta}]$ with $\delta > t$ for Li_xCoO_2 ($x>1$). The presence or not of lithium on the cobalt crystallographic site cannot be ascertained. The most important fact would be the existence of an oxygen deficiency in Li_xCoO_2 ($x>1$) materials. Imanishi et al. [84] assumed that lithium overstoichiometric Li_xCoO_2 materials, with the solid solution limit of excess lithium around 1.15, contain oxygen defects in order to maintain electronic neutrality. In another work, Imanishi et al. [85] carried out an accurate titration of the cobalt oxidation state in various Li_xCoO_2 ($x>1$) samples and concluded that only Co^{3+} ions are present in the lithium overstoichiometric Li_xCoO_2 phases, with a solid solution limit close to $x=1.08$.

In the light of these results and from NMR and magnetic data, in a more recent work, Levasseur et al. [66] deduced that the excess lithium replaces some cobalt ions, and the charge is simply compensated by oxygen vacancies. Considering that no extra Li was found in the tetrahedral site, they inferred that the lithium overstoichiometric Li_xCoO_2 samples have a formula $[Li]_{interslab}[Co_{1-t}Li_t]_{slab}[O_{2-t}]$, $t=(x-1)/(x+1)$ in which all the cobalt ions are trivalent and the charge deficit associated with a Li ion in a cobalt site is compensated for by an O vacancy. They proposed that the trivalent cobalt ions adjacent to oxygen vacancies adopt an intermediate spin state, where the d_{z2} orbital is strongly stabilised due to the oxygen vacancy. A galvanostatic and XRD study of electrochemically deintercalated Li_xCoO_2 ($x=1.10$) [28] showed, unlike stoichiometric $LiCoO_2$, the occurrence of a solid solution in the $0.60<x<1.10$ domain. From XRD and ^7Li MAS NMR measurements [66], it was found that at 900 °C the lithium overstoichiometric material gradually transformed to stoichiometric $LiCoO_2$ by Li_2O loss. Indeed, XRD analysis of lithium deintercalated sample showed the existence of a two-phase domain, typical of stoichiometric $LiCoO_2$, and the NMR spectrum of thermally treated Li_xCoO_2 ($x=1.08$) resembled that of stoichiometric $LiCoO_2$.

3.2.3. $LiCoO_{2-\delta}$

The formation of oxygen deficient lithium cobalt oxide ($LiCoO_{2-\delta}$) was reported by Marini et al. [87]. According to the authors, the values of δ in $LiCoO_{2-\delta}$ were 0.14 for the sample prepared starting from a nominal Li/Co composition = 0.11 and 0.09 for the sample from a nominal Li/Co composition = 0.25.

According to Gorshow et al. [88] and Karelina et al. [89], the nonstoichiometric oxygen content in $LiCoO_{2-\delta}$ and its magnetic susceptibility suggest that Co^{2+} ions and oxygen vacancies are predominant defects in this oxide. Measurements of the electric and thermoelectric force over the temperature range 650–900 °C indicated that $LiCoO_{2-\delta}$ belongs to p-type semiconductors. They found that the production of oxygen vacancies does not give rise to n-type electron conductivity. The authors explained this effect by the localization of electrons on cobalt atoms of the lattice and by the formation of neutral cobalt vacancy complexes, which virtually do not interact with each other.

The NMR spectrum of $LiCoO_{2-\delta}$ sample prepared by Levasseur et al. [66] resembled that of $LiCoO_2$, but for a slight increase in the line width of the central signal. Therefore, it is believed that the amount of defect present in the oxygen-deficient $LiCoO_{2-\delta}$ is small. This result shows that at 900 °C it is very difficult to reduce the low spin trivalent cobalt ions in $LiCoO_2$.

4. Electrochemical behaviour in lithium batteries

4.1. LT-$LiCoO_2$

According to Gummow et al. [9], the electrochemical extraction of lithium ions from LT-$LiCoO_2$ takes place on a constant voltage plateau at 3.6 V (on open circuit) against pure lithium. Fig. 5 shows the electrochemical curve of a Li/LT-$LiCoO_2$ cell, together to those related to Li/HT-$LiCoO_2$ and Li/Li_xCoO_2 ($x=1.10$) cells. After an initial rapid increase in voltage to $x \approx 0.95$, which was attributed to a single-phase reaction process and the generation of a defect rock salt phase $Li_{0.95}CoO_2$, the Li/LT-Li_xCoO_2 cell shows a two-phase, constant-voltage plateau at 3.6 V from $x=0.95$ to $x=0.1$. Li/LT-$LiCoO_2$ cells lose capacity on cycling; this poor performance is attributed to the structural instability of the quasi-spinel LT-$LiCoO_2$ structure on repeated extraction and reinsertion of lithium. Adhikary et al. [19] proposed a model in which oxidation of divalent cobalt explains the electrochemical charge/discharge irreversibility in the initial cycle. According to Garcia et al. [90], the poor cyclability of LT-$LiCoO_2$ can be attributed to the significant reactivity of the oxidized LT-Li_xCoO_2, which results in the formation of passive layer, and a slow transport of lithium into the oxide to repeat the extraction and insertion of lithium. The value

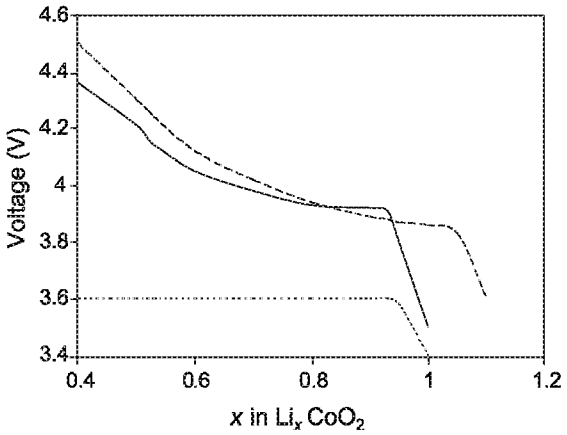


Fig. 5. First galvanostatic charge of Li/LT-$LiCoO_2$ (dotted line) [9], Li/HT-$LiCoO_2$ (full line) [80] and Li/$Li_{1.1}CoO_2$ (dashed line) [28] electrochemical cells.

AMPEREX Ex. 1002
Page 1156

of the first discharge of LT-$LiCoO_2$ was 80 mA h g^{-1} [16], remarkably lower than the values related to HT$LiCoO_2$.

4.2. HT-$LiCoO_2$

The first galvanostatic charge curve of Li/HT-$LiCoO_2$ cell is reported in Fig. 5. The charge curve presents the particular feature associated with the monoclinic distortion expected at $x=0.5$ and the voltage plateau corresponding to the biphasic domain for $0.75 \leq x \leq 0.93$ [78,80]. HT-$LiCoO_2$ samples prepared from different synthesis methods showed a maximum energy capacity in first discharge between 4.5 and 3 V in the range 96–156 mA h g^{-1}, with the most part of the values in the short range 130–140 mA h g^{-1}. The samples of layered $LiCoO_2$ with defect structure show values of the initial discharge slightly higher (156 mA h g^{-1}) [53] and slightly lower (120 mA h g^{-1}) [68] than the average value of 135 mA h g^{-1}. Fig. 6 shows the dependence of the first discharge capacity from various authors on $LiCoO_2$ particle size. As can be seen, the capacity values are scattered and seem to be independent of the particle size. For that regarding the electrochemical cyclability in lithium cells, instead, the capacity fade rate seems to increase with increasing $LiCoO_2$ particle size, as shown in Fig. 7. Because the cells cycled between 3.0 and 4.0 V and between 3.0 and 4.2 V show the capacity fade over 100 cycles of 43.1% and 52.1%, respectively, Kim et al. [91] assumed that the capacity fade is partially ascribed to the phase transition around 4.1 and 4.2 V. As can be seen in Fig. 5, the galvanostatic curve for Li/Li_xCoO_2 ($x>1$) cell is quite different from that of stoichiometric $LiCoO_2$. The feature corresponding to the monoclinic distortion has disappeared. Moreover, the voltage plateau at the beginning of the charge does not exist. According to Imanishi et al. [84], the reversible capacity shows dependence on the composition and the highest one as much as 140 mA h g^{-1} was obtained at Li/Co 1.10. The capacity linearly decreased with Li/Co

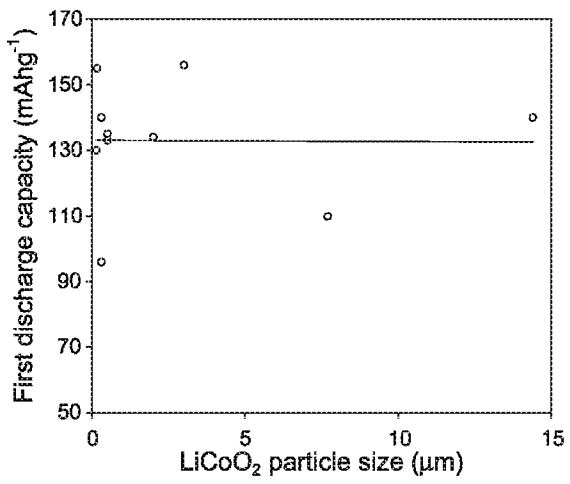


Fig. 6. Dependence of the first discharge capacity from various authors on $LiCoO_2$ particle size.

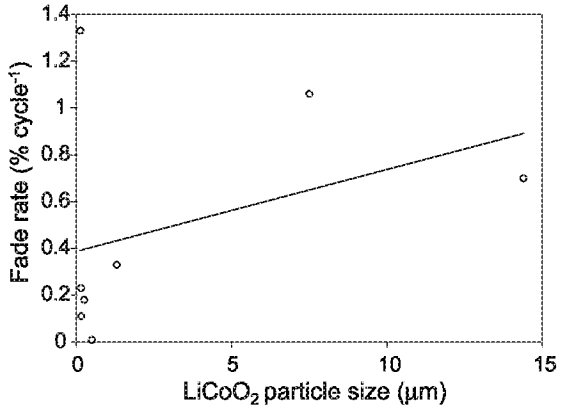


Fig. 7. Capacity fade rate from different authors vs. $LiCoO_2$ particle size.

ratio beyond 1.10 due to decreasing amount of cobalt in the products. Setting the higher cut off voltage as 4.52 V for the charge process, better cycling performance with the reversible capacity of 160 mA h g^{-1} was obtained [84]. Brief, the increase of Li/Co ratio improves the capacity, but too much doping deteriorates the performance. Liu et al. [92] reported that excess lithium in Li_xCoO_2 affects the cycle life of Li-ion batteries, as the capacity fade increases with increasing nominal Li/Co ratio. Comparing the voltage profiles of lithium cells with stoichiometric and lithium overstoichiometric Li_xCoO_2 upon the first 10 cycles, Levasseur et al. [66] noted that the reversibile capacity of these two type of cells are very similar, but the voltage profile upon discharge are significantly different. The voltage drop at the end of discharge is gradual for the lithium overstoichiometric compound in comparison to that of the stoichiometric sample, and this effect becomes more and more important as the cycle number increases. They ascribed the different behaviour of Li_xCoO_2 ($x>1$) to the absence of phase separation in the composition range corresponding to the end of discharge. According to the authors, the more gradual voltage drop at the end of discharge tends to lower the reversible capacity in a fixed cycling voltage range. Furthermore, it has to be remarked that the capacity fade could depend on the large particle size of lithium overstoichiometric Li_xCoO_2. As earlier denoted, the capacity fade increases with increasing $LiCoO_2$ particle size.

5. Transport properties

5.1. Electrical conductivity

The large values of $LiCoO_2$ thermoelectric power are typical of semi-conductor behaviour. The positive value of the Seebeck coefficient revealed that electron holes are the main charge carriers in layered lithium cobalt oxide [32,80]. Since the electrical conductivity of $LiCoO_2$ is an important characteristics for the use of this material in Li-batteries as well as in molten carbonate fuel cells, conductivity measure-

AMPEREX Ex. 1002
Page 1157

ments have been performed in many works [32,35,80,93–99]. The anisotropic temperature dependence of the electrical conductivity in single crystal $LiCoO_2$, grown by a flux method [24], in the temperature range −198 to 27 °C was reported by Takahashi et al. [99]. As shown in Fig. 8, the resistivities both perpendicular and parallel to the *c*-axis show a semiconductive behaviour with large anisotropy of $\rho_c/\rho_a \approx 500$ at 27 °C.

Carewska et al. [35] investigated the temperature dependence of the electrical conductivity of polycrystalline $LiCoO_2$, prepared from various precursors, in the temperature range 550–900 °C. Fig. 9 shows the Arrhenius plot of the electrical conductivity of $LiCoO_2$ samples. Electrical conductivity data matched the following equation, describing the migration of hole by activated hopping process [100]:

$$\sigma = \sigma_0 \exp(-E_a/kT)/T \quad (1)$$

where σ_0 is a pre-exponential factor, E_a is the activation energy and k is the Boltzmann's constant. As can be seen in Fig. 9, the investigated temperature range consisted of two straight portions, a break occurring at around 850 °C. The value of activation energy at lower temperatures (500–800 °C) was 0.37 eV. An increase of the electrical conductivity was observed by increasing lithium content in Li_xCoO_2 ($x \geq 1$) up to $x = 1.35$ [83]. The dependence of conductivity on lithium content in Li_xCoO_2 is shown in Fig. 10. Stoichiometric $LiCoO_2$ exhibited the maximum value of the energy of activation for the electrical conductivity. Electrical conductivity was measured on samples of Li_xCoO_2 ($0.5 < x < 1$) prepared by electrochemical deintercalation from HT-$LiCoO_2$ [80]. Electrical conductivity and thermoelectric power measurements evidenced a gradual change in the electronic properties from localised to delocalised electron upon lithium deintercalation. A strong increase in the conductivity and a transition from semiconductor behaviour to metallic behaviour were reported, as a consequence of the creation of holes in the t_2 band upon deintercalation. According to Menetrier et al. [80], the metal–non-metal transition was the driving force for the existence of the biphasic domain, in agreement with both the experimental results of Imanishi et al. [97] and the theoretical calculations of Van der Ven et al. [100]. The electronic conductivity and thermopower data for deintercalated Li_xCoO_2 ($x>1$) samples are very similar to those reported for stoichiometric $LiCoO_2$ [28]. Fig. 11 shows the dependence of the logarithm of the electrical conductivity on reciprocal temperature of Li_xCoO_2 (nominal $x = 1.10$) deintercalated samples. As in the case of stoichiometric $LiCoO_2$, two different domains can be considered. For materials with $x \geq 0.75$, the electronic conductivity is thermally activated. The decrease in activation energy with decreasing x indicates that more and more electronic holes are created in the cobalt t_2 band. For the most deinterca-

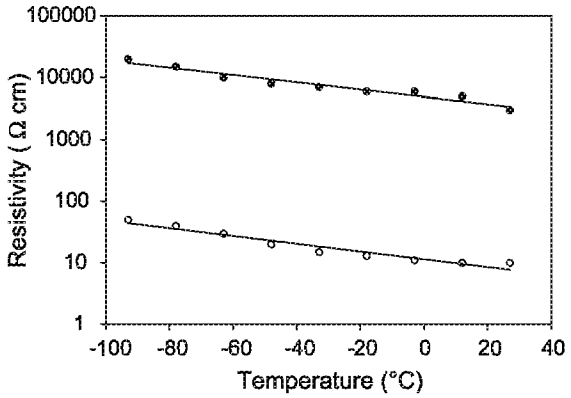


Fig. 8. Temperature dependence of the in-plane (ρ_a, ○) and out-of-plane (ρ_c, ●) resistivity of $LiCoO_2$ single crystals [98].

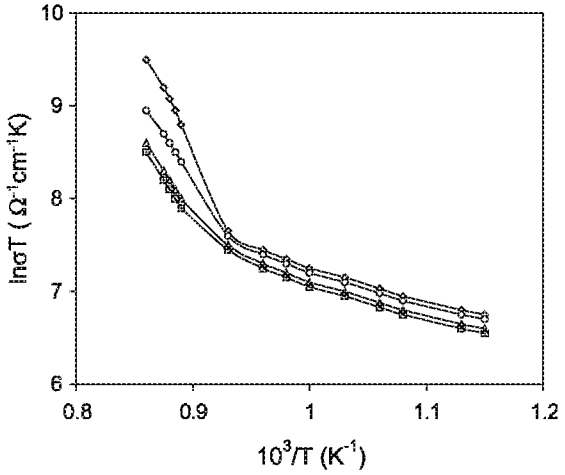


Fig. 9. Arrhenius plot of electrical conductivity of HT-$LiCoO_2$ prepared from different precursors: Li_2CO_3–Co_3O_4 (△); Li(CH_3COO)–Co_3O_4 (△); Li_2CO_3–$2CoCO_3 \cdot 3Co(OH)_2$ (○); Li(CH_3COO)–Co(CH_3COO)$_2$ (◇) [35].

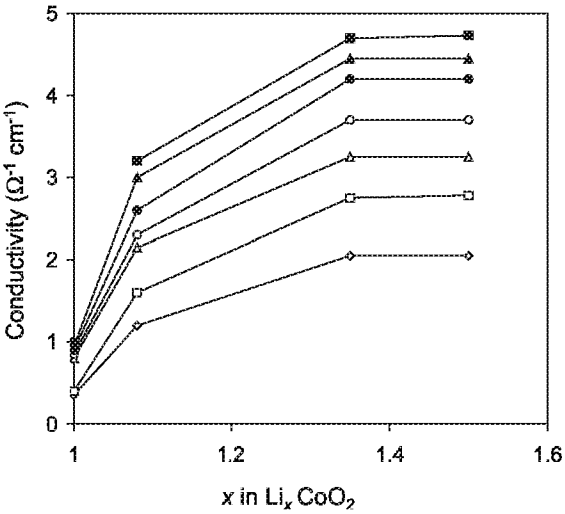


Fig. 10. Isotherms of the electrical conductivity for Li_xCoO_2 samples at various temperatures: 500 °C (◇); 550 °C (△); 598 °C (△); 627 °C (○); 658 °C (●); 677 °C (▲); 698 °C (■) [83].

lated materials ($x \leq 0.60$), pseudometallic behaviour is observed, as conductivity increases with decreasing temperature for $T \leq -23$ °C.

5.2. Chemical diffusion

In a first paper, Nakamura et al. [101] investigated the motion of Li^+ defects in $LiCoO_2$. The spin-lattice relaxation time for ^7Li was measured in $LiCoO_2$ from −196 to 407 °C. The data in the high temperature region were interpreted by the relaxation mechanism of the diffusive motion of Li^+ ion defects. The activation energy for the diffusion of the Li^+ ions in $LiCoO_2$ was estimated to be 0.08 eV. In a more recent work [102], the same authors measured the NMR spectra of ^7Li nucleus in $LiCoO_2$. Line widths of the spectra decreased with increasing temperature above 127 °C. The decrease indicates the motional narrowing originating from diffusing Li^+ defects. A simple ion hopping model pointed out an activation energy of 0.3 eV for lithium ion diffusion in $LiCoO_2$.

Antolini [103] investigated Li loss from $LiCoO_2$ following isochronal thermal treatment for 5 h in the temperature range 850–1300 °C by thermogravimetric and diffractometric measurements. Lithium vaporization starts from 900 °C, and following thermal treatment at 1300 °C 85% of lithium was lost. As shown in Fig. 12, at 1050 °C a change in the mechanism of lithium and oxygen evaporation was observed. At lower temperatures, an activation energy of 3.17 eV, not too far from the heat of reaction from Li_2O to Li_2O_2 vapour, was obtained. Phase transition to cubic $Li_{0.065}Co_{0.935}O$ structure occurred starting from thermal treatment at 1050 °C. Above 1050 °C, an activation energy of the process even to 0.44 eV was found, close to the value of 0.42 eV, the heat of solution of Li_2O to cubic $Li_xNi_{1-x}O$ solid solution with $x = 0.03$. Then, the rate-determining step for the vaporization rate was supposed to be the solution of Li_2O in $Li_{0.065}Co_{0.935}O$.

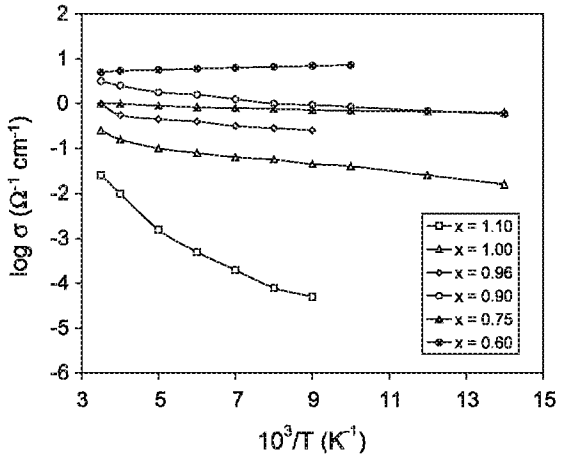


Fig. 11. Variation of the logarithm of the electrical conductivity vs. reciprocal temperature of Li_xCoO_2 ($x = 1.10$) deintercalated samples ($0.60 \leq x \leq 1.10$) [28].

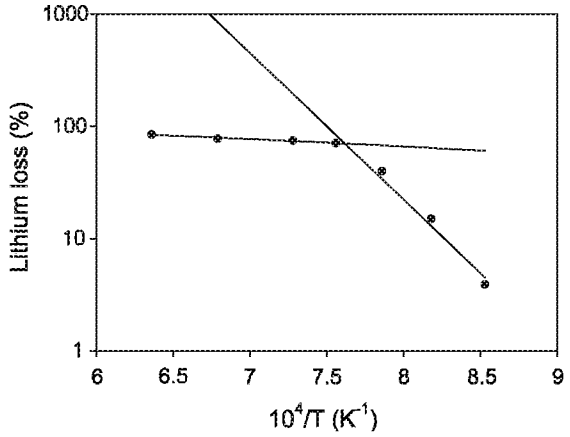


Fig. 12. The logarithm of lithium loss from $LiCoO_2$ samples as a function of the reciprocal temperature [103].

6. Conclusion

From the analysis of more than 40 papers dealing on the way to prepare $LiCoO_2$ by different starting materials and/or different synthesis methods, it can be inferred that:

(i) The reaction mechanism depends on the synthesis method.
(ii) Most synthesis methods lead to the formation of $LiCoO_2$ with particle size <1 μm.
(iii) The presence of Li molten salts gives rise to particle coarsening.
(iv) Maximum discharge specific capacity is independent of $LiCoO_2$ particle size.
(v) Capacity fade rate during cycling in Li-batteries increases with increasing $LiCoO_2$ particle size.

Many efforts have been devoted to synthesize $LiCoO_2$ with structural disordering (nonstoichiometry, cation mixing, and a disturbance of oxygen layers stacking). The structure of these materials should be more stable to intercalation/deintercalation of lithium ions in the course of discharge/charge processes in Li-batteries, thus providing better electrochemical behaviour and preventing structural distortion. The improvement of reversible capacity makes lithium overstoichiometric Li_xCoO_2 ($x>1$) a promising material for Li-batteries, as well as the increase of electrical conducibility makes it an attracting material for molten carbonate fuel cells.

Some uncertainty on the structure (layered or spinel) of delithiated HT-$Li_{0.5}CoO_2$ has still to be clarified.

References

[1] E. Plichta, S. Slane, M. Uchiyama, M. Salomon, D. Chua, W. Ebner, H. Lin, Solid State Ionics 136 (1989) 1865.

AMPEREX Ex. 1002
Page 1159

[2] H.F. Gibbard, J. Power Sources 26 (1989) 81.
[3] T. Nagura, K. Tazawa, Prog. Batteries Sol. Cells 9 (1990) 20.
[4] J.B.J. Veldhuis, F.C. Eckes, L. Plomp, J. Electrochem. Soc. 139 (1992) L6.
[5] J. Han, S.G. Kim, S.P. Yoon, S.W. Nam, T.H. Lim, I.H. Oh, S.A. Hong, H.C. Lim, J. Power Sources 106 (2002) 153.
[6] S.T. Kuk, Y.S. Song, S. Suh, J.Y. Kim, K. Kim, J. Mater. Chem. 11 (2001) 630.
[7] C. Yuh, R. Johnsen, M. Farooque, H. Maru, J. Power Sources 56 (1995) 1.
[8] D.G. Kellermann, Russ. Chem. Rev. 70 (2001) 777.
[9] R.J. Gummow, M.M. Thackeray, W.I.F. David, S. Hull, Mater. Res. Bull. 27 (1992) 327.
[10] R.J. Gummow, M.M. Thackeray, Solid State Ionics 53–56 (1992) 681.
[11] E. Rossen, J.N. Reimers, J.R. Dahn, Solid State Ionics 62 (1993) 53.
[12] R.J. Gummow, D.C. Liles, M.M. Thackeray, W.I.F. David, Mater. Res. Bull. 28 (1993) 1177.
[13] R.J. Gummow, D.C. Liles, M.M. Thackeray, Mater. Res. Bull. 28 (1993) 235.
[14] C.-H. Han, Y.-S. Hong, C.M. Park, K. Kim, J. Power Sources 92 (2001) 95.
[15] I.H. Oh, S.A. Hong, Y.K. Sun, J. Mater. Sci. 32 (1997) 3177.
[16] S.G. Kang, S.Y. Kang, K.S. Ryu, S.H. Chang, Solid State Ionics 120 (1999) 155.
[17] N.V. Kosova, V.F. Anufrienko, T.V. Larina, A. Rougier, L. Aymard, J.M. Tarascon, J. Solid State Chem. 165 (2002) 56.
[18] O.A. Brylev, O.A. Shlyakhtin, T.L. Kulova, A.M. Skundin, Yu.D. Tretyakov, Solid State Ionics 156 (2003) 291.
[19] K. Adhikary, M. Takahashi, S. Kikkawa, Mater. Res. Bull. 33 (1998) 1845.
[20] E. Antolini, J. Eur. Ceram. Soc. 18 (1998) 1405.
[21] Y. Shao-Horn, S.A. Hackney, A.J. Kahaian, M.M. Thackeray, J. Solid State Chem. 168 (2002) 60.
[22] H.J. Orman, P.J. Wiseman, Acta Crystallogr. C 40 (1984) 12.
[23] K. Mizushima, P.C. Jones, P.J. Wiseman, J.B. Goodenough, Mater. Res. Bull. 15 (1980) 783.
[24] J. Akimoto, Y. Gotoh, Y. Oosawa, J. Solid State Chem. 141 (1998) 298.
[25] G.G. Amatucci, J.M. Tarascon, L.C. Klein, J. Electrochem. Soc. 143 (1996) 1114.
[26] W.D. Johnston, R.R. Heikes, D. Sestrich, J. Phys. Chem. Solids 7 (1958) 1.
[27] A. Marini, V. Berbenni, V. Massarotti, D. Capsoni, E. Antolini, J. Solid State Chem. 116 (1995) 23.
[28] S. Levasseur, M. Menetrier, E. Suard, C. Delmas, Solid State Ionics 128 (2000) 11.
[29] J.M. Fernandez-Rodriguez, L. Hernan, J. Morales, J.L. Tirado, Mater. Res. Bull. 23 (1988) 899.
[30] E.F. Sitters, Basic research on MCFC corrosion and improved current density, CEC Contract JOU2-CT93-0286, January to July 1994.
[31] J.R. Dahn, U. von Sacken, C.A. Michal, Solid State Ionics 44 (1990) 87.
[32] A. Honders, J.M. der Kinderen, A.H. van Heeren, J.H.W. de Wit, G.H.J. Broers, Solid State Ionics 14 (1984) 205.
[33] C. Lagergren, A. Lundblad, B. Bergman, J. Electrochem. Soc. 141 (1994) 2959.
[34] P. Parboux, J.M. Tarascon, F.K. Shokoohi, J. Solid State Chem. 94 (1991) 185.
[35] M. Carewska, A. Di Bartolomeo, S. Scaccia, Thermochim. Acta 269/270 (1995) 491.
[36] A. Lundblad, B. Bergman, Solid State Ionics 96 (1997) 173.
[37] A. Lundblad, B. Bergman, Solid State Ionics 96 (1997) 183.
[38] J. Kim, P. Fulmer, A. Manthiram, Mater. Res. Bull. 34 (1999) 571.
[39] S.T. Myung, N. Kumagai, S. Komaba, H.T. Chung, J. Appl. Electrochem. 30 (2000) 1081.
[40] M. Yoshio, H. Tanaka, K. Tominaga, H. Noguchi, J. Power Sources 40 (1992) 347.
[41] C.H. Lu, P.-Y. Yeh, J. Mater. Chem. 10 (2000) 599.
[42] T. Nakamura, A. Kajiyama, Solid State Ionics 123 (1999) 95.
[43] K. Konstantinov, G.X. Wang, J. Yao, H.K. Liu, S.X. Dou, J. Power Sources 119–121 (2003) 195.
[44] Y. Li, C. Wan, Y. Wu, C. Jiang, Y. Zhu, J. Power Sources 85 (2000) 294.
[45] P.N. Kumta, D. Gallet, A. Waghray, G.E. Blomgren, M.P. Setter, J. Power Sources 72 (1998) 92.
[46] T.J. Boyle, D. Ingersoll, T.M. Alam, C.J. Tafoya, M.A. Rodriguez, K. Vanheusden, D.H. Doughty, Chem. Mater. 10 (1998) 2270.
[47] Y.K. Sun, J. Power Sources 83 (1999) 223.
[48] S.M. Lala, L.A. Montoro, E. di Donato, J.M. Rosolen, J. Power Sources 114 (2003) 127.
[49] P. Kalyani, N. Kalaiselvi, N. Muniyandi, J. Power Sources 111 (2002) 232.
[50] S.M. Lala, L.A. Montoro, J.M. Rosolen, J. Power Sources 124 (2003) 118.
[51] E.I. Santiago, A.V.C. Andrade, C.O. Paiva-Santos, L.O.S. Bulhoes, Solid State Ionics 158 (2003) 91.
[52] W.S. Yoon, K.B. Kim, J. Power Sources 81–82 (1999) 517.
[53] W. Tang, H. Kanoh, K. Ooi, Electrochem. Solid-State Lett. 1 (1998) 145.
[54] H. Yan, X. Huang, Z. Lu, H. Huang, R. Xue, L. Chen, J. Power Sources 68 (1997) 530.
[55] S. Tao, Q. Wu, Z. Zhan, G. Meng, Solid State Ionics 124 (1999) 53.
[56] W.T. Jeiong, K.S. Lee, J. Power Sources 104 (2002) 195.
[57] Z.S. Peng, C.R. Wan, C.Y. Jiang, J. Power Sources 72 (1998) 215.
[58] Y.K. Sun, I.H. Oh, S.A. Hong, J. Mater. Sci. 31 (1996) 3617.
[59] B. Garcia, J. Farcy, J.P. Pereira-Ramos, J. Perichon, N. Baffier, J. Power Sources 54 (1995) 373.
[60] E. Zhecheva, R. Stoyanova, M. Gonova, R. Alcantara, J. Morales, J.L. Tirado, Chem. Mater. 8 (1996) 1429.
[61] K. Kanamura, A. Goto, R.H. Ho, T. Umegaki, K. Toyoshima, K. Okada, Y. Hakuta, T. Adschiri, K. Arai, Electrochem. Solid-State Lett. 3 (2000) 256.
[62] A. Burukhin, O. Brylev, P. Hany, B.R. Churagulov, Solid State Ionics 151 (2002) 259.
[63] S.K. Chang, H.J. Kweon, B.K. Kim, D.Y. Jung, Y.U. Kwon, J. Power Sources 104 (2002) 125.
[64] G.G. Amatucci, J.M. Tarascon, D. Larcher, L.C. Klein, Solid State Ionics 84 (1996) 169.
[65] E. Antolini, L. Giorgi, M. Carewska, J. Mater. Sci. Lett. 18 (1999) 325.
[66] S. Levasseur, M. Menetrier, Y. Shao-Horn, L. Gautier, A. Audemer, G. Demazeau, A. Largeteau, C. Delmas, Chem. Mater. 15 (2003) 348.
[67] D. Carlier, I. Saadoune, L. Croguennec, M. Menetrier, E. Suard, C. Delmas, Solid State Ionics 144 (2001) 263.
[68] S. Rodrigues, N. Munichandraiah, A.K. Shukla, J. Power Sources 102 (2001) 322.
[69] M.N. Obrovac, O. Mao, J.R. Dhan, Solid State Ionics 112 (1998) 9.
[70] S. Choi, A. Manthiram, J. Electrochem. Soc. 149 (2002) A162.
[71] S. Choi, A. Manthiram, J. Solid State Chem. 164 (2002) 332.
[72] J. Graetz, C. Julien, R. Yazami, 204th Meeting of The Electrochemical Society, Orlando, FL, Abs. 371.
[73] H. Gabrisch, R. Yazami, B. Fultz, J. Power Sources 119–121 (2003) 674.
[74] R.J. Moore, J. White, J. Mater. Sci. 9 (1974) 1408.
[75] E. Antolini, M. Ferretti, J. Solid State Chem. 117 (1995) 1.
[76] E. Antolini, M. Daturi, M. Ferretti, J. Mater. Sci. Lett. 15 (1996) 416.
[77] M.P.J. Peeters, M.J. Van Bommel, P.M.C. Neilen-ten Wolde, H.A.M. Van Hal, W.C. Keur, A.P.M. Kentgens, Solid State Ionics 112 (1998) 41.
[78] J.N. Reimers, J.R. Dahn, J. Electrochem. Soc. 139 (1992) 2091.

AMPEREX Ex. 1002
Page 1160

[79] T. Ohzuku, A. Ueda, J. Electrochem. Soc. 141 (1994) 2972.
[80] M. Menetrier, I. Saadoune, S. Levasseur, C. Delmas, J. Mater. Chem. 9 (1999) 1135.
[81] J.N. Reimers, J.R. Dahn, U. Von Sacken, J. Electrochem. Soc. 140 (1993) 2752.
[82] Y. Shao-Horn, S. Levasseur, F. Weill, C. Delmas, J. Electrochem. Soc. 150 (2003) A366.
[83] M. Carewska, S. Scaccia, S. Arumugan, Y. Wang, S. Greenbaum, Solid State Ionics 93 (1997) 227.
[84] N. Imanishi, M. Fujii, A. Hirano, Y. Takeda, J. Power Sources 97–98 (2001) 287.
[85] N. Imanishi, M. Fujii, A. Hirano, Y. Takeda, M. Inaba, Z. Ogumi, Solid State Ionics 140 (2001) 45.
[86] P. Ganguly, T.N. Venkatraman, P.R. Rajamohanan, S. Ganapathy, J. Phys. Chem., B 101 (1997) 11099.
[87] A. Marini, V. Berbenni, V. Massarotti, D. Capsoni, G. Bruni, Z. Naturforsch. A 51 (1996) 813.
[88] V.S. Gorshkov, D.G. Kellerman, V.V. Karelina, Russ. J. Phys. Chem. 73 (1999) 921.
[89] V.V. Karelina, D.G. Kellerman, V.S. Gorshkov, I.A. Leonidov, M.V. Patrakeev, Russ. J. Phys. Chem. 75 (2001) 496.
[90] B. Garcia, J. Farcy, J.P. Pereira-Ramos, N. Baffier, J. Electrochem. Soc. 144 (1997) 1179.
[91] K.W. Kim, S.J. Woo, K.H. Choi, K.S. Han, Y.J. Park, Solid State Ionics 159 (2003) 25.
[92] R. Liu, X. Yang, G. Wu, W. Jin, Q. Lin, Extended Abstracts of the 12th International Conference on Solid State Ionics, Halkidiki, Greece 1999.
[93] S. Kikkawa, S. Miyazaki, M. Koizumi, J. Solid State Chem. 62 (1986) 35.
[94] J. Molenda, A. Stoklosa, T. Bak, Solid State Ionics 36 (1989) 53.
[95] M. Shibuya, T. Nishina, T. Matsue, I. Uchida, J. Electrochem. Soc. 143 (1996) 3157.
[96] H. Tukamoto, A.R. West, J. Electrochem. Soc. 144 (1997) 3164.
[97] N. Imanishi, M. Fujiyoshi, Y. Takeda, O. Yamamoto, M. Tabuchi, Solid State Ionics 118 (1999) 121.
[98] Y. Takahashi, Y. Gotoh, J. Akimoto, S. Mizuta, K. Tokiwa, T. Watanabe, J. Solid State Chem. 164 (2002) 1.
[99] R.R. Heikes, W.D. Johnston, J. Chem. Phys. 26 (1957) 582.
[100] A. Van der Ven, M.K. Aydinol, G. Ceder, G. Kresse, J. Hafner, Phys. Rev. B 58 (1998) 2975.
[101] K. Nakamura, M. Yamamoto, K. Okamura, Y. Michihiro, I. Nakabayashi, T. Kanashiro, Solid State Ionics 121 (1999) 301.
[102] K. Nakamura, H. Ohno, K. Okamura, Y. Michihiro, I. Nakabayashi, T. Kanashiro, Solid State Ionics 135 (2000) 143.
[103] E. Antolini, Int. J. Inorg. Mater. 3 (2001) 721.

AMPEREX Ex. 1002
Page 1161

Espacenet

RSS family document

Family list: CN102779976 (A) — 2012-11-14

1 application(s) for: CN102779976 (A)

1. Preparation method of cathode material of LCO (lithium cobaltate)-based lithium ion battery

Inventor:	Applicant:	CPC:	IPC:	Publication info:	Priority date:
XINGLONG GAO LEI LIU (+3)	PULEAD TECHNOLOGY INDUSTRY CO LTD	Y02E60/10	H01M4/1391	CN102779976 (A) 2012-11-14 CN102779976 (B) 2015-05-20 Global Dossier	2011-10-10

Espacenet

Bibliographic data: CN102779976 (A) — 2012-11-14

Preparation method of cathode material of LCO (lithium cobaltate)-based lithium ion battery

Inventor(s): XINGLONG GAO; LEI LIU; WEI WEI; XINHE YANG; HENGHUI ZHOU ± (GAO XINGLONG, ; LIU LEI, ; WEI WEI, ; YANG XINHE, ; ZHOU HENGHUI)

Applicant(s): PULEAD TECHNOLOGY INDUSTRY CO LTD ± (PULEAD TECHNOLOGY INDUSTRY CO., LTD)

Classification: - international: ***H01M4/1391***
- cooperative: Y02E60/10 (EP)

Application number: CN201110305140 20111010 Global Dossier

Priority number (s): CN201110305140 20111010

Also published as: CN102779976 (B)

Abstract of CN102779976 (A)

The invention discloses a preparation method of cathode material of an LCO (lithium cobaltate)-based lithium ion battery, which includes the following steps of: respectively preparing LCO material A with a median particle diameter of 10-25micrometers and LCO material B with a median particle diameter of 1-10micrometers which contain doping element of M; mixing the material A with the material B according to a certain proportion, adding secondary surface doping element M', carrying out ball milling and mixing, roasting and grinding to obtain material C with median particle diameter of 7-15micrometers; and finally coating an element G on the surface of the material C, drying and then conducting heat treatment to obtain the cathode material of the LCO-based lithium ion battery. Through the grading of the LCO materials with different particle diameters, the space utilization rate and the compacted density of the material are effectively improved; through the treatment of secondary surface doping, the stability of the surface structure of the material is improved; and through the coating treatment, the contact area between the LCO and the electrolyte is reduced, and the dissolution of the Co contained in the material in the electrolyte is reduced. Therefore, the cycle performance and the safety performance of the lithium ion battery are improved.

(19)中华人民共和国国家知识产权局

(12)发明专利申请

(10)申请公布号 CN 102779976 A
(43)申请公布日 2012.11.14

(21)申请号 201110305140.6

(22)申请日 2011.10.10

(71)申请人 北大先行科技产业有限公司
地址 102200 北京市昌平区科技园区创新路35号

(72)发明人 高行龙 刘磊 魏伟 杨新河 周恒辉

(74)专利代理机构 北京君尚知识产权代理事务所(普通合伙) 11200
代理人 李稚婷

(51)Int.Cl.
H01M 4/1391(2010.01)

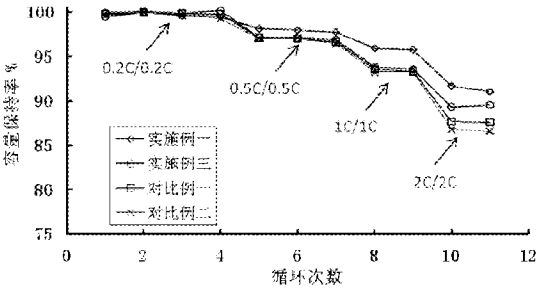
权利要求书 1 页 说明书 6 页 附图 2 页

(54)发明名称

一种钴酸锂基锂离子电池正极材料的制备方法

(57)摘要

本发明公开了一种钴酸锂基锂离子电池正极材料的制备方法，先分别制备中位粒径为10～25μm和1～10μm的含有掺杂元素M的钴酸锂材料A和B；然后将A、B两种材料配比混合，并加入二次表面掺杂元素M′球磨混合，焙烧，粉碎，得中位粒径为7～15μm的材料C；最后在材料C表面包覆元素G，干燥后热处理得所述钴酸锂基锂离子电池正极材料。本发明将不同粒度的钴酸锂进行级配，有效地提高了材料的空间利用率和压实密度，且通过二次表面掺杂提高了材料表面结构的稳定性，而后的包覆处理降低了钴酸锂与电解液的接触面积，减小材料中钴在电解液中的溶解，从而提高了锂离子电池的循环性能和安全性能。



CN 102779976 A

1. 一种钴酸锂基锂离子电池正极材料的制备方法，包括如下步骤：

1) 制备中位粒径为 10 ～ 25μm 的含有掺杂元素 M 的钴酸锂材料 A；

2) 制备中位粒径为 1 ～ 10μm 的含有掺杂元素 M 的钴酸锂材料 B；

3) 将 A、B 两种材料按重量比 3 ： 1 ～ 1 ： 2 的配比混合，并加入二次表面掺杂元素 M′ 进行球磨混合，然后焙烧，粉碎，得到中位粒径为 7 ～ 15μm 的材料 C；

4) 在材料 C 表面包覆元素 G，干燥后在空气气氛下 300-800℃热处理 4-10 小时，得到钴酸锂基锂离子电池正极材料。

2. 如权利要求 1 所述的制备方法，其特征在于，M 选自 Al、Zr、Mg、Ti、Mn、Ni、Sn、Zn、Zr、Ca、Sr、Ba、B、Y、Sm、V、Nb 和 Ta 中的一种或多种；M′ 选自 Al、Zr、Mg、Ti、Mn、Ni、Sn、Zn、Zr、Ca、Sr、Ba、B、Y、Sm、V、Nb、Ta、F、S、N 和 P 的一种或多种。

3. 如权利要求 1 所述的制备方法，其特征在于，步骤 1) 将锂源、钴源和掺杂元素 M 的来源化合物混合，然后在空气气氛中焙烧，再将焙烧后的物料粉碎为中位粒径为 10 ～ 25μm 的材料 A；步骤 2) 将锂源、钴源和掺杂元素 M 的来源化合物混合，然后在空气气氛中焙烧，再将焙烧后的物料粉碎为中位粒径为 1 ～ 10μm 的材料 B。

4. 如权利要求 3 所述的制备方法，其特征在于，所述锂源选自碳酸锂、氢氧化锂和草酸锂中的一种或多种；所述钴源选自碳酸钴、氢氧化钴、草酸钴、四氧化三钴和氧化钴中的一种或多种。

5. 如权利要求 3 所述的制备方法，其特征在于，M 的来源化合物为含有 Al、Zr、Mg、Ti、Mn、Ni、Sn、Zn、Zr、Ca、Sr、Ba、B、Y、Sm、V、Nb 和 / 或 Ta 的氧化物、氢氧化物、碳酸盐、草酸盐中的一种或多种的混合物。

6. 如权利要求 3 所述的制备方法，其特征在于，步骤 1) 中锂、钴、M 原子比例为 (1.00 ～ 1.10) ： 1.00 ： (0.001 ～ 0.05)，焙烧温度为 800 ～ 1100℃，焙烧时间为 6 ～ 24 小时；步骤 2) 中锂、钴、M 原子比例为 (1.00 ～ 1.05) ： 1.00 ： (0.001 ～ 0.05)，焙烧温度为 800 ～ 1100℃，焙烧时间为 6 ～ 24 小时。

7. 如权利要求 1 所述的制备方法，其特征在于，步骤 3) 中掺杂元素 M′ 与钴原子的比例为 0.001 ～ 0.05，将材料 A、材料 B 和 M′ 的来源化合物球磨混合 1 ～ 5 小时，然后在空气气氛中 800 ～ 1100℃焙烧 4 ～ 20 小时，再粉碎成中位粒径为 7 ～ 15μm 的材料 C。

8. 如权利要求 7 所述的制备方法，其特征在于，M′ 的来源化合物为含有 Al、Zr、Mg、Ti、Mn、Ni、Sn、Zn、Zr、Ca、Sr、Ba、B、Y、Sm、V、Nb、Ta、F、S、N 和 / 或 P 的氧化物、氟化物、氢氧化物、草酸盐、碳酸盐中的一种或多种的混合物。

9. 如权利要求 1 所述的制备方法，其特征在于，步骤 4) 中包覆元素 G 的方法是：将材料 C 置于工业酒精中，在搅拌状态下加入溶解在有机溶剂中的包覆元素 G，G 与钴的原子比例为 0.001 ～ 0.05，搅拌 0.5-4 小时后烘干。

10. 如权利要求 9 所述的制备方法，其特征在于，包覆元素 G 的来源为含有 Mg、Ti、Si、Al 和 / 或 Sn 的酯盐、醇盐中的一种或多种的混合物；溶解包覆元素 G 的有机溶剂为乙醇、丙酮和异丙醇中的一种或多种的混合物。

AMPEREX Ex. 1002
Page 1165

一种钴酸锂基锂离子电池正极材料的制备方法

技术领域

[0001] 本发明涉及锂离子电池正极材料的制备，特别涉及高能量密度锂离子电池正极材料钴酸锂的制备方法。

背景技术

[0002] 锂离子电池作为一种新型的二次电池，具有比容量高、电压高、安全性好的特点，广泛应用于移动电话、笔记本电脑、便携式摄像机、DVD、MP3 等便携式电器的驱动电源。随着电子产品的不断升级换代，对其电源的要求也不断提高，

[0003] 在同样的容量发挥前提下，市场需要不断提高电池的体积能量密度，也就是提高电池活性物质的单位体积填充量。对于目前常用的钴酸锂材料来说，其颗粒越大，由于材料的粒度分布变宽，材料的单位体积填充量越大，即压实密度越大，其体积能量密度也就越大。因此，对于常用的钴酸锂材料，其颗粒的中位径 (D50) 不断增大，由 5-10 微米提高到 10 微米以上甚至到 20 微米，目的在于提高活性物质的单位体积填充量，进而提高电池的体积能量密度，如中国专利申请公开说明书 CN 1328351A 提出了一种提高钴酸锂中位径和振实密度的方法，其目的在于提高材料的粒度，进而提高其振实密度、压实密度。中国专利申请公开说明书 CN 101284681A 发明的超大粒径和高密度钴酸锂及其制备方法也是为了提高材料的粒度进而提高其振实密度、压实密度。目前，中位粒径 (D50) 为 12 微米的钴酸锂其正常使用的压实密度为 3.9-4.0g/cm^3，中位粒径 (D50) 为 18 微米的钴酸锂其正常使用的压实密度为 4.0-4.1g/cm^3，中位粒径 (D50) 为 20 微米的钴酸锂其正常使用的压实密度为 4.1-4.2g/cm^3。但是，在对大颗粒钴酸锂材料的评价中发现，当颗粒增大后，正极材料的电化学性能会降低，其循环性能和倍率放电性能变差。因此不能满足日益增长的能量密度的要求。中国专利申请公开说明书 CN 101436666A 进行的提高压实密度及能量密度的钴酸锂制备，其先制备大颗粒的钴酸锂颗粒，再通过碳酸钴和碳酸锂在大的钴酸锂颗粒表面造粒，从而制备出大颗粒钴酸锂表面沾附小颗粒的钴酸锂颗粒，进而提高正极材料的压实密度和体积比容量。但这种经过一次烧结的钴酸锂其结晶性不好，循环性能较差。中国专利申请公开说明书 CN 1665052A 通过颗粒大小不同的钴酸锂进行混合能够提高材料的压实密度，进而提高材料的体积能量密度。然而，通过这种方法制备的钴酸锂，由于其小颗粒的钴酸锂含量较多，小颗粒钴酸锂的充放电速率较快，会给电池带来较大的安全隐患。

发明内容

[0004] 本发明的目的在于解决上述现有技术的问题，提出一种钴酸锂基锂离子电池正极材料制备方法，通过该方法获得的正极材料不仅可提高压实密度，而且能提高锂离子电池的循环性能和安全性能。

[0005] 本发明钴酸锂基锂离子电池正极材料的制备方法，包括如下步骤：

[0006] 1) 制备中位粒径为 10 ～ 25μm 的含有掺杂元素 M 的钴酸锂材料 A；

[0007] 2) 制备中位粒径为 1 ～ 10μm 的含有掺杂元素 M 的钴酸锂材料 B；

AMPEREX Ex. 1002
Page 1166

[0008] 3) 将 A、B 两种材料按重量比 3 ： 1 ～ 1 ： 2 的配比混合，并加入二次表面掺杂元素 M′ 进行球磨混合，然后焙烧，粉碎，得到中位粒径为 7 ～ 15μm 的材料 C；

[0009] 4) 在材料 C 表面包覆元素 G，干燥后在空气气氛下 300-800℃热处理 4-10 小时，得到钴酸锂基锂离子电池正极材料。

[0010] 上述步骤 1) 是制备大粒度的钴酸锂材料，可以采用下述方法：将锂源、钴源和掺杂元素 M 的来源化合物混合，然后在空气气氛中焙烧，再将焙烧后的物料粉碎为粉末粒度 D50 为 10 ～ 25μm 的材料 A。其中，锂源、钴源和掺杂元素 M 的来源化合物按照锂、钴、M 原子比例为 (1.00 ～ 1.10) ： 1.00 ： (0.001 ～ 0.05) 进行混合；焙烧温度为 800 ～ 1100℃，焙烧时间为 6 ～ 24 小时，焙烧过程中不断通入空气做为反应所需要的氧气源；焙烧后的物料通过粗破碎后，使用气流磨进行粉碎，最终得到所需粒径的材料 A。

[0011] 上述步骤 2) 是制备小粒度的钴酸锂材料，可以采用下述方法：将锂源、钴源和掺杂元素 M 的来源化合物混合，然后在空气气氛中焙烧，再将焙烧后的物料粉碎为粉末粒度 D50 为 1 ～ 10μm 的材料 B。其中，锂源、钴源和掺杂元素 M 的来源化合物按照锂、钴、M 原子比例为 (1.00 ～ 1.05) ： 1.00 ： (0.001 ～ 0.05) 进行混合；焙烧温度为 800 ～ 1100℃，焙烧时间为 6 ～ 24 小时，焙烧过程中不断通入空气做为反应所需要的氧气源；焙烧后的物料通过粗破碎后，使用气流磨进行粉碎，最终得到所需粒径的材料 B。

[0012] 上述步骤 3) 是将大小粒度钴酸锂级配，并进行二次表面掺杂，其中，掺杂元素 M′ 与钴原子的比例为 0.001 ～ 0.05，将材料 A、材料 B 和 M′ 的来源化合物球磨混合 1 ～ 5 小时，混合好的物料在空气气氛中进行焙烧，焙烧温度为 800 ～ 1100℃，焙烧时间为 4 ～ 20 小时；将焙烧后的进行粗破碎、精破碎等工序进行粉碎，得到粉末粒度 D50 为 7 ～ 15μm 的材料 C；

[0013] 上述步骤 4) 的包覆方法可以是：将步骤 3) 得到的材料 C 置于工业酒精中，在搅拌状态下加入溶解在有机溶剂中的包覆元素 G，G 与钴的原子比例为 0.001 ～ 0.05，搅拌 0.5-4 小时后烘干，一般在 70-100℃的温度下烘 1-5 小时；将烘干后的物料在空气气氛下热处理，热处理温度为 300-800℃，热处理时间为 4-10 小时。

[0014] 上述步骤 1) 和步骤 2) 中，锂源可选自碳酸锂、氢氧化锂和草酸锂中的一种或多种的混合物。

[0015] 上述步骤 1) 和步骤 2) 中，钴源可选自碳酸钴、氢氧化钴、草酸钴、四氧化三钴和氧化钴中的一种或多种的混合物。

[0016] 上述步骤 1) 和步骤 2) 中，M 代表一种或多种掺杂元素，M 的来源例如含有 Al、Zr、Mg、Ti、Mn、Ni、Sn、Zn、Zr、Ca、Sr、Ba、B、Y、Sm、V、Nb 和 / 或 Ta 的氧化物、氢氧化物、碳酸盐、草酸盐中的一种或多种的混合物。

[0017] 上述步骤 3) 中，M′ 代表一种或多种二次表面掺杂元素，M′ 与 M 可以相同或不同，M′ 的来源例如含有 Al、Zr、Mg、Ti、Mn、Ni、Sn、Zn、Zr、Ca、Sr、Ba、B、Y、Sm、V、Nb、Ta、F、S、N 和 / 或 P 的氧化物、氟化物、氢氧化物、草酸盐、碳酸盐中的一种或多种的混合物。

[0018] 上述步骤 (4) 中，包覆元素 G 的来源例如含有 Mg、Ti、Si、Al 和 / 或 Sn 的酯盐、醇盐中的一种或多种的混合物。溶解包覆元素 G 的有机溶剂可以为乙醇、丙酮、异丙醇中的一种或多种的混合物。

[0019] 本发明的特点及优势为：

AMPEREX Ex. 1002
Page 1167

[0020] 本发明提供的锂离子二次电池正极材料，通过将不同粒度的钴酸锂进行级配，有效地提高了材料的空间利用率，提高了正极材料的压实密度，进而使材料的体积能量密度大大提高。所获得的正极材料在保持中位粒径 (D50) 为 10 微米的基础上，干粉压实密度可达 4.43g/cc，其对应的极片压实密度可达 4.2g/cc。本发明的另一个优势是，对已经掺杂的钴酸锂正极材料进行二次表面掺杂、包覆处理，通过二次表面掺杂获得的表面掺杂层提高了材料表面结构的稳定性，而后的包覆处理降低了钴酸锂与电解液的接触面积，减小材料中钴在电解液中的溶解，从而提高了锂离子电池的循环性能和安全性能。所得锂离子电池 500 次高低温循环容量 (常温 23℃ /45℃，3.0-4.35V) 保持率均大于 90％ ；高温存储膨胀小，85℃存储 4 小时，60℃存储 7 天厚度变化 2-6％。

附图说明

[0021] 图 1 是实施例一制备的具有 Al 包覆层的 $LiCo_{0.98}Ti_{0.01}Mg_{0.01}F_{0.005}O_{1.995}$ 材料的扫描电子显微镜 (SEM) 图。

[0022] 图 2 是实施例一制备的具有 Al 包覆层的 $LiCo_{0.98}Ti_{0.01}Mg_{0.01}F_{0.005}O_{1.995}$ 材料在 3.0-4.3V、45℃条件下的循环测试图。

[0023] 图 3 是实施例一、实施例三和对比例一、对比例二所制备的材料在 3.0 ～ 4.4V 的倍率性能比较图。

具体实施方式

[0024] 下面通过实施例进一步详细描述本发明的方法，但这并非是对本发明的限制，本领域技术人员根据本发明的基本思想，可以做出各种修改或改进，只要不脱离本发明的基本思想，均在本发明的范围之内。

[0025] 实施例一

[0026] 按照锂、钴、钛原子比例为 1.05 ： 1.00 ： 0.01 的比例将碳酸钴、碳酸锂、二氧化钛球磨混合 5 小时 ；将混合后的原料置于焙烧炉中，在空气气氛中 1000℃焙烧 12 小时 ；将焙烧后的产物先通过粗破碎后，再使用气流磨进行精破碎，粉末的平均粒度 D50 为 15μm。

[0027] 按照锂、钴、钛原子比例为 1.01 ： 1.00 ： 0.01 的比例将碳酸钴、碳酸锂、二氧化钛球磨混合 5 小时 ；将混合后的原料置于焙烧炉中，在空气气氛中 1000℃焙烧 12 小时 ；将焙烧后的产物先通过粗破碎后，再使用气流磨进行精破碎，粉末的平均粒度 D50 为 5μm。

[0028] 将 D50 为 15μm 和 D50 为 5μm 的粉末按照重量比为 1 ： 1 的比例称量，加入微米级氧化镁、氟化锂，其中物质的量的比例是 Mg/Co ＝ 0.005，F/Co ＝ 0.002，球磨混合 3 小时 ；球磨后的粉末置于推板隧道窑中，在空气气氛下 980℃焙烧 12 小时 ；将焙烧后的产物先经粗破碎，然后使用气流磨进行精破碎，得到平均粒度 D50 为 10μm 的产物，此时获得镁、钛、氟掺杂的钴酸锂，化学式为 $LiCo_{0.98}Ti_{0.01}Mg_{0.01}F_{0.005}O_{1.995}$，具有层状结构。

[0029] 将获得到的镁、钛、氟掺杂的钴酸锂 ($LiCo_{0.98}Ti_{0.01}Mg_{0.01}F_{0.005}O_{1.995}$) 粉末置于装有工业酒精的搅拌混料罐中，搅拌 10 分钟后，加入溶解在异丙醇中的异丙醇铝溶液 (Al/Co ＝ 0.005) ；在搅拌状态下在 100℃热水浴中干燥 ；将干燥后的物料置于推板隧道窑中，在 500℃下热处理 8 小时，冷却后过筛，即可得到具有 Al 包覆层的 $LiCo_{0.98}Ti_{0.01}Mg_{0.01}F_{0.005}O_{1.995}$ 材料。

AMPEREX Ex. 1002
Page 1168

[0030] 对所得材料进行压实密度和倍率性能测试。

[0031] 压实密度采用干粉压实密度，使用 5g 的样品加入到 Φ10 的模具中，使用 100Mpa 的压力进行干粉压实，保压 1 分钟后退模，测量厚度，根据 ρ = m/v 计算可得，在相当的粒度下，本发明方法制备的材料干粉压实密度为 4.43g/cm^3，压实密度得到较高提高。

[0032] 倍率性能测试使用 2032 型扣式电池测试，扣式电池中正极材料的比例为：活性物质：SP：PVDF = 90：5：5，采用 Clgard2300 型隔膜，负极使用金属锂片，充放电电压为 3.0 ～ 4.4V。级配后的倍率性能实现较大提高，参见图 3。高压 (3.0-4.35V) 高温 (45℃) 循环使用 053450 型电池进行测试，结果如图 2 所示。

[0033] 实施例二

[0034] 按照锂、钴、锆比例为 1.05：1.00：0.01 的比例将碳酸锂、四氧化三钴和二氧化锆球磨混合 5 小时；将混合后的原料置于焙烧炉中，在空气气氛中 1000℃焙烧 12 小时；将焙烧后的产物先通过粗破碎后，再使用气流磨进行精破碎，粉末的平均粒度 D50 为 15μm。

[0035] 按照锂、钴、锆的比例为 1.01：1.00：0.01 比例将碳酸锂、四氧化三钴和二氧化锆球磨混合 5 小时；将混合后的原料置于焙烧炉中，在空气气氛中 1000℃焙烧 12 小时；将焙烧后的产物先通过粗破碎后，再使用气流磨进行精破碎，粉末的平均粒度 D50 为 5μm。

[0036] 将 D50 为 15μm 和 D50 为 5μm 的粉末按照重量比为 1：1 的比例称量，再加入微米级氧化镁、氟化锂，其中物质的量的比例是 Mg/Co = 0.005，F/Co = 0.002，球磨混合 3 小时；球磨后的粉末置于推板隧道窑中，在空气气氛下 980℃焙烧 12 小时；将焙烧后的产物通过粗破碎、精破碎，得到平均粒度 D50 为 10μm 的产物，此时获得镁、锆、氟掺杂的钴酸锂，化学式为 $LiCo_{0.98}Zr_{0.01}Mg_{0.01}F_{0.005}O_{1.995}$，具有层状结构。

[0037] 将获得的镁、锆、氟掺杂的钴酸锂 ($LiCo_{0.98}Zr_{0.01}Mg_{0.01}F_{0.005}O_{1.995}$) 粉末置于装有工业酒精的搅拌混料罐中，搅拌 10 分钟后，加入溶解在异丙醇中的异丙醇铝溶液 (Al/Co = 0.005)，在搅拌状态下在 100℃热水浴中干燥；将干燥后的物料置于推板隧道窑中，在 500℃下热处理 8 小时，冷却后过筛，即可得到具有 Al 包覆层的 $LiCo_{0.98}Zr_{0.01}Mg_{0.01}F_{0.005}O_{1.995}$ 材料。

[0038] 实施例三

[0039] 按照锂、钴、铝比例为 1.05：1.00：0.01 的比例将碳酸锂、四氧化三钴和氧化铝球磨混合 5 小时；将混合后的原料置于焙烧炉中，在空气气氛中 1000℃焙烧 12 小时；将焙烧后的产物先通过粗破碎后，再使用气流磨进行精破碎，粉末的平均粒度 D50 为 15μm。

[0040] 按照锂、钴、铝的比例为 1.01：1.00：0.01 比例将碳酸锂、四氧化三钴和氧化铝球磨混合 5 小时；将混合后的原料置于焙烧炉中，在空气气氛中 1000℃焙烧 12 小时；将焙烧后的产物先通过粗破碎后，再使用气流磨进行精破碎，粉末的平均粒度 D50 为 5μm。

[0041] 将 D50 为 15μm 和 D50 为 5μm 的粉末按照重量比为 2：1 的比例称量，再加入微米级氧化镁、氟化锂，其中物质的量的比例是 Mg/Co = 0.005，F/Co = 0.002，球磨混合 3 小时；球磨后的粉末置于推板隧道窑中，在空气气氛下 980℃焙烧 12 小时；将焙烧后的产物通过粗破碎、精破碎，得到平均粒度 D50 为 10μm 的产物，此时获得铝、镁、氟掺杂的钴酸锂，化学式为 $LiCo_{0.98}Al_{0.01}Mg_{0.01}F_{0.005}O_{1.995}$，具有层状结构。

[0042] 将获得的铝、镁、氟掺杂的钴酸锂 ($LiCo_{0.98}Al_{0.01}Mg_{0.01}F_{0.005}O_{1.995}$) 粉末置于装有工业酒精的搅拌混料罐中，搅拌 10 分钟后，加入溶解在酒精中的醋酸镁溶液 (Mg/Co = 0.005)，

AMPEREX Ex. 1002
Page 1169

在搅拌状态下 100℃热水浴中干燥；将干燥后的物料，置于推板隧道窑中，在 500℃下热处理 8 小时，冷却后过筛，即可得到具有 Mg 包覆层的 $LiCo_{0.98}Al_{0.01}Mg_{0.01}F_{0.005}O_{1.995}$ 材料。

[0043] 对该材料进行倍率性能测试，方法同实施例一，从图 3 可以看出，级配后的倍率性能实现较大提高。

[0044] 实施例四

[0045] 按照锂、钴、钛原子比例为 1.05 ： 1.00 ： 0.01 的比例将碳酸钴、碳酸锂、二氧化钛球磨混合 5 小时；将混合后的原料置于焙烧炉中，在空气气氛中 1000℃焙烧 12 小时；将焙烧后的产物先通过粗破碎后，再使用气流磨进行精破碎，粉末的平均粒度 D50 为 15μm。

[0046] 按照锂、钴、钛原子比例为 1.01 ： 1.00 ： 0.01 的比例将四氧化三钴、碳酸锂、二氧化钛球磨混合 5 小时；将混合后的原料置于焙烧炉中，在空气气氛中 1000℃焙烧 12 小时；将焙烧后的产物先通过粗破碎后，再使用气流磨进行精破碎，粉末的平均粒度 D50 为 5μm。

[0047] 将 D50 为 15μm 和 D50 为 5μm 的粉末按照重量比为 2 ： 1 的比例称量，加入微米级氧化镁、氟化锂，其中物质的量的比例是 Mg/Co = 0.005，F/Co = 0.002，球磨混合 3 小时；球磨后的粉末置于推板隧道窑中，在空气气氛下 980℃焙烧 12 小时；将焙烧后的产物先经粗破碎，然后使用气流磨进行精破碎，得到平均粒度 D50 为 10.5μm 的产物，此时获得镁、钛、氟掺杂的钴酸锂，化学式为 $LiCo_{0.98}Ti_{0.01}Mg_{0.01}F_{0.005}O_{1.995}$，具有层状结构。

[0048] 将获得到的镁、钛、氟掺杂的钴酸锂（$LiCo_{0.98}Ti_{0.01}Mg_{0.01}F_{0.005}O_{1.995}$）粉末置于装有工业酒精的搅拌混料罐中，搅拌 10 分钟后，加入溶解在异丙醇中的异丙醇铝溶液（Al/Co = 0.005）；在搅拌状态下在 100℃热水浴中干燥；将干燥后的物料置于推板隧道窑中，在 500℃下热处理 8 小时，冷却后过筛，即可得到具有 Al 包覆层的 $LiCo_{0.98}Ti_{0.01}Mg_{0.01}F_{0.005}O_{1.995}$ 材料。

[0049] 测量所得材料的压实密度，方法同实施例一所述，测得干粉压实密度为 4.38g/cm^3。

[0050] 实施例五

[0051] 按照锂、钴、钛原子比例为 1.05 ： 1.00 ： 0.01 的比例将碳酸钴、氢氧化锂、二氧化钛球磨混合 5 小时；将混合后的原料置于焙烧炉中，在空气气氛中 1000℃焙烧 12 小时；将焙烧后的产物先通过粗破碎后，再使用气流磨进行精破碎，粉末的平均粒度 D50 为 15μm。

[0052] 按照锂、钴、钛原子比例为 1.01 ： 1.00 ： 0.01 的比例将碳酸钴、碳酸锂、二氧化钛球磨混合 5 小时；将混合后的原料置于焙烧炉中，在空气气氛中 1000℃焙烧 12 小时；将焙烧后的产物先通过粗破碎后，再使用气流磨进行精破碎，粉末的平均粒度 D50 为 5μm。

[0053] 将 D50 为 15μm 和 D50 为 5μm 的粉末按照重量比为 1 ： 2 比例称量，加入微米级氧化镁、氟化锂，其中物质的量的比例是 Mg/Co = 0.005，F/Co = 0.002，球磨混合 3 小时；球磨后的粉末置于推板隧道窑中，在空气气氛下 980℃焙烧 12 小时；将焙烧后的产物先经粗破碎，然后使用气流磨进行精破碎，得到平均粒度 D50 为 8.5μm 的产物，此时获得镁、钛、氟掺杂的钴酸锂，化学式为 $LiCo_{0.98}Ti_{0.01}Mg_{0.01}F_{0.005}O_{1.995}$，具有层状结构。

[0054] 将获得到的镁、钛、氟掺杂的钴酸锂（$LiCo_{0.98}Ti_{0.01}Mg_{0.01}F_{0.005}O_{1.995}$）粉末置于装有工业酒精的搅拌混料罐中，搅拌 10 分钟后，加入溶解在异丙醇中的异丙醇铝溶液（Al/Co

AMPEREX Ex. 1002
Page 1170

= 0.005)；在搅拌状态下在 100℃热水浴中干燥；将干燥后的物料置于推板隧道窑中，在 500℃下热处理 8 小时，冷却后过筛，即可得到具有 Al 包覆层的 $LiCo_{0.98}Ti_{0.01}Mg_{0.01}F_{0.005}O_{1.995}$ 材料。

[0055] 测量所得材料的压实密度，方法同实施例一所述，测得干粉压实密度为 4.20g/cm^3。

[0056] 对比例一

[0057] 按照锂、钴、钛的比例为 1.03 ： 1.00 ： 0.01 的比例将碳酸锂、四氧化三钴、二氧化钛球磨混合 5 小时；将混合后的原料置于焙烧炉中，在空气气氛中 1000℃焙烧 12 小时；将焙烧后的产物先通过粗破碎后，再使用气流磨进行精破碎，粉末的平均粒度 D50 为 12μm。

[0058] 向获得的 D50 为 12μm 的物料中加入微米级氧化镁、氟化锂，其中物质的量的比例是 Mg/Co = 0.005，F/Co = 0.002，球磨混合 3 小时；球磨后的粉末置于推板隧道窑中，在空气气氛下 980℃焙烧 12 小时；将焙烧后的产物通过粗破碎、精破碎，得到平均粒度 D50 为 11.5μm 的产物，此时获得镁、钛、氟掺杂的钴酸锂，化学式为 $LiCo_{0.98}Ti_{0.01}Mg_{0.01}F_{0.005}O_{1.995}$，具有层状结构。

[0059] 将获得的镁、钛、氟掺杂的钴酸锂 ($LiCo_{0.98}Ti_{0.01}Mg_{0.01}F_{0.005}O_{1.995}$) 粉末置于装有工业酒精的搅拌混料罐中，搅拌 10 分钟后，加入溶解在异丙醇中的异丙醇铝溶液 (Al/Co = 0.005)，在搅拌状态下在 100℃热水浴中干燥；将干燥后的物料置于推板隧道窑中，在 500℃下热处理 8 小时，冷却后过筛，即可得到具有 Al 包覆层的 $LiCo_{0.98}Ti_{0.01}Mg_{0.01}F_{0.005}O_{1.995}$ 材料。

[0060] 测量所得材料的压实密度和倍率性能，测试方法同实施例一，干粉压实密度为 4.32g/cm^3，倍率性能见图 3，使用大小颗粒重量比为 1 ： 1 时，其倍率性能最好。

[0061] 对比例二

[0062] 按照锂、钴、钛的比例为 1.03 ： 1.00 ： 0.01 的比例将碳酸锂、四氧化三钴、二氧化锆球磨混合 5 小时；将混合后的原料置于焙烧炉中，在空气气氛中 1000℃焙烧 12 小时；将焙烧后的产物先通过粗破碎后，再使用气流磨进行精破碎，粉末的平均粒度 D50 为 12μm。

[0063] 向获得的 D50 为 12μm 的物料中加入微米级氧化镁、氟化锂，球磨混合 3 小时；球磨后的粉末置于推板隧道窑中，在空气气氛下 960℃焙烧 12 小时；将焙烧后的产物通过破碎后，得到平均粒度 D50 为 12μm 的产物，此时获得镁、锆、氟掺杂的钴酸锂，化学式为 $LiCo_{0.98}Zr_{0.01}Mg_{0.01}F_{0.005}O_{1.995}$，具有层状结构。

[0064] 将获得的镁、锆、氟掺杂的钴酸锂 ($LiCo_{0.98}Zr_{0.01}Mg_{0.01}F_{0.005}O_{1.995}$) 粉末置于装有工业酒精的搅拌混料罐中，搅拌 10 分钟后，加入溶解在异丙醇中的异丙醇铝溶液 (Al/Co = 0.005)，在搅拌状态下在 100℃热水浴中干燥；将干燥后的物料，置于推板隧道窑中，在 500℃下热处理 8 小时，冷却后过筛，即可得到具有 Al 包覆层的 $LiCo_{0.98}Zr_{0.01}Mg_{0.01}F_{0.005}O_{1.995}$ 材料。

[0065] 测量所得材料的倍率性能，测试方法同实施例一，结果见图 3，在粒度相当的条件下，通过大小颗粒级配的钴酸锂的倍率性能优于单一颗粒。

AMPEREX Ex. 1002
Page 1171

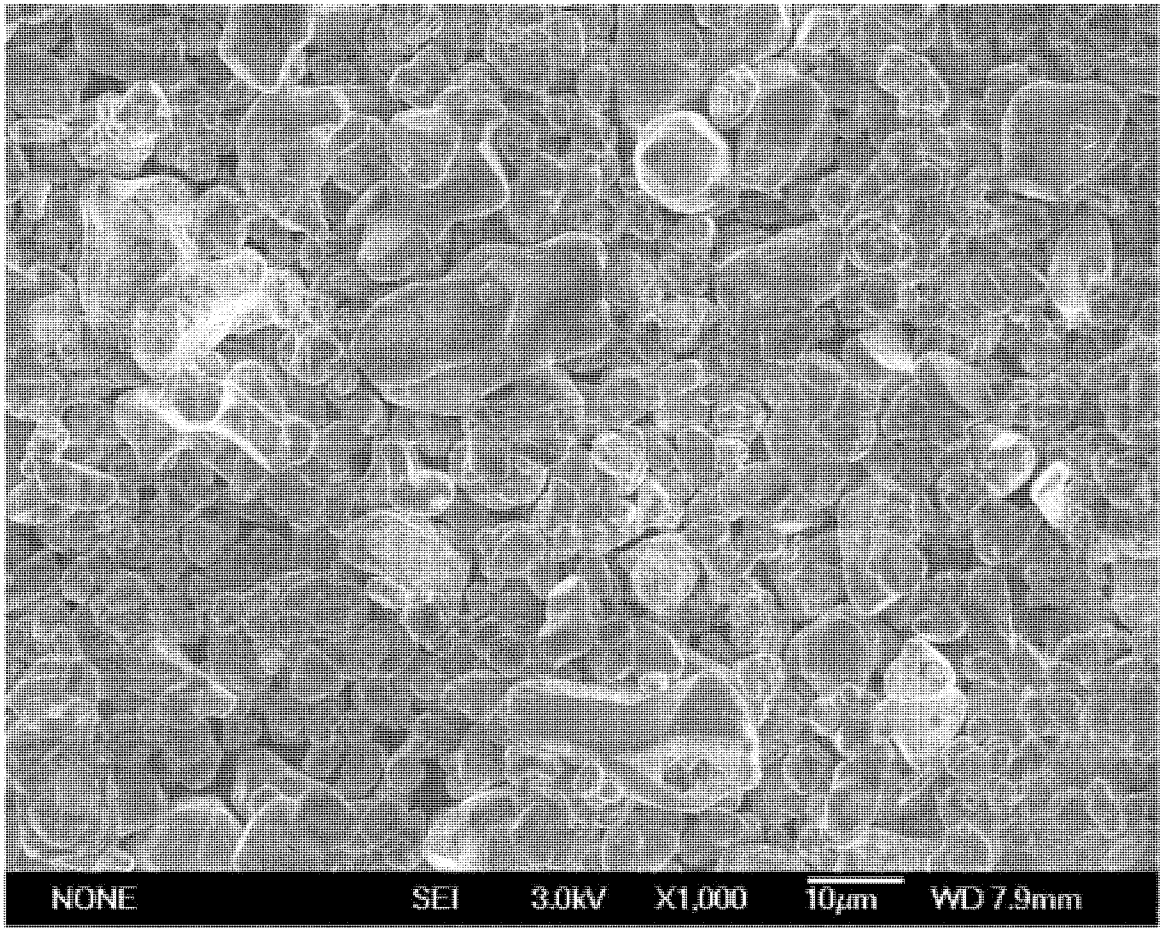


图 1

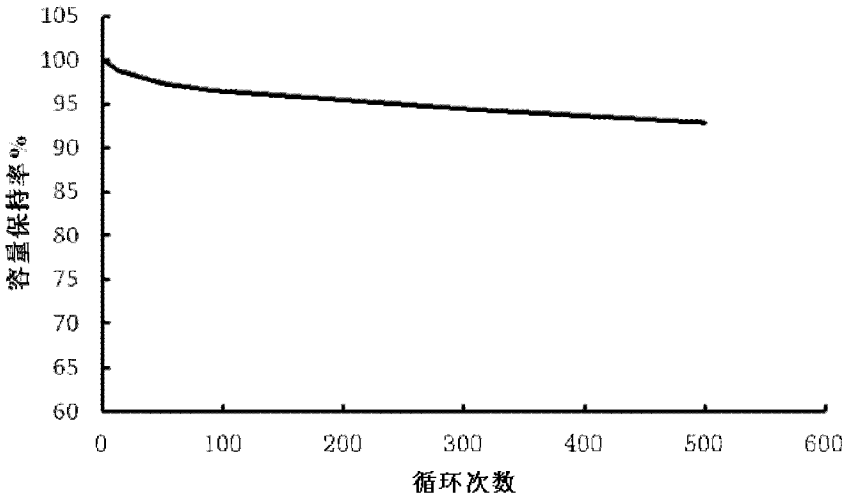


图 2

AMPEREX Ex. 1002
Page 1172

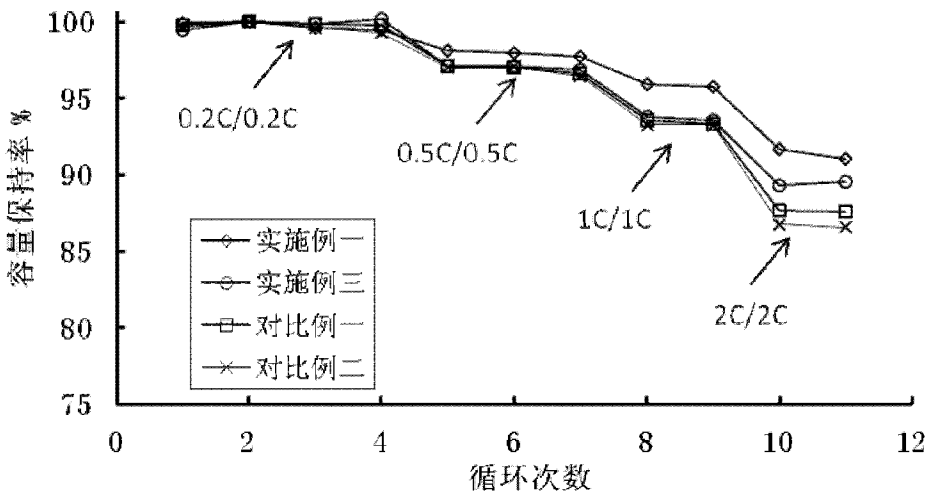


图 3

AMPEREX Ex. 1002
Page 1173

Espacenet

RSS family service

Family list: CN103490060 (A) — 2014-01-01

1 application(s) for: CN103490060 (A)

1. Lithium nickel cobalt manganese positive electrode material and preparation method thereof					
Inventor:	**Applicant:**	**CPC:**	**IPC:**	**Publication info:**	**Priority date:**
WU ZHENHAO LANG YE (+3)	NINGDE AMPEREX TECHNOLOGY LTD	H01M10/0525 H01M4/366 H01M4/505 (+2)	H01M4/505 H01M4/525	CN103490060 (A) 2014-01-01 Global Dossier	2013-10-11

Espacenet

Bibliographic data: CN103490060 (A) — 2014-01-01

Lithium nickel cobalt manganese positive electrode material and preparation method thereof

Inventor(s): WU ZHENHAO; LANG YE; HE JINHUA; WU CHENGREN; XIA HENGTAO ± (WU ZHENHAO, ; LANG YE, ; HE JINHUA, ; WU CHENGREN, ; XIA HENGTAO)

Applicant(s): NINGDE AMPEREX TECHNOLOGY LTD ± (NINGDE AMPEREX TECHNOLOGY LTD)

Classification: - international: ***H01M4/505; H01M4/525***
- cooperative: **H01M10/0525 (CN); H01M4/366 (CN); H01M4/505 (CN); H01M4/525 (CN);** Y02E60/10 (EP)

Application number: CN201310472957 20131011 Global Dossier

Priority number (s): CN201310472957 20131011

Abstract of CN103490060 (A)

The invention discloses a lithium nickel cobalt manganese positive electrode material. The lithium nickel cobalt manganese positive electrode material comprises a lithium nickel cobalt manganese oxide contained core pure phase layer having a thickness of 5-8mum, a surface coat containing oxides, phosphates or fluorides of coating elements comprising Li, Al, Mg, Ti and Zr and having a thickness of 50-100nm, and a superficial doped transition layer positioned between the core pure phase layer and the surface coat, containing doping elements comprising Al, Mg, Ti and Zr or one of rare earth elements and having a thickness of 1-2mum. The lithium nickel cobalt manganese positive electrode material can inhibit the material dissolving in a cycle process without reducing a specific capacity, and has the characteristics of high capability excellent cycle and rate performances, and excellent thermal stability.

(19)中华人民共和国国家知识产权局

(12)发明专利申请

(10)申请公布号 CN 103490060 A
(43)申请公布日 2014.01.01

(21)申请号 201310472957.1

(22)申请日 2013.10.11

(71)申请人 宁德新能源科技有限公司
地址 352100 福建省宁德市东侨经济开发区郑港路1号

(72)发明人 吴振豪 郎野 何金华 吴承仁 夏恒涛

(74)专利代理机构 广州三环专利代理有限公司 44202
代理人 王基才 王冬华

(51)Int.Cl.
H01M 4/505(2010.01)
H01M 4/525(2010.01)

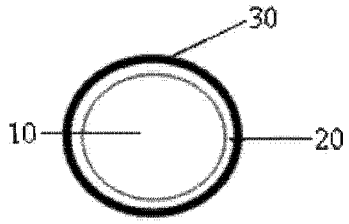
权利要求书1页 说明书6页 附图1页

(54)发明名称

锂镍钴锰正极材料及其制备方法

(57)摘要

本发明公开了一种锂镍钴锰正极材料，其包括：含有锂镍钴锰氧化物的内核纯相层，厚度为5-8μm；含有包覆元素Li、Al、Mg、Ti、Zr的氧化物、磷酸盐或氟化物的表面包覆层，厚度为50-100nm；以及位于内核纯相层和表面包覆层之间含有掺杂元素Al、Mg、Ti、Zr或稀土元素中的一种的浅表掺杂过渡层，厚度为1-2μm。本发明锂镍钴锰正极材料在不降低比容量的前提下，可抑制循环过程中材料的溶解，具有高容量、优异的循环、倍率性能和热稳定性。



CN 103490060 A

1. 一种锂镍钴锰正极材料，其特征在于，所述锂镍钴锰正极材料包括：含有锂镍钴锰氧化物的内核纯相层，厚度为 5-8μm；含有包覆元素 Li、Al、Mg、Ti、Zr 的氧化物、磷酸盐或氟化物的表面包覆层，厚度为 50-100nm；以及位于内核纯相层和表面包覆层之间含有掺杂元素 Al、Mg、Ti、Zr 或稀土元素中的一种的浅表掺杂过渡层，厚度为 1-2μm。

2. 根据权利要求 1 所述的锂镍钴锰正极材料，其特征在于，所述锂镍钴锰正极材料的通式为 $LiNi_xCo_yMn_{1-x-y}A_ZC_wO_2$，其中，$0<x<1$，$0<y<1$，z 为 0.01-0.04，w 为 0.001-0.005；A 为浅表掺杂过渡层中的掺杂元素 Al、Mg、Ti、Zr 或稀土元素；C 为表面包覆元素，选自 Li、Al、Mg、Ti、Zr。

3. 根据权利要求 2 所述的锂镍钴锰正极材料，其特征在于，所述通式 $LiNi_xCo_yMn_{1-x-y}A_ZC_wO_2$ 中，x=0.33，y=0.33；或 x=0.5，y=0.2；或 x=0.4，y=0.4；或 x=0.8，y=0.1；或 x=0.4，y=0.2。

4. 一种锂离子电池，包括正极、负极、间隔于正负极之间的隔离膜，以及电解液，其特征在于，所述正极含有权利要求 1 至 3 中任一项所述的锂镍钴锰正极材料。

5. 一种权利要求 1 至 3 中任一项所述的锂镍钴锰正极材料的制备方法，其特征在于，包括以下步骤：

1) 提供前驱体 $(Ni_xCo_yMn_{1-x-y})(OH)_2$ 粉末，D50=5-8μm；

2) 将掺杂元素 Al、Mg、Ti、Zr 或稀土元素的化合物通过液相法均匀沉积到 $(Ni_xCo_yMn_{1-x-y})(OH)_2$ 前驱体上，沉积后的前驱体 D50=8-10μm，再与锂盐粉末按一定比例均匀混合进行第一次高温烧结，高温煅烧得到体相掺杂锂镍钴锰正极材料初级产品；

3) 在锂镍钴锰正极材料初级产品的表面包覆含有包覆元素 Li、Al、Mg、Ti、Zr 的氧化物、磷酸盐或氟化物的表面包覆层，进行第二次高温处理，在 500-700℃高温处理 3-7h，获得锂镍钴锰正极材料 $LiNi_xCo_yMn_{1-x-y}A_ZC_wO_2$，其中，$0<x<1$，$0<y<1$，z 为 0.01-0.04，w 为 0.001-0.005。

6. 根据权利要求 5 所述的方法，其特征在于，步骤 1) 中，通过将水溶性金属镍盐、钴盐和锰盐按一定的 Ni、Co、Mn 摩尔比配成混合溶液，将混合溶液与沉淀剂、形貌控制剂同时滴加到反应容器中，控制体系的 pH 值和反应温度，反应一段时间后过滤、洗涤、真空干燥后得到前驱体 $(Ni_xCo_yMn_{1-x-y})(OH)_2$ 粉末。

7. 根据权利要求 5 所述的锂镍钴锰正极材料的制备方法，其特征在于，步骤 2) 中，含掺杂元素 Al、Mg、Ti、Zr 或稀土元素的化合物为掺杂元素 Al、Mg、Ti、Zr 或稀土元素的可溶性醋酸盐、氯化盐、硝酸盐、硫酸盐、碳酸盐、纳米氧化物中的一种或多种。

8. 根据权利要求 5 所述的锂镍钴锰正极材料的制备方法，其特征在于，步骤 2) 中，掺杂元素 Al、Mg、Ti、Zr 或稀土元素与镍钴锰金属总和的摩尔比为 0.001-0.20，优选为 0.01-0.04，表面包覆层与正极材料总质量的重量比为 0.001-0.05，优选为 0.005-0.02。

9. 根据权利要求 5 所述的锂镍钴锰正极材料的制备方法，其特征在于，步骤 2) 步中，所述锂盐为碳酸锂、氢氧化锂、醋酸锂中的一种或几种，所述锂盐与前驱体的金属摩尔总和比为 1.01-1.10，优选 1.02-1.05。

10. 根据权利要求 5 所述的锂镍钴锰正极材料的制备方法，其特征在于，步骤 1) 中，金属离子的总浓度为 1-3M，沉淀剂的浓度为 2-6M，体系的 pH 值 10.0-12.0，含掺杂元素 Al、Mg、Ti、Zr 或稀土元素的化合物的尺寸为 5-100nm，高温煅烧的温度为 800-950℃，时间为 10-24h。

AMPEREX Ex. 1002
Page 1177

锂镍钴锰正极材料及其制备方法

技术领域

[0001] 本发明属于锂离子电池领域，更具体地说，本发明涉及一种复合改性锂镍钴锰正极材料及其制备方法。

背景技术

[0002] 正极材料锂镍钴锰（$LiNi_xCo_yMn_{1-x-y}O_2$，$0<x<1$，$0<y<1$）自2000年问世以来，因具有结构稳定、放电比容量大、放电平台高、原料广泛和对环境友好等优点而备受关注，被认为是制备高寿命、高功率、高安全、低成本的锂离子电池的理想正极材料。

[0003] 但是，锂镍钴锰正极材料本身较高的化学活性导致其在循环过程中容易与电解液发生反应，降低了正极材料的稳定性，使用中，正极材料容易出现金属溶出、电解液分解产气等问题，限制了锂镍钴锰正极材料的应用。因此，目前的研究主要集中在如何改善材料的表面稳定性，抑制其与电解液的反应上。为此，现有技术一方面是通过工艺的优化，控制合成过程中材料的晶粒生长，以获取具有较大晶粒且粒度分布均一、比表面积较小的材料，以减小表面与电解液的反应速率，降低电解液消耗；另一方面是通过掺杂和包覆改性提高正极材料的表面稳定性，降低循环过程中金属的溶出。

[0004] 但是，单一的掺杂或包覆往往无法获得综合性能优良的锂镍钴锰正极材料，例如，Al_2O_3、$AlPO_4$表面包覆可以提高锂镍钴锰正极材料的循环性能和安全性能，却会导致容量和倍率性能降低；而Mg，Ti等的掺杂可以提高锂镍钴锰正极材料的倍率性能，但对循环性能提高不大，都达不到改善电池综合性能的需求。

[0005] 有鉴于此，确有必要提供一种具有理想综合性能的锂镍钴锰正极材料及其制备方法。

发明内容

[0006] 本发明的目的在于：克服现有技术的缺陷，提供一种具有理想综合性能的锂镍钴锰正极材料及其制备方法。

[0007] 为了实现上述发明目的，本发明提供了一种锂镍钴锰正极材料，其包括：含有锂镍钴锰氧化物的内核纯相层，厚度为5-8μm，厚度由所合成的前驱体粒径和第一次烧结温度决定；含有包覆元素Li、Al、Mg、Ti、Zr的氧化物、磷酸盐或氟化物的表面包覆层，厚度为50-100nm，厚度由包覆量和第二次热处理温度及时间决定；以及位于内核纯相层和表面包覆层之间含有掺杂元素Al、Mg、Ti、Zr或稀土元素中的一种的浅表掺杂过渡层，厚度为1-2μm，厚度由掺杂前驱体厚度和第一次烧结温度决定。

[0008] 太大的表面包覆层厚度会增加材料的阻抗，降低其循环能力，50-100nm厚的表面包覆层既能起到保护材料表面层免遭电解液的过渡破坏，又能提高材料的循环能力。浅表掺杂过渡层的作用主要是稳定材料的结构，避免材料在长期循环的过程中由于Li+的反复脱嵌产生的应力对材料结构产生破坏，但浅表掺杂过渡层的厚度如果太大，一会降低材料的容量发挥，同时会造成金属混排，降低材料的循环能力，1-2μm的厚度既能增加材料的稳

AMPEREX Ex. 1002
Page 1178

定性，又不会降低材料的循环能力。

[0009] 作为本发明锂镍钴锰正极材料的一种改进，所述锂镍钴锰正极材料的通式为 $LiNi_xCo_yMn_{1-x-y}A_ZC_wO_2$，其中，$0 < x < 1$，$0 < y < 1$，z 为 0.01-0.04，w 为 0.001-0.005；A 为浅表掺杂过渡层中的掺杂元素 Al、Mg、Ti、Zr 或稀土元素；C 为表面包覆元素，选自 Li、Al、Mg、Ti、Zr。

[0010] 作为本发明锂镍钴锰正极材料的一种改进，通式 $LiNi_xCo_yMn_{1-x-y}A_ZC_wO_2$ 中，x=0.33，y=0.33；或 x=0.5，y=0.2；或 x=0.4，y=0.4；或 x=0.8，y=0.1；或 x=0.4，y=0.2。

[0011] 此外，本发明还提供了一种锂离子电池，包括正极、负极、间隔于正负极之间的隔离膜，以及电解液，其中，所述正极含有前述锂镍钴锰正极材料。

[0012] 为了实现上述发明目的，本发明还提供了一种锂镍钴锰正极材料的制备方法，其包括以下步骤：

[0013] 1) 提供前驱体 $(Ni_xCo_yMn_{1-x-y})(OH)_2$ 粉末，D50=5-8μm；

[0014] 2) 将掺杂元素 Al、Mg、Ti、Zr 或稀土元素的化合物通过液相法均匀沉积到 $(Ni_xCo_yMn_{1-x-y})(OH)_2$ 前驱体上，此时前驱体的 D50=8-10μm，再与锂盐粉末按一定比例均匀混合，高温煅烧得到体相掺杂锂镍钴锰正极材料初级产品；

[0015] 3) 在锂镍钴锰正极材料初级产品的表面包覆含有包覆元素 Li、Al、Mg、Ti、Zr 的氧化物、磷酸盐或氟化物的表面包覆层，在 500-700℃高温处理 3-7h，获得锂镍钴锰正极材料 $LiNi_xCo_yMn_{1-x-y}A_ZC_wO_2$，其中，$0 < x < 1$，$0 < y < 1$，z 为 0.01-0.04，w 为 0.001-0.005。

[0016] 作为本发明锂镍钴锰正极材料的制备方法的一种改进，步骤 1) 中，通过将水溶性金属镍盐、钴盐和锰盐按一定的 Ni、Co、Mn 摩尔比配成混合溶液，将混合溶液与沉淀剂、形貌控制剂一起同时滴加到反应容器中，控制体系的 pH 值和反应温度，反应一段时间后经过过滤、洗涤、真空干燥后得到前驱体 $(Ni_xCo_yMn_{1-x-y})(OH)_2$ 粉末。

[0017] 作为本发明锂镍钴锰正极材料的制备方法的一种改进，步骤 2) 中，含掺杂元素 Al、Mg、Ti、Zr 或稀土元素的化合物为掺杂元素 Al、Mg、Ti、Zr 或稀土元素的可溶性醋酸盐、氯化盐、硝酸盐、硫酸盐、碳酸盐、纳米氧化物中的一种或多种。

[0018] 作为本发明锂镍钴锰正极材料的制备方法的一种改进，步骤 2) 中，掺杂元素 Al、Mg、Ti、Zr 或稀土元素与镍钴锰金属总和的摩尔比为 0.001-0.20，优选为 0.01-0.04，表面包覆层与正极材料的质量比为 0.001-0.05，优选为 0.005-0.02。

[0019] 作为本发明锂镍钴锰正极材料的制备方法的一种改进，步骤 2) 步中，所述锂盐为碳酸锂、氢氧化锂、醋酸锂中的一种或几种，所述锂盐与前驱体的金属摩尔总和比为 1.01-1.10，优选 1.02-1.05。

[0020] 作为本发明锂镍钴锰正极材料的制备方法的一种改进，步骤 1) 中，金属离子的总浓度为 1-3M，沉淀剂的浓度为 2-6M，体系的 pH 值 10.0-12.0；步骤 2) 中，含掺杂元素 Al、Mg、Ti、Zr 或稀土元素的化合物的尺寸为 5-100nm，高温煅烧的温度为 800-950℃，时间为 10-24h。

[0021] 相对于现有技术，本发明制备的材料结构更加合理，抗高电压能力更好，实施方法操作简单，易于工业化生产；通过本发明制备方法获得的锂镍钴锰正极材料，改性剂在正极材料内部和表面呈现不同的状态分布，在不降低比容量的前提下，可抑制循环过程中材料的溶解，经过特定的热处理工艺，可在保持较高比容量的同时，具有高容量、优异的循环、倍

AMPEREX Ex. 1002
Page 1179

率性能和热稳定性。

附图说明

[0022] 以下结合附图和具体实施方式，对本发明锂镍钴锰正极材料及其制备方法和其有益效果进行详细说明，其中：

[0023] 图 1 是本发明实施例 1 中制备的锂镍钴锰正极材料的 SEM 图。

[0024] 图 2 是本发明实施例 1-5 和对比例 1 中制备的锂离子电池的循环性能曲线对比图。

[0025] 图 3 是本发明锂镍钴锰正极材料的结构示意图。

具体实施方式

[0026] 为了使本发明的发明目的、技术方案和有益技术效果更加清晰，以下结合附图和实施例，对本发明进行进一步详细说明。应当理解的是，本说明书中描述的实施例仅是为了解释本发明，并非为了限定本发明。

[0027] 下面以 $Li(Ni_{1/3}Co_{1/3}Mn_{1/3})O_2$ 正极材料为例，对本发明进一步详细说明，但本发明的实施例不限于此，在本发明的其他实施例中，各元素的配比可以根据需要适当调整和选择。

[0028] 对比例 1

[0029] 首先，将 $Li(Ni_{1/3}Co_{1/3}Mn_{1/3})O_2$ 前驱体 $(Ni_{1/3}Co_{1/3}Mn_{1/3})(OH)_2$ 和碳酸锂 (Li_2CO_3) 在球磨机中充分混合，然后在空气气氛下进行低温烧结，得到前驱物 A；将前驱物 A 均匀分散到用于表面掺杂的金属元素 Al 的硝酸盐溶液中进行液相热反应，经过滤、洗涤取沉淀物，得到中间体 B；再将中间体 B 均匀分散到 Al 的硝酸盐溶液中，用 NaOH 溶液调节到适当的 pH 值并进行液相热反应，经过滤、洗涤取沉淀物，得到中间体 C；将中间体 C 烘干，球磨和高温烧结得到对比例 1 正极材料 $Al_2O_3/Li_{1.02}Ni_{1/3}Mn_{1/3}Co_{0.31}Al_{0.02}O_2/Li(Ni_{1/3}Co_{1/3}Mn_{1/3})O_2$。

[0030] 实施例 1

[0031] 1) 按分子式 $Li(Ni_{1/3}Co_{1/3}Mn_{1/3})O_2$ 中过渡金属的比例配制 $NiSO_4$、$CoSO_4$、$MnSO_4$ 的混合水溶液，其中，阳离子的浓度为 2mol/L；

[0032] 2) 将步骤 1) 中的混合水溶液和 2mol/L NaOH 溶液、3mol/L 氨水溶液共同滴加到反应容器中，控制体系的 pH 值在 11.0，水浴加热至 50℃，反应 12h 后，过滤、洗涤，在 120℃真空干燥 8h 后得到前驱体 $(Ni_{1/3}Co_{1/3}Mn_{1/3})(OH)_2$，其 D50=5μm；

[0033] 3) 将步骤 2) 中的前驱体 $(Ni_{1/3}Co_{1/3}Mn_{1/3})(OH)_2$、九水硝酸铝与均散剂尿素按摩尔比为前驱体：Al：尿素 =100：0.5：8.35 的比例分别称取 50g 前驱体、3.67g 九水硝酸铝，5.35g 均散剂尿素溶解在 250mL 去离子水中，搅拌分散均匀并升温至 70℃，搅拌保持 1h，过滤得到 $Al(OH)_3$ 包覆的 $(Ni_{1/3}Co_{1/3}Mn_{1/3})(OH)_2$ 前驱体粉末，其 D50=8μm；

[0034] 4) 将步骤 3) 获得的 $Al(OH)_3$ 包覆的 $(Ni_{1/3}Co_{1/3}Mn_{1/3})(OH)_2$ 前驱体粉末与 40.76gLi_2CO_3 粉末混合置于空气氛围的烧结炉中，先在 500℃加热 5 个小时，然后升温至 900℃在空气中烧结 20 个小时，获得内部掺杂 Al 的初级正极材料；

[0035] 5) 将步骤 4) 获得的初级正极材料 50g，置于 50ml 溶解有 1g 九水硝酸铝的无水乙醇中，然后缓慢滴加 10ml 溶解有 0.45g 磷酸二氢铵的水溶液，搅拌 1h 抽滤得到固体粉末，将固体粉末置于空气氛围的烧结炉中，500℃处理 5h，即得到内部掺杂 Al，表面包覆 $AlPO_4$

AMPEREX Ex. 1002
Page 1180

的复合改性锂镍钴锰正极材料，改性后的锂镍钴锰正极材料的结构如图 3 所示（实施例 2 至 5 的锂镍钴锰正极材料的结构大致相同），其中，10 为内核纯相层，其厚度为 5μm；20 为浅表掺杂过渡层，其厚度为 1μm；30 为表面包覆层，其厚度为 100nm。

[0036] 实施例 2

[0037] 1）按分子式 $Li(Ni_{1/3}Co_{1/3}Mn_{1/3})O_2$ 中过渡金属的比例配制 $NiSO_4$、$CoSO_4$、$MnSO_4$ 的混合水溶液，其中，阳离子的浓度为 2mol/L；

[0038] 2）将步骤 1）中的混合水溶液和 2mol/L NaOH 溶液、3mol/L 氨水溶液共同滴加到反应容器中，控制体系的 pH 值在 11.0，水浴加热至 50℃，反应 12h 后，过滤、洗涤，在 120℃真空干燥 8h 后得到前驱体 $(Ni_{1/3}Co_{1/3}Mn_{1/3})(OH)_2$，其 D50=8μm；

[0039] 3）将前驱体 $(Ni_{1/3}Co_{1/3}Mn_{1/3})(OH)_2$、硝酸镁与均散剂尿素按摩尔比为前驱体：Mg：尿素 =100：0.01：8.35 的比例分别称取 50g 前驱体、3.67g 硝酸镁和 5.35g 均散剂尿素溶解在 250mL 去离子水中，搅拌分散均匀并升温至 70℃，搅拌保持 1h，过滤得到 $Mg(OH)_2$ 包覆的前驱体，其 D50=10μm；

[0040] 4）将步骤 3）获得的 $Mg(OH)_2$ 包覆的前驱体粉末与 40.76g Li_2CO_3 粉末混合置于空气氛围的烧结炉中，先在 500℃加热 5 个小时，然后升温至 900℃在空气中烧结 20 个小时，获得内部掺杂 Mg 的初级正极材料；

[0041] 5）将步骤 4）获得的初级正极材料 50g，置于 50ml 溶解有 1g 九水硝酸铝的无水乙醇中，然后缓慢滴加 10ml 溶解有 0.45g 磷酸二氢铵的水溶液，搅拌 1h 抽滤得到固体粉末，将固体粉末置于空气氛围的烧结炉中，500℃处理 5h，即得到内部掺杂 Mg，表面包覆 $AlPO_4$ 的复合改性锂镍钴锰正极材料。其中，内核纯相层厚度为 8μm；浅表掺杂过渡层厚度为 2μm；表面包覆层厚度为 50nm。

[0042] 实施例 3

[0043] 1）按分子式 $Li(Ni_{1/3}Co_{1/3}Mn_{1/3})O_2$ 中过渡金属的比例配制 $NiSO_4$、$CoSO_4$、$MnSO_4$ 的混合水溶液，其中，阳离子的浓度为 2mol/L；

[0044] 2）将步骤 1）中的混合水溶液和 2mol/L NaOH 溶液、3mol/L 氨水溶液共同滴加到反应容器中，控制体系的 pH 值在 11.0，水浴加热至 50℃，反应 12h 后，过滤、洗涤，在 120℃真空干燥 8h 后得到前驱体 $(Ni_{1/3}Co_{1/3}Mn_{1/3})(OH)_2$，其 D50=6μm；

[0045] 3）将 50g 前驱体 $(Ni_{1/3}Co_{1/3}Mn_{1/3})(OH)_2$ 分散在 50ml 无水乙醇和 5ml 去离子水的混合溶液中，然后滴加 0.026M 的钛酸四丁酯的异丙醇溶液，滴加完搅拌 1h，过滤得到 $Ti(OH)_4$ 包覆的前驱体，其 D50=8μm；

[0046] 4）将步骤 3）获得的 $Ti(OH)_4$ 包覆的前驱体粉末与 40.76g Li_2CO_3 粉末混合置于空气氛围的烧结炉中，先在 500℃加热 5 个小时，然后升温至 900℃在空气中烧结 20 个小时，获得内部掺杂 Ti 的初级正极材料；

[0047] 5）将步骤 4）获得的初级正极材料 50g，置于 50ml 溶解有 1g 九水硝酸铝的无水乙醇中，然后缓慢加热搅拌回流 1h，抽滤得到固体粉末，将粉末置于空气氛围的烧结炉中，500℃处理 5h，即得到内部掺杂 Ti，表面包覆 Al_2O_3 的复合改性锂镍钴锰正极材料。其中，内核纯相层厚度为 8μm；浅表掺杂过渡层厚度为 1μm；表面包覆层厚度为 80nm。

[0048] 实施例 4

[0049] 1）按分子式 $Li(Ni_{1/3}Co_{1/3}Mn_{1/3})O_2$ 中过渡金属的比例配制 $NiSO_4$、$CoSO_4$、$MnSO_4$ 的混

AMPEREX Ex. 1002
Page 1181

合水溶液，其中，阳离子的浓度为 2mol/L ；

[0050] 2) 将步骤 1) 中的混合水溶液和 2mol/L NaOH 溶液、3mol/L 氨水溶液共同滴加到反应容器中，控制体系的 pH 值在 11.0，水浴加热至 50℃，反应 12h 后，过滤、洗涤，在 120℃真空干燥 8h 后得到前驱体 $(Ni_{1/3}Co_{1/3}Mn_{1/3})(OH)_2$，其 D50=8μm ；

[0051] 3) 将前驱体 $(Ni_{1/3}Co_{1/3}Mn_{1/3})(OH)_2$、硝酸锆与均散剂尿素按摩尔比为前驱体 :Zr :尿素 =100 :0.03 :8.35 的比例分别称取 50g 前驱体、3.67g 九水硝酸铝、5.35g 均散剂尿素溶解在 250mL 去离子水中，搅拌分散均匀并升温至 70℃，搅拌保持 1h，过滤得到 $Zr(OH)_2$ 包覆的前驱体，其 D50=10μm ；

[0052] 4) 将步骤 3) 获得的 $Zr(OH)_2$ 包覆的前驱体粉末与 40.76gLi_2CO_3 粉末混合置于空气氛围的烧结炉中，先在 500℃加热 5 个小时，然后升温至 900℃在空气中烧结 20 个小时，获得内部掺杂 Zr 的初级正极材料 ；

[0053] 5) 将步骤 4) 获得的初级正极材料 50g，置于 50ml 无水乙醇与 5ml 去离子水的混合溶液中，然后缓慢滴加 10ml0.026M 的钛酸四丁酯的异丙醇溶液，滴加完，搅拌 1h 抽滤得到固体粉末，将固体粉末置于空气氛围的烧结炉中，在 500℃处理 5h，即得到内部掺杂 Zr，表面包覆 TiO_2 的复合改性锂镍钴锰正极材料。其中，内核纯相层厚度为 6μm ；浅表掺杂过渡层厚度为 2μm ；表面包覆层厚度为 90nm。

[0054] 实施例 5

[0055] 1) 按分子式 $Li(Ni_{1/3}Co_{1/3}Mn_{1/3})O_2$ 中过渡金属的比例配制 $NiSO_4$、$CoSO_4$、$MnSO_4$ 的混合水溶液，其中，阳离子的浓度为 2mol/L ；

[0056] 2) 将步骤 1) 中的混合水溶液和 2mol/L NaOH 溶液、3mol/L 氨水溶液共同滴加到反应容器中，控制体系的 pH 值在 11.0，水浴加热至 50℃，反应 12h 后，过滤、洗涤，在 120℃真空干燥 8h 后得到前驱体 $(Ni_{1/3}Co_{1/3}Mn_{1/3})(OH)_2$，其 D50=5μm ；

[0057] 3) 将前驱体 $(Ni_{1/3}Co_{1/3}Mn_{1/3})(OH)_2$、九水硝酸铝与均散剂尿素按摩尔比为前驱体 :Al :尿素 =100 :0.04 :8.35 的比例分别称取 50g 前驱体、3.67g 硝酸铝，5.35g 均散剂尿素溶解在 250mL 去离子水中，搅拌分散均匀并升温至 70℃，搅拌保持 1h，过滤得到 $Al(OH)_3$ 包覆的前驱体，其 D50=10μm ；

[0058] 4) 将步骤 3) 获得的 $Al(OH)_3$ 包覆的前驱体粉末与 40.76gLi_2CO_3 粉末混合置于空气氛围的烧结炉中，先在 500℃加热 5 个小时，然后升温至 900℃并在空气中烧结 20 个小时，获得内部掺杂 Al 的初级正极材料 ；

[0059] 5) 将步骤 4) 获得的初级正极材料 50g，置于 50ml 溶解有 1g 硝酸锆的去离子水中，然后缓慢滴加 0.5M 的氨水溶液，搅拌 1h 抽滤得到固体粉末，将固体粉末置于空气氛围的烧结炉中，500℃处理 5h，即得到内部掺杂 Al、表面包覆 ZrO2 的复合改性锂镍钴锰正极材料。其中，内核纯相层厚度为 5μm ；浅表掺杂过渡层厚度为 2μm ；表面包覆层厚度为 70nm。

[0060] 将对比例 1 和实施例 1 ～ 5 制得的锂离子电池正极材料分别与导电碳、粘结剂聚偏氟乙烯 (PVDF) 按质量比 94:3:3 在 N- 甲基吡咯烷酮 (NMP) 溶剂中混合，常温下搅拌 12h，刮刀涂布在厚度为 16μm 的 Al 箔集流体上，120℃真空干燥 12h，得到正极片 ；负极片为人造石墨 ；中间加聚丙烯 (PP) 隔离膜卷绕，并注入电解液，电解液采用 1mol/L $LiPF_6$，EC/EMC=3:7(V/V)，经焊接卷绕成方形铝壳电池，测试电池的电化学性能。

[0061] 常温循环测试

AMPEREX Ex. 1002
Page 1182

[0062] 将采用对比例 1 和实施例 1 ～ 5 的锂离子电池正极材料组装好的铝壳电池，在 25℃的杭可机中以 0.5C 的电流密度进行充放电循环测试，电压范围为 3.0 ～ 4.4V。图 2 为容量保持率随循环次数变化的对比曲线，从图 2 中可以看出，正极材料经过复合改性后的循环能力显著提高，0.5C100 周循环的容量保持率高达 90% 以上。

[0063] 根据上述说明书的揭示和教导，本发明所属领域的技术人员还可以对上述实施方式进行适当的变更和修改。因此，本发明并不局限于上面揭示和描述的具体实施方式，对本发明的一些修改和变更也应当落入本发明的权利要求的保护范围内。此外，尽管本说明书中使用了一些特定的术语，但这些术语只是为了方便说明，并不对本发明构成任何限制。

AMPEREX Ex. 1002
Page 1183

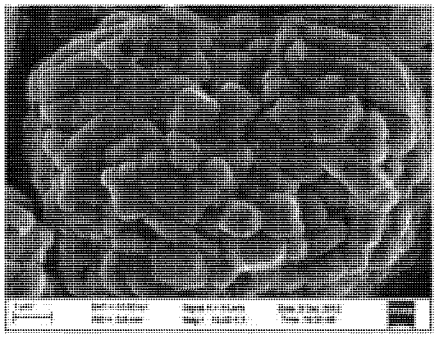


图 1

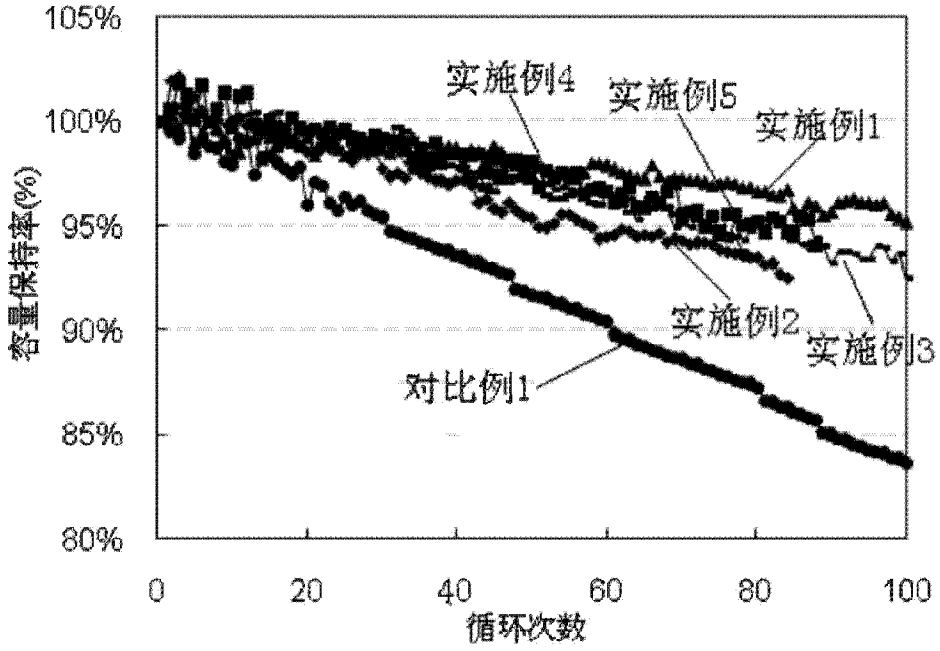


图 2

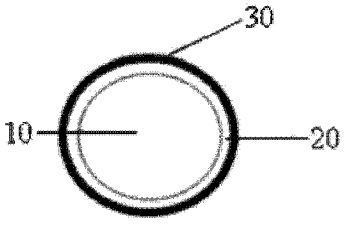


图 3

AMPEREX Ex. 1002
Page 1184

Espacenet

Family list: JP2003068306 (A) — 2003-03-07

1 application(s) for: JP2003068306 (A)

1. LITHIUM NICKEL MANGANESE LAYERED COMPOSITE OXIDE					
Inventor:	**Applicant:**	**CPC:**	**IPC:**	**Publication info:**	**Priority date:**
SHIMA KOJI KIKUCHI KAZUHIRO	MITSUBISHI CHEM CORP	Y02E60/10	H01M10/05 H01M4/131 H01M4/505 (+4)	JP2003068306 (A) 2003-03-07 JP3870846 (B2) 2007-01-24	2001-06-13

Espacenet

Bibliographic data: JP2003068306 (A) — 2003-03-07

LITHIUM NICKEL MANGANESE LAYERED COMPOSITE OXIDE

Inventor(s): SHIMA KOJI; KIKUCHI KAZUHIRO ± (SHIMA KOJI, ; KIKUCHI KAZUHIRO)

Applicant(s): MITSUBISHI CHEM CORP ± (MITSUBISHI CHEMICALS CORP)

Classification: - international: ***H01M10/05; H01M4/131; H01M4/505; H01M4/525;*** (IPC1-7): H01M10/40; H01M4/02; H01M4/58
- cooperative: Y02E60/10 (EP)

Application number: JP20020163894 20020605

Priority number (s): JP20020163894 20020605 ; JP20010178016 20010613

Also published as: JP3870846 (B2)

Abstract of JP2003068306 (A)

PROBLEM TO BE SOLVED: To provide a lithium nickel manganese composite oxide for a secon dary lithium battery good in rate characteristics. SOLUTION: The layered lithium nickel manganese composite oxide in which the atomic ratio of nickel and manganese fills 0.7<=Ni/Mn<=9 and the content of Mg and Ca is both 300 ppm or less. The part of the sites where nickel or manganese exists can be replaced by at least a kind of another metals or the like selected from a group consisting of aluminum, cobalt and iron.

(19)日本国特許庁（ＪＰ）　(12) **公開特許公報**（Ａ）　(11)特許出願公開番号
特開2003－68306
（P2003－68306A）
(43)公開日　平成15年３月７日(2003.3.7)

(51)Int.Cl.[7]	識別記号	ＦＩ		テーマコード（参考）
Ｈ０１Ｍ　4/58		Ｈ０１Ｍ　4/58		５Ｈ０２９
4/02		4/02	Ｃ	５Ｈ０５０
10/40		10/40	Ｚ	

審査請求　未請求　請求項の数７　ＯＬ　（全 11 頁）

(21)出願番号　特願2002－163894(P2002－163894)
(22)出願日　平成14年６月５日(2002.6.5)
(31)優先権主張番号　特願2001－178016(P2001－178016)
(32)優先日　平成13年６月13日(2001.6.13)
(33)優先権主張国　日本（ＪＰ）

(71)出願人　000005968
三菱化学株式会社
東京都千代田区丸の内二丁目５番２号
(72)発明者　島　耕司
神奈川県横浜市青葉区鴨志田町1000番地
三菱化学株式会社内
(72)発明者　菊地　一寛
神奈川県横浜市青葉区鴨志田町1000番地
三菱化学株式会社内
(74)代理人　100103997
弁理士　長谷川　曉司

最終頁に続く

(54)【発明の名称】　層状リチウムニッケルマンガン複合酸化物

(57)【要約】
【目的】　レート特性に優れたリチウム二次電池に使用するリチウムニッケルマンガン複合酸化物を提供する。
【解決手段】　ニッケルとマンガンとの原子比が０．７≦Ｎｉ／Ｍｎ≦９を満たす層状リチウムニッケルマンガン複合酸化物であって、Ｍｇ及びＣａの含有量が共に３００ｐｐｍ以下であることを特徴とする層状リチウムニッケルマンガン複合酸化物。ニッケル及びマンガンの存在するサイトの一部がアルミニウム、コバルト及び鉄からなる群から選ばれる少なくとも一種の金属元素等の他の元素で置換されていてもよい。

AMPEREX Ex. 1002
Page 1187

1

【特許請求の範囲】

【請求項１】　ニッケルとマンガンとの原子比が０．７≦Ｎｉ／Ｍｎ≦９を満たす層状リチウムニッケルマンガン複合酸化物であって、Ｍｇ及びＣａの含有量が共に３００ｐｐｍ以下であることを特徴とする層状リチウムニッケルマンガン複合酸化物。

【請求項２】　ニッケル及びマンガンの存在するサイトの一部が他の元素で置換されていることを特徴とする請求項１に記載の層状リチウムニッケルマンガン複合酸化物。

【請求項３】　他の元素が、Ａｌ、Ｃｏ及びＦｅからなる群から選ばれる少なくとも一種の金属元素である請求項１又は２のいずれかに記載のリチウムニッケルマンガン複合酸化物。

【請求項４】　下記一般式（Ｉ）で表される、請求項１乃至３のいずれかに記載のリチウムニッケルマンガン複合酸化物。

【化１】$Li_xNi_yMn_zQ_{(1-Y-Z)}O_2$　（Ｉ）

（式中、Ｘは０＜Ｘ≦１．２の範囲の数を表す。Ｙ及びＺは、０．７≦Ｙ／Ｚ≦９、及び、０≦０（１－Ｙ－Ｚ）≦０．５の関係を満たし、ＱはＡｌ、Ｃｏ及びＦｅからなる群から選ばれる少なくとも一種を表す。）。

【請求項５】　請求項１乃至４のいずれか１つに記載の層状リチウムニッケルマンガン複合酸化物を含有するリチウム二次電池用正極材料。

【請求項６】　請求項５に記載のリチウム二次電池用正極材料とバインダーとを含有することを特徴とするリチウム二次電池用正極。

【請求項７】　請求項１乃至４のいずれか１つに記載の層状リチウムニッケルマンガン複合酸化物を使用した正極と、負極と、電解質とを有することを特徴とするリチウム二次電池。

【発明の詳細な説明】

【０００１】

【発明の属する技術分野】本発明は、層状リチウムニッケルマンガン複合酸化物、並びにそれを用いたリチウム二次電池用正極材料及びリチウム二次電池に関するものである。

【０００２】

【従来の技術】実使用可能なリチウム二次電池を提供する正極活物質として、リチウム遷移金属複合酸化物が有望視されている。これら化合物の中でも、遷移金属としてコバルト、ニッケル、マンガンを使用する、リチウムコバルト酸化物、リチウムニッケル酸化物、リチウムマンガン酸化物を正極活物質とすると、高性能な電池特性を得られることが知られている。さらに、リチウム遷移金属複合酸化物の安定化や高容量化、安全性向上、高温での電池特性の改良のために、遷移金属サイトの一部を他の金属元素で置換したリチウム遷移金属複合酸化物を用いることも知られている。リチウム遷移金属複合酸化

2

物の例としてスピネル型リチウムマンガン酸化物$LiMn_2O_4$の場合、Ｍｎ価数は形式上３．５価であり、３価と４価が半々ずつ混在している状態であるが、このＭｎ価数より小さい価数の他の遷移金属でＭｎサイトを置換することにより、ヤーンテラー歪みのあるＭｎ３価を減少させて結晶構造を安定化させ、最終的に電池特性が向上する。

【０００３】また、コバルトのような希少で高価な元素を用いる場合、製品としてのリチウム遷移金属複合酸化物の値段を抑えるために置換元素を導入することが考えられる。例えば、$LiCo_{1-x}Ni_xO_2$（０＜ｘ＜１）といったリチウム遷移金属複合酸化物が考えられ、高価なＣｏの比率を下げるためにｘを大きくし、その方向でより性能を上げる研究がなされている。

【０００４】これと同様に、ＮｉとＭｎを比べた場合、Ｎｉの方が高価なことから、$LiNi_{1-x}Mn_xO_2$（０＜ｘ＜１）といったリチウム遷移金属複合酸化物も考えられている。このようなニッケルとマンガンとを含有するリチウムニッケルマンガン複合酸化物は、電池性能の面でも注目すべき点があり、極めて有望な材料である。しかしながら、Ｓｏｌｉｄ　Ｓｔａｔｅ　Ｉｏｎｉｃｓ　３１１－３１８（１９９２）や、Ｊ．　Ｍａｔｅｒ．　Ｃｈｅｍ．　１１４９－１１５５（１９９６）や、Ｊ．　Ｐｏｗｅｒ　Ｓｏｕｒｃｅｓ　６２９－６３３（１９９７）や、Ｊ．　Ｐｏｗｅｒ　Ｓｏｕｒｃｅｓ　４６－５３（１９９８）では、目的生成物として合成可能な範囲は０≦ｘ≦０．５とされており、それよりｘが大きくなると単一相が得られないとされている。

【０００５】一方、第４１回電池討論会２Ｄ２０（２０００）では、ｘ＝０．５に相当するＮｉ：Ｍｎ＝１：１の層状構造をもつ結晶性の高い単一相を共沈法により合成したとの報告がある。それによれば、このリチウム遷移金属複合酸化物は単一相の結晶中にニッケルとマンガンが均一に存在しており、ニッケルとマンガンを均一に存在させるために原料のニッケル化合物とマンガン化合物を原子レベルで均一に分散させる必要があり、そのためには共沈法が好ましいとされる。

【０００６】

【発明が解決しようとする課題】しかしながら、本発明者らの検討によれば、上記のような層状のリチウムニッケルマンガン複合酸化物は、二次電池の活物質としてレート特性が劣ることが判明した。即ち、上記層状リチウムニッケルマンガン複合酸化物においては、結晶中におけるリチウムイオンの拡散速度がリチウムコバルト複合酸化物、あるいはリチウムニッケル複合酸化物と比較し小さく、高いレートでの充放電にリチウムイオンの活物質への脱ドープ・ドープが追従しないため、これを二次電池の活物質として用いたときに高いレートでの充放電容量が劣るのである。

【０００７】

AMPEREX Ex. 1002
Page 1188

3

【課題を解決するための手段】本発明者は、上記層状リチウムニッケルマンガン複合酸化物のレート特性の向上方法について鋭意検討した結果、リチウムニッケルマンガン複合酸化物中には、その原料中に存在する不純物や製造過程で混入する不純物の影響で、通常少なくとも４００ｐｐｍ程度のカルシウムやマグネシウムが存在すること、リチウムニッケルマンガン複合酸化物中に不純物として存在するマグネシウム及びカルシウムの存在量によってレート特性が変化すること、また、上記マグネシウム及びカルシウムの存在量が少ないほどレート特性が向上することを見出し本発明を完成した。

【０００８】即ち、本発明の要旨は、ニッケルとマンガンとの原子比が０．７≦Ｎｉ／Ｍｎ≦９を満たす層状リチウムニッケルマンガン複合酸化物であって、Ｍｇ及びＣａの含有量が共に３００ｐｐｍ以下であることを特徴とする層状リチウムニッケルマンガン複合酸化物に存する。なお、第４１回電池討論会２Ｄ２０（２０００）では、$LiMn_{0.5}Ni_{0.5}O_2$なる組成の層状リチウムニッケルマンガン複合酸化物が報告されているが、レート特性について何も触れられておらず、またマグネシウム及びカルシウムの含有量についても記載されていない。

【０００９】

【発明の実施の形態】本発明の層状リチウムニッケルマンガン複合酸化物は、層状の結晶構造を有し、リチウムとニッケルとマンガンとを含む酸化物である。ニッケルとマンガンの原子比（Ｎｉ／Ｍｎ）は、層状結晶構造が安定に存在し、また電池特性を悪化させない観点で、０．７以上、９以下とする。ニッケルとマンガンの原子比（Ｎｉ／Ｍｎ）として好ましい範囲はいくつか挙げられるが、例えば１つには、下限としては０．８以上、中でも０．９以上、また、上限としては１．２以下、中でも１．１以下である。もう１つには下限としては、１．３以上、中でも１．５以上、また、上限としては、７以下、中でも５以下である。

【００１０】本発明のリチウムニッケルマンガン複合酸化物は、結晶構造の安定化や高容量化、安全性向上、高温での電池特性の改良のためにニッケル及びマンガンの存在するサイトの一部を他の元素（以下「置換元素」ということがある）で置換するのが好ましい。置換元素としては、各種の元素を使用することができるが、好ましくはアルミニウム、コバルト、鉄等の金属元素を挙げることができる。この中でも、アルミニウム、コバルトがさらに好ましく、最も好ましいのはコバルトである。アルミニウム、コバルトは、層状リチウムニッケルマンガン複合酸化物に容易に固溶して単一相を得ることができるという利点があり、さらにアルミニウム及びコバルトは、リチウム二次電池の正極活物質として、高性能な電池特性、特に繰り返し充放電を行った際の放電容量維持率について良好な性能を示すという利点がある。無論、これらの置換元素を複数種使用してもよい。

4

【００１１】置換元素の、置換元素、ニッケル及びマンガンの合計に対する原子比は、通常０．５以下、好ましくは０．３５以下、さらに好ましくは０．２５以下である。置換割合が多きすぎると電池材料として使用した場合の容量が低下する傾向にある。本発明の層状リチウムニッケルマンガン複合酸化物は、通常下記一般式（Ｉ）で示される。

【００１２】

【化２】$LiNiMnQ_{(1-Y-Z)}O_2$　（Ｉ）

ここで、式（Ｉ）中、Ｑは置換元素を表わし、Ｘは０＜Ｘ≦１．２、好ましくは０＜Ｘ≦１．１の範囲の数を表わす。Ｘが大きすぎると、結晶構造が不安定化したり、これを使用したリチウム二次電池の電池容量低下を招く恐れがある。Ｙ及びＺは、Ｙ＋Ｚ≦１を満たす数であり、また０．７≦Ｙ／Ｚ≦９範囲の数を表す。相対的にマンガンの割合が大きくなると単一相のリチウムニッケルマンガン複合酸化物が合成しにくくなる。Ｙ／Ｚの値として好ましい範囲はいくつか挙げられるが、例えば１つには、ニッケル比率を少なくしてコスト上有利でありかつ容易に合成でき、マンガンが多い分、放電電圧が高い故に放電特性として有利である点で、下限としては、０．８以上、中でも０．９以上、上限としては、１．２以下、中でも１．１以下である。もう１つには、ニッケル比率を多くして電池容量を大きくし、嵩密度が高い故に単位体積当たりの電池容量が更に大きくなる点で、下限としては、１．３以上、中でも１．５以上、上限としては、７以下、中でも５以下である。

【００１３】（１－Ｙ－Ｚ）の値は０．５以下、好ましくは０．３５以下、さらに好ましくは０．２５以下とする。置換元素の量が多すぎると、リチウムニッケルマンガン複合酸化物を正極活物質として使用したリチウム二次電池の電池容量が大きく低下することがある。ＱはＡｌ、Ｃｏ及びＦｅからなる群から選ばれる少なくとも一種を表す。これらのうちより好ましいのは、Ａｌ、Ｃｏであり、最も好ましいのはＣｏである。Ａｌ、Ｃｏは、$LiNi_{1-x}Mn_xO_2$（０．７≦Ｎｉ／Ｍｎ≦９）に対して容易に固溶し、単一相のリチウム遷移金属複合酸化物として合成することができる。更に、Ａｌ、Ｃｏに関しては、得られるリチウム遷移金属複合酸化物を正極活物質として用いたリチウム二次電池が高性能な電池特性、特に繰り返し充放電を行った際の放電容量維持率について良好な性能を示す。さらに良好な結晶性を有する層状リチウムニッケルマンガン複合酸化物とするために、層状リチウムニッケルマンガン複合酸化物に対して固溶せずに、焼成時に溶融し、液相を生じる物質（以下、「不活性溶融剤」という）を添加しても良い。これらの不活性溶融剤は常温まで冷却した後は、層状リチウムニッケルマンガン複合酸化物の結晶構造内に取り込まれず、主に表面を被覆、あるいは表面に析出した状態で存在する。上記のような不活性溶融剤としては、ホウ素

AMPEREX Ex. 1002
Page 1189

化合物、アンチモン化合物、あるいはカリウム、バリウム、リチウムのハロゲン化物、硫酸塩、モリブデン酸塩等が挙げられる。これらのうちより好ましいのは、ホウ素化合物、アンチモン化合物である。不活性溶融剤の添加量は、Ｎｉ、Ｍｎ及び置換元素Ｑの合計のモル数を１とした場合、モル比で通常０．０５以下、好ましくは０．０４以下、より好ましくは０．０３以下である。不活性溶融剤の添加量が多すぎると充分な放電容量を得られない場合がある。

【００１４】なお、上記一般式（Ｉ）の組成においては、酸素量に多少の不定比性があってもよい。層状リチウムニッケルマンガン複合酸化物においては、マグネシウム（Ｍｇ）及びカルシウム（Ｃａ）の含有量を共に３００ｐｐｍ以下とする。Ｍｇの含有量及びＣａの含有量は、それぞれ独立に、好ましくは２００ｐｐｍ以下、さらに好ましくは１５０ｐｐｍ以下とする。その結果、レート特性を向上させることができる。Ｍｇ、Ｃａの含有量を低減するとレート特性が改善される理由は明らかではないが、これらの不純物は結晶構造、あるいは１次粒子間の粒界におけるリチウムイオンの移動を阻害するものであると考えられる。ただし、Ｍｇ及びＣａの含有量を必要以上に減らしても、レート特性があまり向上せず、また工業的な負荷が大きくなるので、通常それぞれ１ｐｐｍ以上、好ましくは５ｐｐｍ以上とする。

【００１５】リチウムニッケルマンガン複合酸化物中のＭｇやＣａの含有量を制御するには、製造したリチウムニッケルマンガン複合酸化物に、アンモニウム塩の水溶液による処理を施してＭｇやＣａの含有量を減少させることもできるが、上記処理の結果、リチウムニッケルマンガン複合酸化物の性状に変化を及ぼすことがある。従って、好ましくは、リチウムニッケルマンガン複合酸化物の生成段階においてすでにＭｇやＣａの含有量が上記範囲となるように、製造のための原料の選定や製造条件、製造環境を制御する。具体的には、後述する反応原料中のＭｇ量及びＣａ量をできるだけ減らしておく、あるいは、反応の際に必要な装置又は系外からのＭｇ成分及びＣａ成分の混入をできるだけ避けるようにするのが好ましい。特に、原料として使用するニッケル化合物、マンガン化合物、置換元素化合物中、特にニッケル化合物中には、それらの製造過程において用いられる天然鉱物や水、酸性溶液、アルカリ性溶液に由来して、通常多少なりともＭｇやＣａが含有されるので、原料の選定やその精製程度は、リチウムニッケルマンガン複合酸化物中のＭｇ及びＣａ含有量を所定範囲に制御する上で重要である。リチウムニッケルマンガン複合酸化物中のマグネシウム含有量やカルシウム含有量は、ＩＰＣ発光分析等の方法で測定することができる。

【００１６】層状リチウムニッケルマンガン複合酸化物は、平均１次粒径としては、通常０．０１μｍ以上、好ましくは０．０２μｍ以上、更に好ましくは０．１μｍ以上、通常３０μｍ以下、好ましくは５μｍ以下、更に好ましくは２μｍ以下である。また、平均２次粒径は通常１μｍ以上、好ましくは４μｍ以上、通常５０μｍ以下、好ましくは４０μｍ以下である。さらに、該リチウムニッケルマンガン複合酸化物は、ＢＥＴ比表面積が、通常０．１ｍ²／ｇ以上１０．０ｍ²／ｇ以下、好ましくは０．２ｍ²／ｇ以上９．０ｍ²／ｇ以下である。１次粒子の大きさは、焼成温度、焼成時間等の製造条件等により制御することが可能であり、これらの１つ以上を増加させることにより、１次粒子の粒子径を大きくすることができる。２次粒子の粒子径は、例えば、後述する噴霧乾燥工程における気液比等の噴霧条件等の製造条件により制御することが可能である。比表面積は１次粒子の粒径および２次粒子の粒径により制御することが可能であり、１次粒子の粒径及び／又は２次粒子の粒径を大きくすることにより減少する。上記範囲以下のあまり小さい比表面積では、１次粒子が大きすぎて電池特性が不良である一方、上記範囲以上のあまり大きい比表面積では、これを用いて二次電池を作製する場合の電極作製が困難になる。又、粉体充填密度は、タップ密度（２００回タップ後）で、通常は０．５ｇ／ｃｃ以上、好ましくは０．６ｇ／ｃｃ以上、さらに好ましくは０．８ｇ／ｃｃ以上である。粉体充填密度は高ければ高いほど単位容積あたりのエネルギー密度を大きくすることができるが、現実的には通常３．０ｇ／ｃｃ以下であり、特に２．５ｇ／ｃｃ以下である。

【００１７】なお、本発明においては、前記リチウムニッケルマンガン複合酸化物の比表面積は、公知のＢＥＴ式粉体比表面積測定装置によって測定される。この方法の測定原理は下記の通りである。すなわち、測定方式は連続流動法によるＢＥＴ１点法測定であり、使用する吸着ガス及びキャリアガスはそれぞれ、窒素、ヘリウムである。粉体試料を混合ガスにより４５０℃以下の温度で加熱脱気し、次いで液体窒素温度まで冷却して混合ガスを吸着させる。これを水により室温まで加温して吸着された窒素ガスを脱着させ、熱伝導度検出器によって検出し、脱着ピークとしてその量を求め、試料の比表面積として算出する。

【００１８】本発明のリチウムニッケルマンガン複合酸化物は、例えば、リチウムとニッケルとマンガンと必要に応じて用いられる他金属元素、及び必要に応じて不活性溶融剤とを含む原料を焼成することによって製造することができる。原料として使用するリチウム源としては、例えば、Li_2CO_3、$LiNO_3$、ＬｉＯＨ、$LiOH \cdot H_2O$、ジカルボン酸リチウム、クエン酸リチウム、脂肪酸リチウム、アルキルリチウム、リチウムハロゲン化物等の各種のリチウム化合物を挙げることができる。より具体的には、例えば、Li_2CO_3、$LiNO_3$、ＬｉＯＨ、$LiOH \cdot H_2O$、ＬｉＣｌ、ＬｉＩ、酢酸Ｌｉ、Li_2O等を挙げることができる。これらリ

AMPEREX Ex. 1002
Page 1190

チウム原料の中で好ましいのは、Li_2CO_3、$LiNO_3$、$LiOH \cdot H_2O$、酢酸Li等の水溶性のリチウム化合物である。これらの水溶性化合物は、例えば、分散媒として水を使用したスラリー中に溶解させることによって容易に良好な特性を有するリチウムニッケルマンガン複合酸化物を得ることができる。また、焼成処理の際にＮＯｘ及びＳＯｘ等の有害物質を発生させない点で、窒素原子や硫黄原子を含有しないリチウム化合物が好ましい。最も好ましいリチウム原料は、水溶性でもあり、また窒素原子や硫黄原子を含有しない、$LiOH \cdot H_2O$である。無論、リチウム源として複数種のものを使用してもよい。

【００１９】ニッケル源としては、例えば、$Ni(OH)_2$、NiO、NiOOH、$NiCO_3 \cdot 2Ni(OH)_2 \cdot 4H_2O$、$NiC_2O_4 \cdot 2H_2O$、$Ni(NO_3)_2 \cdot 6H_2O$、$NiSO_4$、$NiSO_4 \cdot 6H_2O$、脂肪酸ニッケル、及びニッケルハロゲン化物からなる群から選ばれた少なくとも一種を挙げることができる。この中でも、焼成処理の際にＮＯｘ及びＳＯｘ等の有害物質を発生させない点で、窒素原子や硫黄原子を含有しない、$Ni(OH)_2$、NiO、NiOOH、$NiCO_3 \cdot 2Ni(OH)_2 \cdot 4H_2O$、$NiC_2O_4 \cdot 2H_2O$のようなニッケル化合物が好ましい。また、さらに工業原料として安価に入手できる観点、及び反応性が高いという観点から、特に好ましいのは$Ni(OH)_2$、NiO、NiOOHである。無論、ニッケル源として複数種のものを使用してもよい。

【００２０】マンガン源としては、例えば、Mn_3O_4、Mn_2O_3、MnO_2、$MnCO_3$、$Mn(NO_3)_2$、$MnSO_4$、ジカルボン酸マンガン、クエン酸マンガン、脂肪酸マンガン、マンガンオキシ水酸化物、マンガン水酸化物、又はマンガンハロゲン化物を挙げることができる。これらマンガン原料の中でも、Mn_2O_3、Mn_3O_4は、最終目的物である複合酸化物のマンガン酸化数に近い価数を有しているため好ましい。さらに工業原料として安価に入手できる観点、及び反応性が高いという観点から、特に好ましいのはMn_2O_3である。マンガン源は、マンガン化合物がスラリー中で電離して生成したマンガンイオンでもよい。無論、マンガン源として複数種のものを使用してもよい。

【００２１】置換元素源としては、上記置換金属のオキシ水酸化物、酸化物、水酸化物、ハロゲン物の他、炭酸塩、硝酸塩、硫酸塩等の無機酸塩や、酢酸塩、シュウ酸塩等の有機酸塩を挙げることができる。具体的なアルミニウム源としては、例えば、AlOOH、Al_2O_3、$Al(OH)_3$、$AlCl_3$、$Al(NO_3)_3 \cdot 9H_2O$及び$Al_2(SO_4)_3$等の各種のアルミニウム化合物を挙げることができる。中でも、焼成工程の際にＮＯｘ及びＳＯｘ等の有害物質を発生させない点で、AlOOH、Al_2O_3及び$Al(OH)_3$が好ましく、さらに好ましくは、工業的に安価に入手できる点及び反応性が高い点でAlOOHである。無論複数のアルミニウム化合物を使用することもできる。

【００２２】具体的なコバルト源としては、例えば、$Co(OH)_2$、CoO、Co_2O_3、Co_3O_4、$Co(OAc)_2 \cdot 4H_2O$、$CoCl_2$、$Co(NO_3)_2 \cdot 6H_2O$、及び$Co(SO_4)_2 \cdot 7H_2O$等の各種のコバルト化合物を挙げることができる。中でも、焼成工程の際にＮＯｘ及びＳＯｘ等の有害物質を発生させない点で、$Co(OH)_2$、CoO、Co_2O_3、Co_3O_4が好ましく、さらに好ましくは、工業的に安価に入手できる点及び反応性が高い点で$Co(OH)_2$である。無論複数のコバルト化合物を使用することもできる。

【００２３】具体的な鉄源としては、例えば、FeO(OH)、Fe_2O_3、Fe_3O_4、$FeCl_2$、$FeCl_3$、$FeC_2O_4 \cdot 2H_2O$、$Fe(NO_3)_3 \cdot 9H_2O$、$FeSO_4 \cdot 7H_2O$及び$Fe_2(SO_4)_3 \cdot nH_2O$等の各種の鉄化合物を挙げることができる。中でも、焼成工程の際にＮＯｘ及びＳＯｘ等の有害物質を発生させない点で、FeO(OH)、Fe_2O_3、Fe_3O_4が好ましく、さらに好ましくは、工業的に安価に入手できる点及び反応性が高い点でFeO(OH)、Fe_2O_3である。無論複数の鉄化合物を使用することもできる。必要に応じて添加される不活性溶融剤の中で、ホウ素化合物としては、具体的には、$Li_2B_4O_7$、$Li_2B_2O_4$、$Li_6B_4O_7$等のホウ酸リチウム、$Na_2B_6O_{10}$、$Na_2B_4O_7$等のホウ酸ナトリウム、$K_2B_{10}O_{16}$、$K_2B_4O_7$等のホウ酸カリウム、B_2O_3、H_3BO_3等から選ばれる１種または２種以上の混合物及びこれらの分解生成物を挙げることができる。同様に不活性溶融剤として添加されるものの中で、アンチモン化合物しては、具体的には、Sb_2O_3、Sb_2O_4、Sb_2O_5等の酸化アンチモン、$LiSbO_3$等のアンチモン酸リチウム等から選ばれる１種または２種以上の混合物を挙げることができる。

【００２４】上記原料については純度が高いことが好ましい。Ｍｇ、Ｃａについては、目的とするモル比にて原料を混合した際に、トータルで３００ｐｐｍ以下となるように原料を選定する必要がある。リチウム、ニッケル、マンガン及び必要に応じて用いられるアルミニウム等の置換元素、の仕込時のモル比は、目的とする層状リチウムニッケルマンガン複合酸化物の組成が得られるように適宜選択すればよい。また、必要に応じて用いられる不活性溶融剤の添加量に関しては、上記リチウム、ニッケル、マンガン及び置換元素の仕込量に応じて適宜選択すれば良い。

【００２５】これらリチウム源、ニッケル源、マンガン源、置換元素源及び不活性溶融剤は、乾式で混合して焼成の原料として用いてもよく、また、湿式（即ちスラリー中）で混合後これを乾燥して焼成の原料としてもよい。湿式で混合する場合は、（１）ニッケル源とマンガ

AMPEREX Ex. 1002
Page 1191

ン源と置換元素源とリチウム源と分散媒とを含有するスラリーを湿式混合、噴霧乾燥した後に焼成する、又は（２）ニッケル源とマンガン源と置換元素源と分散媒とを含有するスラリーを湿式混合、噴霧乾燥した後、これとリチウム源とを混合した後に焼成する、のいずれの方法を用いても良い。各原料は焼成前に十分に混合しておくのが好ましいため、より良好な混合が可能な、少なくともニッケル源とマンガン源と置換元素源とを湿式混合する方法が好ましい。不活性溶融剤は焼成前のいずれの段階で添加しても良い。以下、スラリー中での湿式混合及び乾燥方法について記す。スラリーに用いられる分散媒としては、各種の有機溶媒、水性溶媒を使用することができるが、好ましいのは水である。

【００２６】スラリー全体の重量に対する、リチウム源、ニッケル源、マンガン源及び置換元素源の総重量比、又はリチウム源を除くニッケル源、マンガン源及び置換元素源の総重量比は、通常１０重量％以上、好ましくは１２．５重量％以上、通常５０重量％以下、好ましくは３５重量％以下である。重量比が上記範囲以下の場合は、スラリー濃度が極端に希薄なため噴霧乾燥により生成した球状粒子が必要以上に小さくなったり破損しやすくなったりする一方で、上記範囲以上となると、リチウム源の飽和溶解度を超えることによりリチウム源が溶解しきれない等スラリーの均一性が保ちにくくなる。

【００２７】スラリー中の固形物の平均粒子径は通常２μｍ以下、好ましくは１μｍ以下、さらに好ましくは０．５μｍ以下とする。スラリー中の固形物の平均粒子径が大きすぎると、焼成工程における反応性が低下するだけでなく、球状度が低下し、最終的な粉体充填密度が低くなる傾向にある。この傾向は、平均粒子径で５０μｍ以下の造粒粒子を製造しようとした場合に特に顕著になる。また、必要以上に小粒子化することは、粉砕のコストアップに繋がるので、固形物の平均粒子径は通常０．０１μｍ以上、好ましくは０．０５μｍ以上、さらに好ましくは０．１μｍ以上とする。

【００２８】スラリー中の固形物の平均粒子径を制御する方法としては、原料化合物を予めボールミル、ジェットミル等により乾式粉砕し、これを分散媒に攪拌等によって分散させる方法、原料化合物を分散媒に攪拌等によって分散後、媒体攪拌型粉砕機等を使用して湿式粉砕する方法等を挙げることができる。原料化合物を分散媒に分散後、媒体攪拌型粉砕機等を使用して湿式粉砕する方法を用いることが好ましい。湿式粉砕することによって、本発明の効果が顕著に発揮される。

【００２９】また、スラリーの粘度は、通常５０ｍＰａ・ｓ以上、好ましくは１００ｍＰａ・ｓ以上、特に好ましくは２００ｍＰａ・ｓ以上、通常３０００ｍＰａ・ｓ以下、好ましくは２０００ｍＰａ・ｓ以下、特に好ましくは１６００ｍＰａ・ｓ以下である。粘度が上記範囲以下の場合は、焼成前の乾燥に大きな負荷がかかったり、乾燥により生成した球状粒子が必要以上に小さくなったり破損しやすくなったりする一方で、上記範囲以上となると、乾燥時のスラリー輸送に用いるチューブポンプでの吸引ができなくなる等取り扱いが困難になる。スラリーの粘度測定は、公知のＢＭ型粘度計を用いて行うことができる。ＢＭ型粘度計は、室温大気中において所定の金属製ローターを回転させる方式を採用する測定方法である。スラリーの粘度は、ローターをスラリー中に浸した状態でローターを回転させ、その回転軸にかかる抵抗力（捻れの力）から算出される。但し、室温大気中とは気温１０℃～３５℃、相対湿度２０％ＲＨ～８０％ＲＨの通常考えられる実験室レベルの環境を示す。

【００３０】上記のようにして得られたスラリーは、通常乾燥された後焼成処理に供される。乾燥方法としては噴霧乾燥が好ましい。噴霧乾燥を行うことによって、簡易な方法で球状のリチウムニッケルマンガン複合酸化物を得ることができ、その結果、充填密度を向上させることができる。噴霧乾燥の方法は特に制限されないが、例えば、ノズルの先端に気体流とスラリーとを流入させることによってノズルからスラリー成分の液滴（本明細書においては、これを単に「液滴」という場合がある。）を吐出させ、適当な乾燥ガス温度や送風量を用いて飛散した該液滴を迅速に乾燥させる方法を用いることができる。気体流として供給する気体としては、空気、窒素等を用いることができるが、通常は空気が用いられる。これらは加圧して使用することが好ましい。気体流は、ガス線速として、通常１００ｍ／ｓ以上、好ましくは２００ｍ／ｓ以上、さらに好ましくは３００ｍ／ｓ以上で噴射される。あまり小さすぎると適切な液滴が形成しにくくなる。ただし、あまりに大きな線速は得にくいので、通常噴射速度は１０００ｍ／ｓ以下である。使用されるノズルの形状は、微少な液滴を吐出することができるものであればよく、従来から公知のもの、例えば、特許第２７９７０８０号公報に記載されているような液滴を微細化できるようなノズルを使用することもできる。なお、液滴は環状に噴霧されることが、生産性向上の点で好ましい。飛散した液滴は、これを乾燥する。前述の通り、飛散した該液滴を迅速に乾燥させるように、適当な温度や送風等の処理が施されるが、乾燥塔上部から下部に向かいダウンフローで乾燥ガスを導入するのが好ましい。この様な構造とすることにより、乾燥塔単位容積当たりの処理量を大幅に向上させることができる。また、液滴を略水平方向に噴霧する場合、水平方向に噴霧された液滴をダウンフローガスで抑え込むことにより、乾燥塔の直径を大きく低減させることが可能となり、安価且つ大量に製造することが可能となる。乾燥ガス温度は、通常５０℃以上、好ましくは７０℃以上とし、通常１２０℃以下、好ましくは１００℃以下とする。温度が高すぎると、得られた造粒粒子が中空構造の多いものとなり、粉体の充填密度が低下する傾向にあり、一方、低す

AMPEREX Ex. 1002
Page 1192

ぎると粉体出口部分での水分結露による粉体固着・閉塞等の問題が生じる可能性がある。

【００３１】この様にして噴霧乾燥することによって原料となる造粒粒子が得られる。造粒粒子径としては、平均粒子径で好ましくは５０μｍ以下、さらに好ましくは３０μｍ以下となるようにする。ただし、あまりに小さな粒径は得にくい傾向にあるので、通常は４μｍ以上、好ましくは５μｍ以上である。造粒粒子の粒子径は、噴霧形式、加圧気体流供給速度、スラリー供給速度、乾燥温度等を適宜選定することによって制御することができる。

【００３２】リチウム、マンガン、及びニッケルを含む原料は、焼成処理される。又は、リチウム源を含有しないスラリーを乾燥して得られた、ニッケル、マンガン等を含む原料は、リチウム源と混合された後焼成処理される。焼成処理された後にリチウム源と混合して更に焼成処理に供しても良い。混合方法としては、手振り混合、ボールミル等を用いた機械式混合等が挙げられる。焼成温度としては、原料として使用されるリチウム源、マンガン源、及びニッケル源等の種類によって異なるものの、通常７００℃以上、好ましくは７５０℃以上、さらに好ましくは８００℃以上であり、また通常１０５０℃以下、好ましくは９５０℃以下である。温度が低すぎると、結晶性の良い層状リチウムニッケルマンガン複合酸化物を得るために長時間の焼成時間を要する傾向にある。また、温度が高すぎると、目的とする層状リチウムニッケルマンガン複合酸化物以外の結晶相が生成したり、欠陥が多い層状リチウムニッケルマンガン複合酸化物が生成したりして、該リチウム遷移金属複合酸化物を正極活物質として使用したリチウム二次電池の電池容量が低下あるいは充放電による結晶構造の崩壊による劣化を招くことがある。

【００３３】焼成時間は温度によっても異なるが、通常前述の温度範囲であれば３０分以上、５０時間以下である。焼成時間が短すぎると結晶性の良い層状リチウムニッケルマンガン複合酸化物が得られにくくなり、また長すぎるのはあまり実用的ではない。結晶欠陥が少ない層状リチウムニッケルマンガン複合酸化物を得るためには、焼成反応後、ゆっくりと冷却することが好ましく、例えば５℃／ｍｉｎ．以下の冷却速度で徐冷することが好ましい。

【００３４】焼成時の雰囲気は、製造する化合物の組成や構造に応じて、空気等の酸素含有ガス雰囲気や、窒素やアルゴン等の不活性ガス雰囲気とすることができるが、層状リチウムニッケルマンガン複合酸化物の場合、通常ニッケルは原料の２価から目的生成物の３価へ酸化される必要があることから、好ましくは空気又は酸素である。

【００３５】焼成に使用する加熱装置は、上記の温度、雰囲気を達成できるものであれば特に制限はなく、例えば箱形炉、管状炉、トンネル炉、ロータリーキルン等を使用することができる。なお、上記の製造過程において、装置、容器あるいは外部からＭｇ、Ｃａが混入し、３００ｐｐｍ以上とならないようにする必要がある。なお、本発明においては、スラリー中の固形分の平均粒子径、噴霧乾燥後の造粒粒子の平均粒子径、及び層状リチウムニッケルマンガン複合酸化物の平均粒子径は、公知のレーザー回折／散乱式粒度分布測定装置によって測定される。この方法の測定原理は下記の通りである。すなわち、スラリー又は粉体を分散媒に分散させ、該試料溶液にレーザー光を照射し、粒子に入射されて散乱（回折）した散乱光をディテクタで検出する。検出された散乱光の散乱角θ（入射方向と散乱方向の角度）は、大きい粒子の場合は前方散乱（０＜θ＜９０°）となり、小さい粒子の場合は側方散乱又は後方散乱（９０°＜θ＜１８０°）となる。測定された角度分布値から、入射光波長及び粒子の屈折率等の情報を用いて粒子径分布を算出する。更に得られた粒子径分布から平均粒子径を算出する。測定の際に用いる分散媒としては、例えば０．１重量％ヘキサメタリン酸ナトリウム水溶液を挙げることができる。

【００３６】本発明のリチウムニッケルマンガン複合酸化物を正極活物質（正極材料）として、リチウム二次電池を作製することができる。リチウム二次電池は、通常正極、負極及び電解質層を有する。本発明の二次電池の一例としては、正極、負極、電解液、セパレーターからなる二次電池が挙げられ、この場合正極と負極との間には電解質が存在し、かつセパレーターが正極と負極が接触しないようにそれらの間に配置される。

【００３７】正極は、通常前記リチウムニッケルマンガン複合酸化物とバインダーとを含有する。また、通常、正極は、前記リチウムニッケルマンガン複合酸化物とバインダーとを含有する正極層を集電体上に形成してなる。このような正極層は、リチウムニッケルマンガン複合酸化物、バインダー及び必要に応じて導電剤等を溶媒でスラリー化したものを正極集電体に塗布し、乾燥することにより製造することができる。

【００３８】正極層中には、ＬｉＦｅＰＯ$_4$等のように、リチウム遷移金属複合酸化物以外のリチウムイオンを吸蔵・放出しうる活物質をさらに含有していてもよい。正極層中の活物質の割合は、通常１０重量％以上、好ましくは３０重量％以上、さらに好ましくは５０重量％以上であり、通常９９．９重量％以下、好ましくは９９重量％以下である。多すぎると電極の機械的強度が劣る傾向にあり、少なすぎると容量等電池性能が劣る傾向にある。

【００３９】また、正極に使用されるバインダーとしては、例えば、ポリフッ化ビニリデン、ポリテトラフルオロエチレン、フッ素化ポリフッ化ビニリデン、ＥＰＤＭ（エチレンープロピレンージエン三元共重合体）、ＳＢ

AMPEREX Ex. 1002
Page 1193

Ｒ（スチレン－ブタジエンゴム）、ＮＢＲ（アクリロニトリル－ブタジエンゴム）、フッ素ゴム、ポリ酢酸ビニル、ポリメチルメタクリレート、ポリエチレン、ニトロセルロース等が挙げられる。正極層中のバインダーの割合は、通常０．１重量％以上、好ましくは１重量％以上、さらに好ましくは５重量％以上であり、通常８０重量％以下、好ましくは６０重量％以下、さらに好ましくは４０重量％以下、最も好ましくは１０重量％以下である。バインダーの割合が低すぎると、活物質を十分に保持できずに正極の機械的強度が不足し、サイクル特性等の電池性能を悪化させることがあり、一方高すぎると電池容量や導電性を下げることがある。

【００４０】正極層は、通常導電性を高めるため導電剤を含有する。導電剤としては、天然黒鉛、人造黒鉛等の黒鉛や、アセチレンブラック等のカーボンブラック、ニードルコークス等の無定形炭素等の炭素材料を挙げることができる。正極中の導電剤の割合は、通常０．０１重量％以上、好ましくは０．１重量％以上、さらに好ましくは１重量％以上であり、通常５０重量％以下、好ましくは３０重量％以下、さらに好ましくは１５重量％以下である。導電剤の割合が低すぎると導電性が不十分になることがあり、逆に高すぎると電池容量が低下することがある。

【００４１】また、スラリー溶媒としては、バインダーを溶解あるいは分散するものであれば特に制限はないが、通常は有機溶剤が使用される。例えば、Ｎ－メチルピロリドン、ジメチルホルムアミド、ジメチルアセトアミド、メチルエチルケトン、シクロヘキサノン、酢酸メチル、アクリル酸メチル、ジエチルトリアミン、Ｎ－Ｎ－ジメチルアミノプロピルアミン、エチレンオキシド、テトラヒドロフラン等を挙げることができる。また、水に分散剤、増粘剤等を加えてＳＢＲ等のラテックスで活物質をスラリー化することもできる。

【００４２】正極層の厚さは、通常１～１０００μｍ、好ましくは１０～２００μｍ程度である。厚すぎると導電性が低下する傾向にあり、薄すぎると容量が低下する傾向にある。正極に使用する集電体の材質としては、アルミニウム、ステンレス鋼、ニッケルメッキ鋼等が用いられ、好ましくはアルミニウムである。集電体の厚さは、通常１～１０００μｍ、好ましくは５～５００μｍ程度である。厚すぎるとリチウム二次電池全体としての容量が低下し、薄すぎると機械的強度が不足することがある。

【００４３】なお、塗布・乾燥によって得られた正極層は、活物質の充填密度を上げるためローラープレス等により圧密されるのが好ましい。二次電池の負極に使用される負極の活物質としては、リチウムやリチウムアルミニウム合金等のリチウム合金であっても良いが、より安全性が高く、リチウムを吸蔵、放出できる炭素材料が好ましい。

【００４４】前記炭素材料は特に限定されないが、黒鉛及び、石炭系コークス、石油系コークス、石炭系ピッチの炭化物、石油系ピッチの炭化物、あるいはこれらピッチを酸化処理したものの炭化物、ニードルコークス、ピッチコークス、フェノール樹脂、結晶セルロース等の炭化物等及びこれらを一部黒鉛化した炭素材、ファーネスブラック、アセチレンブラック、ピッチ系炭素繊維等が挙げられる。

【００４５】更に、負極活物質として、ＳｎＯ、SnO_2、$Sn_{1-x}M_xO$（Ｍ＝Ｈｇ、Ｐ、Ｂ、Ｓｉ、ＧｅまたはＳｂ、ただし$0 \leqq x < 1$）、$Sn_3O_2(OH)_2$、$Sn_{3-x}M_xO_2(OH)_2$（Ｍ＝Ｍｇ、Ｐ、Ｂ、Ｓｉ、Ｇｅ、Ｓｂ又はＭｎ、ただし$0 \leqq x < 3$）、$LiSiO_2$、SiO_2又は$LiSnO_2$等を挙げることができる。なお、これらの中から選ばれる２種以上の混合物を負極活物質として用いてもよい。

【００４６】負極は通常、正極の場合と同様、負極層を集電体上に形成されてなる。この際使用するバインダーや、必要に応じて使用される導電剤等やスラリー溶媒としては、正極で使用するものと同様のものを使用することができる。また、負極の集電体としては、銅、ニッケル、ステンレス鋼、ニッケルメッキ鋼等が使用され、好ましくは銅が用いられる。

【００４７】正極と負極との間にセパレーターを使用する場合は、微多孔性の高分子フィルムが用いられ、ポリテトラフルオロエチレン、ポリエステル、ナイロン、セルロースアセテート、ニトロセルロース、ポリスルホン、ポリアクリロニトリル、ポリフッ化ビニリデン、ポリプロピレン、ポリエチレン、ポリブテン等のポリオレフィン高分子を用いることができる。また、ガラス繊維等の不織布フィルターや、ガラス繊維と高分子繊維との不織布フィルターを用いることもできる。セパレータの化学的及び電気化学的安定性は重要な因子である。この点からポリオレフィン系高分子が好ましく、電池セパレータの目的の一つである自己閉塞温度の点からポリエチレン製であることが望ましい。

【００４８】ポリエチレンセパレーターの場合、高温形状維持性の点から超高分子量ポリエチレンであることが好ましく、その分子量の下限は好ましくは５０万、さらに好ましくは１００万、最も好ましくは１５０万である。他方分子量の上限は、好ましくは５００万、更に好ましくは４００万、最も好ましくは３００万である。分子量が大きすぎると、流動性が低すぎて加熱された時セパレーターの孔が閉塞しない場合があるからである。

【００４９】また、本発明のリチウム二次電池における電解質層を構成する電解質には、例えば公知の有機電解液、高分子固体電解質、ゲル状電解質、無機固体電解質等を用いることができるが、中でも有機電解液が好ましい。有機電解液は、有機溶媒と溶質から構成される。有機溶媒としては特に限定されるものではないが、例えば

AMPEREX Ex. 1002
Page 1194

カーボネート類、エーテル類、ケトン類、スルホラン系化合物、ラクトン類、ニトリル類、塩素化炭化水素類、エーテル類、アミン類、エステル類、アミド類、リン酸エステル化合物等を使用することができる。これらの代表的なものを列挙すると、ジメチルカーボネート、ジエチルカーボネート、メチルエチルカーボネート、プロピレンカーボネート、エチレンカーボネート、ブチレンカーボネート、ビニレンカーボネート、テトラヒドロフラン、２－メチルテトラヒドロフラン、１，４－ジオキサン、４－メチル－２－ペンタノン、１，２－ジメトキシエタン、１，２－ジエトキシエタン、γ－ブチロラクトン、１，３－ジオキソラン、４－メチル－１，３－ジオキソラン、ジエチルエーテル、スルホラン、メチルスルホラン、アセトニトリル、プロピオニトリル、ベンゾニトリル、ブチロニトリル、バレロニトリル、１，２－ジクロロエタン、ジメチルホルムアミド、ジメチルスルホキシド、リン酸トリメチル、リン酸トリエチル等の単独もしくは二種類以上の混合溶媒が使用できる。

【００５０】上述の有機溶媒には、電解質を解離させるために高誘電率溶媒が含まれることが好ましい。ここで、高誘電率溶媒とは、２５℃における比誘電率が２０以上の化合物を意味する。高誘電率溶媒の中で、エチレンカーボネート、プロピレンカーボネート及びそれらの水素原子をハロゲン等の他の元素又はアルキル基等で置換した化合物が電解液中に含まれることが好ましい。高誘電率化合物の電解液に占める割合は、好ましくは２０重量％以上、更に好ましくは３０重量％以上、最も好ましくは４０重量％以上である。該化合物の含有量が少ないと、所望の電池特性が得られない場合があるからである。

【００５１】またこの溶媒に溶解させる溶質として特に限定されるものではないが、従来公知のいずれもが使用でき、$LiClO_4$、$LiAsF_6$、$LiPF_6$、$LiBF_4$、$LiB(C_6H_5)_4$、LiCl、LiBr、CH_3SO_3Li、CF_3SO_3Li、$LiN(SO_2CF_3)_2$、$LiN(SO_2C_2F_5)_2$、$LiC(SO_2CF_3)_3$、$LiN(SO_3CF_3)_2$等のリチウム塩が挙げられ、これらのうち少なくとも１種以上のものを用いることができる。また、CO_2、N_2O、CO、SO_2等のガスやポリサルファイドS_x^{2-}など負極表面にリチウムイオンの効率よい充放電を可能にする良好な皮膜を生成する添加剤を任意の割合で上記単独又は混合溶媒に添加してもよい。

【００５２】高分子固体電解質を使用する場合にも、高分子としては、公知のものを用いることができる。特にリチウムイオンに対するイオン導電性の高い高分子を使用することが好ましく、例えば、ポリエチレンオキサイド、ポリプロピレンオキサイド、ポリエチレンイミン等が好ましく使用される。またこの高分子に対して上記の溶質と共に、上記の溶媒を加えてゲル状電解質として使用することも可能である。

【００５３】無機固体電解質を使用する場合にも、この無機物に公知の結晶質、非晶質固体電解質を用いることができる。結晶質の固体電解質としては例えば、ＬｉＩ、Li_3N、$Li_{1+x}M_xTi_{2-x}(PO_4)_3$（Ｍ＝Ａｌ，Ｓｃ，Ｙ，Ｌａ）、$Li_{0.5-3x}RE_{0.5+x}TiO_3$（ＲＥ＝Ｌａ，Ｐｒ，Ｎｄ，Ｓｍ）等が挙げられ、非晶質の固体電解質としては例えば、４．９ＬｉＩ－３４．１Li_2O－６１B_2O_5，３３．３Li_2O－６６．７SiO_2等の酸化物ガラスや０．４５ＬｉＩ－０．３７Li_2S－０．２６B_2S_3，０．３０ＬｉＩ－０．４２Li_2S－０．２８SiS_2等の硫化物ガラス等が挙げられる。これらのうち少なくとも１種以上のものを用いることができる。

【００５４】

【実施例】以下、本発明を実施例を用いて更に説明するが、本発明は、その要旨を超えない限り、以下の実施例に制約されるものではない

＜実施例１＞ＬｉＯＨ・H_2O（本荘ケミカル製）、Ｎｉ$(OH)_2$（和光純薬製）、Mn_2O_3（電解二酸化マンガンを焼成して自製）をそれぞれ最終的な層状リチウムニッケルマンガン複合酸化物中の組成で、Ｌｉ：Ｎｉ：Ｍｎ＝１．０５：０．５０：０．５０（モル比）となるように秤量し、これに純水を加えて固形分濃度１２．５重量％のスラリーを調整した。このスラリーを撹拌しながら、循環式媒体撹拌型湿式粉砕機（シンマルエンタープライゼス社製：ダイノーミルＫＤＬ－Ａ型）を用いて、スラリー中の固形分の平均粒子径が０．３０μｍになるまで粉砕した。３００ｍｌポットを用い、粉砕時間は６時間であった。このスラリーの粘度をＢＭ型粘度計（トキメック社製）により測定した。測定は室温大気中で行い、特定の金属製ローターを装置本体の回転軸に固定し、該ローターをスラリー液面下に浸し、回転軸を回転させてローターにかかる抵抗力（捻れの力）により粘度を算出した。その結果、初期粘度は１５１０ｍＰａ・ｓであった。

【００５５】次にこのスラリーを二流体ノズル型スプレードライヤー（大川原化工機社製：Ｌ－８型スプレードライヤー）を用いて噴霧乾燥を行った。この時の乾燥ガスとして空気を用い、乾燥ガス導入量は４５m^3／ｍｉｎ、乾燥ガス入り口温度は９０℃とした。そして、噴霧乾燥により得られた造粒粒子を９００℃で１０時間空気中で焼成することにより、ほぼ仕込みのモル比組成のリチウムニッケルマンガン複合酸化物（$Li_{1.05}Ni_{0.50}Mn_{0.50}O_2$）を得た。得られたリチウムニッケルマンガン複合酸化物を塩酸に加熱溶解し、ＩＰＣ発光分析にて分析した結果、それぞれ３０ｐｐｍ、１１０ｐｐｍであった。

【００５６】得られたリチウムニッケルマンガン複合酸化物は、平均二次粒子径４．９３μｍ、最大粒径１５μ

AMPEREX Ex. 1002
Page 1195

mのほぼ球状の形状を有する粒子であった。なお、スラリー中の固形分の平均粒子径、及び得られたリチウムニッケルマンガン複合酸化物の平均粒子径・最大粒径は、レーザー回折／散乱式粒度分布測定装置（堀場製作所製：ＬＡ－９２０型粒度分布測定装置）を用いて求めた。具体的には、室温大気中で、スラリー又は焼成物粉末を０．１％ヘキサメタリン酸ナトリウム水溶液に超音波分散及び攪拌により分散させ、透過率を７０％～９５％の間に調節し、測定される粒度分布より平均粒径及び最大粒径を求めた。

【００５７】得られたリチウムニッケルマンガン複合酸化物の粉末Ｘ線回折を測定したところ、菱面体晶の層状リチウムニッケルマンガン複合酸化物の構造を有していることが確認された。この粉末５ｇを１０ｍｌのガラス製メスシリンダーに入れ、２００回タップした後の粉体充填密度（タップ密度）を測定した結果、０．９ｇ／ｃｃであった。

【００５８】この粉末のＢＥＴ比表面積を測定した結果、５．０m^2／ｇであった。比表面積の測定は、ＢＥＴ式粉体比表面積測定装置（大倉理研製：ＡＭＳ８０００型全自動粉体比表面積測定装置）を用いて求めた。続いて、以下の方法で電池評価を行った。得られたリチウムニッケルマンガン複合酸化物を７５重量％、アセチレンブラック２０重量％、ポリテトラフルオロエチレンパウダー５重量％の割合で秤量したものを乳鉢で十分混合し、薄くシート状にしたものを９ｍｍφのポンチを用いて打ち抜いた。この際、全体重量は約８ｍｇになるように調整した。これをＡｌのエキスパンドメタルに圧着して正極とした。

【００５９】得られた前記正極を試験極とし、Ｌｉ金属を対極としてコインセルを組んだ。これに、０．５ｍＡ／cm^2の定電流充電、即ち正極からリチウムイオンを放出させる反応を上限４．３Ｖで行い、０．５ｍＡ／cm^2及び１１ｍＡ／cm^2の定電流放電、即ち正極にリチウムイオンを吸蔵させる反応を下限３．０Ｖで行った際の正極活物質単位重量当たりの放電容量をそれぞれQ_L（ｍＡｈ／ｇ）、Q_H（ｍＡｈ／ｇ）として測定した。

【００６０】表－１に、得られたリチウムニッケルマンガン複合酸化物のＭｇ、Ｃａの分析値と、これらを用いた電池の電流密度０．５ｍＡ／cm^2の放電容量Q_L（ｍＡｈ／ｇ）と１１ｍＡ／cm^2の放電容量Q_H（ｍＡｈ／ｇ）を示す。

＜実施例２＞ＬｉＯＨ・H_2O（本荘ケミカル製）、Ｎｉ（ＯＨ）$_2$（和光純薬製）、Mn_2O_3（電解二酸化マンガンを焼成し自製）、Ｃｏ（ＯＨ）$_2$（伊勢化学製）をそれぞれ最終的な層状リチウムニッケルマンガン複合酸化物中の組成で、Ｌｉ：Ｎｉ：Ｍｎ：Ａｌ＝１．０５：０．４５：０．４５：０．１０（モル比）となるように秤量した以外は、実施例１と同様にしてリチウム遷移金属複合酸化物を得た。

【００６１】得られたリチウム遷移金属複合酸化物の粉末Ｘ線回折を測定したところ、菱面体晶の層状リチウム遷移金属複合酸化物の構造を有していることが確認された。Ｍｇ、Ｃａを分析した結果、それぞれ４０ｐｐｍ、１４０ｐｐｍであった。以下、実施例１と同様にして、電池評価を行なった。結果を表－１に示す。

＜実施例３＞ＬｉＯＨ・H_2O（本荘ケミカル製）、Ｎｉ（ＯＨ）$_2$（和光純薬製）、Mn_2O_3（電解二酸化マンガンを焼成し自製）、Ｃｏ（ＯＨ）$_2$（伊勢化学製）をそれぞれ最終的な層状リチウムニッケルマンガン複合酸化物中の組成で、Ｌｉ：Ｎｉ：Ｍｎ：Ａｌ＝１．０５：０．３３：０．３３：０．３３（モル比）となるように秤量した以外は、実施例１と同様にしてリチウム遷移金属複合酸化物を得た。

【００６２】得られたリチウム遷移金属複合酸化物の粉末Ｘ線回折を測定したところ、菱面体晶の層状リチウム遷移金属複合酸化物の構造を有していることが確認された。Ｍｇ、Ｃａを分析した結果、それぞれ４０ｐｐｍ、９０ｐｐｍであった。以下、実施例１と同様にして、電池評価を行なった。結果を表－１に示す。

＜実施例４＞ＬｉＯＨ・H_2O（本荘ケミカル製）、Ｎｉ（ＯＨ）$_2$（和光純薬製）、Mn_2O_3（電解二酸化マンガンを焼成し自製）、ＡｌＯＯＨ（コンデア社製）をそれぞれ最終的な層状リチウムニッケルマンガン複合酸化物中の組成で、Ｌｉ：Ｎｉ：Ｍｎ：Ａｌ＝１．０５：０．４５：０．４５：０．１０（モル比）となるように秤量した以外は、実施例１と同様にしてリチウム遷移金属複合酸化物を得た。

【００６３】得られたリチウム遷移金属複合酸化物の粉末Ｘ線回折を測定したところ、菱面体晶の層状リチウム遷移金属複合酸化物の構造を有していることが確認された。Ｍｇ、Ｃａを分析した結果、それぞれ３０ｐｐｍ、９０ｐｐｍであった。以下、実施例１と同様にして、電池評価を行なった。結果を表－１に示す。

＜実施例５＞ＬｉＯＨ・H_2O（本荘ケミカル製）、ＮｉO_2（正同化学製）、Mn_2O_3（電解二酸化マンガンを焼成し自製）、Ｃｏ（ＯＨ）$_2$（伊勢化学製）をそれぞれ最終的な層状リチウムニッケルマンガン複合酸化物中の組成で、Ｌｉ：Ｎｉ：Ｍｎ：Ｃｏ＝１．０５：０．６５：０．１５：０．２０（モル比）となるように秤量し、これに純水を加えて固形分濃度２５重量％のスラリーを調整し、実施例１と同様に粉砕した。このスラリーにH_3BO_3をモル比でＢ／（Ｎｉ＋Ｍｎ＋Ｃｏ）＝０．０１となるように添加、溶解した。得られたスラリーを実施例１と同様に噴霧乾燥後、８３０℃で焼成し、リチウム遷移金属複合酸化物を得た。得られたリチウム遷移金属複合酸化物の粉末Ｘ線回折を測定したところ、菱面体晶の層状リチウム遷移金属複合酸化物の構造を有していることが確認された。Ｍｇ、Ｃａを分析した結果、それぞれ１０ｐｐｍ、２０ｐｐｍであった。以下、充電の

AMPEREX Ex. 1002
Page 1196

19

上限電圧を４．２Ｖとした以外は実施例１と同様にして、電池評価を行なった。結果を表－１に示す。

＜比較例１＞Ｎｉ（ＯＨ）$_2$を日本化学産業製に変えた以外は実施例１と同様にして、リチウムニッケルマンガン複合酸化物を得た。

【００６４】得られたリチウムニッケルマンガン複合酸化物の粉末Ｘ線回折を測定したところ、菱面体晶の層状リチウムニッケルマンガン複合酸化物の構造を有していることが確認された。Ｍｇ、Ｃａを分析した結果、それぞれ３３０ｐｐｍ、４２０ｐｐｍであった。以下、実施例１と同様にして、電池評価を行なった。結果を表－１に示す。

【００６５】

【表１】

表－１

	Mg分析値 (ppm)	Ca分析値 (ppm)	Q_L (mAh／g)	Q_H (mAh／g)
実施例1	30	110	147	83
実施例2	40	140	152	80
実施例3	40	90	156	115
実施例4	30	90	125	56
実施例5	10	20	151	114
比較例1	330	420	128	39

20

【００６６】表－１に示すように、実施例１～５のようにＭｇ、Ｃａの含有量が共に３００ｐｐｍ以下である層状リチウム遷移金属複合酸化物は、比較例１のようなＭｇ、Ｃａの含有量が３００ｐｐｍを超える場合に比べ、良好なレート特性を示すことが分かる。

【００６７】

【発明の効果】本発明によれば、容量、レート特性、サイクル特性等の電池性能に優れ、安全性が高く、安価なリチウム二次電池に使用するリチウムニッケルマンガン複合酸化物を得ることができる。特に、本発明によれば、従来の方法に比べてレート特性に優れたリチウム二次電池とすることができるリチウムニッケルマンガン複合酸化物を提供することができる。

フロントページの続き

Ｆターム(参考) 5H029 AJ02 AK03 AL02 AL06 AL12
AM03 AM04 AM05 AM07 BJ03
BJ12 DJ08 DJ12 HJ02
5H050 AA02 BA17 BA18 CA08 CA09
CB02 CB07 CB12 DA02 DA11
EA23 FA02 HA02

AMPEREX Ex. 1002
Page 1197

【公報種別】特許法第１７条の２の規定による補正の掲載
【部門区分】第７部門第１区分
【発行日】平成17年9月8日(2005.9.8)

【公開番号】特開2003-68306(P2003-68306A)
【公開日】平成15年3月7日(2003.3.7)
【出願番号】特願2002-163894(P2002-163894)
【国際特許分類第７版】
　Ｈ０１Ｍ　4/58
　Ｈ０１Ｍ　4/02
　Ｈ０１Ｍ　10/40
【ＦＩ】
　Ｈ０１Ｍ　4/58
　Ｈ０１Ｍ　4/02　C
　Ｈ０１Ｍ　10/40　Z

【手続補正書】
【提出日】平成17年3月15日(2005.3.15)
【手続補正１】
【補正対象書類名】明細書
【補正対象項目名】特許請求の範囲
【補正方法】変更
【補正の内容】
【特許請求の範囲】
【請求項１】
ニッケルとマンガンとの原子比が０．７≦Ｎｉ／Ｍｎ≦7を満たす層状リチウムニッケルマンガン複合酸化物であって、Ｍｇ及びＣａの含有量が共に３００ｐｐｍ以下であることを特徴とする層状リチウムニッケルマンガン複合酸化物。
【請求項２】
ニッケル及びマンガンの存在するサイトの一部が他の元素で置換されていることを特徴とする請求項１に記載の層状リチウムニッケルマンガン複合酸化物。
【請求項３】
他の元素が、Ａｌ、Ｃｏ及びＦｅからなる群から選ばれる少なくとも一種の金属元素である請求項１又は２のいずれかに記載のリチウムニッケルマンガン複合酸化物。
【請求項４】
下記一般式（Ｉ）で表される、請求項１乃至３のいずれかに記載のリチウムニッケルマンガン複合酸化物。
【化１】

$$Li_xNi_YMn_ZQ_{(1-Y-Z)}O_2 \quad (I)$$

（式中、Ｘは０＜Ｘ≦１．２の範囲の数を表す。Ｙ及びＺは、０．７≦Ｙ／Ｚ≦7、及び、０≦（１－Ｙ－Ｚ）≦０．５の関係を満たし、ＱはＡｌ、Ｃｏ及びＦｅからなる群から選ばれる少なくとも一種を表す。）。
【請求項５】
請求項１乃至４のいずれか１つに記載の層状リチウムニッケルマンガン複合酸化物を含有するリチウム二次電池用正極材料。
【請求項６】
請求項５に記載のリチウム二次電池用正極材料とバインダーとを含有することを特徴とするリチウム二次電池用正極。
【請求項７】

請求項１乃至４のいずれか１つに記載の層状リチウムニッケルマンガン複合酸化物を使用した正極と、負極と、電解質とを有することを特徴とするリチウム二次電池。
【手続補正２】
【補正対象書類名】明細書
【補正対象項目名】０００８
【補正方法】変更
【補正の内容】
【０００８】
即ち、本発明の要旨は、ニッケルとマンガンとの原子比が０．７≦Ｎｉ／Ｍｎ≦７を満たす層状リチウムニッケルマンガン複合酸化物であって、Ｍｇ及びＣａの含有量が共に３００ｐｐｍ以下であることを特徴とする層状リチウムニッケルマンガン複合酸化物に存する。
なお、第４１回電池討論会２Ｄ２０（２０００）では、$LiMn_{0.5}Ni_{0.5}O_2$なる組成の層状リチウムニッケルマンガン複合酸化物が報告されているが、レート特性について何も触れられておらず、またマグネシウム及びカルシウムの含有量についても記載されていない。
【手続補正３】
【補正対象書類名】明細書
【補正対象項目名】０００９
【補正方法】変更
【補正の内容】
【０００９】
【発明の実施の形態】
本発明の層状リチウムニッケルマンガン複合酸化物は、層状の結晶構造を有し、リチウムとニッケルとマンガンとを含む酸化物である。ニッケルとマンガンの原子比（Ｎｉ／Ｍｎ）は、層状結晶構造が安定に存在し、また電池特性を悪化させない観点で、０．７以上、７以下とする。ニッケルとマンガンの原子比（Ｎｉ／Ｍｎ）として好ましい範囲はいくつか挙げられるが、例えば１つには、下限としては０．８以上、中でも０．９以上、また、上限としては１．２以下、中でも１．１以下である。もう１つには下限としては、１．３以上、中でも１．５以上、また、上限としては、７以下、中でも５以下である。
【手続補正４】
【補正対象書類名】明細書
【補正対象項目名】００１２
【補正方法】変更
【補正の内容】
【００１２】
【化２】

$$Li_XNi_YMn_ZQ_{(1-Y-Z)}O_2 \quad (I)$$

ここで、式（Ｉ）中、Ｑは置換元素を表わし、Ｘは０＜Ｘ≦１．２、好ましくは０＜Ｘ≦１．１の範囲の数を表わす。Ｘが大きすぎると、結晶構造が不安定化したり、これを使用したリチウム二次電池の電池容量低下を招く恐れがある。Ｙ及びＺは、Ｙ＋Ｚ≦１を満たす数であり、また０．７≦Ｙ／Ｚ≦７の範囲の数を表す。相対的にマンガンの割合が大きくなると単一相のリチウムニッケルマンガン複合酸化物が合成しにくくなる。
Ｙ／Ｚの値として好ましい範囲はいくつか挙げられるが、例えば１つには、ニッケル比率を少なくしてコスト上有利でありかつ容易に合成でき、マンガンが多い分、放電電圧が高い故に放電特性として有利である点で、下限としては、０．８以上、中でも０．９以上、上限としては、１．２以下、中でも１．１以下である。もう１つには、ニッケル比率を多くして電池容量を大きくし、嵩密度が高い故に単位体積当たりの電池容量が更に大きくなる点で、下限としては、１．３以上、中でも１．５以上、上限としては、７以下、中で

も５以下である。
【手続補正５】
【補正対象書類名】明細書
【補正対象項目名】００１３
【補正方法】変更
【補正の内容】
【００１３】
（１－Ｙ－Ｚ）の値は０．５以下、好ましくは０．３５以下、さらに好ましくは０．２５以下とする。置換元素の量が多すぎると、リチウムニッケルマンガン複合酸化物を正極活物質として使用したリチウム二次電池の電池容量が大きく低下することがある。
ＱはＡｌ、Ｃｏ及びＦｅからなる群から選ばれる少なくとも一種を表す。これらのうちより好ましいのは、Ａｌ、Ｃｏであり、最も好ましいのはＣｏである。Ａｌ、Ｃｏは、$LiNi_{1-x}Mn_xO_2$（０．７≦Ｎｉ／Ｍｎ≦７）に対して容易に固溶し、単一相のリチウム遷移金属複合酸化物として合成することができる。更に、Ａｌ、Ｃｏに関しては、得られるリチウム遷移金属複合酸化物を正極活物質として用いたリチウム二次電池が高性能な電池特性、特に繰り返し充放電を行った際の放電容量維持率について良好な性能を示す。
さらに良好な結晶性を有する層状リチウムニッケルマンガン複合酸化物とするために、層状リチウムニッケルマンガン複合酸化物に対して固溶せずに、焼成時に溶融し、液相を生じる物質（以下、「不活性溶融剤」という）を添加しても良い。
これらの不活性溶融剤は常温まで冷却した後は、層状リチウムニッケルマンガン複合酸化物の結晶構造内に取り込まれず、主に表面を被覆、あるいは表面に析出した状態で存在する。
上記のような不活性溶融剤としては、ホウ素化合物、アンチモン化合物、あるいはカリウム、バリウム、リチウムのハロゲン化物、硫酸塩、モリブデン酸塩等が挙げられる。これらのうちより好ましいのは、ホウ素化合物、アンチモン化合物である。
不活性溶融剤の添加量は、Ｎｉ、Ｍｎ及び置換元素Ｑの合計のモル数を１とした場合、モル比で通常０．０５以下、好ましくは０．０４以下、より好ましくは０．０３以下である。不活性溶融剤の添加量が多すぎると充分な放電容量を得られない場合がある。
【手続補正６】
【補正対象書類名】明細書
【補正対象項目名】００１５
【補正方法】変更
【補正の内容】
【００１５】
リチウムニッケルマンガン複合酸化物中のＭｇやＣａの含有量を制御するには、製造したリチウムニッケルマンガン複合酸化物に、アンモニウム塩の水溶液による処理を施してＭｇやＣａの含有量を減少させることもできるが、上記処理の結果、リチウムニッケルマンガン複合酸化物の性状に変化を及ぼすことがある。従って、好ましくは、リチウムニッケルマンガン複合酸化物の生成段階においてすでにＭｇやＣａの含有量が上記範囲となるように、製造のための原料の選定や製造条件、製造環境を制御する。具体的には、後述する反応原料中のＭｇ量及びＣａ量をできるだけ減らしておく、あるいは、反応の際に必要な装置又は系外からのＭｇ成分及びＣａ成分の混入をできるだけ避けるようにするのが好ましい。特に、原料として使用するニッケル化合物、マンガン化合物、置換元素化合物中、特にニッケル化合物中には、それらの製造過程において用いられる天然鉱物や水、酸性溶液、アルカリ性溶液に由来して、通常多少なりともＭｇやＣａが含有されるので、原料の選定やその精製程度は、リチウムニッケルマンガン複合酸化物中のＭｇ及びＣａ含有量を所定範囲に制御する上で重要である。
リチウムニッケルマンガン複合酸化物中のマグネシウム含有量やカルシウム含有量は、ＩＣＰ発光分析等の方法で測定することができる。
【手続補正７】

【補正対象書類名】明細書
【補正対象項目名】００５５
【補正方法】変更
【補正の内容】
【００５５】
次にこのスラリーを二流体ノズル型スプレードライヤー（大川原化工機社製：Ｌ－８型スプレードライヤー）を用いて噴霧乾燥を行った。この時の乾燥ガスとして空気を用い、乾燥ガス導入量は４５m^3／ｍｉｎ、乾燥ガス入り口温度は９０℃とした。そして、噴霧乾燥により得られた造粒粒子を９００℃で１０時間空気中で焼成することにより、ほぼ仕込みのモル比組成のリチウムニッケルマンガン複合酸化物（$Li_{1.05}Ni_{0.50}Mn_{0.50}O_2$）を得た。得られたリチウムニッケルマンガン複合酸化物を塩酸に加熱溶解し、ＩＣＰ発光分析にてＭｇ、Ｃａを分析した結果、それぞれ３０ｐｐｍ、１１０ｐｐｍであった。

UNITED STATES
PATENT AND TRADEMARK OFFICE

P.O. Box 1450
Alexandria, VA 22313 - 1450
www.uspto.gov

ELECTRONIC PAYMENT RECEIPT

APPLICATION #	RECEIPT DATE / TIME	ATTORNEY DOCKET #
16/923,494	12/21/2020 10:02:33 AM ET	12732-2003004

Title of Invention

POSITIVE ELECTRODE ACTIVE MATERIAL, METHOD FOR MANUFACTURING POSITIVE ELECTRODE ACTIVE MATERIAL, AND SECONDARY BATTERY

Application Information

APPLICATION TYPE	Utility - Nonprovisional Application under 35 USC 111(a)	PATENT #	-
CONFIRMATION #	3273	FILED BY	Nikki Krahler
PATENT CENTER #	60122058	AUTHORIZED BY	Heather Flanagan
CUSTOMER #	26171	FILING DATE	07/08/2020
CORRESPONDENCE ADDRESS	-	FIRST NAMED INVENTOR	Teruaki OCHIAI

Payment Information

PAYMENT METHOD	PAYMENT TRANSACTION ID	PAYMENT AUTHORIZED BY
DA / 061050	E2020BKA08323493	Nikki Krahler

FEE CODE	DESCRIPTION	ITEM PRICE($)	QUANTITY	ITEM TOTAL($)
1806	SUBMISSION OF AN INFORMATION DISCLOSURE STATEMENT	260.00	1	260.00
			TOTAL AMOUNT:	$260.00

This Acknowledgement Receipt evidences receipt on the noted date by the USPTO of the indicated documents, characterized by the applicant, and including page counts, where applicable. It serves as evidence of receipt similar to a Post Card, as described in MPEP 503.

New Applications Under 35 U.S.C. 111

If a new application is being filed and the application includes the necessary components for filing date (see 37 CFR 1.53(b)-(d) and MPEP 506), a Filing Receipt (37 CFR 1.54) will be issued in due course and the date shown on this Acknowledgement Receipt will establish the filing date of the application

National Stage of an International Application under 35 U.S.C. 371

If a timely submission to enter the national stage of an international application is compliant with the conditions of 35 U.S.C. 371 and other applicable requirements a Form PCT/DO/EO/903 indicating acceptance of the application as a national stage submission under 35 U.S.C. 371 will be issued in addition to the Filing Receipt, in due course.

New International Application Filed with the USPTO as a Receiving Office

If a new international application is being filed and the international application includes the necessary components for an international filing date (see PCT Article 11 and MPEP 1810), a Notification of the International Application Number and of the International Filing Date (Form PCT/RO/105) will be issued in due course, subject to prescriptions concerning national security, and the date shown on this Acknowledgement Receipt will establish the international filing date of the application.

Available online at www.sciencedirect.com
SCIENCE DIRECT®
Solid State Ionics 159 (2003) 223–232
SOLID STATE IONICS
www.elsevier.com/locate/ssi

Synthesis and electrochemical performance of tetravalent doped $LiCoO_2$ in lithium rechargeable cells

S. Gopukumar[a,*], Yonghyun Jeong[b], Kwang Bum Kim[b]

[a] Central Electrochemical Research Institute (CSIR), Karaikudi-630 006, India
[b] Division of Material Science and Engineering, Yonsei University, 134, Shinchon-dong, Seodaemun-gu, Seoul 120-749, South Korea

Received 29 August 2002; received in revised form 27 January 2003; accepted 6 February 2003

Abstract

Titanium-doped lithium cobalt oxides having the formula $LiTi_xCo_{1-x}O_2$ ($0 \le x \le 0.5$) have been synthesized using high temperature solid-state technique and its performance in a lithium rechargeable cell is reported. The synthesized oxides were structurally analyzed using X-ray diffraction (XRD) and Raman spectroscopy. It has been observed that single-phase materials were below 10% of Ti doping whereas impurity spinel phases were detected at higher concentrations. Electrochemical behaviors of the prepared powders were analyzed using cyclic voltammetry (CV) and galvanostatic charge/discharge cycling studies in the voltage range 3.0–4.25 V (vs. Li metal) using 1 M $LiClO_4$/PC as electrolyte. The composition with $x=0.01$ exhibits an initial charge and discharge capacity of 157 and 148 mA h/g at 0.2*C* rate, respectively, as compared to 137 and 134 mA h/g of $LiCoO_2$. Further, more than 90% of the capacity is retained even after 10 cycles. The role of tetravalent doping on the electrochemical behavior of $LiCoO_2$ has not been reported previously.
© 2003 Elsevier Science B.V. All rights reserved.

Keywords: Lithium Intercalation; Doping; Electrochemical properties; $LiCoO_2$; Capacity

1. Introduction

Lithiated transition metal oxides, namely, $LiMn_2O_4$, $LiCoO_2$ and $LiNiO_2$, are primarily used as cathode materials in lithium ion cells [1–5]. Among these, $LiCoO_2$ is the preferred material in majority of the commercial cells in view of its ease of synthesis and high reversibility [6]. The use of $LiCoO_2$ is considered to deliver a theoretical capacity of 273.8 mA h/g, i.e., when whole of the lithium is deintercalated. Although this high capacity looks very attractive from battery point of view, practically, only 50% of the theoretical capacity, i.e., ~ 137 mA h/g, is possible due to structural degradation and thereby limiting the extraction of lithium to 0.5 [7]. Recently, attempts to modify the pristine $LiCoO_2$ by using techniques like coating [8,9], mixing of ceramic oxide [10], etc. have been made with the idea of enhancing the practical capacity output by stabilizing the layered structure. In spite of the fact that some of these modifications have led to good capacity retention, partial doping of $LiCoO_2$ seems to be most acceptable approach for commercial exploitation consider-

* Corresponding author. Tel.: +91-4565-227750; fax: +91-4565-227779.
E-mail address: deepika_41@rediffmail.com (S. Gopukumar).

0167-2738/03/$ - see front matter © 2003 Elsevier Science B.V. All rights reserved.
doi:10.1016/S0167-2738(03)00081-X

ing the economy and ease of the bulk production process involved.

Ohzuku et al. [11] suggested that partial doping of cobalt with metal ions leads to extended cyclability and increase in capacity of lithium ion cells by enhancing structural stability. Further, theoretical studies suggest [12] that the capacity of layered compounds increased with partial transition metal ion substitution while on the other hand operating voltage increased by doping with nontransition metal ion at the expense of capacity [13–15]. Considering these predictions and a survey of literature suggests that studies on the effect of doping cobalt in $LiCoO_2$ with either of the metal ions like nickel [16], manganese [17], chromium [18], aluminum [19], boron [20], rhodium [21] or iron [22] have been carried out for understanding the electrochemical behavior of $LiM_xCo_{1-x}O_2$ (M = metal ions) in lithium ion cells. Among these materials, aluminum [15,23,24] and nickel [16] have received wide attention but marginal success towards increasing the performance has been reported with only partial nickel substitution. Hence, as evident from literature, doping of $LiCoO_2$ with +2 and +3 valent metal ions does not enhance the capacity over pristine $LiCoO_2$ and therefore alternative dopant ions have to be investigated.

Recently, it was reported by Kim and Amine [25] that the capacity of layered $LiNiO_2$ could be enhanced by doping with tetravalent ions. As $LiNiO_2$ and $LiCoO_2$ are layered materials, therefore, we found it worthwhile to carry out a systematic investigation on the effect of a tetravalent ion by partially substituting cobalt in pristine $LiCoO_2$. We believe that the presence of tetravalent ions leads to the presence of some Co^{2+} charge compensators and, moreover, since both $LiCoO_2$ and $LiTiO_2$ [26] are isostructural, solid solution could be formed thereby enhancing the performance of the end members. A survey of literature points out only a sole publication [27] reporting the IR and Raman spectra of only $LiTi_{0.2}Co_{0.8}O_2$ synthesized at high and low temperatures. We were therefore interested to carry out a detailed investigation on the electrochemical behavior of $LiTi_xCo_{1-x}O_2$ ($x = 0.01–0.5$) as a cathode material for lithium rechargeable cells and present in this communication new electrochemical results hitherto not reported.

2. Experimental

High purity lithium hydroxide, cobalt acetate and titanium dioxide (Aldrich Chemical, USA) were used as received for the synthesis of $LiCoO_2$ and $LiTi_xCo_{1-x}O_2$ by solid-state technique. Stoichiometric amounts of the above chemicals with slight excess of lithium were weighed, mixed thoroughly and then heated initially at 400 °C for 6 h and then annealed at 800 °C for 12 h in a tubular furnace. The heating rate was controlled at 1 °C/min and then cooled at same rate to room temperature. The powders were ground well and used for physical and electrochemical investigations.

The structure of the synthesized powders were evaluated with an automated Rigaku powder X-ray diffractometer using Cu-K_α radiation by measuring the diffraction angle (2θ) between 10° and 80° with an increment of 0.02°/min. XRD of the cycled electrodes were also recorded for analyzing the structural changes.

Room temperature Raman spectra were recorded for the synthesized pristine $LiCoO_2$ as well as Ti-doped $LiCoO_2$ using Jobin-Yvon ISA T64000 Raman spectrometer equipped with a CCD detector and a microscope. Powder samples were put under a microscope objective that allows the laser beam to focus on a small selected area of the surface (~ 1 μm^2) and the backscattered Raman signal was collected. The laser light source was 514.5 nm line excited at 5–10 mW at an Ar ion laser power. A typical spectral run took only a few minutes, hence five Raman spectra, each recorded over the frequency 400–800 cm^{-1} at an acquisition time of 400 s, were averaged to increase the signal to noise ratio.

XANES measurements were recorded for the synthesized materials as detailed elsewhere [40].

Scanning electron microscope (SEM, Hitachi, S2700) was used for observing the morphology of the synthesized powders.

Electrodes for electrochemical measurements consisted of slurry prepared from a mixture of the synthesized powder with carbon black and PVDF binder in the ratio of 85:10:5, respectively, with NMP solvent. The slurry was coated onto an aluminum foil current collector and dried for 3 h. The electrode was hot pressed and stored in an argon-filled glove box prior to use. Cyclic voltammetry (CV) and

AMPEREX Ex. 1002
Page 1205

charge/discharge cycling studies were carried out using a three-electrode glass cell with 1 M $LiClO_4$/PC as electrolyte. Lithium foil was used both as reference and counter electrodes. CV experiments were performed at a scan rate of 25 μV/s in the potential range 3.5–4.25 V. Galvanostatic charge/discharge studies were carried out at a current rate of *C*/5 in the potential range 3–4.25 V. All electrochemical measurements were performed inside an argon-filled glove box and data recorded with an automated battery cycle life tester.

3. Results and discussion

$LiCoO_2$ has an α-$NaFeO_2$ structure belonging to *R*-3*m* space group, in which Li and Co ions are arranged alternatively occupying the 3b and 3a sites, respectively, and sandwiched between oxygen ions. Recently, it has been reported that spinel ($LiTi_2O_4$) [28] compounds of lithium and titanium could be synthesized and can be used in lithium batteries. However, these materials are found to be electrochemically active only in the voltage range below 3 V. In the present investigation, we see that the synthesized materials (below Ti doping of 10%) are capable of cycling at higher voltages, i.e., up to 4.25 V, and hence, no spinel phase lithium titanate is formed below $x=0.10$. Theoretical studies of Ceder et al. [14] suggest the formation of $LiTiO_2$ having the α-$NaFeO_2$ structure, but practically, it was observed by Obrovac et al. [26] that even though layered $LiTiO_2$ could be synthesized, deintercalation of lithium was not possible. Moreover, Pouillerie et al. [29] concluded from their study on $LiNi_{1-x}Mg_xO_2$ that for small values of *x* (below 10%), magnesium ions occupy the lithium sites due to larger ionic radii of magnesium (0.76 Å) than nickel. Following the above views, one may expect that partial introduction of Ti^{4+} ions in place of Co^{3+} in the present case could lead to the presence of titanium in lithium sites since the ionic radii of titanium ions (0.605 Å) are larger as compared to cobalt (0.545 Å) ions. This assumption can also be safely ruled out in view of the smaller ionic size of titanium as compared to lithium and also its high positive charge [30]. Therefore, we can say that addition of low amounts ($x<0.1$) of Ti corresponds to simple replacement of Co in the CoO_2 layers, Co^{2+} being the charge compensator, i.e., $[Li]_{3b}[Co_{1-x}Ti_x]_{3a}O_2$. Similar model has been postulated by Tukamoto and West [31] on their study on Mg-doped $LiCoO_2$. Further, very recent studies of Croguennec et al. [32] on the Rietveld analysis of Ti^{4+}-doped $LiNiO_2$ confirm the presence Ti^{4+} in the nickel site ($[Li_{1-z}Ni_z^{2+}]_{3b}[Ni_{t+z}^{2+}Ti_t^{4+}Ni_{1-z-2t}^{3+}]_{3a}O_2$). Moreover, the materials synthesized in the present study reveal that a layered structure of $LiTi_xCo_{1-x}O_2$ is applicable only up to a value of $x<0.1$ wherein the oxidation state is maintained around 3 [33]. Thus, we may say that true solid solutions of Li_2TiO_3 and $LiCoO_2$ are possible only at low concentration of titanium ions.

Having ascertained the formation of layered $LiTi_xCo_{1-x}O_2$ following the above discussions, we now make structural analysis using XRD and Raman spectroscopy for confirming our postulations. Fig. 1(i) presents the X-ray diffraction patterns of all the synthesized powders of $LiTi_xCo_{1-x}O_2$ in the composition range $0 \le x \le 0.5$. It is observed from the X-ray patterns that the entire fingerprint peaks, viz., 003, 101, 006, 102, 104, 108 and 110, are clearly identifiable thereby suggesting the formation of the α-$NaFeO_2$ structure. The diffraction peaks of the synthesized pristine $LiCoO_2$ are in excellent agreement with the JCPDS card No. 16-0427. The patterns also indicate the existence of additional impurity peaks from a composition of $LiTi_{0.05}Co_{0.95}O_2$ (Fig. 1(c)) and increases in intensity with further increase in titanium composition. Further, at higher compositions of titanium, a shoulder peak emerges alongside the 003 peak and the intensity of doublet peaks (006, 102, 108 and 110) also diminishes. Therefore, we can confirm from the present solid-state synthesis that true solid solutions of the type $LiTi_xCo_{1-x}O_2$ is possible only below the composition of $x=0.05$. The hexagonal parameters of the synthesized materials are presented in Table 1. As is well known, the lattice parameter *a* represents the intralayer metal–metal distance while *c* is ascribed to inter slab distances. It can be seen from Table 1 that the *a* and *c* values for synthesized pristine $LiCoO_2$ are 2.816 and 14.05 Å, respectively. These values are in excellent agreement with the reported values of FM, USA [34] and other researchers [16,23]. Furthermore, *c*/*a* ratio is an indicator of the metal–metal layering distance or in other words hexagonal setting, and is

AMPEREX Ex. 1002
Page 1206

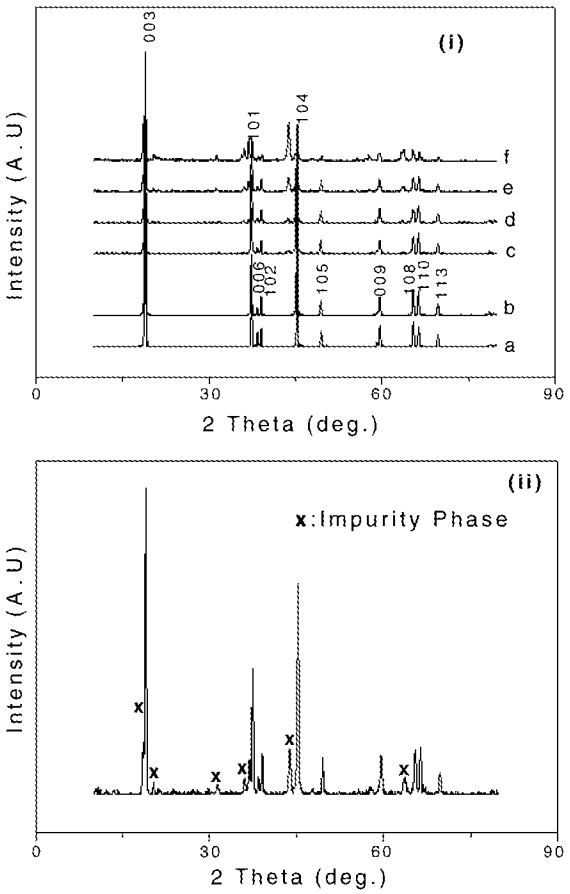


Fig. 1. (i) XRD pattern of $LiTi_xCo_{1-x}O_2$ (a: $x=0$; b: $x=0.01$, c: $x=0.05$; d: $x=0.10$; e: $x=0.25$; f: $x=0.50$). (ii) XRD pattern of $LiTi_{0.25}Co_{0.75}O_2$.

also found to be in close agreement with the reported values, i.e., 4.989.

We have not carried out Rietveld analysis, but to a very good approximation, the intensities of the XRD fingerprint peaks and Raman spectra studies can predict cation mixing. It can be noted that the ratio of the intensities of 003 and 104 (I_{003}/I_{104}) peaks is greater than unity, thereby suggesting no cation disorder which is supplemented by the values of *c*/*a*, i.e., >4.89. Interestingly, it is seen that the ratio of the intensities of 003 and 104 peaks for pristine $LiCoO_2$ is around 2.67 and is the highest [21]. Further, as can be seen from Table 1, the *c*/*a* ratios are in the range of 4.98 thereby indicating no cation mixing. However, coexistence of other impurities with the layered structure is seen by the presence of many additional peaks at higher titanium compositions ($>x=0.10$) and can be ascribed due to inhomogeneous distribution of Ti ions in the $LiCoO_2$ oxide matrix.

Looking at the radius of Ti^{4+} (0.605 Å) [30], we can expect that the partial replacement for low spin Co^{3+} (0.545 Å) should increase the *a* and *c* values thereby facilitating easy lithium insertion and extraction. We observe similar trend up to a value of $x=0.05$ beyond which the values decreases. This could be due to the growth of additional impurity phases at higher titanium concentrations leading to decreased electrochemical activity. Following the suggestions of Reimers et al. [35], we observe that the *R* factor, i.e., the ratio of $[I_{006}/I_{102}]/I_{101}$, is minimum for the lowest dopant composition, viz., $LiTi_{0.01}Co_{0.99}O_2$, and therefore suggesting increased layered characteristics than the pristine $LiCoO_2$ and other titanium compositions. These factors along with the well-defined splitting of doublet peaks at 108 and 110 coupled with high value of lattice constants *a*, *c* as well as *c*/*a* ratio indicate that this composition should have improved electrochemical performance.

The synthesized pristine and Ti-doped $LiCoO_2$ materials has a layered structure and can be assigned to the space group *R*-3*m* and the atoms (Co, Li and O) are located in the Wychoff sites 3a, 3b and 6c, respectively. Factor group analysis [36] of the Raman Spectra for pristine $LiCoO_2$ suggesis a pair of intense peaks located around frequencies of 595 and 485 cm^{-1} and is ascribed to Raman active modes A_{1g} and E_g, respectively. Since Raman modes are entirely due to oxygen atoms, hence the symmetry motions involve Co–O stretching and O–Co–O bending vibrations. The peak at frequency 595 cm^{-1} can be ascribed to symmetric Co–O stretching vibrations of cobalt octohedra [37]. Inaba et al. [38] observed the broadening of the peaks with increasing values of *x* on

Table 1
XRD lattice parameters *a* and *c* (Å) and intensity ratios of 003 and 104 peaks (*I*) for $LiTi_xCo_{1-x}O_2$

x	a	c	*c*/*a*	*I*
0	2.8163	14.051	4.989	2.67
0.01	2.8170	14.072	4.995	1.45
0.05	2.8168	14.070	4.995	1.23
0.25	2.8148	14.068	4.998	–
0.50	2.8121	14.029	4.989	–

AMPEREX Ex. 1002
Page 1207

their study on $LiNi_xCo_{1-x}O_2$. However, broadening of these peaks was ascribed due to polyhedral distortion in pristine $LiCoO_2$ [37]. Based on the intensities of the peaks (Fig. 2a) for pristine $LiCoO_2$, the peaks located at 485.4 and 594.6 cm^{-1} correspond to the optical modes Eg and A_{1g}, respectively, and are as predicted. Thus, A_{1g} stretching mode must be at a higher frequency than the Eg bending mode. Further, with increasing titanium doping, the peaks become broader as predicted by Inaba et al. [38]. It can be clearly seen that the synthesized pristine $LiCoO_2$ has no impurity peaks. However, as seen from Fig. 2b and c, the intensities of the peaks decrease and become broader at lower titanium doping contents, indicating the incorporation of Ti into Co sites. However, at higher doping levels (Fig. 2c), we observe the appearance of additional peaks located at frequencies of 447.8, 604.4 and 686.1 cm^{-1}. Thus, it is clearly seen that a spinel phase coexists with the layered structure and is consistent with our XRD spectrum, wherein we observe a peak growing alongside the 003 peak as also other additional peaks [marked × in Fig. 1(ii)]. Furthermore, due to lack of excess lithium required for the formation of both the phases, Co_3O_4 impurities are also traceable by the appearance of broad Raman peak located at a frequency of 686.1 cm^{-1}. Therefore, we can say that single-phase layered structure is observed only at lower titanium doping levels whereas spinel and impurity phases coexist at higher dopant levels.

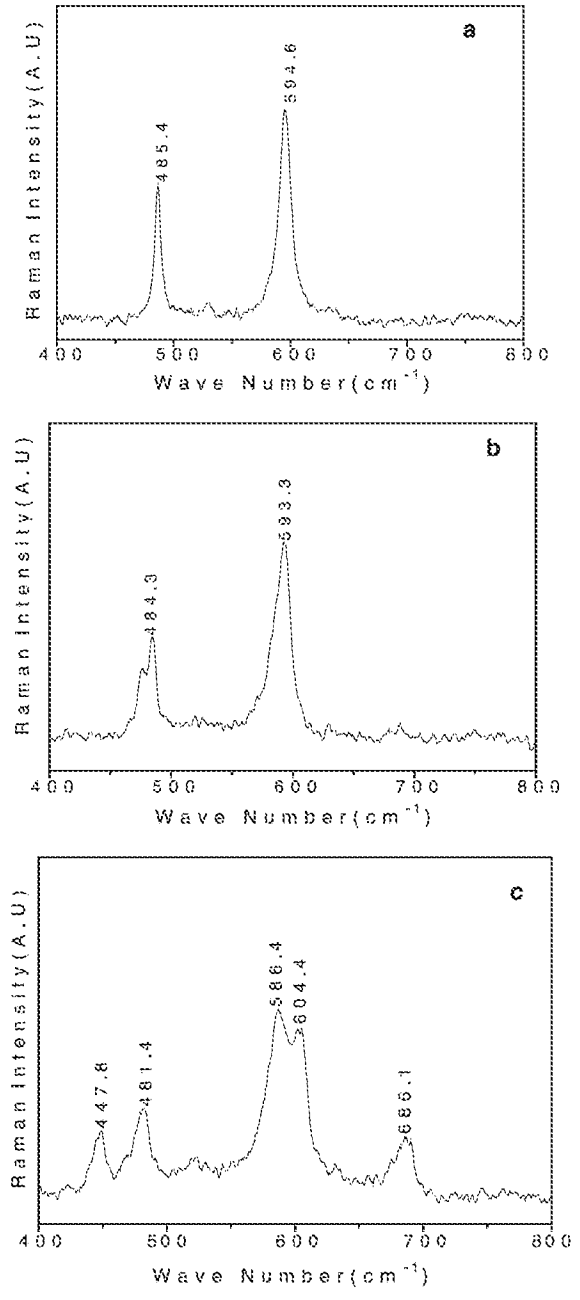


Fig. 2. Raman spectra of $LiTi_xCo_{1-x}O_2$ (a: $x=0$; b: $x=0.01$; c: $x=0.25$).

The synthesized materials were analyzed using XANES spectroscopy technique for obtaining meaningful information on the oxidation state of the metal in the bulk state. Fig. 3a presents the Co K-edge XANES spectra for the synthesized pristine and Ti-doped $LiCoO_2$. It can be clearly seen that the pattern of the spectra for the pristine $LiCoO_2$ is similar to literature reports [40]. The characteristic pre-edge peak 'A', region 'B' and a strong absorption peak 'C' assigned to the dipole-forbidden 1s to 3d, 1s to 4p as well as to the metal ligand transfer- and dipole-allowed 1s to 4p, respectively, are clearly noticeable. Furthermore, it is interesting to note from region 'B' (an indicator of the oxidation state of the metal ion) that the presence of minor amounts of titanium doping shifts the edge energy to slightly lower position thereby suggesting the presence of some Co^{2+} (Fig. 3b-ii) by the incorporation of Ti^{4+}. However, on the other hand, the edge energies shift to higher values with the increase in Ti^{4+} contents indicating the presence of Co^{4+} (Fig. 3b-iii) ions due to the inhomogeneous mixing of Ti ions in the $LiCoO_2$ oxide

AMPEREX Ex. 1002
Page 1208

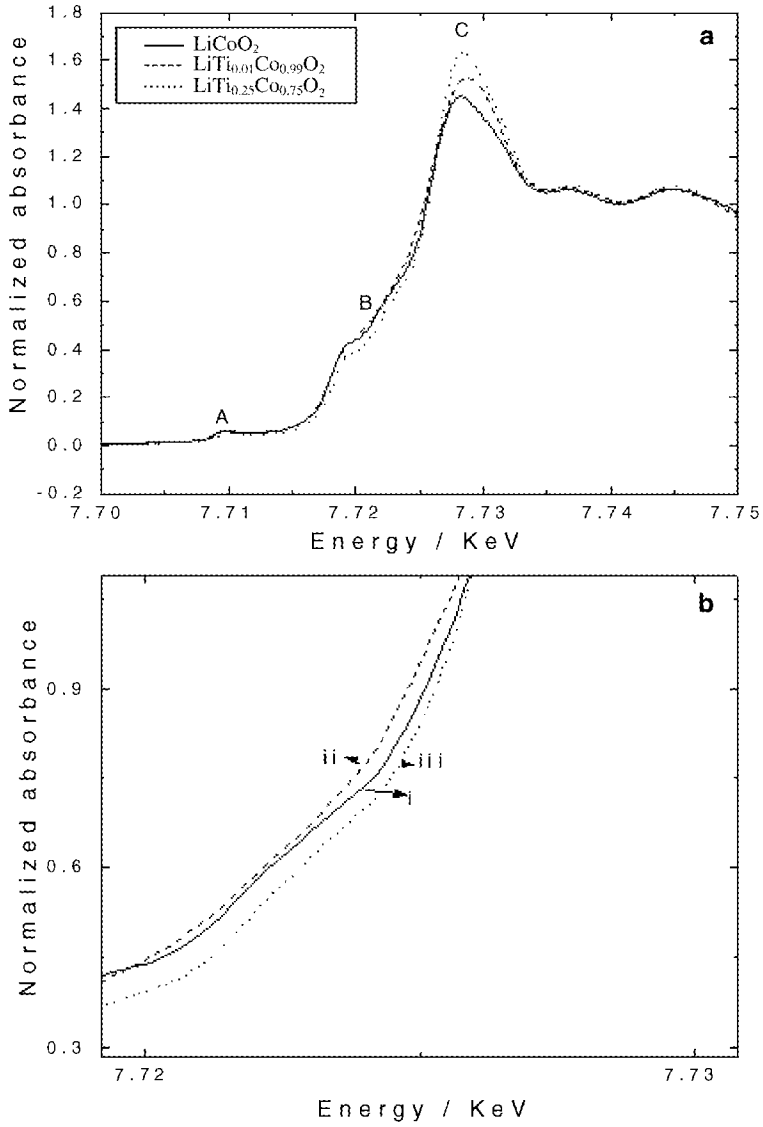


Fig. 3. (a) XANES spectra of $LiTi_xCo_{1-x}O_2$. (b) Magnified view of region B of XANES spectra of $LiTi_xCo_{1-x}O_2$ (i: $x=0$; ii: $x=0.01$; iii: $x=0.25$).

matrix. Detailed discussions on the spectral aspects of the synthesized materials will be presented in a subsequent publication in accordance with Ref. [44].

Morphology of the titanium-doped $LiCoO_2$ depicts that the particles are polydispersed with an average size of less than 1 μm. A typical SEM photograph is presented in Fig. 4.

Cyclic voltammetry is a useful electrochemical tool wherein the changes taking place in an electrochemical reaction are monitored by measuring the current–potential responses. Typical CVs obtained in the present case are depicted in Fig. 5. It is clear from the figures that the major oxidation and reduction peaks are observed at around 3.95 and 3.75 V, respectively, and are representative of lithium deintercalation and reintercalation processes, respectively. These peaks are also signature of hexagonal phase in these types of layered compounds and indicating

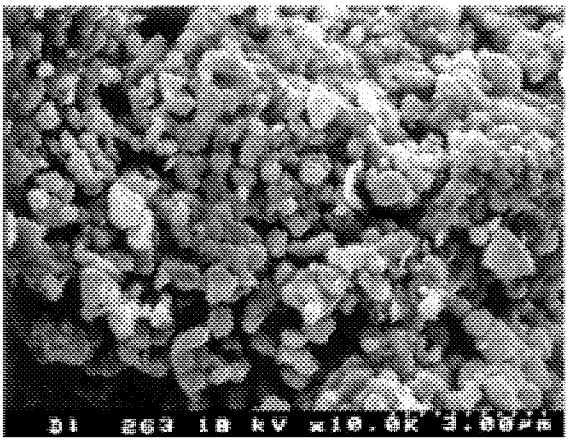


Fig. 4. A typical SEM of $LiTi_{0.01}Co_{0.99}O_2$.

perfect reversibility. Further, two very low intensity small high voltage peaks are also noticed both in the oxidation as well as in the reduction process at around 4.08 and 4.17 V depicting the coexistence of monoclinic phases in the investigated materials. It should be emphasized here that these high voltage peaks in pristine $LiCoO_2$ in the present case are detectable but grow with increase in titanium doping. The high voltage peaks are slightly better visible in the $x=0.01$ concentration and become very prominent at $x=0.25$ (Fig. 5c). This assumption is supported by the fact that in the case of $LiCoO_2$, the high voltage peaks are very prominent with decrease in particle size as observed by Uchida and Saito [39] on their study of thin films and also in the case of sol–gel [40] synthesized $LiCoO_2$. Our results of CV of $LiCoO_2$ are in agreement with Reimers and Dahn [41]. Further, the high voltage peaks are a debatable issue [42] as some of the workers have not observed such peaks. Moreover, these two peaks are assigned due to the phase transition between ordered and disordered lithium ion arrangement in the CoO_2 sheets. It was suggested by Yazami et al. [43] that these high voltage peaks could also arise out of anion absorption on surface impurities. In the present case, we see that these peaks are growing (Fig. 5c) with increasing titanium content (0.25) and therefore we may ascribe this is due to the inhomogeneous distribution of Ti in the $LiCoO_2$ oxide matrix. Similar behavior in CV studies was observed in the case of rhodium-doped $LiCoO_2$ [21]. Furthermore, as these peaks occur at exactly the same voltage as that of monoclinic phase, therefore, the ordering/disordering of Ti–Co ions also takes place reversible to Li ions in this phase. This can be confirmed with the growth of additional peaks in the XRD spectrum more so with the splitting of 104 peak initiating from $x=0.1$ composition.

Fig. 6 depicts the capacities of the synthesized pristine $LiCoO_2$ and titanium-doped $LiCoO_2$ materials over the entire composition range investigated for 10 cycles. It can seen that the composition with $x=0$, i.e., $LiCoO_2$ delivers the charge and discharge capacities of 137 and 134 mA h/g, respectively, for the first cycle at a current rate of $C/5$ in the voltage range of 3–4.25 V. The very low irreversible capacity of 3 mA

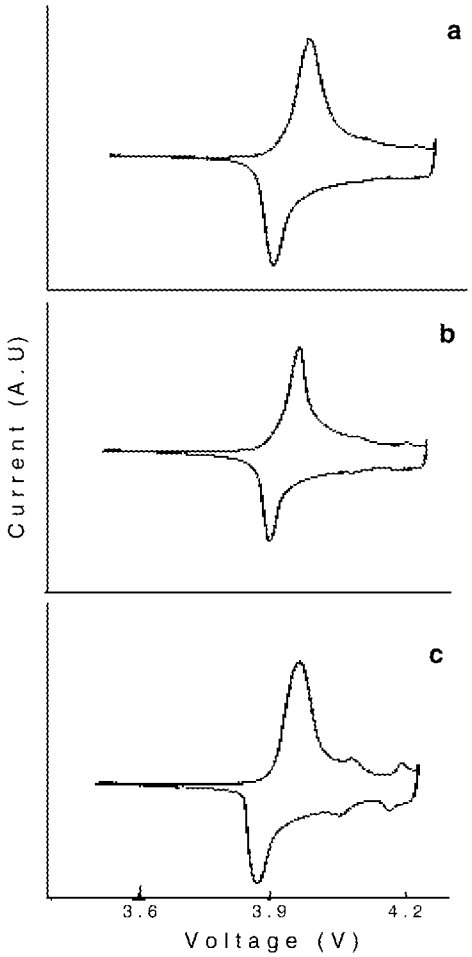


Fig. 5. Cyclic voltammograms of $LiTi_xCo_{1-x}O_2$ (a: $x=0$; b: $x=0.01$; c: $x=0.25$).

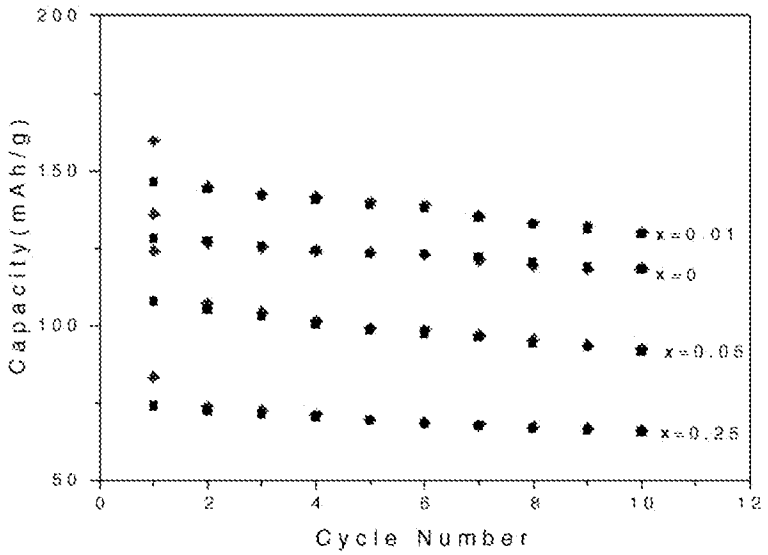


Fig. 6. Capacity (mA h/g) dependence on cycle number for $LiTi_xCo_{1-x}O_2$.

h/g confirms the purity of our sample and from second cycle onwards there is hardly any difference in the charge and discharge capacities. Moreover, we find that about 96% (128 mA h/g) of the initial capacity is retained after 10 cycles and corresponds to ~0.5 of lithium extraction during the charging process. The loss of capacity (3 mA h/g) in the first cycle can be assigned to the formation stage. The obtained values of capacity for pristine $LiCoO_2$ are the highest achieved and compare well with the literature reports [7]. Analysis of the doped $LiCoO_2$ samples indicates that the sample with $x=0.01$ delivers the highest capacity. The fist charge and discharge capacities of $LiTi_{0.01}Co_{0.99}O_2$ are 157 and 148 mA h/g, respectively. This implies a loss of 9 mA h/g in the first cycle as compared to 3 mA h/g for $LiCoO_2$. This slight higher initial loss is understandable in view of the presence of the inactive Ti^{4+} species present in the Co sites. Even though the initial capacity loss is more in the case of $x=0.01$, in subsequent cycles, the loss is not noticed similar to $LiCoO_2$ and the capacities are retained at 135 mA h/g after 10 cycles (Fig. 7). This result is interesting in view of the fact that we have obtained higher capacities than pristine $LiCoO_2$. We confirmed the composition of this particular sample using ICP-AES in view of its superior performance and note that, as expected, the compositions of Ti and Co were 0.009 and 0.991, respectively. Thus, we can confirm the positive effect of tetravalent substitution to the layered structure. Furthermore, as observed in XRD patterns, the well-defined doublets at 006, 102 as well as at 108 and 110 coupled with an increase in the lattice parameters a and c endorse the high electrochemical performance of this investigated composition. Having encouraged by this composition, we investigated other higher compositions and found that the capacities gradually decreased with further increase in titanium content thereby indicating that this composition is the optimum level of dopant. One interesting point to note here is that the presence of higher content of titanium improves the cyclability but

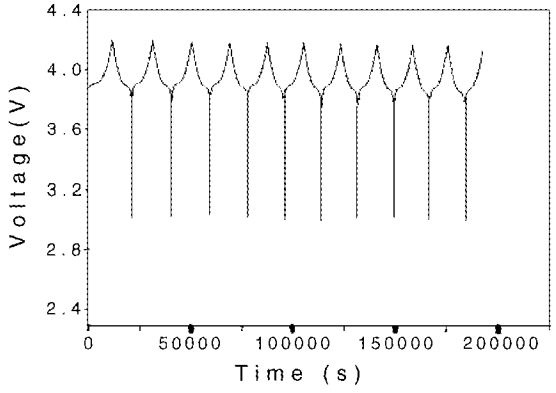


Fig. 7. Cycling behavior of $LiTi_{0.01}Co_{0.99}O_2$.

at the expense of capacity, which is understandable due to the reduction in cobalt ions and as reiterated earlier the electrochemically inactive nature of titanium ions in the investigated voltage range. As observed in the XRD patterns of the cycled $LiTi_{0.01}Co_{1-x}O_2$ cathode (Fig. 8), the structure of the synthesized material is retained even after 10 cycles thereby suggesting the stability of the material. Further, spectral and rate capability studies on this material correlating the present observations have recently been reported elsewhere [44].

Literature survey indicates that various dopants like Ni, Mg, Mn, Zn, Rh, Al, B, Fe, etc. [15,17,21,22,45] substituted for cobalt in $LiCoO_2$ have demonstrated inferior capacities than reported in this study for $LiTi_{0.01}Co_{0.99}O_2$ (Fig. 6) in the voltage range 3–4.25 V.

During the preparation of this manuscript, we came across a recent report by Choblet et al. [10] wherein the authors claim high capacities by the addition of minor amounts of TiO_2 (2 wt.%) as a distinct second phase to $LiCoO_2$ synthesized by complex sol–gel process. Indeed, our results also indicate an enhancement in capacity over pristine $LiCoO_2$ but have several advantages than the former like elimination of chelating agent (ascorbic Acid), pH maintenance (NH_4OH), lower titanium content (1%) and, above all, simple synthesis procedure. Further, our results can be supported by recent findings of Kim and Amine [25] on the role of tetravalent substitution in $LiTi_xNi_{1-x}O_2$ system. The authors also found that a composition of $x=0.025$ gave a enhanced capacity in the voltage range 2.8–4.3 V. The amount of titanium needed to stabilize the $LiNiO_2$ structure is slightly higher than in the present case. Of course, this is understandable in view of the fact that complete oxidation of nickel ions is difficult due to their presence in lithium layers. Therefore, we may conclude that the substitution of low amounts of titanium for cobalt in $LiCoO_2$ results in enhanced electrochemical performance.

4. Conclusion

We have demonstrated that it is possible to prepare solid solutions of $LiCoO_2$ and Li_2TiO_3 using high temperature solid-state technique. Structural characterization using XRD and Raman spectra reveals that single-phase layered compounds with α-$NaFeO_2$ structure are attained at lower titanium doping. The rate of capacity looks similar irrespective of doping amount, even though the initial capacity was enhanced a little for the case of low-doped sample. Further, enhanced stable electrochemical capacities of 135 mA h/g at a current rate of *C*/5 have been achieved for the composition $LiTi_{0.01}Co_{0.99}O_2$ in a lithium rechargeable cell in the voltage range 3–4.25 V using $LiClO_4$/PC as electrolyte.

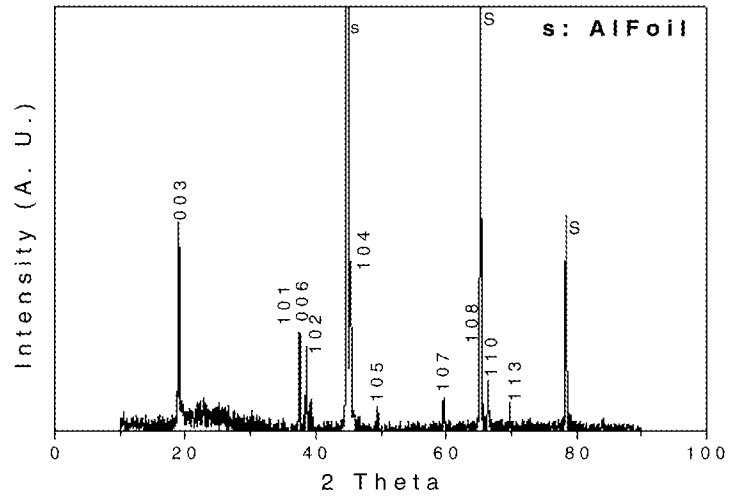


Fig. 8. XRD pattern of cycled $LiTi_{0.01}Co_{0.99}O_2$.

Acknowledgements

One of the authors, GK, would like to thank KOFST, Seoul, Korea, for offering a Brain Pool Visiting Fellowship. GK also thanks CECRI, Karaikudi and CSIR, New Delhi, for grant of leave. The authors thank the referees for their valuable suggestions. This work was also supported by the Ministry of Information and Communication of Korea (Support Project of University Information Technology Research Center supervised by KIPA). The authors would like to thank Cheil Industries Inc. for supporting electrolyte.

References

[1] T. Nagaura, K. Tozawa, Prog. Batteries Sol. Cells 9 (1990) 209.
[2] B. Scrosati, Nature 373 (1993) 557.
[3] L.B. Lave, C.T. Hennekson, F.C. McMicheal, Science 268 (1993) 993.
[4] M. Broussely, P. Biensan, B. Simon, Electrochim. Acta 45 (1999) 3.
[5] C. Delmas, in: G. Pistoia (Ed.), Lithium Batteries—A New Materials Developments and Perspectives, Elsevier, Amsterdam, 1994, pp. 457–489, Chap. 12.
[6] C. Julien, S. Gastro-Garcia, J. Power Sources 97/98 (2001) 290.
[7] Z. Lu, D.D. MacNeil, J.R. Dahn, Electrochem. Solid-State Lett. 4 (2001) A200.
[8] J. Cho, J.Y. Kim, B. Park, Chem. Mater. 12 (2000) 3788.
[9] J. Cho, J.Y. Kim, B. Park, J. Electrochem. Soc. 148 (2001) A1110.
[10] A. Choblet, H.C. Shia, H.-P. Liu, M. Salomon, A. Manivannan, Electrochem. Solid-State Lett. 4 (2001) A65.
[11] T. Ohzuku, A. Udea, M. Nagayama, Y. Iwakoshi, H. Komori, Electrochim. Acta 38 (1993) 1159.
[12] S. Venkatraman, V. Subramanian, S. Gopukumar, N.G. Renganathan, N. Muniyandi, Electrochem. Commun. 2 (2000) 18.
[13] G. Ceder, Y.M. Chiang, D.R. Sadoway, M.K. Aydinol, Y.I. Jang, B. Huang, Nature 392 (1998) 894.
[14] G. Ceder, M.K. Aydinol, A.F. Kohan, Comput. Mater. Sci. 8 (1997) 161.
[15] W. Yoon, K.K. Lee, K.B. Kim, J. Electrochem. Soc. 147 (2000) 2023.
[16] I. Sadoune, C. Delmas, J. Solid State Chem. 136 (1998) 8.
[17] C. Julien, M.A. Camacho-Lopez, T. Mohan, S. Chitra, P. Kalyani, S. Gopukumar, Solid State Ionics 135 (2000) 241.
[18] C.D.W. Jones, E. Rosen, J.R. Dahn, Solid State Ionics 68 (1994) 65.
[19] G.A. Nazri, A. Rougier, K.F. Kia, Mater. Res. Symp. Proc. 453 (1997) 63.
[20] R. Alcantara, P. Lavela, J.L. Tivado, R. Stoyanova, E.J. Zhecheva, Solid State Chem. 134 (1997) 265.
[21] S. Madhavi, G.V. Subba Rao, B.V.R. Chowdari, S.F.Y. Li, J. Electrochem. Soc. 148 (2001) A1279.
[22] H. Kobayashi, S. Shigemura, M. Tabuchi, H. Sakaebe, K. Ado, H. Kageyama, A. Hirano, R. Kanno, M. Wakita, S. Morimotoand Nasu, J. Electrochem. Soc. 147 (2000) 960.
[23] Y.I. Jang, B. Huang, H. Wang, D.R. Sadoway, G. Ceder, Y.M. Chiang, H. Liu, H. Tamura, J. Electrochem. Soc. 146 (1999) 862.
[24] H. Huang, G.V. Subba Rao, B.V.R. Chowdari, J. Power Sources 690 (1999) 81.
[25] J. Kim, K. Amine, Electrochem. Commun. 3 (2001) 52.
[26] M.N. Obrovac, O. Mao, J.R. Dahn, Solid State Ionics 112 (1998) 9.
[27] W. Huang, R. Frech, Solid State Ionics 86–88 (1996) 395.
[28] P. Krtil, D. Fattakhova, J. Electrochem. Soc. 148 (2001) A1045.
[29] C. Pouillerie, L. Croguennec, Ph. Biensan, P. Willmann, C. Delmas, J. Electrochem. Soc. 147 (2000) 2061.
[30] B.V.R. Chowdari, G.V. Subba Rao, S.Y. Chow, Solid State Ionics 140 (2001) 55.
[31] H. Tukamoto, A.R. West, J. Electrochem. Soc. 144 (1997) 3164.
[32] L. Croguennec, E. Suard, P. Willmann, C. Delmas, Chem. Mater. 14 (2002) 2149.
[33] Z. Lu, D.D. MacNeil, J.R. Dahn, Electrochem. Solid-State Lett. 4 (2001) A200.
[34] X.Q. Yang, X. Sun, J. McBreen, Electrochem. Commun. 2 (2000) 100.
[35] J.N. Reimers, E. Rossen, C.D. Jones, J.R. Dahn, Solid State Ionics 61 (1993) 335.
[36] W.G. Fateley, Infrared and Raman Selection Rules for Molecular and Lattice Vibrations: The Correlation Method, Wiley-Interscience, New York, 1972.
[37] C. Julien, M.A. Camacho-Lopez, L. Escobar-Alarcon, E. Haro-Poniatowski, Mater. Chem. Phys. 68 (2001) 210.
[38] M. Inaba, Y. Todzuka, H. Yoshida, Y. Grincourt, A. Tasaka, Y. Tomida, Z. Ogumi, Chem. Lett., (1995) 889.
[39] I. Uchida, H. Saito, J. Electrochem. Soc. 142 (1995) L139.
[40] W.S. Yoon, K.B. Kim, J. Power Sources 81–82 (1999) 517.
[41] J.N. Reimers, J.R. Dahn, J. Electrochem. Soc. 139 (1992) 2091.
[42] T. Ohzuku, A. Ueda, J. Electrochem. Soc. 141 (1994) 2972.
[43] R. Yazami, N. Lebrun, M. Bonneau, M. Molteni, J. Power Sources 54 (1995) 389.
[44] G. Kumar, K.W. Nam, H.S. Jung, K.B. Kim, 11th IMLB, Electrochemical Society Inc., California, 2002, p. 96.
[45] C. Julien, G.A. Nazri, A. Rougier, Solid State Ionics 135 (2000) 121.

AMPEREX Ex. 1002
Page 1213

Identification of cathode materials for lithium batteries guided by first-principles calculations

G. Ceder, Y.-M. Chiang, D. R. Sadoway, M. K. Aydinol, Y.-I. Jang & B. Huang

Department of Materials Science and Engineering, Massachusetts Institute of Technology, Cambridge, Massachusetts 02139-4307, USA

Lithium batteries have the highest energy density of all rechargeable batteries and are favoured in applications where low weight or small volume are desired—for example, laptop computers, cellular telephones and electric vehicles[1]. One of the limitations of present commercial lithium batteries is the high cost of the $LiCoO_2$ cathode material. Searches for a replacement material that, like $LiCoO_2$, intercalates lithium ions reversibly have covered most of the known lithium/transition-metal oxides, but the number of possible mixtures of these[2–5] is almost limitless, making an empirical search labourious and expensive. Here we show that first-principles calculations can instead direct the search for possible cathode materials. Through such calculations we identify a large class of new candidate materials in which non-transition metals are substituted for transition metals. The replacement with non-transition metals is driven by the realization that oxygen, rather than transition-metal ions, function as the electron acceptor upon insertion of Li. For one such material, $Li(Co,Al)O_2$, we predict and verify experimentally that aluminium substitution raises the cell voltage while decreasing both the density of the material and its cost.

The important characteristics of a lithium/metal-oxide compound for battery applications include the voltage at which it exchanges lithium, the amount of lithium that can be reversibly intercalated, and the stability of the material. The first two properties determine the energy density, and the latter limits the lifetime of the battery. Although a high voltage is desirable for obtaining high energy density[3], the practical use of high-voltage cathodes is at present limited by the voltage range over which the electrolyte is stable. The recent development of high-voltage electrolytes[6] is, however, likely to ameliorate this problem.

We demonstrated recently[7,8] that the average potential for intercalation between two compositions x_1 and x_2 can be obtained from the energy change in the reaction:

$$Li_{x_1}MO_2 + (x_2 - x_1)Li \rightarrow Li_{x_2}MO_2 \qquad (1)$$

The advantage of a first-principles computation is that it can be used to calculate the energy of the three compounds in equation (1), and hence the average potential, for any metal M (or combination of them), in any structure, whether these conditions have been experimentally realized or not. To calculate the total energies in equation (1) we use the *ab initio* ultrasoft-pseudopotential method as implemented in ref. 9. For the reactions $Li + Mn_2O_4 \rightarrow LiMn_2O_4$ and $Li + CoO_2 \rightarrow LiCoO_2$ we find average potentials of 4.0 and 3.75 V, respectively. The measured values are approximately 4.1 and 4.0 V, indicating that we have reasonable agreement with experiment, even though there are no adjustable parameters in the theory. The errors are consistent with the systematic underprediction of the potential in these compounds by ~0.2 V (ref. 7). Clearly, the *ab initio* prediction of intercalation voltages is possible. New materials can therefore be pre-screened before attempting their synthesis.

It is traditionally assumed that the intercalation voltage is determined by the redox potential of the transition-metal ion which is believed to change valence on Li insertion. We recently argued that for the late-transition-metal oxides it is instead the oxygen which is in large part responsible for the electron exchange[7]. As electron exchange with oxygen leads to a lower electrostatic energy (hence a higher voltage), we speculated that increased voltage correlates with increased oxygen participation in the electron exchange. If this is correct, part or all of the transition metal in a cathode material could be replaced by non-transition-metal ions, while retaining electrochemical Li-activity, although at a higher voltage. Such substitution would significantly increase the number of compounds that can be considered as cathode-active materials. In particular, elements from the third row of the periodic table would be of interest as they have lower mass than the 3*d* metals.

In this work, we first calculated the hypothetical intercalation voltage in Li_xAlO_2 and found it to be 5.4 V. $LiAlO_2$ has empty Al *p* orbitals well above the filled oxygen *p* states with no *d* states in between (as have all the transition-metal oxides) and electron exchange therefore occurs completely with the oxygen bands. Experimentally, this Li intercalation capacity will probably not be accessible as $LiAlO_2$ is electronically insulating. Electronic conductivity is required in an intercalation oxide, as Li^+ diffusion can occur only when accompanying electron motion is also possible. However, in solid solution with other transition-metal oxides, $LiAlO_2$ may be an attractive component. If our prediction regarding electrochemical activity of the oxygen ion is correct, Al substitution for transition-metal oxides will lead to higher Li intercalation voltage, as the fixed 3+ valence of Al forces more electron exchange with oxygen. However, our calculations indicate potential difficulties for mixing $LiAlO_2$ with other lithium/metal-oxides. We calculated the formation enthalpy for $Li(M,Al)O_2$ mixtures with M = Ti, V, Fe, Co and found them all to be positive, indicating that, at least at low temperature, separate regions of $LiAlO_2$ and $LiMO_2$ are favoured over the solid solution. Only in $Li(Co,Al)O_2$ is the formation enthalpy small enough (30 meV) to allow for entropy-driven mixing. We note that previous investigations of Al-doping of transition-metal oxides show no apparent effect on the intercalation potential[10,11]. However, phase separation at a scale not detectable by X-rays would annihilate the effect of Al doping on the potential, and result in a material with properties indistinguishable from the undoped material.

For $Li(Al_{0.33}Co_{0.67})O_2$ and $Li(Al_{0.67}Co_{0.33})O_2$ in the α-$NaFeO_2$ structure, our first-principles calculations predict an average Li intercalation potential of respectively 4.2 and 4.7 V. Given the

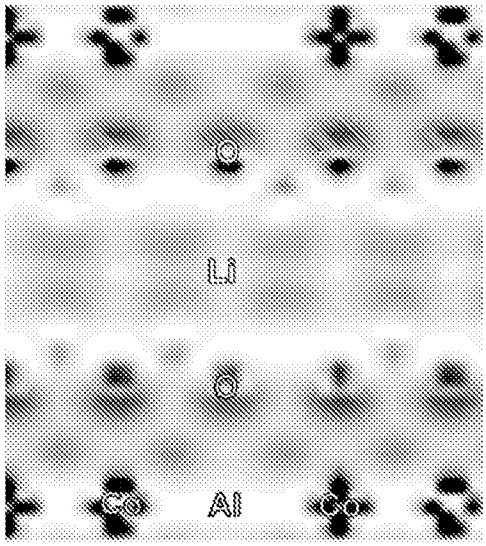


Figure 1 Positive part of the electron density difference between $Li(Al_{0.33}Co_{0.67})O_2$ and $(Al_{0.33}Co_{0.67})O_2$ in a plane perpendicular to the direction of layering in the structure. Darker indicates larger electron density.

Nature © Macmillan Publishers Ltd 1998

AMPEREX Ex. 1002
Page 1214

consistent underestimation of experimental voltages by the calculations[7], the true potential is probably ~0.2 V higher. The increase in voltage over pure $LiCoO_2$ is in agreement with our understanding of the increasing role of oxygen in Al-doped material. Figure 1 shows the change in charge density of the valence electrons when going from $(Al_{0.33}Co_{0.67})O_2$ to $Li(Al_{0.33}Co_{0.67})O_2$. These results are obtained by subtracting the charge density in $(Al_{0.33}Co_{0.67})O_2$ from that in $Li(Al_{0.33}Co_{0.67})O_2$. For these calculations, all atomic positions were assumed to remain unchanged on lithiation (whereas all coordinates were fully relaxed for the voltage calculations). Although Co accepts some charge from the extra lithium atom, none is transferred to Al. Considerable charge transfer to oxygen is clearly visible.

To test the predictions of the computations we developed a method to synthesize homogeneous $Li(Co,Al)O_2$ solid solutions in the α-$NaFeO_2$ structure. First, mixed cobalt–aluminium hydroxides were precipitated from mixed aqueous solutions containing $Co(NO_3)_2$ and $Al(NO_3)_3$, added dropwise to a continuously stirred LiOH aqueous solution kept at pH 10.5. Nitrate ions were removed from the precipitate through a rinsing procedure described in ref. 12. Lithium was then added through a freeze-drying procedure, in which the mixed hydroxide was dispersed in aqueous LiOH solution yielding a total Li/(Co + Al) molar ratio of unity, the suspension was atomized into liquid nitrogen, and the frozen droplets were freeze-dried.

Transmission electron microscopy showed this precursor to consist of crystalline Co,Al hydroxide uniformly mixed with amorphous Li hydroxide at the submicrometre scale. X-ray powder diffraction showed that a single-phase solid solution in the α-$NaFeO_2$ structure (space group $R\bar{3}m$) is obtained on firing this precursor to $T > 400$ °C in air for the compositions $y = 0.25$ and $y = 0.5$. For $y = 0.75$, a two-phase mixture of the α-$NaFeO_2$ solid solution and the tetragonal phase of $LiAlO_2$ was obtained.

Cathodes containing $LiAl_yCo_{1-y}O_2$ were prepared by mixing the oxide powder with carbon black and potting the mixture in a binder of poly(vinylidene fluoride). Pellets weighing 10–35 mg and measuring 1.0 cm^2 in surface area were formed by pressing at 360 MPa. These were dried at 140 °C under primary vacuum for 24 h and transferred to an argon-filled glove box. The test cell consisted of two stainless-steel electrodes in a holder made of Teflon. The anode was a lithium ribbon 0.75 mm thick. The electrolyte consisted of a 1 M solution of $LiPF_6$ in ethylene carbonate–diethyl carbonate, 1:1 by volume. The separator was a film of Celgard 2400 (Celgard LLC, Charlotte, North Carolina). Charge/discharge tests were performed with a Maccor Series 4000 Automated Test System (Maccor Inc., Tulsa, Oklahoma).

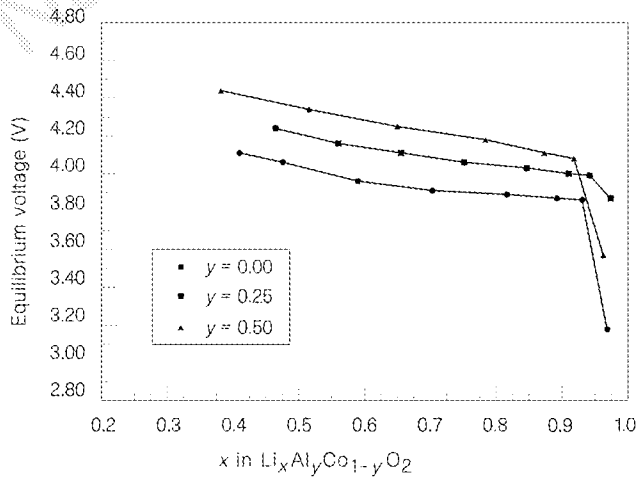


Figure 2 Open-circuit potential as a function of lithium content in pure $LiCoO_2$ and in Al-doped materials.

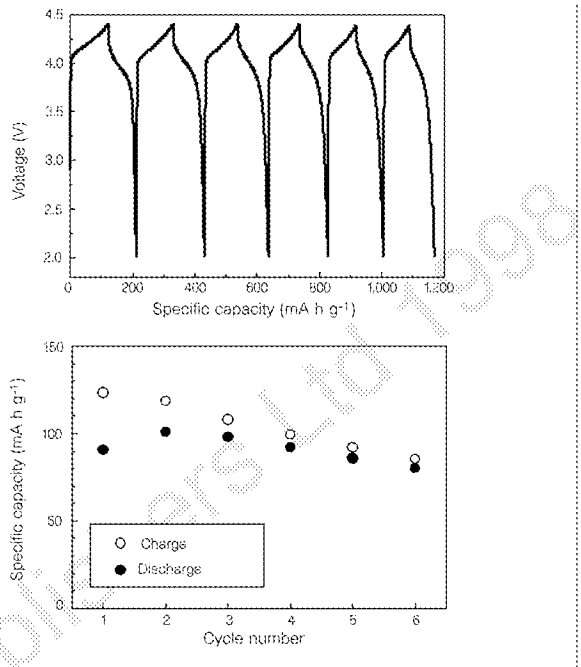


Figure 3 Cycling behaviour of $Li(Al_{0.25}Co_{0.75})O_2$/Li and specific capacity between 2.0 and 4.4 V. The current density was 0.4 mA cm^{-2}.

Figure 2 shows the open-circuit voltage (equilibrium potential) as a function of Li content in the oxide for samples calcined at 850 °C. These results were obtained by charging the cell in steps and allowing it to equilibrate for 15 h after each step. The equilibrium potential of the cells increases systematically with the Al content in the oxide, confirming the theoretical predictions. We note that at a value of $1 - x = 0.4$ the equilibrium voltage of the $Li_{1-x}Al_{0.5}Co_{0.5}O_2$/Li cell was as high as 4.40 V. As the calculations give the average voltage between compositions MO_2 and $LiMO_2$, whereas the cells were charged over only part of this composition range, direct quantitative comparison of the theoretical and experimental voltage is not yet possible.

Figure 3 shows the first few charges and discharges between 2.0 and 4.4 V (current density of 0.4 mA cm^{-2}) for the $LiAl_{0.25}Co_{0.75}O_2$/Li cell. The initial charge and discharge capacity were 120 and 90 mA h g^{-1}, respectively. On the sixth cycle, charge and discharge in the same potential window resulted in a capacity of ~90 and 80 mA h g^{-1}, respectively. The 4.4 V charging limit is imposed by the stability of the electrolyte used in these experiments and it is likely that more capacity could be found at higher potentials. The material clearly shows some capacity fade, as has been the case with many Li insertion materials in the initial stage of their development.

We expect similar results to these in other $LiAl_yM_{1-y}O_2$ solid solutions, where M is a transition metal. The present results show that the intercalation potential of such solid solutions, and probably those of other structures such as the spinel, can be 'quantum-engineered'. Owing to its low weight and price, aluminium can significantly increase energy density while reducing cost. Commercial feasibility of any new material will, however, also rely on successful synthesis and demonstration of high capacity and stability under electrochemical cycling. □

Received 20 August 1997; accepted 9 February 1998.

1. Pistoia, G. *Lithium Batteries* (Elsevier, Amsterdam, 1994).
2. Delmas, C. & Saadoune, I. Electrochemical and physical properties of the $Li_xNi_{1-y}Co_yO_2$ phases. *Solid State Ionics* **53–56**, 370–375 (1992).
3. Fey, G., Li, W. & Dahn, J. R. $LiNiVO_4$: A 4.8 Volt electrode material for lithium cells. *J. Electrochem. Soc.* **141**, 2279–2282 (1994).
4. Reimers, J. N., Rosen, E., Jones, C. D. & Dahn, J. R. Structure and electrochemistry of $Li_xFe_yNi_{1-y}$. *Solid*

Nature © Macmillan Publishers Ltd 1998

AMPEREX Ex. 1002
695
Page 1215

State Ionics **61**, 335–334 (1993).
5. Ohzuku, T., Ueda, A., Nagayama, M., Iwakoshi, Y. & Komori, H. Comparitive study of $LiCoO_2$, $LiNi_{1/2}Co_{1/2}O_2$ and $LiNiO_2$ for 4 volt secondary lithium cells. *Electrochim. Acta* **38**, 1159–1167 (1993).
6. Tarascon, J. M. & Guyomard, D. New electrolyte compositions stable over the 0 to 5 V voltage range and compatible with the $Li_{1+x}Mn_2O_4$/carbon Li-ion cells. *Solid State Ionics* **69**, 293–305 (1994).
7. Aydinol, M. K., Kohan, A. F., Ceder, G., Cho, K. & Joannopoulos, J. Ab-initio study of lithium-intercalation in metal-oxides and metal-dichalcogenides. *Phys. Rev. B* **56**, 1354–1365 (1997).
8. Ceder, G., Aydinol, M. K. & Kohan, A. F. Application of first-principles calculations to the design of rechargeable Li-batteries. *Comput. Mater. Sci.* **8**, 161–169 (1996).
9. Kresse, G. & Furthmüller, J. Efficiency of ab-initio total energy calculations for metals and semiconductors using a plane-wave basis set. *Comput. Mater. Sci.* **6**, 15–50 (1996).
10. Nazri, G. A., Rougier, A. & Kia, K. F. in *Solid State Chemistry of Inorganic Materials* (eds Davies, P. K., Jacobson, A. J., Torardi, C. C. and Vanderah, T. A.) 635–646 (Mater. Res. Soc. Symp. Proc. 453, Materials Research Society, Pittsburgh, 1997).
11. Ohzuku, T., Ueda, A. & Kouguchi, M. Synthesis and characterization of $LiAl_{1/4}Ni_{3/4}O_2$(R3m) for lithium-ion (shuttlecock) batteries. *J. Electrochem. Soc.* **142**, 4033–4039 (1995).
12. Chiang, Y.-M. *et al.* Synthesis of $LiCoO_2$ by decomposition and intercalation of hydroxides. *J. Electrochem. Soc.* **145**, 887–891 (1998).

Acknowledgements. We thank A. Mayes for discussions and comments. This work was sponsored by Furukawa Electric and the US Department of Energy through the Idaho National Engineering Laboratory University Research Consortium.

Correspondence and requests for materials should be addressed to G.C. (e-mail: gerd@lanai-mit.edu).

Surface topography dependence of biomolecular hydrophobic hydration

Yuen-Kit Cheng & Peter J. Rossky

Department of Chemistry and Biochemistry, University of Texas at Austin, Austin, Texas 78712-1167, USA

Many biomolecules are characterized by surfaces containing extended nonpolar regions[1], and the aggregation and subsequent removal of such surfaces from water is believed to play a critical role in the biomolecular assembly in cells[2]. A better understanding of the hydrophobic hydration of biomolecules may therefore yield new insights into intracellular assembly. Conventional views hold that the hydration shell of small hydrophobic solutes is clathrate-like, characterized by local cage-like hydrogen-bonding structures and a distinct loss in entropy[2]. The hydration of extended nonpolar planar surfaces, however, appears to involve structures that are orientationally inverted relative to clathrate-like hydration shells[3,4], with unsatisfied hydrogen bonds that are directed towards the hydrophobic surface. Here we present computer simulations of the interaction between the polypeptide melittin and water that demonstrate that the two different hydration structures also exist near a biomolecular surface. We find that the two structures are distinguished by a substantial difference in the water–water interaction enthalpy, and that their relative contributions depend strongly on the surface topography of the melittin molecule: clathrate-like structures dominate near convex surface patches, whereas the hydration shell near flat surfaces fluctuates between clathrate-like and less-ordered or inverted structures. The strong influence of surface topography on the structure and free energy of hydrophobic hydration is likely to hold in general, and will be particularly important for the many biomolecules whose surfaces contain convex patches, deep or shallow concave grooves and roughly planar areas[5].

The magnitude of the free energy of hydrophobic hydration, as inferred from the solubilities of small hydrocarbons in water, is $\sim$25 cal mol^{-1} Å^{-2} and is typically assumed to depend predominantly on the solute surface area[6]. This, and similar values derived from the data[6], are relatively low when compared with (for instance) the corresponding macroscopic measure of the liquid pentane–water interface, which is[6] $\sim$72 cal mol^{-1} Å^{-2}. Although the origin of this large difference remains controversial (see ref. 7 for a review), it is reasonable to anticipate that the molecularity of the solvent and solute are relevant to the value obtained.

Amphipathic helical polypeptides (with segregation of hydrophilic and hydrophobic moieties) have been chosen as the target in this study. Melittin, a 26-mer polypeptide found in honeybee venom, is one of the most studied archetypes of membrane proteins[8]. It readily self-associates as a tetramer in an aqueous solution of high peptide concentration, high pH, or high ionic strength[8]. Crystallized as a tetrameter, it is spatially a dimer of two almost stereochemically identical amphipathic α-helical dimers related by a two-fold symmetry axis[9]. Each dimer possesses a relatively flat hydrophobic surface, surrounded by convex patches of hydrophobic moieties (Fig. 1); the flat surface is completely buried in the centre of the tetramer on tetramerization[9]. Self-association of α-helical melittin monomers is thought to be important in its lytic activity of membranes, although the actual mechanism is still unknown. (See ref. 8 for a review.)

The interfacial hydration properties are expected to be crucial to the role of hydrophobic hydration of membrane proteins preceding and during membrane association. As the hydration of extended hydrophobic surfaces is apparently common in biological processes (for example, as inferred in the functioning surfaces of chaperonins[10]), results regarding hydrophobic hydration of surfaces, explored in this study, are of significance to a wider range of processes and compounds than the mechanism of melittin in membrane lysis.

In the following analysis, the surface of a melittin dimer is partitioned into two main types, 'flat' and 'convex', according to the local surface curvature (see Fig.1). The coordinates of the dimer were extracted from the crystal structure of melittin tetramer[9] deposited in the Brookhaven Protein Data Bank[11] and its structure was kept rigid throughout the simulation. The use of a fixed protein structure is not implemented as a simplification, but rather is required if one is to specifically identify the nature of hydration that is compatible with a given geometry of the protein surface. It is of interest also to learn how this protein structure might relax in response to full solvent exposure, but the present approach is needed if one is to understand the physical reasons for that process. Studies on the dynamics and other aspects of monomeric melittin in solution can be found elsewhere[12]. The present simulation (see Methods section) was performed at a temperature of 300 K in the

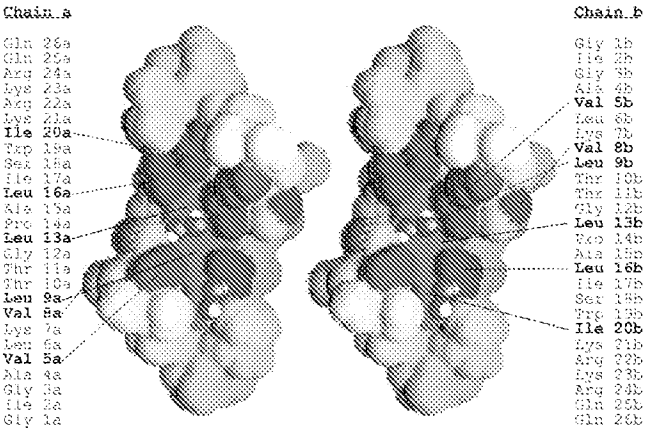


Figure 1 Stereographic image of the hydrophobic surface of the melittin dimer[9]; this is completely buried on tetramerization. The peptide sequences are provided in standard notation and are aligned with the model; the surface carbon centres selected for hydration analysis are indicated in bold. The central contiguous segment (shown green) is relatively flat and long (accessible surface area, 72.4 Å^2); the small convex surface patches are shown blue. Four surface proximal water molecules (rendered with oxygen radius r_{wO} = 1.6 Å and hydrogen radius r_{wH} = 1.0 Å; oxygen atoms are shown in red) are overlaid on the images. Surface regions not considered in this analysis are shown white. The picture is rendered by the program GRASP[22], and accessible surface area calculations by GEPOL93[16].

Nature © Macmillan Publishers Ltd 1998

AMPEREX Ex. 1002
Page 1216

UNITED STATES
PATENT AND TRADEMARK OFFICE

P.O. Box 1450
Alexandria, VA 22313 - 1450
www.uspto.gov

ELECTRONIC ACKNOWLEDGEMENT RECEIPT

APPLICATION #	RECEIPT DATE / TIME	ATTORNEY DOCKET #
16/923,494	**12/21/2020 10:02:33 AM ET**	**12732-2003004**

Title of Invention

POSITIVE ELECTRODE ACTIVE MATERIAL, METHOD FOR MANUFACTURING POSITIVE ELECTRODE ACTIVE MATERIAL, AND SECONDARY BATTERY

Application Information

APPLICATION TYPE	Utility - Nonprovisional Application under 35 USC 111(a)	PATENT #	-
CONFIRMATION #	3273	FILED BY	Nikki Krahler
PATENT CENTER #	60122058	FILING DATE	07/08/2020
CUSTOMER #	26171	FIRST NAMED INVENTOR	Teruaki OCHIAI
CORRESPONDENCE ADDRESS	-	AUTHORIZED BY	Heather Flanagan

Documents

TOTAL DOCUMENTS: 17

DOCUMENT	PAGES	DESCRIPTION	SIZE (KB)
12732-2003004 IDS.pdf	5	Information Disclosure Statement (IDS) Form (SB08)	175 KB
Warning: This is not a USPTO supplied IDS fillable form. Data in the form cannot be automatically loaded to other USPTO systems.			
SolidStateIonics_159_223.pdf	10	Non Patent Literature	7148 KB
SolidStateIonics_170_159.pdf	13	Non Patent Literature	2328 KB
CN001715193.pdf	13	Foreign Reference	1712 KB
CN102339998.pdf	10	Foreign Reference	1584 KB

CN102447107.pdf	10	Foreign Reference	1666 KB
CN102779976.pdf	12	Foreign Reference	2364 KB
CN103022502.pdf	10	Foreign Reference	1689 KB
CN103490060.pdf	11	Foreign Reference	1890 KB
CN104701534.pdf	9	Foreign Reference	1612 KB
CN106099098.pdf	12	Foreign Reference	2453 KB
JP2003-068306.pdf	17	Foreign Reference	19591 KB
JP2008-060033.pdf	25	Foreign Reference	22236 KB
JP2013-087040.pdf	30	Foreign Reference	19808 KB
KR20090111130A.pdf	25	Foreign Reference	1740 KB
KR1020160092946A.pdf	19	Foreign Reference	13542 KB
Nature-392-694-1998.pdf	3	Non Patent Literature	4398 KB

Digest

DOCUMENT	MESSAGE DIGEST(SHA-512)
12732-2003004 IDS.pdf	B00ADE8C8B78FB7276AD55B21075984B5DE3532006066BB59F414818AA41A30F78DD86E0FD9E1FE26AF0068DF0D8F61CB335A2B6DFC4518A478AF1ABFD29F142
SolidStateIonics_159_223.pdf	012C5654245C56AB4B08D6D2E1DB3F113AB0B0DA8149D5946D0207605F4CE07ED6D8BD0F0D13D67BF8F28B8D22491CF229399DCCCF7B088222CB16202E7A87D4
SolidStateIonics_170_159.pdf	A17B2D3376483DE48FE700D4D9578BD756C59C6F4FF57A953

	49888FA96A0268E23AFEAE19E0F53BF464E5F7CB943184F73B A5F017A16386771C335E66EB3EFE8
CN001715193.pdf	3B6AAAFC60B0197CB8BCFEF39336FB99DEC65DD4C4035541 EE83F447CDAB63CCB4C23828F4015A0FE70955F435BFAFF1E 03AC6738E027E44239E41BF88ADC7A5
CN102339998.pdf	27B680FF7F3563906E5783716C8F2F3B0FD477D5C94D968124 6AB250A4521649D53C209B32F9B0EDB23CD0282E2E216E488 7A3E019D628AD4E22F50252F10C46
CN102447107.pdf	E5343AC6F79DC91EC51D33204FB2E06817C41C024466D5BB8 D66BFF6FEF0F43EC43BA70D353AA8B2E967A40F83B24A555E 6D793EB4814D43CC20067FAAFDCB1C
CN102779976.pdf	EA9FDFD795AB02C43CD37015A9A81F6382E34A54E197654AC C75CE5BD265A37536AE17A1B2F165604163DA0E52004DD484 D78F93FCFBAB6313883324EE844947
CN103022502.pdf	16FE405C03F3D1BB075F026E2EBC13F7ED774E6DCD9B5B1B 064F0C01AD3DB839B92B724037F5AD802A5A000CA589F2E35 878C64027816A1DFBC0E8213490E90F
CN103490060.pdf	F57392F60FE3E8D6407F06522B1658EEA0F3C1339F589C6006 BF8216484D8ACEE52641FFF10DB86665DC60944459B1441813 74981E6BFD8A2A079B857779E8F6
CN104701534.pdf	81F1DEB69CAC346D56D3E49B271E1E4C90805E295B31BD018 8EE06DCD3CF761287B12F0EAE6E58A4891B649A1018805EE8 56B1623D6BB198C2B5B2586F192D7E
CN106099098.pdf	A036FA7CEB3BE40321F3734C5578E40E89458876E8EC41C4C 44E163368EAD6F7523D4DA1E9A334ABE39F7C750D821B47C1 B81E6DBD74EDF75A4C6F73FC755134
JP2003-068306.pdf	FAD0C1301DFBEB68001BC4B27CC5BA348378FF3A6DD33575 DDB9F38272FEE74425F7A9E1F315A55EE3109EB7686FCF0C9 74AEC40746D5723E3AC39D90C9959F1
JP2008-060033.pdf	A6803082C45E3CFC5CAEEA65A21EE400B24DDD06D41B3A46

	D54D19D84974BC47667EA950AB17B616514F8823265535AC24A599A607A10E80443F9A2D2C22230D
JP2013-087040.pdf	FEDF5E4EE83807D93F18EAAB45F886D7544395315641BB0B6893408B91AF417D2D64130B1CE9B514D99D20A9EF27C5C5DDED8A89013EF58931AEA5481E02FE52
KR20090111130A.pdf	24A95EABC30F7BF64BFDD756570BE71B4C0BF451154935E55AFC3B3B7A88ED13BADDACF3887125E12F99961EFD4BD9EE3711552330BEDD6978AFE2DC132A8607
KR1020160092946A.pdf	E0497DFDB54A4B108303AF084DA554D0E2A9AD0086426087C93EC6BBEB219FB3293A7D766BC25BB5323C1738F24301E234C597AAED8CA10366FCF66BE80810DA
Nature-392-694-1998.pdf	BE031B71A7C32F390A628C7418E1B183FF48F60F88962E8CA89A8B3A88BF61999873A873F364EA3F385CA525983D1698E0B4BBAE2719DF0731DD983513CE6F76

This Acknowledgement Receipt evidences receipt on the noted date by the USPTO of the indicated documents, characterized by the applicant, and including page counts, where applicable. It serves as evidence of receipt similar to a Post Card, as described in MPEP 503.

New Applications Under 35 U.S.C. 111

If a new application is being filed and the application includes the necessary components for filing date (see 37 CFR 1.53(b)-(d) and MPEP 506), a Filing Receipt (37 CFR 1.54) will be issued in due course and the date shown on this Acknowledgement Receipt will establish the filing date of the application.

National Stage of an International Application under 35 U.S.C. 371

If a timely submission to enter the national stage of an international application is compliant with the conditions of 35 U.S.C. 371 and other applicable requirements a Form PCT/DO/EO/903 indicating acceptance of the application as a national stage submission under 35 U.S.C. 371 will be issued in addition to the Filing Receipt, in due course.

New International Application Filed with the USPTO as a Receiving Office

If a new international application is being filed and the international application includes the necessary components for an international filing date (see PCT Article 11 and MPEP 1810), a Notification of the International Application Number and of the International Filing Date (Form PCT/RO/105) will be issued in due course, subject to prescriptions concerning national security, and the date shown on this Acknowledgement Receipt will establish the international filing date of the application.

Espacenet

RSS family document

Family list: CN102447107 (A) — 2012-05-09

1 application(s) for: CN102447107 (A)

1. High density lithium ion battery cathode material lithium cobalt oxide and preparation method thereof

Inventor:	Applicant:	CPC:	IPC:	Publication info:	Priority date:
LIFENG CUI HUI WANG (+3)	JIANGSU KING LITHIUM CELL CO LTD	Y02E60/10	C01G51/00 H01M4/525	CN102447107 (A) 2012-05-09 Global Dossier	2011-10-17

Espacenet

Bibliographic data: CN102447107 (A) — 2012-05-09

High density lithium ion battery cathode material lithium cobalt oxide and preparation method thereof

Inventor(s): LIFENG CUI; HUI WANG; KETAO YANG; YUNKE GE; XIZHENG WANG ± (CUI LIFENG, ; WANG HUI, ; YANG KETAO, ; GE YUNKE, ; WANG XIZHENG)

Applicant(s): JIANGSU KING LITHIUM CELL CO LTD ± (JIANGSU KING LITHIUM CELL CO.,LTD)

Classification: - international: *C01G51/00; H01M4/525*
- cooperative: Y02E60/10 (EP)

Application number: CN201110314401 20111017 Global Dossier

Priority number (s): CN201110314401 20111017

Abstract of CN102447107 (A)

The invention relates to a manufacture technology of a lithium ion battery cathode material and specifically provides a high density lithium ion battery cathode material lithium cobalt oxide and a preparation method thereof. The high density lithium ion battery cathode material lithium cobalt oxide of the invention has a chemical formula of Li1+xCo(1-a-b-c) MgaTibAlcFdO(2-d), wherein a, b, c, d and x satisfy relations of: 0<=a<=0.03, 0.001<=b<=0.02, 0<=c<=0.01, 0<=d<=0.02 and 0<=x<=0.08; and a preferable value of a, a preferable value of b, a preferable value of c and a preferable value of d satisfy relations of: 0.005<=a<=0.01, 0.002<=b<=0.01, 0<=c<=0.005 and 0<=d<=0.005; and a cation M is doped or cladded by one or a composition of several selected from magnesium, titanium and aluminium. The invention can enhance stability of material structure, cycle performance and safety performance of the lithium ion battery as well as effectively increase space utilization rate of the material and compacted density of the cathode material, thereby substantially raising volume energy density of the material.

(19)中华人民共和国国家知识产权局

(12)发明专利申请

(10)申请公布号 CN 102447107 A
(43)申请公布日 2012.05.09

(21)申请号 201110314401.0

(22)申请日 2011.10.17

(71)申请人 江苏科捷锂电池有限公司
地址 212006 江苏省镇江市京口工业园金阳大道9号

(72)发明人 崔立峰 王辉 杨克涛 葛云科 王熙帧

(74)专利代理机构 镇江京科专利商标代理有限公司 32107
代理人 夏哲华

(51)Int.Cl.
H01M 4/525(2010.01)
C01G 51/00(2006.01)

权利要求书 2 页 说明书 5 页

(54)发明名称

高密度锂离子电池正极材料钴酸锂及其制备方法

(57)摘要

本发明涉及锂离子电池正极材料的制造技术，具体是一种高密度锂离子电池正极材料钴酸锂及其制备方法。本发明的高密度锂离子电池正极材料钴酸锂，其化学式是 $Li_{1+x}Co_{(1-a-b-c)}Mg_aTi_bAl_cF_dO_{(2-d)}$，其中，$0 \leqslant a \leqslant 0.03$，$0.001 \leqslant b \leqslant 0.02$，$0 \leqslant c \leqslant 0.01$，$0 \leqslant d \leqslant 0.02$，$0 \leqslant x \leqslant 0.08$；优选a值为：$0.005 \leqslant a \leqslant 0.01$，b值优选为：$0.002 \leqslant b \leqslant 0.01$，c值优选为 $0 \leqslant c \leqslant 0.005$，d值优选为：$0 \leqslant c \leqslant 0.005$；阳离子M掺杂或包覆为镁、钛、铝几种元素中的一种或多种组合。本发明可以提高材料结构的稳定性，提高锂离子电池的循环性能、安全性能，并且可以有效的提高材料的空间利用率，提高正极材料的压实密度，进而使材料的体积能量密度大大提高。

CN 102447107 A

1. 一种高密度锂离子电池正极材料钴酸锂，其特征是：其化学式是 $Li_{1+x}Co_{(1-a-b-c)}Mg_aTi_bAl_cF_dO_{(2-d)}$，其中，$0 \leqslant a \leqslant 0.03$，$0.001 \leqslant b \leqslant 0.02$，$0 \leqslant c \leqslant 0.01$，$0 \leqslant d \leqslant 0.02$，$0 \leqslant x \leqslant 0.08$。

2. 根据权利要求 1 所述的高密度锂离子电池正极材料钴酸锂，其特征是：a 值优选为：$0.005 \leqslant a \leqslant 0.01$，b 值优选为：$0.002 \leqslant b \leqslant 0.01$，c 值优选为 $0 \leqslant c \leqslant 0.005$，d 值优选为：$0 \leqslant c \leqslant 0.005$。

3. 根据权利要求 1 所述的高密度锂离子电池正极材料钴酸锂，其特征是：上述的钴酸锂材料由两种或三种不同粒度的钴酸锂进行级配，其中钴酸锂的中位径（D50）为 1-4 微米、5-8 微米、12 -25 微米这三种粒径范围中的两种或三种。

4. 根据权利要求 3 所述的高密度锂离子电池正极材料钴酸锂，其特征是：每两种不同粒度的钴酸锂重量比为：小颗粒比大颗粒为 8:1 ～ 1:8。

5. 一种高密度锂离子电池正极材料钴酸锂的制备方法，其特征是：包括以下步骤，

（1）以钴盐和锂盐为原料，按照锂钴比为 1.10-1.05 的比例进行混合，干粉混合均匀后，在 950-1050℃条件下进行第一次合成，并将得到的钴酸锂进行粉碎，得到 A 料；

（2）以钴盐和锂盐（为原料，按照锂钴比为 1.00-1.06 的比例混合，干粉混合均匀后在 900-1000℃条件下进行第一次合成，并将得到的钴酸锂进行粉碎，得到 B 料；

（3）以钴盐和锂盐为原料，按照锂钴比为 1.00-1.06 的比例混合，干粉混合均匀后在 550-650℃条件下进行第一次合成，并将得到的钴混成品进行粉碎，得到 C 料；

（4）将上述 A 料与 B 料混合、或 B 料与 C 料混合、或 A 料、B 料、C 料三者混合，其中，A 料与 B 料的重量比为 A：B=8:1~1:8、或 B 料与 C 料的重量比为 B：C=8:1~1:8、或 A：B：C=(1~8)：(1~8)：(1~8)；混合后升温至 800-1000℃的合成温度下进行保温 5-20 小时，冷却后粉碎。

6. 根据权利要求 5 所述的高密度锂离子电池正极材料钴酸锂的制备方法，其特征是：步骤（1）中所述的钴酸锂是按照如下工艺制备的：以钴盐和锂盐为原料，氧化铝、氧化镁中一种或两种为掺杂剂，按照掺杂阳离子 M：Co =（0.002-0.01）:1 的摩尔比混合均匀，然后将所得的配料进行加热。

7. 根据权利要求 5 所述的高密度锂离子电池正极材料钴酸锂的制备方法，其特征是：步骤（2）中的钴酸锂是按照如下工艺制备的：以钴盐和锂盐为原料，氧化铝、氧化镁中一种或两种为掺杂剂，按照掺杂阳离子 M：Co =（0.002-0.01）:1 的摩尔比混合均匀，然后将所得的配料进行加热。

8. 根据权利要求 5 所述的高密度锂离子电池正极材料钴酸锂的制备方法，其特征是：步骤（3）中的钴酸锂是按照如下工艺制备的：以钴盐和锂盐为原料，氧化铝、氧化镁中一种或两种为掺杂剂，按照 M：Co =（0-0.01）:1 的摩尔比混合均匀，然后将所得的配料进行加热。

9. 根据权利要求 5 所述的高密度锂离子电池正极材料钴酸锂的制备方法，其特征是：步骤（1）中制备的钴酸锂中位径 D50 在 12-25 微米之间，步骤（2）中制备的钴酸锂中位径 D50 在 5-8 微米之间，步骤（3）中制备的钴酸锂中位径 D50 在 1-4 微米之间，且 A、B、C 均为一次粒子或 B、C 为二次球、混合粒子。

10. 根据权利要求 5 所述的高密度锂离子电池正极材料钴酸锂的制备方法，其特征是：在 A 与 B、或 B、C、或 A、B、C 混合的过程中，加入氧化镁，二氧化钛，氟化锂，其中 Mg：Co =

AMPEREX Ex. 1002
Page 1224

(0-0.02):1，Ti :Co=（0.001-0.02）:1，F :Co=（0-0.02）:1，以上比例均为物质的量之比。

AMPEREX Ex. 1002
Page 1225

高密度锂离子电池正极材料钴酸锂及其制备方法

技术领域

[0001] 本发明涉及锂离子电池正极材料的制造技术，具体是一种高密度锂离子电池正极材料钴酸锂及其制备方法。

背景技术

[0002] 锂离子电池作为一种新型的二次电池，具有比容量高、电压高、安全性好的特点，广泛应用于移动电话、笔记本电脑、便携式摄像机、DVD、MP3 等便携式电器的驱动电源。但随着电子产品的不断升级换代，对其电源的要求也不断提高，市场需要电池材料的能量密度以每年 5% 的速度增长。

[0003] 具体来说，锂离子电池的能量密度可以分为体积能量密度和重量能量密度，市场需要的是体积能量密度和重量能量密度的同时提高。

[0004] 1、在提高体积能量方面

在同样的容量发挥前提下，要提高电池的体积能量密度，就需要提高电池活性物质的单位体积填充量。对于目前常用的钴酸锂材料来说，其颗粒越大，由于材料的粒度分布变宽其压实密度也越大，材料的体积填充量就越大，其体积能量密度就越大。因此，目前常用的钴酸锂材料，其颗粒的中位径（D50）不断增大，由 5-10 微米提高到 10 微米以上甚至到 20 微米，目的在于提高活性物质的填充量，进而提高材电池的能量密度，如一种提高钴酸锂中位径和振实密度的方法（CN 1328351），其目的在于提高材料的粒度，进而提高其振实密度、压实密度。专利 CN 101284681 发明的超大粒径和高密度钴酸锂及其制备方法也是为了提高材料的粒度进而提高其振实密度、压实密度。目前，D50 为 12 微米钴酸锂其正常使用的压实密度为 3.8-4.0g/cm^3，D50 为 18 微米为 4.0-4.1g/cm^3，D50 为 20 微米为 4.1-4.2g/cm^3。但是，在对大颗粒钴酸锂材料的评价中发现，当颗粒增大后，正极材料的电化学性能会降低，其循环性能和倍率放电性能变差。因此不能满足日益增长的能量密度的要求。专利 CN 101436666A 进行的提高压实密度及能量密度的钴酸锂制备，其先制备大颗粒的钴酸锂颗粒，再通过碳酸钴和碳酸锂在大的钴酸锂颗粒表面造粒，从而制备出大颗粒钴酸锂表面沾附小颗粒的钴酸锂颗粒，进而提高正极材料的压实密度和体积比容量。但这种经过一次烧结的钴酸锂其结晶性不好，循环性能较差。专利 CN 1665052A 通过不同颗粒大小的钴酸锂进行混合能够提高材料的压实密度，进而提高材料的能量密度。然而，通过这种方法制备的钴酸锂，由于其小颗粒的钴酸锂含量较多，小颗粒钴酸锂的充放电速率较快，会给电池带来较大的安全隐患。

[0005] 2、在提高重量能量密度方面

提高钴酸锂能量密度的另一方面为提高钴酸锂的充电比容量，而提高充电比容量的一个有效方法为提高充电电压。提高充电电压后（>4.2V），一方面由于钴酸锂中锂离子迁出将大于 50%，由此造成钴酸锂的结构不稳定，容易发生结构的坍塌；另一方面，提高电压后材料的表面活性增强，容易与电解液发生反应，进而带来电池的安全隐患。

[0006] 另一方面，提高钴酸锂的重量能量密度就是减小钴酸锂的颗粒尺寸，这样就会导

AMPEREX Ex. 1002
Page 1226

致颗粒数量增多，颗粒间的空隙率增大。出现重量能量密度和体积能量密度不能兼顾的问题。再之，颗粒尺寸的减小，也会给电池的安全性带来隐患。

发明内容

[0007] 本发明所要解决的技术问题是，提供一种兼顾重量能量密度、体积能量密度，同时材料的循环性能、倍率放电性能及安全性能较高的高密度锂离子电池正极材料钴酸锂及其制备方法。

[0008] 本发明的高密度锂离子电池正极材料钴酸锂，其化学式是 $Li_{1+x}Co_{(1-a-b-c)}Mg_aTi_bAl_cF_dO_{(2-d)}$，其中，$0 \leqslant a \leqslant 0.03$，$0.001 \leqslant b \leqslant 0.02$，$0 \leqslant c \leqslant 0.01$，$0 \leqslant d \leqslant 0.02$，$0 \leqslant x \leqslant 0.08$；优选 a 值为：$0.005 \leqslant a \leqslant 0.01$，b 值优选为：$0.002 \leqslant b \leqslant 0.01$，c 值优选为 $0 \leqslant c \leqslant 0.005$，d 值优选为：$0 \leqslant c \leqslant 0.005$；阳离子 M 掺杂或包覆为镁、钛、铝几种元素中的一种或多种组合。

[0009] 上述的钴酸锂材料由两种或三种不同粒度的钴酸锂进行级配，其中钴酸锂的中位径（D50）可以为 1-4 微米、5-8 微米、12 -25 微米这三种粒径范围中的两种或三种。

[0010] 上述每两种不同粒度的钴酸锂重量比可以为：小颗粒比大颗粒为 8:1 ～ 1:8。

[0011] 上述材料的制备方法包括以下步骤：

（1）以钴盐（四氧化三钴、碳酸钴、氢氧化钴等，下同）和锂盐（碳酸锂、氢氧化锂、醋酸锂等，下同）为原料，按照锂钴比为 1.10-1.05 的比例进行混合，干粉混合均匀后，在 950-1050℃条件下进行第一次合成，并将得到的钴酸锂进行粉碎，得到 A 料；

（2）以钴盐（四氧化三钴、碳酸钴、氢氧化钴等，下同）和锂盐（碳酸锂、氢氧化锂、醋酸锂等，下同）为原料，按照锂钴比为 1.00-1.06 的比例混合，干粉混合均匀后在 900-1000℃条件下进行第一次合成，并将得到的钴酸锂进行粉碎，得到 B 料；

（3）以钴盐（四氧化三钴、碳酸钴、氢氧化钴等，下同）和锂盐（碳酸锂、氢氧化锂、醋酸锂等，下同）为原料，按照锂钴比为 1.00-1.06 的比例混合，干粉混合均匀后在 550-650℃条件下进行第一次合成，并将得到的钴混成品进行粉碎，得到 C 料；

（4）将上述 A 料与 B 料混合、或 B 料与 C 料混合、或 A 料、B 料、C 料三者混合，其中，A 料与 B 料的重量比为 A：B=8:1~1:8、或 B 料与 C 料的重量比为 B：C=8:1~1:8、或 A：B：C=(1~8)：(1~8)：(1~8)，升温至 800-1000℃的合成温度下进行保温 5-20 小时，冷却后粉碎。

[0012] 上述步骤（1）中所述的钴酸锂是按照如下工艺制备的：以钴盐和锂盐为原料，氧化铝、氧化镁中一种或两种为掺杂剂，按照掺杂阳离子 M：Co =（0.002-0.01）:1 的摩尔比混合均匀，然后将所得的配料进行加热。

[0013] 上述步骤（2）中的钴酸锂是按照如下工艺制备的：以钴盐和锂盐为原料，氧化铝、氧化镁中一种或两种为掺杂剂，按照掺杂阳离子 M：Co =（0.002-0.01）:1 的摩尔比混合均匀，然后将所得的配料进行加热。

[0014] 上述步骤（3）中的钴酸锂是按照如下工艺制备的：以钴盐和锂盐为原料，氧化铝、氧化镁中一种或两种为掺杂剂，按照 M：Co =（0-0.01）:1 的摩尔比混合均匀，然后将所得的配料进行加热。

[0015] 上述步骤（1）中制备的钴酸锂中位径 D50 在 12-25 微米之间，步骤（2）中制备的钴酸锂中位径 D50 在 5-8 微米之间，步骤（3）中制备的钴酸锂中位径 D50 在 1-4 微米之间，且

AMPEREX Ex. 1002
Page 1227

A、B、C 均为一次粒子或 B、C 为二次球、混合粒子。

[0016] 上述方法中，在 A 与 B、或 B、C、或 A、B、C 混合的过程中，加入氧化镁，二氧化钛，氟化锂，其中 Mg ： Co = (0-0.02) :1，Ti :Co= (0.001-0.02) :1，F :Co= (0-0.02) :1，以上比例均为物质的量之比 ；

本发明的有益效果是 :本发明提供的锂离子二次电池正极材料是在现有二次电池正极材料进行 Al、Mg 晶格(或体相)掺杂，该晶格(或体相)掺杂可以提高材料结构的稳定性，同时使用 Mg、Ti、F 进行表面掺杂或包覆，降低表面钴的丰度或降低钴酸锂与电解液的接触面积，减小材料中钴在电解液中的溶解，从而提高了锂离子电池的循环性能和安全性能。本发明的另一个优势是，通过不同粒度、不同重量的钴酸锂进行级配，可以有效的提供材料的空间利用率，提高正极材料的压实密度，进而使材料的体积能量密度大大提高。

[0017] 经实际测试，本发明材料中的钴酸锂 500 次常温、高温循环容量(常温 25℃、45℃或 60 度，3.0-4.2V) 保持率均大于 90% ；本发明材料中干粉压实密度可达 4.6g/cc，其对应的极片压实密度可达 4.3g/cc~4.4g/cc，甚至 4.5g/cc ；本发明材料中钴酸锂的高温存储膨胀小，85℃存储 48 小时，60℃存储 7 天厚度变化 5% 以内 ；本发明材料中钴酸锂的倍率性能好，1C/0.2C 可达 99%，2C/0.2C 可达 95% 以上 ；本发明材料中钴酸锂的安全性能好，可通过针刺、挤压、撞击、内或外部短路、1C/12V 过充、热滥用等测试。

具体实施方式

[0018] 实施例 1

一种锂离子二次电池正极材料掺杂、包覆型钴酸锂，其化学式为 ：

$Li_{1+x}Co_{(1-a-b-c)}Mg_aTi_bAl_cF_dO_{(2-d)}$，其中，$0 \leqslant a \leqslant 0.03$，$0.001 \leqslant b \leqslant 0.02$，$0 \leqslant c \leqslant 0.01$，$0 \leqslant d \leqslant 0.02$，$0 \leqslant x \leqslant 0.08$ ；具有层状结构。

[0019] 上述锂离子二次电池正极材料镁掺杂型钴酸锂的制备方法如下 :主要包括如下步骤 ：

(1)大颗粒钴酸锂制备 :按照锂、钴、镁原子比例为 1.06 :1.00 :0.005 的比例将钴源、锂源、镁源球磨混合，使用聚氨酯球进行球磨，球磨时间为 5 小时。所使用的钴源可以是碳酸钴、氧化钴等，锂源可以为氢氧化锂、碳酸锂等 ；

(2) 小颗粒钴酸锂制备 :按照锂、钴、镁原子比例为 1.005 :1.00 :0.005 的比例将钴源、锂源、镁源球磨混合，使用聚氨酯球进行球磨，球磨时间为 5 小时。所使用的钴源可以是碳酸钴、氧化钴等，锂源可以为氢氧化锂、碳酸锂等 ；

(3) 将混合后的原料置于焙烧炉中，在空气或氧气的气氛中进行焙烧，焙烧温度为 985℃，焙烧时间为 10 小时 ；

(4) 将焙烧后的产物先通过粗破碎后，再使用气流磨进行精破碎，粉末的平均粒度 D50 为 12μm ～ 16μm 和 5μm ～ 8μm ；

(5) 将钴酸锂粉末置于混料罐中，大小颗粒钴酸锂的重量比为 1 :1，加入微米级镁源、钛源、氟化锂，使用聚氨酯球进行球磨混合，混合时间为 3 小时 ；

(6) 通过筛分后的钴酸锂混合粉末置于推板隧道窑中，在空气气氛下进行焙烧，焙烧温度为 950℃，焙烧时间为 10 小时 ；

(7) 将焙烧后的产物先经粗破碎，然后使用气流磨进行精破碎，得到粒度 D50 为

AMPEREX Ex. 1002
Page 1228

8~12μm的产物，此时获得掺杂镁、钛、氟型钴酸锂，化学式为 $LiCo_{0.988}Ti_{0.002}Mg_{0.01}F_{0.002}O_{1.998}$，具有层状结构。

[0020] 实施例二

(1)大颗粒钴酸锂制备：按照锂、钴、铝原子比例为1.06：1.00：0.005的比例将钴源、锂源、铝源球磨混合，使用聚氨酯球进行球磨，球磨时间为5小时。所使用的钴源可以是碳酸钴、氧化钴等，锂源可以为氢氧化锂、碳酸锂等；

(2)小颗粒钴酸锂制备：按照锂、钴、铝原子比例为1.005：1.00：0.005的比例将钴源、锂源、铝源球磨混合，使用聚氨酯球进行球磨，球磨时间为5小时。所使用的钴源可以是碳酸钴、氧化钴等，锂源可以为氢氧化锂、碳酸锂等；

(3)将混合后的原料置于焙烧炉中，在空气或氧气的气氛中进行焙烧，焙烧温度为985℃，焙烧时间为10小时；

(4)将焙烧后的产物先通过粗破碎后，再使用气流磨进行精破碎，粉末的平均粒度D50为12μm～16μm和5μm～8μm；

(5)将钴酸锂粉末置于混料罐中，大小颗粒钴酸锂的重量比为1：1，加入微米级镁源、钛源、氟化锂，使用聚氨酯球进行球磨混合，混合时间为3小时；

(6)通过筛分后的钴酸锂混合粉末置于推板隧道窑中，在空气气氛下进行焙烧，焙烧温度为950℃，焙烧时间为10小时；

(7)将焙烧后的产物先经粗破碎，然后使用气流磨进行精破碎，得到粒度D50为8~12μm的产物，此时获得掺杂铝、镁、钛、氟型钴酸锂，化学式为 $LiCo_{0.983}Ti_{0.002}Mg_{0.01}Al_{0.005}F_{0.002}O_{1.998}$，具有层状结构。

[0021] 实施例三：

(1)大颗粒钴酸锂制备：按照锂、钴比例为1.08:1.00的比例将锂源、钴源球磨混合5小时；所使用的钴源可以是碳酸钴、氧化钴等，锂源可以为氢氧化锂、碳酸锂等；将混合后的原料置于焙烧炉中，在空气或氧气的气氛中进行焙烧，焙烧温度为995℃，焙烧时间为15小时；

(2)中颗粒钴酸锂制备：按照锂、钴的比例为1.03:1.00比例将将锂源、钴源球磨混合5小时；所使用的钴源可以是碳酸钴、氧化钴等，锂源可以为氢氧化锂、碳酸锂等；将混合后的原料置于焙烧炉中，在空气或氧气的气氛中进行焙烧，焙烧温度为985℃，焙烧时间为10小时；

(3)小颗粒钴酸锂制备：按照锂、钴的比例为1.005:1.00比例将将锂源、钴源在纳米超细搅拌磨中混合至粒度100~500纳米；所使用的钴源可以是碳酸钴、氧化钴等，锂源可以为氢氧化锂、碳酸锂等；将混合后的原料置于焙烧炉中，在空气或氧气的气氛中进行焙烧，焙烧温度为630℃，焙烧时间为6小时；

(4)将焙烧后的产物先通过粗破碎后，再使用气流磨进行精破碎，粉末的平均粒度D50为17μm~23μm、5μm~8μm和1μm ~4μm；

(5)三种物料按照1：1：1混合3小时，添加镁、钛、氟三种添加剂，比例为Mg：Co=0.01，Ti:Co=0.01，F:Co=0.002置于空气气氛的烧结炉中焙烧，焙烧温度为950℃，焙烧时间为10小时；

(6)将焙烧后的产物通过粗破碎、精破碎后，获得中位径为8~12微米钴酸锂粉末；

AMPEREX Ex. 1002
Page 1229

化学式为 $LiCo_{0.98}Mg_{0.01}Ti_{0.01}F_{0.002}O_{1.998}$，具有层状结构；

对比例一

（1）将碳酸锂、四氧化三钴、碱式碳酸镁按照锂、钴、镁的比例为 1.06:1.00:0.005 的比例球磨混合，混合时间为 5 小时；

（2）混合产物置于高温烧结炉中焙烧，焙烧温度为 985℃，焙烧时间 10 小时；

（3）将烧结得到的产物通过粗破碎、精破碎后得到中位径为 10~13 微米的钴酸锂粉末；

（4）向步骤（3）粉末中加入微米级碱式碳酸镁、二氧化钛、氟化锂球磨混合 3 小时；

（5）混合粉末置于高温烧结炉中烧结，在空气气氛下焙烧，焙烧温度为 950℃，烧结时间为 10 小时；

（6）将焙烧后的产物通过粗破碎、经破碎后，得到中位径为 10 ～ 13 微米的产物，此时获得镁、钛、氟掺杂型钴酸锂，化学式为 $LiCo_{0.98}Ti_{0.01}Mg_{0.01}F_{0.002}O_{1.998}$，具有层状结构。

[0022] 对比例二

（1）将碳酸锂、四氧化三钴、氧化铝按照锂、钴、铝的比例为 1.06:1.00:0.005 的比例球磨混合，混合时间为 5 小时；

（2）混合产物置于高温烧结炉中焙烧，焙烧温度为 985℃，焙烧时间 10 小时；

（3）将烧结得到的产物通过粉碎工艺后得到中位径为 10 ～ 13 微米的钴酸锂粉末；

（4）向步骤（3）粉末中加入微米级氧化镁、氧化钛、氟化锂，球磨混合 3 小时；

（5）混合粉末置于高温烧结炉中烧结，在空气气氛下焙烧看，焙烧温度为 950℃，烧结时间为 10 小时；

（6）将焙烧后的产物通过破碎后，得到中位径为 10 ～ 13 微米的产物，此时获得镁、铝、钛、氟掺杂型钴酸锂，化学式为 $LiCo_{0.983}Ti_{0.002}Mg_{0.01}Al_{0.005}F_{0.002}O_{1.998}$ 具有层状结构。

[0023] 本发明上述实施例的材料经 45℃循环测试和 3.0-4.35V 倍率性能测试，其结果均优于对比例的材料。

AMPEREX Ex. 1002
Page 1230

Espacenet

RSS family document

Family list: CN103022502 (A) — 2013-04-03

1 application(s) for: CN103022502 (A)

1. Compounding and coating method of anode material for lithium ion cell					
Inventor:	**Applicant:**	**CPC:**	**IPC:**	**Publication info:**	**Priority date:**
CHEN BOTAO TANG MIAO (+2)	TIANJIN B & M SCIENCE & TECHNOLOGY JOINT STOCK CO LTD	Y02E60/10	H01M4/48 H01M4/62	CN103022502 (A) 2013-04-03 Global Dossier	2012-12-19

Espacenet

Bibliographic data: CN103022502 (A) — 2013-04-03

Compounding and coating method of anode material for lithium ion cell

Inventor(s): CHEN BOTAO; TANG MIAO; CHENG XIAOKUN; XU NING ± (CHEN BOTAO, ; TANG MIAO, ; CHENG XIAOKUN, ; XU NING)

Applicant(s): TIANJIN B & M SCIENCE & TECHNOLOGY JOINT STOCK CO LTD ± (TIANJIN B&M SCIENCE AND TECHNOLOGY JOINT-STOCK CO., LTD)

Classification: - international: ***H01M4/48; H01M4/62***
- cooperative: Y02E60/10 (EP)

Application number: CN201210568755 20121219 Global Dossier

Priority number (s): CN201210568755 20121219

Abstract of CN103022502 (A)

The invention discloses a compounding and coating method of an anode material for a lithium ion cell. The compounding and coating method comprises the steps that fluorides of La, Al and Mg are coprecipitated on the surface of a lithium ion anode material in a liquid phase; and then, the anode material for the lithium ion cell cooperatively coated by La3+, Al3+, Mg2+ and F- is obtained by heat treatment. With the adoption of the coating treatment, the circulating property and the rate discharge property of the anode material under the charge cut-off voltage are improved; and the high-temperature circulating property of a spinel manganese oxide lithium material and the ordinary pressure circulating property of a nickelic anode material are improved.

(19)中华人民共和国国家知识产权局

(12)发明专利申请

(10)申请公布号 CN 103022502 A
(43)申请公布日 2013.04.03

(21)申请号 201210568755.2

(22)申请日 2012.12.19

(71)申请人 天津巴莫科技股份有限公司
地址 300384 天津市滨海新区华苑产业园区(环外)海泰大道8号

(72)发明人 陈勃涛 唐淼 程晓坤 徐宁

(74)专利代理机构 天津才智专利商标代理有限公司 12108
代理人 王颢

(51)Int.Cl.
H01M 4/62(2006.01)
H01M 4/48(2010.01)

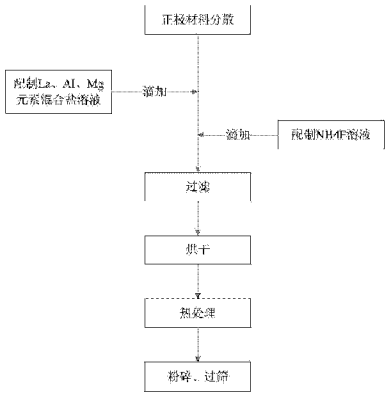
权利要求书 1 页 说明书 5 页 附图 1 页

(54)发明名称

锂离子电池正极材料的复合包覆方法

(57)摘要

本发明公开了一种锂离子电池正极材料的复合包覆的方法。该方法通过在液相中在锂离子正极材料表面共沉淀La、Al、Mg的氟化物，然后再通过热处理得到La^{3+}、Al^{3+}、Mg^{2+}及F^-协同包覆的锂离子电池正极材料。经过此包覆处理后，提高了正极材料在充电截止电压下的循环性能和倍率放电性能，同时也可提高尖晶石氧化锰锂材料的高温循环性能和高镍正极材料的常压循环性能。



CN 103022502 A

1. 一种锂离子电池正极材料的复合包覆方法，其特征在于包括以下步骤：

1）配制含镧、铝和镁中至少两种元素的可溶性盐溶液，使溶液中总金属离子浓度为0.5～2.5mol/L，且三种元素的摩尔比为 La:Al:Mg=0～10:1～5:0～1；

2）配制 NH_4F 溶液，控制溶液浓度为 1～2.5mol/L；

3）将正极材料粉末分散于水中，使固液质量比为 1:1～3，保持溶液温度为 20～60° C;

4）按照可溶性盐溶液中金属离子总质量与正极材料中金属离子总质量比例为 0.01～0.1:1 的比例称取步骤 1）的混合盐溶液，在搅拌状态下滴加到步骤 2）的正极材料浆液中，滴加完毕后搅拌 0.5～2h；

5）将 NH_4F 溶液滴加入步骤 3）得到的浆液中，同时强力搅拌，当浆液的 pH 值达到 8～9 时停止滴加氟化铵溶液；

6）搅拌 0.1～2h 后过滤出沉淀物；

7）将过滤出的沉淀物在 100～150° C 下烘干；

8）将烘干后的沉淀物放入焙烧炉中，在 600～1000° C 下，在空气气氛或氧气气氛下焙烧 4～10h；

9）将焙烧后的产物粉碎、过筛，得到 La^{3+}、Al^{3+}、Mg^{2+} 及 F^- 复合包覆的正极材料。

2. 根据权利要求 1 所述的复合包覆方法，其特征在于：步骤 1）中所述的可溶性盐为硝酸盐、硫酸盐、氯化物或醋酸盐中的一种。

3. 根据权利要求 1 所述的复合包覆方法，其特征在于：步骤 5）中所述的正极材料为 $LiCoO_2$、$LiNi_{1-x-y}Co_xMn_yO_2$、$LiNi_{1-m}Co_mO_2$ 或 $LiMn_2O_4$，其中 $0 < x, y, m < 0.5$。

AMPEREX Ex. 1002
Page 1234

锂离子电池正极材料的复合包覆方法

技术领域

[0001] 本发明涉及锂离子电池用正极材料，特别是涉及一种锂离子电池正极材料的复合包覆方法。

背景技术

[0002] 锂离子电池是目前最炙手可热的二次电池，被广泛用于各种电子设备当中，尤其是在移动电子消费品如笔记本电脑、数码相机和智能手机当中。随着移动电子消费品功能越来越强大，电池的耗电量大幅度增加，同时要求体积越来越小以提高其便携性，因此要求为其配套的锂离子电池能量密度不断提高。虽然锂离子电池自问世以来虽然经过了不断的技术发展，能量密度不断提高，但仍然无法满足电子产品的需求。为了解决能量密度问题，将锂离子电池充电截止电压由原来的 4.2V 提高至 4.3V、4.35V，可使相同体系的锂离子电池放电容量提升 10% ～ 15%，是提高锂离子电池能量密度的有效手段。但是在高充电截止电压下，普通型的正极材料如氧化钴锂材料的循环性能迅速恶化，这主要是由于在高电压下，正极材料具有很强的氧化性，与电解液发生反应而导致正极材料结构分解所致。因此，提高正极材料在高充电截止电压下的循环性能及其它电化学性能是锂离子电池正极材料技术发展的重要方向。

发明内容

[0003] 本发明要解决的技术问题是提供一种能有效地提高锂离子电池正极材料在高充电截止电压下的循环性能和倍率放电性能的复合包覆方法。

[0004] 为此，本发明的技术方案如下：

[0005] 一种锂离子电池正极材料的复合包覆方法，包括以下步骤：

[0006] 1）配制含镧、铝和镁中至少两种元素的可溶性盐溶液，使溶液中总金属离子浓度为 0.5 ～ 2.5mol/L，且三种元素的摩尔比为 La:Al:Mg=0 ～ 10 :1 ～ 5 :0 ～ 1；

[0007] 2）配制 NH_4F 溶液，控制溶液浓度为 1 ～ 2.5mol/L；

[0008] 3）将正极材料粉末分散于水中，使固液质量比为 1:1 ～ 3，保持溶液温度为 20 ～ 60° C;

[0009] 4）按照可溶性盐溶液中金属离子总质量与正极材料中金属离子总质量比例为 0.01 ～ 0.1:1 的比例称取步骤 1）的混合盐溶液，在搅拌状态下滴加到步骤 2）的正极材料浆液中，滴加完毕后搅拌 0.5 ～ 2h；

[0010] 5）将 NH_4F 溶液滴加入步骤 3）得到的浆液中，同时强力搅拌，当浆液的 pH 值达到 8 ～ 9 时停止滴加氟化铵溶液；

[0011] 6）搅拌 0.1 ～ 2h 后过滤出沉淀物；

[0012] 7）将过滤出的沉淀物在 100 ～ 150° C 下烘干；

[0013] 8）将烘干后的沉淀物放入焙烧炉中，在 600 ～ 1000° C 下，在空气气氛或氧气气氛下焙烧 4 ～ 10h；

AMPEREX Ex. 1002
Page 1235

[0014] 9）将焙烧后的产物粉碎、过筛，得到 La^{3+}、Al^{3+}、Mg^{2+} 及 F^- 复合包覆的正极材料。

[0015] 其中，步骤 1）中所述的可溶性盐为硝酸盐、硫酸盐、氯化物或醋酸盐中的一种；步骤 5）中所述的正极材料为 $LiCoO_2$、$LiNi_{1-x-y}Co_xMn_yO_2$、$LiNi_{1-m}Co_mO_2$ 或 $LiMn_2O_4$，其中 $0 < x, y, m < 0.5$。

[0016] 本发明采用阴离子 F^- 与多种阳离子如 Mg^{2+}、Al^{3+} 及稀土元素 La^{3+} 进行复合掺杂，有效地提高了正极材料在高充电截止电压下的循环性能和倍率放电性能。阴离子 F^- 部分替代正极材料中的氧，可抑制在高电位下氧的析出，提高材料结构的稳定性能，同时多种阳离子如 Mg^{2+}、Al^{3+} 和 La^{3+} 元素的表面掺杂与包覆隔绝了正极材料表面结构与电解液的接触，抑制了电解液与正极材料之间的化学反应，稳定了材料的表面结构，因此有效提高了正极材料在高电压下的循环性能和倍率放电性能。

附图说明

[0017] 图 1 是本发明的方法的工艺流程。

具体实施方式

[0018] 参见图 1，本发明的方法包括以下步骤：

[0019] 1）配制含镧、铝和镁中至少两种元素的可溶性盐溶液，使溶液中总金属离子浓度为 0.5 ～ 2.5mol/L，且三种元素的摩尔比为 La:Al:Mg=0 ～ 10 :1 ～ 5 :0 ～ 1；

[0020] 2）配制 NH_4F 溶液，控制溶液浓度为 1 ～ 2.5mol/L；

[0021] 3）将正极材料粉末分散于水中，使固液质量比为 1:1 ～ 3，保持溶液温度为 20 ～ 60° C;

[0022] 4）按照可溶性盐溶液中金属离子总质量与正极材料中金属离子总质量比例为 0.01 ～ 0.1:1 的比例称取步骤 1）的混合盐溶液，在搅拌状态下滴加到步骤 2）的正极材料浆液中，滴加完毕后搅拌 0.5 ～ 2h；

[0023] 5）将 NH_4F 溶液滴加入步骤 3）得到的浆液中，同时强力搅拌，当浆液的 pH 值达到 8 ～ 9 时停止滴加氟化铵溶液；

[0024] 6）搅拌 0.1 ～ 2h 后过滤出沉淀物；

[0025] 7）将过滤出的沉淀物在 100 ～ 150° C 下烘干；

[0026] 8）将烘干后的沉淀物放入焙烧炉中，在 600 ～ 1000° C 下，在空气气氛或氧气气氛下焙烧 4 ～ 10h；

[0027] 9）将焙烧后的产物粉碎、过筛，得到 La^{3+}、Al^{3+}、Mg^{2+} 及 F^- 复合包覆的正极材料。

[0028] 下面结合具体实施例对本发明的方法作进一步说明。

[0029] 实施例 1

[0030] 按照元素的摩尔比 La:Al:Mg=1:1:1 的比例配制硝酸镧、硝酸铝和硝酸镁混合溶液 570ml，La^{3+}、Al^{3+}、Mg^{2+} 的总浓度为 0.5mol/L；配制浓度为 1mol/L 的 NH_4F 溶液。

[0031] 将 3000g 氧化钴锂正极材料投入 5000ml 去离子水中，采用电动搅拌器进行搅拌，保持溶液温度为 20° C。在搅拌过程中将 570ml 硝酸盐溶液滴加入氧化钴锂材料浆料中，滴加完毕后继续搅拌 0.5h。

[0032] 滴加 NH_4F 溶液。用精密 pH 计测定溶液 pH 值，当 pH 值达到 8 ～ 9 时停止滴加 NH_4F

AMPEREX Ex. 1002
Page 1236

溶液，继续搅拌 0.5h。

[0033] 将浆料过滤，过滤物在 100° C 下烘干 10h。烘干后得到的粉末放入马弗炉中在 600° C 下热处理 10h。热处理后的氧化钴锂材料粗料经过粉碎、过筛得到 La、Al、Mg 包覆的氧化钴锂材料。

[0034] 该材料装配成 2032 扣式电池，在 3.0 ～ 4.35V 电压窗口下以 0.1C 倍率电流进行充放电测试，容量达到 167mAh/g。装配成 053048 全电池，在 3.0 ～ 4.35V 电压窗口内以 1C 倍率电流进行充放电，400 周期后放电容量是第 1 周期放电容量的 83%，2C/1C、3C/1C 放电比例分别为 100% 和 98.5%，电池 85° C 下存储 4h 后鼓胀率为 6% ；

[0035] 实施例 2

[0036] 按照摩尔比为 La:Al:Mg=0.5:1:0.5 的比例配制硝酸镧、硝酸铝和硝酸镁混合溶液 1100ml，La、Al、Mg 总浓度为 1mol/L ；配制浓度为 2mol/L 的 NH_4F 溶液。

[0037] 将 5000g 氧化钴锂正极材料投入 15000ml 去离子水中，保持溶液温度为 60℃，采用电动搅拌器进行搅拌。在搅拌过程中将 1100ml 硝酸盐溶液滴加入氧化钴锂材料浆料中，滴加完毕后继续搅拌 0.5h。

[0038] 滴加 NH_4F 溶液。用精密 pH 计测定溶液 pH 值，当 pH 值达到 8 ～ 9 时停止滴加 NH_4F 溶液，继续搅拌 0.5h。

[0039] 将浆料过滤，过滤物在 110° C 下烘干 10h。烘干后得到的粉末放入马弗炉中在 1000° C 下热处理 4h。热处理后的氧化钴锂材料粗料经过粉碎、过筛得到 La、Al、Mg 包覆的氧化钴锂材料。

[0040] 该材料在 3.0 ～ 4.35V 电压窗口下以 0.1C 倍率电流进行充放电测试，容量达到 167mAh/g。装配成 053048 电池，在 3.0 ～ 4.35V 电压窗口内以 1C 倍率电流进行充放电，400 周期后放电容量是第 1 周期放电容量的 85%，2C/1C、3C/1C 放电比例分别为 100% 和 98.3% ；电池 85° C 下存储 4h 后鼓胀率为 8%。

[0041] 实施例 3

[0042] 按照摩尔比为 La:Al:Mg=2:1:1 的比例配制硝酸镧、硝酸铝和硝酸镁混合溶液 2400ml，La、Al、Mg 总浓度为 2.5mol/L ；配制浓度为 2.5mol/L 的 NH_4F 溶液。

[0043] 将 20kg $LiNi_{1/3}Co_{1/3}Mn_{1/3}O_2$ 正极材料投入 40L 去离子水中，保持溶液温度为 30℃，采用电动搅拌器进行搅拌。在搅拌过程中将 2400ml 硝酸盐溶液滴加入 $LiNi_{1/3}Co_{1/3}Mn_{1/3}O_2$ 材料浆料中，滴加完毕后继续搅拌 1h。

[0044] 滴加 NH_4F 溶液。用精密 pH 计测定溶液 pH 值，当 pH 值达到 8 ～ 9 时停止滴加 NH_4F 溶液，继续搅拌 1h。

[0045] 将浆料过滤，过滤物在 150° C 下烘干 10h。烘干后得到的粉末放入马弗炉中在 900° C 下热处理 8h。热处理后的 $LiNi_{1/3}Co_{1/3}Mn_{1/3}O_2$ 材料粗料经过粉碎、过筛得到 La、Al、Mg 包覆的氧化钴锂材料。该材料在 3.0 ～ 4.35V 电压窗口下以 0.1C 倍率电流进行充放电测试，放电容量达到 170mAh/g。

[0046] 将上述材料装配成 053048 电池，在 3.0 ～ 4.35V 电压窗口内以 1C 倍率电流进行充放电，400 周期后放电容量是第 1 周期放电容量的比例为 88%，2C/1C、3C/1C 放电比例分别为 100% 和 99% ；电池 85° C 下存储 4h 后鼓胀率为 10%。

[0047] 实施例 4

AMPEREX Ex. 1002
Page 1237

[0048] 按照摩尔比为 La:Al=1:2 的比例配制硝酸镧和硝酸铝混合溶液 7800ml，La、Al、Mg 总浓度为 1.5mol/L；配制浓度为 2mol/L 的 NH_4F 溶液。

[0049] 将 20kg $LiNi_{1/3}Co_{1/3}Mn_{1/3}O_2$ 正极材料投入 20L 去离子水中，采用电动搅拌器进行搅拌，保持溶液温度为 40° C。在搅拌过程中将 7800ml 硝酸盐溶液滴加入三元材料 $LiNi_{1/3}Co_{1/3}Mn_{1/3}O_2$ 材料浆料中，滴加完毕后继续搅拌 0.5h。

[0050] 滴加 NH_4F 溶液。用精密 pH 计测定溶液 pH 值，当 pH 值达到 8 ～ 9 时停止滴加 NH_4F 溶液，继续搅拌 0.5h。

[0051] 将浆料过滤，过滤物在 120° C 下烘干 10h。烘干后得到的粉末放入马弗炉中在 600° C 下热处理 10h。热处理后的氧化钴锂材料粗料经过粉碎、过筛得到 La、Al、Mg 包覆的氧化钴锂材料。

[0052] 该材料在 3.0 ～ 4.35V 电压窗口下以 0.1C 倍率电流进行充放电测试，容量达到 170mAh/g。装配成 053048 电池，在 3.0 ～ 4.35V 电压窗口内以 1C 倍率电流进行充放电，400 周期后放电容量是第 1 周期放电容量的比例为 83%，2C/1C、3C/1C 放电比例分别为 100% 和 97%；电池 85° C 下存储 4h 后鼓胀率为 16%。

[0053] 实施例 5

[0054] 按照摩尔比为 Al:Mg=1:1 的比例配制硝酸铝和硝酸镁混合溶液 1160ml，Al、Mg 总浓度为 1mol/L，配制浓度为 1mol/L 的 NH_4F 溶液。

[0055] 将 1000g $LiNi_{0.8}Co_{0.2}O_2$ 正极材料投入 1000ml 去离子水中，采用电动搅拌器进行搅拌，保持溶液温度为 40° C。在搅拌过程中将 1160ml 硝酸盐溶液滴加入氧化钴锂材料浆料中，滴加完毕后继续搅拌 0.5h。

[0056] 滴加 NH_4F 溶液。用精密 pH 计测定溶液 pH 值，当 pH 值达到 8 ～ 9 时停止滴加 NH_4F 溶液，继续搅拌 0.5h。

[0057] 将浆料过滤，过滤物在 130° C 下烘干 10h。烘干后得到的粉末放入管式炉中在 800° C 下氧气气氛中热处理 6h。热处理后的 $LiNi_{0.8}Co_{0.2}O_2$ 材料粗料经过粉碎、过筛得到 Al、Mg、F 包覆的 $LiNi_{0.8}Co_{0.2}O_2$ 材料。

[0058] 所得材料在 3.0 ～ 4.3V 电压窗口下以 0.1C 倍率电流进行充放电测试，容量达到 181mAh/g。装配成 053048 电池，以 1C 倍率电流进行充放电，300 周期后放电容量是第 1 周期放电容量的比例为 84%，2C/1C、3C/1C 放电比例分别为 99% 和 96%。

[0059] 实施例 6

[0060] 按照摩尔比为 La:Al:Mg=10:5:1 的比例配制硝酸镧、硝酸铝和硝酸镁混合溶液 125ml，La、Al、Mg 总浓度为 0.5mol/L，配制浓度为 1.5mol/L 的 NH_4F 溶液。

[0061] 将 1000g $LiMn_2O_4$ 正极材料投入 2000ml 去离子水中，采用电动搅拌器进行搅拌，保持溶液温度为 40° C。在搅拌过程中将 125ml 硝酸盐溶液滴加入氧化钴锂材料浆料中，滴加完毕后继续搅拌 0.5h。

[0062] 滴加 NH_4F 溶液。用精密 pH 计测定溶液 pH 值，当 pH 值达到 8 ～ 9 时停止滴加 NH_4F 溶液，继续搅拌 0.5h。

[0063] 将浆料过滤，过滤物在 150° C 下烘干 6h。烘干后得到的粉末放入管式炉中在 800° C 下氧气气氛中热处理 6h。热处理后的 $LiNi_{0.8}Co_{0.2}O_2$ 材料粗料经过粉碎、过筛得到 Al、Mg、F 包覆的 $LiNi_{0.8}Co_{0.2}O_2$ 材料。

AMPEREX Ex. 1002
Page 1238

[0064] 该材料在 3.0 ～ 4.3V 电压窗口下以 0.1C 倍率电流进行充放电测试，容量达到 101mAh/g。装配成 053048 电池，以 1C 倍率电流进行充放电，在 45° C 下 400 周期后放电容量是第 1 周期放电容量的 83%，3C/1C、5C/1C 放电容量比值分别为 99% 和 98%。

[0065] 比较例 1

[0066] 氧化钴锂材料装配成 2032 扣式电池在 3.0 ～ 4.35V 电压窗口内，以 0.1C 倍率电流进行充放电测试，放电容量为 166mAh/g。装配成 053048 电池，在 3.0 ～ 4.35V 电压窗口内以 1C 倍率电流进行充放电，200 周期后放电容量是第 1 周期放电容量的 71%，2C/1C 和 3C/1C 放电容量比值分别为 99%，96%。

[0067] 比较例 2

[0068] 三元材料 $LiNi_{1/3}Co_{1/3}Mn_{1/3}O_2$ 装配成 2032 扣式电池在 3.0 ～ 4.35V 电压窗口内，以 0.1C 倍率电流进行充放电测试，放电容量为 169mAh/g。装配成 053048 电池，在 3.0 ～ 4.35V 电压窗口内以 1C 倍率电流进行充放电，400 周期后放电容量是第 1 周期放电容量的 69%，2C/1C 和 3C/1C 放电容量比值分别为 99% 和 97%。

[0069] 比较例 3

[0070] 镍钴酸锂正极材料 $LiNi_{0.8}Co_{0.2}O_2$ 装配成 2032 扣式电池在 3.0 ～ 4.3V 电压窗口内，以 0.1C 倍率电流进行充放电测试，放电容量为 192mAh/g。装配成 053048 电池，在 3.0 ～ 4.2V 电压窗口内以 1C 倍率电流进行充放电，200 周期后放电容量是第 1 周期放电容量的 70%，2C/1C 和 3C/1C 放电容量比值分别为 97% 和 95%。

[0071] 比较例 4

[0072] 尖晶石氧化锰锂正极材料 $LiMn_2O_4$ 装配成 2032 扣式电池在 3.0 ～ 4.3V 电压窗口内，以 0.1C 倍率电流进行充放电测试，放电容量为 110mAh/g。装配成 053048 电池，在 3.0 ～ 4.2V 电压窗口内在 45° C 环境温度下以 1C 倍率电流进行充放电，300 周期后放电容量是第 1 周期放电容量的 60%，3C/1C 和 5C/1C 放电容量比值分别为 99% 和 97%。

[0073] 从上面的实施例和对比例可知，经本发明的方法处理的氧化钴锂材料，在 3.0 ～ 4.35V 电压范围内以 1C 的倍率充电放电，经过 400 次循环后，材料的容量保持率超过 85%，而原始材料在相同的测试条件下循环 200 周期容量保持率就下降到 71%；经处理的 $LiNi_{1/3}Co_{1/3}Mn_{1/3}O_2$ 材料，在 4.35V 的充电截止电压下，以 1C 的倍率充电放电，经过 400 次循环后，材料的容量保持率超过 88%，达到原始材料在 4.2V 的充电截止电压下的容量保持率，同时电池在 85° C 存储 4h 后鼓胀率降低至 10% 以下；经过包覆处理的 $LiNi_{0.8}Co_{0.2}O_2$ 常压循环性能得到明显提高，容量保持从 200 周期 70% 提高到 300 周期 84%；尖晶石氧化锰锂材料经包覆处理后容量有所下降，但高温循环性能得到改善，如 45° C 下 300 周期容量保持率从 60% 提高到 400 次的 83%。

AMPEREX Ex. 1002
Page 1239

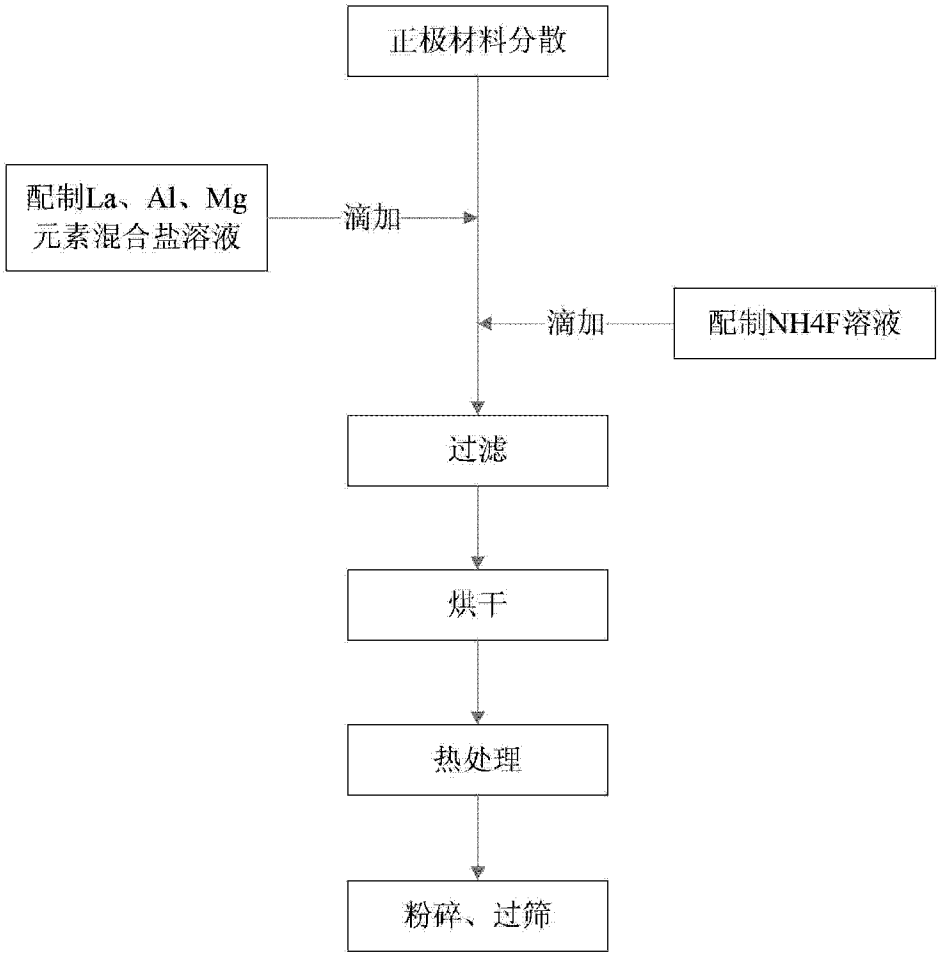


图 1

AMPEREX Ex. 1002
Page 1240

Espacenet

RSS family document

Family list: CN106099098 (A) — 2016-11-09

1 application(s) for: CN106099098 (A)

1. High-voltage cathode material Li delta Co(1-x)MgxO2@AlF3 of lithium ion battery and preparation method of high-voltage cathode material

Inventor:	Applicant:	CPC:	IPC:	Publication info:	Priority date:
LIU XINGQUAN TAN MING (+4)	UNIV ELECTRONIC SCIENCE & TECH CHINA	H01M4/505 H01M4/628 Y02E60/10	H01M4/505 H01M4/62	CN106099098 (A) 2016-11-09 CN106099098 (B) 2020-06-16 Global Dossier	2016-07-07

Espacenet

Bibliographic data: CN106099098 (A) — 2016-11-09

High-voltage cathode material Li delta Co(1-x)MgxO2@AlF3 of lithium ion battery and preparation method of high-voltage cathode material

Inventor(s): LIU XINGQUAN; TAN MING; LIU SHANSHAN; CAI YU; WANG ZHENWEI; ZHAO HONGYUAN ± (刘兴泉, ; 谭铭, ; 刘珊珊, ; 蔡宇, ; 王震伟, ; 赵红远)

Applicant(s): UNIV ELECTRONIC SCIENCE & TECH CHINA ± (电子科技大学)

Classification: - international: ***H01M4/505; H01M4/62***
- cooperative: **H01M4/505 (CN)**; **H01M4/628 (CN)**; Y02E60/10 (EP)

Application number: CN201610531794 20160707 Global Dossier

Priority number (s): CN201610531794 20160707

Also published as: CN106099098 (B)

Abstract of CN106099098 (A)

The invention belongs to the field of lithium ion batteries, and provides a cathode material Li delta Co(1-x)MgxO2@AlF3 of a lithium ion battery and a preparation method of the cathode material. According to the cathode material Li delta Co(1-x) MgxO2@AlF3, delta is larger than or equal to 1 and smaller than or equal to 1.05, x is larger than 0 and smaller than or equal to 0.05, and the defect of poor electrochemical performance of laminar LiCoO2 under high potential is overcome. The bulk-phase doping modification and surface coating combined laminar cathode material Li delta Co (1-x)MgxO2@AlF3 has higher specific discharge capacity and very stable circulation performance; at the room temperature, at 0.5 C rate and within the charge-discharge voltage range of 2.75-4.4 V (vs.Li/Li<+>), the first specific discharge capacity can reach 187.6 mAh/g, the 3.8V platform capacity approaches 100%, the capacity can reach 180 mAh/g after 30 times of circulation, and the capacity retention ratio is 96%. Besides, the provided material preparation method adopts a simple preparation process, the preparation cost is low, and large-scale industrial production is easy to realize.

(19)中华人民共和国国家知识产权局

(12)发明专利申请

(10)申请公布号 CN 106099098 A
(43)申请公布日 2016.11.09

(21)申请号 201610531794.3

(22)申请日 2016.07.07

(71)申请人 电子科技大学
地址 611731 四川省成都市高新区(西区)西源大道2006号

(72)发明人 刘兴泉 谭铭 刘珊珊 蔡宇 王震伟 赵红远

(74)专利代理机构 电子科技大学专利中心 51203
代理人 甘茂

(51)Int.Cl.
H01M 4/505(2010.01)
H01M 4/62(2006.01)

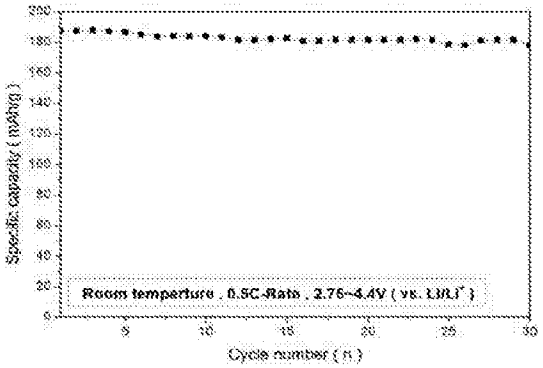
权利要求书1页 说明书5页 附图3页

(54)发明名称

一种锂离子电池高电压正极材料Li δ Co1-xMgxO2@AlF3及其制备方法

(57)摘要

本发明属于锂离子电池领域,提供锂离子电池正极材料Li δ Co1-xMgxO2@AlF3及其制备方法,其中1≤δ≤1.05,0<x≤0.05;用以解决层状LiCoO2在高电位下电化学性能差的缺点。本发明体相掺杂改性与表面包覆相结合的层状正极材料Li δ Co1-xMgxO2@AlF3具有较高的放电比容量和非常稳定的循环性能;在室温和0.5C倍率下,2.75～4.4V(vs.Li/Li+)的充放电电压范围内,首次放电比容量可高达187.6mAh/g,3.8V平台容量接近100%,循环30次以后仍然可达到180mAh/g,容量保持率为96%。同时,本发明提供该材料的制备方法,制备工艺简单、制备成本低,易于实现大规模工业化生产。



CN 106099098 A

1.一种锂离子电池高电压正极材料$Li_{\delta}Co_{1-x}Mg_xO_2@AlF_3$，其特征在于，所述锂离子电池正极材料的分子表达式为$Li_{\delta}Co_{1-x}Mg_xO_2@AlF_3$，其中$1\leqslant\delta\leqslant1.05$，$0<x\leqslant0.05$。

2.按权利要求1所述锂离子电池高电压正极材料$Li_{\delta}Co_{1-x}Mg_xO_2@AlF_3$，其特征在于，所述$AlF_3$的包覆量为1％～5％。

3.按权利要求1所述锂离子电池高电压正极材料$Li_{\delta}Co_{1-x}Mg_xO_2@AlF_3$的制备方法，其特征在于，包括以下步骤：

步骤1.将锂源原料、钴源原料、镁源原料按摩尔比为Li:Co:Mg＝δ:(1-x):x称量后，加入适量无水乙醇混合，得到混合液A，其中，$1\leqslant\delta\leqslant1.05$，$0<x\leqslant0.05$；

步骤2.将混合液A以及适量的球磨珠置于球磨罐中，球磨8～16小时，球磨完成得到混合液B；

步骤3.将混合液B在105℃下干燥10～24小时，之后研磨，得到混合粉末；

步骤4.将步骤3所得混合粉末置于马弗炉中预烧，预烧温度为650～850℃，预烧时间为6～12小时，预烧完成后研磨，得到中间产物；

步骤5.将步骤4所得中间产物置于马弗炉中烧结，烧结温度850～1100℃，烧结时间为8～24小时，烧结完成后研磨，即可制得层状结构锂离子电池正极材料$Li_{\delta}Co_{1-x}Mg_xO_2$；

步骤6.以硝酸铝为铝源，以氟化锂为氟源，采用溶胶凝胶法在粉体产物表面包覆AlF_3，即制备得锂离子电池高电压正极材料$Li_{\delta}Co_{1-x}Mg_xO_2@AlF_3$。

4.按权利要求3所述锂离子电池高电压正极材料$Li_{\delta}Co_{1-x}Mg_xO_2@AlF_3$的制备方法，其特征在于，步骤6中所述$AlF_3$的包覆量为1％～5％。

5.按权利要求3所述锂离子电池高电压正极材料$Li_{\delta}Co_{1-x}Mg_xO_2@AlF_3$的制备方法，其特征在于，步骤1中所述钴源原料为硫酸钴、硝酸钴、碳酸钴、草酸钴以及钴的氢氧化物和氧化物中的至少一种。

6.按权利要求3所述锂离子电池高电压正极材料$Li_{\delta}Co_{1-x}Mg_xO_2@AlF_3$的制备方法，其特征在于，步骤1中所述镁源原料为乙酸镁、碳酸镁、硝酸镁、草酸镁以及镁的氢氧化物和氧化物中的至少一种。

7.按权利要求3所述锂离子电池高电压正极材料$Li_{\delta}Co_{1-x}Mg_xO_2@AlF_3$的制备方法，其特征在于，步骤1中所述锂源原料为醋酸锂、碳酸锂、硝酸锂、柠檬酸锂、草酸锂和氢氧化锂中的至少一种。

AMPEREX Ex. 1002
Page 1244

一种锂离子电池高电压正极材料$Li_\delta Co_{1-x}Mg_xO_2@AlF_3$及其制备方法

技术领域

[0001] 本发明属于锂离子电池领域，涉及锂离子电池正极材料及其制备方法，具体为锂离子电池正极材料$Li_\delta Co_{1-x}Mg_xO_2@AlF_3$及其制备方法，其中$1\leqslant\delta\leqslant1.05$，$0<x\leqslant0.05$。

背景技术

[0002] 锂离子电池因为高电位、高能量密度、长循环寿命、无记忆性等特点，已经广泛应用于手机、笔记本电脑、数码相机等便携式电子设备中；最近几年以来，锂离子电池在电动汽车上的应用也逐渐成熟。目前研究中的锂离子电池正极材料的体系很多，但是大规模工业化生产的商品主要还是钴酸锂($LiCoO_2$)正极材料；而$LiMn_2O_4$较$LiCoO_2$来说，其价格更低、材料热稳定性更好，但是$LiMn_2O_4$的比容量和能量密度较低；$LiFePO_4$材料具有合成资源丰富、成本低、循环性能好、安全性高等诸多优点，但是除了低温性能不佳之外，还有其体积能量密度较低；三元复合材料$LiNi_{1/3}Co_{1/3}Mn_{1/3}O_2$与$LiCoO_2$具有相同的层状结构，它具有常规$LiCoO_2$的高能量密度与良好的循环稳定性等优点，而且成本较低，但是合成较为不易。

[0003] 虽然$LiCoO_2$的理论容量高达274mAh/g，但是其实际容量往往限定在140mAh/g或者更低(充电范围3.0～4.2V，vs.Li/Li^+)，到目前为止，研究者们主要专注的是通过提高其充电电压上限来实现更高的容量。然而，提高电压上限的方法很可能导致材料结构从六方晶系到单斜晶系的不可逆的转变，而且高电位下正极材料与电解液的表面处更容易发生副反应，这些都将破坏$LiCoO_2$材料结构的稳定性，使得其循环性能降低，同时也影响了其容量。为了克服$LiCoO_2$在高电位充放电时遇到的这些困难，提高其在高电位的电化学性能，常见的解决方法有两种：其一是金属阳离子的掺杂，其二是对$LiCoO_2$正极材料表面进行修饰。第一种方法中使用的掺杂元素一般是Al、Mg、Ti、Sr、Zr、V等；金属阳离子的掺杂能够提高材料的导电性，抑制材料的相变，提高材料在高电位下的稳定性，从而实现更好的电化学性能；第二种方法一般是对正极材料表面实现一层很薄的包覆，包覆层从几个纳米到几十个纳米不等，包覆的材料可以选择金属氧化物、金属硅酸盐以及金属氟化物，这些包覆层在维持锂离子通道的同时，使得正极材料不直接和液态电解质接触，抑制了电解质溶液与正极材料的副反应，提高了正极材料的循环稳定性。但是，目前采用上述两种方法提高$LiCoO_2$在高电位的电化学性能的实际效果并不理想，$LiCoO_2$在高电位下的电化学性能有待进一步提高。

发明内容

[0004] 本发明的目的在于针对锂离子电池高电压正极材料层状$LiCoO_2$在高电位下电化学性能差的缺点，提供一种体相掺杂改性与表面包覆相结合的层状正极材料$Li_\delta Co_{1-x}Mg_xO_2@AlF_3$及其制备方法，其中$1\leqslant\delta\leqslant1.05$，$0<x\leqslant0.05$。该锂离子电池正极材料在2.75～4.4V(vs.Li/Li^+)的充放电电压范围内，具有较高的放电比容量和非常稳定的循环性能。其制备方法采用高温固相法制备母体，制备的产品结晶度高、颗粒分布均匀；采用溶胶凝胶法对母体进行表面AlF_3包覆修饰。经过体相掺杂和表面包覆修饰的$Li_\delta Co_{1-x}Mg_xO_2@AlF_3$材料，能量密

AMPEREX Ex. 1002
Page 1245

度高，比普通钴酸锂提高30～50％，电化学性能优良，且制造成本低，工艺设备简单。

[0005] 本发明的技术方案为：一种锂离子电池高电压正极材料$Li_\delta Co_{1-x}Mg_xO_2@AlF_3$，其特征在于，所述锂离子电池正极材料的分子表达式为$Li_\delta Co_{1-x}Mg_xO_2@AlF_3$，其中$1\leqslant\delta\leqslant1.05$，$0<x\leqslant0.05$。

[0006] 进一步的，所述锂离子电池高电压正极材料$Li_\delta Co_{1-x}Mg_xO_2@AlF_3$中$AlF_3$的包覆量为1％～5％。

[0007] 上述锂离子电池高电压正极材料$Li_\delta Co_{1-x}Mg_xO_2@AlF_3$的制备方法，其特征在于，包括以下步骤：

[0008] 步骤1.将锂源原料、钴源原料、镁源原料按摩尔比为Li:Co:Mg＝δ:(1-x):x称量后，加入适量无水乙醇混合，得到混合液A，其中，$1\leqslant\delta\leqslant1.05$，$0<x\leqslant0.05$；

[0009] 步骤2.将混合液A以及适量的球磨珠置于球磨罐中，球磨8～16小时，球磨完成得到混合液B；

[0010] 步骤3.将混合液B在105℃下干燥10～24小时，之后研磨，得到混合粉末；

[0011] 步骤4.将步骤3所得混合粉末置于马弗炉中预烧，预烧温度为650～850℃，预烧时间为6～12小时，预烧完成后研磨，得到中间产物；

[0012] 步骤5.将步骤4所得中间产物置于马弗炉中烧结，烧结温度850～1100℃，烧结时间为8～24小时，烧结完成后研磨，即可制得层状结构锂离子电池正极材料$Li_\delta Co_{1-x}Mg_xO_2$；

[0013] 步骤6.以硝酸铝为铝源，以氟化锂为氟源，采用溶胶凝胶法在粉体产物表面包覆AlF_3，即制备得锂离子电池高电压正极材料$Li_\delta Co_{1-x}Mg_xO_2@AlF_3$。

[0014] 在步骤1中，所述钴源原料为硫酸钴、硝酸钴、碳酸钴、草酸钴以及钴的氢氧化物和氧化物(四氧化三钴与三氧化二钴)中的至少一种。

[0015] 在步骤1中，所述镁源原料为乙酸镁、碳酸镁、硝酸镁、草酸镁以及镁的氢氧化物和氧化物中的至少一种。

[0016] 在步骤1中，所述锂源原料为醋酸锂、碳酸锂、硝酸锂、柠檬酸锂、草酸锂和氢氧化锂中的至少一种。

[0017] 在步骤6中，所述AlF_3的包覆量为1％～5％。

[0018] 本发明通过采用二价金属镁元素取代正极材料中的三价钴元素得到锂离子电池正极材料$Li_\delta Co_{1-x}Mg_xO_2$；二价金属镁元素的引入有如下好处：(1)镁离子可以提高正极材料的导电性，改善其大电流充放电性能；(2)镁离子取代钴离子可以抑制正极材料在充放电时的相变，使得正极材料的稳定性得到增强；(3)由于镁离子的化合价低于钴离子，使得在层状的正极材料中的钴层对氧层的静电作用降低，氧层与氧层之间的距离变大，材料的晶格常数c增加，使锂离子的通道变宽，锂离子能够更好地嵌入与脱嵌。采用AlF_3包覆的$Li_\delta Co_{1-x}Mg_xO_2$表面，能够使正极材料$Li_\delta Co_{1-x}Mg_xO_2$不直接和液态电解质接触，抑制了电解质溶液与正极材料的副反应，提高了正极材料的循环稳定性；由于AlF_3具有较好的离子导电性，进一步改善了$Li_\delta Co_{1-x}Mg_xO_2$的导电性能。

[0019] 本发明采用高温固相法制备锂离子电池正极材料$Li_\delta Co_{1-x}Mg_xO_2$母体，其中$1\leqslant\delta\leqslant1.05$，$0<x\leqslant0.05$。与共沉淀法和溶胶凝胶法相比，高温固相法的工艺更为简单、设备成本低、易于实现大规模生产。

[0020] 综上所述，本发明具有如下优点：

AMPEREX Ex. 1002
Page 1246

[0021] 1、本发明采用高温固相法制备母体，通过原料与分散剂的混磨实现原料的混合以及粒径的控制。而且采用预烧-研磨-终烧的两段烧结方式实现母体材料的均匀制备。

[0022] 2、本发明制备的层状锂离子电池正极材料$Li_8Co_{1-x}Mg_xO_2$，通过少量的二价镁离子掺杂来改善材料的结构和提高电化学性能。

[0023] 3、本发明采用溶胶凝胶法对母体材料进行表面包覆修饰，采用AlF_3包覆的$Li_8Co_{1-x}Mg_xO_2$表面，能够使正极材料$Li_8Co_{1-x}Mg_xO_2$不直接和液态电解质接触，不仅抑制了电解质溶液与正极材料的副反应，提高了正极材料的循环稳定性；而且由于AlF_3具有较好的离子导电性，进一步改善了$Li_8Co_{1-x}Mg_xO_2$的导电性能。

[0024] 4、本发明制备的层状锂离子电池正极材料$Li_8Co_{1-x}Mg_xO_2@AlF_3$具有极高的放电比容量，以及优异的循环性能；在室温0.5C的倍率下，2.75～4.4V(vs.Li/Li^+)的充放电电压范围内，该层状锂离子电池正极材料的首次放电比容量可高达187.6mAh/g，3.8V平台容量接近100％，循环30次以后仍然可达到180mAh/g，容量保持率为96％。

[0025] 5、本发明的制作方法中，工艺步骤与设备简便、成本低廉，易于实现大规模工业化生产。

附图说明

[0026] 图1为本发明制备锂离子电池正极材料母体$Li_8Co_{1-x}Mg_xO_2$的工艺流程图。

[0027] 图2为实施例1制备锂离子电池正极材料母体$Li_{1.05}Co_{0.97}Mg_{0.03}O_2$的XRD图。

[0028] 图3为实施例1制备锂离子电池正极材料母体$Li_{1.05}Co_{0.97}Mg_{0.03}O_2$的SEM图。

[0029] 图4为实施例1制备锂离子电池正极材料$Li_{1.05}Co_{0.97}Mg_{0.03}O_2@AlF_3$的0.5C倍率下的首次充放电曲线图。

[0030] 图5为实施例1制备锂离子电池正极材料$Li_{1.05}Co_{0.97}Mg_{0.03}O_2@AlF_3$在0.5C倍率下的循环30次性能曲线图。

[0031] 图6为实施例1制备锂离子电池正极材料$Li_{1.05}Co_{0.97}Mg_{0.03}O_2@AlF_3$在0.5C倍率下的循环50次性能曲线图。

具体实施方式

[0032] 下面结合具体实施例与附图对本发明做进一步的详细说明。

[0033] 实施例1

[0034] 将0.0525mol(3.8792g)的碳酸锂、0.0323mol(7.7858g)的四氧化三钴、0.0030mol(0.7692g)的六水硝酸镁以及15mL的无水乙醇称量倒入球磨罐中，得到混合液A；

[0035] 将混合液A与100g球磨珠混合后，共同球磨12小时，得到混合液B；将混合液B在105℃的条件下干燥24小时，得到黑色粉末；将所得黑色粉末置于马弗炉中，升温速率为3℃/min，至750℃后保温10小时，保温结束后随炉冷却，待冷却完毕，取出，研磨，得到预烧料中间产物；将预烧料中间产物置于马弗炉中，升温速率仍为3℃/min，至920℃后保温12小时，然后随炉冷却，待冷却完毕，取出，研磨，得到锂离子电池正极材料母体$Li_{1.05}Co_{0.97}Mg_{0.03}O_2$；对锂离子电池正极材料母体$Li_{1.05}Co_{0.97}Mg_{0.03}O_2$进行相应测试其结果如图2、图3所示，从图2中可以看到母体$Li_{1.05}Co_{0.97}Mg_{0.03}O_2$呈完整的层状结构，并含有极少量的$Co_3O_4$杂质，正是由于其中含有极少量的$Co_3O_4$杂质，时材料具备了更好的导电性能；同时材料形貌呈片状叠加

AMPEREX Ex. 1002
Page 1247

外形，表面上分布着及少量的Co_3O_4杂质微粒(图3)。由于片状叠加的外形，使材料具有很好的锂离子脱嵌通道，增加了锂离子的脱嵌能力。

[0036] 在三颈瓶中按AlF_3产量为0.0500g的化学计量称取硝酸铝和氟化锂及0.5g柠檬酸加入10ml无水乙醇中，搅拌直至得到透明溶液，然后将准确称取的5.0000g正极材料母体$Li_{1.05}Co_{0.97}Mg_{0.03}O_2$粉末在搅拌下加入三颈瓶中，搅拌形成均匀的浆状流变态，真空干燥出去无水乙醇溶剂，所得粉末在450-500℃空气中热解2小时，即得到包覆量为1％AlF_3的$Li_{1.05}Co_{0.97}Mg_{0.03}O_2@AlF_3$高电压正极材料。

[0037] 对制备的锂离子电池正极材料$Li_{1.05}Co_{0.97}Mg_{0.03}O_2@AlF_3$进行恒电流充放电测试，其测试结果如图4至图6所示，从测试结果可以看出该正极材料具有很高的放电比容量和优异的循环稳定性能，适用于大倍率充放电需求；在室温环境下，当恒电流充放电倍率为0.5C时，在2.75～4.4V(vs.Li/Li^+)的充放电电压范围内，该层状锂离子电池正极材料$Li_{1.05}Co_{0.97}Mg_{0.03}O_2@AlF_3$的首次放电比容量可高达187.6mAh/g，3.8V平台容量接近100％，循环30次后仍然可达到约180mAh/g，容量保持率约为96％。循环50次后仍然可达到约174mAh/g，容量保持率约为93％。

[0038] 实施例2

[0039] 将0.1050mol(7.7584g)的碳酸锂、0.0646mol(15.5717g)的四氧化三钴、0.0060mol(1.5384g)的六水硝酸镁以及25mL的无水乙醇称量倒入球磨罐中，得到混合液A；

[0040] 将混合液A与150g球磨珠混合后，共同球磨12小时，得到混合液B；将混合液B在105℃的条件下干燥24小时，得到黑色粉末；将所得黑色粉末置于马弗炉中，升温速率为3℃/min，至750℃后保温12小时，保温结束后随炉冷却，待冷却完毕，取出，研磨，得到预烧料中间产物；将预烧料中间产物置于马弗炉中，升温速率为2℃/min，至950℃后保温12小时，保温结束后随炉冷却，待冷却完毕，取出，研磨，得到锂离子电池正极材料母体$Li_{1.05}Co_{0.97}Mg_{0.03}O_2$。

[0041] 在三颈瓶中按AlF_3产量为0.1000g的化学计量称取硝酸铝和氟化锂及1.0g柠檬酸加入10ml乙醇中，搅拌直至得到透明溶液，然后将准确称取的5.0000g正极材料母体$Li_{1.05}Co_{0.97}Mg_{0.03}O_2$粉末在搅拌下加入三颈瓶中，搅拌形成均匀的浆状流变态，真空干燥出去溶剂，粉末在450-500℃空气中热解2小时，即得到包覆量为2％AlF_3的$Li_{1.05}Co_{0.97}Mg_{0.03}O_2@AlF_3$高电压正极材料。经测试，其效果和性能与实施例1基本相同。

[0042] 实施例3

[0043] 将0.0525mol(3.8792g)的碳酸锂、0.0323mol(7.7858g)的四氧化三钴、0.0030mol(0.7692g)的六水硝酸镁以及15mL的无水乙醇称量倒入球磨罐中，得到混合液A；

[0044] 将混合液A与100g球磨珠混合后，共同球磨12小时，得到混合液B；将混合液B在105℃的条件下干燥24小时，得到黑色粉末；将所得黑色粉末置于马弗炉中，升温速率为3℃/min，至750℃后保温10小时，保温结束后随炉冷却，待冷却完毕，取出，研磨，得到预烧料中间产物；将预烧料中间产物置于马弗炉中，升温速率仍为3℃/min，至1000℃后保温12小时，然后随炉冷却，待冷却完毕，取出，研磨，得到锂离子电池正极材料母体$Li_{1.05}Co_{0.97}Mg_{0.03}O_2$。

[0045] 在三颈瓶中按AlF_3产量为0.0500g的化学计量称取硝酸铝和氟化锂及0.5g柠檬酸加入10ml无水乙醇中，搅拌直至得到透明溶液，然后将准确称取的5.0000g正极材料母体$Li_{1.05}Co_{0.97}Mg_{0.03}O_2$粉末在搅拌下加入三颈瓶中，搅拌形成均匀的浆状流变态，真空干燥出

AMPEREX Ex. 1002
Page 1248

去溶剂，粉末在450-500℃空气中热解2小时，即得到包覆量为1％AlF_3的$Li_{1.05}Co_{0.97}Mg_{0.03}O_2$@$AlF_3$高电压正极材料。

[0046] 经测试，其效果和性能与实施例1基本相同。

[0047] 实施例4

[0048] 将0.0525mol(3.8792g)的碳酸锂、0.0323mol(7.7858g)的四氧化三钴、0.0030mol(0.7692g)的六水硝酸镁以及15mL的无水乙醇称量倒入球磨罐中，得到混合液A；

[0049] 将混合液A与100g球磨珠混合后，共同球磨12小时，得到混合液B；将混合液B在105℃的条件下干燥24小时，得到黑色粉末；将所得黑色粉末置于马弗炉中，升温速率为3℃/min，至750℃后保温10小时，保温结束后随炉冷却，待冷却完毕，取出，研磨，得到预烧料中间产物；将预烧料中间产物置于马弗炉中，升温速率仍为3℃/min，至1000℃后保温12小时，然后随炉冷却，待冷却完毕，取出，研磨，得到锂离子电池正极材料母体$Li_{1.05}Co_{0.97}Mg_{0.03}O_2$。

[0050] 在三颈瓶中按AlF_3产量为0.2500g的化学计量称取硝酸铝和氟化锂及2.5g柠檬酸加入15ml无水乙醇中，搅拌直至得到透明溶液，然后将准确称取的5.0000g正极材料母体$Li_{1.05}Co_{0.97}Mg_{0.03}O_2$粉末在搅拌下加入三颈瓶中，搅拌形成均匀的浆状流变态，真空干燥出去溶剂，粉末在450-500℃空气中热解2小时，即得到包覆量为5％AlF_3的$Li_{1.05}Co_{0.97}Mg_{0.03}O_2$@$AlF_3$高电压正极材料。

[0051] 经测试，其效果和性能与实施例1基本相同。

[0052] 实施例5

[0053] 将0.0525mol(3.8792g)的碳酸锂、0.0317mol(7.6255g)的四氧化三钴、0.0050mol(1.2820g)的六水硝酸镁以及15mL的无水乙醇称量倒入球磨罐中，得到混合液A；

[0054] 将混合液A与100g球磨珠混合后，共同球磨12小时，得到混合液B；将混合液B在105℃的条件下干燥24小时，得到黑色粉末；将所得黑色粉末置于马弗炉中，升温速率为3℃/min，至750℃后保温10小时，保温结束后随炉冷却，待冷却完毕，取出，研磨，得到预烧料中间产物；将预烧料中间产物置于马弗炉中，升温速率仍为3℃/min，至920℃后保温12小时，然后随炉冷却，待冷却完毕，取出，研磨，得到锂离子电池正极材料母体$Li_{1.05}Co_{0.95}Mg_{0.05}O_2$。

[0055] 在三颈瓶中按AlF_3产量为0.0500g的化学计量称取硝酸铝和氟化锂及0.5g柠檬酸加入10ml无水乙醇中，搅拌直至得到透明溶液，然后将准确称取的5.0000g正极材料母体$Li_{1.05}Co_{0.97}Mg_{0.03}O_2$粉末在搅拌下加入三颈瓶中，搅拌形成均匀的浆状流变态，真空干燥出去溶剂，粉末在450-500℃空气中热解2小时，即得到包覆量为1％AlF_3的$Li_{1.05}Co_{0.95}Mg_{0.05}O_2$@$AlF_3$高电压正极材料。

[0056] 经测试，其效果和性能与实施例1基本相同。

[0057] 以上所述，仅为本发明的具体实施方式，本说明书中所公开的任一特征，除非特别叙述，均可被其他等效或具有类似目的的替代特征加以替换；所公开的所有特征、或所有方法或过程中的步骤，除了互相排斥的特征和/或步骤以外，均可以任何方式组合。

AMPEREX Ex. 1002
Page 1249

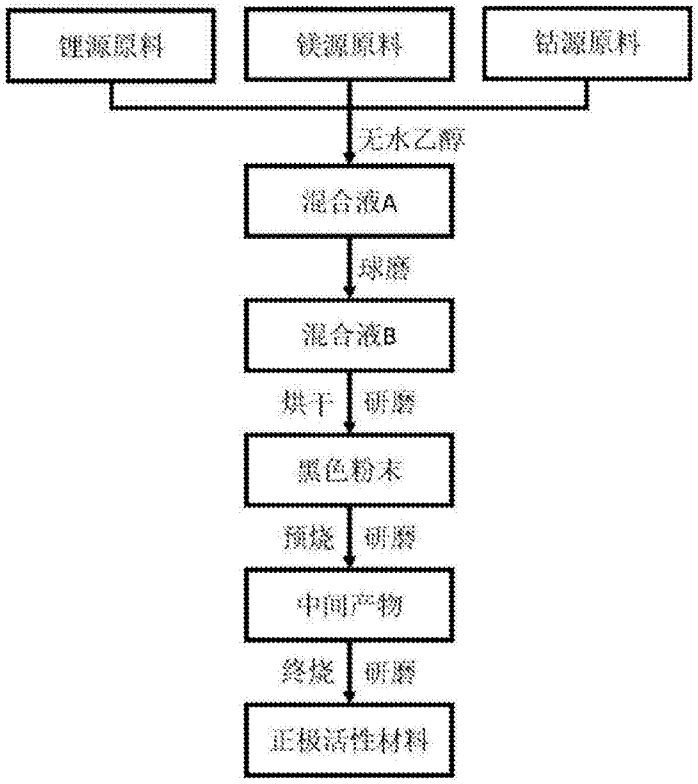


图1

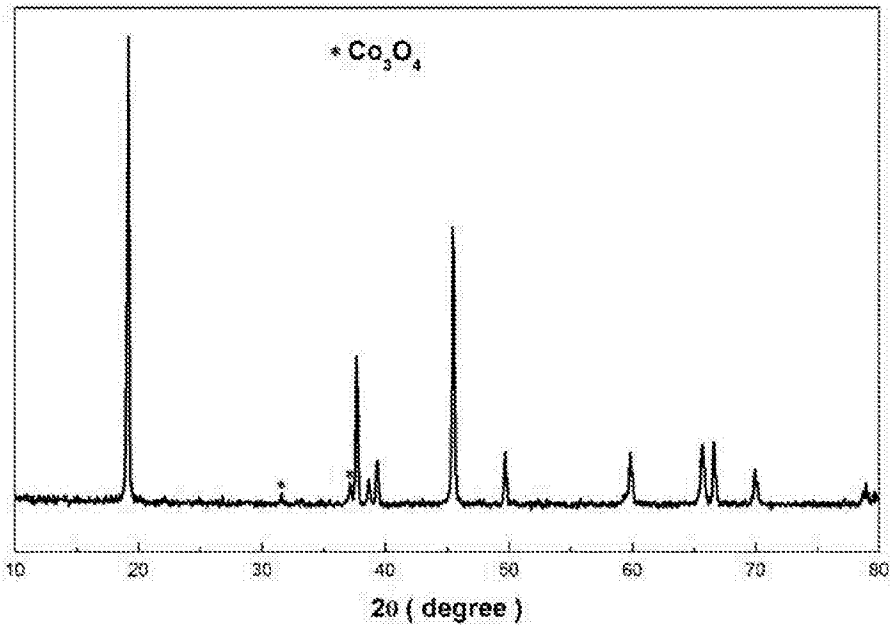


图2

AMPEREX Ex. 1002
Page 1250

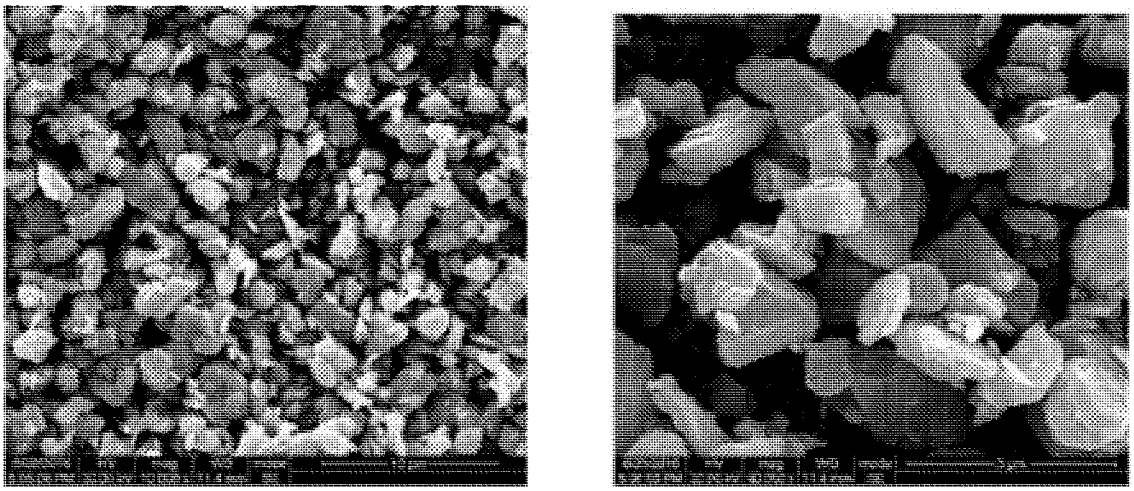


图3

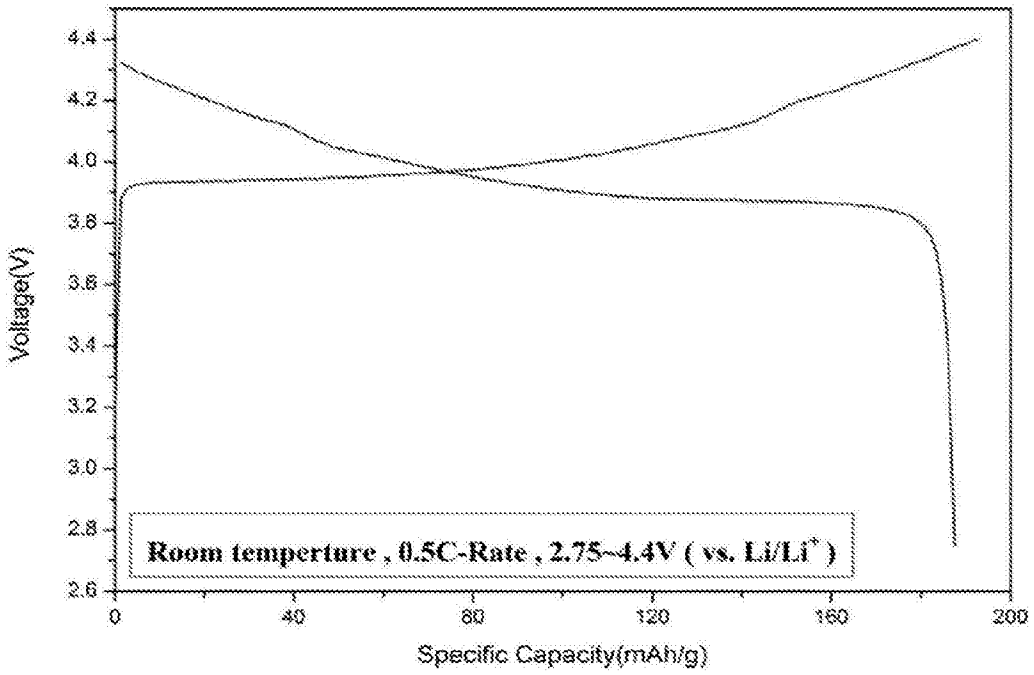


图4

AMPEREX Ex. 1002
Page 1251

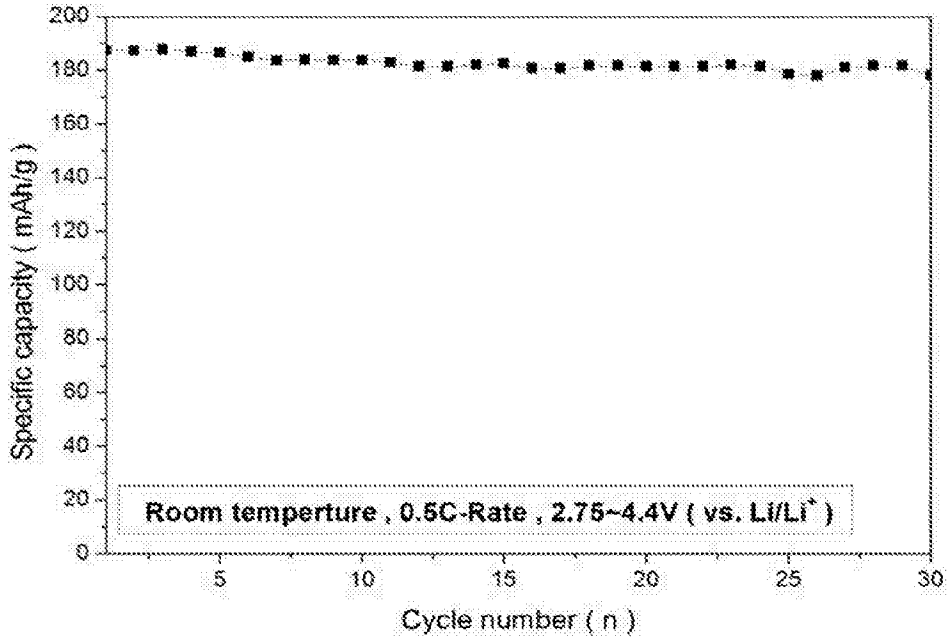


图5

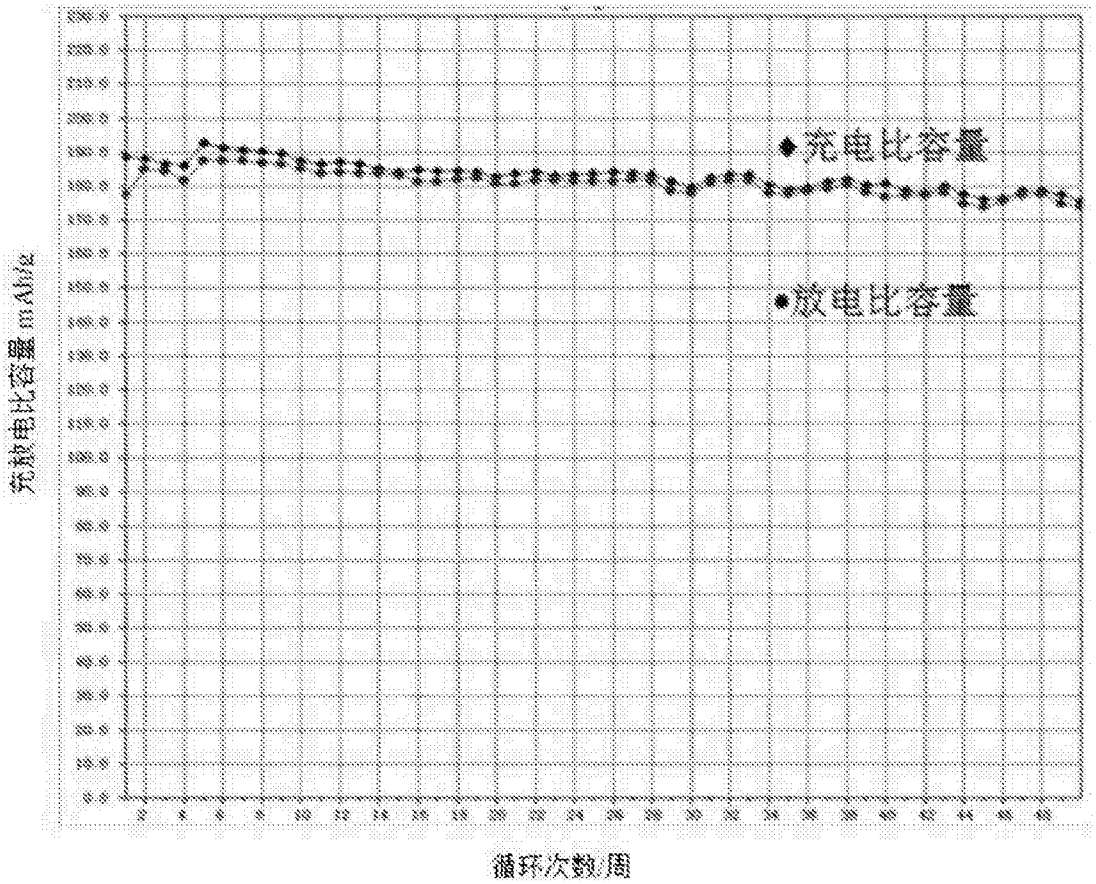


图6

AMPEREX Ex. 1002
Page 1252